Earthquake and Environmental Hazards (EEH)

XXXVII cycle – Academic years 2021-2025

Joining Field Geology, Geodetic and Seismological Observations for seismotectonic analysis

PhD Candidate:

Federico Pietrolungo

Federico Pietrolungo

Supervisor:

Prof. Giusy Lavecchia

Glavecchia

Co-Supervisor:

Prof. Mimmo Palano

Mimmo Palano

Co-Supervisor:

Dott. Daniele Cirillo

Daniele Cirillo

University "G.d'Annunzio" Chieti-Pescara – Dipartimento di Scienze



This work is distributed with Licence Creative Commons (CC BY-NC-SA 4.0)

Attribution-NonCommercial-ShareAlike 4.0 International

https://creativecommons.org/licenses/by-nc-sa/4.0/

A Ginevra.

Ringraziamenti

Ringrazio la prof. Lavecchia G. per avermi dato questa opportunità e per avermi insegnato quanto siano fondamentali la determinazione e la costanza nella ricerca. La sua carriera rappresenta per me un esempio di come la scienza possa essere uno spazio in cui coltivare la più autentica curiosità. Mi ha trasmesso l'importanza del confronto scientifico e del rigore nella discussione. Spero, nel mio percorso futuro, di riuscire a mantenere viva la passione per la ricerca che ho avuto la fortuna di conoscere attraverso il suo esempio.

Ringrazio il prof. Palano M. per il prezioso contributo alla costruzione della mia figura professionale, concedendomi spazi e tempi per sviluppare competenze e tecnicità fondamentali per ogni ricercatore. Il suo supporto è stato determinante non solo per affrontare con consapevolezza questa tesi, ma anche – e soprattutto – per comprendere cosa significhi davvero essere ricercatore e cosa desidero diventare al termine di questo percorso di dottorato.

Ringrazio il dott. Cirillo D. per la sua costante presenza, soprattutto nei momenti più difficili. Il suo supporto, personale e amichevole, è stato imprescindibile per il completamento di questa tesi. Le nostre discussioni sono sempre state un porto sicuro: uno spazio in cui potermi esprimere liberamente, senza timore di errori o incertezze, che fanno naturalmente parte del percorso di ogni dottorando.

Ringrazio la prof. De Nardis R., il prof. Brozzetti F., il dott. Bello S. e il dott. Andrenacci C. per avermi dato l'opportunità di far parte del loro team. La loro disponibilità all'ascolto, unita a consigli e suggerimenti sempre puntuali ed efficaci, è stata per me di grande valore lungo tutto il percorso di ricerca.

Ringrazio i revisori di questa tesi, il dott. Carafa M. C. e il prof. De Guidi G., per i loro preziosi consigli e contributi, che hanno arricchito in modo significativo il lavoro svolto. La loro attenta lettura e le osservazioni puntuali mi hanno permesso di migliorare la qualità complessiva del testo e di affinare ulteriormente l'approccio scientifico adottato.

Ringrazio Gaia, perché so che tante scelte le devo a lei. Perché, comunque andasse, sapevo di avere accanto qualcuno che c'era davvero, in modo semplice, costante e vero. La sua presenza è stata il mio punto fermo, la certezza che non ero mai solo — con o senza un dottorato.

Ringrazio Donato per le risate e per le lunghissime discussioni, informali e piene di idee strampalate che — lo sappiamo bene — non realizzeremo mai. Auguro a ogni dottorando, presente o futuro, di avere la fortuna di incontrare una persona come lui: capace di alleggerire, con intelligenza e ironia, anche il peso più grande di questo percorso.

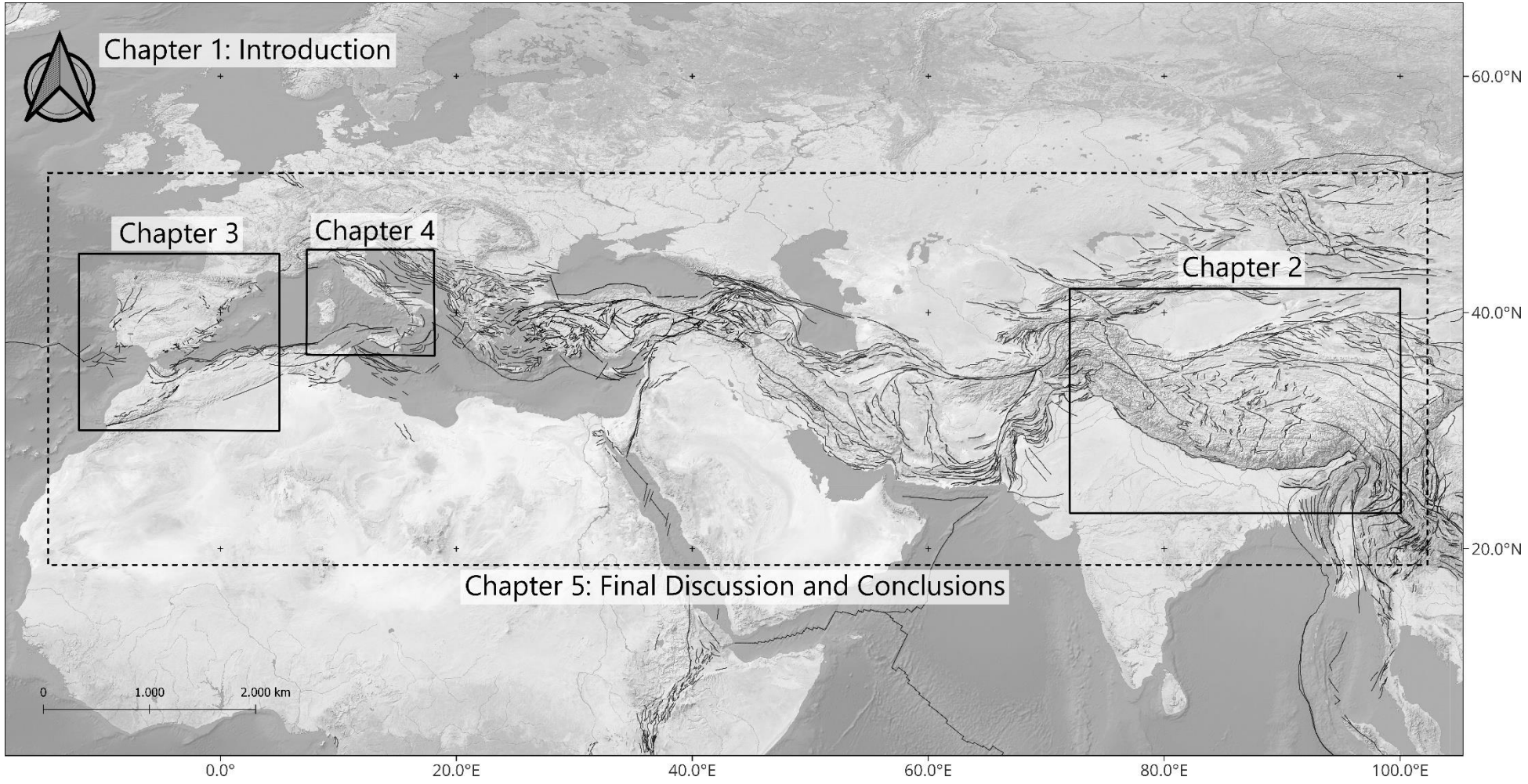
Ringrazio Asier, perché il mio periodo a Palermo sarebbe stato un disastro senza di lui. È una di quelle persone che non sai di aver bisogno finché non le incontri, capace di trasmetterti fiducia quando tu non ne hai, e di farlo con una naturalezza disarmante.

Ringrazio i miei genitori, mia sorella, Marco e i bimbi. La mia famiglia, che forse non ha sempre compreso appieno cosa significasse fare un dottorato o fare ricerca, ma che mi ha sempre sostenuto con amore e pazienza. La loro fiducia in me è qualcosa di davvero ammirevole. Sono grato per il loro sostegno incondizionato, che ha reso ogni passo di questo percorso più significativo.

Ringrazio i miei amici, che pur non essendo sempre consapevoli del peso del mio lavoro, mi hanno sempre dato l'opportunità di fare delle bellissime pause dal dottorato. C'è sempre stato qualcuno con cui parlare, ridere, fare sport. Ho sempre gli stessi amici, e li ringrazio da quando ho preso la mia prima laurea, senza mai stancarmi di farlo. Sappiate che anche in questa tesi c'è qualcosa di voi.

Per tutti coloro che ho dimenticato, scusatemi, tre anni sono tanti. Pensare che una tesi di dottorato sia solo tua è impossibile. Tutti quelli che ho ringraziato hanno sicuramente inserito pezzi fondamentali di questo puzzle, ma ce ne sono molti altri che hanno contribuito allo stesso modo, con una chiacchiera, uno sfogo, un consiglio personale.

Ringrazio tutti coloro che hanno creduto in questo dottorato, anche più di quanto l'abbia fatto io.


Chapter 1: Introduction
Chapter 3
Chapter 4
Chapter 2
Chapter 5: Final Discussion and Conclusions
0
1.000
2.000 km
60.0°N
40.0°N
20.0°N
0.0°
20.0°E
40.0°E
60.0°E
80.0°E
100.0°E

Index

1. Introduction 1

1.1. Thesis abstract 2

1.2. Thesis outline 3

2. Comparison of Crustal Stress and Strain fields in the Himalaya-Tibet Region: Geodynamic Implications 6

2.1. My contribution 7

2.2. Abstract 7

2.3. Introduction 8

2.4. Background 10

2.4.1. Geodynamic Evolution 10

2.4.2. Seismotectonic Framework 12

2.4.3. Geodynamic Models 13

2.5. Data 15

2.5.1. GNSS Data 15

2.5.2. Seismicity and Focal Mechanisms Catalog 16

2.6. Methods 18

2.6.1. Geodetic Strain Rate Field 18

2.6.2. FMS Formal Inversion 20

2.7. Results 21

2.7.1. Strain Rate Field 21

2.7.2. Stress Field 23

2.7.3. Stress-Strain Comparison 24

2.8. Discussion and Conclusions 26

2.9. Supplementary materials 29

3. Active Strain and Stress Fields of Iberia and Northwest Africa: New Insights on Geodynamics from Seismic and GNSS Data 31

3.1. My contribution 32

3.2. Abstract 32

3.3. Introduction 33

3.4. Background setting 36

3.4.1. Geodynamic setting 36

3.4.2. Active Faults 37
3.4.3. Seismicity 39
3.5. Methods 42
3.5.1. Stress field estimation 42
3.5.2. GNSS data processing and velocity and strain field estimation 44
3.6. Results 45
3.6.1. Stress field 45
3.6.1.1. Stress ellipsoids 45
3.6.1.2. Maximum horizontal stress field 48
3.6.2. Velocity field 49
3.6.3. Strain field 51
3.6.3.1. Horizontal strain field 51
3.6.3.2. Minimum horizontal strain 52
3.7. Discussion 53
3.7.1. The stress field of Iberia and Northwest Africa 54
3.7.2. The strain field of Iberia and Northwest Africa 55
3.7.3. The complex Eurasia-Africa plate boundary in the Atlantic-Mediterranean transition 57
3.7.4. Novel insights into the rotation of Iberia 59
3.7.5. The aseismic westward displacement of the Gibraltar Block 61
3.7.6. Low deforming intraplate active regions 65
3.8. Conclusions 66
4. Multi-source deformation maps in the Italian Peninsula: comparison between geological, geodetic and seismological data 69
4.1. My contribution 70
4.2. Abstract 70
4.3. Introduction 70
4.4. Data 72
4.4.1. Host faults and fault systems 72
4.4.2. Fault Striation Pair 74
4.4.3. GNSS velocities 75
4.4.4. Focal Mechanisms Solutions 77
4.5. Methods 78
4.5.1. Geological strain 78
4.5.2. Geodetic strain rate map 80

4.5.3. Building a common grid – Angular difference 83
4.6. Results 85
4.7. Conclusion and discussion 86
4.7.1. New methodological approaches for multi-source strain 86
4.7.2. Multi-source strain patterns 87
5. Final discussion and conclusion 91
5.1. Stress inversion 92
5.2. Geodetic strain rate 94
5.3. Seismotectonic comparative analysis 95
5.3.1. Strain and Stress Patterns Across Orogenic Belts 95
5.3.2. Indenter-escape tectonics across scale 97
5.4. The Complementary Role of Geodetic, Seismological, and Geological Data 98
5.5. Concluding remarks 101
6. Scientific Production 103
6.1. Published articles 104
6.1.1. Paleo-Earthquake Fingerprints and Along-Strike Slip Variation of the Silent Mt. Morrone Normal Fault (Central Italy): A Structural-Geochemical Approach 104
6.1.2. QUIN 2.0 - new release of the QUaternary fault strain INdicators database from the Southern Apennines of Italy 105
6.1.3. Slowly Deforming Megathrusts within the Continental Lithosphere: A Case from Italy 105
6.1.4. Reappraisal and Analysis of Macroseismic Data for Seismotectonic Purposes: The Strong Earthquakes of Southern Calabria, Italy 106
6.2. Conference Oral presentations 106
6.2.1. Crustal deformation at the Himalaya region and South Tibet: a 3D structural model from a multidisciplinary perspective 107
6.2.2. Himalaya-Tibet crustal stress and strain 107
6.2.3. Crustal strain-rate and stress field in the Himalaya-Tibet Region 108
6.1. Conference Poster presentations 109
6.1.1. Crustal deformation at the Himalaya region and South Tibet: a 3D structural model from a multidisciplinary perspective 109
6.1.2. The November 9, 2022, compressional seismic sequence (Mw 5.5) - another piece of information to the 3D seismotectonic fault model of the coastal Marche-Adriatic offshore area (Italy) 110
7. References 112
8. Supplementary material 133
8.1. Supplementary material for Chapter 2 134

8.1.1. Table – Focal Mechanism Solutions catalog 134
8.1.2. Table – GNSS velocities 263
8.1.3. Table – Stress results values 298
8.1.4. Table – Geodetic strain 307
8.1.5. Figures – Stress inversion results 373
8.2. Supplementary material for Chapter 3 436
8.2.1. Image – Focal Mechanism Solutions 436
8.2.2. Table – Historical Earthquakes 436
8.2.3. Table – Focal Mechanism Solutions 439
8.2.4. Table – Stress Inversion Results 519
8.2.5. Table – σ_{Hmax} directions 525
8.2.6. Table – GNSS Networks used for velocity field computation 535
8.2.7. Table – GNSS velocities 536
8.3. Supplementary material for Chapter 4 564
8.3.1. Table – Stress2GRID results – Geological (SS) vs Geodetic strain (GPS) 564
8.3.2. Table – Stress2GRID results – Geological (SS) vs Seismological strain (FM) 576
8.3.3. Table – Stress2GRID results – Geodetic (GPS) vs Seismological strain (FMS) 581

1.Introduction

1.1. Thesis abstract

The study of stress and strain fields is fundamental to understand the active deformation of the Earth's crust and its implications for seismotectonics and geodynamics. This thesis integrates field geology, geodetic data, and seismological observations to investigate the relationship between stress and strain in different tectonic settings. The main objectives are: i) Update GNSS based velocity fields and Focal Mechanisms catalogs; ii) Identify the most effective stress-strain analysis methods to gain deeper insights into the seismotectonic of the areas; iii) Observe the results to discuss the seismotectonic and geodynamic models proposed in the literature and identify areas that need further investigation.

This comparative approach offers valuable insights into the interaction between strain and stress in different regions of the Alpine-Himalayan Belt (Read and Watson, 1975). The first two case studies primarily focus on comparing stress fields, derived from earthquake focal mechanisms, with strain fields, interpolated from GNSS velocity data. The third case study incorporates a broader dataset, integrating fault-striation pairs from structural geology alongside seismic and GNSS data. This multi-source approach enables a more refined interpretation of fault activity and strain patterns, improving our understanding of the region's seismotectonics.

A key finding of this research is that in many regions, the alignment between maximum horizontal stress (σ_{Hmax}) and minimum horizontal strain (ε_{Hmin}) suggests a mechanically elastic response of the crust, where deformation occurs in the same direction as the applied stress. However, significant deviations from this expected pattern highlight the influence of additional factors such as lateral variations in crustal properties, gravitational forces, and deep-seated geodynamic processes. In the Himalaya-Tibet region, the stress and strain fields indicate a combination of compressional forces from the India-Eurasia convergence and widespread eastward extrusion of the Tibetan Plateau, controlled by a combination of indenter-escape tectonics, undethrusting of the Indian Plate and topographic loading. In the Iberia and Northwest Africa, the convergence of Eurasia and Africa in the Mediterranean results in complex geodynamic processes, influencing multiple crustal blocks at different stages of subduction and collision. This study reveals that strain is primarily concentrated along the plate boundary, with the Gibraltar Block undergoing westward displacement due to subduction rollback and/or mantle flow, while tectonically active intraplate regions exhibit low horizontal strain rates, mainly controlled by vertical stress and isostatic adjustments. We also introduce a high-detail, multi-source strain model for the Apennines (Italy) by synthesizing Quaternary fault-slip data, earthquake focal mechanism solutions, and GNSS-derived strain parameters to map principal strain orientations and reveal the interplay between long-term fault slip patterns, seismic strain release, and current crustal deformation.

The integrated approach confirms a predominantly extensional regime—with regional strain correlating over the past 3.5 million years and evidence for an eastward migration of the extensional front—thereby offering a significant step toward a unified seismotectonic model for Italy and providing valuable tools for future geodynamic research and seismic hazard assessment.

The thesis concludes with a discussion of the used methodology for formal stress inversion and strain computation and about the broader implications of these methods in seismotectonics and geodynamics. We also underscore both the similarities and differences among various seismotectonic domains by evaluating the effectiveness of our approach across diverse regions along the Alpine-Himalyan Belt. This synthesis of updated data leads to the most refined interpretation of the underlying deformation processes, ultimately enhancing our understanding of regional tectonic dynamics.

This thesis highlights the importance of a multidisciplinary approach in seismotectonic research and emphasizes the need to study different seismotectonic domains to obtain new insight and provide refined answers to key scientific questions.

1.2. Thesis outline

The study is structured into eight chapters, with the first five forming the main body of the thesis. These chapters provide a comprehensive analysis of the stress-strain relationship and its geodynamic implications.

The first chapter contains the thesis abstract, which contains the aims of the research project described together with the objectives achieved. The chapter also contains this thesis outline.

The chapters 2, 3 and 4 present case studies from regions along the Alpine-Himalayan Belt characterized by different tectonic strain rates:

- Chapter 2: Himalaya-Tibet (high strain rate)
- Chapter 3: Iberia and Northwest Africa (low strain rate)
- Chapter 4: Italian Apennines (medium strain rate)

These case studies analyse the spatial relationships between geodetically derived strain fields (from GNSS velocity data) and stress fields inferred from earthquake focal mechanisms. The first two case studies primarily focus on stress-strain comparisons, while the third one employs a multi-source approach by incorporating structural geology data (fault-striation pairs) alongside geodetic and seismological observations.

In detail:

Chapter 2 presents a published article on Remote Sensing (https://doi.org/10.3390/rs16244765). In the Himalaya-Tibet region, we compiled all available Focal Mechanism Solutions (FMSs) for the period between June 1933 and March 2024, gathering approximately 1,300 FMSs related to earthquakes with Mw > 4. Additionally, we updated the velocity field by processing ~120 GNSS stations and merging the results with velocity fields from the literature using the Helmert Transformation. Based on this dataset, we performed stress inversion of the seismological data using a novel approach, applying STRESSINVERSE (Vavryčuk, 2014) within a regular grid-search framework. To enable an optimal comparison between stress and strain, we computed the strain rate field from the GNSS velocity field using VISR (Shen et al., 2015). This comparison allowed us to characterize the seismotectonic domains and analyse the forces driving the observed stress and strain fields.

Chapter 3 is an article submitted on Gondwana Research journal. In this chapter we applied the same methodology, adjusting some parameters, in Iberia and Northwest Africa. We collect all the FMSs for the area, and we processed by GAMIT/GLOBK (Herring et al., 2018) software GNSS data to obtain the updated velocity field in the area. We applied here the new approach to obtain the horizontal maximum stress, the geometry of the stress axes and the stress ratio from the formal inversion of the FMSs with the methodology proposed in the Chapter 2. This study focuses on understanding where strain accumulates and how it relates to the regional stress field in the westernmost Mediterranean. Key findings reveal that strain is mainly concentrated along the Eurasia-Africa boundary, with distinct deformation behaviours in different crustal domains, while intraplate regions exhibit low horizontal strain rates, primarily influenced by vertical stress.

The Chapter 4 is a manuscript in preparation on the Italian Apennines. In this chapter we focused on the strain fields and how it can be described by different data. This study presents a new high-resolution strain map for peninsular Italy by integrating Quaternary fault-slip data, focal mechanisms, and GNSS-derived strain field. The results highlight a predominantly extensional regime with a SW-NE to NW-SE trending stretching directions, consistent with long-term geological deformation and ongoing seismic activity, supporting the eastward migration of the extensional front along the Italian Apennines. Beyond mapping strain, this work provides a novel framework for comparing multi-source deformation data, improving seismotectonic zoning and seismic hazard assessment in Italy.

The main of the thesis concludes with the Chapter 5 that discusses the new methodology used for computing the formal stress inversion and the methodology applied for strain rate computation. This chapter also presents an important and insightful discussion by

comparing the seismotectonics and geodynamics of different orogenic belts across the Alpine-Himalayan Belt, as well as the deformation model of indenter-escape tectonics by comparing the Tibetan Plateau and the Alboran Sea. The discussion highlights how integrating stress and strain data from multiple sources enhances our ability to characterize active deformation and assess seismic hazard.

In Chapter 6, the scientific output is presented, showing the scientific articles I have collaborated on, as well as the oral presentations and posters presented at various national and international conferences.

In Chapter 7, all the references from Chapters 2, 3, 4, 5 and 6 are listed. References for supplementary materials (Chapter 8) are provided in the same chapter.

2. Comparison of Crustal Stress and Strain fields in the Himalaya-Tibet Region: Geodynamic Implications

This paper is authored by: Pietrolungo F., Lavecchia G., Madarieta-Txurruka A., Sparacino F., Srivastava E., Daniele Cirillo., de Nardis R., Andrenacci C., Bello S., Parrino N., Sulli A & Palano M.

Published in December 2024 by Remote Sensing – MDPI, 2024, 16(24), 4765; https://doi.org/10.3390/rs16244765

2.1. My contribution

In this research, my primary task was to gather all available data for the study area from both seismological and geodetic perspectives. I aimed to identify the stations for which RINEX data (the fundamental input for deriving a velocity field) could be obtained, as well as pre-existing velocity solutions from the literature that could be integrated into our analysis. Additionally, I developed scripts to collect focal mechanisms based on well-defined criteria (such as the calculation method and magnitude) while ensuring that the final database did not contain multiple solutions for the same seismic event.

From a computational standpoint, I assisted for generating the velocity field and processing the data using GAMIT/GLOBK. I then carried out the strain rate calculations presented in this study, testing various methods and input parameters beforehand.

On the seismological side, after gathering the necessary data, I personally developed a script to apply the STRESSINVERSE algorithm (see next in the main text) over a predefined grid, automatically generating graphical and tabulated outputs, which were included in both the figures of the article and the supplementary materials.

Finally, I authored the manuscript, following an in-depth review of the existing seismotectonic and geodynamic models for the study area. This involved a critical analysis of these models, highlighting their limitations. I personally drafted the first version of the article, carefully refining both the text and figures.

2.2. Abstract

The Himalaya–Tibet region represents a complex region of active deformation related to the ongoing India–Eurasia convergence process. To provide additional constraints on the active processes shaping this region, we used a comprehensive dataset of GNSS and focal mechanisms data and derived crustal strain and stress fields. The results allow the detection of features such as the arc-parallel extension along the Himalayan Arc and the coexistence of strike-slip and normal faulting across Tibet. We discuss our findings concerning the relevant geodynamic models proposed in the literature. While earlier studies largely emphasized the role of either compressional or extensional processes, our findings suggest a more complex interaction between them. In general, our study highlights the critical role of both surface and deep processes in shaping the geodynamic processes. The alignment between tectonic stress and strain patterns indicates that the crust is highly elastic and influenced by present-day tectonics. Stress and strain orientations show a clockwise rotation at 31°N, reflecting deep control by the underthrusted Indian Plate. South of this boundary,

compression is driven by basal drag from the underthrusting Indian Plate, while northward, escape tectonics dominate, resulting in eastward movement of the Tibetan Plateau. Localized stretching along the Himalaya is likely driven by the oblique convergence resulting from the India–Eurasia collision generating a transtensional regime over the Main Himalayan Thrust. In Tibet, stress variations appear mainly related to changes in the vertical axis, driven by topographically induced stresses linked to the uniform elevation of the plateau. From a broader perspective, these findings improve the understanding of driving crustal forces in the Himalaya–Tibet region and provide insights into how large-scale geodynamics drives surface deformation. Additionally, they contribute to the ongoing debate regarding the applicability of the stress–strain comparison and offer a more comprehensive framework for future research in similar tectonic settings worldwide.

2.3. Introduction

The spatial comparison of crustal stress and strain patterns is one of the most compelling approaches in a geodynamically complex framework. It provides useful constraints on driving forces and highlights those regions which accumulate stress and encourage seismic deformation. This approach has been widely applied in the literature to describe crustal behavior and deformation models (Chang et al., 2003; Dobretsov et al., 2013; Keiding et al., 2009; Palano et al., 2013; Rashidi and Derakhshani, 2022; Reyners, 2010). For instance, Chang et al., 2003, studying Taiwan Island, found that both stress and strain fields perceptively reflect the long-term collision mechanism and that inherited structure can play a role in redirecting the stress–strain orientation. In Japan, Townend and Zoback, 2006 found that observed geodetic velocities are mainly driven by the crustal collision rather than the subduction zone locking; Palano et al., 2013 applied the comparison to the Gibraltar Orogenic Arc, finding a significant coherence between well-constrained stress indicators and GNSS-derived strain, therefore suggesting that deep dynamic processes control both crustal stress and surface deformation. Other studies have been conducted both in geothermal-active regions (Keiding et al., 2009) and in volcanically active areas (Reyners, 2010), providing information on the seismicity distribution and deformation behavior of these areas.

Himalaya–Tibet (Figure 2.1) represents a complex region of active deformation related to the long-lasting and still active India–Eurasia convergence process (Van Hinsbergen et al., 2019). Although the Indian-Eurasian convergence is a puzzling geodynamic process that generates active deformation and seismicity across different geographical areas, such as the Kachchh region (Bhatia et al., 1999; Khattri et al., 1984; Malik et al., 2024; Srivastava et al., 2023), most of the crustal deformation is currently concentrated along the Himalayan Arc, driven by the high convergence rate between the Indian and Eurasian Plates (Tian et al., 2015). In the central sector of the Himalayan Arc (Nepal), the convergence is predominantly arc-normal

(Bettinelli et al., 2006; Bilham et al., 1997), while to the east and west, a significant arc-parallel component of deformation has been observed both by geological and geodetic data (De Sarkar et al., 2013; Hetényi et al., 2016; Kumar et al., 2023b, 2023a; Panda and Lindsey, 2024; Styron et al., 2015). Despite the ongoing N–S convergence, southern and central Tibet are also experiencing significant E–W extension. This complex structural configuration, characterized by the concurrent presence of active strike-slip and normal fault systems traversing Tibet (Dasgupta et al., 2021; Zhang and Wang, 2007), hampers effective kinematic zonation in the region that still lack definitive characterization.

Due to its complexity, different models have been proposed for the ongoing deformation (at least for the last few Ma) of the Himalaya–Tibet region: the topographic loading (Dewey, 1988), the indenter-escape tectonic (Tapponnier and Molnar, 1976), the thinning model (Styron et al., 2015), the oblique convergence (McCaffrey and Nabelek, 1998), and the channel flow (Bird, 1991).

We employ the latest and most comprehensive geodetic crustal motion data, along with a novel estimation of the seismological stress and geodetic strain rate fields. Using these results, we aim to furnish a critical bridge among current geodynamic models proposed for the Himalaya–Tibet region, providing therefore an empirical evaluation of their applicability through a detailed stress–strain comparison. Such a detailed comparison will offer a refined perspective on ongoing tectonic processes, enhancing understanding of the driving forces behind crustal deformation in complex tectonic settings.

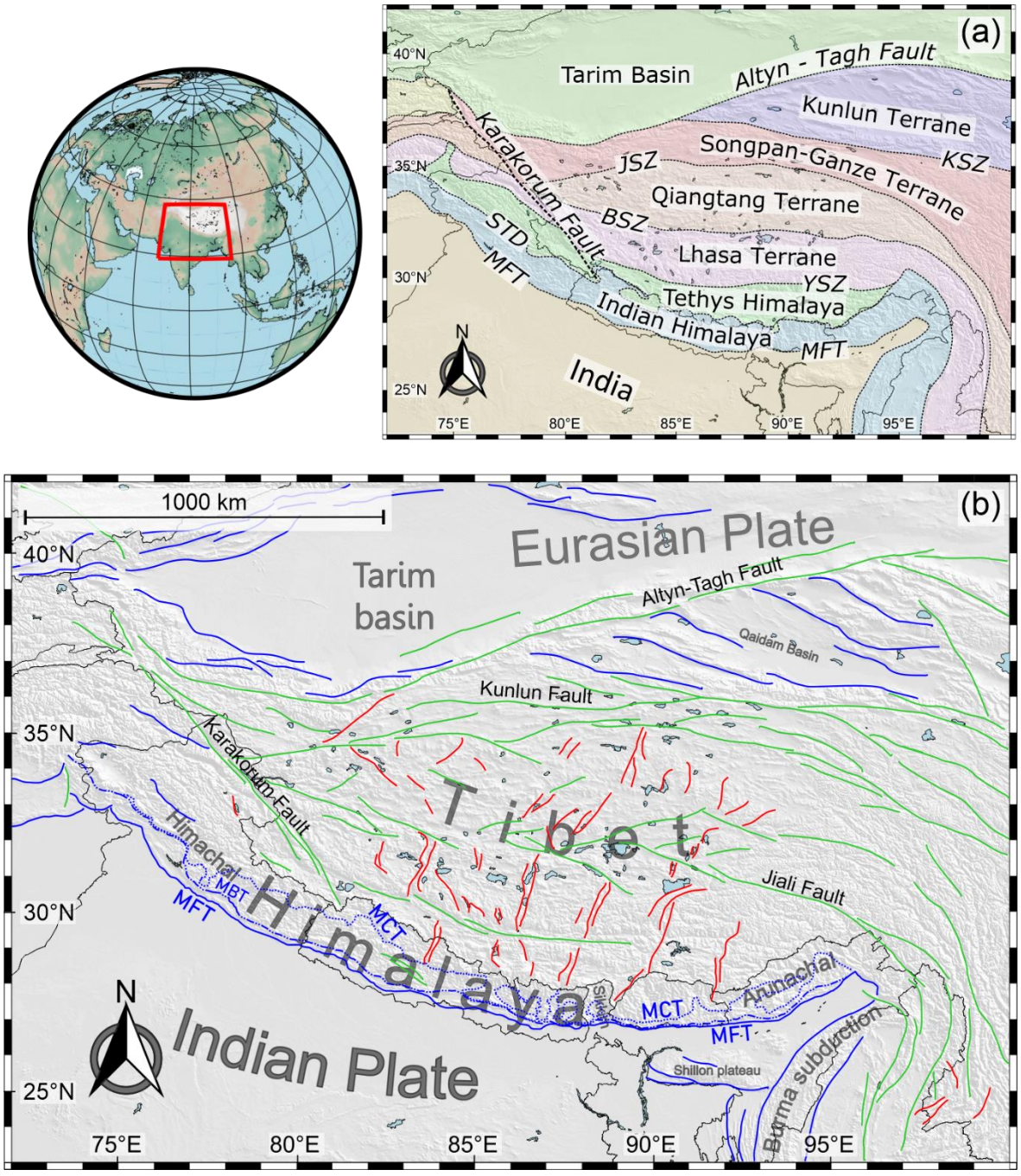


Figure 2.1: Geological background of the Himalaya-Tibet region. a) Main terranes, suture zones and principal tectonic lineaments on the study region (modified from Li et al., 2015). KSZ: Kunlun Suture Zone; JSZ: Jinsha Suture Zone; BSZ: Bangong-Nujiang Suture Zone; YSZ: Yarlung-Tsangpo Suture Zone; STD: South Tibetan Detachment; MFT: Main Frontal Thrust. b) Active and main faults from Zelenin et al., 2022: blue: thrust; red: normal fault; green strike-slip fault. MCT: Main Central Thrust; MBT: Main Boundary Thrust; MFT: Main Frontal Thrust. The terrain model is from GEBCO Bathymetric Compilation Group 2023, 2023, accessed on 31 October 2024

2.4. Background

2.4.1. Geodynamic Evolution

Tibet (i.e., the region in central Asia located between the Tarim Basin to the north and the Indian Plate to the south) has an extensive geological history (Van Hinsbergen et al., 2019).

The current geological setting of Tibet resulted from the occurrence of sequential geodynamic events such as microcontinent collision, the building of orogenic belts, and the formation of island arcs, at least since the early Paleozoic (Xiao et al., 2015). Nowadays, from north to south, the Kunlun (KUT), Songpan-Ganze (SGT), Qiangtang (QT), Lhasa (LHT), the Tethys Himalaya (THT), and the Indian Himalaya (INT) terranes represent the pronounced horizontal heterogeneity of the plateau (Hetényi et al., 2016) (Figure 2.1). These terranes are separated by suture zones, including the Kunlun (KSZ), Jinsha (JSZ), Bangong-Nujiang (BSZ), and Yarlung-Tsangpo sutures (YSZ) (Figure 2.1). All these suture lines are the result of a succession of subductions, from the closure of the Paleo-Tethys in the Late Triassic (Kunlun and Jinsha suture zones) up to the closure of the Bangong-Nujiang Ocean, the northern branch of the Neo-Tethys, with the formation of the Bangong-Nujiang suture zone in the Late Cretaceous (Zhu et al., 2022).

Since the Late Cretaceous, India began its northward drift, separating Gondwana. During this process, the Tethys Himalaya Terrane moved away from India, leading to the opening of the North Indian Sea. Both India and the Tethys Himalaya moved towards the Eurasian plate at a rate of approximately 15–18 cm/yr until they collided around 60–55 Ma (Van Hinsbergen et al., 2019). Around 50 Ma, the convergence rates significantly slowed to 6 cm/yr, marking the onset of the continent–continent collision phase (Bilham, 2019). This latest phase of shortening has been accommodated by the continuous underthrusting of the Indian shield beneath the Tethyan Himalaya and the Lhasa Terrane (Molnar and Tapponnier, 1975), as also evidenced by recent seismic observations (Nábělek et al., 2009) which imaged a distinct cold body beneath the Lhasa Terrane. The underthrusting also explains the uplift in Tibet during the last 40 Ma (Rowley and Currie, 2006; Wu et al., 2022). However, other hypotheses have been suggested (Finch et al., 2014; Powell, 1986; Wiesmayr and Grasemann, 2002).

Following the India–Eurasia collision, the deformation fronts progressively shifted southward from the YSZ, giving rise to the imbricated fold-and-thrust belt of the Himalayas. Southward, Tibet is bounded by the South Tibetan Detachment (STD), which represents the lower boundary of the stacked Tethyan Himalaya sequence. The STD is a lithospheric shear zone in which both reverse and normal faulting episodes have been recorded (Burchfiel et al., 1992; Finch et al., 2014; Wiesmayr and Grasemann, 2002). The detachment acted as a shortening structure during the Eocene (Aikman et al., 2008), meanwhile the normal faulting was probably active during the Miocene (Godin et al., 2006). Different hypotheses have been proposed for the reactivation of the STD with normal faulting features (Kellett et al., 2019) such as gravitational collapse (Hodges et al., 1993), wedge extrusion (Kellett and Grujic, 2012), channel flow (Jamieson et al., 2006), or tectonic wedging/duplexing (Webb et al., 2011, 2007).

In the southern part of the STD, the Indian Himalaya Terrane is affected by a complex thrust system formed by the Main Central Thrust (MCT), the Main Boundary Thrust (MBT), and the Main Frontal Thrust (MFT). While activity on the MCT started around ~22–18 Ma and may have remained episodically active up to the present day (Dal Zilio et al., 2020; Ghoshal et al., 2020), the MBT developed from 11 Ma until the Pleistocene. The MFT defines the southernmost margin of the orogenic arc and represents the near-surface expression of the deep basal décollement (Main Himalayan Thrust; hereinafter, MHT). The MHT separates the Indian shield from the Indian Himalaya terrane and is currently acting as the gently inclined basal detachment with a ramp-flat geometry underlying this complex structure (Panda and Lindsey, 2024). The MHT appears to be segmented by subsurface transverse tectonic lineaments and faults, with normal to strike-slip features in regions with low seismic coupling values (Dal Zilio et al., 2020). These regions are marked at depth by the presence of subsurface paleo-basement ridges, such as the Delhi–Haridwar (DHR), the Faizabad (FR) and the Munger–Saharsa (MSR) (Dasgupta et al., 1987).

2.4.2. Seismotectonic Framework

Past seismic activity highlights the Himalaya–Tibet region as an area of high seismic risk, with numerous moderate-to-large earthquakes (6 < Mw < 7) distributed across the region (Bilham et al., 2001). By inspecting the USGS catalog (https://earthquake.usgs.gov, accessed on 31 May 2024), ~15,000 earthquakes with Mw > 2.5 spanning the 1960–March 2024 time interval have been selected (Figure 2.2). Despite being one of the most seismically active regions in the world, instrumental hypocenters in the area are poorly constrained due to the lack of local seismic networks, especially in Tibet. Instrumental seismicity occurs within approximately 100 km of the Main Himalayan Thrust (MHT) downdip, with notable seismic gaps in Bhutan (Li et al., 2020). In more detail, it is sparsely distributed in a clustered pattern along the collisional arc, following some of the strike-slip lineaments and in a N–S aligned pattern around a few normal faults. It is also primarily concentrated within the upper 30–35 km of the crust, though intermediate-depth (>40 km Michailos et al., 2021) seismic events have been locally recorded beneath the Himalayas (GEBCO Bathymetric Compilation Group 2023, 2023). In the last century, Himalaya has experienced four large seismic events (Mw > 7) such as the Mw 8.9 1950 Assam earthquake (Ben-Menahem et al., 1974; Coudurier-Curveur et al., 2020), the Mw 7.8 and Mw 7.3 2015 Gorkha (Galetzka et al., 2015; Lindsey et al., 2015), and the Mw 7.6 2005 Kashmir ones (Avouac et al., 2006).

The southern border of Tibet is currently experiencing a marked E-W crustal stretching, which is accommodated by N-S-oriented normal (Armijo et al., 1986) and active strike-slip faults (Armijo et al., 1986; Taylor, 2009). These active faults are associated with widespread

seismicity with Mw > 6, e.g., the Mw 6.2 2004 and the Mw 6.3 2005 Zhongba earthquakes (Ryder et al., 2012), the Mw 6.3 2008 Damxung earthquake (Bie et al., 2014), and the Mw 6.1 2020 Nima earthquake (Hu et al., 2022), also including notable seismic sequences. Strike-slip faults, predominantly oriented NW-SE or NE-SW, have generated several significant seismic events, including the Mw 7.7 1951 Beng Co earthquake (Li et al., 2022), the Mw 6.9 2014 Yutian earthquake (Li et al., 2021), and the Mw 7.6 2001 Kunlun earthquake (Xie et al., 2014).

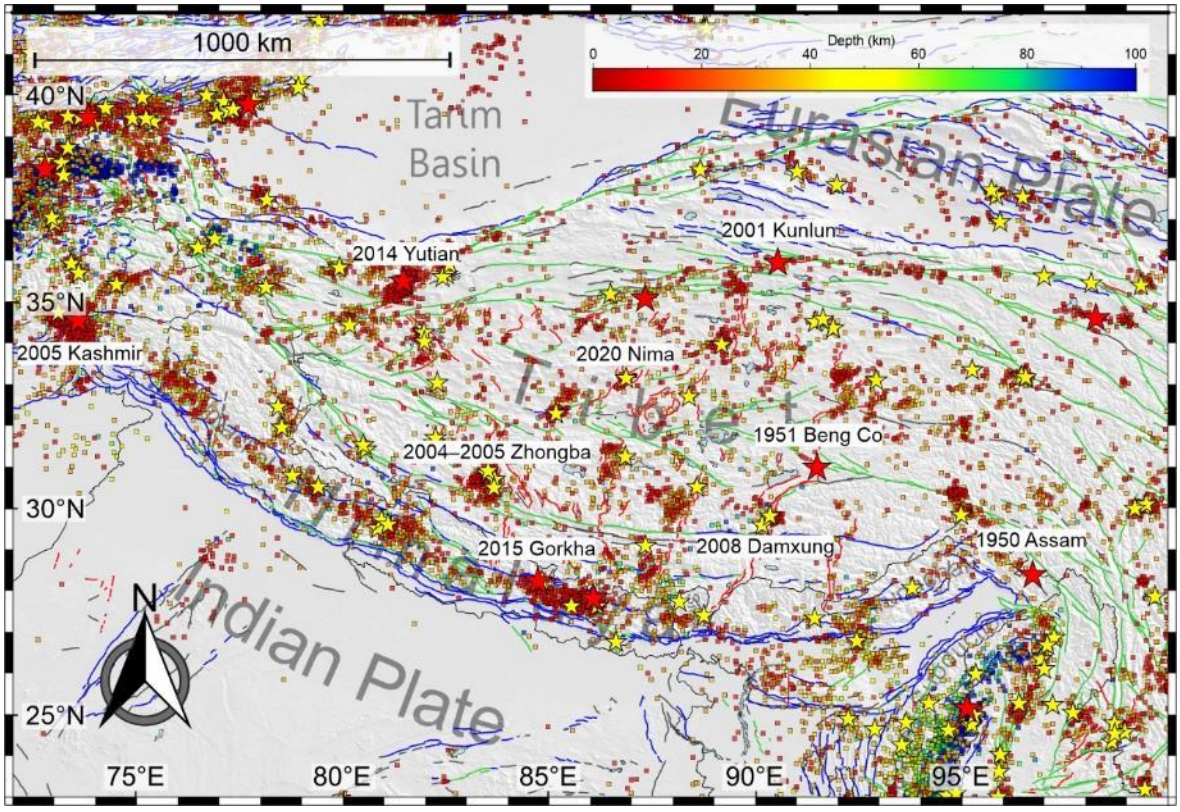


Figure 2.2: Instrumental seismicity (Mw > 2.5) from 1960 to 2024 (USGS catalog; https://earthquake.usgs.gov), colored according to focal depth with a rainbow color scale. Yellow and red stars are seismic events with 6<Mw≤7 and Mw>7, respectively. Earthquakes before 1960 (1950 Assam and 1951 Beng Co) are from Coudurier-Curveur et al., 2020 and (Li et al., 2022), respectively. Active and main faults from Zelenin et al., 2022: blue: thrust; red: normal fault; green strike-slip fault; grey unknown kinematics fault. The terrain model is from GEBCO (GEBCO Bathymetric Compilation Group 2023, 2023), accessed on 31 October 2024.

2.4.3. Geodynamic Models

Several geodynamic models have been proposed to explain the complex fragmentation and kinematic heterogeneity of the Himalaya–Tibet region. All models primarily aim to interpret the synchronous coexistence of (i) a roughly N-S striking compression, as resulting from the collisional process between Indian and Eurasian plates, with (ii) an E–W extension, related to a general eastward motion of Tibet.

N-S trending normal faults in Tibet are commonly thought to represent the active deformation due to topographic loading (Dewey, 1988; England and Houseman, 1989; Harrison et al., 1992). Collapse occurs in response to the isostatic compensation in the highly thickened Tibetan crust (~70 km Teng et al., 2014). The topographic loading model is only able to explain extension in the Tibet region, without fully accounting for the eastward motion of all the Tibetan terranes and the distributed active strike-slip faults.

Tapponnier and Molnar, 1976 explain the eastward motion of Tibet by suggesting an indenter-escape tectonic model. According to this model, the weak Tibetan lithosphere is tectonically pushed eastward because of the N-S convergence of the highly rigid lithosphere of India and the Tarim Basin (Eurasia). The indenter block was too buoyant to subduct, so lithospheric accommodation is mainly achieved by the eastward extrusion of Tibet. This model well explains the clockwise rotation of eastern Tibet (Cao et al., 2009) and the bending of faults such as the Jiali Fault (Zhang et al., 2021). However, the indenter-escape tectonic model assumes that deformation is mainly confined to the horizontal plane, neglecting vertical deformations, which would be relevant, especially in the Himalaya–Tibet region where the crust is the thickest in the world. Furthermore, such an explanation is insufficient as it considers extensional tectonics isolated from the compressive forces arising from the ongoing India–Eurasia convergence. These compressive forces would be crucial in driving the uplift of the plateau from the Paleogene up to the present, as testified by the ongoing uplift inferred by recent leveling and GNSS measurements (Wu et al., 2022).

A primary piece of information for enhancing the understanding of the active geodynamics of the Himalaya–Tibet region is the precise location of the Indian Plate beneath Tibet. A gently northward-dipping surface has been presented by different authors (Kind et al., 2002; Nábělek et al., 2009; Shi et al., 2016; Xu et al., 2017; Zhang et al., 2014), revealing similar seismic characteristics of the layers up to 31°N. The presence of the underthrusted Indian crust has led to the proposal of two additional models closely related to the active dynamics.

The thinning model (Styron et al., 2015) suggests that the subsequent extension reflects the thinning of the upper crust in response to thickening due to the underthrusted Indian Plate. This model has two significant limitations: (i) extension does not cease at 31°N but also affects the Qiangtang Terrane and (ii) while extension should theoretically activate progressively from south to north, it appears to have started fairly uniformly across the plateau during the Miocene (Harrison et al., 1992; Styron et al., 2015).

Beyond that, other authors have proposed the oblique convergence model (McCaffrey and Nabelek, 1998; Panda et al., 2018; Saylor et al., 2010; Styron et al., 2011) which also assumes the underthrusting of India but explains the extension through the relative movement between the Indian and Eurasian plates. McCaffrey and Nabelek, 1998 observed that the

former plate moves as a whole towards the north, evidencing that the convergence is perpendicular only in a limited sector of the Himalayas, having its contact zone with the Eurasian Plate in a semicircular shape. Such a feature highlights that in the other sectors, the overall convergence is also partitioned into a parallel component. In such a context, the E-W extension would result from a basal shear caused by the Indian oblique underthrusting beneath Tibet. However, this model is unable to properly explain the deformation northward of the underthrusted Indian Plate, as similarly observed for the thinning model. Additionally, this model requires higher deformation values moving west and south where, according to some authors (e.g., Xiao et al., 2015), the convergence is less perpendicular and shallower, with the maximum rates occurring in the western Himalayan region.

An additional attempt to explain the complexity of deformation was the channel flow model by Bird, 1991. This author was the first to theorize, through numerical models, the possible presence of a deep zone in the Tibetan crust hosting a planar channel flow. Beaumont et al., 2001, using thermal-mechanical models, explain that the effect of surface denudation could be due to crustal channel flow which, as also noted by Copley and McKenzie, 2007, causes the Himalayan Arc to expand both radially and circumferentially. Rey et al., 2010 suggested that the critical thickness required to weaken the lower crust would be 50 km, raising the question of how a real thickness of ~70 km (Teng et al., 2014) could be attained. In this context, the observed uplift may be difficult to explain since the channel flow model is typically considered a consequence of uplift rather than its cause (Rey et al., 2010).

2.5. Data

2.5.1. GNSS Data

As a first step, raw observations of more than 150 continuous GNSS stations encompassing the Himalaya–Tibet region were collected from UNAVCO (https://www.unavco.org (accessed on 31 May 2024)). After a preliminary check, 37 stations were removed because they were characterized by a limited temporal coverage of raw data (less than 2.5 years), while the remaining stations were processed by using the GAMIT/GLOBK v.10.7 software (Herring et al., 2018), following the standard approach described in Billi et al., 2023, in order to estimate a consistent set of positions and velocities in a fixed ITRF14 reference frame (Altamimi et al., 2016). To enhance the spatial density of the geodetic velocity field across the studied area, the obtained solution has been integrated with the solutions reported in the recent literature (Frohling and Szeliga, 2016; Hao et al., 2019; Wang and Shen, 2020). Published solutions were aligned with our solution by determining the Helmert transformation parameters that minimize the root mean square of velocity differences at common sites (e.g., Sparacino et

al., 2020). All sites displaying significant inconsistencies with neighboring stations were removed from the unified velocity field, resulting in a final dataset of approximately 1142 GNSS sites. The resulting velocity field (Figure 2.3) has been rotated to an Eurasian reference frame by using the Euler pole parameters reported in Altamimi et al., 2017.

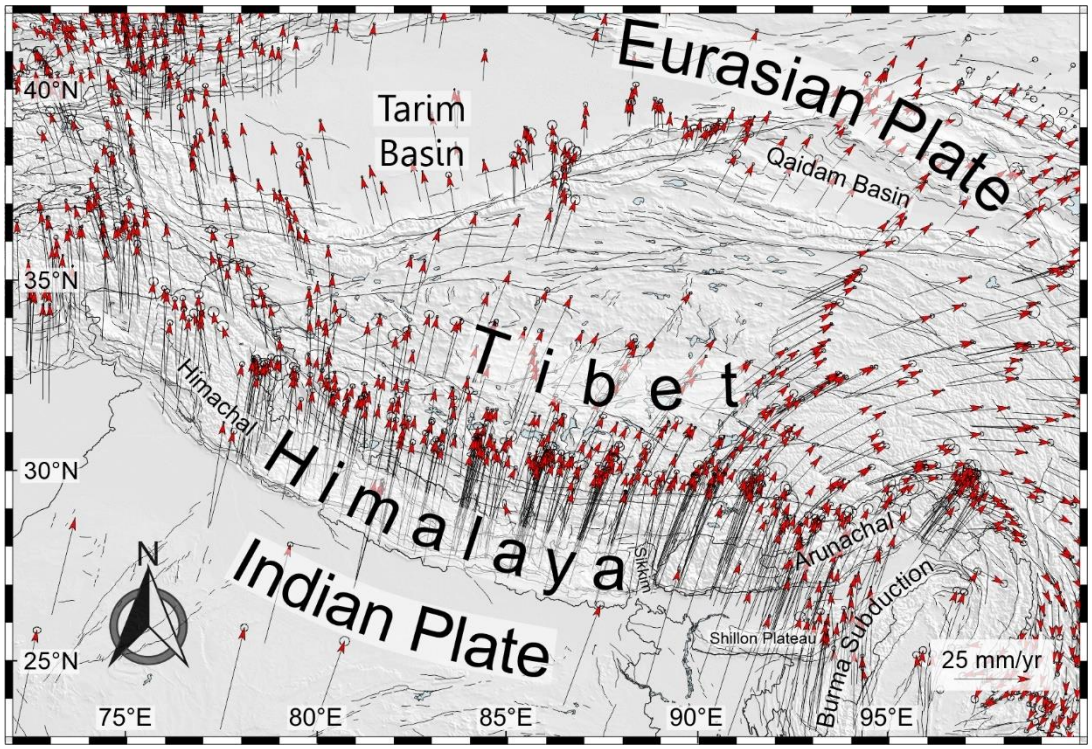


Figure 2.3: Thin red head arrows represent the GNSS horizontal velocities and 95% confidence ellipses in an Eurasian reference frame (Hao et al., 2019). The terrain model is from GEBCO (GEBCO Bathymetric Compilation Group 2023, 2023), accessed on 31 October 2024.

2.5.2. Seismicity and Focal Mechanisms Catalog

Mechanical stress acting in the Earth's crust can be estimated by inverting earthquake focal mechanisms. Therefore, to provide a reliable estimation of the crustal stress in the study area, a dataset of FMSs has been compiled. In a first step we collected all available FMSs over the Himalaya–Tibet area by inspecting the following sources:

- GCMT (https://www.globalcmt.org/ accessed on 31 May 2024);
- ISC (http://www.isc.ac.uk/iscgem/index.php accessed on 31 May 2024);
- World Stress Map (Heidbach et al., 2018) (https://www.world-stress-map.org/download accessed on 31 May 2024).

Multiple solutions for the same event have been removed, selecting the solution having the least difference concerning the hypocentral parameters reported in the USGS seismic catalog (Figure 2.2).

In the second step, data from the literature have been integrated into the general catalog by preferring the solutions coming from local seismic networks or computed by using refined velocity models (Ali and Shanker, 2017; Bai et al., 2016; Chandra, 1978; Chen and Molnar, 1990; Dasgupta et al., 1987; De La Torre et al., 2007; Hao et al., 2019; Kayal et al., 2012; Kumar et al., 2015; Luo et al., 2016; Mukhopadhyay and Dasgupta, 1988; Nandy and Dasgupta, 1991; O'Kane et al., 2022; Parija et al., 2018; Paul et al., 2015; Rastogi, 1974; Wang et al., 2017; Yadav et al., 2017; Zhu and Helmberger, 1996). Moreover, since the procedure of the waveform-inversion FMSs is generally more stable and robust than solutions obtained by first-motion polarity (e.g., Adinolfi et al., 2022; Kusumawati et al., 2023), the former was selected when both types of solutions were available for the same earthquake.

The final catalog contains ~1300 FMSs related to $M_w > 4$ earthquakes that occurred in the June 1933–March 2024 period (Figure 2.4). About ~80% of the collected FMSs have been obtained by waveform inversion, while the remaining has been computed by first-motion polarity and are related to the earthquakes that occurred before the advent of the digital epoch in the 1980s. In the study area, most of the FMSs have focal depths less than 30 km; ~8% have focal depths up to 80 km. Among these last solutions, the most remarkable ones are those related to the 2011 Sikkim seismic sequence (Baruah et al., 2016) that occurred beneath the MHT, and those related to the Burma active subduction and the Pamir–Hindu Kush lithospheric subduction (Zhang et al., 2011).

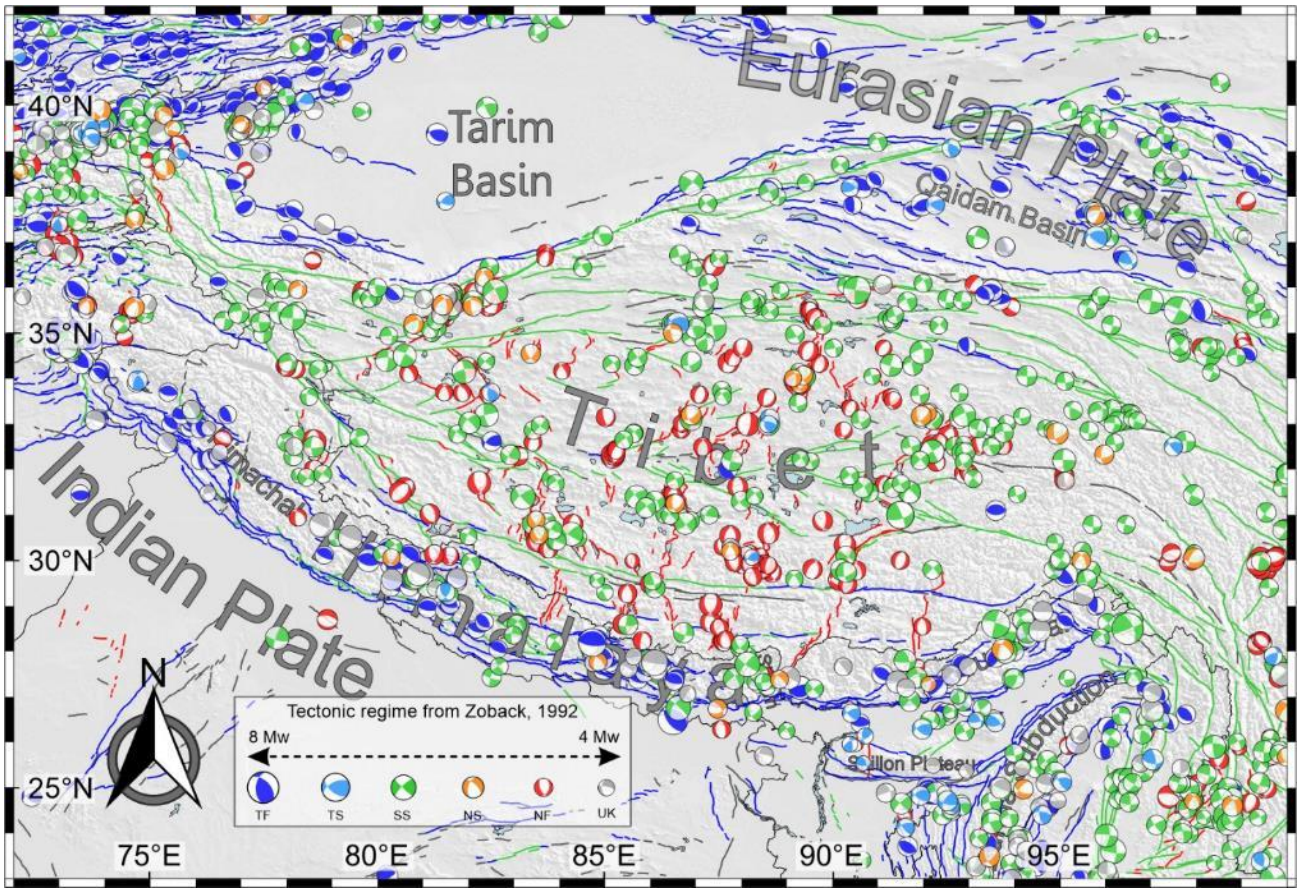


Figure 2.4: Lower hemisphere, equal area projection for FMSs with M>4 spanning the June 1933 - February 2024 time period. FMSs are colored according to kinematics classification (Zoback, 1992): blue, thrust faulting (TF); light blue, thrust with strike-slip component (TS); green, pure strike-slip (SS); orange, normal faulting with strike-slip component (NS); red, normal faulting (NF); grey, unknown kinematics (UK). Other features are as Figure 2. The terrain model is from GEBCO (GEBCO Bathymetric Compilation Group 2023, 2023), acccessed on the 31 October 2024

2.6. Methods

2.6.1. Geodetic Strain Rate Field

The horizontal strain rate pattern and associated uncertainties over the study area have been calculated using the method described by Shen et al., 2015. This algorithm employs discretized geodetic observations and applies a least-squares procedure to interpolate velocities on an optimally regular grid. Interpolated velocities are then used to derive strain rate values by assuming the medium to be elastic. After some preliminary tests, we chose a value of 18 as the weighting threshold, according to the inter-stations distance of the GNSS network (Palano et al., 2018) and the comparative analysis conducted by Nucci et al., 2024.

This study examines the minimum and maximum stretching, ε_{Hmin} and ε_{Hmax}, respectively, as eigenvalues of the computed strain rate tensor, alongside their corresponding azimuths. The two eigenvectors are assumed to be orthogonal to each other and oriented at 45° relative to the azimuth of the maximum shear strain rate. Additionally, a crucial parameter is the

dilatation strain rate, which quantifies the rate of the areal change as the sum of the ε_{Hmin} and ε_{Hmax} values.

The adopted grid nodes are evenly spaced at intervals of 0.25° × 0.25°. The distribution of stations across the area is irregular (Figure 2.3); therefore, the results for these regions, such as north–central Tibet and the Tarim Basin, must be interpreted keeping this aspect in mind. Achieved results are reported in Figure 2.5.

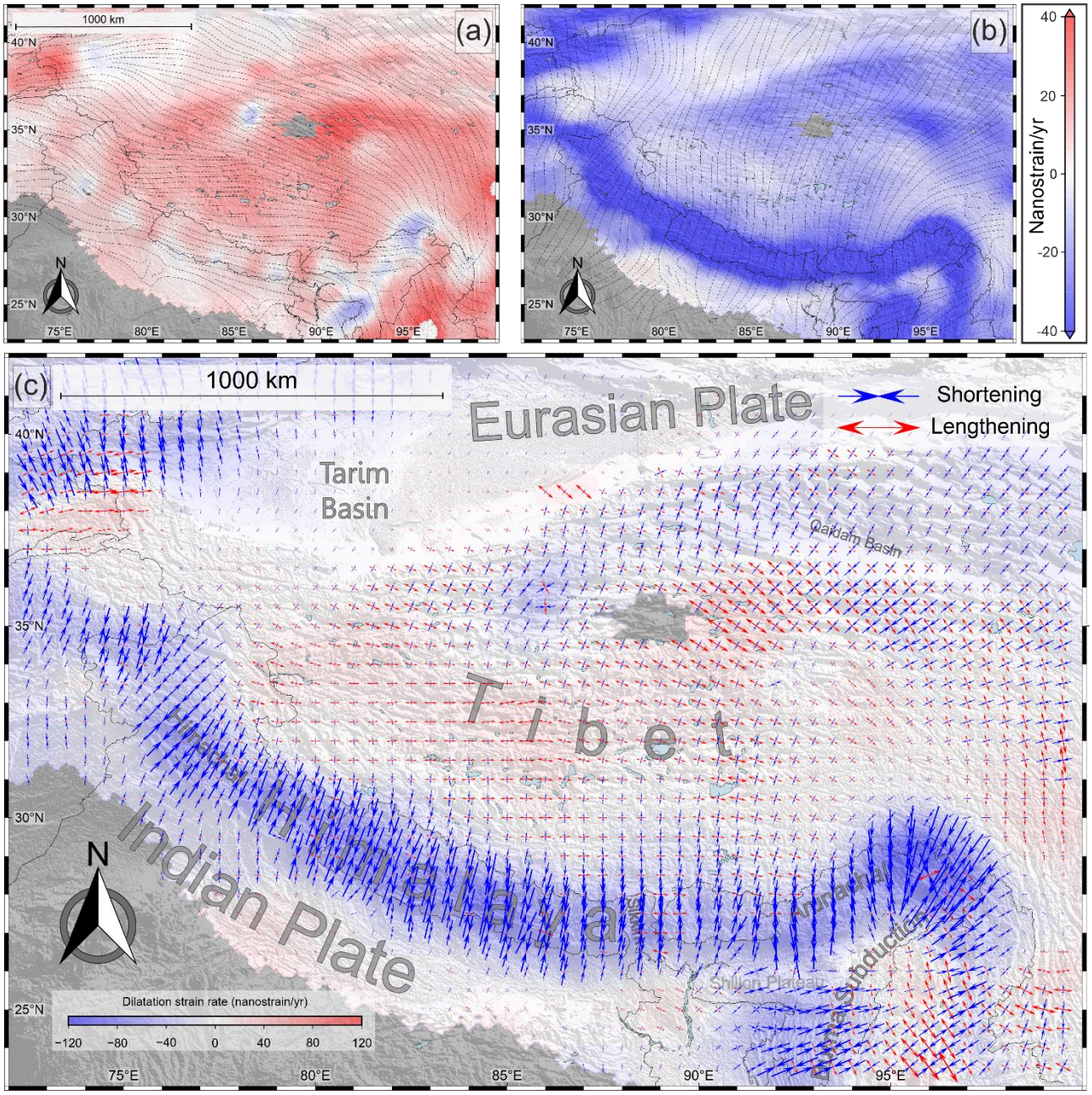


Figure 2.5: Strain rate maps from GNSS data. a) ε_{Hmax} (greatest extensional horizontal strain rate) trajectories are reported as dotted black lines. The background color indicates the magnitude of ε_{Hmax}; negative and positive values for shortening and lengthening, respectively. b) ε_{Hmin} (greatest contractional horizontal strain rate) trajectories are reported as dotted black lines. The background color indicates the magnitude of ε_{Hmin}; negative values for shortening and positive values for lengthening. c)

Horizontal strain rate axes red and blue arrows represent the greatest extensional (ε_{Hmax}) and contractional (ε_{Hmin}) horizontal strain rates. The colors in the background show the 2D dilatation strain rate, blue and red for areal contraction and dilatation, respectively. The terrain model is from GEBCO (GEBCO Bathymetric Compilation Group 2023, 2023), acccessed on 31 October 2024.

2.6.2. FMS Formal Inversion

The stress tensor over the study area has been calculated by using the FMSs database (see Section 16) fusing of the STRESSINVERSE code (Mw > 4 earthquakes) (Vavryčuk, 2014) as the input. This code calculates the stress tensor parameters assuming: (i) the tectonic stress is uniform and homogeneous in the considered volume, (ii) earthquakes occur on pre-existing faults, and (iii) the slip vector points to the direction of shear stress on the fault (Bott, 1959; Vavryčuk, 2014; Wallace, 1951). This method can determine the 3D stress tensor, defining trend, and plunge of the three axes, σ_1, σ_2, and σ_3 (with $\sigma_1 \geq \sigma_2 \geq \sigma_3$, under the compression-positive stress convention), and the dimensionless stress ratio, R (Gephart and Forsyth, 1984):

$$R = \frac{\sigma_1 - \sigma_2}{\sigma_1 - \sigma_3} \qquad (1)$$

The stress ratio R varies from 0 to 1.0; when R = 0, σ_1 and σ_2 are equal in magnitude, while R = 1 means that σ_2 and σ_3 have the same values.

To ensure more accurate estimations of stress ratio values, the STRESSINVERSE code selects the optimal nodal plane (Vavryčuk, 2014) by quantifying the fault instability (Vavryčuk et al., 2013), following the Mohr–Coulomb failure criterion (Lund and Slunga, 1999). To properly evaluate the sensitivity of the inversion procedure to friction parameters, needed in the instability constraint, the inversion was run repeatedly with friction ranging from 0.4 to 1 in steps of 0.05. Thus, the code performs a set of iterations aimed at determining the orientation of the stress axes and the estimation of the stress ratio, considering all possible nodal plane combinations, until the stress parameters converge toward the best model (Michael, 1984). In this way, the instability of the nodal planes of all FMSs is calculated, selecting those most susceptible to shear faulting.

The inversion has been performed on a moving 2° × 2° equally spaced grid with a 1° overlap on each side. The inversion is only performed in cells containing at least 8 FMSs. Based on the measured stress field geometry and stress ratio, the so-called maximum sub-horizontal compressive stress, σ_{Hmax}, is also calculated (Lund and Townend, 2007) (see Figure 2.6).

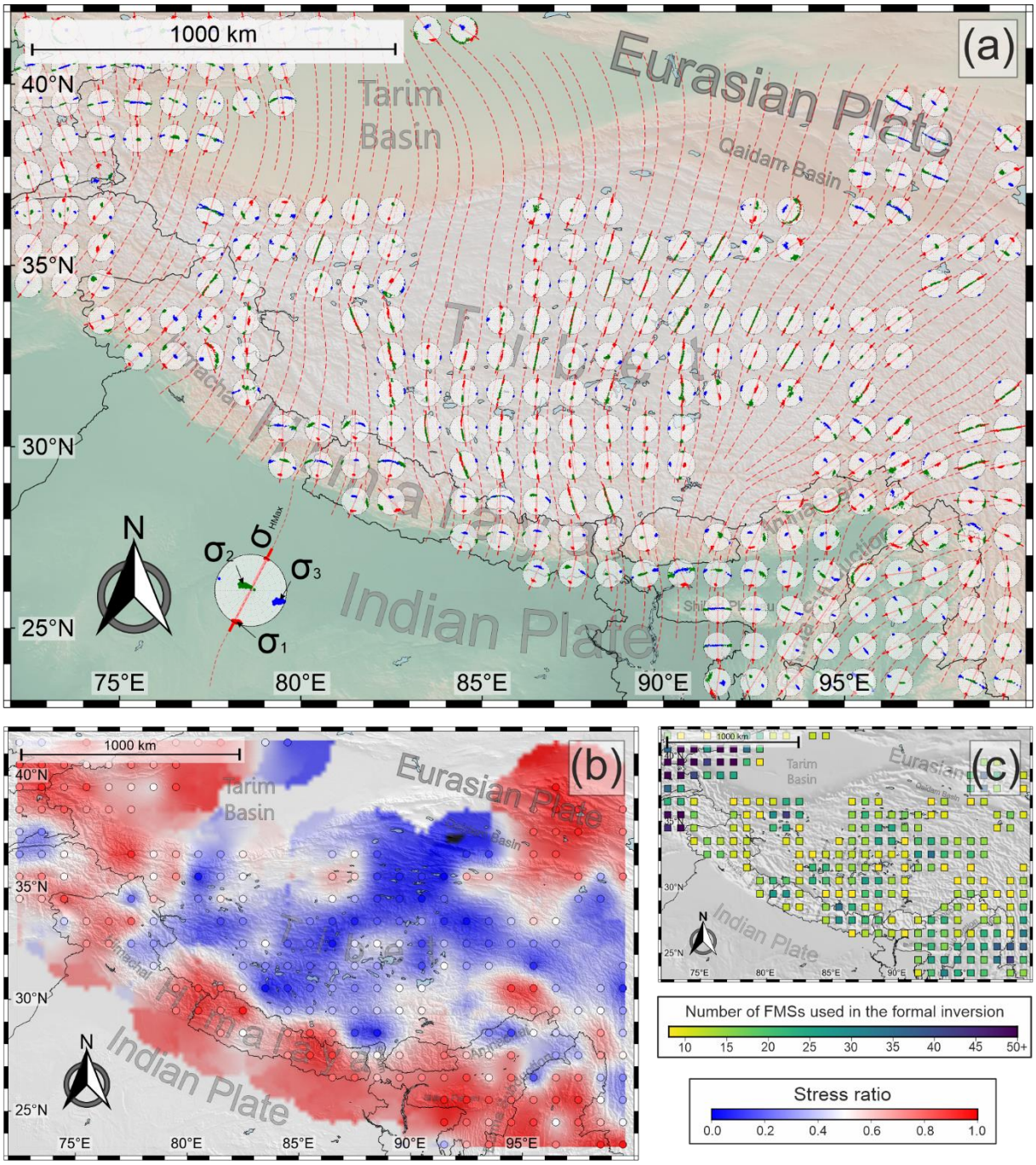


Figure 2.6: Results from formal stress inversion a) Stereoplots (lower hemisphere) showing achieved results. σ_1, σ_2 and σ_3 axes are reported in red, green and blue, respectively. The σ_{Hmax} trajectories are reported as red dashed lines. b) Spatial pattern of the stress ratio values. c) Coloured squares showing the number of FMSs used in the gridded stress inversions. The terrain model is from GEBCO (GEBCO Bathymetric Compilation Group 2023, 2023), accessed on 31 October 2024.

2.7. Results

2.7.1. Strain Rate Field

Strain rate results are reported in Figure 5 as ε_{Hmax} and ε_{Hmin} values along with the associated azimuthal pattern (i.e., arrows and trajectories). Despite some very localized artifacts, our

results align well with previous solutions (Ge et al., 2015; Hao et al., 2019), providing, moreover, an improved resolution of the deformation field thanks to the high spatial density of the geodetic velocity field across the studied area.

The ε_{Hmax} strain parameter has positive values with very small variability over most of the study area. The largest positive values (up to 30 nanostrain/yr) are observed in the entire of Tibet, while values ranging from 0 to ~25–30 nanostrain/yr can be observed along six localized N-S oriented strips along the Himalayan Arc. Some small patches with negative values (~25 nanostrain/yr) can be observed close to Arunachal, the Shillong plateau, and the Himachal regions. The ε_{Hmax} trajectories outline a general E-W trend, gradually rotating, moving eastward. Along the Himalayan Arc, the ε_{Hmax} trajectories pass from a roughly WNW-ESE attitude in the western Himalaya to E-W and N-S attitudes in central and eastern Himalaya (Figure 2.5).

The ε_{Hmin} values effectively depict the general contraction of the study areas, with low values (ca. −25 nanostrain/yr) mainly characterizing the Tibetan region and high values along the Himalayan Arc (up to −100 nanostrain/yr) and at the northern margin of Tibet, along the Altyn-Tagh and Kunlun faults (up to −40 nanostrain/yr). The ε_{Hmin} trajectories show a general NNE-SSW trend over most of the study area. Such a pattern is roughly orthogonal to the general attitude of the Himalayan Arc. A marked rotation is observed in proximity to the Arunachal area, where the ε_{Hmin} trajectories follow the clockwise rotation of the orogenic belt, aligning NE-SW. Another interesting feature is the gradual rotation of the ε_{Hmin} trajectories observed in the Tibetan Plateau. In the southern part of the plateau, the ε_{Hmin} trajectories show a predominant N-S orientation, while north of the 31°N parallel, the trajectories gradually rotate clockwise about 30°. The horizontal dilatation rate map (sum of ε_{Hmin} and ε_{Hmax}) is dominated by the contractional pattern (up to −120 nanostrain/yr) along the Himalayan orogen, clearly evidencing the ongoing India–Eurasia convergence. Such a general contraction concentrated within 100 km north of the MFT indicates the active contraction of the Indian Himalaya above the MHT. In the Tibetan region, the areal change values are close to zero or show small local variations, indicating no significant change in areal strain. However, given that ε_{Hmax} and ε_{Hmin} have similar (not zero) values, it can be inferred that crustal deformation in the Tibetan region occurs prevalently as shear strain, in a generally constant area strain in the map view (Milnes, 1994). Such a feature aligns well with the presence of abundant strike-slip faults, responsible for several large earthquakes. The dilatation rate is close to zero in the Tarim Basin where, in contrast to Tibet's results, ε_{Hmin} and ε_{Hmax} have very small or close to zero values, suggesting a small/null deformation of the region. Estimated strain rate parameters over this area would be poorly constrained because of the lack of GNSS stations; however, the small/null deformation within the Tarim Basin is also confirmed by geological data, clearly documenting no active deformation since

the onset of the India–Eurasia convergence (Chang et al., 2014; Yang and Liu, 2002). Moreover, both the southern and northern margins of the Tarim Basin show negative areal changes that appear related to the presence of active faults/structures, such as the Altyn Tagh fault and the Tianshan orogeny, respectively.

2.7.2. Stress Field

The estimated stress parameters over the study area are reported in Figure 6 (see Supplementary Material for additional details in Paragraphs 8.1.3 and 8.1.5). As already mentioned, most of the collected FMSs are related to earthquakes located in the uppermost part of the crust, within the first 30–35 km. Therefore, our stress results must be considered as representative only of the shallow crust, being the average crustal thickness of ~70 km (Teng et al., 2014) beneath most of the study area. Figure 2.6a shows achieved results for each inverted cell in terms of stereoplot representations and stress trajectories. As mentioned previously, the stress tensor inversion has been performed only for those cells containing at least eight FMSs. Only a few cells contain eight FMSs, and their resulting stress parameters agree with the ones obtained for the neighboring cells, evidencing acceptable reliability of the estimations. Each stereoplot shows the retrieved principal stress (σ_1, σ_2 and σ_3) 3D spatial pattern along with the associated confidence limits, while the stress trajectories refer to the σ_{Hmax} pattern.

Along the Himalayan Arc, the σ_1 stress axis is roughly sub-horizontal (estimated plunge in the 0–35° range), pointing toward a rough N-S orientation, while the σ_2 and σ_3 axes represent, alternatively, the vertical stress. In this region, only the σ1 axis is well constrained by the inversion, while the σ_2 and σ_3 axes sometimes show a partial overlap of their estimated 95% confidence limits, suggesting that they are approximately equal in magnitude ($R > 0.75$). As a result, there are alternating sectors of the Himalayan Arc where σ_2 is sub-horizontal, like in most of the central Himalaya, and areas where it becomes vertical, such as in the Sikkim region, Himachal, and Bhutan. However, the σ_{Hmax} pattern along the Himalayan Arc effectively reflects the primary compression arising from the India–Eurasia convergence.

In Tibet, the best constrained stress axis is σ_3, which is always sub-horizontal with a W-E to NW-SE average strike. σ_1 and σ_2 axes are alternatively sub-vertical, with partial overlap of their estimated 95% confidence limits; therefore, they are approximately equal in magnitude ($R < 0.25$) and their possible flipping over the entire Tibet (Figure 2.6) is admittable. Indeed, the flipping in the position of the σ_1 and σ_2 axes is consistent with the main features of active faults in the region (Figure 2.2). Tibet is currently deformed by both normal faults, which account for the vertical σ_1, and strike-slip faults, coherent with sub-horizontal σ_1 and σ_3.

Areas such as the central Tibetan region or the transition zone between the central Himalaya and Tibet are characterized by FMSs with heterogeneous kinematics, i.e., strike-slip, normal, and reverse faulting in the former and thrust (southward) and normal (northern) faulting in the latter, respectively. Despite these complex patterns, the achieved results are quite similar to the ones obtained for the neighboring cells, also evidencing an acceptable reliability for these estimations.

The σ_{Hmax} trajectories show a perpendicular trend with respect to the Himalayan Arc, mainly in the westernmost part, in the easternmost part of Nepal, and the Assam region (Figure 2.6). The σ_{Hmax} on the Tibetan Plateau shows a pattern predominantly oriented along the N-S attitude till latitude 31°N. To the north, it rotates clockwise at approximately 30° and aligns NE-SW. This main direction can be observed northward, up to the Kunlun Fault. To the southeast, the σ_{Hmax} trajectories depict a clockwise rotation, passing from NW-SE to N-S and NE-SW above the Burma subduction system.

Figure 2.6b provides the spatial distribution of the estimated stress ratio (R) values. As previously mentioned, the stress ratio R varies from 0 ($\sigma_1 = \sigma_2$) to 1 ($\sigma_2 = \sigma_3$); therefore, in the following, we defined three main groups with $0.25 < R < 0.75$, $R \geq 0.75$ and $R \leq 0.25$. Regions with $0.25 < R < 0.75$ are sparsely distributed throughout the study area, generally lacking a distinct pattern and representing transitional values for the other two groups. Regions with $R < 0.25$ can be recognized across a large sector of Tibet, where, as pointed out before, σ_1 and σ_2 axes flip among them, evidencing that the crustal deformation is accommodated by the coexistence of active strike-slip and normal faults.

Regions with $R > 0.75$ are the Himalayan Arc, the area north of the Qaidam Basin and the northwest border of the Tarim Basin. In all these zones, the σ_1 axis is sub-horizontal, while σ_2 and σ_3 can alternatively represent the vertical stress, therefore evidencing the coexistence of the strike-slip and reverse faulting regimes.

2.7.3. Stress-Strain Comparison

The comparison of geodetic strain and seismological stress is carried out by comparing the azimuthal pattern of the ε_{Hmin} (shortening axis) and the σ_{Hmax} (maximum horizontal stress) (Figure 2.7). Strain and stress parameters have been estimated on grids with different sizes which, however, share several nodes; therefore, the comparison of their azimuthal patterns has been performed by considering the estimated values at the shared nodes. A remarkable feature of this comparison is that, in 90% of cases, the estimated angular discrepancy is less than 15°, even in those regions where strain and stress axes show spectacular rotations (Figure 2.7). Considering uncertainties associated with both strain and stress fields (see Supplementary Material in Paragraph 8.1.3 and 8.1.4), the methodology used, the type of data, and their spatial distribution, these cases could be considered almost concordant.

Based on this last consideration. This alignment is consistent with a macroscopically elastic mechanical response of the sampled upper crust, in which deformation tends to occur in the same direction as the applied stress. However, we acknowledge that this interpretation relies on a simplified model of isotropic elasticity, which may not apply in the presence of elastic anisotropy or more complex behaviors such as plasticity or viscoelasticity. At a regional scale, this correlation between the principal axes of stress and strain rate has been reported in previous studies (Palano, 2015; Townend and Zoback, 2006). Moreover, moderate-to-large azimuthal discrepancies can be recognized along the western (Himachal region) and eastern sectors of the Himalaya and along the NW border of the Tarim Basin, evidencing either a significant heterogeneity of the upper crust or the superposition of different stress sources.

We also observe that along the Himalayan Arc, as well as the southern sector of the Tibetan Plateau, stress and strain azimuthal patterns are roughly sub-parallel to the predicted India–Eurasia relative motion (Figure 2.7). At a northern of latitude 31°N, the stress–strain azimuthal pattern shows a significant oblique relationship with the predicted one. We therefore suggest that the forces arising from the convergence process control both crustal stress and surface strain, at least along the southern sector of the orogenic belt. The observed perturbation of this general pattern would be related to local complexities and/or to the superposition of secondary stress sources. Furthermore, the significant discrepancies between the observed stress and the predicted one northward of the 31° parallel provide significant evidence of a different driving mechanism that is actively shaping the ongoing tectonic setting of the Tibetan area.

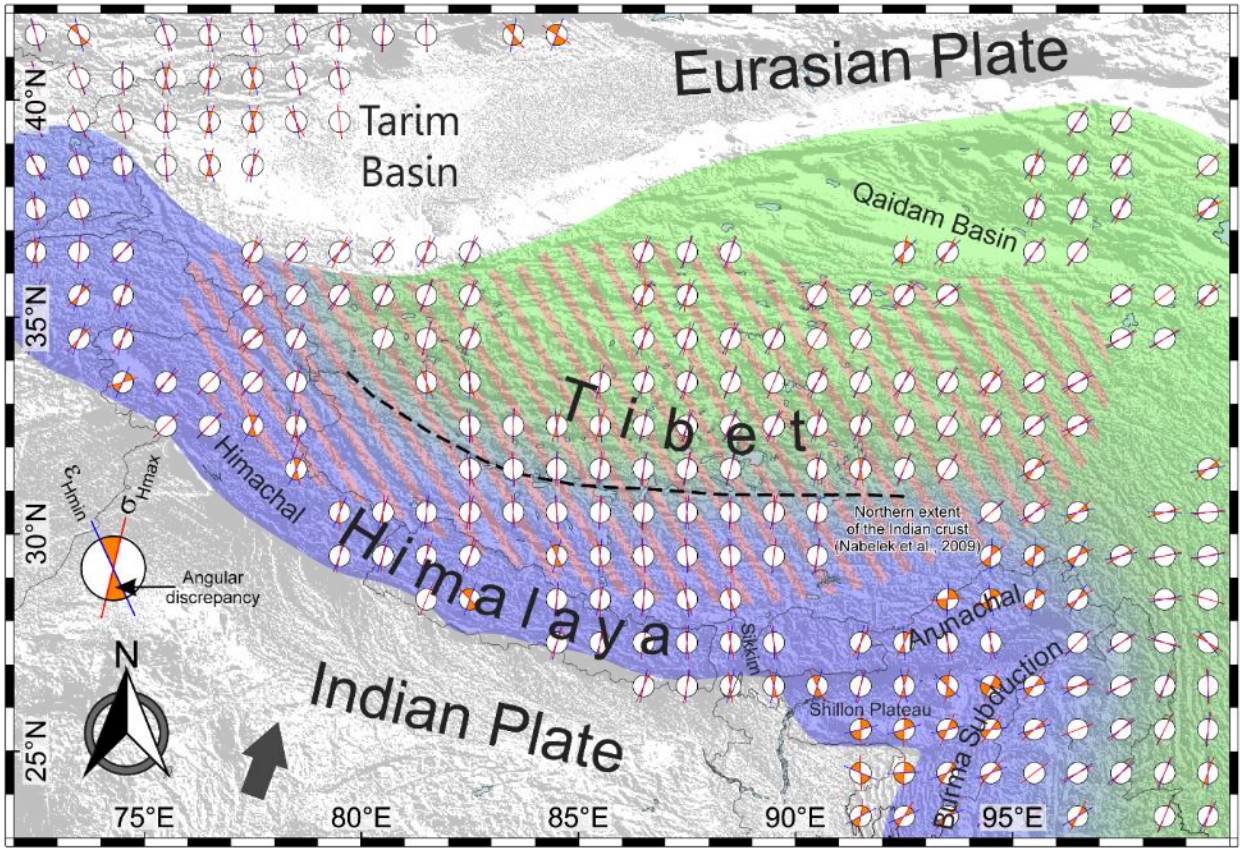


Figure 2.7: Azimuthal comparison between ε_{Hmin} in blue and σ_{Hmax} in red. The discrepancy angle between the horizontal axes is colored in orange. The northern limit of the underthrusted Indian crust (Nábělek et al., 2009) is marked by a black dashed line. Background colors are related to the zones largely affected by the suggested geodynamic models: the area mainly driven by escape tectonics (Tapponnier et al., 1986) is reported in green, the area with the underthrusted Indian crust (Nábělek et al., 2009) is reported in blue and the area affected by topographic loading is reported in red oblique strips. The black arrow stands for the relative India-Eurasia motion, as resulting from the analyzed GNSS data (Table S1 in Supplementary materials). The terrain model is from GEBCO (GEBCO Bathymetric Compilation Group 2023, 2023), accessed on 31 October 2024.

2.8. Discussion and Conclusions

The compiled and analysed database of GNSS data and earthquake focal mechanism solutions (see the Supplementary Material for details) allow an enhanced understanding of the kinematic zonation across the Himalaya–Tibet region. In particular, the computed GNSS velocity field, referred to the Eurasian reference frame (Altamimi et al., 2017), shows a fan-shaped feature (Figure 2.3) along the whole Himalayan Arc coupled with a large-scale clockwise rotation around the eastern sector of the Himalaya (Figure 2.4). Both features have been already detected by previous studies focusing on the area (Gan et al., 2007; Vernant et al., 2014; Wang and Shen, 2020; Wang et al., 2001; Zhang et al., 2004). The fan-shaped feature along the Himalayan Arc effectively depicts the ongoing convergence between Indian and Eurasian plates, with rates decreasing northward, while the large-scale clockwise rotation appears related to deep processes involving the subducting lithosphere (Wang and Shen, 2020). This computed GNSS velocity field has been used to estimate the horizontal strain-

rate fields (Figure 2.5). The achieved results highlight a contractional pattern along the Himalayan orogeny, related to the India–Eurasia convergence. Tibet is prevalently deforming due to shear strain, coupled with a small fraction of crustal stretching, in agreement with Liu et al., 2024. Deformation in the inner part of the Tarim Basin is null, despite being currently trapped between the Altyn Tagh Fault and the Tianshan orogeny southward and northward, respectively. In such a context, the Tarim Basin behaves as a rigid block, as already suggested by Chang et al., 2014 and Yang and Liu, 2002.

The reverse FMSs located along the Himalayan Arc, effectively suggests active thrusting occurring along the MHT (Figure 2.4). Reverse FMSs are also located along a roughly E-W oriented belt, extending from Pamir and Tian Shan to the west, up to the Qaidam Basin to the east. All these FMSs highlight the intense deformation accounted by the reverse faults, therefore evidencing that most of the convergence between Tarim and Eurasia is absorbed farther north, along the southern margin of the Kazakh platform, in central Asia (Zubovich et al., 2010). FMSs with strike-slip features dominated the Tibetan Plateau, while numerous FMSs with normal faulting can also be observed. Abundant FMSs with strike-slip features can also be observed eastward of the Burma subduction zone. The achieved stress field is in agreement with previous studies (Wang et al., 2017) and highlights that along the Himalayan Arc, the σ_1 stress axis is roughly sub-horizontal with a prevailing N-S orientation, while the σ_2 and σ_3 axes represent, alternatively, the vertical stress, being both approximately equal in magnitude ($R > 0.75$). Conversely, the adjacent Tibetan region is experiencing both strike-slip and normal faulting, with the σ_3 being always sub-horizontal, with average strikes ranging from W-E to NW-SE, and the σ_2 and σ_1 axes approximately equal in magnitude ($R < 0.25$). The computed σ_{Hmax} trajectories (Figure 2.6a) show a main N-S orientation in both the Himalayan Arc and the southern part of Tibet, while at the latitude 31°N, the σ_{Hmax} orientations rotate toward a NE-SW strike. To the southeast, the σ_{Hmax} trajectories describe a large clockwise rotation, with orientations ranging from NW-SE to N-S and NE-SW above the Burma subduction system.

The azimuthal patterns of the geodetic shortening axis (ε_{Hmin}) and the seismological horizontal stress (σ_{Hmax}) have been compared by considering their estimates at the shared nodes of the computational grids. Over most of the study area, ε_{Hmin} and σ_{Hmax} are nearly parallel. Such a general alignment implies that the crust exhibits significant elasticity, as it is contracting along the σ_{Hmax} direction.

Novel stress–strain maps (Figure 2.5 and Figure 2.6) provide new insights into the active geodynamic models suggested to explain the complex geodynamic setting of the Himalaya–Tibet region. We observed that stress and strain are roughly sub-parallel to the predicted motion of the India–Eurasia convergence, which therefore represents the main mechanism in controlling both crustal stress and surface strain. Along the orogenic belt, the general

pattern is locally modulated by some significant perturbations; considering available geological information along with our stress results we infer that these perturbations would be related to crustal lateral density changes, strength contrasts and active faults. Evidence of crustal lateral density changes and strength contrasts along the orogenic arc have been provided by local tomographic studies (Mukhopadhyay and Sharma, 2010; Raoof et al., 2017; Thirunavukarasu et al., 2017). Moreover, along the Himalayan orogenic arc, the magnitude of ε_{Hmax} reveals several regions of arc-parallel stretching, consistent with the presence of N-S-oriented normal faults (Stevens and Avouac, 2021) and reoriented strike-slip faults (Berthet et al., 2014; Malik et al., 2023). Such a feature, coupled with the fan-shaped pattern of both ε_{Hmin} and σ_{Hmax} along the orogeny, aligns well with the oblique convergence model proposed by McCaffrey and Nabelek, 1998.

Along Tibet, we inferred small stress ratio values ($R \leq 0.25$), which suggests that at the local scale, σ_1 and σ_2 can act as the σ_{Hmax}. Given the close relationship between stress and strain, it can be inferred that the magnitude of the σ_{Hmax} axis is elastically proportional to the magnitude of the ε_{Hmin} axis, leading to a uniform distribution across Tibet (Figure 2.5c). This uniformity supports the idea that any variations in stress magnitude are more likely to occur along the vertical axis, rather than on the horizontal axis. Therefore, we propose that variation in the vertical stress is related to topographic loading, which would effectively modulate the stress related to the convergence process.

At the latitude of 31°N, our results show a ~30° rotation of the ε_{Hmin} and σ_{Hmax} axis. Such a boundary coincides at depth with the location of the northern extent of the underthrusted Indian Plate, as suggested by geophysical data (Nábělek et al., 2009; Van Hinsbergen, 2022). At the surface, the boundary is not geologically well-defined; the normal and strike-slip faults (Armijo et al., 1986; Rothery and Drury, 1984; Taylor and Peltzer, 2006) are quasi-homogeneously distributed at the scale of the whole Tibet. We therefore suggest that southern Tibet deforms in response to the stress field arising from the regional India–Eurasia convergence and local topographic loading, in agreement with the progressive underthrusting of the Indian Plate beneath southern Tibet. Conversely, in northern Tibet, the regional stress field related to the India–Eurasia convergence is largely modulated by the superposition of other stress sources.

Among the models proposed to explain the recent geodynamic evolution of the Tibetan region, the indenter-escape tectonic (Tapponnier and Molnar, 1976) model assumes that deformation is mainly confined to the horizontal plane and implies that compressive forces must be transmitted across plate boundaries, which in turn implies that the rate of the escaping must be equal to or less than the convergence rate. Moreover, this model also implies the eastward extrusion of Tibet. Such features can be easily observed on the GNSS-based velocity field (Figure 2.4), but limited toward the north of 31°N. Therefore, the

indenter-escape tectonic model provides a plausible explanation of the motion of northern Tibet. However, it is unable to explain the vertical motion; therefore, other stress sources acting on the vertical component, such as the topographic loading, must be considered. Indeed, the combined action of both indenter-escape tectonic and topographic loading would provide a reasonable mechanism to properly explain the ongoing geodynamic evolution of this region.

An additional attempt to explain the complex deformation of the Himalaya–Tibet region was the channel flow model proposed by Bird, 1991. This author hypothesized the presence of a deep zone in the Tibetan crust, hosting a planar channel flow which allowed the Himalayan Arc to expand both radially and circumferentially. However, our stress and strain trajectories do not support the channel flow model.

In conclusion, we support the combination of different geodynamic models, refining the model proposed by Copley et al., 2011. South of the 31°N latitude, compression is driven by basal drag from the underthrusting Indian Plate, while northward, escape tectonics dominate, where the eastward extrusion of the Tibetan Plateau becomes evident. All over Tibet, we can see no difference in terms of E-W stretching, leading to the idea that the normal faulting regime is due to topographic loading, given the uniform elevation of the plateau (Copley et al., 2011; Dewey, 1988; Rey et al., 2001).

Geodetic and seismological data collected and analyzed in this study are provided as Supplementary Material so that they can be used as input for additional studies. Future efforts should point toward an improved estimation of the crustal vertical motion, making this pattern a significant key element of the complex geodynamic processes of the Himalaya–Tibet region.

2.9. Supplementary materials

Supporting information are reported in Paragraph 8.1, in detail:

- Paragraph 8.1.1: catalog of Focal Mechanism Solutions with time, coordinates, magnitude, type of magnitude, depth, strike-dip-rake, reference and methods used.
- Paragraph 8.1.2: coordinates and velocities referred to ITRF14 and Eurasian reference frame for GNSS sites analyzed in the study area.
- Paragraph 8.1.3: stress inversion results with an ID number, coordinates of the node, number of FMSs considered in the inversion, stress ratio (R), frictional coefficient, trend/plunge of the three principal axes (σ_1, σ_2 and σ_3), azimuth of the σ_{Hmax}.
- Paragraph 8.1.4: geodetic strain rate node-by-node with azimuth, magnitude and uncertainties on ε_{Hmax}, ε_{Hmin} and dilatation.

- Paragraph 8.1.5: all the results and uncertainties in the calculation of node-by-node stress inversion.

Georeferenced KML trajectory files can be downloaded at: https://www.mdpi.com/article/10.3390/rs16244765/s1. In particular:

1. Georeferenced KML trajectory file S1: trajectories of the greatest contractional horizontal strain rate (ε_{Hmin}), same in Figure 2.5b.
2. Georeferenced KML trajectory file S2: trajectories of the maximum horizontal stress (σ_{Hmax}), same in Figure 2.6a.

3. Active Strain and Stress Fields of Iberia and Northwest Africa: New Insights on Geodynamics from Seismic and GNSS Data

This manuscript is authored by: Madarieta-Txurruka A., Prieto J. F., Escayo J., Pietrolungo F., Pelaez J. A., Galindo-Zaldivar J., Henares J., Sparacino F., Ercilia G., Fernández J. & Palano M.

Submitted to Gondwana Research – Elsevier journal

3.1. My contribution

In this study, my contribution involved assisting in the collection of focal mechanisms reported in the database (detailed in the supplementary chapter), ensuring an optimal selection based on a complex hierarchy of factors described in the main text. I contributed in obtaining the velocity field to the preliminary phase preceding the computation by analyzing time series and identifying potential issues related to the initial processing stage performed with GAMIT.

I subsequently assisted the first author in the strain rate calculation, as well as in generating the various figures, initially created using GMT (Generic Mapping Tools) and included in the main text. Additionally, I carried out the stress calculations using a previously developed script from our first study, adapting it to the Iberian context by incorporating new parameters discussed with the co-authors.

Finally, I contributed to the final seismotectonic and geodynamic discussion.

3.2. Abstract

The convergence of Eurasia and Africa in the Mediterranean area drives complex geodynamic processes, involving multiple crustal blocks at various stages of subduction and collision. The westernmost region includes not only the two main plates but also the former Iberian microplate and the ALKAPECA domains. These blocks, composed of continental and oceanic crust of varying ages, exhibit distinct deformation behaviors under the regional stress regime. We estimated detailed stress and strain fields using a new earthquake focal mechanism catalog and an updated GNSS velocity field, to better understand where strain accumulates and its relationship to the stress field. Three key findings emerged. First, strain is primarily concentrated along the Eurasia-Africa boundary due to the regional NW-SE compression. In the Atlantic segment, stresses are directly transferred to Iberia, while in the Alboran and Mediterranean segments they are absorbed by the thinned continental crust of the Alboran Domain and the detached margins of the Tell in Algeria and eastern Betic Cordillera in southern Spain. This tectonic framework, combined with the oblique regional convergence respect to the SW Iberian margin, could facilitate clockwise rotation of Iberia. Second, the highest shortening strain concentrates in the aseismic westward displacing Gibraltar Block. Its distinct displacement is likely driven by a terminal subduction with rollback and mantle flow. Third, tectonically active intraplate regions exhibit low horizontal strain rates. The data suggest that these areas are also governed by vertical stress. This study highlights the value of combined stress and strain field analysis for understanding

geodynamic processes in complex regions. It also clarifies how stresses are accommodated in different crustal types, both seismically and aseismically.

3.3. Introduction

The Alpine Orogeny resulted from the closure of the Tethys Ocean (e.g., Schmid et al., 2004) due to counterclockwise convergence of the African plate relative to the Eurasian plate (e.g., Van Hinsbergen et al., 2014). Beyond the interaction of the two major plates, other microplates such as Anatolia (e.g., Taymaz et al., 2007), Adria (e.g., Kissling, 2024), and Iberia, as well as smaller crustal blocks like the ALKAPECA domain –formed by Alboran, Kabylia, Peloritani and Calabria– (e.g., Alvarez et al., 1974; Bouillin et al., 1986), played a significant tectonic role (Figure 3.1). The interplay between these continental blocks gave rise to various geodynamic processes that shaped the evolution of the Mediterranean region. These processes include inversion of rifted margins (Guiraud, 1998; Martínez-García et al., 2013), subduction with or without rollback and associated back-arc extension (Doglioni et al., 1999; Jolivet and Faccenna, 2000; Le Pichon et al., 1982; Schildgen et al., 2014), rifting and post-rift thermal subsidence (Banda and Santanach, 1992; Civile et al., 2010), continental collision (McQuarrie and Van Hinsbergen, 2013; Reilinger et al., 2006; Schmid et al., 2004; Vissers and Meijer, 2012), syn/post orogenic collapse (Jolivet and Faccenna, 2000; Madarieta-Txurruka et al., 2023; Madarieta-Txurruka et al., 2024) among others.

Iberia represented the westernmost major microplate involved in the Alpine Orogeny in the Mediterranean (Figure 3.1). The spatial and temporal distribution of Cenozoic deformation led to complex evolutionary timelines across its margins, giving rise to orogens shaped by diverse processes at different stages of tectonic development. Initially, the northern margin underwent deformation through subduction, followed by collision with the southwesternmost edge of Eurasia, resulting in the formation of the Pyrenees (e.g., Beaumont et al., 2000; Pedrera et al., 2023), the Cantabrian Mountains (Alonso and García-Olalla, 1997; Gallastegui et al., 2002) and the inversion of the Basque-Cantabrian Basin (Pedrera et al., 2021). Today, the main compressional phase has ended, and the region is primarily affected by extension (Lacan and Ortuño, 2012). Deformation also influenced the internal regions of Iberia, reactivating Variscan structures (De Vicente et al., 2007) and inverting previously thinned chains (Guimerà et al., 2004). Later, northeastern Iberia underwent extension during the opening of Valencia Trough (Roca and Guimerà, 1992), driven by subduction with rollback of the Tethys (Fang et al., 2021). Currently, deformation is concentrated along the southern Iberian margin from the Azores-Gibraltar Fracture zone to the Tell Cordillera, including the development of the Gibraltar Arc. However, these regions are not governed by the same processes. For instance, the subduction with rollback that

previously led to the formation of the Valencia Through initially collide with northern Africa forming the Tell Cordillera (Van Hinsbergen et al., 2014) and is now driving the evolution of the Gibraltar Arc (Chertova et al., 2014; De Galdeano, 1990; De Vicente et al., 2007; Rosenbaum et al., 2002) causing the westward displacement of the Alboran Domain (Gonzalez-Castillo et al., 2015) and back-arc extension (Jolivet et al., 2008; Tendero-Salmerón et al., 2022). Meanwhile, African push to the north include indentation tectonics in the Alboran Sea (Estrada et al., 2018; Galindo-Zaldivar et al., 2018). To the east, the back arc extension produced the Algero-Balearic oceanic crust which is now interacting with Iberia and Africa in the eastern Betic Cordillera and Tell Cordillera (Coppier et al., 1989; Ercilla et al., 2022; Tendero-Salmerón et al., 2024). Finally, thrusting between SE Iberian margin and Africa is observed in the Atlantic region (e.g., Martínez-Loriente et al., 2013; Tortella et al., 1997). Alpine Orogeny also played a significant role in Northwest Africa, leading to the inversion of the Atlas Cordillera (Anahnah et al., 2011; Chalouan et al., 2023; Mora et al., 2006).

This complex interaction of geodynamic processes at various evolutionary stages makes this region an extraordinary laboratory for studying the dynamics of continental and oceanic crustal blocks during the Alpine Orogeny.

The geodynamic processes mentioned above determine the stresses in each region. Strain, on the other hand, is the result of the stress acting across the crust. Typically, there is always a direct geometric relationship between the two. In the case of perfectly elastic materials, if the strain and stress fields are expressions of the same process, they are observed to be parallel (e.g., Townend and Zoback, 2006). However, in anisotropic and inhomogeneous materials, such as a heterogeneously deformed crust, the relationship between strain and stress can become oblique (e.g., Flesch et al., 2000; Lachenbruch and Sass, 1992; Zoback et al., 1987). Determining stress through earthquake focal mechanism solutions provides insights into the stress released during seismic events (Aki and Richards, 2002). In contrast, strain estimates derived from regional dense GNSS networks capture crustal deformation resulting from stress that may be released either seismically or aseismically (e.g., Kreemer et al., 2014). By integrating and comparing these two approaches, it is possible to achieve a more comprehensive understanding of tectonic and geodynamic processes, as applied in other regions worldwide, such as Italy (Palano, 2015; Palano et al., 2011), Dead Sea Fault System (Palano et al., 2013), the Himalaya-Tibet region (e.g., Pietrolungo et al., 2024) or Japan (Townend and Zoback, 2006).

This manuscript aims to elucidate the principal geodynamic processes influencing the westernmost Mediterranean by analyzing and comparing the current stress and strain fields with seismicity patterns and major active faults. To achieve this, a comprehensive compilation of all available earthquake focal mechanism solutions (FMSs) has been conducted to

estimate the stress field affecting the region. Additionally, a new velocity field is computed, and a corresponding strain field is derived.

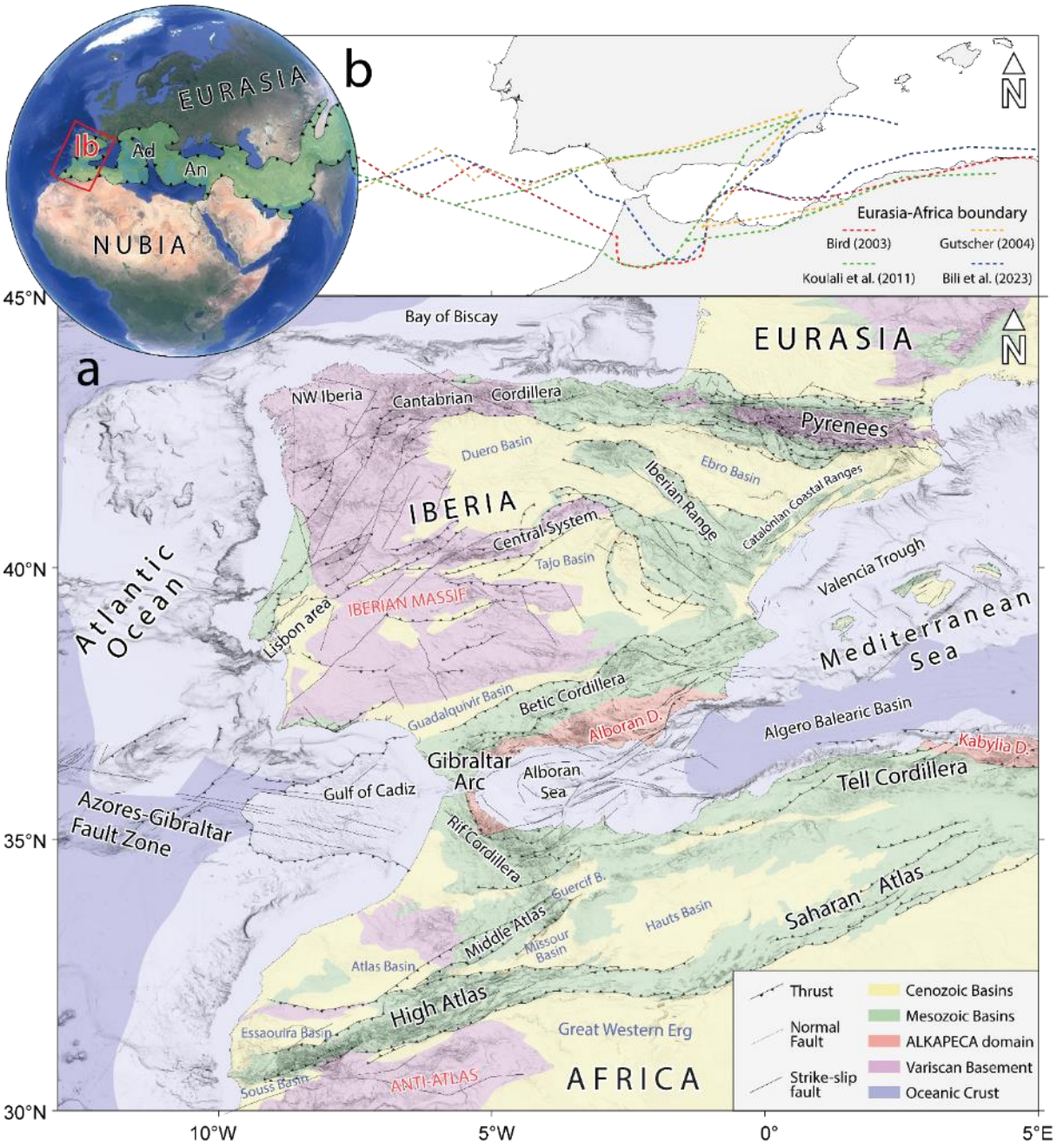


Figure 3.1: Geological context of Iberia and Northwest Africa. a) Simplified geological map modified from Vergés et al., 2019 and Palano et al., 2015 in Iberia and from Anahnah et al., 2011 and Persits et al., 1997 in Northwest Africa. The oceanic crust is obtained from Druet et al., 2023. b) Eurasia-Africa plate boundary from Billi et al., 2023; Bird, 2003; Gutscher, 2004; Koulali et al., 2011. Inset: Global map with the location of the study area at the westernmost end of the Alpine orogenic belt (highlighted in green). Ib: Iberia, Ad: Adria, An: Anatolia.

3.4. Background setting

3.4.1. Geodynamic setting

The Alpine geodynamic evolution of westernmost Mediterranean began during the Permo-Triasssic rifting of Pangea which thinned the Variscan lithosphere, delineating the future margins of the Iberian microplate and the rifted margins within Iberia and Northwest Africa (Angrand et al., 2020; Arche and López-Gómez, 1996; López-Gómez et al., 2019). The resulting rifted zones facilitated the breakup of the lithosphere during the Jurassic-Cretaceous extensional phase. The northward migration of the central Atlantic rifting during the early-middle Jurassic separated Eurasia, Iberia, and Africa from North America, opening the Atlantic Ocean. First, the extension localized in northwest Africa forming different rift basins (e.g., Jacobshagen et al., 1988; Teixell et al., 2003). Later, rifting migrate to the southern and eastern margins of Iberia and the northern margin of Africa, forming Ligurian-Tethys basins (Pedrera et al., 2020; Schettino and Turco, 2011). In the upper Jurassic, the central Atlantic rifting evolved northward and later eastward opening the Bay of Biscay and Pyrenean Basin between north Iberian margin and Eurasia (García-Senz et al., 2020; Pedrera et al., 2021; Sibuet et al., 2004; Thinon et al., 2001; Tugend et al., 2014). The internal part of Iberia underwent extension, leading to the formation of the Iberian Basin (e.g., Aurell et al., 2019; Omodeo Salè et al., 2014). The opening of the margins of Iberia and rifted basins in Northwest Africa continues till the late Cretaceous, when African plate began to push northward, modifying the displacement of Iberia (e.g., Srivastava et al., 1990).

During this Cenozoic, the central Atlantic continued opening, and the western Iberian margin remained almost undeformed. However, mainland Iberia and the other margins have been inverted due to the Eurasia-Africa convergence (e.g., Casas-Sainz and De Vicente, 2009; Vergés and Fernàndez, 2006). The Alpine Orogeny started in the north Iberian margin. During the late Cretaceous-middle Miocene the Pyrenean Basin and the southern margin of the Bay of Biscay were inverted, resulting in the Pyrenean Cordillera and Cantabrian Mountains, respectively (Alvarez-Marron et al., 1997; Fillon et al., 2016; Gallastegui et al., 2002; Pedrera et al., 2023; Teixell, 1998). The Iberian Massif and the Iberian Chain were also deformed during the late Eocene-early Miocene leading to the formation of the Central System and the Iberian Range (De Vicente et al., 2018; De Vicente and Vegas, 2009). Meanwhile, Africa continued its northwestward motion, inverted the rift basins and the Middle Atlas, High Atlas and Saharan Atlas were developed (e.g., Frizon De Lamotte et al., 2000) (Figure 3.1).

Since middle Miocene the Iberian northern margins have remained almost stable while the convergence is mainly concentrated in the south Iberian and northwest African margins (Figure 3.1). The subduction with rollback of the Tethys below Eurasia displaced ALKAPECA

Domain towards the south, fragmenting the LAKAPECA in four smaller domains. While the Peloritani and Calabria domains were displaced toward the southwest, the Kabylia Domain moved south, colliding with the African Margin and developing the Tell Cordillera (Mauffret, 2007; Van Hinsbergen et al., 2014). The Alboran Domain, on the opposite, shifted to southwest and later to the west colliding with the SE Iberian and NW African margins. During this process the Gibraltar Arc was developed, formed by the Betic Cordillera in Iberia and Rif Cordillera in Africa (Chertova et al., 2014; Romagny et al., 2020; Rosenbaum et al., 2002; Schettino and Turco, 2011; Spakman and Wortel, 2004).

Currently, the continuous NW-SE convergence between Eurasia and Africa produces a transpressional boundary along the Azores-Gibraltar Fault System (Buforn et al., 1988; Custódio et al., 2015; Duarte et al., 2013; Galindo-Zaldívar, 2003; Jiménez-Munt et al., 2010; Martínez-Loriente et al., 2021; Martínez-Loriente et al., 2018, 2013; Sallarès et al., 2013), indentation along the Alboran Sea and SE Iberian margin(Borque et al., 2019; Estrada et al., 2018; Galindo-Zaldivar et al., 2018; Tendero-Salmerón et al., 2024) and compression along the Tell Cordillera and the Atlas Mountains (e.g., Frizon De Lamotte et al., 2000) defining the actual diffuse plate boundary (e.g., Billi et al., 2023; Bird, 2003; Gómez De La Peña et al., 2022; Gutscher, 2004; Koulali et al., 2011) (Figure 3.1b).

3.4.2. Active Faults

Ongoing geodynamic processes control the distribution of stress and the localization of active structures that currently shape the region. Active faults facilitate the displacement of crustal blocks and determine strain patterns. Over the past decades, extensive research had led to the identification and characterization of numerous active faults. Figure 3.2 illustrates the active faults, color-coded according to their kinematics, compiled from the Quaternary Fault Database of Iberia (QAFI) (García-Mayordomo et al., 2012) and the GEM Global Active Faults database (Styron and Pagani, 2020) for Northwest Africa. Faults classified as active in the QAFI database are shown with solid lines, while those "debated faults" are represented by dashed lines. In this study, the latter are considered potentially active.

Active faults are mainly concentrated in the Eurasian-African plate boundary and in the Atlas and Pyrenean cordilleras (Figure 3.2). The Atlantic sector of the Eurasian-African plate boundary is formed by the Azores-Gibraltar fracture zone (Buforn et al., 1988; Jiménez-Munt et al., 2001; Laughton and Whitmarsh, 1974; Sartori et al., 1994). It represents a dextral to reverse plate boundary forming transpressive positive flower structures (Bartolome et al., 2012; Zitellini et al., 2009). Between the plate boundary and SW Iberia, the main active structures are NNE-SSW to ENE-WSW striking reverse to reverse sinistral faults (e.g., Gràcia et al., 2003; Martínez-Loriente et al., 2018, 2013; Zitellini et al., 2004).

Active faults along the Gibraltar Arc are diverse: reverse, strike-slip, and normal faulting occurs. In the western Betic Cordillera, no major faults are considered active. However, continuous seismicity in the Morón de la Frontera area (Ruiz-Constán et al., 2009) and GNSS data (Gonzalez-Castillo et al., 2015) suggest that an ENE-WSW to NE-SW striking basal thrust could be active, producing surface folding (Gonzalez-Castillo et al., 2015; Gutscher et al., 2012; Pedrera et al., 2011). The western Rif Cordillera is also characterized by active thrusts striking NW-SE to E-W (e.g., (Koulali et al., 2011). The central Betic Cordillera is primarily characterized by normal faulting (Martin-Rojas et al., 2023; Sanz De Galdeano et al., 2012, 2003). Most active faults are NW-SE striking normal faults (Alfaro et al., 2008; Galindo-Zaldívar et al., 1999; Madarieta-Txurruka et al., 2022, 2021) but E-W normal faulting also occurs (Araque-Pérez et al., 2025, 2024; Madarieta-Txurruka et al., 2024; Martínez-Martos et al., 2017; Reicherter et al., 2003; Ruano et al., 2004). NE-SW strike-slip faults are also present (Medina-Cascales et al., 2021).

The eastern Rif Cordillera, the Alboran Sea, and the eastern Betic Cordillera are deformed by the active Trans-Alboran Shear Zone (TASZ) (Hernandez et al., 1987) and the Eastern Betic Shear Zone (EBSZ) (Coppier et al., 1989), a NE-SW striking corridor mainly formed by sinistral strike-slip and reverse faults. The development of this system is related to the central Alboran indenter, bounded by N-S sinistral and E-W dextral faults (Estrada et al., 2018; Galindo-Zaldivar et al., 2018; Gómez De La Peña et al., 2022) and it deforms the coastal part of the central Betic Cordillera, where NW-SE dextral-normal faults occur (García-Mayordomo et al., 2012; Pedrera et al., 2012). The Eastern Betic Shear Zone develops in association with the eastern Betic indenter (Silva et al., 1993; Tendero-Salmerón et al., 2024), mainly bounded by N-S to NE-SW sinistral to sinistral-reverse faults to the east and thrusts in the north (Booth-Rea et al., 2004; Borque et al., 2019; Martínez-Díaz, 1999). Between the two indenters lies the Carboneras Fault (Faulkner et al., 2003; Moreno et al., 2015), connecting the shear zones.

In the Tell Cordillera, the main active faults are E-W to ENE-WSW reverse faults (Bouhadad, 2001; Heddar et al., 2013; Maouche et al., 2011; Meghraoui, 1991). These reverse faults are cut by WNW-ESE dextral-reverse faults (Basili et al., 2013; Domzig, 2006; Mauffret, 2007). ENE-WSW trending thrust faults are also present in the High Atlas (Arboleya et al., 2004; Sébrier et al., 2006; Tesón and Teixell, 2008). In the Middle Atlas, particularly near the Rif Cordillera, sinistral and sinistral-reverse faults are also recognized (Gomez et al., 1996).

The Pyrenees, the Iberian Range, and the NW coast of Iberia are dominated by active normal faulting, mostly parallel to the mountain ranges. In the Pyrenees, the faults strike E-W (Lacan and Ortuño, 2012; Ortuño et al., 2013). Normal faults in the Iberian Range are oriented NW-SE to N-S (Lafuente et al., 2011; Peiro et al., 2023, 2020), while in the Catalonia Coastal Ranges, they are oriented NE-SW (Masana et al., 2001; Perea et al., 2012). In the Cantabrian Mountains, two NW-SE dextral faults are considered potentially active (Fernández-Viejo et

al., 2021; López-Fernández et al., 2018). Finally, eastern Iberia is affected by large NNE-SSW sinistral faults (Ribeiro et al., 1990; Rockwell et al., 2009; Villamor et al., 2012) and NE-SW reverse faults (Cabral, 2012).

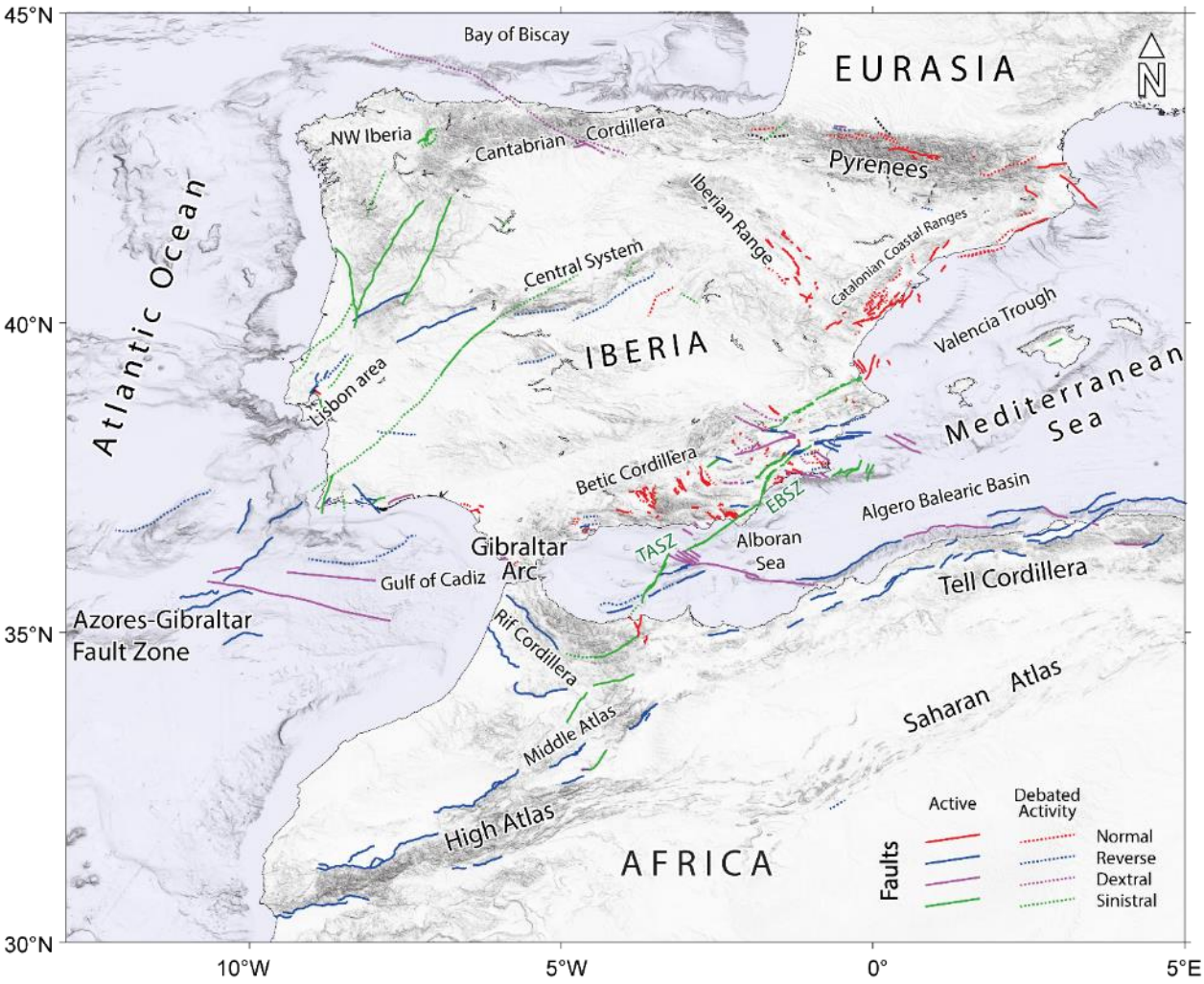


Figure 3.2: Active faults in Iberia and Northwest Africa, color-coded according to the kinematics from the QAFI (García-Mayordomo et al., 2012) and GEM (Styron and Pagani, 2020) databases. TASZ: Trans-Alboran Shear Zone. EBSZ: Eastern Betic Shear Zone Gb: Granada Basin. GBb: Guadix-Baza Basin.

3.4.3. Seismicity

The study region is affected by historical earthquakes over Mw 6 mainly located in the Eurasia-Africa plate boundary (Grünthal and Wahlström, 2012; Hamdache et al., 2010; Pelaez et al., 2007; Stucchi et al., 2013) (Figure 3.3 and Paragraph 8.2.2). The main earthquakes close to Iberia is the 1755 Lisbon earthquake (Baptista et al., 1998; Martinez Solares et al., 1979) with an estimated Mw 8.7, occurred between SW Iberia and the Azores-Gibraltar Fault Zone. In this region another four historical earthquakes with Mw > 7 occurred (AD 1309, 1724,

1816, 1858). Other earthquakes with Mw > 7 occurred in the Tell Cordillera (AD 1365, 1716, 1825, 1867, 1891, 1922 and 10 October 1980). Earthquakes with Mw > 6 are more widespread and they also occur onshore near Lisbon (e.g., AD 1531), Pyrenees (e.g., AD 1428), Gulf of Cádiz (e.g., AD 1722, 1773), Betic cordillera (e.g., AD 1522, 1680, 1829, 1884), Alboran Sea (e.g., AD 1804), Rif Cordillera (e.g., AD 1624) and westernmost High Atlas (e.g., AD 1731).

The instrumental seismicity provided by the Spanish Instituto Geographic Nacional (IGN, 2022) is mainly distributed along the Eurasia-Africa plate boundary, delineating a diffuse contact from the Azores-Gibraltar Fault Zone to the Tell Cordillera, but also in the Pyrenees, High and Middle Atlas, NW Iberia and other Iberian intraplate regions (Figure 3.3 and Figure 3.4). Along the Azores-Gibraltar Fault Zone the seismicity is concentrated along NE-SW striking clusters reaching the SW Iberian margin. Most of the seismicity is above 50 km depth and the maximum magnitude is related to the Mw 7.9 February 1969 earthquake. The seismicity in SW Iberia and adjacent western Iberian margin is more widespread, also reaches 50 km and magnitude hardly exceed M 5.0. Earthquake focal mechanism solutions (FMSs) along these regions suggest main reverse and strike-slip faulting (e.g., Buforn et al., 1988; Custódio et al., 2015).

The Gibraltar Arc is affected by a crustal seismicity mainly concentrated in the Betic Cordillera, Eastern Rift and the Alboran Sea. The maximum magnitude reached Mw 6.3, during the 2016 series in the Alboran Sea (Hamdache et al., 2022). Along the Betic Cordillera only a few earthquakes exceed Mw 5.0. FMSs suggest reverse and strike-slip faulting in the western Betic Cordillera (Ruiz-Constán et al., 2009); mainly normal faulting in the central Betic Cordillera (Lozano et al., 2022; Madarieta-Txurruka et al., 2022, 2021), strike-slip faulting along a NE-SW band from the eastern Rif Cordillera to the eastern Betic Cordillera crossing the Alboran Sea (Galindo-Zaldivar et al., 2018; Grevemeyer et al., 2015; Rodríguez-Escudero et al., 2014) and reverse and strike-slip faulting in the western Rif Cordillera. At the internal part of the Gibraltar Arc intermediate seismicity occurs along a N-S sharp band reaching 100 km depth. Maximum magnitudes are around M 5.0 and FMSs suggest reverse to normal and strike-slip kinematics (Ruiz-Constán et al., 2011; Santos-Bueno et al., 2019) (Figure 3.3 and Paragraph 8.2.1). Deep earthquakes, above 600 km depth, also occur below the central Betic Cordillera at least since 1954 when the M 7.8 Durcal earthquake occurred (Buforn, 2005; Buforn et al., 2011, 1991) (depicted in pink in Figure 3.3 and Paragraph 8.2.1).

Along the Tell Cordillera the seismicity is widespread concentrated in crustal depths (Hamdache et al., 2010). However, the seismicity increases in some clusters located close to the Mediterranean coast reaching magnitudes close to M 7.0 during the 1954 and 1980 El Asnan (Bezzeghoud et al., 1995), and 2003 Zemmouri earthquakes (Hamdache et al., 2004). Seismicity is mainly related to reverse and strike slip faulting as shown by the FMSs (Figure

3.4). Along the Moroccan Atlas seismicity is less frequent. Two clusters highlight in the western and central High Atlas. Main earthquakes are the M 6.0, 1960 Agadir, earthquake, and the M 6.8, September 2023, earthquake (Peláez, 2023). FMSs suggest thrusting and strike-slip faulting related to the main earthquakes (Cheloni et al., 2024; Udías and Buforn, 1991).

Along the Pyrenees the seismicity is also crustal and concentrates mostly in the western half. The magnitude of earthquakes hardly exceeds Mw 5.0. FMSs suggest a main normal faulting but also strike-slip faulting, and some reverse solutions (Rigo et al., 2015; Ruiz et al., 2023). The NE Iberian margin is affected by low magnitude seismicity following the axis of the Catalonian Coastal Ranges, related to strike-slip to normal FMSs. In the internal part of Iberia scarce seismicity occurs, concentrated around the Iberian Range (e.g., Peiro et al., 2024) with normal and strike slip FMSs. Finally, in the north Iberian margin seismicity is scarce except in NW Iberia. This region is characterized by low to moderate magnitude crustal clusters, reaching sporadically over M 5.0. The seismicity is mainly related to strike-slip and normal FMSs (Martín-González et al., 2023).

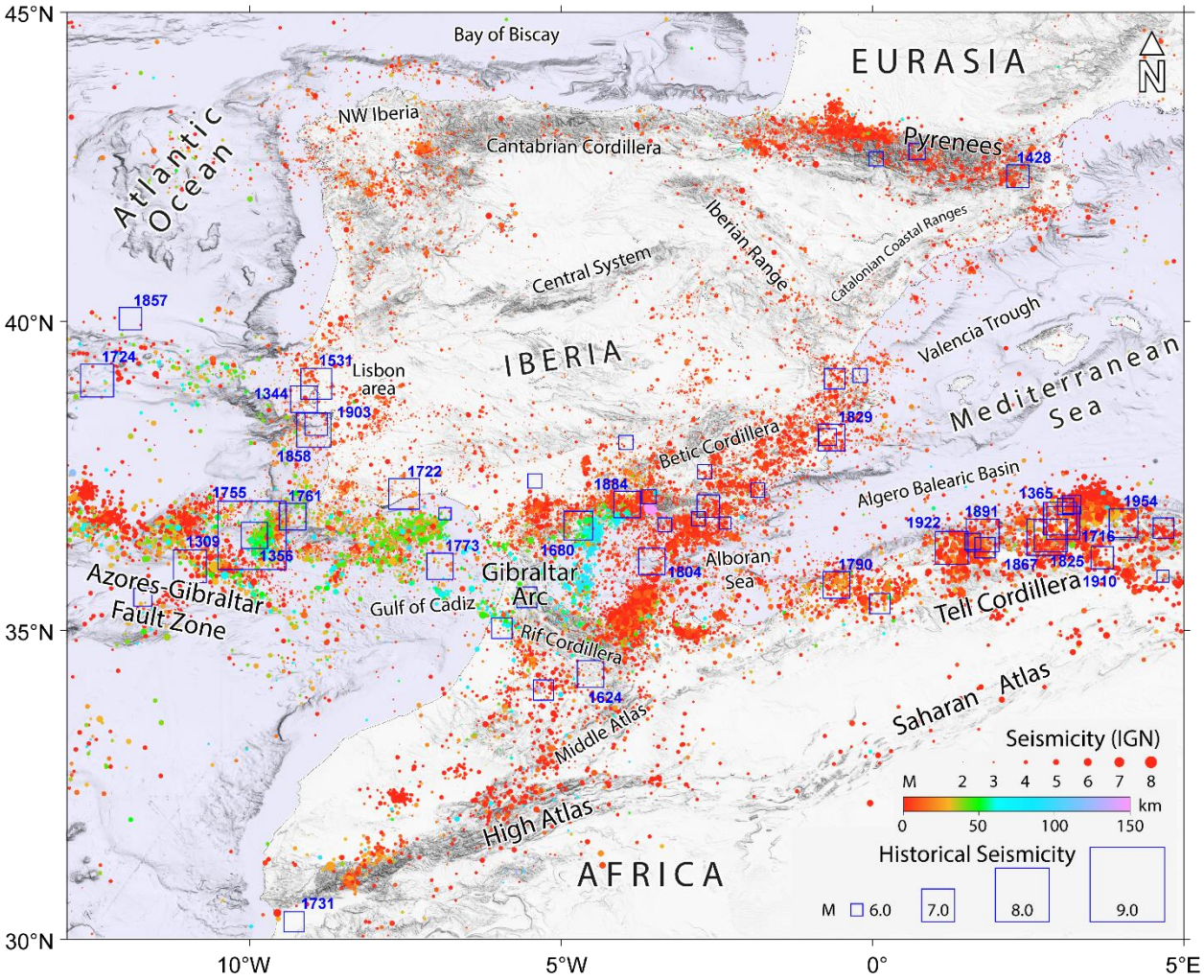


Figure 3.3: Historical and instrumental seismicity in Iberia and Northwest Africa. The historical seismicity (Paragraph 8.2.2) shows all the earthquakes with Mw > 6.0 and the earthquakes with Mw > 6.5 are represented by the year of occurrence. The instrumental seismicity with M > 2.0 belongs to the Spanish Instituto Geográfico Nacional database (IGN, 2022).

3.5. Methods

3.5.1. Stress field estimation

The slip direction along a fault during an earthquake reflects the stress conditions at the source. Consequently, earthquake focal parameters provide valuable insights into the current tectonic stress field across the seismogenic layer. For this reason, earthquake focal mechanism solutions (FMSs) are essential and widely used indicators of stress, and their formal inversion enables the determination of the regional stress field.

The FMS dataset compiled here considered mostly available solutions along Iberia and Northwest Africa, onshore and offshore. An exhaustive compilation has been made from research works and specific catalogs to increase the coverage of the entire study area. In many cases, a seismic event had multiple although similar FMSs proposed by different

sources. It was therefore necessary to establish criteria for selecting the solution to use for a given seismic event. Overall, the following criteria was considered: 1-Detailed calculation of FMSs from peer-review papers analyzing specific earthquakes or study areas are preferred over solutions from catalogs, giving preference to the most recent publications. 2-Waveform inversion solutions are preferred over polarities. 3-The Iberian and European catalogs are preferred over global catalogs due to their better coverage of stations and the use of more detailed velocity models.

The final catalog comprises ~2200 FMSs from 1910 to 2024 reaching M 8, which are shown in Paragraph 8.2.1 and resumed in Paragraph 8.2.3. Most of the FMSs are in the Eurasia-Africa boundary (~80%), along the Azores-Gibraltar Fault Zone, Gibraltar Arc and Tell Cordillera. There are also solutions along the Pyrenees (~10%) and some widespread solutions along NW Iberia, Lisbon area and Atlas. Most of the FMSs, around 89%, are crustal (< 30 km) and are widespread along the active areas noted before. Solutions with depths of up to 50 km account for 6% of the data and are predominantly located to the southwest of Iberia, mainly in offshore regions. Solutions with intermediate depth (50-150 km) account for ~5% and are mainly located in the internal part of the Gibraltar Arc. Finally, five deep earthquake FMSs (> 600 km) are situated beneath the central Betic Cordillera.

For the inversion of the crustal stress field earthquake FMSs deeper than 50 km and with less than M 2.0 are discarded (Paragraph 8.2.3). The remaining ~1800 earthquake FMSs (Figure 3.4) are inverted using the STRESSINVERSE software developed by Vavryčuk, 2014. This software calculates the geometry of the three stress axes (σ_1, σ_2 and σ_3) and stress ratio, R, (eq. 1), by means of an iterative inversion, considering all the nodal plane combinations, till obtaining the combination more susceptible to shear faulting. The inversion is applied along a 0.5º resolution grid and computed with a half-cell overlapping in every cell with a minimum of 8 solutions (Figure 3.5 and Paragraph 8.2.4).

$$R = \frac{\sigma_1 - \sigma_2}{\sigma_1 - \sigma_3} \qquad (1)$$

Finally, to estimate the trajectories of the σ_{Hmax} field (Figure 3.5), the maximum horizontal stress (σ_{Hmax}) in each cell is calculated, following the methodology proposed by Lund and Townend, 2007, which considers the main stress axes and stress ratio (R). To increase the coverage of σ_{Hmax} data, the former solutions are combined with σ_{Hmax} indicators from individual FMSs with M > 4.5, along with other stress indicators obtained from World Stress Map (Heidbach et al., 2018) (Paragraph 8.2.5).

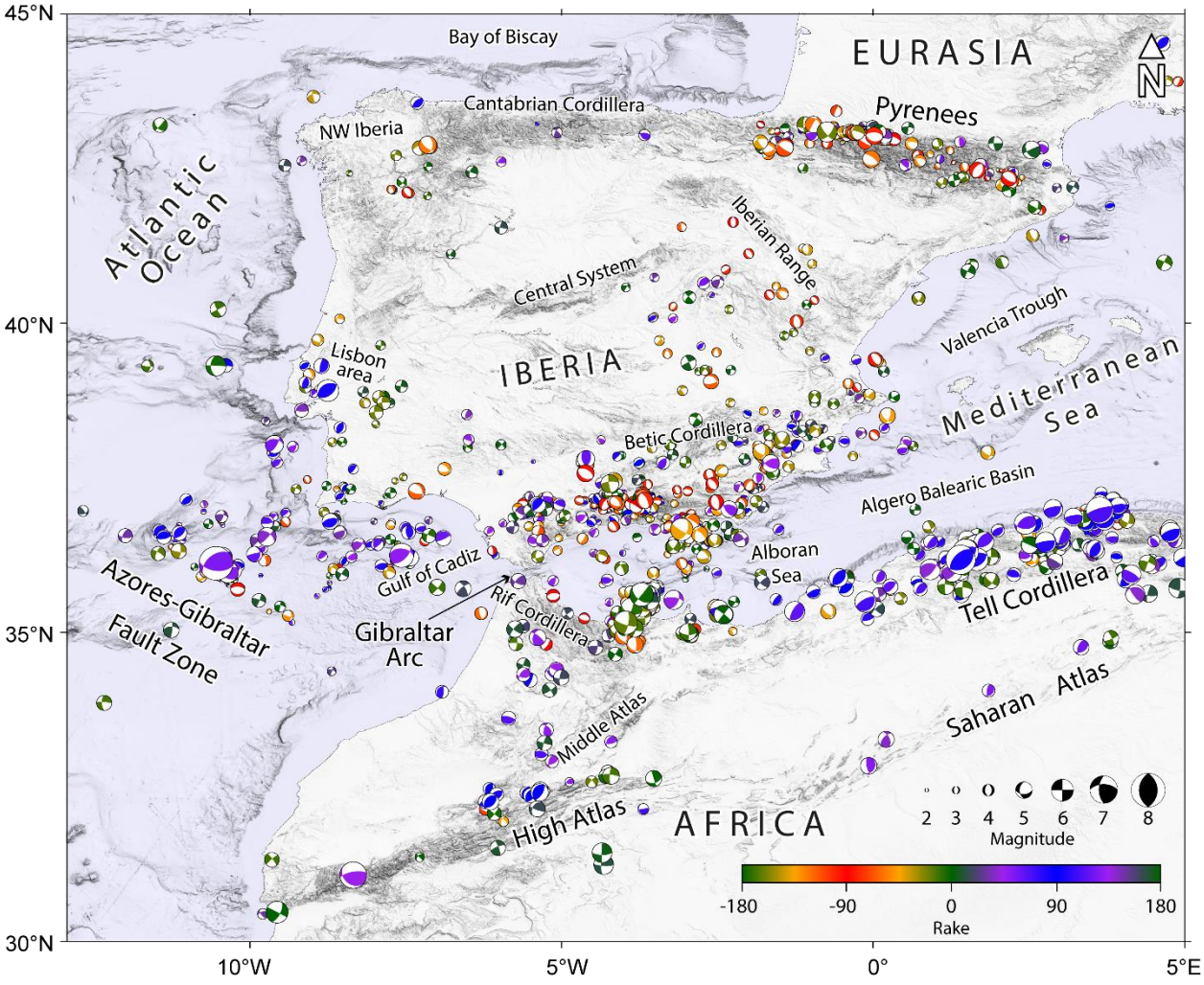


Figure 3.4: FMSs in Iberia and Northwest Africa. The solutions reported here, with a magnitude greater than Mw 2 and a depth less than 50 km, were used in the stress inversion. The compressive quadrants are color-coded according to the rake.

3.5.2. GNSS data processing and velocity and strain field estimation

The GNSS dataset used here includes 530 continuous stations belonging to the EUREF permanent network, SONEL database, Portuguese RENEP and SERVIR networks, Spanish ERGNSS network, French RGP network and other 15 networks developed by regional institutions (Paragraph 8.2.6), with time interval of the longest observations covering almost 25 years, from 1999.00 to 2024.00. In addition to continuous GNSS sites, we included data from 25 episodic GNSS sites located in Morocco (Koulali et al., 2011) with surveys spanning the 1999.80–2006.71 time interval, available in the UNAVCO archive (www.unavco.org). This dataset increases the number of stations and/or time-interval of the previous studies in Iberia and Northwest Africa (Fernandes et al., 2007; Garate et al., 2015; Koulali et al., 2011; Palano et al., 2015, 2013; Serpelloni et al., 2022; Sparacino et al., 2020).

The GNSS data are processed using the GAMIT/GLOBK software (Herring et al., 2018) (www-gpsg.mit.edu), by adopting the strategy described by Palano et al., 2020. By using the GLORG module of GLOBK, all the GAMIT solutions and their full covariance matrices are combined to estimate a consistent set of positions and velocities in the ITRF2014 reference frame Altamimi et al., 2017. To improve the density of the velocity field we aligned velocity fields available in literature (Bougrine et al., 2019; Cabral et al., 2017; Echeverria et al., 2015, 2013; Garate et al., 2015; Rigo et al., 2015) to the ITRF2014 solution computed here by applying a Helmert transformation (Paragraph 8.2.7). We align the ITRF14 velocities into a fixed Eurasian and African reference frames (Altamimi et al., 2017) to adequately show the crustal deformation pattern over the study area (Figure 3.6 and Paragraph 8.2.7). Finally, 85 stations with anomalous velocities compared to neighboring ones, have been discarded from the velocity solutions, likely due to a non-tectonic deformation (Paragraph 8.2.7).

The strain field is computed following the method outlined by Shen et al., 2015 considering a total of 647 stations (Figure 3.6). First, we interpolate the GNSS velocity field into a 0.5° resolution grid using Voronoi spatial and Gaussian distance weighting, following the comparative analysis conducted by Nucci et al., 2024, ensuring nodes do not coincide with any GNSS stations locations (Palano et al., 2013). The weighting threshold (Wt) is strongly influenced by the inter-station distances of GNSS velocities and the measurement uncertainties (Shen et al., 2015), therefore, we tested multiple values. Based on the results, we selected an optimal weighting threshold of 10, which preserves the observed velocity field while ensuring that the model-observed discrepancy exceeds the mean uncertainty of GNSS measurements. Later, the horizontal strain-rate tensor is computed as the derivative of the velocities. From the horizontal strain-rate field, the areal change rate is calculated, as it represents the sum of the ε_{Hmin} and ε_{Hmax} rates and it is indicative of the crustal dilatation rate (Figure 3.7). Moreover, the second invariant is computed (Eq. 2), which represents the total deformation of the area (Figure 3.8). Finally, the ε_{Hmin} trajectories are estimated to achieve an optimal comparison with the σ_{Hmax} (Figure 3.8).

3.6. Results

3.6.1. Stress field

3.6.1.1. Stress ellipsoids

The stress field (Figure 3.5 and Paragraph 8.2.4) is depicted through stereoplots representing the principal stress axes derived from each iterative solution during the inversion process (Figure 3.5a). Each stereoplot is color-coded according to the principal stress axis (or axes) situated close to the vertical, considering the most probable solution available in Paragraph

8.2.4. Stress ratio (R) for each computing cell is also shown (Figure 3.5b). As previously quoted, the FMSs included in the inversion are predominantly from events within the upper 30 km, none of which exceeding 50 km depth. Therefore, the resulting stress field basically reflects the stress distribution within the crust.

Overall, the inversion results are of high quality, as indicated by the low dispersion of iterative solutions in most cells. However, the dispersion is higher in cells where FMSs display variable kinematics, particularly in transition zones between different seismotectonic regions, such as the internal part of the Gibraltar Arc. The dispersion increases in regions with limited FMSs such as northwest or central Iberia. In some cells, only the σ_1 axis is well-constrained, while the σ_2 and σ_3 axes partially overlap in their estimated 95% confidence limits. Most of these solutions exhibit R values above 0.75, suggesting that the magnitudes of the σ_2 and σ_3 axes are nearly equal, making difficult to define them properly and accurately constrain the stress tensor.

Due to the distribution of available FMSs (Figure 3.4) the inverted cells are mostly widespread along the Eurasia-Africa plate boundary (Figure 3.5). Towards the southwest of Iberia, most of the stress tensors located offshore suggest a NW-SE to NNW-SSE horizontal σ_1, NE-SW horizontal σ_3 and close to vertical σ_2, with stress ratio mostly upper than 0.7, suggesting a prolate stress ellipsoid. In some cells, mainly located in the Gulf of Cádiz, the σ_2 and σ_3 axes interchange, positioning σ_3 close to the vertical. In the coastal area and onshore the stress tensors are also characterized by NW-SE horizontal σ_1, NE-SW subhorizontal σ_3 and subvertical σ_2. The stress ratio decreases from ~0.7 in the south, to 0.5-0.2, near Lisbon, suggesting a prolate shape of the stress ellipsoid in the south and a triaxial to oblate shape in the north.

The Gibraltar Arc is characterized by a complex stress regime, with varying ellipsoid shapes and orientations depending on the location. In the western Betic Cordillera, stress inversion indicates a NW-SE trending subhorizontal σ_1 and subvertical σ_3, with stress ratios above 0.7. The central Betic Cordillera is divided into two distinct regions. The southern part is characterized by a vertical σ1 and NE-SW trending σ_3. To the north, near the Guadalquivir Basin, σ_1 becomes horizontal trending NW-SE and, being σ_2 vertical. In both regions, R values are greater than 0.5, mostly above 0.7, suggesting a triaxial to mainly prolate shape of the stress ellipsoid. In the eastern Betic Cordillera the σ_1 is horizontal striking NW-SE to N-S, while σ_3 is horizontal and σ_2 subvertical. Some cells show vertical σ_3 or both inclined σ_2 and σ_3 axes. The stress ratio is irregular in the area, suggesting all prolate, oblate and triaxial shapes. The stress ellipsoids in the eastern Rif Cordillera, the Alboran Sea and on the coast of the central-eastern Betic Cordillera are mainly characterized by NW-SE σ_1 and vertical σ_2, and very different stress ratios. Some ellipsoids with vertical or highly inclined σ_1 and NW-

SE striking inclined σ_2 occur surrounding the Alboran Ridge. Finally, the stress ellipsoid in the western Rif has a N-S horizontal σ_1, ENE-WSW inclined σ_2 and σ_3, and prolate shape.

The stress field in the Tell Cordillera is more homogeneous. It is mostly characterized by a horizontal σ_1 striking NW-SE and vertical σ_3, with a prolate shape, as indicated by R > 0.6-0.7. In some cells, the high R values result in an overlap between the σ_2 and σ_3 axes. In the easternmost sector, this results in a reversal, σ_2 becoming vertical. Following this pattern, the three available stress ellipsoids in the High-Middle Atlas show horizontal σ_1 striking NW-SE and vertical σ_3. However, R values close to 0.5 suggest a triaxial shape.

The Pyrenees are predominantly characterized by stress ellipsoids with nearly vertical σ_1 and N-S to NE-SW striking σ_3. In the easternmost sector, however, σ_1 becomes subhorizontal, striking NNW-SSE to NNE-SSW while both subvertical σ_2 and σ_3 are present. R values generally range between 0.4 and 0.8, suggesting triaxial to prolate ellipsoid shapes.

In NW Iberia the inverted four cells illustrate stress ellipsoid with NNW-SSE striking σ_1 and subvertical σ_2, and triaxial to oblate shapes. Stress inversion is possible also in other internal regions of Iberia. To the south of the Central System stress ellipsoids are characterized by NW-SE striking subhorizontal σ_1 and subvertical σ_2 and prolate shape. Finally, the available stress ellipsoids in the southeastern Iberian Range and NE Iberian margin show inclined σ_1 and σ_3 axes striking NE-SW, and triaxial to prolate shapes.

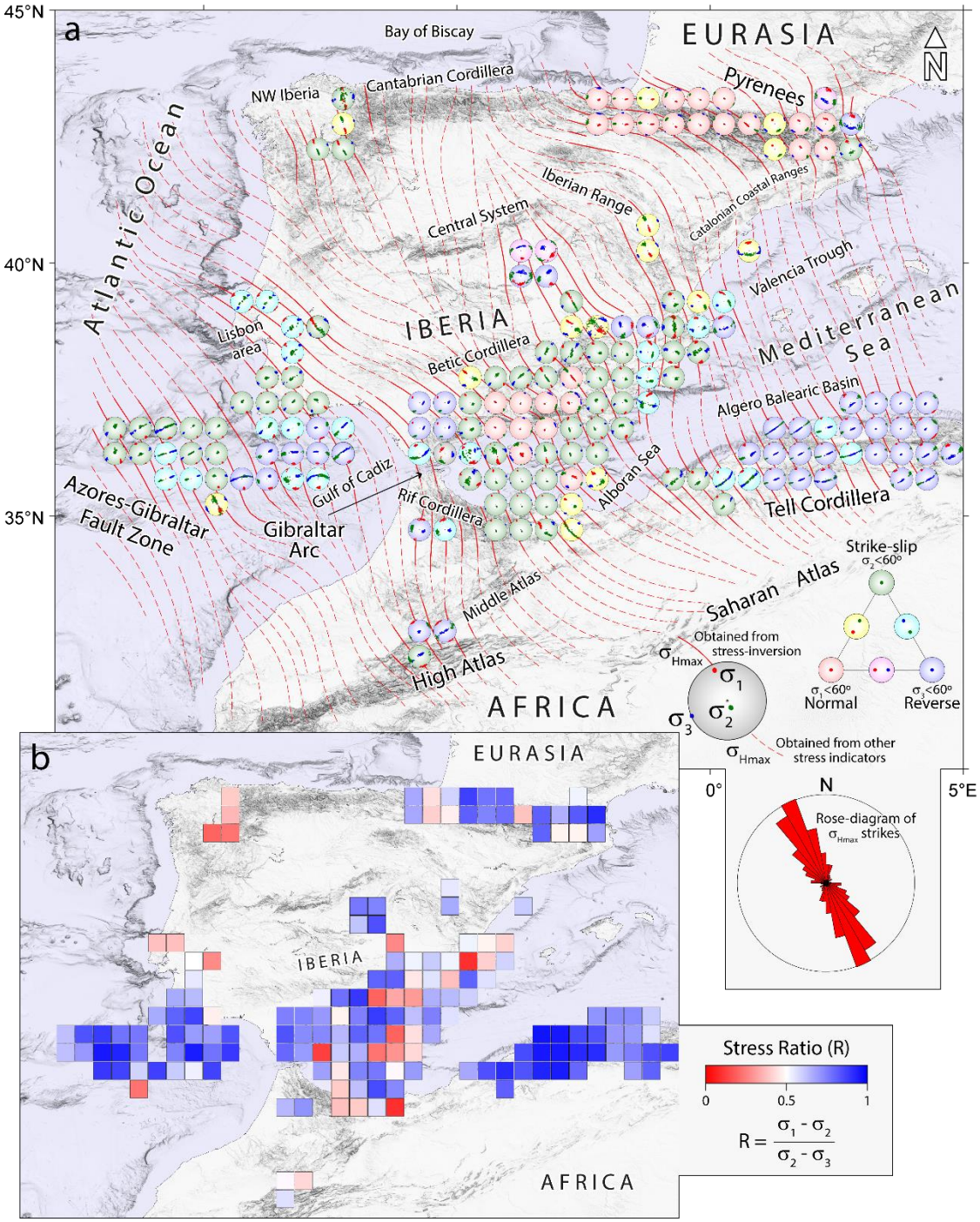


Figure 3.5: Stress field in Iberia and Northwest Africa. a) Stereoplots depict the stress field by representing the main stress axes (σ_1 in red, σ_2 in green and σ_3 in blue), derived from each iterative solution during the inversion process. Each stereoplot is color-coded according to the principal stress axis (or axes) situated close to the vertical, considering the final solution available in Paragraph 8.2.4. The red lines represent σ_{Hmax} trajectories. The lower-right inset represents the rose-diagram of the σ_{Hmax} strikes in each grid cell and the average strike of the σ_{Hmax}. b) The stress ratio (R) in each cell.

3.6.1.2. Maximum horizontal stress field

The horizontal maximum stress (σ_{Hmax}) field shows generally good coverage across the study area (Figure 3.5a). Data obtained from stress inversion results (represented by continuous

dark red lines) cover the Africa Eurasia plate boundary, the Pyrenees, the Atlas Cordillera and several regions in Northwest and eastern Iberia. The σ_{Hmax} field is further complemented by individual FMSs with M > 4.5 and other stress indicators (Paragraph 8.2.5); however, these results should be interpreted with caution due to their higher uncertainty.

The general pattern of the σ_{Hmax} along Iberia and Northwest Africa is mostly striking N150º-160ºE (Inset in Figure 3.5). This general pattern slightly rotates anticlockwise in southwestern Iberia and clockwise in the Cantabrian region and eastern Iberia. The Betic-Rif Cordillera has the most complex σ_{Hmax} pattern of the study area. In the western Betic Cordillera the σ_{Hmax} slightly rotate clockwise to ~N130ºE while in the western Rif rotates clockwise to ~N020ºE. In this way, the σ_{Hmax} pattern locates oblique to the western Gibraltar Arc. The central Betic Cordillera is characterized by a local anticlockwise rotation of the trajectories to ~N120ºE. To the easternmost Betic Cordillera the pattern rotates clockwise to ~N005ºE. The pattern changes more strongly in the Pyrenees and the Iberian Range, where the σ_{Hmax} rotates to ~N100ºE, subparallel to the axis of each mountain range.

3.6.2. Velocity field

The velocity field shown in Figure 3.6 provides extensive coverage of the study area. It is depicted using velocity vectors accompanied by the 95% confidence ellipses. GNSS station density is notably higher in Iberia and France compared to Northwest Africa, with the densest regions being the Pyrenees, the eastern Central System, southwestern Iberia, and the eastern Betic Cordillera. This higher density is due to the inclusion of various episodic networks in these areas. However, although station density is greater, the precision of the measurements is slightly lower, as indicated by the larger error ellipses.

In the Eurasia reference frame (Figure 3.6a), the most distinct observation is the Eurasia-Africa convergence represented by the NW directed motion in the east and WNW directed motion in the west of Africa respect to Eurasia, at rates of 4.5–6 mm/yr. Along the Tell Cordillera the convergence rate decreases to 2–3 mm/yr in the coast. Iberia shows an almost stable pattern respect Eurasia, mainly in the northern half. However, velocities increase from 0–0.5 mm/yr in the northeast to 2–3 mm/yr at the southern and southwestern margins. Additionally, the direction of motion rotates from predominantly southwestward in the northeast to WSW/Wward in the south-central region, and to WNWward in the southwest. This general pattern shifts in the western Gibraltar Arc and the eastern Betic Cordillera. The Gibraltar Arc is characterized by westward velocities exceeding 3 mm/yr in the western and central-south Betic Cordillera and reaching 5–6 mm/yr in the Rif Cordillera. Meanwhile, the coastal areas of the eastern Betic Cordillera exhibit a radial motion pattern, with northwestward to northward velocities reaching up to 2 mm/yr.

In the Africa reference frame (Figure 3.6b) the Eurasia-Africa convergence is also observed. It is represented by the SEward motion in northeast Iberia to ESEward motion in southwest Iberia. The African reference frame allow to better observe the motions of different tectonic regions in Africa. Most of the stations located in mainland regions show velocities below 1-1.5 mm/yr. Moreover, it perfectly shows the southwestward motion up to 3.5 mm/yr of the Rif Cordillera. Finally, the Tell Cordillera undergoes southeastward decreasing from 2-3 mm/yr in the coast to almost stable in the internal region.

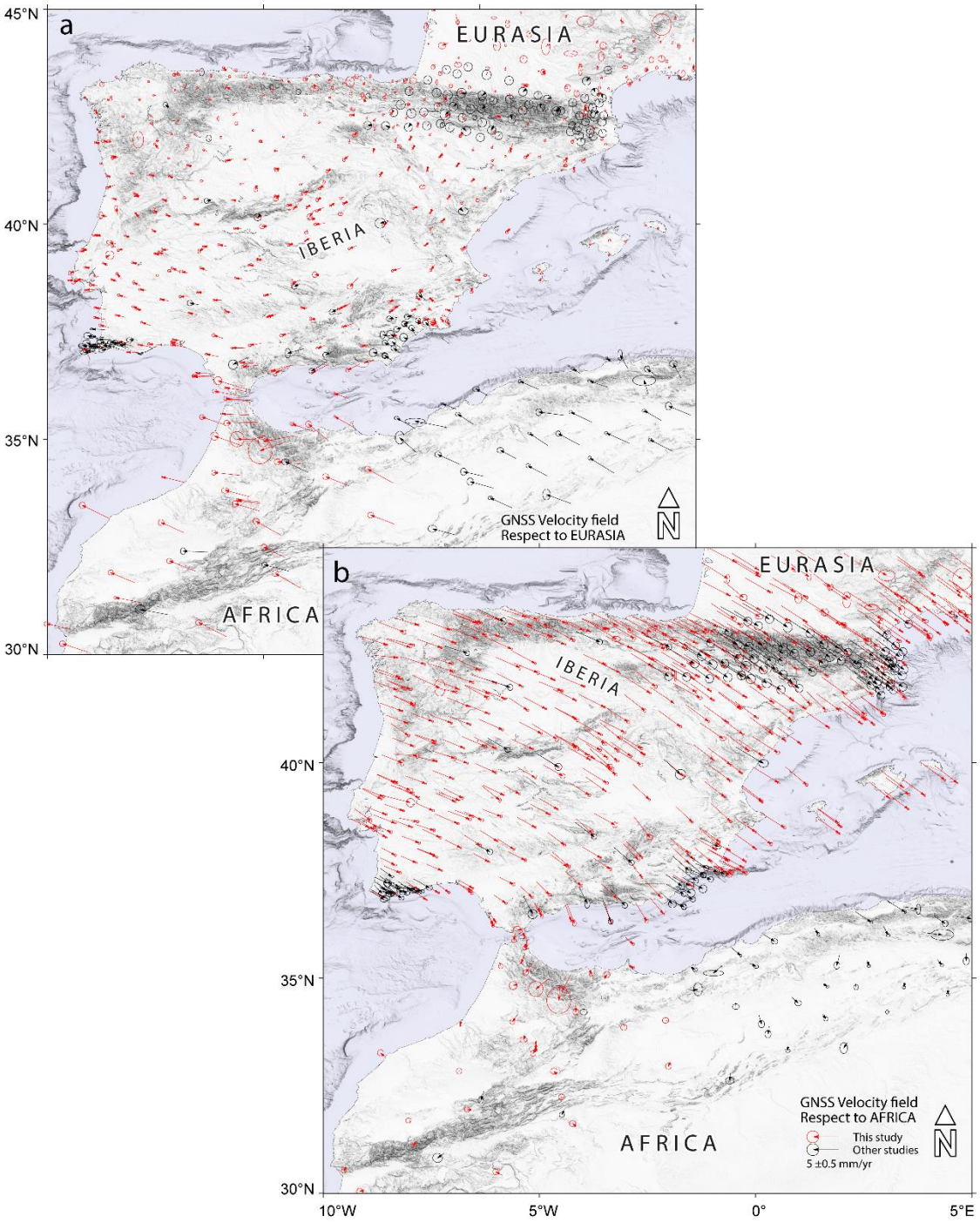


Figure 3.6: Velocity field of Iberia and Northwestern Africa. a) GNSS velocities and 95% confidence ellipses in a fixed Eurasia. b) GNSS velocities and 95% confidence ellipses in a fixed Africa.

3.6.3. Strain field

3.6.3.1. Horizontal strain field

The strain field is represented by the horizontal maximum and minimum strain axes, the second invariant of the strain (Figure 3.7) and the areal change rates (Figure 3.8). The highest strain-rate and second invariant values (> 10 nanostrain/yr) are located along the Gibraltar Arc and the Alboran Sea, followed by the Tell Cordillera and Lisbon area (Figure 3.7).

In the Gibraltar Arc and the Alboran Sea, three sectors can be differentiated (Figure 3.8). First, the westernmost Gibraltar Arc characterized by 2D shortening up to -20 nanostrain/yr in E-W direction and -7 nanostrain/yr in N-S direction. Therefore, this area stands out with the highest negative areal change rates in the region, up to -22 nanostrain/yr. Second, a NE-SW striking corridor from the eastern Rif to the eastern Betic Cordillera, crossing the Alboran Sea, characterized by NNW-SSE shortening up to -24 nanostrain/yr and WSW-ENE stretching up to 22 nanostrain/yr. The areal change rates in the former region varies between null and slightly negative areas, the latter affecting the central Alboran Sea and the easternmost Betic Cordillera. Third, the central Betic Cordillera is characterized by a NE-SW to NNE-SSW stretching up to 17 nanostrain/yr and limited perpendicular shortening. Therefore, it lies under positive areal change rates close to 8-10 nanostrain/yr.

The Tell Cordillera is affected by NW-SE shortening between 12 and 17 nanostrain/yr (Figure 3.8). The central sector is distinct due to the highest shortening values and the simultaneous NE-SW stretching, which reaches up to 12 nanostrain/yr. Overall, the mountain range undergoes negative areal change rates between 6-10 nanostrain/yr. In southwestern Iberia the strain field suggests NE-SW stretching up to 17 nanostrain/yr together with a NE-SW shortening of 6-7 nanostrain/yr resulting in slightly positive areal change rates.

The internal regions of Iberia and Northwest Africa and the Pyrenees undergo low horizontal strain rates, mostly with second invariant values lower than 10 nanostrain/yr. They depict a disordered pattern of horizontal strain axes and areal changes rates, leading to their classification as nearly tectonically stable regions.

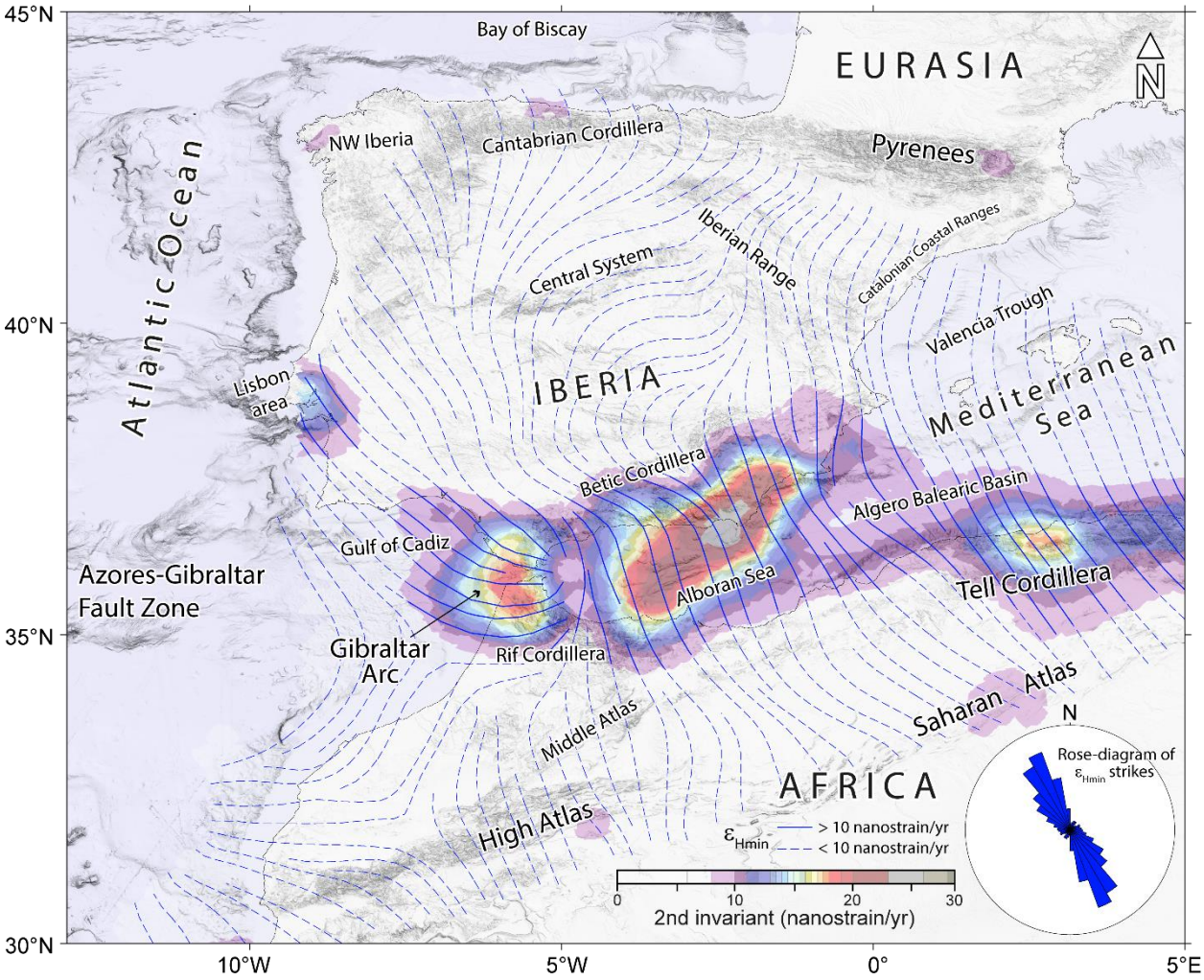


Figure 3.7: Second invariant of the 2D strain rate field of Iberia and Northwest Africa. The blue lines represent ε_{Hmin} trajectories. The lower-right inset represents the rose-diagram of the ε_{Hmin} strikes in each grid cell.

3.6.3.2. Minimum horizontal strain

The minimum horizontal strain (ε_{Hmin}) is represented by trajectories obtained by the combination of the ε_{Hmin} strikes estimated in each cell (Figure 3.7). The trajectories are only estimated considering the cells with less than 30º axis error. Therefore, the region is mostly covered except for the Pyrenees and NW Iberia. This error during the computations shows the disordered pattern of the strain rate axes along these regions mentioned before. The trajectories in areas with second invariant >10 nanostrain/yr are considered representative to the strain field while areas with <10 nanostrain/yr should be considered with caution due to the low values of the strain rate.

As represented in the rose-diagram most of the estimated ε_{Hmin} strikes indicate that the region is affected by N150º-160ºE shortening (Inset in Figure 3.7). This general shortening affects the Tell and Atlas Cordilleras, the easternmost Rif and the Alboran Sea, as well as

southwestern Iberia. This general pattern rotates anticlockwise in the central Betic Cordillera, up to N110ºE, and clockwise in the eastern Betic Cordillera, up to N010ºE. The main strike-change of the trajectories occurs in the western Gibraltar Arc. This region is characterized by a radial pattern of the trajectories respect to the curved axis of the arc; striking NE-SW in the western Betic Cordillera, E-W in the Strait of Gibraltar and WSW-ENE in the western Rif Cordillera.

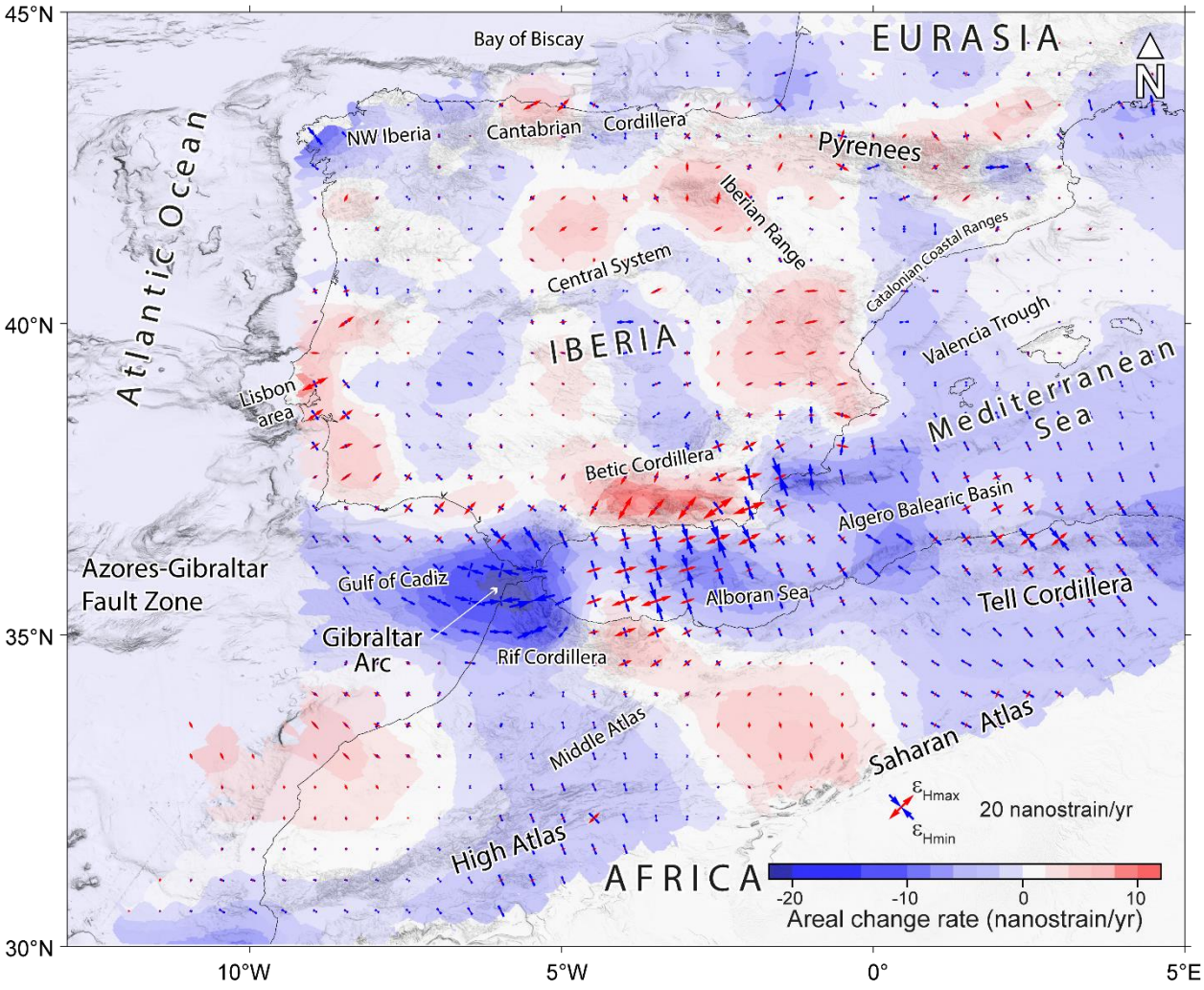


Figure 3.8: Strain-rate field of Iberia and Northwest Africa. Areal change and $\varepsilon_{Hmax}/\varepsilon_{Hmin}$ axes of the 2D strain-rates.

3.7. Discussion

The newly obtained stress and strain fields offer a fresh perspective on the tectonic and geodynamic processes affecting Iberia and Northwest Africa. These results allow a more refined understanding of tectonic activity in each region. Additionally, the combined interpretation of stress and strain fields reveals the internal deformation of the primary tectonic blocks in response to regional stresses, facilitating a discussion of the geodynamic processes that drive them.

3.7.1. The stress field of Iberia and Northwest Africa

Usually, the stress inversion methodology requires the definition of stress provinces or seismotectonic zones (e.g., Rigo et al., 2015; Villani et al., 2024; Zoback and Zoback, 1980). This process needs a deep geological and seismological understanding of the region, which is not free from interpretative errors and biases. Additionally, Neogene geological information sometimes differs from explicitly active processes (e.g., Madarieta-Txurruka et al., 2024), a discrepancy that becomes more pronounced in tectonically complex settings such as the Eurasia-Africa plate boundary between Iberia and Northwest Africa. For this reason, this study employs a method that is not constrained by prior knowledge—whether accurate, limited, or erroneous—of each study area. At present, a vast number of FMSs is available, increasing data density in tectonically active regions. This allows for stress inversion within a grid-based approach covering the study area. The results presented here depict the regional stress field using a 0.5º × 0.5º grid.

In addition, the principal stress axes in a region suggests the type of faults that should affect the area and therefore, the earthquake kinematics. Assuming an ideal scenario where the principal stress axes are oriented vertically and horizontally, normal faulting occurs when σ_1 is vertical, strike-slip faulting occurs when σ_2 is vertical and thrusting occurs when σ_3 is vertical (Heidbach et al., 2018). Following these criteria, we can discuss the relation between faulting (Figure 3.2), earthquake kinematics (Figure 3.4) and stress field (Figure 3.5a). The comparison reflects a general good quality of the inversion.

The area from the Azores-Gibraltar Fault Zone, Gulf of Cádiz and SW Iberia is characterized by NW-SE striking σ_1 and alternating vertical σ_2 and σ_3. This data reflects properly the reverse to strike-slip FMSs with NE-SW striking nodal planes, and is tectonically coherent with NE-SW reverse, WNW-ESE dextral and NNW-SSE sinistral faults (Gràcia et al., 2003; Martínez-Loriente et al., 2021; Martínez-Loriente et al., 2018, 2013; Zitellini et al., 2004). However, the main earthquakes associated with these faults mainly presents reverse to strike-slip FMSs, suggesting also a sinistral kinematics of the faults (Buforn et al., 1988; Pro et al., 2013). To the north, closer to the Lisbon area, a slight anticlockwise rotation of s_1 facilitates the mainly reverse behavior of the NNE-SSW faults (Baptista et al., 2014; Cabral et al., 2004; Carvalho et al., 2011), as reflected with the largest FMSs in the Lisbon area (Stich et al., 2005).

In the Gibraltar Arc the results show mostly a good fit between the computes stress field and recognized faults. The stress ellipsoids with vertical σ_2 are mainly located following a seismic corridor crossing the Alboran Sea, characterized by strike-slip FMSs. It corresponds to the Trans-Alboran and the Eastern Betic shear zones, mainly formed by strike-slip faults (Silva et al., 1993). In the southern part central Betic Cordillera the stress field suggest vertical σ_1 and NE-SW to ENE-WSW striking σ_3, perpendicular to the active normal faults in the Granada

and Baza extensional basin (Madarieta-Txurruka et al., 2024, 2021; Sanz De Galdeano et al., 2012). To the north, close to the Guadalquivir Basin, the σ_2 is vertically oriented, in a zone affected by N-S strike-slip faulting (Marín-Lechado et al., 2017; Morales et al., 2015; Pedrera et al., 2013; Tendero-Salmerón et al., 2021). In the western Gibraltar Arc the inversion of the scarce available FMSs depict a stress ellipsoid with NW-SE striking σ_1, perpendicular to arc shape (Ruiz-Constán et al., 2009). However, no active faults are recognized in the eastern Betic Cordillera. In the eastern Rif, on the contrary, the single stress ellipsoid depicts a N-S horizontal σ_1 and subvertical σ_3, oblique the main thrusts (Koulali et al., 2011).

The stress ellipsoid with NW-SE horizontal σ_1 and mainly vertical σ_3 in the Tell and the High Atlas is in accordance with the main recognized reverse faults in both mountain ranges (Bouhadad, 2001; Meghraoui, 1991). The stress ellipsoids with inclined σ_2 and σ_3, and with vertical σ_2 in some cells along the Tell Cordillera fit well with the strike-slip fault that segments the mountain range (Mauffret, 2007).

The vertical σ_1 along the Pyrenees and the inclined σ_1 the Iberian Range with R values over 0.5 perfectly reflects the occurrence of the normal and normal to strike-slip FMSs. This stress pattern is coherent with active normal faults described in both mountain ranges (Gutierrez et al., 2012; Lacan and Ortuño, 2012). In NW Iberia the stress ellipsoids suggest horizontal σ_3 with inclined σ_1 and σ_2 coherent with the normal and strike-slip FMSs. However, known active faults suggest just strike-slip faulting (García-Mayordomo et al., 2012) (Figure 3.2). Considering that the studied earthquakes have low magnitude they could correspond to a normal segment of strike-slip major faults or the influence of fluids.

As shown here, the results are in general accordance with the structural data, and respect the different zonation proposed in the literature (e.g., De Vicente et al., 2008; Herraiz et al., 2000; Stich et al., 2006). Therefore, this methodology may become a valuable tool for determining or redefining seismotectonic zones. However, it also implies some limitations. First, it is a method dependent on FMS availability, which is correlated with the densest seismic areas (Figure 3.5). Thus, some areas could present a lack of inverted cells due to the low available FMSs, as occurred in the Atlas and NW Iberia. Second, the inversion is not ideal in cells bordering/over two different seismotectonic zones, because the method considers FMSs derived from different stress regimes (Figure 3.5). On the other hand, this limitation could help in detecting unknown seismotectonic boundaries. Additionally, the scale of observation depends on the resolution of the grid and the cell size. For local studies higher resolution is required and thus, the number and spatial coverage of available FMSs must increase. Therefore, while this approach is valuable for regional-scale research, such as the westernmost Mediterranean, its relevance in local studies needs further evaluation.

3.7.2. The strain field of Iberia and Northwest Africa

The velocity field presented here aligns with previous studies (e.g., Koulali et al., 2011; Palano et al., 2015; Serpelloni et al., 2022). Regionally, three are the main features driving the plates motion in the region: a) The NW-SE convergence among Eurasia and Africa, b) the westward displacement of the Gibraltar Arc, and c) the slight clockwise rotation of Iberia respect to Eurasia, mainly affecting its southern part (Figure 3.6).

Locally, the recognition of tectonically active structures is closely linked to the active surface deformation that the GNSS velocity field has successfully identified. The second invariant of the strain field (Figure 3.7) reflects the zones with maximum deformation and serves to compare with the activity or density of active faults in each area (Figure 3.2). On the other hand, the areal change (Figure 3.8) provides a valuable metric for comparison of contraction/dilatation within the crust with kinematics of faults.

The second invariant of the strain field shows the higher degree of strain along the Eurasia-Africa plate boundary. These zones largely coincide with regions characterized by a higher density of faults and greater seismic activity. The most deforming zone corresponds to the Trans-Alboran and the Eastern Betic shear zones (Figure 3.7). This fault corridor consists of a densely faulted zone extending from the eastern Rif to the eastern Betic Cordillera ((Borque et al., 2019; Echeverria et al., 2013; Galindo-Zaldivar et al., 2018). The western Gibraltar Arc is notable for a local maximum in the second invariant strain, but in contrast, it lacks seismic activity and recognized faults in the western Betic Cordillera. To a lesser extent, other regions such as the Tell Cordillera, the central Betic Cordillera, and the Lisbon area also exhibit second invariant strain values above 10 nanostrain/yr which agree with a higher density of faults and historical and instrumental seismicity (Cabral, 2012; Mauffret, 2007; Sanz De Galdeano et al., 2012). Second invariant strain rates in mainland Iberia, the Pyrenees, and the Atlas Cordillera are significantly lower compared to regions along the plate boundary (Figure 3.7). The low values contrast with the location of recognized faults in some of these areas (Figure 3.2). This data suggest that they correspond to structures with very low Quaternary activity, undetectable within the measurement period, and/or that they respond to processes governed by vertical deformations.

The areal change rate indicates that the Eurasia-Africa convergence generally results in moderate shortening. The highest deforming zone (Figure 3.7) along the Trans-Alboran and Eastern Betic shear zones, suggests oblique shortening of up to 8 nanostrain/yr respect to the main faults (Figure 3.8). This aligns well with the sinistral to sinistral-reverse kinematics observed in most faults (Stich et al., 2006) Coherently, the shortening direction is perpendicular to the NE-SW folds of the Alboran Ridge and Águilas Arc (Coppier et al., 1989; Gómez De La Peña et al., 2022). In the Tell Cordillera, there is also a clear coherence between the shortening and the structures. The ENE-WSW to NE-SW thrust faults and WNW-ESE dextral faults (Bouhadad, 2001; Mauffret, 2007; Meghraoui, 1991) accommodate the

moderate perpendicular shortening. The maximum shortening up to -20 nanostrain/yr in the study area occurs in the western Gibraltar Arc where only two active thrusts are recognized, both located in the Rif (Koulali et al., 2011). The other two deforming regions reflect stretching values (Figure 3.8). First, the central Betic Cordillera extends in ENE-WSW to NE-SW direction, in accordance with the main normal faulting in the region (Sanz De Galdeano et al., 2012). On the other hand, the E-W stretching observed in the Lisbon area contrasts with the NNE-SSW thrust and sinistral strike-slip faults and with the main earthquake in the region (Stich et al., 2005).

The strain field derived from the new velocity field provides the opportunity to discuss the affecting stresses and geodynamic processes causing the superficial deformation, both seismically and aseismically. The superficial strain should be the consequence of the main stresses affecting the crust. Assuming the macroscopically homogeneous and elastic crustal blocks, the regional ε_{Hmin} and σ_{Hmax} fields should be parallel. In the westernmost Mediterranean, the presented trajectories of ε_{Hmin} and σ_{Hmax} suggest that it is mostly occurring along the studied regions. Both ε_{Hmin} and σ_{Hmax} present a similar value, mainly striking between N150º-160ºE (Figure 3.5 and Figure 3.7). The discrepancies may be related to the very heterogeneous crust involved in the region (e.g., Druet et al., 2023; Gómez De La Peña et al., 2018; Sallarès et al., 2013, 2011) and the diverse pattern of the ε_{Hmin} along the western Gibraltar Arc. In this region the trajectories exhibit a clear angular discrepancy of up to 90º. While the σ_{Hmax} maintains a NW-SE orientation, the ε_{Hmin} is oriented radially with respect to the arc. This region is characterized by relatively low seismicity compared to surrounding areas, resulting in a limited availability of earthquake focal mechanism solutions. Consequently, the ε_{Hmin} just reflects the NW-SE compression between Eurasia and Africa, while the ε_{Hmin} indicates the aseismic displacement of the Gibraltar Arc toward the west, also supported by geological observations (e.g., Gonzalez-Castillo et al., 2015; Pedrera et al., 2011).

3.7.3. The complex Eurasia-Africa plate boundary in the Atlantic-Mediterranean transition

The convergence between the Eurasian and African plates results in compression and shortening along the southern margin of Iberia. This convergence results in a complex interaction between the involved crustal blocks. A good example of the complexity is the ongoing debate to define the Eurasia-Africa plate boundary in the region (e.g., Billi et al., 2023, p. 202; Bird, 2003; Gómez De La Peña et al., 2018; Gutscher, 2004).

Our results led to divide the plate boundary in four segments —Atlantic, Gibraltar, Alboran and Mediterranean—based on the stress pattern, the localization of deformations, and the number and nature of the involved crustal blocks (Figure 3.9 and Table 3.1). From east to west, the segments are as follows:

a) The *Atlantic segment* is the result of the direct interaction between the SW Iberian margin (Eurasia) and the old and cold oceanic lithosphere (Martínez-Loriente et al., 2014, 2013; Sallarès et al., 2013). Hypocenters and FMSs suggest that the deformation localize in NE-SW/NNE-SSW reverse to sinistral and WNW-ESE dextral faults (Buforn et al., 1988; Pro et al., 2013), cutting the entire oceanic lithosphere (Figure 3.3 and Figure 3.4). This pattern occurs in response to the NW-SE compression with alternating vertical σ_2 and σ_3 stress field affecting the segment. This segment constitutes a transpressive boundary formed by en-echelon thrusts and large WNW-ESE dextral faults, where the Gulf of Cadiz oceanic crust (GCOC) and the thinned southwest Iberian margin overthrust each other (Galindo-Zaldívar, 2003; Jiménez-Munt et al., 2010; Martínez-Loriente et al., 2021; Sallarès et al., 2013).

b) The *Gibraltar segment* involves a crustal block here referred to as the Gibraltar Block, located between the two main plates. As shown by the velocity field the Gibraltar Block displaces westward and overthrust the Iberian and African margins (Figure 3.5). From the areal change (Figure 3.8) and seismicity (Figure 3.2) comparison its limit can be constrained. The northern limit of this block could correspond to a seismic dextral corridor extending from Morón de la Frontera to the Torcal Shear Zone (TSZ) (Ruiz-Constán et al., 2011). The southwestern limit, perfectly observed in the velocity field (Figure 3.6b), correspond to a seismic normal to sinistral zone to the west of the Togrout Fault (TF) (d'Acremont et al., 2014; Galindo-Zaldivar et al., 2015; Poujol et al., 2014; Tahayt et al., 2009). To the east seems to be detached from the rest of the Alboran domain as suggested by the highly thinned crust in the central Alboran Sea (Torne et al., 2000) and ENE-WSW extension from the central Betic Cordillera to the eastern Rif Cordillera (Figure 3.8). This configuration fits well with the crustal block division suggested by Crespo-Blanc et al., 2016. They suggest four blocks that behave independently. The western ones constitute the western Betic and the Rif blocks, coinciding with the crustal block referred to here. The approximate N-S ε_{Hmin} axes suggest that nowadays both blocks are attached probably due to the continues NW-SE Eurasia-Africa convergence.

c) The *Alboran segment* is characterized by an Alboran thinned continental crust (AlTCC) between the Betic Cordillera and Africa. The second invariant of the strain fields

(Figure 3.7) suggest that most of the convergence along these segments is accommodated in the Alboran Sea, and the northern coastal areas, in accordance with the velocity field published by Galindo-Zaldivar et al., 2022. The stress ellipsoids and the areal change rates suggest that the Central Alboran indentation (CAI), formed by the African Continental Crust (AfCC), deforms the thinned and weak continental crust (Estrada et al., 2018; Galindo-Zaldivar et al., 2018) by means of a strike-slip faults mainly along the Trans Alboran Shear Zone (TASZ).

d) The *Mediterranean segment* involves the young Algero-Balearic oceanic crust (ABOC) situated between the southeastern margin of Iberia and Africa. The horizontal strain rates (Figure 3.8) show a NW-SE to N-S shortening localized in the eastern Betic Cordillera (Bougrine et al., 2019; Echeverria et al., 2013) and in the Tell Cordillera (Coppier et al., 1989; Silva et al., 1993; Tendero-Salmerón et al., 2024) which accommodate the NW-SE compression. In contrast the rigid oceanic crust undergoes low internal deformation (Palano et al., 2015). This pattern involves thrusting in the African margin and the development of the Eastern Betic indentation (EBI) in the Iberian margin.

3.7.4. Novel insights into the rotation of Iberia

The new velocity field depicts a clockwise rotation of Iberia, mainly observed in southwestern Iberia (Figure 3.6), which was first described by Palano et al., 2015. This rotation could result from; a) the angular relation between the Eurasia-Africa convergence and the orientation of the Iberian margins in each segment and b) the structural differences between the distinct segment of the Eurasia-African boundary, as outlined in the previous section.

The velocity field presented here also reflects a counterclockwise rotation of Africa relative to Eurasia, previously shown by Calais et al., 2003, McClusky et al., 2003, Serpelloni et al., 2007, Palano et al., 2015, Neres et al., 2016, among others. This plate motion implies a convergence shifting from a WNW-ESE direction in the Atlantic to a NW-SE direction in the Mediterranean (Figure 3.5). This pattern implies that the convergence in the Mediterranean is nearly perpendicular to the southeastern Iberian margin, whereas in the Atlantic, it is oblique to the southwestern Iberian margin. This contrast in convergence angles likely contributes to the observed rotational deformation in southwestern Iberia. On the other hand, this phenomenon could be further influenced by the Alboran Domain, located between the major plates in the Mediterranean. While in the Mediterranean the new map of the second invariant of the strain shows that the Alboran Domain and the detached margins absorb most of the convergence (Figure 3.7), in the Atlantic zone, there are no microplates

between Iberia and Africa, resulting in direct interaction between the two plates. Although seismicity suggests that most of the deformation is accommodated in the Atlantic segment described earlier, some of this stress is probably transferred to Iberia. Additionally, the continuous westward displacement of the Gibraltar block, pushing against southwestern Iberia, could further enhance its clockwise rotation.

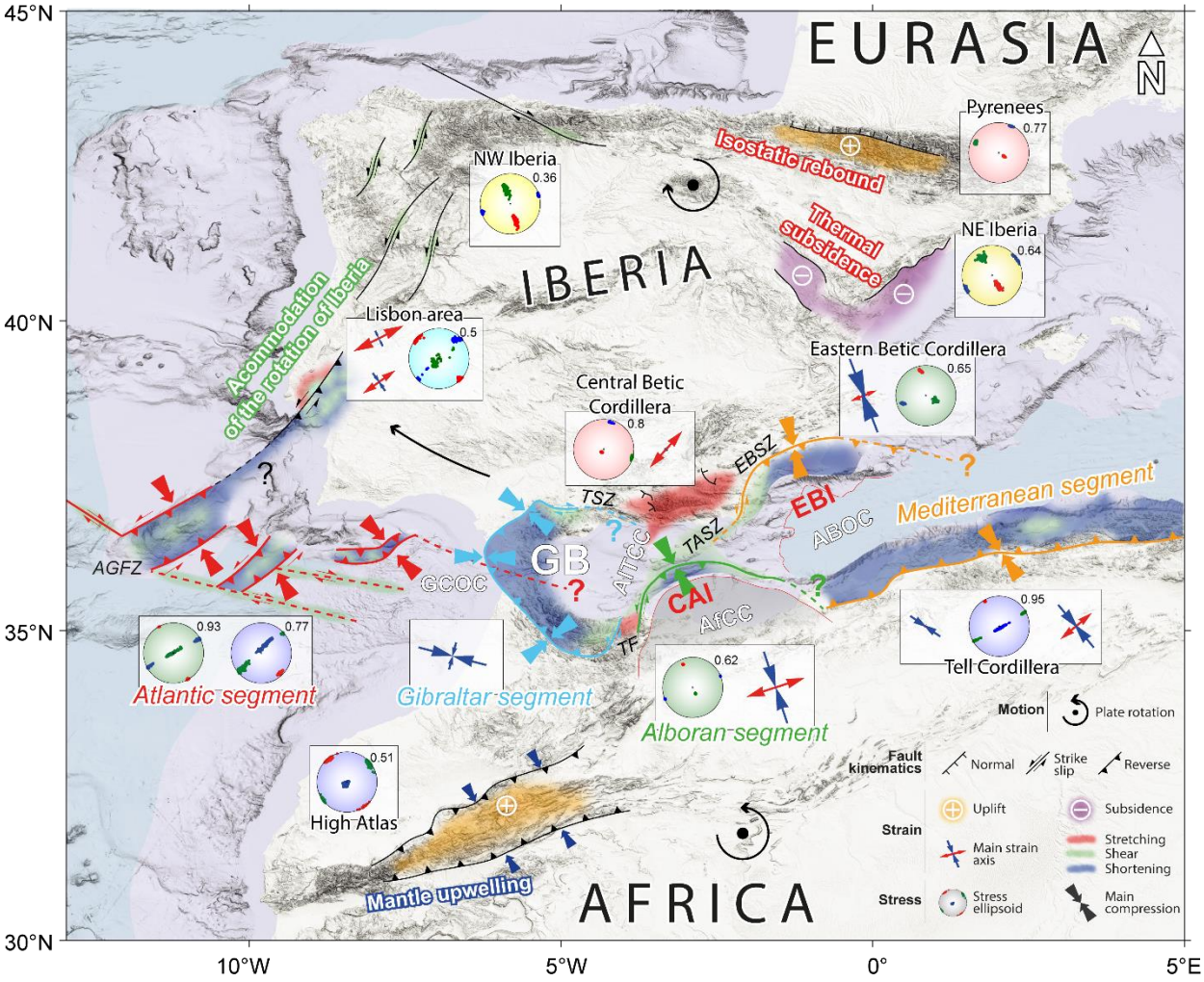


Figure 3.9: Geodynamic model of Iberia and Northwest Africa. The four segments along the Eurasia-Africa plate boundary are depicted. Boxes represent the most representative stress and strain axes in each region. The number adjacent to the stereoplots indicates the stress ratio (R). GB: Gibraltar block. ABOC: Algero-Balearic Oceanic Crust. AlTCC: Alboran thinned continental crust. AfCC; African continental Crust. CAI: Central Alboran indentation. EBI: Eastern Alboran indentation. AGFZ: Azores-Gibraltar Fracture Zone. TF: Trougout Fault. EBSZ: Eastern Betic Shear Zone. TASZ: Tran-Alboran Shear Zone. TSZ: Torcal shear zone. MdlF: Morón de la Frontera. Gb: Granada Basin. GBb: Guadix-Baza Basin.

As stated by Palano et al., 2015, the clockwise rotation of SW Iberia implies active thrusting and NNE-SSW sinistral or NW-SE dextral faulting as mechanisms to accommodate stress in NW Iberia. The velocity field presented here suggests that rotation terminates in the Lisbon area, while the NW Iberia remains practically stable (Figure 3.6). Historical and instrumental

seismicity data, focal mechanisms with reverse kinematics, and the presence of reverse to sinistral faults in the Lisboan area indicate that a significant portion of the deformation is concentrated there (Figure 3.9 and Table 3.1). This is further supported by the highest values of the second invariant (Figure 3.7). However, ε_{Hmin} axes suggest extension subparallel to compression. The Lisbon area is characterized by the thick Cenozoic sedimentary cover (Carvalho et al., 2017), making it possible that this deformation results from shallow adjustment processes linked to the displacement of deep-blind thrusts (Cabral et al., 2013). The August 2024, Mw 5.3, earthquake, located in the western Iberian margin (Figure 3.4), with a focal mechanism showing reverse to sinistral motion, suggests that this front may continue offshore. Indeed, the southern part of the western Iberian margin is characterized by Alpine compressional structures (Alves, 2024). However, seismicity in the area is significantly lower offshore compared to onshore.

As shown, the data suggest that a significant portion of the stresses is accommodated in Lisboan area; however, part of it may be transferred toward NW Iberia (Figure 3.9 and Table 3.1), activating low-rate sinistral and dextral faults in NW Iberia (López-Fernández et al., 2018; Martín-González et al., 2023). The frequent low to moderate magnitude seismicity in the region (Figure 3.2) suggests this behavior, in response to a NW-SE compression (Figure 3.5).

3.7.5. The aseismic westward displacement of the Gibraltar Block

The Gibraltar block haghlights as the most unconventional crustal block along the study area (Figure 3.9 and Table 3.1). An interesting observation is the lack of seismicity along the Gibraltar Block (Figure 3.2) (with the exception of the shear zones bounding it in the north and in the southeast), despite being the region exhibiting the highest shortening rates in the study area (Figure 3.5 and Figure 3.8). This pattern is also reflected in the angular discrepancies between σ_{Hmax} and ε_{Hmin}, discussed before. The lack of seismicity is in accordance with the known low seismic coupling values (Sparacino et al., 2020) and suggests aseismic deformation, such as creeping or elastic storage, that could be released by future earthquakes. The continuous decrease of the velocities towards the foreland depicted in the velocity field (Figure 3.5) is in accordance with the deformation accommodated by folding suggested by Gonzalez-Castillo et al., 2015. This observation implies the continuous slip of the basal thrust. This main thrust is rooted in the Keuper formation of the Triassic and the Olistrostomic Complex, characterized by their ductile rheology (Anahnah et al., 2011; Pedrera et al., 2020), which could absorb deformation by creeping. However, the occurrence of larger earthquakes with long recurrence period cannot be discarded, given that some events over Mw 5.0, and reaching Mw 6.7 (Figure 3.3), have been documented in the region within

historical records (Pelaez et al., 2007). More detailed studies in the area are required to clarify this issue.

Another open question is the geodynamic process driving the displacement of the Gibraltar Block. Some models suggest that the principal driver is the ongoing subduction with rollback (Duarte et al., 2024; Fadil et al., 2006; Gonzalez-Castillo et al., 2015; Pedrera et al., 2011; Pérouse et al., 2010) or terminal subduction where the displacement of the overriding plate is mainly driven by mantle flow due to slab sinking (Civiero et al., 2020; Gea et al., 2023; Neres et al., 2016). Although there is consensus that subduction with rollback was responsible for the westward displacement of the Alboran Domain, its role in the present-day geodynamics remains debated. In fact, the westward escape of the Gibraltar Block due to indentation in central Alboran is also proposed (Chalouan et al., 2006; Fernández-Ibáñez et al., 2007; Rebaï et al., 1992). This model attributes the westward motion to the indentation tectonics affecting the central Alboran region due to northward displacement of Africa (Estrada et al., 2018; Tendero-Salmerón et al., 2022). The GNSS pattern of subduction with roll-back should show velocities decreasing from the west, near the arc front, toward the east. The mantle flow model should show a similar pattern but with big shortening in the front, as shown by numerical modelling (e.g., Gea et al., 2023). Alternatively, escape tectonics suggest a decreasing strain-rate and fault slip far from the indenter (Ježek et al., 2002; Tapponnier et al., 1982) and therefore, it should result in a velocity decrease from the east, near the indenter, toward the west (Galindo-Zaldivar et al., 2022; Pietrolungo et al., 2024). The velocity fields presented here shows higher westward motion in the western Gibraltar Arc respect to the central Alboran supporting subduction models. In addition, the strain field depicts shortening in the front pointing to a surface deformation driven by mantle flow. This is further supported by the absence of a clear Wadati-Benioff zone (Platt and Houseman, 2003) and vertical intermediate seismicity with FMSs with vertical nodal planes pointing to the slab sinking and tearing (Meighan et al., 2013; Ruiz-Constán et al., 2011; Santos-Bueno et al., 2019).

In this setting, the extension in the central Betic Cordillera may result from the opening between the western Betic Cordillera and eastern Betic Cordillera (Figure 3.9 and Table 3.1). However, this region underwent the highest uplift since the middle Miocene (Braga et al., 2003; Reinhardt et al., 2007) and constitute the highest elevation in entire Iberia (Sanz De Galdeano and Alfaro, 2004). Additionally, the active normal faulting mainly occurs surrounding this elevated area (Martínez-Martos et al., 2017; Martin-Rojas et al., 2023; Sanz De Galdeano et al., 2012). This observation suggests the possibility of an extension parallel to the arc, oriented perpendicular to the regional compressive stress. However, the vertical σ_1 with R values over 0.75 supports radial extension, a therefore, the area is not under NW-SE compression. Moreover, ε_{Hmin} axis show values close to zero, much smaller than those in

the close Alboran Sea (Galindo-Zaldivar et al., 2022), supporting that the area is not shortening. These observations endorse that actual compression and shortening are not the main features controlling the extension but the vertical stresses, probably related to gravitational forces (Madarieta-Txurruka et al., 2023; Madarieta-Txurruka et al., 2024).

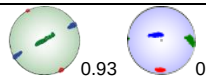
REGION			SEISMICITY	CRUSTAL STRESS	HORIZONTAL SURFACE STRAIN RATE		TECTONICS / GEODYNAMICS
					Strain rate	2nd invariant	
Eurasia-Africa plate boundary	Atlantic segment		Frequent < 50 km depth moderate to high magnitude seismicity R and SS FMSs		- - - -		Oblique transpression between SW Iberian margin and Gulf of Cádiz Oceanic Crust (GCOC) / Eurasia-Africa convergence
	Gibraltar segment		Mostly aseismic Crustal low to moderate magnitude seismicity in the limits. Intermediate seismicity N, R and SS FMSs	- - - -		10 - 20 nanostrain/yr	Westward aseismic displacements of the Gibraltar Block / Subduction with rollback or mantle flow
	Alboran segment		Frequent crustal low-to moderate magnitude seismicity R and SS FMSs			15 - 30 nanostrain/yr	African Continental Crust (AfCC) indents the Alboran Thinned Continental Crust (AlTCC) / Eurasia-Africa convergence
	Mediterranean segment	Eastern Betic Cordillera	Crustal low magnitude seismicity SS and R FMSs			10 - 30 nanostrain/yr	Algero-Balearic Oceanic Crust (ABOC) indents the SE Iberian margin / Eurasia-Africa convergence
		Tell Cordillera	Frequent crustal moderate to high magnitude seismicity R and SS FMSs			10 - 20 nanostrain/yr	Underthrusting of the Algero-Balearic Oceanic Crust (ABOC) below Tell Cordillera / Eurasia-Africa convergence
Margin regions	Central Betic Cordillera		Frequent crustal low to moderate magnitude seismicity Mainly N FMSs			10 - 18 nanostrain/yr	Orogen parallel extension / Gravitational stress
	Lisbon area		Scarce crustal low to moderate magnitude seismicity SS and R FMSs			10 - 15 nanostrain/yr	Transpression accommodating and stretching at the / Clockwise rotation of SW Iberia + Eurasia-Africa convergence
Intraplate regions	NW Iberia		Scarce crustal low to moderate seismicity SS and R FMSs		- - - -	< 10 nanostrain/yr	Large scale slow-rate strike-slip faulting / Clockwise rotation of SW Iberia + Eurasia-Africa convergence
	Pyrenees		Frequent crustal low to moderate magnitude seismicity N and SS FMSs				Orogen perpendicular extension / Isostatic rebound in the eroding highlands
	NE Iberia		Scarce crustal low magnitude seismicity SS and N FMSs				Orogen perpendicular extension / Post-rift thermal subsidence + regional compression
	High Atlas		Scarce crustal moderate magnitude seismicity R and SS FMSs				Thrusting and uplift / Mantle upwelling

Table 3.1 Geodynamics of Iberia and Northwestern Africa. Comparison between seismicity, stress, strain and the proposed tectonics/geodynamic models for each region. The stress and strain columns depict the most representative stress and strain axes in each region. The number adjacent to the stereoplots indicates the stress ratio (R).

3.7.6. Low deforming intraplate active regions

In contrast to the Eurasia-Africa plate boundary, the other tectonically active regions exhibit low strain rates, typically below 10 nanostrain/yr (Figure 3.7). As discased before, the moderate magnitude seismicity related to sinistral and dextral faults in the NW Iberia fit in the general NW-SE compressional regime of Iberia. In addition, other regions exhibit tectonic activity, including the Pyrenees, NE Iberia, and the Atlas Cordillera.

The new deformation field presented here suggests low strain rates across the Pyrenees (Figure 3.7). Both the strain and velocity fields do not show a clear pattern of shortening or stretching at the scale of the entire range. This low level of deformation contrasts with the recurrent seismicity, which primarily occurs in the western part of the Pyrenees (Figure 3.2). Main earthquakes in the area occur in normal faults (Figure 3.3) and respond to the stress regime with vertical σ_1 and N-S to NW-SE σ_3 calculated here (Figure 3.5), suggesting approximate N-S extension. These data support the model proposed by Lacan and Ortuño, 2012 suggesting an uplift of the of the mountain range due to the isostatic adjustment in response to erosion, as occurred in the western Alps (Vernant et al., 2013). As pointed by Lacan and Ortuño, 2012 the normal faults and the seismicity occurs to the north of the highest massifs of the cordillera, which undergo continuous uplift (e.g., Ortuño et al., 2013). Bouguer anomaly maps (Ayala et al., 2016) show that to the south of these faults the crustal root is deeper and suggest that the faults are rooted in crustal thickness transition zones. Therefore, they may accommodate the isostatic disequilibrium between crustal blocks (Figure 3.9 and Table 3.1). In fact, local studies in the westernmost part suggest a up to 2 mm/yr N-S stretching of the region (Asensio et al., 2012).

In the easternmost Pyrenees, the vertical σ_1 change into a vertical σ_2 or σ_3 (Figure 3.5). This data suggests that the region is not undergoing extension but is instead influenced by horizontal compression parallel to the regional main stress. The absence of lithospheric crustal root (Gunnell et al., 2008) explains an isostatic equilibrium which derives to a lower activity of normal faults. In fact, according to Fillon et al., 2021, exhumation in the eastern part of the Pyrenees occurred before 20 Ma, opposite to the ongoing exhumation in the western as described before. During the late Oligocene-middle Miocene the northeastern Iberia underwent extension and thinning due to the opening of the Gulf of Lyon and the Valencia Trough (Cabrera et al., 2004; Roca and Guimerà, 1992) removing the crustal root of the eastern Pyrenees. Consequently, the region is primarily undergoing deformation in response to the moderate regional compressional stress, rather than vertical stresses, as it may have already reached isostatic equilibrium.

Towards the south NE Iberia experiences similar geological history. However, the stress ellipsoids along the Iberian Range show vertical stress ellipsoids with inclined σ_1 and σ_2, and

horizontal σ_3 (Figure 3.5). The stress field could result from a combination of extensional processes related to rifting in the Valencia Trough and regional compression. Since the Middle Miocene, this region has experienced post-rift subsidence (Cabrera et al., 2004; Roca and Guimerà, 1992). Associated with this process, the area between the Iberian Range and Catalonian Coastal Ranges undergoes relative uplift compared to the subsidence observed along them (Gómez, 1984, p. 19; Peiro et al., 2023; Scotti et al., 2014). These extensional processes, combined with regional compression, could explain the NW-SE striking highly inclined σ_1 and the normal to strike-slip character of the FMSs (Figure 3.9 and Table 3.1). In addition, this process could be accentuated by the slow gravitational dismantling of the mentioned mountain ranges.

In the case of the High Atlas, surface deformation is also minimal, with shortening rates of less than 0.5 mm/year, as reported previously (Chalouan et al., 2023; Koulali et al., 2011). However, from moderate-to-high magnitude FMSs reveal active thrust faulting, e.g., the September 2023 earthquake (Cheloni et al., 2024), and strike-slip faulting, e.g., the 1960 Agadir earthquake, which operate under a NW-SE compressional regime (Figure 3.5). Moreover, the High Atlas is characterized by the highest elevations in the study area. However, our data suggest that this is not a result of crustal shortening. Instead, gravimetric and seismic data (Fullea et al., 2007; Miller and Becker, 2014; Teixell et al., 2005) and magnetotelluric studies (Anahnah et al., 2011) show the absence of a significant crustal root beneath the High Atlas, and the presence of an anomalous mantle. Therefore, the presence of ascending mantle dome is proposed to explain the elevation. Nevertheless, this phenomenon would imply an increase in vertical stress (σ_v), which contrasts with the subvertical values of σ_3. Therefore, compression due to the Eurasia-Africa convergence is necessary to orient σ_1 in a NW-SE direction. This compression would result in low shortening values but thrust fault activity with long recurrence periods, in a region uplifting due to mantle upwelling (Figure 3.9 and Table 3.1).

3.8. Conclusions

The methodology presented here demonstrates its utility as an effective tool for determining stress from large databases of FMSs along extended areas. Overall, the stress field presents a good fit with FMSs and the main active faults, highlighting its quality. The strain rate field presented here also highlights the main deformations affecting the study region. The directions of the ε_{Hmin} mostly fits with the σ_{Hmax}, active faulting and seismicity pattern. Moreover, it serves a great tool for analyzing the surface deformation in aseismic region and the possible stresses producing it, such as in the western Gibraltar Arc.

As shown, computed new stress and strain fields in the Eurasia-Africa plate boundary results in complex deformation patterns along Iberia and Northwest Africa. The integrated analysis of the stress and strain field with active faulting and seismicity pattern serves as proper methodology to infer geodynamic processes in each region. Two distinct active tectonic regions emerge from the strain rate field analysis: the highly deformed Eurasia-Africa plate boundary and the relatively stable internal areas of Iberia and Northwest Africa.

Four main segments can be distinguished along the Eurasia-Africa plate boundary. From west to east: a) the Atlantic segment, characterized by direct plate interaction between the Iberian southwestern margin and the African oceanic crust, b) the Gibraltar segment, comprising the westward displacing Gibraltar Block, c) the Alboran segment, where the Alboran thinned continental crust separates the two main plates, and d) the Mediterranean segment, where Algero-Balearic oceanic crust lies between Iberia and Africa. The Atlantic and Mediterranean segments are characterized by a NW-SE oriented horizontal σ_1 stress axis, with alternating vertical σ_2 and σ_3 axes. The resulting nearly parallel shortening is accommodated through thrust and localized strike-slip faults, primarily concentrated along the Iberian margins and within the Tell Cordillera, while oceanic crusts undergo minimal deformation. The Alboran segment, on the other hand, is characterized by NW-SE horizontal σ_1 and vertical σ_2, with parallel shortening accommodated the mostly in the Alboran Domain through the sinistral Trans-Alboran Shear Zone, likely due to indentation tectonics.

The new computed velocity field confirms the clockwise rotation of southwestern Iberia. The angular relationship between the Eurasia-Africa convergence and the orientation of the Iberian margins could explain this rotation. In the Atlantic sector, the convergence is oblique to the E-W margin of Iberia, with direct plate interaction. In contrast, in the Mediterranean, the convergence is perpendicular to the margin, and most of the deformation is accommodated within the Alboran domain and detached margins. This rotation may be mostly accommodated by NE-SW thrusting front from Lisbon area, as shown by earthquake FMSs.

Along the plate boundary, a crustal block behaves differently: the Gibraltar Block. Unlike the rest of the region, the area exhibits E-W shortening, nearly perpendicular to the Eurasia-Africa convergence, and the seismicity is scarce, even in the historical record. The strain pattern could be explained by terminal subduction with rollback/mantle flow. The lack of seismicity may result from a deformation being accommodated by folding over a creeping thrust rooted in the Triassic Keuper.

The intraplate regions undergo low horizontal strain rates. In the Pyrenees, they present vertical σ_1 and high R values, along with active normal faulting close to the uplifting regions support the ongoing isostatic rebound. The stress ellipsoids with incline σ_1 and σ_2 in NE Iberia

support the ongoing thermal subsidence under regional compression. Finally, the stress ellipsoids with a NW-SE oriented σ_1 and a vertical σ_3, along with the ongoing uplift, point to the combination of regional NW-SE stresses and mantle upwelling as the processes governing the stresses in the High Atlas.

4. Multi-source deformation maps in the Italian Peninsula: comparison between geological, geodetic and seismological data

This manuscript is authored by: Lavecchia G., Andrenacci C., Bello S., Pietrolungo F., Cirillo D., Brozzetti F. & de Nardis R.

4.1. My contribution

My contribution to this work includes the collection of geodetic data and the calculation of strain using various software. Additionally, I focused on finding the optimal way to compare the different datasets by using the Stress2Grid software and Python codes. I created most of the figures in this thesis to effectively visualize the results. I also collaborated in discussing the various topics addressed in the study and in drafting the paper presented here.

4.2. Abstract

Understanding the strain regime is fundamental for seismotectonic and geodynamic studies, yet many regions still lack high-resolution, multi-source strain datasets. In this study, we introduce a multi-source strain map that synthesizes Quaternary fault-slip data (QUIN 1.0 and 2.0) with focal mechanism solutions and GNSS-derived strain parameters.

Using formal Bingham statistics and a refined methodological approach, we map the principal strain orientations across the region, highlighting the relationships between long-term fault slip patterns, seismic strain release, and present-day crustal deformation. Our results confirm a predominantly extensional regime, characterized by a large-scale SW-NE (Northern Apennines) to NW-SE (Southern Apennines) trending strain field, with local variations reflecting structural complexities and fault segmentation. The integration of these datasets reveals a strong correlation between long-term geological strain, ongoing seismic deformation, and geodetic extension, indicating a remarkable continuity in the regional stress field over the past 3.5 million years. Additionally, our findings support the hypothesis of an eastward migration of the extensional front, with progressive activation of faults along the Apennine chain.

Beyond providing a high-resolution strain model, this study introduces a novel methodological framework for comparing deformation indicators from different timescales and data sources. This integrated approach enhances seismotectonic zoning, improves the assessment of active fault systems, and contributes to a better understanding of crustal-scale deformation processes in a high-seismicity region. The strain database represents a significant step toward a unified seismotectonic model for Italy, offering a valuable tool for future geodynamic research and seismic hazard assessment.

4.3. Introduction

Since the late 1980s, intraplate stress regime studies have become central in contemporary geodynamic and seismotectonic studies (Zoback et al., 1989). Researchers approach this subject by analysing focal mechanisms and in-situ stress data from borehole breakout analysis and measurements, complemented by geological features and Quaternary fault-slip

data. In addition to the worldwide compilation of stress indicators from the World Stress Map project (Heidbach et al., 2018), several other regional databases are available. Notably, recent ones for North America (Lundstern and Zoback, 2020), for Italy (Mariucci and Montone, 2020), for the Pannonian basin (Békési et al., 2023), for the Mediterranean (Martínez-Garzón et al., 2020), for north Africa (Rashwan et al., 2021; Soumaya et al., 2018), for Australia (Rajabi et al., 2017), among others, provide valuable resources and stress inversion results. Also, high-intensity datasets often contain only the orientation of the horizontal component of the 3D stress tensor systematically compiled (Reiter et al., 2024). Less frequently, they contain principal stress attitudes and relative magnitude derived from formal stress inversions (Soumaya et al., 2018). Performing the latter requires extensive input data. While databases containing thousands of focal mechanisms are available for specific regions, such as the USA, particularly California (Yang and Hauksson, 2013), rich seismological databases are lacking for other regions, including Italy.

In contrast, Italy benefits from two geological databases, encompassing ~8000 Quaternary fault-slip records (QUIN 1.0 (Lavecchia et al., 2022) and 2.0 (Lavecchia et al., 2024a), located along well-exposed host faults (hereinafter HF). These databases comprehensively cover the Extensional Intramountain Seismogenic Province of Peninsular Italy (Figure 4.1a). This Province encompasses a region of the Italian Peninsula characterized by active extensional tectonics, mountainous terrain, and significant seismic hazard (Pondrelli et al., 2020). Its surface boundaries are defined by the presence of active fault systems associated with crustal extension, contributing to the seismic activity observed in the region (Lavecchia et al., 2021).

In the present study, the integration and elaboration of the two QUIN databases (Lavecchia et al., 2022, 2024a) and some additional structural data, allow us to obtain a new database which for the first time cover peninsular Italy with high-detail multiscale strain parameters. This is done considering the detailed surface geometry and spatial distribution of the associated interconnected, predominantly extensional faults.

The principal strain trend obtained through statistics methods are juxtaposed with the geometry, timing and multi-scale segmentation pattern of the outcropping intra-Apennine fault system and, with deformation trends derived from seismological and geodetic information. This comparison aims to verify the consistency between long-term and current strain fields, fulfilling the image of ongoing deformation. Focal mechanism data are derived from available catalogues (Pondrelli et al., 2020; Scognamiglio et al., 2006), while extensional strain attitudes from geodetic data are here computed starting from Serpelloni et al., 2022 velocity field.

For the first time, we:

1. parametrize in high detail the regional strain pattern of Italian Apennines, during the last prevailingly extensional phase that started since Late Pliocene times;
2. verify the degree of strain compatibility between long-term geological patterns and ongoing seismological and geodetic ones to refine seismotectonic zoning and to understand crustal-scale deformation processes overtime.

4.4. Data

4.4.1. Host faults and fault systems

The Host Faults (HF) represented in our figures (Figure 4.1) includes the fault traces dating from the Late Pliocene to the Quaternary period, encompassing intra-Apennine normal and normal oblique faults that host the Structural Sites (SS) of the QUIN databases (Figure 4.1). Fault traces are compiled from the two fault traces datasets released together with the QUIN databases (Lavecchia et al., 2022, 2024a), with additional traces from other literature integrated in a more western position with respect to the QUIN HF traces (see references in (Lavecchia et al., 2022, 2024a).

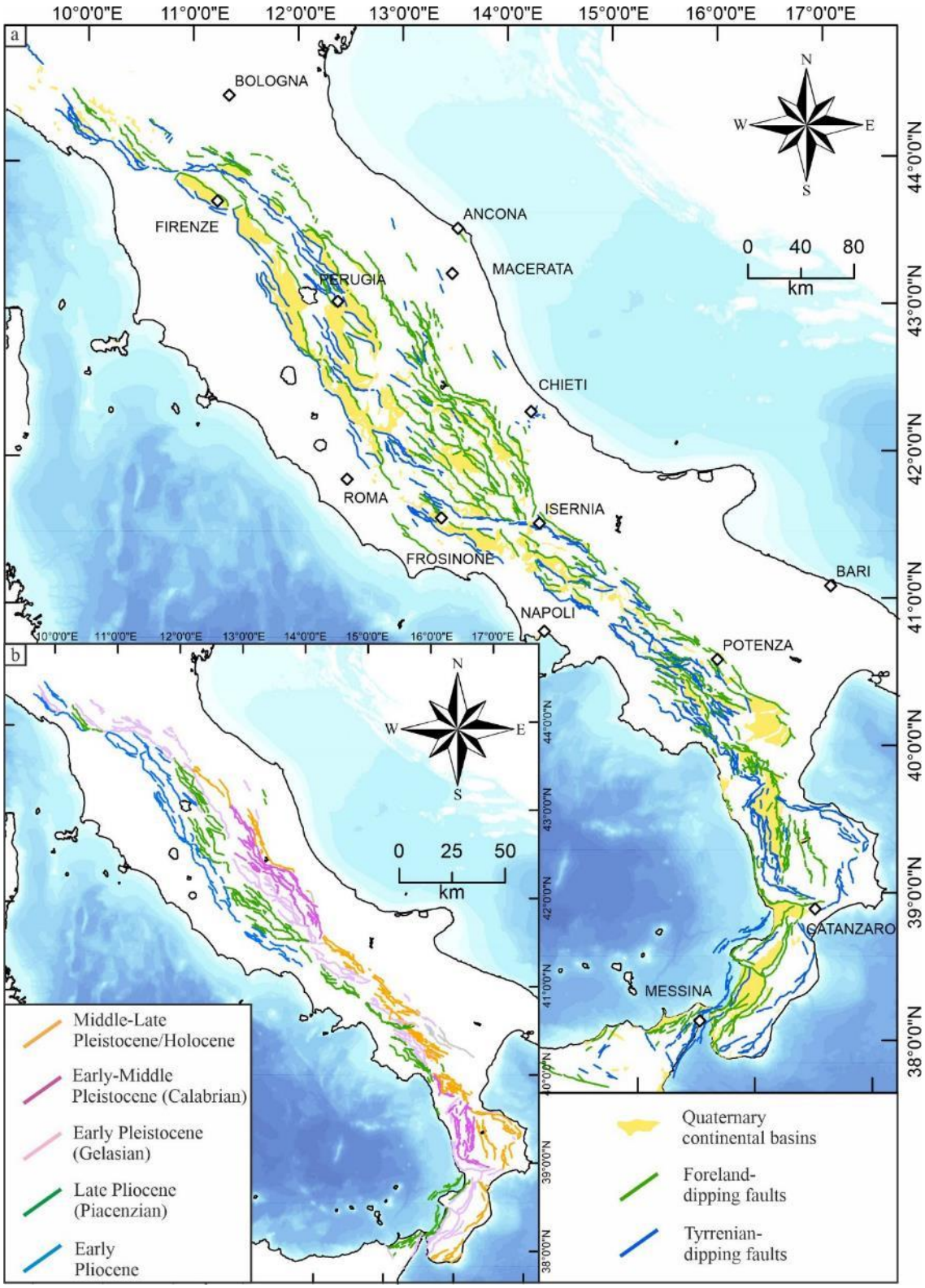


Figure 4.1: a) Plio-Quaternary fault segmentation pattern in Peninsular Italy with hierarchy order and timing. a. Fault traces of major Plio-Quaternary fault systems divided based on the prevailing dip-direction (Tyrrhenian-dipping, in blue or foreland-dipping, in green) with their corresponding Quaternary continental basins (in yellow). B) Temporal hierarchization of the main fault systems from Early Pliocene to middle-Late Pleistocene/Holocene.

HFs datasets include information on the fault name, dip-direction (toward the Tyrrhenian hinterland or the Adriatic-Aegean foreland), the belonging of groups of kinematically coherent and essentially contemporaneous faults in a major FS and the onset timing of such FS. Together, they encompass a total of ~500 faults that cover ~1000 km of the intra-Apennine extensional belt from Lunigiana-Garfagnana regions in the Northern Apennines to the Peloritani Mountains in northeastern Sicily, passing through the Central-Southern Apennines and the Calabrian arc (Figure 4.1a).

Based on the age of the oldest syntectonic deposits associated with each FS, four major alignments of extensional features, mainly rejuvenating eastward, with local out-of-sequence internal activity, may be identified (Figure 4.1b). From East to West, the corresponding extensional tectonic stages, in average lasting 0.8-1 My, may be schematically referred to:

- Middle Pleistocene (Ionian 0,781 - 0.126 My) to Late Pleistocene-Holocene (0,126 - 0 My; duration ~0.8 my)
- Early-Middle Pleistocene (Calabrian, 1.8 - 0.781 My; duration ~1 my);
- Early Pleistocene (Gelasian, 2.59 to 1.8 My; duration ~0.8 my);
- Late Pliocene (Piacenzian, 3,6 to 2.59 My; duration ~1 my).

In northern Italy, in a still more internal position, corresponding to the Apennine's western foothills, another extensional fault alignment may be identified, which dates to the upper part of Early Pliocene times (upper Zanclean, 5.332 to 3.6 My; duration ~1.7 my).

4.4.2. Fault Striation Pair

The Fault-Striation Pairs (FSP) dataset is an updated and reorganized compilation from QUIN 1.0 (Lavecchia et al., 2022) and 2.0 (Lavecchia et al., 2024a), integrated with additional data (Bertotti et al., 1997; Cardello et al., 2021; De Paola et al., 2008; Smeraglia et al., 2018; Testa et al., 2023). It comprises 7,959 FSPs distributed across peninsular Italy.

To enhance strain analyses while preserving local detail, Structural Sites (SS) with closely spaced FSPs were sometimes merged into Composite Structural Sites (CSS) based on spatial proximity and fault association. The final dataset includes 818 SSs (500 individual, 318 composite), with 65% located on faults.

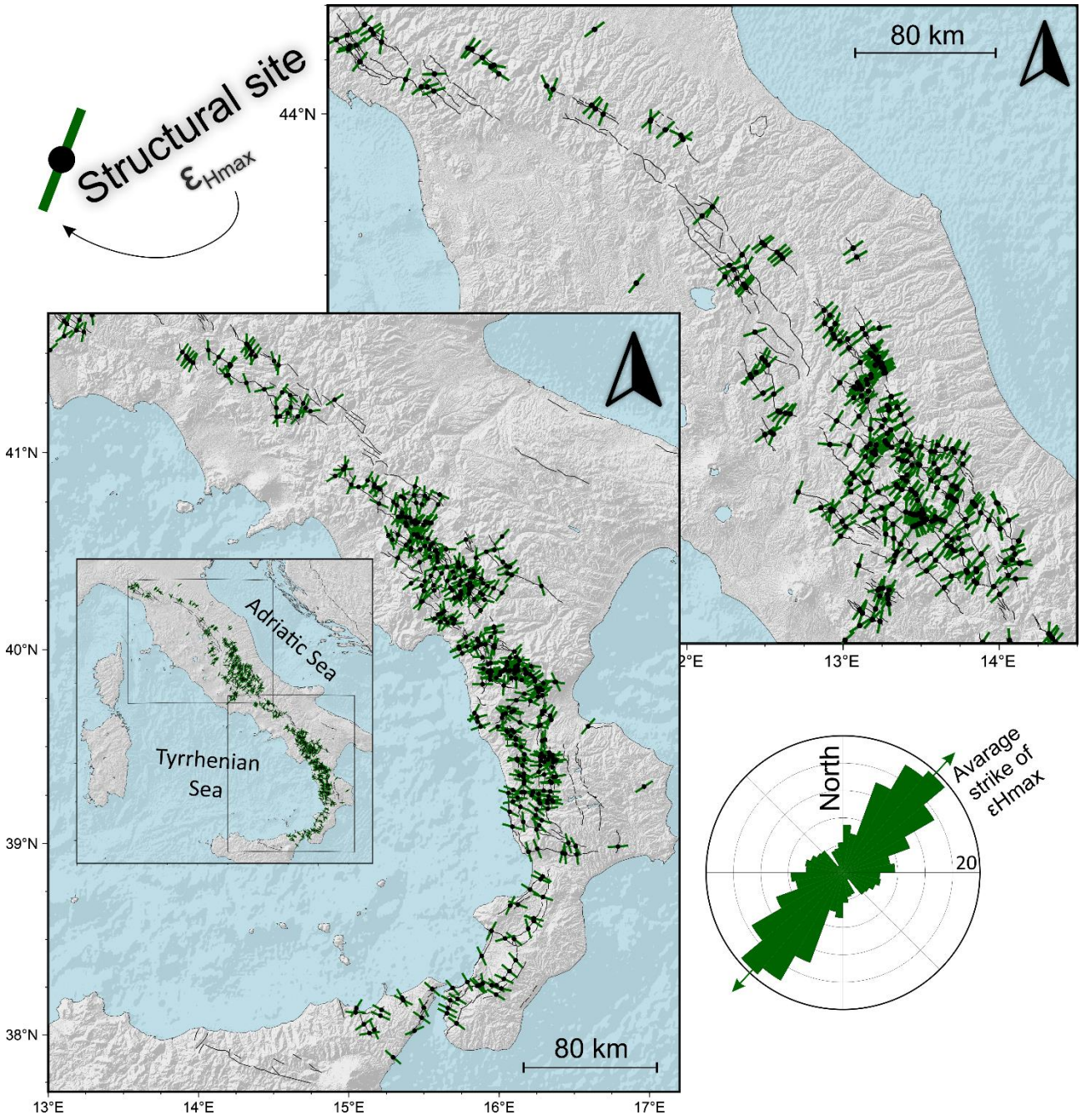


Figure 4.2: ε_{Hmax} calculated assuming θ angles of 30°. The rose diagram represents ε_{Hmax} axes attitudes. Background colors represent the interpolation of the standard deviation of the PTB deviation angle.

4.4.3. GNSS velocities

We select velocity solutions of GNSS stations from Serpelloni et al., 2022 as it represents the most recent and comprehensive update of GNSS station data in the Euro-Mediterranean region, improving upon previously available solutions (Antonio Avallone et al., 2010; Devoti et al., 2017; Serpelloni et al., 2005). It is the result of the processing done by GAMIT/GLOBK software and incorporating data from over 4000 ~GNSS stations. In the Italian region we

count more than ~800 stations spanning from 2.5 years of acquisition time up to 25 years (Figure 4.3).

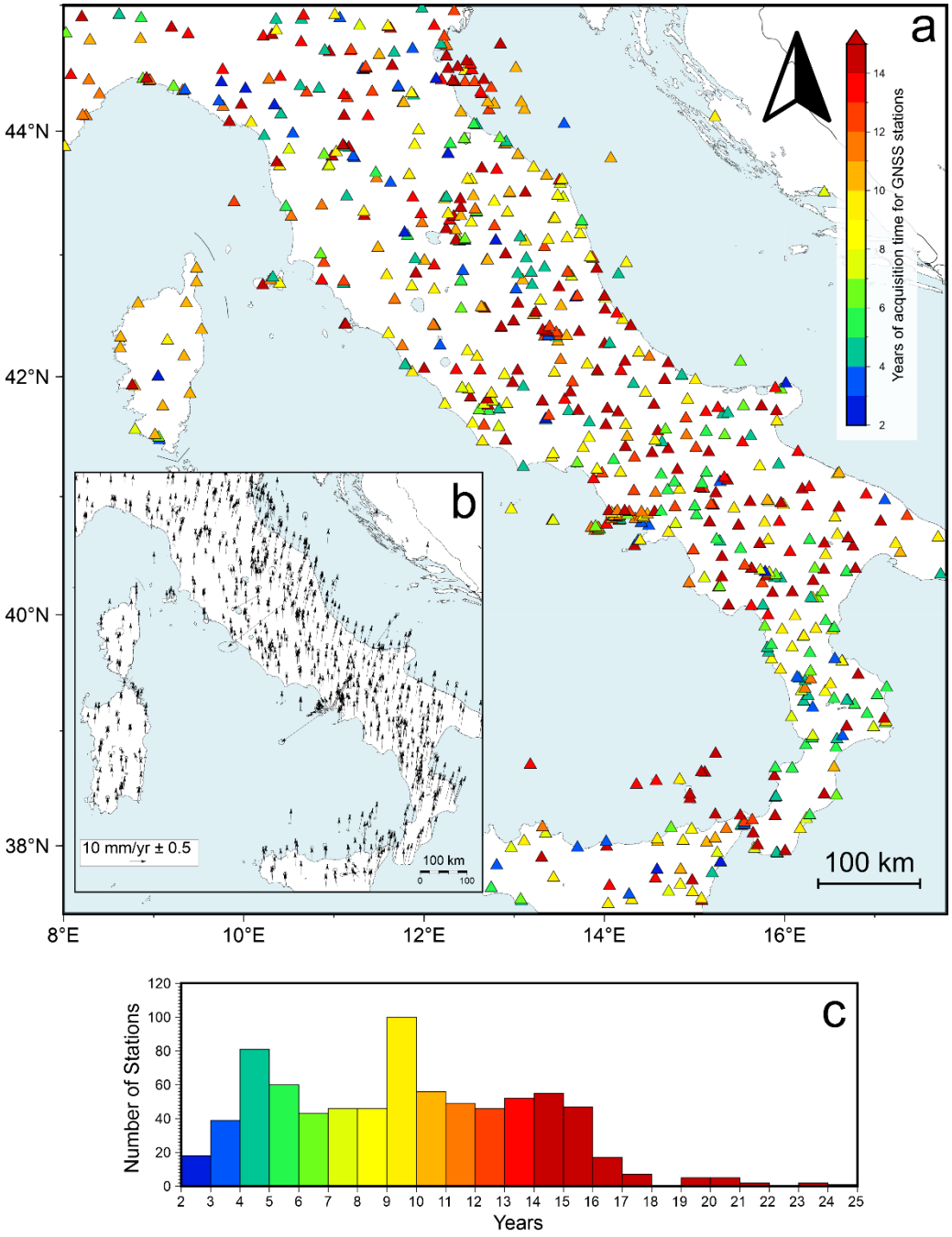


Figure 4.3: a) GNSS stations distribution coloured by acquisition years; b) GNSS velocity field from Serpelloni et al., 2022 in IGb14 reference frame; c) histogram showing the number of GNSS stations relative to the acquisition years.

4.4.4. Focal Mechanisms Solutions

We collect Focal Mechanisms (FMSs) to have a complete catalog to analyze the seismological data respect the other sources. The catalog is a synthesis of the RCMT Catalog (Pondrelli et al., 2020) and TDMT Catalog (Scognamiglio et al., 2006), covering the time period from 1908 to December 31, 2023. To focus on crustal deformation, we select focal mechanisms from the first 18 km of depth. Specifically, to study the activity of normal faults along the Apennines, we include FMSs ranging from normal (NF) to normal-to-strike (NS) (Zoback, 1992). Since our interest lies in the maximum deformation axes, we assume that the T-axis represents the ε_{Hmax}. This assumption is valid because, in the selected FMSs, only NF and NS mechanisms are included, meaning the plunge of the T-axis is always sub-horizontal (Figure 4.4).

FMSs are predominantly concentrated in the Central Apennines and are associated with the 2016 Central Italy Seismic Sequence (Chiaraluce et al., 2017). The magnitude distribution ranges from M 3 to M 7, with over 90% of the events not exceeding M 5. Additionally, less than 10% of the FMS correspond to depths greater than 12 km. Based on this dataset, we assume that the deformation of the upper crust is reliably represented by this catalog of FMSs.

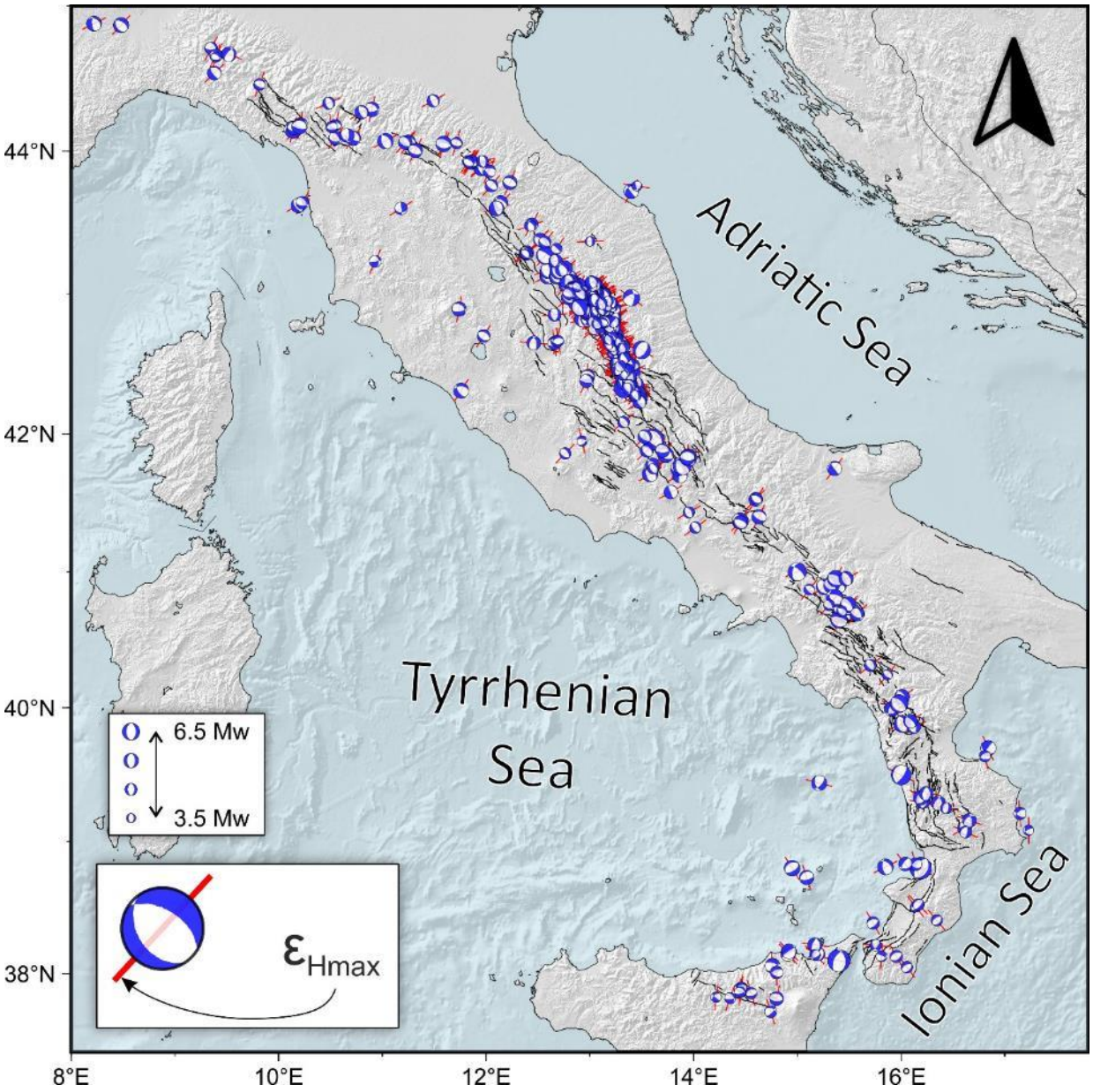


Figure 4.4: FMS database used for this work. FMS dimension is scaled by magnitude. The red axis represents the azimuth of the T-axes assumed to be the maximum horizontal axes (ε_{Hmax}). In black lines are reported the HF.

4.5. Methods

4.5.1. Geological strain

We conducted the first comprehensive deformation analysis of the entire late Pliocene–Quaternary Apennine extensional belt, producing the first strain map of peninsular Italy. Approximately 800 distinct Structural Sites (SS) were identified by grouping all the FSPs data. ~85% of these sites are located along HF traces, while the remainder are off-fault or within associated continental basins. The SSs are further classified into individual SSs when all FSPs are surveyed at precisely the same position, and CSSs (Composite SSs) where we have

grouped neighboring FSPs. In grouping the FSPs data, we preferred to retain many SSs to preserve local geometric and kinematic variations. Such a choice implies that some SSs consist of a small amount of data, but they are valuable as they are specifically located on a distinct structure and are crucial for highlighting local deviations of the strain pattern.

The resulting strain parameters at any SS relies on the Mohr-Coulomb fracture criterion, referred to as the PBT-Method (Sippel et al., 2009), and on the assumption that the variation of the theta (θ) angle, the angle between the P axis and the striation, favors the verticalization of the vertical stress.

For each SS, we obtained the most representative strain solution, expressed through P, B, T deformation axes, hereafter denoted as S_1, S_2, and S_3, plus the corresponding Strain Ratio (R) and Strain Index index (R'), along with uncertainty parameters and quality ratings. We also computed the maximum and minimum horizontal deformation axes (ε_{Hmax} and ε_{Hmin}) determined using the Lund and Townend, 2007 correction for any SS.

To calculate the average fault solution and corresponding S_1-S_2-S_3 (i.e., P-B-T) strain tensor axes at each SS, we used Bingham's statistics to process an unweighted moment tensor solution, starting from the FSPs input data. The procedure involves the calculation of a 3x3 matrix derived from the direction cosines of the P and T axes (composed of the sums of the products and squares of the direction cosines of the P and T axes) (Angelier, 1979).

The calculation is organized into eight consequential steps, here organized in an ad hoc MATLAB flow:

1. Calculation of the P-B-T axes for any FSP of any given SS (Andrenacci et al., 2021);
2. Evaluation of the kinematic compatibility among the FPS within each SS, through calculation of a first SS strain tensor (P', T', B') and corresponding PTB deviation;
3. Rejection for any SS of the kinematically incompatible FSPs, e.g. those with PTB deviation values greater than the mean plus one standard deviation of all PTB deviation values;
4. Calculation from the remaining kinematically compatible FSPs of a second strain tensor (P", T", B", after referred to as S_1, S_2, S_3), which represents the best-fit solution for the investigated SS;
5. Calculation from such second tensor of the attitude of the best-fit fault plane and striation;
6. Calculation of the Strain Ratio value $R = (S_2 - S_3) / (S_1 - S_3)$ and subsequent calculation of the Strain Index R', where R' = R for normal faults, R' = 2 -R for strike-slip faults, and R' = 2 + R for reverse faults (Delvaux et al., 1997);
7. Computation of the maximum horizontal strain (ε_{Hmax}) according to Lund and Townend, 2007's methodology;

8. Definition of quality parameters, ranging from A (the best) to D (the worst), assigned to each computed SS strain tensor. These parameters are inspired by those of the World Stress Map (Sperner et al., 2003);

4.5.2. Geodetic strain rate map

The strain rate was computed using four different methods: three based on interpolating the velocities of neighbouring measurements and one following elasticity criteria. This analysis was made possible by the method published by Maurer and Materna, 2023. To focus on the direction of the maximum strain (ε_{Hmax}), we tested these methods and selected GNSS stations on a uniformly distributed 0.5° × 0.5° grid to evaluate the reliability of the results.

The VISR software (Shen et al., 2015) applies a least-squares procedure to interpolate velocities on an optimally regular grid (see Paragraph 4.5.1). The interpolated velocities are then used to derive strain rate values, assuming an elastic medium. Our primary interest lies in calculating long-term strain rates, primarily driven by tectonic processes. The geostatistical (Geostats) method, as described by Maurer and Materna, 2023, employs kriging interpolation to estimate surface strain rates from geodetic velocity data. It determines optimal weights for observed velocities using spatial covariance models (e.g., Gaussian or exponential functions), producing a smooth, data-driven interpolate velocity field. By incorporating variogram analysis, this method improves strain rate reliability, particularly in regions with sparse GNSS data, and allows for aleatoric uncertainty estimation. The Local Average Gradient method, also described by Maurer and Materna, 2023, is a neighborhood-based approach for estimating strain rates. It defines a local window around each estimation point and applies a local linear regression to determine velocity gradients. Unlike global interpolation methods, this technique focuses on capturing local variations in strain while maintaining computational efficiency. It does not apply additional weighting based on spatial covariance, distinguishing it from geostatistical approaches like kriging. The GPSGRIDDER method (Sandwell and Wessel, 2016) interpolates 2D vector data using elasticity constraints, specifically Green's functions for an elastic body subjected to in-plane forces. This ensures coupling between horizontal velocity components, which can be adjusted by varying Poisson's ratio. The interpolation is performed by solving for a set of body forces applied at measurement locations, optimized to match observed velocities. Implemented in GMT as GPSGRIDDER, this method provides a robust means of estimating strain rates while accounting for spatial variability and smoothing. All these methods were tested by selecting input parameters optimally selected for the area. The tests have been done for different initial datasets based on the acquisition time of GNSS stations. The

selection process began by considering all available solutions in the velocity field, followed by filtering the data based on acquisition time lengths of 3, 5, and 7 years (Figure 4.5).

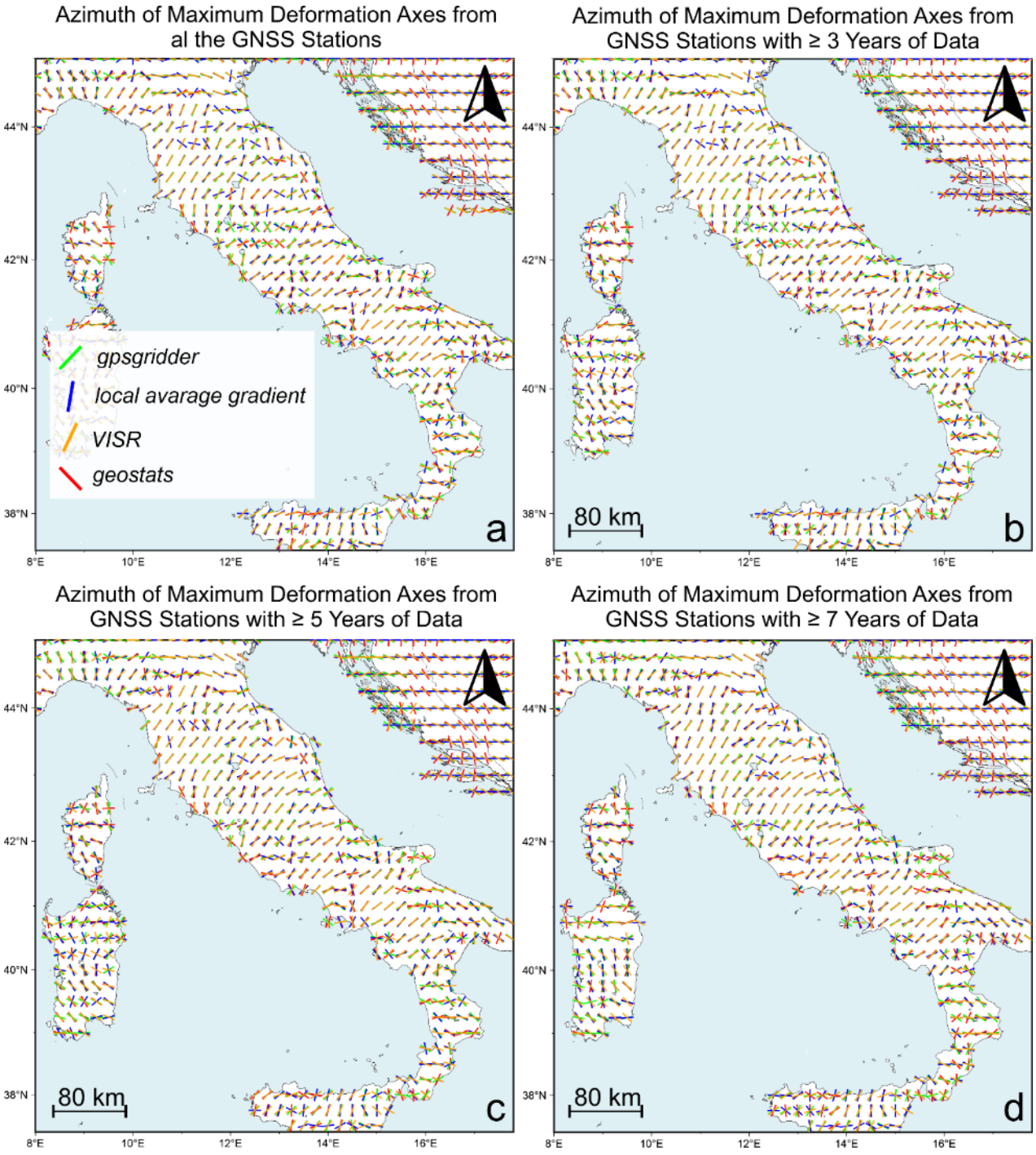


Figure 4.5: a) directions of ε_{Hmax} computed starting from all the GNSS stations in Serpelloni et al., 2022, computed by different methods: gpsgridder, local average gradient, VISR and geostats. In b), c) and d) same methodology selecting GNSS stations with acquisition years ≥ 3, ≥ 5 and ≥ 7.

Our primary goal is to determine the correct azimuth of the maximum strain (ε_{Hmax}). To assess the consistency of the input data, we compared the results obtained from different methodologies. Since we are particularly interested in the orientation of the maximum

deformation axes, the comparison was conducted by evaluating the solutions at homogeneous grid nodes.

The results show greater variability as the acquisition time of the stations decreases. The outcomes from calculations using all stations (Figure 4.5a) and those with at least 3 years of data (Figure 4.5b) exhibit some variability in the calculated azimuth of ε_{Hmax}. In contrast, solutions derived from data with 5 and 7 years of acquisition show reduced variability, with nearly identical results. Our objective is to obtain the most reliable solution with the highest possible resolution in the region, as we need to compare geodetic data with higher-resolution datasets, such as structural data (SS). For this reason, we choose to select stations with at least 5 years of data.

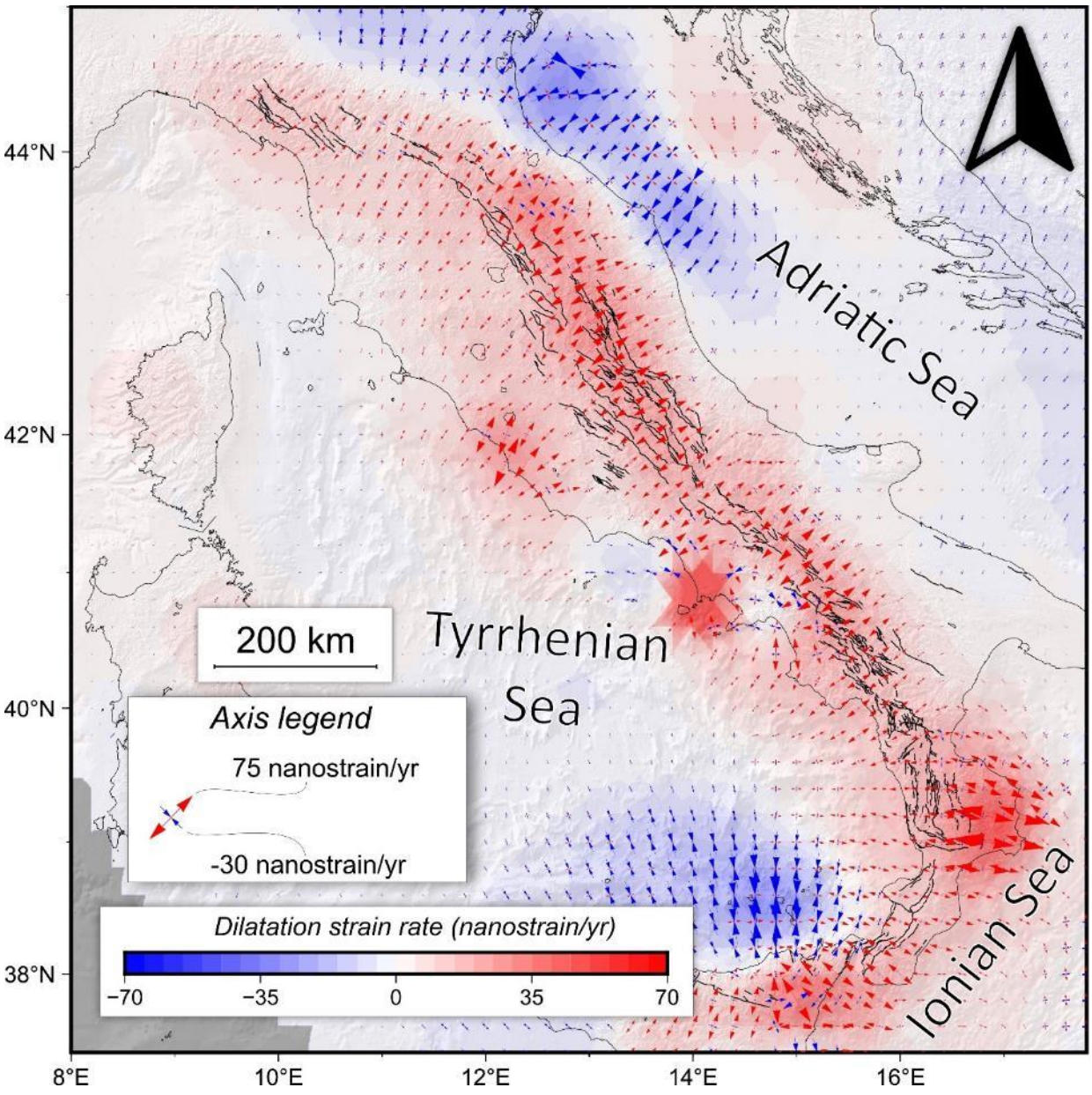


Figure 4.6: Strain-rate map showing the dilatation strain rate and the magnitude and directions of ε_{Hmax} and ε_{hmin} computed by VISR software and selecting GNSS stations with at least 5 years of acquisition.

Among the most constrained solutions (5-7 years, Figure 4.5c-d), the angular difference between the various methods is particularly high in coastal areas, where the geodetic data is more interpolated due to the lack of measurements that could constrain the results. Along the Apennine chain (the area of interest in this study), the axes consistently show a difference of around 15 degrees. The method that, likely due to its simpler mathematical approach, exhibits the greatest variability is the Local Average Gradient. The geostats, on the other hand, shows a deviation from the other methods in areas where the station density differs from the "average" distribution. It provides excellent results in regions where station distribution is uniform, as it is the only method that, through the variogram, allows for the determination of interpolation parameters (sill, range, and nuggets) directly from the dataset. The results between VISR and GPSGRIDDER show angular differences that, in 95% of the cases, are around 5°, values that do not significantly affect the outcome of the study. We opted for VISR as we have greater expertise with the choice of the initial parameters.

4.5.3. Building a common grid – Angular difference

We evaluated three evenly spaced point data grids covering square cells of different sizes: 5 x 5 km, 10 x 10 km, and 20 x 20 km. Considering the obtained results and the distribution of all the three types of data, we choose a grid size 10 x 10 km. This size effectively balances the need to maintain local geological detail while capturing sufficient focal mechanisms and geodetic data.

We used the Fishnet Tool from ESRI ArcGIS Desktop 10.8 to create the grid, applying Lambert Conformal Conic projection, hence using kilometric coordinates. This approach ensures a consistently equidistant grid, overcoming the variability in kilometres distances associated with measurements in WGS84 degrees across Italy.

For interpolation of structural data and focal mechanisms, we modified the stress2grid software (Ziegler and Heidbach, 2019), integrating our grid directly into the Matlab code. The software is builded to facilitate the analysis of the horizontal stress (σ_{Hmax}) based on non-uniform data distribution on a specific area. It employs two approaches to calculate the mean horizontal stress on regular grids: the first uses a fixed search radius around a grid points, while the second approach is by using a variable search radius, determining the radius for which the standard deviation of the mean σ_{Hmax} is below a given threshold. Given the methodology, we assume that the mathematical process used by the software is also suitable for strain axes, and therefore it can be applied to interpolate ε_{Hmax} azimuths as well. In this case, we considered the first approach the most appropriate workflow for our purpose, as the multi-source data have significantly different spatial distributions along the Apennines.

In the case of Structural Site data, we opted against interpolating neighboring cell grids to retain discrete information, particularly for ε_{Hmax} values. Instead, we averaged the ε_{Hmax} values within each 10 x 10 km square cell. Structural sites with a quality class D were excluded to avoid dispersion caused by less reliable structural data. We also excluded Subset ES (Early Stage), which represents sites in an early deformation stage observed in the field, and Subset T, which includes local transverse discontinuities to the main fault trend.

For FMSs, we applied a 10 km search radius within the 10 x 10 km grid to interpolate neighboring ε_{Hmax}. Seismological data were weighted according to the linear distance from the grid node (Inverse Distance Weighting) and the quality of each focal mechanism. Given the integration of multiple data sources in our catalog, we selected the moment magnitude (Mw) as the primary quality parameter, as lower magnitudes are associated with more limited data availability, resulting in higher uncertainties in the solution (Adinolfi et al., 2022). Quality classes were defined as follows: quality A for events with Mw > 4.5, quality B for events between Mw 4.0 and 4.5, and class C for events < 4.0 Mw. In stress2grid default parameters are weighted 1/15, 1/20 and 1/25 respectively for quality A, B and C (see Paragraph 4.5.1).

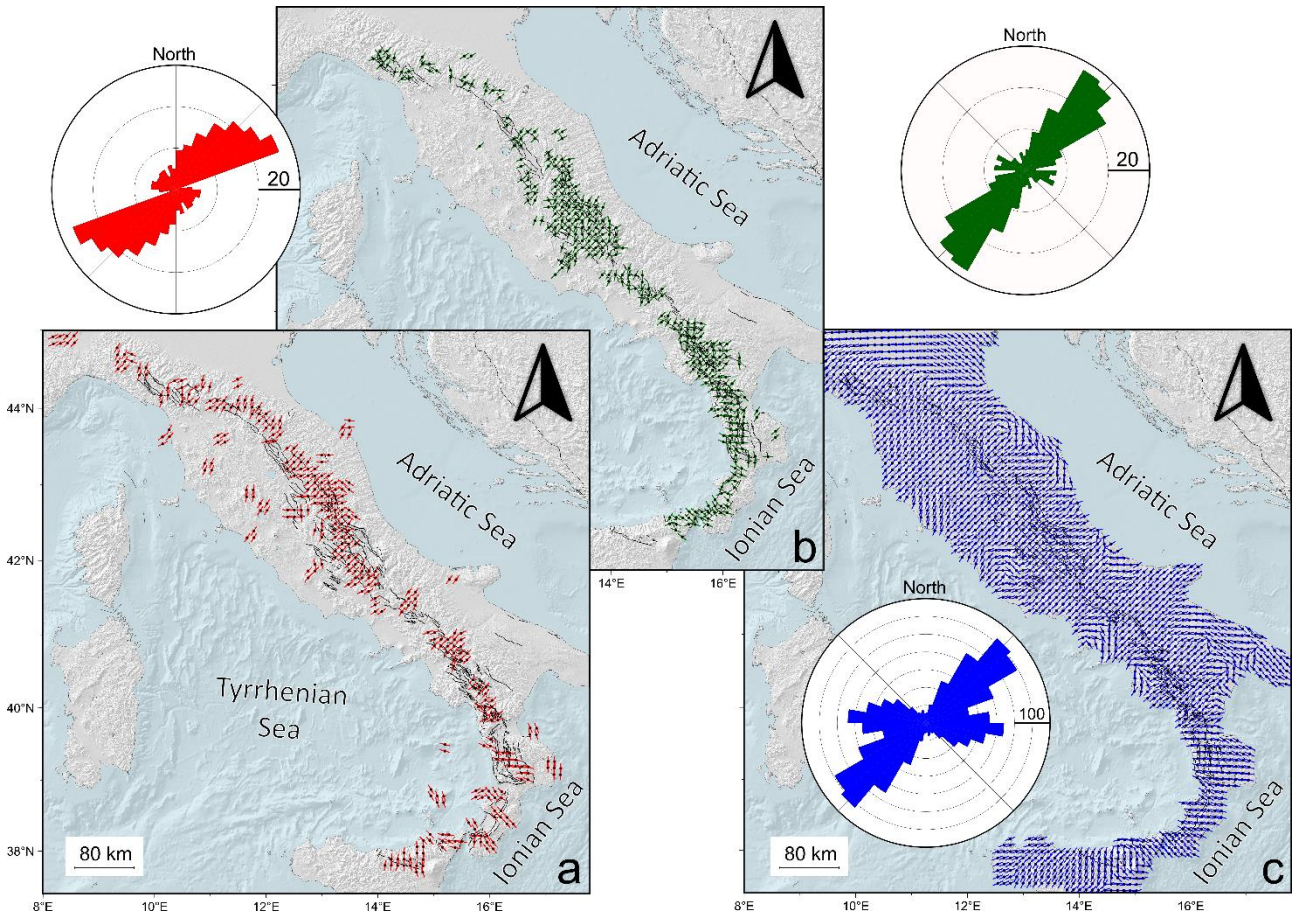


Figure 4.7: a) stress2grid results on 10 x 10 km starting from FMS ε_{Hmax}. b) stress2grid results on 10 x 10km starting from SS ε_{Hmax}. c) stress2grid results on 10x10 km starting from geodetic ε_{Hmax}.

Extensional strain directions (ε_{Hmax}) from geodetic data were first interpolated independently and subsequently sampled on the same 10 x 10 km regular grid containing the geological and seismological ε_{Hmax}. The step procedure was necessary because the VISR software for interpolating the geodetic data (Shen et al., 2015) does not allow the input of external projected grids. Therefore, we performed processing with parameters suitable for interpolation but requested the software to output a particularly dense grid (0.01/0.01°). Subsequently, we resampled the nearest strain rate values using QGIS software (Find Nearest feature), ensuring that the resampled point was at most 200m away.

To measure the angular divergence between geological (SS) and seismological (FMSs) data, between geological and geodetic (GNSS) data, and between geodetic and seismological data, we selected grid cells having at least two data type on each node of the Italian Peninsula. We measured the acute angle between two directions at each grid point, compared only high-quality ε_{Hmax} data and handling the calculation in Python.

4.6. Results

Considering that the studied area prevailingly undergoes extension, we find it more representative to visualize the ε_{Hmax} axis. At the regional scale, ε_{Hmax} rotate roughly perpendicularly to the major fault alignments moving southward. Locally, at the individual fault scale, ε_{Hmax} exhibit a slight rotation perpendicular to the fault strike, even in cases where a strike-slip component might prevail (Figure 4.2b). The strain map obtained in this study is compared with the geometry and multi-scale segmentation pattern of the outcropping FS, as well as with deformation trends derived from earthquake data and geodetic information. To better analyse the statistics of ε_{Hmax} azimuth measurements, we divided the study area into the Northern and Southern Apennines (Figure 4.8). In general, the axes are sub-parallel, with angular discrepancies around 15° in 90% of the cases. In the northern Apennines all the data confirm a general SW-NE stretching direction. Meanwhile, the southern Apennines maintain a SW-NE trend up to approximately 40°N latitude, after which, proceeding southward a sharp clockwise rotation occurs. This rotation initially aligns the axes in a NW-SE direction in Calabria and then shifts to a N-S orientation in Sicily. Using a 10 × 10 km grid, the mean long-term geological trend of ε_{Hmax} deviates on average by ~± 16° from the geodetic extensional direction and by approximately ± 14° from the ε_{Hmax} trend derived from focal mechanisms. However, this divergence is not a uniform average value but is influenced by localized high-discrepancy areas, where angular deviations exceed 45° and can reach up to 90°. These high angular deviations are generally associated with low-quality geological strain tensors, primarily due to the uncertainty and non-uniqueness of the input fault slip parameters (FSPs), as well as the uncertainties in the seismological and geodetic ε_{Hmax} axes.

In the comparison between geodetic and seismological strain, most interpolated nodes exhibit similar angular values. However, areas with higher angular deviation (> 30°) are generally found farther from the central Apennines, where dilatation strain rate is lower (see Figure 4.6) and FMSs are sparse. Additionally, the angular difference tends to increase offshore and further East and West of the main Apennine deformation zone (see Figure 4.5). Comparing the seismological and geological data, we observe that the number of points where the azimuth of ε_{Hmax} can be measured is generally lower in the geological dataset. Overall, the angular misfit is low, but localized areas show discrepancies reaching up to 45°. In general, the geological ε_{Hmax} appear less uniform and homogeneous compared to the seismological data. The geological dataset provides a more detailed representation of the strain pattern, whereas the seismological data exhibit a smoother pattern of strain axes. Regarding the structural and geodetic data, a general angular agreement is also observed. Like the seismological data, the geological strain pattern appears more detailed than the geodetic one, in which ε_{Hmax} values generally show lower angular differences between neighboring nodes.

4.7. Conclusion and discussion

4.7.1. New methodological approaches for multi-source strain

In this study, we evaluate the spatial distribution of various datasets and the type of deformation they represent. Geodetic data may capture deformation that is not directly linked to tectonic processes, while FMSs provide insight into deformation at depth. In contrast, geological data (SS) primarily reflect surface tectonic activity. Many studies have combined data from seismology and geology to create unified strain or stress maps (Delvaux and Barth, 2010; Heidbach et al., 2018; Villani et al., 2024), often without distinguishing between datasets that may represent different deformation processes. In contrast, this work emphasizes the unique characteristics of each dataset to highlight its specific seismotectonic significance.

For this approach, it is crucial to develop a methodological framework that allows for the comparison of datasets with varying spatial distributions (see Figure 4.7) on a unified grid. This study introduces a new methodological approach, offering the scientific community a more reliable and straightforward means of comparing strain data from geological, geodetic, and seismological sources.

Structural data have been extensively analysed and placed at the core of this study, as they are the only available data that can describe a surface process with a temporal resolution longer than geodetic and seismological data. This also results in considerable data variability,

sometimes showing directions that deviate from the current deformational trend. Furthermore, while the QUIN 1.0 (Lavecchia et al., 2022) and QUIN 2.0 (Lavecchia et al., 2024a) structural databases provide an abundant collection of data along the Apennine chain, structural data remain heavily dependent on the lithological composition, which may or may not preserve kinematic data. These types of data are crucial for describing the deformation of a specific fault at a scale that only geological-structural data can achieve. However, they are spatially constrained to the faults and their possibility of being identified at the surface.

The literature includes various studies on the uncertainty of strain rate calculations for a specific area, as well as the reliability of GNSS station velocity measurements relative to their acquisition duration (Maurer and Materna, 2023; Nucci et al., 2024). Nucci et al., 2025a analyzed the misfit angle between GNSS strain field and the sum of the moment tensor of the focal mechanisms in hexagonal cells. They also compare the seismic strain axes respect three the Nearest Neighbours, VISR and Wavelet-based methods (Tape et al., 2009). Their results, like ours, support the hypothesis that the geodetic strain rate is representative of the accumulated and released through earthquakes (Carafa et al., 2017; D'Agostino, 2014; Nucci et al., 2025a), although some strain peaks appear to be associated with the viscoelastic relaxation resulting from recent earthquakes, with effects persisting over decadal timescales (Carafa et al., 2024). A high misfit angle between the two datasets is observed in regions distant from the Apennines, such as the Adriatic side of the Italian Peninsula. This discrepancy is likely due to the limited availability of data. In fact, in these peripheral areas, the results may be more influenced by interpolation rather than the original data.

However, our focus here is on how these factors impact the calculation of the ε_{Hmax} direction. We find that ε_{Hmax} directions remain stable when selecting stations with at least 5 years of data. The methods, excluding simpler approaches like the Local Average Gradient (Huang et al., 2022), show similar strain patterns across the datasets.

4.7.2. Multi-source strain patterns

It is well known that the intra-Apennine extensional belt results from the latest phase of lithospheric-scale deformation, which, since the late Miocene, has driven the progressive counterclockwise rotation of the Adriatic block and the opening of the Tyrrhenian Basin (Doglioni et al., 2004; Lavecchia, 1988). The onset of this most recent deformation phase has been variably dated to the late Pliocene (3.5 million years ago) by some authors (Barchi, 2010; Martini et al., 2001) and to the Early Pleistocene (1.8 million years ago) or even the Middle Pleistocene (0.8 million years ago) by others (Bonini et al., 2016, p. 201; Faure Walker et al., 2021). Furthermore, several studies suggest that extensional deformation in Southern

Italy began later than in the Northern Apennines (Brozzetti et al., 2017; Galli and Bosi, 2003; Papanikolaou and Roberts, 2007). Accurately defining the timing and spatial distribution of long-term extensional structures associated with this phase, which remains active and continues to generate destructive earthquakes, is particularly relevant for seismotectonic analyses.

The results of this study support the hypothesis that the most recent phase of extensional deformation began in the late Pliocene. Since then, the extensional front has migrated eastward while locally remaining active in the background. From West to East, four distinct structural alignments spanning the entire belt can be identified. These structures are generally continuous along their trend, though some major transfer faults accommodate the eastward shift of the extensional front.

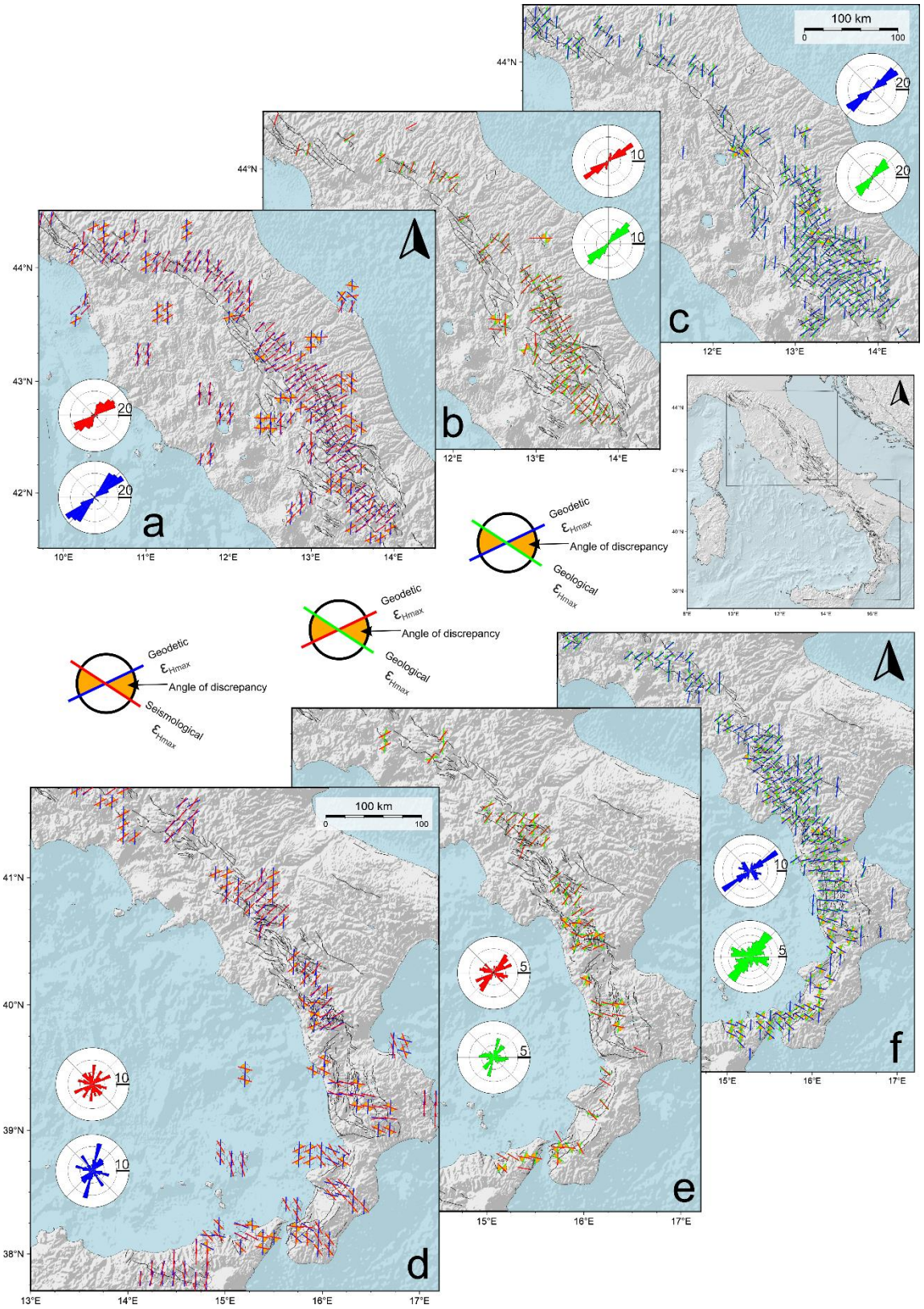


Figure 4.8: gridded representation of the computed deformation pattern compared with geodetic, seismological and geological data. a), b) and c) comparison of ε_{Hmax} respectively from geodetic and FMS, FMS and SS, geodetic and SS for the northern Apennines. d), e) and f) comparison of ε_{Hmax} respectively from geodetic and FMS, FMS and SS, geodetic and SS for the southern Apennines. Data in supplementary in Paragraph 8.3.1, 8.3.2 and 8.3.3

The correspondence between ongoing tectonic processes evidenced by recent stresses obtained from geological data (such as fault-slip data, as well as veins and pressure-solution, known as stylolites), and contemporary stresses derived from borehole breakouts, earthquake focal mechanism inversions, and GPS measurements have been extensively documented in the literature globally (Carafa and Barba, 2013; Cirillo et al., 2022; De Matteis et al., 2012; Ferrarini et al., 2015; Lavecchia et al., 2017), as well as in Italy.

From a tectonic perspective, the similarity between present-day strain patterns and those associated with long-term deformation suggests a remarkable continuity in the regional kinematics. This observation indicates that the overall strain field has remained relatively stable over extended periods, preserving the large-scale tectonic regime and associated plate motions (Lacombe, 2012).

The appropriate time window for neotectonics and seismotectonic studies has been widely debated (Wu and Hu, 2024). A conservative approach considers only deformation occurring after the Last Glacial Maximum (LGM) (Galadini et al., 2012). Others extend the timeframe to include active faults that have been deforming for over 40,000 years, primarily based on potassium-argon dating (SM Working Group, 2015). Additionally, some researchers advocate considering the entire period during which the regional strain field has remained unchanged, estimated to be approximately 2.5–3 million years in Italy, spanning the late Pliocene and Quaternary (Christophersen et al., 2015; Machette, 2000).

In conclusion, this study does not analyse past strain regimes that are no longer active but rather investigates the long-term strain field that has persisted for the last 3.5 million years and continues to evolve eastward. A long-term strain analysis provides a more comprehensive view of the region, bridging gaps in earthquake records and revealing persistent deformation zones and structural discontinuities that influence strain partitioning and regional tectonics.

5. Final discussion and conclusion

Previous chapter investigate three different areas (Himalaya-Tibet, Iberia-Northwest Africa, Italian Apennines) in which we applied the comparison between different data sources, from seismic to geodetic and geological to understand the geodynamics and the seismotectonic of different areas.

5.1. Stress inversion

To analyse the regional stress field, two main approaches have been employed by researchers: the seismotectonic-based selection of Focal Mechanism Solutions (FMSs) (Sheikholeslami et al., 2021) and the grid-search selection of FMSs (Han et al., 2019; Yang et al., 2018).

The first approach relies on a stress inversion guided by seismotectonic knowledge, where the selection of focal mechanisms is selected based on predefined zoning criteria (Delvaux and Barth, 2010). However, because seismotectonic zoning is constrained by the knowledge available at the time of computation, this method may sometimes introduce selection biases. As seismic event density and catalog completeness have increased over the years, the need for a more objective and systematic methodology to delineate seismotectonically homogeneous zones has become increasingly evident.

As discussed in Chapters 2 and 3, applying stress inversion through a grid-search approach has proven instrumental in identifying areas with a relatively uniform stress field, thereby facilitating the recognition of seismotectonically homogeneous regions (Paragraph 3.7.1). We consider this method a valuable tool for obtaining a first order estimate of the stress field in each study area.

In this thesis, we propose a novel approach to stress inversion using a grid search by integrating the STRESSINVERSE software (Vavryčuk, 2014) into a Python-based framework. This method determines the stress field across a region by considering only the density of available Focal Mechanism Solutions and the spatial resolution of the analysis. While this is not the first tool to apply stress inversion on a grid, the MATLAB-based MSATSI (Martinez-Garzon et al., 2014) methodology also represents a significant contribution to this field. As described in Bala et al., 2021 the differences between two approaches are diverse: for first STRESSINVERSE (Vavryčuk, 2014) determine the fault orientations by the fault instability criteria (Vavryčuk et al., 2013). This allows for the exclusion of planes that are less susceptible to fault slip from the final stress inversion. Even though the stress ratio remains a highly complex parameter to determine in stress inversion MSATSI (Martínez-Garzón et al., 2016), the results from STRESSINVERSE provide a have a more accurate estimation of it (Paragraphs

2.7.2 and 3.6.1.1) compared to MSATSI (Andrei Bala et al., 2021; Vavryčuk, 2014). The R parameter is an important value to determine the orientation of the σ_{Hmax}, as the azimuth of the σ_{Hmax} may differ by tens of degrees (Lund and Townend, 2007). In Chapter 2 and 3 we have extensively used the stress ratio also in the interpretative phase, as a clear pattern has been observed in Himalaya-Tibet area and in Iberia and Northwestern Africa areas. Secondly, while MSATSI performs stress inversion using a grid search, adjacent cells are not independent, as a damping parameter is applied to ensure a gradual transition between grid nodes (Martínez-Garzón et al., 2016). This approach is particularly powerful when describing regions where the stress field geometry is relatively homogeneous but exhibits small spatial variations (Das et al., 2023). In our case, however, since we are primarily interested in obtaining the less smoothed estimation of horizontal stresses (σ_{Hmax}), we opted for a moving window approach. Although in the transition areas between two seismotectonically homogeneous zones it generates less constrained solutions (see Figure 2.6 and Figure 3.2), it still provides the best possible estimates of σ_{Hmax} for the given crustal volume.

A critical discussion is required regarding the selection of the minimum magnitude for focal mechanisms used as input for stress inversion. Specifically, it is necessary to determine the lowest magnitude at which a focal mechanism can reliably represent the regional crustal stress field. An important question arises: is it appropriate to perform stress inversion using focal mechanisms with magnitudes lower than the magnitude of completeness? This issue is particularly relevant because smaller magnitude earthquakes may be influenced by local heterogeneities, fault-specific conditions, or transient stress variations rather than the broader regional stress field (Luo and Liu, 2021). Different researchers have approached this problem using various methodologies. Delvaux and Barth, 2010 proposed selecting focal mechanisms for inversion based on the magnitude of completeness within each seismotectonic homogeneous area, as this value varies depending on seismic activity and the density of the seismic network. In contrast, Keiding et al., 2009 adopted a uniform magnitude threshold of approximately M 3 for the Reykjanes Peninsula, southwest Iceland, when defining the magnitude of completeness. Establishing a precise threshold is challenging, as stress inversion has been performed in diverse tectonic settings. For instance, in the Himalaya-Tibet region, the database of focal mechanisms predominantly includes events with Mw > 5 (Paragraph 2.4.2), whereas in Iberia-Northwest Africa, seismic events rarely exceed Mw 4 (Paragraph 3.4.3). Based on these regional characteristics, we adopted a minimum magnitude of M 4 for the Himalaya-Tibet region and M 2 for the Iberia-Northwest Africa region. We also tested lower magnitude thresholds, but in many cases, the resulting solutions appeared poorly constrained. Despite these limitations, the stress inversion results in both regions are consistent with the observed kinematics of surface faulting (Paragraphs 2.4.2 and 3.4.2). Additionally, the trajectories of σ_{Hmax} broadly align with the convergence of

the Indian-Eurasian plates and the African-Eurasian plates, further supporting the reliability of the selected magnitude thresholds in the two cases.

5.2. Geodetic strain rate

The calculation of strain rates is a key aspect of this thesis. It has been the common thread throughout all the chapters (Paragraphs 2.7.2, 3.6.3 and 4.5.2), as geodetic data is one of the most valuable datasets for defining surface deformation.

Despite the high number and density of GNSS measurements in the study areas, selecting a precise methodology remains crucial for a reliable result. In the three case studies, we chose the solution computed by the VISR algorithm (Shen et al., 2015). However, in Paragraph 4.5.2, we explored alternative methodologies by using the tool Strain_2d from Maurer and Materna, 2023 to assess the reliability of the directions of the ε_{Hmin} and ε_{Hmax} axes. As observed, the differences between the results are primarily due to the selection of GNSS data as the starting dataset, particularly concerning the acquisition time and the quality of the final velocity solution.

The strain maps described in Paragraphs 2.7.2 and 3.6.3 are in good agreement with previous studies conducted in the Himalaya-Tibet region (Stevens and Avouac, 2021; Wang et al., 2019) and in Iberia and Northwest Africa (Koulali et al., 2011; Palano et al., 2015; Serpelloni et al., 2022). The new insights derived from the updated strain maps are primarily due to the increased resolution of the input data, which has allowed us to minimize the impact of interpolation (thus reducing the threshold) and to highlight new aspects of surface deformation.

In Paragraph 2.7.1., we identified several well-defined areas where stretching occurs parallel to the Himalayan Arc, potentially accommodating the extensively described arc-parallel stretching of the region (Kumar et al., 2023a). In Paragraph 3.6.3, a refined strain rate calculation allowed us to pinpoint a region experiencing relatively high strain rates (> 20 nanostrain/yr, Figure 3.8). This area is particularly noteworthy, as it exhibits low instrumental seismicity (Paragraph 3.4.3) and therefore warrants further attention.

In Italy, the approach is different. The main result concerning strain rates lies in their comparison with other datasets. The greatest challenge was integrating geodetic, seismological, and geological data onto a common grid to achieve the most reliable comparison possible, using the dataset from Serpelloni et al., 2022 as a reference. Our strain map results do not differ significantly from those previously presented along the Apennines (Di Luccio et al., 2022; Nucci et al., 2025b; Palano, 2015).

Another important observation, primarily emerging from Paragraphs 3.7.6. and 4.6., is that the greatest difficulty in determining the axes of maximum and minimum deformation arises when the dilatation rate falls between -10 and 10 nanostrain/yr. Such low deformation on surface can be attributed to various factors other than tectonics (see Paragraph 3.7.6). Analyses of deformation axes are certainly more reliable in areas experiencing higher strain rates (Paragraph 2.7.1).

5.3. Seismotectonic comparative analysis

5.3.1. Strain and Stress Patterns Across Orogenic Belts

The power of this thesis is that the study areas is different in each chapter, also following similar approach and this permits a discussion on different seismotectonic settings and which are the geodynamic processes proposed in literature.

We describe 4 main extensional domain and their relationship with the compressional domain:

1. In the Tibetan Plateau, normal faulting is widespread and is systematically accompanied by strike-slip faulting, as evidenced by both FMSs and active surface faults (Dasgupta et al., 2021; Zhang and Wang, 2007). This extensional domain spans ~1,000 km in the north-south direction and ~1,300 km in the west-east direction. While compressional stresses are predominantly directed N-S, the extensional ones are oriented W-E, perpendicular to the average strike of the orogen. In contrast, the primary compressional domain is represented by the Himalayan Arc, where high-magnitude earthquakes—reaching up to M 8—occur along the Main Himalayan Thrust (Dal Zilio et al., 2020, Paragraph 2.4.2). This major detachment fault dips northward at an angle of approximately 5–6° and features localized ramp structures described by numerous authors (Panda and Lindsey, 2024). In this tectonic setting, the maximum horizontal stress (σ_{Hmax}) trajectories align with the minimum horizontal strain (ε_{Hmin}). Medium-to-high dilatation strain rates (~40 nanostrain/yr) remain relatively constant across the Tibetan Plateau, extending northward as far as the Tarim Basin – Altyn Tagh region (Figure 2.5). Moreover, the Tibetan Plateau exhibits both N-S contractional strain values and stress ratio values close to 0 (Figure 2.6), indicating similar magnitudes of σ_1 and σ_2. These two factors demonstrate that compressional stress and its associated contractional effects are not confined to the Himalayan Arc alone but persist within the plateau itself.
2. In the Pyrenees, normal faulting is well-documented through both surface faults (Paragraph 3.4.2) and focal mechanism solutions (FMSs) (Paragraph 3.4.3). Strike-slip

faulting, however, is limited to the easternmost part of the orogen (Paragraph 3.6.1). The extensional domain forms a narrow W-E oriented strip, ~100 km wide in the N-S direction and extending ~400 km from west to east. The primary compressional domain is no longer active, as the Pyrenean orogeny resulted from the Iberian-Eurasian collision during the Mesozoic-Cenozoic Alpine orogeny (Lacan and Ortuño, 2012). The maximum horizontal stress (σ_{Hmax}) trajectories are oriented NNW-SSE, while the minimum horizontal strain (ε_{Hmin}) axes are poorly constrained in the region. This uncertainty is attributed to the very low dilatation strain rates (< 10 nanostrain/yr) recorded at the surface by GNSS stations (Paragraph 3.5.2). The stress ratio is generally higher than 0.75 (Paragraph 3.6.1.1), with σ_1 often plunging at angles close to 80–90°, indicating a dominant vertical stress axis compared to the horizontal ones.

3. In the Betic Cordillera, seismicity is predominantly characterized by FMSs indicating normal fault kinematics. The extensional domain extends ~150 km in the N-S direction and ~250 km in the W-E direction. The compressional domain is located to the south, in the Alboran segment, where both strike-slip and thrust faulting occur (Paragraphs 3.4.2 and 3.4.3). In both the compressional and extensional domains, seismicity is generally of low to moderate magnitude (Paragraph 3.4.2). The maximum horizontal stress (σ_{Hmax}) trajectories and the minimum horizontal strain (ε_{Hmin}) are consistently oriented NW-SE throughout the Betic Cordillera. The dilatation strain rate is moderate, ranging from 10 to 18 nanostrain per year. As in other regions, σ_1 remains consistently subvertical, with a stress ratio greater than 0.75.
4. Along the Apennines, focal mechanism solutions (FMSs) (Paragraph 4.4.4) and fault kinematics (Paragraph 4.4.1) predominantly indicate normal faulting. Only in a few cases do strike-slip focal solutions reveal fault complexities. The extensional domain extends along the entire length of the Apennine orogen, forming a belt that varies in width from ~40 km to ~90 km. The compressional domain is primarily characterized by moderate-to-high magnitude events (Lavecchia et al., 2024b), with a compressional direction consistently perpendicular to the orogen. This direction rotates from NE-SW in the Northern Apennines to NW-SE in the Calabria region (Polonia et al., 2011). In Italy, stress inversion is not performed, as multi-source strain rate maps and FMSs are considered sufficient to describe the seismotectonic framework of the region. The extensional domain is mainly characterized by an ε_{Hmax} direction perpendicular to the orogen, as confirmed by geological, seismological, and geodetic data, all of which consistently indicate the same orientation for the ε_{Hmax} axes. Dilatation values range between ~50 and ~60 nanostrain/yr.

Observing the strain directions, we notice a distinctive pattern along the Apennines of the Italian Peninsula. Here, the ε_{Hmin} direction in the compressional domain aligns parallel to the

ε_{Hmax} direction in the extensional domain (Paragraph 4.5.2). This behaviour contrasts with other cases reported in the Tibet-Himalaya and Betic Cordillera regions. In the Pyrenees, no comparison can be made, as there is no evidence of recent active compressional domain.

In the Tibetan Plateau, both the stress and strain fields indicate ongoing extensional/stretching affecting the entire region, accompanied by compressional/contraction processes. This widespread contraction may explain the differences observed in the seismotectonic setting of Italy. We believe that, in the Tibetan Plateau, the crust is unable to stretch effectively to dissipate topographic loading (England and Houseman, 1989), except in the W-E direction, precisely because the shortening process is still ongoing in the N-S direction. This contrasts with Italy, where contractional deformation in the extensional domain (ε_{Hmin} values) are very low and only occur locally (Figure 4.6).

Along the Betic Cordillera, the strain map reveals a strong stretching component with no significant contraction. The stretching direction forms an almost 90° angle with the contraction recorded in the compressive domain further south in the Alboran Segment (Paragraphs 3.6.1.2 and 3.6.3.2). In this case, fault activity appears to be primarily driven by gravitational forces in response to the rapid uplift of the Betic Cordillera (Braga et al., 2003). Stress inversion further supports this interpretation, revealing a predominantly low value for sub-horizontal σ_2 and σ_3 along the orogen, as indicated by a stress ratio greater than 0.75 (Paragraph 3.6.1.1).

5.3.2. Indenter-escape tectonics across scale

In Paragraph 2.8, we describe the geodynamic processes shaping the Himalaya-Tibet region, applying the same approach in Paragraph 3.7.3 for the Alboran domain. In the Tibetan Plateau, the observed stress-strain patterns strongly support the indenter-escape tectonic model proposed by Tapponnier et al., 1986. Similarly, in the Eastern Betics, an indenter-like deformation is clearly recognizable. Despite the significant differences in size and spatial extent between the two regions, the indenter-like behavior is evident in both cases. However, a key distinction lies in the presence of escape tectonics, which is a dominant feature in the Tibetan Plateau but much less evident in the Eastern Betics.

The primary difference between these two regions—Himalaya-Tibet and the Eastern Betics—is the crustal thickness. In the Himalaya-Tibet region, the crust reaches an estimated thickness of ~70 km, whereas in the Eastern Betics, it varies from 4–6 km in hyperextended domains to 18–20 km in thicker zones.

In both cases, the indenter-like deformation is primarily controlled by the contrast in crustal rigidity between the colliding lithospheres. In the Himalaya-Tibet region, this contrast arises

from the rigid Indian plate colliding with the thickened Tibetan crust, while in the Alboran domain, it results from the interaction between the rigid African plate and the hyperthinned Alboran crust. This contrast in mechanical properties is identified as the preconditioning factor for the development of indenter-like deformation.

However, a fundamental difference between the two regions emerges in the mechanical behavior of the crust undergoing indentation—namely, the Tibetan Plateau and the central-northern sector of the Alboran Sea. In Tibet, stress data indicate that the vertical stress axis is consistently high and alternates between being σ_1 (maximum compressive stress) and σ_2 (intermediate stress), depending on local conditions (Paragraph 2.7.2). Conversely, in the Alboran Sea, the vertical stress axis is invariably σ_2, as also demonstrated by the predominance of strike-slip faulting in the region, as reported by Gómez De La Peña et al., 2018.

This difference highlights the influence of escape tectonics in the Tibetan Plateau, where crustal deformation is significantly affected by lateral extrusion. Furthermore, the presence of high vertical stress values in Tibet suggests that topographic loading plays a key role in controlling deformation, requiring stress dissipation through normal faulting. In contrast, in the Alboran Sea, the absence of significant vertical loading and escape tectonics implies a different stress regime, where strike-slip faulting dominates as the primary mode of crustal deformation.

5.4. The Complementary Role of Geodetic, Seismological, and Geological Data

One of the most compelling aspects of this study is its multidisciplinary approach, which underscores the importance of understanding data and what they represent. From the experience gained through the research presented in this thesis, we emphasize that each dataset describes a specific phenomenon and is particularly valuable because of its ability to precisely capture that phenomenon.

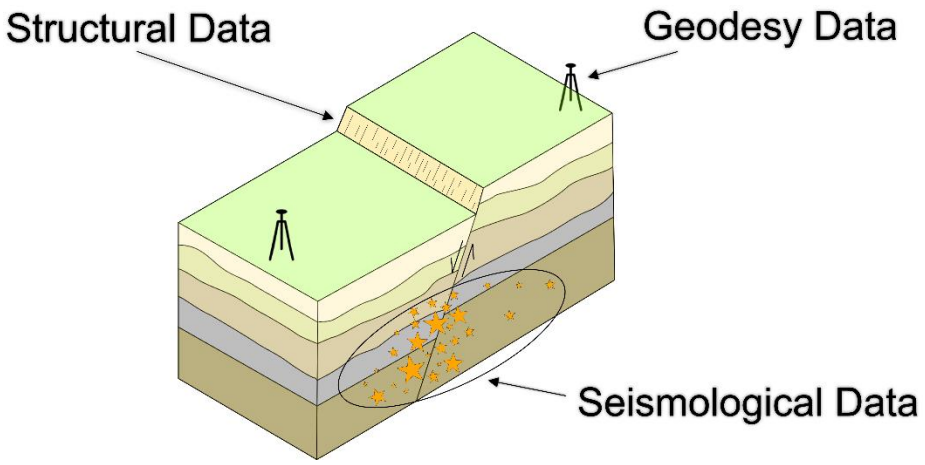


Figure 5.1: Schematic representation of spatial relative distribution of Geological, Geodetic and Seismological data

Geodetic data excellently describe surface deformation, making them fundamental for analysing tectonic processes. However, it is crucial—and sometimes challenging—to distinguish non-tectonic phenomena that may influence GNSS stations movements. As discussed in Paragraph 3.7.5, GNSS stations can also detect aseismic tectonic deformations, which are not recorded by seismological data due to the absence of seismic events. Additionally, the temporal coverage of geodetic data varies significantly. In the best cases, records date back to the 1980s, but a tectonically relevant coverage in many areas only became available from the 2000s onwards.

Seismological data have the great advantage of providing insights into strain and stress conditions within the crust, as they describe subsurface deformation processes. Historical seismic data exist since the early 1900s, but their quality is generally poor because they were not derived from direct instrumental observations but rather from macroseismic intensity fields.

Geological data, on the other hand, have the longest temporal coverage, as they record surface tectonic deformation over geological timescales. However, their precision in dating events is often low due to the inherent limitations in determining the exact timing of past deformations. Nevertheless, geological data are the only means to accurately determine the true orientation of active faults, allowing for a more comprehensive discussion of fault geometry within a seismotectonic and geodynamic framework.

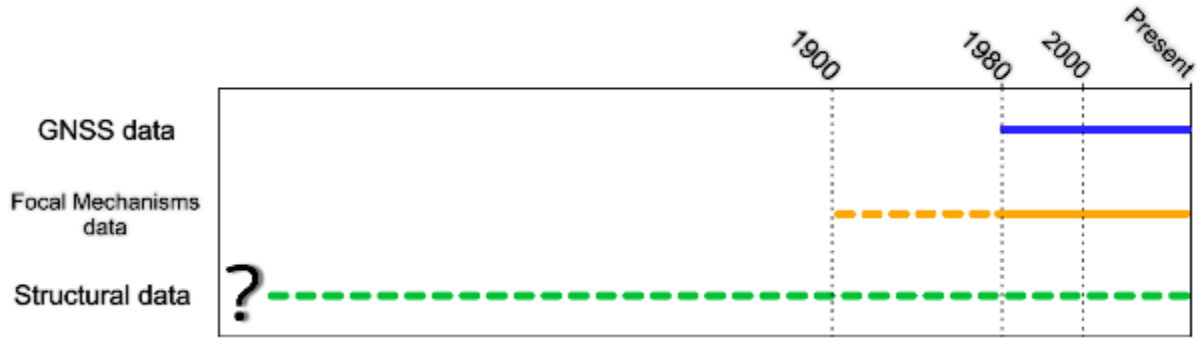


Figure 5.2: Temporal distribution of Geological, Seismological and Geodetic data

Another key aspect to consider is the spatial distribution of the data, which varies significantly depending on the type of data being analyzed. For geological data, there are only a few cases where we have sufficient information to reliably determine a homogeneous geological strain in each area. Along the Apennines, such analyses are possible thanks to the extensive work of Lavecchia et al. (2022, 2024). However, in most other regions of the world, this level of data coverage is lacking. Fault kinematics also influence the quantity of data that can be collected. Normal faults tend to preserve kinematic indicators more effectively than strike-slip or thrust faults. Similarly, geodetic results depend on the availability of GNSS velocity measurements. The distance between stations is rarely as close as 20 km and is more commonly around 50–60 km. This leads to large, interpolated areas where the strain rate is not directly constrained by real data, as observed in the Tarim Basin or specific regions of Tibet (see Chapter 2). The distribution of seismicity is another limiting factor, as it often occurs in clustered patterns. This poses a challenge when performing formal stress inversions, especially when aiming to obtain representative stress values across an entire region.

Nevertheless, the continuous integration of geodetic and seismological datasets is progressively improving both the spatial and temporal resolution of such analyses, thereby enhancing the overall effectiveness of the approach.

This thesis advocates for a multidisciplinary approach that enables an effective methodology for cross-referencing different datasets. It also highlights the necessity of recognizing that each type of data describes a specific process and has unique capabilities. By integrating geodetic, seismological, and geological data, this study demonstrates how combining different perspectives can lead to a more complete and robust understanding of tectonic deformation and seismic hazard.

5.5. Concluding remarks

In this PhD thesis, we present and discuss the application of a multidisciplinary approach to seismotectonic studies, integrating geological, geodetic, and seismological data to analyse stress and strain fields across different tectonic settings. The primary objective is to construct a reliable and constrained deformation model that summarizes the structural and geodynamic evolution of various regions, including high-strain (Himalaya-Tibet), low-strain (Iberia and Northwest Africa), and intermediate-strain (Apennines) domains. This comprehensive framework enhances our understanding of active deformation processes and their implications for seismic hazard assessment.

In the Himalaya and Iberia, we updated the focal mechanism and GNSS velocity databases to enhance the spatial resolution and improve the reliability of the results. In both cases, we have highlighted new seismotectonic and geodynamic aspects by calculating crustal stress and strain rate in the most accurate way possible based on the updated datasets.

In Italy we obtain a comparative analysis between geological, geodetic and seismological data. The aim of this work is to understand the power of each data and what it represents. The comparative analysis better constrain the seismotectonic assessment and the seismic hazard, leading to a discussion on the activity of normal faults on the Apennines.

As seen in this thesis the use of stress-strain analysis is essential in these geodynamic contexts, where traditional methods may be limited by complex tectonic interactions, heterogeneous crustal properties, and variable seismicity rates. By incorporating multiple data sources, we overcome these limitations and provide new insights into seismotectonic assessments.

Specifically:

In the Himalaya-Tibet region (Chapter 2), a comprehensive analysis of GNSS and focal mechanism data reveals complex deformation, characterized by arc-parallel extension along the Himalayan Arc and a coexistence of strike-slip and normal faulting across Tibet. Stress and strain rate patterns indicate a highly elastic crust influenced by deep tectonic processes, with a clockwise rotation at approximately 31°N reflecting the control of the underthrusting Indian Plate; south of this boundary, compression is driven by basal drag, while northward, escape tectonics result in eastward movement of the Tibetan Plateau. These findings enhance our understanding of the intricate interplay between surface and deep processes in driving regional deformation and provide a robust framework for future research in similar tectonic settings.

In Iberia and Northwest Africa (Chapter 3), our analysis demonstrates how the methodology used in the Himalaya-Tibet region can also be applied in low-strain areas. In fact, stress inversion results align with the main active faults reported in regional databases, underscoring the quality of the methodology and the newly presented focal mechanism database. With this comprehensive overview and the new GNSS velocity and strain rate field computations, we were able to describe the complex interaction between the Eurasian and African plates, in fact strain is predominantly concentrated along this boundary, with stresses in the Atlantic segment directly transmitted to Iberia and those in the Alboran and Mediterranean segments absorbed by thinned continental crust. The aseismic Gibraltar Block exhibits the highest degree of shortening, likely driven by terminal subduction with rollback and mantle flow. In contrast, tectonically active intraplate regions show low horizontal strain rates, suggesting that vertical stress is the dominant mechanism in these areas.

In the Italian Peninsula (Chapter 4), a novel multi-source approach has been implemented, integrating structural geology, GNSS data, and focal mechanism solutions to characterize strain patterns. The similarity found in the maximum deformation axes between present-day strain patterns (GNSS and focal mechanism solutions) and those associated with long-term deformation suggests a remarkable continuity in the regional kinematics and eastward propagation of the extensional domain during the last 3.5 million years.

While the methodologies applied in this study are robust, their results remain dependent on the quality and distribution of seismic, geodetic, and structural datasets. The uncertainty assessment of stress and strain models is therefore a fundamental aspect of this research, ensuring that interpretations remain constrained and geologically meaningful.

In conclusion, this thesis presents a novel multi-parametric approach that significantly improves our ability to analyse seismotectonic processes deforming compressional and extensional domains. The integration of geological, geodetic, and geophysical data allows for a deeper understanding of crustal deformation and its implications for earthquake generation. This innovative framework paves the way for further investigations on different areas in trying to improve the methodology and the seismotectonic and geodynamic knowledge. The results of these studies represent a significant advancement in the offering new methodologies and applications that will foster further progress within the scientific community.

6. Scientific Production

6.1. Published articles

6.1.1. Paleo-Earthquake Fingerprints and Along-Strike Slip Variation of the Silent Mt. Morrone Normal Fault (Central Italy): A Structural-Geochemical Approach

Bello S., Galli P., Perna M.G., Peronace E., Messina P., Rosatelli G., Andrenacci C., Lavecchia G., Pietrolungo F., Consalvo A., Mouslopoulou V., Brozzetti F.

February 2025, Geochemistry, Geophysics, Geosystems 26(2) - DOI: 10.1029/2024GC011868

Abstract:

This study provides insights into the tectonic evolution of the normal Mt Morrone Fault System (MMFS) in Central Italy and highlights the utility of multidisciplinary approaches in reconstructing the seismic history of dormant fault systems. The MMFS comprises two parallel normal faults that traverse the western slope of Mt. Morrone, and although the system can produce M > 6 earthquakes, it has been aseismic in post Roman times. Here, we combine geochemical analysis of carbonate fault-scarp samples with new structural fault data and Lidar-based topographic analysis to provide new constraints on fault geometries and kinematics, the paleo-earthquake history of MMFS since the Last Glacial Maximum and its slip rates. Structural analysis reveals kinematic similarities between the two parallel strands, reflecting their response to the same stress regime. Rare Earth Elements analyses on 53 limestone samples reveal a minimum of eight concentration fluctuations upscarp, here interpreted as tectonic exhumation of the fault scarp due to post LGM earthquakes. Slip per event ranges from 30 to 110 cm typical of earthquakes with 6.3 ≤ M ≤ 6.8. Lidar analysis reveals triangular slip profiles on both fault strands. We estimate that an earthquake with an average M = 6.5–6.6 would have a recurrence interval of ~2,125 ± 125 years. Slip rates were calculated to be 0.5–0.65 mm/yr on the lower and 0.65–0.7 mm/yr on the upper fault strand, with the combined system having slip rates of 0.62–0.69 mm/yr. Our findings indicate that both strands of the MMFS are active and accumulate slip interdependently, a finding that is critical for seismic hazard assessment.

6.1.2. QUIN 2.0 - new release of the QUaternary fault strain INdicators database from the Southern Apennines of Italy

Lavecchia G., Bello S., Andrenacci C., Cirillo D., Pietrolungo F., Talone D., Ferrarini F., de Nardis R., Galli P., Faure Walker J., Sgambato C., Menichetti M., Monaco C., Gambino S., De Guidi G., Barreca G., Carnemolla F., Brighenti F., Giuffrida S., Pirrotta C., Carboni F., Ferranti L., Valoroso L., Toscani G., Barchi M. R., Roberts G., Brozzetti F.

February 2024, Scientific Data 11(1) - DOI: 10.1038/s41597-024-03008-6

Abstract:

QUIN database integrates and organizes structural-geological information from published and unpublished sources to constrain deformation in seismotectonic studies. The initial release, QUIN1.0, comprised 3,339 Fault Striation Pairs, mapped on 445 sites exposed along the Quaternary faults of central Italy. The present Data Descriptor introduces the QUIN 2.0 release, which includes 4,297 Fault Striation Pairs on 738 Structural Sites from southern Italy. The newly investigated faults span ~500 km along the Apennines chain, with strikes transitioning from ~SE to ~SW and comprehensively details Fault Striation Pairs' location, attitude, kinematics, and deformation axes. Additionally, it offers a shapefile of the fault traces hosting the data. The QUIN 2.0 release offers a significant geographic extension to the QUIN 1.0, with comprehensive description of local geometric-kinematic complexities of the regional pattern. The QUIN data may be especially relevant for constraining intra-Apennine potential seismogenic deformation patterns, where earthquake data only offer scattered or incomplete information. QUIN's data will support studies aimed at enhancing geological understanding, hazard assessment and comprehension of fault rupture propagation and barriers.

6.1.3. Slowly Deforming Megathrusts within the Continental Lithosphere: A Case from Italy

Lavecchia G., Pietrolungo F., Bello S., Talone D., Pandolfi C., Andrenacci C., Carducci A., de Nardis R.

December 2023, GSA Today 34(1):4 - DOI: 10.1130/GSATG573A.1

Abstract:

The Late Pliocene–Quaternary Outer Thrust System of the Apennine-Maghrebides fold-and-thrust belt extends ~2000 km from northern Italy to Sicily. Its northernmost arc is seismically active and represents a test case to study geometries and seismogenesis of slowly deforming megathrusts developed within the continental lithosphere. Two distinct SW-dipping reverse shear zones (T1 and T2) in the Outer Thrust System of eastern Central Italy have been recently unveiled thanks to geological and integrated seismological information. These shear zones penetrate the Adria continental lithosphere to a maximum depth of ~60 km, with an outward convex shape associated with an outwarddiverging radial pattern.

6.1.4. Reappraisal and Analysis of Macroseismic Data for Seismotectonic Purposes: The Strong Earthquakes of Southern Calabria, Italy

Andrenacci C., Bello S., Barbano M.S., de Nardis R., Pirrotta C., Pietrolungo F., Lavecchia G.

July 2023, Geosciences 13(7):212 - DOI: 10.3390/geosciences13070212

Abstract:

In tectonically active areas, such as the Italian peninsula, studying the faults responsible for strong earthquakes is often challenging, especially when the earthquakes occurred in historical times. In such cases, geoscientists need to integrate all the available information from historical reports, surface geology, and geophysics to constrain the faults responsible for the earthquakes from a seismotectonic point of view. In this paper, we update and review, according to the EMS-98 scale, the macroseismic fields of the five main events of the 1783 Calabria sequence (5, 6, and 7 February, 1 and 28 March, Mw 5.9 to 7.1), two other destructive events within the same epicentral area of the 1783 sequence (1791, Mw 6.1 and 1894, Mw 6.1), plus the Messina Strait 1908 earthquake (Mw 7.1). For the 1783 seismic sequence, we also elaborate an updated and new catalog of coseismic effects. The new macroseismic fields were analyzed using a series of MATLAB algorithms to identify (1) the unitarity of the field or its partitioning in sub-sources and (2) the field and sub-fields' main elongation. A collection of earthquake scale laws from literature was used to compute the average source parameters (length, width, and area) with their range of variability, and an elliptical map-view representation of the source geometry was calculated and made available. The analyses of such data allow us to speculate on the earthquakes/faults association, as well as propose new interpretations and reconstruct the space–time evolution of the significant southern Calabria seismic sequences in the last five centuries.

6.2. Conference Oral presentations

6.2.1. Crustal deformation at the Himalaya region and South Tibet: a 3D structural model from a multidisciplinary perspective

Pietrolungo F., Palano M., Sparacino F., Cirillo D., De Nardis, R. & Lavecchia G.

Presented to: BEGEO Scientists 2nd conference 2023

Abstract:

The Nepal and India regions are highly complex tectonically. While there is a strongly collisional zone accommodated by the Main Himalayan Thrust and its splays, in close proximity to this domain, there are several examples of strike-slip and extensional focal mechanisms. Consequently, the area is highly active, but the existing seismic networks, with limited coverage, do not allow for accurate localization of these events, especially regarding depth constraints. However, in the months following the 2015 Gorkha event with a magnitude of 7.8 Mw, the NAMASTE project provided a well-located sequence that allows us to reconstruct the geometry of the active thrusts in the area. On the other hand, in 2011, further west, the region of Sikkim was struck by another moderate-magnitude event (6.9 Mw). In this sequence, most of the focal mechanisms are observed to be right-lateral strike-slip. The majority of authors (Dasgupta et al., 2021) attribute these right-lateral movements to deep strike-slip lineaments within the Indian crust being underthrust. These two seismic sequences provide an excellent opportunity to reconstruct the three-dimensional tectonic setting, both at the shallow and deeper levels, and to understand the resulting surface deformation using processed GPS data and so clarify the role of trascurrence on the Main Himalayan Thrust.

6.2.2. Himalaya-Tibet crustal stress and strain

Pietrolungo F., Palano M., Madarieta-Txurruka A., Srivastava E., Sparacino F., Sulli A., Parrino N., Andrenacci C., Cirillo D., Bello S. and Lavecchia G.

Presented to: SGI-SIMP (Società Geologica Italiana – Società Italiana di Mineralogia e Petrografia) Congresso 3-5 Settembre 2024 "Geology for a Sustainable management of our Planet"

Abstract:

The India-Eurasia collision zone is one of the most complex and destructive collisional zones globally. The Indian plate converges with the Tibetan Plateau to the north, exhibiting a convergence rate increasing from ~16.5 mm/yr (Kumar et al., 2023b) in the west to ~21 mm/yr in the Bhutan region (Dal Zilio et al., 2020). Compression is primarily accommodated

by the basal detachment commonly referred to as the Main Himalayan Thrust, whose surface expression is represented by the Main Frontal Thrust. To describe the destructiveness of this zone, historical and instrumental events such as the 1505 Lo Mustang earthquake (8.2-8.8 Mw), the 2015 Gorkha earthquake (7.8 Mw), and the 1714 Bhutan earthquake (8.1 Mw) are remembered. The Tibetan region, on the other hand, is primarily affected by extensional earthquakes that accommodate a west-east directed extension with moderate to high magnitude earthquakes, ranging between 5.5 Mw and 6.8 Mw, such as the 2008 Xizang earthquake (6.7 Mw) and the 2008 Damxung earthquake (6.3 Mw) on the Yadung-Gulu rift. Active strike-slip faults are also present, bordering much of the Tibetan plateau and intersecting its central zones (Wang and Barbot, 2023). Notable examples include the Altyn-Tagh fault, the Karakoram fault, and the Gyaring Co fault. Although the region is particularly affected by high rates of seismicity, seismic and geodetic networks are not well-distributed. In such cases, a multidisciplinary approach allows for drawing from several data types to obtain a more comprehensive understanding of the seismotectonic setting. We have computed a new velocity field by processing continuous stations throughout the Tibetan-Nepal-Indian territory. Additionally, through a set of Helmert transformations, all pre-existing velocity fields documented in the literature have been merged into a unified large-scale velocity field. This unified velocity field constructed has been utilized to compute a fine strain rate map over the entire study area. A unified catalog for instrumental seismicity and focal mechanisms, registered in the area since 1980, have been collected too. Such a unified catalog is the outcome of a meticulous compilation of data sourced from various national and international catalogues, aimed to improving the completeness magnitude of the area (approximately 4 Mw). The same care has been applied to gather historical events preceding 1980, ensuring a comprehensive understanding of the seismic history (Cheng et al., 2017). A complete understanding of the deformation pattern can be achieved by comparing strain rate maps with focal mechanism inversions. This approach allows us to compare stress and strain and to discriminate the contributions of several sources of different kinematics.

6.2.3. Crustal strain-rate and stress field in the Himalaya-Tibet Region

Pietrolungo F., Palano M., Madarieta-Txurruka A., Srivastava E., Sparacino F., Sulli A., Parrino N., Andrenacci C., Cirillo D., Bello S. and Lavecchia G.

Presented to: Workshop CRUST 2024 - Chieti

Abstract:

In tectonically active areas, such as the Italian peninsula, studying the faults responsible for strong earthquakes is often challenging, especially when the earthquakes occurred in

historical times. In such cases, geoscientists need to integrate all the available information from historical reports, surface geology, and geophysics to constrain the faults responsible for the earthquakes from a seismotectonic point of view. In this paper, we update and review, according to the EMS-98 scale, the macroseismic fields of the five main events of the 1783 Calabria sequence (5, 6, and 7 February, 1 and 28 March, Mw 5.9 to 7.1), two other destructive events within the same epicentral area of the 1783 sequence (1791, Mw 6.1 and 1894, Mw 6.1), plus the Messina Strait 1908 earthquake (Mw 7.1). For the 1783 seismic sequence, we also elaborate an updated and new catalog of coseismic effects. The new macroseismic fields were analyzed using a series of MATLAB algorithms to identify (1) the unitarity of the field or its partitioning in sub-sources and (2) the field and sub-fields' main elongation. A collection of earthquake scale laws from literature was used to compute the average source parameters (length, width, and area) with their range of variability, and an elliptical map-view representation of the source geometry was calculated and made available. The analyses of such data allow us to speculate on the earthquakes/faults association, as well as propose new interpretations and reconstruct the space–time evolution of the significant southern Calabria seismic sequences in the last five centuries.

6.1. Conference Poster presentations

6.1.1. Crustal deformation at the Himalaya region and South Tibet: a 3D structural model from a multidisciplinary perspective

Pietrolungo F., Palano M., Sparacino F., Cirillo D., De Nardis, R. & Lavecchia G.

Presented to: SGI-SIMP-SOGEI-AIV (Società Geologica Italiana – Società Italiana di Mineralogia e Petrografia – Società Geochimica Italiana – Associazione Italiana di Vulcanologia) Congresso Congiunto 2023 "The Geoscience paradigm: resources, risks and future perspectives"

Abstract:

One of the most reliable techniques for defining deformation rates is GNSS technology, which can provide an accuracy of less than 1 mm. In addition, significant progress has been made in 3D modelling to evaluate and connect seismogenic faults and seismicity distribution (De Nardis et al., 2022). Our primary objective is to integrate all available GNSS measurements in the literature (Wang and Shen, 2020) and combine them with our processing results for the Himalayan region and its surrounding areas in order to understand the long-term velocities and deformation rates of Quaternary active faults. The region is

characterized by a long history of seismicity (Dasgupta et al., 2021), providing abundant data which are useful to construct a highly detailed 3D structure accommodating active compressional and extensional deformations. To better estimate the geometry of the Main Himalayan Thrust, its splays (Main Frontal Thrust, Main Central Thrust, and South Tibetan Detachment) and other high-angle normal faults, we collect a large number of crustal-scale geological and tomographic cross-sections, from the literature, in a 3D environment using ArcGIS and MOVE software. Contextualizing the strain calculated from continuous measurements of permanent GNSS stations to the reconstructed 3D surface fault model will be the major challenge of this work. This could allow us to answer major questions about lithospheric deformation, such as the compression-distension coupling in the Himalayan-Tibetan region. Furthermore, it could help us to identify areas of deep detachment or high-angle faults, where a particularly high strain rate is detected along with a lack of released seismicity (Sparacino et al., 2020).

6.1.2. The November 9, 2022, compressional seismic sequence (Mw 5.5) - another piece of information to the 3D seismotectonic fault model of the coastal Marche-Adriatic offshore area (Italy)

Pietrolungo F., Palano M., Sparacino F., Cirillo D., De Nardis, R. & Lavecchia G.

Presented to: Tectonic Studies Group 2023 in Leeds

Abstract:

The coastal Marche-Adriatic region of eastern-Central Italy has been long questioned in the literature whether being active or not and, in case of activity, whether under a compressional or a strike-slip regime (De Nardis et al., 2022 with references). Our recent paper integrates high-quality seismological data from a local network with long-term geological constraints to build a 3D crust-scale seismotectonic fault model. Late Pliocene-to-Quaternary NE-verging fold-and-thrust structures develops at the hangingwall of the Adriatic Basal Thrust (ABT), a SW-dipping reverse shear zones which penetrate across the entire crust and is seismogenic at upper and lower crust depths.

The November 9, 2022 seismic sequence activated one offshore ABT upper crustal splay with pure compressional kinematics. Two major events (Mw 5.5 and 5.2) enucleated within 1 minute, at depths of ~5 km and ~7.5 km, respectively, and ~8 km away in map view. At a depth of a few kilometres, the seismogenic thrust intercepts two deep extraction wells (Pesaro Mare 4 and Bice 1), re-opening the question of triggered and induced seismicity. Geological section, serial hypocentral cross-sections, focal mechanisms, and available

information from exploration wells are used to build a detailed nonplanar 3D geometric and kinematic fault model of the structures responsible for the sequence and to test its fits with the previously built regional model. Preliminary observations highlight a synchronous activity of the upper crust segment activated by the sequence with that of surrounding multi-depth fault structures, and Coulomb stress scenarios are built for analysing such an aspect.

7. References

- *Adinolfi, G.M., De Matteis, R., De Nardis, R., Zollo, A., 2022. A functional tool to explore the reliability of micro-earthquake focal mechanism solutions for seismotectonic purposes. Solid Earth 13, 65–83. https://doi.org/10.5194/se-13-65-2022*
- *Aikman, A.B., Harrison, T.M., Lin, D., 2008. Evidence for Early (> 44 Ma) Himalayan Crustal Thickening, Tethyan Himalaya, southeastern Tibet. Earth Planet. Sci. Lett. 274, 14–23. https://doi.org/10.1016/j.epsl.2008.06.038*
- *Aki, K., Richards, P.G., 2002. Quantitative Seismology, 2nd Ed., Quantitative Seismology.*
- *Alexandre, P., 1990. Les séismes en Europe occidentale de 394 à 1259 Nouveau catalogue critique. Obersavoire R. Belg.*
- *Alfaro, P., Delgado, J., De Galdeano, C.S., Galindo-Zaldívar, J., García-Tortosa, F.J., López-Garrido, A.C., López-Casado, C., Marín-Lechado, C., Gil, A., Borque, M.J., 2008. The Baza Fault: a major active extensional fault in the central Betic Cordillera (south Spain). Int. J. Earth Sci. 97, 1353–1365. https://doi.org/10.1007/s00531-007-0213-z*
- *Ali, S.M., Shanker, D., 2017. Study of seismicity in the NW Himalaya and adjoining regions using IMS network. J. Seismol. 21, 317–334. https://doi.org/10.1007/s10950-016-9603-7*
- *Alonso, I., García-Olalla, C., 1997. Mineral Composition of Soils and Vegetation from Six Mountain Grassland Communities in Northern Spain. J. Sci. Food Agric. 73, 200–206. https://doi.org/10.1002/(SICI)1097-0010(199702)73:2<200::AID-JSFA701>3.0.CO;2-L*
- *Altamimi, Z., Métivier, L., Rebischung, P., Rouby, H., Collilieux, X., 2017. ITRF2014 plate motion model. Geophys. J. Int. 209, 1906–1912. https://doi.org/10.1093/gji/ggx136*
- *Altamimi, Z., Rebischung, P., Métivier, L., Collilieux, X., 2016. ITRF2014: A new release of the International Terrestrial Reference Frame modeling nonlinear station motions. J. Geophys. Res. Solid Earth 121, 6109–6131. https://doi.org/10.1002/2016JB013098*
- *Alvarez, W., Cocozza, T., Wezel, F.C., 1974. Fragmentation of the Alpine orogenic belt by microplate dispersal. Nature 248, 309–314. https://doi.org/10.1038/248309a0*
- *Alvarez-Marron, J., Rubio, E., Torne, M., 1997. Subduction-related structures in the North Iberian Margin. J. Geophys. Res. Solid Earth 102, 22497–22511. https://doi.org/10.1029/97JB01425*
- *Alves, T.M., 2024. Networks of geometrically coherent faults accommodate Alpine tectonic inversion offshore southwestern Iberia. Solid Earth 15, 39–62. https://doi.org/10.5194/se-15-39-2024*
- *Ambraseys, N.N., Vogt, J., Adams, R.D., 1991. The Algerian earthquake of 24 June 1910: A case history. Tectonophysics 193, 205–213. https://doi.org/10.1016/0040-1951(91)90200-C*
- *Anahnah, F., Galindo-Zaldívar, J., Chalouan, A., Pous, J., Ruano, P., Pedrera, A., Ruiz-Constán, A., Ahmamou, M., Benmakhlouf, M., Ibarra, P., Asensio, E., 2011. Crustal resistivity structure of the southwestern transect of the Rif Cordillera (Morocco): CRUSTAL STRUCTURE RIF CORDILLERA. Geochem. Geophys. Geosystems 12, n/a-n/a. https://doi.org/10.1029/2011GC003783*
- *Andrei Bala, Mircea Radulian, Dragos Toma-Danila, 2021. Present-day stress field pattern in the Vrancea seismic zone (Romania) deduced from earthquake focal mechanism inversion. Ann. Geophys. 64, PE660. https://doi.org/10.4401/ag-8632*
- *Andrenacci, C., Bello, S., de Nardis, R., Lavecchia, G., 2021. FAULT-STRIATION PAIR ANALYSIS (F-SPA) Tool. https://doi.org/10.5281/ZENODO.5910783*
- *Angelier, J., 1979. Determination of the mean principal directions of stresses for a given fault population. Tectonophysics 56, T17–T26. https://doi.org/10.1016/0040-1951(79)90081-7*
- *Angrand, P., Mouthereau, F., Masini, E., Asti, R., 2020. A reconstruction of Iberia accounting for Western Tethys–North Atlantic kinematics since the late-Permian–Triassic. Solid Earth 11, 1313–1332. https://doi.org/10.5194/se-11-1313-2020*
- *Antonio Avallone, Giulio Selvaggi, Elisabetta D'Anastasio, Nicola D'Agostino, Grazia Pietrantonio, Federica Riguzzi, Enrico Serpelloni, Marco Anzidei, Giuseppe Casula, Gianpaolo Cecere, Ciriaco D'Ambrosio, Prospero De Martino, Roberto Devoti, Luigi Falco, Mario Mattia, Massimo Rossi, Francesco Obrizzo, Umberto Tammaro, Luigi Zarrilli, 2010. The RING network: improvement of a GPS velocity field in the central Mediterranean. Ann. Geophys. 53. https://doi.org/10.4401/ag-4549*
- *Araque-Pérez, C.J., Mancilla, F., López-Comino, J.A., Stich, D., Morales, J., Teixido, T., 2025. New geological insights from legacy seismic sections: Decoding the Granada Basin (Spain). Mar. Pet. Geol. 174, 107294. https://doi.org/10.1016/j.marpetgeo.2025.107294*
- *Araque-Pérez, C.J., Teixidó, T., De Lis Mancilla, F., Morales, J., 2024. Reprocessing and interpretation of legacy seismic data using machine learning from the Granada Basin, Spain. Tectonophysics 885, 230414. https://doi.org/10.1016/j.tecto.2024.230414*
- *Arboleya, M.L., Teixell, A., Charroud, M., Julivert, M., 2004. A structural transect through the High and Middle Atlas of Morocco. J. Afr. Earth Sci. 39, 319–327. https://doi.org/10.1016/j.jafrearsci.2004.07.036*
- *Arche, A., López-Gómez, J., 1996. Origin of the Permian-Triassic Iberian Basin, central-eastern Spain. Tectonophysics 266, 443–464. https://doi.org/10.1016/S0040-1951(96)00202-8*
- *Armijo, R., Tapponnier, P., Mercier, J.L., Han, T., 1986. Quaternary extension in southern Tibet: Field observations and tectonic implications. J. Geophys. Res. Solid Earth 91, 13803–13872. https://doi.org/10.1029/JB091iB14p13803*
- *Asensio, E., Khazaradze, G., Echeverria, A., King, R.W., Vilajosana, I., 2012. GPS studies of active deformation in the Pyrenees: GPS active deformation in the Pyrenees. Geophys. J. Int. 190, 913–921. https://doi.org/10.1111/j.1365-246X.2012.05525.x*
- *Aurell, M., Fregenal-Martínez, M., Bádenas, B., Muñoz-García, M.B., Élez, J., Meléndez, N., De Santisteban, C., 2019. Middle Jurassic–Early Cretaceous tectono-sedimentary evolution of the southwestern Iberian Basin (central Spain): Major palaeogeographical changes in the geotectonic framework of the Western Tethys. Earth-Sci. Rev. 199, 102983. https://doi.org/10.1016/j.earscirev.2019.102983*
- *Avouac, J.-P., Ayoub, F., Leprince, S., Konca, O., Helmberger, D.V., 2006. The 2005, Mw 7.6 Kashmir earthquake: Sub-pixel correlation of ASTER images and seismic waveforms analysis. Earth Planet. Sci. Lett. 249, 514–528. https://doi.org/10.1016/j.epsl.2006.06.025*

- Ayala, C., Bohoyo, F., Maestro, A., Reguera, M.I., Torne, M., Rubio, F., Fernàndez, M., García-Lobón, J.L., 2016. Updated Bouguer anomalies of the Iberian Peninsula: a new perspective to interpret the regional geology. J. Maps 12, 1089–1092. https://doi.org/10.1080/17445647.2015.1126538
- Bai, L., Liu, H., Ritsema, J., Mori, J., Zhang, T., Ishikawa, Y., Li, G., 2016. Faulting structure above the Main Himalayan Thrust as shown by relocated aftershocks of the 2015 M_w 7.8 Gorkha, Nepal, earthquake. Geophys. Res. Lett. 43, 637–642. https://doi.org/10.1002/2015GL066473
- Banda, E., Santanach, P., 1992. The Valencia trough (western Mediterranean): An overview. Tectonophysics 208, 183–202. https://doi.org/10.1016/0040-1951(92)90344-6
- Baptista, M.A., Miranda, J.M., Batllo, J., 2014. The 1531 Lisbon Earthquake: A Tsunami in the Tagus Estuary? Bull. Seismol. Soc. Am. 104, 2149–2161. https://doi.org/10.1785/0120130316
- Baptista, M.A., Miranda, P.M.A., Miranda, J.M., Victor, L.M., 1998. Constrains on the source of the 1755 Lisbon tsunami inferred from numerical modelling of historical data on the source of the 1755 Lisbon tsunami. J. Geodyn. 25, 159–174. https://doi.org/10.1016/S0264-3707(97)00020-3
- Barchi, M.R., 2010. The Neogene-Quaternary evolution of the Northern Apennines: crustal structure, style of deformation and seismicity. J. Virtual Explor. 36. https://doi.org/10.3809/jvirtex.2010.00220
- Bartolome, R., Gracia, E., Stich, D., Martinez-Loriente, S., Klaeschen, D., De Lis Mancilla, F., Lo Iacono, C., Danobeitia, J.J., Zitellini, N., 2012. Evidence for active strike-slip faulting along the Eurasia-Africa convergence zone: Implications for seismic hazard in the southwest Iberian margin. Geology 40, 495–498. https://doi.org/10.1130/G33107.1
- Baruah, Santanu, Saikia, S., Baruah, Saurabh, Bora, P.K., Tatevossian, R., Kayal, J.R., 2016. The September 2011 Sikkim Himalaya earthquake Mw 6.9: is it a plane of detachment earthquake? Geomat. Nat. Hazards Risk 7, 248–263. https://doi.org/10.1080/19475705.2014.895963
- Basili, R., Kastelic, V., Demircioglu Tumsa, M.B., Garcia Moreno, D., Nemser, E.S., Petricca, P., Sboras, S.P., Besana-Ostman, G.M., Cabral, J., Camelbeeck, T., Caputo, R., Danciu, L., Domaç, H., Fonseca, J.F. de B.D., García-Mayordomo, J., Giardini, D., Glavatovic, B., Gulen, L., Ince, Y., Pavlides, S., Sesetyan, K., Tarabusi, G., Tiberti, M.M., Utkucu, M., Valensise, G., Vanneste, K., Vilanova, S.P., Wössner, J., 2013. European Database of Seismogenic Faults (EDSF). https://doi.org/10.6092/INGV.IT-SHARE-EDSF
- Beaumont, C., Jamieson, R.A., Nguyen, M.H., Lee, B., 2001. Himalayan tectonics explained by extrusion of a low-viscosity crustal channel coupled to focused surface denudation. Nature 414, 738–742. https://doi.org/10.1038/414738a
- Beaumont, C., Muñoz, J.A., Hamilton, J., Fullsack, P., 2000. Factors controlling the Alpine evolution of the central Pyrenees inferred from a comparison of observations and geodynamical models. J. Geophys. Res. Solid Earth 105, 8121–8145. https://doi.org/10.1029/1999JB900390
- Békési, E., Porkoláb, K., Wesztergom, V., Wéber, Z., 2023. Updated stress dataset of the Circum-Pannonian region: Implications for regional tectonics and geo-energy applications. Tectonophysics 856, 229860. https://doi.org/10.1016/j.tecto.2023.229860
- Ben-Menahem, A., Aboodi, E., Schild, R., 1974. The source of the great Assam earthquake — an interplate wedge motion. Phys. Earth Planet. Inter. 9, 265–289. https://doi.org/10.1016/0031-9201(74)90056-9
- Berthet, T., Ritz, J.-F., Ferry, M., Pelgay, P., Cattin, R., Drukpa, D., Braucher, R., Hetenyi, G., 2014. Active tectonics of the eastern Himalaya: New constraints from the first tectonic geomorphology study in southern Bhutan. Geology 42, 427–430. https://doi.org/10.1130/G35162.1
- Bertotti, G., Capozzi, R., Picotti, V., 1997. Extension controls Quaternary tectonics, geomorphology and sedimentation of the N-Appennies foothills and adjacent Po Plain (Italy). Tectonophysics 282, 291–301. https://doi.org/10.1016/S0040-1951(97)00229-1
- Bettinelli, P., Avouac, J.-P., Flouzat, M., Jouanne, F., Bollinger, L., Willis, P., Chitrakar, G.R., 2006. Plate Motion of India and Interseismic Strain in the Nepal Himalaya from GPS and DORIS Measurements. J. Geod. 80, 567–589. https://doi.org/10.1007/s00190-006-0030-3
- Bezzeghoud, M., Dimitro, D., Ruegg, J.C., Lammali, K., 1995. Faulting mechanism of the El Asnam (Algeria) 1954 and 1980 earthquakes from modelling of vertical movements. Tectonophysics 249, 249–266. https://doi.org/10.1016/0040-1951(95)00032-I
- Bhatia, S.C., Kumar, M.R., Gupta, H.K., 1999. A probabilistic seismic hazard map of India and adjoining regions. Probabilistic Seism. Hazard Map India Adjoin. Reg. 42.
- Bie, L., Ryder, I., Nippress, S.E.J., Bürgmann, R., 2014. Coseismic and post-seismic activity associated with the 2008 Mw 6.3 Damxung earthquake, Tibet, constrained by InSAR. Geophys. J. Int. 196, 788–803. https://doi.org/10.1093/gji/ggt444
- Bilham, R., 2019. Himalayan earthquakes: a review of historical seismicity and early 21st century slip potential. Geol. Soc. Lond. Spec. Publ. 483, 423–482. https://doi.org/10.1144/SP483.16
- Bilham, R., Gaur, V.K., Molnar, P., 2001. Himalayan Seismic Hazard. Science 293, 1442–1444. https://doi.org/10.1126/science.1062584
- Bilham, R., Larson, K., Freymueller, J., 1997. GPS measurements of present-day convergence across the Nepal Himalaya. Nature 386, 61–64. https://doi.org/10.1038/386061a0
- Billi, A., Cuffaro, M., Orecchio, B., Palano, M., Presti, D., Totaro, C., 2023. Retracing the Africa–Eurasia nascent convergent boundary in the western Mediterranean based on earthquake and GNSS data. Earth Planet. Sci. Lett. 601, 117906. https://doi.org/10.1016/j.epsl.2022.117906
- Bird, P., 2003. An updated digital model of plate boundaries. Geochem. Geophys. Geosystems 4, 2001GC000252. https://doi.org/10.1029/2001GC000252
- Bird, P., 1991. Lateral extrusion of lower crust from under high topography in the isostatic limit. J. Geophys. Res. Solid Earth 96, 10275–10286. https://doi.org/10.1029/91JB00370

- *Bonini, M., Corti, G., Donne, D.D., Sani, F., Piccardi, L., Vannucci, G., Genco, R., Martelli, L., Ripepe, M., 2016. Seismic sources and stress transfer interaction among axial normal faults and external thrust fronts in the Northern Apennines (Italy): A working hypothesis based on the 1916–1920 time–space cluster of earthquakes. Tectonophysics 680, 67–89. https://doi.org/10.1016/j.tecto.2016.04.045*
- *Booth-Rea, G., Azañón, J.-M., Azor, A., García-Dueñas, V., 2004. Influence of strike-slip fault segmentation on drainage evolution and topography. A case study: the Palomares Fault Zone (southeastern Betics, Spain). J. Struct. Geol. 26, 1615–1632. https://doi.org/10.1016/j.jsg.2004.01.007*
- *Borque, M.J., Sánchez-Alzola, A., Martin-Rojas, I., Alfaro, P., Molina, S., Rosa-Cintas, S., Rodríguez-Caderot, G., De Lacy, C., García-Armenteros, J.A., Avilés, M., Herrera-Olmo, A., García-Tortosa, F.J., Estévez, A., Gil, A.J., 2019. How Much Nubia-Eurasia Convergence Is Accommodated by the NE End of the Eastern Betic Shear Zone (SE Spain)? Constraints From GPS Velocities. Tectonics 38, 1824–1839. https://doi.org/10.1029/2018TC004970*
- *Bott, M.H.P., 1959. The Mechanics of Oblique Slip Faulting. Geol. Mag. 96, 109–117. https://doi.org/10.1017/S0016756800059987*
- *Bougrine, A., Yelles-Chaouche, A.K., Calais, E., 2019. Active deformation in Algeria from continuous GPS measurements. Geophys. J. Int. 217, 572–588. https://doi.org/10.1093/gji/ggz035*
- *Bouhadad, Y., 2001. [No title found]. J. Seismol. 5, 541–558. https://doi.org/10.1023/A:1012039900248*
- *Bouillin, J.-P., Durand-Delga, M., Olivier, Ph., 1986. Betic-Rifian and Tyrrhenian Arcs : Distinctive Features, Genesis and Development Stages, in: Developments in Geotectonics. Elsevier, pp. 281–304. https://doi.org/10.1016/B978-0-444-42688-8.50017-5*
- *Braga, J.C., Martín, J.M., Quesada, C., 2003. Patterns and average rates of late Neogene–Recent uplift of the Betic Cordillera, SE Spain. Geomorphology 50, 3–26. https://doi.org/10.1016/S0169-555X(02)00205-2*
- *Brozzetti, F., Cirillo, D., De Nardis, R., Cardinali, M., Lavecchia, G., Orecchio, B., Presti, D., Totaro, C., 2017. Newly identified active faults in the Pollino seismic gap, southern Italy, and their seismotectonic significance. J. Struct. Geol. 94, 13–31. https://doi.org/10.1016/j.jsg.2016.10.005*
- *Buforn, E., 2005. Study of the Damaging Earthquakes of 1911, 1999, and 2002 in the Murcia, Southeastern Spain, Region: Seismotectonic and Seismic-Risk Implications. Bull. Seismol. Soc. Am. 95, 549–567. https://doi.org/10.1785/0120040041*
- *Buforn, E., Pro, C., Cesca, S., Udias, A., Del Fresno, C., 2011. The 2010 Granada, Spain, Deep Earthquake. Bull. Seismol. Soc. Am. 101, 2418–2430. https://doi.org/10.1785/0120110022*
- *Buforn, E., Udías, A., Colombás, M.A., 1988. Seismicity, source mechanisms and tectonics of the Azores-Gibraltar plate boundary. Tectonophysics 152, 89–118. https://doi.org/10.1016/0040-1951(88)90031-5*
- *Buforn, E., Udías, A., Madariaga, R., 1991. Intermediate and deep earthquakes in Spain. Pure Appl. Geophys. 136, 375–393. https://doi.org/10.1007/BF00878576*
- *Burchfiel, B.C., Zhiliang, C., Hodges, K.V., Yuping, L., Royden, L.H., Changrong, D., Jiene, X., 1992. The South Tibetan Detachment System, Himalayan Orogen: Extension Contemporaneous With and Parallel to Shortening in a Collisional Mountain Belt, in: Geological Society of America Special Papers. Geological Society of America, pp. 1–41. https://doi.org/10.1130/SPE269-p1*
- *Cabral, J., 2012. Neotectonics of mainland Portugal: state of the art and future perspectives. J. Iber. Geol. 38, 71–84. https://doi.org/10.5209/rev_JIGE.2012.v38.n1.39206*
- *Cabral, J., Mendes, V.B., Figueiredo, P., Silveira, A.B.D., Pagarete, J., Ribeiro, A., Dias, R., Ressurreição, R., 2017. Active tectonics in Southern Portugal (SW Iberia) inferred from GPS data. Implications on the regional geodynamics. J. Geodyn. 112, 1–11. https://doi.org/10.1016/j.jog.2017.10.002*
- *Cabral, J., Moniz, C., Batlló, J., Figueiredo, P., Carvalho, J., Matias, L., Teves-Costa, P., Dias, R., Simão, N., 2013. The 1909 Benavente (Portugal) earthquake: search for the source. Nat. Hazards 69, 1211–1227. https://doi.org/10.1007/s11069-011-0062-8*
- *Cabral, J., Ribeiro, P., Figueiredo, P., Pimentel, N., Martins, A., 2004. The Azambuja fault: An active structure located in an intraplate basin with significant seismicity (Lower Tagus Valley, Portugal). J. Seismol. 8, 347–362. https://doi.org/10.1023/B:JOSE.0000038450.23032.68*
- *Cabrera, L., Roca, E., Garces, M., Porta, J., 2004. Estratigraf'ia y evolución tectonosedimentaria oligocena superior-neógena del sector central del margen catalán (Cadena Costero-Catalana), in: Geología de España. pp. 569–573.*
- *Calais, E., DeMets, C., Nocquet, J.-M., 2003. Evidence for a post-3.16-Ma change in Nubia–Eurasia–North America plate motions? Earth Planet. Sci. Lett. 216, 81–92. https://doi.org/10.1016/S0012-821X(03)00482-5*
- *Cao, J., Shi, Y., Zhang, H., Wang, H., 2009. Numerical simulation of GPS observed clockwise rotation around the eastern Himalayan syntax in the Tibetan Plateau. Sci. Bull. 54, 1398–1410. https://doi.org/10.1007/s11434-008-0588-7*
- *Cara, M., Alasset, P.-J., Sira, C., 2008. Magnitude of Historical Earthquakes, from Macroseismic Data to Seismic Waveform Modelling: Application to the Pyrenees and a 1905 Earthquake in the Alps, in: Fréchet, J., Meghraoui, M., Stucchi, M. (Eds.), Historical Seismology, Modern Approaches in Solid Earth Sciences. Springer Netherlands, Dordrecht, pp. 369–384. https://doi.org/10.1007/978-1-4020-8222-1_18*
- *Carafa, M.M.C., Barba, S., 2013. The stress field in Europe: optimal orientations with confidence limits. Geophys. J. Int. 193, 531–548. https://doi.org/10.1093/gji/ggt024*
- *Carafa, M.M.C., Bird, P., Verdecchia, A., Taroni, M., Doglioni, C., 2024. Empirical evidence for multi-decadal transients affecting geodetic velocity fields and derived seismicity forecasts in Italy. Sci. Rep. 14, 19941. https://doi.org/10.1038/s41598-024-70816-6*
- *Carafa, M.M.C., Valensise, G., Bird, P., 2017. Assessing the seismic coupling of shallow continental faults and its impact on seismic hazard estimates: a case-study from Italy. Geophys. J. Int. ggx002. https://doi.org/10.1093/gji/ggx002*

- *Cardello, G.L., Vico, G., Consorti, L., Sabbatino, M., Carminati, E., Doglioni, C., 2021. Constraining the Passive to Active Margin Tectonics of the Internal Central Apennines: Insights from Biostratigraphy, Structural, and Seismic Analysis. Geosciences 11, 160. https://doi.org/10.3390/geosciences11040160*
- *Carvalho, J., Pinto, C., Dias, R., Rabeh, T., Torres, L., Borges, J., Torres, R., Duarte, H., 2017. Tectonic evolution of an intraplate basin: the Lower Tagus Cenozoic Basin, Portugal. Basin Res. 29, 636–657. https://doi.org/10.1111/bre.12193*
- *Carvalho, J., Rabeh, T., Bielik, M., Szalaiová, E., Torres, L., Silva, M., Carrilho, F., Matias, L., Miranda, J.M., 2011. Geophysical study of the Ota–VF Xira–Lisbon–Sesimbra fault zone and the lower Tagus Cenozoic basin. J. Geophys. Eng. 8, 395–411. https://doi.org/10.1088/1742-2132/8/3/001*
- *Casas-Sainz, A.M., De Vicente, G., 2009. On the tectonic origin of Iberian topography. Tectonophysics 474, 214–235. https://doi.org/10.1016/j.tecto.2009.01.030*
- *Chalouan, A., Galindo-Zaldívar, J., Akil, M., Marín, C., Chabli, A., Ruano, P., Bargach, K., Sanz De Galdeano, C., Benmakhlouf, M., Ahmamou, M., Gourari, L., 2006. Tectonic wedge escape in the southwestern front of the Rif Cordillera (Morocco). Geol. Soc. Lond. Spec. Publ. 262, 101–118. https://doi.org/10.1144/GSL.SP.2006.262.01.06*
- *Chalouan, A., Gil, A.J., Chabli, A., Bargach, K., Liemlahi, H., El Kadiri, K., Tendero-Salmerón, V., Galindo-Zaldívar, J., 2023. cGPS Record of Active Extension in Moroccan Meseta and Shortening in Atlasic Chains under the Eurasia-Nubia Convergence. Sensors 23, 4846. https://doi.org/10.3390/s23104846*
- *Chandra, U., 1978. Seismicity, earthquake mechanisms and tectonics along the Himalayan mountain range and vicinity. Phys. Earth Planet. Inter. 16, 109–131. https://doi.org/10.1016/0031-9201(78)90083-3*
- *Chang, C.-P., Chang, T.-Y., Angelier, J., Kao, H., Lee, J.-C., Yu, S.-B., 2003. Strain and stress field in Taiwan oblique convergent system: constraints from GPS observation and tectonic data. Earth Planet. Sci. Lett. 214, 115–127. https://doi.org/10.1016/S0012-821X(03)00360-1*
- *Chang, H., An, Z., Liu, W., Ao, H., Qiang, X., Song, Y., Lai, Z., 2014. Quaternary structural partitioning within the rigid Tarim plate inferred from magnetostratigraphy and sedimentation rate in the eastern Tarim Basin in China. Quat. Res. 81, 424–432. https://doi.org/10.1016/j.yqres.2013.10.018*
- *Cheloni, D., Famiglietti, N.A., Tolomei, C., Caputo, R., Vicari, A., 2024. The 8 September 2023, M_W 6.8, Morocco Earthquake: A Deep Transpressive Faulting Along the Active High Atlas Mountain Belt. Geophys. Res. Lett. 51, e2023GL106992. https://doi.org/10.1029/2023GL106992*
- *Chen, W., Molnar, P., 1990. Source parameters of earthquakes and intraplate deformation beneath the Shillong Plateau and the Northern Indoburman Ranges. J. Geophys. Res. Solid Earth 95, 12527–12552. https://doi.org/10.1029/JB095iB08p12527*
- *Cheng, J., Rong, Y., Magistrale, H., Chen, G., Xu, X., 2017. An Mw-Based Historical Earthquake Catalog for Mainland China. Bull. Seismol. Soc. Am. 107, 2490–2500. https://doi.org/10.1785/0120170102*
- *Chertova, M.V., Spakman, W., Geenen, T., Van Den Berg, A.P., Van Hinsbergen, D.J.J., 2014. Underpinning tectonic reconstructions of the western Mediterranean region with dynamic slab evolution from 3-D numerical modeling. J. Geophys. Res. Solid Earth 119, 5876–5902. https://doi.org/10.1002/2014JB011150*
- *Chiaraluce, L., Di Stefano, R., Tinti, E., Scognamiglio, L., Michele, M., Casarotti, E., Cattaneo, M., De Gori, P., Chiarabba, C., Monachesi, G., Lombardi, A., Valoroso, L., Latorre, D., Marzorati, S., 2017. The 2016 Central Italy Seismic Sequence: A First Look at the Mainshocks, Aftershocks, and Source Models. Seismol. Res. Lett. 88, 757–771. https://doi.org/10.1785/0220160221*
- *Christophersen, A., Litchfield, N., Berryman, K., Thomas, R., Basili, R., Wallace, L., Ries, W., Hayes, G.P., Haller, K.M., Yoshioka, T., Koehler, R.D., Clark, D., Wolfson-Schwehr, M., Boettcher, M.S., Villamor, P., Horspool, N., Ornthammarath, T., Zuñiga, R., Langridge, R.M., Stirling, M.W., Goded, T., Costa, C., Yeats, R., 2015. Development of the Global Earthquake Model's neotectonic fault database. Nat. Hazards 79, 111–135. https://doi.org/10.1007/s11069-015-1831-6*
- *Cirillo, D., Totaro, C., Lavecchia, G., Orecchio, B., De Nardis, R., Presti, D., Ferrarini, F., Bello, S., Brozzetti, F., 2022. Structural complexities and tectonic barriers controlling recent seismic activity in the Pollino area (Calabria–Lucania, southern Italy) – constraints from stress inversion and 3D fault model building. Solid Earth 13, 205–228. https://doi.org/10.5194/se-13-205-2022*
- *Civiero, C., Custódio, S., Duarte, J.C., Mendes, V.B., Faccenna, C., 2020. Dynamics of the Gibraltar Arc System: A Complex Interaction Between Plate Convergence, Slab Pull, and Mantle Flow. J. Geophys. Res. Solid Earth 125, e2019JB018873. https://doi.org/10.1029/2019JB018873*
- *Civile, D., Lodolo, E., Accettella, D., Geletti, R., Ben-Avraham, Z., Deponte, M., Facchin, L., Ramella, R., Romeo, R., 2010. The Pantelleria graben (Sicily Channel, Central Mediterranean): An example of intraplate 'passive' rift. Tectonophysics 490, 173–183. https://doi.org/10.1016/j.tecto.2010.05.008*
- *Copley, A., Avouac, J.-P., Wernicke, B.P., 2011. Evidence for mechanical coupling and strong Indian lower crust beneath southern Tibet. Nature 472, 79–81. https://doi.org/10.1038/nature09926*
- *Copley, A., McKenzie, D., 2007. Models of crustal flow in the India-Asia collision zone. Geophys. J. Int. 169, 683–698. https://doi.org/10.1111/j.1365-246X.2007.03343.x*
- *Coppier, G., Griveaud, P., De Larouziere, F.-D., Montenat, C., Ott d'Estevou, P., 1989. Example of Neogene tectonic indentation in the Eastern Betic Cordilleras: the Arc of Aguilas (Southeastern Spain). Geodin. Acta 3, 37–51. https://doi.org/10.1080/09853111.1989.11105173*
- *Coudurier-Curveur, A., Tapponnier, P., Okal, E., Van Der Woerd, J., Kali, E., Choudhury, S., Baruah, S., Etchebes, M., Karakaş, Ç., 2020. A composite rupture model for the great 1950 Assam earthquake across the cusp of the East Himalayan Syntaxis. Earth Planet. Sci. Lett. 531, 115928. https://doi.org/10.1016/j.epsl.2019.115928*
- *Crespo-Blanc, A., Comas, M., Balanyá, J.C., 2016. Clues for a Tortonian reconstruction of the Gibraltar Arc: Structural pattern, deformation diachronism and block rotations. Tectonophysics 683, 308–324. https://doi.org/10.1016/j.tecto.2016.05.045*

- *Custódio, S., Dias, N.A., Carrilho, F., Góngora, E., Rio, I., Marreiros, C., Morais, I., Alves, P., Matias, L., 2015. Earthquakes in western Iberia: improving the understanding of lithospheric deformation in a slowly deforming region. Geophys. J. Int. 203, 127–145. https://doi.org/10.1093/gji/ggv285*
- *d'Acremont, E., Gutscher, M.-A., Rabaute, A., Mercier De Lépinay, B., Lafosse, M., Poort, J., Ammar, A., Tahayt, A., Le Roy, P., Smit, J., Do Couto, D., Cancouët, R., Prunier, C., Ercilla, G., Gorini, C., 2014. High-resolution imagery of active faulting offshore Al Hoceima, Northern Morocco. Tectonophysics 632, 160–166. https://doi.org/10.1016/j.tecto.2014.06.008*
- *D'Agostino, N., 2014. Complete seismic release of tectonic strain and earthquake recurrence in the Apennines (Italy). Geophys. Res. Lett. 41, 1155–1162. https://doi.org/10.1002/2014GL059230*
- *Dal Zilio, L., Jolivet, R., Van Dinther, Y., 2020. Segmentation of the Main Himalayan Thrust Illuminated by Bayesian Inference of Interseismic Coupling. Geophys. Res. Lett. 47, e2019GL086424. https://doi.org/10.1029/2019GL086424*
- *Das, S., Sandeep, Devi, S., Mittal, H., Kumar, P., Monika, 2023. Spatial Distribution of Stress Orientation by Inversion of Focal Mechanism Solutions Using MSATSI: A Case Study Across Japan Trench, in: Shrikhande, M., Agarwal, P., Kumar, P.C.A. (Eds.), Proceedings of 17th Symposium on Earthquake Engineering (Vol. 4), Lecture Notes in Civil Engineering. Springer Nature Singapore, Singapore, pp. 243–256. https://doi.org/10.1007/978-981-99-1459-3_20*
- *Dasgupta, S., Mukhopadhyay, B., Mukhopadhyay, M., Pande, P., 2021. Geo- and seismo- tectonics of Eastern Himalaya: Exploring earthquake source zones from foredeep to Tibetan hinterland. Phys. Chem. Earth Parts ABC 123, 103013. https://doi.org/10.1016/j.pce.2021.103013*
- *Dasgupta, S., Mukhopadhyay, M., Nandy, D.R., 1987. Active transverse features in the central portion of the Himalaya. Tectonophysics 136, 255–264. https://doi.org/10.1016/0040-1951(87)90028-X*
- *De Galdeano, C.S., 1990. Geologic evolution of the Betic Cordilleras in the Western Mediterranean, Miocene to the present. Tectonophysics 172, 107–119. https://doi.org/10.1016/0040-1951(90)90062-D*
- *De La Torre, T.L., Monsalve, G., Sheehan, A.F., Sapkota, S., Wu, F., 2007. Earthquake processes of the Himalayan collision zone in eastern Nepal and the southern Tibetan Plateau. Geophys. J. Int. 171, 718–738. https://doi.org/10.1111/j.1365-246X.2007.03537.x*
- *De Matteis, R., Matrullo, E., Rivera, L., Stabile, T.A., Pasquale, G., Zollo, A., 2012. Fault Delineation and Regional Stress Direction from the Analysis of Background Microseismicity in the southern Apennines, Italy. Bull. Seismol. Soc. Am. 102, 1899–1907. https://doi.org/10.1785/0120110225*
- *De Nardis, R., Pandolfi, C., Cattaneo, M., Monachesi, G., Cirillo, D., Ferrarini, F., Bello, S., Brozzetti, F., Lavecchia, G., 2022. Lithospheric double shear zone unveiled by microseismicity in a region of slow deformation. Sci. Rep. 12, 21066. https://doi.org/10.1038/s41598-022-24903-1*
- *De Paola, N., Collettini, C., Faulkner, D.R., Trippetta, F., 2008. Fault zone architecture and deformation processes within evaporitic rocks in the upper crust. Tectonics 27, 2007TC002230. https://doi.org/10.1029/2007TC002230*
- *De Sarkar, S., Mathew, G., Pande, K., 2013. Arc parallel extension in Higher and Lesser Himalayas, evidence from western Arunachal Himalaya, India. J. Earth Syst. Sci. 122, 715–727. https://doi.org/10.1007/s12040-013-0298-7*
- *De Vicente, G., Cloetingh, S., Muñoz-Martín, A., Olaiz, A., Stich, D., Vegas, R., Galindo-Zaldívar, J., Fernández-Lozano, J., 2008. Inversion of moment tensor focal mechanisms for active stresses around the microcontinent Iberia: Tectonic implications. Tectonics 27, 2006TC002093. https://doi.org/10.1029/2006TC002093*
- *De Vicente, G., Cunha, P.P., Muñoz-Martín, A., Cloetingh, S.A.P.L., Olaiz, A., Vegas, R., 2018. The Spanish-Portuguese Central System: An Example of Intense Intraplate Deformation and Strain Partitioning. Tectonics 37, 4444–4469. https://doi.org/10.1029/2018TC005204*
- *De Vicente, G., Vegas, R., 2009. Large-scale distributed deformation controlled topography along the western Africa–Eurasia limit: Tectonic constraints. Tectonophysics 474, 124–143. https://doi.org/10.1016/j.tecto.2008.11.026*
- *De Vicente, G., Vegas, R., Muñoz Martín, A., Silva, P.G., Andriessen, P., Cloetingh, S., González Casado, J.M., Van Wees, J.D., Álvarez, J., Carbó, A., Olaiz, A., 2007. Cenozoic thick-skinned deformation and topography evolution of the Spanish Central System. Glob. Planet. Change 58, 335–381. https://doi.org/10.1016/j.gloplacha.2006.11.042*
- *Delvaux, D., Barth, A., 2010. African stress pattern from formal inversion of focal mechanism data. Tectonophysics 482, 105–128. https://doi.org/10.1016/j.tecto.2009.05.009*
- *Delvaux, D., Moeys, R., Stapel, G., Petit, C., Levi, K., Miroshnichenko, A., Ruzhich, V., San'kov, V., 1997. Paleostress reconstructions and geodynamics of the Baikal region, Central Asia, Part 2. Cenozoic rifting. Tectonophysics 282, 1–38. https://doi.org/10.1016/S0040-1951(97)00210-2*
- *Devoti, R., D'Agostino, N., Serpelloni, E., Pietrantonio, G., Riguzzi, F., Avallone, A., Cavaliere, A., Cheloni, D., Cecere, G., D'Ambrosio, C., Franco, L., Selvaggi, G., Metois, M., Esposito, A., Sepe, V., Galvani, A., Anzidei, M., 2017. A Combined Velocity Field of the Mediterranean Region. Ann. Geophys. 60, 1. https://doi.org/10.4401/ag-7059*
- *Dewey, J.F., 1988. Extensional collapse of orogens. Tectonics 7, 1123–1139. https://doi.org/10.1029/TC007i006p01123*
- *Di Luccio, F., Palano, M., Chiodini, G., Cucci, L., Piromallo, C., Sparacino, F., Ventura, G., Improta, L., Cardellini, C., Persaud, P., Pizzino, L., Calderoni, G., Castellano, C., Cianchini, G., Cianetti, S., Cinti, D., Cusano, P., De Gori, P., De Santis, A., Del Gaudio, P., Diaferia, G., Esposito, A., Galluzzo, D., Galvani, A., Gasparini, A., Gaudiosi, G., Gervasi, A., Giunchi, C., La Rocca, M., Milano, G., Morabito, S., Nardone, L., Orlando, M., Petrosino, S., Piccinini, D., Pietrantonio, G., Piscini, A., Roselli, P., Sabbagh, D., Sciarra, A., Scognamiglio, L., Sepe, V., Tertulliani, A., Tondi, R., Valoroso, L., Voltattorni, N., Zuccarello, L., 2022. Geodynamics, geophysical and geochemical observations, and the role of CO2 degassing in the Apennines. Earth-Sci. Rev. 234, 104236. https://doi.org/10.1016/j.earscirev.2022.104236*
- *Dobretsov, N.L., Koulakov, I.Yu., Polyansky, O.P., 2013. Geodynamics and stress–strain patterns in different tectonic settings. Russ. Geol. Geophys. 54, 357–380. https://doi.org/10.1016/j.rgg.2013.03.001*

- *Doglioni, C., Harabaglia, P., Merlini, S., Mongelli, F., Peccerillo, A., Piromallo, C., 1999. Orogens and slabs vs. their direction of subduction. Earth-Sci. Rev. 45, 167–208. https://doi.org/10.1016/S0012-8252(98)00045-2*
- *Doglioni, C., Innocenti, F., Morellato, C., Procaccianti, D., Scrocca, D., 2004. On the tyrrhenian sea opening. Mem Descr Carta Geol It XLIV, 147–164.*
- *Domzig, A., 2006. Déformation active et récente, et structuration tectonosédimentaire de la marge sous-marine algérienne.*
- *Druet, M., Bohoyo, F., Maestro, A., Mink, S., García-Senz, J., Pedrera, A., Rodríguez Fernández, R., 2023. Tectonics of the Iberian continental margins and abyssal plains. J. Maps 19, 2237980. https://doi.org/10.1080/17445647.2023.2237980*
- *Duarte, J.C., Riel, N., Rosas, F.M., Popov, A., Schuler, C., Kaus, B.J.P., 2024. Gibraltar subduction zone is invading the Atlantic. Geology 52, 331–335. https://doi.org/10.1130/G51654.1*
- *Duarte, J.C., Rosas, F.M., Terrinha, P., Schellart, W.P., Boutelier, D., Gutscher, M.-A., Ribeiro, A., 2013. Are subduction zones invading the Atlantic? Evidence from the southwest Iberia margin. Geology 41, 839–842. https://doi.org/10.1130/G34100.1*
- *Echeverria, A., Khazaradze, G., Asensio, E., Gárate, J., Dávila, J.M., Suriñach, E., 2013. Crustal deformation in eastern Betics from CuaTeNeo GPS network. Tectonophysics 608, 600–612. https://doi.org/10.1016/j.tecto.2013.08.020*
- *Echeverria, A., Khazaradze, G., Asensio, E., Masana, E., 2015. Geodetic evidence for continuing tectonic activity of the Carboneras fault (SE Spain). Tectonophysics 663, 302–309. https://doi.org/10.1016/j.tecto.2015.08.009*
- *England, P., Houseman, G., 1989. Extension during continental convergence, with application to the Tibetan Plateau. J. Geophys. Res. Solid Earth 94, 17561–17579. https://doi.org/10.1029/JB094iB12p17561*
- *Ercilla, G., Galindo-Zaldívar, J., Estrada, F., Valencia, J., Juan, C., Casas, D., Alonso, B., Comas, M.C., Tendero-Salmerón, V., Casalbore, D., Azpiroz-Zabala, M., Bárcenas, P., Ceramicola, S., Chiocci, F.L., Idárraga-García, J., López-González, N., Mata, P., Palomino, D., Rodríguez-García, J.A., Teixeira, M., Nespereira, J., Vázquez, J.T., Yenes, M., 2022. Understanding the complex geomorphology of a deep sea area affected by continental tectonic indentation: The case of the Gulf of Vera (Western Mediterranean). Geomorphology 402, 108126. https://doi.org/10.1016/j.geomorph.2022.108126*
- *Estrada, F., Galindo-Zaldívar, J., Vázquez, J.T., Ercilla, G., D'Acremont, E., Alonso, B., Gorini, C., 2018. Tectonic indentation in the central Alboran Sea (westernmost Mediterranean). Terra Nova 30, 24–33. https://doi.org/10.1111/ter.12304*
- *Fadil, A., Vernant, P., McClusky, S., Reilinger, R., Gomez, F., Ben Sari, D., Mourabit, T., Feigl, K., Barazangi, M., 2006. Active tectonics of the western Mediterranean: Geodetic evidence for rollback of a delaminated subcontinental lithospheric slab beneath the Rif Mountains, Morocco. Geology 34, 529. https://doi.org/10.1130/G22291.1*
- *Fang, Y., Fang, L., Deng, S., Lu, Y., Wang, B., Zhao, X., Wang, Y., Zhang, H., Zhang, X., Sha, J., 2021. Carbon isotope stratigraphy across the Triassic-Jurassic boundary in the high-latitude terrestrial Junggar Basin, NW China. Palaeogeogr. Palaeoclimatol. Palaeoecol. 577, 110559. https://doi.org/10.1016/j.palaeo.2021.110559*
- *Faulkner, D.R., Lewis, A.C., Rutter, E.H., 2003. On the internal structure and mechanics of large strike-slip fault zones: field observations of the Carboneras fault in southeastern Spain. Tectonophysics 367, 235–251. https://doi.org/10.1016/S0040-1951(03)00134-3*
- *Faure Walker, J., Boncio, P., Pace, B., Roberts, G., Benedetti, L., Scotti, O., Visini, F., Peruzza, L., 2021. Fault2SHA Central Apennines database and structuring active fault data for seismic hazard assessment. Sci. Data 8, 87. https://doi.org/10.1038/s41597-021-00868-0*
- *Fernandes, R.M.S., Miranda, J.M., Meijninger, B.M.L., Bos, M.S., Noomen, R., Bastos, L., Ambrosius, B.A.C., Riva, R.E.M., 2007. Surface velocity field of the Ibero-Maghrebian segment of the Eurasia-Nubia plate boundary. Geophys. J. Int. 169, 315–324. https://doi.org/10.1111/j.1365-246X.2006.03252.x*
- *Fernández-Ibáñez, F., Soto, J.I., Zoback, M.D., Morales, J., 2007. Present-day stress field in the Gibraltar Arc (western Mediterranean). J. Geophys. Res. Solid Earth 112, 2006JB004683. https://doi.org/10.1029/2006JB004683*
- *Fernández-Viejo, G., Llana-Fúnez, S., Acevedo, J., López-Fernández, C., 2021. The Cantabrian Fault at Sea. Low Magnitude Seismicity and Its Significance Within a Stable Setting. Front. Earth Sci. 9, 645061. https://doi.org/10.3389/feart.2021.645061*
- *Ferrarini, F., Lavecchia, G., De Nardis, R., Brozzetti, F., 2015. Fault Geometry and Active Stress from Earthquakes and Field Geology Data Analysis: The Colfiorito 1997 and L'Aquila 2009 Cases (Central Italy). Pure Appl. Geophys. 172, 1079–1103. https://doi.org/10.1007/s00024-014-0931-7*
- *Fillon, C., Mouthereau, F., Calassou, S., Pik, R., Bellahsen, N., Gautheron, C., Stockli, D., Brichau, S., Daril, N., Mouchené, M., Van Der Beek, P., 2021. Post-orogenic exhumation in the western Pyrenees: evidence for extension driven by pre-orogenic inheritance. J. Geol. Soc. 178, jgs2020-079. https://doi.org/10.1144/jgs2020-079*
- *Fillon, C., Pedreira, D., Van Der Beek, P.A., Huismans, R.S., Barbero, L., Pulgar, J.A., 2016. Alpine exhumation of the central Cantabrian Mountains, Northwest Spain: ALPINE EXHUMATION OF THE CANTABRIANS. Tectonics 35, 339–356. https://doi.org/10.1002/2015TC004050*
- *Finch, M., Hasalova, P., Weinberg, R.F., Fanning, C.M., 2014. Switch from thrusting to normal shearing in the Zanskar shear zone, NW Himalaya: Implications for channel flow. Geol. Soc. Am. Bull. 126, 892–924. https://doi.org/10.1130/B30817.1*
- *Flesch, L.M., Holt, W.E., Haines, A.J., Shen-Tu, B., 2000. Dynamics of the Pacific-North American Plate Boundary in the Western United States. Science 287, 834–836. https://doi.org/10.1126/science.287.5454.834*
- *Frizon De Lamotte, D., Saint Bezar, B., Bracène, R., Mercier, E., 2000. The two main steps of the Atlas building and geodynamics of the western Mediterranean. Tectonics 19, 740–761. https://doi.org/10.1029/2000TC900003*
- *Frohling, E., Szeliga, W., 2016. GPS constraints on interplate locking within the Makran subduction zone. Geophys. J. Int. 205, 67–76. https://doi.org/10.1093/gji/ggw001*

- *Fullea, J., Fernàndez, M., Zeyen, H., Vergés, J., 2007. A rapid method to map the crustal and lithospheric thickness using elevation, geoid anomaly and thermal analysis. Application to the Gibraltar Arc System, Atlas Mountains and adjacent zones. Tectonophysics 430, 97–117. https://doi.org/10.1016/j.tecto.2006.11.003*
- *Galadini, F., Falcucci, E., Galli, P., Giaccio, B., Gori, S., Messina, P., Moro, M., Saroli, M., Scardia, G., Sposato, A., 2012. Time intervals to assess active and capable faults for engineering practices in Italy. Eng. Geol. 139–140, 50–65. https://doi.org/10.1016/j.enggeo.2012.03.012*
- *Galetzka, J., Melgar, D., Genrich, J.F., Geng, J., Owen, S., Lindsey, E.O., Xu, X., Bock, Y., Avouac, J.-P., Adhikari, L.B., Upreti, B.N., Pratt-Sitaula, B., Bhattarai, T.N., Sitaula, B.P., Moore, A., Hudnut, K.W., Szeliga, W., Normandeau, J., Fend, M., Flouzat, M., Bollinger, L., Shrestha, P., Koirala, B., Gautam, U., Bhatterai, M., Gupta, R., Kandel, T., Timsina, C., Sapkota, S.N., Rajaure, S., Maharjan, N., 2015. Slip pulse and resonance of the Kathmandu basin during the 2015 Gorkha earthquake, Nepal. Science 349, 1091–1095. https://doi.org/10.1126/science.aac6383*
- *Galindo-Zaldívar, J., 2003. Active faulting in the internal zones of the central Betic Cordilleras (SE, Spain). J. Geodyn. 36, 239–250. https://doi.org/10.1016/S0264-3707(03)00049-8*
- *Galindo-Zaldivar, J., Ercilla, G., Estrada, F., Catalán, M., d'Acremont, E., Azzouz, O., Casas, D., Chourak, M., Vazquez, J.T., Chalouan, A., Sanz De Galdeano, C., Benmakhlouf, M., Gorini, C., Alonso, B., Palomino, D., Rengel, J.A., Gil, A.J., 2018. Imaging the Growth of Recent Faults: The Case of 2016–2017 Seismic Sequence Sea Bottom Deformation in the Alboran Sea (Western Mediterranean). Tectonics 37, 2513–2530. https://doi.org/10.1029/2017TC004941*
- *Galindo-Zaldivar, J., Gil, A.J., Sanz De Galdeano, C., Lacy, M.C., García-Armenteros, J.A., Ruano, P., Ruiz, A.M., Martínez-Martos, M., Alfaro, P., 2015. Active shallow extension in central and eastern Betic Cordillera from CGPS data. Tectonophysics 663, 290–301. https://doi.org/10.1016/j.tecto.2015.08.035*
- *Galindo-Zaldivar, J., Gil, A.J., Tendero-Salmerón, V., Borque, M.J., Ercilla, G., González-Castillo, L., Sánchez-Alzola, A., Lacy, M.C., Estrada, F., Avilés, M., Alfaro, P., Madarieta-Txurruka, A., Chacón, F., 2022. The Campo de Dalias GNSS Network Unveils the Interaction between Roll-Back and Indentation Tectonics in the Gibraltar Arc. Sensors 22, 2128. https://doi.org/10.3390/s22062128*
- *Galindo-Zaldívar, J., Jabaloy, A., Serrano, I., Morales, J., González-Lodeiro, F., Torcal, F., 1999. Recent and present-day stresses in the Granada Basin (Betic Cordilleras): Example of a late Miocene-present-day extensional basin in a convergent plate boundary. Tectonics 18, 686–702. https://doi.org/10.1029/1999TC900016*
- *Gallastegui, J., Pulgar, J.A., Gallart, J., 2002. Initiation of an active margin at the North Iberian continent-ocean transition. Tectonics 21. https://doi.org/10.1029/2001TC901046*
- *Galli, P., Bosi, V., 2003. Catastrophic 1638 earthquakes in Calabria (southern Italy): New insights from paleoseismological investigation. J. Geophys. Res. Solid Earth 108. https://doi.org/10.1029/2001JB001713*
- *Gan, W., Zhang, P., Shen, Z., Niu, Z., Wang, M., Wan, Y., Zhou, D., Cheng, J., 2007. Present-day crustal motion within the Tibetan Plateau inferred from GPS measurements. J. Geophys. Res. Solid Earth 112, 2005JB004120. https://doi.org/10.1029/2005JB004120*
- *Garate, J., Martin-Davila, J., Khazaradze, G., Echeverria, A., Asensio, E., Gil, A.J., De Lacy, M.C., Armenteros, J.A., Ruiz, A.M., Gallastegui, J., Alvarez-Lobato, F., Ayala, C., Rodríguez-Caderot, G., Galindo-Zaldívar, J., Rimi, A., Harnafi, M., 2015. Topo-Iberia project: CGPS crustal velocity field in the Iberian Peninsula and Morocco. GPS Solut. 19, 287–295. https://doi.org/10.1007/s10291-014-0387-3*
- *García-Mayordomo, J., Insua-Arévalo, J.M., Martínez-Díaz, J.J., Jiménez-Díaz, A., Martín-Banda, R., Martín-Alfageme, S., Álvarez-Gómez, J.A., Rodríguez-Peces, M., Pérez-López, R., Rodríguez-Pascua, M.A., Masana, E., Perea, H., Martín-González, F., Giner-Robles, J., Nemser, E.S., Cabral, J., 2012. The Quaternary Active Faults Database of Iberia (QAFI v.2.0). J. Iber. Geol. 38, 285–302. https://doi.org/10.5209/rev_JIGE.2012.v38.n1.39219*
- *García-Senz, J., Pedrera, A., Ayala, C., Ruiz-Constán, A., Robador, A., Rodríguez-Fernández, L.R., 2020. Inversion of the north Iberian hyperextended margin: the role of exhumed mantle indentation during continental collision. Geol. Soc. Lond. Spec. Publ. 490, 177–198. https://doi.org/10.1144/SP490-2019-112*
- *Ge, W., Molnar, P., Shen, Z., Li, Q., 2015. Present-day crustal thinning in the southern and northern Tibetan Plateau revealed by GPS measurements. Geophys. Res. Lett. 42, 5227–5235. https://doi.org/10.1002/2015GL064347*
- *Gea, P.J., Negredo, A.M., Mancilla, F.D.L., 2023. The Gibraltar slab dynamics and its influence on past and present-day Alboran domain deformation: Insights from thermo-mechanical numerical modelling. Front. Earth Sci. 11, 995041. https://doi.org/10.3389/feart.2023.995041*
- *GEBCO Bathymetric Compilation Group 2023, 2023. The GEBCO_2023 Grid - a continuous terrain model of the global oceans and land. https://doi.org/10.5285/f98b053b-0cbc-6c23-e053-6c86abc0af7b*
- *Gephart, J.W., Forsyth, D.W., 1984. An improved method for determining the regional stress tensor using earthquake focal mechanism data: Application to the San Fernando Earthquake Sequence. J. Geophys. Res. Solid Earth 89, 9305–9320. https://doi.org/10.1029/JB089iB11p09305*
- *Ghoshal, S., McQuarrie, N., Robinson, D.M., Adhikari, D.P., Morgan, L.E., Ehlers, T.A., 2020. Constraining Central Himalayan (Nepal) Fault Geometry Through Integrated Thermochronology and Thermokinematic Modeling. Tectonics 39, e2020TC006399. https://doi.org/10.1029/2020TC006399*
- *Goded, T., Buforn, E., Munoz, D., 2008. The 1494 and 1680 Malaga (Southern Spain) Earthquakes. Seismol. Res. Lett. 79, 707–715. https://doi.org/10.1785/gssrl.79.5.707*
- *Godin, L., Grujic, D., Law, R.D., Searle, M.P., 2006. Channel flow, ductile extrusion and exhumation in continental collision zones: an introduction. Geol. Soc. Lond. Spec. Publ. 268, 1–23. https://doi.org/10.1144/GSL.SP.2006.268.01.01*
- *Gómez De La Peña, L., R. Ranero, C., Gràcia, E., Booth-Rea, G., Azañón, J.M., Tinivella, U., Yelles-Chaouche, A., 2022. Evidence for a developing plate boundary in the western Mediterranean. Nat. Commun. 13, 4786. https://doi.org/10.1038/s41467-022-31895-z*

- *Gómez De La Peña, L., Ranero, C.R., Gràcia, E., 2018. The Crustal Domains of the Alboran Basin (Western Mediterranean). Tectonics 37, 3352–3377. https://doi.org/10.1029/2017TC004946*
- *Gomez, F., Barazangi, M., Bensaid, M., 1996. Active tectonism in the intracontinental Middle Atlas Mountains of Morocco: synchronous crustal shortening and extension. J. Geol. Soc. 153, 389–402. https://doi.org/10.1144/gsjgs.153.3.0389*
- *Gómez, J.L.M., 1984. Comprensión y distensión alpinas en la cadena Ibérica Oriental.*
- *Gonzalez-Castillo, L., Galindo-Zaldivar, J., De Lacy, M.C., Borque, M.J., Martinez-Moreno, F.J., García-Armenteros, J.A., Gil, A.J., 2015. Active rollback in the Gibraltar Arc: Evidences from CGPS data in the western Betic Cordillera. Tectonophysics 663, 310–321. https://doi.org/10.1016/j.tecto.2015.03.010*
- *Gràcia, E., Dañobeitia, J., Vergés, J., Bartolomé, R., Córdoba, D., 2003. Crustal architecture and tectonic evolution of the Gulf of Cadiz (SW Iberian margin) at the convergence of the Eurasian and African plates. Tectonics 22, 2001TC901045. https://doi.org/10.1029/2001TC901045*
- *Grevemeyer, I., Gràcia, E., Villaseñor, A., Leuchters, W., Watts, A.B., 2015. Seismicity and active tectonics in the Alboran Sea, Western Mediterranean: Constraints from an offshore-onshore seismological network and swath bathymetry data. J. Geophys. Res. Solid Earth 120, 8348–8365. https://doi.org/10.1002/2015JB012073*
- *Grünthal, G., Wahlström, R., 2012. The European-Mediterranean Earthquake Catalogue (EMEC) for the last millennium. J. Seismol. 16, 535–570. https://doi.org/10.1007/s10950-012-9302-y*
- *Guimerà, J., Mas, R., Alonso, Á., 2004. Intraplate deformation in the NW Iberian Chain: Mesozoic extension and Tertiary contractional inversion. J. Geol. Soc. 161, 291–303. https://doi.org/10.1144/0016-764903-055*
- *Guiraud, R., 1998. Mesozoic rifting and basin inversion along the northern African Tethyan margin: an overview. Geol. Soc. Lond. Spec. Publ. 132, 217–229. https://doi.org/10.1144/GSL.SP.1998.132.01.13*
- *Gunnell, Y., Zeyen, H., Calvet, M., 2008. Geophysical evidence of a missing lithospheric root beneath the Eastern Pyrenees: Consequences for post-orogenic uplift and associated geomorphic signatures. Earth Planet. Sci. Lett. 276, 302–313. https://doi.org/10.1016/j.epsl.2008.09.031*
- *Gutierrez, F., Linares, R., Roque, C., Zarroca, M., Rosell, J., Galve, J.P., Carbonel, D., 2012. Investigating gravitational grabens related to lateral spreading and evaporite dissolution subsidence by means of detailed mapping, trenching, and electrical resistivity tomography (Spanish Pyrenees). Lithosphere 4, 331–353. https://doi.org/10.1130/L202.1*
- *Gutscher, M.-A., 2004. What Caused the Great Lisbon Earthquake? Science 305, 1247–1248. https://doi.org/10.1126/science.1101351*
- *Gutscher, M.-A., Dominguez, S., Westbrook, G.K., Le Roy, P., Rosas, F., Duarte, J.C., Terrinha, P., Miranda, J.M., Graindorge, D., Gailler, A., Sallares, V., Bartolome, R., 2012. The Gibraltar subduction: A decade of new geophysical data. Tectonophysics 574–575, 72–91. https://doi.org/10.1016/j.tecto.2012.08.038*
- *Hamdache, M., Peláez, J.A., Gospodinov, D., Henares, J., Galindo-Zaldívar, J., Sanz De Galdeano, C., Ranguelov, B., 2022. Stochastic Modeling of the Al Hoceima (Morocco) Aftershock Sequences of 1994, 2004 and 2016. Appl. Sci. 12, 8744. https://doi.org/10.3390/app12178744*
- *Hamdache, M., Pelaez, J.A., Talbi, A., Casado, C.L., 2010. A Unified Catalog of Main Earthquakes for Northern Algeria from A.D. 856 to 2008. Seismol. Res. Lett. 81, 732–739. https://doi.org/10.1785/gssrl.81.5.732*
- *Hamdache, M., Pelaez, J.A., Yelles-Chauche, A.K., 2004. The Algiers, Algeria Earthquake (Mw 6. 8) of 21 May 2003: Preliminary Report. Seismol. Res. Lett. 75, 360–367. https://doi.org/10.1785/gssrl.75.3.360*
- *Han, C., Huang, Z., Xu, M., Wang, L., Mi, N., Yu, D., Li, H., 2019. Focal mechanism and stress field in the northeastern Tibetan Plateau: insight into layered crustal deformations. Geophys. J. Int. 218, 2066–2078. https://doi.org/10.1093/gji/ggz267*
- *Hao, M., Li, Y., Zhuang, W., 2019. Crustal movement and strain distribution in East Asia revealed by GPS observations. Sci. Rep. 9, 16797. https://doi.org/10.1038/s41598-019-53306-y*
- *Harbi, A., Peresan, A., Panza, G.F., 2010. Seismicity of Eastern Algeria: a revised and extended earthquake catalogue. Nat. Hazards 54, 725–747. https://doi.org/10.1007/s11069-009-9497-6*
- *Harrison, T.M., Copeland, P., Kidd, W.S.F., Yin, A., 1992. Raising Tibet. Science 255, 1663–1670. https://doi.org/10.1126/science.255.5052.1663*
- *Heddar, A., Authemayou, C., Djellit, H., Yelles, A.K., Déverchère, J., Gharbi, S., Boudiaf, A., Van Vliet Lanoe, B., 2013. Preliminary results of a paleoseismological analysis along the Sahel fault (Algeria): New evidence for historical seismic events. Quat. Int. 302, 210–223. https://doi.org/10.1016/j.quaint.2012.09.007*
- *Heidbach, O., Rajabi, M., Cui, X., Fuchs, K., Müller, B., Reinecker, J., Reiter, K., Tingay, M., Wenzel, F., Xie, F., Ziegler, M.O., Zoback, M.-L., Zoback, M., 2018. The World Stress Map database release 2016: Crustal stress pattern across scales. Tectonophysics 744, 484–498. https://doi.org/10.1016/j.tecto.2018.07.007*
- *Hernandez, J., De Larouziere, F.D., Bolze, J., Bordet, P., 1987. Le magmatisme neogene betico-rifain et le couloir de decrochement trans-Alboran. Bull. Société Géologique Fr. III, 257–267. https://doi.org/10.2113/gssgfbull.III.2.257*
- *Herraiz, M., De Vicente, G., Lindo-Ñaupari, R., Giner, J., Simón, J.L., González-Casado, J.M., Vadillo, O., Rodríguez-Pascua, M.A., Cicuéndez, J.I., Casas, A., Cabañas, L., Rincón, P., Cortés, A.L., Ramírez, M., Lucini, M., 2000. The recent (upper Miocene to Quaternary) and present tectonic stress distributions in the Iberian Peninsula. Tectonics 19, 762–786. https://doi.org/10.1029/2000TC900006*
- *Herring, T.A., Floyd, M., Perry, M., 2018. Herring et al., 2018 - GAMIT-GLOBK for GNSS. GAMIT-GLOBK GNSS 1–48.*
- *Hetényi, G., Cattin, R., Berthet, T., Le Moigne, N., Chophel, J., Lechmann, S., Hammer, P., Drukpa, D., Sapkota, S.N., Gautier, S., Thinley, K., 2016. Segmentation of the Himalayas as revealed by arc-parallel gravity anomalies. Sci. Rep. 6, 33866. https://doi.org/10.1038/srep33866*

- *Hodges, K.V., Burchfiel, B.C., Royden, L.H., Chen, Z., Liu, Y., 1993. The metamorphic signature of contemporaneous extension and shortening in the central Himalayan orogen: data from the Nyalam transect, southern Tibet. J. Metamorph. Geol. 11, 721–737. https://doi.org/10.1111/j.1525-1314.1993.tb00183.x*
- *Hu, X., He, P., Zhang, J., 2022. Source mechanism of the 2020 Mw 6.3 Nima earthquake derived from Bayesian inversions with InSAR observations: Insight into E-W extensional activity in the central Tibet. Adv. Space Res. 70, 1721–1736. https://doi.org/10.1016/j.asr.2022.06.065*
- *Huang, M., Udell Lopez, K., Olsen, K.G., 2022. Icequake-Magnitude Scaling Relationship Along a Rift Within the Ross Ice Shelf, Antarctica. Geophys. Res. Lett. 49, e2022GL097961. https://doi.org/10.1029/2022GL097961*
- *IGN, 2022. Catálogo de terremotos. Centro Nacional de Información Geográfica (Ministerio de Transportes, Movilidad y Agenda Urbana), ES.*
- *Jacobshagen, V., Brede, R., Hauptmann, M., Heinitz, W., Zylka, R., 1988. Structure and post-Palaeozoic evolution of the central High Atlas, in: Jacobshagen, V.H. (Ed.), The Atlas System of Morocco, Lecture Notes in Earth Sciences. Springer-Verlag, Berlin/Heidelberg, pp. 245–271. https://doi.org/10.1007/BFb0011596*
- *Jamieson, R.A., Beaumont, C., Nguyen, M.H., Grujic, D., 2006. Provenance of the Greater Himalayan Sequence and associated rocks: predictions of channel flow models. Geol. Soc. Lond. Spec. Publ. 268, 165–182. https://doi.org/10.1144/GSL.SP.2006.268.01.07*
- *Ježek, J., Schulmann, K., Thompson, A.B., 2002. Strain partitioning in front of an obliquely convergent indenter. Stephan Mueller Spec. Publ. Ser. 1, 93–104. https://doi.org/10.5194/smsps-1-93-2002*
- *Jiménez-Munt, I., Fernàndez, M., Torne, M., Bird, P., 2001. The transition from linear to diffuse plate boundary in the Azores–Gibraltar region: results from a thin-sheet model. Earth Planet. Sci. Lett. 192, 175–189. https://doi.org/10.1016/S0012-821X(01)00442-3*
- *Jiménez-Munt, I., Fernàndez, M., Vergés, J., Afonso, J.C., Garcia-Castellanos, D., Fullea, J., 2010. Lithospheric structure of the Gorringe Bank: Insights into its origin and tectonic evolution: GORRINGE BANK STRUCTURE AND EVOLUTION. Tectonics 29, n/a-n/a. https://doi.org/10.1029/2009TC002458*
- *Jolivet, L., Augier, R., Faccenna, C., Negro, F., Rimmele, G., Agard, P., Robin, C., Rossetti, F., Crespo-Blanc, A., 2008. Subduction, convergence and the mode of backarc extension in the Mediterranean region. Bull. Société Géologique Fr. 179, 525–550. https://doi.org/10.2113/gssgfbull.179.6.525*
- *Jolivet, L., Faccenna, C., 2000. Mediterranean extension and the Africa-Eurasia collision. Tectonics 19, 1095–1106. https://doi.org/10.1029/2000TC900018*
- *Kayal, J.R., Arefiev, S.S., Baruah, Saurabh, Hazarika, D., Gogoi, N., Gautam, J.L., Baruah, Santanu, Dorbath, C., Tatevossian, R., 2012. Large and great earthquakes in the Shillong plateau–Assam valley area of Northeast India Region: Pop-up and transverse tectonics. Tectonophysics 532–535, 186–192. https://doi.org/10.1016/j.tecto.2012.02.007*
- *Keiding, M., Lund, B., Árnadóttir, T., 2009. Earthquakes, stress, and strain along an obliquely divergent plate boundary: Reykjanes Peninsula, southwest Iceland. J. Geophys. Res. Solid Earth 114, 2008JB006253. https://doi.org/10.1029/2008JB006253*
- *Kellett, D.A., Cottle, J.M., Larson, K.P., 2019. The South Tibetan Detachment System: history, advances, definition and future directions. Geol. Soc. Lond. Spec. Publ. 483, 377–400. https://doi.org/10.1144/SP483.2*
- *Kellett, D.A., Grujic, D., 2012. New insight into the South Tibetan detachment system: Not a single progressive deformation. Tectonics 31, 2011TC002957. https://doi.org/10.1029/2011TC002957*
- *Khattri, K.N., Rogers, A.M., Perkins, D.M., Algermissen, S.T., 1984. A seismic hazard map of India and adjacent areas. Tectonophysics 108, 93–134. https://doi.org/10.1016/0040-1951(84)90156-2*
- *Kind, R., Yuan, X., Saul, J., Nelson, D., Sobolev, S.V., Mechie, J., Zhao, W., Kosarev, G., Ni, J., Achauer, U., Jiang, M., 2002. Seismic Images of Crust and Upper Mantle Beneath Tibet: Evidence for Eurasian Plate Subduction. Science 298, 1219–1221. https://doi.org/10.1126/science.1078115*
- *Kissling, E., 2024. Adria microplate: a puzzling key stone in west-central Mediterranean geodynamics. Ann. Geophys. 67, G431. https://doi.org/10.4401/ag-9160*
- *Koulali, A., Ouazar, D., Tahayt, A., King, R.W., Vernant, P., Reilinger, R.E., McClusky, S., Mourabit, T., Davila, J.M., Amraoui, N., 2011. New GPS constraints on active deformation along the Africa–Iberia plate boundary. Earth Planet. Sci. Lett. 308, 211–217. https://doi.org/10.1016/j.epsl.2011.05.048*
- *Kreemer, C., Blewitt, G., Klein, E.C., 2014. A geodetic plate motion and Global Strain Rate Model. Geochem. Geophys. Geosystems 15, 3849–3889. https://doi.org/10.1002/2014GC005407*
- *Kumar, A., Mitra, S., Suresh, G., 2015. Seismotectonics of the eastern Himalayan and indo-burman plate boundary systems: Seismotectonics of Northeast of India. Tectonics 34, 2279–2295. https://doi.org/10.1002/2015TC003979*
- *Kumar, P., Malik, J.N., Gahalaut, V.K., 2023a. Arc-Parallel Shear and Orogenic Deformation Along the Oblique Himalayan Convergent Plate Margin: Implications from Topographic- and Gradient-Anomaly Profiling in the Himalaya. Pure Appl. Geophys. 180, 2169–2189. https://doi.org/10.1007/s00024-023-03246-6*
- *Kumar, P., Malik, J.N., Gahalaut, V.K., Yadav, R.K., Singh, G., 2023b. Evidence of Strain Accumulation and Coupling Variation in the Himachal Region of NW Himalaya From Short Term Geodetic Measurements. Tectonics 42, e2022TC007690. https://doi.org/10.1029/2022TC007690*
- *Kusumawati, D., Sahara, D.P., Puspito, N.T., Baskara, A.W., Kurniawan, A., Tanihaha, W., Solihin, L.J.J., Pratama, M.D., Patimah, S.H., Sasmi, A.T., Muhammad, Hilmy, Muhammad, Hammam, Natafrisca, W.C.C., Bening, M.A., 2023. Moment tensor inversion implementation in determining focal mechanism solution of Palu-Koro and Matano fault events: processing strategy. IOP Conf. Ser. Earth Environ. Sci. 1227, 012043. https://doi.org/10.1088/1755-1315/1227/1/012043*

- *Lacan, P., Ortuño, M., 2012. Active Tectonics of the Pyrenees: A review. J. Iber. Geol. 38, 9–30. https://doi.org/10.5209/rev_JIGE.2012.v38.n1.39203*
- *Lachenbruch, A.H., Sass, J.H., 1992. Heat flow from Cajon Pass, fault strength, and tectonic implications. J. Geophys. Res. Solid Earth 97, 4995–5015. https://doi.org/10.1029/91JB01506*
- *Lacombe, O., 2012. Do fault slip data inversions actually yield "paleostresses" that can be compared with contemporary stresses? A critical discussion. Comptes Rendus Géoscience 344, 159–173. https://doi.org/10.1016/j.crte.2012.01.006*
- *Lafuente, P., Arlegui, L.E., Liesa, C.L., Simón, J.L., 2011. Paleoseismological analysis of an intraplate extensional structure: the Concud fault (Iberian Chain, eastern Spain). Int. J. Earth Sci. 100, 1713–1732. https://doi.org/10.1007/s00531-010-0542-1*
- *Laughton, A.S., Whitmarsh, R.B., 1974. The Azores-Gibraltar Plate Boundary, in: Kristjansson, L. (Ed.), Geodynamics of Iceland and the North Atlantic Area. Springer Netherlands, Dordrecht, pp. 63–81. https://doi.org/10.1007/978-94-010-2271-2_5*
- *Lavecchia, G., 1988. The tyrrhenian-apennines system: structural setting and seismotectogenesis. Tectonophysics 147, 263–296. https://doi.org/10.1016/0040-1951(88)90190-4*
- *Lavecchia, G., Adinolfi, G.M., De Nardis, R., Ferrarini, F., Cirillo, D., Brozzetti, F., De Matteis, R., Festa, G., Zollo, A., 2017. Multidisciplinary inferences on a newly recognized active east-dipping extensional system in Central Italy. Terra Nova 29, 77–89. https://doi.org/10.1111/ter.12251*
- *Lavecchia, G., Bello, S., Andrenacci, C., Cirillo, D., Ferrarini, F., Vicentini, N., De Nardis, R., Roberts, G., Brozzetti, F., 2022. QUaternary fault strain INdicators database - QUIN 1.0 - first release from the Apennines of central Italy. Sci. Data 9, 204. https://doi.org/10.1038/s41597-022-01311-8*
- *Lavecchia, G., Bello, S., Andrenacci, C., Cirillo, D., Pietrolungo, F., Talone, D., Ferrarini, F., De Nardis, R., Galli, P., Faure Walker, J., Sgambato, C., Menichetti, M., Monaco, C., Gambino, S., De Guidi, G., Barreca, G., Carnemolla, F., Brighenti, F., Giuffrida, S., Pirrotta, C., Carboni, F., Ferranti, L., Valoroso, L., Toscani, G., Barchi, M.R., Roberts, G., Brozzetti, F., 2024a. QUIN 2.0 - new release of the QUaternary fault strain INdicators database from the Southern Apennines of Italy. Sci. Data 11, 189. https://doi.org/10.1038/s41597-024-03008-6*
- *Lavecchia, G., De Nardis, R., Ferrarini, F., Cirillo, D., Bello, S., Brozzetti, F., 2021. Regional Seismotectonic Zonation of Hydrocarbon Fields in Active Thrust Belts: A Case Study from Italy, in: Bonali, F.L., Pasquaré Mariotto, F., Tsereteli, N. (Eds.), Building Knowledge for Geohazard Assessment and Management in the Caucasus and Other Orogenic Regions, NATO Science for Peace and Security Series C: Environmental Security. Springer Netherlands, Dordrecht, pp. 89–128. https://doi.org/10.1007/978-94-024-2046-3_7*
- *Lavecchia, G., Pietrolungo, F., Bello, S., Talone, D., Pandolfi, C., Andrenacci, C., Carducci, A., De Nardis, R., 2024b. Slowly Deforming Megathrusts within the Continental Lithosphere: A Case from Italy. GSA Today 34, 4–10. https://doi.org/10.1130/GSATG573A.1*
- *Le Pichon, X., Lybéris, N., Angelier, J., Renard, V., 1982. Strain distribution over the east Mediterranean ridge: A synthesis incorporating new Sea-Beam data. Tectonophysics 86, 243–274. https://doi.org/10.1016/0040-1951(82)90069-5*
- *Li, K., Tapponnier, P., Xu, X., Ren, J., Wang, S., Zhao, J., 2022. Holocene Slip Rate Along the Beng Co Fault and Dextral Strike-Slip Extrusion of Central Eastern Tibet. Tectonics 41, e2022TC007230. https://doi.org/10.1029/2022TC007230*
- *Li, Q., Li, C., Tan, K., Lu, X., Zuo, X., 2021. Slip Model of the 2020 Yutian (Northwestern Tibetan Plateau) Earthquake Derived From Joint Inversion of InSAR and Teleseismic Data. Earth Space Sci. 8, e2020EA001409. https://doi.org/10.1029/2020EA001409*
- *Li, S., Tao, T., Gao, F., Qu, X., Zhu, Y., Huang, J., Wang, Q., 2020. Interseismic Coupling beneath the Sikkim–Bhutan Himalaya Constrained by GPS Measurements and Its Implication for Strain Segmentation and Seismic Activity. Remote Sens. 12, 2202. https://doi.org/10.3390/rs12142202*
- *Li, Y., Wang, C., Dai, J., Xu, G., Hou, Y., Li, X., 2015. Propagation of the deformation and growth of the Tibetan–Himalayan orogen: A review. Earth-Sci. Rev. 143, 36–61. https://doi.org/10.1016/j.earscirev.2015.01.001*
- *Lindsey, E.O., Natsuaki, R., Xu, X., Shimada, M., Hashimoto, M., Melgar, D., Sandwell, D.T., 2015. Line-of-sight displacement from ALOS-2 interferometry: M_w 7.8 Gorkha Earthquake and M_w 7.3 aftershock. Geophys. Res. Lett. 42, 6655–6661. https://doi.org/10.1002/2015GL065385*
- *Liu, C., Ji, L., Zhu, L., Xu, C., Zhao, C., Lu, Z., Wang, Q., 2024. Kilometer-resolution three-dimensional crustal deformation of Tibetan Plateau from InSAR and GNSS. Sci. China Earth Sci. 67, 1818–1835. https://doi.org/10.1007/s11430-023-1289-4*
- *LNEC, 1986. A Sismicidade Histórica e a Revisão do Catálogo Sísmico. Laboratorio Nacional de Engenharia Civil, 189 pp.*
- *López-Fernández, C., Fernández-Viejo, G., Olona, J., Llana-Fúnez, S., 2018. Intraplate Seismicity in Northwest Iberia along the Trace of the Ventaniella Fault: A Case for Fault Intersection at Depth. Bull. Seismol. Soc. Am. 108, 604–618. https://doi.org/10.1785/0120170215*
- *López-Gómez, J., Alonso-Azcárate, J., Arche, A., Arribas, J., Fernández Barrenechea, J., Borruel-Abadía, V., Bourquin, S., Cadenas, P., Cuevas, J., De La Horra, R., Díez, J.B., Escudero-Mozo, M.J., Fernández-Viejo, G., Galán-Abellán, B., Galé, C., Gaspar-Escribano, J., Gisbert Aguilar, J., Gómez-Gras, D., Goy, A., Gretter, N., Heredia Carballo, N., Lago, M., Lloret, J., Luque, J., Márquez, L., Márquez-Aliaga, A., Martín-Algarra, A., Martín-Chivelet, J., Martín-González, F., Marzo, M., Mercedes-Martín, R., Ortí, F., Pérez-López, A., Pérez-Valera, F., Pérez-Valera, J.A., Plasencia, P., Ramos, E., Rodríguez-Méndez, L., Ronchi, A., Salas, R., Sánchez-Fernández, D., Sánchez-Moya, Y., Sopeña, A., Suárez-Rodríguez, Á., Tubía, J.M., Ubide, T., Valero Garcés, B., Vargas, H., Viseras, C., 2019. Permian-Triassic Rifting Stage, in: Quesada, C., Oliveira, J.T. (Eds.), The Geology of Iberia: A Geodynamic Approach, Regional Geology Reviews. Springer International Publishing, Cham, pp. 29–112. https://doi.org/10.1007/978-3-030-11295-0_3*
- *Lozano, L., Cantavella, J.V., Gaite, B., Ruiz-Barajas, S., Antón, R., Barco, J., 2022. Seismic Analysis of the 2020–2021 Santa Fe Seismic Sequence in the Granada Basin, Spain: Relocations and Focal Mechanisms. Seismol. Res. Lett. 93, 3246–3265. https://doi.org/10.1785/0220220097*
- *Lund, B., Slunga, R., 1999. Stress tensor inversion using detailed microearthquake information and stability constraints: Application to Ölfus in southwest Iceland. J. Geophys. Res. Solid Earth 104, 14947–14964. https://doi.org/10.1029/1999JB900111*

- *Lund, B., Townend, J., 2007. Calculating horizontal stress orientations with full or partial knowledge of the tectonic stress tensor. Geophys. J. Int. 170, 1328–1335. https://doi.org/10.1111/j.1365-246X.2007.03468.x*
- *Lundstern, J.-E., Zoback, M.D., 2020. Multiscale variations of the crustal stress field throughout North America. Nat. Commun. 11, 1951. https://doi.org/10.1038/s41467-020-15841-5*
- *Luo, J., Zhao, C., Lü, J., Zhou, L., Zheng, S., 2016. Characteristics of Focal Mechanisms and the Stress Field in the Southeastern Margin of the Tibetan Plateau. Pure Appl. Geophys. 173, 2687–2710. https://doi.org/10.1007/s00024-016-1350-8*
- *Luo, Y., Liu, Z., 2021. Fault zone heterogeneities explain depth-dependent pattern and evolution of slow earthquakes in Cascadia. Nat. Commun. 12, 1959. https://doi.org/10.1038/s41467-021-22232-x*
- *Machette, M.N., 2000. Active, capable, and potentially active faults — a paleoseismic perspective. J. Geodyn. 29, 387–392. https://doi.org/10.1016/S0264-3707(99)00060-5*
- *Madarieta-Txurruka, A., Galindo-Zaldívar, J., González-Castillo, L., Peláez, J.A., Ruiz-Armenteros, A.M., Henares, J., Garrido-Carretero, M.S., Avilés, M., Gil, A.J., 2021. High- and Low-Angle Normal Fault Activity in a Collisional Orogen: The Northeastern Granada Basin (Betic Cordillera). Tectonics 40, e2021TC006715. https://doi.org/10.1029/2021TC006715*
- *Madarieta-Txurruka, A., González-Castillo, L., Peláez, J.A., Catalán, M., Henares, J., Gil, A.J., Lamas-Fernández, F., Galindo-Zaldívar, J., 2022. The Role of Faults as Barriers in Confined Seismic Sequences: 2021 Seismicity in the Granada Basin (Betic Cordillera). Tectonics 41, e2022TC007481. https://doi.org/10.1029/2022TC007481*
- *Madarieta-Txurruka, A., González-Castillo, L., Peláez, J.A., Galindo-Zaldívar, J., Borque, M.J., Lacy, M.C., Ruiz-Armenteros, A.M., Henares, J., Ruano, P., Sánchez-Alzola, A., Avilés, M., Rodríguez-Caderot, G., Martínez-Moreno, F.J., Tendero-Salmerón, V., Vinardell-Peña, R., Gil, A.J., 2024. Active Shortening Simultaneous to Normal Faulting Based on GNSS, Geophysical, and Geological Data: The Seismogenic Ventas de Zafarraya Fault (Betic Cordillera, Southern Spain). Tectonics 43, e2023TC007956. https://doi.org/10.1029/2023TC007956*
- *Madarieta-Txurruka, A., Peláez, J.A., González-Castillo, L., Gil, A.J., Galindo-Zaldívar, J., 2023. Active Collapse in the Central Betic Cordillera: Development of the Extensional System of the Granada Basin. Appl. Sci. 13, 9138. https://doi.org/10.3390/app13169138*
- *Malik, J.N., Arora, S., Gadhavi, M.S., Singh, G., Kumar, P., Johnson, F.C., Thakur, M., Raoof, J., 2023. Geological evidence of paleo-earthquakes on a transverse right-lateral strike-slip fault along the NW Himalayan front: Implications towards fault segmentation and strain partitioning. J. Asian Earth Sci. 244, 105518. https://doi.org/10.1016/j.jseaes.2022.105518*
- *Malik, J.N., Srivastava, E., Gadhavi, M.S., Livio, F., Sharma, N., Arora, S., Parrino, N., Burrato, P., Sulli, A., 2024. Holocene surface-rupturing paleo-earthquakes along the Kachchh Mainland Fault: shaping the seismic landscape of Kachchh, Western India. Sci. Rep. 14, 11612. https://doi.org/10.1038/s41598-024-62086-z*
- *Maouche, S., Meghraoui, M., Morhange, C., Belabbes, S., Bouhadad, Y., Haddoum, H., 2011. Active coastal thrusting and folding, and uplift rate of the Sahel Anticline and Zemmouri earthquake area (Tell Atlas, Algeria). Tectonophysics 509, 69–80. https://doi.org/10.1016/j.tecto.2011.06.003*
- *Marín-Lechado, C., Pedrera, A., Peláez, J.A., Ruiz-Constán, A., González-Ramón, A., Henares, J., 2017. Deformation style and controlling geodynamic processes at the eastern Guadalquivir foreland basin (Southern Spain). Tectonics 36, 1072–1089. https://doi.org/10.1002/2017TC004556*
- *Mariucci, M.T., Montone, P., 2020. Database of Italian present-day stress indicators, IPSI 1.4. Sci. Data 7, 298. https://doi.org/10.1038/s41597-020-00640-w*
- *Martinez Solares, J.M., Lopez Arroyo, A., Mezcua, J., 1979. Isoseismal map of the 1755 Lisbon earthquake obtained from Spanish data. Tectonophysics 53, 301–313. https://doi.org/10.1016/0040-1951(79)90075-1*
- *Martínez Solares, J.M.M., 2003. Historical Seismicity of the Iberian Peninsula.*
- *Martínez-Díaz, J.J., 1999. Sismotectónica de la falla de Alhama de Murcia, implicaciones sismogenéticas del terremoto de Lorca de junio-1977 (Mb: 4,2). Estud. Geológicos 55, 251–266. https://doi.org/10.3989/egeol.99555-6165*
- *Martínez-García, P., Comas, M., Soto, J.I., Lonergan, L., Watts, A.B., 2013. Strike-slip tectonics and basin inversion in the Western Mediterranean: the Post-Messinian evolution of the Alboran Sea. Basin Res. 25, 361–387. https://doi.org/10.1111/bre.12005*
- *Martínez-Garzón, P., Heidbach, O., Bohnhoff, M., 2020. Contemporary stress and strain field in the Mediterranean from stress inversion of focal mechanisms and GPS data. Tectonophysics 774, 228286. https://doi.org/10.1016/j.tecto.2019.228286*
- *Martinez-Garzon, P., Kwiatek, G., Ickrath, M., Bohnhoff, M., 2014. MSATSI: A MATLAB Package for Stress Inversion Combining Solid Classic Methodology, a New Simplified User-Handling, and a Visualization Tool. Seismol. Res. Lett. 85, 896–904. https://doi.org/10.1785/0220130189*
- *Martínez-Garzón, P., Vavryčuk, V., Kwiatek, G., Bohnhoff, M., 2016. Sensitivity of stress inversion of focal mechanisms to pore pressure changes. Geophys. Res. Lett. 43, 8441–8450. https://doi.org/10.1002/2016GL070145*
- *Martínez-Loriente, S., Gràcia, E., Bartolome, R., Perea, H., Klaeschen, D., Dañobeitia, J.J., Zitellini, N., Wynn, R.B., Masson, D.G., 2018. Morphostructure, tectono-sedimentary evolution and seismic potential of the Horseshoe Fault, SW Iberian Margin. Basin Res. 30, 382–400. https://doi.org/10.1111/bre.12225*
- *Martínez-Loriente, S., Gràcia, E., Bartolome, R., Sallarès, V., Connors, C., Perea, H., Lo Iacono, C., Klaeschen, D., Terrinha, P., Dañobeitia, J.J., Zitellini, N., 2013. Active deformation in old oceanic lithosphere and significance for earthquake hazard: Seismic imaging of the Coral Patch Ridge area and neighboring abyssal plains (SW Iberian Margin). Geochem. Geophys. Geosystems 14, 2206–2231. https://doi.org/10.1002/ggge.20173*
- *Martínez-Loriente, S., Sallarès, V., Gràcia, E., 2021. The Horseshoe Abyssal plain Thrust could be the source of the 1755 Lisbon earthquake and tsunami. Commun. Earth Environ. 2, 145. https://doi.org/10.1038/s43247-021-00216-5*

- *Martínez-Loriente, S., Sallarès, V., Gràcia, E., Bartolome, R., Dañobeitia, J.J., Zitellini, N., 2014. Seismic and gravity constraints on the nature of the basement in the Africa-Eurasia plate boundary: New insights for the geodynamic evolution of the SW Iberian margin. J. Geophys. Res. Solid Earth 119, 127–149. https://doi.org/10.1002/2013JB010476*
- *Martínez-Martos, M., Galindo-Zaldívar, J., Sanz De Galdeano, C., García-Tortosa, F.J., Martínez-Moreno, F.J., Ruano, P., González-Castillo, L., Azañón, J.M., 2017. Latest extension of the Laujar fault in a convergence setting (Sierra Nevada, Betic Cordillera). J. Geodyn. 104, 15–26. https://doi.org/10.1016/j.jog.2016.12.002*
- *Martínez-Solares, J.M., Mezcua-Rodríguez, J., 2002. Catálogo sísmico de la Península Ibérica:(880 aC-1900). Dir. Gen. Intituto Geográfico Nac. DL 2002.*
- *Martín-González, F., Crespo-Martín, C., Cesca, S., González-Muñoz, S., 2023. Understanding seismicity and seismotectonics in a stable continental region (NW Iberian Peninsula): Implications for the nature of intraplate seismicity. Glob. Planet. Change 227, 104177. https://doi.org/10.1016/j.gloplacha.2023.104177*
- *Martini, I.P., Sagri, M., Colella, A., 2001. Neogene—Quaternary basins of the inner Apennines and Calabrian arc, in: Vai, G.B., Martini, I.P. (Eds.), Anatomy of an Orogen: The Apennines and Adjacent Mediterranean Basins. Springer Netherlands, Dordrecht, pp. 375–399. https://doi.org/10.1007/978-94-015-9829-3_22*
- *Martin-Rojas, I., Alfaro, P., Galindo-Zaldivar, J., Borque-Arancón, M.J., García-Tortosa, F.J., Sanz De Galdeano, C., Avilés, M., Sánchez-Alzola, A., González-Castillo, L., Ruano, P., Medina-Cascales, I., Tendero-Salmerón, V., Madarieta-Txurruka, A., Pedrosa-González, M.T., Gil-Cruz, A.J., 2023. Insights of Active Extension Within a Collisional Orogen From GNSS (Central Betic Cordillera, S Spain). Tectonics 42, e2022TC007723. https://doi.org/10.1029/2022TC007723*
- *Masana, E., Villamarín, J.A., Cabañero, J.S., Plaza, J., Santanach, P., 2001. Seismogenic faulting in an area of low seismic activity: Paleoseismicity of the El Camp fault (Northeast Spain). Neth. J. Geosci. 80, 229–241. https://doi.org/10.1017/S0016774600023854*
- *Mauffret, A., 2007. The Northwestern (Maghreb) boundary of the Nubia (Africa) Plate. Tectonophysics 429, 21–44. https://doi.org/10.1016/j.tecto.2006.09.007*
- *Maurer, J., Materna, K., 2023. Quantification of geodetic strain rate uncertainties and implications for seismic hazard estimates. Geophys. J. Int. 234, 2128–2142. https://doi.org/10.1093/gji/ggad191*
- *McCaffrey, R., Nabelek, J., 1998. Role of oblique convergence in the active deformation of the Himalayas and southern Tibet plateau. Geology 26, 691. https://doi.org/10.1130/0091-7613(1998)026<0691:ROOCIT>2.3.CO;2*
- *McClusky, S., Reilinger, R., Mahmoud, S., Ben Sari, D., Tealeb, A., 2003. GPS constraints on Africa (Nubia) and Arabia plate motions. Geophys. J. Int. 155, 126–138. https://doi.org/10.1046/j.1365-246X.2003.02023.x*
- *McQuarrie, N., Van Hinsbergen, D.J.J., 2013. Retrodeforming the Arabia-Eurasia collision zone: Age of collision versus magnitude of continental subduction. Geology 41, 315–318. https://doi.org/10.1130/G33591.1*
- *Medina-Cascales, I., García-Tortosa, F.J., Martin-Rojas, I., Pérez-Peña, J.V., Alfaro, P., 2021. Tectonic geomorphology of an active slow-moving, intrabasinal fault: The Galera Fault (Guadix-Baza Basin, central Betic Cordillera, southern Spain). Geomorphology 393, 107941. https://doi.org/10.1016/j.geomorph.2021.107941*
- *Meghraoui, M., 1991. Blind reverse faulting system associated with the Mont Chenoua-Tipaza earthquake of 29 October 1989 (north-central Algeria). Terra Nova 3, 84–92. https://doi.org/10.1111/j.1365-3121.1991.tb00847.x*
- *Meighan, H.E., Ten Brink, U., Pulliam, J., 2013. Slab tears and intermediate-depth seismicity. Geophys. Res. Lett. 40, 4244–4248. https://doi.org/10.1002/grl.50830*
- *Michael, A.J., 1984. Determination of stress from slip data: Faults and folds. J. Geophys. Res. Solid Earth 89, 11517–11526. https://doi.org/10.1029/JB089iB13p11517*
- *Michailos, K., Carpenter, N.S., Hetényi, G., 2021. Spatio-Temporal Evolution of Intermediate-Depth Seismicity Beneath the Himalayas: Implications for Metamorphism and Tectonics. Front. Earth Sci. 9, 742700. https://doi.org/10.3389/feart.2021.742700*
- *Miller, M.S., Becker, T.W., 2014. Reactivated lithospheric-scale discontinuities localize dynamic uplift of the Moroccan Atlas Mountains. Geology 42, 35–38. https://doi.org/10.1130/G34959.1*
- *Milnes, A.G., 1994. Aspects of "strike-slip" or wrench tectonics an introductory discussion. Norwegian Journal of Geology 74.*
- *Molnar, P., Tapponnier, P., 1975. Cenozoic Tectonics of Asia: Effects of a Continental Collision: Features of recent continental tectonics in Asia can be interpreted as results of the India-Eurasia collision. Science 189, 419–426. https://doi.org/10.1126/science.189.4201.419*
- *Mora, A., Parra, M., Strecker, M.R., Kammer, A., Dimaté, C., Rodríguez, F., 2006. Cenozoic contractional reactivation of Mesozoic extensional structures in the Eastern Cordillera of Colombia. Tectonics 25, 2005TC001854. https://doi.org/10.1029/2005TC001854*
- *Morales, J., Azañón, J.M., Stich, D., Roldán, F.J., Pérez-Peña, J.V., Martín, R., Cantavella, J.V., Martín, J.B., Mancilla, F., González-Ramón, A., 2015. The 2012–2013 earthquake swarm in the eastern Guadalquivir basin (South Spain): A case of heterogeneous faulting due to oroclinal bending. Gondwana Res. 28, 1566–1578. https://doi.org/10.1016/j.gr.2014.10.017*
- *Moreno, X., Masana, E., Pallàs, R., Gràcia, E., Rodés, Á., Bordonau, J., 2015. Quaternary tectonic activity of the Carboneras Fault in the La Serrata range (SE Iberia): Geomorphological and chronological constraints. Tectonophysics 663, 78–94. https://doi.org/10.1016/j.tecto.2015.08.016*
- *Mukhopadhyay, M., Dasgupta, S., 1988. Deep structure and tectonics of the burmese arc: constraints from earthquake and gravity data. Tectonophysics 149, 299–322. https://doi.org/10.1016/0040-1951(88)90180-1*
- *Mukhopadhyay, S., Sharma, J., 2010. Attenuation characteristics of Garwhal–Kumaun Himalayas from analysis of coda of local earthquakes. J. Seismol. 14, 693–713. https://doi.org/10.1007/s10950-010-9192-9*

- *Nábělek, J., Hetényi, G., Vergne, J., Sapkota, S., Kafle, B., Jiang, M., Su, H., Chen, J., Huang, B.-S., Team, T.H.-C., 2009. Underplating in the Himalaya-Tibet Collision Zone Revealed by the Hi-CLIMB Experiment. Science 325, 1371–1374. https://doi.org/10.1126/science.1167719*
- *Nandy, D.R., Dasgupta, S., 1991. Seismotectonic domains of northeastern India and adjacent areas. Phys. Chem. Earth 18, 371–384. https://doi.org/10.1016/0079-1946(91)90010-D*
- *Neres, M., Carafa, M.M.C., Fernandes, R.M.S., Matias, L., Duarte, J.C., Barba, S., Terrinha, P., 2016. Lithospheric deformation in the Africa-Iberia plate boundary: Improved neotectonic modeling testing a basal-driven Alboran plate. J. Geophys. Res. Solid Earth 121, 6566–6596. https://doi.org/10.1002/2016JB013012*
- *Nucci, R., Serpelloni, E., Faenza, L., Garcia, A., Belardinelli, M.E., 2025a. Geodetic Strain Rates and Seismicity Rates Along the Apennines (Italy). J. Geophys. Res. Solid Earth 130, e2024JB029848. https://doi.org/10.1029/2024JB029848*
- *Nucci, R., Serpelloni, E., Faenza, L., Garcia, A., Belardinelli, M.E., 2025b. Geodetic Strain Rates and Seismicity Rates Along the Apennines (Italy). J. Geophys. Res. Solid Earth 130, e2024JB029848. https://doi.org/10.1029/2024JB029848*
- *Nucci, R., Serpelloni, E., Faenza, L., Garcia, A., Belardinelli, M.E., 2024. Comparative Analysis of Methods to Estimate Geodetic Strain Rates from GNSS Data in Italy. Ann. Geophys. 66, DM531. https://doi.org/10.4401/ag-9015*
- *O'Kane, A., Copley, A., Mitra, S., Wimpenny, S., 2022. The geometry of active shortening in the northwest Himalayas and the implications for seismic hazard. Geophys. J. Int. 231, 2009–2033. https://doi.org/10.1093/gji/ggac303*
- *Olivera, C., Redondo, E., Lambert, J., Riera-Melis, A., Roca, A., 2008. Review of Historical Earthquakes in the Lower Middle Ages: Earthquakes of the XIV and XV Centuries in Catalonia (NE Spain), in: Fréchet, J., Meghraoui, M., Stucchi, M. (Eds.), Historical Seismology, Modern Approaches in Solid Earth Sciences. Springer Netherlands, Dordrecht, pp. 147–162. https://doi.org/10.1007/978-1-4020-8222-1_7*
- *Omodeo Salè, S., Guimerà, J., Mas, R., Arribas, J., 2014. Tectono-stratigraphic evolution of an inverted extensional basin: the Cameros Basin (north of Spain). Int. J. Earth Sci. 103, 1597–1620. https://doi.org/10.1007/s00531-014-1026-5*
- *Ortuño, M., Martí, A., Martín-Closas, C., Jiménez-Moreno, G., Martinetto, E., Santanach, P., 2013. Palaeoenvironments of the Late Miocene Prüedo Basin: implications for the uplift of the Central Pyrenees. J. Geol. Soc. 170, 79–92. https://doi.org/10.1144/jgs2011-121*
- *Palano, M., 2015. On the present-day crustal stress, strain-rate fields and mantle anisotropy pattern of Italy. Geophys. J. Int. 200, 969–985. https://doi.org/10.1093/gji/ggu451*
- *Palano, M., Cannavò, F., Ferranti, L., Mattia, M., Mazzella, M.E., 2011. Strain and stress fields in the Southern Apennines (Italy) constrained by geodetic, seismological and borehole data: Strain and stress in Southern Apennines. Geophys. J. Int. 187, 1270–1282. https://doi.org/10.1111/j.1365-246X.2011.05234.x*
- *Palano, M., González, P.J., Fernández, J., 2015. The Diffuse Plate boundary of Nubia and Iberia in the Western Mediterranean: Crustal deformation evidence for viscous coupling and fragmented lithosphere. Earth Planet. Sci. Lett. 430, 439–447. https://doi.org/10.1016/j.epsl.2015.08.040*
- *Palano, M., González, P.J., Fernández, J., 2013. Strain and stress fields along the Gibraltar Orogenic Arc: Constraints on active geodynamics. Gondwana Res. 23, 1071–1088. https://doi.org/10.1016/j.gr.2012.05.021*
- *Palano, M., Imprescia, P., Agnon, A., Gresta, S., 2018. An improved evaluation of the seismic/geodetic deformation-rate ratio for the Zagros Fold-and-Thrust collisional belt. Geophys. J. Int. 213, 194–209. https://doi.org/10.1093/gji/ggx524*
- *Palano, M., Pezzo, G., Serpelloni, E., Devoti, R., D'Agostino, N., Gandolfi, S., Sparacino, F., Anderlini, L., Poluzzi, L., Tavasci, L., Macini, P., Pietrantonio, G., Riguzzi, F., Antoncecchi, I., Ciccone, F., Rossi, G., Avallone, A., Selvaggi, G., 2020. Geopositioning time series from offshore platforms in the Adriatic Sea. Sci. Data 7, 373. https://doi.org/10.1038/s41597-020-00705-w*
- *Panda, D., Kundu, B., Santosh, M., 2018. Oblique convergence and strain partitioning in the outer deformation front of NE Himalaya. Sci. Rep. 8, 10564. https://doi.org/10.1038/s41598-018-28774-3*
- *Panda, D., Lindsey, E.O., 2024. Overriding Plate Deformation Controls Inferences of Interseismic Coupling Along the Himalayan Megathrust. J. Geophys. Res. Solid Earth 129, e2024JB029819. https://doi.org/10.1029/2024JB029819*
- *Papanikolaou, I.D., Roberts, G.P., 2007. Geometry, kinematics and deformation rates along the active normal fault system in the southern Apennines: Implications for fault growth. J. Struct. Geol. 29, 166–188. https://doi.org/10.1016/j.jsg.2006.07.009*
- *Parija, M.P., Kumar, S., Tiwari, V.M., Rao, N.P., Kumar, N., Biswal, S., Singh, I., 2018. Microseismicity, tectonics and seismic potential in the Western Himalayan segment, NW Himalaya, India. J. Asian Earth Sci. 159, 1–16. https://doi.org/10.1016/j.jseaes.2018.03.016*
- *Paul, H., Mitra, S., Bhattacharya, S.N., Suresh, G., 2015. Active transverse faulting within underthrust Indian crust beneath the Sikkim Himalaya. Geophys. J. Int. 201, 1072–1083. https://doi.org/10.1093/gji/ggv058*
- *Pedrera, A., García-Senz, J., Peropadre, C., Robador, A., López-Mir, B., Díaz-Alvarado, J., Rodríguez-Fernández, L.R., 2021. The Getxo crustal-scale cross-section: Testing tectonic models in the Bay of Biscay-Pyrenean rift system. Earth-Sci. Rev. 212, 103429. https://doi.org/10.1016/j.earscirev.2020.103429*
- *Pedrera, A., García-Senz, J., Pueyo, E.L., López-Mir, B., Silva-Casal, R., Díaz-Alvarado, J., 2023. Inhomogeneous rift inversion and the evolution of the Pyrenees. Earth-Sci. Rev. 245, 104555. https://doi.org/10.1016/j.earscirev.2023.104555*
- *Pedrera, A., Marín-Lechado, C., Stich, D., Ruiz-Constán, A., Galindo-Zaldívar, J., Rey-Moral, C., De Lis Mancilla, F., 2012. Nucleation, linkage and active propagation of a segmented Quaternary normal-dextral fault: the Loma del Viento fault (Campo de Dalías, Eastern Betic Cordillera, SE Spain). Tectonophysics 522–523, 208–217. https://doi.org/10.1016/j.tecto.2011.12.001*
- *Pedrera, A., Ruiz-Constán, A., Galindo-Zaldívar, J., Chalouan, A., Sanz De Galdeano, C., Marín-Lechado, C., Ruano, P., Benmakhlouf, M., Akil, M., López-Garrido, A.C., Chabli, A., Ahmamou, M., González-Castillo, L., 2011. Is there an active subduction beneath the*

Gibraltar orogenic arc? Constraints from Pliocene to present-day stress field. J. Geodyn. 52, 83–96. https://doi.org/10.1016/j.jog.2010.12.003

- *Pedrera, A., Ruiz-Constán, A., García-Senz, J., Azor, A., Marín-Lechado, C., Ayala, C., Díaz De Neira, J.A., Rodríguez-Fernández, L.R., 2020. Evolution of the South-Iberian paleomargin: From hyperextension to continental subduction. J. Struct. Geol. 138, 104122. https://doi.org/10.1016/j.jsg.2020.104122*
- *Pedrera, A., Ruiz-Constán, A., Marín-Lechado, C., Galindo-Zaldívar, J., González, A., Peláez, J.A., 2013. Seismic transpressive basement faults and monocline development in a foreland basin (Eastern Guadalquivir, SE Spain): ACTIVE TRANSPRESSION IN BETICS FORELAND. Tectonics 32, 1571–1586. https://doi.org/10.1002/2013TC003397*
- *Peiro, A., Lozano, L., Arlegui, L.E., Cantavella, J.V., Ruiz-Barajas, S., Simón, J.L., 2024. Present-day incipient fault coalescence at a relay zone (Jiloca extensional basin, Spain): Evidence from instrumental seismicity. Tectonophysics 893, 230541. https://doi.org/10.1016/j.tecto.2024.230541*
- *Peiro, A., Simón, J.L., Martín-Bello, L., Arlegui, L.E., Ezquerro, L., Luzón, A., Medialdea, A., Corral, B., Liesa, C.L., 2023. Recent activity and paleoseismicity of an intraplate extensional fault: the Calamocha fault (Jiloca graben, central Iberian Chain). Int. J. Earth Sci. 112, 513–537. https://doi.org/10.1007/s00531-022-02265-3*
- *Peiro, A., Simón, J.L., Román-Berdiel, T., 2020. Fault relay zones evolving through distributed longitudinal fractures: The case of the Teruel graben system (Iberian Chain, Spain). J. Struct. Geol. 131, 103942. https://doi.org/10.1016/j.jsg.2019.103942*
- *Peláez, J.A., 2023. Deadly Morocco quake resulted from Africa's ongoing collision with Europe. Temblor. https://doi.org/10.32858/temblor.321*
- *Pelaez, J.A., Chourak, M., Tadili, B.A., Brahim, L.A., Hamdache, M., Casado, C.L., Solares, J.M.M., 2007. A Catalog of Main Moroccan Earthquakes from 1045 to 2005. Seismol. Res. Lett. 78, 614–621. https://doi.org/10.1785/gssrl.78.6.614*
- *Perea, H., 2009. The Catalan seismic crisis (1427 and 1428; NE Iberian Peninsula): Geological sources and earthquake triggering. J. Geodyn. 47, 259–270. https://doi.org/10.1016/j.jog.2009.01.002*
- *Perea, H., Masana, E., Santanach, P., 2012. An active zone characterized by slow normal faults, the northwestern margin of the València trough (NE Iberia): a review. J. Iber. Geol. 38, 31–52. https://doi.org/10.5209/rev_JIGE.2012.v38.n1.39204*
- *Pérouse, E., Vernant, P., Chéry, J., Reilinger, R., McClusky, S., 2010. Active surface deformation and sub-lithospheric processes in the western Mediterranean constrained by numerical models. Geology 38, 823–826. https://doi.org/10.1130/G30963.1*
- *Persits, F.M., Ahlbrandt, T.S., Tuttle, M.L.W., Charpentier, R.R., Brownfield, M.E., Takahashi, K.I., 1997. Maps showing geology, oil and gas fields and geological provinces of Africa.*
- *Pietrolungo, F., Lavecchia, G., Madarieta-Txurruka, A., Sparacino, F., Srivastava, E., Cirillo, D., De Nardis, R., Andrenacci, C., Bello, S., Parrino, N., Sulli, A., Palano, M., 2024. Comparison of Crustal Stress and Strain Fields in the Himalaya–Tibet Region: Geodynamic Implications. Remote Sens. 16, 4765. https://doi.org/10.3390/rs16244765*
- *Platt, J., Houseman, G., 2003. Evidence for active subduction beneath Gibraltar: Comment and Reply. Geology 31, e22–e22. https://doi.org/10.1130/0091-7613-31.1.e22*
- *Polonia, A., Torelli, L., Mussoni, P., Gasperini, L., Artoni, A., Klaeschen, D., 2011. The Calabrian Arc subduction complex in the Ionian Sea: Regional architecture, active deformation, and seismic hazard. Tectonics 30, 2010TC002821. https://doi.org/10.1029/2010TC002821*
- *Pondrelli, S., Visini, F., Rovida, A., D'Amico, V., Pace, B., Meletti, C., 2020. Style of faulting of expected earthquakes in Italy as an input for seismic hazard modeling. Nat. Hazards Earth Syst. Sci. 20, 3577–3592. https://doi.org/10.5194/nhess-20-3577-2020*
- *Poujol, A., Ritz, J.-F., Tahayt, A., Vernant, P., Condomines, M., Blard, P.-H., Billant, J., Vacher, L., Tibari, B., Hni, L., Idrissi, A.K., 2014. Active tectonics of the Northern Rif (Morocco) from geomorphic and geochronological data. J. Geodyn. 77, 70–88. https://doi.org/10.1016/j.jog.2014.01.004*
- *Powell, C.McA., 1986. Continental underplating model for the rise of the Tibetan Plateau. Earth Planet. Sci. Lett. 81, 79–94. https://doi.org/10.1016/0012-821X(86)90102-0*
- *Pro, C., Buforn, E., Bezzeghoud, M., Udías, A., 2013. The earthquakes of 29 July 2003, 12 February 2007, and 17 December 2009 in the region of Cape Saint Vincent (SW Iberia) and their relation with the 1755 Lisbon earthquake. Tectonophysics 583, 16–27. https://doi.org/10.1016/j.tecto.2012.10.010*
- *Rajabi, M., Heidbach, O., Tingay, M., Reiter, K., 2017. Prediction of the present-day stress field in the Australian continental crust using 3D geomechanical–numerical models. Aust. J. Earth Sci. 64, 435–454. https://doi.org/10.1080/08120099.2017.1294109*
- *Raoof, J., Mukhopadhyay, S., Koulakov, I., Kayal, J.R., 2017. 3-D seismic tomography of the lithosphere and its geodynamic implications beneath the northeast India region. Tectonics 36, 962–980. https://doi.org/10.1002/2016TC004375*
- *Rashidi, A., Derakhshani, R., 2022. Strain and Moment Rates from GPS and Seismological Data in Northern Iran: Implications for an Evaluation of Stress Trajectories and Probabilistic Fault Rupture Hazard. Remote Sens. 14, 2219. https://doi.org/10.3390/rs14092219*
- *Rashwan, M., Sawires, R., Radwan, A.M., Sparacino, F., Peláez, J.A., Palano, M., 2021. Crustal Strain and Stress Fields in Egypt from Geodetic and Seismological Data. Remote Sens. 13, 1398. https://doi.org/10.3390/rs13071398*
- *Rastogi, B.K., 1974. Earthquake mechanisms and plate tectonics in the Himalayan region. Tectonophysics 21, 47–56. https://doi.org/10.1016/0040-1951(74)90061-4*
- *Read, H.H., Watson, J., 1975. The Alpine-Himalayan Belt and the Eurasian Craton, in: Introduction to Geology. Macmillan Education UK, London, pp. 179–222. https://doi.org/10.1007/978-1-349-15613-9_7*
- *Rebaï, S., Philip, H., Taboada, A., 1992. Modern tectonic stress field in the Mediterranean region: evidence for variation in stress directions at different scales. Geophys. J. Int. 110, 106–140. https://doi.org/10.1111/j.1365-246X.1992.tb00717.x*

- *Reicherter, K.R., Jabaloy, A., Galindo-Zaldívar, J., Ruano, P., Becker-Heidmann, P., Morales, J., Reiss, S., González-Lodeiro, F., 2003. Repeated palaeoseismic activity of the Ventas de Zafarraya fault (S Spain) and its relation with the 1884 Andalusian earthquake. Int. J. Earth Sci. 92, 912–922. https://doi.org/10.1007/s00531-003-0366-3*
- *Reilinger, R., McClusky, S., Vernant, P., Lawrence, S., Ergintav, S., Cakmak, R., Ozener, H., Kadirov, F., Guliev, I., Stepanyan, R., Nadariya, M., Hahubia, G., Mahmoud, S., Sakr, K., ArRajehi, A., Paradissis, D., Al-Aydrus, A., Prilepin, M., Guseva, T., Evren, E., Dmitrotsa, A., Filikov, S.V., Gomez, F., Al-Ghazzi, R., Karam, G., 2006. GPS constraints on continental deformation in the Africa-Arabia-Eurasia continental collision zone and implications for the dynamics of plate interactions. J. Geophys. Res. Solid Earth 111, 2005JB004051. https://doi.org/10.1029/2005JB004051*
- *Reinhardt, L.J., Dempster, T.J., Shroder, J.F., Persano, C., 2007. Tectonic denudation and topographic development in the Spanish Sierra Nevada. Tectonics 26, 2006TC001954. https://doi.org/10.1029/2006TC001954*
- *Reiter, K., Heidbach, O., Ziegler, M.O., 2024. Impact of faults on the remote stress state. Solid Earth 15, 305–327. https://doi.org/10.5194/se-15-305-2024*
- *Rey, P., Vanderhaeghe, O., Teyssier, C., 2001. Gravitational collapse of the continental crust: definition, regimes and modes. Tectonophysics 342, 435–449. https://doi.org/10.1016/S0040-1951(01)00174-3*
- *Rey, P.F., Teyssier, C., Whitney, D.L., 2010. Limit of channel flow in orogenic plateaux. Lithosphere 2, 328–332. https://doi.org/10.1130/L114.1*
- *Reyners, M., 2010. Stress and strain from earthquakes at the southern termination of the Taupo Volcanic Zone, New Zealand. J. Volcanol. Geotherm. Res. 190, 82–88. https://doi.org/10.1016/j.jvolgeores.2009.02.016*
- *Ribeiro, A., Quesada, C., Dallmeyer, R. D., 1990. Geodynamic Evolution of the Iberian Massif, in: Dallmeyer, R. David, Garcia, E.M. (Eds.), Pre-Mesozoic Geology of Iberia. Springer Berlin Heidelberg, Berlin, Heidelberg, pp. 399–409. https://doi.org/10.1007/978-3-642-83980-1_28*
- *Rigo, A., Vernant, P., Feigl, K.L., Goula, X., Khazaradze, G., Talaya, J., Morel, L., Nicolas, J., Baize, S., Chery, J., Sylvander, M., 2015. Present-day deformation of the Pyrenees revealed by GPS surveying and earthquake focal mechanisms until 2011. Geophys. J. Int. 201, 947–964. https://doi.org/10.1093/gji/ggv052*
- *Roca, E., Guimerà, J., 1992. The Neogene structure of the eastern Iberian margin: Structural constraints on the crustal evolution of the Valencia trough (western Mediterranean). Tectonophysics 203, 203–218. https://doi.org/10.1016/0040-1951(92)90224-T*
- *Rockwell, T., Fonseca, J., Madden, C., Dawson, T., Owen, L.A., Vilanova, S., Figueiredo, P., 2009. Palaeoseismology of the Vilariça Segment of the Manteigas-Bragança Fault in northeastern Portugal. Geol. Soc. Lond. Spec. Publ. 316, 237–258. https://doi.org/10.1144/SP316.15*
- *Rodríguez-Escudero, E., Martínez-Díaz, J.J., Álvarez-Gómez, J.A., Insua-Arévalo, J.M., Capote Del Villar, R., 2014. Tectonic setting of the recent damaging seismic series in the Southeastern Betic Cordillera, Spain. Bull. Earthq. Eng. 12, 1831–1854. https://doi.org/10.1007/s10518-013-9551-3*
- *Romagny, A., Jolivet, L., Menant, A., Bessière, E., Maillard, A., Canva, A., Gorini, C., Augier, R., 2020. Detailed tectonic reconstructions of the Western Mediterranean region for the last 35 Ma, insights on driving mechanisms. BSGF - Earth Sci. Bull. 191, 37. https://doi.org/10.1051/bsgf/2020040*
- *Rosenbaum, G., Lister, G.S., Duboz, C., 2002. Relative motions of Africa, Iberia and Europe during Alpine orogeny. Tectonophysics 359, 117–129. https://doi.org/10.1016/S0040-1951(02)00442-0*
- *Rothery, D.A., Drury, S.A., 1984. The neotectonics of the Tibetan Plateau. Tectonics 3, 19–26. https://doi.org/10.1029/TC003i001p00019*
- *Rowley, D.B., Currie, B.S., 2006. Palaeo-altimetry of the late Eocene to Miocene Lunpola basin, central Tibet. Nature 439, 677–681. https://doi.org/10.1038/nature04506*
- *Ruano, P., Galindo-Zaldívar, J., Jabaloy, A., 2004. Recent Tectonic Structures in a Transect of the Central Betic Cordillera. Pure Appl. Geophys. 161, 541–563. https://doi.org/10.1007/s00024-003-2462-5*
- *Ruiz, M., Díaz, J., Canari, A., Ortuño, M., Vergés, J., 2023. Seismic activity at the eastern Pyrenean termination. Tectonophysics 862, 229977. https://doi.org/10.1016/j.tecto.2023.229977*
- *Ruiz-Constán, A., Galindo-Zaldívar, J., Pedrera, A., Célérier, B., Marín-Lechado, C., 2011. Stress distribution at the transition from subduction to continental collision (northwestern and central Betic Cordillera): FROM SUBDUCTION TO CONTINENTAL COLLISION. Geochem. Geophys. Geosystems 12, n/a-n/a. https://doi.org/10.1029/2011GC003824*
- *Ruiz-Constán, A., Stich, D., Galindo-Zaldívar, J., Morales, J., 2009. Is the northwestern Betic Cordillera mountain front active in the context of the convergent Eurasia–Africa plate boundary? Terra Nova 21, 352–359. https://doi.org/10.1111/j.1365-3121.2009.00886.x*
- *Ryder, I., Bürgmann, R., Fielding, E., 2012. Static stress interactions in extensional earthquake sequences: An example from the South Lunggar Rift, Tibet. J. Geophys. Res. Solid Earth 117, 2012JB009365. https://doi.org/10.1029/2012JB009365*
- *Sallarès, V., Gailler, A., Gutscher, M.-A., Graindorge, D., Bartolomé, R., Gràcia, E., Díaz, J., Dañobeitia, J.J., Zitellini, N., 2011. Seismic evidence for the presence of Jurassic oceanic crust in the central Gulf of Cadiz (SW Iberian margin). Earth Planet. Sci. Lett. 311, 112–123. https://doi.org/10.1016/j.epsl.2011.09.003*
- *Sallarès, V., Martínez-Loriente, S., Prada, M., Gràcia, E., Ranero, C., Gutscher, M.-A., Bartolome, R., Gailler, A., Dañobeitia, J.J., Zitellini, N., 2013. Seismic evidence of exhumed mantle rock basement at the Gorringe Bank and the adjacent Horseshoe and Tagus abyssal plains (SW Iberia). Earth Planet. Sci. Lett. 365, 120–131. https://doi.org/10.1016/j.epsl.2013.01.021*
- *Sandwell, D.T., Wessel, P., 2016. Interpolation of 2-D vector data using constraints from elasticity. Geophys. Res. Lett. 43. https://doi.org/10.1002/2016GL070340*

- *Santos-Bueno, N., Fernández-García, C., Stich, D., Mancilla, F.D.L., Martín, R., Molina-Aguilera, A., Morales, J., 2019. Focal Mechanisms for Subcrustal Earthquakes Beneath the Gibraltar Arc. Geophys. Res. Lett. 46, 2534–2543. https://doi.org/10.1029/2018GL081587*
- *Sanz De Galdeano, C., Alfaro, P., 2004. Tectonic significance of the present relief of the Betic Cordillera. Geomorphology 63, 175–190. https://doi.org/10.1016/j.geomorph.2004.04.002*
- *Sanz De Galdeano, C., García-Tortosa, F.J., Peláez, J.A., Alfaro, P., Azañón, J.M., Galindo-Zaldívar, J., López Casado, C., López Garrido, A.C., Rodríguez-Fernández, J., Ruano, P., 2012. Main active faults in the Granada and Guadix-Baza Basins (Betic Cordillera). J. Iber. Geol. 38, 209–223. https://doi.org/10.5209/rev_JIGE.2012.v38.n1.39215*
- *Sanz De Galdeano, C., Peláez Montilla, J.A., López Casado, C., 2003. Seismic Potential of the Main Active Faults in the Granada Basin (Southern Spain). Pure Appl. Geophys. 160, 1537–1556. https://doi.org/10.1007/s00024-003-2359-3*
- *Sartori, R., Torelli, L., Zitellini, N., Peis, D., Lodolo, E., 1994. Eastern segment of the Azores-Gibraltar line (central-eastern Atlantic): An oceanic plate boundary with diffuse compressional deformation. Geology 22, 555. https://doi.org/10.1130/0091-7613(1994)022<0555:ESOTAG>2.3.CO;2*
- *Saylor, J., DeCelles, P., Gehrels, G., Murphy, M., Zhang, R., Kapp, P., 2010. Basin formation in the High Himalaya by arc-parallel extension and tectonic damming: Zhada basin, southwestern Tibet. Tectonics 29, n/a-n/a. https://doi.org/10.1029/2008TC002390*
- *Schettino, A., Turco, E., 2011. Tectonic history of the western Tethys since the Late Triassic. Geol. Soc. Am. Bull. 123, 89–105. https://doi.org/10.1130/B30064.1*
- *Schildgen, T.F., Yıldırım, C., Cosentino, D., Strecker, M.R., 2014. Linking slab break-off, Hellenic trench retreat, and uplift of the Central and Eastern Anatolian plateaus. Earth-Sci. Rev. 128, 147–168. https://doi.org/10.1016/j.earscirev.2013.11.006*
- *Schmid, S.M., Fügenschuh, B., Kissling, E., Schuster, R., 2004. Tectonic map and overall architecture of the Alpine orogen. Eclogae Geol. Helvetiae 97, 93–117. https://doi.org/10.1007/s00015-004-1113-x*
- *Scognamiglio, L., Tinti, E., Quintiliani, M., 2006. Time Domain Moment Tensor (TDMT). https://doi.org/10.13127/TDMT*
- *Scotti, V.N., Molin, P., Faccenna, C., Soligo, M., Casas-Sainz, A., 2014. The influence of surface and tectonic processes on landscape evolution of the Iberian Chain (Spain): Quantitative geomorphological analysis and geochronology. Geomorphology 206, 37–57. https://doi.org/10.1016/j.geomorph.2013.09.017*
- *Sébrier, M., Siame, L., Zouine, E.M., Winter, T., Missenard, Y., Leturmy, P., 2006. Active tectonics in the Moroccan High Atlas. Comptes Rendus Géoscience 338, 65–79. https://doi.org/10.1016/j.crte.2005.12.001*
- *Serpelloni, E., Anzidei, M., Baldi, P., Casula, G., Galvani, A., 2005. Crustal velocity and strain-rate fields in Italy and surrounding regions: new results from the analysis of permanent and non-permanent GPS networks. Geophys. J. Int. 161, 861–880. https://doi.org/10.1111/j.1365-246X.2005.02618.x*
- *Serpelloni, E., Cavaliere, A., Martelli, L., Pintori, F., Anderlini, L., Borghi, A., Randazzo, D., Bruni, S., Devoti, R., Perfetti, P., Cacciaguerra, S., 2022. Surface Velocities and Strain-Rates in the Euro-Mediterranean Region From Massive GPS Data Processing. Front. Earth Sci. 10, 907897. https://doi.org/10.3389/feart.2022.907897*
- *Serpelloni, E., Vannucci, G., Pondrelli, S., Argnani, A., Casula, G., Anzidei, M., Baldi, P., Gasperini, P., 2007. Kinematics of the Western Africa-Eurasia plate boundary from focal mechanisms and GPS data. Geophys. J. Int. 169, 1180–1200. https://doi.org/10.1111/j.1365-246X.2007.03367.x*
- *Sheikholeslami, M.R., Mobayen, P., Javadi, H.R., Ghassemi, M.R., 2021. Stress field and tectonic regime of Central Iran from inversion of the earthquake focal mechanisms. Tectonophysics 813, 228931. https://doi.org/10.1016/j.tecto.2021.228931*
- *Shen, Z., Wang, M., Zeng, Y., Wang, F., 2015. Optimal Interpolation of Spatially Discretized Geodetic Data. Bull. Seismol. Soc. Am. 105, 2117–2127. https://doi.org/10.1785/0120140247*
- *Shi, D., Zhao, W., Klemperer, S.L., Wu, Z., Mechie, J., Shi, J., Xue, G., Su, H., 2016. West–east transition from underplating to steep subduction in the India–Tibet collision zone revealed by receiver-function profiles. Earth Planet. Sci. Lett. 452, 171–177. https://doi.org/10.1016/j.epsl.2016.07.051*
- *Sibuet, J., Srivastava, S.P., Spakman, W., 2004. Pyrenean orogeny and plate kinematics. J. Geophys. Res. Solid Earth 109, 2003JB002514. https://doi.org/10.1029/2003JB002514*
- *Silva, P.G., Goy, J.L., Somoza, L., Zazo, C., Bardají, T., 1993. Landscape response to strike-slip faulting linked to collisional settings: Quaternary tectonics and basin formation in the Eastern Betics, southeastern Spain. Tectonophysics 224, 289–303. https://doi.org/10.1016/0040-1951(93)90034-H*
- *Sippel, J., Scheck-Wenderoth, M., Reicherter, K., Mazur, S., 2009. Paleostress states at the south-western margin of the Central European Basin System — Application of fault-slip analysis to unravel a polyphase deformation pattern. Tectonophysics 470, 129–146. https://doi.org/10.1016/j.tecto.2008.04.010*
- *Smeraglia, L., Bernasconi, S.M., Berra, F., Billi, A., Boschi, C., Caracausi, A., Carminati, E., Castorina, F., Doglioni, C., Italiano, F., Rizzo, A.L., Uysal, I.T., Zhao, J., 2018. Crustal-scale fluid circulation and co-seismic shallow comb-veining along the longest normal fault of the central Apennines, Italy. Earth Planet. Sci. Lett. 498, 152–168. https://doi.org/10.1016/j.epsl.2018.06.013*
- *Soumaya, A., Ben Ayed, N., Rajabi, M., Meghraoui, M., Delvaux, D., Kadri, A., Ziegler, M., Maouche, S., Braham, A., 2018. Active Faulting Geometry and Stress Pattern Near Complex Strike-Slip Systems Along the Maghreb Region: Constraints on Active Convergence in the Western Mediterranean. Tectonics 37, 3148–3173. https://doi.org/10.1029/2018TC004983*
- *Spakman, W., Wortel, R., 2004. A Tomographic View on Western Mediterranean Geodynamics, in: Cavazza, W., Roure, F., Spakman, W., Stampfli, G.M., Ziegler, P.A. (Eds.), The TRANSMED Atlas. The Mediterranean Region from Crust to Mantle. Springer Berlin Heidelberg, Berlin, Heidelberg, pp. 31–52. https://doi.org/10.1007/978-3-642-18919-7_2*

- *Sparacino, F., Palano, M., Peláez, J.A., Fernández, J., 2020. Geodetic Deformation versus Seismic Crustal Moment-Rates: Insights from the Ibero-Maghrebian Region. Remote Sens. 12, 952. https://doi.org/10.3390/rs12060952*
- *Sperner, B., Müller, B., Heidbach, O., Delvaux, D., Reinecker, J., Fuchs, K., 2003. Tectonic stress in the Earth's crust: advances in the World Stress Map project. Geol. Soc. Lond. Spec. Publ. 212, 101–116. https://doi.org/10.1144/GSL.SP.2003.212.01.07*
- *Srivastava, E., Malik, J.N., Parrino, N., Burrato, P., Sharma, N., Gadhavi, M., Sulli, A., Di Maggio, C., Morticelli, M.G., 2023. Extremely fast Holocene coastal landscape evolution in the Kachchh Upland (NW India): Clues from a multidisciplinary review. J. Maps 19, 2167617. https://doi.org/10.1080/17445647.2023.2167617*
- *Srivastava, S.P., Roest, W.R., Kovacs, L.C., Oakey, G., Lévesque, S., Verhoef, J., Macnab, R., 1990. Motion of Iberia since the Late Jurassic: Results from detailed aeromagnetic measurements in the Newfoundland Basin. Tectonophysics 184, 229–260. https://doi.org/10.1016/0040-1951(90)90442-B*
- *Stevens, V.L., Avouac, J.-P., 2021. On the relationship between strain rate and seismicity in the India–Asia collision zone: implications for probabilistic seismic hazard. Geophys. J. Int. 226, 220–245. https://doi.org/10.1093/gji/ggab098*
- *Stich, D., Batlló, J., Macià, R., Teves-Costa, P., Morales, J., 2005. Moment tensor inversion with single-component historical seismograms: The 1909 Benavente (Portugal) and Lambesc (France) earthquakes. Geophys. J. Int. 162, 850–858. https://doi.org/10.1111/j.1365-246X.2005.02680.x*
- *Stich, D., Serpelloni, E., De Lis Mancilla, F., Morales, J., 2006. Kinematics of the Iberia–Maghreb plate contact from seismic moment tensors and GPS observations. Tectonophysics 426, 295–317. https://doi.org/10.1016/j.tecto.2006.08.004*
- *Stucchi, M., Rovida, A., Gomez Capera, A.A., Alexandre, P., Camelbeeck, T., Demircioglu, M.B., Gasperini, P., Kouskouna, V., Musson, R.M.W., Radulian, M., Sesetyan, K., Vilanova, S., Baumont, D., Bungum, H., Fäh, D., Lenhardt, W., Makropoulos, K., Martinez Solares, J.M., Scotti, O., Živčić, M., Albini, P., Batllo, J., Papaioannou, C., Tatevossian, R., Locati, M., Meletti, C., Viganò, D., Giardini, D., 2013. The SHARE European Earthquake Catalogue (SHEEC) 1000–1899. J. Seismol. 17, 523–544. https://doi.org/10.1007/s10950-012-9335-2*
- *Styron, R., Pagani, M., 2020. The GEM Global Active Faults Database. Earthq. Spectra 36, 160–180. https://doi.org/10.1177/8755293020944182*
- *Styron, R., Taylor, M., Sundell, K., 2015. Accelerated extension of Tibet linked to the northward underthrusting of Indian crust. Nat. Geosci. 8, 131–134. https://doi.org/10.1038/ngeo2336*
- *Styron, R.H., Taylor, M.H., Murphy, M.A., 2011. Oblique convergence, arc-parallel extension, and the role of strike-slip faulting in the High Himalaya. Geosphere 7, 582–596. https://doi.org/10.1130/GES00606.1*
- *Tahayt, A., Feigl, K.L., Mourabit, T., Rigo, A., Reilinger, R., McClusky, S., Fadil, A., Berthier, E., Dorbath, L., Serroukh, M., Gomez, F., Ben Sari, D., 2009. The Al Hoceima (Morocco) earthquake of 24 February 2004, analysis and interpretation of data from ENVISAT ASAR and SPOT5 validated by ground-based observations. Remote Sens. Environ. 113, 306–316. https://doi.org/10.1016/j.rse.2008.09.015*
- *Tape, C., Musé, P., Simons, M., Dong, D., Webb, F., 2009. Multiscale estimation of GPS velocity fields. Geophys. J. Int. 179, 945–971. https://doi.org/10.1111/j.1365-246X.2009.04337.x*
- *Tapponnier, P., Molnar, P., 1976. Slip-line field theory and large-scale continental tectonics. Nature 264, 319–324. https://doi.org/10.1038/264319a0*
- *Tapponnier, P., Peltzer, G., Armijo, R., 1986. On the mechanics of the collision between India and Asia. Geol. Soc. Lond. Spec. Publ. 19, 113–157. https://doi.org/10.1144/GSL.SP.1986.019.01.07*
- *Tapponnier, P., Peltzer, G., Le Dain, A.Y., Armijo, R., Cobbold, P., 1982. Propagating extrusion tectonics in Asia: New insights from simple experiments with plasticine. Geology 10, 611. https://doi.org/10.1130/0091-7613(1982)10<611:PETIAN>2.0.CO;2*
- *Taylor, M., 2009. Active structures of the Himalayan-Tibetan orogen and their relationships to earthquake distribution, contemporary strain field, and Cenozoic volcanism.*
- *Taylor, M., Peltzer, G., 2006. Current slip rates on conjugate strike-slip faults in central Tibet using synthetic aperture radar interferometry. J. Geophys. Res. Solid Earth 111, 2005JB004014. https://doi.org/10.1029/2005JB004014*
- *Taymaz, T., Yilmaz, Y., Dilek, Y., 2007. The geodynamics of the Aegean and Anatolia: introduction. Geol. Soc. Lond. Spec. Publ. 291, 1–16. https://doi.org/10.1144/SP291.1*
- *Teixell, A., 1998. Crustal structure and orogenic material budget in the west central Pyrenees. Tectonics 17, 395–406. https://doi.org/10.1029/98TC00561*
- *Teixell, A., Arboleya, M., Julivert, M., Charroud, M., 2003. Tectonic shortening and topography in the central High Atlas (Morocco). Tectonics 22, 2002TC001460. https://doi.org/10.1029/2002TC001460*
- *Teixell, A., Ayarza, P., Zeyen, H., Fernàndez, M., Arboleya, M., 2005. Effects of mantle upwelling in a compressional setting: the Atlas Mountains of Morocco. Terra Nova 17, 456–461. https://doi.org/10.1111/j.1365-3121.2005.00633.x*
- *Tendero-Salmerón, V., Ercilla, G., González-Castillo, L., Madarieta-Txurruka, A., Martínez-Moreno, F.J., Estrada, F., Galindo-Zaldivar, J., 2024. Gravimetric survey and modelling of a tectonic indenter boundary: The Palomares Fault Zone (Betic Cordillera, Iberia). Tectonophysics 872, 230147. https://doi.org/10.1016/j.tecto.2023.230147*
- *Tendero-Salmerón, V., Galindo-Zaldivar, J., d'Acremont, E., Catalán, M., Martos, Y.M., Ammar, A., Ercilla, G., 2022. New insights on the Alboran Sea basin extension and continental collision from magnetic anomalies related to magmatism (western Mediterranean). Mar. Geol. 443, 106696. https://doi.org/10.1016/j.margeo.2021.106696*
- *Tendero-Salmerón, V., Lafosse, M., d'Acremont, E., Rabaute, A., Azzouz, O., Ercilla, G., Makkaoui, M., Galindo-Zaldivar, J., 2021. Application of Automated Throw Backstripping Method to Characterize Recent Faulting Activity Migration in the Al Hoceima Bay (Northeast Morocco): Geodynamic Implications. Front. Earth Sci. 9, 645942. https://doi.org/10.3389/feart.2021.645942*

- *Teng, J., Deng, Y., Badal, J., Zhang, Y., 2014. Moho depth, seismicity and seismogenic structure in China mainland. Tectonophysics 627, 108–121. https://doi.org/10.1016/j.tecto.2013.11.008*
- *Tesón, E., Teixell, A., 2008. Sequence of thrusting and syntectonic sedimentation in the eastern Sub-Atlas thrust belt (Dadès and Mgoun valleys, Morocco). Int. J. Earth Sci. 97, 103–113. https://doi.org/10.1007/s00531-006-0151-1*
- *Testa, A., Boncio, P., Baize, S., Mirabella, F., Pucci, S., Pace, B., Riesner, M., Pauselli, C., Ercoli, M., Benedetti, L., Di Chiara, A., Civico, R., 2023. Paleoseismological Constraints on the Anghiari Normal Fault (Northern Apennines, Italy) and Potential Implications for the Activity of the Altotiberina Low-Angle Normal Fault. Tectonics 42, e2023TC007798. https://doi.org/10.1029/2023TC007798*
- *Thinon, I., Fidalgo-González, L., Réhault, J.-P., Olivet, J.-L., 2001. Déformations pyrénéennes dans le golfe de Gascogne. Comptes Rendus Académie Sci. - Ser. IIA - Earth Planet. Sci. 332, 561–568. https://doi.org/10.1016/S1251-8050(01)01576-2*
- *Thirunavukarasu, A., Kumar, A., Mitra, S., 2017. Lateral variation of seismic attenuation in Sikkim Himalaya. Geophys. J. Int. 208, 257–268. https://doi.org/10.1093/gji/ggw384*
- *Tian, X., Chen, Y., Tseng, T.-L., Klemperer, S.L., Thybo, H., Liu, Z., Xu, T., Liang, X., Bai, Z., Zhang, X., Si, S., Sun, C., Lan, H., Wang, E., Teng, J., 2015. Weakly coupled lithospheric extension in southern Tibet. Earth Planet. Sci. Lett. 430, 171–177. https://doi.org/10.1016/j.epsl.2015.08.025*
- *Torne, M., Fernàndez, M., Comas, M.C., Soto, J.I., 2000. Lithospheric Structure Beneath the Alboran Basin: Results from 3D Gravity Modeling and Tectonic Relevance. J. Geophys. Res. Solid Earth 105, 3209–3228. https://doi.org/10.1029/1999JB900281*
- *Tortella, D., Torne, M., Pérez-Estáun, A., 1997. [No title found]. Mar. Geophys. Res. 19, 211–230. https://doi.org/10.1023/A:1004258510797*
- *Townend, J., Zoback, M.D., 2006. Stress, strain, and mountain building in central Japan. J. Geophys. Res. Solid Earth 111, 2005JB003759. https://doi.org/10.1029/2005JB003759*
- *Tugend, J., Manatschal, G., Kusznir, N.J., Masini, E., Mohn, G., Thinon, I., 2014. Formation and deformation of hyperextended rift systems: Insights from rift domain mapping in the Bay of Biscay-Pyrenees. Tectonics 33, 1239–1276. https://doi.org/10.1002/2014TC003529*
- *Udías, A., Buforn, E., 1991. Regional Stresses Along the Eurasia-Africa Plate Boundary Derived from Focal Mechanisms of Large Earthquakes, in: Udías, A., Buforn, E. (Eds.), Source Mechanism and Seismotectonics. Birkhäuser Basel, Basel, pp. 433–448. https://doi.org/10.1007/978-3-0348-8654-3_6*
- *Van Hinsbergen, D.J.J., 2022. Indian plate paleogeography, subduction and horizontal underthrusting below Tibet: paradoxes, controversies and opportunities. Natl. Sci. Rev. 9, nwac074. https://doi.org/10.1093/nsr/nwac074*
- *Van Hinsbergen, D.J.J., Lippert, P.C., Li, S., Huang, W., Advokaat, E.L., Spakman, W., 2019. Reconstructing Greater India: Paleogeographic, kinematic, and geodynamic perspectives. Tectonophysics 760, 69–94. https://doi.org/10.1016/j.tecto.2018.04.006*
- *Van Hinsbergen, D.J.J., Vissers, R.L.M., Spakman, W., 2014. Origin and consequences of western Mediterranean subduction, rollback, and slab segmentation. Tectonics 33, 393–419. https://doi.org/10.1002/2013TC003349*
- *Vavryčuk, V., 2014. Iterative joint inversion for stress and fault orientations from focal mechanisms. Geophys. J. Int. 199, 69–77. https://doi.org/10.1093/gji/ggu224*
- *Vavryčuk, V., Bouchaala, F., Fischer, T., 2013. High-resolution fault image from accurate locations and focal mechanisms of the 2008 swarm earthquakes in West Bohemia, Czech Republic. Tectonophysics 590, 189–195. https://doi.org/10.1016/j.tecto.2013.01.025*
- *Vergés, J., Fernàndez, M., 2006. Ranges and basins in the Iberian Peninsula: their contribution to the present topography. Geol. Soc. Lond. Mem. 32, 223–234. https://doi.org/10.1144/GSL.MEM.2006.032.01.13*
- *Vergés, J., Kullberg, J.C., Casas-Sainz, A., De Vicente, G., Duarte, L.V., Fernàndez, M., Gómez, J.J., Gómez-Pugnaire, M.T., Jabaloy Sánchez, A., López-Gómez, J., Macchiavelli, C., Martín-Algarra, A., Martín-Chivelet, J., Muñoz, J.A., Quesada, C., Terrinha, P., Torné, M., Vegas, R., 2019. An Introduction to the Alpine Cycle in Iberia, in: Quesada, C., Oliveira, J.T. (Eds.), The Geology of Iberia: A Geodynamic Approach, Regional Geology Reviews. Springer International Publishing, Cham, pp. 1–14. https://doi.org/10.1007/978-3-030-11295-0_1*
- *Vernant, P., Bilham, R., Szeliga, W., Drupka, D., Kalita, S., Bhattacharyya, A.K., Gaur, V.K., Pelgay, P., Cattin, R., Berthet, T., 2014. Clockwise rotation of the Brahmaputra Valley relative to India: Tectonic convergence in the eastern Himalaya, Naga Hills, and Shillong Plateau. J. Geophys. Res. Solid Earth 119, 6558–6571. https://doi.org/10.1002/2014JB011196*
- *Vernant, P., Hivert, F., Chéry, J., Steer, P., Cattin, R., Rigo, A., 2013. Erosion-induced isostatic rebound triggers extension in low convergent mountain ranges. Geology 41, 467–470. https://doi.org/10.1130/G33942.1*
- *Vilanova, S.P., Fonseca, J.F.B.D., 2007. Probabilistic Seismic-Hazard Assessment for Portugal. Bull. Seismol. Soc. Am. 97, 1702–1717. https://doi.org/10.1785/0120050198*
- *Villamor, P., Capote, R., Stirling, M.W., Tsige, M., Berryman, K.R., Martínez-Díaz, J.J., Martín-González, F., 2012. Contribution of active faults in the intraplate area of Iberia to seismic hazard: The Alentejo-Plasencia Fault. J. Iber. Geol. 38, 85–111. https://doi.org/10.5209/rev_JIGE.2012.v38.n1.39207*
- *Villani, F., Antonioli, A., Pastori, M., Baccheschi, P., Ciaccio, M.G., 2024. Stress Patterns and Crustal Anisotropy in the Eastern Alps: Insights From Seismological and Geological Observations. Tectonics 43, e2023TC008033. https://doi.org/10.1029/2023TC008033*
- *Vissers, R.L.M., Meijer, P.Th., 2012. Mesozoic rotation of Iberia: Subduction in the Pyrenees? Earth-Sci. Rev. 110, 93–110. https://doi.org/10.1016/j.earscirev.2011.11.001*
- *Wallace, R.E., 1951. Geometry of Shearing Stress and Relation to Faulting. J. Geol. 59, 118–130. https://doi.org/10.1086/625831*
- *Wang, H., Wright, T.J., Liu-Zeng, J., Peng, L., 2019. Strain Rate Distribution in South-Central Tibet From Two Decades of InSAR and GPS. Geophys. Res. Lett. 46, 5170–5179. https://doi.org/10.1029/2019GL081916*

- *Wang, L., Barbot, S., 2023. Three-dimensional kinematics of the India–Eurasia collision. Commun. Earth Environ. 4, 164. https://doi.org/10.1038/s43247-023-00815-4*
- *Wang, M., Shen, Z., 2020. Present-Day Crustal Deformation of Continental China Derived From GPS and Its Tectonic Implications. J. Geophys. Res. Solid Earth 125, e2019JB018774. https://doi.org/10.1029/2019JB018774*
- *Wang, Q., Zhang, P.-Z., Freymueller, J.T., Bilham, R., Larson, K.M., Lai, X., You, X., Niu, Z., Wu, J., Li, Y., Liu, J., Yang, Z., Chen, Q., 2001. Present-Day Crustal Deformation in China Constrained by Global Positioning System Measurements. Science 294, 574–577. https://doi.org/10.1126/science.1063647*
- *Wang, X., Wei, S., Wu, W., 2017. Double-ramp on the Main Himalayan Thrust revealed by broadband waveform modeling of the 2015 Gorkha earthquake sequence. Earth Planet. Sci. Lett. 473, 83–93. https://doi.org/10.1016/j.epsl.2017.05.032*
- *Webb, A.A.G., Schmitt, A.K., He, D., Weigand, E.L., 2011. Structural and geochronological evidence for the leading edge of the Greater Himalayan Crystalline complex in the central Nepal Himalaya. Earth Planet. Sci. Lett. 304, 483–495. https://doi.org/10.1016/j.epsl.2011.02.024*
- *Webb, A.A.G., Yin, A., Harrison, T.M., Célérier, J., Burgess, W.P., 2007. The leading edge of the Greater Himalayan Crystalline complex revealed in the NW Indian Himalaya: Implications for the evolution of the Himalayan orogen. Geology 35, 955. https://doi.org/10.1130/G23931A.1*
- *Wiesmayr, G., Grasemann, B., 2002. Eohimalayan fold and thrust belt: Implications for the geodynamic evolution of the NW-Himalaya (India). Tectonics 21. https://doi.org/10.1029/2002TC001363*
- *Wu, Y., Zheng, Z., Nie, J., Chang, L., Su, G., Yin, H., Liang, H., Pang, Y., Chen, C., Jiang, Z., Bo, W., 2022. High-Precision Vertical Movement and Three-Dimensional Deformation Pattern of the Tibetan Plateau. J. Geophys. Res. Solid Earth 127, e2021JB023202. https://doi.org/10.1029/2021JB023202*
- *Wu, Z., Hu, M., 2024. Definitions, Classification Schemes for Active Faults, and Their Application. Geosciences 14, 68. https://doi.org/10.3390/geosciences14030068*
- *Xiao, W., Windley, B.F., Sun, S., Li, J., Huang, B., Han, C., Yuan, C., Sun, M., Chen, H., 2015. A Tale of Amalgamation of Three Permo-Triassic Collage Systems in Central Asia: Oroclines, Sutures, and Terminal Accretion. Annu. Rev. Earth Planet. Sci. 43, 477–507. https://doi.org/10.1146/annurev-earth-060614-105254*
- *Xie, C., Lei, X., Wu, X., Hu, X., 2014. Short- and long-term earthquake triggering along the strike-slip Kunlun fault, China: Insights gained from the Ms 8.1 Kunlun earthquake and other modern large earthquakes. Tectonophysics 617, 114–125. https://doi.org/10.1016/j.tecto.2014.01.023*
- *Xu, Q., Zhao, J., Yuan, X., Liu, H., Pei, S., 2017. Detailed Configuration of the Underthrusting Indian Lithosphere Beneath Western Tibet Revealed by Receiver Function Images. J. Geophys. Res. Solid Earth 122, 8257–8269. https://doi.org/10.1002/2017JB014490*
- *Yadav, D.K., Kumar, N., Hazarika, D., Yadav, D.N., Wadhawan, M., 2017. Seismicity and Tectonics of Kinnaur Himalaya and adjoining region inferred from focal mechanism solutions and stress tensor inversion. Seism. Tecton. Kinnaur Himalaya Adjoin. Reg. Inferred Focal Mech. Solut. Stress Tensor Inversion 38(1), 49–55.*
- *Yang, W., Hauksson, E., 2013. The tectonic crustal stress field and style of faulting along the Pacific North America Plate boundary in Southern California. Geophys. J. Int. 194, 100–117. https://doi.org/10.1093/gji/ggt113*
- *Yang, Y., Liang, C., Fang, L., Su, J., Hua, Q., 2018. A Comprehensive Analysis on the Stress Field and Seismic Anisotropy in Eastern Tibet. Tectonics 37, 1648–1657. https://doi.org/10.1029/2018TC005011*
- *Yang, Y., Liu, M., 2002. Cenozoic deformation of the Tarim plate and the implications for mountain building in the Tibetan Plateau and the Tian Shan. Tectonics 21. https://doi.org/10.1029/2001TC001300*
- *Zelenin, E., Bachmanov, D., Garipova, S., Trifonov, V., Kozhurin, A., 2022. The Active Faults of Eurasia Database (AFEAD): the ontology and design behind the continental-scale dataset. Earth Syst. Sci. Data 14, 4489–4503. https://doi.org/10.5194/essd-14-4489-2022*
- *Zhang, L., Liang, S., Yang, X., Gan, W., Dai, C., 2021. Geometric and kinematic evolution of the Jiali fault, eastern Himalayan Syntaxis. J. Asian Earth Sci. 212, 104722. https://doi.org/10.1016/j.jseaes.2021.104722*
- *Zhang, P.-Z., Shen, Z., Wang, M., Gan, W., Bürgmann, R., Molnar, P., Wang, Q., Niu, Z., Sun, J., Wu, J., Hanrong, S., Xinzhao, Y., 2004. Continuous deformation of the Tibetan Plateau from global positioning system data. Geology 32, 809. https://doi.org/10.1130/G20554.1*
- *Zhang, X., Wang, Y., 2007. Seismic and GPS evidence for the kinematics and the state of stress of active structures in south and south-central Tibetan Plateau. J. Asian Earth Sci. 29, 283–295. https://doi.org/10.1016/j.jseaes.2006.03.008*
- *Zhang, Z., Klemperer, S., Bai, Z., Chen, Y., Teng, J., 2011. Crustal structure of the Paleozoic Kunlun orogeny from an active-source seismic profile between Moba and Guide in East Tibet, China. Gondwana Res. 19, 994–1007. https://doi.org/10.1016/j.gr.2010.09.008*
- *Zhang, Z., Wang, Y., Houseman, G.A., Xu, T., Wu, Z., Yuan, X., Chen, Y., Tian, X., Bai, Z., Teng, J., 2014. The Moho beneath western Tibet: Shear zones and eclogitization in the lower crust. Earth Planet. Sci. Lett. 408, 370–377. https://doi.org/10.1016/j.epsl.2014.10.022*
- *Zhu, L., Helmberger, D.V., 1996. Intermediate depth earthquakes beneath the India-Tibet Collision Zone. Geophys. Res. Lett. 23, 435–438. https://doi.org/10.1029/96GL00385*
- *Zhu, R., Zhao, P., Zhao, L., 2022. Tectonic evolution and geodynamics of the Neo-Tethys Ocean. Sci. China Earth Sci. 65, 1–24. https://doi.org/10.1007/s11430-021-9845-7*
- *Ziegler, M., Heidbach, O., 2019. Manual of the Matlab Script Stress2Grid v1.1, WSM Technical Report; 19-02. GFZ German Research Centre for Geosciences. https://doi.org/10.2312/WSM.2019.002*

- *Zitellini, N., Gràcia, E., Matias, L., Terrinha, P., Abreu, M.A., DeAlteriis, G., Henriet, J.P., Dañobeitia, J.J., Masson, D.G., Mulder, T., Ramella, R., Somoza, L., Diez, S., 2009. The quest for the Africa–Eurasia plate boundary west of the Strait of Gibraltar. Earth Planet. Sci. Lett. 280, 13–50. https://doi.org/10.1016/j.epsl.2008.12.005*
- *Zitellini, N., Rovere, M., Terrinha, P., Chierici, F., Matias, L., 2004. Neogene Through Quaternary Tectonic Reactivation of SW Iberian Passive Margin. Pure Appl. Geophys. 161, 565–587. https://doi.org/10.1007/s00024-003-2463-4*
- *Zoback, M.D., Zoback, M.L., Mount, V.S., Suppe, J., Eaton, J.P., Healy, J.H., Oppenheimer, D., Reasenberg, P., Jones, L., Raleigh, C.B., Wong, I.G., Scotti, O., Wentworth, C., 1987. New Evidence on the State of Stress of the San Andreas Fault System. Science 238, 1105–1111. https://doi.org/10.1126/science.238.4830.1105*
- *Zoback, M.L., 1992. First- and second-order patterns of stress in the lithosphere: The World Stress Map Project. J. Geophys. Res. Solid Earth 97, 11703–11728. https://doi.org/10.1029/92JB00132*
- *Zoback, M.L., Zoback, M., 1980. State of stress in the conterminous United States. J. Geophys. Res. Solid Earth 85, 6113–6156. https://doi.org/10.1029/JB085iB11p06113*
- *Zoback, M.L., Zoback, M.D., Adams, J., Assumpção, M., Bell, S., Bergman, E.A., Blümling, P., Brereton, N.R., Denham, D., Ding, J., Fuchs, K., Gay, N., Gregersen, S., Gupta, H.K., Gvishiani, A., Jacob, K., Klein, R., Knoll, P., Magee, M., Mercier, J.L., Müller, B.C., Paquin, C., Rajendran, K., Stephansson, O., Suarez, G., Suter, M., Udias, A., Xu, Z.H., Zhizhin, M., 1989. Global patterns of tectonic stress. Nature 341, 291–298. https://doi.org/10.1038/341291a0*
- *Zubovich, A.V., Wang, X., Scherba, Y.G., Schelochkov, G.G., Reilinger, R., Reigber, C., Mosienko, O.I., Molnar, P., Michajljow, W., Makarov, V.I., Li, J., Kuzikov, S.I., Herring, T.A., Hamburger, M.W., Hager, B.H., Dang, Y., Bragin, V.D., Beisenbaev, R.T., 2010. GPS velocity field for the Tien Shan and surrounding regions: GPS VELOCITY FIELD FOR THE TIEN SHAN. Tectonics 29, n/a-n/a. https://doi.org/10.1029/2010TC002772*

8. Supplementary material

8.1. Supplementary material for Chapter 2

8.1.1. Table – Focal Mechanism Solutions catalog

Date	*Lon*	*Lat*	*Depth*	*Mag*	*MagType*	*Biblio*	*Strike*	*Dip*	*Rake*	*Method*
yyyy-mm-dd hh:mm:ss	deg	deg	km	\	\	\	deg	deg	deg	\
1933-06-07 19:46:08	99.9	27.5	20	6.3	Ms	WSM2016	318	52	0	First Motion
1933-08-11 16:54:06	98.4	25.9	39	6.5	Ms	WSM2016	270	65	11	First Motion
1933-09-25 00:00:00	86.9	38.3	0	6.8	Ms	WSM2016	308	75	179	First Motion
1934-01-15 16:43:18	86.5	26.5	22	8.3	Ms	WSM2016	291	35	63	First Motion
1937-01-07 21:20:41	97.6	35.5	20	7.5	Ms	WSM2016	296	80	-4	First Motion
1941-04-19 15:53:45	97	39.1	26	6	Ms	WSM2016	87	70	-18	First Motion
1944-10-18 02:36:56	83.2	31.4	33	6.8	Ms	WSM2016	232	72	11	First Motion
1946-11-07 03:56:23	80.6	34.5	39	6.3	Ms	WSM2016	299	74	5	First Motion
1947-07-29 21:43:33	93.6	28.6	0	7.7	Ms	WSM2016	287	82	7	First Motion
1948-05-25 15:11:21	100.5	29.5	18	7.3	Ms	WSM2016	237	70	-179	First Motion
1949-02-23 00:00:00	84	42	0	7.3	Ms	WSM2016	148	75	-5	First Motion
1949-02-24 00:08:11	84	42	0	7.3	Ms	WSM2016	148	75	-5	First Motion
1949-05-25 16:23:49	83.6	42	0	6.3	Ms	WSM2016	241	70	-159	First Motion
1949-07-10 11:53:38	70.8	39.2	16	7.4	Ms	WSM2016	118	49	36	First Motion
1950-02-03 10:51:52	99.9	22.1	0	6.8	Ms	WSM2016	149	84	0	First Motion
1950-08-15 22:09:34	96.7	28.4	0	8.6	Ms	WSM2016	327	60	168	First Motion
1950-08-19 00:58:46	96.6	28.7	0	5.8	Ms	WSM2016	337	80	0	First Motion
1950-08-24 02:46:58	96.6	28.7	0	5.8	Ms	WSM2016	57	84	3	First Motion
1951-03-12 22:52:20	94.2	28.7	0	5.8	Ms	WSM2016	224	66	-174	First Motion
1951-04-15 07:40:59	93.8	28.4	0	6.5	Ms	WSM2016	174	75	166	First Motion
1951-04-22 11:37:40	94.2	28.7	0	5.5	Ms	WSM2016	175	76	170	First Motion
1951-12-21 16:37:29	100	26.7	0	6.3	Ms	WSM2016	324	55	-154	First Motion
1951-12-27 00:30:52	95.7	39.6	0	6	Ms	WSM2016	245	75	-16	First Motion
1952-01-23 11:29:25	95.7	39.8	0	5.5	Ms	WSM2016	13	69	-170	First Motion
1952-02-06 13:27:16	95.2	39.9	0	5.3	Ms	WSM2016	359	62	-165	First Motion

1952-05-26 10:46:32	94.5	28.5	0	5.5	Ms	WSM2016	192	72	-12	First Motion
1952-06-15 23:16:05	90.8	31.5	0	5.3	Ms	WSM2016	5	60	8	First Motion
1952-06-19 20:12:59	99.8	22.7	0	6.5	Ms	WSM2016	243	77	0	First Motion
1952-08-17 00:00:00	91.5	31	0	7.5	Ms	WSM2016	72	66	8	First Motion
1952-08-18 00:02:11	91.5	31	0	7.5	Ms	WSM2016	72	66	8	First Motion
1952-08-25 09:44:48	94	28	0	5.3	Ms	WSM2016	170	75	5	First Motion
1952-10-05 00:00:00	93.2	37.1	0	6	Ms	WSM2016	193	64	-7	First Motion
1952-10-06 06:04:30	93.2	37.1	0	6	Ms	WSM2016	193	64	-7	First Motion
1953-12-03 22:54:08	85.7	31.4	0	6.3	Ms	WSM2016	232	68	1	First Motion
1954-01-23 00:00:00	72.5	37.4	33	6.1	NaN	WSM2016	122	29	128	NaN
1954-02-11 08:30:15	101.3	39	10	7.3	Ms	WSM2016	303	20	90	First Motion
1954-02-23 14:40:35	91.6	27.8	0	6	Ms	WSM2016	346	60	161	First Motion
1954-08-18 00:00:00	70.6	39.1	33	4.4	NaN	WSM2016	62	43	73	NaN
1955-01-29 01:02:38	82.4	33.2	0	6.5	Ms	WSM2016	167	75	-4	First Motion
1955-03-22 14:14:12	98.4	25.9	0	6	Ms	WSM2016	299	84	4	First Motion
1955-03-27 22:38:50	90.2	29.8	0	5.8	Ms	WSM2016	8	65	11	First Motion
1955-04-14 09:29:02	101.8	30	0	7.5	Ms	WSM2016	338	80	-3	First Motion
1955-04-15 11:40:58	74.6	39.9	0	7	Ms	WSM2016	277	69	-1	First Motion
1955-06-07 08:48:54	101.1	26.5	20	6	Ms	WSM2016	302	80	0	First Motion
1955-06-23 00:00:00	71.1	42	33	4.4	NaN	WSM2016	307	45	97	NaN
1955-06-27 18:14:09	78.6	32.5	0	5.8	Ms	WSM2016	179	69	-171	First Motion
1955-07-19 00:00:00	68	39.7	33	5.6	NaN	WSM2016	260	44	149	NaN
1955-08-21 00:00:00	69.67	38.6	20	4.4	NaN	WSM2016	45	42	69	NaN
1955-09-23 23:06:23	101.8	26.6	10	6.8	Ms	WSM2016	120	80	177	First Motion
1955-12-29 16:25:35	90.3	30.1	0	5.5	Ms	WSM2016	37	70	6	First Motion
1956-03-05 00:00:00	77.1	37.8	33	5.6	NaN	WSM2016	40	45	63	NaN
1956-06-08 00:00:00	67.5	35.2	33	6.1	NaN	WSM2016	112	15	-90	NaN
1956-06-09 00:00:00	67.5	35	33	7.2	NaN	WSM2016	301	20	-90	NaN
1956-09-22 00:00:00	69.32	38.45	5	5.6	NaN	WSM2016	261	83	174	NaN
1956-10-10 00:00:00	77.8	28.3	20	6.5	NaN	WSM2016	105	72	168	NaN

1957-01-28 00:00:00	69.3	38.45	5	4.4	NaN	WSM2016	19	49	29	NaN
1957-04-14 15:11:56	84.27	30.58	0	6.5	Ms	WSM2016	222	68	17	First Motion
1957-08-30 00:00:00	72.9	39.3	33	4.4	NaN	WSM2016	39	15	90	NaN
1958-03-22 00:00:00	67.5	35.05	33	5.6	NaN	WSM2016	32	48	63	NaN
1958-12-28 00:00:00	79.8	30	30	6.2	NaN	WSM2016	282	36	90	NaN
1959-04-26 20:35:00	100.7	26.2	20	5.8	Ms	WSM2016	200	90	0	First Motion
1959-11-15 00:00:00	75.3	38.8	40	6.4	Ms	WSM2016	165	72	-168	First Motion
1960-02-12 00:00:00	70.1	38.88	20	4.4	NaN	WSM2016	208	58	12	NaN
1960-02-21 00:00:00	71.6	40.2	15	4.4	NaN	WSM2016	31	45	-54	NaN
1960-08-03 00:00:00	72.8	41.7	10	4.4	NaN	WSM2016	309	69	7	NaN
1961-04-01 23:18:26	77.8	39.9	20	6.8	Ms	WSM2016	116	68	-21	First Motion
1961-04-13 00:00:00	77.7	39.8	20	6.8	Ms	WSM2016	157	60	2	First Motion
1961-04-14 00:34:39	77.7	39.8	20	6.8	Ms	WSM2016	221	32	105	First Motion
1961-06-04 15:33:03	81.9	34.15	11	6.5	Ms	WSM2016	256	74	172	First Motion
1961-06-14 00:00:00	69.2	38.45	2	4.4	NaN	WSM2016	71	57	34	NaN
1961-06-27 15:03:41	99.75	27.73	10	6	Ms	WSM2016	36	60	17	First Motion
1961-07-17 00:00:00	72.4	41.2	10	4.4	NaN	WSM2016	270	28	58	NaN
1962-01-31 00:00:00	70.13	38.67	5	5	NaN	WSM2016	10	36	54	NaN
1962-05-21 20:02:52	96	37.1	25	6.8	Mb	WSM2016	272	30	90	First Motion
1962-05-21 21:15:44	95.9	37.2	25	5.9	Ms	WSM2016	238	70	-14	First Motion
1962-06-19 00:00:00	69.1	38.45	10	4.4	NaN	WSM2016	186	71	-5	NaN
1962-06-24 09:21:18	101.2	25.2	18	6.2	Ms	WSM2016	52	15	90	First Motion
1962-08-01 23:47:46	98.6	39.2	25	5.4	Ms	WSM2016	314	23	90	First Motion
1962-09-22 14:51:52	97	26.5	33	6.4	Ms	WSM2016	3	16	90	First Motion
1962-12-18 00:00:00	71.5	40	30	5	NaN	WSM2016	124	58	168	NaN
1963-02-27 00:00:00	69.87	38.7	5	4.4	NaN	WSM2016	335	42	111	NaN
1963-04-07 01:48:56	82.5	33.7	0	5	Ms	WSM2016	187	55	145	First Motion
1963-04-12 08:41:31	78.8	31.9	35	5	Ms	WSM2016	215	83	-1	First Motion
1963-04-19 15:35:21	97	35.7	0	7	Ms	WSM2016	9	86	-176	First Motion
1963-04-23 17:55:07	99.5	25.8	20	6	Ms	WSM2016	93	84	-2	First Motion

1963-06-11 00:00:00	69.65	38.42	5	4.4	NaN	WSM2016	208	37	111	NaN
1963-06-12 02:07:22	87.3	31	0	5	Ms	WSM2016	207	55	18	First Motion
1963-06-19 10:47:24.6	92.1	25	51	5.9	Mb	Chandra, 1978	261	25	90	First Motion
1963-06-21 15:26:29.3	92.1	24.9	53	5.7	Mb	Chandra, 1978	226	15	47	First Motion
1963-07-02 05:10:34	96.1	37.1	0	5	Ms	WSM2016	334	72	-173	First Motion
1963-08-29 00:00:00	74.2	39.8	0	6.5	Ms	WSM2016	47	43	90	First Motion
1963-09-02 01:34:31.6	74.7	33.9	44	5.1	Mb	Chandra, 1978	325	20	90	First Motion
1963-10-19 00:00:00	71.5	40.1	5	4.4	NaN	WSM2016	14	35	54	NaN
1963-12-18 14:40:18	82.6	41.9	30	5.1	Ms	WSM2016	205	62	-11	First Motion
1964-02-13 18:03:53	101	26.1	24	5.4	Ms	WSM2016	263	62	163	First Motion
1964-02-13 21:53:18	72.9	39.5	38	5.1	Ms	WSM2016	281	60	-154	First Motion
1964-02-18 03:48:35.6	91.1	27.5	30	5.6	Mb	Chandra, 1978	302	40	90	First Motion
1964-03-27 23:03:41.7	89.3	27.2	32	6.3	Mb	Chandra, 1978	76	19	90	First Motion
1964-03-28 07:13:00	89.3	27.2	32	6.3	Ms	WSM2016	76	19	90	First Motion
1964-04-02 00:00:00	95.42	5.75	65	5.6	Mb	Dasgupta & Mukhopadhyuay, 1993	331	86	0	First Motion
1964-04-15 00:00:00	88	21.7	36	5.3	Mb	WSM2016	252	27	45	First Motion
1964-05-03 07:34:00	100.7	26.1	19	4.5	Ms	WSM2016	139	55	149	First Motion
1964-06-11 01:55:35	93.1	31.8	7	5	Ms	WSM2016	220	84	175	First Motion
1964-06-13 00:00:00	93.95	23	60	5.2	Mb	Mukhopadhyay, 1988	68	42	-166	First Motion
1964-06-15 00:00:00	96.82	5.28	46	5.3	Mb	Dasgupta & Mukhopadhyuay, 1993	81	39	53	First Motion
1964-06-27 00:00:00	77.5	40.4	23	4.4	NaN	WSM2016	299	49	-143	NaN
1964-07-28 00:00:00	96.12	14.17	22	5.9	Mb	Dasgupta & Mukhopadhyuay, 1993	231	41	-117	First Motion
1964-08-30 10:35:07	88.4	27.5	21	5.1	Ms	WSM2016	328	79	5	First Motion
1964-09-01 13:22:36.6	92.3	27.2	33	5.7	Mb	Chandra, 1978	224	20	90	First Motion
1964-09-26 00:46:2.8	80.7	30.1	50	6.2	Mb	Chandra, 1978	306	17	90	First Motion
1964-10-21 00:00:00	93.75	28.04	37	5.9	Mb	Nandy et al., 1991	307	59	-150	First Motion
1964-10-22 07:09:19	93.8	28	37	6.6	Ms	WSM2016	299	68	-159	First Motion
1964-11-10 00:12:51	86.05	29.55	33	5	Ms	WSM2016	80	52	10	First Motion
1964-11-20 14:34:32	101.4	25.2	33	5	Ms	WSM2016	153	84	0	First Motion

1964-12-20 11:31:32	81.1	29.4	9	5.3	Ms	WSM2016	243	74	7	First Motion
1965-01-12 13:32:24.1	87.84	27.4	23	5.8	Mb	Dasgupta et al., 1987	329	72	-165	First Motion
1965-01-21 21:31:35	87	35.1	34	5.5	Ms	WSM2016	168	65	155	First Motion
1965-01-29 00:00:00	73.6	35.6	33	5.7	Mb	WSM2016	72	32	-142	First Motion
1965-02-02 15:56:51	73.4	37.5	33	5.8	Mb	Chandra, 1978	206	81	6	First Motion
1965-02-18 00:00:00	94.21	24.97	53	5.4	M	Chen & Molnar, 1990	220	60	216	First Motion
1965-04-02 00:00:00	66.7	36.8	5	4.4	NaN	WSM2016	250	61	0	NaN
1965-04-10 22:11:20	73.13	37.45	35	5.3	Ms	WSM2016	357	37	-35	First Motion
1965-05-31 10:04:43	78	32.6	28	5.1	Ms	WSM2016	237	58	-165	First Motion
1965-06-01 07:52:25.1	83.06	28.59	20	5.3	Mb	Dasgupta et al., 1987	318	64	-168	First Motion
1965-06-15 07:59:19.4	95.6	29.6	30	5.6	Mb	Chandra, 1978	131	70	0	First Motion
1965-06-17 20:14:49.800	87.7	32	16	5.3	M	Rastogi, 1974	315	78	90	First Motion
1965-06-18 08:17:40	93.7	25	66	5.8	Mb	Chandra, 1978	216	30	13	First Motion
1965-07-03 19:26:12	101.6	22.4	15	6.1	Ms	WSM2016	301	73	-167	First Motion
1965-08-02 04:09:22	93.2	32.9	35	5.2	Ms	WSM2016	108	76	0	First Motion
1965-09-22 00:00:00	99.4	20.6	11	6.1	Ms	WSM2016	261	76	0	First Motion
1965-12-09 00:00:00	92.51	27.43	29	5.2	Mb	Nandy et al., 1991	105	82	-7	First Motion
1966-01-05 00:00:00	69.22	38.25	2	4.4	NaN	WSM2016	251	44	138	NaN
1966-01-24 07:23:09.7	69.7	29.9	26	5.6	Mb	Chandra, 1978	210	27	43	First Motion
1966-01-31 10:35:03	99.7	27.9	13	5.1	Ms	WSM2016	1	51	29	First Motion
1966-02-07 04:26:10.6	69.7	29.9	10	6	Mb	Chandra, 1978	237	45	90	First Motion
1966-02-07 23:06:36.7	69	30.3	11	5.8	Mb	Chandra, 1978	231	43	58	First Motion
1966-03-06 02:10:53.6	80.6	31.6	12	5.7	Mb	Chandra, 1978	45	35	-90	First Motion
1966-03-06 02:15:57.2	80.5	31.5	50	6	Mb	Chandra, 1978	225	45	-90	First Motion
1966-03-14 12:42:49	97.5	32.5	33	5.1	Ms	WSM2016	250	50	23	First Motion
1966-04-11 00:00:00	70.5	39	15	4.4	NaN	WSM2016	348	50	32	NaN
1966-04-14 00:00:00	70.5	39	10	5	NaN	WSM2016	354	49	33	NaN
1966-05-12 19:42:51	78	40.2	40	5	Ms	WSM2016	264	82	5	First Motion
1966-06-27 10:41:08.1	80.83	29.62	33	6	Mb	Dasgupta et al., 1987	200	74	-9	First Motion
1966-06-27 18:59:18	80.9	29.7	36	6.5	Ms	WSM2016	297	2	90	First Motion

1966-06-27 21:55:52	80.8	29.6	15	5	Ms	WSM2016	314	84	4	First Motion
1966-08-01 21:02:59.5	68.6	30.1	33	6	Mb	Chandra, 1978	97	82	173	First Motion
1966-08-05 09:03:00	79.6	32.7	31	5.1	Ms	WSM2016	160	69	-10	First Motion
1966-08-10 00:00:00	69.55	38.45	2	5	NaN	WSM2016	281	34	135	NaN
1966-08-11 00:00:00	69.55	38.45	2	4.4	NaN	WSM2016	268	80	176	NaN
1966-08-15 02:15:34.4	78.9	28.7	53	5.6	Mb	Chandra, 1978	101	30	-90	First Motion
1966-09-19 13:03:53	97.7	24	33	5.4	Ms	WSM2016	261	69	-5	First Motion
1966-09-21 07:37:22	97.7	24.1	0	5.2	Ms	WSM2016	172	82	174	First Motion
1966-09-26 05:10:56	92.6	27.5	19	5.5	Mb	Chandra, 1978	253	20	90	First Motion
1966-09-28 14:00:22.3	100.1	27.5	27	6.1	Mb	Chandra, 1978	320	40	-90	First Motion
1966-10-14 09:04:43	87.4	36.5	14	6	Ms	WSM2016	205	24	-90	Centroid Moment Tensor
1966-10-20 08:53:41	78.5	33.6	25	4.9	Ms	WSM2016	185	64	-24	First Motion
1966-10-22 00:00:00	94.28	23.04	72	5.1	Mb	Mukhopadhyay, 1988	37	71	178	First Motion
1966-11-06 02:53:00	83.9	28.2	33	4.8	Ms	WSM2016	310	75	14	First Motion
1966-12-16 20:52:16.3	80.79	29.62	19	5.7	Mb	Dasgupta et al., 1987	178	69	-19	First Motion
1966-12-17 04:52:16	80.8	29.6	19	6.1	Ms	WSM2016	290	24	90	Centroid Moment Tensor
1966-12-22 06:10:59	80.8	29.7	21	5.2	Mb	WSM2016	237	47	48	First Motion
1967-01-30 00:00:00	96.14	26.1	39	5.4	Mb	Mukhopadhyay, 1988	216	77	176	First Motion
1967-02-14 00:00:00	96.47	13.75	13	5.6	Mb	Dasgupta & Mukhopadhyuay, 1993	240	35	-90	First Motion
1967-02-15 00:00:00	93.99	20.33	51	5.4	Mb	Mukhopadhyay, 1988	217	55	6	First Motion
1967-02-20 23:06:36.7	69.9	30.3	11	5.8	Mb	Chandra, 1978	149	45	100	First Motion
1967-02-21 12:37:46.100	75.4	33.7	41	5.1	M	Rastogi, 1974	100	60	90	First Motion
1967-03-11 00:00:00	94.3	28.3	12	5.3	NaN	WSM2016	273	30	90	First Motion
1967-03-12 00:56:51	94.4	28.5	15	5.2	Ms	WSM2016	276	32	90	First Motion
1967-03-14 00:00:00	94.29	28.41	20	5.7	Mb	Nandy et al., 1991	151	69	22	First Motion
1967-04-12 00:00:00	96.45	5.32	45	5.4	Mb	Dasgupta & Mukhopadhyuay, 1993	98	28	90	First Motion
1967-04-22 00:00:00	96.39	5.12	44	5.4	Mb	Dasgupta & Mukhopadhyuay, 1993	68	56	36	First Motion

1967-05-11 22:50:59	73.8	39.3	33	5.9	Ms	WSM2016	215	65	11	First Motion
1967-05-14 00:00:00	70.7	39.8	5	4.4	NaN	WSM2016	277	72	-169	NaN
1967-05-27 00:00:00	77.7	36.1	10	5.9	Ms	WSM2016	258	72	5	First Motion
1967-05-28 03:05:48	77.7	36.1	10	5.9	Ms	WSM2016	258	72	5	First Motion
1967-06-13 00:00:00	78.2	42.9	3	4.4	Mb	WSM2016	130	46	37	Centroid Moment Tensor
1967-07-02 00:00:00	93.59	8.65	44	5.7	Mb	Dasgupta & Mukhopadhyuay, 1993	351	76	0	First Motion
1967-08-15 17:21:04	93.6	31.1	25	5.5	Ms	WSM2016	271	38	90	First Motion
1967-08-21 00:00:00	95.74	3.72	40	6.1	Mb	Dasgupta & Mukhopadhyuay, 1993	293	12	90	First Motion
1967-08-30 12:22:03	100.3	31.6	8	6.8	Ms	WSM2016	245	45	-70	First Motion
1967-08-30 19:08:51	100.33	31.7	10	6	Ms	WSM2016	53	40	-90	First Motion
1967-09-06 00:00:00	93.55	14.65	36	5.5	Mb	Dasgupta & Mukhopadhyuay, 1993	196	14	-90	First Motion
1967-09-15 00:00:00	91.86	27.42	19	5.8	Mb	Nandy et al., 1991	248	64	-24	First Motion
1967-10-03 00:00:00	68.7	38.67	10	5	NaN	WSM2016	321	54	167	NaN
1967-12-10 00:00:00	73.75	17.4	6.12	6	Mb	WSM2016	302	70	170	First Motion
1968-01-05 14:42:49	79.1	30.5	11	4.7	Ms	WSM2016	172	74	15	First Motion
1968-01-31 19:45:19	92.2	29.8	11	5.2	Ms	WSM2016	318	76	-176	First Motion
1968-02-11 00:00:00	78.7	34.2	24	5.1	Ms	WSM2016	43	65	15	Centroid Moment Tensor
1968-03-03 00:17:16	100.3	29.9	10	5.7	Ms	WSM2016	334	76	-12	First Motion
1968-03-13 00:00:00	66.37	42.55	30	5	NaN	WSM2016	107	36	-125	NaN
1968-03-16 20:26:35	101.1	25.3	13	5.1	Ms	WSM2016	131	22	90	First Motion
1968-04-14 00:00:00	66.4	42.4	30	5	NaN	WSM2016	108	36	-123	NaN
1968-04-21 00:00:00	68.65	38.47	15	5	NaN	WSM2016	259	41	119	NaN
1968-06-12 00:00:00	91.94	24.83	41	5.3	M	Chen & Molnar, 1990	123	60	135	First Motion
1968-07-08 00:00:00	67.5	38.3	20	5	NaN	WSM2016	67	38	-122	NaN
1968-07-19 00:00:00	93.67	8.86	36	5.5	Mb	Dasgupta & Mukhopadhyuay, 1993	255	79	-9	First Motion
1968-08-18 00:00:00	90.62	26.42	29	5.1	M	Chen & Molnar, 1990	90	60	90	First Motion
1968-09-03 00:00:00	69.2	36.3	38	5.2	NaN	WSM2016	244	39	55	First Motion

1968-11-05 00:00:00	76.5	32.3	33	4.9	NaN	WSM2016	316	24	74	First Motion
1968-12-22 17:06:36	101.9	36.2	7	5.4	Ms	WSM2016	141	20	90	First Motion
1968-12-27 00:00:00	91.61	24.12	29	5.1	M	Chen & Molnar, 1990	140	72	138	First Motion
1969-01-21 00:00:00	69.67	38.42	2	5	NaN	WSM2016	36	52	38	NaN
1969-01-25 00:00:00	92.4	22.98	49	5.2	Mb	Mukhopadhyay, 1988	349	17	66	First Motion
1969-02-09 23:34:45	101.4	22	9	5.4	Ms	WSM2016	309	64	-174	First Motion
1969-02-11 00:00:00	79.4	41.5	10	6.3	Ms	WSM2016	234	40	90	First Motion
1969-02-12 06:08:54	79.3	41.5	10	6.3	Ms	WSM2016	234	40	90	First Motion
1969-03-03 00:00:00	79.9	30.2	18	5.3	NaN	WSM2016	125	40	82	NaN
1969-03-22 00:00:00	70.4	38.8	25	5	NaN	WSM2016	7	75	-11	NaN
1969-04-28 00:00:00	95.2	25.93	68	5	Mb	Mukhopadhyay, 1988	259	32	-40	First Motion
1969-05-15 20:39:45.8	70.9	34.6	22	5.6	Mb	Chandra, 1978	233	15	90	First Motion
1969-06-22 09:33:23	79.4	30.5	15	5.1	Ms	WSM2016	96	30	30	First Motion
1969-07-02 00:00:00	99.5	21	33	5.3	Ms	WSM2016	249	74	4	First Motion
1969-08-28 11:58:36	73.5	39	9	5.6	Ms	WSM2016	110	78	-169	First Motion
1969-08-29 00:00:00	96.06	26.35	72	5.2	Mb	Mukhopadhyay, 1988	34	32	90	First Motion
1969-09-15 00:15:26	74.8	39.7	38	5.5	Ms	WSM2016	269	37	123	First Motion
1969-09-28 00:00:00	73.5	39.4	38	5	NaN	WSM2016	15	34	135	NaN
1969-10-24 00:00:00	72.4	24.8	15	5.3	Mb	WSM2016	128	55	135	First Motion
1969-11-06 04:25:14	90.24	27.66	13	5	Ms	WSM2016	240	27	7	First Motion
1969-11-21 00:00:00	94.61	1.94	20	6.4	Mb	Dasgupta & Mukhopadhyuay, 1993	280	74	166	First Motion
1970-02-06 00:00:00	101	23.1	15	6.2	Ms	WSM2016	43	70	13	First Motion
1970-02-07 06:10:40	101.03	23.08	15	6.2	Ms	WSM2016	43	70	13	First Motion
1970-02-10 00:00:00	93.96	27.4	12	5.4	Mb	Nandy et al., 1991	10	64	163	First Motion
1970-02-12 01:51:48.4	81.57	29.24	25	5.3	Mb	Dasgupta et al., 1987	206	60	-4	First Motion
1970-02-19 07:10:01.8	94	27.4	18	5.5	Mb	Chandra, 1978	274	59	153	First Motion
1970-03-10 00:00:00	96.98	26.83	24	5.2	Mb	Nandy et al., 1991	247	79	-176	First Motion
1970-03-23 00:00:00	73	21.7	3	5.4	Mb	WSM2016	162	38	132	First Motion
1970-05-06 00:00:00	92.91	9.81	32	5.3	Mb	Dasgupta & Mukhopadhyuay, 1993	150	10	-90	First Motion

1970-05-21 00:00:00	66.8	38.83	5	4.4	NaN	WSM2016	303	35	-48	NaN
1970-05-29 00:00:00	94.06	23.96	61	5.1	M	Chen & Molnar, 1990	151	70	158	First Motion
1970-06-05 12:53:05	78.88	42.48	12	6.8	Ms	WSM2016	105	25	90	First Motion
1970-06-21 00:00:00	73	40.6	35	4.4	NaN	WSM2016	230	40	53	NaN
1970-07-25 00:00:00	88.5	25.7	33	5.2	NaN	WSM2016	177	42	-19	NaN
1970-07-29 10:16:19.3	95.4	26	59	6.5	Mb	Chandra, 1978	289	28	-1	First Motion
1970-07-29 13:50:57	77.77	40.05	13	5.9	Ms	WSM2016	271	29	136	First Motion
1970-08-03 00:00:00	97.94	2.54	69	5.7	Mb	Dasgupta & Mukhopadhyuay, 1993	201	31	-16	First Motion
1970-09-05 21:37:33	101.33	32.15	20	5.5	Ms	WSM2016	68	17	-66	First Motion
1970-11-08 17:15:56	101.4	32.15	0	5.5	Ms	WSM2016	268	69	169	First Motion
1970-11-18 01:59:30	101.9	25.2	0	4.4	Ms	WSM2016	111	81	172	First Motion
1971-02-02 00:00:00	91.66	23.71	46	5.4	Mb	Chen & Molnar, 1990	119	36	90	First Motion
1971-02-04 00:00:00	98.72	0.53	40	6.2	Mb	Dasgupta & Mukhopadhyuay, 1993	265	72	164	First Motion
1971-02-05 17:10:33	99.4	25.1	14	5.8	Ms	WSM2016	112	74	-176	First Motion
1971-03-23 17:52:10	79.3	41.4	20	6	Ms	WSM2016	228	38	90	First Motion
1971-03-24 04:47:15	79.4	41.3	20	6.1	Ms	WSM2016	251	44	90	Centroid Moment Tensor
1971-03-24 21:54:18	98.1	35.5	13	6.3	Ms	WSM2016	164	30	90	First Motion
1971-03-28 08:23:21.5	95.22	12.12	22.2	5.2	Mb	Eguchi, 1979	90	87	0	First Motion
1971-03-29 17:55:43	95.11	11.16	16.5	5.1	Mb	Eguchi, 1979	281	79	10	First Motion
1971-04-03 12:49:01	95.1	32.2	20	6.3	Ms	WSM2016	180	82	176	First Motion
1971-04-28 23:32:01	101.1	23	15	6.7	Ms	WSM2016	255	74	0	First Motion
1971-05-03 08:33:23	84.3	30.8	20	5.4	Ms	WSM2016	10	32	-90	Centroid Moment Tensor
1971-05-10 22:51:45	71.29	42.85	33	5.6	Ms	WSM2016	37	48	57	Centroid Moment Tensor
1971-05-22 00:00:00	92.2	32.4	20	6.5	Ms	WSM2016	328	87	0	Centroid Moment Tensor
1971-05-23 04:03:30	92.2	32.4	20	6.5	Ms	WSM2016	328	87	0	Centroid Moment Tensor
1971-05-30 15:44:15.7	96.4	25.2	15	5.8	Mb	Chandra, 1978	37	80	-174	First Motion

1971-05-31 00:00:00	96.51	25.22	22	5.2	Mb	Mukhopadhyay, 1988	18	70	-174	First Motion
1971-06-05 00:00:00	92.46	9.38	25	5.3	Mb	Dasgupta & Mukhopadhyuay, 1993	150	10	-90	First Motion
1971-06-16 06:04:10	79.28	41.52	12	5.8	Ms	WSM2016	256	35	90	First Motion
1971-06-16 08:58:37	79.23	41.52	29	5.6	Ms	WSM2016	315	60	156	First Motion
1971-06-26 00:00:00	94.78	24.6	74	5	Mb	Mukhopadhyay, 1988	10	37	60	First Motion
1971-08-12 04:17:03	95.08	12.5	19.7	5.3	Mb	Eguchi, 1979	77	72	-1	First Motion
1971-09-06 20:00:29	101.8	26.4	0	5.1	ML	WSM2016	80	89	0	First Motion
1971-09-14 11:11:06	100.8	23	0	6.2	Ms	WSM2016	146	67	0	First Motion
1971-10-10 00:00:00	95.92	23	46	4.9	Mb	Mukhopadhyay, 1988	227	61	-13	First Motion
1971-10-14 00:00:00	95.86	23.04	47	5.1	Mb	Mukhopadhyay, 1988	235	57	-7	First Motion
1971-11-05 00:00:00	92.93	10.11	53	5.9	Mb	Dasgupta & Mukhopadhyuay, 1993	0	21	71	First Motion
1971-11-18 00:00:00	66.6	38.6	27	5	NaN	WSM2016	209	50	36	NaN
1971-12-29 22:27:02	94.7	25.1	33	5.5	Mb	Chandra, 1978	350	33	157	First Motion
1972-01-15 00:00:00	79	40.3	6	6.2	Ms	WSM2016	253	37	45	First Motion
1972-01-16 04:21:50	79	40.3	6	6.2	Ms	WSM2016	279	22	108	First Motion
1972-02-22 00:00:00	92.48	10.42	4	5.4	Mb	Dasgupta & Mukhopadhyuay, 1993	116	61	-168	First Motion
1972-03-15 00:00:00	84.4	30.5	0	5.1	Ms	WSM2016	277	67	25	First Motion
1972-03-24 16:11:48	87.73	42.83	39	4.9	Ms	WSM2016	242	15	62	First Motion
1972-04-08 17:33:39	101.8	29.6	28	5.2	Ms	WSM2016	0	58	11	First Motion
1972-04-09 12:10:50	84.8	42.3	30	5.6	Ms	WSM2016	319	43	132	First Motion
1972-04-21 00:00:00	81.2	35	21	4.8	Ms	WSM2016	184	78	-174	First Motion
1972-06-02 00:00:00	96.64	3.49	17	5.4	Mb	Dasgupta & Mukhopadhyuay, 1993	203	45	0	First Motion
1972-06-24 15:29:22	69.69	36.28	24	6	Mb	WSM2016	43	21	109	Centroid Moment Tensor
1972-07-07 20:04:00	98.1	20.5	27	5.7	Ms	WSM2016	175	55	143	First Motion
1972-07-22 00:00:00	91.7	31.5	15	6	Ms	WSM2016	212	65	-17	Centroid Moment Tensor
1972-07-23 00:41:01	91.7	31.5	15	6	Ms	WSM2016	212	65	-17	Centroid Moment Tensor

1972-08-10 00:00:00	93.5	32.5	34	5	Ms	WSM2016	261	70	18	First Motion
1972-08-30 23:14:06	96.4	36.7	15	5.5	Ms	WSM2016	287	47	141	First Motion
1972-08-31 02:51:32	96.5	36.6	15	5.3	Ms	WSM2016	91	58	38	First Motion
1972-09-03 16:48:28.8	73.4	36	36	6.3	Mb	Chandra, 1978	127	29	90	First Motion
1972-09-03 23:03:52.1	73.3	35.9	33	5.6	Mb	Chandra, 1978	128	30	90	First Motion
1972-09-04 13:42:18.1	73.4	35.9	33	5.8	Mb	Chandra, 1978	127	35	90	First Motion
1972-09-07 18:35:55	100.45	26.08	10	4.2	Ms	WSM2016	123	51	140	Centroid Moment Tensor
1972-09-27 08:08:31	101.7	30.4	13	5.6	Ms	WSM2016	168	79	11	First Motion
1972-09-30 00:21:35	101.7	30.5	16	5.6	Ms	WSM2016	301	80	-10	First Motion
1972-09-30 04:24:41	101.9	30.4	20	5.7	Ms	WSM2016	210	70	-14	First Motion
1972-10-27 00:00:00	75.33	42.63	5	4.4	NaN	WSM2016	73	16	90	NaN
1972-11-13 23:34:11.8	95.23	12.44	24.1	5	Mb	Eguchi, 1979	73	79	-6	First Motion
1972-11-24 00:00:00	85.34	11.67	27	5.2	Mb	WSM2016	97	40	108	Centroid Moment Tensor
1972-12-28 16:57:45	70.4	34.7	63	5.6	Mb	Chandra, 1978	238	3	90	First Motion
1972-12-30 00:00:00	87.6	33.6	33	4.7	Ms	WSM2016	234	57	-8	First Motion
1973-01-16 21:31:26	75.7	33.2	42	5.1	Mb	Chandra, 1978	87	50	48	First Motion
1973-01-20 00:00:00	68.7	29.3	19	5.6	NaN	WSM2016	209	82	-7	NaN
1973-02-06 18:37:07	100.7	31.3	11	7.6	Ms	WSM2016	125	87	0	Centroid Moment Tensor
1973-02-07 17:20:57	100.9	31.4	20	5	Ms	WSM2016	329	59	-175	First Motion
1973-02-08 00:06:28	100.5	31.6	10	6	Ms	WSM2016	30	30	-90	First Motion
1973-03-24 03:14:54	100	31.9	20	5.5	Ms	WSM2016	65	65	-28	First Motion
1973-04-07 00:00:00	91.32	7	39	5.8	Mb	Dasgupta & Mukhopadhyuay, 1993	124	82	-174	First Motion
1973-05-31 00:00:00	93.52	24.31	56	5.8	Mb	Chen & Molnar, 1990	253	80	13	Centroid Moment Tensor
1973-06-01 21:03:01	98.7	24.9	0	4.9	Ms	WSM2016	9	51	168	First Motion
1973-06-02 00:39:49	98.5	24.9	0	5	Ms	WSM2016	285	83	-4	First Motion
1973-06-09 16:19:46.7	92.59	10.66	43.8	5.6	Mb	Eguchi, 1979	83	66	173	First Motion
1973-06-16 15:22:49	95.8	37.6	0	5.1	Ms	WSM2016	338	15	118	First Motion

1973-07-09 00:00:00	92.59	10.66	44	5.6	Mb	Dasgupta & Mukhopadhyuay, 1993	226	66	7	First Motion
1973-07-14 21:39:29	86.6	35.2	30	6	Ms	WSM2016	156	40	-144	First Motion
1973-07-16 00:00:00	86.5	35	0	5.2	Ms	WSM2016	273	52	-158	First Motion
1973-07-21 00:00:00	86.5	35.2	9	4.9	NaN	WSM2016	210	25	22	NaN
1973-07-27 00:00:00	94.49	23.27	60	5.4	Mb	Mukhopadhyay, 1988	4	16	130	First Motion
1973-08-01 14:05:15.5	89.17	29.59	63	4.9	Mb	Dasgupta et al., 1987	220	60	-24	First Motion
1973-08-02 05:33:11	101.2	30.9	13	4.7	Ms	WSM2016	81	90	0	AR
1973-08-16 11:58:11	101.2	23.1	7	6.3	Ms	WSM2016	188	47	-61	First Motion
1973-08-16 16:02:50	86.9	33.2	10	5.5	Ms	WSM2016	160	55	-154	Centroid Moment Tensor
1973-08-30 00:00:00	84.33	7.15	27	5.8	Mb	WSM2016	70	46	59	Centroid Moment Tensor
1973-09-01 00:00:00	75.08	42.57	10	4.4	NaN	WSM2016	133	25	141	NaN
1973-09-08 15:25:42	86.9	33.1	0	6	Ms	WSM2016	119	60	-161	Centroid Moment Tensor
1973-09-09 10:13:41	100.1	31.6	32	5.8	Ms	WSM2016	74	75	5	First Motion
1973-10-16 09:50:43.7	82.99	28.36	34	5	Mb	Dasgupta et al., 1987	184	70	-15	First Motion
1973-10-24 00:00:00	75.9	33.1	33	5.4	NaN	WSM2016	163	41	73	First Motion
1973-11-09 00:00:00	93.9	5.98	44	5.1	Mb	Dasgupta & Mukhopadhyuay, 1993	82	18	32	First Motion
1973-11-28 00:00:00	81.5	37.9	33	4.9	Ms	WSM2016	219	57	34	First Motion
1974-01-01 00:00:00	95.87	4.64	74	5.1	Mb	Dasgupta & Mukhopadhyuay, 1993	198	18	-12	First Motion
1974-02-16 00:00:00	92.32	11.47	19	5.2	Mb	Dasgupta & Mukhopadhyuay, 1993	9	7	90	First Motion
1974-03-14 07:13:13	101.2	24.8	10	4	Ms	WSM2016	326	44	-8	First Motion
1974-03-24 00:00:00	86	27.66	20	5.4	Mb	Nandy et al., 1991	212	60	-17	First Motion
1974-04-05 00:00:00	93.68	21.33	47	5	Mb	Mukhopadhyay, 1988	223	56	173	First Motion
1974-04-06 20:34:17	99.8	27.55	20	4.2	ML	WSM2016	213	55	-169	First Motion
1974-06-05 08:02:08	99.6	29.4	10	5.2	Ms	WSM2016	357	82	176	First Motion
1974-06-15 18:19:28	99.9	31.6	13	5	Ms	WSM2016	277	79	10	First Motion
1974-08-12 04:05:31	73.6	39.5	33	5.9	Ms	WSM2016	325	22	-90	First Motion

1974-08-12 05:21:38	73.5	39.4	33	6.4	Ms	WSM2016	261	2	-90	First Motion
1974-08-27 20:56:01	73.9	39.9	33	6	Ms	WSM2016	129	55	-144	First Motion
1974-09-27 05:26:33.6	85.51	28.59	20	5.5	Mb	Dasgupta et al., 1987	181	72	14	First Motion
1974-09-29 23:51:50	77.9	40.5	18	5.5	Ms	WSM2016	268	31	45	First Motion
1974-10-13 00:00:00	87.2	34.8	33	5.1	Ms	WSM2016	246	62	155	First Motion
1974-12-28 12:11:43.8	72.9	35.1	22	6	Mb	Chandra ,1978	231	22	90	First Motion
1975-01-04 00:00:00	97.5	38.6	33	5.3	Ms	WSM2016	213	38	27	First Motion
1975-01-04 17:22:22	100.35	26.35	26	4	Ms	WSM2016	305	60	154	Centroid Moment Tensor
1975-01-05 00:00:00	94.39	7.39	26	5.3	Mb	Dasgupta & Mukhopadhyuay, 1993	61	39	141	First Motion
1975-01-12 05:22:28	101.6	24.9	34	5.4	Ms	WSM2016	282	79	170	First Motion
1975-01-15 19:34:42	101.9	29.4	25	6.2	Ms	WSM2016	10	65	-17	First Motion
1975-01-19 16:02:03	78.6	32.6	30	6.9	Ms	WSM2016	180	40	-90	Centroid Moment Tensor
1975-01-29 20:06:02.4	73.6	35.6	33	5.7	Mb	Chandra ,1978	72	32	-142	First Motion
1975-01-31 12:38:50.8	84.77	28.09	19	5	Mb	Dasgupta et al., 1987	212	60	-4	First Motion
1975-02-01 00:00:00	93.6	32.6	7	4.7	Ms	WSM2016	182	63	-151	First Motion
1975-03-16 17:15:18	102	25.4	0	4	ML	WSM2016	218	85	4	First Motion
1975-03-18 15:01:23	99.42	25.5	0	4.5	ML	WSM2016	306	75	-175	First Motion
1975-03-19 02:44:16	86.5	35.2	28	6	Ms	WSM2016	353	65	-152	First Motion
1975-04-28 00:00:00	80	36	31	5.2	Ms	WSM2016	273	65	24	First Motion
1975-04-29 00:00:00	79.9	35.8	0	5	Ms	WSM2016	163	65	157	First Motion
1975-05-05 13:18:46	92.9	33.2	12	6.4	Ms	WSM2016	343	77	-168	Centroid Moment Tensor
1975-05-19 00:00:00	80.8	35.1	6	5.5	Ms	WSM2016	319	78	-178	First Motion
1975-05-20 03:47:44	80.8	35.2	11	5.4	Ms	WSM2016	3	46	-146	Centroid Moment Tensor
1975-05-21 00:00:00	94.09	23.86	43	5.3	Mb	Chen & Molnar, 1990	243	40	0	First Motion
1975-05-31 00:44:58	96.92	26.55	30	5.7	Mb	WSM2016	330	27	90	Centroid Moment Tensor
1975-06-03 00:00:00	96.9	26.6	0.1	5.4	NaN	WSM2016	161	69	-19	NaN

1975-06-04 10:24:29	79.7	35.9	0	6.1	Ms	WSM2016	52	41	-46	Centroid Moment Tensor
1975-06-09 11:16:41	100.1	27.03	0	4.2	Ms	WSM2016	49	68	160	Centroid Moment Tensor
1975-06-10 19:50:11	95.9	28.3	33	4.9	Ms	WSM2016	333	59	-161	First Motion
1975-07-19 14:10:54	78.6	32	31	5.3	Ms	WSM2016	180	50	-125	Centroid Moment Tensor
1975-07-23 00:00:00	96.36	26.58	22	5.2	Mb	Mukhopadhyay, 1988	269	66	-161	First Motion
1975-09-04 05:50:30	99.9	25.9	5	5	Ms	WSM2016	242	53	15	First Motion
1975-11-07 00:00:00	95.3	33.3	27	5.1	Ms	WSM2016	190	60	159	First Motion
1975-11-12 00:00:00	76.1	33	2	5	NaN	WSM2016	347	18	90	NaN
1975-12-01 02:22:22	100.3	27.2	18	4.9	Ms	WSM2016	206	29	-32	First Motion
1975-12-13 00:00:00	94.27	23.62	62	5.2	Mb	Mukhopadhyay, 1988	8	15	27	First Motion
1975-12-17 00:00:00	95.83	5.25	40	5.6	Mb	Dasgupta & Mukhopadhyuay, 1993	220	61	5	First Motion
1975-12-29 13:07:59	97.1	26.7	0	5.3	Ms	WSM2016	40	69	-170	First Motion
1976-01-01 00:00:00	76.1	32.9	40	5.3	NaN	WSM2016	336	33	88	NaN
1976-01-10 20:51:28	83.3	42.2	33	5.8	Ms	WSM2016	288	20	90	First Motion
1976-02-16 22:45:39	100.7	22.8	10	5.8	Ms	WSM2016	353	63	2	First Motion
1976-03-11 00:00:00	74.3	36.7	22	4.9	NaN	WSM2016	168	30	142	NaN
1976-05-10 00:00:00	81.5	29.3	0	5.2	Ms	WSM2016	144	58	33	First Motion
1976-05-29 12:23:29.900	98.65	24.39	15	6.7	Mw	GCMT	232	82	-10	Centroid Moment Tensor
1976-05-30 03:36:55	98.8	24.6	22	5.7	Ms	WSM2016	230	55	-31	First Motion
1976-05-30 12:18:39	98.8	24.4	27	5.6	Ms	WSM2016	268	50	41	First Motion
1976-05-31 05:08:35.400	98.6	24.26	15	6.1	Mw	GCMT	249	80	-18	Centroid Moment Tensor
1976-06-01 02:35:04	98.7	24.2	18	6	Ms	WSM2016	44	64	-6	First Motion
1976-06-09 08:20:35	98.7	24.8	10	6.2	Ms	WSM2016	358	75	-179	First Motion
1976-07-04 00:33:21	98.8	24.3	22	6	Ms	WSM2016	52	75	-16	First Motion
1976-07-10 00:00:00	70.5	32.2	39	5.1	NaN	WSM2016	333	30	-90	NaN
1976-07-10 00:00:00	68.1	30.8	7	5.2	NaN	WSM2016	127	51	39	NaN

1976-07-21 15:10:52.200	98.57	24.74	15	6.1	Mw	GCMT	248	88	-2	Centroid Moment Tensor
1976-08-12 00:00:00	97.04	26.7	31	6.2	Mb	Nandy et al., 1991	135	42	-14	First Motion
1976-09-03 17:57:28	100.2	28.1	0	5.2	Ms	WSM2016	260	58	-171	First Motion
1976-09-14 06:43:51.6	89.57	29.81	75	5.4	Mb	Dasgupta et al., 1987	360	40	-122	First Motion
1976-09-19 21:56:11	101.07	22.48	20	5.2	Ms	WSM2016	22	36	71	First Motion
1976-10-29 21:11:48	101.1	27.5	25	4	Ms	WSM2016	288	63	153	Centroid Moment Tensor
1976-11-03 00:00:00	95.19	4.22	54	5.5	Mb	Dasgupta & Mukhopadhyuay, 1993	227	51	164	First Motion
1976-11-06 00:00:00	101.1	27.6	21	6.7	Ms	WSM2016	23	50	-3	First Motion
1976-11-07 02:50:12	101.1	27.5	3	5.6	Ms	WSM2016	301	77	179	First Motion
1976-11-07 09:57:44	101.2	27.4	20	5.1	Ms	WSM2016	99	69	-169	First Motion
1976-11-07 16:13:54	101.07	27.43	20	4.9	ML	WSM2016	349	61	22	First Motion
1976-11-09 07:27:39	101.3	27.6	20	4.7	Ms	WSM2016	112	69	169	First Motion
1976-11-13 05:27:11	101.1	27.5	9	5.1	ML	WSM2016	121	54	-167	First Motion
1976-11-16 19:19:20	101.1	27.5	20	4.9	Ms	WSM2016	108	74	-170	First Motion
1976-12-11 00:00:00	93.9	7.65	13	5.4	Mb	Dasgupta & Mukhopadhyuay, 1993	244	79	0	First Motion
1976-12-13 14:36:57	101	27.4	21	6.4	Ms	WSM2016	24	70	6	First Motion
1976-12-13 15:23:45	101	27.3	20	5	Ms	WSM2016	16	74	10	First Motion
1976-12-22 02:54:05	101	27.4	0	4	Ms	WSM2016	185	69	-5	Centroid Moment Tensor
1977-01-01 21:39:46.000	90.67	38.22	10	6	Mw	GCMT	98	61	65	Centroid Moment Tensor
1977-01-06 00:00:00	88	31.3	0	5.5	Ms	WSM2016	137	74	175	First Motion
1977-01-15 12:23:48	101.3	27.5	0	4.8	Ms	WSM2016	241	59	-23	First Motion
1977-01-19 00:00:00	95.8	37.1	18	6.3	Ms	WSM2016	246	43	34	First Motion
1977-02-07 08:57:30	101.1	27.3	20	5.1	Ms	WSM2016	91	75	168	First Motion
1977-02-18 00:28:27	101.1	27.43	20	5	ML	WSM2016	19	53	-24	First Motion
1977-02-25 14:02:53	100.9	27.33	0	4.7	Ms	WSM2016	279	79	-175	First Motion
1977-03-17 07:54:53	99.68	25.85	20	5.4	Ms	WSM2016	0	54	-19	First Motion
1977-04-04 12:13:35	100.95	27.5	20	4.9	Ms	WSM2016	116	62	-173	First Motion

1977-04-16 20:20:13	100.8	27.4	20	4.7	Ms	WSM2016	16	54	-9	First Motion
1977-05-03 20:26:31	101.1	27.3	23	5.1	Ms	WSM2016	293	71	-165	First Motion
1977-05-06 23:36:15	101.1	27.4	0	4.5	Ms	WSM2016	282	60	-160	First Motion
1977-05-12 00:00:00	92.96	21.68	39	5.4	Mb	Mukhopadhyay, 1988	242	66	15	First Motion
1977-06-09 00:00:00	91.5	30	25	5	Ms	WSM2016	200	45	-90	First Motion
1977-06-09 19:14:42	100.27	26.98	20	4.7	Ms	WSM2016	15	59	12	First Motion
1977-07-13 08:09:19.400	67.13	29.69	15	5.5	Mw	GCMT	109	75	166	Centroid Moment Tensor
1977-07-18 14:22:56.200	69.89	35.62	77.6	5.1	Mw	GCMT	109	30	-47	Centroid Moment Tensor
1977-07-23 06:57:08.900	83.59	42.2	33	5.4	Mw	GCMT	90	74	81	Centroid Moment Tensor
1977-10-13 00:00:00	93.9	9.43	24	5	Mb	Dasgupta & Mukhopadhyuay, 1993	247	62	-17	First Motion
1977-10-13 11:32:13.500	93.16	23.27	60.8	5.4	Mw	GCMT	48	84	-49	Centroid Moment Tensor
1977-10-17 11:46:47	98.9	26	16	4.9	Ms	WSM2016	334	75	-176	First Motion
1977-10-19 00:00:00	91	39.2	0	5.2	Ms	WSM2016	236	60	-12	First Motion
1977-10-24 01:14:42	102	24.3	20	4.3	ML	WSM2016	280	75	-172	First Motion
1977-11-04 00:00:00	81.3	29.5	17	4.8	Ms	WSM2016	189	62	20	First Motion
1977-11-18 05:20:18.400	88.14	33	10	6.4	Mw	GCMT	9	71	-91	Centroid Moment Tensor
1977-12-03 00:00:00	95.91	3.52	21	5.8	Mb	Dasgupta & Mukhopadhyuay, 1993	313	7	90	First Motion
1977-12-18 16:47:21.500	77.44	39.92	15	5.9	Mw	GCMT	68	68	74	Centroid Moment Tensor
1978-02-07 00:00:00	93	12.81	10	5.5	Mb	Dasgupta & Mukhopadhyuay, 1993	210	62	-17	First Motion
1978-02-10 17:29:47.1	84.7	28.03	33	5.3	Mb	Dasgupta et al., 1987	221	55	-6	First Motion
1978-02-19 00:00:00	85	29.3	22	4.5	Ms	WSM2016	254	63	-168	First Motion
1978-03-16 02:00:06.500	66.43	29.83	39.2	6.1	Mw	GCMT	12	83	-13	Centroid Moment Tensor
1978-03-24 21:05:55.800	78.69	42.37	34.7	6.9	Mw	GCMT	155	67	129	Centroid Moment Tensor
1978-04-04 00:40:35.100	82.03	33.03	10	5.9	Mw	GCMT	223	59	-8	Centroid Moment Tensor

1978-04-14 06:11:34.400	75.45	41.5	33	5	Mw	GCMT	90	57	90	Centroid Moment Tensor
1978-04-19 00:00:00	82.68	27.67	51	4.9	Mb	Nandy et al., 1991	236	79	-176	First Motion
1978-04-22 00:00:00	85.9	42	0	5.3	Ms	WSM2016	290	47	61	First Motion
1978-05-19 20:58:56	100.3	25.53	10	5.1	Ms	WSM2016	330	44	-172	First Motion
1978-05-31 02:05:17	101.6	30.4	20	4.9	Ms	WSM2016	35	71	169	First Motion
1978-06-14 00:00:00	76.1	32.2	7	5	NaN	WSM2016	348	19	90	NaN
1978-07-31 11:55:45.800	81.78	35.68	10	5.5	Mw	GCMT	219	28	-32	Centroid Moment Tensor
1978-08-08 18:12:29	83.1	32.3	3	5.3	Ms	WSM2016	230	38	-133	First Motion
1978-08-31 03:26:53.500	101.04	27.41	10	5.3	Mw	GCMT	5	58	-26	Centroid Moment Tensor
1978-09-09 23:11:14.800	101.03	23.2	10	5.3	Mw	GCMT	131	84	158	Centroid Moment Tensor
1978-09-30 09:04:34.400	95.94	16.64	10	5.7	Mw	GCMT	17	76	-168	Centroid Moment Tensor
1978-10-04 13:53:50.7	85.93	27.82	19	5.2	Mb	Dasgupta et al., 1987	246	62	-18	First Motion
1978-11-17 00:00:00	97.1	37.3	15	5	Ms	WSM2016	327	52	0	First Motion
1978-12-18 00:00:00	95.44	4.2	66	5.3	Mb	Dasgupta & Mukhopadhyuay, 1993	204	62	-11	First Motion
1979-01-01 00:00:00	70.08	37.98	18	4.8	NaN	WSM2016	68	15	47	NaN
1979-01-08 00:00:00	72.9	38.6	0	4.8	NaN	WSM2016	187	51	-11	NaN
1979-01-19 00:00:00	86.6	35.2	7	6.3	NaN	WSM2016	246	43	34	NaN
1979-02-14 00:00:00	69.97	40.22	20	4.6	NaN	WSM2016	340	49	-47	NaN
1979-03-13 00:00:00	70.8	35.9	0	4.7	NaN	WSM2016	261	52	-167	NaN
1979-03-15 12:52:30.400	101.61	23.24	10	6	Mw	GCMT	33	62	-3	Centroid Moment Tensor
1979-03-29 02:01:35.400	83.69	41.93	15	5.6	Mw	GCMT	80	63	81	Centroid Moment Tensor
1979-03-29 07:07:25	97.75	32.61	12	5.8	Mw	Luo et al., 2016	266	84	-15	Centroid Moment Tensor
1979-04-01 00:00:00	75.7	39.1	0	4.5	NaN	WSM2016	165	39	-106	NaN
1979-04-06 00:00:00	77.4	42	0	5.2	NaN	WSM2016	159	49	-151	NaN
1979-04-16 00:00:00	70.57	38.86	7	4.4	NaN	WSM2016	125	38	141	NaN

1979-04-25 00:00:00	96.63	27.43	23	4.9	Mb	Nandy et al., 1991	215	61	-23	First Motion
1979-05-20 22:59:14.700	80.32	29.58	15	5.8	Mw	GCMT	105	83	91	Centroid Moment Tensor
1979-05-22 00:00:00	75.98	42.1	10	4.4	NaN	WSM2016	149	30	90	NaN
1979-06-19 16:29:08	87.48	26.74	20	5.2	Mb	Dasgupta et al., 1987	72	52	-146	First Motion
1979-07-05 00:00:00	82.88	11.98	45	5	Mb	Dasgupta & Mukhopadhyuay, 1993	31	38	45	First Motion
1979-08-05 00:00:00	73.5	39.4	0	4.6	NaN	WSM2016	175	50	146	NaN
1979-08-30 00:00:00	68.5	36.1	0	5	NaN	WSM2016	292	38	-158	NaN
1979-08-31 00:00:00	68.5	36.1	0	4.9	NaN	WSM2016	298	37	-155	NaN
1979-09-28 07:46:50.800	90.45	37.81	15	5.1	Mw	GCMT	129	23	42	Centroid Moment Tensor
1979-09-29 00:00:00	95.8	29	35	5	Ms	WSM2016	122	30	32	First Motion
1979-10-20 00:00:00	70.61	38.93	15	4.7	NaN	WSM2016	59	32	-100	NaN
1979-11-09 00:00:00	70.5	39.9	0	4.5	NaN	WSM2016	355	40	-60	NaN
1979-11-21 00:00:00	97.04	27.1	42	5.5	Mb	Nandy et al., 1991	229	32	21	First Motion
1979-11-25 02:40:49.200	96.32	25.21	10	5.2	Mw	GCMT	266	85	-11	Centroid Moment Tensor
1979-11-27 00:00:00	68.6	36.3	0	4.6	NaN	WSM2016	41	15	118	NaN
1979-12-06 00:00:00	95.48	30	22	5.2	Mb	Nandy et al., 1991	220	54	-33	First Motion
1979-12-21 06:32:00	97.78	26.61	10	5.3	Mw	Luo et al., 2016	119	42	72	Centroid Moment Tensor
1980-01-01 00:00:00	95.18	12.36	21	5	Mb	Dasgupta & Mukhopadhyuay, 1993	132	40	-165	First Motion
1980-01-13 00:00:00	72.8	39.5	0	5.2	NaN	WSM2016	160	50	-55	NaN
1980-01-17 00:00:00	71.1	35.2	0	4.5	NaN	WSM2016	253	38	-35	NaN
1980-01-17 00:00:00	71.6	39.4	0	5.1	NaN	WSM2016	180	50	128	NaN
1980-02-02 12:29:20.200	101.38	27.6	10	5.5	Mw	GCMT	213	74	-6	Centroid Moment Tensor
1980-02-14 00:00:00	69.3	37.1	0	4.8	NaN	WSM2016	352	21	-109	NaN
1980-02-19 00:00:00	92.59	6.73	32	5.1	Mb	Dasgupta & Mukhopadhyuay, 1993	263	69	19	First Motion
1980-02-22 00:00:00	88.6	30.6	14	5.8	NaN	WSM2016	338	45	-110	NaN
1980-03-06 00:00:00	92	36.1	0	5	Ms	WSM2016	239	65	-16	First Motion

1980-03-22 00:00:00	69.3	36.5	0	4.8	NaN	WSM2016	278	38	22	NaN
1980-04-10 00:00:00	70.23	38.02	8	4.7	NaN	WSM2016	87	33	-116	NaN
1980-04-13 00:00:00	95.5	30.2	30	5.1	Ms	WSM2016	202	62	30	First Motion
1980-04-14 10:17:18.200	69.12	36.19	17	5.5	Mw	GCMT	69	59	135	Centroid Moment Tensor
1980-04-17 00:00:00	99.1	37.9	15	5.2	Ms	WSM2016	202	45	-139	First Motion
1980-05-01 00:00:00	68.7	36.1	0	4.7	NaN	WSM2016	283	40	-24	NaN
1980-05-15 00:00:00	71.9	37.4	0	4.4	NaN	WSM2016	210	42	-40	NaN
1980-06-01 00:00:00	95.6	39.1	20	5.6	Ms	WSM2016	116	41	99	First Motion
1980-06-22 14:38:58.400	81.59	30.1	15	5.1	Mw	GCMT	28	36	-51	Centroid Moment Tensor
1980-06-24 00:00:00	88.6	33	3	5.1	Ms	WSM2016	249	63	-2	First Motion
1980-06-24 00:00:00	88.6	33	15	6.1	Ms	WSM2016	251	59	-18	First Motion
1980-06-26 00:00:00	68.4	37.2	0	4.5	NaN	WSM2016	281	44	133	NaN
1980-07-05 00:00:00	77.5	42.1	33	5.4	Ms	WSM2016	261	39	101	First Motion
1980-07-10 00:00:00	72.2	35.8	0	4.6	NaN	WSM2016	225	38	-22	NaN
1980-07-11 00:00:00	70.5	40.2	0	5.1	NaN	WSM2016	45	50	55	NaN
1980-07-12 00:00:00	93.8	36.9	25	5.1	Ms	WSM2016	196	33	126	First Motion
1980-07-20 00:00:00	72.04	41.37	20	4.6	NaN	WSM2016	115	41	142	NaN
1980-07-26 00:00:00	70.3	40	0	4.6	NaN	WSM2016	245	10	-90	NaN
1980-07-29 12:23:15.900	81.11	28.96	10	5.5	Mw	GCMT	98	65	90	Centroid Moment Tensor
1980-07-29 14:58:40.800	81.092	29.598	16	6.4	Mw	ISC (NEIC)	102	65	97	Centroid Moment Tensor
1980-07-31 00:00:00	74.9	39.6	0	5.2	NaN	WSM2016	105	38	-57	NaN
1980-08-14 00:00:00	88.6	33	33	4.9	Ms	WSM2016	169	50	148	First Motion
1980-08-15 05:45:02	88.63	33.12	20	5.2	Ms	WSM2016	169	50	148	First Motion
1980-08-17 00:00:00	75.7	39	0	4.6	NaN	WSM2016	184	41	150	NaN
1980-08-23 00:00:00	94.9	30.4	34	4.7	Ms	WSM2016	354	63	166	First Motion
1980-08-23 21:36:55.200	75.37	32.59	15	5.5	Mw	GCMT	140	81	95	Centroid Moment Tensor
1980-08-27 04:30:20.900	94.76	15.72	20	5.2	Mw	GCMT	114	40	86	Centroid Moment Tensor

1980-09-20 10:45:29.400	73.58	17.31	15	5	Mw	GCMT	139	29	-111	Centroid Moment Tensor
1980-10-07 00:00:00	82.1	35.6	0	5.4	Ms	WSM2016	285	43	-154	First Motion
1980-11-12 00:00:00	70.5	36.3	0	4.6	NaN	WSM2016	33	0	0	NaN
1980-11-19 19:00:55.900	89.05	27.42	44.1	6.2	Mw	GCMT	209	51	-2	Centroid Moment Tensor
1980-11-20 00:00:00	93.92	22.74	30	5.2	Mb	Mukhopadhyay, 1988	357	77	170	First Motion
1980-12-06 00:00:00	78.4	40.1	33	5.3	Ms	WSM2016	211	47	27	First Motion
1980-12-06 00:00:00	78.6	39.9	0	5	NaN	WSM2016	139	11	-45	NaN
1980-12-11 00:00:00	69.05	41.33	10	5.3	NaN	WSM2016	88	52	139	NaN
1980-12-30 00:00:00	69.11	41.31	10	4.8	NaN	WSM2016	230	50	52	NaN
1981-01-23 21:13:55.600	101.35	30.86	10	6.5	Mw	GCMT	51	86	-163	Centroid Moment Tensor
1981-02-04 00:00:00	73	37.5	0	4.9	NaN	WSM2016	215	42	-40	NaN
1981-02-15 00:00:00	74	39.5	0	4.7	NaN	WSM2016	176	41	160	NaN
1981-03-03 05:52:39.300	72.5	39.14	15	5.4	Mw	GCMT	1	88	-46	Centroid Moment Tensor
1981-04-12 10:18:34	85.74	8.48	15	5	Mb	WSM2016	340	73	-177	Centroid Moment Tensor
1981-04-23 00:00:00	75.6	40	0	4.6	NaN	WSM2016	168	40	98	NaN
1981-05-07 00:00:00	72.6	39.5	0	4.6	NaN	WSM2016	147	42	-157	NaN
1981-05-13 10:07:53	82.51	32.62	33	5.4	Ms	WSM2016	112	55	137	First Motion
1981-05-22 19:36:21	101.18	27.33	10	5	Ms	WSM2016	298	66	165	First Motion
1981-06-09 00:00:00	91.3	34.3	15	6.1	Ms	WSM2016	104	79	-5	First Motion
1981-06-10 00:00:00	72.7	37.6	0	4.6	NaN	WSM2016	66	35	82	NaN
1981-06-13 07:29:17.200	67.74	36.19	15	5.6	Mw	GCMT	107	34	157	Centroid Moment Tensor
1981-06-30 21:55:57	95.45	23	10	4.9	Mw	Luo et al., 2016	7	40	142	Centroid Moment Tensor
1981-07-07 10:29:08	97.67	25.42	25	5.1	Ms	WSM2016	80	49	168	First Motion
1981-08-14 06:09:39	98.51	25.61	10	5.2	Mw	Luo et al., 2016	33	63	-52	Centroid Moment Tensor
1981-08-16 18:55:45.700	97.02	25.53	37	5.1	Mw	GCMT	30	83	-156	Centroid Moment Tensor

1981-09-12 00:00:00	73.5	35.5	15	6.3	Ms	WSM2016	294	25	90	First Motion
1981-09-19 06:51:02.300	101.54	22.84	10	5.3	Mw	GCMT	50	82	-19	Centroid Moment Tensor
1981-10-08 00:00:00	74	39.3	0	4.5	NaN	WSM2016	314	45	-110	NaN
1981-10-23 00:00:00	95	30	33	5.4	Ms	WSM2016	31	80	177	First Motion
1981-10-24 00:00:00	68.5	36.4	0	4.6	NaN	WSM2016	159	48	120	NaN
1981-10-24 07:44:49	95.02	30.03	33	5.4	Ms	WSM2016	31	80	177	First Motion
1981-11-09 00:00:00	73.6	35.6	0	4.7	NaN	WSM2016	235	51	-39	NaN
1981-11-30 00:00:00	70.75	38.76	4	4.7	NaN	WSM2016	208	41	-70	NaN
1981-12-02 00:00:00	75.3	39.8	0	5	NaN	WSM2016	182	47	-35	NaN
1982-01-20 00:00:00	93.95	7.06	28	5.5	Mb	Dasgupta & Mukhopadhyuay, 1993	4	36	-118	First Motion
1982-01-20 00:00:00	93.88	7.15	40	5.6	Mb	Dasgupta & Mukhopadhyuay, 1993	1	47	-154	First Motion
1982-01-22 04:30:04.800	89.79	30.87	10	5.5	Mw	GCMT	7	64	-64	Centroid Moment Tensor
1982-01-23 17:37:36.900	82.24	31.71	10	6.3	Mw	GCMT	17	38	-58	Centroid Moment Tensor
1982-02-22 17:59:57.500	73.4	35.15	15	5.2	Mw	GCMT	123	43	76	Centroid Moment Tensor
1982-04-05 00:00:00	88.84	27.38	9	5	Mb	Nandy et al., 1991	206	49	-24	First Motion
1982-04-08 00:00:00	93.92	7.49	26	5.1	Mb	Dasgupta & Mukhopadhyuay, 1993	197	39	156	First Motion
1982-04-08 02:41:19	85.84	18.01	31.7	5.5	Mb	WSM2016	324	50	130	Centroid Moment Tensor
1982-04-22 00:00:00	70.2	37.7	0	4.6	NaN	WSM2016	198	50	-50	NaN
1982-05-06 00:00:00	71.5	40.22	20	5.5	NaN	WSM2016	85	34	90	NaN
1982-05-16 00:00:00	68.5	36	0	4.9	NaN	WSM2016	290	49	173	NaN
1982-05-22 08:53:04.800	94.39	7.61	12.2	5.5	Mw	GCMT	19	23	-98	Centroid Moment Tensor
1982-06-01 06:12:16	102.36	21.97	10	5.5	Mw	Luo et al., 2016	49	66	-3	Centroid Moment Tensor
1982-06-15 23:24:38	100.55	31.9	10	5.6	Mw	Luo et al., 2016	105	72	-3	Centroid Moment Tensor
1982-07-03 08:13:37	100.27	26.59	10	5.3	Mw	Luo et al., 2016	166	64	-90	Centroid Moment Tensor

1982-07-04 18:34:28	90.65	19.56	29.4	5.2	Mb	WSM2016	240	73	0	Centroid Moment Tensor
1982-08-12 00:00:00	73.6	35.5	0	4.6	NaN	WSM2016	239	50	-12	NaN
1982-08-18 00:00:00	72	37.5	0	4.8	NaN	WSM2016	87	14	90	NaN
1982-09-27 00:00:00	73.6	39.4	0	4.9	NaN	WSM2016	334	43	-90	NaN
1982-09-29 04:24:18.400	73.11	37.34	10	5.5	Mw	GCMT	180	46	-69	Centroid Moment Tensor
1982-10-08 13:34:58	99.61	25.69	10	5.2	Mw	Luo et al., 2016	146	23	-112	Centroid Moment Tensor
1982-10-27 00:00:00	69.4	36.2	0	4.7	NaN	WSM2016	251	48	138	NaN
1982-10-27 15:36:35	105.85	23.97	10	5.2	Mw	Luo et al., 2016	33	74	6	Centroid Moment Tensor
1982-10-31 18:40:57.800	82.36	36.07	10	5.4	Mw	GCMT	215	45	-15	Centroid Moment Tensor
1982-11-08 00:00:00	69.6	36.1	0	4.7	NaN	WSM2016	299	41	33	NaN
1982-11-13 00:00:00	69.1	36.1	0	4.7	NaN	WSM2016	307	41	-114	NaN
1982-11-20 07:58:47.000	70.35	34.46	10	5.7	Mw	GCMT	57	63	80	Centroid Moment Tensor
1982-11-22 00:00:00	77.5	39.8	0	4.6	NaN	WSM2016	176	47	121	NaN
1982-12-01 00:00:00	69.3	36.3	0	4.6	NaN	WSM2016	242	49	127	NaN
1982-12-16 00:00:00	68.7	36	0	4.6	NaN	WSM2016	342	45	53	NaN
1982-12-16 00:40:48.720	69.011	36.148	13	6.4	Mw	ISC (NEIC)	32	46	77	Centroid Moment Tensor
1982-12-16 08:56:42.600	92.57	11.58	63	5.6	Mw	GCMT	158	67	138	Centroid Moment Tensor
1982-12-31 19:46:49.700	77.01	42.75	15	5.3	Mw	GCMT	57	69	75	Centroid Moment Tensor
1983-01-03 00:00:00	68.8	36	0	4.6	NaN	WSM2016	279	42	-138	NaN
1983-01-24 23:09:28.900	93.39	12.99	72.7	6.8	Mw	GCMT	174	62	133	Centroid Moment Tensor
1983-01-30 00:00:00	94.96	5.47	67	5.2	Mb	Dasgupta & Mukhopadhyuay, 1993	214	42	-43	First Motion
1983-02-02 00:00:00	92.87	26.9	45	5.2	Mb	Nandy et al., 1991	38	70	160	First Motion
1983-02-06 00:00:00	68.6	36.2	0	5.3	NaN	WSM2016	146	43	31	NaN
1983-02-13 00:00:00	75.3	40.1	0	5.1	NaN	WSM2016	141	46	120	NaN

1983-02-13 01:40:17.200	75.11	39.94	15	6.2	Mw	GCMT	230	60	-7	Centroid Moment Tensor
1983-02-17 00:00:00	75.2	40.1	0	4.9	NaN	WSM2016	167	46	131	NaN
1983-02-26 20:07:51.700	70.16	38.93	10	5.3	Mw	GCMT	42	46	94	Centroid Moment Tensor
1983-02-27 20:33:06.300	78.15	32.29	10	5.2	Mw	GCMT	192	71	-7	Centroid Moment Tensor
1983-03-01 00:00:00	96.05	28.63	27	5.1	Mb	Nandy et al., 1991	45	79	-176	First Motion
1983-03-09 00:00:00	73.1	38.2	0	4.6	NaN	WSM2016	188	47	-52	NaN
1983-03-16 00:00:00	95.8	3.51	22	5.3	Mb	Dasgupta & Mukhopadhyuay, 1993	344	46	-149	First Motion
1983-03-30 00:00:00	75.3	40	0	5.1	NaN	WSM2016	175	45	133	NaN
1983-03-30 00:00:00	75.3	40.1	0	5.4	NaN	WSM2016	101	43	101	NaN
1983-04-05 00:00:00	70.65	41.78	20	4.6	NaN	WSM2016	51	37	72	NaN
1983-04-05 00:00:00	75.2	40	0	6.1	NaN	WSM2016	117	45	113	NaN
1983-04-06 00:00:00	71.41	38.87	5	5.3	NaN	WSM2016	315	50	-132	NaN
1983-04-22 00:00:00	68.32	39.37	15	4.5	NaN	WSM2016	7	41	49	NaN
1983-04-22 00:37:43.700	99.06	14.52	10.1	5.8	Mw	GCMT	85	33	89	Centroid Moment Tensor
1983-04-22 03:21:42.200	99.08	14.93	15	5	Mw	GCMT	130	29	139	Centroid Moment Tensor
1983-05-01 00:00:00	71.42	38.87	10	4.4	NaN	WSM2016	308	50	-139	NaN
1983-05-08 00:00:00	70.7	36.8	0	4.4	NaN	WSM2016	328	42	73	NaN
1983-06-05 00:00:00	73.6	39.5	0	4.4	NaN	WSM2016	331	40	76	NaN
1983-06-05 00:00:00	75.6	39.2	0	5.1	NaN	WSM2016	295	44	-126	NaN
1983-06-24 07:18:27	103.67	21.85	10	6.2	Mw	Luo et al., 2016	20	66	0	Centroid Moment Tensor
1983-07-02 00:00:00	94.68	5.71	78	5.6	Mb	Dasgupta & Mukhopadhyuay, 1993	240	58	145	First Motion
1983-07-15 04:48:54	103.29	21.93	15	5.3	Mw	Luo et al., 2016	34	78	10	Centroid Moment Tensor
1983-08-20 00:00:00	73.7	39.5	0	5.1	NaN	WSM2016	312	52	46	NaN
1983-08-25 11:05:33.900	73.87	39.09	15	5.1	Mw	GCMT	119	86	142	Centroid Moment Tensor

1983-08-30 10:39:34.200	94.9	25.34	68.9	5.7	Mw	GCMT	161	65	159	Centroid Moment Tensor
1983-09-17 04:40:43.100	93.15	8	35.2	5.2	Mw	GCMT	199	43	-43	Centroid Moment Tensor
1983-10-01 00:00:00	79.1	42.72	15	4.6	NaN	WSM2016	166	42	114	NaN
1983-10-09 00:00:00	72.4	38.7	0	4.6	NaN	WSM2016	307	49	-130	NaN
1983-11-05 00:00:00	72.6	41.37	20	4.7	NaN	WSM2016	105	40	98	NaN
1983-11-19 00:00:00	71.29	40.24	20	4.4	NaN	WSM2016	100	38	71	NaN
1983-12-07 00:00:00	68.8	36.1	0	5.3	NaN	WSM2016	345	45	52	NaN
1983-12-15 10:52:59.600	87.64	43.1	56.3	5.1	Mw	GCMT	165	44	132	Centroid Moment Tensor
1983-12-16 00:00:00	73	39.4	0	4.9	NaN	WSM2016	143	44	-111	NaN
1983-12-16 13:16:01.600	72.48	39.32	15	5.9	Mw	GCMT	60	51	97	Centroid Moment Tensor
1983-12-21 00:00:00	77.45	42.07	15	4.8	NaN	WSM2016	66	36	90	NaN
1983-12-22 00:00:00	68.8	36.2	0	5.2	NaN	WSM2016	293	44	31	NaN
1984-01-20 00:00:00	96.36	28.65	26	5	Mb	Nandy et al., 1991	48	60	-173	First Motion
1984-02-01 00:00:00	70.4	34.3	10	6.2	NaN	WSM2016	289	41	33	NaN
1984-02-02 00:00:00	70.1	34.3	10	4.7	NaN	WSM2016	287	42	40	NaN
1984-02-02 00:00:00	71.4	42.87	15	4.8	NaN	WSM2016	80	43	120	NaN
1984-02-03 00:00:00	70	34.3	10	4.6	NaN	WSM2016	292	41	52	NaN
1984-02-05 00:00:00	71.36	39.05	30	4.4	NaN	WSM2016	55	46	115	NaN
1984-02-15 00:00:00	71.1	40.9	15	4.9	NaN	WSM2016	88	38	105	NaN
1984-02-15 00:00:00	67.65	40	15	5.2	NaN	WSM2016	105	39	117	NaN
1984-02-16 00:00:00	71.1	40.93	15	4.8	NaN	WSM2016	258	47	132	NaN
1984-02-17 00:00:00	71.06	40.93	10	4.8	NaN	WSM2016	189	44	56	NaN
1984-02-17 00:00:00	71.08	40.86	15	4.9	NaN	WSM2016	356	54	25	NaN
1984-02-17 23:26:58.500	70.84	41.13	12	5.5	Mw	GCMT	104	60	116	Centroid Moment Tensor
1984-02-23 15:22:49.600	67.43	39.91	15	5	Mw	GCMT	77	71	84	Centroid Moment Tensor
1984-03-13 00:00:00	71.06	40.91	15	4.4	NaN	WSM2016	55	37	53	NaN
1984-03-21 00:00:00	93.3	26.76	35	5	Mb	Nandy et al., 1991	146	65	11	First Motion

1984-04-13 09:50:11.200	94.72	12.12	10	5.2	Mw	GCMT	43	59	-90	Centroid Moment Tensor
1984-04-21 00:00:00	69.1	36.3	10	5	NaN	WSM2016	230	47	124	NaN
1984-04-23 22:30:04.300	99.62	21.79	17	5.9	Mw	GCMT	84	69	13	Centroid Moment Tensor
1984-05-06 00:00:00	93.52	24.22	57	5.7	Mb	Chen & Molnar, 1990	252	76	18	Centroid Moment Tensor
1984-05-29 00:00:00	97.14	3.64	72	5.7	Mb	Dasgupta & Mukhopadhyuay, 1993	192	50	-27	First Motion
1984-06-20 00:00:00	73	39.4	10	4.9	NaN	WSM2016	294	47	-126	NaN
1984-07-05 00:00:00	94.76	11.27	18	5.4	Mb	Dasgupta & Mukhopadhyuay, 1993	249	61	165	First Motion
1984-07-19 16:16:10.600	94.58	11.11	25.1	4.8	Mw	GCMT	96	47	-58	Centroid Moment Tensor
1984-07-20 20:06:29.500	94.53	11.26	10	5	Mw	GCMT	74	63	-79	Centroid Moment Tensor
1984-07-23 02:07:29.500	94.24	10.95	10	5	Mw	GCMT	76	73	-89	Centroid Moment Tensor
1984-09-05 00:00:00	71.9	38.7	20	4.5	NaN	WSM2016	178	50	-21	NaN
1984-09-22 00:00:00	92.15	26.49	28	5.2	Mb	Nandy et al., 1991	33	61	5	First Motion
1984-10-26 20:22:21.830	71.328	39.155	11	6.1	Mw	ISC (NEIC)	36	54	42	Centroid Moment Tensor
1984-11-28 10:29:29.500	96.96	26.52	16	5.7	Mw	GCMT	210	77	138	Centroid Moment Tensor
1985-01-11 00:00:00	72.9	39.5	7	4.4	NaN	WSM2016	87	69	-179	NaN
1985-03-16 00:00:00	71.34	39.21	5	4.4	NaN	WSM2016	307	66	168	NaN
1985-04-04 08:40:47.100	95.09	11.31	17.8	5.3	Mw	GCMT	79	89	50	Centroid Moment Tensor
1985-04-18 05:52:55	102.64	25.39	10	5.7	Mw	Luo et al., 2016	5	82	-33	Centroid Moment Tensor
1985-04-21 13:21:33.200	87.18	35.72	10	5.6	Mw	GCMT	155	90	140	Centroid Moment Tensor
1985-04-24 06:47:51.500	95.97	25.83	56.4	5.2	Mw	GCMT	182	58	113	Centroid Moment Tensor
1985-04-25 15:30:20.800	93.37	8.31	54.1	5.5	Mw	GCMT	78	88	8	Centroid Moment Tensor
1985-04-27 00:00:00	71.1	40.9	10	5	NaN	WSM2016	85	41	110	NaN

1985-05-05 00:00:00	73.1	39.3	10	4.4	NaN	WSM2016	152	60	175	NaN
1985-05-18 00:00:00	71.14	40.9	5	4.4	NaN	WSM2016	119	38	145	NaN
1985-05-20 15:11:46.500	87.16	35.58	10	5.8	Mw	GCMT	156	79	175	Centroid Moment Tensor
1985-06-01 00:00:00	69.11	41.32	5	4.4	NaN	WSM2016	39	54	166	NaN
1985-06-15 15:17:46.500	83.37	34.55	10	5.3	Mw	GCMT	40	61	-30	Centroid Moment Tensor
1985-06-28 00:00:00	72.22	39.9	7	4.4	NaN	WSM2016	1	54	41	NaN
1985-07-01 02:23:52	87.43	18.4	10	5.3	Mb	WSM2016	60	59	1	Centroid Moment Tensor
1985-07-21 00:00:00	72.9	39.4	10	4.4	NaN	WSM2016	69	16	90	NaN
1985-08-01 12:13:52	95.53	29.24	40	5.7	Mw	Luo et al., 2016	176	15	153	Centroid Moment Tensor
1985-08-03 00:00:00	70.5	36.7	7	4.4	NaN	WSM2016	61	29	68	NaN
1985-08-15 00:00:00	70.5	38.93	5	4.4	NaN	WSM2016	45	32	75	NaN
1985-08-23 12:41:56.160	75.224	39.431	36	6.7	Mw	ISC (NEIC)	64	85	90	Centroid Moment Tensor
1985-08-24 00:00:00	75.3	39.2	10	4.4	NaN	WSM2016	241	50	46	NaN
1985-08-29 23:39:55.200	75.14	39.25	10	5.2	Mw	GCMT	81	27	57	Centroid Moment Tensor
1985-09-05 18:30:26	98.23	25.29	61	5.5	Mw	Luo et al., 2016	14	65	177	Centroid Moment Tensor
1985-09-08 00:00:00	71.7	37.6	10	4.4	NaN	WSM2016	277	49	49	NaN
1985-10-03 00:00:00	75.5	39.5	10	4.4	NaN	WSM2016	215	55	-153	NaN
1985-10-10 00:00:00	73.22	41.67	15	5	NaN	WSM2016	253	43	95	NaN
1985-10-13 00:00:00	69.83	40.28	10	4.4	NaN	WSM2016	104	51	127	NaN
1985-10-13 15:59:51.220	69.823	40.301	13	5.8	Mw	ISC (NEIC)	8	47	62	Centroid Moment Tensor
1985-11-07 00:00:00	72.55	40.13	15	4.4	NaN	WSM2016	200	65	24	NaN
1985-11-19 00:00:00	71.1	37.9	10	4.4	NaN	WSM2016	337	52	-135	NaN
1985-11-27 00:00:00	69.68	37.89	3	4.4	NaN	WSM2016	72	46	118	NaN
1985-12-15 00:00:00	69.88	38.81	8	4.4	NaN	WSM2016	159	48	120	NaN
1985-12-20 00:00:00	75.4	39.5	10	5	NaN	WSM2016	168	51	129	NaN
1986-01-28 00:00:00	75.6	39.5	10	4.4	NaN	WSM2016	194	50	21	NaN

1986-01-28 12:32:18.600	94.01	8.81	15	5.9	Mw	GCMT	256	88	-4	Centroid Moment Tensor
1986-02-19 17:34:30.300	91.18	24.89	18	5.3	Mw	GCMT	70	90	40	Centroid Moment Tensor
1986-03-13 08:41:22	101.02	25.45	15	5.3	Mw	Luo et al., 2016	165	66	-84	Centroid Moment Tensor
1986-03-21 00:00:00	69.03	39.9	10	4.4	NaN	WSM2016	34	37	25	NaN
1986-04-25 16:12:35.200	77.07	39.83	15	5.4	Mw	GCMT	48	45	45	Centroid Moment Tensor
1986-04-26 07:35:16	76.35	32.23	13	5.5	Mw	O Kane et al., 2022	299	20	58	Centroid Moment Tensor
1986-05-15 14:38:12.800	69.11	29.54	15	5.2	Mw	GCMT	31	79	65	Centroid Moment Tensor
1986-05-24 15:31:53.700	68.69	35.99	17	5	Mw	GCMT	163	55	117	Centroid Moment Tensor
1986-06-20 17:12:51.700	86.77	30.82	15	6	Mw	GCMT	51	78	-4	Centroid Moment Tensor
1986-06-29 09:55:41.400	96.12	15.45	15	5.5	Mw	GCMT	50	74	-94	Centroid Moment Tensor
1986-07-06 00:00:00	80.2	34.4	9	6.1	Ms	WSM2016	270	68	-13	First Motion
1986-07-19 20:12:58.700	86.88	30.88	15	5	Mw	GCMT	51	78	4	Centroid Moment Tensor
1986-07-26 20:24:55.700	94.19	23.86	64.9	5.4	Mw	GCMT	36	76	162	Centroid Moment Tensor
1986-08-06 19:55:20	101.2	29.15	15	5.3	Mw	Luo et al., 2016	40	41	-162	Centroid Moment Tensor
1986-08-20 21:24:03.000	91.96	34.58	15	6.4	Mw	GCMT	253	69	-18	Centroid Moment Tensor
1986-08-26 09:43:00.390	101.496	37.724	6	6	Mw	ISC (NEIC)	230	13	144	Centroid Moment Tensor
1986-09-15 21:42:29.290	71.092	36.714	77	5.6	Mw	ISC (NEIC)	113	63	164	Centroid Moment Tensor
1986-09-20 10:04:58.700	93.16	12.82	21.6	5.1	Mw	GCMT	185	71	102	Centroid Moment Tensor
1986-10-16 19:54:11.200	66.45	27.24	46.6	5	Mw	GCMT	1	60	28	Centroid Moment Tensor
1986-10-31 00:00:00	71.4	39.2	10	4.4	NaN	WSM2016	296	43	-137	NaN
1986-11-01 19:59:53	96.91	25.53	70	5.2	Mw	Luo et al., 2016	28	45	132	Centroid Moment Tensor

1986-11-12 00:00:00	73	38.7	40	5	NaN	WSM2016	205	73	12	NaN
1987-01-05 00:00:00	81.2	42.17	4	5.6	NaN	WSM2016	140	47	-58	NaN
1987-01-07 18:19:11	103.86	34.23	15	5.4	Mw	Luo et al., 2016	68	65	152	Centroid Moment Tensor
1987-01-24 08:09:21.300	79.318	41.529	14	6	Mw	ISC (NEIC)	27	42	53	Centroid Moment Tensor
1987-01-25 00:00:00	79.6	41.3	8	4.4	NaN	WSM2016	226	43	42	NaN
1987-02-06 00:00:00	69.6	37	9	4.4	NaN	WSM2016	312	52	52	NaN
1987-02-14 00:00:00	79.3	41.4	9	4.4	NaN	WSM2016	183	49	-21	NaN
1987-02-23 00:00:00	79	41.3	8	4.4	NaN	WSM2016	227	45	38	NaN
1987-02-23 00:21:24.000	70.14	39.12	33	4.9	Mw	GCMT	61	61	139	Centroid Moment Tensor
1987-03-03 09:41:33.100	79.52	41.3	33	5	Mw	GCMT	42	21	96	Centroid Moment Tensor
1987-03-09 00:00:00	74.7	38.2	4	4.4	NaN	WSM2016	197	54	-179	NaN
1987-03-16 00:00:00	73.9	39.3	10	4.4	NaN	WSM2016	325	39	36	NaN
1987-03-26 00:00:00	69.95	41.81	20	5	NaN	WSM2016	326	47	-65	NaN
1987-04-17 00:00:00	73	39.4	5	4.4	NaN	WSM2016	2	57	-5	NaN
1987-04-30 05:17:43.200	74.67	39.67	15	5.7	Mw	GCMT	113	44	86	Centroid Moment Tensor
1987-06-08 00:00:00	74.7	39.8	10	5.3	NaN	WSM2016	272	48	57	NaN
1987-06-24 00:00:00	73.93	40.9	10	5	NaN	WSM2016	118	54	136	NaN
1987-07-11 00:00:00	72.7	36.9	5	5	NaN	WSM2016	214	45	-15	NaN
1987-09-25 23:16:34.200	90.34	29.47	15	5	Mw	GCMT	21	45	-90	Centroid Moment Tensor
1987-12-21 00:00:00	70.8	38.8	5	5.3	NaN	WSM2016	324	49	-159	NaN
1987-12-22 00:16:42.900	89.75	41.27	19	5.5	Mw	GCMT	186	49	128	Centroid Moment Tensor
1987-12-26 00:00:00	72.1	41.1	10	4.4	NaN	WSM2016	132	41	151	NaN
1988-01-25 01:12:27.400	94.87	29.8	33	5.2	Mw	GCMT	37	69	159	Centroid Moment Tensor
1988-02-06 00:00:00	91.52	24.65	31	5.8	Mb	Chen & Molnar, 1990	225	77	5	Centroid Moment Tensor
1988-03-19 20:19:20.300	68.1	30.41	15	5.7	Mw	GCMT	142	6	-7	Centroid Moment Tensor

1988-06-17 13:30:47.100	77.51	43.01	15	5.7	Mw	GCMT	29	12	25	Centroid Moment Tensor
1988-07-20 06:20:54.300	72.83	36.91	15	5.5	Mw	GCMT	137	38	-96	Centroid Moment Tensor
1988-08-20 23:09:09.560	86.616	26.755	44	6.8	Mw	ISC (NEIC)	217	54	-10	Centroid Moment Tensor
1988-09-03 12:52:56	97.38	29.95	15	4.8	Mw	Luo et al., 2016	88	57	-79	Centroid Moment Tensor
1988-09-23 04:46:44.300	74.47	39.66	15	5.1	Mw	GCMT	106	23	64	Centroid Moment Tensor
1988-09-25 20:52:22.200	71.64	37.51	44.5	5.5	Mw	GCMT	43	89	-15	Centroid Moment Tensor
1988-10-23 11:43:10.900	94.67	20.74	45.6	5.1	Mw	GCMT	168	27	-58	Centroid Moment Tensor
1988-10-29 09:11:00.800	85.73	27.39	18	5.2	Mw	GCMT	106	62	79	Centroid Moment Tensor
1988-11-06 13:03:31	99.68	23	15	7	Mw	Luo et al., 2016	64	84	12	Centroid Moment Tensor
1988-11-07 02:40:03	99.42	23.38	15	5.2	Mw	Luo et al., 2016	6	58	138	Centroid Moment Tensor
1988-11-15 10:28:13.200	99.23	22.8	15	5.3	Mw	GCMT	63	90	20	Centroid Moment Tensor
1988-11-25 22:29:44.100	91.77	34.29	15	5.5	Mw	GCMT	169	84	150	Centroid Moment Tensor
1988-11-27 04:17:58.500	100.17	22.7	15	5.5	Mw	GCMT	71	61	14	Centroid Moment Tensor
1988-11-30 08:13:28	99.54	22.15	15	6	Mw	Luo et al., 2016	76	87	-15	Centroid Moment Tensor
1988-12-14 11:46:06.000	71.56	39.72	15	5.3	Mw	GCMT	3	51	127	Centroid Moment Tensor
1989-01-18 18:22:53.900	100.13	29.88	15	5.2	Mw	GCMT	120	50	-20	Centroid Moment Tensor
1989-02-12 07:55:56	96.83	26.18	33	5.3	Mw	Luo et al., 2016	193	69	147	Centroid Moment Tensor
1989-02-19 01:46:01.600	94.47	7.65	15	5.3	Mw	GCMT	43	83	-32	Centroid Moment Tensor
1989-03-01 03:25:10	98.3	21.61	58	5.7	Mw	Luo et al., 2016	73	79	9	Centroid Moment Tensor
1989-04-13 00:00:00	92.431	24.404	32	5.5	Mb	Kumar et al., 2015	226	75	18	Centroid Moment Tensor

1989-04-15 20:34:21	99.37	29.92	15	6.4	Mw	Luo et al., 2016	74	62	-99	Centroid Moment Tensor
1989-04-25 02:13:20.830	99.419	30.048	7	6.1	Mw	ISC (NEIC)	43	38	-126	Centroid Moment Tensor
1989-05-01 07:05:00	99.43	29.98	10	5.4	Ms	WSM2016	297	53	18	First Motion
1989-05-03 05:53:12	99.69	30	15	6.2	Mw	Luo et al., 2016	95	52	-67	Centroid Moment Tensor
1989-05-03 15:41:40	99.43	29.83	15	5.8	Mw	Luo et al., 2016	91	45	-90	Centroid Moment Tensor
1989-05-07 00:38:20	99.65	23.46	15	5.6	Mw	Luo et al., 2016	68	79	15	Centroid Moment Tensor
1989-05-13 23:19:47.800	91.65	35.69	15	5.3	Mw	GCMT	157	88	156	Centroid Moment Tensor
1989-07-21 03:09:22	99.54	29.79	15	5.6	Mw	Luo et al., 2016	59	38	-127	Centroid Moment Tensor
1989-09-22 02:25:56	102.83	30.87	15	6.1	Mw	Luo et al., 2016	202	74	99	Centroid Moment Tensor
1989-09-28 21:52:21.300	99.06	20.32	15	5.8	Mw	GCMT	76	72	-1	Centroid Moment Tensor
1990-01-14 03:03:19.230	91.971	37.819	14	6	Mw	ISC (NEIC)	94	41	116	Centroid Moment Tensor
1990-03-08 18:57:05	96.61	25.11	56	5.2	Mw	Luo et al., 2016	32	72	173	Centroid Moment Tensor
1990-03-29 16:19:21.000	73.09	39.04	22	5.3	Mw	GCMT	6	89	34	Centroid Moment Tensor
1990-04-17 01:59:35.100	74.78	39.29	15	6	Mw	GCMT	118	68	156	Centroid Moment Tensor
1990-04-19 22:41:34.500	69.52	34.16	33	5.3	Mw	GCMT	3	85	-26	Centroid Moment Tensor
1990-04-26 09:37:15.040	100.245	35.986	10	6.1	Mw	ISC (NEIC)	123	35	61	Centroid Moment Tensor
1990-04-27 05:29:30.000	66.46	28.7	15	5.5	Mw	GCMT	264	84	147	Centroid Moment Tensor
1990-05-05 20:47:01	73.02	36.91	22	6	Ms	WSM2016	168	31	-56	NaN
1990-08-14 00:50:39.300	65.8	26.93	15	5.5	Mw	GCMT	194	80	-19	Centroid Moment Tensor
1990-08-18 18:52:43.300	93.86	7.75	15	6	Mw	GCMT	185	73	180	Centroid Moment Tensor

1990-11-14 18:45:05.000	65.84	27.45	28.7	5.5	Mw	GCMT	97	59	151	Centroid Moment Tensor
1990-12-25 01:06:56.300	93.47	12.36	17.1	5.3	Mw	GCMT	58	51	-117	Centroid Moment Tensor
1990-12-29 13:23:55.200	93.93	8.14	21	6	Mw	GCMT	77	89	4	Centroid Moment Tensor
1991-01-05 14:57:24	96.18	23.61	21	6.9	Mw	Luo et al., 2016	2	68	166	Centroid Moment Tensor
1991-02-25 14:30:34.600	79.2	40.34	15	6	Mw	GCMT	68	50	94	Centroid Moment Tensor
1991-06-06 16:02:07	87.25	42.68	33	5.2	Ms	WSM2016	326	14	139	First Motion
1991-07-18 09:50:41.600	94.29	8.37	41.9	5.5	Mw	GCMT	73	87	1	Centroid Moment Tensor
1991-10-19 21:23:14.300	78.774	30.78	19	6.8	Mw	ISC (NEIC)	18	38	172	Centroid Moment Tensor
1991-11-08 15:13:00	70.66	26.38	26	5.4	Mw	Bai et al., 2017	56	43	46	Centroid Moment Tensor
1991-12-21 00:00:00	88.14	27.9	70	4.9	Mb	Zhu & Helmberger 1996	295	85	180	Centroid Moment Tensor
1992-01-11 06:16:57	86.67	9.45	17.1	5.6	Mb	WSM2016	296	49	137	Centroid Moment Tensor
1992-01-20 08:58:24.200	65.93	27.37	15	5.5	Mw	GCMT	99	72	170	Centroid Moment Tensor
1992-01-21 22:08:00.100	67.49	26.9	15	5.4	Mw	GCMT	15	44	75	Centroid Moment Tensor
1992-03-17 02:14:44.200	93.3	8.87	60.8	5.1	Mw	GCMT	137	89	161	Centroid Moment Tensor
1992-03-28 10:17:45.100	67.36	26.75	15	4.9	Mw	GCMT	3	33	91	Centroid Moment Tensor
1992-04-04 00:00:00	87.98	28.15	80	4.9	Mb	Zhu & Helmberger 1996	46	68	-23	Centroid Moment Tensor
1992-04-23 15:32:54.000	98.85	22.4	15	6.1	Mw	GCMT	252	84	-22	Centroid Moment Tensor
1992-04-24 07:07:23.910	66.065	27.55	33	6.2	Mw	ISC (NEIC)	254	69	158	Centroid Moment Tensor
1992-05-10 04:04:00	72.93	37.17	5	5.8	Mw	Bai et al., 2017	186	45	-55	Centroid Moment Tensor
1992-05-20 12:20:35.100	71.27	32.95	15	6	Mw	GCMT	68	85	91	Centroid Moment Tensor

1992-06-15 02:49:02	96.03	23.95	23	6.3	Mw	Luo et al., 2016	8	69	-173	Centroid Moment Tensor
1992-06-27 13:21:27.200	81.12	35.18	33	5	Mw	GCMT	12	30	-90	Centroid Moment Tensor
1992-07-09 21:34:02	90.2	20.96	30	5.4	Mb	WSM2016	79	58	12	Centroid Moment Tensor
1992-07-30 08:24:46.650	90.163	29.584	10	6.1	Mw	ISC (NEIC)	107	48	-64	Centroid Moment Tensor
1992-08-19 02:04:45.800	73.32	42.19	17	7.2	Mw	GCMT	88	60	99	Centroid Moment Tensor
1992-10-28 07:02:11.300	96.29	18.88	48.9	5.4	Mw	GCMT	68	65	7	Centroid Moment Tensor
1992-11-22 11:42:48.200	94.51	20.43	71.4	5.2	Mw	GCMT	187	29	-43	Centroid Moment Tensor
1992-11-23 23:11:07.900	72.38	38.7	43.6	5.6	Mw	GCMT	211	33	-49	Centroid Moment Tensor
1992-12-17 17:43:12.700	68.52	37.3	28.8	5.2	Mw	GCMT	172	45	114	Centroid Moment Tensor
1992-12-22 16:42:43.900	88.03	34.67	15	5.2	Mw	GCMT	29	65	-57	Centroid Moment Tensor
1992-12-24 05:09:47.200	72.23	42.45	26.1	5.3	Mw	GCMT	79	35	57	Centroid Moment Tensor
1993-01-18 12:42:12.600	90.28	30.34	15	5.9	Mw	GCMT	25	48	-57	Centroid Moment Tensor
1993-01-26 20:32:08.700	100.88	22.86	24.4	5.6	Mw	GCMT	50	82	-5	Centroid Moment Tensor
1993-02-03 00:05:13	86.06	42.16	33	5.4	Ms	WSM2016	60	69	167	First Motion
1993-03-20 14:51:00	87.33	29.03	16	6.2	Mw	Bai et al., 2017	161	46	-121	Centroid Moment Tensor
1993-04-18 04:55:44.800	95.52	12	17.3	5.2	Mw	GCMT	77	63	-48	Centroid Moment Tensor
1993-06-15 23:12:23.200	77.53	35.19	15	5	Mw	GCMT	95	74	-13	Centroid Moment Tensor
1993-07-17 09:46:39	99.82	27.42	15	5.4	Mw	Luo et al., 2016	140	33	-54	Centroid Moment Tensor
1993-08-14 14:30:07.900	101.8	25.63	33	5.2	Mw	GCMT	115	76	165	Centroid Moment Tensor
1993-09-29 22:25:48.620	76.451	18.066	5	6.2	Mw	ISC (NEIC)	123	41	92	Centroid Moment Tensor

1993-09-30 17:04:51.700	92.06	11.84	22.8	5.3	Mw	GCMT	173	65	94	Centroid Moment Tensor
1993-10-02 08:42:00	88.66	38.17	11	6.1	Mw	Bai et al., 2017	326	42	146	Centroid Moment Tensor
1993-11-16 15:52:47.300	66.88	30.54	33	5.6	Mw	GCMT	24	89	-13	Centroid Moment Tensor
1994-01-11 00:52:04	97.4	24.8	15	6.1	Mw	Luo et al., 2016	106	25	-85	Centroid Moment Tensor
1994-04-06 07:03:31	97.05	25.62	15	5.8	Mw	Luo et al., 2016	96	57	26	Centroid Moment Tensor
1994-05-25 18:42:23.600	94.37	7.7	41.4	5.8	Mw	GCMT	148	85	177	Centroid Moment Tensor
1994-05-29 14:11:59.300	94.17	20.45	49.1	6.5	Mw	GCMT	220	32	-8	Centroid Moment Tensor
1994-06-29 18:22:33.580	93.673	32.567	8	5.8	Mw	ISC (NEIC)	13	45	-98	Centroid Moment Tensor
1994-06-30 00:48:38.300	93.76	32.53	15	5	Mw	GCMT	200	57	-70	Centroid Moment Tensor
1994-08-03 00:00:00	93.979	21.503	58	5.5	Mb	Kumar et al., 2015	206	81	9	Centroid Moment Tensor
1994-08-14 07:38:35.000	89.18	34.97	33	5.2	Mw	GCMT	61	68	5	Centroid Moment Tensor
1994-08-19 21:02:45.620	96.415	17.974	14	5.8	Mw	ISC (NEIC)	194	66	176	Centroid Moment Tensor
1994-09-23 19:15:51.300	100.05	36.07	15	5.3	Mw	GCMT	123	31	71	Centroid Moment Tensor
1994-11-21 08:16:40	96.83	25.37	43	5.9	Mw	Luo et al., 2016	34	76	179	Centroid Moment Tensor
1994-11-22 15:38:35.400	95.51	13.64	22.7	5.2	Mw	GCMT	17	74	-164	Centroid Moment Tensor
1994-12-28 03:56:22.500	90.57	35.75	33	5.2	Mw	GCMT	31	25	-116	Centroid Moment Tensor
1994-12-29 18:58:34	103.59	28.8	33	5.1	Mw	Luo et al., 2016	38	55	146	Centroid Moment Tensor
1995-02-17 02:44:32.200	92.62	27.48	35	5.4	Mw	GCMT	226	84	-44	Centroid Moment Tensor
1995-02-20 04:12:27.500	70.84	39.62	27	5.3	Mw	GCMT	1	71	-6	Centroid Moment Tensor
1995-02-20 08:07:34	72.4	41.73	33	5	Mb	WSM2016	267	30	110	Centroid Moment Tensor

1995-03-19 02:02:36	87.12	42.32	22	5	Ms	WSM2016	73	64	13	First Motion
1995-04-24 16:13:14	103.16	22.88	33	5.2	Mw	Luo et al., 2016	11	83	-10	Centroid Moment Tensor
1995-06-11 21:55:49	70.13	32.44	16	5.1	Mb	WSM2016	212	28	53	Centroid Moment Tensor
1995-07-09 15:56:28	100.35	35.55	33	5.2	Mb	WSM2016	100	33	76	Centroid Moment Tensor
1995-07-09 20:31:38	99.28	21.92	15	5.9	Mw	Luo et al., 2016	64	66	3	Centroid Moment Tensor
1995-07-11 21:46:50	99.22	21.89	15	6.8	Mw	Luo et al., 2016	60	85	1	Centroid Moment Tensor
1995-07-27 15:16:32.800	93.97	9.18	26.7	5.2	Mw	GCMT	93	69	-30	Centroid Moment Tensor
1995-09-26 04:39:10.500	81.4	42.02	43	5.1	Mw	GCMT	82	54	100	Centroid Moment Tensor
1995-10-08 08:55:50	71.87	41.23	20	5.9	Mb	WSM2016	247	40	66	Centroid Moment Tensor
1995-10-23 22:46:57	102.54	25.87	15	6.2	Mw	Luo et al., 2016	13	75	-9	Centroid Moment Tensor
1995-11-01 12:29:29	80.31	42.99	15	5.5	Mb	WSM2016	270	13	90	Centroid Moment Tensor
1995-12-18 04:57:11.900	97.63	34.74	33	5.7	Mw	GCMT	46	81	176	Centroid Moment Tensor
1995-12-23 10:32:04.400	73.26	38.4	33	5.2	Mw	GCMT	174	31	-77	Centroid Moment Tensor
1995-12-24 09:36:12.000	78.16	37.72	33	5.1	Mw	GCMT	138	23	114	Centroid Moment Tensor
1996-01-18 09:33:51	77.98	42.1	20.4	5.2	Mb	WSM2016	54	32	111	Centroid Moment Tensor
1996-02-03 11:14:31	100.28	27.15	15	5.7	Mw	Luo et al., 2016	153	57	-105	Centroid Moment Tensor
1996-02-04 07:36:21	100.12	27.52	15	5.5	Mw	Luo et al., 2016	18	58	-40	Centroid Moment Tensor
1996-02-04 16:58:14	100.38	26.84	15	6.6	Mw	Luo et al., 2016	173	57	-93	Centroid Moment Tensor
1996-03-19 15:00:36.300	76.8	39.93	22.2	6.3	Mw	GCMT	72	66	81	Centroid Moment Tensor
1996-04-01 08:08:00	73.46	31.46	40	5.2	Mw	Bai et al., 2017	98	33	101	Centroid Moment Tensor

1996-04-13 10:45:22.400	94.57	7.28	48.1	5.3	Mw	GCMT	56	89	-3	Centroid Moment Tensor
1996-06-21 00:32:50.200	69	28.61	33	5.1	Mw	GCMT	216	87	-28	Centroid Moment Tensor
1996-06-25 07:28:59.100	93.87	8.65	29.9	5.2	Mw	GCMT	82	84	3	Centroid Moment Tensor
1996-07-03 06:44:00	88.19	30.11	4	5.6	Mw	Bai et al., 2017	172	45	-102	Centroid Moment Tensor
1996-07-03 10:10:34	88.19	29.92	33	5	Mb	WSM2016	175	27	-90	Centroid Moment Tensor
1996-07-24 17:23:58.500	68.19	36.08	35.8	5	Mw	GCMT	27	41	78	Centroid Moment Tensor
1996-07-26 13:09:09.600	96.53	24.68	67.6	5.3	Mw	GCMT	93	70	11	Centroid Moment Tensor
1996-07-31 08:00:34.000	88.67	29.74	15	5.4	Mw	GCMT	23	32	-41	Centroid Moment Tensor
1996-08-02 11:36:12	67.63	29.29	33	4.9	Mb	WSM2016	247	24	130	Centroid Moment Tensor
1996-09-24 19:24:54.500	100.7	27.18	15	5.5	Mw	GCMT	151	50	-83	Centroid Moment Tensor
1996-11-11 09:22:27.760	95.013	19.33	80	5.9	Mw	ISC (NEIC)	81	69	154	Centroid Moment Tensor
1996-11-19 00:12:18.680	92.641	24.498	46	5.4	Mw	ISC (NEIC)	88	40	50	Centroid Moment Tensor
1996-11-19 10:44:46.060	78.133	35.345	38	6.9	Mw	ISC (NEIC)	3	88	174	Centroid Moment Tensor
1996-11-20 18:09:19	96.23	40.23	15	5	Mb	WSM2016	101	46	59	Centroid Moment Tensor
1996-11-23 01:59:45	76.84	39	33	5	Mb	WSM2016	344	18	113	Centroid Moment Tensor
1996-12-21 08:39:49.000	99.9	30.67	15	5.4	Mw	GCMT	28	71	-167	Centroid Moment Tensor
1997-01-05 08:47:25	80.29	29.43	15	5.6	Mb	WSM2016	277	18	67	Centroid Moment Tensor
1997-01-09 13:43:31	74.16	41	15	5.7	Mb	WSM2016	280	32	115	Centroid Moment Tensor
1997-01-21 01:48:28.600	77.26	39.51	33	5.9	Mw	GCMT	224	87	-15	Centroid Moment Tensor
1997-01-23 18:56:27	77.183	39.638	19	4.7	Ms	WSM2016	340	46	66	Centroid Moment Tensor

1997-01-24 20:42:55	77.017	39.467	20	4.7	Ms	WSM2016	8	26	-132	Centroid Moment Tensor
1997-01-25 07:58:42	77.117	39.533	21	4.8	Ms	WSM2016	351	29	-157	Centroid Moment Tensor
1997-01-29 08:20:17.900	77.42	38.97	33	5.2	Mw	GCMT	42	43	10	Centroid Moment Tensor
1997-01-31 05:57:39	77.083	39.517	21	4.5	Ms	WSM2016	141	53	176	Centroid Moment Tensor
1997-02-09 11:28:14	95.82	35.7	15	4.7	Mb	WSM2016	1	70	-173	Centroid Moment Tensor
1997-02-12 04:20:58	77.083	39.45	27	5	Ms	WSM2016	155	75	-175	Centroid Moment Tensor
1997-02-15 13:26:08	77.083	39.65	22	4.6	Ms	WSM2016	142	72	175	Centroid Moment Tensor
1997-02-21 22:29:11	77.133	39.6	23	4.9	Ms	WSM2016	218	39	-96	Centroid Moment Tensor
1997-02-26 23:09:09	77.1	38.583	23	4.5	Ms	WSM2016	51	40	-104	Centroid Moment Tensor
1997-02-27 21:08:13.600	68.13	29.74	15.3	7.1	Mw	GCMT	85	77	82	Centroid Moment Tensor
1997-03-01 06:04:14	76.89	39.4	22	5.2	Mb	WSM2016	180	80	-173	Centroid Moment Tensor
1997-03-01 12:25:25	77.083	39.583	20	4.5	Ms	WSM2016	230	29	-90	Centroid Moment Tensor
1997-03-01 17:35:08	77.033	39.617	9	4.5	Ms	WSM2016	283	36	-31	Centroid Moment Tensor
1997-03-02 01:52:05	77.067	39.567	24	4.6	Ms	WSM2016	246	78	4	Centroid Moment Tensor
1997-03-04 13:03:47	68.65	28.95	33	5.4	Mb	WSM2016	139	73	174	Centroid Moment Tensor
1997-03-20 08:50:40.350	68.022	30.136	18	5.7	Mw	ISC (NEIC)	70	89	71	Centroid Moment Tensor
1997-03-21 21:04:57.500	85.02	33.15	15	5.3	Mw	GCMT	35	26	-43	Centroid Moment Tensor
1997-04-01 03:12:47	76.95	39.467	24	4.8	Ms	WSM2016	153	79	176	Centroid Moment Tensor
1997-04-03 02:42:05	77.017	39.467	21	4.6	Ms	WSM2016	265	55	23	Centroid Moment Tensor
1997-04-05 23:46:00	76.88	39.54	18	5.9	Mw	Bai et al., 2017	161	78	-172	Centroid Moment Tensor

1997-04-06 04:36:00	77	39.54	15	5.9	Mw	Bai et al., 2017	253	43	-36	Centroid Moment Tensor
1997-04-06 08:06:28	76.97	39.5	18	4.6	Ms	WSM2016	148	74	171	Centroid Moment Tensor
1997-04-06 10:20:27	77	39.6	19	4.6	Ms	WSM2016	240	11	-49	Centroid Moment Tensor
1997-04-06 12:58:18	76.99	39.48	33	5.2	Mb	WSM2016	227	36	-60	Centroid Moment Tensor
1997-04-06 13:09:27	77.017	39.5	20	5.1	Ms	WSM2016	148	74	171	Centroid Moment Tensor
1997-04-06 14:57:56	77	39.533	21	4.6	Ms	WSM2016	239	74	3	Centroid Moment Tensor
1997-04-06 19:01:55	77.017	39.45	22	4.7	Ms	WSM2016	70	70	-13	Centroid Moment Tensor
1997-04-06 23:14:08	77.017	39.567	24	4.5	Ms	WSM2016	239	61	5	Centroid Moment Tensor
1997-04-07 12:43:22	77.083	39.617	22	4.6	Ms	WSM2016	146	76	170	Centroid Moment Tensor
1997-04-07 16:28:25	76.983	39.433	19	4.6	Ms	WSM2016	147	78	169	Centroid Moment Tensor
1997-04-08 05:22:53	77	39.6	22	4.5	Ms	WSM2016	10	43	-149	Centroid Moment Tensor
1997-04-08 09:29:05	76.967	39.567	26	4.5	Ms	WSM2016	38	42	-113	Centroid Moment Tensor
1997-04-08 11:34:17	77.1	39.583	23	4.6	Ms	WSM2016	178	33	-114	Centroid Moment Tensor
1997-04-09 12:02:41	77.017	39.567	28	4.9	Ms	WSM2016	355	52	-164	Centroid Moment Tensor
1997-04-10 10:58:33	77	39.617	21	4.5	Ms	WSM2016	182	39	-110	Centroid Moment Tensor
1997-04-11 05:34:00	76.95	39.56	17	6.1	Mw	Bai et al., 2017	240	37	-82	Centroid Moment Tensor
1997-04-11 06:17:42	77.05	39.567	17	4.4	Ms	WSM2016	252	54	-38	Centroid Moment Tensor
1997-04-11 11:33:45	77.03	39.617	20	4.5	Ms	WSM2016	154	79	176	Centroid Moment Tensor
1997-04-11 12:29:11	77	39.65	17	4.5	Ms	WSM2016	154	77	175	Centroid Moment Tensor
1997-04-11 16:16:26	76.983	39.517	21	4.6	Ms	WSM2016	75	65	-17	Centroid Moment Tensor

1997-04-11 17:05:15	77.017	39.6	25	4.5	Ms	WSM2016	73	31	71	Centroid Moment Tensor
1997-04-11 17:12:47	77.033	39.583	20	4.6	Ms	WSM2016	75	77	-9	Centroid Moment Tensor
1997-04-11 19:25:33	77.05	39.567	20	4.6	Ms	WSM2016	148	73	173	Centroid Moment Tensor
1997-04-11 20:32:17	77.033	39.567	25	4.8	Ms	WSM2016	148	76	173	Centroid Moment Tensor
1997-04-12 21:09:09	77.2	39.64	16	5.2	Mb	WSM2016	244	48	-64	Centroid Moment Tensor
1997-04-15 18:19:15.600	76.99	39.69	23	5.8	Mw	GCMT	73	74	-25	Centroid Moment Tensor
1997-04-16 02:51:26	77	39.683	23	4.6	Ms	WSM2016	265	56	19	Centroid Moment Tensor
1997-04-16 09:23:24	77.033	39.617	21	4.9	Ms	WSM2016	7	50	-142	Centroid Moment Tensor
1997-04-17 11:56:24	77.033	39.6	24	4.5	Ms	WSM2016	254	3	90	Centroid Moment Tensor
1997-05-08 02:53:00	92.28	24.89	36	5.9	Mw	Bai et al., 2017	347	86	-167	Centroid Moment Tensor
1997-05-17 11:58:22	77.017	39.65	26	5.4	Ms	WSM2016	151	74	179	Centroid Moment Tensor
1997-05-21 22:51:31.800	80.22	23.06	38	5.8	Mw	GCMT	61	70	73	Centroid Moment Tensor
1997-05-30 17:54:54.400	78.06	37.18	33	5	Mw	GCMT	117	23	91	Centroid Moment Tensor
1997-06-06 08:23:04	76.917	39.467	22	4.5	Ms	WSM2016	202	37	-23	Centroid Moment Tensor
1997-06-09 06:16:13	77.017	39.617	18	4.5	Ms	WSM2016	58	64	-29	Centroid Moment Tensor
1997-06-17 11:18:45.400	68.07	29.72	33	5.2	Mw	GCMT	82	64	95	Centroid Moment Tensor
1997-06-24 09:24:51.200	77.18	39.8	33.8	5.1	Mw	GCMT	251	78	-18	Centroid Moment Tensor
1997-06-24 18:06:40	76.9	39.6	21	4.5	Ms	WSM2016	226	39	-96	Centroid Moment Tensor
1997-07-31 15:59:39.700	93.43	23.8	41.8	5.2	Mw	GCMT	201	80	103	Centroid Moment Tensor
1997-08-09 04:48:07	97.46	30.16	33	5.2	Mw	Luo et al., 2016	72	27	-91	Centroid Moment Tensor

1997-08-24 13:15:27.400	67.99	29.71	23	5.6	Mw	GCMT	96	63	98	Centroid Moment Tensor
1997-09-07 10:15:25	67.92	29.5	18	5.5	Mb	WSM2016	282	29	90	Centroid Moment Tensor
1997-10-15 20:30:58.500	81.02	35.75	33	5.2	Mw	GCMT	69	49	-4	Centroid Moment Tensor
1997-10-17 17:35:17.600	77.07	39.59	33	5.3	Mw	GCMT	70	88	9	Centroid Moment Tensor
1997-10-23 02:44:27	77.1	39.483	20	4.5	Ms	WSM2016	288	22	25	Centroid Moment Tensor
1997-10-23 12:28:38.200	100.55	27.14	15	5.1	Mw	GCMT	153	20	-110	Centroid Moment Tensor
1997-11-03 02:29:52	85.39	28.6	33	5.4	Mb	WSM2016	20	31	-71	Centroid Moment Tensor
1997-11-04 16:83:85	76.983	39.433	27	4.8	Ms	WSM2016	239	43	2	Centroid Moment Tensor
1997-11-08 10:02:00	87.37	35.12	10	7.5	Mw	Bai et al., 2017	348	88	-168	Centroid Moment Tensor
1997-11-09 00:24:54	88.56	33.58	33	5.1	Mb	WSM2016	45	31	-64	Centroid Moment Tensor
1997-11-21 11:23:06.310	92.702	22.212	50	6.1	Mw	ISC (NEIC)	161	33	169	Centroid Moment Tensor
1997-12-13 03:41:35	68.26	29.1	36.7	4.9	Mb	WSM2016	246	34	47	Centroid Moment Tensor
1997-12-30 13:43:23	96.52	25.01	54	5.7	Mw	Luo et al., 2016	32	85	174	Centroid Moment Tensor
1998-02-04 14:33:21	69.92	37.13	33.8	5.6	Mb	WSM2016	211	77	-2	Centroid Moment Tensor
1998-03-19 13:51:38.700	76.88	39.94	32.7	5.6	Mw	GCMT	75	68	95	Centroid Moment Tensor
1998-05-15 08:41:26.200	93.82	10.57	45.4	5.2	Mw	GCMT	8	78	-174	Centroid Moment Tensor
1998-05-28 21:11:44.130	78.843	37.388	10	5.6	Mw	ISC (NEIC)	122	87	-75	Centroid Moment Tensor
1998-05-29 22:49:34.140	75.655	41.173	17	5.2	Mw	ISC (NEIC)	87	43	100	Centroid Moment Tensor
1998-05-30 06:22:29.000	70.139	37.135	33	6.6	Mw	MOS	199	64	-3	Centroid Moment Tensor
1998-06-06 13:37:11.400	69.91	37.21	33	5.1	Mw	GCMT	153	77	179	Centroid Moment Tensor

1998-06-25 06:39:19.900	80.44	41.16	15.1	5.1	Mw	GCMT	39	69	72	Centroid Moment Tensor
1998-06-26 01:23:55.800	69.68	30	33	5.1	Mw	GCMT	8	68	24	Centroid Moment Tensor
1998-06-29 20:35:55.200	70.07	37.03	33	5.1	Mw	GCMT	7	81	-17	Centroid Moment Tensor
1998-07-12 20:52:16	68.24	29.93	15	4.8	Mb	WSM2016	255	15	47	Centroid Moment Tensor
1998-07-20 01:06:07.000	88.47	29.83	15	5.7	Mw	GCMT	16	32	-83	Centroid Moment Tensor
1998-07-21 14:40:45	88.5	29.93	15.7	5	Mb	WSM2016	34	43	-90	Centroid Moment Tensor
1998-07-28 04:51:47.000	81.58	41.93	46.9	5.1	Mw	GCMT	83	48	92	Centroid Moment Tensor
1998-08-02 04:40:00	77.03	39.57	16	5.6	Mw	Bai et al., 2017	231	30	-91	Centroid Moment Tensor
1998-08-09 00:34:58	94.42	7.43	28	5.2	Mb	WSM2016	240	80	9	Centroid Moment Tensor
1998-08-10 09:52:15	94.39	7.58	23.7	5.9	Mb	WSM2016	237	84	0	Centroid Moment Tensor
1998-08-25 07:41:40.190	88.109	30.079	11	5.7	Mw	ISC (NEIC)	24	64	-53	Centroid Moment Tensor
1998-08-27 09:03:40.800	77.22	39.51	32	6.3	Mw	GCMT	240	78	0	Centroid Moment Tensor
1998-08-28 22:02:02.400	88.41	30.08	15	5	Mw	GCMT	19	45	-90	Centroid Moment Tensor
1998-09-03 06:43:04	77.3	39.47	31.7	5.1	Mb	WSM2016	234	32	-90	Centroid Moment Tensor
1998-09-26 18:27:05	93.6	27.87	33	5.4	Mb	WSM2016	233	26	116	Centroid Moment Tensor
1998-09-30 02:29:59.100	88.25	29.64	33	5.1	Mw	GCMT	139	32	-112	Centroid Moment Tensor
1998-10-02 12:49:38	101.52	27.45	15	5.3	Mw	Luo et al., 2016	151	74	-90	Centroid Moment Tensor
1998-10-05 10:24:49	88.6	29.89	33	4.8	Mb	WSM2016	26	28	-78	Centroid Moment Tensor
1998-10-15 19:05:26.600	94.34	7.73	52.1	5.3	Mw	GCMT	66	90	-12	Centroid Moment Tensor
1998-10-25 20:06:04.000	68.21	36.24	41.4	5.1	Mw	GCMT	79	62	137	Centroid Moment Tensor

1998-11-06 22:52:09	92.23	10.93	22	5.2	Mb	WSM2016	322	11	90	Centroid Moment Tensor
1998-11-19 11:38:17.700	101.47	27.25	15	5.5	Mw	GCMT	31	79	-9	Centroid Moment Tensor
1999-01-20 22:09:21.100	68.22	37.18	34.1	5	Mw	GCMT	194	20	104	Centroid Moment Tensor
1999-01-30 03:51:05.420	88.463	41.674	23.3	5.4	Mw	ISC (NEIC)	110	40	90	Centroid Moment Tensor
1999-02-11 14:08:00	69.24	34.31	18	6	Mw	Bai et al., 2017	194	66	-30	Centroid Moment Tensor
1999-02-22 11:37:53.300	93.99	23.15	51	5	Mw	GCMT	47	35	-103	Centroid Moment Tensor
1999-03-15 10:43:01.000	82.38	41.98	17	5.4	Mw	GCMT	52	77	76	Centroid Moment Tensor
1999-03-28 19:05:11.030	79.403	30.512	15	6.6	Mw	ISC (NEIC)	111	82	95	Centroid Moment Tensor
1999-04-05 00:00:00	93.716	24.935	49	5.5	Mb	Kumar et al., 2015	344	69	169	Centroid Moment Tensor
1999-05-29 20:10:50.600	93.77	32.81	33	5.3	Mw	GCMT	261	80	-3	Centroid Moment Tensor
1999-06-26 21:54:10.940	69.444	30.098	33	5.6	Mw	ISC (NEIC)	15	38	43	Centroid Moment Tensor
1999-06-29 00:57:58.600	69.76	30.02	33	4.9	Mw	GCMT	68	45	82	Centroid Moment Tensor
1999-06-29 08:04:08.200	73.1	38.47	55.9	5.3	Mw	GCMT	209	86	-22	Centroid Moment Tensor
1999-07-12 03:42:00	69.46	29.99	19	5.6	Mw	Bai et al., 2017	269	60	152	Centroid Moment Tensor
1999-08-03 12:02:30	69.23	36.37	24.3	5.1	Mb	WSM2016	193	48	16	Centroid Moment Tensor
1999-08-04 00:09:00	86.88	37.39	33	5	Mb	WSM2016	330	38	145	Centroid Moment Tensor
1999-08-15 16:18:36.600	96.23	18.46	38.9	5.2	Mw	GCMT	265	83	-2	Centroid Moment Tensor
1999-08-29 03:44:52	93.52	8.88	24.8	4.9	Mb	WSM2016	187	58	167	Centroid Moment Tensor
1999-09-23 20:45:17	84.47	42.35	30	5.1	Ms	WSM2016	300	5	90	First Motion
1999-10-05 00:00:00	91.982	26.293	40	5.5	Mb	Kumar et al., 2015	129	57	140	Centroid Moment Tensor

1999-10-31 17:09:14.200	66.44	38.94	55	5	Mw	GCMT	35	58	156	Centroid Moment Tensor
1999-12-06 07:33:11	76.25	42.75	32.6	5.3	Mb	WSM2016	238	38	90	Centroid Moment Tensor
1999-12-18 00:50:33.500	94.56	7.05	25	5.2	Mw	GCMT	54	67	-5	Centroid Moment Tensor
1999-12-25 13:28:11.600	65.95	38.73	63.7	4.9	Mw	GCMT	52	66	107	Centroid Moment Tensor
2000-01-14 22:09:06.300	101.28	25.34	33	5.5	Mw	GCMT	25	77	-2	Centroid Moment Tensor
2000-01-14 23:37:10	101.4	25.39	33	5.9	Mw	Luo et al., 2016	27	78	-6	Centroid Moment Tensor
2000-01-19 20:59:26.200	101.33	19.92	15	5.4	Mw	GCMT	64	80	4	Centroid Moment Tensor
2000-01-26 21:38:02.100	95.72	30.79	33	5.1	Mw	GCMT	1	80	160	Centroid Moment Tensor
2000-01-31 07:25:59.740	88.604	38.114	33	5.4	Mw	ISC (NEIC)	63	86	5	Centroid Moment Tensor
2000-02-12 00:04:22	90.88	34.05	33	4.6	Mb	WSM2016	257	79	6	Centroid Moment Tensor
2000-03-12 18:03:56	73.93	17.45	15	4.9	Mb	WSM2016	352	23	-90	Centroid Moment Tensor
2000-04-15 09:32:38.800	95.65	32.85	33	5.2	Mw	GCMT	90	68	-4	Centroid Moment Tensor
2000-04-20 08:41:29.590	66.445	38.616	10	5.3	Mw	ISC (NEIC)	75	44	82	Centroid Moment Tensor
2000-06-07 21:46:00	97.19	26.8	13	6.3	Mw	Bai et al., 2017	290	38	41	Centroid Moment Tensor
2000-06-08 12:21:12	97.41	26.43	19	5.1	Mw	Luo et al., 2016	126	33	67	Centroid Moment Tensor
2000-06-19 22:41:49.600	77.43	35.24	40.4	5.4	Mw	GCMT	89	89	-13	Centroid Moment Tensor
2000-07-10 04:25:15	92.55	32.74	15	5.6	Mb	WSM2016	4	38	-115	Centroid Moment Tensor
2000-08-08 01:15:09.400	76.83	41.9	33	5	Mw	GCMT	128	43	95	Centroid Moment Tensor
2000-09-05 00:32:42	73.93	17.26	15	5.4	Mb	WSM2016	355	21	-90	Centroid Moment Tensor
2000-09-12 00:27:00	99.37	35.37	6	6.1	Mw	Bai et al., 2017	343	80	-170	Centroid Moment Tensor

2000-09-13 15:11:23.000	95.12	33.94	15	5	Mw	GCMT	84	77	1	Centroid Moment Tensor
2000-09-20 19:21:17.600	99.61	35.32	15	5	Mw	GCMT	262	87	-31	Centroid Moment Tensor
2000-10-06 12:05:41	97.13	24.18	73	5.4	Mw	Luo et al., 2016	144	77	166	Centroid Moment Tensor
2000-10-12 07:54:39	92.89	10.38	36.9	5.1	Mb	WSM2016	175	26	116	Centroid Moment Tensor
2000-10-30 22:39:09.400	69.22	37.47	28.7	5.1	Mw	GCMT	85	28	122	Centroid Moment Tensor
2000-11-05 12:47:04	92.97	9.97	32.6	5.2	Mb	WSM2016	195	23	128	Centroid Moment Tensor
2000-11-13 08:56:56.300	93.04	21.94	74	5.4	Mw	GCMT	216	83	-5	Centroid Moment Tensor
2001-01-02 16:22:37	68.3	35.95	33	5.1	Mb	WSM2016	187	20	34	Centroid Moment Tensor
2001-01-14 22:09:06	101.28	25.34	33	5.5	Mw	Luo et al., 2016	25	77	-3	Centroid Moment Tensor
2001-01-18 08:41:41.600	66.14	38.61	26.6	5.3	Mw	GCMT	61	40	114	Centroid Moment Tensor
2001-01-26 03:16:40.500	70.232	23.419	16	7.6	Mw	ISC (NEIC)	81	52	63	Centroid Moment Tensor
2001-01-28 01:02:10.700	70.517	23.507	10	5.8	Mw	ISC (NEIC)	81	52	63	Centroid Moment Tensor
2001-01-28 11:10:44.700	70.48	23.74	15	5.3	Mw	GCMT	32	81	67	Centroid Moment Tensor
2001-02-14 15:27:28	101.08	29.4	8	5	Ms	WSM2016	19	70	160	First Motion
2001-02-15 22:39:07.00	92.59	26.68	44	4	Mw	Kayal et al., 2012	60	80	35	Centroid Moment Tensor
2001-02-19 08:24:23.400	70.07	23.72	15	5.4	Mw	GCMT	90	49	101	Centroid Moment Tensor
2001-02-23 00:09:23.690	101.129	29.513	33	5.6	Mw	ISC (NEIC)	117	42	-39	Centroid Moment Tensor
2001-02-27 01:46:08.00	90.73	26.14	17	4.4	Mw	Kayal et al., 2012	170	55	30	Centroid Moment Tensor
2001-03-03 22:56:05.100	93.43	23.99	64.1	5.2	Mw	GCMT	19	66	-57	Centroid Moment Tensor
2001-03-05 05:50:00	86.9	34.37	13	5.6	Mw	Bai et al., 2017	170	64	-153	Centroid Moment Tensor

2001-03-09 01:07:09	69.32	32.15	33	5	Mb	WSM2016	190	68	13	Centroid Moment Tensor
2001-03-10 00:20:16.00	91.87	27.67	11	4.1	Mw	Kayal et al., 2012	235	30	-95	Centroid Moment Tensor
2001-03-15 00:39:11.000	94.08	8.76	28.3	5.3	Mw	GCMT	250	81	-2	Centroid Moment Tensor
2001-03-15 01:22:44.300	94.11	8.79	29.9	5.9	Mw	GCMT	258	88	-9	Centroid Moment Tensor
2001-04-12 10:47:08	98.81	24.77	15	5.6	Mw	Luo et al., 2016	57	63	-29	Centroid Moment Tensor
2001-04-18 20:47:48.00	91.65	24.19	56.9	4	Mw	Kayal et al., 2012	330	40	175	Centroid Moment Tensor
2001-05-16 11:00:22.100	70.19	30.13	17.5	5.1	Mw	GCMT	2	38	9	Centroid Moment Tensor
2001-05-23 21:10:45.600	101.11	27.53	33	5.4	Mw	GCMT	8	87	-2	Centroid Moment Tensor
2001-06-01 14:00:43	69.39	35.17	62.1	5	Mb	Ali & Shanker, 2017	209	61	74	Catalog collection
2001-06-30 11:48:34	69.77	30.98	35.2	5.2	Mb	Ali & Shanker, 2017	158	61	-4	Catalog collection
2001-07-25 16:02:57.800	95.85	33.27	33	5.5	Mw	GCMT	251	77	-38	Centroid Moment Tensor
2001-08-09 23:51:34	101.25	24.89	33	5.1	Mw	Luo et al., 2016	143	89	140	Centroid Moment Tensor
2001-09-02 16:58:01	72.03	39.4	15	4.4	Mb	WSM2016	118	25	-44	Centroid Moment Tensor
2001-09-25 14:56:44.250	80.214	11.956	10	5.1	Mw	ISC (NEIC)	92	41	113	Centroid Moment Tensor
2001-09-28 04:37:58.700	75.46	33	40.5	4.9	Mw	GCMT	125	59	81	Centroid Moment Tensor
2001-10-13 20:54:49	91.8	18.69	15	5	Mb	WSM2016	94	33	-76	Centroid Moment Tensor
2001-10-27 05:35:46	101.01	26.36	15	5.5	Mw	Luo et al., 2016	35	69	1	Centroid Moment Tensor
2001-11-07 00:00:00	85.6	29.99	22	4	Mw	De La Torre et al., 2007	154	37	-112	Centroid Moment Tensor
2001-11-14 09:26:10.010	90.541	35.946	10	7.5	Mw	ISC (NEIC)	99	90	-9	Centroid Moment Tensor
2001-11-18 21:59:52.530	93.691	35.726	10	5.5	Mw	ISC (NEIC)	87	56	97	Centroid Moment Tensor

2001-11-19 17:45:23.450	93.672	35.763	10	5.4	Mw	ISC (NEIC)	111	50	113	Centroid Moment Tensor
2001-11-27 07:31:57.100	81.75	29.61	15	5.5	Mw	GCMT	104	87	92	Centroid Moment Tensor
2001-11-27 08:53:54	81.75	29.55	33	5.4	Mb	Ali & Shanker, 2017	280	28	74	Catalog collection
2001-11-30 10:43:21.800	91.11	36.07	15	5.2	Mw	GCMT	71	74	-60	Centroid Moment Tensor
2001-12-01 12:25:19	93.93	35.58	15	5.1	Mb	WSM2016	254	35	-142	Centroid Moment Tensor
2001-12-02 00:00:00	88.31	27.34	13	4.8	Mw	De La Torre et al., 2007	225	62	9	Centroid Moment Tensor
2001-12-08 04:12:47	93.13	36.07	15	5.1	Mb	WSM2016	90	31	-40	Centroid Moment Tensor
2002-01-27 22:33:43.400	75.91	33.32	28.8	5.2	Mw	GCMT	225	20	-11	Centroid Moment Tensor
2002-03-07 00:00:00	84.83	29.56	66	4	Mw	De La Torre et al., 2007	232	78	6	Centroid Moment Tensor
2002-03-22 02:02:18.000	70.4	37.48	75.7	4.9	Mw	GCMT	4	83	7	Centroid Moment Tensor
2002-03-23 04:56:26.090	88	29.98	5	4.3	Mw	HIMNT	194	34	-59	Centroid Moment Tensor
2002-03-25 14:56:33.820	69.315	36.062	8	6	Mw	ISC (NEIC)	197	46	102	Centroid Moment Tensor
2002-03-25 21:45:10.000	69.59	36.22	15	5.1	Mw	GCMT	36	16	171	Centroid Moment Tensor
2002-03-27 08:52:52.270	69.338	36.023	10	5.6	Mw	ISC (NEIC)	28	26	136	Centroid Moment Tensor
2002-04-12 04:00:00	69.42	35.96	5	5.7	Mw	Bai et al., 2017	204	46	96	Centroid Moment Tensor
2002-04-12 16:26:01	68.8	35.89	15	4.9	Mb	WSM2016	157	50	31	Centroid Moment Tensor
2002-06-04 14:36:05	81.25	30.13	15	5.4	Mb	WSM2016	158	50	-131	Centroid Moment Tensor
2002-06-20 05:40:46.040	89	26.25	28	4.6	Mw	De La Torre et al., 2007	237	72	-9	Centroid Moment Tensor
2002-06-29 06:54:48.000	94.28	34.06	33	5.6	Mw	GCMT	0	87	177	Centroid Moment Tensor
2002-07-13 20:06:27.540	69.979	30.797	33	5.6	Mw	ISC (NEIC)	167	55	-6	Centroid Moment Tensor

2002-08-08 11:42:10	99.95	30.69	55	5.3	Mw	Luo et al., 2016	92	41	-87	Centroid Moment Tensor
2002-08-22 04:50:09.980	88.23	30.07	17	4.3	Mw	De La Torre et al., 2007	110	53	144	Centroid Moment Tensor
2002-08-31 12:40:34.870	88.12	29.92	6	4.7	Mw	HIMNT	188	19	-56	Centroid Moment Tensor
2002-09-13 22:28:29.460	93.068	13.036	21	6.5	Mw	ISC (NEIC)	191	40	137	Centroid Moment Tensor
2002-09-14 19:58:36.950	93.157	13.055	33	5.8	Mw	ISC (NEIC)	173	39	109	Centroid Moment Tensor
2002-09-18 12:01:36.310	93.168	13.112	33	5.5	Mw	ISC (NEIC)	221	61	121	Centroid Moment Tensor
2002-09-27 17:14:44.100	93.49	32.95	33	5.1	Mw	GCMT	80	81	-9	Centroid Moment Tensor
2002-10-12 18:30:50.43	92.95	25.37	29.5	4	Mw	Kayal et al., 2012	260	10	20	Centroid Moment Tensor
2002-10-16 01:31:20.800	93.16	21.16	45.9	5.1	Mw	GCMT	177	57	-60	Centroid Moment Tensor
2002-10-19 07:24:40.800	92.87	35.72	33	5.1	Mw	GCMT	92	76	-14	Centroid Moment Tensor
2002-10-26 20:28:51.000	96.14	35.18	33	5.3	Mw	GCMT	11	78	176	Centroid Moment Tensor
2002-11-01 22:09:29	74.65	35.52	33	5.4	Mb	Ali & Shanker, 2017	216	42	-90	Catalog collection
2002-11-03 07:33:38	74.6	35.42	33	5.3	Mb	Ali & Shanker, 2017	201	62	-102	Catalog collection
2002-11-20 21:32:36.200	74.66	35.52	15	6.3	Mw	GCMT	55	64	-75	Centroid Moment Tensor
2002-12-04 00:00:00	94.529	19.387	52	5.7	Mb	Kumar et al., 2015	100	25	-152	Centroid Moment Tensor
2002-12-13 01:45:33.900	94.54	8.54	15	5	Mw	GCMT	58	84	20	Centroid Moment Tensor
2002-12-14 13:27:29.100	97.443	39.736	22	5.6	Mw	ISC (NEIC)	101	50	99	Centroid Moment Tensor
2002-12-25 12:57:03.200	75.254	39.57	10	5.7	Mw	ISC (NEIC)	71	78	35	Centroid Moment Tensor
2003-01-13 16:35:01.900	95.65	12.93	15	5.2	Mw	GCMT	11	52	-180	Centroid Moment Tensor
2003-01-17 14:31:12.700	93.89	8	17.1	5.2	Mw	GCMT	3	84	-160	Centroid Moment Tensor

2003-01-20 12:54:38.00	94.95	22.37	10	4.1	Mw	Kayal et al., 2012	45	85	65	Centroid Moment Tensor
2003-01-26 10:49:30.400	95.36	12.98	26	5.1	Mw	GCMT	245	32	-6	Centroid Moment Tensor
2003-01-30 17:21:09.400	94.32	7.8	37.1	5.1	Mw	GCMT	237	85	-5	Centroid Moment Tensor
2003-02-15 21:37:33.84	90.39	25.96	36.6	4.3	Mw	Kayal et al., 2012	240	60	150	Centroid Moment Tensor
2003-02-24 02:03:41.450	77.23	39.61	11	6.3	Mw	ISC (NEIC)	90	60	90	Centroid Moment Tensor
2003-02-24 21:18:48.800	77.04	39.35	15	5.2	Mw	GCMT	69	64	69	Centroid Moment Tensor
2003-02-25 03:52:48.200	77.62	39.52	15	5.3	Mw	GCMT	110	77	166	Centroid Moment Tensor
2003-03-12 04:47:00	77.43	39.36	12	5.4	Mw	Bai et al., 2017	245	33	79	Centroid Moment Tensor
2003-03-15 22:59:32.500	77.47	39.74	15	5	Mw	GCMT	61	89	33	Centroid Moment Tensor
2003-03-25 00:00:00	89.6	27.18	28	5.2	Mw	De La Torre et al., 2007	141	83	177	Centroid Moment Tensor
2003-03-25 04:30:04.00	94.62	23.68	22.7	4	Mw	Kayal et al., 2012	5	25	125	Centroid Moment Tensor
2003-03-26 04:22:30.070	92.564	12.518	33	5.9	Mw	ISC (NEIC)	251	55	-10	Centroid Moment Tensor
2003-03-30 23:15:51.200	77.46	39.02	41.6	5.2	Mw	GCMT	93	56	90	Centroid Moment Tensor
2003-04-17 00:48:38.580	96.476	37.529	14	6.2	Mw	ISC (NEIC)	115	65	90	Centroid Moment Tensor
2003-05-05 06:34:47.000	72.24	40.97	46	5.1	Mw	GCMT	71	55	78	Centroid Moment Tensor
2003-05-20 18:34:43.600	93.23	32.53	33	5.1	Mw	GCMT	40	31	-38	Centroid Moment Tensor
2003-05-22 18:11:57.400	72.78	42.81	27.6	5.5	Mw	GCMT	62	46	34	Centroid Moment Tensor
2003-05-24 11:28:02.300	92.29	32.16	33	5	Mw	GCMT	158	73	-93	Centroid Moment Tensor
2003-05-24 19:32:43.300	92.36	32.59	33	5	Mw	GCMT	186	62	-83	Centroid Moment Tensor
2003-05-29 14:18:56.000	80.38	35.87	33	5	Mw	GCMT	88	23	45	Centroid Moment Tensor

2003-05-30 10:27:53.30	92.76	27.01	57.5	4.2	Mw	Kayal et al., 2012	240	50	160	Centroid Moment Tensor
2003-06-04 16:28:37	77.69	39.66	15	5.1	Mb	WSM2016	90	36	90	Centroid Moment Tensor
2003-07-07 06:55:43.020	89.475	34.606	17.7	5.5	Mw	ISC (NEIC)	23	47	-89	Centroid Moment Tensor
2003-07-13 23:38:46.400	95.25	12.49	15	5	Mw	GCMT	247	72	-16	Centroid Moment Tensor
2003-07-17 20:28:25.28	90.68	25.54	20.8	4.1	Mw	Kayal et al., 2012	90	60	40	Centroid Moment Tensor
2003-07-21 15:16:38	101.32	25.98	15	5.9	Mw	Luo et al., 2016	200	80	-6	Centroid Moment Tensor
2003-07-26 23:18:17.960	92.306	22.854	10	5.6	Mw	ISC (NEIC)	145	52	106	Centroid Moment Tensor
2003-07-27 12:07:33.300	92.34	22.83	15	5.4	Mw	GCMT	2	16	88	Centroid Moment Tensor
2003-08-05 11:08:01	70.43	23.69	15	5.1	Mb	WSM2016	221	24	67	Centroid Moment Tensor
2003-08-18 09:03:03.520	95.605	29.573	33	5.5	Mw	ISC (NEIC)	67	77	-11	Centroid Moment Tensor
2003-09-01 23:16:00	75.32	38.6	4	5.7	Mw	Bai et al., 2017	107	47	-153	Centroid Moment Tensor
2003-09-16 08:00:46.300	100.97	29.03	33	4.9	Mw	GCMT	61	23	-119	Centroid Moment Tensor
2003-09-21 18:16:13.410	95.672	19.917	10	6.6	Mw	ISC (NEIC)	97	71	-10	Centroid Moment Tensor
2003-09-26 23:35:30	77.05	40.2	15	5.2	Mb	WSM2016	289	13	55	Centroid Moment Tensor
2003-10-16 12:28:09.070	101.254	25.954	33	5.5	Mw	ISC (NEIC)	97	60	178	Centroid Moment Tensor
2003-10-25 12:41:35.250	100.951	38.4	10	5.8	Mw	ISC (NEIC)	145	45	110	Centroid Moment Tensor
2003-10-25 12:47:58.830	100.975	38.383	10	5.7	Mw	ISC (NEIC)	91	47	56	Centroid Moment Tensor
2003-10-30 15:22:21.800	95.73	19.82	15	5.2	Mw	GCMT	121	42	63	Centroid Moment Tensor
2003-11-10 14:45:51	68.2	41.06	15	5	Mb	WSM2016	121	27	90	Centroid Moment Tensor
2003-11-20 14:05:04.000	93.07	13.21	39.2	5.3	Mw	GCMT	216	59	115	Centroid Moment Tensor

2003-12-01 01:38:32	80.5	42.93	15	6	Mb	WSM2016	281	14	122	Centroid Moment Tensor
2003-12-19 00:11:58.230	95.698	19.852	10	5.2	Mw	ISC (NEIC)	150	35	90	Centroid Moment Tensor
2004-01-03 15:44:57.80	94.19	23.4	28.2	4.2	Mw	Kayal et al., 2012	70	10	-150	Centroid Moment Tensor
2004-01-08 23:35:47.14	94.18	25.44	45	4.4	Mw	Kayal et al., 2012	100	90	-80	Centroid Moment Tensor
2004-01-13 23:16:56.85	92.12	27.28	15.3	4.2	Mw	Kayal et al., 2012	10	60	-140	Centroid Moment Tensor
2004-01-16 09:06:22.900	75.39	42.65	30.2	4.8	Mw	GCMT	88	48	90	Centroid Moment Tensor
2004-02-09 22:13:14.81	91.6	24.38	40.9	4.1	Mw	Kayal et al., 2012	320	40	-60	Centroid Moment Tensor
2004-02-10 05:39:43	83.42	32.6	28.8	4.9	Mb	WSM2016	350	37	-118	Centroid Moment Tensor
2004-02-14 10:30:22.180	73.216	34.774	11	5.5	Mw	ISC (NEIC)	127	42	82	Centroid Moment Tensor
2004-02-14 11:56:57.530	73.206	34.798	11	5.4	Mw	ISC (NEIC)	119	46	82	Centroid Moment Tensor
2004-02-15 23:23:10.900	78.58	36.6	21.6	4.8	Mw	GCMT	92	59	-100	Centroid Moment Tensor
2004-02-23 07:18:39.800	93.83	7.13	62.1	4.8	Mw	GCMT	149	74	136	Centroid Moment Tensor
2004-02-24 20:21:52.200	96.61	37.66	23	5	Mw	GCMT	51	89	-3	Centroid Moment Tensor
2004-03-02 12:30:23	96.52	37.61	21.1	5.1	Mb	WSM2016	100	41	90	Centroid Moment Tensor
2004-03-06 10:21:32	93.19	13.05	24.7	5.2	Mb	WSM2016	214	51	157	Centroid Moment Tensor
2004-03-06 11:54:43	92.13	33.26	12	5	Mb	WSM2016	195	46	-131	Centroid Moment Tensor
2004-03-07 13:29:46	91.33	31.6	20.7	5.3	Mb	WSM2016	326	80	-173	Centroid Moment Tensor
2004-03-16 21:23:24.300	96.56	37.6	13	5.1	Mw	GCMT	127	42	116	Centroid Moment Tensor
2004-03-27 00:43:10.600	68.99	40.15	27.3	5	Mw	GCMT	66	26	58	Centroid Moment Tensor
2004-03-27 18:47:29.200	89.179	33.954	8	6	Mw	ISC (NEIC)	25	53	-94	Centroid Moment Tensor

2004-03-27 20:05:57.500	89.19	33.87	18.4	5	Mw	GCMT	44	36	-49	Centroid Moment Tensor
2004-03-28 22:05:46.500	89.37	34.07	17.7	5.2	Mw	GCMT	51	62	-30	Centroid Moment Tensor
2004-03-28 22:27:31.400	89.28	33.91	16.9	5.1	Mw	GCMT	46	50	-39	Centroid Moment Tensor
2004-04-06 10:30:32	89.25	33.83	12	5.3	Mb	WSM2016	174	49	-124	Centroid Moment Tensor
2004-04-10 15:57:02	93.09	13.19	33.4	5	Mb	WSM2016	358	30	70	Centroid Moment Tensor
2004-04-15 21:20:42.000	94.1	8.8	18.6	5.3	Mw	GCMT	157	80	173	Centroid Moment Tensor
2004-04-15 23:02:15.000	94.15	8.85	17.6	5	Mw	GCMT	54	75	-53	Centroid Moment Tensor
2004-04-16 02:06:15.300	94.14	8.88	21.1	5.6	Mw	GCMT	64	84	-12	Centroid Moment Tensor
2004-04-16 11:29:48.700	94.05	8.9	22.5	4.8	Mw	GCMT	149	72	176	Centroid Moment Tensor
2004-04-21 13:54:05.35	94.79	25.23	13.6	4.4	Mw	Kayal et al., 2012	300	70	100	Centroid Moment Tensor
2004-04-22 10:02:21.600	89.33	33.88	17.7	5.2	Mw	GCMT	36	49	-50	Centroid Moment Tensor
2004-04-23 23:38:26.76	94.67	25.27	21.8	4.3	Mw	Kayal et al., 2012	220	20	120	Centroid Moment Tensor
2004-04-30 14:11:22.700	71.1	37.5	73.2	4.8	Mw	GCMT	141	69	155	Centroid Moment Tensor
2004-05-03 17:41:29	93.19	13.18	27.8	5.3	Mb	WSM2016	1	34	68	Centroid Moment Tensor
2004-05-04 05:04:58	96.65	37.6	18.6	5.4	Mb	WSM2016	145	84	175	Centroid Moment Tensor
2004-05-04 11:36:03	96.62	37.61	21.6	5.3	Mb	WSM2016	140	86	-178	Centroid Moment Tensor
2004-05-10 23:27:25	96.58	37.55	12	5.4	Mb	WSM2016	273	33	70	Centroid Moment Tensor
2004-05-13 04:00:49.100	68.34	29.31	12.4	5	Mw	GCMT	93	78	89	Centroid Moment Tensor
2004-05-18 02:58:18.700	93.81	7.4	73.3	4.9	Mw	GCMT	130	76	165	Centroid Moment Tensor
2004-05-23 02:21:06.700	89.36	34.05	12	4.8	Mw	GCMT	220	53	-54	Centroid Moment Tensor

2004-05-23 07:38:12.900	89.42	34.04	12	5.3	Mw	GCMT	53	72	-26	Centroid Moment Tensor
2004-05-23 14:46:27.300	89.29	33.87	12.1	4.8	Mw	GCMT	54	56	-27	Centroid Moment Tensor
2004-05-24 01:39:53.10	94.96	24.72	43	4.5	Mw	Kayal et al., 2012	170	10	170	Centroid Moment Tensor
2004-05-24 22:01:02.500	97.21	27.06	26.5	4.9	Mw	GCMT	136	48	74	Centroid Moment Tensor
2004-06-03 13:01:17.80	94.74	25.39	24.8	4.5	Mw	Kayal et al., 2012	190	70	170	Centroid Moment Tensor
2004-06-26 23:45:52.500	95	10.93	22	5	Mw	GCMT	4	55	-156	Centroid Moment Tensor
2004-06-29 08:11:31.800	92.54	35.75	17.1	5.3	Mw	GCMT	93	63	-15	Centroid Moment Tensor
2004-07-11 23:08:00	83.67	30.69	4	6.3	Mw	Bai et al., 2017	359	45	-96	Centroid Moment Tensor
2004-07-15 08:18:31.500	70.48	35.89	50.7	5.4	Mw	GCMT	25	74	143	Centroid Moment Tensor
2004-07-18 08:31:48.700	69.63	33.43	17.2	5.2	Mw	GCMT	217	71	-16	Centroid Moment Tensor
2004-07-22 03:56:34	65.32	28.65	10	5.1	Mb	Ali & Shanker, 2017	164	84	-150	Catalog collection
2004-07-25 19:49:01.300	95.15	12.46	12	5.5	Mw	GCMT	39	22	-163	Centroid Moment Tensor
2004-07-28 22:22:16.200	83.63	30.35	13.7	5	Mw	GCMT	9	47	-64	Centroid Moment Tensor
2004-07-29 01:44:07.400	95.06	12.36	12	5.8	Mw	GCMT	22	43	-142	Centroid Moment Tensor
2004-07-29 02:01:52.700	95.07	12.3	20.4	5	Mw	GCMT	52	49	-80	Centroid Moment Tensor
2004-07-29 02:18:42.300	95.25	12.49	12	4.8	Mw	GCMT	27	44	-139	Centroid Moment Tensor
2004-07-29 13:23:03.280	95.003	12.445	24.1	5.6	Mw	ISC (NEIC)	28	76	-95	Centroid Moment Tensor
2004-07-31 04:15:47.900	95.22	12.37	12.1	5	Mw	GCMT	17	64	-124	Centroid Moment Tensor
2004-08-04 01:09:12.10	90.52	25.97	19.4	4.2	Mw	Kayal et al., 2012	320	50	-130	Centroid Moment Tensor
2004-08-06 14:35:27	95.09	12.3	12	5.7	Mb	WSM2016	18	48	-142	Centroid Moment Tensor

2004-08-13 10:48:42.700	69.92	30.76	12.4	5.3	Mw	GCMT	89	80	144	Centroid Moment Tensor
2004-08-24 10:05:34.470	92.19	32.542	10	5.4	Mw	ISC (NEIC)	215	55	-55	Centroid Moment Tensor
2004-09-17 11:25:51.000	95.83	15.76	12	5.7	Mw	GCMT	95	32	-31	Centroid Moment Tensor
2004-09-27 17:05:40.800	95.7	29.78	31.1	5	Mw	GCMT	35	86	-11	Centroid Moment Tensor
2004-10-07 16:14:17	77.51	40.38	16.9	5	Mb	WSM2016	243	13	90	Centroid Moment Tensor
2004-10-26 02:11:33.440	81.154	31.024	10.1	5.5	Mw	ISC (NEIC)	140	44	-107	Centroid Moment Tensor
2004-10-31 00:18:38.900	74.44	34.91	20.3	4.7	Mw	GCMT	70	68	-89	Centroid Moment Tensor
2004-10-31 06:02:56.300	74.37	35.2	14.7	4.9	Mw	GCMT	39	74	-164	Centroid Moment Tensor
2004-10-31 06:10:37.500	74.34	35.16	12	5.1	Mw	GCMT	42	58	-107	Centroid Moment Tensor
2004-11-02 08:23:23.10	92.22	25.49	25	4.2	Mw	Kayal et al., 2012	210	20	30	Centroid Moment Tensor
2004-11-17 07:34:32.100	71.75	39.44	25.5	5.1	Mw	GCMT	104	86	173	Centroid Moment Tensor
2004-11-17 20:58:00	71.86	39.19	6	5.8	Mw	Bai et al., 2017	185	88	11	Centroid Moment Tensor
2004-11-18 02:30:37.500	71.74	39.14	26.8	4.9	Mw	GCMT	49	75	-5	Centroid Moment Tensor
2004-11-18 21:18:58.200	71.71	39.28	12	4.8	Mw	GCMT	102	74	152	Centroid Moment Tensor
2004-11-19 20:05:14.400	92.89	32.17	21.8	4.8	Mw	GCMT	54	73	-23	Centroid Moment Tensor
2004-11-21 20:45:28.600	71.7	39.3	74.8	5	Mw	GCMT	162	50	-77	Centroid Moment Tensor
2004-12-09 00:00:00	92.536	24.715	34	5.5	Mb	Kumar et al., 2015	213	66	34	Centroid Moment Tensor
2004-12-09 08:48:58.90	92.47	24.89	43.7	4	Mw	Kayal et al., 2012	10	20	10	Centroid Moment Tensor
2004-12-10 03:44:00	93.35	35.83	19.4	5.2	Mb	WSM2016	341	48	133	Centroid Moment Tensor
2004-12-26 09:20:11.400	92.45	8.58	12	6.6	Mw	GCMT	163	53	96	Centroid Moment Tensor

2004-12-26 10:18:14.600	94.11	8.91	33.3	6.3	Mw	GCMT	61	54	70	Centroid Moment Tensor
2004-12-26 11:05:05.800	92.84	13.49	14	6.2	Mw	GCMT	29	56	158	Centroid Moment Tensor
2004-12-26 14:48:43.500	92.86	13.52	13	5.7	Mw	GCMT	38	78	145	Centroid Moment Tensor
2004-12-26 18:42:46.000	92.94	13.77	20.3	5.4	Mw	GCMT	144	69	174	Centroid Moment Tensor
2004-12-27 00:36:10.300	92.29	8.25	34.1	5.5	Mw	GCMT	139	39	-109	Centroid Moment Tensor
2004-12-27 00:39:46.900	93.69	8.98	15.8	5.3	Mw	GCMT	34	52	-62	Centroid Moment Tensor
2004-12-27 00:49:31.500	92.37	13.05	21.4	5.7	Mw	GCMT	229	60	-59	Centroid Moment Tensor
2004-12-27 02:04:25.600	94.29	8.07	12	5.1	Mw	GCMT	223	32	-23	Centroid Moment Tensor
2004-12-27 05:50:11.800	92.01	8.04	17.6	5.2	Mw	GCMT	24	84	-30	Centroid Moment Tensor
2004-12-27 06:01:50.900	93.45	7.6	59.8	5	Mw	GCMT	171	69	131	Centroid Moment Tensor
2004-12-27 09:57:55.900	92.74	7.65	12	5.7	Mw	GCMT	109	52	65	Centroid Moment Tensor
2004-12-27 10:46:41.700	93.11	13.85	12	5.4	Mw	GCMT	247	12	-7	Centroid Moment Tensor
2004-12-27 11:57:56.500	92.35	7.88	16.4	5.1	Mw	GCMT	14	70	-74	Centroid Moment Tensor
2004-12-27 12:14:04.900	92.51	12.86	29.8	5	Mw	GCMT	48	52	-106	Centroid Moment Tensor
2004-12-27 14:30:36.400	93.9	8.63	12	5.2	Mw	GCMT	215	34	-23	Centroid Moment Tensor
2004-12-27 14:46:48.600	92.72	12.39	27	5.5	Mw	GCMT	191	19	-64	Centroid Moment Tensor
2004-12-27 15:20:35.300	93.7	10.61	16.2	5.2	Mw	GCMT	182	44	-41	Centroid Moment Tensor
2004-12-27 18:24:02.800	94.21	8.81	25.2	5	Mw	GCMT	151	65	174	Centroid Moment Tensor
2004-12-27 19:13:21.800	92.28	11.72	25.4	5.5	Mw	GCMT	22	20	-77	Centroid Moment Tensor
2004-12-27 19:18:27.800	92.41	8.95	18.5	5	Mw	GCMT	111	61	169	Centroid Moment Tensor

2004-12-27 19:26:57.200	92.14	7.51	12	5.2	Mw	GCMT	10	59	-41	Centroid Moment Tensor
2004-12-27 19:28:53.300	93.93	8.72	12	5.3	Mw	GCMT	177	24	-79	Centroid Moment Tensor
2004-12-27 20:23:44.900	91.78	7.04	13.9	5.7	Mw	GCMT	10	74	-11	Centroid Moment Tensor
2004-12-27 20:36:19.800	93.8	8.93	12	5.2	Mw	GCMT	178	30	-83	Centroid Moment Tensor
2004-12-27 23:20:10.100	93.12	9.72	29.2	4.9	Mw	GCMT	63	48	-113	Centroid Moment Tensor
2004-12-27 23:58:04.000	91.89	8.19	12	5.3	Mw	GCMT	182	27	-56	Centroid Moment Tensor
2004-12-28 00:04:47.800	93.13	8.89	41.7	5.1	Mw	GCMT	171	53	100	Centroid Moment Tensor
2004-12-28 00:37:53.500	94.32	7.61	22	5.5	Mw	GCMT	52	84	-8	Centroid Moment Tensor
2004-12-28 05:36:14.300	93.77	9.48	12	5.4	Mw	GCMT	0	55	-101	Centroid Moment Tensor
2004-12-28 10:51:50.600	92.2	10.61	12	5.3	Mw	GCMT	22	8	130	Centroid Moment Tensor
2004-12-28 17:11:14.400	93.99	9.9	13.9	5.3	Mw	GCMT	62	89	3	Centroid Moment Tensor
2004-12-28 17:46:22.000	92.2	8.33	15	4.9	Mw	GCMT	146	66	162	Centroid Moment Tensor
2004-12-28 19:55:12.900	93.76	9.44	12	5.1	Mw	GCMT	1	54	-101	Centroid Moment Tensor
2004-12-28 20:41:57.900	93.22	10.12	19.7	4.9	Mw	GCMT	176	69	-23	Centroid Moment Tensor
2004-12-28 21:47:33.000	93.78	9.06	12	5.4	Mw	GCMT	205	37	-49	Centroid Moment Tensor
2004-12-28 22:16:54.100	93.06	13.6	15.4	5	Mw	GCMT	53	62	-179	Centroid Moment Tensor
2004-12-28 23:40:02.100	92.04	11.12	12	5	Mw	GCMT	209	57	-55	Centroid Moment Tensor
2004-12-29 01:39:41.240	93.156	8.378	34	5.8	Mw	ISC (NEIC)	162	78	87	Centroid Moment Tensor
2004-12-29 01:50:52.570	93.756	9.109	8	6.1	Mw	ISC (NEIC)	201	36	-59	Centroid Moment Tensor
2004-12-29 05:56:47.540	93.198	8.791	12	6.2	Mw	ISC (NEIC)	53	52	-40	Centroid Moment Tensor

2004-12-29 06:05:19.100	93.24	8.74	12	5.8	Mw	GCMT	181	89	-81	Centroid Moment Tensor
2004-12-29 06:19:06.900	93.9	9.55	12	5.3	Mw	GCMT	210	30	-61	Centroid Moment Tensor
2004-12-29 06:30:45.400	92.75	13.28	12.3	5.3	Mw	GCMT	243	11	-10	Centroid Moment Tensor
2004-12-29 06:35:41.200	92.99	9.29	45.7	5	Mw	GCMT	53	48	120	Centroid Moment Tensor
2004-12-29 10:09:23.800	93.81	7.61	12	5	Mw	GCMT	47	46	-122	Centroid Moment Tensor
2004-12-29 11:58:44.900	93.11	13.66	14.1	5.1	Mw	GCMT	21	66	168	Centroid Moment Tensor
2004-12-29 17:12:38.500	93.91	10.32	12	5.2	Mw	GCMT	53	41	-113	Centroid Moment Tensor
2004-12-29 22:55:44.600	93.78	7.67	19.6	4.8	Mw	GCMT	79	44	-89	Centroid Moment Tensor
2004-12-29 23:14:06.200	92.14	7.84	12	5.2	Mw	GCMT	18	89	-33	Centroid Moment Tensor
2004-12-30 03:12:49.100	92.31	9.15	35	4.9	Mw	GCMT	184	58	-64	Centroid Moment Tensor
2004-12-30 06:38:21.000	92.6	9.18	41	4.7	Mw	GCMT	4	76	-54	Centroid Moment Tensor
2004-12-30 17:58:14.500	92.35	12.28	12	5.6	Mw	GCMT	29	13	138	Centroid Moment Tensor
2004-12-31 02:24:00.520	92.533	7.12	14	6	Mw	ISC (NEIC)	188	33	114	Centroid Moment Tensor
2004-12-31 05:53:57.000	91.98	11.15	12.5	5	Mw	GCMT	7	48	-151	Centroid Moment Tensor
2004-12-31 09:57:00.020	93.947	7.636	22.2	5.6	Mw	ISC (NEIC)	14	29	-96	Centroid Moment Tensor
2004-12-31 16:15:47.700	93.99	7.56	12	4.9	Mw	GCMT	20	53	-89	Centroid Moment Tensor
2004-12-31 22:09:26.500	94.06	9.41	20	5.2	Mw	GCMT	53	87	-8	Centroid Moment Tensor
2005-01-01 01:42:23.800	93.96	7.24	12	5	Mw	GCMT	28	73	-136	Centroid Moment Tensor
2005-01-01 01:43:41.500	92.46	7.08	13.9	5.1	Mw	GCMT	205	55	-37	Centroid Moment Tensor
2005-01-01 11:53:14.100	91.67	11.14	21.6	5	Mw	GCMT	1	37	-112	Centroid Moment Tensor

2005-01-01 14:29:16.600	93.32	8.14	12	5.5	Mw	GCMT	164	85	94	Centroid Moment Tensor
2005-01-01 19:08:05.800	94.49	7.15	19.8	6.1	Mw	GCMT	63	77	-13	Centroid Moment Tensor
2005-01-01 22:23:16.600	92.56	7.12	12	5.1	Mw	GCMT	167	70	117	Centroid Moment Tensor
2005-01-01 22:28:13.780	92.765	7.192	10	5.5	Mw	ISC (NEIC)	159	45	89	Centroid Moment Tensor
2005-01-01 22:40:51	92.42	8.33	18.2	5	Mb	WSM2016	111	67	171	Centroid Moment Tensor
2005-01-04 04:18:23	93.02	7.08	34.1	4.9	Mb	WSM2016	292	52	-128	Centroid Moment Tensor
2005-01-04 09:13:12	92.03	10.65	24	6	Mb	WSM2016	5	20	90	Centroid Moment Tensor
2005-01-04 12:15:33	93.64	8.83	12	5	Mb	WSM2016	199	21	-118	Centroid Moment Tensor
2005-01-04 19:14:49	91.56	10.48	12	5.6	Mb	WSM2016	359	21	90	Centroid Moment Tensor
2005-01-05 08:32:56	92.62	13.02	19.4	5.2	Mb	WSM2016	32	46	-114	Centroid Moment Tensor
2005-01-06 10:38:44	93.07	13.71	15.1	5.1	Mb	WSM2016	44	61	174	Centroid Moment Tensor
2005-01-06 11:55:44	91.99	11.01	13	5.4	Mb	WSM2016	210	27	-50	Centroid Moment Tensor
2005-01-07 10:49:14	93.61	8.89	12	5.5	Mb	WSM2016	219	48	-60	Centroid Moment Tensor
2005-01-08 05:30:47	92.03	10.41	12	5.2	Mb	WSM2016	15	31	131	Centroid Moment Tensor
2005-01-09 01:59:13	92.29	7.39	12	5	Mb	WSM2016	312	30	65	Centroid Moment Tensor
2005-01-10 01:04:17	93.91	9.56	12	4.9	Mb	WSM2016	23	77	-11	Centroid Moment Tensor
2005-01-11 05:49:29	93.85	8.16	12.9	4.9	Mb	WSM2016	18	43	-117	Centroid Moment Tensor
2005-01-11 22:55:49	92.22	11.95	19.6	4.9	Mb	WSM2016	345	74	173	Centroid Moment Tensor
2005-01-13 05:30:22.400	92.28	11.9	23.2	4.7	Mw	GCMT	149	77	174	Centroid Moment Tensor
2005-01-13 19:56:21.300	92.31	14.53	14.5	4.7	Mw	GCMT	246	75	-51	Centroid Moment Tensor

2005-01-14 16:22:08.200	93.29	8.53	25.2	5.1	Mw	GCMT	9	89	66	Centroid Moment Tensor
2005-01-15 07:46:53.260	92.387	14.57	25.7	5.5	Mw	ISC (NEIC)	34	37	-112	Centroid Moment Tensor
2005-01-17 02:45:16.800	92.21	14.57	16.5	5	Mw	GCMT	45	27	-80	Centroid Moment Tensor
2005-01-17 03:55:46.700	93.13	14.48	30.6	4.8	Mw	GCMT	31	58	-133	Centroid Moment Tensor
2005-01-18 02:36:46.700	91.93	10.57	12	5	Mw	GCMT	26	37	135	Centroid Moment Tensor
2005-01-18 15:30:22.000	67.61	35.68	19.9	5.3	Mw	GCMT	250	88	170	Centroid Moment Tensor
2005-01-18 22:04:46.700	93.97	8.34	26.1	4.8	Mw	GCMT	82	83	-8	Centroid Moment Tensor
2005-01-19 22:46:59.900	92.27	13.08	30.9	4.8	Mw	GCMT	33	54	-92	Centroid Moment Tensor
2005-01-22 18:38:14.900	92.22	14.59	12	5.5	Mw	GCMT	14	23	-128	Centroid Moment Tensor
2005-01-23 08:22:17.600	92.84	13.64	26.6	4.8	Mw	GCMT	4	83	-149	Centroid Moment Tensor
2005-01-23 16:55:48.700	92.91	13.64	14.4	5	Mw	GCMT	139	49	-8	Centroid Moment Tensor
2005-01-24 04:16:47.440	92.482	7.33	30	6.3	Mw	ISC (NEIC)	202	70	-12	Centroid Moment Tensor
2005-01-26 17:30:30.400	94.14	8.2	12	5.5	Mw	GCMT	69	72	-20	Centroid Moment Tensor
2005-01-26 22:47:00.600	94.14	7.92	21.4	5.4	Mw	GCMT	67	90	-20	Centroid Moment Tensor
2005-01-26 23:03:08.600	94.23	7.94	14.6	5.1	Mw	GCMT	46	74	-56	Centroid Moment Tensor
2005-01-27 03:58:45.600	94.2	7.94	19.5	5.4	Mw	GCMT	62	87	-26	Centroid Moment Tensor
2005-01-27 04:02:50.100	94.21	7.89	12.7	5.1	Mw	GCMT	53	89	-41	Centroid Moment Tensor
2005-01-27 05:22:20.300	94.18	7.9	19.7	5.3	Mw	GCMT	62	85	-25	Centroid Moment Tensor
2005-01-27 05:35:22.600	92.87	13.28	13.8	4.9	Mw	GCMT	141	59	-4	Centroid Moment Tensor
2005-01-27 05:48:12.900	94.2	7.99	14.9	5.2	Mw	GCMT	58	88	-42	Centroid Moment Tensor

2005-01-27 05:51:04.400	91.72	10.72	37.3	5.2	Mw	GCMT	20	47	108	Centroid Moment Tensor
2005-01-27 06:14:31.000	94.18	7.94	12	5	Mw	GCMT	36	74	-54	Centroid Moment Tensor
2005-01-27 06:56:58.600	94.17	7.92	18.5	5.5	Mw	GCMT	74	81	-12	Centroid Moment Tensor
2005-01-27 07:20:26.400	94.19	7.95	14	5.2	Mw	GCMT	52	75	-51	Centroid Moment Tensor
2005-01-27 07:26:01.800	94.21	7.99	21.6	5.3	Mw	GCMT	153	62	178	Centroid Moment Tensor
2005-01-27 07:28:32.200	94.22	7.98	22.9	5.1	Mw	GCMT	9	54	-139	Centroid Moment Tensor
2005-01-27 07:35:46.900	94.2	7.96	17	5.2	Mw	GCMT	170	89	166	Centroid Moment Tensor
2005-01-27 07:41:26.200	94.25	7.9	22.2	4.9	Mw	GCMT	50	86	-32	Centroid Moment Tensor
2005-01-27 08:07:26.300	94.2	7.93	14.2	5.1	Mw	GCMT	71	77	-37	Centroid Moment Tensor
2005-01-27 08:19:09.100	94.17	7.93	12	5.5	Mw	GCMT	78	88	-7	Centroid Moment Tensor
2005-01-27 08:31:12.100	94.22	7.96	14.6	5.2	Mw	GCMT	138	75	178	Centroid Moment Tensor
2005-01-27 08:36:52.000	94.21	7.89	16.5	5.2	Mw	GCMT	63	83	-55	Centroid Moment Tensor
2005-01-27 08:42:16.100	94.22	7.83	14.8	5.4	Mw	GCMT	53	87	-39	Centroid Moment Tensor
2005-01-27 09:11:28.800	94.26	8.11	16.1	5.2	Mw	GCMT	240	43	-27	Centroid Moment Tensor
2005-01-27 09:25:28.700	94.16	7.94	17.7	5.1	Mw	GCMT	79	85	-29	Centroid Moment Tensor
2005-01-27 09:52:21.300	94.25	7.87	20	5.3	Mw	GCMT	144	65	177	Centroid Moment Tensor
2005-01-27 09:59:31.800	94.22	7.98	25.2	5.2	Mw	GCMT	76	84	-25	Centroid Moment Tensor
2005-01-27 10:08:13.500	94.16	7.92	19.5	5.3	Mw	GCMT	62	76	-37	Centroid Moment Tensor
2005-01-27 10:58:07.500	94.11	7.91	13.9	5.3	Mw	GCMT	174	90	180	Centroid Moment Tensor
2005-01-27 11:44:06.300	94.15	8.02	12	5.2	Mw	GCMT	246	58	-29	Centroid Moment Tensor

2005-01-27 11:47:36.900	94.2	7.92	12	5.5	Mw	GCMT	76	86	0	Centroid Moment Tensor
2005-01-27 11:56:43.400	94.16	7.88	15.5	5	Mw	GCMT	60	67	-57	Centroid Moment Tensor
2005-01-27 12:11:55.300	94.28	7.98	12	5.4	Mw	GCMT	184	86	178	Centroid Moment Tensor
2005-01-27 13:15:20.400	94.14	7.86	17.1	5.3	Mw	GCMT	60	87	-29	Centroid Moment Tensor
2005-01-27 13:18:05.700	94.25	7.92	23.3	5.3	Mw	GCMT	55	84	-28	Centroid Moment Tensor
2005-01-27 13:25:21.700	94.2	7.77	18.1	5.2	Mw	GCMT	150	69	178	Centroid Moment Tensor
2005-01-27 13:26:33.600	94.24	7.84	22.2	5.3	Mw	GCMT	154	67	177	Centroid Moment Tensor
2005-01-27 13:54:15.400	94.17	7.92	19.5	5.4	Mw	GCMT	76	87	-11	Centroid Moment Tensor
2005-01-27 13:57:07.200	94.16	7.97	16.3	5.5	Mw	GCMT	62	81	-23	Centroid Moment Tensor
2005-01-27 14:13:18.000	94.14	7.95	17.3	5.1	Mw	GCMT	41	74	-58	Centroid Moment Tensor
2005-01-27 14:35:09.200	94.2	7.95	22.3	5.1	Mw	GCMT	67	85	-28	Centroid Moment Tensor
2005-01-27 15:24:51.500	94.21	7.66	24.7	5.2	Mw	GCMT	2	85	-140	Centroid Moment Tensor
2005-01-27 15:27:53.800	94.16	7.94	12	5.3	Mw	GCMT	1	77	-150	Centroid Moment Tensor
2005-01-27 15:34:30.400	94.25	7.74	23	5.2	Mw	GCMT	56	70	-41	Centroid Moment Tensor
2005-01-27 16:00:57.900	94.18	7.76	32.5	5	Mw	GCMT	162	66	160	Centroid Moment Tensor
2005-01-27 16:02:22.300	94.25	8.04	31.6	5	Mw	GCMT	80	85	-12	Centroid Moment Tensor
2005-01-27 16:48:28.500	94.14	7.94	12	4.9	Mw	GCMT	81	82	-2	Centroid Moment Tensor
2005-01-27 16:58:52.300	94.24	7.81	19.5	5.7	Mw	GCMT	58	84	-12	Centroid Moment Tensor
2005-01-27 17:25:01.900	94.25	7.78	19	5.3	Mw	GCMT	156	62	178	Centroid Moment Tensor
2005-01-27 17:40:49.500	94.17	7.92	13	5.4	Mw	GCMT	48	61	-67	Centroid Moment Tensor

2005-01-27 18:52:39.300	94.24	7.85	15.9	5.6	Mw	GCMT	53	84	-25	Centroid Moment Tensor
2005-01-27 19:20:21.900	94.17	7.91	12	5.3	Mw	GCMT	52	56	-63	Centroid Moment Tensor
2005-01-27 19:31:11.100	94.2	8	19.3	5.2	Mw	GCMT	56	69	-45	Centroid Moment Tensor
2005-01-27 19:40:39.500	94.07	8.16	15.3	5.2	Mw	GCMT	58	60	-70	Centroid Moment Tensor
2005-01-27 20:17:39.200	94.19	8.01	22.6	5.1	Mw	GCMT	62	78	-33	Centroid Moment Tensor
2005-01-27 20:31:02.800	94.19	7.97	16.3	5.2	Mw	GCMT	57	73	-52	Centroid Moment Tensor
2005-01-27 20:45:20.100	94.19	7.89	15.1	5	Mw	GCMT	63	72	-69	Centroid Moment Tensor
2005-01-27 20:51:10.900	94.18	8.11	16.6	5.2	Mw	GCMT	93	82	-9	Centroid Moment Tensor
2005-01-27 21:00:44.900	93.7	9.74	12.2	5.3	Mw	GCMT	57	82	-1	Centroid Moment Tensor
2005-01-27 21:05:05.300	94.26	7.99	15.4	5.1	Mw	GCMT	32	87	-41	Centroid Moment Tensor
2005-01-27 21:32:20.000	94.17	7.98	17	5.2	Mw	GCMT	54	76	-34	Centroid Moment Tensor
2005-01-27 21:47:56.100	94.17	7.95	12	5.1	Mw	GCMT	31	63	-90	Centroid Moment Tensor
2005-01-27 22:40:48.400	94.18	8	12	5.3	Mw	GCMT	12	54	-119	Centroid Moment Tensor
2005-01-27 22:56:51.400	94.31	8.05	21.9	4.9	Mw	GCMT	52	68	-56	Centroid Moment Tensor
2005-01-27 23:20:09.100	94.2	8.02	12	5.3	Mw	GCMT	54	77	-39	Centroid Moment Tensor
2005-01-27 23:27:03.200	94.23	7.89	22.8	5	Mw	GCMT	142	60	160	Centroid Moment Tensor
2005-01-27 23:40:49.500	94.25	8	21.6	4.9	Mw	GCMT	45	61	-51	Centroid Moment Tensor
2005-01-28 00:15:46.500	94.21	7.84	17.6	5.2	Mw	GCMT	62	85	-28	Centroid Moment Tensor
2005-01-28 01:01:29.600	94.17	7.94	12	4.8	Mw	GCMT	55	54	-66	Centroid Moment Tensor
2005-01-28 01:36:20.200	94.23	7.96	12	5.2	Mw	GCMT	38	63	-84	Centroid Moment Tensor

2005-01-28 01:43:39.800	94.23	7.96	28.2	5	Mw	GCMT	31	54	-85	Centroid Moment Tensor
2005-01-28 02:23:15.600	94.2	7.87	15.5	5.3	Mw	GCMT	43	78	-43	Centroid Moment Tensor
2005-01-28 02:28:58.300	94.15	7.99	12	5.2	Mw	GCMT	4	66	-122	Centroid Moment Tensor
2005-01-28 03:31:26.900	94.2	8.06	12	5.3	Mw	GCMT	4	56	-134	Centroid Moment Tensor
2005-01-28 04:34:41.600	94.23	7.89	17.6	5.1	Mw	GCMT	164	54	174	Centroid Moment Tensor
2005-01-28 05:38:27.100	94.2	7.82	17.4	5.1	Mw	GCMT	51	81	-41	Centroid Moment Tensor
2005-01-28 06:06:55.500	94.21	7.73	16.8	5.3	Mw	GCMT	31	64	-29	Centroid Moment Tensor
2005-01-28 06:10:30.100	94.17	7.85	12	5.5	Mw	GCMT	49	82	-30	Centroid Moment Tensor
2005-01-28 06:13:27.600	94.16	7.79	17.8	5.7	Mw	GCMT	57	79	-24	Centroid Moment Tensor
2005-01-28 07:49:17.500	94.23	7.82	16	5.6	Mw	GCMT	47	80	-30	Centroid Moment Tensor
2005-01-28 08:21:23.800	94.17	8.01	12	5.2	Mw	GCMT	27	54	-96	Centroid Moment Tensor
2005-01-28 08:29:47.200	94.27	7.82	18.4	5.3	Mw	GCMT	43	77	-48	Centroid Moment Tensor
2005-01-28 08:47:18.700	94.11	7.84	13.1	5.2	Mw	GCMT	51	88	-35	Centroid Moment Tensor
2005-01-28 09:14:46.400	94.21	8	22	5.1	Mw	GCMT	69	88	-27	Centroid Moment Tensor
2005-01-28 10:21:20.500	93.91	7.66	19.4	5.1	Mw	GCMT	45	39	-34	Centroid Moment Tensor
2005-01-28 11:53:03.700	94.23	7.84	17.2	5.3	Mw	GCMT	51	81	-24	Centroid Moment Tensor
2005-01-28 12:37:13.200	94.22	8.07	12	5.1	Mw	GCMT	14	53	-116	Centroid Moment Tensor
2005-01-28 17:49:41.500	94.3	8.12	12	5	Mw	GCMT	14	61	-103	Centroid Moment Tensor
2005-01-28 19:18:54.600	94.2	7.86	12	5.4	Mw	GCMT	47	79	-29	Centroid Moment Tensor
2005-01-28 22:29:04.400	94.23	7.75	20.6	5.3	Mw	GCMT	155	68	177	Centroid Moment Tensor

2005-01-28 22:35:29.500	94.01	7.71	15.3	5.1	Mw	GCMT	5	65	-109	Centroid Moment Tensor
2005-01-28 23:32:11.800	94.24	8.05	12	5	Mw	GCMT	14	54	-112	Centroid Moment Tensor
2005-01-29 01:13:44.200	92.56	7.21	12	5.3	Mw	GCMT	107	40	-157	Centroid Moment Tensor
2005-01-29 01:50:22.100	94.23	7.77	21.3	5.3	Mw	GCMT	68	86	-9	Centroid Moment Tensor
2005-01-29 03:38:03.600	94.25	8.09	12	5.1	Mw	GCMT	11	58	-113	Centroid Moment Tensor
2005-01-29 05:26:48.800	94.2	7.82	12	5.2	Mw	GCMT	50	85	-26	Centroid Moment Tensor
2005-01-29 05:44:13.600	93.07	13.18	20.6	5.2	Mw	GCMT	118	44	44	Centroid Moment Tensor
2005-01-29 09:27:40.100	94.29	7.76	15.4	5	Mw	GCMT	54	85	-38	Centroid Moment Tensor
2005-01-29 16:12:50.900	94.25	8.18	25.4	5	Mw	GCMT	59	86	-29	Centroid Moment Tensor
2005-01-29 16:36:55.600	94.26	8.05	12	5	Mw	GCMT	10	60	-108	Centroid Moment Tensor
2005-01-29 18:37:58.400	94.33	8.11	15.6	4.8	Mw	GCMT	5	55	-125	Centroid Moment Tensor
2005-01-29 19:06:16.600	94.29	7.72	15.1	5.3	Mw	GCMT	40	82	-28	Centroid Moment Tensor
2005-01-29 20:01:57.700	94.22	8.1	12	5.2	Mw	GCMT	242	57	-37	Centroid Moment Tensor
2005-01-29 20:28:24.500	94.21	7.75	19	5.6	Mw	GCMT	63	84	-15	Centroid Moment Tensor
2005-01-29 20:54:26.000	94.2	7.82	12.4	5	Mw	GCMT	42	82	-59	Centroid Moment Tensor
2005-01-29 20:58:34.600	94.19	8.01	12	5	Mw	GCMT	38	62	-87	Centroid Moment Tensor
2005-01-29 22:03:52.600	94.18	7.8	12	5.4	Mw	GCMT	51	78	-23	Centroid Moment Tensor
2005-01-30 00:07:35.000	94.21	8.13	19.7	5.3	Mw	GCMT	84	80	-11	Centroid Moment Tensor
2005-01-30 00:34:11.400	94.21	8.07	13.6	5	Mw	GCMT	8	58	-129	Centroid Moment Tensor
2005-01-30 02:25:43.700	94.18	8.03	12	5	Mw	GCMT	12	50	-130	Centroid Moment Tensor

2005-01-30 02:35:17.800	94.23	8.06	12	5.2	Mw	GCMT	1	62	-151	Centroid Moment Tensor
2005-01-30 03:44:13.300	94.08	8	12	4.7	Mw	GCMT	64	41	-49	Centroid Moment Tensor
2005-01-30 06:26:16.800	93.02	13.8	14.1	5	Mw	GCMT	46	71	173	Centroid Moment Tensor
2005-01-30 07:02:25.100	92.97	13.2	23.1	5.1	Mw	GCMT	8	77	158	Centroid Moment Tensor
2005-01-30 08:49:39.500	94.18	7.94	12	5.1	Mw	GCMT	68	56	-56	Centroid Moment Tensor
2005-01-30 10:32:55.400	94.22	8.04	12	5	Mw	GCMT	1	69	-155	Centroid Moment Tensor
2005-01-30 15:33:13.510	94.056	8.117	18.6	5.3	Mw	ISC (NEIC)	40	51	-95	Centroid Moment Tensor
2005-01-30 21:39:05.400	94.24	8.13	15.8	5.3	Mw	GCMT	6	90	160	Centroid Moment Tensor
2005-01-31 02:20:43.800	94.23	8.02	18.5	4.8	Mw	GCMT	40	54	-122	Centroid Moment Tensor
2005-01-31 08:15:07.200	94.22	8.09	12	5.1	Mw	GCMT	262	77	-21	Centroid Moment Tensor
2005-01-31 13:14:34.700	94.22	8.03	12	5.1	Mw	GCMT	1	88	-178	Centroid Moment Tensor
2005-01-31 16:30:20.400	94.26	8.09	12	5.1	Mw	GCMT	239	52	-41	Centroid Moment Tensor
2005-02-01 10:35:17	94.18	9.99	12	5.3	Mb	WSM2016	23	39	-114	Centroid Moment Tensor
2005-02-01 13:41:53	94.22	8.08	12	5.2	Mb	WSM2016	24	42	-120	Centroid Moment Tensor
2005-02-01 13:54:38	94.1	9.94	12	5.1	Mb	WSM2016	33	38	-115	Centroid Moment Tensor
2005-02-02 00:52:45.300	94.32	8.09	12	4.8	Mw	GCMT	18	59	-110	Centroid Moment Tensor
2005-02-02 01:30:22.280	93.96	9.962	39.5	5.3	Mw	ISC (NEIC)	24	51	-85	Centroid Moment Tensor
2005-02-02 13:22:38.500	94.27	8.09	12	5.1	Mw	GCMT	89	86	0	Centroid Moment Tensor
2005-02-04 09:44:53	94.2	7.76	13	5.1	Mb	WSM2016	157	75	-171	Centroid Moment Tensor
2005-02-05 08:00:27	94.26	8.06	12	5.7	Mb	WSM2016	220	36	-79	Centroid Moment Tensor

2005-02-05 17:35:47	94.27	8.08	15	5.5	Mb	WSM2016	2	85	176	Centroid Moment Tensor
2005-02-08 07:20:59	96.05	19.61	16	5.2	Mb	WSM2016	129	46	53	Centroid Moment Tensor
2005-02-10 01:34:31	94.2	8.01	12	5	Mb	WSM2016	184	46	-136	Centroid Moment Tensor
2005-02-14 13:21:55.700	93.73	14.78	12	4.9	Mw	GCMT	29	59	166	Centroid Moment Tensor
2005-02-14 23:38:08.660	79.44	41.728	22	6	Mw	ISC (NEIC)	81	83	79	Centroid Moment Tensor
2005-02-15 11:15:13.700	92.61	24.52	27.2	5	Mw	GCMT	52	86	-38	Centroid Moment Tensor
2005-02-15 13:05:53.800	94.62	24.4	60.4	5.2	Mw	GCMT	171	65	147	Centroid Moment Tensor
2005-02-16 08:19:41.470	93.945	8.097	11	5.9	Mw	ISC (NEIC)	265	84	-5	Centroid Moment Tensor
2005-02-20 11:43:46.100	92.07	11.51	30	4.8	Mw	GCMT	43	47	135	Centroid Moment Tensor
2005-02-20 23:08:05.600	93.84	10.3	12	5.4	Mw	GCMT	223	44	-44	Centroid Moment Tensor
2005-02-22 17:12:01.500	91.72	10.81	12	5.5	Mw	GCMT	188	63	101	Centroid Moment Tensor
2005-02-24 15:06:51.700	93.76	8.68	28	4.8	Mw	GCMT	9	45	-65	Centroid Moment Tensor
2005-02-25 13:31:14.870	94.101	7.831	22.7	5.5	Mw	ISC (NEIC)	60	88	-12	Centroid Moment Tensor
2005-03-07 21:32:33	91.31	9.05	29.2	4.9	Mb	WSM2016	312	32	47	Centroid Moment Tensor
2005-03-12 22:43:33	91.6	9.72	12	5.1	Mb	WSM2016	51	61	167	Centroid Moment Tensor
2005-03-14 04:27:18.700	93.05	9.47	54.7	5	Mw	GCMT	2	35	100	Centroid Moment Tensor
2005-03-14 09:43:50.000	73.79	17.1	13	4.9	Mw	GCMT	189	55	-68	Centroid Moment Tensor
2005-03-22 09:38:29.500	92.57	13.08	32	5	Mw	GCMT	27	62	-94	Centroid Moment Tensor
2005-03-23 05:59:10.600	95.43	26.17	79	4.9	Mw	GCMT	132	42	177	Centroid Moment Tensor
2005-03-23 09:17:09.400	92.11	12.4	20	5.2	Mw	GCMT	17	22	111	Centroid Moment Tensor

2005-03-24 07:38:03.900	77.99	39.81	30.7	4.8	Mw	GCMT	70	73	120	Centroid Moment Tensor
2005-03-26 20:32:15.700	87.95	28.08	69.6	4.7	Mw	GCMT	109	62	179	Centroid Moment Tensor
2005-04-03 14:42:49	93.71	9.75	12	5.2	Mb	WSM2016	184	37	-140	Centroid Moment Tensor
2005-04-06 08:44:57	78.7	41.48	29.8	5.2	Mb	WSM2016	288	41	107	Centroid Moment Tensor
2005-04-07 20:04:00	83.66	30.49	6	6.3	Mw	Bai et al., 2017	170	43	-67	Centroid Moment Tensor
2005-04-08 19:51:35	83.76	30.25	19.6	5.1	Mb	WSM2016	181	45	-79	Centroid Moment Tensor
2005-04-17 21:37:56.000	93.89	10.2	12	5.3	Mw	GCMT	219	35	-43	Centroid Moment Tensor
2005-04-26 14:01:43.900	94.04	7.74	12	4.9	Mw	GCMT	219	37	-57	Centroid Moment Tensor
2005-04-27 14:04:47.400	93.72	8.66	17.9	4.9	Mw	GCMT	227	50	-53	Centroid Moment Tensor
2005-05-04 02:32:41	91.64	9.19	12	5.4	Mb	WSM2016	42	59	154	Centroid Moment Tensor
2005-05-23 04:13:50.000	67.69	30.39	12	5.2	Mw	GCMT	86	4	-66	Centroid Moment Tensor
2005-06-01 20:06:00	94.63	28.88	19	5.6	Mw	Bai et al., 2017	209	6	28	Centroid Moment Tensor
2005-06-13 19:28:17.300	94.06	7.68	12	5.3	Mw	GCMT	235	41	-32	Centroid Moment Tensor
2005-06-16 16:06:37.800	92.13	7.73	16.8	4.8	Mw	GCMT	108	81	176	Centroid Moment Tensor
2005-06-22 07:48:23.900	69.37	36.41	23.2	4.8	Mw	GCMT	78	44	150	Centroid Moment Tensor
2005-06-23 03:05:07.900	73.05	39.83	31.9	4.7	Mw	GCMT	62	57	59	Centroid Moment Tensor
2005-06-30 16:02:35.200	91.88	7.79	12	4.8	Mw	GCMT	20	88	-34	Centroid Moment Tensor
2005-07-04 16:07:36	93.8	10.33	12	4.9	Mb	WSM2016	220	35	-59	Centroid Moment Tensor
2005-07-13 00:29:29.810	92.903	10.351	49.6	5.5	Mw	ISC (NEIC)	49	36	141	Centroid Moment Tensor
2005-07-15 12:50:07.700	94.3	7.56	13.9	4.9	Mw	GCMT	51	71	-48	Centroid Moment Tensor

2005-07-16 02:17:20.130	69.461	30.003	10	5.2	Mw	ISC (NEIC)	69	68	80	Centroid Moment Tensor
2005-07-24 15:42:06.210	92.19	7.92	16	7.1	Mw	ISC (NEIC)	122	77	172	Centroid Moment Tensor
2005-07-25 02:17:16.000	92.07	7.79	12	5	Mw	GCMT	110	87	158	Centroid Moment Tensor
2005-07-25 03:26:17.600	91.926	8.123	31.3	5.5	Mw	ISC (NEIC)	174	42	-52	Centroid Moment Tensor
2005-07-25 12:43:45.700	92.22	7.85	12	5.2	Mw	GCMT	36	85	-25	Centroid Moment Tensor
2005-07-26 06:32:11.200	91.56	8.44	12	5.3	Mw	GCMT	218	56	-61	Centroid Moment Tensor
2005-07-29 12:27:04.700	92.27	8.49	27.3	5.3	Mw	GCMT	118	84	169	Centroid Moment Tensor
2005-07-30 12:24:41.800	92.01	7.61	20.8	5.1	Mw	GCMT	45	73	-74	Centroid Moment Tensor
2005-08-09 11:23:00	94.33	7.78	24	5.3	Mb	WSM2016	147	74	175	Centroid Moment Tensor
2005-08-24 22:32:47.800	79.66	39.88	46.4	5	Mw	GCMT	48	56	24	Centroid Moment Tensor
2005-08-25 21:08:18.000	79.35	37.13	15	5.4	Mw	GCMT	89	23	68	Centroid Moment Tensor
2005-08-29 14:44:48.800	91.92	11.04	21	5.2	Mw	GCMT	179	74	97	Centroid Moment Tensor
2005-08-31 12:45:41.800	68.98	36.44	22.3	5	Mw	GCMT	93	61	169	Centroid Moment Tensor
2005-09-06 11:10:29	92.28	7.76	28.5	5	Mb	WSM2016	194	40	-66	Centroid Moment Tensor
2005-09-13 14:32:58.600	91.92	8.11	12	5.5	Mw	GCMT	203	31	-50	Centroid Moment Tensor
2005-09-14 08:17:01.500	91.93	8.14	16.7	4.9	Mw	GCMT	196	29	-54	Centroid Moment Tensor
2005-09-18 00:00:00	94.748	24.615	78	5.5	Mb	Kumar et al., 2015	275	47	50	Centroid Moment Tensor
2005-09-18 03:47:41.800	94.16	7.6	12	5.1	Mw	GCMT	15	70	-88	Centroid Moment Tensor
2005-09-23 05:00:58.400	82.46	41.97	12	4.8	Mw	GCMT	105	37	111	Centroid Moment Tensor
2005-09-26 16:41:02.600	69.6	38.59	12	5	Mw	GCMT	49	51	-79	Centroid Moment Tensor

2005-09-26 21:49:44.500	69.63	38.88	15	5.1	Mw	GCMT	60	32	-51	Centroid Moment Tensor
2005-10-06 02:53:01	93.98	7.74	18.6	5	Mb	WSM2016	231	36	-43	Centroid Moment Tensor
2005-10-07 21:25:49	92.96	34.71	15	5	Mb	WSM2016	123	38	35	Centroid Moment Tensor
2005-10-08 03:50:41	73.47	34.38	12	6.9	Mb	WSM2016	333	40	122	Centroid Moment Tensor
2005-10-08 10:46:00	73.1	34.73	8	6.1	Mw	Bai et al., 2017	328	39	77	Centroid Moment Tensor
2005-10-08 12:08:28	73.06	34.58	14.3	5.3	Mb	WSM2016	319	30	101	Centroid Moment Tensor
2005-10-08 12:25:00	73.12	34.77	3	5.9	Mw	Bai et al., 2017	96	47	39	Centroid Moment Tensor
2005-10-08 21:13:32	73.1	34.68	12	5.9	Mb	WSM2016	7	41	116	Centroid Moment Tensor
2005-10-08 21:45:10	73.06	34.6	12	5.5	Mb	WSM2016	338	33	120	Centroid Moment Tensor
2005-10-08 22:04:27	72.86	34.69	12	5	Mb	WSM2016	279	25	32	Centroid Moment Tensor
2005-10-08 22:53:39	73.17	34.93	12	5	Mb	WSM2016	352	23	114	Centroid Moment Tensor
2005-10-09 04:58:55	72.94	34.7	12	4.9	Mb	WSM2016	282	28	90	Centroid Moment Tensor
2005-10-09 07:09:19	73.01	34.57	12	5.5	Mb	WSM2016	316	28	102	Centroid Moment Tensor
2005-10-09 08:30:00	73.18	34.67	6	5.7	Mw	Bai et al., 2017	344	37	122	Centroid Moment Tensor
2005-10-09 08:59:34	72.86	34.64	12	4.9	Mb	WSM2016	280	22	41	Centroid Moment Tensor
2005-10-09 09:22:34	73.26	34.6	12	4.9	Mb	WSM2016	151	62	154	Centroid Moment Tensor
2005-10-09 11:21:44	73.02	34.55	15.7	4.9	Mb	WSM2016	327	21	126	Centroid Moment Tensor
2005-10-09 12:38:14	73.03	34.74	12	4.9	Mb	WSM2016	283	38	107	Centroid Moment Tensor
2005-10-09 19:20:37	73.58	34.33	12	5.5	Mb	WSM2016	285	36	101	Centroid Moment Tensor
2005-10-09 19:47:01	72.87	34.62	17	4.9	Mb	WSM2016	258	47	64	Centroid Moment Tensor

2005-10-10 12:38:11.500	73.26	34.65	12	4.9	Mw	GCMT	71	62	56	Centroid Moment Tensor
2005-10-11 03:37:57	92.02	10.89	24	5.5	Mb	WSM2016	360	22	90	Centroid Moment Tensor
2005-10-12 20:23:38	73.08	34.88	12	5.6	Mb	WSM2016	317	41	100	Centroid Moment Tensor
2005-10-13 20:49:26.000	73.1	34.69	13.6	4.9	Mw	GCMT	131	57	66	Centroid Moment Tensor
2005-10-14 19:37:48.100	73	34.91	20.4	4.8	Mw	GCMT	117	33	49	Centroid Moment Tensor
2005-10-17 10:43:10.000	73.08	34.81	21.2	4.9	Mw	GCMT	116	51	79	Centroid Moment Tensor
2005-10-18 21:20:07.800	73.09	34.72	12	5	Mw	GCMT	104	59	82	Centroid Moment Tensor
2005-10-19 02:33:28.310	73.037	34.751	5	5.5	Mw	ISC (NEIC)	140	53	92	Centroid Moment Tensor
2005-10-19 03:16:26.200	73.14	34.78	12	5.4	Mw	GCMT	110	47	78	Centroid Moment Tensor
2005-10-19 12:47:32.600	72.73	34.98	12	5.1	Mw	GCMT	165	63	110	Centroid Moment Tensor
2005-10-21 08:04:02.400	67.29	32.03	15	5	Mw	GCMT	212	80	-16	Centroid Moment Tensor
2005-10-23 15:04:20.890	73.042	34.854	10	5.2	Mw	ISC (NEIC)	172	49	115	Centroid Moment Tensor
2005-10-23 19:28:27.300	73.11	34.75	12	4.8	Mw	GCMT	75	62	70	Centroid Moment Tensor
2005-10-24 13:14:14.900	73.18	34.76	16.9	4.8	Mw	GCMT	68	43	54	Centroid Moment Tensor
2005-10-26 01:42:44.500	73.85	34.11	21.9	4.8	Mw	GCMT	140	70	115	Centroid Moment Tensor
2005-10-28 21:34:14.540	73.196	34.661	10	5.2	Mw	ISC (NEIC)	156	43	85	Centroid Moment Tensor
2005-10-29 16:52:54.200	89.14	34.01	31.3	4.8	Mw	GCMT	241	58	-35	Centroid Moment Tensor
2005-10-31 05:51:18.600	81.28	29.39	47	4.7	Mw	GCMT	8	52	176	Centroid Moment Tensor
2005-10-31 10:34:05.000	92.68	17.58	19.1	4.7	Mw	GCMT	5	50	-127	Centroid Moment Tensor
2005-10-31 21:47:59.500	84.88	28.38	22.5	4.7	Mw	GCMT	120	42	97	Centroid Moment Tensor

2005-11-20 05:35:06.300	73.12	34.68	20.5	4.8	Mw	GCMT	144	50	76	Centroid Moment Tensor
2005-11-21 08:26:11.920	73.126	34.65	10	5.1	Mw	ISC (NEIC)	129	35	118	Centroid Moment Tensor
2005-12-01 15:38:27	73.14	34.79	13.2	5	Mb	WSM2016	103	41	102	Centroid Moment Tensor
2005-12-14 07:09:54.900	78.83	30.12	34.2	5.1	Mw	GCMT	117	67	92	Centroid Moment Tensor
2005-12-25 08:02:10.300	73.2	34.65	15.2	5.2	Mw	GCMT	5	10	170	Centroid Moment Tensor
2005-12-28 22:04:36.600	73.15	34.84	28.6	5.1	Mw	GCMT	12	71	-174	Centroid Moment Tensor
2005-12-29 07:20:57.400	96.29	24.74	18.5	5.1	Mw	GCMT	104	72	-1	Centroid Moment Tensor
2006-01-06 04:25:06	95.2	12.06	12	5.5	Mb	WSM2016	15	50	-140	Centroid Moment Tensor
2006-01-18 00:23:52.900	87.82	34.47	12	4.9	Mw	GCMT	210	70	-62	Centroid Moment Tensor
2006-01-21 04:07:03.710	93.245	13.002	44	5.6	Mw	ISC (NEIC)	51	40	120	Centroid Moment Tensor
2006-02-01 22:24:16	80.31	30.06	30.7	4.9	Mb	WSM2016	157	54	-141	Centroid Moment Tensor
2006-02-02 21:49:03.700	73.18	34.83	18.8	4.9	Mw	GCMT	160	42	120	Centroid Moment Tensor
2006-02-03 01:57:47	86.7	26.94	30.9	5	Mb	WSM2016	278	30	90	Centroid Moment Tensor
2006-02-05 13:40:33	91.75	11.03	15.8	4.9	Mb	WSM2016	359	35	-101	Centroid Moment Tensor
2006-02-08 12:57:28	72.99	34.75	33.1	4.9	Mb	WSM2016	306	33	90	Centroid Moment Tensor
2006-02-14 00:55:28.800	88.64	27.22	19.2	5.3	Mw	GCMT	68	68	73	Centroid Moment Tensor
2006-02-14 19:17:28	80.2	30.3	38.6	4.3	NaN	WSM2016	262	28	90	NaN
2006-02-15 01:55:06.900	81.47	33.7	30.5	4.8	Mw	GCMT	210	50	-49	Centroid Moment Tensor
2006-02-21 15:10:22.500	95.13	31.75	14.5	4.9	Mw	GCMT	70	36	-13	Centroid Moment Tensor
2006-02-23 20:04:53.550	91.705	26.912	10	5.8	Mw	ISC (NEIC)	225	87	-4	Centroid Moment Tensor

2006-02-26 02:13:50.400	89.598	35.28	10	5.4	Mw	ISC (NEIC)	29	65	-82	Centroid Moment Tensor
2006-03-07 18:20:46	70.77	23.72	12	5.2	Mb	WSM2016	224	76	0	Centroid Moment Tensor
2006-03-09 14:48:55	94.48	10.79	12	5.1	Mb	WSM2016	86	34	-71	Centroid Moment Tensor
2006-03-09 15:03:13	94.55	10.87	17.1	5.1	Mb	WSM2016	57	36	-109	Centroid Moment Tensor
2006-03-09 15:12:03	94.51	10.78	12	5.2	Mb	WSM2016	89	35	-59	Centroid Moment Tensor
2006-03-09 15:19:15	94.68	10.89	12	5.1	Mb	WSM2016	60	32	-111	Centroid Moment Tensor
2006-03-09 15:46:52	94.49	10.81	12	4.9	Mb	WSM2016	83	35	-78	Centroid Moment Tensor
2006-03-09 17:09:11	94.47	10.83	18.2	4.9	Mb	WSM2016	70	35	-79	Centroid Moment Tensor
2006-03-09 18:21:52	94.69	10.82	12	5.1	Mb	WSM2016	83	39	-79	Centroid Moment Tensor
2006-03-09 18:26:27	94.51	10.79	12	5	Mb	WSM2016	110	27	-41	Centroid Moment Tensor
2006-03-09 19:15:44	94.55	10.79	12.1	5	Mb	WSM2016	72	39	-90	Centroid Moment Tensor
2006-03-09 20:25:46	94.52	10.79	12	4.9	Mb	WSM2016	60	27	-115	Centroid Moment Tensor
2006-03-09 21:18:55	94.66	10.86	12	4.9	Mb	WSM2016	79	30	-79	Centroid Moment Tensor
2006-03-09 21:37:01	94.49	10.76	12	5.1	Mb	WSM2016	64	36	-109	Centroid Moment Tensor
2006-03-09 22:30:47	94.46	10.75	12	5	Mb	WSM2016	76	32	-90	Centroid Moment Tensor
2006-03-10 01:13:41	94.67	10.72	18.1	4.9	Mb	WSM2016	267	27	-61	Centroid Moment Tensor
2006-03-10 04:05:43	94.37	10.73	12	5.2	Mb	WSM2016	66	34	-90	Centroid Moment Tensor
2006-03-10 04:43:34	94.35	10.64	12	5.2	Mb	WSM2016	59	34	-90	Centroid Moment Tensor
2006-03-10 05:06:09	94.41	10.69	12	4.9	Mb	WSM2016	41	33	-120	Centroid Moment Tensor
2006-03-10 07:50:14	73.89	33.13	10	4.9	Mb	Ali & Shanker, 2017	246	21	61	Catalog collection

2006-03-10 12:03:58	94.53	10.79	12	5	Mb	WSM2016	70	29	-90	Centroid Moment Tensor
2006-03-11 11:48:52	94.4	10.69	12	5	Mb	WSM2016	40	45	-106	Centroid Moment Tensor
2006-03-12 22:59:21	93.6	13.94	36.7	5.1	Mb	WSM2016	22	36	133	Centroid Moment Tensor
2006-03-16 13:59:23.800	94.45	10.75	12	5.4	Mw	GCMT	71	34	-91	Centroid Moment Tensor
2006-03-19 02:49:00	73.2	34.62	13.5	4.9	Mb	Ali & Shanker, 2017	319	35	91	Catalog collection
2006-03-19 19:12:16.200	94.52	10.78	12	4.9	Mw	GCMT	78	33	-84	Centroid Moment Tensor
2006-03-19 21:57:16.600	94.46	10.77	12	5	Mw	GCMT	86	35	-80	Centroid Moment Tensor
2006-03-20 17:40:44.810	73.747	34.756	12	5.2	Mw	ISC (NEIC)	62	46	97	Centroid Moment Tensor
2006-03-21 06:52:07.700	68.27	29.28	12	5.1	Mw	GCMT	95	66	72	Centroid Moment Tensor
2006-03-21 07:08:13	67.94	29.28	18.8	4.9	Mb	WSM2016	270	22	43	Centroid Moment Tensor
2006-03-25 20:13:36.700	93.91	23.33	46	5.1	Mw	GCMT	51	86	-14	Centroid Moment Tensor
2006-03-29 23:38:54.800	95.62	35.53	24.3	5.3	Mw	GCMT	204	79	163	Centroid Moment Tensor
2006-04-04 09:12:22.500	73.22	34.52	12	4.6	Mw	GCMT	98	44	57	Centroid Moment Tensor
2006-04-04 09:12:23	73.14	34.6	10	4.6	Mb	Ali & Shanker, 2017	320	54	117	Catalog collection
2006-04-06 12:02:55	70.64	23.68	12	4.9	Mb	WSM2016	246	31	49	Centroid Moment Tensor
2006-04-06 17:59:16	70.35	23.25	30.2	5.5	Mb	WSM2016	238	67	7	Centroid Moment Tensor
2006-04-14 09:27:40.100	89.669	35.314	10	5.6	Mw	ISC (NEIC)	52	44	-92	Centroid Moment Tensor
2006-04-14 10:26:15.000	92.9	9.6	62.4	5	Mw	GCMT	9	41	124	Centroid Moment Tensor
2006-04-19 21:05:43.600	90.67	31.61	23.2	5.7	Mw	GCMT	235	89	-10	Centroid Moment Tensor
2006-04-28 18:01:28.500	80.62	41.74	20.8	4.9	Mw	GCMT	72	53	90	Centroid Moment Tensor

2006-05-11 00:00:00	94.27	23.359	31	5.7	Mb	Kumar et al., 2015	58	59	124	Centroid Moment Tensor
2006-05-25 06:50:00.600	91.62	10.18	12	4.9	Mw	GCMT	57	67	168	Centroid Moment Tensor
2006-05-30 19:43:47.100	92.04	20.54	21	4.9	Mw	GCMT	63	85	-2	Centroid Moment Tensor
2006-06-08 11:34:58	77.64	40.53	30.2	4.9	Mb	WSM2016	289	35	111	Centroid Moment Tensor
2006-06-23 05:34:08.000	70.26	23.36	20.8	4.8	Mw	GCMT	75	60	72	Centroid Moment Tensor
2006-06-27 15:02:22.000	93.75	8.81	19.5	5	Mw	GCMT	29	71	-20	Centroid Moment Tensor
2006-07-06 03:57:00	71.82	39.13	5	5.8	Mw	Bai et al., 2017	285	59	145	Centroid Moment Tensor
2006-07-17 20:41:56.000	96.4	33.07	22.1	5.2	Mw	GCMT	27	89	-160	Centroid Moment Tensor
2006-07-19 09:53:08.300	96.27	33.06	24.6	5.5	Mw	GCMT	210	86	154	Centroid Moment Tensor
2006-07-23 12:44:34.300	96.17	32.99	27	4.8	Mw	GCMT	11	75	-168	Centroid Moment Tensor
2006-07-29 00:11:51.340	68.828	37.255	34.2	5.4	Mw	ISC (NEIC)	178	42	107	Centroid Moment Tensor
2006-07-29 10:57:15.540	68.808	37.13	10	5.4	Mw	ISC (NEIC)	159	49	87	Centroid Moment Tensor
2006-08-02 10:41:59	95.74	19.08	20.7	5	Mb	WSM2016	4	86	-178	Centroid Moment Tensor
2006-08-06 14:26:19	74.67	37.57	24	5.3	Mb	WSM2016	126	84	-175	Centroid Moment Tensor
2006-08-12 20:46:11	92.86	24.59	32.7	4.9	Mb	WSM2016	256	61	19	Centroid Moment Tensor
2006-08-30 08:05:49.300	77.43	39.47	21.5	4.8	Mw	GCMT	205	88	-12	Centroid Moment Tensor
2006-09-01 20:08:03	89.62	35.35	23.6	4.8	Mb	WSM2016	11	39	-107	Centroid Moment Tensor
2006-09-06 07:51:46	76.87	40.2	31.8	5	Mb	WSM2016	257	37	90	Centroid Moment Tensor
2006-09-11 18:12:22	78.23	35.47	14.9	5.5	Mb	Ali & Shanker, 2017	260	68	-21	Catalog collection
2006-09-27 18:46:06.300	100.18	11.89	16.7	4.7	Mw	GCMT	191	41	-77	Centroid Moment Tensor

2006-09-28 14:39:18.400	95.15	11.79	16.9	5	Mw	GCMT	44	43	-84	Centroid Moment Tensor
2006-10-01 03:25:44	95.23	11.88	12	4.8	Mb	WSM2016	22	39	-117	Centroid Moment Tensor
2006-10-07 21:12:26	100.15	11.78	12	4.9	Mb	WSM2016	171	37	-90	Centroid Moment Tensor
2006-11-03 14:43:10	93.26	21.99	34.5	4.9	Mb	WSM2016	216	70	1	Centroid Moment Tensor
2006-11-08 02:21:27	75.32	42.65	23.8	4.8	Mb	WSM2016	83	40	90	Centroid Moment Tensor
2006-11-10 13:21:24	92.61	24.61	31.8	4.9	Mb	WSM2016	141	46	155	Centroid Moment Tensor
2006-12-22 19:50:44.630	92.361	10.653	24	6.1	Mw	ISC (NEIC)	45	23	154	Centroid Moment Tensor
2006-12-24 01:58:34.400	74.56	39.83	17.3	5	Mw	GCMT	66	54	52	Centroid Moment Tensor
2006-12-25 20:01:00.450	76.163	42.156	11.6	5.8	Mw	ISC (NEIC)	90	15	90	Centroid Moment Tensor
2007-01-07 10:47:06	98.3	22.04	20	4.8	Mb	WSM2016	92	71	-1	Centroid Moment Tensor
2007-01-08 12:48:40	92.3	8.03	12	5.7	Mb	WSM2016	317	32	65	Centroid Moment Tensor
2007-01-08 17:21:00	70.31	39.8	9	6.1	Mw	Bai et al., 2017	187	65	16	Centroid Moment Tensor
2007-01-29 19:48:40.800	93.76	8.37	77.3	5.4	Mw	GCMT	136	60	167	Centroid Moment Tensor
2007-01-31 10:52:37.300	70.04	39.82	19.8	5.2	Mw	GCMT	57	50	117	Centroid Moment Tensor
2007-02-02 22:02:48.800	71.12	39.15	16.6	5.2	Mw	GCMT	75	53	118	Centroid Moment Tensor
2007-02-02 22:32:18.790	91.768	37.688	10	5.3	Mw	ISC (NEIC)	123	57	111	Centroid Moment Tensor
2007-02-11 04:39:18	73	36.79	26.5	4.9	Mb	WSM2016	140	53	-136	Centroid Moment Tensor
2007-02-25 01:49:42.400	90.63	33.1	20.5	5.3	Mw	GCMT	66	67	-19	Centroid Moment Tensor
2007-03-12 12:44:46	69.3	36.52	32.2	4.9	Mb	Ali & Shanker, 2017	225	42	88	Catalog collection
2007-03-15 18:30:08.600	89.49	35.5	18.6	5	Mw	GCMT	41	46	-51	Centroid Moment Tensor

2007-03-16 21:51:22.200	89.5	35.56	16.5	5	Mw	GCMT	41	45	-47	Centroid Moment Tensor
2007-04-01 07:09:00	91.54	9.18	12	4.9	Mb	WSM2016	16	68	176	Centroid Moment Tensor
2007-04-09 16:23:40	89.51	35.5	20.8	4.6	Mb	WSM2016	36	47	-55	Centroid Moment Tensor
2007-04-10 13:56:54	92.59	13.13	18.3	5.5	Mb	WSM2016	239	49	-42	Centroid Moment Tensor
2007-04-15 13:59:32.800	72.62	39.5	17.8	5	Mw	GCMT	93	53	126	Centroid Moment Tensor
2007-04-15 22:20:14.400	74.81	39.6	26.4	4.9	Mw	GCMT	41	89	-19	Centroid Moment Tensor
2007-04-26 05:23:48.100	96.16	15.47	12	4.9	Mw	GCMT	6	72	-167	Centroid Moment Tensor
2007-05-05 08:51:39.090	81.967	34.248	9	5.8	Mw	ISC (NEIC)	45	75	-90	Centroid Moment Tensor
2007-05-05 17:38:21.100	90.03	34.67	24.5	5	Mw	GCMT	77	89	16	Centroid Moment Tensor
2007-05-07 11:59:48	97.95	31.44	14.5	5.6	Mb	WSM2016	210	73	-174	Centroid Moment Tensor
2007-05-16 08:56:14.120	100.732	20.503	9	6.2	Mw	ISC (NEIC)	235	75	-35	Centroid Moment Tensor
2007-05-20 14:18:21.600	88.56	27.23	13.6	4.9	Mw	GCMT	204	58	-4	Centroid Moment Tensor
2007-05-31 23:18:05.100	94.03	8.31	12	5.4	Mw	GCMT	124	63	178	Centroid Moment Tensor
2007-06-02 21:34:58	101.13	23.02	12	5.7	Mb	WSM2016	146	63	156	Centroid Moment Tensor
2007-06-03 02:49:03	101.12	22.93	24.4	4.7	Mb	WSM2016	239	79	10	Centroid Moment Tensor
2007-06-03 12:21:00	75.27	39.4	24	4.1	Ms	WSM2016	245	80	-4	Centroid Moment Tensor
2007-06-06 11:09:29.400	75.36	42.71	28.3	5	Mw	GCMT	89	38	86	Centroid Moment Tensor
2007-06-22 04:51:29.130	68.903	37.296	31.1	5.2	Mw	ISC (NEIC)	59	7	154	Centroid Moment Tensor
2007-06-23 08:17:20.600	100	21.49	16.1	5.6	Mw	GCMT	61	81	8	Centroid Moment Tensor
2007-06-23 08:27:49.200	99.93	21.46	17.6	5.4	Mw	GCMT	237	79	-31	Centroid Moment Tensor

2007-06-29 23:23:57.900	96.79	25.4	14.1	5.2	Mw	GCMT	105	82	-4	Centroid Moment Tensor
2007-07-10 08:03:00	74.5	39.72	22	4.7	Ms	WSM2016	171	71	-178	Centroid Moment Tensor
2007-07-20 10:06:52.040	82.378	42.913	10	5.5	Mw	ISC (NEIC)	65	76	47	Centroid Moment Tensor
2007-07-21 22:44:16.600	70.17	38.98	12.4	5.2	Mw	GCMT	71	63	135	Centroid Moment Tensor
2007-07-22 09:34:34.300	101.37	38.42	24.1	5	Mw	GCMT	159	85	176	Centroid Moment Tensor
2007-07-22 23:02:13	78.25	30.95	24.9	4.9	NaN	WSM2016	304	42	-138	NaN
2007-07-25 23:37:31.520	92.518	7.157	15	6.1	Mw	ISC (NEIC)	184	40	97	Centroid Moment Tensor
2007-07-30 22:42:06.800	95.77	19.06	12	5.6	Mw	GCMT	127	47	79	Centroid Moment Tensor
2007-07-31 02:47:11.900	71.24	39.25	17.5	5	Mw	GCMT	50	41	83	Centroid Moment Tensor
2007-07-31 08:43:42.500	95.79	19.05	13.5	5	Mw	GCMT	138	47	94	Centroid Moment Tensor
2007-08-11 18:39:11	100.03	25.42	7	4.3	Mw	Luo et al., 2016	147	62	-162	Centroid Moment Tensor
2007-08-25 17:03:08.300	94.01	14.31	41.1	5.2	Mw	GCMT	124	81	-32	Centroid Moment Tensor
2007-09-09 02:00:41.900	69.97	30.43	12	5.3	Mw	GCMT	82	88	170	Centroid Moment Tensor
2007-10-10 12:25:33.700	91.64	9.71	12	5.2	Mw	GCMT	17	71	173	Centroid Moment Tensor
2007-10-19 07:19:53.300	66.14	28.38	16.6	5.5	Mw	GCMT	197	86	-2	Centroid Moment Tensor
2007-10-26 06:50:10.100	76.62	35.27	12	5.2	Mw	GCMT	8	80	-156	Centroid Moment Tensor
2007-11-06 09:38:06	70.49	21.04	12	5	Mb	WSM2016	325	65	172	Centroid Moment Tensor
2007-11-07 00:00:00	92.366	22.13	24	5.5	Mb	Kumar et al., 2015	199	27	-75	Centroid Moment Tensor
2007-11-21 19:04:02.100	93.79	7.76	17.8	4.9	Mw	GCMT	60	41	-105	Centroid Moment Tensor
2007-11-25 13:53:48.000	69.72	29.53	12	5.1	Mw	GCMT	67	61	98	Centroid Moment Tensor

2007-12-11 15:56:38	77.48	34.99	15.5	5.1	Mb	Ali & Shanker, 2017	263	53	-13	Catalog collection
2007-12-17 15:30:00	74.62	39.68	8	4.2	Ms	WSM2016	352	44	-80	Centroid Moment Tensor
2007-12-18 00:16:54	103.65	27.18	8	4.1	Mw	Luo et al., 2016	150	82	-13	Centroid Moment Tensor
2007-12-18 05:56:18.600	70.02	30.48	13	4.9	Mw	GCMT	74	88	163	Centroid Moment Tensor
2007-12-26 04:45:32.400	73.05	40.34	24.8	5.1	Mw	GCMT	117	49	106	Centroid Moment Tensor
2007-12-30 09:55:30.700	84.51	36.44	24.4	5	Mw	GCMT	146	90	154	Centroid Moment Tensor
2007-12-31 18:23:38.900	71.97	41.11	19.6	5	Mw	GCMT	94	56	75	Centroid Moment Tensor
2008-01-01 06:32:27.960	72.985	40.288	6	5.5	Mw	ISC (NEIC)	95	52	106	Centroid Moment Tensor
2008-01-09 08:26:00	85.17	32.29	8	6.3	Mw	Bai et al., 2017	206	46	-78	Centroid Moment Tensor
2008-01-12 22:44:47	92.33	22.76	33.8	5	Mb	WSM2016	352	35	102	NaN
2008-01-14 03:21:46.900	85.25	32.33	14.1	4.9	Mw	GCMT	34	45	-67	Centroid Moment Tensor
2008-01-14 13:38:35.990	92.869	10.413	34	5.9	Mw	ISC (NEIC)	161	70	87	Centroid Moment Tensor
2008-01-14 17:49:54	98.57	25.93	7	4	Mw	Luo et al., 2016	71	63	-16	Centroid Moment Tensor
2008-01-16 11:54:44.120	85.158	32.331	9	5.8	Mw	ISC (NEIC)	220	50	-54	Centroid Moment Tensor
2008-01-17 07:09:59.900	85.26	32.42	18.3	4.9	Mw	GCMT	7	31	-115	Centroid Moment Tensor
2008-01-17 23:07:02.500	100.35	38.02	20.7	4.9	Mw	GCMT	134	42	74	Centroid Moment Tensor
2008-01-22 16:23:27	98.95	25.88	4	4.1	Mw	Luo et al., 2016	24	46	-75	Centroid Moment Tensor
2008-01-22 18:43:37.600	85.22	32.31	12.6	5.5	Mw	GCMT	45	35	-60	Centroid Moment Tensor
2008-02-01 21:06:45	104.8	28.3	4	4.5	Mw	Luo et al., 2016	311	60	56	Centroid Moment Tensor
2008-02-18 02:44:45	99.7	25.7	14	4.7	Mw	Luo et al., 2016	37	78	14	Centroid Moment Tensor

2008-02-26 17:49:58	101.92	30.1	5	5	Mw	Luo et al., 2016	72	82	-166	Centroid Moment Tensor
2008-03-20 22:32:58	81.47	35.49	10	6.3	Mb	WSM2016	358	41	-110	NaN
2008-03-21 06:16:07.900	81.65	35.89	29.9	5.2	Mw	GCMT	199	40	-62	Centroid Moment Tensor
2008-03-21 06:33:03	81.44	35.81	21	7.4	Ms	WSM2016	174	16	-158	First Motion
2008-03-21 12:03:00.200	81.43	35.39	19.5	5.2	Mw	GCMT	200	40	-73	Centroid Moment Tensor
2008-03-21 12:37:00.200	97.81	24.54	18.1	5.1	Mw	GCMT	79	89	8	Centroid Moment Tensor
2008-03-21 20:52:17.900	81.16	35.09	27.8	5	Mw	GCMT	222	56	-21	Centroid Moment Tensor
2008-03-22 07:12:03	81.44	35.62	20	5.6	Ms	WSM2016	231	55	-40	First Motion
2008-03-23 08:26:16	81.52	35.67	0	5.8	NaN	WSM2016	106	56	-9	First Motion
2008-03-23 20:56:18.500	81.65	35.86	16.1	5.1	Mw	GCMT	206	47	-46	Centroid Moment Tensor
2008-03-24 04:56:09	81.56	35.81	11	5.2	Mb	WSM2016	246	41	12	First Motion
2008-03-24 07:58:36.700	81.64	35.8	27.5	5.1	Mw	GCMT	131	83	157	Centroid Moment Tensor
2008-03-24 12:03:22	81.62	35.49	0	4.9	NaN	WSM2016	115	59	2	First Motion
2008-03-25 14:16:05	81.52	35.84	0	4.8	NaN	WSM2016	17	77	174	First Motion
2008-03-26 10:39:32.000	81.66	35.85	17.7	5.2	Mw	GCMT	141	80	172	Centroid Moment Tensor
2008-03-26 20:02:58	81.49	35.34	0	5	NaN	WSM2016	259	49	-131	First Motion
2008-03-30 08:32:28.200	101.94	37.91	18.8	5.1	Mw	GCMT	64	75	1	Centroid Moment Tensor
2008-04-10 07:17:20	74.96	39.35	10	4.9	Mb	WSM2016	303	45	120	NaN
2008-04-10 15:17:00	74.8	39.63	8	4.8	Ms	WSM2016	113	43	95	Centroid Moment Tensor
2008-04-17 08:29:07.200	91.77	8.25	12.4	5.1	Mw	GCMT	6	43	-90	Centroid Moment Tensor
2008-04-18 03:01:56.200	81.29	35.28	35.3	5	Mw	GCMT	128	73	177	Centroid Moment Tensor
2008-04-25 12:03:55.500	85.42	32.65	26.6	5	Mw	GCMT	235	84	-30	Centroid Moment Tensor
2008-05-02 15:56:20	101.72	27.4	8	4.5	Mw	Luo et al., 2016	318	60	-124	Centroid Moment Tensor

2008-05-05 20:55:12	104.52	25.95	4	4.1	Mw	Luo et al., 2016	94	90	180	Centroid Moment Tensor
2008-05-06 05:25:33	81.26	35.1	10	4.9	Mb	Ali & Shanker, 2017	190	34	-71	Catalog collection
2008-06-02 21:57:00	74.85	39.58	26	4	Ms	WSM2016	226	82	-4	Centroid Moment Tensor
2008-06-08 17:56:20	92.12	33.17	10	5.2	Mb	WSM2016	154	63	-155	NaN
2008-06-08 18:24:44	85.24	32.45	10	4.9	Mb	WSM2016	353	41	-114	NaN
2008-06-10 10:04:58	91.96	33.18	10	5.5	Mb	WSM2016	159	57	-146	NaN
2008-06-10 11:36:45	92.09	33.24	10	5	Mb	WSM2016	242	53	-27	NaN
2008-06-10 14:15:38	92.09	33.16	10	5.3	Mb	WSM2016	170	47	-131	NaN
2008-06-18 05:23:34.500	91.33	35.31	22.5	5.4	Mw	GCMT	162	90	178	Centroid Moment Tensor
2008-06-18 08:12:18.200	92.21	33.09	18.7	5.2	Mw	GCMT	52	69	-31	Centroid Moment Tensor
2008-06-19 22:36:59.200	92.19	33.13	18.3	4.9	Mw	GCMT	65	67	-16	Centroid Moment Tensor
2008-06-27 11:40:13.990	91.824	11.005	17	6.6	Mw	ISC (NEIC)	35	62	-63	Centroid Moment Tensor
2008-06-27 13:07:14.700	91.95	11.09	12.1	5.9	Mw	GCMT	216	28	-41	Centroid Moment Tensor
2008-06-27 18:05:16.500	91.84	10.8	17.3	5	Mw	GCMT	5	34	-59	Centroid Moment Tensor
2008-06-28 03:26:54.800	92.06	10.95	13.7	5.1	Mw	GCMT	207	28	-55	Centroid Moment Tensor
2008-06-28 04:35:04.000	91.96	10.87	17.2	5	Mw	GCMT	5	67	-96	Centroid Moment Tensor
2008-06-28 12:54:46.360	91.712	10.847	15	6.1	Mw	ISC (NEIC)	2	78	-107	Centroid Moment Tensor
2008-06-28 15:29:13.900	92.1	11	13.2	5.4	Mw	GCMT	206	19	-56	Centroid Moment Tensor
2008-06-29 00:32:16.100	91.87	11.07	14.6	5	Mw	GCMT	237	41	-29	Centroid Moment Tensor
2008-06-29 04:14:38.600	91.96	10.81	12	5.2	Mw	GCMT	216	29	-49	Centroid Moment Tensor
2008-06-29 08:41:59.800	88.2	35.73	34.3	5	Mw	GCMT	71	87	14	Centroid Moment Tensor
2008-06-29 12:47:26.620	88.307	35.658	10	5.4	Mw	ISC (NEIC)	80	88	2	Centroid Moment Tensor

2008-07-02 20:22:57	88.36	35.78	10	4.8	Mb	WSM2016	250	82	-8	NaN
2008-07-07 02:50:39.200	95.34	25.95	70	4.9	Mw	GCMT	137	45	135	Centroid Moment Tensor
2008-07-11 02:03:47	69.58	35.4	31.5	4.8	Mb	Ali & Shanker, 2017	190	43	88	Catalog collection
2008-07-16 22:58:24.300	92.24	33.15	16.6	5.3	Mw	GCMT	61	71	-23	Centroid Moment Tensor
2008-07-18 12:47:06.300	87.26	37.85	20.2	5	Mw	GCMT	137	81	166	Centroid Moment Tensor
2008-07-26 05:35:35.800	91.64	11.61	12	5.1	Mw	GCMT	196	60	102	Centroid Moment Tensor
2008-08-01 01:29:31	71.42	41.56	24.8	4.8	Mb	WSM2016	212	47	68	NaN
2008-08-05 10:08:12	93.58	13.86	35	5.2	Mb	WSM2016	11	39	130	NaN
2008-08-05 21:59:44	91.97	33.12	10	5.2	Mb	WSM2016	49	60	-27	NaN
2008-08-08 21:49:02.000	83.92	31.7	21	4.8	Mw	GCMT	239	75	-21	Centroid Moment Tensor
2008-08-10 08:20:32	91.81	11.04	10	5.7	Mb	WSM2016	49	77	-8	NaN
2008-08-10 09:27:57	91.76	11.02	29.5	5.3	Mb	WSM2016	348	49	-127	NaN
2008-08-10 12:21:12	91.71	10.95	13	5.4	Mb	WSM2016	217	44	-41	NaN
2008-08-10 13:01:32	91.79	10.98	10	5.1	Mb	WSM2016	219	30	-36	NaN
2008-08-10 17:57:24	92.05	33.16	14.1	4.1	Mb	WSM2016	49	49	-52	NaN
2008-08-10 22:53:56	91.93	32.26	10	4.6	Mb	WSM2016	59	71	-9	NaN
2008-08-17 17:58:21	70.263	38.693	4	4	Mw	WSM2016	88	11	0	NaN
2008-08-18 14:11:10.000	91.93	33.65	23.2	5.2	Mw	GCMT	79	88	-6	Centroid Moment Tensor
2008-08-19 21:35:16.500	98.03	25.09	18.7	5	Mw	GCMT	21	42	-117	Centroid Moment Tensor
2008-08-21 12:24:30.930	97.697	25.039	10	6	Mw	ISC (NEIC)	235	85	-10	Centroid Moment Tensor
2008-08-25 13:22:08.500	83.51	30.61	17.3	6.7	Mw	GCMT	30	48	-48	Centroid Moment Tensor
2008-08-25 19:13:56.700	83.48	30.41	19.2	5.1	Mw	GCMT	8	54	-71	Centroid Moment Tensor
2008-08-25 20:40:49.200	83.72	30.85	23.7	5	Mw	GCMT	225	68	-19	Centroid Moment Tensor
2008-08-26 07:46:58.800	91.51	31.69	21.4	4.9	Mw	GCMT	60	89	-8	Centroid Moment Tensor

2008-08-29 09:43:20.200	83.52	30.58	17.9	4.9	Mw	GCMT	171	39	-90	Centroid Moment Tensor
2008-08-30 08:30:53.010	101.889	26.241	11	5.8	Mw	ISC (NEIC)	104	71	179	Centroid Moment Tensor
2008-08-30 12:46:49.700	83.96	42.79	12.8	5.3	Mw	GCMT	50	57	69	Centroid Moment Tensor
2008-08-30 21:31:17.200	83.67	30.73	22.2	5	Mw	GCMT	209	74	-15	Centroid Moment Tensor
2008-08-31 08:31:10.700	101.97	26.232	10	5.3	Mw	ISC (NEIC)	86	76	-177	Centroid Moment Tensor
2008-08-31 17:34:49	101.92	26.18	0	5.2	ML	WSM2016	180	87	0	Centroid Moment Tensor
2008-08-31 19:00:29	101.92	26.19	14	4.7	ML	WSM2016	97	86	177	Centroid Moment Tensor
2008-09-01 04:24:33	68.942	37.417	15	5	Mw	WSM2016	321	40	63	NaN
2008-09-03 06:27:25	97.78	24.87	10	4.8	Mb	WSM2016	276	84	0	NaN
2008-09-04 12:53:11	80.35	30.28	10	5	Mb	Ali & Shanker, 2017	333	59	-163	Catalog collection
2008-09-05 16:24:12	101.93	26.25	16	4.1	ML	WSM2016	11	66	-6	Centroid Moment Tensor
2008-09-10 01:14:31	83.59	30.78	10	5.3	Mb	Ali & Shanker, 2017	206	77	-12	Catalog collection
2008-09-10 01:28:06	83.4	30.8	7.3	5.4	Mb	Ali & Shanker, 2017	317	68	-163	Catalog collection
2008-09-11 17:27:55	72.696	39.264	15	4	Mw	WSM2016	77	36	128	NaN
2008-09-18 20:32:50.100	91.83	10.97	27	5	Mw	GCMT	36	49	-55	Centroid Moment Tensor
2008-09-22 13:30:37.500	96.15	15.46	12	5.2	Mw	GCMT	33	39	-121	Centroid Moment Tensor
2008-09-25 01:47:11.190	83.487	30.836	4	5.9	Mw	ISC (NEIC)	206	75	-5	Centroid Moment Tensor
2008-09-25 20:17:30.300	83.71	30.72	23.2	4.9	Mw	GCMT	204	62	-12	Centroid Moment Tensor
2008-09-30 09:16:37	101.92	26.23	13	4.6	ML	WSM2016	100	73	0	Centroid Moment Tensor
2008-10-03 21:20:24	91.66	10.76	21.6	5.5	Mb	WSM2016	206	48	-57	NaN
2008-10-05 15:52:00	73.82	39.53	4	6.4	Mw	Bai et al., 2017	246	38	102	Centroid Moment Tensor
2008-10-05 16:11:05	73.871	39.517	9	5.4	Mw	WSM2016	79	47	128	NaN
2008-10-05 18:27:36	73.768	39.455	9	4.7	Mw	WSM2016	57	30	90	NaN

2008-10-05 18:34:32	73.829	39.517	9	4	Mw	WSM2016	288	40	117	NaN
2008-10-05 21:46:00	73.981	39.634	6	4.5	Mw	WSM2016	278	44	124	NaN
2008-10-05 22:56:00	69.47	33.89	31	5.8	Mw	Bai et al., 2017	218	80	10	Centroid Moment Tensor
2008-10-06 00:11:00	73.67	39.4	40	6	Ms	WSM2016	77	30	171	Centroid Moment Tensor
2008-10-06 02:27:00	73.64	39.44	28	5.1	Ms	WSM2016	78	36	120	Centroid Moment Tensor
2008-10-06 05:45:00	73.71	39.67	9	4.6	Ms	WSM2016	290	47	138	Centroid Moment Tensor
2008-10-06 07:50:26	73.872	39.538	4	4.4	Mw	WSM2016	140	26	176	NaN
2008-10-06 08:30:00	90.35	29.81	4	6.3	Mw	Bai et al., 2017	44	48	-75	Centroid Moment Tensor
2008-10-06 12:10:33	90.32	29.65	10	5.4	Mb	WSM2016	173	43	-122	NaN
2008-10-06 15:50:00	73.74	39.46	10	4.7	Ms	WSM2016	134	42	161	Centroid Moment Tensor
2008-10-07 15:06:41	73.93	39.609	4	4	Mw	WSM2016	50	37	64	NaN
2008-10-07 23:13:15	73.783	39.508	4	4	Mw	WSM2016	36	42	52	NaN
2008-10-08 07:13:00	73.37	39.52	10	4.1	Ms	WSM2016	219	45	84	Centroid Moment Tensor
2008-10-08 14:07:16	90.31	29.74	10	5.6	Mb	WSM2016	69	62	-25	NaN
2008-10-08 23:31:15	73.818	39.525	9	4.1	Mw	WSM2016	269	25	111	NaN
2008-10-09 03:13:41	73.925	39.518	9	4.4	Mw	WSM2016	216	41	-14	NaN
2008-10-09 14:43:18	73.962	39.612	6	4.3	Mw	WSM2016	235	45	124	NaN
2008-10-10 17:39:05	73.956	39.583	6	4	Mw	WSM2016	120	58	157	NaN
2008-10-11 02:01:43	73.926	39.602	4	4	Mw	WSM2016	49	38	61	NaN
2008-10-12 17:02:31	73.947	39.578	4	4	Mw	WSM2016	323	44	-166	NaN
2008-10-13 09:23:34.500	73.88	39.54	21.1	5.1	Mw	GCMT	128	88	162	Centroid Moment Tensor
2008-10-13 16:05:24.900	73.69	39.5	12	5.2	Mw	GCMT	92	72	126	Centroid Moment Tensor
2008-10-13 17:16:14.400	70.1	38.8	22.3	5.2	Mw	GCMT	47	28	128	Centroid Moment Tensor
2008-10-14 00:05:00	73.74	39.44	9	5.4	Ms	WSM2016	217	47	51	Centroid Moment Tensor

2008-10-18 09:28:58	73.799	39.512	6	4.4	Mw	WSM2016	312	19	152	NaN
2008-10-20 14:26:35.000	91.32	35.26	22.9	5	Mw	GCMT	251	87	-4	Centroid Moment Tensor
2008-10-20 15:08:49.000	92.8	33.69	21.3	4.8	Mw	GCMT	95	89	-4	Centroid Moment Tensor
2008-10-23 05:50:47.100	73.73	39.52	20	4.8	Mw	GCMT	76	44	109	Centroid Moment Tensor
2008-10-25 10:13:57	101.91	26.25	15	4.3	ML	WSM2016	95	54	171	Centroid Moment Tensor
2008-10-28 22:33:12.900	67.43	30.47	16.6	5.3	Mw	GCMT	128	70	151	Centroid Moment Tensor
2008-10-28 23:09:57.650	67.351	30.639	15	6.4	Mw	ISC (NEIC)	51	64	34	Centroid Moment Tensor
2008-10-29 11:32:48.600	67.57	30.29	12	6.4	Mw	GCMT	233	88	-22	Centroid Moment Tensor
2008-10-30 10:44:57	73.469	39.62	9	4.3	Mw	WSM2016	309	78	176	NaN
2008-11-03 16:08:14	67.67	30.4	10	4.9	Mb	Ali & Shanker, 2017	285	43	108	Catalog collection
2008-11-04 14:22:22	74.018	39.591	9	4.4	Mw	WSM2016	251	40	122	NaN
2008-11-06 14:23:52	74.02	39.48	35	4.8	Mb	WSM2016	259	29	134	NaN
2008-11-07 09:21:14	74.035	39.569	4	4	Mw	WSM2016	355	23	19	NaN
2008-11-08 01:30:41	74.017	39.6	9	4.1	Mw	WSM2016	228	44	90	NaN
2008-11-08 04:04:22	69.017	38.447	6	4.2	Mw	WSM2016	333	49	173	NaN
2008-11-09 19:22:45	73.832	39.506	6	4	Mw	WSM2016	83	43	117	NaN
2008-11-10 01:22:00	95.83	37.56	17	6	Mw	Bai et al., 2017	252	28	63	Centroid Moment Tensor
2008-11-10 03:22:00	73.64	39.51	27	4	Ms	WSM2016	79	43	98	Centroid Moment Tensor
2008-11-11 21:56:04.600	95.82	37.52	23.9	5.1	Mw	GCMT	104	76	51	Centroid Moment Tensor
2008-11-13 20:52:04	74.04	39.601	9	4.2	Mw	WSM2016	248	41	113	NaN
2008-11-15 15:21:11.500	67.56	30.31	19.6	4.8	Mw	GCMT	28	78	-10	Centroid Moment Tensor
2008-11-16 12:20:38.800	91.82	10.88	12	5.5	Mw	GCMT	216	49	-55	Centroid Moment Tensor
2008-11-19 17:14:20.600	93.76	8.76	18.9	5.2	Mw	GCMT	199	48	-72	Centroid Moment Tensor

2008-11-27 15:49:47	74.042	39.602	9	4.1	Mw	WSM2016	257	43	114	NaN
2008-12-05 23:24:37	94.08	8.74	28.3	5.2	Mb	WSM2016	161	55	-160	NaN
2008-12-06 00:43:09	93.98	8.72	38.2	5.3	Mb	WSM2016	156	60	-168	NaN
2008-12-08 08:59:11	82.05	29.95	35.6	5.3	Mb	Ali & Shanker, 2017	230	62	-17	Catalog collection
2008-12-09 02:46:32	67.56	30.34	10	5.2	Mb	Ali & Shanker, 2017	333	83	169	Catalog collection
2008-12-09 05:53:43	67.45	30.39	10	5.3	Mb	Ali & Shanker, 2017	330	80	163	Catalog collection
2008-12-11 13:16:13	81.37	35.27	33.3	4.9	Mb	Ali & Shanker, 2017	209	46	-66	Catalog collection
2008-12-20 23:22:51.200	96.09	22.65	14.8	5.3	Mw	GCMT	90	82	11	Centroid Moment Tensor
2008-12-25 20:20:49.900	97.86	23.97	17.3	4.8	Mw	GCMT	84	84	14	Centroid Moment Tensor
2009-01-09 12:40:14.8	78.269	31.87	9.9	4	ML	Yadav et al., 2017	48	56	-22	First Motion
2009-01-17 20:08:17	73.478	39.623	6	4.5	Mw	WSM2016	308	73	179	NaN
2009-01-18 04:08:00	73.32	39.56	6	4.7	Ms	WSM2016	310	64	168	Centroid Moment Tensor
2009-01-21 01:42:22.500	96.11	15.49	19.3	5	Mw	GCMT	12	83	176	Centroid Moment Tensor
2009-01-25 21:16:24.400	72.04	38.67	29.4	5	Mw	GCMT	200	89	-24	Centroid Moment Tensor
2009-01-28 20:29:56.900	92.75	13.62	18.5	5.1	Mw	GCMT	16	78	-132	Centroid Moment Tensor
2009-01-31 04:27:37.900	95.08	11.73	12	5.1	Mw	GCMT	18	60	-126	Centroid Moment Tensor
2009-02-02 08:36:49.000	66.37	26.98	21.3	5.1	Mw	GCMT	189	81	-6	Centroid Moment Tensor
2009-02-02 08:36:51	66.32	27.23	35	5.1	Mb	Ali & Shanker, 2017	189	81	-6	Catalog collection
2009-02-16 23:13:53	75.57	38.809	15	4.2	Mw	WSM2016	237	18	164	NaN
2009-02-18 10:11:43	83.86	30.67	35	5.1	Mb	Ali & Shanker, 2017	206	68	3	Catalog collection
2009-02-20 03:48:48.520	73.9	34.203	12	5.4	Mw	ISC (NEIC)	140	65	99	Centroid Moment Tensor
2009-02-20 10:02:32.100	78.63	40.74	16.6	5.2	Mw	GCMT	81	54	89	Centroid Moment Tensor
2009-02-28 08:43:42.500	81.39	35.57	22.5	4.8	Mw	GCMT	219	54	-51	Centroid Moment Tensor
2009-03-01 00:05:20	72.161	38.559	6	4.1	Mw	WSM2016	2	54	-35	NaN

2009-03-03 14:22:15.900	71.38	38.39	19.7	5.1	Mw	GCMT	230	64	-21	Centroid Moment Tensor
2009-03-05 15:49:53	95.99	15.58	7.9	5.2	Mb	WSM2016	33	34	-121	NaN
2009-03-11 12:58:43	91.69	10.67	10	5	Mb	WSM2016	215	21	-45	NaN
2009-03-17 23:14:48.800	67.42	25.84	12	5	Mw	GCMT	12	47	75	Centroid Moment Tensor
2009-04-01 02:34:36	82.44	33.66	10	5	Mb	Ali & Shanker, 2017	342	46	-119	Catalog collection
2009-04-09 01:46:58	70.75	27.14	44.3	5.1	Mb	Ali & Shanker, 2017	243	89	30	Catalog collection
2009-04-16 21:27:52.900	70.11	34.14	12	5.2	Mw	GCMT	63	61	103	Centroid Moment Tensor
2009-04-19 04:08:20.200	78.32	41.29	25.9	5.4	Mw	GCMT	127	90	177	Centroid Moment Tensor
2009-04-19 12:08:00	78.3	41.3	30	5.5	Ms	WSM2016	40	80	-1	Centroid Moment Tensor
2009-04-22 09:26:06.000	77.27	40.21	15.9	5	Mw	GCMT	38	51	57	Centroid Moment Tensor
2009-04-26 23:54:15.800	72.62	41.06	36.2	4.9	Mw	GCMT	11	28	63	Centroid Moment Tensor
2009-04-27 20:04:15.700	72.35	42.9	19.9	5	Mw	GCMT	98	50	117	Centroid Moment Tensor
2009-04-29 18:53:11.800	71.26	41.62	19.7	4.8	Mw	GCMT	54	49	97	Centroid Moment Tensor
2009-05-10 17:34:05	67.567	38.197	12	4.8	Mw	WSM2016	193	34	90	NaN
2009-05-25 15:18:53	70.563	38.871	6	4.4	Mw	WSM2016	65	14	139	NaN
2009-05-25 23:27:03	73.728	39.521	4	4	Mw	WSM2016	280	17	90	NaN
2009-06-04 02:54:48	81.76	32.78	7.2	5	Mb	Ali & Shanker, 2017	211	70	-13	Catalog collection
2009-06-06 09:44:42.400	86.43	30.99	31.9	4.9	Mw	GCMT	218	76	-9	Centroid Moment Tensor
2009-06-15 12:05:27.300	93.8	9.12	12	5.2	Mw	GCMT	208	40	-61	Centroid Moment Tensor
2009-06-17 09:22:16	69.809	38.12	4	4.3	Mw	WSM2016	85	20	178	NaN
2009-06-21 04:46:28.200	90.31	36.05	18.2	4.9	Mw	GCMT	259	85	-5	Centroid Moment Tensor
2009-06-22 23:10:06.200	95.12	12.11	12	5.2	Mw	GCMT	45	35	-95	Centroid Moment Tensor
2009-06-22 23:16:33.200	95.16	12.19	12	5.1	Mw	GCMT	9	54	-140	Centroid Moment Tensor

2009-07-01 00:29:27	73.45	39.59	39.9	5	Mb	WSM2016	35	84	1	NaN
2009-07-09 11:19:16	101.1	25.63	7	5.5	Mb	WSM2016	204	84	-3	NaN
2009-07-10 09:02:04	101.03	25.67	10	5	Mb	WSM2016	21	83	4	NaN
2009-07-24 03:11:56.830	85.902	31.158	13.4	5.5	Mw	ISC (NEIC)	231	84	-14	Centroid Moment Tensor
2009-07-24 11:11:00	86.1	31.3	13	5.6	Ms	WSM2016	333	74	-177	Centroid Moment Tensor
2009-07-26 07:12:08.500	94.57	10.82	12	5	Mw	GCMT	85	38	-69	Centroid Moment Tensor
2009-07-26 07:40:18.600	94.53	10.8	12	5.1	Mw	GCMT	64	32	-99	Centroid Moment Tensor
2009-07-26 08:11:21.700	94.53	10.82	12	5.2	Mw	GCMT	64	29	-96	Centroid Moment Tensor
2009-07-26 08:41:01.400	94.54	10.81	12	5.1	Mw	GCMT	71	34	-93	Centroid Moment Tensor
2009-07-26 09:06:50.200	94.68	10.83	12	5	Mw	GCMT	51	42	-125	Centroid Moment Tensor
2009-07-26 09:40:30.500	94.47	10.79	12	5.1	Mw	GCMT	70	31	-94	Centroid Moment Tensor
2009-07-26 10:14:17.800	94.51	10.78	12	5	Mw	GCMT	65	30	-103	Centroid Moment Tensor
2009-07-26 10:58:05.700	94.52	10.78	12	5.1	Mw	GCMT	65	34	-103	Centroid Moment Tensor
2009-07-26 11:55:51.100	94.53	10.77	12	5.1	Mw	GCMT	60	37	-103	Centroid Moment Tensor
2009-07-26 12:25:55.300	94.39	10.74	12	4.9	Mw	GCMT	77	31	-63	Centroid Moment Tensor
2009-07-26 12:34:37.400	94.58	10.8	13.5	4.8	Mw	GCMT	81	41	-83	Centroid Moment Tensor
2009-07-26 12:48:40.500	94.53	10.76	12	5	Mw	GCMT	64	41	-99	Centroid Moment Tensor
2009-07-26 13:29:20.700	94.55	10.82	12	5	Mw	GCMT	55	29	-112	Centroid Moment Tensor
2009-07-26 13:49:00.300	94.53	10.79	12	4.9	Mw	GCMT	62	40	-100	Centroid Moment Tensor
2009-07-26 14:58:20.900	94.55	10.83	12	5	Mw	GCMT	59	28	-103	Centroid Moment Tensor
2009-07-26 15:27:01.200	94.48	10.76	12	5	Mw	GCMT	65	36	-99	Centroid Moment Tensor

2009-07-26 15:51:07.700	94.44	10.8	12	5	Mw	GCMT	67	26	-97	Centroid Moment Tensor
2009-07-26 17:47:58.900	94.41	10.76	12	5	Mw	GCMT	68	30	-93	Centroid Moment Tensor
2009-07-26 21:49:25.700	94.46	10.76	12	5.1	Mw	GCMT	66	38	-96	Centroid Moment Tensor
2009-07-27 02:09:18.800	94.29	10.64	12	4.9	Mw	GCMT	62	39	-70	Centroid Moment Tensor
2009-07-27 03:32:02.200	94.42	10.71	12	4.9	Mw	GCMT	56	37	-104	Centroid Moment Tensor
2009-07-27 06:23:52.800	73.01	34.93	25.9	5	Mw	GCMT	113	65	67	Centroid Moment Tensor
2009-07-27 21:15:05.900	94.32	10.71	12	5	Mw	GCMT	85	40	-65	Centroid Moment Tensor
2009-07-28 03:17:50	74.028	39.61	9	4.3	Mw	WSM2016	246	41	125	NaN
2009-07-28 05:15:00.400	94.23	10.64	12	5.2	Mw	GCMT	55	40	-93	Centroid Moment Tensor
2009-07-28 19:14:10.500	94.23	10.61	12	5	Mw	GCMT	39	43	-95	Centroid Moment Tensor
2009-08-09 04:02:07	81.65	35.58	10	5.1	Mb	Ali & Shanker, 2017	226	43	-8	Catalog collection
2009-08-10 19:55:36	92.89	14.1	4.7	6.9	Mb	WSM2016	39	36	-90	NaN
2009-08-13 09:21:35.750	92.821	14.052	35	5.8	Mw	ISC (NEIC)	259	77	-5	Centroid Moment Tensor
2009-08-14 19:39:52.800	93.02	14.08	19.7	5	Mw	GCMT	9	33	-124	Centroid Moment Tensor
2009-08-19 10:44:44.10	92.3	26.49	10	5.1	Mw	Kayal et al., 2012	342	80	-175	Centroid Moment Tensor
2009-08-19 14:57:24.10	92.38	26.67	10	4.9	Mw	Kayal et al., 2012	200	40	-120	Centroid Moment Tensor
2009-08-26 07:26:42.000	70.5	39.09	22.4	4.8	Mw	GCMT	83	79	178	Centroid Moment Tensor
2009-08-27 04:06:10	73.957	39.577	4	4.1	Mw	WSM2016	225	50	34	NaN
2009-08-28 01:52:12.700	95.76	37.64	12	6.3	Mw	GCMT	101	60	83	Centroid Moment Tensor
2009-08-28 09:52:00	95.8	37.6	10	6.4	Ms	WSM2016	266	18	57	Centroid Moment Tensor
2009-08-28 10:14:00	95.8	37.6	6	5.3	Ms	WSM2016	271	48	-31	Centroid Moment Tensor

2009-08-28 16:28:43.800	95.76	37.75	17	5	Mw	GCMT	56	80	-3	Centroid Moment Tensor
2009-08-29 00:28:00	95.8	37.7	10	5	Ms	WSM2016	261	19	25	Centroid Moment Tensor
2009-08-30 17:15:52.700	95.57	37.66	16.8	5.4	Mw	GCMT	55	51	64	Centroid Moment Tensor
2009-08-30 19:27:51.100	95.06	25.13	78	5.3	Mw	GCMT	150	65	138	Centroid Moment Tensor
2009-08-31 01:15:00	95.7	37.7	10	5	Ms	WSM2016	99	27	151	Centroid Moment Tensor
2009-08-31 10:15:29.770	95.831	37.606	6	5.7	Mw	ISC (NEIC)	110	65	90	Centroid Moment Tensor
2009-08-31 22:27:54.000	95.93	37.62	12	4.8	Mw	GCMT	107	45	94	Centroid Moment Tensor
2009-09-01 03:10:54	73.668	39.401	9	4.1	Mw	WSM2016	272	51	140	NaN
2009-09-10 00:20:12	95.91	37.65	10	5.2	Mb	WSM2016	281	35	98	NaN
2009-09-21 00:00:00	94.862	20.384	67	5.5	Mb	Kumar et al., 2015	304	79	-65	Centroid Moment Tensor
2009-09-21 08:53:05.910	91.437	27.332	14	6.1	Mw	ISC (NEIC)	12	4	-173	Centroid Moment Tensor
2009-09-28 02:43:25.600	95.9	35.82	24.4	4.8	Mw	GCMT	178	61	178	Centroid Moment Tensor
2009-09-29 06:01:18.800	83.55	30.56	21.1	5	Mw	GCMT	36	56	-31	Centroid Moment Tensor
2009-10-02 13:49:10	96.07	39.49	10	5.1	Mb	WSM2016	194	81	0	NaN
2009-10-13 12:47:20.400	70.71	38.76	19.6	5	Mw	GCMT	47	86	3	Centroid Moment Tensor
2009-10-16 02:56:39.700	77.03	39.9	18.8	5	Mw	GCMT	74	62	75	Centroid Moment Tensor
2009-10-16 19:29:15.000	92.34	35.17	20.6	4.9	Mw	GCMT	40	89	11	Centroid Moment Tensor
2009-10-20 06:14:59	72.962	39.411	1.5	4.3	ML	WSM2016	280	66	-175	NaN
2009-10-25 11:40:52.000	80.25	34.94	17.6	5	Mw	GCMT	84	88	28	Centroid Moment Tensor
2009-10-29 17:00:40.200	91.62	27.2	15.1	5.1	Mw	GCMT	96	83	88	Centroid Moment Tensor
2009-11-01 21:07:21	100.82	25.96	24.5	5	Mb	WSM2016	286	84	0	NaN

2009-11-02 05:07:00	100.7	26	10	5	Ms	WSM2016	192	84	0	Centroid Moment Tensor
2009-11-02 21:35:44	92.97	14.03	15.7	5.5	Mb	WSM2016	239	19	-68	NaN
2009-11-04 21:56:09	95.76	37.65	3	5.6	Mb	WSM2016	313	51	151	NaN
2009-11-05 05:56:00	95.8	37.6	5	5.1	Ms	WSM2016	342	21	135	Centroid Moment Tensor
2009-11-07 20:08:46	86.01	29.49	5.7	5.7	Mb	WSM2016	178	43	-90	NaN
2009-11-08 02:11:12	69.65	38.528	4	4.4	Mw	WSM2016	335	48	18	NaN
2009-11-08 04:08:00	86.1	29.4	10	5.6	Ms	WSM2016	139	79	-173	Centroid Moment Tensor
2009-11-10 02:48:47	91.9	8.08	23	6.1	Mb	WSM2016	124	76	170	NaN
2009-11-12 15:17:01	69.648	38.512	9	4	Mw	WSM2016	329	69	6	NaN
2009-11-14 13:03:36.200	73.74	17.1	12	4.8	Mw	GCMT	181	47	-67	Centroid Moment Tensor
2009-11-15 01:56:20	72.829	39.398	6	4.5	Mw	WSM2016	84	66	165	NaN
2009-11-20 07:17:01.800	83.71	30.6	18.9	5	Mw	GCMT	115	46	-136	Centroid Moment Tensor
2009-11-26 00:15:03.500	81.38	35.39	25.8	4.9	Mw	GCMT	222	49	-4	Centroid Moment Tensor
2009-11-26 06:13:03.000	92.8	13.58	29	5.1	Mw	GCMT	258	77	-24	Centroid Moment Tensor
2009-12-01 11:40:46	92.79	13.62	33.6	5.4	Mb	WSM2016	252	73	-17	NaN
2009-12-06 04:33:16	77.35	35.78	72.2	5.2	Mb	Ali & Shanker, 2017	348	19	158	Catalog collection
2009-12-12 11:51:25.100	73.74	17.02	12	4.8	Mw	GCMT	163	43	-79	Centroid Moment Tensor
2009-12-12 16:22:10.500	66.56	28.28	17.8	4.8	Mw	GCMT	198	66	-11	Centroid Moment Tensor
2009-12-13 14:41:56.600	91.74	21.87	12	4.9	Mw	GCMT	160	51	87	Centroid Moment Tensor
2009-12-14 00:03:00	94.5	41.9	5	5.1	Ms	WSM2016	150	15	120	Centroid Moment Tensor
2009-12-21 05:15:13.600	96.68	37.57	22.1	5	Mw	GCMT	122	43	112	Centroid Moment Tensor
2009-12-21 13:15:00	96.7	37.5	6	5	Ms	WSM2016	140	68	164	Centroid Moment Tensor
2010-01-01 02:22:27.100	83.91	30.43	16.4	5.2	Mw	GCMT	114	81	161	Centroid Moment Tensor

2010-01-02 02:15:05	71.456	38.274	6	5.3	Mw	WSM2016	228	54	-38	NaN
2010-01-16 05:44:28.200	88.25	35.66	25.8	4.9	Mw	GCMT	54	89	6	Centroid Moment Tensor
2010-02-13 16:37:32	72.728	39.395	6	4.1	Mw	WSM2016	28	47	5	NaN
2010-02-14 20:32:43	71.753	39.701	6	4.1	Mw	WSM2016	357	35	-147	NaN
2010-02-17 00:39:05	74.847	39.572	12	4.1	Mw	WSM2016	48	34	90	NaN
2010-02-23 12:13:29.400	91.3	35.3	23.9	4.8	Mw	GCMT	74	86	5	Centroid Moment Tensor
2010-02-24 11:18:16	73.73	39.503	6	4.1	Mw	WSM2016	157	27	164	NaN
2010-02-25 04:56:54.600	102.04	25.4	24.6	5.2	Mw	GCMT	14	76	-9	Centroid Moment Tensor
2010-02-26 04:42:30	86.73	28.41	10	5.6	Mb	WSM2016	12	70	-15	NaN
2010-03-02 01:55:39	75.633	42.402	9	4.8	Mw	WSM2016	188	34	-27	NaN
2010-03-10 14:32:22	86.97	36.43	10	4.6	Mb	WSM2016	160	84	179	NaN
2010-03-15 05:56:48	72.152	38.544	9	4	Mw	WSM2016	278	81	174	NaN
2010-03-15 20:17:19.900	82	30.53	22.5	4.9	Mw	GCMT	202	76	-19	Centroid Moment Tensor
2010-03-19 19:53:38.100	99.99	21.47	15.2	4.9	Mw	GCMT	234	63	-19	Centroid Moment Tensor
2010-03-23 15:02:06.800	74.66	37.5	19.4	5.1	Mw	GCMT	25	58	-31	Centroid Moment Tensor
2010-03-23 15:51:23.900	74.7	37.65	24.1	5	Mw	GCMT	212	61	-11	Centroid Moment Tensor
2010-03-24 02:06:10.630	92.708	32.509	7	5.5	Mw	ISC (NEIC)	68	66	-23	Centroid Moment Tensor
2010-03-24 02:44:53.500	92.92	32.37	19.1	5.4	Mw	GCMT	66	83	-10	Centroid Moment Tensor
2010-03-30 16:54:54.400	92.76	13.58	30.5	6.6	Mw	GCMT	255	60	-20	Centroid Moment Tensor
2010-04-07 09:22:31	73.311	39.487	6	4.1	Mw	WSM2016	246	21	90	NaN
2010-04-13 20:15:00.500	91.94	7.83	28.5	5.2	Mw	GCMT	38	81	-30	Centroid Moment Tensor
2010-04-13 21:40:01.000	96.71	33.08	27.4	4.9	Mw	GCMT	116	81	-19	Centroid Moment Tensor
2010-04-13 23:49:38.330	96.548	33.165	17	6.9	Mw	ISC (NEIC)	208	86	178	Centroid Moment Tensor

2010-04-14 01:25:17.800	96.53	33.18	17.9	6.1	Mw	GCMT	205	89	155	Centroid Moment Tensor
2010-04-17 00:59:00.200	92.84	32.38	17.3	5.3	Mw	GCMT	70	73	-24	Centroid Moment Tensor
2010-04-18 20:28:50.290	67.658	35.633	13	5.4	Mw	ISC (NEIC)	83	77	-172	Centroid Moment Tensor
2010-04-20 10:58:28	71.48	38.269	4	4	Mw	WSM2016	354	40	-136	NaN
2010-04-27 00:07:12	73.962	39.613	12	4.2	Mw	WSM2016	306	64	168	NaN
2010-04-27 20:22:30.500	101.63	30.51	25.4	5.1	Mw	GCMT	236	79	176	Centroid Moment Tensor
2010-04-28 16:48:38.600	96.6	33.12	25.4	4.8	Mw	GCMT	182	79	178	Centroid Moment Tensor
2010-04-28 18:01:22.800	93.01	19.18	31.2	5.2	Mw	GCMT	179	66	-67	Centroid Moment Tensor
2010-05-11 22:58:31	71.945	41.411	18	4.3	Mw	WSM2016	252	34	90	NaN
2010-05-14 07:02:08	71.432	38.328	4	4	Mw	WSM2016	40	59	-15	NaN
2010-05-16 08:55:46.290	93.18	14.423	38.7	5.3	Mw	ISC (NEIC)	178	49	-66	Centroid Moment Tensor
2010-05-27 05:38:20	71.454	38.328	6	4	Mw	WSM2016	181	26	-90	NaN
2010-05-29 02:29:48.640	96.07	33.165	7	5.8	Mw	ISC (NEIC)	78	79	-3	Centroid Moment Tensor
2010-05-30 10:19:26	71.171	37.028	12	4	Mw	WSM2016	326	68	-158	NaN
2010-05-30 23:54:13	69.75	37.759	9	4	Mw	WSM2016	20	1	90	NaN
2010-05-31 00:22:08	69.74	37.77	4	4.5	Mw	WSM2016	128	2	-90	NaN
2010-06-03 05:35:45	96.15	33.33	23.8	5.2	Mb	WSM2016	177	80	177	NaN
2010-06-03 20:47:05	96.09	33.3	10	5	Mb	WSM2016	171	82	-174	NaN
2010-06-05 16:59:16	65.97	28.17	10	5	Mb	Ali & Shanker, 2017	196	83	6	Catalog collection
2010-06-06 16:42:43.400	96.27	33.18	18.1	4.9	Mw	GCMT	171	85	168	Centroid Moment Tensor
2010-06-10 06:38:10	74.464	40.064	21	4.9	Mw	WSM2016	263	23	107	NaN
2010-06-13 06:26:04.300	91.82	7.71	12	5.2	Mw	GCMT	20	83	-28	Centroid Moment Tensor
2010-06-13 07:05:36.500	91.92	7.98	18.9	5.2	Mw	GCMT	196	47	-51	Centroid Moment Tensor
2010-06-15 23:24:25.800	91.67	7.41	12	5	Mw	GCMT	34	89	-28	Centroid Moment Tensor

2010-06-15 23:39:11	71.9	38.588	9	4.1	Mw	WSM2016	336	35	-90	NaN
2010-06-18 23:09:34.300	93.12	13.21	20.1	5.9	Mw	GCMT	116	38	59	Centroid Moment Tensor
2010-06-19 12:58:27	71.585	37.102	12	4.3	Mw	WSM2016	142	49	-156	NaN
2010-06-19 14:41:59	71.566	37.115	6	4.2	Mw	WSM2016	152	27	-137	NaN
2010-06-24 04:08:35.060	91.958	7.696	20.5	5.5	Mw	ISC (NEIC)	105	79	175	Centroid Moment Tensor
2010-06-24 17:06:21.700	91.96	7.72	16.6	4.9	Mw	GCMT	134	58	173	Centroid Moment Tensor
2010-06-25 07:28:59.700	91.85	7.65	14.4	5.2	Mw	GCMT	19	87	-11	Centroid Moment Tensor
2010-06-27 09:43:51.800	95.88	13.43	12	5	Mw	GCMT	67	31	-67	Centroid Moment Tensor
2010-06-27 10:51:45.900	96	13.5	12	5	Mw	GCMT	40	33	-131	Centroid Moment Tensor
2010-07-06 19:08:25	80.4	29.84	32.8	5	Mb	Ali & Shanker, 2017	318	25	140	Catalog collection
2010-07-08 13:46:58	93.26	14.37	35	5.2	Mb	WSM2016	12	77	-170	NaN
2010-08-03 16:26:25	69.64	38.45	23.7	5.4	Mb	WSM2016	228	31	75	NaN
2010-08-09 22:21:43	92.82	13.61	20.9	5.4	Mb	WSM2016	250	46	-28	NaN
2010-08-14 20:18:00.900	66.31	28.1	19.9	5.2	Mw	GCMT	208	83	-5	Centroid Moment Tensor
2010-08-17 01:39:30.900	95.13	11.54	12.4	5.4	Mw	GCMT	263	87	-12	Centroid Moment Tensor
2010-09-07 15:41:38	73.84	39.45	10	5.5	Mb	WSM2016	312	83	177	NaN
2010-09-07 20:50:57	96.31	33.28	2.4	5	Mb	WSM2016	178	84	-178	NaN
2010-09-10 17:24:17	90.66	23.41	10	4.8	Mb	WSM2016	150	77	171	NaN
2010-09-11 11:43:09	94.06	7.79	10	5.4	Mb	WSM2016	154	84	-179	NaN
2010-11-06 02:12:44	87.51	36.64	10	4.9	Mb	WSM2016	141	85	179	NaN
2010-11-15 00:51:56.600	70.51	34.46	25.4	5.2	Mw	GCMT	60	59	77	Centroid Moment Tensor
2010-11-30 08:40:00.400	90.53	29.78	20.8	5.3	Mw	GCMT	199	49	-59	Centroid Moment Tensor
2010-12-09 23:17:32	70.08	31.53	14.1	5.4	Mb	Ali & Shanker, 2017	162	16	52	Catalog collection
2010-12-11 15:34:30	69.46	30.42	28	5	Mb	Ali & Shanker, 2017	237	30	82	Catalog collection

2010-12-29 18:31:05.100	86.73	30.92	27	5.1	Mw	GCMT	9	59	-73	Centroid Moment Tensor
2011-01-01 01:56:07.800	75.16	39.44	12	4.9	Mw	GCMT	98	47	100	Centroid Moment Tensor
2011-01-01 15:31:58	97.92	24.72	10	4.6	Ms	WSM2016	231	72	7	Centroid Moment Tensor
2011-01-02 03:36:15	68.97	36.19	28.4	4.8	Mb	Ali & Shanker, 2017	350	52	78	Catalog collection
2011-01-02 07:33:34	97.92	24.72	10	4.8	Ms	WSM2016	232	74	9	Centroid Moment Tensor
2011-01-02 07:44:30	97.92	24.72	10	4	Ms	WSM2016	229	67	12	Centroid Moment Tensor
2011-01-14 22:50:34	97.93	24.73	10	4.3	Ms	WSM2016	243	73	13	Centroid Moment Tensor
2011-02-01 13:39:48	94.12	10.697	25	5.5	Mw	WSM2016	188	27	-137	NaN
2011-02-01 15:11:20	97.95	24.73	10	4.8	Ms	WSM2016	249	79	10	Centroid Moment Tensor
2011-02-04 00:00:00	94.735	24.609	76	6.4	Mb	Kumar et al., 2015	130	57	130	Centroid Moment Tensor
2011-03-10 04:58:15	97.927	24.728	10	5.6	Mw	WSM2016	245	66	4	NaN
2011-03-10 12:58:10	97.92	24.72	10	5.8	Ms	WSM2016	154	71	166	Centroid Moment Tensor
2011-03-10 13:04:50	97.92	24.68	10	4.5	Ms	WSM2016	167	74	175	Centroid Moment Tensor
2011-03-17 15:34:33.800	78.9	40.39	16.5	4.9	Mw	GCMT	104	67	125	Centroid Moment Tensor
2011-03-23 05:55:58.000	76.51	36.13	77	4.8	Mw	GCMT	89	48	81	Centroid Moment Tensor
2011-03-24 13:55:17.600	100.02	20.62	13.2	6.8	Mw	GCMT	70	85	11	Centroid Moment Tensor
2011-03-24 15:54:35.800	99.9	20.61	14.4	5.7	Mw	GCMT	80	79	18	Centroid Moment Tensor
2011-03-25 00:22:40.200	99.95	20.6	12	5	Mw	GCMT	8	63	166	Centroid Moment Tensor
2011-03-26 05:57:31.600	100.29	20.68	14.9	5	Mw	GCMT	146	88	168	Centroid Moment Tensor
2011-04-04 11:31:44.300	80.71	29.43	18.8	5.4	Mw	GCMT	96	67	70	Centroid Moment Tensor
2011-04-19 16:27:29.100	89.72	34.33	16.4	4.9	Mw	GCMT	5	42	-108	Centroid Moment Tensor

2011-06-03 07:27:11	92.38	9.57	34	5.5	Mw	WSM2016	191	25	-90	NaN
2011-06-20 10:16:52.400	98.8	25	15.7	5	Mw	GCMT	103	46	98	Centroid Moment Tensor
2011-06-26 07:48:15.100	95.98	32.33	15.9	5.3	Mw	GCMT	77	63	-31	Centroid Moment Tensor
2011-07-19 19:35:43.480	71.41	40.081	20	6.1	Mw	ISC (NEIC)	90	30	90	Centroid Moment Tensor
2011-07-24 10:38:55.900	66.17	28.03	13.4	4.9	Mw	GCMT	120	83	154	Centroid Moment Tensor
2011-07-28 21:59:46	100.88	27.76	10	4.1	Mw	Luo et al., 2016	147	70	-70	Centroid Moment Tensor
2011-08-01 19:40:53	87.57	33.74	13.6	5.1	Mb	WSM2016	319	81	-176	NaN
2011-08-09 11:50:17	98.7	25	11	5.6	Mw	Luo et al., 2016	160	89	168	Centroid Moment Tensor
2011-08-11 10:06:35	77.198	39.913	19	5.6	Mw	WSM2016	264	41	97	NaN
2011-08-17 23:52:03.400	69.19	36.48	29.6	4.9	Mw	GCMT	78	37	151	Centroid Moment Tensor
2011-08-30 16:23:50	97.98	24.73	10	4.8	Mw	Luo et al., 2016	251	83	21	Centroid Moment Tensor
2011-09-08 19:46:50	70.7	38.98	30	5	Mb	WSM2016	344	61	24	NaN
2011-09-15 15:27:04.600	82.46	36.45	12	5.3	Mw	GCMT	245	89	-8	Centroid Moment Tensor
2011-09-18 00:00:00	88.491	27.332	27.73	4.8	Mb	Paul et al. 2015	180	70	10	Centroid Moment Tensor
2011-09-18 00:00:00	88.518	27.474	48.95	4.8	Mb	Paul et al. 2015	10	65	-50	Centroid Moment Tensor
2011-09-18 00:00:00	88.136	27.718	53	6.9	Mb	Paul et al. 2015	219	78	9	Centroid Moment Tensor
2011-09-23 13:38:34	98.17	24.35	6	4	Mw	Luo et al., 2016	339	77	163	Centroid Moment Tensor
2011-10-01 12:48:57	95.78	12.99	15.1	5.1	Mb	WSM2016	11	48	-148	NaN
2011-10-20 17:18:35.300	70.44	20.98	12	5.1	Mw	GCMT	236	83	-29	Centroid Moment Tensor
2011-10-20 20:52:40.100	81.57	35.63	24	5	Mw	GCMT	228	72	-19	Centroid Moment Tensor
2011-11-05 21:34:32	105.07	29.4	20	4.5	Mw	Luo et al., 2016	166	48	62	Centroid Moment Tensor

2011-11-28 15:06:50	97.6	25.1	18	5.1	Mw	Luo et al., 2016	289	87	-9	Centroid Moment Tensor
2011-11-30 19:42:32.600	93.843	7.805	6	5.6	Mw	ISC (NEIC)	30	30	-90	Centroid Moment Tensor
2011-12-01 03:50:57	83.82	31.8	6.7	5.1	Mb	Ali & Shanker, 2017	329	84	-176	Catalog collection
2011-12-01 12:48:18	76.89	38.31	31.7	5.3	Mb	WSM2016	52	37	33	NaN
2011-12-02 19:37:46	93.73	7.86	10	5	Mw	WSM2016	190	32	-80	NaN
2011-12-05 18:55:43	92.89	32.55	16.5	4.7	Mb	WSM2016	333	82	-176	NaN
2011-12-05 20:37:46	103.2	27.4	5	4.2	Mw	Luo et al., 2016	352	72	-16	Centroid Moment Tensor
2011-12-16 15:47:27.400	94.11	7.84	15.8	5.1	Mw	GCMT	222	28	-20	Centroid Moment Tensor
2011-12-22 23:42:57.600	86.54	31.76	26.1	4.9	Mw	GCMT	244	79	-15	Centroid Moment Tensor
2011-12-23 12:02:03.800	68.24	28.72	12	5.1	Mw	GCMT	118	55	81	Centroid Moment Tensor
2012-01-04 16:51:44	66.17	26.74	10	4.8	Mb	WSM2016	93	64	-158	NaN
2012-01-08 06:20:06	87.47	42.2	15.7	5	Mb	WSM2016	130	38	90	NaN
2012-02-05 07:10:17	74.78	41.44	10	5.2	Mb	WSM2016	79	40	106	NaN
2012-02-17 15:44:25.800	82.92	32.32	20.9	5.4	Mw	GCMT	118	70	172	Centroid Moment Tensor
2012-02-20 13:59:26.300	79.64	35.8	25	4.9	Mw	GCMT	239	78	-11	Centroid Moment Tensor
2012-02-20 14:18:07.300	79.65	35.76	28.8	5.1	Mw	GCMT	238	77	-11	Centroid Moment Tensor
2012-03-04 17:11:45	101.8	30.1	9	4.3	Mw	Luo et al., 2016	71	63	-150	Centroid Moment Tensor
2012-03-06 02:52:42	93.73	8.62	10	5.3	Mw	WSM2016	358	44	-104	NaN
2012-03-08 22:50:00	81.31	39.38	45	5.9	Mw	Bai et al., 2017	132	46	128	Centroid Moment Tensor
2012-03-12 06:06:00	73.15	36.74	6	5.7	Mw	Bai et al., 2017	212	53	-5	Centroid Moment Tensor
2012-04-10 08:08:38	82.39	34.38	34.1	4.7	Mb	WSM2016	223	83	6	NaN
2012-04-14 20:31:21	100.08	29.28	10	4.5	Mw	Luo et al., 2016	101	45	-121	Centroid Moment Tensor
2012-04-24 14:57:14	93.91	8.95	12	5.6	Mw	WSM2016	60	67	-25	NaN

2012-04-25 07:42:23.380	93.945	9.011	9	5.7	Mw	ISC (NEIC)	64	85	-15	Centroid Moment Tensor
2012-04-25 16:31:02.400	94.11	8.82	19.6	5	Mw	GCMT	37	66	-66	Centroid Moment Tensor
2012-04-30 13:06:58.740	93.327	14.405	35	5.2	Mw	ISC (NEIC)	77	90	22	Centroid Moment Tensor
2012-05-03 10:19:37	98.53	40.51	10	5.2	Mb	WSM2016	69	73	-10	NaN
2012-05-04 00:00:00	95.164	27.406	22	4.4	Mb	Kumar et al., 2015	181	60	-168	Centroid Moment Tensor
2012-05-11 00:00:00	92.906	26.246	42	5.4	Mb	Kumar et al., 2015	332	84	175	Centroid Moment Tensor
2012-05-12 01:34:43	89.43	38.31	10	4.8	Mb	WSM2016	345	54	170	NaN
2012-05-12 23:28:00	70.35	38.61	12	5.7	Mw	Bai et al., 2017	62	34	139	Centroid Moment Tensor
2012-05-19 14:02:35.300	87.08	33.65	22.2	4.9	Mw	GCMT	9	39	-96	Centroid Moment Tensor
2012-05-24 19:39:28.500	93.34	14.4	23.5	4.8	Mw	GCMT	90	88	-22	Centroid Moment Tensor
2012-05-27 20:50:22.100	83.57	30.67	20.3	4.9	Mw	GCMT	214	50	-20	Centroid Moment Tensor
2012-06-11 05:29:00	69.35	36.02	16	5.7	Mw	Bai et al., 2017	329	71	17	Centroid Moment Tensor
2012-06-12 13:40:39	104.28	28.1	9	4.9	Mw	Luo et al., 2016	274	86	-178	Centroid Moment Tensor
2012-06-14 21:51:26.280	84.279	42.166	13	5.2	Mw	ISC (NEIC)	113	42	103	Centroid Moment Tensor
2012-06-19 20:14:01.600	70.24	23.52	14.8	5.1	Mw	GCMT	13	89	-26	Centroid Moment Tensor
2012-06-24 07:59:33	100.69	27.71	11	6	Mw	Luo et al., 2016	165	47	-77	Centroid Moment Tensor
2012-06-24 07:59:35.500	100.75	27.72	12.5	5.6	Mw	GCMT	179	55	-59	Centroid Moment Tensor
2012-06-26 06:21:15	100.68	27.79	7	4.1	Mw	Luo et al., 2016	180	60	-51	Centroid Moment Tensor
2012-06-29 22:22:26	101.18	28.13	7	4.1	Mw	Luo et al., 2016	192	72	-20	Centroid Moment Tensor
2012-07-01 00:00:00	94.73	25.6	53	5.5	Mb	Kumar et al., 2015	143	78	174	Centroid Moment Tensor
2012-07-03 19:11:41	88.01	29.91	10	4.9	Mb	WSM2016	179	40	-85	NaN

2012-07-10 00:00:00	93.164	26.48	46	4.5	Mb	Kumar et al., 2015	331	48	153	Centroid Moment Tensor
2012-07-14 19:55:17.950	94.48	25.424	52.1	5.2	Mw	ISC (NEIC)	148	76	163	Centroid Moment Tensor
2012-07-17 20:18:45	102.26	29.01	11	4	Mw	Luo et al., 2016	182	81	-12	Centroid Moment Tensor
2012-07-22 02:11:11.600	96.43	24.86	17.9	5.1	Mw	GCMT	95	77	-7	Centroid Moment Tensor
2012-07-22 16:44:22.000	88.32	29.93	24.8	5	Mw	GCMT	200	31	-47	Centroid Moment Tensor
2012-07-22 20:29:43.100	87.28	36.09	23.6	5.2	Mw	GCMT	66	83	-2	Centroid Moment Tensor
2012-07-29 02:21:12.600	94.299	22.935	75.3	5.7	Mw	ISC (NEIC)	71	83	-27	Centroid Moment Tensor
2012-07-29 16:05:32	101.22	23.08	10	4.7	Mw	Luo et al., 2016	25	82	22	Centroid Moment Tensor
2012-08-11 09:34:22	78.14	39.96	10	5.3	Mw	WSM2016	83	38	99	NaN
2012-08-12 10:47:00	82.52	35.67	12	6.2	Mw	Bai et al., 2017	215	47	-52	Centroid Moment Tensor
2012-08-13 20:32:57.800	73.75	34.88	18.1	5	Mw	GCMT	7	65	61	Centroid Moment Tensor
2012-08-19 00:00:00	92.601	26.601	40	4	Mb	Kumar et al., 2015	120	77	-149	Centroid Moment Tensor
2012-08-23 16:30:22.900	82.65	28.05	28.9	5	Mw	GCMT	114	69	85	Centroid Moment Tensor
2012-08-26 05:18:24.100	89.79	35.17	17.8	5	Mw	GCMT	65	76	-10	Centroid Moment Tensor
2012-09-07 03:19:40	104	27.5	12	5.4	Mw	Luo et al., 2016	250	69	158	Centroid Moment Tensor
2012-09-07 03:58:00	104.01	27.58	9	4.1	Mw	Luo et al., 2016	0	58	74	Centroid Moment Tensor
2012-09-07 04:16:29	104	27.6	10	5.2	Mw	Luo et al., 2016	229	44	141	Centroid Moment Tensor
2012-09-07 05:12:46	104	27.54	8	4.3	Mw	Luo et al., 2016	280	85	169	Centroid Moment Tensor
2012-09-10 06:19:21	92.85	13.64	30.5	4.9	Mb	WSM2016	258	58	-12	NaN
2012-09-10 14:35:43	93.62	10.46	38.7	5.2	Mb	WSM2016	66	38	-99	NaN
2012-09-11 00:00:00	94.208	23.966	27	4	Mb	Kumar et al., 2015	335	75	75	Centroid Moment Tensor

2012-09-11 03:20:16	99.18	24.67	8	4.9	Mw	Luo et al., 2016	46	50	-61	Centroid Moment Tensor
2012-09-11 03:21:20	99.18	24.66	14	5.3	Mw	Luo et al., 2016	31	43	-72	Centroid Moment Tensor
2012-09-17 23:28:34	100.08	23.34	14	4.7	Mw	Luo et al., 2016	291	86	-169	Centroid Moment Tensor
2012-09-22 20:42:47.700	96.89	25.49	15	4.7	Mw	GCMT	122	78	-30	Centroid Moment Tensor
2012-09-25 08:32:59.700	69.06	36.46	26.5	5.2	Mw	GCMT	43	25	83	Centroid Moment Tensor
2012-10-02 00:00:00	92.95	26.78	36	5.2	Mb	Kumar et al., 2015	89	53	44	Centroid Moment Tensor
2012-10-08 17:46:20	78.444	31.832	21	4.9	Mw	Parija et al., 2018	124	88	-166	Centroid Moment Tensor
2012-10-14 23:07:00	101.9	25.15	10	4.8	Mw	Luo et al., 2016	55	73	34	Centroid Moment Tensor
2012-10-19 02:44:16	102.86	30.14	26	4.6	Mw	Luo et al., 2016	149	30	27	Centroid Moment Tensor
2012-11-10 14:19:33	105.22	29.32	25	4.6	Mw	Luo et al., 2016	126	44	64	Centroid Moment Tensor
2012-11-10 22:01:32	105.23	29.32	22	4.7	Mw	Luo et al., 2016	117	45	52	Centroid Moment Tensor
2012-11-11 00:59:00	105.24	29.31	12	4.9	Mw	Luo et al., 2016	356	63	117	Centroid Moment Tensor
2012-11-11 01:12:38.870	95.885	23.005	13.7	6.8	Mw	ISC (NEIC)	15	80	175	Centroid Moment Tensor
2012-11-11 10:54:41.350	95.832	22.72	6	5.8	Mw	ISC (NEIC)	262	81	-20	Centroid Moment Tensor
2012-11-11 18:19:43.800	96.07	23.06	20.1	5.6	Mw	GCMT	93	78	20	Centroid Moment Tensor
2012-11-11 20:23:12	76.331	32.294	5	4	Mw	Parija et al., 2018	114	63	-89	Centroid Moment Tensor
2012-11-13 18:28:13.100	95.98	22.83	16.4	4.9	Mw	GCMT	0	60	174	Centroid Moment Tensor
2012-11-14 11:42:56	102.52	26.49	13	4.6	Mw	Luo et al., 2016	107	89	173	Centroid Moment Tensor
2012-11-19 17:25:52.100	96.1	22.94	19.9	4.8	Mw	GCMT	0	72	174	Centroid Moment Tensor
2012-11-19 17:54:07.100	67.57	30.31	12	5.3	Mw	GCMT	228	81	-25	Centroid Moment Tensor

2012-11-26 05:33:48.800	90.355	40.411	10	5	Mw	ISC (NEIC)	63	46	56	Centroid Moment Tensor
2012-11-26 23:13:53.100	93.52	13.97	41.3	5	Mw	GCMT	10	36	136	Centroid Moment Tensor
2012-12-03 11:55:27	95.89	23.11	35.4	4.6	Mb	WSM2016	360	67	-174	NaN
2012-12-25 17:36:29.700	66.45	28.32	16.5	4.9	Mw	GCMT	108	60	160	Centroid Moment Tensor
2012-12-26 13:59:45.600	95.87	22.77	26.8	5	Mw	GCMT	1	60	171	Centroid Moment Tensor
2013-01-18 12:42:50.810	99.546	31.056	8	5.4	Mw	ISC (NEIC)	129	71	-2	Centroid Moment Tensor
2013-01-22 15:09:23.100	68.71	36.5	25.5	5.2	Mw	GCMT	90	52	160	Centroid Moment Tensor
2013-01-28 16:38:53.580	79.708	42.605	15	6.1	Mw	ISC (NEIC)	148	88	178	Centroid Moment Tensor
2013-01-30 09:27:03.500	94.86	32.86	19.6	5.2	Mw	GCMT	85	83	-9	Centroid Moment Tensor
2013-02-04 12:04:55	94.7	32.9	10	4.8	Mb	WSM2016	342	86	-178	NaN
2013-02-07 00:57:19	104.08	28.03	10	4.1	Mw	Luo et al., 2016	360	42	28	Centroid Moment Tensor
2013-02-11 19:13:02	92.37	38.48	16.9	5.3	Mb	WSM2016	319	40	98	NaN
2013-02-19 02:46:58	103	27.1	4	4.8	Mw	Luo et al., 2016	99	77	-163	Centroid Moment Tensor
2013-02-19 07:55:30	104.9	28.3	6	4.4	Mw	Luo et al., 2016	192	64	33	Centroid Moment Tensor
2013-02-20 05:01:57.500	101.7	23.19	15.4	4.7	Mw	GCMT	131	72	137	Centroid Moment Tensor
2013-02-25 05:11:07.520	85.651	34.292	10	5.4	Mw	ISC (NEIC)	135	87	177	Centroid Moment Tensor
2013-03-02 01:30:39	92.22	24.68	38.7	5.5	Mb	WSM2016	332	36	147	NaN
2013-03-03 03:12:28.900	71.5	38.64	23.5	5.1	Mw	GCMT	135	87	178	Centroid Moment Tensor
2013-03-03 05:41:15	99.7	25.9	7	5.3	Mw	Luo et al., 2016	0	46	-77	Centroid Moment Tensor
2013-03-30 20:04:47.100	96.07	22.94	12	5.2	Mw	GCMT	3	75	-180	Centroid Moment Tensor
2013-04-03 16:35:47	95.62	19.24	10	5.3	Mw	WSM2016	128	42	66	NaN

2013-04-04 15:16:27.400	95.77	19.08	12	5.1	Mw	GCMT	150	46	103	Centroid Moment Tensor
2013-04-11 03:47:04	95.64	19.36	10	5.2	Mw	WSM2016	166	24	130	NaN
2013-04-16 08:34:13.000	95.12	28.67	39.6	4.9	Mw	GCMT	120	51	90	Centroid Moment Tensor
2013-04-17 01:45:54	99.8	25.9	8	4.8	Mw	Luo et al., 2016	360	50	-78	Centroid Moment Tensor
2013-04-20 00:02:46	103	30.5	18	6.3	Mw	Luo et al., 2016	30	47	79	Centroid Moment Tensor
2013-04-20 03:34:17	102.9	30.1	12	5.1	Mw	Luo et al., 2016	48	41	90	Centroid Moment Tensor
2013-04-21 09:30:24	103	30.3	18	5	Mw	Luo et al., 2016	42	51	74	Centroid Moment Tensor
2013-04-24 09:25:30.040	70.22	34.526	63.8	5.5	Mw	ISC (NEIC)	188	34	135	Centroid Moment Tensor
2013-05-01 06:57:15	75.73	33.1	15	5.6	Mw	O Kane et al., 2022	299	14	80	Centroid Moment Tensor
2013-05-15 10:54:29.000	86.55	31.25	17.4	5.2	Mw	GCMT	57	50	-37	Centroid Moment Tensor
2013-05-16 03:34:17.100	86.52	31.26	16.2	5.1	Mw	GCMT	53	37	-34	Centroid Moment Tensor
2013-05-24 22:18:33.910	69.171	40.912	19.2	5.3	Mw	ISC (NEIC)	69	39	157	Centroid Moment Tensor
2013-05-26 06:08:15.960	67.314	39.956	18	5.7	Mw	ISC (NEIC)	46	50	90	Centroid Moment Tensor
2013-06-04 17:34:50	76.601	32.672	28	4.9	Mw	Parija et al., 2018	294	27	-92	Centroid Moment Tensor
2013-06-05 00:43:36	95.93	37.6	9	5.4	Mb	WSM2016	266	34	82	NaN
2013-06-05 22:04:03	76.286	32.907	40	4	Mw	Parija et al., 2018	235	12	10	Centroid Moment Tensor
2013-06-21 20:51:55.100	73.24	37	19	4.8	Mw	GCMT	142	41	-116	Centroid Moment Tensor
2013-06-26 05:48:47.800	91.26	9.44	25	4.9	Mw	GCMT	198	39	-72	Centroid Moment Tensor
2013-06-28 11:40:50.600	82.18	28.49	18.2	5	Mw	GCMT	109	64	88	Centroid Moment Tensor
2013-06-30 04:59:34	73.47	39.27	28.8	5	Mb	WSM2016	193	79	7	NaN
2013-07-09 13:49:18	78.197	32.765	8	5	Mw	Parija et al., 2018	311	87	-162	Centroid Moment Tensor

2013-07-09 14:50:57	78.17	32.743	38	4.1	Mw	Parija et al., 2018	144	75	-117	Centroid Moment Tensor
2013-07-13 17:49:36	76.535	32.383	5	4.4	Mw	Parija et al., 2018	1	3	-33	Centroid Moment Tensor
2013-08-02 02:32:48	75.87	33.23	15	5.1	Mw	O Kane et al., 2022	327	42	122	Centroid Moment Tensor
2013-08-02 21:37:43	75.89	33.31	14	5.1	Mw	O Kane et al., 2022	326	42	110	Centroid Moment Tensor
2013-08-06 15:31:22	86.45	31.44	8.9	5.2	Mb	WSM2016	31	41	-66	NaN
2013-08-06 16:13:53	86.49	31.47	10	4.8	Mb	WSM2016	348	44	-127	NaN
2013-08-11 12:40:06	97.97	30.06	10	4.8	Mb	WSM2016	205	46	-141	NaN
2013-08-11 21:23:00	97.96	30.05	2	5.8	Mw	Bai et al., 2017	90	54	-40	Centroid Moment Tensor
2013-08-11 23:48:19	97.91	29.98	10	4.9	Mb	WSM2016	215	52	-128	NaN
2013-08-12 08:09:38	97.96	30.15	10	4.9	Mb	WSM2016	199	61	-158	NaN
2013-08-24 02:35:52.400	71.62	37.28	24.5	4.8	Mw	GCMT	38	70	-6	Centroid Moment Tensor
2013-08-24 16:56:29.500	71.7	37.26	24.2	4.8	Mw	GCMT	126	79	176	Centroid Moment Tensor
2013-08-26 14:35:59.500	94.18	33.17	18.8	4.8	Mw	GCMT	80	74	-26	Centroid Moment Tensor
2013-08-27 20:44:52	99.33	28.2	5	5	Mw	Luo et al., 2016	296	57	-68	Centroid Moment Tensor
2013-08-27 23:53:04	99.36	28.19	6	4.5	Mw	Luo et al., 2016	291	55	-73	Centroid Moment Tensor
2013-08-29 10:13:24	76.273	31.479	47	4.4	Mw	Parija et al., 2018	78	89	132	Centroid Moment Tensor
2013-08-31 00:04:19	99.35	28.15	9	5.6	Mw	Luo et al., 2016	299	53	-73	Centroid Moment Tensor
2013-08-31 00:13:27	99.44	28.24	12	4.4	Mw	Luo et al., 2016	308	41	-97	Centroid Moment Tensor
2013-08-31 00:27:03	99.45	28.2	7	4.8	Mw	Luo et al., 2016	323	56	-79	Centroid Moment Tensor
2013-08-31 02:18:45	99.41	28.26	10	4.5	Mw	Luo et al., 2016	283	57	-81	Centroid Moment Tensor
2013-08-31 23:17:46	99.49	28.19	10	4.3	Mw	Luo et al., 2016	273	75	-99	Centroid Moment Tensor

2013-09-02 14:52:32	99.37	28.19	9	4.4	Mw	Luo et al., 2016	275	51	-90	Centroid Moment Tensor
2013-09-03 14:32:34	99.46	28.19	8	4.7	Mw	Luo et al., 2016	268	41	-117	Centroid Moment Tensor
2013-09-06 15:08:04	99.47	28.22	7	4.6	Mw	Luo et al., 2016	141	58	-72	Centroid Moment Tensor
2013-09-09 03:28:34.400	96.05	22.91	22.6	4.9	Mw	GCMT	3	68	179	Centroid Moment Tensor
2013-09-19 21:37:03.400	101.65	37.73	19.5	5.1	Mw	GCMT	135	34	59	Centroid Moment Tensor
2013-09-20 11:53:27.500	96.04	22.81	12	5	Mw	GCMT	91	85	13	Centroid Moment Tensor
2013-09-20 12:24:49.200	96.04	22.88	12	5.7	Mw	GCMT	1	77	164	Centroid Moment Tensor
2013-10-03 06:12:39	88.4	27.29	9.9	5.2	Ms	WSM2016	304	37	123	NaN
2013-10-18 13:18:24.200	66.51	28.21	15.5	5.4	Mw	GCMT	31	90	-33	Centroid Moment Tensor
2013-10-20 02:43:29	104.49	33.57	6.4	4.1	Mw	Han et al. 2019	149	33	90	Centroid Moment Tensor
2013-10-20 10:03:36	104.25	34.49	4.2	4.4	Mw	Han et al. 2019	190	63	9	Centroid Moment Tensor
2013-10-21 02:27:13.100	76.95	35.44	16.5	5.6	Mw	GCMT	3	63	-160	Centroid Moment Tensor
2013-10-22 23:59:49	104.78	34.05	7.6	4.1	Mw	Han et al. 2019	302	58	59	Centroid Moment Tensor
2013-10-24 17:57:36.970	93.0654	14.2917	23	5.4	Mw	ISC (NEIC)	52	65	-97	Centroid Moment Tensor
2013-10-25 22:50:59	97.36	39.88	15.4	4.5	Mw	Han et al. 2019	123	63	64	Centroid Moment Tensor
2013-11-02 16:17:21	97.72	38.53	8.3	4.3	Mw	Han et al. 2019	326	74	81	Centroid Moment Tensor
2013-11-03 07:02:05	88.23	35.53	10	4.5	Ms	WSM2016	138	82	-177	NaN
2013-11-06 00:00:00	93.55	26.5	33	5.3	Mb	Kumar et al., 2015	310	75	161	Centroid Moment Tensor
2013-11-06 20:26:25	102.93	30.33	28.2	4.4	Mw	Han et al. 2019	234	90	71	Centroid Moment Tensor
2013-11-10 05:15:11	69.08	38.4	22	4.9	Mw	WSM2016	334	79	6	NaN
2013-11-18 07:43:49.200	88.18	35.62	27.5	4.9	Mw	GCMT	131	88	177	Centroid Moment Tensor

2013-11-20 10:09:18.430	95.1481	12.3975	10.3	5.5	Mw	ISC (NEIC)	82	62	-39	Centroid Moment Tensor
2013-11-23 23:30:42.550	86.8448	36.5757	7.2	5.4	Mw	ISC (NEIC)	68	84	-6	Centroid Moment Tensor
2013-11-27 07:58:49	106.21	39.58	4.2	4.2	Mw	Han et al. 2019	70	70	-35	Centroid Moment Tensor
2013-11-28 08:23:56.000	100.68	25.54	20.4	4.8	Mw	GCMT	160	41	-71	Centroid Moment Tensor
2013-11-29 06:25:28.200	71.17	36.92	27.6	5	Mw	GCMT	149	80	173	Centroid Moment Tensor
2013-12-01 08:34:27	78.94	40.29	10	5.2	Mw	WSM2016	242	41	97	NaN
2013-12-05 18:11:07	73.21	36.75	35	4.8	Ms	WSM2016	294	73	163	NaN
2013-12-07 18:30:59	100.22	41.04	9.3	4.6	Mw	Han et al. 2019	70	43	21	Centroid Moment Tensor
2013-12-11 16:14:39	89.19	34.01	25.6	4.9	Ms	WSM2016	48	44	-48	NaN
2013-12-19 19:28:40.940	67.4543	27.5175	10.1	5.4	Mw	ISC (NEIC)	4	76	95	Centroid Moment Tensor
2013-12-20 03:04:38.400	93.02	14.29	36.1	4.9	Mw	GCMT	14	85	-170	Centroid Moment Tensor
2013-12-21 14:21:41.100	71.23	36.43	77	4.9	Mw	GCMT	233	64	123	Centroid Moment Tensor
2013-12-25 06:29:04	104.92	32.25	15.3	4.1	Mw	Han et al. 2019	200	37	51	Centroid Moment Tensor
2014-01-07 23:16:21	103.24	31.44	25.1	4.1	Mw	Han et al. 2019	59	74	16	Centroid Moment Tensor
2014-01-16 17:47:33.500	90.38	31.86	26.9	5.1	Mw	GCMT	235	87	-10	Centroid Moment Tensor
2014-01-19 15:33:14.700	93.84	33.01	24.5	4.8	Mw	GCMT	64	61	-6	Centroid Moment Tensor
2014-01-20 18:55:18	103.97	32.93	16	4	Mw	Han et al. 2019	71	68	38	Centroid Moment Tensor
2014-01-21 02:01:50	96.69	37.4	5	4.2	Mw	Han et al. 2019	98	43	59	Centroid Moment Tensor
2014-01-21 20:46:36.490	75.101	42.0873	7	4	Mw	ISC (NEIC)	97	72	146	Centroid Moment Tensor
2014-01-25 00:18:34	97.67	38.49	3.9	4	Mw	Han et al. 2019	289	46	74	Centroid Moment Tensor
2014-01-26 12:38:37	95.94	23.07	19	5	Mw	WSM2016	357	84	-177	NaN

2014-01-29 13:46:55.200	94.08	23.71	53.8	5.1	Mw	GCMT	249	60	0	Centroid Moment Tensor
2014-01-29 21:04:06	103.45	31.31	30.5	4.1	Mw	Han et al. 2019	310	66	24	Centroid Moment Tensor
2014-02-02 23:44:00.300	95.15	12.24	12	5.4	Mw	GCMT	16	50	-140	Centroid Moment Tensor
2014-02-11 01:15:28	89.26	33.93	25	5.2	Mw	WSM2016	199	42	-98	NaN
2014-02-12 09:19:00	82.59	35.91	6	6.9	Mw	Bai et al., 2017	332	85	-161	Centroid Moment Tensor
2014-02-13 00:08:46.300	82.33	36.09	35.4	4.8	Mw	GCMT	230	74	-15	Centroid Moment Tensor
2014-02-22 04:56:16	102.27	37.61	4.2	4.7	Mw	Han et al. 2019	77	63	-3	Centroid Moment Tensor
2014-02-27 18:52:59	106.79	39.31	12.1	4.4	Mw	Han et al. 2019	93	75	-7	Centroid Moment Tensor
2014-02-28 08:10:41	96.57	42.94	28.4	4.8	Mw	Han et al. 2019	183	77	-30	Centroid Moment Tensor
2014-03-07 08:41:57	91.13	31.68	15.5	4.7	Ms	WSM2016	9	41	-102	NaN
2014-03-11 11:23:55	92.86	13.6	33	4.8	Mw	WSM2016	268	61	-11	NaN
2014-03-13 13:05:01	103.78	33.15	14.2	4.2	Mw	Han et al. 2019	252	64	39	Centroid Moment Tensor
2014-03-14 13:38:06.400	94.253	7.7556	8	5.4	Mw	ISC (NEIC)	45	81	-38	Centroid Moment Tensor
2014-03-15 06:30:46	93.98	7.64	26	4.9	Mw	WSM2016	173	82	173	NaN
2014-03-21 13:41:14.000	94.53	7.57	19.5	6.4	Mw	ISC (NEIC)	63	79	0	Centroid Moment Tensor
2014-03-21 14:11:19.200	94.34	7.65	13.8	5.6	Mw	GCMT	53	77	-37	Centroid Moment Tensor
2014-03-21 14:25:14.400	94.35	7.57	14.8	5.5	Mw	GCMT	64	86	-25	Centroid Moment Tensor
2014-03-21 21:03:45.300	94.41	7.48	17.4	5.4	Mw	GCMT	53	78	-27	Centroid Moment Tensor
2014-03-22 12:58:20.700	82.35	36.23	25.3	5.2	Mw	GCMT	218	47	-26	Centroid Moment Tensor
2014-03-30 17:10:17.700	86.53	31.25	14.3	5.3	Mw	GCMT	48	45	-43	Centroid Moment Tensor
2014-04-02 06:04:43	103.6	31.17	19.1	4.5	Mw	Han et al. 2019	314	36	-11	Centroid Moment Tensor

2014-04-04 22:40:31	103.6	28.1	12	4.8	Mw	Luo et al., 2016	224	66	114	Centroid Moment Tensor
2014-04-11 02:31:00	103.18	31.69	15.6	4.8	Mw	Han et al. 2019	207	73	-17	Centroid Moment Tensor
2014-04-26 20:10:26	106.02	37.13	3.8	4	Mw	Han et al. 2019	299	80	20	Centroid Moment Tensor
2014-04-28 02:08:35	96.85	39.25	2	4.4	Mw	Han et al. 2019	287	79	81	Centroid Moment Tensor
2014-05-05 11:08:43.900	99.6826	19.7026	6	6.1	Mw	ISC (NEIC)	159	88	175	Centroid Moment Tensor
2014-05-05 23:04:56.100	99.6	19.64	12	4.8	Mw	GCMT	158	86	173	Centroid Moment Tensor
2014-05-06 00:50:18	99.69	19.72	15	5.2	Mw	WSM2016	344	73	-162	NaN
2014-05-06 00:58:22	99.49	19.71	13	5.2	Mw	WSM2016	234	55	-26	NaN
2014-05-08 22:51:16	68.36	26.39	14.7	4.5	Ms	WSM2016	122	42	69	NaN
2014-05-16 06:32:11.800	67.75	29.3	15.8	4.8	Mw	GCMT	56	42	95	Centroid Moment Tensor
2014-05-21 16:21:54.100	88.0176	18.1994	47	6	Mw	ISC (NEIC)	50	87	10	Centroid Moment Tensor
2014-05-23 20:49:00	97.84	24.97	17	5.7	Mw	Bai et al., 2017	334	85	-165	Centroid Moment Tensor
2014-05-30 01:20:17.500	97.9	24.93	14.7	5.9	Mw	GCMT	82	79	5	Centroid Moment Tensor
2014-06-06 00:16:33.900	89.26	34.15	18.9	4.7	Mw	GCMT	231	89	-17	Centroid Moment Tensor
2014-06-09 12:51:16	100.16	38.12	6	4	Mw	Han et al. 2019	258	62	-31	Centroid Moment Tensor
2014-06-09 23:54:15	105.17	32.58	15.2	4.8	Mw	Han et al. 2019	172	50	42	Centroid Moment Tensor
2014-06-10 01:28:07	105.17	32.57	15.7	4.1	Mw	Han et al. 2019	118	70	62	Centroid Moment Tensor
2014-06-13 06:17:05	66.02	27.74	31	5.3	Mw	WSM2016	197	69	21	NaN
2014-06-14 07:27:30	104.14	31.57	25	4.3	Mw	Han et al. 2019	16	53	58	Centroid Moment Tensor
2014-06-20 19:36:00.400	75.976	40.0217	22	4.1	Mw	ISC (NEIC)	11	50	42	Centroid Moment Tensor
2014-07-10 19:10:56	99.07	37.11	3	4	Mw	Han et al. 2019	338	52	3	Centroid Moment Tensor

2014-07-13 16:23:45.400	67.67	36.5	26	5	Mw	GCMT	122	74	158	Centroid Moment Tensor
2014-07-20 10:03:46	104.08	31.5	25.3	4.3	Mw	Han et al. 2019	178	58	31	Centroid Moment Tensor
2014-07-25 20:03:45	98.99	37.16	19.3	4.4	Mw	Han et al. 2019	326	69	24	Centroid Moment Tensor
2014-07-29 07:07:07.500	93.0516	14.4151	12	5.3	Mw	ISC (NEIC)	190	90	142	Centroid Moment Tensor
2014-07-29 08:20:14	105.24	31.46	25.4	5.4	Mw	Han et al. 2019	49	78	0	Centroid Moment Tensor
2014-07-29 09:09:36	105.22	31.43	12.5	4.8	Mw	Han et al. 2019	230	76	-24	Centroid Moment Tensor
2014-07-31 13:41:03.200	95.19	12.3	12	5.8	Mw	GCMT	28	42	-116	Centroid Moment Tensor
2014-07-31 17:33:33	95.39	12.62	15	4.8	Mw	WSM2016	38	44	124	NaN
2014-08-03 05:57:31	85.5	29.28	10	5.2	Ms	WSM2016	202	42	-61	NaN
2014-08-03 08:30:10	103.3	27.1	12	5.9	Mw	Luo et al., 2016	71	79	165	Centroid Moment Tensor
2014-08-09 06:53:41	104.13	31.83	23.7	4.5	Mw	Han et al. 2019	197	36	82	Centroid Moment Tensor
2014-08-11 10:50:05	99.02	34.84	4.7	4.6	Mw	Han et al. 2019	360	43	-65	Centroid Moment Tensor
2014-08-12 10:42:17	103.99	31.6	25	4.1	Mw	Han et al. 2019	170	61	51	Centroid Moment Tensor
2014-08-15 21:42:33.400	77.29	43.19	26.9	4.8	Mw	GCMT	58	23	64	Centroid Moment Tensor
2014-08-16 22:07:58	103.5	28.1	8	4.8	Mw	Luo et al., 2016	319	69	4	Centroid Moment Tensor
2014-08-21 19:29:36	105.27	32.56	15.9	4	Mw	Han et al. 2019	190	59	37	Centroid Moment Tensor
2014-08-23 03:58:48	105.05	32.71	2	4	Mw	Han et al. 2019	114	56	90	Centroid Moment Tensor
2014-08-26 01:10:09	101.2	39.11	16.6	4	Mw	Han et al. 2019	240	85	-35	Centroid Moment Tensor
2014-08-29 01:04:02.000	71.3	39.17	12	4.9	Mw	GCMT	92	61	156	Centroid Moment Tensor
2014-08-29 23:05:43	109.74	42.37	8.3	4.3	Mw	Han et al. 2019	132	33	49	Centroid Moment Tensor

2014-09-05 11:31:50	102.36	38.59	11.3	4.2	Mw	Han et al. 2019	108	47	71	Centroid Moment Tensor
2014-09-09 09:28:23.300	93.1631	22.1586	16	5.4	Mw	ISC (NEIC)	26	81	179	Centroid Moment Tensor
2014-09-13 01:58:00.900	72.08	37.77	28.2	5	Mw	GCMT	40	80	-13	Centroid Moment Tensor
2014-09-14 01:21:05.700	71.4121	36.8985	71	4.7	Mw	ISC (NEIC)	67	55	141	Centroid Moment Tensor
2014-09-26 04:21:24.900	95.18	12.36	12	5.5	Mw	GCMT	44	38	-100	Centroid Moment Tensor
2014-09-27 20:11:58	103.45	31.3	18.9	4.2	Mw	Han et al. 2019	299	59	-4	Centroid Moment Tensor
2014-09-27 22:49:05.300	69.8143	36.4493	28	5	Mw	ISC (NEIC)	226	87	-76	Centroid Moment Tensor
2014-10-02 15:56:32	97.79	36.42	2	5.4	Mw	Han et al. 2019	293	22	90	Centroid Moment Tensor
2014-10-07 13:49:39	100.5	23.4	16	6.5	Mw	Luo et al., 2016	61	84	-162	Centroid Moment Tensor
2014-10-07 21:14:06	102.91	30.13	16.2	4.4	Mw	Han et al. 2019	207	23	82	Centroid Moment Tensor
2014-10-13 17:21:22.000	94.43	7.51	16.6	4.7	Mw	GCMT	141	61	179	Centroid Moment Tensor
2014-10-18 02:46:20	103.04	34.13	16.8	4.5	Mw	Han et al. 2019	290	59	-7	Centroid Moment Tensor
2014-10-20 00:32:24	105.2	31.46	15.3	4.2	Mw	Han et al. 2019	233	77	-15	Centroid Moment Tensor
2014-10-25 02:26:01	102.39	34.3	25.3	5.1	Mw	Han et al. 2019	196	82	-173	Centroid Moment Tensor
2014-10-26 02:58:47.400	94.41	7.48	18.8	5	Mw	GCMT	54	79	-29	Centroid Moment Tensor
2014-10-26 22:07:18.300	94.4	7.53	15.4	5	Mw	GCMT	53	77	-29	Centroid Moment Tensor
2014-11-06 15:46:19	94.19	7.4	17	5.1	Mw	WSM2016	141	78	171	NaN
2014-11-08 17:37:45	96.92	37.56	3.4	4.6	Mw	Han et al. 2019	99	68	70	Centroid Moment Tensor
2014-11-11 05:04:48.900	94.38	7.52	22.1	5.1	Mw	GCMT	57	88	-18	Centroid Moment Tensor
2014-11-11 07:50:09.200	94.327	7.443	8	5.3	Mw	ISC (NEIC)	68	82	-12	Centroid Moment Tensor

2014-11-11 08:04:39.200	94.39	7.55	26.9	5.3	Mw	GCMT	73	89	-31	Centroid Moment Tensor
2014-11-14 01:24:15.500	77.3176	42.1365	9	5.2	Mw	ISC (NEIC)	79	40	107	Centroid Moment Tensor
2014-11-14 23:03:16	103.74	37.12	4.3	5	Mw	Han et al. 2019	281	71	2	Centroid Moment Tensor
2014-11-17 04:34:13.500	94.4317	20.7609	66	5.3	Mw	ISC (NEIC)	104	21	-160	Centroid Moment Tensor
2014-11-17 05:08:14.400	94.38	7.52	18.2	5	Mw	GCMT	43	84	-49	Centroid Moment Tensor
2014-11-18 03:25:37.500	94.3581	7.4832	8	5.6	Mw	ISC (NEIC)	140	78	165	Centroid Moment Tensor
2014-11-18 06:06:29.400	94.43	7.45	15.1	5.1	Mw	GCMT	50	84	-45	Centroid Moment Tensor
2014-11-19 01:56:48	105.43	42.78	3	4.7	Mw	Han et al. 2019	65	54	-163	First Motion
2014-11-19 02:49:19	105.47	42.75	7.2	4.1	Mw	Han et al. 2019	0	23	90	Centroid Moment Tensor
2014-11-19 03:05:45	105.44	42.84	2	4.7	Mw	Han et al. 2019	349	30	81	Centroid Moment Tensor
2014-11-19 03:14:08	105.5	42.71	17.9	4.3	Mw	Han et al. 2019	213	73	10	Centroid Moment Tensor
2014-11-20 06:05:47.700	94.42	7.49	19.3	4.8	Mw	GCMT	25	60	-64	Centroid Moment Tensor
2014-11-20 18:14:40.000	93.46	23.49	35.2	5.7	Mw	GCMT	49	66	-37	Centroid Moment Tensor
2014-11-21 03:15:25	101.42	33.04	16.3	4.8	Mw	Han et al. 2019	111	73	-21	Centroid Moment Tensor
2014-11-22 08:55:25	101.7	23.3	9	5.9	Mw	Luo et al., 2016	143	81	-11	Centroid Moment Tensor
2014-11-22 13:45:29.000	66.48	36.63	27.5	5.4	Mw	GCMT	139	47	127	Centroid Moment Tensor
2014-11-22 14:55:30	102.36	34.35	11.9	4.8	Mw	Han et al. 2019	214	73	-14	Centroid Moment Tensor
2014-11-22 18:16:38	104.44	32.09	15.3	4.1	Mw	Han et al. 2019	310	47	74	Centroid Moment Tensor
2014-11-25 15:19:09.000	101.7795	30.2169	12	5.6	Mw	ISC (NEIC)	152	82	-3	Centroid Moment Tensor
2014-11-28 01:18:46.500	92.79	12.4	36.2	5.1	Mw	GCMT	159	80	162	Centroid Moment Tensor

2014-12-05 18:43:44	100.5	23.3	8	5.6	Mw	Luo et al., 2016	163	69	-180	Centroid Moment Tensor
2014-12-06 10:20:00	100.5	23.3	8	5.6	Mw	Luo et al., 2016	160	77	180	Centroid Moment Tensor
2014-12-07 19:58:48	99.5	38.42	2	4.2	Mw	Han et al. 2019	110	27	83	Centroid Moment Tensor
2014-12-08 03:43:52	97.02	41.54	7	4.1	Mw	Han et al. 2019	35	76	5	First Motion
2014-12-16 03:03:39	103.06	30.32	5.8	4.1	Mw	Han et al. 2019	92	43	90	Centroid Moment Tensor
2014-12-18 15:32:15.400	86.56	27.46	30.3	5	Mw	GCMT	117	72	110	Centroid Moment Tensor
2014-12-19 02:36:19.200	94.42	7.61	24.6	5	Mw	GCMT	55	86	-41	Centroid Moment Tensor
2014-12-21 23:49:37	105.36	34.4	17.8	4.1	Mw	Han et al. 2019	220	30	-1	Centroid Moment Tensor
2015-01-04 01:47:13	109.91	38.47	4.5	4	Mw	Han et al. 2019	194	56	77	Centroid Moment Tensor
2015-01-07 03:36:20	106.22	32.95	5	4	Mw	Han et al. 2019	46	16	-5	Centroid Moment Tensor
2015-02-04 10:44:17	83.43	32.87	10	5.1	Ms	WSM2016	215	84	2	NaN
2015-02-04 11:53:17	99.06	34.72	5.9	4.5	Mw	Han et al. 2019	139	53	-90	Centroid Moment Tensor
2015-02-04 22:18:44	106.09	36.69	13.8	4.2	Mw	Han et al. 2019	283	77	8	Centroid Moment Tensor
2015-02-11 03:30:14	92.27	13.1	33	5.2	Mw	WSM2016	159	57	-173	NaN
2015-02-24 00:52:06	104.01	31.67	29.1	4.5	Mw	Han et al. 2019	228	59	80	Centroid Moment Tensor
2015-02-26 21:59:05.100	73.28	34.57	19.7	5.1	Mw	GCMT	125	53	92	Centroid Moment Tensor
2015-02-28 00:50:56	103.91	33.15	22	4	Mw	Han et al. 2019	158	69	-7	Centroid Moment Tensor
2015-03-01 04:38:12	104.09	31.78	20.7	4.1	Mw	Han et al. 2019	249	28	21	Centroid Moment Tensor
2015-03-01 10:24:43	98.78	23.63	17	5.2	Mw	WSM2016	340	86	179	NaN
2015-03-02 06:28:07	105.6	37.47	10.1	4	Mw	Han et al. 2019	76	55	-90	Centroid Moment Tensor
2015-03-04 14:32:10	103.7	38.04	14.2	4.2	Mw	Han et al. 2019	280	39	31	Centroid Moment Tensor

2015-03-20 13:10:01	99.2	35.98	14.5	4.2	Mw	Han et al. 2019	42	54	-17	Centroid Moment Tensor
2015-04-07 04:41:53	83.58	32.97	16	5	Mw	WSM2016	130	87	-177	NaN
2015-04-09 19:37:02	105.57	34.65	17	4.2	Mw	Han et al. 2019	89	72	33	Centroid Moment Tensor
2015-04-09 22:49:44	92.83	14.08	39	4.8	Mw	WSM2016	240	42	-61	NaN
2015-04-15 07:08:36	104.03	35.36	24.9	5	Mw	Han et al. 2019	192	85	-8	Centroid Moment Tensor
2015-04-15 07:39:27	106.37	39.76	9.9	5.7	Mw	Han et al. 2019	357	85	-179	Centroid Moment Tensor
2015-04-15 10:49:57	106.36	39.81	13	4.1	Mw	Han et al. 2019	69	70	-30	Centroid Moment Tensor
2015-04-16 09:16:19	106.45	39.79	36	4.1	Mw	Han et al. 2019	55	64	-64	First Motion
2015-04-21 00:17:29.800	92.8	14.12	26.4	4.9	Mw	GCMT	5	66	-122	Centroid Moment Tensor
2015-04-21 14:02:17.500	82.35	28.65	26.4	5	Mw	GCMT	118	44	66	Centroid Moment Tensor
2015-04-23 23:58:22	94.99	12.3	34.4	4.9	Ms	WSM2016	241	42	-60	NaN
2015-04-25 06:11:23.600	84.726	28.194	10	7.6	Mw	MOS	281	19	94	Centroid Moment Tensor
2015-04-25 06:45:29.400	84.93	27.86	21	6.7	Mw	GCMT	85	73	74	Centroid Moment Tensor
2015-04-25 06:56:00	85.767	27.805	12.1	4.85	Mw	Wang et al., 2017	336	21	149	Centroid Moment Tensor
2015-04-25 07:07:00	85.922	27.745	14.7	4.54	Mw	Wang et al., 2017	55	74	60	Centroid Moment Tensor
2015-04-25 07:47:00	85.63	27.884	14.9	4.58	Mw	Wang et al., 2017	334	22	161	Centroid Moment Tensor
2015-04-25 08:20:00	85.115	27.726	7.9	4.35	Mw	Wang et al., 2017	79	56	95	Centroid Moment Tensor
2015-04-25 08:29:00	84.68	27.947	9.4	4.47	Mw	Wang et al., 2017	249	16	75	Centroid Moment Tensor
2015-04-25 08:55:00	85.516	27.619	7.3	4.88	Mw	Wang et al., 2017	304	85	-58	Centroid Moment Tensor
2015-04-25 12:44:00	84.665	28.105	7.4	4.73	Mw	Wang et al., 2017	13	28	180	Centroid Moment Tensor
2015-04-25 17:42:50.900	85.824	28.2406	9	5.1	Mw	ISC (NEIC)	192	77	-71	Centroid Moment Tensor

2015-04-25 23:16:15.000	84.8504	27.7701	14	5	Mw	ISC (NEIC)	197	50	-37	Centroid Moment Tensor
2015-04-26 07:09:00	86.0147	27.7677	13.1	6.66	Mw	Wang et al., 2017	304	19	110	Centroid Moment Tensor
2015-04-26 16:26:00	85.815	27.807	13	5.02	Mw	Wang et al., 2017	304	20	122	Centroid Moment Tensor
2015-04-27 12:35:52.900	88.27	26.66	26.5	5	Mw	GCMT	52	71	-35	Centroid Moment Tensor
2015-05-12 07:05:00	86.097	27.752	11.6	7.14	Mw	Wang et al., 2017	329	8	141	Centroid Moment Tensor
2015-05-12 07:34:00	86.264	27.694	14.8	4.72	Mw	Wang et al., 2017	222	34	50	Centroid Moment Tensor
2015-05-12 07:36:00	86.148	27.584	10	5.92	Mw	Wang et al., 2017	270	32	68	Centroid Moment Tensor
2015-05-12 08:13:00	85.852	27.764	11.5	4.6	Mw	Wang et al., 2017	300	15	120	Centroid Moment Tensor
2015-05-13 21:38:00	86.072	27.638	10.4	4.44	Mw	Wang et al., 2017	236	16	45	Centroid Moment Tensor
2015-05-15 01:42:00	84.738	27.862	10	4.45	Mw	Wang et al., 2017	258	44	102	Centroid Moment Tensor
2015-05-16 08:33:04	103.56	31.47	24.1	4	Mw	Han et al. 2019	307	77	-13	Centroid Moment Tensor
2015-05-16 11:34:00	86.151	27.588	9.5	5.22	Mw	Wang et al., 2017	322	11	131	Centroid Moment Tensor
2015-05-17 01:20:16	100.15	39.26	26.7	4.1	Mw	Han et al. 2019	280	80	-27	Centroid Moment Tensor
2015-05-20 03:31:41.900	70.2332	38.6719	11	5.2	Mw	ISC (NEIC)	76	29	160	Centroid Moment Tensor
2015-05-30 00:04:48.400	91.13	34.67	12.5	4.6	Mw	GCMT	30	35	-95	Centroid Moment Tensor
2015-06-24 19:12:54.600	88.4058	41.8061	33	5	Mw	ISC (NEIC)	133	46	98	Centroid Moment Tensor
2015-06-28 01:05:28.600	90.4247	26.6388	15	5.1	Mw	ISC (NEIC)	134	61	146	Centroid Moment Tensor
2015-06-30 19:44:50.400	73.6597	39.5964	14	4.1	Mw	ISC (NEIC)	14	31	-110	Centroid Moment Tensor
2015-07-13 18:25:07.500	72.61	39.18	26.1	4.9	Mw	GCMT	43	70	-15	Centroid Moment Tensor
2015-07-15 10:26:13	103.71	37.12	6.3	4.4	Mw	Han et al. 2019	282	81	5	Centroid Moment Tensor

2015-07-17 19:51:18.100	69.2666	36.8498	14	4.1	Mw	ISC (NEIC)	25	29	-77	Centroid Moment Tensor
2015-07-21 01:27:09.000	96.25	19.15	18.9	4.8	Mw	GCMT	166	40	118	Centroid Moment Tensor
2015-08-02 11:09:24	100.14	39.26	23.8	4.1	Mw	Han et al. 2019	270	82	7	Centroid Moment Tensor
2015-08-11 23:11:52	103.63	31.25	2	4.2	Mw	Han et al. 2019	59	23	83	Centroid Moment Tensor
2015-08-20 05:39:09	106.55	39.29	6.5	4	Mw	Han et al. 2019	269	57	-82	Centroid Moment Tensor
2015-08-23 19:14:14	103.44	31.3	19.6	4	Mw	Han et al. 2019	304	55	-4	Centroid Moment Tensor
2015-08-28 11:44:44	103.39	31.32	19.4	4.1	Mw	Han et al. 2019	309	57	7	Centroid Moment Tensor
2015-08-31 13:56:06	104.41	31.89	17.8	4.1	Mw	Han et al. 2019	190	42	50	Centroid Moment Tensor
2015-09-02 01:47:48	104.94	32.42	25.4	4.3	Mw	Han et al. 2019	91	59	83	Centroid Moment Tensor
2015-09-22 17:43:10.000	71.9187	41.3059	25	4.3	Mw	ISC (NEIC)	56	27	69	Centroid Moment Tensor
2015-09-22 18:01:36	105.38	32.61	3	4.4	Mw	Han et al. 2019	159	38	28	Centroid Moment Tensor
2015-10-21 00:36:03	109.78	38.4	3	4.2	Mw	Han et al. 2019	147	67	59	Centroid Moment Tensor
2015-10-23 00:27:42.300	70.3633	29.669	11	5.4	Mw	ISC (NEIC)	32	47	112	Centroid Moment Tensor
2015-10-28 20:12:11.200	100.38	27.62	13.6	4.8	Mw	GCMT	6	46	78	Centroid Moment Tensor
2015-10-30 11:26:43.600	99.57	24.98	15.9	5	Mw	GCMT	35	51	-64	Centroid Moment Tensor
2015-11-17 17:29:36.000	73.131	40.371	16	5.6	Mw	IPGP	74	35	117	Centroid Moment Tensor
2015-11-20 04:45:49.900	73.2169	40.4008	18	4.5	Mw	ISC (NEIC)	51	61	112	Centroid Moment Tensor
2015-11-22 14:53:42	106.71	39.95	8.2	4	Mw	Han et al. 2019	259	44	29	Centroid Moment Tensor
2015-11-22 21:02:41	100.39	38.01	12	5.3	Mw	Han et al. 2019	113	59	17	Centroid Moment Tensor
2015-11-22 22:13:46	100.41	37.94	11.4	4	Mw	Han et al. 2019	301	73	30	Centroid Moment Tensor

2015-11-27 08:34:01.900	94.99	22.38	16.6	5.4	Mw	GCMT	92	37	38	Centroid Moment Tensor
2015-12-06 04:35:02	106.12	39.14	3.5	4	Mw	Han et al. 2019	140	43	51	Centroid Moment Tensor
2015-12-18 22:17:01.000	81.6	29.04	23.1	5.2	Mw	GCMT	102	60	72	Centroid Moment Tensor
2016-01-12 17:11:25	106.28	36.37	4	4.4	Mw	Han et al. 2019	114	52	-20	Centroid Moment Tensor
2016-01-13 14:19:27.800	71.2	36.5126	74	4.5	Mw	ISC (NEIC)	38	34	63	Centroid Moment Tensor
2016-01-13 20:35:00.400	91.73	32.52	23	5.4	Mw	GCMT	72	82	-3	Centroid Moment Tensor
2016-01-13 21:18:16.300	84.11	42.11	22.5	5.1	Mw	GCMT	111	62	106	Centroid Moment Tensor
2016-01-13 21:37:39.200	73.21	38.78	23.4	4.9	Mw	GCMT	45	83	-32	Centroid Moment Tensor
2016-01-20 17:13:12	101.65	37.66	3.8	6.2	Mw	Han et al. 2019	131	66	73	Centroid Moment Tensor
2016-01-20 17:57:20	101.64	37.66	12	4.6	Mw	Han et al. 2019	317	44	31	Centroid Moment Tensor
2016-01-20 19:25:06	101.6	37.69	12.6	4	Mw	Han et al. 2019	135	73	26	Centroid Moment Tensor
2016-01-21 09:55:26	101.65	37.65	7.7	4.1	Mw	Han et al. 2019	138	69	41	Centroid Moment Tensor
2016-01-23 08:02:50	101.6	37.69	2	4.2	Mw	Han et al. 2019	11	23	-90	Centroid Moment Tensor
2016-01-24 21:43:31	105.5	40.8	5.5	4.1	Mw	Han et al. 2019	22	39	-90	Centroid Moment Tensor
2016-02-02 10:25:33	101.67	37.64	5.7	4.1	Mw	Han et al. 2019	139	55	61	Centroid Moment Tensor
2016-02-23 00:33:37.700	95.11	31.86	20.6	4.9	Mw	GCMT	39	53	-71	Centroid Moment Tensor
2016-03-18 16:11:00.100	72.4418	38.0049	22	5.3	Mw	ISC (NEIC)	127	75	179	Centroid Moment Tensor
2016-03-21 14:48:51.300	66.0911	27.7707	17	5.6	Mw	ISC (NEIC)	83	87	168	Centroid Moment Tensor
2016-04-19 20:33:01.000	93.83	10.29	12	5.1	Mw	GCMT	47	47	-146	Centroid Moment Tensor
2016-04-23 09:32:56.800	95.08	31.76	23.9	4.8	Mw	GCMT	44	54	-64	Centroid Moment Tensor

2016-05-13 07:01:10.300	66.3842	30.6604	7	5.5	Mw	ISC (NEIC)	110	74	177	Centroid Moment Tensor
2016-05-17 16:48:51.900	99.64	26.07	19.4	5	Mw	GCMT	23	87	4	Centroid Moment Tensor
2016-05-17 17:05:14.000	99.63	26.1	25.3	4.8	Mw	GCMT	14	45	-56	Centroid Moment Tensor
2016-05-22 01:32:37.500	87.66	28.26	22.7	4.8	Mw	GCMT	189	41	-66	Centroid Moment Tensor
2016-05-22 01:48:49.200	87.62	28.22	12	5.3	Mw	GCMT	203	45	-46	Centroid Moment Tensor
2016-05-22 02:05:55.400	87.6	28.22	12	5.2	Mw	GCMT	175	37	-83	Centroid Moment Tensor
2016-06-26 11:17:08.800	73.464	39.447	11	6.5	Mw	MOS	75	42	137	Centroid Moment Tensor
2016-06-27 05:08:22.300	73.4918	39.4844	21	4.3	Mw	ISC (NEIC)	200	71	-22	Centroid Moment Tensor
2016-06-27 06:25:38.600	73.3494	39.4908	15	4.6	Mw	ISC (NEIC)	185	52	-13	Centroid Moment Tensor
2016-06-27 19:28:48.900	73.42	39.5	18	4.9	Mw	GCMT	91	54	96	Centroid Moment Tensor
2016-06-28 12:43:16.100	73.3726	39.4984	20	4.8	Mw	ISC (NEIC)	179	34	-68	Centroid Moment Tensor
2016-06-28 21:38:03.800	73.3318	39.4686	19	5.4	Mw	ISC (NEIC)	88	87	171	Centroid Moment Tensor
2016-06-29 08:08:15.500	73.46	39.49	20.4	4.8	Mw	GCMT	60	47	50	Centroid Moment Tensor
2016-07-19 12:32:56.800	79.26	41.58	14.4	4.8	Mw	GCMT	54	53	87	Centroid Moment Tensor
2016-08-13 08:29:50.500	101.7	37.72	22.9	4.8	Mw	GCMT	127	40	78	Centroid Moment Tensor
2016-09-15 02:30:46.500	91.45	10.13	12	4.9	Mw	GCMT	72	77	-167	Centroid Moment Tensor
2016-09-22 16:47:17.300	99.78	30.1	20.2	5.2	Mw	GCMT	56	53	-122	Centroid Moment Tensor
2016-09-22 17:23:16.000	99.75	30.08	21.1	5.2	Mw	GCMT	69	51	-117	Centroid Moment Tensor
2016-09-23 22:27:22.500	94.21	8.29	19.8	5	Mw	GCMT	73	86	-29	Centroid Moment Tensor
2016-09-26 19:04:19.000	94.19	8.34	16.5	5	Mw	GCMT	73	86	-32	Centroid Moment Tensor

2016-10-17 07:14:49.600	94.95	32.79	20.9	6	Mw	GCMT	63	59	-33	Centroid Moment Tensor
2016-10-20 04:53:53.700	69.93	30.83	24.2	5	Mw	GCMT	84	52	-180	Centroid Moment Tensor
2016-11-17 21:45:58.700	96.21	32.59	22.3	4.9	Mw	GCMT	79	73	1	Centroid Moment Tensor
2016-11-25 14:19:04.000	73.86	39.13	21.5	5.2	Mw	ISC (NEIC)	24	89	37	Centroid Moment Tensor
2016-11-25 14:24:39.000	74.01	39.67	11.5	6.6	Mw	ISC (NEIC)	107	76	174	Centroid Moment Tensor
2016-11-25 19:46:19.500	74.3071	39.24	29	4.3	Mw	ISC (NEIC)	183	69	-16	Centroid Moment Tensor
2016-11-26 09:23:28.000	74.26	39.26	20	5	Mw	GCMT	104	86	179	Centroid Moment Tensor
2016-11-27 23:35:26.000	86.53	27.35	35.4	5.2	Mw	GCMT	100	67	80	Centroid Moment Tensor
2016-12-14 08:14:33.000	90.18	38.7	24.6	4.9	Mw	GCMT	143	89	177	Centroid Moment Tensor
2016-12-20 10:04:39.360	84.9583	37.1442	10	5.4	Mw	ISC (NEIC)	165	62	156	Centroid Moment Tensor
2017-01-18 15:42:41.900	95.04	12.04	12.1	4.9	Mw	GCMT	80	58	-54	Centroid Moment Tensor
2017-01-20 09:54:05.800	76.93	38.33	19.3	5	Mw	GCMT	122	26	43	Centroid Moment Tensor
2017-01-31 06:16:02.700	94.07	31.46	22.3	4.8	Mw	GCMT	68	80	-11	Centroid Moment Tensor
2017-03-13 14:19:08.100	96.09	17.23	12	5.2	Mw	GCMT	7	86	175	Centroid Moment Tensor
2017-03-14 11:07:14.700	73.47	39.28	17.2	5	Mw	GCMT	14	70	-7	Centroid Moment Tensor
2017-03-22 11:27:01.940	71.9527	37.5003	9.9	4.9	Mw	ISC (NEIC)	229	89	-22	Centroid Moment Tensor
2017-03-24 01:23:31.100	67.37	28.9	25.2	5	Mw	GCMT	121	90	156	Centroid Moment Tensor
2017-03-26 23:40:32.000	99.82	25.75	23	5	Mw	GCMT	51	89	5	Centroid Moment Tensor
2017-03-26 23:55:04.100	99.84	25.82	20.3	5.1	Mw	GCMT	48	89	5	Centroid Moment Tensor
2017-04-18 09:13:10.600	100.17	20.68	21.5	4.9	Mw	GCMT	145	87	174	Centroid Moment Tensor

2017-04-28 05:01:24.680	76.8073	41.8946	6.9	4.3	Mw	ISC (NEIC)	55	26	45	Centroid Moment Tensor
2017-05-16 14:04:44.700	95.16	11.61	27.9	4.8	Mw	GCMT	266	85	-1	Centroid Moment Tensor
2017-05-22 09:23:09.100	73.54	39.43	14.8	4.7	Mw	GCMT	103	77	168	Centroid Moment Tensor
2017-06-13 19:38:18.800	91.3	33.59	12	4.9	Mw	GCMT	59	57	-64	Centroid Moment Tensor
2017-06-26 00:39:47.040	73.5158	39.5189	10	4	Mw	ISC (NEIC)	116	42	139	Centroid Moment Tensor
2017-06-29 21:45:31.440	73.3632	39.4748	10	4.1	Mw	ISC (NEIC)	62	89	32	Centroid Moment Tensor
2017-07-23 10:36:37.120	75.2771	41.133	3.5	4.2	Mw	ISC (NEIC)	92	40	121	Centroid Moment Tensor
2017-08-21 11:20:17.200	88.63	35.49	29.2	4.8	Mw	GCMT	54	82	-6	Centroid Moment Tensor
2017-09-09 07:48:36.560	74.9524	38.8091	10	4.2	Mw	ISC (NEIC)	37	33	-143	Centroid Moment Tensor
2017-09-16 10:11:33.470	83.5155	42.2053	16	5.4	Mw	ISC (NEIC)	88	55	92	Centroid Moment Tensor
2017-09-29 13:49:57.000	67.8665	40.0326	13.5	5.1	Mw	ISC (NEIC)	44	18	77	Centroid Moment Tensor
2017-11-17 22:34:25.200	95.14	29.69	12	6.5	Mw	GCMT	119	24	72	Centroid Moment Tensor
2017-12-14 18:54:27.300	101.7555	35.2516	11.5	5	Mw	ISC (NEIC)	106	70	50	Centroid Moment Tensor
2017-12-22 15:58:48.100	93.1114	10.1077	40.5	4.8	Mw	ISC (NEIC)	168	58	97	Centroid Moment Tensor
2017-12-27 13:56:58.800	72.33	38.98	20.9	4.8	Mw	GCMT	27	78	12	Centroid Moment Tensor
2017-12-29 11:29:41.000	92.46	8.48	20.5	5.1	Mw	GCMT	195	48	-44	Centroid Moment Tensor
2018-01-17 01:25:22.800	86.94	35.03	28.4	5	Mw	GCMT	209	56	-57	Centroid Moment Tensor
2018-01-25 01:15:58.000	91.783	8.27	10	5.9	Mw	IPGP	35	56	-51	Centroid Moment Tensor
2018-01-25 03:48:27.450	91.728	8.241	12	5.2	Mw	ISC (GFZ)	190	29	-79	Centroid Moment Tensor
2018-01-31 04:58:45.300	66.49	26.07	14.6	4.8	Mw	GCMT	70	67	62	Centroid Moment Tensor

2018-02-13 02:39:45.230	92.962	12.216	59	5.1	Mw	ISC (GFZ)	120	39	123	Centroid Moment Tensor
2018-02-14 23:58:54.540	86.893	34.904	11	4.8	Mw	ISC (GFZ)	147	86	178	Centroid Moment Tensor
2018-02-15 10:17:26.900	82.11	35.92	25.5	4.9	Mw	GCMT	209	49	-60	Centroid Moment Tensor
2018-03-17 19:59:02.500	96.21	18.24	18.5	4.8	Mw	GCMT	174	44	102	Centroid Moment Tensor
2018-04-22 23:39:30.460	73.068	38.7307	21.1	4.3	Mw	ISC (NEIC)	222	63	-22	Centroid Moment Tensor
2018-04-28 15:14:21.500	70.946	36.3463	70.5	5.3	Mw	ISC (NEIC)	47	59	41	Centroid Moment Tensor
2018-05-05 19:56:35.000	88.86	35.93	13.4	4.7	Mw	GCMT	83	64	-6	Centroid Moment Tensor
2018-05-13 18:20:58.500	93.581	7.3523	30.5	5.1	Mw	ISC (NEIC)	17	4	114	Centroid Moment Tensor
2018-06-06 18:15:55.500	78.25	35.96	17.3	5	Mw	GCMT	243	65	-47	Centroid Moment Tensor
2018-06-17 13:21:30.200	96.0775	18.181	11.5	5	Mw	ISC (NEIC)	127	28	67	Centroid Moment Tensor
2018-06-17 14:21:28.900	70.4403	30.1769	11.5	5.1	Mw	ISC (NEIC)	89	46	166	Centroid Moment Tensor
2018-06-21 20:29:23.700	94.51	7.23	25.3	5	Mw	GCMT	62	88	-19	Centroid Moment Tensor
2018-07-20 01:27:34.140	73.2124	38.7797	35	4.2	Mw	ISC (NEIC)	207	76	-14	Centroid Moment Tensor
2018-07-21 00:40:39.000	80.97	35.15	22.2	5	Mw	GCMT	247	80	-20	Centroid Moment Tensor
2018-08-13 16:07:10.200	93.24	13.98	26.7	4.9	Mw	GCMT	32	85	149	Centroid Moment Tensor
2018-09-14 07:51:24.400	94.25	7.18	71	5.1	Mw	GCMT	101	60	150	Centroid Moment Tensor
2018-09-14 22:15:05.270	77.2122	41.9386	20	4.2	Mw	ISC (NEIC)	88	55	76	Centroid Moment Tensor
2018-09-27 21:13:19.900	80.6914	34.1183	11.5	5	Mw	ISC (NEIC)	200	43	-43	Centroid Moment Tensor
2018-10-18 07:52:03.400	89.25	33.46	14.6	5	Mw	GCMT	76	64	-20	Centroid Moment Tensor
2018-10-22 16:49:39.200	87.85	29.96	23.8	5	Mw	GCMT	6	51	-72	Centroid Moment Tensor

2018-10-29 14:43:35.800	78.0096	34.2401	17.5	4.9	Mw	ISC (NEIC)	33	47	-87	Centroid Moment Tensor
2018-10-30 02:22:21.010	75.1483	39.4323	19.5	4.6	Mw	ISC (NEIC)	14	89	25	Centroid Moment Tensor
2018-10-31 23:09:04.000	87.83	30.04	18.9	4.9	Mw	GCMT	158	37	-95	Centroid Moment Tensor
2018-11-14 17:10:52.500	84.06	34.17	24.1	4.7	Mw	GCMT	209	47	-38	Centroid Moment Tensor
2018-11-28 10:17:06.970	96.9185	27.1986	11	5.3	Mw	ISC (NEIC)	68	62	50	Centroid Moment Tensor
2018-11-28 14:44:25.100	68.8072	35.8103	23.5	4.9	Mw	ISC (NEIC)	43	57	109	Centroid Moment Tensor
2018-12-20 11:08:11.700	74.76	39.11	19.1	5.1	Mw	GCMT	190	85	-10	Centroid Moment Tensor
2018-12-22 00:32:27.400	71.6867	37.7941	5	4	Mw	ISC (NEIC)	73	45	113	Centroid Moment Tensor
2018-12-23 19:32:21.000	87.752	30.539	10	5.7	Mw	IPGP	199	50	-70	Centroid Moment Tensor
2019-01-14 10:54:51.200	101.8	21.33	12	4.8	Mw	GCMT	54	90	21	Centroid Moment Tensor
2019-01-16 21:39:38.900	96.4	24.79	23.4	4.7	Mw	GCMT	35	68	-165	Centroid Moment Tensor
2019-01-20 14:28:30.030	87.597	30.305	10	4.9	Mw	ISC (GFZ)	6	50	-71	Centroid Moment Tensor
2019-01-20 15:06:42.800	87.81	30.21	21	4.8	Mw	GCMT	193	43	-59	Centroid Moment Tensor
2019-02-20 09:05:42.500	99.6	19.24	16	4.7	Mw	GCMT	82	68	9	Centroid Moment Tensor
2019-03-16 06:00:05.900	67.68	29.62	22.8	4.9	Mw	GCMT	27	65	93	Centroid Moment Tensor
2019-03-23 11:29:27.400	93	14.1178	17.5	5.2	Mw	ISC (NEIC)	29	52	-106	Centroid Moment Tensor
2019-03-25 11:25:28.100	70.16	30.87	19.6	4.7	Mw	GCMT	260	78	175	Centroid Moment Tensor
2019-03-27 21:36:34.800	90.94	38.37	14.6	4.8	Mw	GCMT	130	54	80	Centroid Moment Tensor
2019-03-28 03:08:15.500	95.12	11.17	12	4.7	Mw	GCMT	24	43	-58	Centroid Moment Tensor
2019-03-31 23:44:43.300	94.3	7.5	12	5	Mw	GCMT	65	86	-23	Centroid Moment Tensor

2019-04-04 07:45:30.100	94	25.759	60.5	5.1	Mw	ISC (NEIC)	80	70	1	Centroid Moment Tensor
2019-04-13 16:12:59.300	94.42	7.34	12	5.4	Mw	GCMT	55	83	-9	Centroid Moment Tensor
2019-04-13 20:43:31.170	94.205	7.314	13	5	Mw	ISC (GFZ)	148	82	162	Centroid Moment Tensor
2019-04-14 18:31:11.000	89.3	32.23	25.7	4.7	Mw	GCMT	232	86	-17	Centroid Moment Tensor
2019-04-18 21:52:10.560	94.206	7.633	10	4.9	Mw	ISC (GFZ)	153	89	165	Centroid Moment Tensor
2019-04-23 20:15:50.000	94.564	28.463	15	6.1	Mw	IPGP	92	87	97	Centroid Moment Tensor
2019-04-27 20:27:38.100	97.42	39.14	16.9	5	Mw	GCMT	119	44	89	Centroid Moment Tensor
2019-04-29 00:23:17.660	73.7091	39.1983	35	4.6	Mw	ISC (NEIC)	109	85	106	Centroid Moment Tensor
2019-05-17 19:05:23.500	94.34	7.61	18.7	5.1	Mw	GCMT	67	78	-24	Centroid Moment Tensor
2019-05-22 00:39:34.960	92.9916	13.8921	29	5.6	Mw	ISC (NEIC)	13	70	-118	Centroid Moment Tensor
2019-05-24 21:23:39.900	92.87	13.86	24.7	5	Mw	GCMT	246	42	-18	Centroid Moment Tensor
2019-05-26 01:44:58.200	87.76	30.2	15.1	4.9	Mw	GCMT	209	56	-41	Centroid Moment Tensor
2019-05-26 02:09:28.400	87.77	30.3	15	4.8	Mw	GCMT	204	30	-25	Centroid Moment Tensor
2019-06-17 22:20:01.500	92.77	12.14	31.1	4.9	Mw	GCMT	246	69	-18	Centroid Moment Tensor
2019-07-15 17:41:31.900	91.32	31.63	20.1	4.7	Mw	GCMT	25	54	-76	Centroid Moment Tensor
2019-07-19 09:22:15.510	92.8302	27.7188	15	5.3	Mw	ISC (NEIC)	38	69	92	Centroid Moment Tensor
2019-07-19 22:54:27.900	92.99	27.67	26.1	4.9	Mw	GCMT	51	81	98	Centroid Moment Tensor
2019-07-21 12:23:31.400	100.77	26.11	21.8	5	Mw	GCMT	27	77	-7	Centroid Moment Tensor
2019-08-18 03:24:23.400	94.64	18.4	24	5.4	Mw	GCMT	78	25	-156	Centroid Moment Tensor
2019-08-21 20:10:47.600	69.37	36.4	22.3	4.7	Mw	GCMT	4	39	79	Centroid Moment Tensor

2019-08-28 13:40:06.200	93.01	13.15	66	4.8	Mw	GCMT	14	56	-178	Centroid Moment Tensor
2019-08-31 15:09:22.590	95.395	22.787	11	5.4	Mw	ISC (GFZ)	188	85	177	Centroid Moment Tensor
2019-09-09 06:40:33.300	75.87	32.92	30.1	4.9	Mw	GCMT	118	55	89	Centroid Moment Tensor
2019-09-16 12:48:42.400	100.31	38.55	22.4	5.1	Mw	GCMT	137	44	101	Centroid Moment Tensor
2019-09-24 11:01:54.990	73.7936	33.0779	10	5.6	Mw	ISC (NEIC)	106	90	106	Centroid Moment Tensor
2019-09-27 10:58:34.300	88.79	38	19	4.8	Mw	GCMT	85	85	17	Centroid Moment Tensor
2019-09-29 09:02:13.600	91.38	10.87	18.3	4.8	Mw	GCMT	15	25	96	Centroid Moment Tensor
2019-10-22 01:30:40.680	95.695	19.2642	10	4.3	Mw	ISC (NEIC)	174	63	111	Centroid Moment Tensor
2019-10-27 05:29:49.100	78.75	41.22	12	4.9	Mw	GCMT	91	43	114	Centroid Moment Tensor
2019-10-27 10:52:41.340	78.8603	41.3098	10	4.3	Mw	ISC (NEIC)	83	47	97	Centroid Moment Tensor
2019-11-17 06:47:09.800	94.55	7.17	13.3	4.8	Mw	GCMT	57	82	-21	Centroid Moment Tensor
2019-11-17 23:05:58.000	93	11.4	26.7	5	Mw	GCMT	20	87	-97	Centroid Moment Tensor
2019-11-19 13:30:56.600	81.217	29.358	12	4.9	Mw	ISC (GFZ)	106	77	87	Centroid Moment Tensor
2019-11-20 21:03:57.830	101.2534	19.4452	10	5.6	Mw	ISC (NEIC)	69	87	-11	Centroid Moment Tensor
2019-11-20 23:50:43.000	101.356	19.453	10	6.6	Mw	ISC-PPSM	133	63	173	Centroid Moment Tensor
2019-11-26 11:05:57.500	94.4139	19.6306	70.5	5.3	Mw	ISC (NEIC)	71	51	172	Centroid Moment Tensor
2019-11-28 14:39:13.800	96.0424	23.18	11.5	5.2	Mw	ISC (NEIC)	94	54	0	Centroid Moment Tensor
2019-12-14 18:53:21.160	79.1662	38.9262	37.7	4.2	Mw	ISC (NEIC)	39	28	-155	Centroid Moment Tensor
2019-12-19 12:07:58.600	87.15	32.5	28.5	5	Mw	GCMT	205	54	-57	Centroid Moment Tensor
2019-12-30 17:18:58.000	74.65	35.57	12	5.6	Mw	GCMT	234	57	-42	Centroid Moment Tensor

2019-12-30 17:49:59.900	74.52	35.49	12	5.1	Mw	GCMT	59	46	-55	Centroid Moment Tensor
2020-01-16 08:32:38.500	83.5418	41.6107	11.5	5.2	Mw	ISC (NEIC)	64	81	-32	Centroid Moment Tensor
2020-01-17 16:05:50.560	77.139	39.741	12	5.2	Mw	ISC (GFZ)	80	86	-175	Centroid Moment Tensor
2020-01-19 13:27:56.630	77.1084	39.8353	5.5	6	Mw	ISC (NEIC)	67	81	88	Centroid Moment Tensor
2020-01-19 14:23:04.400	77.38	39.67	18.1	5.1	Mw	GCMT	84	68	88	Centroid Moment Tensor
2020-01-23 09:48:07.800	93.48	20.37	32.3	4.9	Mw	GCMT	15	53	-70	Centroid Moment Tensor
2020-01-24 07:09:15.700	71.5332	39.1619	11.5	5.5	Mw	ISC (NEIC)	32	21	110	Centroid Moment Tensor
2020-01-24 22:56:06.100	95.1	31.87	22.5	5.3	Mw	GCMT	25	44	-89	Centroid Moment Tensor
2020-01-29 09:10:50.300	70.43	38.81	22.5	5	Mw	GCMT	30	25	101	Centroid Moment Tensor
2020-01-29 21:45:35.600	91.98	28.55	22	4.8	Mw	GCMT	188	42	-75	Centroid Moment Tensor
2020-02-15 03:31:56.900	79.75	41.77	28	5.1	Mw	GCMT	79	31	49	Centroid Moment Tensor
2020-02-20 18:01:39.000	85.72	34.47	26.1	5.3	Mw	GCMT	56	87	0	Centroid Moment Tensor
2020-02-21 15:39:18.300	77.42	39.84	13.6	4.8	Mw	GCMT	44	65	51	Centroid Moment Tensor
2020-02-28 21:36:26.000	81.19	41.86	17.4	4.6	Mw	GCMT	65	85	-11	Centroid Moment Tensor
2020-03-15 16:17:07.500	85.63	32.79	26.3	5	Mw	GCMT	228	82	-16	Centroid Moment Tensor
2020-03-20 00:49:02.410	77.1901	42.0498	13.9	4.5	Mw	ISC (NEIC)	71	45	75	Centroid Moment Tensor
2020-03-20 01:33:15.140	87.331	28.648	13	5.7	Mw	ISC (GFZ)	185	40	-67	Centroid Moment Tensor
2020-03-22 19:21:43.000	81.19	41.88	17.7	4.8	Mw	GCMT	66	90	-19	Centroid Moment Tensor
2020-03-26 04:44:31.270	70.4159	40.7584	10	4.6	Mw	ISC (NEIC)	49	69	117	Centroid Moment Tensor
2020-04-16 11:45:23.000	94.029	22.8	36.2	6.3	Mw	ISC-PPSM	180	32	104	Centroid Moment Tensor

2020-04-21 00:09:11.000	92.95	9.37	29.8	4.8	Mw	GCMT	45	66	-130	Centroid Moment Tensor
2020-04-24 22:32:50.430	68.7379	37.5452	10	4.8	Mw	ISC (NEIC)	206	56	110	Centroid Moment Tensor
2020-04-24 22:43:21.850	68.7544	37.7227	10	4.4	Mw	ISC (NEIC)	184	29	95	Centroid Moment Tensor
2020-04-30 20:17:54.800	89.52	32.18	23.4	4.8	Mw	GCMT	70	85	3	Centroid Moment Tensor
2020-05-22 13:44:53.300	85.65	32.8	21.8	4.9	Mw	GCMT	242	82	-10	Centroid Moment Tensor
2020-05-22 18:38:19.500	85.64	32.8	23.4	5	Mw	GCMT	238	79	-20	Centroid Moment Tensor
2020-05-22 18:38:19.500	85.64	32.8	23.4	5	Mw	GCMT	238	79	-20	Centroid Moment Tensor
2020-05-25 14:42:17.870	93.892	24.333	65	5.1	Mw	ISC (GFZ)	247	63	-11	Centroid Moment Tensor
2020-06-21 10:46:29.000	93.23	23.89	33.8	5	Mw	GCMT	143	80	156	Centroid Moment Tensor
2020-06-21 22:40:52.780	93.326	23.192	13	5.5	Mw	ISC (GFZ)	15	88	175	Centroid Moment Tensor
2020-06-25 20:29:43.000	82.32	35.75	16.6	5	Mw	GCMT	233	66	-52	Centroid Moment Tensor
2020-06-25 21:05:18.000	82.452	35.628	10	6.3	Mw	IPGP	23	35	-80	Centroid Moment Tensor
2020-07-17 13:29:11.100	94.8613	11.6428	11.5	5.1	Mw	ISC (NEIC)	268	76	-3	Centroid Moment Tensor
2020-07-17 14:03:40.430	94.9362	11.8485	10	6.1	Mw	ISC (NEIC)	184	88	173	Centroid Moment Tensor
2020-07-17 14:43:17.000	95.03	11.77	12.1	5	Mw	GCMT	5	47	-174	Centroid Moment Tensor
2020-07-17 16:33:54.200	93.27	23.12	23.5	5.2	Mw	GCMT	9	69	176	Centroid Moment Tensor
2020-07-17 18:32:58.710	94.9745	12.0979	5.1	5.7	Mw	ISC (NEIC)	165	49	174	Centroid Moment Tensor
2020-07-22 20:07:19.190	86.8637	33.1438	10	6.1	Mw	ISC (NEIC)	28	48	-72	Centroid Moment Tensor
2020-07-23 10:50:11.300	86.86	33.09	13.6	5.1	Mw	GCMT	20	44	-91	Centroid Moment Tensor
2020-07-28 14:38:50.300	93.36	23.1	20	4.7	Mw	GCMT	16	87	-175	Centroid Moment Tensor

2020-07-31 11:20:13.200	86.7	33.01	27.4	4.9	Mw	GCMT	39	40	-69	Centroid Moment Tensor
2020-08-17 11:23:43.200	86.68	32.88	20.9	4.9	Mw	GCMT	17	39	-72	Centroid Moment Tensor
2020-08-26 00:48:54.400	82.39	35.78	23	4.8	Mw	GCMT	204	49	-67	Centroid Moment Tensor
2020-08-27 12:07:15.620	93.3258	23.1636	10	5.3	Mw	ISC (NEIC)	100	84	-6	Centroid Moment Tensor
2020-09-15 23:34:08.000	85.88	27.53	27.5	5.1	Mw	GCMT	106	69	83	Centroid Moment Tensor
2020-09-18 17:47:49.000	73.66	38.04	28.9	5.2	Mw	GCMT	32	82	-3	Centroid Moment Tensor
2020-09-25 10:57:14.270	78.205	34.208	10	5.1	Mw	ISC (GFZ)	28	41	-94	Centroid Moment Tensor
2020-09-27 17:27:48.200	78.03	34.35	18.1	5.1	Mw	GCMT	2	52	-164	Centroid Moment Tensor
2020-10-10 17:38:00.760	93.4997	24.6661	53	5.5	Mw	ISC (NEIC)	164	74	168	Centroid Moment Tensor
2020-10-21 13:12:37.300	90.4	33.35	19.6	4.7	Mw	GCMT	19	43	-98	Centroid Moment Tensor
2020-10-29 09:32:41.700	71.53	37.65	26	4.8	Mw	GCMT	111	51	138	Centroid Moment Tensor
2020-11-14 02:56:55.620	67.435	30.3659	12	5.5	Mw	ISC (NEIC)	36	72	-2	Centroid Moment Tensor
2020-12-23 23:51:50.400	98.33	34.14	21	4.8	Mw	GCMT	19	78	-170	Centroid Moment Tensor
2020-12-24 08:09:48.500	96.78	25.53	16.4	4.8	Mw	GCMT	24	58	178	Centroid Moment Tensor
2020-12-26 10:28:38.000	71.48	40.27	27.9	4.9	Mw	GCMT	46	27	92	Centroid Moment Tensor
2021-02-02 02:31:16.100	87.52	28.52	17.8	5	Mw	GCMT	159	43	-96	Centroid Moment Tensor
2021-02-25 02:34:26.000	96.03	22.69	19.9	4.9	Mw	GCMT	1	67	-167	Centroid Moment Tensor
2021-03-19 06:11:27.110	92.9151	31.9246	8	5.7	Mw	ISC (NEIC)	0	48	-136	Centroid Moment Tensor
2021-03-22 17:23:37.300	93	31.93	22.7	4.8	Mw	GCMT	203	46	-66	Centroid Moment Tensor
2021-03-23 21:14:20.300	81.17	41.8	12	5.3	Mw	GCMT	154	64	157	Centroid Moment Tensor

2021-03-26 00:18:34.000	91.38	35.4	28.1	4.8	Mw	GCMT	69	82	1	Centroid Moment Tensor
2021-03-26 19:02:08.900	92.8	27.45	28	4.9	Mw	GCMT	83	80	100	Centroid Moment Tensor
2021-03-29 17:27:23.000	87.719	34.352	8	5.7	Mw	IPGP	207	59	-75	Centroid Moment Tensor
2021-04-18 13:24:36.500	94.38	22.41	37.9	5.1	Mw	GCMT	14	63	106	Centroid Moment Tensor
2021-04-21 19:34:44.100	94.15	10.51	16	4.8	Mw	GCMT	75	40	-47	Centroid Moment Tensor
2021-04-28 02:21:29.100	92.5	26.62	39.8	6	Mw	GCMT	85	55	47	Centroid Moment Tensor
2021-05-13 03:42:38.600	99.36	24.35	18.5	4.7	Mw	GCMT	64	85	24	Centroid Moment Tensor
2021-05-14 09:54:04.540	73.0747	39.4026	10	4.3	Mw	ISC (NEIC)	59	87	111	Centroid Moment Tensor
2021-05-19 12:06:01.900	100.06	25.66	24.2	4.8	Mw	GCMT	226	79	-17	Centroid Moment Tensor
2021-05-21 13:21:33.800	100.0148	25.6892	11.5	5.2	Mw	ISC (NEIC)	11	62	-71	Centroid Moment Tensor
2021-05-21 13:48:37.190	100.0082	25.7274	9	5.9	Mw	ISC (NEIC)	45	89	-5	Centroid Moment Tensor
2021-05-21 14:31:19.900	99.9912	25.6809	15.5	5.1	Mw	ISC (NEIC)	43	64	-38	Centroid Moment Tensor
2021-05-21 18:04:15.900	98.263	34.569	15	7.4	Mw	ISC (GFZ)	102	84	-4	Centroid Moment Tensor
2021-05-22 02:29:37.700	97.54	34.9	18.4	5.2	Mw	GCMT	35	66	-175	Centroid Moment Tensor
2021-05-22 03:21:20.300	98.11	34.68	31.1	5.2	Mw	GCMT	55	44	-79	Centroid Moment Tensor
2021-05-22 07:06:24.900	98.89	34.48	26.6	5.1	Mw	GCMT	265	71	-5	Centroid Moment Tensor
2021-05-22 09:39:37.900	97.59	34.81	24.7	4.9	Mw	GCMT	36	88	-162	Centroid Moment Tensor
2021-05-22 12:14:39.900	100.08	25.55	16.5	4.8	Mw	GCMT	194	59	-65	Centroid Moment Tensor
2021-05-27 08:54:33.600	66.22	30.11	19.7	5	Mw	GCMT	17	81	-5	Centroid Moment Tensor
2021-05-27 13:06:10.000	99.14	34.55	19.1	5	Mw	GCMT	142	48	103	Centroid Moment Tensor

2021-05-28 03:58:09.100	66.41	27.77	12	4.7	Mw	GCMT	14	70	16	Centroid Moment Tensor
2021-05-30 04:50:10.300	98.27	34.71	25.3	5	Mw	GCMT	33	79	-161	Centroid Moment Tensor
2021-05-30 06:55:16.600	98.44	34.66	25.2	5.1	Mw	GCMT	35	77	-141	Centroid Moment Tensor
2021-06-15 14:46:06.500	97.23	26.48	27.3	4.8	Mw	GCMT	6	67	165	Centroid Moment Tensor
2021-06-16 08:48:58.000	93.723	38.206	14	5.7	Mw	ISC-PPSM	90	49	58	Centroid Moment Tensor
2021-06-28 00:40:38.000	77.95	34.28	12	4.7	Mw	GCMT	54	42	-56	Centroid Moment Tensor
2021-07-07 06:43:50.000	101.23	19.59	14.9	4.9	Mw	GCMT	251	87	-22	Centroid Moment Tensor
2021-07-20 23:54:27.200	69.84	29.07	12	5.1	Mw	GCMT	54	34	120	Centroid Moment Tensor
2021-07-26 05:03:34.300	94.56	24.58	47.2	4.9	Mw	GCMT	174	88	143	Centroid Moment Tensor
2021-08-13 04:21:39.700	97.65	34.6	19.1	5.7	Mw	GCMT	16	86	-162	Centroid Moment Tensor
2021-08-15 10:41:12.800	70.1	37.51	12.1	5.2	Mw	GCMT	2	40	26	Centroid Moment Tensor
2021-08-25 23:38:28.600	95.5261	38.9098	11.5	5.3	Mw	ISC (NEIC)	127	45	72	Centroid Moment Tensor
2021-09-17 19:12:02.800	69.39	29.97	12	5	Mw	GCMT	68	61	96	Centroid Moment Tensor
2021-09-19 19:24:05.100	95	25.17	58.8	4.7	Mw	GCMT	60	72	-57	Centroid Moment Tensor
2021-09-24 15:04:17.800	94.13	8.61	14.1	5.3	Mw	GCMT	79	81	-10	Centroid Moment Tensor
2021-09-27 05:40:42.900	73.1483	38.2431	17.5	5.1	Mw	ISC (NEIC)	2	50	-62	Centroid Moment Tensor
2021-11-13 21:42:07.400	68.89	32.13	21	4.8	Mw	GCMT	223	87	-11	Centroid Moment Tensor
2021-11-16 05:22:49.730	101.7446	22.2085	10	4.7	Mw	ISC (NEIC)	127	67	162	Centroid Moment Tensor
2021-11-16 07:54:48.800	101.84	22.26	15.9	4.7	Mw	GCMT	112	60	179	Centroid Moment Tensor
2021-11-25 23:45:44.700	93.43	22.62	42	6.2	Mw	GCMT	149	89	160	Centroid Moment Tensor

2021-11-30 13:53:41.740	87.922	31.618	13	5.5	Mw	ISC (GFZ)	177	44	-91	Centroid Moment Tensor
2021-12-14 22:17:16.200	69.76	37.42	23.2	4.8	Mw	GCMT	22	45	107	Centroid Moment Tensor
2021-12-18 23:54:31.200	92.62	39.07	26.5	5.1	Mw	GCMT	179	61	141	Centroid Moment Tensor
2021-12-19 21:06:15.040	101.3109	19.5613	10	5.3	Mw	ISC (NEIC)	64	86	-4	Centroid Moment Tensor
2021-12-21 21:08:37.300	93.77	10.17	14.8	4.7	Mw	GCMT	62	36	-70	Centroid Moment Tensor
2021-12-23 22:39:10.000	92.52	7.07	13.4	4.9	Mw	GCMT	207	59	-34	Centroid Moment Tensor
2021-12-24 13:43:22.920	101.6708	22.3699	9.5	5.6	Mw	ISC (NEIC)	211	78	-7	Centroid Moment Tensor
2021-12-24 14:02:30.900	101.76	22.29	16.4	4.9	Mw	GCMT	218	73	-4	Centroid Moment Tensor
2021-12-27 13:31:05.300	74.878	35.419	12	5.1	Mw	ISC (GFZ)	28	68	-24	Centroid Moment Tensor
2021-12-29 00:01:00.300	93.44	9.83	79.9	4.7	Mw	GCMT	108	45	155	Centroid Moment Tensor
2021-12-31 14:53:03.900	101.76	22.36	19.9	4.8	Mw	GCMT	129	82	177	Centroid Moment Tensor
2022-01-21 10:12:32.520	93.862	23.078	66	5.3	Mw	ISC (GFZ)	121	63	120	Centroid Moment Tensor
2022-01-23 02:21:19.920	97.3425	38.4613	10	5.4	Mw	ISC (NEIC)	167	76	177	Centroid Moment Tensor
2022-01-24 01:20:52.600	69.12	36.06	28	5.1	Mw	GCMT	46	84	178	Centroid Moment Tensor
2022-03-16 13:35:25.100	74.94	35.64	30.8	5.2	Mw	GCMT	32	85	-37	Centroid Moment Tensor
2022-03-17 00:26:05.200	97.65	39.04	21.5	5.1	Mw	GCMT	73	81	-10	Centroid Moment Tensor
2022-03-17 13:41:18.500	77.94	35.97	22.5	5.1	Mw	GCMT	88	70	37	Centroid Moment Tensor
2022-03-25 16:21:04.000	97.2796	38.5288	12	5.6	Mw	ISC (NEIC)	174	82	178	Centroid Moment Tensor
2022-03-25 16:28:42.000	97.29	38.59	24.6	5	Mw	GCMT	87	66	-5	Centroid Moment Tensor
2022-03-25 18:50:06.500	97.32	38.51	20.3	4.9	Mw	GCMT	91	87	-2	Centroid Moment Tensor

2022-04-15 01:26:16.280	97.27	38.458	21	5.1	Mw	ISC (GFZ)	88	71	-7	Centroid Moment Tensor
2022-04-16 00:32:18.200	100.67	27.76	24.5	4.8	Mw	GCMT	91	79	-176	Centroid Moment Tensor
2022-04-19 22:44:41.100	70.37	38.92	17.6	4.8	Mw	GCMT	116	49	150	Centroid Moment Tensor
2022-05-26 07:48:51.400	91.93	32.2	24.2	5.1	Mw	GCMT	226	86	-11	Centroid Moment Tensor
2022-06-21 20:54:37.520	69.4887	33.0316	20	6.2	Mw	ISC (AUST)	21	89	-11	Centroid Moment Tensor
2022-06-29 18:54:45.600	99.95	21.12	16.7	4.9	Mw	GCMT	228	73	-23	Centroid Moment Tensor
2022-07-18 12:22:45.380	69.5572	33.049	11	5.2	Mw	ISC (AUST)	17	83	9	Centroid Moment Tensor
2022-07-21 16:40:16.700	99.9696	20.9024	11.5	4.9	Mw	ISC (NEIC)	223	83	-36	Centroid Moment Tensor
2022-07-21 17:07:26.500	99.8632	21.1499	10	5.8	Mw	ISC (NEIC)	62	85	-5	Centroid Moment Tensor
2022-07-29 09:58:49.900	99.97	21.09	12	4.8	Mw	GCMT	78	37	-35	Centroid Moment Tensor
2022-07-29 10:17:22.600	99.8939	21.0572	5	4.3	Mw	ISC (NEIC)	59	63	-59	Centroid Moment Tensor
2022-07-30 05:56:33.800	85.15	34.32	26.4	4.8	Mw	GCMT	57	90	22	Centroid Moment Tensor
2022-07-31 02:28:12.200	86.82	27.07	14.7	4.7	Mw	GCMT	214	85	-66	Centroid Moment Tensor
2022-08-14 08:20:01.300	92.7992	33.1244	6	5.5	Mw	ISC (NEIC)	245	78	-4	Centroid Moment Tensor
2022-08-15 08:30:37.900	99.23	38.55	24.3	5.1	Mw	GCMT	135	43	92	Centroid Moment Tensor
2022-08-15 13:05:09.900	90.25	32.86	23.4	4.8	Mw	GCMT	51	41	-38	Centroid Moment Tensor
2022-08-31 09:13:14.600	81.86	33.69	23.1	4.9	Mw	GCMT	182	45	-61	Centroid Moment Tensor
2022-09-15 22:49:40.340	77.7681	36.0018	14	5	Mw	ISC (AUST)	59	87	2	Centroid Moment Tensor
2022-10-16 08:54:32.700	78.22	39.41	13.2	4.7	Mw	GCMT	12	53	111	Centroid Moment Tensor
2022-10-19 04:35:39.100	92.26	37.82	15.1	5.3	Mw	GCMT	131	63	144	Centroid Moment Tensor

2022-10-23 15:07:00.400	77.98	37.65	14.1	5	Mw	GCMT	103	49	89	Centroid Moment Tensor
2022-11-27 19:58:45.700	74.46	39.72	27.4	4.9	Mw	GCMT	93	27	85	Centroid Moment Tensor
2022-12-14 20:46:31.600	95.9211	21.8715	15	4.8	Mw	ISC (NEIC)	8	41	-160	Centroid Moment Tensor
2022-12-22 02:47:07.200	99.31	35.67	26.7	5.1	Mw	GCMT	85	83	-12	Centroid Moment Tensor
2022-12-28 17:16:35.700	79.561	41.7941	20	5.1	Mw	ISC (NEIC)	66	81	72	Centroid Moment Tensor
2023-01-24 08:58:31.400	81.729	29.591	18	5.5	Mw	ISC (GFZ)	100	69	90	Centroid Moment Tensor
2023-01-25 19:49:46.400	102.21	29.57	12.5	5.4	Mw	GCMT	170	55	-90	Centroid Moment Tensor
2023-01-29 23:49:40.300	82.41	39.96	31.1	5.8	Mw	GCMT	158	79	151	Centroid Moment Tensor
2023-02-22 10:25:54.400	81.99	41.87	17	4.8	Mw	GCMT	102	52	94	Centroid Moment Tensor
2023-02-23 00:37:39.010	73.291	38.062	10	6.8	Mw	ISC (GFZ)	26	68	-18	Centroid Moment Tensor
2023-02-26 23:58:08.900	79.93	41.8	30.5	4.9	Mw	GCMT	156	80	154	Centroid Moment Tensor
2023-02-28 04:21:00.200	73.18	38.03	21.2	4.9	Mw	GCMT	206	88	-6	Centroid Moment Tensor
2023-02-28 14:46:58.400	102.0079	29.668	10	5	Mw	ISC (AUST)	166	39	-76	Centroid Moment Tensor
2023-03-15 02:32:25.200	81.31	35.12	25	5.1	Mw	GCMT	240	77	-13	Centroid Moment Tensor
2023-03-17 10:39:42.700	96.46	30.79	24.7	5.1	Mw	GCMT	106	90	-11	Centroid Moment Tensor
2023-03-22 20:07:44.100	69.9679	39.4456	14	5.7	Mw	ISC (NEIC)	84	84	172	Centroid Moment Tensor
2023-04-04 17:17:46.900	94	9.13	12	4.9	Mw	GCMT	227	50	-51	Centroid Moment Tensor
2023-04-13 03:21:25.100	94.02	8.97	17.7	4.9	Mw	GCMT	51	81	-40	Centroid Moment Tensor
2023-04-24 10:58:35.300	94.04	9.34	13.4	4.9	Mw	GCMT	46	67	-7	Centroid Moment Tensor
2023-04-27 19:45:56.400	81.57	29.41	22.1	4.9	Mw	GCMT	109	63	77	Centroid Moment Tensor

2023-04-28 20:07:04.500	94.19	8.4	12	5.1	Mw	GCMT	11	48	-139	Centroid Moment Tensor
2023-05-17 15:23:53.200	98.3963	23.3534	9	4.1	Mw	ISC (NEIC)	250	73	-7	Centroid Moment Tensor
2023-05-29 02:33:31.820	92.388	26.691	17	4.9	Mw	ISC (GFZ)	77	36	87	Centroid Moment Tensor
2023-05-31 11:20:17.060	96.212	25.099	11	5.8	Mw	ISC (GFZ)	224	77	177	Centroid Moment Tensor
2023-06-13 08:03:45.300	75.9572	33.2081	10	5	Mw	ISC (AUST)	144	86	177	Centroid Moment Tensor
2023-06-17 16:14:28.000	79.81	35.75	30.4	4.7	Mw	GCMT	228	70	-11	Centroid Moment Tensor
2023-06-19 01:40:25.400	96.35	15.31	12	5.5	Mw	GCMT	43	33	-131	Centroid Moment Tensor
2023-06-21 02:47:21.500	96.38	15.32	12	4.7	Mw	GCMT	40	63	-157	Centroid Moment Tensor
2023-06-22 00:12:58.500	96.4	15.34	14.4	4.8	Mw	GCMT	60	43	-113	Centroid Moment Tensor
2023-06-26 13:32:07.600	94	9.3	12	5	Mw	GCMT	51	83	-19	Centroid Moment Tensor
2023-06-26 18:05:41.300	94.05	9.32	12	4.7	Mw	GCMT	235	81	-4	Centroid Moment Tensor
2023-08-14 14:49:50.300	92.36	24.94	26.6	5.3	Mw	GCMT	152	49	134	Centroid Moment Tensor
2023-08-18 07:32:43.200	93.99	9.35	17.9	4.8	Mw	GCMT	48	77	-20	Centroid Moment Tensor
2023-08-20 15:28:26.300	77.49	39.87	20.8	4.7	Mw	GCMT	95	47	133	Centroid Moment Tensor
2023-08-31 18:45:17.600	73.05	38.11	26.5	4.9	Mw	GCMT	22	85	17	Centroid Moment Tensor
2023-09-09 10:18:33.900	92.84	24.65	38.9	4.9	Mw	GCMT	134	50	127	Centroid Moment Tensor
2023-09-24 16:34:35.400	94.61	6.99	17.9	5	Mw	GCMT	61	77	-26	Centroid Moment Tensor
2023-10-13 00:03:17.700	68.65	36.13	17.5	4.8	Mw	GCMT	186	51	103	Centroid Moment Tensor
2023-10-22 01:54:22.100	84.75	27.75	24.8	4.9	Mw	GCMT	260	29	-6	Centroid Moment Tensor
2023-10-22 15:14:12.600	97.31	39.36	14.9	4.7	Mw	GCMT	183	79	171	Centroid Moment Tensor

2023-10-23 06:10:42.800	91.34	33.52	21.3	4.8	Mw	GCMT	55	54	-43	Centroid Moment Tensor
2023-10-23 08:43:40.700	88.29	31.42	22.2	4.8	Mw	GCMT	232	74	-20	Centroid Moment Tensor
2023-10-24 11:32:13.000	97.308	39.265	12	5.3	Mw	IPGP	177	58	123	Centroid Moment Tensor
2023-10-25 10:49:06.200	71.583	39.1741	8	4.4	Mw	ISC (NEIC)	50	48	75	Centroid Moment Tensor
2023-10-25 15:52:19.700	83.7	36.76	12	4.9	Mw	GCMT	232	57	-47	Centroid Moment Tensor
2023-10-25 18:35:41.900	83.69	36.65	12.9	4.6	Mw	GCMT	4	52	-114	Centroid Moment Tensor
2023-11-13 12:16:38.400	72.27	38.51	26	5.2	Mw	GCMT	217	90	0	Centroid Moment Tensor
2023-11-17 01:37:12.900	99.37	21.16	12	5.8	Mw	GCMT	77	73	4	Centroid Moment Tensor
2023-11-23 10:01:51.200	71.78	38.81	12.8	4.9	Mw	GCMT	171	38	-72	Centroid Moment Tensor
2023-12-18 10:18:54.100	76.7029	33.2057	17.5	5	Mw	ISC (NEIC)	127	28	63	Centroid Moment Tensor
2024-01-22 18:09:07.890	78.837	41.4549	15.5	7.2	Mw	ISC (AUST)	111	79	104	Centroid Moment Tensor
2024-01-29 22:27:41.000	78.715	41.187	17	5.8	Mw	IPGP	27	53	62	Centroid Moment Tensor
2024-02-18 11:20:35.230	67.0174	36.6677	9	4.9	Mw	ISC (AUST)	21	76	27	Centroid Moment Tensor
2024-02-25 04:15:01.120	78.4258	41.1198	9	5.3	Mw	ISC (AUST)	69	38	88	Centroid Moment Tensor

8.1.2. Table – GNSS velocities

Lon	*Lat*	*Ve_ITRF14*	*Vn_ITRF14*	*Ve_EurasianRF*	*Vn_EurasianRF*	*dVe*	*dVn*	*Name*
deg	deg	mm/a	mm/a	mm/a	mm/a	mm/a	mm/a	\
72.68	32.73	31.15	28.04	2.26	25.66	0.7	0.7	0705_GPS
74.42	35.41	22.77	22.25	-6.17	20.37	0.4	0.6	0901_GPS
94.108	28.257	46.17	13.19	17.57	16.98	3.2	3.5	13KM_GPS
73.2	33.5	30.34	28.98	1.43	26.75	0.3	0.3	1405_GPS
74.87	36.43	25.24	24.88	-3.7	23.13	0.99	1.03	1700_GPS
74.6	35.43	20.87	23.65	-8.07	21.82	0.47	0.51	1801_GPS
73.76	35.52	24.36	21.53	-4.57	19.46	0.4	0.5	1802_GPS
75.23	35	25.27	23.67	-3.69	22.03	0.3	0.4	1902_GPS
75.5	35.07	25.08	22.07	-3.88	20.5	0.2	0.3	1903_GPS
74.58	35.49	21.77	22.15	-7.17	20.32	0.5	0.7	2001_GPS
73.54	34.07	27.42	29.88	-1.5	27.75	0.5	0.6	2003_GPS
72.45	32.61	30.47	28.83	1.59	26.39	0.6	0.7	2004_GPS
74.61	35.51	22.77	22.95	-6.17	21.13	0.55	0.53	2101_GPS
74.73	35.24	23.57	22.56	-5.38	20.77	0.52	0.69	2201_GPS
75.39	35.48	24.56	22.39	-4.4	20.79	0.61	0.82	2203_GPS
73.13	33.82	29.22	27.67	0.31	25.42	0.2	0.3	2204_GPS
75.74	35.36	25.78	20.8	-3.18	19.3	0.48	0.58	2205_GPS
94.047	28.325	48.98	12.61	20.38	16.39	2.7	3.3	35KM_GPS
72.05	41.784	25.82	4.71	-2.84	2.15	0.3	0.3	ABD4_GPS
73.12	37.461	24.39	20.44	-4.49	18.19	1.5	1.6	ABLA_GPS
90.672	26.357	42.25	26.45	13.68	29.27	1.2	1.3	ABPH_GPS
85.358	27.697	36.64	34.54	7.89	35.83	0.9	0.7	AIRP_GPS
77.323	40.332	30.37	13.34	1.52	12.3	0.4	0.4	AJ02_GPS

73.28	38.902	19.27	16.49	-9.57	14.29	1.3	1.4	AJLA_GPS
73.821	38.503	22.08	23.54	-6.79	21.49	0.6	0.6	AKBA_GP1
73.618	38.56	19.17	21.79	-9.69	19.68	1.4	1.5	AKBA_GPS
78.542	41.795	29.9	11.39	1.11	10.7	0.4	0.4	AKH4_GPS
72.145	41.557	26.03	5.88	-2.65	3.35	0.3	0.3	AKJ4_GPS
75.967	40.717	28.03	13.62	-0.78	12.19	0.3	0.3	AKS4_GPS
92.945	26.174	41.57	25.32	13.07	28.79	1.9	1.8	AKSG_GPS
78.966	39.877	28.99	15.48	0.1	14.92	0.4	0.4	AKTA_GPS
72.258	39.421	20.92	14.16	-7.87	11.66	0.6	0.6	ALD4_GPS
79.65	29.59	36.3	36.04	7.43	35.67	0.7	0.7	ALMO_GPS
74.244	40.331	26.23	15.51	-2.57	13.58	0.4	0.4	ALUN_GPS
88.702	27.024	35.74	31.5	7.08	33.75	1.4	0.9	AMBK_GPS
96.469	28.059	39.88	16.15	11.37	20.61	3	3.6	AMLG_GPS
95.901	28.778	46.54	9.7	17.98	14	0.7	0.8	AMOL_GPS
82.247	28.03	36	36.41	7.21	36.8	0.9	0.9	AMP0_GPS
92.484	26.156	36.48	30.24	7.97	33.57	2.3	2.1	AMSO_GPS
95.845	28.567	39.52	6.46	10.96	10.74	0.7	0.6	ANGO_GPS
95.902	28.801	44.44	10.2	15.88	14.5	0.3	0.3	ANIN_GPS
85.456	37.387	28.1	10.67	-0.84	11.99	1.2	1.1	AQIN_GPS
77.75	41.86	29.19	10.81	0.42	9.89	0.4	0.4	ARA4_GPS
76.665	41.693	28.5	10.12	-0.27	8.89	0.7	0.7	ARC4_GPS
73.653	33.978	26.91	32.61	-2.01	30.51	0.3	0.3	ARJA_GPS
74.827	40.838	27.52	10.04	-1.27	8.28	0.4	0.4	ARP4_GPS
72.982	41.244	25.37	7.05	-3.35	4.76	0.4	0.5	ARS4_GPS
75.272	34.1	28.93	30.95	-0.02	29.32	0.6	0.6	ARUU_GPS
95.829	28.491	41.73	13.92	13.18	18.2	2.1	2.8	ARZO_GPS
76.856	38.449	26.62	20.38	-2.3	19.21	1	0.8	AS25_GPS
92.491	37.259	37.01	8.31	8.24	11.64	1.3	1.1	AS40_GPS
73.538	40.075	28.93	9.81	0.13	7.68	0.7	0.7	ASK4_GPS
80.34	29.76	36.11	30.75	7.23	30.58	0.8	0.7	ASKO_GPS

86.38	37.413	30.38	12.51	1.45	14.09	2.2	2.3	AT01_GPS
86.327	37.336	32.48	12.53	3.55	14.1	1.7	1.9	AT02_GPS
86.309	37.232	35.18	12.73	6.25	14.29	1.3	1.4	AT03_GPS
86.264	36.994	32.09	13.24	3.15	14.79	1.8	1.9	AT04_GPS
86.25	36.428	32.29	16.95	3.34	18.5	1.6	1.6	AT06_GPS
86.056	36.253	31.1	17.01	2.15	18.5	1.4	1.4	AT07_GPS
86.119	36.026	34.2	13.99	5.24	15.5	1.4	1.4	AT08_GPS
86.283	35.657	34.99	16.45	6.03	18.01	1.5	1.6	AT09_GPS
86.056	35.853	34.4	18.11	5.44	19.6	1.4	1.5	AT10_GPS
85.646	37.871	28.29	10.82	-0.64	12.19	1.7	1.7	AT12_GPS
86.167	37.62	28.68	11.77	-0.25	13.29	2	2.1	AT14_GPS
86.333	37.213	33.88	12.12	4.95	13.69	2.2	2.4	AT3X_GPS
73.106	38.554	20.57	20.63	-8.28	18.38	1.4	1.4	ATSA_GPS
85.144	37.057	28.81	13.96	-0.14	15.19	1.3	1.1	ATUB_GPS
79.559	30.531	34.48	30.82	5.57	30.43	4.19	2.41	AULI_GPS
72.46	32.608	30.07	28.25	1.19	25.81	0.3	0.2	AWAN_GPS
73.268	39.513	25.54	12.48	-3.28	10.27	0.6	0.6	BAB4_GPS
79.493	30.743	27.66	22.08	-1.26	21.67	1.3	1.1	BADR_GPS
79.77	29.82	33.21	35.21	4.33	34.88	0.7	0.6	BAGR_GPS
85.794	27.745	36.24	32.62	7.49	34.03	1	0.9	BAL0_GPS
95.847	28.091	40.41	20.12	11.88	24.4	1.8	2.7	BALK_GPS
91.293	26.005	41	30.88	12.47	33.88	0.6	0.5	BAMU_GPS
80.18	29.1	36.58	34.59	7.73	34.38	0.8	0.7	BANB_GPS
78.115	30.452	35.24	29.97	6.34	29.16	1.4	1.3	BATA_GPS
75.019	41.576	27.78	6.78	-0.97	5.08	0.4	0.4	BAU4_GPS
75.083	41.079	27.11	10.07	-1.67	8.38	0.4	0.4	BAY4_GPS
94.728	29.684	44.22	2.12	15.58	6.09	3.5	1.2	BAYI_GPS
82.094	28.196	40.15	38.39	11.35	38.73	0.99	1.01	BBP0_GPS
83.82573	27.45737	36.84	36.15	8.09	37	0.41	0.83	BELT_GPS
83.561	28.348	36.51	30.24	7.71	31.01	0.5	0.5	BENI_GPS

84.37967	28.22861	36.08	31	7.29	32.01	0.32	0.49	BESI_GPS
75.03	40.646	27.93	11.08	-0.87	9.38	0.4	0.4	BET4_GPS
88.569	26.889	33.43	35.23	4.78	37.44	1.5	1.1	BGKT_GPS
83.418	27.507	36.16	35.58	7.41	36.31	1.1	0.6	BHAI_GPS
84.43	27.678	34.85	37.6	6.09	38.62	1.7	1.1	BHAR_GPS
78.617	30.806	30.96	27.73	2.04	27.07	1.1	1.1	BHAT_GPS
90.72	27.54	39.83	26.93	11.18	29.76	1.1	1.4	BHUM_GPS
85.339	28.389	38.68	26.73	9.89	28.01	1.9	1.4	BI01_GPS
87.782	28.319	39.75	25.35	11	27.34	0.9	0.7	BI02_GPS
87.687	28.08	39.03	26.08	10.29	28.04	0.9	0.7	BI03_GPS
89.077	27.661	40.17	28.59	11.48	30.95	1.7	1.4	BI04_GPS
87.264	26.484	38.93	34.91	10.29	36.75	0.5	0.4	BIRB_GPS
90.995	29.562	45.64	16.15	16.89	19.06	1.2	1	BJ01_GPS
86.159	31.897	38.84	20.3	9.92	21.82	0.4	0.4	BJ03_GPS
81.232	30.55	28.84	21.39	-0.08	21.48	0.9	0.5	BJ04_GPS
75.426	40.757	27.83	12.27	-0.97	10.68	0.7	0.7	BKE4_GPS
81.71437	28.65582	36.02	34.53	7.19	34.76	0.27	0.35	BMCL_GPS
95.665	28.159	46.52	19.57	17.98	23.8	1.9	2.7	BMJR_GPS
82.54	27.786	35.78	37.33	7.01	37.8	1	0.9	BMT0_GPS
84.39508	27.94947	37.42	35.86	8.65	36.87	1.69	1.81	BNDP_GPS
89.66479	26.11916	40.22	34.18	11.65	36.71	0.2	0.26	BNGM_GPS
90.38	26.437	41.66	34.53	13.08	37.26	2.4	3.1	BNGP_GPS
75.938	31.479	31.28	31.38	2.36	29.94	0.9	0.9	BOHA_GPS
92.438	27.272	41.56	19.66	12.97	22.98	0.7	0.6	BOMD_GPS
92.415	27.27	41.07	20.96	12.48	24.27	0.2	0.3	BOMP_GPS
90.569	26.473	42.56	30.68	13.98	33.47	1.9	1.7	BONG_GPS
73.235	41.648	26.85	6.58	-1.86	4.36	0.4	0.4	BOR4_GPS
72.668	39.495	27.96	14.66	-0.84	12.28	3	6.7	BRDB_GPS
88.738	26.751	43.32	36.69	14.68	38.95	1.1	0.8	BRDH_GPS
87.2722	26.51972	38.95	34.85	10.31	36.69	0.24	0.25	BRN2_GPS

87.28126	26.43868	38.56	35.52	9.92	37.36	0.53	0.7	BRNG_GPS
80.398	31.527	27.19	19.02	-1.76	18.87	0.7	0.5	BS02_GPS
82.184	30.66	30.94	20.72	2.02	21.09	0.9	0.5	BS04_GPS
82.518	32.524	34.11	19.12	5.14	19.59	1.6	1.3	BS05_GPS
83.274	32.417	33.7	18.01	4.73	18.7	2.2	1.4	BS06_GPS
84.915	32.094	35.57	19.15	6.63	20.31	0.5	0.4	BS07_GPS
85.607	30.077	36.87	22.16	8	23.52	0.7	0.5	BS09_GPS
85.8	29.419	37.24	23.61	8.4	25.03	0.8	0.7	BS10_GPS
89.573	28.914	41.54	21.85	12.79	24.35	1	0.8	BS11_GPS
88.18	29.176	40.18	21.93	11.39	24.03	1	0.7	BS15_GPS
85.336	33.14	37.58	18.62	8.62	19.9	0.8	0.8	BS16_GPS
92.854	34.63	47.11	4.92	18.31	8.36	1.2	1.1	BS19_GPS
91.79	29.252	44.5	14.62	15.79	17.76	1	0.6	BS23_GPS
82.008	32.077	33.2	19.66	4.24	19.98	1.3	1.1	BS27_GPS
90.616	29.195	43.53	17.96	14.79	20.76	1.2	0.9	BS28_GPS
91.288	30.527	46.37	13.86	17.59	16.85	1	0.8	BS29_GPS
92.027	31.533	48.99	9.66	20.2	12.86	0.7	0.5	BS30_GPS
85.187	31.561	35.44	20.37	6.51	21.61	0.6	0.5	BS34_GPS
90.298	26.596	40.47	36.45	11.87	39.16	3.3	3.7	BSBR_GPS
84.267	32.282	33.08	18.23	4.12	19.2	1.6	0.9	BT02_GPS
91.722	32.171	48.21	8.94	19.4	12.06	0.7	0.6	BT05_GPS
84.179	29.654	33.08	22.76	4.21	23.71	1	0.6	BT07_GPS
85.29	28.842	37.12	24.15	8.31	25.42	0.8	0.7	BT08_GPS
87.171	28.622	38.07	23.02	9.29	24.83	1.6	1.4	BT10_GPS
88.891	29.214	40.57	21.14	11.79	23.45	0.9	0.7	BT11_GPS
89.289	28.071	40.29	25.13	11.58	27.55	0.8	0.7	BT13_GPS
94.387	29.622	47.63	2.21	18.98	6.08	0.4	0.3	BT14_GPS
90.587	30.175	46.77	15.96	17.99	18.75	1.4	0.9	BT15_GPS
87.434	31.785	40.21	18.43	11.31	20.32	0.7	0.5	BT17_GPS
75.02	41.186	26.9	10.38	-1.87	8.68	0.4	0.4	BTR4_GPS

97.076	32.858	49.53	0.38	20.9	5.01	0.65	0.59	BTX4_GPS
99.647	33.758	44.71	-2.92	16.2	2.42	0.5	0.5	BUDR_GPS
96.48	32.204	52.04	-1.86	23.39	2.6	0.4	0.4	BUNQ_GPS
92.013	26.246	39.3	28.98	10.77	32.18	1.3	1.1	BURA_GPS
72.374	32.805	29.67	33.47	0.79	31	0.2	0.2	BUT1_GPS
99.98	35.59	39.59	-0.51	11.12	4.92	0.6	0.6	BUXH_GPS
95.295	32.894	52.9	1.56	24.2	5.69	0.4	0.4	BUZD_GPS
90.854	31.404	44.12	13.28	15.3	16.15	0.8	0.5	BX06_GPS
87.576	29.118	40.39	22.61	11.59	24.54	0.4	0.3	BX08_GPS
86.723	29.419	38.43	23.25	9.6	24.93	1.2	0.7	BX09_GPS
85.214	29.441	36.45	23.57	7.6	24.82	0.4	0.3	BX10_GPS
83.325	30.133	31.91	21.4	3.02	22.1	1	0.6	BX11_GPS
81.2007	29.47418	33.99	27.65	5.12	27.73	0.38	0.48	BYNA_GPS
73.415	37.793	23.49	22.35	-5.39	20.18	1.5	1.6	BZRA_GPS
97.122	31.164	47.49	-6.13	18.89	-1.49	1	0.8	CAD1_GPS
72.09	40.199	26.7	9.81	-2.05	7.26	0.4	0.4	CAUV_GPS
75.75	40.686	28.34	13.28	-0.47	11.79	0.7	0.7	CEK4_GPS
94.199	25.652	35.5	23.77	7.07	27.59	0.6	0.5	CHAK_GPS
80.09	29.33	32.99	33.82	4.13	33.58	0.8	0.7	CHAM_GPS
78.365	30.404	37.16	31.79	8.26	31.05	2.42	1.54	CHAM_GPS
76.673	31.919	31.6	34.86	2.66	33.63	1.4	1.3	CHBG_GPS
72.954	31.755	29.15	34.81	0.28	32.51	0.4	0.4	CHIN_GPS
77.739	41.527	29.01	12.62	0.22	11.7	0.6	0.6	CHK4_GPS
85.31409	28.20723	37.49	27.57	8.71	28.85	0.23	0.33	CHLM_GPS
78.368	30.394	32.84	31.4	3.94	30.66	0.9	0.8	CHMB_GPS
82.504	27.951	39.09	37.94	10.31	38.4	1	0.9	CHP0_GPS
76.052	41.334	27.91	12.09	-0.87	10.68	0.7	0.7	CHT4_GPS
90.498	27.484	40.23	27.49	11.58	30.26	0.5	0.4	CHUC_GPS
78.655	33.576	26.94	16.3	-2.05	15.65	2.7	1.1	CHUS_GPS
84.38535	27.66824	33.39	34.1	4.63	35.11	0.66	0.21	CHWN_GPS

97.456	28.65	41.87	-11.83	13.37	-7.1	1.1	0.8	CHY1_GPS
72.875	41.966	27.42	4.18	-1.26	1.86	0.4	0.4	CHY4_GPS
72.362	32.722	30.27	30.38	1.39	27.91	0.2	0.2	CNJP_GPS
74.837	34.13	27.22	29.77	-1.73	28.01	0.2	0.2	CONV_GPS
95.766	27.912	44.3	17.64	15.77	21.9	1.3	2.4	CPKW_GPS
99.879	35.802	37.79	-0.38	9.32	5.02	0.6	0.6	CS24_GPS
91.856	25.567	39.05	29.92	10.56	33.08	0.3	0.3	CSOS_GPS
86.904	30.445	41.17	21.29	12.3	23.03	0.4	0.5	CUOM_GPS
80.602	29.334	35.59	32.07	6.73	31.98	0.9	0.8	DAD2_GPS
91.363	29.664	45.83	15.14	17.09	18.15	0.3	0.3	DAGZ_GPS
75.993	32.536	28.7	29.46	-0.24	28.04	0.8	0.8	DALH_GPS
85.108	27.608	36.74	34.81	8	36.03	0.3	0.3	DAMA_GPS
75.041	40.782	27.72	11.08	-1.07	9.38	0.4	0.4	DAR4_GPS
72.286	39.573	26.12	10.15	-2.67	7.66	0.6	0.6	DAT4_GPS
74.689	36.312	25.13	30	-3.81	28.2	1.7	2	DDAS_GPS
77.126	28.482	33.93	35.76	5.13	34.66	0.3	0.3	DELH_GPS
77.172	28.544	36.73	32.14	7.93	31.06	1	1	DELO_GPS
96.292	27.899	44.28	10.7	15.77	15.11	2.6	3.2	DEMW_GPS
74.431	35.894	24.03	23.77	-4.91	21.9	0.3	0.3	DENY_GPS
91.46	26.86	38.66	30.32	10.07	33.36	1.5	2.3	DEOT_GPS
98.907	28.488	39.71	-14.71	11.28	-9.58	0.4	0.4	DEQN_GPS
90.54	27.52	40.24	26.08	11.59	28.86	0.6	0.7	DGON_GPS
90.284	26.618	42.37	33.26	13.77	35.97	1.9	2.7	DGPR_GPS
80.56	29.86	36.81	25.68	7.92	25.58	0.8	0.7	DHAR_GPS
78.155	30.342	32.34	32.46	3.44	31.66	1.1	1.1	DHAU_GPS
73.935	33.93	27.41	32.83	-1.52	30.81	0.4	0.4	DHUL_GPS
99.89	26.461	30.24	-19.88	1.95	-14.48	0.8	0.7	DIAN_GPS
95.594	31.415	51.66	-1.12	22.99	3.09	0.4	0.4	DING_GPS
76.498	41.245	27.82	13.37	-0.97	12.09	0.7	0.7	DJA4_GPS
73.956	41.896	27.45	6.18	-1.26	4.17	0.3	0.3	DJE4_GPS

74.469	40.987	27.4	9.84	-1.37	7.98	0.5	0.5	DJR4_GPS
97.378	37.38	37.09	1.38	8.53	6.09	0.1	0.1	DLHA_GPS
82.81789	28.98368	34.65	25.13	5.81	25.68	0.14	0.17	DLPA_GPS
84.26519	27.97335	33.44	33.94	4.67	34.91	0.52	0.64	DMAU_GPS
95.616	28.27	46.52	16.38	17.97	20.6	1.7	2.6	DMBK_GPS
73.619	40.925	25.19	10.17	-3.57	8.06	0.6	0.6	DNG4_GPS
80.58179	28.75445	37.62	36.12	8.79	36.02	0.26	0.23	DNGD_GPS
83.76347	28.34509	35.5	27.55	6.7	28.38	0.16	0.2	DNSG_GPS
89.632	27.59	40.16	27.94	11.48	30.46	0.5	0.5	DODI_GPS
78.187	30.191	33.73	33.25	4.84	32.46	0.9	0.9	DOIW_GPS
93.066	26.193	39.97	30.28	11.47	33.78	2	1.9	DOKM_GPS
75.769	34.424	25.04	29.61	-3.92	28.12	0.6	0.6	DRAS_GPS
80.50094	29.73381	32.31	29.78	3.43	29.66	0.27	0.29	DRCL_GPS
97.27	33.9	47.29	-1.35	18.67	3.33	2.3	2.2	DS39_GPS
98.197	33.06	47.05	-1.35	18.47	3.59	1.2	1	DS40_GPS
98.315	34.94	45.38	-1.66	16.81	3.31	2.1	1.7	DT01_GPS
74.366	41.476	26.57	7.47	-2.17	5.58	0.4	0.4	DYU4_GPS
76.468	41.82	27.69	9.67	-1.07	8.38	0.3	0.3	ELB4_GPS
74.452	41.821	27.27	7.14	-1.45	5.27	0.3	0.3	EME4_GPS
76.422	41.494	28.71	12.69	-0.07	11.39	0.7	0.7	ENG4_GPS
86.813	27.958	35.84	25.82	7.09	27.53	1.2	0.6	EVE1_GPS
99.075	40.275	30.19	-3.58	1.85	1.6	0.2	0.2	G041_GPS
86.251	38.077	27.67	10.75	-1.24	12.3	1.5	1.5	G0BB_GPS
77.001	36.444	25.05	22.36	-3.92	21.23	0.4	0.5	G0BK_GPS
79.257	35.937	25.76	17.82	-3.23	17.34	0.4	0.4	G0BL_GPS
93.067	36.89	35.4	7.05	6.64	10.55	0.9	0.9	G0CS_GPS
97.054	41.853	30.71	-2.15	2.35	2.47	0.2	0.2	G122_GPS
95.464	41.07	30.94	-0.61	2.45	3.56	0.2	0.2	G123_GPS
96.714	40.637	30.7	-1.45	2.25	3.07	0.2	0.3	G125_GPS
97.677	40.271	30.46	-2.6	2.04	2.19	0.2	0.2	G127_GPS

97.085	40.286	30.2	-1.65	1.75	2.98	0.2	0.2	G128_GPS
97.44	40.027	30.49	-1.44	2.04	3.28	0.5	0.5	G129_GPS
96.746	40.036	30.42	-1.35	1.94	3.18	0.2	0.2	G130_GPS
95.712	40.08	30.38	-0.48	1.85	3.76	0.2	0.2	G131_GPS
98.892	39.906	30.52	-3.53	2.15	1.6	0.3	0.3	G132_GPS
99.6	39.7	30.29	-3.82	1.95	1.5	0.2	0.2	G133_GPS
98.501	39.713	29.95	-2.93	1.54	2.09	0.4	0.4	G135_GPS
98.188	39.841	30.76	-1.54	2.34	3.39	0.4	0.4	G136_GPS
97.921	39.854	30.37	-2.57	1.94	2.29	0.2	0.2	G137_GPS
97.703	39.569	31	-1.31	2.54	3.49	0.2	0.2	G138_GPS
96.748	39.903	30.53	-1.16	2.04	3.37	0.5	0.5	G139_GPS
98.798	39.409	31.35	-3	2.94	2.1	0.3	0.3	G142_GPS
99.613	39.145	30.71	-3.22	2.34	2.11	0.3	0.4	G143_GPS
97.997	39.186	31.4	-1.19	2.94	3.69	0.3	0.3	G144_GPS
95.606	39.71	31.31	-0.15	2.75	4.06	0.2	0.2	G145_GPS
99.62	38.834	31.52	-3.02	3.13	2.31	0.4	0.4	G146_GPS
98.266	38.967	32.5	-1.06	4.04	3.89	0.5	0.5	G147_GPS
99.565	38.445	32.84	-2.41	4.43	2.9	0.4	0.5	G148_GPS
98.853	37.979	35.09	-1.11	6.62	4.01	0.3	0.2	G149_GPS
98.656	37.578	36.22	-0.66	7.73	4.4	0.3	0.3	G150_GPS
95.803	37.513	36.26	3.01	7.63	7.28	0.5	0.5	G151_GPS
99.491	37.133	36.39	-1.08	7.93	4.21	0.5	0.5	G152_GPS
99.01	37.297	36.21	-0.05	7.73	5.11	0.5	0.5	G153_GPS
98.345	37.307	36.14	0.42	7.62	5.4	0.4	0.4	G154_GPS
96.699	37.363	35.62	1.67	7.02	6.19	0.3	0.3	G156_GPS
99.895	36.693	36.77	-1.19	8.32	4.21	0.3	0.2	G157_GPS
99.067	36.795	36.81	-0.37	8.32	4.81	0.3	0.3	G158_GPS
98.462	36.943	36.85	0.89	8.33	5.9	0.3	0.3	G159_GPS
94.998	40.549	30.79	-0.08	2.25	3.96	0.2	0.2	G160_GPS
94.813	40.172	30.62	0.37	2.05	4.36	0.2	0.2	G161_GPS

94.555	39.716	30.75	0.84	2.15	4.76	0.2	0.2	G162_GPS
93.489	39.645	30.9	1.63	2.25	5.25	0.2	0.3	G163_GPS
94.857	39.514	31.55	1.16	2.95	5.16	0.4	0.4	G164_GPS
93.003	39.287	31.83	2.57	3.14	6.05	0.2	0.2	G165_GPS
94.355	38.809	33.89	1.6	5.24	5.46	0.4	0.4	G167_GPS
94.998	38.056	34.69	2.03	6.04	6.07	0.5	0.5	G169_GPS
93.499	37.902	35.95	4.33	7.23	7.95	0.4	0.3	G170_GPS
90.804	38.287	36.15	7.07	7.35	9.92	0.4	0.4	G171_GPS
89.196	38.717	29.58	5.72	0.75	8.11	0.3	0.4	G172_GPS
93.854	41.888	31.57	0.53	3.06	4.25	0.4	0.4	G304_GPS
96.918	41.233	30.46	-2.4	2.06	2.18	0.4	0.4	G305_GPS
98.55	39.939	30.43	-3.54	2.04	1.49	0.4	0.4	G308_GPS
97.967	39.677	31.18	-2.58	2.74	2.29	0.4	0.4	G309_GPS
94.327	39.615	30.97	0.6	2.35	4.45	0.4	0.4	G311_GPS
94.258	39.413	32.38	1.52	3.75	5.35	0.4	0.4	G312_GPS
97.088	39.457	32.74	-0.25	4.24	4.38	0.4	0.4	G313_GPS
94.311	39.158	33.88	1.11	5.24	4.96	0.4	0.4	G314_GPS
95.457	39.25	33.22	-0.01	4.64	4.16	0.4	0.4	G315_GPS
90.728	38.869	30.93	4.8	2.15	7.63	0.5	0.6	G316_GPS
91.497	38.758	33.31	4.88	4.55	7.93	0.4	0.4	G319_GPS
89.557	38.517	30.28	6.92	1.45	9.42	0.4	0.4	G322_GPS
93.425	38.533	34.04	2.35	5.34	5.95	0.7	0.7	G323_GPS
89.868	38.439	31.17	6.93	2.35	9.52	0.4	0.3	G324_GPS
94.613	38.33	34.9	1.03	6.24	4.96	0.4	0.4	G325_GPS
90.102	38.351	34.27	7.97	5.45	10.62	0.4	0.4	G326_GPS
90.269	38.285	34.66	8.32	5.84	11.02	0.3	0.4	G328_GPS
92.419	38.072	35.29	5.33	6.54	8.64	0.6	0.6	G332_GPS
89.339	38.11	33.99	7.98	5.14	10.41	0.7	0.7	G333_GPS
91.677	37.853	36.32	7.93	7.53	11.03	0.4	0.4	G335_GPS
99.411	37.618	36.78	-2.36	8.33	2.91	0.4	0.4	G336_GPS

90.918	37.025	35.26	9.75	6.43	12.64	0.4	0.4	G339_GPS
95.482	37.216	35.88	3.19	7.22	7.37	0.5	0.6	G341_GPS
95.367	36.955	36.19	3.62	7.52	7.77	0.4	0.4	G344_GPS
93.62	36.746	35.17	5.5	6.43	9.15	0.6	0.7	G346_GPS
91.886	37.038	36.03	9.18	7.23	12.34	0.5	0.5	G347_GPS
96.448	36.437	36.66	4.53	8.03	8.98	0.5	0.5	G349_GPS
99.775	36.255	37.38	-0.46	8.91	4.91	0.4	0.4	G351_GPS
96.886	41.128	30.67	-1.99	2.26	2.58	0.9	0.8	GA01_GPS
99.696	40.463	29.84	-3.24	1.54	2.11	0.7	0.7	GA02_GPS
98.666	40.71	30.3	-4.17	1.96	0.89	0.9	0.8	GA03_GPS
94.324	39.955	29.95	1.6	1.35	5.45	1	0.8	GA05_GPS
99.956	39.581	29.87	-4.01	1.54	1.41	0.7	0.6	GA08_GPS
95.318	39.333	32.93	-1.17	4.34	2.96	1.1	0.9	GA12_GPS
96.058	38.971	37.06	-1.44	8.49	2.9	2.2	2.1	GA13_GPS
98.777	38.805	33.15	-0.6	4.71	4.5	2	2	GA15_GPS
99.329	38.646	31.44	-1.45	3.03	3.8	0.8	0.8	GA18_GPS
96.821	37.599	33.72	2.35	5.14	6.9	2.3	2.3	GA20_GPS
97.812	37.349	34.98	2.01	6.44	6.84	2.2	2.1	GA24_GPS
99.322	37.337	34.71	0.24	6.25	5.49	2.1	2	GA25_GPS
98.462	36.441	36.41	1.84	7.88	6.85	2	2	GA28_GPS
84.062	32.306	36.28	18.18	7.32	19.09	0.5	0.5	GAIZ_GPS
89.534	27.223	39.64	30.77	10.99	33.26	0.5	0.5	GANG_GPS
83.643	28.599	36.22	26.82	7.4	27.61	0.7	0.6	GANS_GPS
89.733	27.907	43.88	23.6	15.19	26.15	0.3	0.3	GASA_GPS
75.479	38.853	28.6	23.56	-0.29	21.99	0.5	0.5	GAZE_GPS
93.339	29.9	48.58	5.6	19.88	9.18	1	0.8	GBD1_GPS
88.569	27.365	38.87	28.33	10.19	30.54	0.2	0.3	GBSK_GPS
97.012	40.285	29.51	-1.93	1.05	2.68	0.9	1	GC24_GPS
94.758	40.157	30.52	0.38	1.95	4.35	0.7	0.7	GC27_GPS
89.52	26.927	42.51	35.37	13.87	37.86	0.7	0.7	GEDU_GPS

90.43	26.91	39.59	30.92	10.97	33.67	1.8	2.5	GELE_GPS
89.575	27.319	39.44	29.05	10.78	31.55	0.6	0.6	GENE_GPS
90.959	29.278	46.63	17.36	17.89	20.26	1.5	1.5	GGAR_GPS
84.40973	28.3746	38.61	20.05	9.81	21.06	0.61	0.64	GHER_GPS
79.09	30.298	33.14	29.9	4.24	29.37	1.3	1.1	GHOL_GPS
91.661	26.153	39.3	29.88	10.77	32.98	0.2	0.3	GHTU_GPS
91.741	26.135	39.9	27.76	11.37	30.88	0.6	0.5	GHTY_GPS
74.363	35.925	26.73	28.99	-2.2	27.1	0.7	0.7	GILG_GPS
80.6262	29.17652	34.6	34.31	5.74	34.23	0.21	0.37	GNTW_GPS
93.242	29.883	48.58	7.13	19.88	10.68	0.4	0.4	GONG_GPS
82.4912	27.95082	36.73	34.99	7.95	35.45	0.42	0.57	GRHI_3PS
85.156	36.986	29.41	14.35	0.45	15.58	1.5	1.4	GRUB_GPS
95.761	40.516	31.06	-0.79	2.55	3.47	0.3	0.3	GSAX_GPS
94.685	40.144	30.63	-0.1	2.05	3.85	0.3	0.3	GSDH_GPS
99.814	39.41	30.79	-3.97	2.44	1.41	0.2	0.2	GSGT_GPS
98.215	39.808	31.36	-2.35	2.94	2.59	0.3	0.3	GSJY_GPS
85.877	27.91	36.15	28.68	7.39	30.12	0.3	0.3	GUMB_GPS
81.353	28.824	36.45	37.26	7.61	37.39	0.9	0.9	GUT0_GPS
97.217	29.153	42.1	-9.86	13.57	-5.19	1	0.8	GYX1_GPS
99.168	30.094	43.06	-11.98	14.58	-6.77	0.3	0.3	H069_GPS
99.667	30.294	44.25	-13.61	15.79	-8.27	0.5	0.5	H184_GPS
98.599	29.671	43.37	-12.13	14.88	-7.08	0.4	0.3	H186_GPS
98.687	29.244	41.95	-13.05	13.48	-7.98	0.3	0.3	H187_GPS
99.254	28.844	39.31	-15.91	10.88	-10.68	0.6	0.5	H188_GPS
99.745	29	40.79	-17.24	12.37	-11.88	0.3	0.3	H189_GPS
99.757	28.32	37.86	-17.84	9.47	-12.47	0.3	0.2	H190_GPS
98.914	28.442	38.91	-15.02	10.48	-9.88	0.3	0.2	H191_GPS
99.708	27.829	34.42	-19.57	6.05	-14.22	1.3	1.3	H192_GPS
99.027	27.611	34.15	-15.45	5.76	-10.28	0.3	0.3	H193_GPS
98.668	27.759	35.57	-14.15	7.16	-9.08	0.2	0.3	H194_GPS

99.645	27.313	33.01	-18.01	4.67	-12.67	0.2	0.2	H195_GPS
99.293	27.18	32.52	-16.12	4.17	-10.88	0.3	0.3	H196_GPS
98.878	26.909	30.72	-14.2	2.37	-9.07	0.3	0.3	H197_GPS
99.933	26.45	30.14	-17.79	1.86	-12.37	0.2	0.2	H198_GPS
98.923	26.548	29	-14.71	0.67	-9.57	0.2	0.2	H200_GPS
99.987	26.144	29.62	-17.8	1.36	-12.37	0.3	0.3	H201_GPS
98.815	25.987	28.76	-12.88	0.46	-7.77	0.5	0.5	H203_GPS
99.924	25.716	27.7	-16.28	-0.54	-10.87	0.2	0.2	H204_GPS
99.535	25.463	26.6	-15.47	-1.63	-10.16	0.7	0.7	H205_GPS
99.11	25.652	25.82	-15.36	-2.44	-10.17	0.2	0.2	H206_GPS
99.148	25.07	26.08	-14.47	-2.14	-9.27	0.3	0.2	H207_GPS
97.928	25.151	22.73	-7.95	-5.54	-3.09	0.8	0.7	H308_GPS
98.197	25.454	23.85	-9.62	-4.44	-4.68	1	0.9	H309_GPS
98.808	31.208	49.11	-6.98	20.58	-1.87	0.5	0.5	H311_GPS
98.851	25.195	23.7	-14.09	-4.54	-8.97	0.6	0.5	H313_GPS
98.873	27.297	32.74	-14.71	4.36	-9.59	0.5	0.4	H314_GPS
99	29.715	41.75	-12.74	13.27	-7.58	0.5	0.5	H316_GPS
99.339	28.218	38.07	-15.73	9.67	-10.48	0.7	0.6	H318_GPS
99.433	27.764	36.24	-16.35	7.86	-11.07	0.4	0.4	H319_GPS
99.578	31.038	45.77	-10.9	17.28	-5.58	0.6	0.6	H321_GPS
99.789	26.017	28.42	-17.34	0.16	-11.96	0.5	0.4	H323_GPS
99.862	26.807	30.27	-18.77	1.96	-13.37	0.5	0.5	H324_GPS
99.998	26.759	31.27	-19	2.97	-13.57	0.5	0.5	H325_GPS
79.51	29.21	33.38	36.38	4.53	35.97	0.8	0.7	HALD_GPS
89.968	38.391	34.47	4.9	5.65	7.51	1.4	1.3	HAPI_GPS
78.754	31.037	31.27	24.19	2.34	23.57	1.1	1.1	HARS_GPS
78.021	30.459	32.64	32	3.74	31.16	0.7	0.7	HATI_GP1
91.481	26.175	39.62	29.33	11.08	32.38	0.9	0.8	HATI_GPS
90.907	38.285	34.24	3.85	5.44	6.73	1.3	1	HATU_GPS
73.249	34.42	24.9	29.52	-4.02	27.31	0.7	0.9	HAZU_GPS

99.7	31.694	47.49	-8.43	19	-3.08	0.4	0.4	HB16_GPS
99.537	30.284	44.15	-12.88	15.68	-7.57	0.4	0.4	HB17_GPS
85.008	27.316	36.82	36.24	8.09	37.43	1	0.9	HET0_GPS
85.05161	27.41486	36.86	34.54	8.13	35.74	0.26	0.41	HETA_GPS
87.327	27.049	38.57	33.58	9.89	35.44	0.5	0.4	HILE_GPS
75.363	32.565	33.1	31.43	4.16	29.82	1.5	1.4	HIRA_GPS
96.543	28.076	41.88	12.93	13.37	17.41	2	2.8	HLNG_GPS
99.436	26.468	28.66	-15.95	0.36	-10.67	1	0.9	HN01_GPS
95.966	28.325	45.11	13.79	16.57	18.11	0.4	0.3	HUNL_GPS
90.972	26.425	42.35	29.97	13.78	32.87	0.8	0.8	HWLI_GPS
85.518	41.908	31.34	7.23	2.59	8.56	0.4	0.4	I030_GPS
87.194	40.835	30.56	7.27	1.78	9.09	0.3	0.4	I032_GPS
88.251	40.267	29.55	6.27	0.76	8.39	0.4	0.5	I033_GPS
88.183	39.024	29.62	5.91	0.78	8.01	1.2	1.2	I034_GPS
86.977	38.508	29.25	7.74	0.36	9.5	0.4	0.4	I035_GPS
81.803	41.815	31.59	7.87	2.8	8.13	0.3	0.3	I055_GPS
84.245	41.78	30.77	11.49	1.99	12.46	0.4	0.4	I056_GPS
82.969	41.715	30.29	11.38	1.5	11.98	1.2	1.2	I057_GPS
82.346	41.485	30.91	12.82	2.1	13.24	0.3	0.4	I058_GPS
81.345	41.601	32.81	8.3	4	8.43	0.5	0.5	I059_GPS
82.785	41.216	30.61	12.7	1.79	13.24	0.4	0.4	I060_GPS
80.239	41.143	30.83	15.52	2	15.33	0.5	0.5	I061_GPS
80.392	40.643	30.06	14.68	1.2	14.53	0.4	0.4	I062_GPS
84.337	40.217	29.63	9.07	0.77	10.06	0.5	0.5	I063_GPS
83.61	39.015	28.69	11.48	-0.23	12.26	0.2	0.2	I064_GPS
83.159	38.257	26.82	13.21	-2.13	13.86	0.4	0.4	I065_GPS
83.811	37.594	26.52	11.73	-2.44	12.57	0.2	0.2	I066_GPS
82.696	37.046	26.14	13.15	-2.84	13.67	0.3	0.3	I067_GPS
81.664	36.84	25.25	14.14	-3.73	14.36	0.2	0.2	I068_GPS
82.993	36.739	25.94	13.27	-3.04	13.87	0.2	0.2	I069_GPS

81.478	36.455	25.05	15.39	-3.94	15.55	0.3	0.3	I070_GPS
78.451	40.942	29.95	15.92	1.12	15.21	0.2	0.2	I072_GPS
79.035	40.503	29.66	15.26	0.8	14.72	0.2	0.2	I073_GPS
76.889	40.204	29.37	14.86	0.52	13.7	0.2	0.2	I074_GPS
78.037	39.714	28.19	18.35	-0.7	17.52	0.2	0.2	I075_GPS
78.54	39.776	28.89	18.2	0	17.51	0.3	0.4	I076_GPS
76.512	39.806	29.38	15.88	0.51	14.61	0.4	0.4	I077_GPS
75.25	39.718	27.76	14.23	-1.09	12.59	0.2	0.2	I078_GPS
76.734	39.497	28.69	19.01	-0.19	17.8	0.2	0.2	I079_GPS
75.899	39.196	29.59	21.25	0.71	19.8	0.3	0.3	I081_GPS
77.624	38.904	27.71	19.26	-1.21	18.31	0.4	0.4	I082_GPS
76.174	38.935	28.41	21.47	-0.49	20.1	0.2	0.2	I083_GPS
77.277	38.174	25.83	21.57	-3.11	20.52	0.3	0.3	I084_GPS
78.246	37.559	25.94	20	-3.02	19.23	0.2	0.2	I086_GPS
79.964	37.098	25.95	16.82	-3.03	16.55	0.3	0.3	I087_GPS
75.447	36.851	24.54	22.79	-4.4	21.21	0.2	0.2	I088_GPS
74.336	39.842	27.75	15.68	-1.08	13.78	0.3	0.3	I089_GPS
74.951	38.662	23.3	21.92	-5.58	20.2	0.2	0.2	I090_GPS
83.041	41.958	31.98	7.83	3.2	8.45	0.4	0.4	I382_GPS
82.44	41.858	30.89	11.2	2.1	11.64	0.6	0.6	I383_GPS
79.715	41.661	30.61	11.76	1.81	11.41	0.3	0.4	I384_GPS
80.065	41.663	30.31	10.06	1.51	9.82	0.4	0.5	I385_GPS
89.125	41.644	29.47	5.43	0.78	7.8	1	1.1	I386_GPS
87.436	41.292	30.33	6.8	1.58	8.69	0.4	0.4	I387_GPS
77.949	40.877	28.95	14.96	0.12	14.1	0.3	0.4	I388_GPS
91.33	41.015	31.12	3.62	2.46	6.62	0.5	0.5	I389_GPS
83.188	41.082	30.81	12.09	1.98	12.75	0.4	0.4	I390_GPS
81.303	40.495	31.16	15.22	2.29	15.33	0.4	0.4	I391_GPS
75.367	40.501	28.14	12.49	-0.68	10.89	0.4	0.5	I392_GPS
77.622	40.343	29.57	15.35	0.71	14.4	0.4	0.4	I393_GPS

79.435	40.035	28.88	16.75	0	16.32	0.4	0.4	I394_GPS
77.444	39.631	28.99	18.01	0.1	17.01	0.4	0.4	I395_GPS
76.009	39.56	28.98	17.92	0.11	16.5	0.4	0.4	I396_GPS
75.579	39.321	29.78	20.94	0.91	19.4	0.4	0.5	I397_GPS
88.214	39.276	29.29	6.99	0.46	9.1	0.4	0.4	I398_GPS
74.427	39.025	23.48	20.86	-5.38	18.99	0.3	0.3	I399_GPS
88.931	38.988	28.89	6.09	0.06	8.41	0.4	0.4	I400_GPS
75.401	38.96	29.19	22.89	0.31	21.3	0.3	0.4	I401_GPS
74.833	38.862	24.59	21.94	-4.29	20.18	0.4	0.4	I402_GPS
74.924	38.225	24.71	22.03	-4.19	20.3	0.4	0.4	I403_GPS
76.661	38.38	27.22	20.84	-1.7	19.61	0.4	0.5	I404_GPS
85.575	38.065	27.68	10.24	-1.24	11.59	0.4	0.4	I405_GPS
80.3	37.891	26.05	16.31	-2.91	16.13	0.4	0.4	I406_GPS
75.768	37.84	25.62	22.39	-3.3	20.9	0.4	0.4	I407_GPS
86.171	37.588	29.78	11.07	0.85	12.59	0.3	0.3	I408_GPS
77.356	37.501	26.84	20.85	-2.11	19.82	0.4	0.4	I409_GPS
75.383	37.354	25.03	22.9	-3.9	21.3	0.4	0.4	I410_GPS
77.04	37.138	25.64	21.24	-3.32	20.12	0.4	0.4	I411_GPS
84.524	37.133	26.82	11.53	-2.14	12.58	0.3	0.3	I412_GPS
76.981	36.848	25.45	21.85	-3.51	20.71	0.4	0.4	I413_GPS
79.915	36.825	24.96	17.43	-4.02	17.14	0.4	0.4	I414_GPS
83.6	36.723	26.93	12.1	-2.05	12.88	0.9	0.9	I415_GPS
77.838	37.394	25.15	19.61	-3.81	18.72	0.6	0.7	I416_GPS
79.99	36.399	24.66	17.51	-4.33	17.24	0.4	0.4	I418_GPS
78.069	36.338	24.85	19.86	-4.13	19.04	0.5	0.5	I419_GPS
78.973	32.779	26.22	19.81	-2.76	19.25	0.6	0.4	IAOH_GPS
73.796	39.654	28.75	12.13	-0.07	10.07	0.7	0.6	IKZ4_GPS
78.21	41.601	29.81	12.08	1.02	11.3	0.4	0.5	ISH4_GPS
98.098	36.27	37.27	2.19	8.71	7.1	0.3	0.3	J002_GPS
99.972	35.622	37.89	-0.41	9.42	5.01	0.2	0.2	J003_GPS

95.528	34.552	48.61	2.29	19.91	6.48	0.5	0.4	J004_GPS
98.209	34.894	44.29	0.27	15.72	5.21	0.3	0.3	J005_GPS
99.688	33.804	43.81	-2.53	15.3	2.82	0.3	0.3	J006_GPS
95.257	32.894	52.6	1.97	23.9	6.09	0.5	0.5	J008_GPS
99.193	31.938	48.11	-6.9	19.59	-1.69	0.5	0.4	J009_GPS
97.169	31.162	48.69	-4.85	20.09	-0.2	0.4	0.4	J010_GPS
95.601	29.939	46.7	-1.22	18.08	2.99	0.3	0.2	J011_GPS
97.997	29.709	42.1	-8.57	13.58	-3.69	0.3	0.3	J012_GPS
92.438	34.207	50.14	7.57	21.33	10.89	1.7	1.7	J016_GPS
91.675	32.246	48.21	9.75	19.4	12.85	0.3	0.2	J018_GPS
94.096	31.917	50.33	4.79	21.6	8.58	0.5	0.4	J019_GPS
92.068	31.509	49.59	9.85	20.8	13.07	0.3	0.2	J020_GPS
91.112	30.479	46.03	16.25	17.25	19.19	1.3	1.3	J021_GPS
93.146	29.94	48.7	9.45	20	12.97	1.1	1.2	J022_GPS
91.105	32.012	47.63	11.12	18.8	14.06	0.3	0.2	J025_GPS
88.694	31.129	43.86	17.68	15	19.93	0.3	0.3	J026_GPS
90.55	30.088	45.57	15.47	16.79	18.25	0.3	0.3	J027_GPS
92.87	30.751	49.33	8.23	20.59	11.67	0.3	0.2	J028_GPS
88.56	28.244	39.33	24.64	10.6	26.85	0.4	0.4	J029_GPS
87.06	28.587	37.27	23.75	8.49	25.53	0.3	0.3	J030_GPS
92.399	28.422	44.94	13.47	16.28	16.78	0.2	0.2	J032_GPS
90.558	28.419	42.09	21.47	13.39	24.25	0.2	0.2	J033_GPS
91.91	27.971	42.73	16.9	14.08	20.07	0.2	0.2	J034_GPS
89.197	31.985	44.28	15.74	15.41	18.13	0.3	0.3	J035_GPS
86.442	31.927	40.33	19.02	11.41	20.62	0.2	0.3	J036_GPS
88.837	29.359	40.98	20.75	12.19	23.04	0.3	0.3	J037_GPS
87.085	29.32	38.52	22.35	9.7	24.14	0.3	0.3	J038_GPS
89.556	28.911	41.34	21.75	12.59	24.25	0.3	0.3	J039_GPS
85.442	28.959	37.02	24.11	8.2	25.42	0.2	0.2	J040_GPS
85.975	28.149	36.86	25.76	8.09	27.23	0.2	0.2	J041_GPS

89.154	27.721	39.88	27.47	11.19	29.85	0.4	0.4	J042_GPS
84.129	32.297	35.38	19.07	6.42	20	0.2	0.2	J043_GPS
81.19	32.382	30.61	18.39	1.64	18.47	0.2	0.2	J044_GPS
81.176	30.29	31.13	21.9	2.22	21.98	0.2	0.2	J045_GPS
82.832	30.389	32.12	21.04	3.21	21.6	0.2	0.2	J046_GPS
77.005	36.577	24.75	22.56	-4.22	21.43	0.4	0.3	J047_GPS
79.94	33.564	29.74	17.54	0.75	17.26	0.2	0.2	J049_GPS
78.722	36.205	25.36	18.37	-3.63	17.74	0.4	0.4	J301_GPS
79.159	35.995	25.16	17.65	-3.83	17.14	0.4	0.4	J302_GPS
77.844	35.568	25.76	20.12	-3.23	19.23	0.4	0.4	J303_GPS
79.516	35.615	25.07	17.05	-3.93	16.65	0.4	0.4	J304_GPS
79.427	35.774	25.96	17.48	-3.04	17.05	0.4	0.4	J305_GPS
79.473	35.235	26.36	16.86	-2.64	16.44	0.4	0.4	J306_GPS
76.162	38.669	28.1	21.77	-0.81	20.4	0.4	0.4	J307_GPS
79.098	31.887	27.7	20.09	-1.26	19.56	0.4	0.4	J308_GPS
79.738	35.015	25.76	16.89	-3.24	16.55	0.4	0.4	J309_GPS
79.809	33.214	28.93	17.18	-0.06	16.86	0.4	0.4	J310_GPS
79.814	31.498	28.28	19.58	-0.67	19.26	0.4	0.4	J311_GPS
79.862	34.947	26.66	16.75	-2.34	16.45	0.4	0.4	J312_GPS
80.001	32.612	29.32	18.12	0.34	17.86	0.3	0.3	J313_GPS
80.293	31.71	28.99	18.95	0.03	18.77	0.4	0.4	J314_GPS
80.341	34.438	28.16	18.12	-0.84	17.96	0.4	0.4	J315_GPS
80.323	33.771	29.84	17.13	0.84	16.96	0.4	0.4	J316_GPS
80.413	33.041	29.53	17.41	0.54	17.27	0.4	0.4	J317_GPS
80.429	30.961	29.17	20.31	0.24	20.17	0.4	0.4	J318_GPS
95.79	29.819	47.29	-1.78	18.68	2.49	0.4	0.4	J319_GPS
81.856	30.716	31.75	20.51	2.83	20.78	0.3	0.3	J320_GPS
82.167	34.245	32.74	16.71	3.74	17.07	0.5	0.5	J321_GPS
82.192	32.243	31.6	18.71	2.63	19.08	0.4	0.4	J322_GPS
82.248	31.512	32.17	19.8	3.22	20.19	0.5	0.4	J323_GPS

82.503	34.081	32.84	17.21	3.85	17.67	0.4	0.4	J324_GPS
82.803	35.023	33.84	15.53	4.84	16.08	0.5	0.4	J325_GPS
83.241	29.795	33.39	22.22	4.51	22.9	0.6	0.6	J326_GPS
83.325	32.411	34.39	18.59	5.42	19.29	0.3	0.3	J327_GPS
83.556	30.769	33.83	20.03	4.91	20.8	0.5	0.5	J328_GPS
83.682	31.652	35.17	19.29	6.23	20.09	0.4	0.4	J329_GPS
83.974	31.034	35.33	20.41	6.41	21.3	0.4	0.4	J330_GPS
84.02	33.164	34.51	17.49	5.54	18.39	0.4	0.4	J331_GPS
84.039	29.721	34.08	22.8	5.21	23.71	0.5	0.5	J332_GPS
83.779	35.347	33.63	16.55	4.64	17.38	0.5	0.5	J333_GPS
85.07	31.354	36.83	19.8	7.91	21.01	0.6	0.6	J334_GPS
85.269	32.022	36.86	19.35	7.92	20.61	0.4	0.4	J335_GPS
85.198	30.688	37.41	20.57	8.51	21.81	0.5	0.6	J336_GPS
85.64	29.441	36.34	21.85	7.5	23.22	0.8	0.7	J337_GPS
85.693	29.961	36.97	21.74	8.11	23.13	0.8	0.7	J338_GPS
86.387	28.687	36.29	24.24	7.5	25.83	0.5	0.5	J339_GPS
86.52	30.001	39.76	21.5	10.91	23.12	0.6	0.6	J340_GPS
87.167	31.203	41.3	18.82	12.41	20.63	0.5	0.5	J341_GPS
87.004	30.619	40.37	19.56	11.5	21.32	0.5	0.5	J342_GPS
84.827	35.467	34.72	14.15	5.74	15.28	0.4	0.4	J343_GPS
85.714	35.47	34.11	15.71	5.14	17.1	0.6	0.6	J344_GPS
87.355	31.602	41.61	18.65	12.71	20.51	0.5	0.5	J345_GPS
87.769	28.538	39.56	24.46	10.8	26.44	1.4	1.2	J346_GPS
88.238	29.429	40.89	20.92	12.09	23.04	0.4	0.4	J347_GPS
88.672	33.258	42.82	15.19	13.91	17.43	0.5	0.4	J348_GPS
88.639	30.629	41.64	18.41	12.8	20.64	0.5	0.5	J349_GPS
89.028	31.428	43.36	17.09	14.5	19.44	0.4	0.4	J350_GPS
90.075	31.42	45.04	15.2	16.2	17.85	0.5	0.5	J351_GPS
89.305	27.931	40.79	24.93	12.09	27.36	0.9	0.8	J352_GPS
89.627	28.315	38.5	23.93	9.78	26.45	0.8	0.7	J353_GPS

90.021	31.357	44.34	16.01	15.5	18.64	0.5	0.4	J354_GPS
90.069	30.517	43.91	15.8	15.1	18.44	0.4	0.4	J355_GPS
89.911	28.619	42.11	21.75	13.38	24.35	0.5	0.5	J356_GPS
90.107	28.932	42.23	19.9	13.49	22.56	0.5	0.5	J357_GPS
90.153	29.444	43.05	18.09	14.29	20.76	0.4	0.4	J358_GPS
90.266	29.324	43.85	18.06	15.09	20.76	0.4	0.4	J359_GPS
90.562	30.206	44.58	15.36	15.79	18.15	0.5	0.4	J360_GPS
90.819	32.005	47.33	11.89	18.5	14.75	0.4	0.4	J361_GPS
90.899	31.445	46.62	12.27	17.8	15.15	0.5	0.4	J362_GPS
91.654	30.902	48.47	12.66	19.69	15.76	0.4	0.4	J363_GPS
91.695	31.865	49.01	10.05	20.2	13.16	0.4	0.4	J364_GPS
91.787	31.229	48.89	10.33	20.1	13.47	0.4	0.4	J365_GPS
91.846	32.56	48.52	7.6	19.7	10.75	0.4	0.4	J366_GPS
91.889	28.96	44.98	14.11	16.28	17.27	0.4	0.4	J367_GPS
91.948	33.478	48.83	8.27	20.01	11.45	0.6	0.5	J368_GPS
91.92	32.873	48.32	8.98	19.5	12.15	0.4	0.4	J369_GPS
92.606	34.373	49.02	6.59	20.21	9.96	0.4	0.4	J370_GPS
92.731	34.462	46.91	5.15	18.11	8.55	0.6	0.6	J371_GPS
92.83	31.794	50.07	8.13	21.3	11.56	0.4	0.4	J373_GPS
93.073	29.044	46.15	9.47	17.48	12.97	0.4	0.4	J375_GPS
93.218	30.643	49.42	7.43	20.69	10.97	0.4	0.4	J378_GPS
94.364	35.874	36.25	4.21	7.52	8.07	0.4	0.4	J380_GPS
94.457	33.449	49.54	3.59	20.8	7.48	0.7	0.7	J381_GPS
94.631	31.585	51	2.54	22.29	6.48	0.4	0.3	J382_GPS
94.797	35.925	36.54	4.79	7.83	8.78	0.4	0.4	J383_GPS
95.231	35.74	39.61	4.87	10.91	8.98	0.4	0.4	J385_GPS
95.369	33.826	48.61	2.33	19.91	6.48	0.6	0.6	J386_GPS
95.813	30.754	48.83	-1.78	20.19	2.49	0.6	0.6	J388_GPS
96.095	29.75	44.48	-3.76	15.88	0.59	0.4	0.4	J389_GPS
96.406	31.495	50.23	-2.64	21.59	1.8	0.4	0.4	J390_GPS

96.416	35.727	39.76	3.65	11.11	8.09	0.4	0.4	J391_GPS
96.633	32.742	51.55	-2.51	22.9	1.99	0.4	0.4	J392_GPS
96.885	30.055	45.16	-6.37	16.58	-1.8	0.4	0.4	J393_GPS
97.054	28.451	41.38	-4.41	12.87	0.21	0.6	0.6	J394_GPS
97.181	29.282	41.61	-8.55	13.07	-3.89	0.4	0.4	J395_GPS
97.176	33.712	47.63	0.44	19	5.09	0.4	0.4	J396_GPS
97.288	33.06	45.82	-1.19	17.2	3.49	0.5	0.4	J397_GPS
97.469	28.72	41.28	-10.03	12.78	-5.29	0.6	0.6	J398_GPS
97.502	34.022	46.32	-0.04	17.71	4.7	0.5	0.4	J399_GPS
97.956	34.4	47.19	0.74	18.6	5.61	0.4	0.4	J400_GPS
97.959	35.501	40.49	2.13	11.91	7	0.3	0.3	J401_GPS
98.23	31.514	48.75	-6.13	20.19	-1.18	0.4	0.4	J402_GPS
98.621	32.377	47.35	-4.84	18.8	0.21	0.4	0.4	J403_GPS
98.604	35.016	43.77	-0.65	15.22	4.4	0.5	0.5	J404_GPS
98.874	35.126	42.35	-0.32	13.81	4.8	0.4	0.3	J405_GPS
99.196	34.271	44.33	-0.9	15.8	4.31	0.4	0.4	J406_GPS
99.222	35.358	38.53	0.69	10.01	5.91	0.5	0.5	J407_GPS
98.323	33.053	47.47	-3.16	18.9	1.81	0.5	0.4	J420_GPS
98.592	31.871	48.74	-6.44	20.19	-1.39	0.6	0.5	J421_GPS
97.403	28.992	41.39	-10.41	12.87	-5.69	0.7	0.6	J422_GPS
97.513	29.959	44.83	-8.34	16.28	-3.59	0.4	0.4	J423_GPS
97.097	30.554	47.37	-5.83	18.79	-1.2	0.3	0.3	J424_GPS
97.337	30.808	52.23	-5.76	23.65	-1.06	1.1	1.1	J425_GPS
97.782	31.37	48.77	-5.51	20.19	-0.69	0.5	0.5	J426_GPS
92.352	33.953	50.52	7.26	21.71	10.56	0.6	0.4	J427_GPS
88.399	29.331	42.19	22.67	13.4	24.84	1.3	1.2	J428_GPS
83.742	29.866	31.89	26.98	3.01	27.8	1.3	1.2	J430_GPS
92.01908	25.17943	40.13	30.55	11.68	33.75	0.27	0.4	JAFL_GPS
92.204	26.117	39.28	28.23	10.76	31.48	1.4	1.2	JAGI_GPS
90.76	27.538	40.33	23.12	11.68	25.96	0.8	0.7	JAKR_GPS

83.658	28.508	35.92	27.71	7.11	28.51	0.7	0.6	JALT_GPS
91.237	25	42.82	30.29	14.37	33.27	0.5	0.5	JAML_GPS
85.924	26.711	38.26	36.38	9.58	37.83	1.9	1.2	JANK_GPS
95.8	40.514	30.46	-1	1.96	3.27	0.2	0.2	JB28_GPS
94.873	36.433	37.73	5.06	9.03	9.07	0.3	0.3	JB30_GPS
93.412	38.809	34.63	2.36	5.94	5.95	0.2	0.2	JB31_GPS
90.982	38.588	34.83	5.73	6.05	8.63	0.3	0.3	JB32_GPS
98.498	25.018	24	-11.3	-4.24	-6.28	0.3	0.3	JB41_GPS
85.538	38.081	27.48	10.35	-1.45	11.69	0.2	0.2	JB46_GPS
75.923	39.517	30.48	17.94	1.61	16.5	0.2	0.2	JB48_GPS
96.988	32.997	48.53	-0.81	19.9	3.79	0.4	0.5	JB49_GPS
96.868	29.391	43.64	-9.07	15.09	-4.5	0.3	0.3	JB50_GPS
93.052	35.088	46.41	5.16	17.62	8.65	0.5	0.4	JB51_GPS
91.985	32.986	47.83	7.26	19.01	10.45	0.4	0.3	JB52_GPS
87.766	31.891	42.31	17.24	13.41	19.22	0.3	0.3	JB53_GPS
86.967	28.392	37.46	24.58	8.69	26.33	0.3	0.3	JB54_GPS
79.581	35.459	26.56	17.03	-2.44	16.64	0.2	0.2	JB55_GPS
79.8	32.427	28.92	18.99	-0.05	18.67	0.2	0.2	JB56_GPS
73.0239	26.2064	36.27	34.03	7.67	31.75	0.1	0.1	JDPR_GPS
78.608	25.452	37.01	33.16	8.41	32.49	0.9	0.8	JHAN_GPS
77.175	32.634	23.62	19.62	-5.34	18.54	1.4	1.4	JIPA_GPS
86.187	27.65705	35.14	20.76	6.4	22.29	0.47	0.65	JIR2_GPS
86.23	27.635	36.53	28.39	7.8	29.93	0.9	0.6	JIRI_GPS
88.936	26.965	41.33	32.43	12.68	34.75	1.1	0.7	JITI_GPS
73.686	40.637	25.2	9.95	-3.57	7.86	0.5	0.5	JLK4_GPS
82.19258	29.27782	33.36	26.24	4.5	26.61	0.17	0.22	JMLA_GPS
83.7433	28.80528	35.81	25.23	6.98	26.05	0.17	0.22	JMSM_GPS
83.718	28.781	35.13	26	6.3	26.81	0.4	0.4	JOMO_GPS
98.496	39.758	32.05	-5.22	3.64	-0.2	1.1	1	JQ13_GPS
85.057	30.729	37.81	22.6	8.91	23.8	0.5	0.5	JRGR_GPS

94.159	26.739	40.27	20.78	11.76	24.59	2.8	2.7	JRHT_GPS
76.294	31.897	31.29	30.48	2.36	29.14	0.9	0.9	JWLM_GPS
89.731	27.785	41.67	27.01	12.98	29.56	0.4	0.4	KABU_GPS
76.101	41.173	27.22	12.98	-1.57	11.59	0.5	0.5	KAI4_GPS
89.45	26.89	39.31	31.99	10.68	34.46	0.6	1.3	KAMJ_GPS
92.65	26.163	43.08	31.2	14.57	34.58	2.7	2.3	KAMP_GPS
91.52	27.29	38.59	24.41	9.98	27.47	1.2	1.8	KANG_GPS
79.9	29.78	33.81	32.47	4.93	32.18	0.8	0.7	KAPK_GPS
76.776	41.733	28.3	11.08	-0.47	9.88	0.4	0.4	KAR4_GPS
80.781	41.38	30.02	14.86	1.2	14.82	1	0.8	KARA_GPS
76.162	34.559	27.34	25.1	-1.63	23.73	0.2	0.2	KARG_GPS
73.46	38.957	21.17	24.86	-7.67	22.71	0.6	0.6	KARL_GPS
76.84	41.132	28.12	13.27	-0.69	12.09	0.3	0.3	KASU_GPS
84.12986	27.64797	35.79	35.15	7.03	36.08	0.4	0.24	KAWA_GPS
77.921	32.364	23.81	18.52	-5.15	17.65	1.9	1.7	KAZA_GPS
73.94352	41.38494	27.13	7.48	-1.61	5.47	0.19	0.16	KAZA_GPS
95.819	28.178	45.51	15.92	16.97	20.2	2.1	2.8	KBLI_GPS
77.906	37.258	24.75	19.59	-4.21	18.72	1	1	KELI_GPS
87.206	27.38	38.39	33.91	9.69	35.73	1.6	1.2	KHAN_GPS
92.08	26.126	41.29	28.56	12.77	31.78	1.2	1.1	KHET_GPS
90.612	27.288	38.51	27.57	9.87	30.37	0.9	0.8	KHOS_GPS
93.4	26.571	41.58	26.69	13.06	30.28	1.6	1.6	KHRA_GPS
72.297	40.362	27.79	7.55	-0.96	5.06	0.6	0.6	KHZ4_GPS
93.968	27.313	41.42	25.64	12.87	29.39	2	2.8	KIMN_GPS
85.28817	27.68188	39.9	29.9	11.15	31.17	0.57	1.61	KIRT_GPS
76.463	38.656	27.31	21.99	-1.6	20.7	0.6	0.6	KIZI_GPS
73.19	41.001	25.58	8.99	-3.16	6.76	0.5	0.5	KJA6_GPS
72.894	41.695	26.74	6.18	-1.95	3.86	0.4	0.4	KKA4_GPS
72.735	39.678	27.32	9.83	-1.48	7.47	0.6	0.6	KKB4_GPS
74.928	41.737	27.87	6.81	-0.87	5.08	0.4	0.4	KKC4_GPS

76.205	41.902	27.58	9.64	-1.17	8.28	0.5	0.5	KKD4_GPS
85.27881	27.80073	36.73	30.87	7.97	32.14	0.17	0.39	KKN4_GPS
75.55	41.018	27.22	11.23	-1.57	9.68	0.8	0.7	KKY4_GPS
86.169	41.708	31.24	7.55	2.49	9.07	1	0.9	KL19_GPS
83.6033	27.76685	37.22	35.06	8.45	35.84	0.21	0.27	KLDN_GPS
83.612	27.767	38.27	34.34	9.5	35.12	0.43	0.36	KLDN_GPS
89.905	38.409	32.97	4.32	4.15	6.92	1.4	1.1	KLSA_GPS
78.19922	41.8678	30.77	6.4	1.99	5.61	0.17	1.08	KMTR_GPS
74.817	34.109	30.92	32.77	1.97	31.01	1.3	1.3	KNEW_GPS
96.359	27.756	40.27	14.48	11.77	18.91	0.6	0.6	KNGR_GPS
76.408	41.892	26.88	9.99	-1.87	8.69	0.7	0.7	KOG4_GPS
77.175	37.396	25.54	19.7	-3.41	18.62	1	1	KOKY_GPS
76.52	40.918	28.23	14.26	-0.58	12.99	0.7	0.7	KOS4_GPS
76.69	37.862	25.23	22.03	-3.71	20.81	1	1	KOSR_GPS
77.192	32.317	25.71	25.72	-3.24	24.64	1.4	1.4	KOT1_GPS
73.881	41.808	27.15	5.3	-1.56	3.27	0.5	0.5	KOVK_GPS
86.828	27.994	38.94	24.82	10.19	26.53	1.2	1.1	KPFB_GPS
76.072	41.781	27.99	9.28	-0.77	7.88	0.3	0.3	KRB4_GPS
73.46	38.956	22.29	21.03	-6.55	18.88	1.3	1.4	KRKA_GPS
76.434	41.122	27.63	12.89	-1.17	11.59	0.4	0.4	KRL6_GPS
82.785	27.568	34.56	37.26	5.8	37.8	1	0.9	KRN2_GPS
75.048	41.487	27.49	7.98	-1.27	6.28	0.4	0.4	KRT4_GPS
76.443	40.734	28.24	13.59	-0.58	12.3	0.7	0.7	KRU4_GPS
73.667	41.344	26.78	7.26	-1.95	5.17	0.5	0.5	KRV4_GPS
79.62	29.638	39.83	34.27	10.95	33.9	4.12	3.08	KTML_GPS
85.53853	27.61841	35.38	33.31	6.64	34.65	0.47	0.39	KUGE_GPS
75.761	41.749	28.48	8.08	-0.27	6.59	0.8	0.8	KUK4_GPS
76.298	40.816	28.53	13.23	-0.28	11.89	0.3	0.3	KUL4_GPS
77.108	32.067	26.3	25.04	-2.65	23.94	0.9	0.9	KULU_GPS
92.248	26.196	40.89	28.51	12.37	31.78	1	0.9	KUMO_GPS

78.19	41.864	32.74	11.89	3.96	11.1	0.39	0.41	KUMT_GPS
75.569	41.358	27.3	10.73	-1.47	9.18	0.3	0.3	KUN4_GPS
90.7	27.61	41.44	26.73	12.79	29.56	1.7	1.6	KURJ_GPS
82.095	28.01	33.79	33.75	5	34.09	0.9	0.9	KUS0_GPS
83.678	28.211	36.7	33.51	7.91	34.31	0.7	0.7	KUSU_GPS
73.323	39.379	22.85	18.06	-5.97	15.87	0.7	0.7	KYZY_GPS
75.977	40.523	29.24	12.82	0.42	11.39	0.7	0.7	KZY4_GPS
93.082	29.082	46.95	9.07	18.28	12.57	1.1	0.9	LAC1_GPS
72.792	31.856	28.85	33.56	-0.02	31.21	0.3	0.3	LALI_GPS
78.68	29.848	37.82	33.31	8.94	32.66	1.6	1.4	LAN2_GPS
89.69	28.064	39.09	24.51	10.39	27.05	0.6	0.6	LAYA_GPS
80.95597	26.91256	38.2	34.68	9.48	34.69	0.62	1.1	LCK2_GPS
80.95562	26.91215	35.67	35.23	6.95	35.24	0.14	0.18	LCK4_GPS
80.9559	26.91244	37.85	34.54	9.13	34.55	0.6	0.98	LCKI_GPS
91.10403	29.65733	46.31	16.21	17.56	19.15	0.34	0.22	LHAZ_GPS
91.15	27.72	39.73	25.31	11.08	28.26	3.4	2.8	LHUE_GPS
94.36	29.648	48.54	3.52	19.89	7.38	0.4	0.3	LINZ_GPS
73.221	41.572	27.05	7.08	-1.66	4.86	0.4	0.4	LJM4_GPS
78.414	33.999	25.65	18.17	-3.34	17.45	2.7	1	LKNG_GPS
94.724	29.737	48.03	1.02	19.38	4.99	1	0.8	LLZ1_GPS
84.57342	28.17412	34.4	26.23	5.62	27.29	0.31	0.33	LMJG_GPS
81.116	28.613	39.04	34.73	10.21	34.79	1.5	1.5	LMK1_GPS
92.46	28.414	45.64	13.55	16.98	16.88	0.4	0.3	LNGZ_GPS
88.265	39.446	29.89	6.38	1.06	8.51	1	0.8	LOBU_GPS
92.439	28.432	43.44	12.36	14.78	15.68	2.1	1.9	LOZ1_GPS
80.943	26.891	37.73	32.68	9.01	32.69	1	1	LUCK_GPS
86.726	27.686	37.22	26.65	8.49	28.33	0.5	0.4	LUKL_GPS
94.475	26.22	36.73	21.8	8.27	25.7	0.3	0.3	LUMA_GPS
94.418	29.601	47.93	2.01	19.28	5.89	0.9	0.8	LZX1_GPS
75.037	33.595	31.92	31.02	2.97	29.32	1.2	1.2	MAAL_GPS

73.638	38.146	20.39	26.79	-8.48	24.69	1.5	1.6	MADA_GPS
80.148	28.963	36.16	34.5	7.32	34.28	0.9	0.8	MAH0_GPS
91.572	25.699	36.97	33.6	8.47	36.67	1.7	1.5	MAWP_GPS
88.185	26.883	34.44	35.74	5.78	37.84	1.4	1	MIRK_GPS
98.595	29.691	43.87	-12.63	15.38	-7.58	1	0.9	MKZ1_GPS
94.184	29.189	46.62	3.97	17.98	7.79	1	0.8	MLX1_GPS
97.45	25.435	23.47	-5.32	-4.84	-0.59	0.5	0.5	MMMZ_GPS
73.194	34.329	25.3	31.24	-3.62	29.01	0.4	0.4	MNK2_GPS
96.806	25.325	26.08	-4.44	-2.25	0.11	1.2	1.2	MOGA_GPS
77.868	30.147	36.03	29.74	7.14	28.86	1.3	1.1	MOHA_GPS
75.038	41.669	27.58	7.38	-1.16	5.68	0.3	0.3	MOL4_GPS
91.435	25.233	41.64	28.29	13.17	31.33	0.7	0.6	MOPE_GPS
92.269	26.218	38.39	28.4	9.87	31.67	1.1	1	MRGN_GPS
83.953	29.178	32.05	23.92	3.21	24.8	1.6	1.1	MST2_GPS
83.895	29.179	35.05	24.24	6.21	25.11	0.6	0.4	MSTG_GPS
76.572	41.129	27.02	12.95	-1.78	11.69	0.9	0.9	MUD4_GPS
82.347	28.249	36.81	37.18	8.01	37.6	0.9	0.9	MUL0_GPS
74.484	34.095	27.42	31.98	-1.52	30.12	0.5	0.5	MULG_GPS
88.4	26.98	37.34	35.28	8.68	37.45	0.5	0.4	MUNG_GPS
91.842	25.413	39.74	30.03	11.27	33.18	0.6	0.5	MUNN_GPS
80.24	30.06	30.52	23.77	1.62	23.58	0.5	0.5	MUNS_GPS
73.391	33.895	25.7	29.88	-3.22	27.71	0.7	0.7	MURE_GPS
73.796	38.137	21.79	25.44	-7.09	23.38	0.6	0.6	MURG_GPS
78.704	33.191	23.43	17.49	-5.55	16.85	2.6	1	MUTH_GPS
95.913	28.28	43.61	16.2	15.07	20.5	1.6	2.5	MY65_GPS
95.909	28.233	41.71	12.3	13.17	16.6	2.9	3.4	MYDA_GPS
76.307	32.248	28.3	29.47	-0.64	28.14	0.8	0.8	NADI_GPS
85.521	27.693	36.75	33.83	8	35.17	0.61	0.58	NAGA_GPS
86.715	27.803	38.43	26.55	9.69	28.23	0.7	0.5	NAMC_GPS
97.024	25.359	25.68	-5.1	-2.64	-0.49	1.2	1.2	NAMT_GPS

96.562	25.626	33.41	10.22	5.05	14.7	1.2	1.1	NAMY_GPS
92.061	31.48	50.59	9.15	21.8	12.36	0.4	0.4	NAQU_GPS
76.255	41.446	27.91	11.44	-0.87	10.09	0.4	0.4	NAR5_GPS
74.974	34.353	27.63	28.73	-1.32	27.01	0.6	0.6	NARA_GPS
91.54	27	38.97	22.8	10.37	25.87	3.2	4	NARP_GPS
85.32773	27.65669	31.61	33.44	2.86	34.72	0.56	0.35	NAST_GPS
88.35	26.711	35.23	34.19	6.59	36.34	1.9	1.5	NBUV_GPS
90.963	30.773	42.36	20.6	17.29	18.15	0.5	0.5	NCRS_GPS
81.615	28.049	36	34.69	7.21	34.89	0.6	0.6	NEPJ_GPS
75.73	41.875	27.27	7.48	-1.47	5.98	0.8	0.8	NGS4_GPS
89.63	38.468	31.97	3.9	3.14	6.42	1.3	1.1	NICE_GPS
85.187	27.183	36.47	37.48	7.75	38.72	1.09	1.01	NIJ0_GPS
88.68	27	37.94	34.7	9.28	36.95	0.8	0.6	NIMC_GPS
74.889	34.12	27.32	30.35	-1.63	28.61	1.4	1.4	NISH_GPS
86.034	28.303	36.77	24.64	7.99	26.12	1	0.7	NL10_GPS
94.142	27.235	40.31	23.39	11.77	27.19	1.5	2.4	NLKP_GPS
95.348	27.186	45.54	19.18	17.04	23.32	1.7	1.6	NMRP_GPS
91.863	25.9	38.88	30.22	10.37	33.38	0.5	0.5	NONG_GPS
81.59531	28.11718	36.68	35.68	7.88	35.88	0.15	0.18	NPGJ_GPS
81.575	28.134	37.51	37.3	8.71	37.49	0.9	0.9	NPJ0_GPS
74.69	41.82	27.57	7.18	-1.16	5.38	0.4	0.4	NRK4_GPS
73.763	40.88	25.29	10.23	-3.47	8.16	0.4	0.4	NSB4_GPS
75.881	32.304	31.1	31.39	2.16	29.93	0.8	0.8	NURP_GPS
78.66	33.209	27.94	17.4	-1.04	16.75	0.7	0.7	NYOM_GPS
75.849	41.433	27.4	11.75	-1.37	10.29	0.7	0.7	OBO4_GPS
87.39214	26.86609	39.81	35.76	11.14	37.64	0.29	0.34	ODRE_GPS
73.933	41.383	26.8	8.44	-1.94	6.42	0.3	0.3	OKI4_GPS
75.983	41.577	27.5	9.31	-1.27	7.88	0.8	0.8	ONA4_GPS
72.743	40.522	26.6	8.63	-2.16	6.27	0.4	0.5	OSH4_GPS
72.7775	40.52994	27.01	8.38	-1.75	6.03	0.24	0.48	OSHK_GPS

75.827	41.655	24.96	9.77	-3.8	8.3	0.6	0.6	OTTU_GPS
74.076	40.436	26.32	12.16	-2.47	10.18	0.4	0.4	OYT4_GPS
76	39.48	29.08	18.32	0.21	16.9	1.3	1.2	P007_GPS
79.926	36.743	24.06	16.13	-4.93	15.84	1.2	1.1	P008_GPS
75.13	40.848	27.32	10.85	-1.47	9.18	0.4	0.4	PAK4_GPS
72.764	39.917	26.48	5.1	-2.31	2.75	2.5	2.6	PAMA_GPS
77.575	34.711	24.56	21	-4.43	20.03	1.3	1.3	PAN2_GPS
92.825	25.717	41.74	30.95	13.27	34.38	2.5	1.9	PANI_GPS
89.44	27.39	40.65	28.69	11.98	31.15	0.7	0.7	PARO_GPS
72.998	35.112	25.01	27.18	-3.9	24.89	0.3	0.3	PATA_GPS
72.352	33.134	29.67	32.08	0.78	29.61	0.3	0.3	PATH_GPS
96.417	27.992	40.08	13.96	11.57	18.4	1.9	2.8	PAYA_GPS
96.318	25.615	34.02	10.9	5.66	15.32	1.2	1.2	PHAK_GPS
86.823	27.894	38.84	25.02	10.1	26.73	0.8	0.6	PHE1_GPS
80.191	29.599	33.4	31.79	4.52	31.58	0.5	0.5	PITH_GPS
74.57	35.79	24.05	21.56	-4.89	19.73	0.5	0.5	PK18_GPS
73.96	35.47	24.87	20.13	-4.06	18.12	0.3	0.4	PK20_GPS
74.85	36.65	25.64	23.17	-3.29	21.42	1.8	1.7	PK28_GPS
73.44	33.12	30.55	30.17	1.64	28.01	0.3	0.3	PK34_GPS
85.398	27.575	39.03	34.93	10.29	36.23	1	0.9	PKI0_GPS
72.88	32.74	29.85	27.05	0.96	24.73	1	1.1	PM01_GPS
88.753	26.881	42.93	35.58	14.28	37.85	1	0.6	PMSM_GPS
77.567	34.727	24.56	20.71	-4.43	19.74	2.1	0.9	PNMK_GPS
83.978	28.199	35.8	33.22	7.01	34.11	0.5	0.4	POKH_GPS
79.194	30.329	30.94	30.57	2.04	30.07	1.2	1.1	POKH_GPS
91.105	25.668	41.48	30.73	12.97	33.67	0.6	0.6	PORL_GPS
88.849	39.027	28.89	6.72	0.06	9.01	0.6	0.6	POWR_GPS
94.892	29.541	46.31	-0.52	17.68	3.49	1	0.8	PQX1_GPS
73.06	33.67	28.62	29.68	-0.29	27.41	0.1	0.1	PS01_GPS
72.94	34.8	26.39	27.18	-2.52	24.88	0.4	0.5	PS07_GPS

91.185	26.503	39.15	31.81	10.58	34.77	0.8	0.8	PSLA_GPS
95.745	28.316	47.22	17.34	18.67	21.59	2.1	2.8	PTCM_GPS
75.088	40.578	27.93	11.26	-0.88	9.58	0.4	0.4	PTU4_GPS
73.627	41.288	25.58	7.77	-3.16	5.67	0.4	0.4	PUR4_GPS
97.4	27.35	36	-8.8	7.56	-4.08	1.2	1.2	PUTA_GPS
82.98671	28.10126	36.67	34.41	7.88	35.01	0.36	0.28	PYUT_GPS
77.63	30.276	33.73	32.31	4.84	31.36	0.8	0.8	QASI_GPS
98.097	36.296	37.87	2.09	9.31	7	0.3	0.4	QHDL_GPS
94.772	36.145	37.23	4.2	8.52	8.18	0.3	0.3	QHGE_GPS
93.331	38.744	34.83	2.08	6.13	5.65	0.3	0.4	QHLH_GPS
98.208	34.92	45.29	-0.03	16.72	4.91	0.5	0.5	QHMD_GPS
90.801	38.475	35.54	6.67	6.75	9.52	0.5	0.5	QHMY_GPS
92.438	34.217	49.12	6.64	20.31	9.96	0.4	0.4	QHTT_GPS
97.015	33.01	48.33	-1.01	19.7	3.6	0.6	0.5	QHYS_GPS
75.404	40.094	28.95	12.78	0.11	11.19	0.4	0.4	QIAK_GPS
76.978	40.844	28.54	11.34	-0.28	10.2	0.4	0.4	QIQI_GPS
85.427	37.582	26.8	10.98	-2.14	12.29	1.1	1.2	QUIS_GPS
92.629	26.073	43.77	30.2	15.27	33.58	2.3	1.9	RAJA_GP1
77.979	30.095	34.23	36.31	5.34	35.46	1.2	1.1	RAJA_GPS
74.252	41.912	27.26	6.4	-1.45	4.48	0.3	0.3	RAL4_GPS
95.855	28.449	42.52	13.32	13.97	17.61	0.7	0.7	RALI_GPS
85.222	28.015	38.76	28.78	9.99	30.03	1	0.9	RAM0_GPS
79.08	29.23	34.98	33.4	6.13	32.87	0.7	0.7	RAMR_GPS
91.719	25.256	40.13	33.26	11.67	36.38	0.7	0.7	RANG_GPS
79.43	29.64	33.6	36.2	4.72	35.77	0.9	0.8	RANI_GP1
82.573	28.062	35.7	32.92	6.91	33.4	2	1.3	RANJ_GPS
74.593	33.993	25.62	31.75	-3.32	29.92	0.9	0.9	RANK_GPS
74.347	33.395	30.31	32.52	1.38	30.62	0.3	0.3	RAUJ_GPS
73.752	33.871	29.01	33.48	0.09	31.41	0.3	0.2	RAWL_GPS
89.392	26.849	40.51	30.91	11.88	33.36	1.4	1.5	RBIT_GPS

76.815	31.634	30.68	32.23	1.75	31.04	0.8	0.8	REWL_GPS
79.142	41.964	28.69	11.92	-0.09	11.41	0.8	0.8	RKA4_GPS
74.742	41.726	27.47	6.76	-1.27	4.98	0.4	0.4	RKR4_GPS
86.55001	27.30513	37.99	30.21	9.28	31.84	0.28	0.32	RMJT_GPS
86.59706	26.99095	39.36	34.31	10.67	35.96	0.56	0.27	RMTE_GPS
95.845	28.147	42.21	16.62	13.67	20.9	2.3	3.1	RON1_GPS
86.827	28.194	40.65	24.92	11.89	26.63	1.7	1.2	RONG_GPS
77.6	34.128	23.94	20.6	-5.04	19.64	0.3	0.3	RSCL_GPS
75.37	41.76	28.48	7.19	-0.27	5.59	0.3	0.3	RSO4_GPS
75.732	41.697	27.89	8.18	-0.87	6.68	0.3	0.3	RSR4_GPS
96.763	29.505	43.94	-8.64	15.38	-4.1	0.9	0.8	RWZ1_GPS
77.86	30.329	34.63	32.84	5.73	31.96	0.8	0.7	SABA_GPS
77.613	34.13	26.54	19.49	-2.44	18.53	0.7	0.7	SABU_GPS
88.791	27.01	39.24	31.87	10.59	34.15	1.7	1.4	SAMS_GPS
78.436	39.95	27.78	18.03	-1.1	17.31	1	0.8	SANC_GPS
89.926	38.408	33.67	4.12	4.85	6.72	1.7	1.7	SCAN_GPS
86.929	27.973	39.54	25.79	10.79	27.53	3.7	3.5	SCOL_GPS
99.803	28.937	41.49	-17.25	13.08	-11.87	0.3	0.3	SCXC_GPS
94.013	25.261	30.67	22.02	2.26	25.79	0.2	0.2	SENA_GPS
89.056	38.968	28.18	6.66	-0.65	9.01	0.6	0.7	SFEE_GPS
77.248	38.412	26.53	22.07	-2.4	21.01	0.9	0.7	SHAC_GPS
72.173	34.232	28.09	31.42	-0.8	28.9	0.6	0.6	SHAH_GPS
77.808	33.972	26.44	17.54	-2.54	16.64	1.2	1.1	SHAK_GPS
80.721	29.527	35.2	30.84	6.33	30.79	0.9	0.8	SHB0_GPS
72.08	39.861	30.04	9.42	1.27	6.87	0.9	0.9	SHB4_GPS
88.705	30.932	44.15	17.18	15.3	19.43	0.3	0.4	SHEN_GPS
91.885	25.566	38.35	31.22	9.86	34.38	0.3	0.3	SHIL_GPS
80.098	32.509	35.42	20.38	6.45	20.14	1.73	1.39	SHIQ_GPS
74.828	37.54	24.31	22.75	-4.61	20.99	0.8	0.9	SHMA_GPS
85.741	29.591	37.55	22.02	8.7	23.42	0.5	0.4	SHOT_GPS

80.636	29.012	36.46	36.96	7.61	36.88	0.9	0.9	SHP0_GPS
72.789	41.302	25.56	6.9	-3.15	4.55	1	1	SHY5_GPS
94.629	26.99	38.47	20.16	9.96	24.1	1.7	2.5	SIBS_GPS
84.99	27.17	38.95	34.59	10.23	35.77	0.63	0.5	SIM4_GPS
81.826	29.967	32.92	24.72	4.03	24.99	1.2	1	SIMI_GPS
84.984	27.165	38.71	35.94	9.99	37.12	0.5	0.5	SIMP_GPS
81.634	28.583	34.14	33.98	5.32	34.19	0.9	0.9	SKA0_GPS
75.772	40.476	28.34	12.87	-0.48	11.38	0.6	0.6	SME4_GPS
81.80655	29.96939	32.71	22.51	3.82	22.77	0.19	0.2	SMKT_GPS
77.627	41.918	28.59	10.94	-0.18	9.99	0.4	0.4	SMO4_GPS
85.79886	27.38483	36.22	33.02	7.5	34.44	0.3	0.27	SNDL_GPS
75.325	34.292	26.83	28.63	-2.13	27.01	0.7	0.7	SON1_GPS
75.423	41.914	27.27	7.56	-1.47	5.97	0.3	0.3	SON4_GPS
93.783	31.88	50.14	2.07	21.4	5.77	3.3	1.1	SOSH_GPS
81.691	28.407	37.53	36.57	8.72	36.8	0.9	0.9	SPS2_GPS
72.472	32.263	28.85	33.55	-0.02	31.11	0.2	0.2	SPUR_GPS
77.425	32.798	27.02	17.95	-1.94	16.94	1.8	1.7	SRCH_GPS
83.93581	28.26021	36.72	31.51	7.93	32.39	0.22	0.45	SRNK_GPS
74.185	37.836	20.71	19.03	-8.18	17.09	1.3	1.4	STSA_GPS
78.676	30.997	27.76	23.41	-1.17	22.76	2.4	1.5	SUKI_GPS
75.045	34.227	29.12	27.91	0.17	26.21	0.8	0.8	SUMB_GPS
85.329	28.171	37.37	28.74	8.59	30.02	1	1	SYA0_GPS
86.71246	27.81424	37.65	23.2	8.91	24.88	0.21	0.75	SYBC_GPS
73.257	39.732	27.73	10.78	-1.08	8.57	0.6	0.6	SYT4_GPS
90.65	27.08	38.4	30.06	9.78	32.87	3.6	3.9	TAMA_GPS
96.73	26.332	35.67	8.18	7.27	12.71	1.2	1.2	TANA_GPS
83.554	27.874	35.58	36.14	6.81	36.91	0.7	0.6	TANS_GPS
77.805	41.729	28.8	10.29	0.02	9.39	0.6	0.6	TAR2_GPS
75.234	37.775	25.92	22.84	-3	21.2	0.1	0.1	TASH_GPS
75.211	37.847	23.21	26.95	-5.7	25.3	0.9	0.8	TAXK_GPS

96.396	27.973	41.78	13.07	13.27	17.51	0.3	0.3	TDNG_GPS
73.333	41.785	26.74	5.55	-1.96	3.36	0.4	0.4	TEM4_GPS
86.765	27.835	38.33	24.84	9.59	26.54	0.7	0.6	TENG_GPS
90.085	38.391	34.66	6.17	5.84	8.82	1.1	0.8	TERR_GPS
74.722	41.511	27.28	7.17	-1.47	5.38	0.4	0.4	TGU4_GPS
96.332	27.913	40.18	15.59	11.67	20.01	2.1	2.8	THGM_GPS
75.263	40.889	27.52	11.21	-1.27	9.58	0.4	0.4	THR4_GPS
89.63485	27.47193	41.7	27.92	13.03	30.44	0.35	0.69	TIMP_GPS
87.155	28.63	38.17	23.73	9.39	25.54	1.2	1	TING_GPS
78.178	34.031	25.15	19.03	-3.84	18.24	2.2	0.8	TNGS_GPS
95.085	30.103	48.83	1.43	20.18	5.5	1.9	1.7	TOM1_GPS
95.067	30.099	47.41	3.16	18.76	7.22	1.88	1.66	TOM3_GPS
73.16	41.895	27.33	4.7	-1.36	2.46	0.4	0.4	TOR4_GPS
87.70982	27.35225	37.9	31.2	9.2	33.17	0.22	0.22	TPLJ_GPS
75.383	40.578	28.04	12.38	-0.77	10.78	0.4	0.4	TRG4_GPS
77.619	34.568	30.56	20.69	1.57	19.74	2.2	0.8	TRTH_GPS
83.645	28.71	35.13	26.72	6.31	27.51	0.8	0.7	TUKO_GPS
75.388	40.517	28.14	12.88	-0.67	11.28	0.6	0.6	TURG_GPS
95.834	28.224	44.61	15.82	16.07	20.1	0.7	0.8	TWGN_GPS
73.334	40.569	26.7	9.36	-2.07	7.17	0.5	0.5	TZB4_GPS
92.78	26.618	40.31	27.36	11.77	30.78	0.2	0.3	TZPR_GPS
73.427	39.226	19.32	24.12	-9.51	21.96	1.6	1.8	UBLA_GPS
79.27	41.99	28.29	12.28	-0.49	11.8	1.4	1.2	UCH4_GPS
76.689	32.698	26.12	23.96	-2.84	22.74	0.9	0.9	UDAI_GPS
94.36	25.109	30.34	18.93	1.96	22.8	0.3	0.2	UKHR_GPS
75.959	41.934	27.58	8.21	-1.17	6.78	0.3	0.3	UKO4_GPS
90.31	26.781	39.88	34.85	11.27	37.56	1.9	2.7	ULTP_GPS
92.725	25.526	41.73	27.49	13.27	30.89	2.5	1.7	UMRA_GPS
76.307	31.538	32.97	31.98	4.05	30.65	1	1	UNAN_GPS
73.478	41.219	26.28	8.91	-2.46	6.76	0.4	0.4	UUM4_GPS

74.929	41.936	27.56	6.9	-1.17	5.17	0.3	0.3	UZB4_GPS
74.78	41.069	27	9.65	-1.77	7.88	0.5	0.5	UZG4_GPS
72.498	41.98	27.71	4.89	-0.95	2.46	0.4	0.4	UZU4_GPS
87.072	38.709	28.34	9.31	-0.54	11.09	0.7	0.9	V403_GPS
78.032	36.349	25.15	20.57	-3.83	19.74	0.6	0.6	V407_GPS
97.016	28.131	40.97	2.1	12.48	6.71	0.5	0.5	WALG_GPS
91.53	27.11	39.28	22.3	10.68	25.36	2.8	4.2	WAMR_GPS
78.014	30.329	33.14	32.4	4.24	31.56	0.7	0.7	WIH2_GPS
77.974	30.285	34.43	31.51	5.53	30.66	0.8	0.7	WILD_GPS
91.858	33.234	48.93	7.9	20.11	11.05	0.6	0.5	WQ15_GPS
93.913	35.52	44.28	2.63	15.53	6.37	1.3	1.3	WT02_GPS
92.056	33.649	49.43	6.25	20.61	9.46	1.2	1.1	WT04_GPS
91.996	31.445	49.29	9.87	20.5	13.06	0.3	0.3	WT07_GPS
89.604	28.916	42.04	22.24	13.29	24.75	0.3	0.3	WT09_GPS
86.02	28.29	37.47	24.14	8.69	25.62	3.6	1.9	WT11_GPS
88.906	27.489	40.57	27.34	11.89	29.65	0.6	0.6	WT15_GPS
75.51	39.311	29.98	20.15	1.11	18.59	0.5	0.5	WUPA_GPS
75.124	39.697	27.66	16.26	-1.19	14.59	1.1	0.8	WUQO_GPS
79.21	41.202	30.04	14.81	1.22	14.32	0.1	0.1	WUSH_GPS
81.926	32.047	30.5	18.08	1.54	18.37	2.5	2.3	XGBA_GPS
78.77	39.814	29.39	16.93	0.5	16.31	0.3	0.3	XJBC_GPS
74.971	38.651	24.9	21.71	-3.99	19.99	0.3	0.4	XJBL_GPS
79.045	37.162	25.96	18.37	-3.01	17.83	0.3	0.4	XJHT_GPS
82.978	41.725	31.89	10.65	3.1	11.25	0.3	0.3	XJKC_GPS
86.189	41.792	31.44	8.45	2.69	9.98	0.3	0.3	XJKE_GPS
85.53	38.119	28.98	8.65	0.06	9.99	0.3	0.3	XJQM_GPS
88.171	39.022	29.5	6.2	0.66	8.3	0.3	0.3	XJRQ_GPS
83.659	38.969	29.39	11.06	0.47	11.86	0.3	0.4	XJTZ_GPS
75.238	39.74	29.16	14.43	0.31	12.79	0.3	0.4	XJWU_GPS
77.446	37.85	26.93	21.12	-2.02	20.12	0.4	0.4	XJYC_GPS

81.969	36.433	25.25	13.65	-3.74	13.96	0.4	0.4	XJYT_GPS
91.693	32.275	48.71	9.34	19.9	12.45	0.4	0.3	XZ06_GPS
93.784	31.89	51.54	7.67	22.8	11.37	1.3	1	XZ14_GPS
87.184	29.268	40.4	21.42	11.59	23.24	0.4	0.4	XZAR_GPS
81.428	30.837	32.85	19.43	3.92	19.58	0.5	0.5	XZBG_GPS
97.174	31.135	49.79	-4.95	21.19	-0.3	0.5	0.4	XZCD_GPS
97.466	28.661	42.07	-9.83	13.57	-5.1	0.5	0.5	XZCY_GPS
91.097	30.48	46.47	14.12	17.69	17.06	0.4	0.4	XZDX_GPS
80.107	32.52	30.42	18.19	1.44	17.96	0.3	0.3	XZGE_GPS
84.071	32.292	36.68	19.28	7.72	20.2	0.7	0.7	XZGZ_GPS
87.234	31.796	42.22	18.99	13.31	20.82	1.3	1.4	XZNM_GPS
92.109	31.492	50.89	8.54	22.11	11.77	0.6	0.7	XZNQ_GPS
88.865	29.249	41.77	21.14	12.99	23.44	0.4	0.3	XZRK_GPS
79.718	33.392	29.74	17.7	0.75	17.35	0.6	0.5	XZRT_GPS
88.906	27.437	40.46	27.94	11.78	30.25	0.7	0.6	XZYD_GPS
84.156	29.68	35.78	23.07	6.91	24.01	0.5	0.4	XZZB_GPS
86.941	28.357	38.86	24.19	10.09	25.94	0.5	0.4	XZZF_GPS
88.153	39.029	28.5	6.21	-0.34	8.3	0.5	0.4	Y033_GPS
79.774	37.135	25.85	17.87	-3.13	17.54	0.9	0.9	Y035_GPS
80.078	32.53	31.02	16.2	2.04	15.96	2.1	1.7	Y036_GPS
90.442	37.274	35.67	9.98	6.83	12.73	1.4	1.4	Y196_GPS
81.481	32.616	31.01	18.31	2.03	18.48	0.4	0.4	Y204_GPS
82.801	32.456	33.2	19.14	4.23	19.69	0.4	0.4	Y205_GPS
84.423	33.634	36.71	18.47	7.73	19.49	0.4	0.4	Y208_GPS
85.834	32.827	39.17	20.18	10.22	21.61	0.4	0.4	Y209_GPS
99.661	33.96	43.31	-2.72	14.8	2.62	0.3	0.4	Y222_GPS
97.391	33.181	51.49	-2.75	22.87	1.96	1.3	1.2	Y224_GPS
96.5	32.27	51.54	0.64	22.89	5.1	2.1	2.2	Y226_GPS
81.389	30.812	31.65	20.64	2.72	20.78	0.3	0.3	Y240_GPS
83.238	30.153	32.81	24.52	3.92	25.19	0.3	0.3	Y241_GPS

85.141	29.481	35.85	23.19	7	24.42	0.3	0.3	Y246_GPS
85.064	31.033	37.72	21.3	8.81	22.5	0.4	0.4	Y247_GPS
86.515	28.581	37.28	23.41	8.49	25.03	0.3	0.3	Y250_GPS
88.924	27.446	40.76	28.04	12.08	30.36	0.3	0.3	Y251_GPS
92.952	31.86	49.97	7.1	21.2	10.57	0.7	0.7	Y252_GPS
92.036	31.469	48.49	9.76	19.7	12.97	0.4	0.3	Y254_GPS
90.484	31.091	44.12	14.19	15.3	16.95	0.6	0.6	Y256_GPS
90.798	29.736	45.35	16.71	16.59	19.56	0.3	0.3	Y258_GPS
90.746	28.75	42.9	19.22	14.18	22.06	0.3	0.3	Y264_GPS
92.576	28.432	45.74	12.52	17.09	15.88	0.3	0.3	Y265_GPS
99.108	30.011	43.46	-12.97	14.98	-7.78	0.5	0.4	Y273_GPS
99.14	27.311	33.33	-15.68	4.96	-10.48	0.5	0.5	Y293_GPS
99.95	25.69	28.19	-15.98	-0.04	-10.56	0.4	0.4	Y299_GPS
95.377	37.834	36.18	1.82	7.54	5.97	0.6	0.7	Y345_GPS
97.73	37.377	38.17	0.89	9.62	5.7	0.6	0.6	Y347_GPS
84.043	29.534	35.67	24.6	6.81	25.51	0.5	0.5	YARE_GPS
96.633	39.839	31.44	-0.42	2.94	4.08	1.1	1.1	YC20_GPS
99.269	26.492	28.47	-16.4	0.16	-11.17	0.5	0.5	YD02_GPS
99.764	26.529	29.45	-17.04	1.16	-11.67	0.6	0.6	YD03_GPS
98.625	26.018	25.77	-11.93	-2.54	-6.87	0.6	0.6	YD07_GPS
98.78	25.947	25.36	-13.77	-2.94	-8.67	0.7	0.7	YD08_GPS
98.94	25.836	25.74	-13.71	-2.54	-8.57	0.7	0.6	YD11_GPS
99.575	25.761	26.71	-15.78	-1.54	-10.46	0.7	0.6	YD13_GPS
99.372	25.885	27.53	-16.83	-0.74	-11.57	0.3	0.4	YNYL_GPS
99.698	27.823	34.03	-20.32	5.66	-14.97	0.3	0.3	YNZD_GPS
75.741	41.979	27.57	8.07	-1.17	6.57	0.3	0.3	YUZ4_GPS
99.38	39.247	30.62	-3.06	2.24	2.2	1.2	1.2	YZ46_GPS
73.207	41.335	26.37	7.89	-2.35	5.66	0.7	0.6	YZG4_GPS
75.009	41.092	27.01	10.09	-1.77	8.38	0.4	0.4	ZBA4_GPS
90.684	27.183	40.9	28.15	12.27	30.97	0.9	0.8	ZHEM_GPS

93.841	27.619	43.25	16.37	14.68	20.09	1.7	2.5	ZIRO_GPS
95.738	29.87	48.4	-3.76	19.79	0.49	1.2	0.9	ZMZ1_GPS
94.035	25.718	37.31	24.22	8.87	27.99	0.6	0.5	ZUBU_GPS
97.778	29.727	43.01	-10.91	14.48	-6.09	1.3	1.1	ZUG1_GPS

8.1.3. Table – Stress results values

GRID_ID	*N_FMS*	*Lon_GRID*	*Lat_GRID*	*shape_ratio*	*friction*	σ_1 *trend*	σ_1 *plunge*	σ_2 *trend*	σ_2 *plunge*	σ_3 *trend*	σ_3 *plunge*	σ_{Hmax}
\	\	deg	deg	\	\	deg	deg	deg	deg	deg	deg	deg
11	45	72.5	34.5	0.57	0.4	217.69	5.32	127.25	4.69	356.06	82.9	38.02
12	49	72.5	35.5	0.66	0.5	215.58	5.31	125.24	3.61	1.17	83.57	35.76
13	23	72.5	36.5	0.3	0.55	354.94	6.03	102.54	70.73	262.95	18.23	173.58
14	36	72.5	37.5	0.39	0.5	343.48	10.17	177.55	79.53	73.93	2.49	163.76
15	71	72.5	38.5	0.68	0.85	339.78	1.25	222.85	87.23	69.83	2.47	159.79
16	77	72.5	39.5	0.76	0.9	159.05	1.84	265.82	83.64	68.85	6.09	159
17	36	72.5	40.5	0.88	0.85	164.42	3.15	255.6	20.53	66.08	69.2	164.28
18	17	72.5	41.5	0.42	0.55	346.39	5.01	255.9	5.49	118.48	82.56	167.04
30	53	73.5	34.5	0.65	0.5	222.93	2.93	132.7	4.5	345.91	84.63	43.06
31	58	73.5	35.5	0.75	0.65	225.12	8.73	134.15	6.26	8.93	79.23	45.44
32	23	73.5	36.5	0.33	0.4	353.35	23.84	230.27	51	97.44	28.84	2.49
33	25	73.5	37.5	0.26	0.4	344.07	28.33	159.74	61.6	253.09	1.81	163.3
34	63	73.5	38.5	0.75	0.8	338.57	1.1	243.88	76.78	68.83	13.18	158.64
35	113	73.5	39.5	0.93	0.85	337.85	3.07	238.35	72.03	68.83	17.69	157.92
36	66	73.5	40.5	0.88	0.85	341.62	2.99	73.46	31.59	246.78	58.24	161.45
37	8	73.5	41.5	0.37	0.65	309.35	7.8	218.15	8.68	80.7	78.29	131.34
48	10	74.5	33.5	0.41	0.55	246.58	15.99	152.08	15.34	20.5	67.55	72.81
49	14	74.5	34.5	0.87	0.95	33.07	12.34	294.92	32.94	140.76	54.24	33.9
50	17	74.5	35.5	0.52	0.6	246.05	65.54	19.14	17.26	114.52	16.78	30.11
51	10	74.5	36.5	0.52	0.95	223.74	29.34	8.09	55.32	123.97	16.8	38.57
53	41	74.5	38.5	0.83	0.8	167.36	0.74	261.35	79.43	77.22	10.54	167.34
54	101	74.5	39.5	0.8	0.85	350.5	0.17	260.4	29.67	80.8	60.33	170.52

55	69	74.5	40.5	0.81	0.8	354.6	6.46	85.29	6.06	218.12	81.13	174.43
66	17	75.5	32.5	0.72	0.65	226.29	18.36	318.54	6.75	67.91	70.35	45.28
67	16	75.5	33.5	0.67	0.7	225.72	15.12	316.31	2.18	54.3	74.72	45.41
72	21	75.5	38.5	0.72	0.75	358.6	6.26	123.54	79.15	267.62	8.82	178.32
73	42	75.5	39.5	0.81	0.9	184.56	1.78	93.09	39.42	276.72	50.53	4.75
74	28	75.5	40.5	0.58	0.6	193.47	2.2	284.84	31.96	99.95	57.95	12.87
75	8	75.5	41.5	0.88	0.85	168.26	1.88	258.9	18.63	72.7	71.26	168.18
85	18	76.5	32.5	0.71	0.9	222.23	4.04	313.13	12.53	114.68	76.81	41.87
86	13	76.5	33.5	0.77	0.8	222.84	14.02	132.54	1.2	37.73	75.92	42.94
91	26	76.5	38.5	0.66	0.85	192.69	13.06	78.24	60.72	289.1	25.7	14.65
92	87	76.5	39.5	0.53	0.45	198.51	11.31	77.36	68.86	292.15	17.61	20.17
93	65	76.5	40.5	0.56	0.45	198.96	7.19	88.29	70.33	291.33	18.2	19.96
94	12	76.5	41.5	0.54	0.4	2.69	8.84	268.35	25.92	110	62.39	5.34
104	11	77.5	32.5	0.32	0.4	351.53	16.62	97.92	43.39	245.98	41.92	162.79
105	10	77.5	33.5	0.81	0.85	52.88	53.65	201.94	32.26	301.63	14.93	44.81
106	12	77.5	34.5	0.15	0.4	30.48	71.98	218.33	17.86	127.59	2.3	37.47
107	15	77.5	35.5	0.68	0.4	210.12	20.15	39.1	69.61	301.19	2.93	30.49
108	8	77.5	36.5	0.92	0.75	196.78	8.29	301.75	60.58	102.33	28.01	16.48
110	25	77.5	38.5	0.79	0.9	197.27	6.88	295.64	50.35	101.71	38.81	16.47
111	93	77.5	39.5	0.62	0.65	199.15	19.72	313.9	49.43	95.27	33.78	14.69
112	78	77.5	40.5	0.77	0.95	194.02	17.18	317.28	60.58	96.44	23.1	12.4
113	15	77.5	41.5	0.66	0.4	353.97	7.88	260.3	24.8	100.32	63.82	175.41
122	10	78.5	31.5	0.44	0.6	170.28	39.18	335.45	49.87	74.25	7.35	166.2
123	11	78.5	32.5	0.31	0.6	7.79	61.64	170.74	27.3	264.43	7.11	175.63
124	12	78.5	33.5	0.4	0.55	133.79	70.14	12.79	10.54	279.61	16.64	7.27
125	10	78.5	34.5	0.62	0.95	198.32	19.02	46.02	68.73	291.51	9.18	19.61
126	9	78.5	35.5	0.56	0.45	213.18	8.1	60.3	80.91	303.77	4.09	33.45
127	9	78.5	36.5	0.54	0.6	33.49	30.71	212.19	59.29	303.15	0.57	33.31
130	21	78.5	39.5	0.51	0.65	153.18	19.96	244.44	3.47	343.89	69.71	151.59
131	34	78.5	40.5	0.69	0.4	164.82	13.44	256.08	5.26	6.99	75.54	164.22

132	26	78.5	41.5	0.72	0.4	165.9	3.75	256.33	6.57	46.38	82.43	165.73
139	12	79.5	29.5	0.77	0.55	187.24	31.82	40.03	53.57	287.39	15.86	10
140	14	79.5	30.5	0.74	0.7	178.6	19.59	81.59	18.92	311.04	62.19	0.98
145	8	79.5	35.5	0.72	0.7	209.79	2.62	99.2	82.59	300.11	6.92	29.88
146	10	79.5	36.5	0.65	0.4	26.94	28.31	201.8	61.59	295.78	2.15	26.47
149	8	79.5	39.5	0.88	0.95	175.15	29.88	292.07	38.24	59.1	37.38	172.8
150	20	79.5	40.5	0.84	0.5	165.54	15.34	261.77	21.58	42.87	63.06	164.5
151	25	79.5	41.5	0.73	0.7	171.55	10.68	262.47	4.82	16.42	78.26	171.2
158	28	80.5	29.5	0.91	0.7	189.1	26.96	283.55	8.67	29.83	61.46	8.57
159	22	80.5	30.5	0.88	0.7	184.91	28.88	302.2	39.73	70.57	36.76	2.56
163	21	80.5	34.5	0.25	0.4	201.27	49.8	14.62	40.01	107.38	3.28	17.85
164	29	80.5	35.5	0.04	0.4	18.14	23.07	210.25	66.46	110.03	4.42	19.96
165	11	80.5	36.5	0.35	0.5	25.71	15.95	229.04	72.72	117.58	6.49	26.96
170	12	80.5	41.5	0.72	0.85	180.34	7.45	87.36	21.66	288.25	66.98	1.3
176	12	81.5	28.5	0.7	0.5	197.45	26.58	98.32	17.59	338.71	57.32	22.01
177	28	81.5	29.5	0.77	0.7	188.25	31.01	279.42	1.95	12.65	58.91	7.7
178	19	81.5	30.5	0.84	0.95	184.41	35.34	300.97	32.24	60.62	38.11	0.13
181	10	81.5	33.5	0.15	0.5	162.14	45.87	331.65	43.65	66.69	5.27	157.13
182	25	81.5	34.5	0.54	0.65	203.56	68.07	13.74	21.64	105.09	3.39	16.29
183	42	81.5	35.5	0.35	0.5	203.18	52.78	14.57	36.91	107.7	4.15	18.6
184	24	81.5	36.5	0.29	0.5	196.99	49.23	8.08	40.42	101.85	4.41	12.63
189	10	81.5	41.5	0.88	0.95	176.88	25.95	347.23	63.73	85.01	3.82	176.6
195	10	82.5	28.5	0.5	0.7	138.64	23.23	232.14	8.09	340.09	65.24	133.85
196	12	82.5	29.5	0.95	0.5	192.47	22.07	289.43	16.63	53.31	61.81	12.05
197	11	82.5	30.5	0.55	0.7	180.76	32.06	356.82	57.88	89.65	1.78	0.17
198	8	82.5	31.5	0.33	0.65	347.91	49.08	168.28	40.91	78.12	0.18	168.08
199	9	82.5	32.5	0.37	0.6	333.23	55.51	152.35	34.48	242.63	0.41	152.73
200	12	82.5	33.5	0.24	0.6	334.64	45.32	174.07	43	74.75	9.85	163.37
201	8	82.5	34.5	0.46	0.8	17.81	68.27	215.59	20.78	123.27	6.07	31.67
202	24	82.5	35.5	0.48	0.55	199.48	42.05	9.87	47.55	105.14	4.8	16.61

203	22	82.5	36.5	0.54	0.45	198.47	37.58	16.74	52.41	107.83	0.84	18.1
216	24	83.5	30.5	0.03	0.5	331.55	61.45	179.88	25.59	84.14	11.8	173.97
217	22	83.5	31.5	0.27	0.65	351.28	40.19	183.04	49.21	86.24	5.84	175.34
218	8	83.5	32.5	0.5	0.95	5.18	29.35	177.77	60.45	273.39	3.18	4.17
227	12	83.5	41.5	0.39	0.4	148.16	14.43	240.8	10.15	4.76	72.23	143.69
232	13	84.5	27.5	0.72	0.7	202.33	27.13	293.61	2.5	28.46	62.73	21.63
233	15	84.5	28.5	0.72	0.6	180.13	28.69	86.21	7.12	343.57	60.28	2.26
234	8	84.5	29.5	0.34	0.55	332.06	46.27	159.79	43.47	66.11	3.87	155.32
235	20	84.5	30.5	0.08	0.45	342.8	41.37	187.92	45.8	84.37	12.83	173.8
236	22	84.5	31.5	0.23	0.65	359.64	34.42	191.25	55.03	93.4	5.46	2.76
237	11	84.5	32.5	0.18	0.4	48	75.25	192.99	12.17	284.77	8.21	15.16
246	11	84.5	41.5	0.16	0.4	138.42	19.17	229.64	3.49	329.54	70.49	123.07
251	29	85.5	27.5	0.89	0.5	188.74	31.07	281.44	4.47	18.79	58.54	8.28
252	34	85.5	28.5	0.86	0.65	181.75	31.51	311.01	45.9	73.27	27.34	179.16
253	9	85.5	29.5	0.34	0.95	166.66	30.02	353	59.83	258.25	2.75	167.81
254	10	85.5	30.5	0.18	0.4	6.72	19.9	181.57	70.03	276.12	1.65	6.22
255	13	85.5	31.5	0.18	0.85	14.1	23.45	191.65	66.53	283.71	0.9	13.77
256	12	85.5	32.5	0.18	0.4	91.21	80.91	195.12	2.2	285.46	8.82	15.53
257	9	85.5	33.5	0.25	0.5	0.57	2.2	105.71	81.62	270.26	8.08	0.34
269	8	86.5	26.5	0.78	0.95	205.47	45.44	115.42	0.05	25.37	44.56	25.5
270	25	86.5	27.5	0.88	0.7	189.48	39.53	281.93	2.96	15.5	50.31	8.87
271	23	86.5	28.5	0.73	0.75	185.38	36.17	337.81	50.49	85.08	13.75	1.77
272	8	86.5	29.5	0.36	0.95	171.57	2.63	338.84	87.3	81.55	0.59	171.56
273	16	86.5	30.5	0.31	0.65	3.74	21.87	177.64	68.02	272.89	2.12	3.13
274	15	86.5	31.5	0.28	0.55	4.36	18.33	186.67	71.66	94.59	0.69	4.53
275	12	86.5	32.5	0.04	0.45	13.21	52.77	188.75	37.15	280.38	2.15	10.43
276	15	86.5	33.5	0.12	0.4	10.87	36.74	190.2	53.26	280.63	0.32	10.65
277	14	86.5	34.5	0.49	0.75	188.34	10.3	18.06	79.55	278.65	1.73	8.5
278	15	86.5	35.5	0.65	0.8	187.17	13.28	15.18	76.6	277.59	1.8	7.32
279	9	86.5	36.5	0.39	0.45	193.89	5.4	18.15	84.59	283.92	0.4	13.91

288	13	87.5	26.5	0.82	0.65	195.54	33.14	310.94	33.31	73.36	39.21	11.03
289	21	87.5	27.5	0.59	0.65	178.28	24.24	320.83	60.44	80.92	15.87	175.08
290	12	87.5	28.5	0.12	0.45	341.21	22.77	171.34	66.91	72.74	3.65	162.58
291	20	87.5	29.5	0.35	0.45	294.76	71.3	176.35	9.15	83.67	16.16	172.11
292	27	87.5	30.5	0.25	0.55	342.84	54.66	182.7	33.7	86.35	9.41	175.01
293	14	87.5	31.5	0.38	0.65	10.27	29.62	185.11	60.28	279.01	2.22	9.41
294	12	87.5	32.5	0.44	0.65	12.62	61.75	191.11	28.24	281.45	0.63	11.62
295	14	87.5	33.5	0.06	0.45	359.01	74.66	193.1	14.9	102.15	3.57	12.09
296	17	87.5	34.5	0.34	0.65	191.59	27.59	13.53	62.4	282	0.8	11.88
297	22	87.5	35.5	0.58	0.65	189.76	7.24	347.24	82.17	99.38	2.97	9.6
298	16	87.5	36.5	0.51	0.4	200.67	2.09	320.91	85.86	110.54	3.57	20.61
307	15	88.5	26.5	0.63	0.95	171.82	0.11	262.2	74.3	81.79	15.7	171.81
308	20	88.5	27.5	0.52	0.85	348.31	7.33	227.82	75.78	79.89	12.11	169.05
309	9	88.5	28.5	0.04	0.4	338.64	18.41	176.43	70.73	70.47	5.49	160.4
310	22	88.5	29.5	0.4	0.45	332.81	75.69	175.07	13.28	83.83	5.23	173.05
311	25	88.5	30.5	0.34	0.5	333.05	71.58	177.68	16.85	85.47	7.24	174.45
312	8	88.5	31.5	0.31	0.65	20.53	46.61	192.98	43.14	286.52	3.78	17.24
313	10	88.5	32.5	0.5	0.9	205.95	1.82	314.37	84.27	115.77	5.43	25.86
314	26	88.5	33.5	0.17	0.5	199.15	13.55	21.74	76.43	289.29	0.59	19.27
315	24	88.5	34.5	0.11	0.4	192.93	48.76	19.97	41.03	286.92	3.49	16.72
316	13	88.5	35.5	0.12	0.45	20.11	37.52	192.35	52.23	287.22	3.76	17.44
317	10	88.5	36.5	0.15	0.5	16.55	25	188.69	64.79	285.14	3.02	15.32
326	12	89.5	26.5	0.78	0.95	163.62	2.52	258.4	62.1	72.29	27.77	163.38
327	10	89.5	27.5	0.6	0.7	168.93	0.99	262.66	75.11	78.67	14.86	168.83
329	13	89.5	29.5	0.49	0.5	81.94	75.17	185.49	3.55	276.4	14.38	7.4
330	14	89.5	30.5	0.5	0.6	91.38	78.32	181.84	0.09	271.86	11.68	1.88
332	10	89.5	32.5	0.45	0.55	208.87	12.09	37.72	77.77	299.26	1.83	29.09
333	24	89.5	33.5	0.2	0.45	200.87	12.21	34.75	77.43	291.51	2.92	21.38
334	25	89.5	34.5	0.08	0.4	184	69.55	22.21	19.51	290.11	5.91	19.94
335	14	89.5	35.5	0.07	0.4	202.45	0.04	111.94	85.04	292.45	4.96	22.45

345	8	90.5	26.5	0.74	0.95	166.95	17.83	67.26	27.61	285.74	56.25	169.69
348	10	90.5	29.5	0.53	0.8	76.89	70.64	186.44	6.71	278.64	18.07	11.57
349	10	90.5	30.5	0.49	0.75	71.92	75.22	179.56	4.57	270.7	14.03	1.94
350	8	90.5	31.5	0.15	0.7	176.5	18.92	18.52	69.71	268.93	7.06	178.59
351	10	90.5	32.5	0.13	0.45	187.74	5.44	60.22	81.11	278.41	7.01	8.32
352	8	90.5	33.5	0.15	0.4	28.95	12.78	220.96	76.94	119.54	2.63	29.46
353	16	90.5	34.5	0.03	0.5	199.98	79.52	31.82	10.26	301.44	2.1	31.43
354	17	90.5	35.5	0.1	0.4	36.44	69.56	211.09	20.36	301.74	1.75	31.8
361	10	91.5	23.5	0.43	0.4	202.75	19.22	305.19	31.69	86.58	51.68	13.61
362	16	91.5	24.5	0.94	0.95	178.05	4.85	86.97	12.53	288.82	76.54	178.12
363	18	91.5	25.5	0.95	0.65	180.29	7.01	89.26	8.28	310.04	79.12	0.34
364	15	91.5	26.5	0.79	0.9	189.65	20.31	30.55	68.39	282.29	7.08	10.25
365	11	91.5	27.5	0.78	0.85	209.3	21.77	28.42	68.23	119.18	0.3	29.27
369	15	91.5	31.5	0.5	0.95	151.96	56.41	5.08	29.09	266.31	15.32	170.6
370	27	91.5	32.5	0.36	0.6	2.89	53.88	188.92	35.97	96.84	2.88	6.18
371	20	91.5	33.5	0.08	0.4	22.08	12.05	212.53	77.76	112.54	2.16	22.5
372	14	91.5	34.5	0.19	0.5	211.36	39.48	28.75	50.49	120.3	1.28	30.43
373	13	91.5	35.5	0.01	0.4	27.31	65.77	209.65	24.21	119.26	0.88	29.26
380	20	92.5	23.5	0.66	0.9	215.29	19.99	331.59	50.61	111.99	32.32	31.47
381	26	92.5	24.5	0.81	0.85	184.06	4.47	277.99	41.25	89	48.4	3.59
382	22	92.5	25.5	0.93	0.95	183.01	2.48	273.77	17.05	85	72.76	2.96
383	22	92.5	26.5	0.87	0.8	195.36	14.57	97.17	28.72	309.1	57.15	16.32
384	22	92.5	27.5	0.61	0.9	200.72	22.27	98.46	27.42	324.17	53.39	27.02
388	16	92.5	31.5	0.31	0.6	31.73	65.7	196.97	23.59	289.39	5.51	20.26
389	35	92.5	32.5	0.18	0.45	30.31	74.78	201.71	15.06	292.3	2.17	22.41
390	24	92.5	33.5	0.02	0.4	203.23	28.34	25.85	61.64	293.82	1.1	23.81
392	9	92.5	35.5	0.65	0.95	31.13	10.59	147.48	67.15	297.23	20	29.86
393	8	92.5	36.5	0.1	0.4	178.45	36.07	29.31	49.68	280.16	15.56	9.3
399	31	93.5	23.5	0.8	0.9	222.87	14.65	334.75	54.94	123.81	31.04	41.41
400	25	93.5	24.5	0.67	0.8	212.88	2.9	306.02	47.24	120.21	42.61	32.32

401	16	93.5	25.5	0.86	0.8	23.88	2.69	290.86	48.23	116.28	41.65	24.08
402	17	93.5	26.5	0.53	0.65	188.33	10.11	92.31	30.46	294.61	57.56	11.69
403	23	93.5	27.5	0.55	0.55	159.48	24.89	66.16	7.12	321.33	63.97	163.3
404	14	93.5	28.5	0.27	0.5	94.32	10.16	187.99	19.65	338.44	67.69	87.27
407	8	93.5	31.5	0.4	0.6	34.55	5.32	162.72	81.43	303.92	6.7	34.17
408	21	93.5	32.5	0.16	0.45	212.24	32.21	34.85	57.76	302.98	1.18	32.89
409	17	93.5	33.5	0.17	0.4	208.34	12.81	38.75	76.99	298.86	2.27	28.77
411	10	93.5	35.5	0.6	0.8	60.69	11.21	154.56	18.83	301.54	67.86	58.37
412	13	93.5	36.5	0.13	0.45	199.87	7.78	104.95	32.12	301.89	56.72	27.88
418	24	94.5	23.5	0.91	0.95	231.84	10.19	325.36	18.87	114.9	68.37	51.51
419	28	94.5	24.5	0.86	0.95	41.31	3.53	308.74	35.97	136.15	53.8	41.56
420	24	94.5	25.5	0.81	0.95	33.82	8.99	292.29	51.65	130.64	36.91	34.75
421	11	94.5	26.5	0.79	0.85	24.56	21.57	229.89	66.38	118.22	9.17	25.4
422	12	94.5	27.5	0.75	0.6	176.73	28.38	81.67	9.28	335.32	59.88	179.04
423	15	94.5	28.5	0.13	0.4	169.04	26.91	77.49	3.07	341.48	62.89	62.88
424	13	94.5	29.5	0.65	0.95	229.58	15.11	132.53	24.44	348.37	60.73	52.72
425	8	94.5	30.5	0.89	0.95	226.47	14.21	136.19	1.09	41.89	75.75	46.51
427	16	94.5	32.5	0.26	0.4	206.81	9.97	14.67	79.81	116.44	2.1	26.53
428	13	94.5	33.5	0.39	0.5	206.6	0.48	304.57	86.58	116.57	3.39	26.58
437	23	95.5	23.5	0.92	0.6	219.51	9.26	59.32	80.16	310.04	3.28	39.55
438	22	95.5	24.5	0.89	0.9	52.52	2.21	321.05	33.45	145.86	56.46	52.63
439	26	95.5	25.5	0.77	0.95	48.62	3.42	315.96	37.85	143	51.94	49.07
440	10	95.5	26.5	0.17	0.6	335.32	44.02	233.09	12.37	131.14	43.35	36.35
442	9	95.5	28.5	0.49	0.95	224.36	21.62	123.96	24.47	350.86	56.33	53.08
443	17	95.5	29.5	0.71	0.95	230.43	15.74	133.51	23.15	351.65	61.47	52.86
444	12	95.5	30.5	0.88	0.95	224.64	13.17	103.14	65.87	319.49	19.84	45.17
445	8	95.5	31.5	0.09	0.4	38.4	49.78	210.43	39.95	303.74	3.94	33.92
446	21	95.5	32.5	0.27	0.4	42.3	10.63	227.96	79.32	132.49	1.03	42.44
447	16	95.5	33.5	0.59	0.6	229.62	6.31	352.1	78.36	138.53	9.74	49.18
450	8	95.5	36.5	0.79	0.95	212.26	2.9	119.98	38.12	305.95	51.73	32.61

451	22	95.5	37.5	0.75	0.4	199.19	13.42	294.7	21.91	80	63.93	17.59
452	20	95.5	38.5	0.76	0.55	195.97	17.23	291.75	18.01	65.08	64.65	14.17
456	20	96.5	23.5	0.76	0.85	207.25	2.08	108.82	76.06	297.76	13.78	27.37
457	17	96.5	24.5	0.49	0.6	243.09	8.98	106.95	77.64	334.44	8.42	63.78
458	24	96.5	25.5	0.87	0.55	248.69	6.23	128.2	77.86	339.84	10.38	68.84
459	23	96.5	26.5	0.7	0.5	261.68	4.51	169.56	25.08	1.18	64.47	82.39
460	15	96.5	27.5	0.32	0.45	197.98	31.61	103.85	6.68	3.24	57.53	46.56
461	9	96.5	28.5	0.42	0.95	65.97	39.26	219.52	47.61	324.7	13.44	58.24
462	13	96.5	29.5	0.64	0.95	72.85	54.21	234.14	34.33	330.29	8.91	65.11
463	8	96.5	30.5	0.36	0.95	214.4	69.21	49.08	20.16	317.29	4.84	46.45
465	16	96.5	32.5	0.31	0.45	232.04	13.39	31.82	75.76	140.9	4.74	51.25
466	15	96.5	33.5	0.5	0.65	233.56	10.1	18.08	77.66	142.31	7.01	52.94
469	12	96.5	36.5	0.87	0.65	217.95	3.12	126.07	30.94	313.12	58.87	38.14
470	36	96.5	37.5	0.86	0.45	201.05	9.62	293.35	13.32	76.22	73.46	20.7
471	39	96.5	38.5	0.96	0.7	201.7	5.83	293.04	12.9	87.9	75.8	21.65
472	16	96.5	39.5	0.96	0.6	29.69	5.4	298.38	13.58	140.89	75.34	29.74
476	33	97.5	24.5	0.83	0.95	221.88	11.37	11.02	76.81	130.55	6.59	41.64
477	37	97.5	25.5	0.92	0.85	226.59	12.92	351.54	68.18	132.5	17.27	46.26
478	22	97.5	26.5	0.76	0.65	244.75	11.34	150.27	21.27	1.03	65.63	65.97
479	14	97.5	27.5	0.36	0.7	230.9	17.94	135.98	14.84	8.67	66.39	59.9
481	9	97.5	29.5	0.46	0.75	64.83	64.52	238.42	25.34	329.6	2.49	60.3
486	9	97.5	34.5	0.29	0.45	245.26	20.16	65.39	69.84	335.27	0.04	65.27
487	12	97.5	35.5	0.67	0.7	239.35	11.36	77.52	78.06	330.08	3.63	59.6
489	15	97.5	37.5	0.93	0.55	21.01	8.97	287.94	18.76	135.37	69.06	21.23
490	23	97.5	38.5	0.92	0.7	25.7	6.66	118.43	22.2	279.97	66.72	25.49
491	13	97.5	39.5	0.82	0.7	32.02	6.12	122.37	3.2	239.87	83.09	31.95
494	15	98.5	23.5	0.94	0.45	204.2	7.09	319.4	73.73	112.35	14.57	24.09
495	42	98.5	24.5	0.65	0.65	206	5.98	18.5	83.97	115.92	0.78	25.98
496	38	98.5	25.5	0.51	0.8	205.3	4.23	358.55	85.27	115.14	2.12	25.22
497	8	98.5	26.5	0.38	0.95	208.03	0.74	318.73	87.9	118	1.96	28.01

498	11	98.5	27.5	0.69	0.4	219.25	77.42	105.38	5.16	14.33	11.44	101.7
499	10	98.5	28.5	0.71	0.4	221.71	85.9	92.16	2.61	2.02	3.16	91.67
500	8	98.5	29.5	0.16	0.4	249.74	24.89	57.69	64.62	157.58	4.66	67.87
501	9	98.5	30.5	0.38	0.45	73.73	21.33	262.53	68.44	164.9	3	74.5
505	14	98.5	34.5	0.17	0.7	54.59	37.93	240.97	51.9	147.01	3.1	56.74
506	17	98.5	35.5	0.34	0.75	52.14	9.55	246.69	80.14	142.55	2.43	52.41
513	15	99.5	23.5	0.96	0.4	195.33	5.97	102.49	25.39	297.62	63.82	15.43
514	20	99.5	24.5	0.48	0.65	199.86	8.88	46.67	80.07	290.55	4.41	20.22
515	37	99.5	25.5	0.3	0.65	9.18	2.23	178.15	87.73	279.16	0.43	9.16
516	32	99.5	26.5	0.27	0.6	174.47	26.73	3.23	63	266.26	3.54	175.85
517	26	99.5	27.5	0.52	0.65	359.68	82.11	118.89	3.87	209.36	6.87	119.87
518	20	99.5	28.5	0.38	0.65	65.32	76.85	288.65	9.64	197.13	8.85	106.21
519	13	99.5	29.5	0.3	0.6	253.58	50.81	80.29	39	347.62	3.29	77.04
520	14	99.5	30.5	0.08	0.4	82.54	17.03	250.57	72.62	351.5	3.4	81.57
521	9	99.5	31.5	0.29	0.6	225.1	39.35	58.87	49.83	320.73	6.82	49.63
525	10	99.5	35.5	0.77	0.95	38.29	34.04	178.68	48.76	293.75	20.38	34.25
527	8	99.5	37.5	0.76	0.8	59.41	19.43	298.47	55.56	159.86	27.22	61.72
528	11	99.5	38.5	0.78	0.9	45.16	0.9	142.46	82.94	315.05	7	45.14

8.1.4. Table – Geodetic strain

Lon	Lat	Ve	dVe	Vn	dVn	ε_{Hmax}	$d\varepsilon_{Hmax}$	Azi ε_{Hmax}	ε_{Hmin}	$d\varepsilon_{Hmin}$	Azi ε_{Hmin}	dAzi	Dilatation	dDilatation	nsite
deg	deg	mm/a	mm/a	mm/a	mm/a	nanostrain/yr	nanostrain/yr	deg	nanostrain/yr	nanostrain/yr	deg	deg	nanostrain/yr	nanostrain/yr	
86.5	25.5	39.2	0.4	33.8	0.4	1.4	2.9	-44.1	-0.1	3.1	45.9	78.7	1.2	4.2	25
83	25.5	38	0.5	36.5	0.5	2.2	11.6	-73.9	-4.6	8.4	16.1	68.1	-2.5	14.1	50
82	25	38.1	0.5	35.3	0.5	4.1	3.2	-130.6	1.8	3.1	-40.6	54.4	5.9	4.4	50
82.5	25	38.2	0.6	36.1	0.6	1.7	5.5	-102.4	-2.1	4.5	-12.4	51.9	-0.3	7	31
78	30	33.8	0.5	32.6	0.5	3.8	15	-83	-8.8	17.3	7	51.6	-5	22.9	43
81.5	25.5	37.5	0.4	35.1	0.4	3.4	2.5	-120.1	1.3	2.8	-30.1	51.5	4.7	3.7	31
82.5	25.5	37.9	0.5	36.2	0.5	1.2	5.8	-77.5	-4.7	6.4	12.5	43.7	-3.4	8.6	28
81	25.5	37.4	0.4	34.5	0.4	4.6	2.3	-158	2.3	2.6	-68	42.7	6.9	3.5	65
80	27.5	36.5	0.4	35	0.4	5	3.4	-150	1.4	4.1	-60	42.1	6.4	5.2	32
81	26	37	0.4	34.8	0.4	3.6	2.3	-139	1	3	-49	41.6	4.6	3.8	43
86	36	31.2	0.3	14.3	0.3	-22.7	5.9	-29.2	-28	4.6	60.8	40.5	-50.7	7.5	53
80.5	27	36.6	0.3	35	0.3	5.7	5.2	-5	-1.4	7.6	85	39.1	4.3	9.2	41
87	25.5	39.1	0.3	34.2	0.3	1.9	2.6	-67	-1.1	2.3	23	34.9	0.7	3.5	40
86	35.5	31.7	0.3	15.6	0.3	-21.6	6.3	-3.2	-27.9	3.8	86.8	33.3	-49.5	7.3	57
81	26.5	36.6	0.3	34.9	0.3	3.6	2.6	-148.8	-0.2	3.6	-58.8	33.1	3.4	4.4	49
81.5	25	37.9	0.5	34.6	0.5	5.7	2.6	-159.2	2.5	2.5	-69.2	32.8	8.2	3.7	77
83	26	37.6	0.4	36.2	0.5	3.2	7.7	-67.7	-5.5	4.4	22.3	32.3	-2.4	8.7	59
80.5	26	36.9	0.3	34.4	0.3	4.5	2.3	-159.3	0.9	3.3	-69.3	32.2	5.4	4	43
80.5	25.5	37.2	0.4	34	0.4	5.6	2.4	-175	2.3	2.8	-85	31.8	7.9	3.7	37
83	24.5	38.8	0.6	35.7	0.6	4.4	3.7	-45.7	-0.5	3.8	44.3	31.5	3.9	5.3	33
82	25.5	37.7	0.5	35.7	0.5	3.1	3	-93.8	-1.4	3.6	-3.8	30	1.6	4.7	42
81.5	26	37.2	0.4	35.3	0.4	3	2.7	-101	-1.1	3.1	-11	28.7	1.9	4.1	34
81	27	36.5	0.2	34.8	0.3	5.5	4.8	-178.9	-3.8	8	-88.9	28.3	1.7	9.4	47
80	26	36.8	0.3	34.1	0.3	5.3	2.7	-170.2	0.5	3.8	-80.2	27.5	5.8	4.6	36
75	37	24.7	0.2	23.1	0.2	1.9	3.5	-84.9	-2.6	2.1	5.1	26.8	-0.7	4.1	65
82.5	26	37.5	0.4	36	0.4	1.3	3.8	-75.2	-4.9	3.9	14.8	26.8	-3.5	5.4	32

83	25	38.4	0.5	36.4	0.5	2.7	4.4	-69.1	-4.3	4.1	20.9	25.8	-1.6	6.1	39
82	26	37.4	0.4	35.7	0.4	2.8	3	-86.9	-3.1	3.8	3.1	24.4	-0.2	4.9	37
91.5	25	40.3	0.1	31	0.1	-16.2	1.9	-40.5	-19.2	1.5	49.5	23.3	-35.3	2.4	43
80.5	26.5	36.6	0.3	34.6	0.3	4.6	2.4	-159.1	-1.3	4.1	-69.1	22.9	3.3	4.8	45
83.5	26	37.8	0.5	36.1	0.5	10.2	13.4	-60.6	-6.5	3.6	29.4	22.8	3.8	13.9	45
74.5	36.5	24.7	0.2	23.3	0.2	2.4	3	-42	-1.9	1.8	48	22.7	0.5	3.4	26
86	24.5	39.9	0.5	32.7	0.5	3.8	2.6	-164.9	-2.1	3.6	-74.9	22.2	1.7	4.4	46
93.5	26.5	39	0.2	24.3	0.2	-5.9	4.8	-137.2	-12.8	2.4	-47.2	21.9	-18.7	5.3	43
88	41.5	30.6	0.1	6	0.2	-3.2	2.3	-52.3	-7	1.6	37.7	21.4	-10.2	2.8	38
79.5	27	36.1	0.2	34.6	0.2	7.2	1.6	-41	4.1	1.8	49	21.1	11.3	2.3	39
77.5	29	34.2	0.6	34.3	0.6	6.7	15.4	-87.6	-21.7	13.7	2.4	20.9	-15	20.6	37
100	41	30.9	0.1	-4.6	0.1	0.3	2.9	-57.8	-4	1.1	32.2	20.9	-3.7	3.1	34
87	24	40	0.4	33.5	0.4	0.8	2.7	-105.6	-5.5	3.3	-15.6	20.6	-4.8	4.3	27
98.5	27	31.6	0.2	-12.9	0.2	-2.6	3.2	-128.2	-8.1	2.3	-38.2	20.1	-10.7	3.9	31
88.5	39.5	29.5	0.2	6.5	0.2	3.3	2.9	-71	-2.6	2.8	19	19.7	0.7	4	44
75	36.5	24.7	0.1	23	0.2	3.6	2.8	-43.3	-1.5	2.2	46.7	19.5	2.2	3.5	42
80.5	27.5	36.8	0.2	35.2	0.3	4.5	2	-179.7	-3.3	4.8	-89.7	19.3	1.3	5.2	44
86	25	39.5	0.4	33.3	0.4	5.2	2.4	-21.5	-1	3.3	68.5	19.3	4.2	4	47
80	26.5	36.7	0.3	34.4	0.3	6.7	4.1	-166.2	-5.2	6.8	-76.2	19	1.5	7.8	45
80	27	36.7	0.3	34.7	0.3	5.5	2.3	-164.7	-2.2	4.4	-74.7	18.9	3.3	4.9	38
87.5	25	39.3	0.3	34.3	0.3	3.6	2.1	-85.2	-1	2	4.8	18.7	2.6	2.9	49
87	40.5	30.2	0.1	7.4	0.2	0	1.7	-61.1	-3.8	1.8	28.9	18.5	-3.8	2.4	38
88.5	42	30.8	0.2	5.3	0.2	-2	2.1	-77.5	-6.3	1.7	12.5	18	-8.3	2.7	48
92	33.5	49	0.3	7.8	0.2	8.4	11.2	-22.4	-20.8	13.4	67.6	18	-12.3	18.5	43
89.5	26	40.4	0.2	34.6	0.3	-3.7	5.8	-57.9	-20.9	10	32.1	17.9	-24.7	11.3	44
74.5	37	24.6	0.2	22.9	0.3	3.7	3.2	-98.3	-2.7	2	-8.3	17.8	1.1	3.8	30
91	24.5	40.6	0.1	32.6	0.1	-14.5	1.6	-31.7	-17.6	1.1	58.3	17.7	-32.1	2	41
87.5	24.5	39.5	0.3	34.1	0.4	2.6	2.3	-92.4	-3.4	2.7	-2.4	17.6	-0.8	3.6	47
87.5	40	29.8	0.2	7.1	0.2	0.5	1.9	-46.4	-4.2	2.3	43.6	17.5	-3.7	2.9	38
87.5	40.5	30.1	0.1	7	0.2	-0.5	1.8	-45.2	-5.3	2.4	44.8	17.5	-5.8	2.9	46

87	25	39.4	0.3	33.7	0.3	2.9	2.4	-143.1	-2.8	2.7	-53.1	17.4	0.1	3.4	35
98.5	27.5	34.3	0.1	-13	0.2	-3.3	2.2	-161.4	-9.3	2.7	-71.4	17.4	-12.6	3.5	40
88	40	29.7	0.1	6.7	0.2	0.6	2.1	-40.7	-5.3	3.1	49.3	17.2	-4.6	3.5	44
87.5	41.5	30.8	0.1	6.4	0.1	-2.9	2.2	-53.2	-7.9	1.9	36.8	16.3	-10.8	2.8	43
88	42	31	0.1	5.7	0.2	-2.3	2	-64.7	-6.8	1.4	25.3	16.1	-9.1	2.5	44
86	24	40.2	0.5	32.4	0.5	4.8	3.5	-153.4	-3	2.8	-63.4	16	1.8	4.3	41
75.5	37	24.8	0.1	22.8	0.1	3.7	2.8	-92.2	-2.7	2.1	-2.2	15.7	1.1	3.5	45
81.5	26.5	36.8	0.3	35.2	0.3	1.5	2.9	-81.2	-5.8	2.8	8.8	15.5	-4.4	4	29
87.5	41	30.4	0.1	6.8	0.2	-2.1	2.1	-42.6	-8.1	2.6	47.4	15.5	-10.2	3.3	42
87	41	30.6	0.1	7.2	0.2	-0.9	1.8	-60.7	-5.9	2	29.3	15.4	-6.8	2.7	35
79.5	26.5	36.4	0.2	34.3	0.3	8.2	2	-27.6	3.2	1.9	62.4	15.3	11.4	2.6	37
88	39.5	29.5	0.2	6.8	0.2	2.6	2.4	-60.3	-3.6	2.2	29.7	15.2	-0.9	3.3	47
79	29.5	34.8	0.4	33.3	0.4	6.4	10.4	-156.2	-21.9	10.6	-66.2	15.1	-15.5	14.9	38
88.5	40	29.8	0.2	6.3	0.2	2.4	2.1	-60.9	-3.6	2.4	29.1	15.1	-1.2	3.1	42
88.5	41.5	30.5	0.2	5.6	0.2	-1.2	1.9	-67.8	-5.8	1.5	22.2	15	-7	2.4	38
76	28.5	34.1	0.4	34.3	0.4	-0.3	2.6	-102.8	-13.8	6.5	-12.8	14.9	-14.1	7	87
77.5	28	34.5	0.5	35.3	0.5	11.9	7.3	-61.5	-6	6.1	28.5	14.7	6	9.4	46
88	41	30.2	0.2	6.3	0.2	-1.9	2.1	-38.8	-8.1	2.4	51.2	14.7	-10.1	3.1	40
76.5	28.5	34	0.1	35.3	0.1	2.7	2.9	-63.5	-3.7	1.7	26.5	14.6	-1	3.3	76
88	40.5	29.9	0.2	6.5	0.2	-0.6	1.9	-32.4	-8.1	3.2	57.6	14.3	-8.7	3.6	55
79.5	26	36.8	0.3	33.9	0.3	8.4	1.8	-29.5	3.2	1.9	60.5	14.2	11.6	2.5	41
88.5	40.5	30	0.2	6.1	0.2	1	1.8	-56.7	-4.5	2	33.3	14	-3.5	2.7	42
88.5	41	30.3	0.2	5.9	0.2	-0.2	1.8	-61.8	-5.1	1.6	28.2	14	-5.3	2.4	42
76.5	28	34.5	0.1	35.3	0.1	6.7	4	-30.9	-2.1	0.7	59.1	13.9	4.6	4.1	89
99	27	31.4	0.1	-15	0.1	1	3	-112.9	-6.5	2.5	-22.9	13.9	-5.4	3.8	41
78	28	34.8	0.8	36.3	0.8	7.8	4.9	-87	-14.6	9.4	3	13.7	-6.8	10.6	46
87.5	42	31.1	0.1	6.1	0.1	-2.3	1.9	-61	-7.4	1.5	29	13.7	-9.7	2.4	54
87.5	39.5	29.4	0.2	7.3	0.2	2.4	2.4	-52	-4.2	2	38	13.6	-1.7	3.1	24
80	28	36.7	0.3	35.6	0.3	2.6	2.4	-56.1	-5.1	2.7	33.9	13.4	-2.5	3.6	36
82.5	26.5	37.1	0.3	35.7	0.3	1.7	2.4	-70.9	-6.4	2.6	19.1	13.4	-4.8	3.6	26

84	26	37.9	0.5	36	0.5	5.4	6.5	-64.1	-8.6	2.7	25.9	13.4	-3.2	7	39
86.5	25	39.7	0.4	33	0.4	5.2	2.4	-157.9	-6.3	4.3	-67.9	13.4	-1	4.7	24
91	26.5	40.7	0.3	29.9	0.3	-10	5.3	-50.8	-29.8	7.8	39.2	13.4	-39.7	9.3	39
97	42	30.9	0.1	-2	0.1	1.6	2.6	-31.4	-5.7	2.2	58.6	13.2	-4.2	3.4	37
74.5	36	24.6	0.2	23.2	0.2	6.3	3.3	-35.5	-1.4	1.9	54.5	12.9	4.9	3.6	36
91.5	24.5	39.6	0.1	32	0.1	-19.6	1.6	-157.3	-23.9	1.2	-67.3	12.8	-43.5	2	44
87	40	29.8	0.1	7.6	0.2	1.4	1.6	-62.1	-3.4	1.4	27.9	12.6	-2.1	2.1	45
100	40.5	30.6	0.1	-4.4	0.1	0.9	2.2	-68.6	-4.6	1.1	21.4	12.6	-3.7	2.4	47
85.5	24.5	39.6	0.5	33.5	0.5	6.7	2.3	-34.5	-1.8	2.9	55.5	12.5	4.9	3.7	39
87	41.5	30.9	0.1	6.9	0.1	-1.7	2	-61.4	-8	2	28.6	12.5	-9.7	2.8	40
84	25.5	38.3	0.6	35.9	0.5	7.9	6.1	-55.2	-7.5	2.9	34.8	12.4	0.4	6.9	36
87.5	26.5	38.5	0.3	35.2	0.2	-12.3	9.4	-83.8	-31.1	4.7	6.2	12.4	-43.4	10.3	30
83.5	24.5	38.9	0.6	35.6	0.6	8.5	3.5	-45	-4	4	45	12.3	4.5	5.3	50
78	29	34.3	0.3	34.5	0.3	5.6	6.6	-88	-19.7	8.4	2	12.2	-14.2	10.7	45
79	26	36.6	0.3	33.8	0.3	8.9	1.5	-34.5	3.1	2	55.5	12.2	12	2.4	46
86	25.5	38.9	0.4	33.9	0.4	5.1	2.4	-57.4	-2.8	2.3	32.6	12.2	2.3	3.3	40
77	29	33.8	0.5	34.6	0.5	5.9	8.4	-87.1	-20.2	6.9	2.9	12	-14.3	10.9	24
78	27.5	35.1	0.3	34.9	0.2	10	1.8	-55	2.2	2.8	35	12	12.1	3.2	43
81.5	27	36.4	0.2	34.8	0.3	-0.9	3.2	-66.7	-9.7	2	23.3	12	-10.6	3.8	29
90.5	24	41.1	0.1	33.7	0.1	-8.3	1.2	-41.4	-12.2	1.2	48.6	11.9	-20.5	1.6	47
99	27.5	34.1	0.1	-15.2	0.1	0.1	2.8	-132.9	-8.1	2.2	-42.9	11.8	-8	3.4	48
78	27	35.5	0.2	34.5	0.2	9.8	1.2	-44.3	3.1	2.6	45.7	11.7	12.9	2.8	41
79	27	35.9	0.2	34.6	0.2	8.6	1.2	-43.2	3.6	1.8	46.8	11.7	12.2	2	36
87.5	39	29.1	0.2	7.4	0.2	5.8	3.2	-58.5	-4.8	2.4	31.5	11.7	1	4.2	24
79	26.5	36.3	0.2	34.2	0.2	9.1	1.4	-32.2	3.2	2	57.8	11.6	12.4	2.3	57
87	39.5	29.4	0.2	7.8	0.2	2.6	2	-60.9	-3.6	1.5	29.1	11.6	-1	2.5	43
77.5	37.5	25.9	0.1	20.9	0.1	1.8	1.8	-64.8	-5	2	25.2	11.5	-3.2	2.7	34
77.5	27	35.1	0.3	34.6	0.3	10.1	1.4	-49.2	2.5	2.7	40.8	11.4	12.6	3	44
78	26.5	35.8	0.3	34.2	0.2	9.6	1.2	-43.3	3	2.4	46.7	11.2	12.5	2.6	38
86.5	41	30.6	0.1	7.6	0.2	0.6	1.4	-71.4	-5.2	1.7	18.6	11.1	-4.7	2.3	34

77	29.5	33.4	0.7	33.9	0.6	8.3	8.8	-79.4	-17.2	4.3	10.6	11	-8.9	9.8	28
78.5	27	35.7	0.2	34.5	0.2	9.3	1.1	-42.8	3.5	2	47.2	11	12.8	2.3	33
79	27.5	35.6	0.2	34.9	0.2	8.1	1.1	-62.6	2.7	1.7	27.4	11	10.8	2	44
78.5	26.5	36	0.3	34.1	0.2	9.3	1.2	-39	3.2	2.1	51	10.9	12.5	2.3	32
86.5	40.5	30.1	0.1	7.8	0.2	1.1	1.3	-69.2	-3.7	1.3	20.8	10.9	-2.6	1.8	38
95	27	40.8	0.4	18.9	0.4	7	6.3	-103.4	-17.2	7.3	-13.4	10.9	-10.2	9.5	55
77	37.5	25.8	0.1	21.3	0.1	1.7	1.4	-82.4	-4.7	1.9	7.6	10.7	-3	2.4	36
87	39	29	0.2	8	0.2	6.5	3	-58	-4.1	2.1	32	10.7	2.4	3.9	46
78.5	27.5	35.4	0.2	34.9	0.2	9.1	1.3	-57.1	2.6	2	32.9	10.6	11.6	2.4	30
87	42	31.3	0.1	6.5	0.1	-1.4	1.8	-64.7	-7.9	1.6	25.3	10.6	-9.3	2.4	41
99.5	40.5	30.6	0.1	-4.1	0.1	2	2.3	-72.3	-5	1.3	17.7	10.5	-3	2.6	50
87.5	25.5	39	0.3	34.5	0.3	4.4	1.9	-80.6	-3.7	2.2	9.4	10.4	0.7	2.9	45
75	36	24.7	0.1	23	0.2	7.1	2.4	-69.9	-1.5	1.7	20.1	10.3	5.6	2.9	38
76	37	25	0.1	22.4	0.1	3.8	1.6	-90.2	-3.2	2	-0.2	10.3	0.7	2.6	41
79.5	27.5	35.9	0.2	34.9	0.2	7.1	1.1	-67.2	1.4	1.6	22.8	10.3	8.5	2	40
83	26.5	37.2	0.3	35.9	0.3	4.1	3.6	-63.3	-8.4	2.5	26.7	10.3	-4.3	4.2	62
87	23.5	40.2	0.4	33.9	0.4	1	2.8	-103.8	-12.4	4	-13.8	10.1	-11.3	5	70
88	39	29.3	0.2	6.9	0.2	5.9	2.8	-65.8	-5.6	2.8	24.2	10.1	0.3	4	38
81	27.5	36.6	0.2	35	0.2	2.6	2.2	-15.8	-9.8	3.7	74.2	10	-7.2	4.4	43
84	25	38.8	0.6	35.4	0.6	12.1	4.8	-44.7	-6.1	3.9	45.3	10	6	6.4	40
91.5	26.5	40.1	0.3	29	0.3	-6.6	5.2	-72.6	-28.8	5.8	17.4	10	-35.4	7.8	39
77	38	26.4	0.1	21.1	0.1	0.4	1.7	-94.3	-7.1	1.9	-4.3	9.9	-6.8	2.6	40
77.5	29.5	33.7	0.5	33.5	0.5	6.5	7.3	-84.4	-18.7	4.8	5.6	9.8	-12.2	8.7	35
82	26.5	37	0.3	35.5	0.3	2	2.4	-81.7	-8.5	2.6	8.3	9.8	-6.5	3.6	34
87	24.5	39.8	0.4	33.5	0.4	4.6	3	-137	-7.1	3.1	-47	9.8	-2.6	4	21
98.5	26.5	28.9	0.2	-12.3	0.2	3	3.3	-71.2	-8.8	2.1	18.8	9.8	-5.8	4	34
100	40	30.4	0.1	-4.2	0.1	0.5	1.6	-61.7	-5.3	1.2	28.3	9.8	-4.8	2	54
74	33.5	29.7	0.1	31.7	0.1	9.7	2.3	-52.1	-0.6	2.6	37.9	9.7	9.2	3.5	39
77.5	38	26.5	0.1	20.6	0.1	-0.3	1.9	-78.8	-8.8	2.1	11.2	9.7	-9.2	2.8	49
88.5	39	29.5	0.2	6.6	0.2	7.2	2.8	-67.1	-6.2	3.7	22.9	9.7	1	4.7	45

89	41.5	30.6	0.2	5.3	0.2	1.1	1.6	-72.8	-5.3	1.5	17.2	9.6	-4.2	2.2	45
97.5	42	30.9	0.1	-2.4	0.1	3.9	1.6	-44.7	-4	2.1	45.3	9.6	0	2.7	31
74	36	24.7	0.2	23.6	0.2	1.4	2.5	-66.2	-8.5	1.8	23.8	9.5	-7	3.1	56
79	29	35.7	0.4	34.2	0.4	8.2	4.3	-70.1	-22.2	8.9	19.9	9.5	-14	9.8	47
99.5	41	30.8	0.1	-4.2	0.1	2.8	2.1	-60	-4.4	1.2	30	9.5	-1.6	2.4	44
86.5	24	40.2	0.5	32.4	0.5	7.1	4.2	-142.6	-7.7	3.2	-52.6	9.4	-0.6	4.9	43
89	41	30.4	0.2	5.5	0.2	1.9	1.5	-69.3	-4.6	1.5	20.7	9.4	-2.7	2.1	37
89	42	30.9	0.2	5	0.2	1.1	1.6	-75.2	-5.7	1.6	14.8	9.4	-4.6	2.3	49
75.5	36.5	24.9	0.1	22.8	0.1	5.1	2	-65.8	-3	1.7	24.2	9.2	2.1	2.6	43
86.5	40	29.7	0.1	8	0.2	1.8	1.2	-67.3	-3.6	1.2	22.7	9.1	-1.8	1.7	56
96.5	42	31	0.1	-1.7	0.1	1.1	1.6	-38.7	-5.8	1.5	51.3	9.1	-4.8	2.2	42
86.5	41.5	31	0.1	7.3	0.2	0.2	1.6	-71	-7.5	1.9	19	9	-7.3	2.5	42
76.5	37.5	25.7	0.1	21.8	0.1	2.7	1.3	-92.8	-4.3	1.8	-2.8	8.9	-1.6	2.2	41
87	38.5	29.1	0.2	8	0.2	30.9	10.7	-47.5	-9.1	6	42.5	8.9	21.8	12.4	44
92.5	33.5	48.9	0.2	6.7	0.2	9.5	5.7	-55.2	-10.4	2.3	34.8	8.9	-0.9	6.2	40
99	40.5	30.6	0.1	-3.7	0.1	2	2.1	-69.3	-6.1	1.5	20.7	8.9	-4.1	2.5	55
99.5	27.5	34.1	0.1	-17.1	0.1	3.5	2.3	-130.1	-5.8	2.1	-40.1	8.9	-2.4	2.9	47
78.5	28	35.2	0.2	35.3	0.3	8.7	1.7	-72.2	-2.1	2.7	17.8	8.8	6.5	3.2	30
79.5	29.5	34	0.3	33.5	0.3	0.2	8	-70	-35.2	7.3	20	8.8	-34.9	10.7	42
86	40.5	30.1	0.1	8.2	0.1	1.6	1.1	-70.6	-3.8	1.2	19.4	8.8	-2.2	1.6	35
86.5	36.5	30	0.4	13.1	0.4	-3.5	5.5	-65.4	-25.2	3.6	24.6	8.6	-28.7	6.5	41
86.5	42	31.3	0.1	6.9	0.1	-0.1	1.7	-71.2	-8.4	1.9	18.8	8.6	-8.5	2.6	42
92	33	48.6	0.2	7.7	0.2	17.2	7.9	-57	-11.9	3.3	33	8.5	5.3	8.8	38
93	26	38	0.2	26.8	0.2	-5	3	-7.6	-19.4	3.2	82.4	8.5	-24.4	4.5	43
97	41.5	30.7	0.1	-2	0.1	2.6	2	-41	-6.1	1.6	49	8.5	-3.5	2.6	39
83.5	25.5	38.1	0.4	36.2	0.3	4.5	3.3	-62.7	-9.2	2.2	27.3	8.4	-4.6	4	44
89.5	26.5	40.4	0.2	33.3	0.2	7.1	9.6	-79.7	-29.3	6.1	10.3	8.4	-22.2	11.3	43
92.5	34	48.8	0.2	6.5	0.2	5.9	5.2	-63.7	-12.5	1.9	26.3	8.4	-6.5	5.5	45
96	28.5	44.3	0.3	12.3	0.2	35.5	26	-112.7	-65.3	9.2	-22.7	8.4	-29.9	27	47
99.5	27	31.6	0.1	-17.1	0.1	3.5	2.2	-96.8	-8	2.7	-6.8	8.4	-4.5	3.5	48

76.5	37	25.2	0.1	22	0.1	3.6	1.3	-80.7	-4.1	1.9	9.3	8.3	-0.5	2.3	38
87.5	24	39.9	0.4	34.1	0.4	2	2.2	-93.4	-11	3.4	-3.4	8.3	-9	4.1	45
99	26.5	29	0.1	-14.8	0.1	12.1	4.3	-83.5	-5.6	2.8	6.5	8.3	6.5	5.1	40
86	41	30.5	0.1	8	0.2	1.5	1.1	-72.1	-5	1.4	17.9	8.2	-3.5	1.8	43
89	39	28.9	0.2	6.7	0.2	17.7	5.9	-23.1	-18.1	8.6	66.9	8.2	-0.4	10.4	46
95	26.5	38.4	0.3	19.2	0.3	14.6	2.8	-176.3	-4.3	4.2	-86.3	8.2	10.2	5.1	38
73.5	33.5	29.5	0.1	30.7	0.1	7.9	2	-77.6	-3.3	2.4	12.4	8.1	4.6	3.1	43
75.5	37.5	25.3	0.1	22.6	0.1	8.2	2.9	-96.8	-3.6	1.7	-6.8	8.1	4.6	3.3	41
83	38.5	27.8	0.1	12.6	0.1	4.6	1.5	-73.4	-1.6	1	16.6	8.1	3	1.8	54
85.5	40.5	30.1	0.1	8.7	0.1	2	1.1	-67.8	-3.8	1.1	22.2	8.1	-1.8	1.6	54
89	40.5	30.2	0.2	5.7	0.2	3.7	1.5	-67.7	-4.3	1.6	22.3	8.1	-0.6	2.2	42
94.5	27	40.7	0.5	19.9	0.5	2.2	5.1	-111.1	-24.6	5.7	-21.1	8.1	-22.5	7.4	47
74.5	35.5	24.6	0.1	23	0.2	4.1	2.1	-76	-10.4	3.3	14	8	-6.3	3.9	30
76	29	33.4	0.3	34.2	0.3	1	1.6	-86.8	-7.8	1.9	3.2	8	-6.7	2.5	23
77	37	25.4	0.1	21.5	0.1	3.7	1.5	-71.2	-4.7	1.8	18.8	8	-1	2.3	48
83.5	26.5	37.3	0.3	35.8	0.3	5.6	4.1	-63.6	-11.2	2.4	26.4	8	-5.6	4.7	40
86.5	38.5	28.4	0.2	8.8	0.2	31.5	9.2	-48.8	-9	6.2	41.2	8	22.5	11.3	38
96.5	41.5	30.8	0.1	-1.6	0.1	1.5	1.8	-41.3	-6.2	1.2	48.7	8	-4.6	2.2	43
86.5	24.5	40	0.5	32.5	0.5	7.4	3.4	-145.9	-10.5	4	-55.9	7.9	-3.1	4.9	30
86.5	39.5	29.4	0.1	8.2	0.2	2.6	1.3	-66.4	-4	1.3	23.6	7.9	-1.4	1.8	41
91	27	40	0.3	27.9	0.3	-7.7	6.6	-59	-52	11.9	31	7.9	-59.7	12.9	44
85.5	25	39.2	0.4	33.8	0.4	8.4	2.1	-41.4	-3	2.4	48.6	7.8	5.4	3.1	35
86	38.5	27.8	0.3	9.5	0.3	28.4	7.9	-48.9	-7.8	5.7	41.1	7.8	20.5	9.9	40
87.5	38.5	29.4	0.2	7.7	0.2	13.4	4.6	-61.2	-11.3	4.5	28.8	7.8	2.1	6.6	50
90	26.5	40.5	0.3	32.2	0.3	0	7	-75.7	-31.7	5	14.3	7.8	-31.7	8.7	46
76	37.5	25.5	0.1	22.2	0.1	4.4	1.6	-95.4	-4	1.6	-5.4	7.7	0.4	2.3	44
78	37.5	26	0.1	20.2	0.1	3.1	1.7	-55.8	-6.4	1.9	34.2	7.7	-3.3	2.5	50
83	38	27.1	0.1	12.7	0.1	5.2	1.5	-75.4	-1.6	1	14.6	7.7	3.5	1.8	46
83.5	38.5	27.9	0.1	11.9	0.1	4.9	1.7	-76.7	-2.4	1	13.3	7.7	2.5	1.9	38
85	40.5	30	0.1	9.1	0.1	2.3	1.3	-60.9	-3.9	1	29.1	7.7	-1.6	1.6	44

86	40	29.7	0.1	8.5	0.1	1.9	1.1	-70.2	-3.8	1.1	19.8	7.7	-1.9	1.5	48
86.5	39	29	0.2	8.5	0.2	3.8	1.5	-67.1	-4.7	1.7	22.9	7.7	-0.9	2.4	34
99	28	36.6	0.1	-15.2	0.1	3.1	1.8	-153.3	-7.8	2.3	-63.3	7.7	-4.7	2.9	51
85.5	38.5	28.5	0.2	9.7	0.2	4.4	1.3	-80.3	-4.6	2	9.7	7.6	-0.2	2.4	40
85.5	40	29.6	0.1	8.9	0.1	2	1.1	-69.8	-3.9	1.1	20.2	7.6	-1.9	1.6	53
89.5	42	31.1	0.2	4.6	0.2	2.6	1.4	-73.1	-5	1.5	16.9	7.6	-2.5	2.1	46
91.5	26	40.1	0.2	30.1	0.2	-9.3	4.2	-17.7	-34.2	5.4	72.3	7.6	-43.5	6.8	37
98.5	28	36.9	0.1	-13	0.1	0.7	1.6	-3.6	-10.1	2.4	86.4	7.6	-9.4	2.9	44
76.5	41	28.2	0.1	12.9	0.1	8.1	4.3	-75.4	-15.2	4.3	14.6	7.5	-7.1	6.1	39
78.5	30	33.8	0.4	32.2	0.4	0.4	5.8	-63.4	-42.7	9.2	26.6	7.5	-42.4	11	54
81.5	27.5	36.2	0.2	34.5	0.2	-1.6	2.8	-49.6	-14.6	1.8	40.4	7.5	-16.1	3.4	32
83.5	39	28.6	0.1	11.7	0.1	4.8	1.8	-66.5	-3.4	1.2	23.5	7.5	1.4	2.1	49
85	40	29.6	0.1	9.3	0.1	2.2	1.3	-64.2	-4.1	1	25.8	7.5	-1.9	1.6	44
82.5	38.5	27.7	0.1	13.2	0.1	4.5	1.1	-70.3	-0.9	0.9	19.7	7.3	3.6	1.4	42
84	39	28.7	0.1	10.9	0.1	4.6	2	-70.3	-4.6	1.3	19.7	7.3	0	2.3	30
85.5	38	28.1	0.2	10	0.2	6.3	1.7	-78.8	-5.3	2.5	11.2	7.3	1	3	40
89.5	41.5	30.8	0.2	4.9	0.2	2.9	1.4	-73	-4.7	1.5	17	7.3	-1.8	2	38
91	24	40.4	0.1	33.4	0.1	-11.1	1.2	-23.7	-17.8	1.1	66.3	7.3	-28.9	1.7	42
92	26	39.5	0.1	29.4	0.2	7.7	4.6	-67.3	-14.8	3	22.7	7.3	-7.1	5.4	39
92.5	25	37.7	0.1	29.2	0.1	-20.6	3	-166.2	-34.5	1.9	-76.2	7.3	-55.1	3.6	34
94	27	40.4	0.4	20.1	0.4	-8.5	3.4	-94.7	-31.4	4.2	-4.7	7.3	-39.9	5.4	45
96	41.5	31	0.1	-1.2	0.1	0.9	1.4	-42.7	-6.2	1.1	47.3	7.3	-5.3	1.8	45
83	39	28.5	0.1	12.4	0.1	4.6	1.4	-65	-2.4	1	25	7.2	2.2	1.7	62
84	38	27.4	0.1	11.5	0.1	5.7	1.7	-81.3	-2.3	1.1	8.7	7.2	3.4	2	33
84	38.5	28.1	0.1	11.3	0.1	5.7	1.9	-80.7	-3.3	1.2	9.3	7.2	2.4	2.3	33
84.5	39.5	29.2	0.1	10	0.2	3	1.7	-64.1	-5.4	1.3	25.9	7.2	-2.4	2.1	41
85	24.5	39.4	0.5	34.1	0.5	10.5	2.2	-38.5	-3.5	2.9	51.5	7.2	7.1	3.5	44
98	24	24.1	0.1	-7.9	0.1	14.5	5.9	-57.9	-18.5	6	32.1	7.2	-4	8.3	44
99.5	40	30.5	0.1	-3.8	0.1	1.3	1.6	-59.8	-6.1	1	30.2	7.2	-4.8	1.9	54
77.5	37	25.5	0.1	21	0.1	5.1	2	-57.2	-5.5	1.7	32.8	7.1	-0.4	2.6	34

77.5	38.5	27.2	0.1	20	0.1	-2.6	2.1	-83.7	-13.6	1.7	6.3	7.1	-16.2	2.7	48
84.5	41	30.4	0.1	9.4	0.1	2.5	1.5	-56.6	-5.2	1.2	33.4	7.1	-2.7	1.9	51
85.5	41	30.5	0.1	8.4	0.1	2.1	1.1	-69	-4.8	1.2	21	7.1	-2.8	1.7	38
90	26	40.2	0.2	33.8	0.2	4.4	4	-63.1	-24.4	6.3	26.9	7.1	-20	7.4	50
82.5	39	28.4	0.1	13.1	0.1	4.3	1.1	-68.2	-1.4	0.9	21.8	7	2.9	1.4	44
83.5	25	38.6	0.4	36.1	0.4	6.1	2.5	-57.4	-7.9	2.2	32.6	7	-1.8	3.4	41
84.5	40	29.6	0.1	9.8	0.1	2.7	1.5	-55.8	-4.7	1.1	34.2	7	-2	1.8	26
76	31.5	31.8	0.4	31.9	0.4	-5.9	7	-44.7	-46.7	6.8	45.3	6.9	-52.7	9.8	43
77	38.5	27.2	0.1	20.7	0.1	-2.8	2.1	-93	-14.6	1.9	-3	6.9	-17.4	2.8	41
79	28	35.5	0.2	35.3	0.2	8.1	1.1	-76.4	-1.9	2.1	13.6	6.9	6.1	2.4	50
83.5	41	30.5	0.1	10.7	0.1	0.9	1.6	-51.7	-8.3	1.5	38.3	6.9	-7.4	2.2	44
84	41	30.5	0.1	10	0.1	2.1	1.6	-51.2	-6.4	1.4	38.8	6.9	-4.4	2.1	30
84.5	25.5	38.5	0.5	35.4	0.5	8.1	3.1	-56.3	-8.5	2.4	33.7	6.9	-0.4	4	42
85	39.5	29.2	0.1	9.6	0.2	2.4	1.3	-71.5	-5.1	1.2	18.5	6.9	-2.6	1.8	45
89	40	30.2	0.2	6	0.2	6	1.6	-70	-4.3	1.8	20	6.9	1.7	2.4	45
89.5	41	30.6	0.2	5.1	0.2	3.7	1.3	-70.8	-4.5	1.5	19.2	6.9	-0.8	2	37
84	41.5	30.9	0.1	10	0.1	-0.5	1.9	-73.7	-11.5	1.7	16.3	6.8	-12	2.6	30
84.5	39	28.8	0.1	10.3	0.2	4.2	1.7	-77	-5.2	1.3	13	6.8	-1.1	2.2	42
84.5	40.5	30	0.1	9.6	0.1	2.8	1.4	-53.1	-4.6	1.1	36.9	6.8	-1.8	1.7	32
85.5	25.5	38.8	0.4	34.4	0.4	6.9	2	-56.2	-5.6	2.2	33.8	6.8	1.2	2.9	36
90	42	31.2	0.2	4.3	0.2	3.2	1.3	-69.9	-4.8	1.4	20.1	6.8	-1.6	1.9	39
95.5	30	47.2	0.2	-0.6	0.1	-12.7	2.8	-64.5	-28.8	2.6	25.5	6.8	-41.5	3.9	36
96	42	31.1	0.1	-1.3	0.1	1.3	1.2	-40.9	-6	1.3	49.1	6.8	-4.7	1.7	44
76.5	38	26.3	0.1	21.5	0.1	2.4	1.5	-102.3	-7.3	1.7	-12.3	6.7	-4.9	2.3	42
78	29.5	33.9	0.4	33.4	0.3	6.2	4.6	-84.6	-20	4.1	5.4	6.7	-13.8	6.1	47
84	39.5	29.2	0.1	10.6	0.1	3.9	1.9	-56.1	-6	1.4	33.9	6.7	-2	2.3	39
85	38.5	28.4	0.2	10.2	0.2	4.8	1.4	-83.5	-4.1	1.5	6.5	6.7	0.8	2.1	40
85	41	30.5	0.1	8.9	0.1	2.2	1.2	-64.5	-5.1	1.1	25.5	6.7	-2.8	1.7	38
87.5	23.5	40.1	0.4	34.8	0.3	2	2.2	-94	-12.9	3.4	-4	6.7	-10.8	4	42
90	41.5	30.9	0.2	4.5	0.2	3.8	1.3	-71.9	-4.3	1.5	18.1	6.7	-0.5	1.9	45

92	25.5	39.2	0.2	30	0.2	-3.4	2.5	-18	-26.9	5.1	72	6.7	-30.3	5.7	28
99.5	28	36.5	0.1	-16.9	0.1	5.7	1.9	-148.7	-5.8	2.1	-58.7	6.7	-0.1	2.7	49
78	38	26.5	0.1	19.8	0.1	0.1	1.6	-73.2	-10.2	1.8	16.8	6.6	-10.1	2.4	46
81	38	26.7	0.1	15.3	0.1	1.9	0.9	-64.9	-4.1	1.1	25.1	6.6	-2.2	1.4	67
84.5	25	38.9	0.5	35	0.5	10.8	2.7	-45.9	-5.7	2.6	44.1	6.6	5.1	3.8	43
84.5	38.5	28.2	0.1	10.7	0.1	5.4	1.6	-83.1	-3.8	1.3	6.9	6.6	1.6	2.1	54
85.5	39.5	29.2	0.1	9.2	0.2	2.4	1.1	-72.2	-4.7	1.2	17.8	6.6	-2.3	1.6	56
86	39	28.9	0.2	8.9	0.2	3.3	1.2	-71.9	-5.1	1.6	18.1	6.6	-1.7	2	46
86	41.5	30.9	0.1	7.8	0.2	1.6	1.3	-72.6	-7.8	1.8	17.4	6.6	-6.2	2.2	50
84.5	38	27.6	0.1	11	0.1	6.3	1.6	-83.7	-2.9	1.3	6.3	6.5	3.4	2.1	58
86	39.5	29.3	0.1	8.7	0.2	2.6	1.1	-70.5	-4.4	1.2	19.5	6.5	-1.8	1.6	48
88	25	39.2	0.3	34.6	0.3	7.5	1.7	-77.3	-3.2	1.9	12.7	6.5	4.3	2.5	38
90	41	30.7	0.2	4.7	0.2	4.8	1.3	-70	-4.5	1.7	20	6.5	0.3	2.1	44
92.5	26	40.1	0.3	28.9	0.3	15	5.8	-77.3	-18.3	5.2	12.7	6.5	-3.3	7.7	49
100	41.5	30.9	0.1	-4.6	0.1	3.3	1.6	-49	-4.6	0.8	41	6.5	-1.3	1.8	39
75	37.5	24.7	0.2	22.8	0.2	17.4	4.3	-98.5	-3.9	1.8	-8.5	6.4	13.4	4.7	77
82	38.5	27.6	0.1	13.9	0.1	1.2	0.9	-77.3	-4.1	0.8	12.7	6.4	-2.8	1.2	38
85	38	27.8	0.2	10.5	0.2	6.1	1.5	-83.8	-3.6	1.6	6.2	6.4	2.5	2.2	45
85	39	28.8	0.2	9.9	0.2	3.4	1.3	-77.3	-5	1.4	12.7	6.4	-1.6	1.9	43
85.5	39	28.8	0.2	9.4	0.2	3.1	1.1	-75.5	-5.2	1.5	14.5	6.4	-2.1	1.9	49
91.5	37	35.7	0.2	9.4	0.2	7.5	3.8	-77.7	-20.7	4.9	12.3	6.4	-13.2	6.3	46
74	35.5	24.5	0.1	23	0.2	-0.3	3.3	-71.3	-27.3	4.5	18.7	6.3	-27.6	5.7	52
82.5	38	27	0.1	13.3	0.1	5.5	1.2	-69.6	-1.3	0.9	20.4	6.3	4.2	1.5	39
83.5	38	27.3	0.1	12.1	0.1	6.1	1.6	-77.7	-2.5	1	12.3	6.3	3.6	1.9	31
86	36.5	30.1	0.3	13	0.3	1.6	4.8	-61.6	-26.9	4.1	28.4	6.3	-25.3	6.3	43
88	24.5	39.3	0.3	34.7	0.3	7.2	2	-77.7	-6.7	2.3	12.3	6.3	0.5	3.1	39
94.5	26.5	38.5	0.3	21.6	0.3	13.8	3	-158.1	-9.3	3.6	-68.1	6.3	4.5	4.6	46
99	28.5	38.8	0.1	-14.9	0.1	7.3	1.7	-172.7	-4.5	2.2	-82.7	6.3	2.8	2.8	53
90.5	24.5	41.3	0.1	33.2	0.1	-4.3	1.6	-34.3	-14.1	1.5	55.7	6.2	-18.4	2.2	44
95	30	47.7	0.2	1.3	0.2	-5.4	2.3	-50.6	-21.1	2.5	39.4	6.2	-26.5	3.4	76

95.5	42	31.2	0.1	-0.9	0.1	1.5	1	-41.9	-6.2	1.3	48.1	6.2	-4.7	1.7	45
75	42	27.6	0.1	6.6	0.1	4.4	4.2	-99.1	-25.6	4.8	-9.1	6.1	-21.2	6.4	20
76.5	31.5	30.7	0.4	31.3	0.4	-7	7.4	-49.5	-53.7	6.5	40.5	6.1	-60.7	9.9	29
80.5	38	26.5	0.1	16	0.1	1.8	1	-61	-5.6	1.3	29	6.1	-3.8	1.6	46
81.5	38	26.8	0.1	14.7	0.1	2.1	0.9	-69.2	-3.9	0.9	20.8	6.1	-1.8	1.3	29
85	25	39.1	0.4	34.4	0.4	10.2	2.2	-45.6	-4.8	2.3	44.4	6.1	5.4	3.2	47
90.5	37.5	34.7	0.3	8.9	0.3	11.4	5.9	-76.7	-23.2	4.6	13.3	6.1	-11.8	7.5	48
94	26.5	38.7	0.2	23.1	0.3	9	3.5	-155.7	-12	2.6	-65.7	6.1	-3	4.2	42
95.5	41.5	31.1	0.1	-0.8	0.1	1.1	1.1	-44.5	-6.3	1.1	45.5	6.1	-5.3	1.6	46
99	23.5	25.1	0.2	-9.5	0.2	25.5	7.1	-73.7	-19.3	6.1	16.3	6.1	6.2	9.7	54
100	24	26.7	0.2	-13.3	0.1	10.6	3.7	-85.3	-10.8	2.8	4.7	6.1	-0.2	4.6	31
75.5	40.5	28.3	0.2	12.5	0.2	10.7	4.7	-103.6	-19.2	4.1	-13.6	6	-8.5	6.2	35
75	41	27.4	0.1	10.2	0.1	6.4	5.7	-105.9	-28.7	4.6	-15.9	5.9	-22.4	7.3	26
81	37.5	26	0.1	15.4	0.1	3.6	1.2	-54.3	-5.1	1.3	35.7	5.9	-1.5	1.8	56
86	42	31.3	0.1	7.3	0.1	2.2	1.7	-73.9	-10.5	2.1	16.1	5.9	-8.4	2.7	48
90.5	41	30.9	0.2	4.3	0.2	5.6	1.3	-65.8	-4.9	1.7	24.2	5.9	0.6	2.1	39
90.5	42	31.3	0.2	3.9	0.2	3.5	1.2	-65.4	-5	1.4	24.6	5.9	-1.6	1.8	39
95	42	31.3	0.1	-0.4	0.1	1.9	0.9	-42.5	-6.3	1.4	47.5	5.9	-4.4	1.7	43
96	41	30.8	0.1	-1.1	0.1	1.9	1.4	-48	-6.7	1.1	42	5.9	-4.9	1.8	46
97.5	41.5	30.7	0.1	-2.5	0.1	3.9	1.2	-48.9	-5.2	1.4	41.1	5.9	-1.3	1.9	38
72	40.5	26.6	0.2	8.2	0.2	2.4	3.1	-100.4	-20	2.9	-10.4	5.8	-17.6	4.2	47
72.5	40.5	26.7	0.1	8.7	0.2	1.9	2.9	-100.3	-19.9	3.4	-10.3	5.8	-18	4.4	50
76	41	27.9	0.2	12.4	0.2	7.5	4.2	-98.7	-23.3	4.6	-8.7	5.8	-15.8	6.2	45
80.5	28	37	0.2	35.8	0.2	2.4	2.1	-39.8	-14.8	2.7	50.2	5.8	-12.4	3.4	43
82	38	26.9	0.1	14	0.1	2.4	1	-72.6	-4.1	0.9	17.4	5.8	-1.7	1.3	41
82.5	39.5	29.1	0.1	12.9	0.1	4	1	-66.5	-2.9	1	23.5	5.8	1.1	1.4	43
84	40.5	30	0.1	10.2	0.1	3.5	1.5	-46.1	-6.2	1.3	43.9	5.8	-2.8	2	36
86	38	28.6	0.2	9.7	0.2	14.3	4.1	-72.5	-15.7	4.5	17.5	5.8	-1.4	6.1	29
95.5	41	30.9	0.1	-0.6	0.1	1.5	1.3	-47.8	-6.8	1.1	42.2	5.8	-5.2	1.7	38
99	40	30.6	0.1	-3.4	0.1	2.3	1.7	-58.9	-7.8	1.1	31.1	5.8	-5.4	2.1	59

74.5	37.5	23.8	0.3	22.7	0.3	19.7	4.1	-98.9	-4.1	2.1	-8.9	5.7	15.6	4.6	30
75.5	36	25.1	0.1	23	0.1	8.2	2	-75.2	-4.6	1.5	14.8	5.7	3.6	2.5	40
76	36.5	25	0.1	22.6	0.1	5.8	1.5	-64.3	-5	1.6	25.7	5.7	0.8	2.2	35
78.5	29	34.6	0.2	34.5	0.2	9	3.7	-85.6	-24.8	5.5	4.4	5.7	-15.8	6.6	40
81.5	38.5	27.5	0.1	14.5	0.1	1.3	0.8	-78.8	-4.3	0.8	11.2	5.7	-3	1.1	37
83	39.5	29.2	0.1	12.2	0.1	4.2	1.3	-56.1	-4.5	1.2	33.9	5.7	-0.3	1.8	62
83	41	30.7	0.1	11.4	0.1	-0.3	1.5	-61.9	-11	1.5	28.1	5.7	-11.3	2.1	42
83.5	39.5	29.2	0.1	11.4	0.1	4.6	1.7	-52	-6.7	1.5	38	5.7	-2.1	2.3	56
84	40	29.6	0.1	10.4	0.1	3.8	1.6	-48.6	-6.3	1.3	41.4	5.7	-2.5	2	43
85.5	41.5	30.9	0.1	8.2	0.2	2.5	1.2	-71.2	-8.3	1.7	18.8	5.7	-5.8	2.1	39
86.5	38	29.1	0.3	9.4	0.3	14.8	4.6	-70.2	-17.8	4.7	19.8	5.7	-3	6.6	46
87	36.5	30.6	0.5	13.1	0.5	1.9	4.3	-73.6	-22.8	2.2	16.4	5.7	-20.9	4.9	46
73.5	38	22.1	0.2	20.9	0.2	22.6	1.8	-102.1	-2.2	4.6	-12.1	5.6	20.4	4.9	23
79.5	38	26.4	0.1	17.5	0.1	1.3	1.4	-57.3	-9.7	1.6	32.7	5.6	-8.4	2.2	36
84.5	26	38.1	0.4	36	0.4	5.3	3	-68.2	-13.9	2.6	21.8	5.6	-8.6	3.9	38
84.5	41.5	30.9	0.1	9.3	0.1	1.9	1.6	-68.7	-9.8	1.6	21.3	5.6	-7.9	2.2	42
89	39.5	30.2	0.2	6.2	0.2	9.1	1.7	-74.3	-4.8	2.1	15.7	5.6	4.3	2.8	46
91	41	31.1	0.2	3.9	0.2	5.8	1.5	-60.6	-6.1	1.8	29.4	5.6	-0.3	2.3	42
95.5	27.5	41.5	0.3	15.2	0.3	0.2	5.2	-49.9	-29.9	3	40.1	5.6	-29.7	5.9	68
96	30	46.4	0.2	-2.5	0.1	-9.4	2.7	-58.8	-28.1	2.5	31.2	5.6	-37.5	3.7	33
98.5	40.5	30.6	0.1	-3.2	0.1	3.3	1.6	-61.9	-7.5	1.3	28.1	5.6	-4.3	2.1	39
75.5	31.5	30.6	0.4	32	0.4	5.3	2.3	-65.6	-18.8	4	24.4	5.5	-13.5	4.6	48
75.5	32	30.4	0.3	31.2	0.3	4.4	2.3	-57.6	-18.5	3.7	32.4	5.5	-14.1	4.4	45
77.5	28.5	34.3	0.1	35.6	0.1	8.3	3.1	-86	-21.9	4.7	4	5.5	-13.6	5.7	53
78.5	37.5	26	0.1	19.4	0.1	5.1	1.7	-49.7	-8.1	1.9	40.3	5.5	-3	2.5	44
81.5	37.5	26.1	0.1	14.7	0.1	3.9	1.1	-62.2	-4.5	1.1	27.8	5.5	-0.5	1.6	26
85	25.5	38.7	0.4	34.9	0.4	8	2.1	-56.3	-7.9	2.1	33.7	5.5	0.1	3	49
85.5	35.5	33	0.2	15	0.2	-3.1	3.3	-52.1	-27	3.3	37.9	5.5	-30.1	4.6	48
89.5	40.5	30.5	0.2	5.3	0.2	5.5	1.3	-68.5	-5	1.5	21.5	5.5	0.5	2	48
95.5	27	39.5	0.3	15.2	0.3	8.6	4.7	-34.9	-19.3	2.8	55.1	5.5	-10.7	5.4	67

96.5	41	30.7	0.1	-1.5	0.1	2.4	1.4	-48.1	-6.8	1.1	41.9	5.5	-4.4	1.8	44
75	35.5	24.8	0.1	23	0.2	9.3	2.1	-82.3	-9.3	2.6	7.7	5.4	0	3.4	40
78.5	38	26.5	0.1	19	0.1	0.4	1.3	-66.9	-10.4	1.6	23.1	5.4	-9.9	2	32
79	30	33.1	0.4	31.5	0.3	-3.7	5.9	-63.8	-50.7	6.6	26.2	5.4	-54.4	8.9	40
80	38	26.3	0.1	16.7	0.1	1.7	1.2	-55.9	-9.2	1.7	34.1	5.4	-7.5	2.1	39
82	37.5	26.2	0.1	14	0.1	4.2	1.2	-69.8	-4.3	1.1	20.2	5.4	-0.1	1.6	39
82	39	28.3	0.1	13.7	0.1	1.1	0.8	-81.7	-4.9	0.8	8.3	5.4	-3.9	1.1	39
83.5	27.5	36.6	0.2	36.1	0.2	7.4	6.2	-79.2	-40.6	7.8	10.8	5.4	-33.2	10.1	56
84	26.5	37.5	0.3	35.9	0.3	5.1	3.2	-67.1	-15.6	2.5	22.9	5.4	-10.4	4.1	44
87	38	29.6	0.3	9	0.3	14.1	4.2	-69.2	-18.6	4.4	20.8	5.4	-4.5	6.2	43
88	38.5	29.8	0.2	7.4	0.2	12.2	2.9	-64.6	-13.8	3.8	25.4	5.4	-1.6	4.9	40
90.5	41.5	31.1	0.2	4.1	0.2	4.3	1.1	-65.7	-4.9	1.3	24.3	5.4	-0.6	1.7	43
92.5	25.5	38.3	0.2	28.8	0.2	-8.9	2.3	-15.8	-28	2.6	74.2	5.4	-36.9	3.6	45
94.5	42	31.4	0.1	0	0.1	2.4	0.9	-43.2	-6.4	1.4	46.8	5.4	-4	1.7	50
97	41	30.7	0.1	-1.9	0.1	2.8	1.3	-48	-6.9	1.3	42	5.4	-4.1	1.8	43
98	42	30.9	0.1	-2.9	0.1	4.1	0.9	-49.3	-4.7	1.3	40.7	5.4	-0.6	1.6	28
98.5	28.5	38.9	0.1	-12.8	0.1	5.6	1.6	-10	-7.7	2.1	80	5.4	-2.1	2.7	48
99.5	28.5	38.7	0.1	-16.5	0.1	9.2	1.9	-164.6	-5.2	2.3	-74.6	5.4	4	2.9	50
78	28.5	34.7	0.2	35.7	0.2	9	3	-85.5	-22.4	4.9	4.5	5.3	-13.4	5.7	44
78	38.5	27.1	0.1	19.2	0.1	-1.6	1.5	-82.9	-12	1.2	7.1	5.3	-13.7	1.9	53
85	41.5	30.9	0.1	8.7	0.2	2.8	1.3	-68.8	-8.8	1.6	21.2	5.3	-6	2.1	24
95	41.5	31.2	0.1	-0.3	0.1	1.5	1	-44.4	-6.6	1.2	45.6	5.3	-5.2	1.5	45
96	40.5	30.7	0.1	-0.9	0.1	2.6	1.4	-51.8	-8.1	1.5	38.2	5.3	-5.5	2	41
99	26	27.1	0.1	-14.5	0.1	19.9	4.1	-77.3	-7.5	2.9	12.7	5.3	12.4	5	35
99	41	30.7	0.1	-3.7	0.1	3.5	1.2	-56.5	-5.2	1	33.5	5.3	-1.7	1.6	46
100	39.5	30.4	0.1	-4	0.1	4	2.2	-47.4	-14.8	2.7	42.6	5.3	-10.8	3.5	50
72	42	26.7	0.1	4.7	0.1	4.1	2.7	-109.2	-16.6	2.6	-19.2	5.2	-12.5	3.7	33
79	38	26.5	0.1	18.2	0.1	0.8	1.2	-61.8	-10.1	1.5	28.2	5.2	-9.3	2	35
80	37.5	25.9	0.1	16.9	0.1	4.3	1.6	-48.6	-9.4	1.9	41.4	5.2	-5.1	2.5	28
81	38.5	27.4	0.1	15.1	0.1	1.2	0.7	-78.5	-4.8	0.8	11.5	5.2	-3.6	1.1	70

83.5	40.5	30.1	0.1	10.9	0.1	3	1.3	-46.1	-7.6	1.4	43.9	5.2	-4.6	1.9	56
85.5	36	31.6	0.3	14	0.3	-2.4	3.5	-49.3	-29.4	3.4	40.7	5.2	-31.8	4.9	54
92.5	34.5	48.4	0.2	5.7	0.2	8.4	4.3	-71.3	-16.7	2.2	18.7	5.2	-8.3	4.7	43
95	41	31	0.1	-0.2	0.1	1.5	1.2	-46.6	-7.3	1.1	43.4	5.2	-5.9	1.6	38
72	37.5	19.4	0.2	19	0.2	18.8	5.9	-106.7	-21.2	3.9	-16.7	5.1	-2.3	7	53
74	42	27.4	0.1	5.7	0.1	0	4.1	-105.1	-30	3.4	-15.1	5.1	-30	5.3	37
76.5	38.5	27.2	0.1	21.3	0.1	0.2	2.1	-106.6	-16.6	2.2	-16.6	5.1	-16.3	3	42
78.5	28.5	35.2	0.3	35.9	0.3	10.5	2.9	-83.7	-23.3	5.2	6.3	5.1	-12.8	5.9	29
80.5	37.5	25.8	0.1	16.1	0.1	4.1	1.3	-49.3	-8.2	1.8	40.7	5.1	-4.1	2.2	36
80.5	38.5	27.3	0.1	15.7	0.1	1	0.8	-77.6	-5.8	0.9	12.4	5.1	-4.9	1.2	44
82	39.5	29	0.1	13.4	0.1	0.9	0.8	-81.8	-5.8	0.9	8.2	5.1	-4.9	1.2	48
88	25.5	39.1	0.2	34.6	0.3	7.3	1.5	-78.8	-5.3	2	11.2	5.1	2	2.4	42
91	37.5	35.1	0.2	8.6	0.2	11.5	4.9	-78.5	-22.6	3.5	11.5	5.1	-11.2	6.1	28
91.5	33	48.1	0.2	9.2	0.2	19.9	5.8	-58.3	-13.7	1.9	31.7	5.1	6.2	6.1	32
94.5	29.5	47.4	0.2	3.7	0.2	-9.5	2.9	-85.5	-43.2	4.8	4.5	5.1	-52.8	5.7	28
95	27.5	42.1	0.4	16.9	0.5	11.5	6.7	-101	-44.1	7.2	-11	5.1	-32.6	9.6	63
96.5	30	45.8	0.1	-4.4	0.1	-1	2.3	-34.5	-18.7	2.1	55.5	5.1	-19.7	3.1	26
72.5	32	28.9	0.1	33.7	0.1	3.8	4.3	-94.3	-23.7	2.2	-4.3	5	-19.9	4.8	44
73	40.5	26.8	0.1	9.4	0.2	0.9	2.9	-105.9	-25.4	3.5	-15.9	5	-24.5	4.6	32
74.5	42	27.4	0.1	6.2	0.1	6.2	4.3	-101.8	-30.8	4.8	-11.8	5	-24.6	6.4	37
75	32	30.2	0.3	31.8	0.3	5.4	1.7	-73.9	-11.6	2.4	16.1	5	-6.1	2.9	41
77	27.5	35.1	0.2	34.9	0.2	9.8	1.9	-31.2	-1.9	0.6	58.8	5	7.9	2	36
77	41	28.5	0.1	13	0.1	8.8	2.8	-94	-15.4	2.9	-4	5	-6.6	4	49
78.5	30.5	32.2	0.4	29.4	0.4	-4	10.6	-71	-81	8.7	19	5	-85	13.6	31
79	40.5	29.5	0.1	15.8	0.1	1.6	2.2	-96.4	-13.4	1.4	-6.4	5	-11.8	2.6	23
80	38.5	27.2	0.1	16.3	0.1	0.3	1	-74.6	-7.5	1	15.4	5	-7.2	1.4	44
83.5	41.5	31	0.1	10.4	0.1	-1.7	1.8	-80.7	-16	1.7	9.3	5	-17.7	2.5	22
90	24	41.2	0.1	34.1	0.1	0.2	1.3	-66.2	-9.9	1	23.8	5	-9.7	1.6	44
90.5	23.5	41	0.1	34.2	0.1	-3	1	-58.7	-10.4	0.9	31.3	5	-13.4	1.3	45
98.5	23.5	24.6	0.2	-8.4	0.2	15.8	2.3	-68.5	-18.7	5.2	21.5	5	-2.9	5.7	47

76	38	26.2	0.1	22	0.1	6.6	1.8	-98.3	-7.4	1.6	-8.3	4.9	-0.7	2.4	41
76.5	30	32.4	0.4	33.6	0.4	7.1	4.1	-67.4	-22.1	2.7	22.6	4.9	-15	5	16
77.5	39	27.8	0.1	19.3	0.1	-4.3	1.8	-100.7	-18.4	1.6	-10.7	4.9	-22.7	2.4	52
78	37	25.6	0.1	20.2	0.1	7.3	1.7	-48.7	-6.3	1.7	41.3	4.9	1	2.3	42
79.5	38.5	27.1	0.1	17	0.1	-0.6	1.1	-71.3	-9.5	1.1	18.7	4.9	-10	1.5	35
79.5	39	27.7	0.1	16.7	0.1	-0.3	1.2	-85.9	-8.8	0.8	4.1	4.9	-9.2	1.5	35
83	37.5	26.5	0.1	12.8	0.1	7.6	1.4	-70.8	-2.9	1.1	19.2	4.9	4.7	1.8	30
83	40	29.7	0.1	11.9	0.1	3.3	1.1	-53.9	-6.3	1.2	36.1	4.9	-3	1.6	48
83.5	40	29.7	0.1	11.2	0.1	3.8	1.3	-46.5	-7.5	1.4	43.5	4.9	-3.7	1.9	63
88	24	39.7	0.3	34.9	0.3	5.3	1.8	-83	-10.2	2.2	7	4.9	-4.9	2.9	47
92	25	39.2	0.1	30.3	0.1	-18.4	2.5	-172.9	-38.9	2.9	-82.9	4.9	-57.2	3.8	26
94	29	46.4	0.3	6.9	0.3	-1.6	3.4	-85.2	-35.1	4.5	4.8	4.9	-36.6	5.7	37
94	42	31.5	0.1	0.5	0.1	2.9	0.9	-44.5	-6.6	1.3	45.5	4.9	-3.8	1.6	47
96	30.5	47.8	0.2	-2.3	0.1	4.5	1.9	-22.3	-12.4	2.2	67.7	4.9	-7.9	2.9	25
98	23.5	24.4	0.3	-7.2	0.3	14.8	2.7	-63.7	-20.4	5.3	26.3	4.9	-5.6	5.9	32
72	40	26.3	0.2	9.3	0.2	4.8	3.7	-117.6	-28.6	3.9	-27.6	4.8	-23.8	5.4	45
75	32.5	30.2	0.3	31.3	0.3	4.5	1.8	-65.9	-12.4	2.2	24.1	4.8	-8	2.8	36
76	40.5	28.5	0.1	13.3	0.1	7.2	2.8	-94.6	-19.1	3.4	-4.6	4.8	-11.9	4.4	46
78	39	27.7	0.1	18.8	0.1	-2.3	1.7	-99.8	-14.9	1.3	-9.8	4.8	-17.2	2.1	43
78.5	39	27.7	0.1	18.1	0.1	-1.9	1.4	-89.8	-11.9	1	0.2	4.8	-13.8	1.7	42
78.5	42	29.7	0.1	10.9	0.1	8.5	4.5	-72.7	-28	4.4	17.3	4.8	-19.5	6.3	46
79	39	27.7	0.1	17.4	0.1	-1.2	1.2	-86.2	-10.2	0.9	3.8	4.8	-11.4	1.5	49
82.5	40	29.8	0.1	12.6	0.1	3.3	0.9	-60.5	-5.6	1.2	29.5	4.8	-2.3	1.5	44
84	37.5	27	0.1	11.8	0.1	8.3	1.6	-74.4	-4	1.3	15.6	4.8	4.3	2.1	30
89	25.5	39.6	0.2	34.4	0.2	12	1.6	-71.9	-1.5	2	18.1	4.8	10.4	2.3	53
90.5	27	40.4	0.3	29	0.3	-1.1	5.1	-75.4	-39.9	3.8	14.6	4.8	-41	6.3	49
91	41.5	31.2	0.1	3.6	0.2	4.5	1.1	-61.3	-5.6	1.3	28.7	4.8	-1.1	1.7	48
91	42	31.3	0.1	3.4	0.2	3.9	1	-60.7	-5.4	1.2	29.3	4.8	-1.6	1.6	47
97.5	24	24.4	0.2	-6.3	0.2	11.1	4.5	-44	-27.2	4.6	46	4.8	-16	6.4	36
73.5	34	27.9	0.1	30.3	0.1	1.8	1.4	-64.1	-13.2	2	25.9	4.7	-11.4	2.4	46

76	29.5	32.6	0.4	35	0.4	8.4	3.5	-71	-19.2	2.9	19	4.7	-10.8	4.5	43
76.5	36.5	25.2	0.1	22.2	0.1	6.2	1.4	-62.7	-6.4	1.6	27.3	4.7	-0.1	2.1	42
78.5	29.5	34	0.3	33.2	0.3	7.5	3.3	-84.6	-23.9	3.9	5.4	4.7	-16.4	5.1	41
78.5	38.5	27.1	0.1	18.5	0.1	-1.1	1.3	-77.1	-11.4	1.1	12.9	4.7	-12.6	1.7	44
79	37.5	26	0.1	18.6	0.1	5.3	1.6	-48	-8.7	1.7	42	4.7	-3.4	2.3	46
79.5	37.5	25.9	0.1	17.7	0.1	5.3	1.7	-47.3	-9.1	1.7	42.7	4.7	-3.8	2.4	39
82	40	29.7	0.1	13.3	0.1	0.4	0.8	-76.7	-8.4	1.2	13.3	4.7	-8	1.5	45
83	40.5	30.3	0.1	11.7	0.1	2.4	1.2	-49	-8.8	1.4	41	4.7	-6.3	1.8	42
93	26.5	39.9	0.2	26.8	0.2	-3.5	4.2	-90.1	-48.4	5.7	-0.1	4.7	-51.9	7.1	40
94.5	27.5	42.4	0.5	17	0.6	8	5.7	-105.2	-45.5	6.2	-15.2	4.7	-37.5	8.3	42
98	27	32.9	0.2	-8.9	0.3	-3	2.1	-31.4	-24	2.7	58.6	4.7	-26.9	3.5	32
98	41.5	30.8	0.1	-2.9	0.1	4	0.9	-51.6	-5.1	1.2	38.4	4.7	-1.1	1.5	33
99	23	25.8	0.3	-8.8	0.2	23.8	4.2	-64.4	-23.7	5.5	25.6	4.7	0.1	7.2	55
100	36.5	37	0.1	-1.1	0.1	5.9	2.4	-60	-15.7	2.6	30	4.7	-9.8	3.5	28
100	42	30.9	0.1	-4.7	0.1	3.8	1.3	-49.7	-5.2	0.8	40.3	4.7	-1.4	1.5	40
73	42	27.2	0.1	5.1	0.1	5.4	3.2	-102	-23.1	3.2	-12	4.6	-17.7	4.6	52
74	38	22.8	0.3	22.5	0.3	22.4	3.5	-90.2	-7.1	3.2	-0.2	4.6	15.2	4.8	52
77	30	32.5	0.3	33	0.3	8.4	4.2	-70.9	-20.8	2.2	19.1	4.6	-12.4	4.7	36
77	36.5	25.3	0.1	21.6	0.1	7	1.5	-58.5	-6.4	1.6	31.5	4.6	0.6	2.2	46
77.5	36.5	25.4	0.1	20.9	0.1	9	1.7	-51.7	-6	1.7	38.3	4.6	3	2.4	42
79	38.5	27.1	0.1	17.7	0.1	-1	1.1	-72.8	-10.8	1.1	17.2	4.6	-11.8	1.6	35
81.5	39	28.2	0.1	14.2	0.1	1.2	0.7	-84.8	-5.2	0.8	5.2	4.6	-3.9	1	50
87	26	39	0.4	37.2	0.4	3.9	4.6	-78.1	-32.7	4.5	11.9	4.6	-28.9	6.4	34
88	23.5	40	0.3	35.5	0.3	4.4	1.8	-86.2	-10.5	2.1	3.8	4.6	-6.1	2.7	46
95.5	30.5	48.2	0.2	-0.5	0.1	3.6	1.7	-31.4	-13.3	2.1	58.6	4.6	-9.7	2.7	39
99.5	41.5	30.9	0.1	-4.2	0.1	4.1	1.2	-50.2	-4.8	0.9	39.8	4.6	-0.7	1.4	33
100	28.5	38.6	0.1	-17.6	0.1	12.2	1.9	-153.8	-5.5	2.2	-63.8	4.6	6.6	2.9	52
72.5	42	26.9	0.1	4.9	0.1	7.3	2.8	-105.1	-18.7	2.8	-15.1	4.5	-11.3	4	52
73	32	29.2	0.1	33.7	0.1	5.8	4.1	-95.3	-23.5	2.1	-5.3	4.5	-17.7	4.6	47
75.5	41	27.6	0.1	11.4	0.1	9.8	4.3	-108	-28.2	4.2	-18	4.5	-18.4	6	27

75.5	42	27.7	0.1	7.1	0.1	4.1	4.4	-105.3	-36	4.6	-15.3	4.5	-31.9	6.4	36
77.5	30	32.7	0.4	32.3	0.4	8.3	4.3	-74.6	-21.5	2	15.4	4.5	-13.2	4.7	38
81.5	39.5	28.9	0.1	14	0.1	1.3	0.7	-87.5	-5.9	0.9	2.5	4.5	-4.5	1.1	56
82	27	36.6	0.2	35.3	0.3	0.7	2.3	-81.5	-18.4	2.1	8.5	4.5	-17.7	3.1	38
82.5	37.5	26.4	0.1	13.4	0.1	7.8	1.3	-67.6	-2.7	1.1	22.4	4.5	5.1	1.7	36
83.5	37.5	26.8	0.1	12.3	0.1	8.2	1.5	-72.9	-3.7	1.1	17.1	4.5	4.5	1.9	21
86	26	38.7	0.5	36.6	0.5	7	2.6	-72.9	-23.3	3.8	17.1	4.5	-16.3	4.7	47
87.5	38	30.2	0.4	8.8	0.4	14.6	3.3	-68.4	-19.7	4.1	21.6	4.5	-5.1	5.3	39
91.5	25.5	40.4	0.1	30.4	0.1	0.7	2.8	-14	-34.1	4.7	76	4.5	-33.5	5.4	40
92.5	33	49.1	0.2	7	0.2	14.4	3.5	-64.9	-11.2	2	25.1	4.5	3.2	4.1	42
94.5	41.5	31.3	0.1	0.2	0.1	2	0.9	-44.9	-7.1	1.1	45.1	4.5	-5.2	1.4	46
97.5	29.5	43	0.1	-8.5	0.1	7.5	2.5	-12.6	-13.8	2.2	77.4	4.5	-6.3	3.4	34
99.5	26.5	29.7	0.1	-16.5	0.1	13.8	2.5	-90.2	-8.8	2.6	-0.2	4.5	5	3.6	49
100	24.5	27.7	0.1	-13.9	0.1	11.8	3.4	-93.3	-18.2	3.1	-3.3	4.5	-6.4	4.6	32
72	37	20.6	0.2	19.8	0.2	10.5	4.5	-85.3	-23.5	1.9	4.7	4.4	-13	4.9	60
72	41.5	26.3	0.1	5.7	0.1	1.8	2.7	-108	-23.3	3	-18	4.4	-21.6	3.9	35
73	38	21.3	0.2	20.1	0.2	24.4	2	-107.4	-13.1	5.5	-17.4	4.4	11.3	5.8	38
80.5	37	25.6	0.1	16.2	0.1	4.4	1.3	-47.3	-9.1	1.6	42.7	4.4	-4.7	2.1	38
88.5	25.5	39.3	0.2	34.5	0.2	9.7	1.4	-77.6	-3.9	2	12.4	4.4	5.8	2.3	42
90	27	40.6	0.2	30	0.2	-2.1	5.6	-78.3	-40.6	2.6	11.7	4.4	-42.7	6.2	42
91.5	41	31.2	0.1	3.4	0.2	5.6	1.2	-55.2	-7.4	1.6	34.8	4.4	-1.8	2	41
93	34	49	0.2	5.9	0.2	8.5	2.6	-62.7	-11.1	1.7	27.3	4.4	-2.6	3	44
95	40.5	30.9	0.1	0	0.1	3.1	1.5	-50.2	-8.8	1.1	39.8	4.4	-5.7	1.8	36
95.5	40.5	30.9	0.1	-0.5	0.1	3	1.4	-51.1	-8.4	1.2	38.9	4.4	-5.4	1.8	40
96	31	49	0.2	-1.9	0.1	8.7	1.6	-18	-7.9	2.1	72	4.4	0.8	2.6	34
96.5	40.5	30.7	0.1	-1.3	0.1	3	1.2	-52.5	-8.5	1.3	37.5	4.4	-5.5	1.8	47
99	29	40.6	0.1	-14.2	0.1	14.5	1.8	-5	-3.6	2.2	85	4.4	10.8	2.8	47
72	41	26.4	0.1	7	0.1	0.6	2.8	-99.9	-24	2.4	-9.9	4.3	-23.4	3.6	38
73.5	42	27.3	0.1	5.4	0.1	3.4	3.3	-104.2	-28.5	3.3	-14.2	4.3	-25.1	4.7	33
79	41	29.9	0.1	15.1	0.1	2.7	1.9	-94.4	-14.7	1.6	-4.4	4.3	-12	2.5	31

80	39	27.9	0.1	16.1	0.1	0.8	1	-87.6	-7.5	0.8	2.4	4.3	-6.6	1.2	44
81.5	40	29.7	0.1	14	0.1	1.4	0.8	-86	-8.6	1.3	4	4.3	-7.2	1.5	59
82.5	40.5	30.3	0.1	12.4	0.1	2.2	1	-58.7	-8.9	1.3	31.3	4.3	-6.7	1.7	49
84	27.5	36.5	0.2	36	0.2	-13.9	6.7	-76.2	-69.5	7.9	13.8	4.3	-83.4	10.5	27
85.5	29	36.8	0.1	24.1	0.1	8.3	3.7	-78.3	-22.5	2.9	11.7	4.3	-14.2	4.7	46
86.5	37.5	29.5	0.3	10.5	0.3	13.7	3.9	-76.5	-19.8	3.2	13.5	4.3	-6.1	5.1	54
88.5	38.5	30.4	0.2	7.2	0.2	13.2	2.3	-64.3	-15.4	3.8	25.7	4.3	-2.2	4.4	44
89.5	25.5	40.2	0.1	34.5	0.2	13.8	2.1	-59.6	-4.4	2.8	30.4	4.3	9.4	2.9	42
89.5	39	30.4	0.2	6.1	0.2	15.4	1.9	-67.6	-13.9	4.2	22.4	4.3	1.5	4.6	34
90	40.5	30.7	0.2	4.9	0.2	6.7	1.1	-65.9	-5.7	1.4	24.1	4.3	0.9	1.8	43
90.5	26.5	40.4	0.3	31	0.3	3.4	3.2	-72.8	-33.3	4.5	17.2	4.3	-29.9	5.6	40
93.5	26	36.7	0.2	24.8	0.2	6.8	2.5	-177	-17.6	2.5	-87	4.3	-10.8	3.6	41
93.5	42	31.5	0.1	1	0.1	3.4	0.9	-46.3	-6.6	1.2	43.7	4.3	-3.2	1.5	57
94	29.5	47.4	0.2	5.2	0.2	5.2	2.6	-59.6	-18.9	2.8	30.4	4.3	-13.6	3.7	40
97	30	45.2	0.1	-6.3	0.1	5.6	2.2	-13.2	-14.3	2.2	76.8	4.3	-8.7	3.1	28
98	27.5	35.4	0.2	-9.2	0.2	-0.7	2	-27.6	-22.5	2.7	62.4	4.3	-23.2	3.4	27
99.5	26	28.1	0.1	-16.1	0.1	21.3	2.9	-98.5	-6	2.9	-8.5	4.3	15.3	4.1	42
100	37	36.6	0.1	-1.6	0.1	5.3	2.2	-58.6	-16.9	2.5	31.4	4.3	-11.5	3.3	42
72	31.5	28.9	0.3	34.2	0.3	2.7	2.6	-98.8	-17.4	1.5	-8.8	4.2	-14.7	2.9	37
73	41	26.4	0.1	8.1	0.2	0.8	2.8	-104.5	-27	3.1	-14.5	4.2	-26.2	4.2	40
75	31.5	30.2	0.3	32.5	0.3	5.7	1.5	-75.6	-14.3	2.5	14.4	4.2	-8.6	2.9	36
76.5	32	29.1	0.3	29.2	0.3	-7.9	6.3	-48.6	-67.3	6.1	41.4	4.2	-75.1	8.8	37
77	39	28	0.1	19.9	0.1	-6.2	1.9	-97.5	-25.5	2	-7.5	4.2	-31.7	2.8	37
78.5	37	25.7	0.1	19.4	0.1	8.1	1.5	-45.4	-7.6	1.7	44.6	4.2	0.5	2.3	46
79.5	28	35.8	0.2	35.3	0.2	7.2	1	-76	-6.8	1.8	14	4.2	0.5	2.1	34
81	37	25.6	0.1	15.5	0.1	5.1	1.3	-50.9	-8	1.4	39.1	4.2	-2.8	1.9	45
82.5	41	30.9	0.1	12.1	0.1	-1.2	1.6	-72.5	-16.7	1.7	17.5	4.2	-17.9	2.3	57
85.5	42	31.3	0.1	7.8	0.1	3.4	1.5	-72.5	-12.9	1.9	17.5	4.2	-9.4	2.4	41
90	23.5	41	0.1	34.6	0.1	0.3	1.1	-68.6	-9.4	0.8	21.4	4.2	-9.1	1.4	44
94.5	30	48	0.2	3.1	0.2	3.6	1.9	-43.7	-16.5	2.4	46.3	4.2	-12.9	2.9	21

95.5	31	49.2	0.2	-0.3	0.1	7.6	1.5	-26.7	-8.5	1.8	63.3	4.2	-0.8	2.3	40
96.5	30.5	47.4	0.2	-4	0.1	8.6	2	-13	-11	2.3	77	4.2	-2.4	3	30
97.5	41	30.7	0.1	-2.4	0.1	3.8	1	-52.3	-6.5	1.2	37.7	4.2	-2.8	1.5	46
98.5	41	30.7	0.1	-3.3	0.1	3.8	0.9	-55.5	-5.8	1	34.5	4.2	-2	1.4	31
98.5	41.5	30.8	0.1	-3.3	0.1	4.1	0.8	-51.9	-5.1	1.1	38.1	4.2	-1.1	1.3	32
99	41.5	30.8	0.1	-3.7	0.1	4.2	0.9	-51.1	-4.9	1	38.9	4.2	-0.7	1.3	41
99.5	23	26.6	0.2	-10.4	0.2	26	5.1	-63.3	-27.7	5.1	26.7	4.2	-1.7	7.5	56
99.5	29	40.5	0.1	-15.8	0.1	15	1.8	-1.3	-4.2	2.1	88.7	4.2	10.8	2.8	48
75.5	32.5	30.4	0.3	30.8	0.3	5.5	2.6	-43.6	-40.7	6.1	46.4	4.1	-35.2	6.7	36
79	39.5	28.4	0.1	17.1	0.1	0.3	1.4	-96.5	-12.7	1.2	-6.5	4.1	-12.5	1.9	38
80	37	25.6	0.1	16.9	0.1	5.2	1.4	-44.7	-9.3	1.5	45.3	4.1	-4.1	2	37
80.5	39	28	0.1	15.4	0.1	1.3	0.8	-87.6	-6.4	0.8	2.4	4.1	-5.1	1.1	28
81	39	28.1	0.1	14.8	0.1	1.3	0.7	-86.3	-5.6	0.7	3.7	4.1	-4.3	1	73
84.5	37.5	27.5	0.1	11.4	0.1	9.3	1.6	-74.5	-5.7	1.4	15.5	4.1	3.6	2.1	49
89.5	40	30.5	0.2	5.6	0.2	8	1.2	-68.9	-5.9	1.5	21.1	4.1	2.1	1.9	45
91.5	42	31.4	0.1	3	0.1	3.9	0.9	-56.2	-5.8	1.1	33.8	4.1	-1.9	1.4	39
97	40.5	30.7	0.1	-1.8	0.1	3.3	1.1	-52.7	-9.2	1.4	37.3	4.1	-5.9	1.8	48
98.5	26	26.3	0.2	-11.7	0.2	20.7	4.1	-66.3	-13.3	2.6	23.7	4.1	7.4	4.9	33
98.5	29	40.7	0.1	-12.5	0.1	12.9	1.7	-9.3	-5.5	2.1	80.7	4.1	7.4	2.8	53
99.5	24	26.2	0.2	-11.9	0.1	12.9	3.9	-77.3	-19.5	2.8	12.7	4.1	-6.6	4.8	50
99.5	39.5	30.7	0.1	-3.5	0.1	4.4	2	-48.6	-17.4	2.4	41.4	4.1	-12.9	3.1	62
100	28	36.8	0.1	-18.2	0.1	14.7	2	-131.3	-4.3	1.9	-41.3	4.1	10.4	2.7	50
72	32.5	28.9	0.2	32.7	0.2	4.4	2.5	-87.7	-19.1	1.7	2.3	4	-14.7	3.1	47
72.5	40	26.3	0.2	10	0.2	7.6	3.7	-111.5	-33	4.2	-21.5	4	-25.4	5.7	45
72.5	41	26.5	0.1	7.5	0.2	1.1	2.5	-100.4	-23.7	2.7	-10.4	4	-22.6	3.6	47
77.5	42	28.7	0.1	10.5	0.1	10.4	3.6	-91.3	-35.8	5.1	-1.3	4	-25.4	6.2	42
79.5	31.5	28.3	0.2	20.5	0.2	10.7	2.9	-79.2	-17	2.7	10.8	4	-6.3	3.9	50
79.5	39.5	28.5	0.1	16.6	0.1	1.7	1.3	-96.8	-10.4	1	-6.8	4	-8.7	1.7	45
80	34	28.6	0.1	17.6	0.1	17.7	2.6	-74.6	-4.5	1.7	15.4	4	13.2	3.1	36
81	39.5	28.8	0.1	14.6	0.1	1.9	0.8	-91.5	-6.3	0.9	-1.5	4	-4.4	1.1	47

86	37.5	28.9	0.3	10.8	0.3	14.3	3.1	-78.4	-18.7	3.4	11.6	4	-4.4	4.6	46
86.5	26	38.7	0.6	38.4	0.6	7	3.9	-77.5	-40.4	5.5	12.5	4	-33.4	6.8	41
87	26.5	38.8	0.2	35.6	0.2	2.4	4.8	-80.4	-38.2	4.5	9.6	4	-35.8	6.6	39
88.5	25	39.3	0.2	34.8	0.3	11.3	1.5	-72.8	-4.2	1.7	17.2	4	7.1	2.2	39
90	24.5	41.3	0.1	33.9	0.1	5.6	1.5	-55.4	-9.4	1.5	34.6	4	-3.7	2	39
91.5	41.5	31.3	0.1	3.2	0.1	4.5	1	-56.4	-6.3	1.1	33.6	4	-1.8	1.5	39
92	42	31.5	0.1	2.5	0.1	4	0.9	-53.2	-6	1	36.8	4	-2	1.4	47
92.5	42	31.5	0.1	2	0.1	4	0.9	-50.7	-6.2	1	39.3	4	-2.2	1.4	48
93	42	31.5	0.1	1.6	0.1	3.8	0.9	-48.2	-6.5	1.1	41.8	4	-2.7	1.4	48
94.5	40.5	31	0.1	0.5	0.1	3.1	1.5	-48.5	-9.1	0.9	41.5	4	-6	1.7	43
95.5	26.5	37.4	0.3	15.2	0.3	17.8	3.3	-13.7	-13	2.8	76.3	4	4.8	4.3	55
96	40	31	0.1	-0.6	0.1	4.5	1.4	-52.4	-11.2	1.7	37.6	4	-6.7	2.2	44
98	41	30.7	0.1	-2.8	0.1	3.9	0.9	-54.4	-6.2	1.1	35.6	4	-2.3	1.4	37
98.5	42	30.9	0.1	-3.3	0.1	4.1	0.8	-50.2	-5.2	1	39.8	4	-1.1	1.3	39
73	37.5	21.5	0.2	20.1	0.2	22.1	1.6	-99.1	-6	3.6	-9.1	3.9	16.1	3.9	31
75.5	35.5	25.3	0.1	23.1	0.2	13.2	2.3	-85.2	-11.2	2	4.8	3.9	2	3.1	36
75.5	38	25.9	0.1	22.4	0.1	17.7	2.8	-94.7	-6.4	1.7	-4.7	3.9	11.3	3.3	37
79.5	37	25.7	0.1	17.7	0.1	6.6	1.5	-43.8	-8.9	1.5	46.2	3.9	-2.4	2.1	51
81.5	37	25.7	0.1	14.8	0.1	6	1.2	-60.2	-7.1	1.3	29.8	3.9	-1	1.8	28
85	26	38.4	0.4	36	0.4	6.1	1.9	-69.2	-17.6	2.6	20.8	3.9	-11.4	3.2	45
88.5	23	40	0.2	36.4	0.2	5.3	1.5	-80.2	-8.5	1.5	9.8	3.9	-3.2	2.1	38
88.5	23.5	40.1	0.2	35.8	0.2	5.8	1.6	-78.6	-9.2	1.4	11.4	3.9	-3.4	2.2	38
89	26	39.7	0.2	34.4	0.2	8.7	1.8	-78.6	-11.8	2.5	11.4	3.9	-3.1	3	37
91	25	40.8	0.1	31.9	0.1	-1.4	1.9	-41.2	-18.2	1.3	48.8	3.9	-19.6	2.3	39
91	40.5	31.1	0.2	4.1	0.2	7.3	1.3	-57.3	-8.1	1.7	32.7	3.9	-0.8	2.1	43
94	41.5	31.4	0.1	0.7	0.1	2.5	0.9	-45.7	-7.4	1	44.3	3.9	-4.9	1.4	46
94.5	41	31.2	0.1	0.3	0.1	2	1	-45.9	-8.1	0.9	44.1	3.9	-6	1.4	40
95.5	40	31	0.1	-0.2	0.1	5.2	1.6	-52.3	-10.6	1.5	37.7	3.9	-5.4	2.2	43
96.5	31	48.7	0.2	-3.4	0.1	12	1.8	-8.6	-7.9	2.2	81.4	3.9	4.1	2.8	31
97	29.5	43.7	0.1	-6.6	0.1	0.2	2.6	-39.7	-26.1	2.4	50.3	3.9	-25.9	3.6	31

72.5	38	20.6	0.3	19.2	0.3	27	3.2	-112.1	-24.3	6.1	-22.1	3.8	2.7	6.9	41
73.5	40.5	26.7	0.1	10.4	0.2	2.5	3.3	-111	-34.2	3.2	-21	3.8	-31.6	4.5	34
74.5	33	30.2	0.2	31.9	0.2	5.2	1.9	-79.2	-14.9	1.9	10.8	3.8	-9.6	2.7	29
76	36	25.3	0.1	22.9	0.1	7.6	1.6	-67.3	-8.1	1.4	22.7	3.8	-0.5	2.1	37
76.5	41.5	28	0.1	11.4	0.1	11	5.4	-101.5	-38.8	3.9	-11.5	3.8	-27.8	6.7	52
78	36.5	25.5	0.1	20.1	0.1	10.5	1.7	-47.7	-8	1.8	42.3	3.8	2.5	2.4	36
78	42	29.3	0.1	10.8	0.1	24.9	4.5	-79.5	-26.3	4.9	10.5	3.8	-1.4	6.7	40
79	28.5	35.5	0.2	35.7	0.2	9.5	1.6	-82.8	-18.5	3.5	7.2	3.8	-9	3.8	39
79	37	25.7	0.1	18.5	0.1	7.6	1.4	-43.9	-8.4	1.6	46.1	3.8	-0.8	2.2	45
79	40	29.1	0.1	16.7	0.1	2.4	1.9	-97.5	-16.3	1.7	-7.5	3.8	-14	2.5	20
80	28.5	37.1	0.3	36.7	0.3	8	2.9	-76	-30.8	5	14	3.8	-22.8	5.8	38
85	29.5	36.1	0.1	23.3	0.1	12.6	2.8	-79.9	-16.7	2.8	10.1	3.8	-4.1	3.9	45
88.5	24	39.9	0.2	35.3	0.3	8.1	1.6	-76	-9.4	1.6	14	3.8	-1.3	2.3	45
88.5	24.5	39.4	0.2	35.1	0.3	11.6	1.6	-71.7	-7.4	1.7	18.3	3.8	4.2	2.4	45
90.5	40.5	30.9	0.2	4.5	0.2	7.3	1.2	-62.1	-6.7	1.4	27.9	3.8	0.6	1.8	48
95	30.5	48.5	0.2	1.2	0.1	5.2	1.5	-36.1	-12.9	1.9	53.9	3.8	-7.7	2.4	62
97	31	48.4	0.2	-4.7	0.2	14.5	2	-0.4	-8.8	2.4	89.6	3.8	5.7	3.1	37
97.5	24.5	24.2	0.3	-6.2	0.2	16.8	3.7	-39.1	-26	4.4	50.9	3.8	-9.2	5.8	37
98	24.5	23.7	0.2	-8.4	0.2	23.4	4.9	-57.2	-20.4	3.1	32.8	3.8	3	5.8	46
98.5	40	30.5	0.1	-3	0.1	4.3	1.9	-56.1	-17.7	2.2	33.9	3.8	-13.4	2.9	32
100	36	37.7	0.1	-0.7	0.1	9.4	2.6	-50.1	-15.9	2.2	39.9	3.8	-6.5	3.3	34
72.5	31	29.3	0.2	35	0.2	1	2	-106.7	-17	1.4	-16.7	3.7	-16	2.4	31
73.5	41	26.3	0.1	8.9	0.2	4.5	3.6	-105	-37.6	3.6	-15	3.7	-33.1	5.1	36
74.5	32.5	30.2	0.2	32.4	0.2	5.9	1.8	-86.9	-13	1.7	3.1	3.7	-7.2	2.4	33
76	32	30.6	0.3	30.8	0.3	0	4.3	-45.1	-60.2	6.5	44.9	3.7	-60.2	7.8	39
77.5	34	25.3	0.2	21.2	0.2	8	2.4	-40.3	-21.6	3.1	49.7	3.7	-13.5	3.9	47
78	34	25.9	0.2	20.2	0.2	14.2	1.9	-55.3	-9.5	2.6	34.7	3.7	4.7	3.1	41
80	39.5	28.6	0.1	16.1	0.1	3.2	1.2	-100.1	-9	1	-10.1	3.7	-5.8	1.5	20
80.5	39.5	28.7	0.1	15.4	0.1	2.7	0.9	-96.7	-7.3	0.9	-6.7	3.7	-4.6	1.3	24
82	40.5	30.4	0.1	13.2	0.1	-0.3	1	-75.4	-14.3	1.5	14.6	3.7	-14.6	1.9	48

85	37.5	27.9	0.2	11.1	0.2	9.9	1.6	-73.4	-8.4	1.7	16.6	3.7	1.5	2.4	53
85.5	26	38.5	0.4	36.1	0.4	6.4	1.9	-71.3	-20.5	2.8	18.7	3.7	-14.1	3.4	33
85.5	27	37.9	0.4	36.1	0.3	5.2	5.2	-63.3	-64.1	7.3	26.7	3.7	-58.9	8.7	47
89	23	40.3	0.2	36.2	0.2	5.2	1.3	-75.2	-8	1.2	14.8	3.7	-2.8	1.8	45
90	36.5	35.3	0.5	11.5	0.5	16.8	3.2	-69.2	-22.3	4	20.8	3.7	-5.5	5.2	41
90.5	26	40.2	0.2	32.5	0.2	8	2.1	-63	-25.2	3.8	27	3.7	-17.2	4.5	40
91	26	40	0.2	31.4	0.2	8.9	2.6	-50.7	-21.4	2.9	39.3	3.7	-12.5	3.9	47
91.5	40.5	31.3	0.2	3.7	0.2	6.4	1.2	-51	-10.7	1.9	39	3.7	-4.3	2.2	40
92	37	36.1	0.2	8.4	0.2	12.1	2.9	-63.8	-21.5	3.1	26.2	3.7	-9.4	4.3	40
93	30.5	49	0.1	8	0.1	15.3	2.5	-61	-11.9	2.4	29	3.7	3.4	3.5	47
93.5	30.5	49.1	0.2	6.3	0.1	12.6	2.1	-51.5	-10.9	2	38.5	3.7	1.8	3	43
94.5	26	35.4	0.2	21.1	0.2	17.8	2	-178.6	-15.7	3.4	-88.6	3.7	2.2	4	45
94.5	31.5	50.5	0.2	3.1	0.1	13.3	2.3	-41.8	-8.7	1.8	48.2	3.7	4.7	2.9	63
95	31	49.4	0.2	1.3	0.1	8	1.5	-34.3	-9.4	1.7	55.7	3.7	-1.4	2.2	49
97.5	40.5	30.7	0.1	-2.2	0.1	3.7	1.1	-55.1	-9	1.3	34.9	3.7	-5.3	1.7	51
98	26.5	30.3	0.2	-8.2	0.2	1.3	2.4	-37	-23.8	2.2	53	3.7	-22.5	3.3	34
98	29	41.2	0.1	-10.4	0.1	7.7	1.8	-21.8	-12.9	2	68.2	3.7	-5.2	2.7	43
98	40.5	30.7	0.1	-2.7	0.1	3.9	1.1	-57.4	-8.4	1.1	32.6	3.7	-4.5	1.6	38
99.5	42	30.9	0.1	-4.2	0.1	4.3	1	-49.7	-5.3	0.8	40.3	3.7	-1	1.2	35
100	23.5	26.4	0.2	-12.7	0.2	16	3.7	-62	-21.1	2.9	28	3.7	-5.1	4.7	39
100	30	42.9	0.1	-14.6	0.1	23.6	2.8	-2.5	-5.5	2.6	87.5	3.7	18.2	3.8	59
73.5	37.5	22.2	0.2	20.7	0.2	21.5	1.3	-105.8	-3.1	2.9	-15.8	3.6	18.4	3.2	34
74	37.5	23	0.2	21.4	0.2	21.3	1.8	-109.1	-2.7	2.4	-19.1	3.6	18.6	3	48
74	41.5	27	0.1	7.3	0.1	6.3	3.5	-102.8	-33.6	3.5	-12.8	3.6	-27.3	5	38
74.5	41.5	27.2	0.1	7.7	0.1	6.9	3.3	-102.1	-32.4	3.8	-12.1	3.6	-25.6	5	42
78.5	39.5	28.4	0.1	17.9	0.1	0.4	1.7	-101.3	-19.3	1.8	-11.3	3.6	-18.9	2.5	35
79	32	27.6	0.2	20.4	0.2	15.8	3	-79.4	-13.8	2.4	10.6	3.6	2.1	3.8	45
79	42	29.6	0.1	11.2	0.1	0.5	3.3	-88.8	-37.4	2.5	1.2	3.6	-36.9	4.1	50
81	40	29.6	0.1	14.7	0.1	3	0.9	-93.1	-9.7	1.3	-3.1	3.6	-6.6	1.6	40
83	41.5	31.1	0.1	10.8	0.1	-1.8	1.8	-86.8	-22.7	1.9	3.2	3.6	-24.5	2.6	43

84	42	31.2	0.1	9.2	0.1	-0.2	1.8	-80.5	-20.2	1.7	9.5	3.6	-20.3	2.5	45
85.5	29.5	36.9	0.1	23	0.1	16.8	3.2	-84.1	-16.4	2.7	5.9	3.6	0.4	4.2	48
86	29	37.2	0.1	23.7	0.1	9	2.4	-83.7	-20.2	2.7	6.3	3.6	-11.2	3.6	21
87	37	30.6	0.4	11.5	0.4	11.7	3.6	-74.9	-21.9	2.1	15.1	3.6	-10.2	4.2	41
87	37.5	30	0.3	10.3	0.4	12.9	3.2	-74.9	-20.6	2.7	15.1	3.6	-7.7	4.2	38
87.5	27	38.5	0.1	33.3	0.1	-4.8	5	-79.1	-46.6	3.4	10.9	3.6	-51.4	6	38
89.5	23	40.6	0.1	35.6	0.1	4.5	1.3	-73.2	-7.8	1	16.8	3.6	-3.3	1.6	46
90	23	40.8	0.1	35.1	0.1	3.2	1.1	-73.7	-7.9	0.9	16.3	3.6	-4.8	1.4	52
91	36.5	36.7	0.3	10	0.3	23.4	3.3	-58.3	-17.7	4.1	31.7	3.6	5.7	5.2	32
91.5	37.5	35.4	0.2	8.2	0.2	11.1	3.5	-74.2	-24.5	2.8	15.8	3.6	-13.5	4.5	43
92	34	48.3	0.2	7.3	0.2	14.2	3.2	-63	-11.9	1.4	27	3.6	2.3	3.4	40
94	26	36.1	0.2	23.4	0.2	16.1	2.2	-176.7	-15.7	3	-86.7	3.6	0.4	3.7	45
95	26	35.1	0.3	18.1	0.3	18.8	2.2	-5	-11.3	3	85	3.6	7.5	3.7	23
96	31.5	50.1	0.2	-1.4	0.1	11.6	1.6	-19.1	-7.5	1.9	70.9	3.6	4.1	2.5	43
96.5	40	30.9	0.1	-1	0.1	4.5	1.3	-54.6	-13.2	1.8	35.4	3.6	-8.8	2.3	42
97	30.5	46.9	0.1	-5.6	0.1	13	2	-2.1	-10.6	2.3	87.9	3.6	2.3	3	33
98	28	37.7	0.2	-9.6	0.2	1.1	1.9	-30.5	-22.4	2.4	59.5	3.6	-21.3	3	21
99	42	30.9	0.1	-3.8	0.1	4.2	0.9	-50	-5.3	0.9	40	3.6	-1.1	1.2	38
99.5	23.5	26	0.2	-11.2	0.2	25	4.9	-61.5	-24.6	3.9	28.5	3.6	0.4	6.2	56
100	29	40.3	0.1	-16.9	0.1	15.6	1.9	-171.6	-8.4	2.3	-81.6	3.6	7.2	3	47
100	30.5	44.1	0.2	-13.4	0.1	20.5	2.6	-2	-10.9	2.8	88	3.6	9.6	3.8	53
100	39	31.2	0.1	-3.6	0.1	5.2	2.1	-48.1	-20.2	2.4	41.9	3.6	-15	3.2	44
72.5	32.5	29.1	0.1	32.5	0.1	4.7	2.4	-88.7	-20.8	1.5	1.3	3.5	-16.1	2.8	51
73	32.5	29.3	0.1	32.5	0.1	4.3	2.9	-93.5	-21.9	1.5	-3.5	3.5	-17.6	3.2	47
77	41.5	28.4	0.1	11.7	0.1	10.4	3.6	-99.5	-29.9	3	-9.5	3.5	-19.6	4.7	52
78.5	36.5	25.6	0.1	19.2	0.1	10.1	1.4	-45.7	-8.1	1.7	44.3	3.5	2	2.2	35
78.5	40.5	29.4	0.1	15.9	0.1	3	1.7	-102.4	-15.6	1.5	-12.4	3.5	-12.6	2.3	41
79.5	34.5	27.4	0.2	17.8	0.1	17.9	2.3	-66.9	-8.1	2	23.1	3.5	9.7	3.1	35
79.5	35	26.8	0.1	17.6	0.1	14.3	1.9	-60.2	-11	2.3	29.8	3.5	3.3	3.1	44
79.5	40.5	29.7	0.1	15.6	0.1	4.5	1.7	-95.4	-14.1	1.5	-5.4	3.5	-9.6	2.3	44

79.5	41	30	0.1	14.8	0.1	4.1	1.8	-90.7	-16	1.7	-0.7	3.5	-11.9	2.5	50
80	33.5	29.1	0.1	17.8	0.1	15.2	2.2	-81.2	-6.3	1.5	8.8	3.5	8.9	2.7	40
84.5	42	31.2	0.1	8.8	0.1	2.2	1.7	-74.9	-18.4	1.8	15.1	3.5	-16.2	2.5	41
85	42	31.2	0.1	8.3	0.1	3.6	1.5	-71.9	-15.5	1.8	18.1	3.5	-11.9	2.3	27
85.5	37.5	28.3	0.2	10.8	0.2	10.8	1.8	-73.4	-11.8	2.1	16.6	3.5	-1.1	2.8	36
87.5	26	38.9	0.3	36.2	0.3	5.4	2.3	-77.8	-26.7	3.5	12.2	3.5	-21.2	4.2	36
90	25.5	40.6	0.1	34	0.1	12.2	1.6	-42.8	-14.8	3.1	47.2	3.5	-2.6	3.3	47
92	41.5	31.4	0.1	2.7	0.1	4.4	0.9	-53.2	-6.8	1	36.8	3.5	-2.4	1.4	45
93	31	49.5	0.1	7.7	0.1	14.8	2.3	-59.7	-12.3	2.2	30.3	3.5	2.5	3.3	43
93	33.5	49.2	0.2	6	0.2	11.7	2.1	-58.8	-9.7	1.5	31.2	3.5	2	2.6	40
93	34.5	48.5	0.2	5.5	0.2	10.3	2.7	-62.1	-15.9	1.9	27.9	3.5	-5.6	3.2	40
93.5	31	49.8	0.2	6.2	0.1	14.1	2.5	-53.1	-11.2	1.8	36.9	3.5	2.9	3.1	42
93.5	41.5	31.4	0.1	1.2	0.1	3.1	0.9	-47.1	-7.5	1	42.9	3.5	-4.4	1.3	66
94	30	48.2	0.2	4.8	0.2	7.8	1.8	-48.7	-14.5	2.1	41.3	3.5	-6.7	2.7	45
94.5	31	49.7	0.2	2.9	0.1	10.3	1.8	-39	-9.6	1.7	51	3.5	0.7	2.4	54
95	31.5	50.4	0.2	1.5	0.1	11.5	1.7	-33.8	-8.3	1.6	56.2	3.5	3.3	2.4	51
95	40	31.1	0.1	0.2	0.1	6.8	1.8	-53.3	-11.1	1.3	36.7	3.5	-4.2	2.2	44
95.5	28	44.1	0.4	16.3	0.4	-8.8	5.4	-64.3	-65.9	4.7	25.7	3.5	-74.8	7.1	69
97.5	29	41.9	0.2	-8.2	0.2	1.2	2.4	-43.1	-26.6	2.4	46.9	3.5	-25.4	3.4	34
98.5	23	25.4	0.3	-7.6	0.3	18.2	2	-63.9	-22.7	4	26.1	3.5	-4.6	4.6	44
99.5	37	36.6	0.1	-1	0.1	6.9	2	-57.1	-19	2.6	32.9	3.5	-12.1	3.2	29
72.5	37.5	21	0.3	19.8	0.3	28.4	3.3	-94.4	-15	3.9	-4.4	3.4	13.5	5.1	41
72.5	41.5	26.4	0.1	6.2	0.1	5.9	2.5	-106.7	-26.6	3	-16.7	3.4	-20.6	3.9	54
73	41.5	26.4	0.1	6.7	0.2	9.5	3.7	-106.3	-36.3	4	-16.3	3.4	-26.8	5.5	52
74	34	28	0.1	30.9	0.1	5.8	1.9	-74.5	-18.6	2.3	15.5	3.4	-12.8	3	32
74.5	32	30.1	0.3	32.7	0.3	6	1.7	-83.9	-14.3	1.7	6.1	3.4	-8.4	2.4	39
74.5	38	23.5	0.2	22.5	0.2	28.8	3.6	-94.2	-7.1	2.3	-4.2	3.4	21.7	4.2	30
75	33	30.5	0.3	31.1	0.3	7.3	2.4	-55.3	-22.2	2.6	34.7	3.4	-14.9	3.5	38
77	32	27.9	0.3	27.5	0.3	-2.1	5.9	-58	-72.2	5.7	32	3.4	-74.3	8.2	41
77	42	28.4	0.1	9.9	0.1	3.9	4.2	-105.8	-55.6	5.7	-15.8	3.4	-51.7	7	60

77.5	34.5	25.4	0.2	21.1	0.2	6.6	2.3	-33.5	-18.3	1.8	56.5	3.4	-11.7	3	40
78.5	36	25.7	0.1	19.1	0.1	12.2	1.6	-46.7	-9	1.9	43.3	3.4	3.2	2.5	44
79	31.5	28.3	0.3	21.8	0.2	10.8	3.5	-70	-27.8	3.1	20	3.4	-17	4.7	45
79	36.5	25.7	0.1	18.4	0.1	9.2	1.4	-42.8	-8.6	1.6	47.2	3.4	0.6	2.1	50
79.5	32	28.3	0.1	19.7	0.1	14.2	2.4	-85.8	-11.3	2	4.2	3.4	2.8	3.1	48
84.5	26.5	37.7	0.4	36.5	0.4	4.9	2.4	-71.3	-25.1	2.9	18.7	3.4	-20.3	3.7	39
85	29	36.4	0.1	24.3	0.1	10.6	2.7	-77.9	-21.2	2.7	12.1	3.4	-10.6	3.8	43
85.5	33	38.4	0.2	19.4	0.2	25.8	2.6	-100	-2.8	2.3	-10	3.4	23.1	3.5	42
85.5	35	34	0.2	15.9	0.2	2.1	2.2	-62.6	-20.9	1.7	27.4	3.4	-18.8	2.8	31
86	27	37.8	0.4	34.9	0.2	24.2	6.9	-72.3	-67.7	7.4	17.7	3.4	-43.5	10.1	43
86.5	36	31.4	0.3	14.1	0.3	3	2.4	-63.3	-23.6	2	26.7	3.4	-20.6	3.1	40
86.5	37	30.2	0.3	11.7	0.4	12.6	3.3	-74.2	-21.5	2.3	15.8	3.4	-8.8	4	51
87	29	38.6	0.1	23	0.1	18.8	3.1	-92.8	-18.3	3.2	-2.8	3.4	0.5	4.5	46
89	23.5	40.4	0.2	35.7	0.2	6.2	1.4	-72.3	-8.9	1.1	17.7	3.4	-2.6	1.8	42
89	26.5	39.2	0.3	34.4	0.3	23.4	6.2	-79.7	-43.2	5.7	10.3	3.4	-19.8	8.5	41
92.5	41.5	31.4	0.1	2.2	0.1	4.2	0.9	-50.9	-7.1	0.9	39.1	3.4	-2.9	1.3	48
93.5	34	49.2	0.2	5.3	0.2	11.3	1.9	-54.4	-9.3	1.5	35.6	3.4	1.9	2.4	46
94	31	49.8	0.2	4.6	0.1	12.4	2.2	-45.7	-10	1.6	44.3	3.4	2.4	2.6	43
95	28	43.5	0.4	13.9	0.4	-2.8	4.5	-103.3	-56.9	4.2	-13.3	3.4	-59.7	6.3	70
95.5	31.5	50.2	0.2	0	0.1	11.3	1.6	-26.6	-7.7	1.7	63.4	3.4	3.6	2.3	45
97	40	30.9	0.1	-1.4	0.1	4.3	1.3	-55.8	-15.4	1.9	34.2	3.4	-11.1	2.3	38
98	28.5	39.6	0.1	-10.1	0.2	2.8	1.6	-31.4	-19.8	2.1	58.6	3.4	-17	2.7	35
98	29.5	42.6	0.1	-10.2	0.1	16.1	2.3	-5.7	-9	2	84.3	3.4	7.1	3	44
98.5	24	24.6	0.2	-9.1	0.1	16.9	2.8	-69.5	-23.4	3.8	20.5	3.4	-6.5	4.6	50
99.5	30	43.1	0.1	-13.4	0.1	22.7	2.3	-6.7	-4.7	2.3	83.3	3.4	17.9	3.2	53
73.5	32	29.5	0.2	33.9	0.2	6.5	2.8	-96.6	-21.8	1.8	-6.6	3.3	-15.3	3.3	43
74.5	31.5	29.9	0.3	33.3	0.3	5.8	1.6	-81.9	-15.7	1.9	8.1	3.3	-9.9	2.5	47
78	30.5	32.6	0.4	30.9	0.4	6.9	5.8	-63.3	-62.2	5.5	26.7	3.3	-55.3	8.1	46
78	33.5	26.2	0.2	20.6	0.2	16.3	1.7	-63.7	-13.7	3	26.3	3.3	2.7	3.4	39
78.5	40	29	0.1	16.9	0.1	1.7	1.7	-101	-19.3	1.8	-11	3.3	-17.6	2.5	45

79.5	40	29.3	0.1	16.5	0.1	4.7	1.7	-96.3	-15.5	1.6	-6.3	3.3	-10.8	2.3	45
80.5	33.5	29.7	0.1	17.7	0.1	14.4	1.8	-85.2	-5.5	1.4	4.8	3.3	8.9	2.3	52
82	37	25.8	0.1	14.1	0.1	8.2	1.3	-68.2	-7.3	1.2	21.8	3.3	0.9	1.8	50
83.5	42	31.2	0.1	9.4	0.1	-1	1.8	-86.7	-22.7	1.7	3.3	3.3	-23.7	2.5	31
86.5	29	37.9	0.1	23.3	0.1	13.3	2.3	-91	-17.4	2.7	-1	3.3	-4.1	3.5	38
87.5	29	39.4	0.2	22.8	0.1	17.5	2.9	-94	-24.1	3.7	-4	3.3	-6.6	4.7	47
89	24	40.3	0.2	35.3	0.2	9	1.5	-70.6	-9	1.1	19.4	3.3	0	1.9	42
89	38.5	30.9	0.2	7.2	0.2	14.8	1.9	-67	-19.8	3.7	23	3.3	-5	4.1	41
89.5	23.5	40.8	0.1	35.2	0.1	4.7	1.3	-69.8	-9.1	0.9	20.2	3.3	-4.3	1.6	46
89.5	24	40.8	0.1	34.9	0.1	6.9	1.4	-67.5	-9.3	1	22.5	3.3	-2.4	1.7	40
89.5	37	34	0.5	10.7	0.5	14.4	2.7	-73.5	-25.3	3.8	16.5	3.3	-11	4.6	38
89.5	39.5	30.7	0.2	5.9	0.2	10.5	1.3	-70.5	-8.6	1.8	19.5	3.3	2	2.2	42
90.5	23	40.9	0.1	34.6	0.1	1.4	0.9	-65.5	-8.6	0.9	24.5	3.3	-7.2	1.2	40
92	26.5	40	0.2	27.4	0.2	2.3	3.1	-94.4	-50.2	4.9	-4.4	3.3	-48	5.7	45
92	41	31.3	0.1	2.9	0.1	5.2	1	-52.3	-8.1	1.2	37.7	3.3	-2.9	1.6	42
94	31.5	50.4	0.2	4.6	0.1	15.5	2.5	-51.3	-10.5	1.8	38.7	3.3	5	3	44
94	41	31.3	0.1	0.8	0.1	2.7	0.9	-46	-8.4	0.9	44	3.3	-5.7	1.3	39
96	26.5	36.4	0.3	11.3	0.3	18	3.6	-20	-20.8	2.7	70	3.3	-2.8	4.5	56
97.5	30	44.7	0.1	-7.8	0.1	13	2.2	-179.8	-12.1	2	-89.8	3.3	0.9	3	35
98	26	27.3	0.2	-8.1	0.2	10.4	2.8	-46.1	-19.3	2	43.9	3.3	-8.9	3.5	34
98	40	30.6	0.1	-2.5	0.1	4.5	1.8	-57	-20.4	2.2	33	3.3	-15.9	2.9	37
99	29.5	42	0.1	-13.2	0.1	20.1	1.9	-10.6	-5.1	2.1	79.4	3.3	15	2.8	53
72	36.5	22	0.1	21.2	0.2	3.6	3.2	-71.9	-32	2.1	18.1	3.2	-28.4	3.8	58
73	33.5	29.1	0.1	30.5	0.1	2	0.9	-75.4	-15.1	1.4	14.6	3.2	-13.1	1.7	48
73.5	41.5	26.7	0.1	7.1	0.1	9.2	3.7	-103.6	-36.9	3.6	-13.6	3.2	-27.7	5.2	30
74.5	31	29.9	0.3	34.1	0.3	6.1	1.4	-79.8	-16.5	2.1	10.2	3.2	-10.4	2.5	70
76.5	31	32.6	0.5	32.6	0.5	6.2	3.8	-53.2	-52.5	5.4	36.8	3.2	-46.2	6.6	25
78	34.5	25.9	0.2	20.2	0.2	11.4	1.9	-49.7	-11.1	1.7	40.3	3.2	0.4	2.5	53
79	35.5	26.1	0.1	18.2	0.1	13.2	1.6	-52.3	-10.3	2.1	37.7	3.2	2.9	2.6	43
79	36	25.8	0.1	18.3	0.1	11.1	1.4	-45.7	-9.1	1.7	44.3	3.2	2	2.2	43

80	31.5	28.8	0.2	19.9	0.1	14.1	2.4	-87.1	-13.7	2.1	2.9	3.2	0.3	3.2	44
80	34.5	28	0.1	17.5	0.1	18.2	2	-71.1	-6	1.7	18.9	3.2	12.2	2.7	38
82	27.5	36.2	0.2	35.2	0.2	-1.3	2.4	-82.8	-28.9	2.3	7.2	3.2	-30.2	3.3	38
86	37	29.7	0.3	11.9	0.3	14.1	2.9	-73.4	-21	2.6	16.6	3.2	-6.9	3.9	36
86.5	28.5	37.3	0.1	24.4	0.1	10.5	2.9	-83.1	-27.5	3.1	6.9	3.2	-17	4.3	42
89	25	39.6	0.2	35	0.2	15	1.5	-66.5	-4.1	1.7	23.5	3.2	11	2.1	50
89	33	43.5	0.2	14.9	0.1	20.8	2.8	-67.9	-12.1	2.4	22.1	3.2	8.7	3.7	40
90	40	30.8	0.2	5.2	0.2	8.6	1.1	-65.1	-7.3	1.4	24.9	3.2	1.4	1.8	40
91.5	32.5	48	0.2	9.5	0.1	21.2	3.9	-65.4	-17.7	1.9	24.6	3.2	3.5	4.3	37
93	41.5	31.4	0.1	1.7	0.1	3.7	0.8	-48.8	-7.4	0.9	41.2	3.2	-3.7	1.2	48
93.5	30	48.3	0.2	6.6	0.2	12.7	2.2	-56.9	-14.7	2.1	33.1	3.2	-2.1	3.2	46
94	27.5	41.9	0.4	16.3	0.5	-5.2	4.1	-91.4	-59.2	4	-1.4	3.2	-64.4	5.7	48
94	30.5	49	0.2	4.6	0.1	10.9	1.8	-43.4	-11.3	1.8	46.6	3.2	-0.4	2.5	42
94.5	30.5	48.7	0.2	2.9	0.1	7.4	1.5	-39.7	-12.2	1.7	50.3	3.2	-4.8	2.2	41
94.5	32	50.9	0.2	3.3	0.1	17.5	2.3	-46.4	-8.7	1.7	43.6	3.2	8.8	2.9	78
96	39.5	31.8	0.1	-0.3	0.1	7.6	1.7	-51.3	-14.9	1.8	38.7	3.2	-7.3	2.5	44
96.5	39.5	31.8	0.2	-0.5	0.2	6.6	1.6	-53.6	-16.9	2.1	36.4	3.2	-10.3	2.6	43
97.5	40	30.8	0.1	-1.9	0.1	4.5	1.6	-56.9	-20.4	2.2	33.1	3.2	-15.9	2.8	46
98.5	29.5	42.2	0.1	-11.6	0.1	18.7	2	-8.9	-6.4	1.9	81.1	3.2	12.2	2.8	51
99.5	29.5	41.9	0.1	-14.6	0.1	20.8	1.9	-8.2	-5.2	2.1	81.8	3.2	15.6	2.8	49
99.5	36.5	37.2	0.1	-0.4	0.1	7.1	1.9	-52.1	-18.8	2.2	37.9	3.2	-11.7	2.8	34
100	29.5	41.6	0.1	-15.8	0.1	20.4	2	-179.2	-7.2	2.2	-89.2	3.2	13.2	3	50
72	31	30.2	0.2	33	0.2	0.4	1.5	-129.3	-17.9	1.3	-39.3	3.1	-17.5	2	44
72	33	29	0.1	31.7	0.1	3.4	1.5	-80.9	-17.5	1.5	9.1	3.1	-14.1	2.1	35
73	40	26.7	0.2	10.9	0.2	11.7	3.4	-110.6	-35.7	4	-20.6	3.1	-23.9	5.3	48
75	41.5	27.4	0.1	8.3	0.1	9.8	3.9	-106.8	-40.9	3.9	-16.8	3.1	-31.1	5.5	22
76	30	32.2	0.3	34.2	0.3	7.6	2.2	-67	-23.1	2.4	23	3.1	-15.6	3.3	25
76	32.5	29.3	0.3	29.2	0.3	2.5	3.9	-45.6	-68.3	6.6	44.4	3.1	-65.8	7.7	47
76.5	30.5	31.9	0.3	32.7	0.3	5.9	2.9	-59.1	-29.9	2.5	30.9	3.1	-24	3.9	20
78.5	32	27.4	0.3	21.9	0.3	15.6	3.1	-69.7	-22.9	2.9	20.3	3.1	-7.3	4.2	42

78.5	32.5	26.9	0.3	20.7	0.2	17.5	2.7	-75.9	-16.5	2.6	14.1	3.1	0.9	3.7	51
78.5	41	29.7	0.1	15	0.1	4.8	1.6	-100.7	-17.3	1.8	-10.7	3.1	-12.5	2.4	52
79.5	33.5	28.3	0.2	18.1	0.1	19.2	2.6	-79.1	-7.3	1.7	10.9	3.1	11.9	3.1	36
79.5	35.5	26.3	0.1	17.5	0.1	12.3	1.7	-51.7	-11.3	1.9	38.3	3.1	1	2.5	41
79.5	36.5	25.7	0.1	17.6	0.1	8.3	1.3	-42.3	-9.5	1.4	47.7	3.1	-1.2	1.9	48
83	27	36.8	0.3	36.7	0.3	3	2.4	-78.4	-30.9	2.7	11.6	3.1	-27.9	3.6	55
85.5	32.5	38.1	0.1	19.5	0.1	24.7	2.1	-95.6	-2.3	2.1	-5.6	3.1	22.4	3	46
87	29.5	39.4	0.2	22.1	0.1	17.5	2.7	-93.7	-15.1	2.6	-3.7	3.1	2.4	3.8	36
91	37	35.5	0.2	9.8	0.2	11.8	2.8	-72.4	-25.3	2.8	17.6	3.1	-13.5	4	32
92	24.5	38	0.1	31.4	0.1	-19.2	1.9	-173.1	-40	1.6	-83.1	3.1	-59.2	2.5	30
93.5	28.5	45.4	0.3	10.5	0.3	3.8	3.5	-87.5	-41.8	3.7	2.5	3.1	-38	5.1	41
93.5	29	46.6	0.2	7.9	0.2	11.9	3.4	-64.3	-21.4	2	25.7	3.1	-9.4	3.9	46
93.5	31.5	50.1	0.2	6	0.1	15.3	2.4	-57.8	-12.6	1.9	32.2	3.1	2.7	3	44
94	40.5	31.2	0.1	1	0.1	3.7	1.2	-48	-9.7	0.8	42	3.1	-6	1.5	35
94.5	40	31.1	0.1	0.7	0.1	8.5	1.9	-53.6	-11.7	1.1	36.4	3.1	-3.2	2.2	41
95	32	51	0.2	1.9	0.1	14.8	2	-37.4	-8.7	1.7	52.6	3.1	6.1	2.6	48
96.5	31.5	49.8	0.2	-2.7	0.1	13.1	1.7	-12.7	-9.7	2	77.3	3.1	3.4	2.6	39
97	39.5	31.7	0.1	-0.7	0.1	5.4	1.6	-56	-20.9	2.3	34	3.1	-15.5	2.8	39
100	25	28.2	0.1	-14.9	0.1	15.3	2.8	-86	-19.7	2.6	4	3.1	-4.4	3.9	40
72	33.5	28.9	0.1	30.8	0.1	1.6	1.1	-72.4	-17.1	1.6	17.6	3	-15.4	1.9	43
72	39.5	24.8	0.3	11.2	0.3	6.8	3.7	-123.4	-50.9	4.4	-33.4	3	-44.1	5.9	47
73.5	38.5	22	0.3	21.4	0.3	20.1	3.9	-101.8	-33.5	4	-11.8	3	-13.4	5.6	32
74	32	29.9	0.3	33.6	0.3	6.7	2.1	-91.5	-18.5	1.6	-1.5	3	-11.8	2.6	51
75	38	24.8	0.1	22.5	0.1	29.7	3.5	-95	-7.4	1.8	-5	3	22.3	3.9	78
76	41.5	27.7	0.1	10.6	0.1	10.1	4.5	-105.3	-51.7	4.6	-15.3	3	-41.6	6.5	44
76.5	32.5	28.3	0.3	27.5	0.3	0.7	4	-44.7	-55.7	4.2	45.3	3	-55	5.9	43
76.5	40.5	28.8	0.1	13.9	0.1	7.6	2.8	-88.8	-29.1	2.5	1.2	3	-21.5	3.7	36
77	31.5	29.9	0.4	29.9	0.4	5.4	5	-55.5	-67.2	5.7	34.5	3	-61.7	7.6	50
77	34.5	25.8	0.1	22.5	0.1	4.8	2.3	-41.7	-25.9	2.3	48.3	3	-21.1	3.3	49
77.5	41	29	0.1	13.7	0.1	12.8	2.1	-106.6	-21.3	2.9	-16.6	3	-8.5	3.6	55

78	36	25.6	0.1	20.1	0.1	12.1	1.6	-47.3	-10.6	1.7	42.7	3	1.5	2.4	43
78.5	33.5	26.6	0.2	19.5	0.2	20.2	1.7	-72.9	-8.3	2.4	17.1	3	11.9	2.9	40
78.5	35.5	25.8	0.1	19.1	0.1	12.7	1.7	-50.9	-10.8	1.8	39.1	3	1.9	2.5	46
79.5	32.5	28.4	0.1	19.1	0.1	15.4	2.3	-87.3	-11.1	1.8	2.7	3	4.3	2.9	33
79.5	34	27.8	0.2	18	0.1	20.4	2.3	-72	-6.5	1.7	18	3	13.9	2.9	42
80	33	29.2	0.1	18.2	0.1	14	2	-87	-9	1.5	3	3	5	2.5	39
80	36.5	25.6	0.1	16.9	0.1	7.3	1.4	-43	-10	1.2	47	3	-2.7	1.8	47
80	40	29.5	0.2	16.1	0.2	6	1.3	-97.4	-13.5	1.5	-7.4	3	-7.5	2	22
80.5	33	29.9	0.1	18	0.1	13.3	1.7	-89.8	-8	1.5	0.2	3	5.4	2.3	40
86	28.5	36.9	0.1	24.9	0.1	3.1	2.8	-75.2	-36.2	3	14.8	3	-33.1	4.1	42
86	29.5	37.8	0.2	22.7	0.1	16.8	2.3	-88.8	-16.1	2.6	1.2	3	0.8	3.4	15
86	32	39.1	0.1	19.5	0.1	23.6	1.8	-84.4	-2.6	2.1	5.6	3	21.1	2.8	71
87.5	29.5	40	0.2	21.7	0.1	14.3	2.3	-91.8	-17.3	2.6	-1.8	3	-3.1	3.4	54
87.5	37.5	30.6	0.4	10.1	0.4	13.7	2.5	-73.9	-21.3	2.6	16.1	3	-7.6	3.6	42
88	29	40	0.2	22.6	0.2	12	2.6	-93.8	-28.2	3.4	-3.8	3	-16.2	4.2	35
89	24.5	39.9	0.2	35.1	0.2	13	1.5	-66.7	-7.6	1.4	23.3	3	5.4	2	40
89.5	24.5	40.6	0.1	34.7	0.2	12.2	1.4	-63	-7.9	1.3	27	3	4.3	1.9	37
89.5	27	40.6	0.2	30.9	0.2	14.4	5.4	-84.3	-41.8	2.8	5.7	3	-27.4	6.1	43
89.5	37.5	33.4	0.4	9.5	0.4	14.7	2.5	-71.7	-26.8	3.6	18.3	3	-12.2	4.4	42
92	40.5	31.3	0.1	3.1	0.1	5.9	1.1	-49	-10.9	1.4	41	3	-5	1.8	42
92.5	24.5	35.9	0.1	30.2	0.1	-13.7	2.1	-2.3	-38.5	1.7	87.7	3	-52.1	2.7	25
92.5	41	31.4	0.1	2.4	0.1	4.6	1	-50.5	-8.4	1	39.5	3	-3.7	1.4	47
93	41	31.4	0.1	1.9	0.1	4	0.9	-49.1	-8.5	0.9	40.9	3	-4.5	1.3	46
93.5	41	31.4	0.1	1.4	0.1	3.3	0.9	-47.2	-8.6	0.8	42.8	3	-5.3	1.2	67
95.5	26	34.6	0.3	14.4	0.3	22.8	2.8	-11.5	-12.5	2.4	78.5	3	10.3	3.6	34
97.5	39.5	31.5	0.1	-1.1	0.1	4.7	1.7	-55.5	-24	2.4	34.5	3	-19.4	3	47
99	24	25.4	0.2	-10.5	0.1	18.7	3.3	-76.1	-24.2	3	13.9	3	-5.5	4.5	58
99	25.5	25.9	0.1	-14.2	0.1	28.5	3.8	-71.8	-16	2.7	18.2	3	12.5	4.6	41
100	27.5	34.6	0.1	-18.4	0.1	20.2	2.1	-120.2	-7.9	2.1	-30.2	3	12.3	2.8	46
72	38	20.2	0.3	17.9	0.3	24.3	5.1	-123.9	-42.4	4.9	-33.9	2.9	-18.1	6.9	55

74.5	33.5	30	0.2	31.6	0.2	11.6	2.4	-66.3	-23.1	2.6	23.7	2.9	-11.4	3.6	26
76	38.5	27	0.1	21.6	0.1	10.9	1.9	-102	-16.3	2	-12	2.9	-5.5	2.8	49
76	42	27.9	0.1	8	0.1	11.7	4.3	-107.2	-50	4.7	-17.2	2.9	-38.3	6.3	39
76.5	39	28.1	0.1	20.4	0.1	-2.6	1.9	-99.2	-30.7	2.1	-9.2	2.9	-33.3	2.8	38
77.5	35	25.8	0.2	21.2	0.1	8	2.2	-41.5	-17.3	1.4	48.5	2.9	-9.3	2.6	44
78	39.5	28.4	0.1	18.3	0.1	-0.3	1.6	-103.8	-26.7	2.2	-13.8	2.9	-27.1	2.7	45
79	32.5	27.5	0.2	19.7	0.2	17.9	2.5	-83.2	-12.4	2	6.8	2.9	5.6	3.2	43
79	35	26.4	0.2	18.3	0.1	15.7	1.7	-61.3	-10.4	1.9	28.7	2.9	5.3	2.6	40
79.5	33	28.5	0.2	18.5	0.1	17.1	2.4	-85.4	-9.8	1.7	4.6	2.9	7.3	2.9	33
80	32	28.9	0.1	19.3	0.1	13.9	1.9	-90.3	-10.9	1.7	-0.3	2.9	3	2.5	39
80	40.5	30	0.1	15.4	0.1	6.8	1.4	-95	-15.6	1.8	-5	2.9	-8.7	2.3	27
80.5	34	29.4	0.1	17.5	0.1	18.7	1.8	-79.5	-4.2	1.5	10.5	2.9	14.6	2.4	62
80.5	40	29.8	0.2	15.8	0.2	6.5	1.2	-98	-13.1	1.6	-8	2.9	-6.6	2	36
82.5	27	36.8	0.3	35.9	0.3	1.3	1.9	-78.9	-27.4	2.3	11.1	2.9	-26.1	3	28
83	42	31.3	0.1	9.4	0.1	-0.4	2	-92	-27.7	2	-2	2.9	-28.1	2.8	42
85	33	37.3	0.2	19	0.2	24.5	2.2	-100.1	-5.3	2.1	-10.1	2.9	19.2	3.1	37
85.5	30	37.3	0.2	22.2	0.2	20.3	2.6	-88.6	-13.7	2.2	1.4	2.9	6.6	3.5	39
85.5	36.5	30.3	0.2	13	0.2	10.4	2.5	-60.8	-24.8	2.6	29.2	2.9	-14.4	3.6	58
86.5	29.5	38.6	0.2	22.4	0.1	16.6	2.2	-93.2	-15.3	2.5	-3.2	2.9	1.3	3.3	47
88	29.5	40.6	0.2	21.3	0.1	12	2.1	-91.7	-19.8	2.5	-1.7	2.9	-7.8	3.3	41
88	38	30.8	0.3	8.6	0.3	14.4	1.9	-69.8	-19.7	2.9	20.2	2.9	-5.3	3.5	41
90	25	41	0.1	34	0.1	13.5	1.7	-47.5	-10.8	2.2	42.5	2.9	2.7	2.5	36
90	27.5	41	0.2	27.7	0.2	-4	3.9	-91.8	-61.5	4.3	-1.8	2.9	-65.5	5.9	45
91	23.5	40.6	0.1	33.8	0.1	-3.7	0.8	-36.7	-16.5	1.1	53.3	2.9	-20.2	1.3	43
91	38	34.3	0.2	7.3	0.2	15.9	3.5	-74.6	-26.8	2.3	15.4	2.9	-10.9	4.2	38
92	32.5	48.7	0.2	8.4	0.1	19.2	3.1	-66.3	-16.9	1.9	23.7	2.9	2.2	3.7	39
93	30	48.1	0.2	8.6	0.1	16.6	2.7	-63.2	-15.6	2	26.8	2.9	0.9	3.3	46
95.5	32	50.9	0.2	0.5	0.1	13.8	1.7	-31.1	-9.2	1.6	58.9	2.9	4.6	2.4	44
95.5	39.5	31.9	0.1	0.1	0.1	9.6	1.9	-51.2	-14.7	1.6	38.8	2.9	-5.1	2.4	40
97	31.5	49.3	0.2	-3.8	0.2	14.7	1.8	-7.9	-11.1	2	82.1	2.9	3.7	2.7	39

97.5	31	48	0.2	-5.8	0.2	17.5	1.9	-176.8	-10.1	2.1	-86.8	2.9	7.4	2.8	41
97.5	31.5	48.9	0.2	-4.8	0.2	16.7	2	-6.1	-11.1	2	83.9	2.9	5.7	2.8	42
98.5	30	43.8	0.1	-10.4	0.1	21.3	2.1	-2.5	-7.5	1.8	87.5	2.9	13.8	2.8	55
98.5	39.5	31.1	0.1	-2.4	0.1	6	2	-55.3	-21.7	2.1	34.7	2.9	-15.7	2.8	26
99	30	43.4	0.1	-11.9	0.1	22.7	2	-6.6	-6.1	2	83.4	2.9	16.6	2.9	47
99	37	36.7	0.1	-0.3	0.1	5.9	1.8	-54.7	-21	2.2	35.3	2.9	-15.2	2.8	38
99	39.5	30.9	0.1	-2.9	0.1	5.3	1.8	-52.2	-20	2	37.8	2.9	-14.6	2.6	62
99.5	39	31.6	0.1	-3	0.1	6.2	2.2	-49.1	-23.4	2.1	40.9	2.9	-17.2	3	57
100	23	26.9	0.2	-11.8	0.2	16.6	3.6	-61.5	-31.9	3.2	28.5	2.9	-15.3	4.8	48
72	32	29	0.2	33.5	0.2	2.7	1.5	-91.3	-17	1	-1.3	2.8	-14.3	1.8	35
72.5	33.5	29	0.1	30.6	0.1	2	0.9	-72.5	-16.6	1.4	17.5	2.8	-14.6	1.7	36
73.5	32.5	29.7	0.2	32.9	0.2	7.4	2.4	-97.7	-21.9	1.6	-7.7	2.8	-14.6	2.8	38
74	40.5	26.6	0.1	12	0.1	7.9	3.5	-100.9	-42.8	2.9	-10.9	2.8	-34.8	4.6	38
75.5	41.5	27.5	0.1	9.5	0.1	7.2	4.5	-110.9	-55.5	4.3	-20.9	2.8	-48.3	6.2	31
76	35.5	25.7	0.1	23.2	0.1	10	1.8	-73.1	-14.7	1.6	16.9	2.8	-4.8	2.4	37
76.5	36	25.5	0.1	22.4	0.1	7.8	1.4	-60.4	-11	1.3	29.6	2.8	-3.2	1.9	39
76.5	42	28.2	0.1	8.9	0.1	13.7	4.9	-106.5	-59.7	5.4	-16.5	2.8	-46	7.2	54
77	35	26	0.1	22.3	0.1	6	2.2	-47.4	-21.5	1.6	42.6	2.8	-15.5	2.7	48
77.5	36	25.6	0.1	21	0.1	10.8	1.6	-49.5	-11.4	1.5	40.5	2.8	-0.6	2.2	43
78	33	26.2	0.3	21	0.3	19.1	2.3	-69.1	-20.5	3	20.9	2.8	-1.4	3.8	33
78	35	25.9	0.2	20.2	0.1	11.2	1.8	-49.5	-12.9	1.4	40.5	2.8	-1.7	2.3	47
78.5	33	26.5	0.3	19.9	0.2	21	2.2	-78.4	-12.6	2.5	11.6	2.8	8.4	3.3	37
79	30.5	31.6	0.4	28	0.3	0.4	5.5	-66.9	-73	4.5	23.1	2.8	-72.6	7.1	48
79.5	31	29.4	0.3	23	0.3	6.3	3.5	-67	-49.3	3.9	23	2.8	-43	5.3	57
79.5	36	25.9	0.1	17.6	0.1	10.2	1.4	-45	-10.2	1.4	45	2.8	0	2	48
80	32.5	29.1	0.1	18.7	0.1	13.8	1.8	-90.1	-10.5	1.7	-0.1	2.8	3.3	2.5	38
81	32.5	30.4	0.1	18.4	0.1	14	1.6	-93.6	-9.7	1.7	-3.6	2.8	4.4	2.3	39
81	33	30.5	0.1	18	0.1	14.1	1.5	-92.5	-7.4	1.5	-2.5	2.8	6.7	2.1	45
81.5	40.5	30.6	0.1	14.2	0.1	2.2	1.2	-84.6	-20.5	2	5.4	2.8	-18.3	2.3	56
82.5	42	31.3	0.1	9.2	0.1	0.3	1.9	-91.6	-28	1.9	-1.6	2.8	-27.7	2.7	56

85	30	36.4	0.2	22.4	0.2	17.7	2.5	-89.3	-14.3	2.1	0.7	2.8	3.4	3.2	41
85.5	32	38	0.1	19.6	0.1	23.1	1.7	-89.5	-4	2	0.5	2.8	19.1	2.6	47
86	30	38.3	0.2	21.9	0.2	20.6	2.3	-89.7	-13.8	2.5	0.3	2.8	6.8	3.4	62
86.5	30	39.3	0.2	21.6	0.2	19.1	2.4	-92.2	-14.5	2.4	-2.2	2.8	4.6	3.4	54
87	28.5	38	0.2	24.4	0.2	18.6	3.8	-93.3	-30.2	3.4	-3.3	2.8	-11.5	5.1	45
88	26.5	39.1	0.2	35	0.3	5.1	2.6	-77.9	-40.4	3.7	12.1	2.8	-35.3	4.6	39
88.5	29	40.5	0.2	22.3	0.1	10.8	2.6	-93	-28.1	2.9	-3	2.8	-17.3	3.9	42
89	31	43.4	0.1	17.3	0.1	13.3	1.9	-80	-13.8	1.8	10	2.8	-0.5	2.6	37
89.5	25	40.3	0.1	34.6	0.2	15.4	1.5	-59.8	-5.3	1.8	30.2	2.8	10.1	2.1	42
90.5	38	33.7	0.2	7.6	0.2	16.3	3.2	-73.6	-27.1	2.6	16.4	2.8	-10.9	4.1	47
92	37.5	35.5	0.2	7.5	0.2	9.4	2.7	-67.4	-26.4	2.1	22.6	2.8	-16.9	3.5	40
93.5	33.5	49.5	0.2	5.3	0.2	13.6	1.6	-54.2	-8.1	1.4	35.8	2.8	5.5	2.1	45
94.5	28	43.4	0.4	14	0.4	-0.2	3.7	-103.6	-58.1	4.2	-13.6	2.8	-58.4	5.6	41
97.5	27.5	36.8	0.3	-4.5	0.3	6.7	2.9	-36.1	-38.1	3.4	53.9	2.8	-31.3	4.4	40
97.5	37	37.3	0.1	1.7	0.1	6.9	1.6	-56.6	-18.5	1.7	33.4	2.8	-11.7	2.4	56
98	30	44.2	0.1	-9.1	0.1	19.8	2.2	-176.5	-9.8	1.8	-86.5	2.8	10	2.9	46
98	37.5	36.5	0.1	0.5	0.1	5.4	2	-52	-22.6	1.8	38	2.8	-17.2	2.7	34
98	39.5	31.3	0.1	-1.7	0.1	5.6	1.8	-55.4	-23.6	2.2	34.6	2.8	-18	2.9	39
99.5	30.5	44.6	0.1	-12	0.1	24.7	2.2	-3.5	-11.1	2.8	86.5	2.8	13.6	3.5	49
99.5	37.5	35.9	0.1	-1.5	0.1	10	2.1	-51.5	-22.3	2.5	38.5	2.8	-12.2	3.2	34
100	27	32.4	0.1	-18.3	0.1	22.5	2.3	-105.2	-14.5	2.7	-15.2	2.8	8	3.6	51
100	37.5	35.8	0.1	-2.1	0.1	9.9	2.2	-49.1	-22.9	2.3	40.9	2.8	-13	3.2	43
72.5	31.5	29	0.2	34.5	0.2	3.8	1.6	-93.8	-17.7	1.1	-3.8	2.7	-14	1.9	37
72.5	33	29.1	0.1	31.5	0.1	3.8	1.3	-81.8	-18.1	1.2	8.2	2.7	-14.3	1.8	32
73	33	29.3	0.1	31.4	0.1	4.3	1.3	-87.1	-17.7	1.2	2.9	2.7	-13.5	1.8	45
73.5	40	27	0.2	12	0.2	12.8	3.7	-116.2	-39.9	3.4	-26.2	2.7	-27.1	4.9	25
74	32.5	30	0.2	33	0.2	7.4	2	-95.1	-18.8	1.6	-5.1	2.7	-11.3	2.5	54
74	33	30.1	0.2	32.4	0.2	8.9	1.8	-96.5	-17.7	1.8	-6.5	2.7	-8.8	2.5	55
74	40	27.1	0.1	13.8	0.1	9.9	3.7	-110.9	-40	3	-20.9	2.7	-30.1	4.7	35
77	32.5	27.5	0.3	25.8	0.3	4.9	3.6	-50.6	-47.1	3.2	39.4	2.7	-42.2	5	41

77	36	25.6	0.1	21.8	0.1	9.2	1.5	-54.4	-11.7	1.3	35.6	2.7	-2.5	2	40
77	40.5	29.1	0.1	14.2	0.1	5.2	2.5	-97.8	-30.2	2.2	-7.8	2.7	-24.9	3.3	49
77.5	32	27.7	0.3	25.7	0.3	9.6	4.4	-62.8	-63.8	5	27.2	2.7	-54.2	6.6	39
78	35.5	25.8	0.1	20.1	0.1	12	1.8	-48.5	-12.8	1.5	41.5	2.7	-0.8	2.3	46
78.5	34	26.5	0.2	19.4	0.2	19.2	1.6	-65.4	-8	2.1	24.6	2.7	11.3	2.6	48
79	31	30.1	0.3	24.8	0.3	4.3	4.6	-65.1	-57.4	3.7	24.9	2.7	-53.2	5.9	41
79	33	27.4	0.2	19.1	0.2	20.5	2.4	-82.9	-10.3	1.9	7.1	2.7	10.2	3	41
79	33.5	27.3	0.2	18.7	0.2	22.4	2.2	-77.9	-7.8	1.9	12.1	2.7	14.7	2.9	53
80	31	29.2	0.2	21.6	0.2	12.4	3	-72.9	-39.2	3.7	17.1	2.7	-26.8	4.8	52
80.5	32.5	29.8	0.1	18.5	0.1	13.6	1.6	-91.9	-10.1	1.6	-1.9	2.7	3.5	2.2	30
80.5	36.5	25.7	0.1	16.2	0.1	7.5	1.3	-47.7	-10.7	1.1	42.3	2.7	-3.2	1.7	61
80.5	40.5	30.4	0.1	15.3	0.1	7.6	1.3	-93.3	-19.6	2.3	-3.3	2.7	-12	2.7	41
81	28	36.6	0.2	35.2	0.2	3.2	2.1	-46	-27.5	2	44	2.7	-24.3	2.9	39
81.5	32.5	31.2	0.1	18.5	0.1	15.3	1.5	-95.1	-9.5	1.7	-5.1	2.7	5.8	2.3	38
81.5	42	31.2	0.1	8.9	0.1	3.1	2	-89.4	-28.3	2	0.6	2.7	-25.1	2.8	34
82	42	31.3	0.1	9.1	0.1	1.2	1.9	-95.9	-27.3	1.9	-5.9	2.7	-26.1	2.7	48
82.5	37	26.1	0.1	13.6	0.1	12.1	1.3	-65.2	-7.1	1.2	24.8	2.7	5	1.8	31
84.5	29.5	35.6	0.1	23.5	0.1	11.3	1.8	-76.4	-20.1	2.6	13.6	2.7	-8.8	3.1	30
85	32.5	37.1	0.2	19.2	0.1	23.1	1.9	-97.2	-5.6	2	-7.2	2.7	17.4	2.7	42
88	26	39.1	0.2	35.6	0.3	6.7	1.4	-79.9	-23.7	3	10.1	2.7	-17	3.3	46
88.5	29.5	41.1	0.2	20.9	0.1	11.4	2.2	-91.4	-21.7	2.5	-1.4	2.7	-10.2	3.3	41
89	38	32.1	0.3	8.4	0.3	15	1.8	-67.8	-25.7	3.5	22.2	2.7	-10.7	3.9	40
89.5	38.5	31.4	0.2	7	0.2	17.1	1.9	-67.4	-25.8	3.7	22.6	2.7	-8.7	4.1	39
90	38	33.1	0.2	7.9	0.2	16.6	2.8	-71.9	-27.9	3.2	18.1	2.7	-11.3	4.2	41
90.5	27.5	40.8	0.3	26.4	0.2	0.6	3.6	-80.2	-51.7	3.4	9.8	2.7	-51.1	4.9	49
90.5	40	31	0.2	4.8	0.2	8.9	1.1	-61.4	-9.5	1.3	28.6	2.7	-0.6	1.7	48
91	40	31.2	0.2	4.4	0.2	8.6	1.2	-56.3	-10.5	1.4	33.7	2.7	-1.9	1.8	34
92.5	30.5	48.4	0.1	9.8	0.1	17.2	2.1	-67.9	-15.5	2.2	22.1	2.7	1.7	3.1	40
93.5	40.5	31.3	0.1	1.5	0.1	4.4	1.1	-48	-10	0.8	42	2.7	-5.7	1.4	71
94	28.5	45	0.4	10.9	0.4	-1.2	2.7	-95.8	-56.7	4.5	-5.8	2.7	-57.9	5.2	36

94	32	50.5	0.2	4.5	0.1	17	2.1	-55.2	-11	1.7	34.8	2.7	6.1	2.6	47
96	26	33.7	0.3	10.7	0.3	28.8	3.8	-11.4	-17.9	2.2	78.6	2.7	10.9	4.4	42
97.5	26	29.1	0.3	-3.2	0.3	15.2	3.4	-24.3	-29.6	2.5	65.7	2.7	-14.4	4.2	28
97.5	30.5	46.4	0.1	-6.8	0.1	18.4	1.9	-174	-11.2	2.1	-84	2.7	7.2	2.8	38
98	31.5	48.4	0.2	-5.7	0.2	19.3	2.1	-9.5	-11.4	1.9	80.5	2.7	7.9	2.9	38
98.5	25.5	25	0.2	-11.4	0.2	28.3	3.6	-63.2	-19.3	2.8	26.8	2.7	9.1	4.5	41
100	26	29.4	0.1	-17	0.1	37.6	3.7	-104.1	-20.9	3.9	-14.1	2.7	16.8	5.3	45
100	26.5	30.8	0.1	-17.8	0.1	29.9	3.7	-100.4	-19.8	2.8	-10.4	2.7	10.2	4.7	43
74	38.5	22.5	0.3	22.1	0.3	27.3	3.5	-93.9	-24.5	3.1	-3.9	2.6	2.7	4.7	52
74.5	41	27	0.1	9.9	0.1	11.3	3.5	-95.8	-44.3	3.5	-5.8	2.6	-33	5	62
75	40.5	27.7	0.1	12.3	0.1	15.8	3.4	-83.7	-34.4	3	6.3	2.6	-18.6	4.5	47
77	30.5	31.6	0.3	31.7	0.3	7.5	2.8	-60.9	-30	2	29.1	2.6	-22.6	3.4	42
77	34	25.8	0.2	22.9	0.2	5.8	2.2	-42.4	-32.8	2.7	47.6	2.6	-27.1	3.5	44
77.5	33.5	26.2	0.2	22	0.2	10.9	1.8	-50.6	-28.4	3.1	39.4	2.6	-17.5	3.5	46
77.5	39.5	28.5	0.1	18.4	0.1	-2.6	1.6	-103.9	-30.8	2	-13.9	2.6	-33.4	2.6	57
78	32	27.6	0.3	23.9	0.3	14.9	3.4	-64.5	-41.7	3.9	25.5	2.6	-26.9	5	29
78	32.5	26.9	0.3	22.3	0.3	14.9	2.6	-66.7	-28.3	3	23.3	2.6	-13.5	3.9	34
78.5	35	26.1	0.2	19.2	0.1	13.9	1.6	-56.3	-11.5	1.6	33.7	2.6	2.4	2.3	47
79.5	30	32.4	0.3	29.9	0.3	5.4	5.6	-68.1	-73.5	4.5	21.9	2.6	-68.1	7.1	46
80	35	27.2	0.1	17.2	0.1	15.7	1.6	-63.3	-10	1.5	26.7	2.6	5.6	2.3	46
80	41	30.4	0.1	14.5	0.1	6.2	1.5	-89.4	-20.3	2	0.6	2.6	-14.1	2.5	34
80.5	28.5	37.6	0.2	37	0.2	1.6	2.8	-63.3	-50.1	4.1	26.7	2.6	-48.5	4.9	50
80.5	32	29.6	0.1	19.1	0.1	14.3	1.6	-92.2	-11	1.6	-2.2	2.6	3.2	2.3	23
81.5	32	31.1	0.1	19	0.1	15.6	1.7	-93.5	-11.4	1.7	-3.5	2.6	4.1	2.4	34
82	32	31.9	0.1	19.1	0.1	16.8	1.7	-94.6	-11.2	1.8	-4.6	2.6	5.7	2.5	48
82.5	27.5	36.1	0.3	37.2	0.3	1.5	2.9	-81.6	-51.8	4.1	8.4	2.6	-50.4	5	40
82.5	41.5	31.2	0.1	10.9	0.1	-1.3	1.8	-89.1	-30.6	2	0.9	2.6	-31.9	2.7	54
83.5	27	37	0.3	37	0.3	4	2.6	-76.8	-37.3	3	13.2	2.6	-33.3	4	48
84.5	32.5	36.2	0.2	19	0.1	20.6	1.7	-94.7	-7.4	1.8	-4.7	2.6	13.2	2.5	46
85	33.5	36.9	0.2	18.4	0.2	17.3	1.8	-87.3	-9.8	1.6	2.7	2.6	7.5	2.5	45

85.5	28.5	36.9	0.1	25.9	0.1	4.4	3.2	-77.1	-40	2.6	12.9	2.6	-35.6	4	41
86	32.5	39.1	0.1	19.1	0.1	21.1	1.4	-81.3	-5.7	2	8.7	2.6	15.4	2.4	72
87	30	40	0.2	21.2	0.2	15.6	2.2	-89.9	-14.9	1.8	0.1	2.6	0.7	2.8	42
88.5	33	42.7	0.2	15.6	0.1	19.1	2.1	-68.7	-10.9	1.7	21.3	2.6	8.2	2.7	44
89	29	41	0.2	21.9	0.1	12.9	2.4	-89.6	-26.9	2.8	0.4	2.6	-14	3.7	46
89.5	36.5	34.5	0.4	11.6	0.4	16.2	1.9	-73	-22.1	2.9	17	2.6	-5.9	3.5	39
89.5	38	32.5	0.2	8.2	0.3	16	2.2	-69.6	-28.1	3.5	20.4	2.6	-12.1	4.1	43
92.5	40.5	31.4	0.1	2.6	0.1	5.5	1	-48.8	-10.6	1.1	41.2	2.6	-5.1	1.5	40
93	31.5	49.7	0.2	7.3	0.1	15.3	1.8	-62.5	-14.4	1.9	27.5	2.6	0.9	2.7	39
93	40.5	31.3	0.1	2.1	0.1	5	1	-48.5	-10.3	0.9	41.5	2.6	-5.3	1.4	46
93.5	29.5	47.4	0.2	7.1	0.2	13.2	2.5	-60.1	-18.6	1.8	29.9	2.6	-5.5	3.1	42
93.5	34.5	48.7	0.2	5.1	0.1	15.1	2.2	-52.6	-15.1	1.7	37.4	2.6	-0.1	2.7	47
94	33.5	49.8	0.2	4.4	0.2	16.2	1.5	-49	-7.3	1.4	41	2.6	8.8	2.1	43
94	34	49.5	0.2	4.5	0.2	15	1.6	-44.9	-9.3	1.5	45.1	2.6	5.6	2.2	40
94.5	33.5	50.1	0.2	3.6	0.2	17.7	1.6	-43.7	-8.4	1.7	46.3	2.6	9.3	2.4	58
96	27	38.7	0.3	11.5	0.3	15.4	3.6	-34.6	-37.1	3.2	55.4	2.6	-21.8	4.8	64
96	32	50.7	0.2	-0.7	0.1	14.2	1.7	-23.1	-10.9	1.7	66.9	2.6	3.3	2.4	45
97	37.5	36.5	0.1	1.5	0.1	10.4	1.8	-60.2	-19.2	1.8	29.8	2.6	-8.8	2.6	48
97.5	23.5	25.1	0.2	-5.6	0.2	13.9	3.5	-48.3	-30.4	2.1	41.7	2.6	-16.5	4.1	33
98	37	37.2	0.1	1.1	0.1	5	1.4	-52.5	-20.7	1.7	37.5	2.6	-15.7	2.3	48
98.5	37	36.9	0.1	0.4	0.1	4.4	1.5	-52.4	-21.5	1.8	37.6	2.6	-17.1	2.3	38
99	39	31.9	0.1	-2.4	0.1	8.7	2.3	-51.1	-25	2.1	38.9	2.6	-16.3	3	42
72	34	28.4	0.1	29.9	0.1	1.8	1.1	-63.3	-21.1	1.7	26.7	2.5	-19.3	2	28
73	34	28.1	0.1	29.7	0.1	3.1	1.1	-58.3	-18.6	1.6	31.7	2.5	-15.5	1.9	50
73.5	33	29.6	0.1	31.7	0.1	5.5	1.4	-94	-17.7	1.3	-4	2.5	-12.2	1.9	43
74	31	29.6	0.3	34.8	0.3	5.7	1.4	-83.2	-17.7	1.5	6.8	2.5	-12	2.1	13
74	36.5	23.8	0.1	22.5	0.2	11.3	1.3	-90.3	-10.5	1.5	-0.3	2.5	0.9	2	39
74	37	23.2	0.2	21.7	0.2	16.9	1.3	-100.5	-7.1	1.8	-10.5	2.5	9.8	2.2	36
75.5	33	29.6	0.3	29.8	0.3	6.2	2.3	-50.7	-31.5	2.3	39.3	2.5	-25.3	3.2	30
77.5	32.5	27.1	0.3	24	0.3	11.9	3.3	-60.9	-41.4	3.2	29.1	2.5	-29.4	4.5	40

79	34	27	0.2	18.5	0.2	22.5	1.9	-70.7	-7	1.8	19.3	2.5	15.5	2.6	48
79	34.5	26.6	0.2	18.4	0.2	19.6	1.7	-67	-8.6	1.7	23	2.5	11	2.5	40
79.5	28.5	35.9	0.2	35.7	0.2	8.7	1.3	-81	-24.1	2.6	9	2.5	-15.3	3	39
80.5	29	36.2	0.2	34.6	0.2	18.5	6.6	-68.6	-76.5	6.1	21.4	2.5	-58	8.9	40
81	32	30.4	0.1	19	0.1	15	1.7	-92.6	-11.5	1.6	-2.6	2.5	3.5	2.3	45
81	33.5	30.5	0.1	17.7	0.1	16.1	1.4	-88.5	-5.9	1.3	1.5	2.5	10.2	1.9	37
81	40.5	30.8	0.1	15.2	0.1	6.7	1.4	-89.9	-26.8	2.6	0.1	2.5	-20.1	2.9	33
82.5	32	32.7	0.1	19.1	0.1	18.1	1.7	-88.5	-10.9	1.8	1.5	2.5	7.2	2.5	31
83	37	26.5	0.1	13.1	0.1	13.7	1.4	-67.8	-8.3	1.2	22.2	2.5	5.4	1.9	15
84	32	35.2	0.1	19.3	0.1	18.5	1.7	-91.1	-10	1.7	-1.1	2.5	8.5	2.4	35
84	32.5	35.3	0.2	18.8	0.1	19.1	1.6	-91.9	-8.3	1.7	-1.9	2.5	10.8	2.4	49
84.5	32	36.1	0.2	19.4	0.1	19.4	1.6	-92.5	-9.2	1.8	-2.5	2.5	10.2	2.4	45
84.5	33	36.3	0.1	18.6	0.1	21.3	1.8	-95	-7.4	1.8	-5	2.5	13.9	2.5	42
85	26.5	38.1	0.5	38	0.4	6.2	2	-73.2	-43.3	3.9	16.8	2.5	-37.1	4.4	48
85	32	37	0.1	19.6	0.1	21.3	1.5	-91.9	-6.8	1.9	-1.9	2.5	14.5	2.4	37
85	34	36.1	0.2	17.6	0.2	11.6	1.7	-79	-13.9	1.4	11	2.5	-2.3	2.2	44
85	34.5	35.1	0.2	16.7	0.2	8.1	1.8	-71.7	-17.1	1.3	18.3	2.5	-9	2.2	44
85	35	34.2	0.2	15.8	0.2	8.3	1.9	-65.7	-20.2	1.5	24.3	2.5	-11.9	2.5	45
86.5	31.5	40	0.1	19.5	0.1	22.1	1.7	-78.7	-8.2	2.1	11.3	2.5	13.9	2.7	40
87	30.5	40.4	0.2	20.4	0.2	16.8	2.1	-84	-13.9	1.7	6	2.5	2.8	2.7	36
87.5	30	40.6	0.1	20.8	0.1	12.9	1.9	-89.8	-16.1	1.7	0.2	2.5	-3.2	2.5	53
88	27	38.6	0.2	33	0.2	4	3.8	-79.8	-53.8	3.8	10.2	2.5	-49.8	5.3	28
88.5	30.5	42.3	0.1	18.9	0.1	12.9	1.9	-85.6	-15.7	1.5	4.4	2.5	-2.8	2.4	43
88.5	38	31.4	0.3	8.5	0.3	14.8	1.5	-69.2	-21.7	3	20.8	2.5	-6.9	3.3	42
89	30.5	42.9	0.1	18.2	0.1	13.3	2	-82.3	-16.1	1.6	7.7	2.5	-2.8	2.5	34
89	37.5	32.9	0.3	9.6	0.4	14.8	1.7	-70.9	-25.8	3.3	19.1	2.5	-11	3.7	39
89.5	27.5	41	0.2	28.3	0.2	21.2	5.4	-92.6	-72.7	5.9	-2.6	2.5	-51.5	8	45
89.5	31	44	0.1	16.5	0.1	14.7	1.7	-77.2	-14.2	1.8	12.8	2.5	0.5	2.5	44
90	39.5	30.9	0.2	5.5	0.2	10.8	1.1	-66.2	-11.7	1.5	23.8	2.5	-0.9	1.9	40
91	23	40.7	0.1	34.1	0.1	0.9	0.8	-48.6	-12.3	0.9	41.4	2.5	-11.4	1.2	40

91.5	24	39.2	0.1	32.8	0.1	-9.3	1.2	-22	-27.4	1.1	68	2.5	-36.7	1.6	39
91.5	36.5	37.7	0.3	8.8	0.2	29.6	2.6	-51.4	-18.6	3.5	38.6	2.5	11	4.2	42
91.5	40	31.5	0.1	3.9	0.2	7.5	1.1	-51.1	-12.8	1.5	38.9	2.5	-5.3	1.8	43
92.5	31	49	0.1	9.1	0.1	17.2	1.8	-66.5	-15.9	2.2	23.5	2.5	1.3	2.8	46
92.5	32.5	49.2	0.2	7.4	0.2	16.5	2.1	-64.5	-15.2	1.8	25.5	2.5	1.3	2.8	40
93	33	49.4	0.2	6.2	0.2	14.5	1.7	-60.1	-11	1.5	29.9	2.5	3.5	2.2	42
93.5	27	40.4	0.3	20.4	0.3	-8.6	3	-83.2	-63.8	3.8	6.8	2.5	-72.4	4.8	37
94	40	31.2	0.1	1.2	0.1	8.8	1.6	-52.8	-12.5	0.9	37.2	2.5	-3.7	1.9	36
94.5	32.5	50.8	0.2	3.4	0.2	19.6	2	-49.6	-9	1.5	40.4	2.5	10.6	2.5	73
94.5	33	50.5	0.2	3.5	0.2	19.4	1.8	-48.4	-8.3	1.7	41.6	2.5	11.1	2.4	63
94.5	34	49.8	0.2	3.8	0.2	16.8	1.6	-36.9	-11.7	1.8	53.1	2.5	5.1	2.5	45
95	25.5	31.8	0.2	16.8	0.2	20	2.1	-11.1	-17	2.5	78.9	2.5	2.9	3.3	26
96.5	26	32.8	0.4	6.9	0.4	34.7	4.9	-12	-32.2	3.4	78	2.5	2.5	5.9	44
96.5	26.5	35.7	0.4	7.7	0.4	18.2	4	-29.3	-55.4	5	60.7	2.5	-37.1	6.4	53
96.5	37.5	36.3	0.1	1.9	0.1	10.9	1.7	-63.8	-18.7	1.9	26.2	2.5	-7.8	2.5	38
97	37	37.3	0.1	2.2	0.1	9.6	1.7	-60.1	-17.3	1.5	29.9	2.5	-7.6	2.3	49
97.5	25	24.5	0.2	-5.3	0.2	24.1	3	-38.5	-30.9	3.8	51.5	2.5	-6.8	4.9	21
97.5	37.5	36.6	0.1	1.1	0.1	8.3	1.9	-54.9	-21.2	1.7	35.1	2.5	-12.8	2.6	47
98	25	23.8	0.2	-8.4	0.2	30	3.6	-54.6	-22.2	2.9	35.4	2.5	7.8	4.7	47
98	25.5	25	0.2	-8.3	0.2	23.8	3.1	-53.5	-19.4	2.3	36.5	2.5	4.4	3.8	45
98	31	47.5	0.2	-6.8	0.2	19.9	1.8	-177.9	-10.8	1.9	-87.9	2.5	9.1	2.6	51
98.5	31.5	48.1	0.2	-6.6	0.2	23	2.4	-13.2	-14	2.2	76.8	2.5	9	3.3	45
98.5	37.5	36.2	0.1	-0.2	0.1	6	2	-50.5	-22.9	1.7	39.5	2.5	-16.9	2.5	40
99	37.5	36	0.1	-0.9	0.1	8.3	2.1	-50.9	-22.9	1.9	39.1	2.5	-14.6	2.7	39
99.5	25.5	27.2	0.1	-15.4	0.1	27.3	2.8	-85.6	-15.8	2.5	4.4	2.5	11.6	3.7	30
100	25.5	28.5	0.1	-15.9	0.1	26.6	2.8	-93.7	-18	2.7	-3.7	2.5	8.6	3.9	41
72.5	37	21.3	0.2	20.3	0.2	15.8	2.4	-84.7	-21.9	1.9	5.3	2.4	-6	3.1	45
74	31.5	29.7	0.2	34.1	0.2	5.3	1.4	-85.7	-17.5	1.3	4.3	2.4	-12.1	1.9	57
74	41	26.5	0.1	9.6	0.1	13	3.6	-100	-45.4	3.1	-10	2.4	-32.4	4.7	38
75.5	30	32	0.2	34.8	0.2	7.7	1.3	-68.3	-22.2	2.1	21.7	2.4	-14.5	2.5	55

76.5	34.5	26.6	0.1	24.1	0.1	4.7	2.1	-56.8	-37.2	2.7	33.2	2.4	-32.5	3.5	51
76.5	35	26.3	0.1	23.2	0.1	7.1	1.9	-62.2	-27.1	2	27.8	2.4	-20	2.8	47
76.5	35.5	25.8	0.1	22.8	0.1	8.6	1.7	-62.4	-17.1	1.3	27.6	2.4	-8.5	2.1	44
77	31	32.1	0.4	31.8	0.4	9.1	3.3	-56.7	-61.8	5	33.3	2.4	-52.7	6	41
77	39.5	28.7	0.1	18.4	0.1	-5.2	1.7	-99.6	-37.8	2	-9.6	2.4	-43	2.7	40
77.5	30.5	31.5	0.3	30.5	0.3	8.6	2.9	-63.1	-31	1.6	26.9	2.4	-22.3	3.3	41
77.5	35.5	25.8	0.1	21.1	0.1	10.5	1.7	-48.7	-15.5	1.3	41.3	2.4	-4.9	2.1	43
77.5	41.5	28.9	0.1	12.2	0.1	15.6	2.7	-100.7	-32.4	2.9	-10.7	2.4	-16.8	4	38
78	40	28.9	0.1	16.9	0.1	1.5	1.4	-105.3	-26.1	1.8	-15.3	2.4	-24.6	2.3	44
78	40.5	29.3	0.1	15.6	0.1	4.3	1.4	-107.7	-21.5	1.7	-17.7	2.4	-17.2	2.2	44
78	41	29.4	0.1	14.5	0.1	8.3	1.5	-104.1	-22.5	2.2	-14.1	2.4	-14.2	2.7	46
78.5	31	30.6	0.3	26.6	0.3	9.9	5.1	-64.5	-61.4	3.3	25.5	2.4	-51.5	6	31
78.5	34.5	26.3	0.2	19.3	0.2	16.4	1.6	-60.1	-10.2	1.7	29.9	2.4	6.2	2.3	46
79.5	41.5	30.2	0.1	13.2	0.1	5.3	2.6	-86.1	-38.2	2.5	3.9	2.4	-33	3.6	45
79.5	42	29.9	0.1	10.8	0.2	11.3	3.4	-80.2	-41.4	2.2	9.8	2.4	-30	4	49
80	29	36.1	0.2	35.3	0.2	17.2	3.5	-70.3	-65.6	6.6	19.7	2.4	-48.3	7.3	41
80	36	25.9	0.1	16.9	0.1	9.9	1.3	-48.1	-11.2	1.1	41.9	2.4	-1.3	1.7	42
81.5	33	31.2	0.1	18	0.1	15.6	1.4	-94.4	-7.7	1.4	-4.4	2.4	7.9	2	41
82	32.5	32	0.1	18.5	0.1	16.8	1.4	-95.8	-9.4	1.6	-5.8	2.4	7.3	2.2	42
82.5	32.5	32.8	0.1	18.6	0.1	17.7	1.4	-89.1	-9.3	1.7	0.9	2.4	8.4	2.2	33
83.5	32.5	34.4	0.1	18.7	0.1	18.3	1.6	-89.9	-8.7	1.6	0.1	2.4	9.6	2.3	45
84.5	31	36	0.2	20.8	0.2	19.7	1.9	-92.4	-15.5	2.1	-2.4	2.4	4.2	2.8	45
84.5	31.5	36	0.2	20	0.2	19.2	1.6	-91.7	-12.1	1.9	-1.7	2.4	7.1	2.5	47
84.5	33.5	36.1	0.2	18.2	0.2	18.1	1.7	-89.5	-9.7	1.5	0.5	2.4	8.5	2.3	40
85	31.5	37	0.2	20.1	0.2	20.7	1.6	-90	-10.5	1.9	0	2.4	10.3	2.5	25
85.5	31.5	37.9	0.2	20.1	0.2	22.7	1.7	-86.3	-8	1.9	3.7	2.4	14.7	2.5	44
86	31.5	39	0.1	19.9	0.2	23.3	1.7	-82.1	-6.7	1.9	7.9	2.4	16.7	2.6	67
86	35	34.2	0.2	15.4	0.2	8	1.8	-59.7	-21.5	1.7	30.3	2.4	-13.4	2.5	54
86.5	32	40	0.1	19	0.1	20.5	1.3	-76.4	-7.5	1.8	13.6	2.4	13.1	2.3	34
87.5	36.5	32.1	0.3	12.5	0.4	12.3	2.2	-74.3	-22.7	1.9	15.7	2.4	-10.4	2.9	47

88	30	41.2	0.1	20.3	0.1	12.2	1.8	-89.4	-17	1.6	0.6	2.4	-4.9	2.4	44
88.5	33.5	42.3	0.2	15.2	0.2	21.7	2	-66.9	-11.9	2	23.1	2.4	9.9	2.8	50
89	29.5	41.7	0.1	20.5	0.1	13.4	2.1	-88.2	-23	2.3	1.8	2.4	-9.6	3.2	40
89	33.5	43.2	0.2	14.3	0.2	22.9	2.1	-66.4	-13	2.2	23.6	2.4	9.9	3	38
90	31	44.6	0.1	15.6	0.1	17.5	1.8	-76.5	-14.6	1.9	13.5	2.4	2.9	2.6	42
90	31.5	45.1	0.1	14.8	0.1	18.7	1.7	-76.9	-15.8	2.3	13.1	2.4	2.9	2.9	42
90	37	34.5	0.3	10.5	0.3	14.5	2.2	-73.1	-26.4	2.7	16.9	2.4	-11.9	3.5	42
90	37.5	33.8	0.2	9.2	0.2	15.3	2.3	-73.3	-26.3	2.6	16.7	2.4	-11.1	3.5	41
90.5	25	41	0.1	33.1	0.1	11.6	1.8	-38.3	-17.6	1.8	51.7	2.4	-6	2.5	38
91	30	45.7	0.1	15.3	0.1	21.3	2.8	-81.4	-19.5	2.2	8.6	2.4	1.8	3.5	42
91	31.5	47	0.2	12.5	0.1	28	3.2	-77.7	-20.1	2.5	12.3	2.4	7.8	4.1	46
91	32	47.3	0.1	11.5	0.1	22.2	2.4	-72.2	-19.5	2.3	17.8	2.4	2.7	3.3	41
92	40	31.6	0.1	3.4	0.1	6.9	1.1	-47.3	-15.1	1.5	42.7	2.4	-8.2	1.9	44
92.5	26.5	40	0.1	27.7	0.2	5.7	3.3	-100.3	-78.4	5.9	-10.3	2.4	-72.7	6.8	49
93	25	35.6	0.1	27.3	0.1	-7.3	2.7	-15.9	-43.8	1.5	74.1	2.4	-51.1	3	46
93	25.5	36.6	0.2	26.8	0.2	-5.2	2.5	-18.2	-40.8	2	71.8	2.4	-46	3.2	45
93	28.5	45.5	0.2	11.5	0.2	12.1	3.1	-81.7	-34.9	2.5	8.3	2.4	-22.8	4	38
93	29	46.4	0.2	10	0.2	16.8	2.9	-67.1	-21.4	1.7	22.9	2.4	-4.6	3.4	42
94.5	29	46.1	0.3	7.7	0.3	-7.3	2.8	-96	-72.9	4.3	-6	2.4	-80.2	5.2	38
95	32.5	51	0.2	2.2	0.1	18.2	1.8	-41.4	-10.4	1.6	48.6	2.4	7.8	2.4	48
95	39.5	32	0.1	0.5	0.1	12.3	1.9	-52.7	-15	1.4	37.3	2.4	-2.7	2.3	47
95.5	25.5	31.5	0.3	13	0.3	25.3	2.6	-16.9	-14.9	2	73.1	2.4	10.3	3.3	29
96	28	43.2	0.3	15.3	0.3	-0.2	5.3	-56.8	-104	7.2	33.2	2.4	-104.2	8.9	61
96.5	32	50.3	0.2	-1.9	0.2	15.2	1.7	-17.9	-13.4	1.9	72.1	2.4	1.9	2.5	46
96.5	37	37.1	0.1	2.6	0.1	11	1.7	-62.1	-17.2	1.5	27.9	2.4	-6.2	2.3	36
97.5	25.5	26.1	0.3	-4.3	0.3	24	3.1	-34.8	-28.4	3	55.2	2.4	-4.4	4.3	22
97.5	26.5	32	0.3	-3.1	0.3	6	2.7	-30.1	-36.3	2.2	59.9	2.4	-30.3	3.5	36
97.5	27	34.5	0.3	-3.6	0.3	2.9	2.4	-35.5	-39	2.5	54.5	2.4	-36.1	3.5	38
97.5	28	39	0.2	-5	0.2	0.6	2.7	-51	-56.5	4.1	39	2.4	-56	4.8	38
98.5	31	47.1	0.2	-7.9	0.2	22.4	1.9	-0.2	-11.3	2	89.8	2.4	11.1	2.8	43

98.5	39	32.2	0.1	-1.7	0.1	10.8	2.1	-52.7	-25.7	2.4	37.3	2.4	-14.8	3.1	26
99	36.5	37.4	0.1	0.2	0.1	8.3	1.7	-49.4	-21.1	1.8	40.6	2.4	-12.8	2.5	35
99.5	24.5	26.9	0.1	-13.1	0.1	21.6	3.1	-87.5	-26.6	2.7	2.5	2.4	-5	4.1	42
99.5	36	38.1	0.1	-0.2	0.1	11.4	2.1	-42.8	-20.7	1.8	47.2	2.4	-9.3	2.7	37
99.5	38	34.6	0.1	-2	0.1	16.2	2.9	-46.4	-28.2	2.3	43.6	2.4	-12	3.7	37
99.5	38.5	33	0.1	-2.4	0.1	11	2.7	-46	-28.9	1.9	44	2.4	-17.9	3.3	51
72.5	34	28.3	0.1	29.8	0.1	2.9	1	-59.8	-20.1	1.7	30.2	2.3	-17.2	1.9	30
75	33.5	29.9	0.2	30.7	0.2	12.5	2.9	-63.4	-33.7	2.3	26.6	2.3	-21.1	3.7	35
76.5	29.5	32.7	0.2	34.2	0.2	7.7	1.9	-70.9	-22.8	1.4	19.1	2.3	-15.1	2.4	68
77.5	33	26.7	0.3	22.9	0.3	12.4	2.2	-56.5	-30.8	2.7	33.5	2.3	-18.4	3.5	46
80.5	31.5	29.6	0.1	19.7	0.1	16.8	1.9	-90.2	-13.3	1.6	-0.2	2.3	3.5	2.5	19
81	28.5	37.4	0.2	36.2	0.2	-2.1	2.9	-62.7	-67.8	4.7	27.3	2.3	-69.8	5.6	38
81	36.5	25.8	0.1	15.6	0.1	9.2	1.2	-54.8	-11.6	1.2	35.2	2.3	-2.4	1.7	45
82	31	31.9	0.1	20.4	0.1	10.4	1.6	-88.9	-16.8	1.5	1.1	2.3	-6.4	2.2	54
82	31.5	31.9	0.1	19.7	0.1	14.6	1.7	-93.1	-12.2	1.4	-3.1	2.3	2.4	2.2	49
83	32	33.5	0.1	19.2	0.1	18.3	1.6	-88.6	-10.4	1.6	1.4	2.3	7.9	2.3	68
83	32.5	33.6	0.1	18.6	0.1	18.1	1.4	-88.9	-9	1.6	1.1	2.3	9.1	2.2	63
83.5	31	34.1	0.1	20.4	0.1	19.8	2	-92.6	-15.5	2	-2.6	2.3	4.3	2.8	30
83.5	31.5	34.3	0.1	19.7	0.1	19.5	2	-90.8	-11.9	1.7	-0.8	2.3	7.5	2.7	24
83.5	32	34.4	0.1	19.2	0.1	18.2	1.7	-89.8	-10	1.6	0.2	2.3	8.2	2.4	47
84	33	35.4	0.1	18.4	0.1	19.6	1.5	-92.4	-8.1	1.6	-2.4	2.3	11.6	2.2	50
84.5	29	36	0.1	24.7	0.1	9.2	1.9	-77.6	-29.1	2.5	12.4	2.3	-19.9	3.1	26
84.5	34	35.6	0.2	17.4	0.2	13.7	1.6	-81.2	-12.9	1.3	8.8	2.3	0.7	2.1	40
85	30.5	36.7	0.2	21.6	0.2	19.9	2	-91	-14.2	1.8	-1	2.3	5.7	2.7	42
85	31	36.9	0.2	20.9	0.2	20.2	1.7	-90.3	-13.1	1.8	-0.3	2.3	7.1	2.5	38
85	35.5	33.3	0.2	14.9	0.2	11.3	2	-59.8	-24.4	2	30.2	2.3	-13.1	2.9	43
85.5	30.5	37.6	0.2	21.5	0.2	20.8	2	-87.9	-13	1.7	2.1	2.3	7.8	2.7	44
85.5	37	29.4	0.2	11.9	0.2	16.2	2.1	-69	-20.7	2.1	21	2.3	-4.5	3	51
86.5	27	38.2	0.2	33.9	0.2	10.5	3.8	-78.8	-70.8	5	11.2	2.3	-60.3	6.5	72
86.5	30.5	39.6	0.2	20.8	0.2	20.4	2.1	-84.6	-12.9	1.7	5.4	2.3	7.4	2.7	58

87.5	30.5	41.1	0.1	19.9	0.2	14.6	1.7	-84.4	-14.7	1.5	5.6	2.3	-0.1	2.3	40
87.5	31	41.5	0.1	19.1	0.2	16.5	1.6	-80.9	-13.9	1.8	9.1	2.3	2.7	2.4	34
88	28.5	39.3	0.2	24.4	0.2	10.9	2.9	-90.8	-35.9	2.4	-0.8	2.3	-25	3.8	44
88	30.5	41.7	0.1	19.4	0.1	13.7	1.6	-85.5	-15.3	1.5	4.5	2.3	-1.6	2.2	46
88.5	26	39.3	0.2	35.1	0.2	7.9	1.3	-81.4	-22.8	2.7	8.6	2.3	-14.9	3	39
88.5	28.5	39.8	0.2	24	0.2	11.6	2.9	-89.6	-33.1	2.4	0.4	2.3	-21.5	3.8	43
88.5	30	41.7	0.1	19.9	0.1	12.4	1.9	-88.1	-17.9	1.6	1.9	2.3	-5.5	2.5	50
88.5	31	42.8	0.1	18	0.1	14.6	1.5	-81.2	-13.8	1.5	8.8	2.3	0.7	2.2	52
88.5	31.5	43.1	0.1	17.2	0.1	15.7	1.5	-76.8	-12	1.5	13.2	2.3	3.6	2.1	47
88.5	32.5	42.9	0.1	16.1	0.1	18.3	1.7	-69.9	-11	1.5	20.1	2.3	7.3	2.2	45
89	27	40.3	0.3	33.1	0.3	23	5.5	-86.6	-101.4	7.4	3.4	2.3	-78.4	9.2	49
89	31.5	43.7	0.1	16.5	0.1	16.1	1.6	-75	-12.7	1.6	15	2.3	3.5	2.2	37
89	32.5	43.7	0.1	15.4	0.1	19.8	1.9	-68.9	-12	1.7	21.1	2.3	7.8	2.5	43
90	28	41.7	0.1	24.4	0.1	7	3.1	-81.8	-44.7	3	8.2	2.3	-37.7	4.3	46
90	38.5	31.9	0.2	6.6	0.2	20.8	2.3	-68	-31	3.6	22	2.3	-10.2	4.3	41
90	39	31.2	0.2	5.8	0.2	15.2	1.5	-68.7	-18.6	2.2	21.3	2.3	-3.3	2.7	42
90.5	30.5	45.1	0.1	15.4	0.1	23.3	2.5	-79.2	-16.9	2	10.8	2.3	6.4	3.2	39
90.5	31.5	46	0.1	13.7	0.1	22	2.1	-78	-18.2	2.4	12	2.3	3.8	3.2	50
90.5	38.5	32.6	0.2	6.2	0.2	20.3	2.6	-70.4	-30.7	3.1	19.6	2.3	-10.4	4	41
91.5	32	48.1	0.1	10.2	0.1	21.3	2.6	-68.9	-19.7	2	21.1	2.3	1.6	3.3	47
91.5	33.5	47.7	0.2	8.8	0.2	23.2	2.7	-64.2	-12.3	1.5	25.8	2.3	10.9	3	37
91.5	38	34.6	0.2	6.9	0.2	12.1	2.6	-69.3	-28.3	1.9	20.7	2.3	-16.3	3.3	44
92.5	31.5	49.2	0.1	8.5	0.1	16.9	1.7	-65.6	-16	2	24.4	2.3	0.9	2.6	46
92.5	40	31.4	0.1	2.8	0.1	7.1	1.2	-47.4	-14.6	1.3	42.6	2.3	-7.5	1.7	40
93	29.5	47.2	0.2	9.2	0.2	16.6	2.5	-64	-18.2	1.4	26	2.3	-1.7	2.9	44
93.5	40	31.2	0.1	1.7	0.1	8.5	1.5	-51.4	-13	0.9	38.6	2.3	-4.5	1.7	68
94	28	43.5	0.4	14.2	0.4	-0.7	3.2	-97.6	-58.6	3.7	-7.6	2.3	-59.3	4.9	42
94	33	50.1	0.2	4.4	0.2	17.5	1.6	-53	-8.3	1.4	37	2.3	9.3	2.1	42
95	29.5	46.9	0.2	3.1	0.2	-16.2	3	-91.1	-76.9	3.9	-1.1	2.3	-93.2	4.9	81
95	33	50.8	0.2	2.5	0.2	18.9	1.6	-41.5	-11.1	1.8	48.5	2.3	7.8	2.4	47

95	33.5	50.4	0.2	2.8	0.2	18.2	1.5	-36.5	-13.8	2.1	53.5	2.3	4.4	2.6	46
95.5	32.5	51	0.2	1	0.1	16.6	1.7	-33.8	-12.4	1.7	56.2	2.3	4.2	2.4	46
95.5	37.5	36	0.1	2.7	0.1	8.7	1.3	-64.9	-18.6	1.7	25.1	2.3	-9.8	2.2	44
96	37.5	36.1	0.1	2.3	0.1	9.8	1.4	-65	-18.7	1.8	25	2.3	-8.9	2.3	41
96	39	33.2	0.2	0.3	0.2	9.4	1.6	-53.3	-18.9	1.6	36.7	2.3	-9.5	2.3	45
97	24	25.9	0.2	-2.8	0.3	20.6	3.9	-33.1	-38.9	2.3	56.9	2.3	-18.3	4.7	35
97	26	31.5	0.3	2.4	0.3	28.8	4.6	-16.8	-46.4	3.8	73.2	2.3	-17.6	5.9	38
98	36.5	38	0.1	1.5	0.1	7.5	1.3	-48.3	-21.2	1.8	41.7	2.3	-13.7	2.2	51
99	30.5	45.1	0.1	-10.5	0.1	24.3	1.8	-1.3	-10.4	2.1	88.7	2.3	13.9	2.8	45
99	38	34.8	0.1	-1.4	0.1	15	2.8	-48.3	-26.5	2	41.7	2.3	-11.6	3.4	40
99	38.5	33.3	0.1	-1.8	0.1	12.6	2.5	-46.6	-29.2	2.4	43.4	2.3	-16.6	3.4	41
99.5	25	27.2	0.1	-14.5	0.1	27.3	3	-82.6	-23.3	3	7.4	2.3	4.1	4.3	39
100	35.5	39	0.1	-0.8	0.1	15.1	2.1	-38.5	-20.4	1.9	51.5	2.3	-5.3	2.8	46
72.5	39.5	24.6	0.3	12.7	0.3	15.9	3.8	-114.6	-58.4	4.2	-24.6	2.2	-42.5	5.8	51
74.5	40	27.4	0.1	14.7	0.1	12.3	2.9	-91.2	-41.3	2.9	-1.2	2.2	-29	4.1	64
75	31	30.9	0.2	33.5	0.2	7.6	1	-72.2	-18	1.7	17.8	2.2	-10.4	2	39
75.5	31	31.1	0.2	32.9	0.2	7	1.1	-67.2	-21.7	1.8	22.8	2.2	-14.7	2.2	44
76.5	34	26.8	0.2	24.9	0.2	5.6	2.2	-48.8	-37.9	2.5	41.2	2.2	-32.3	3.3	48
77	33	26.9	0.3	24.6	0.3	6.8	2.4	-45.6	-41.9	2.7	44.4	2.2	-35.1	3.7	42
77	35.5	25.8	0.1	22	0.1	9.2	1.7	-53.5	-17.7	1.3	36.5	2.2	-8.5	2.1	47
78.5	31.5	28.7	0.3	24	0.3	14.9	3.4	-64.7	-41.8	3	25.3	2.2	-26.9	4.4	36
79	41.5	30	0.1	13.4	0.1	3.6	2.1	-93.7	-38	2.3	-3.7	2.2	-34.5	3.1	44
80	35.5	26.5	0.1	17	0.1	12.8	1.4	-56.1	-11.4	1.2	33.9	2.2	1.5	1.9	41
80.5	31	29.7	0.1	20.7	0.1	18.1	2.4	-82.9	-24.5	2.3	7.1	2.2	-6.4	3.3	17
80.5	34.5	28.7	0.1	17.3	0.1	20.2	1.6	-73.2	-6.9	1.3	16.8	2.2	13.3	2.1	34
81	34	30.2	0.1	17.4	0.1	19.7	1.4	-82.4	-5.1	1.3	7.6	2.2	14.6	1.9	42
81.5	28	36.2	0.2	34.7	0.2	-0.7	2.2	-59.4	-36	1.8	30.6	2.2	-36.7	2.9	41
81.5	31	31.3	0.1	20.5	0.1	12.5	1.8	-86.9	-17.7	1.5	3.1	2.2	-5.2	2.4	27
81.5	31.5	31.2	0.1	19.7	0.1	15.1	1.8	-91.3	-13	1.3	-1.3	2.2	2.1	2.2	30
81.5	33.5	31.3	0.1	17.6	0.1	17	1.3	-91.2	-6.7	1.3	-1.2	2.2	10.3	1.8	46

82	33	32	0.1	18.1	0.1	16.7	1.3	-95.5	-8.3	1.4	-5.5	2.2	8.4	1.9	40
82	41	31	0.1	12.9	0.1	0.1	1.6	-89.8	-33.4	2.1	0.2	2.2	-33.3	2.6	44
82.5	31	32.5	0.1	20.4	0.1	11.9	1.6	-85.1	-16.3	1.5	4.9	2.2	-4.5	2.2	42
82.5	31.5	32.6	0.1	19.7	0.1	16.4	1.6	-88.7	-11.9	1.4	1.3	2.2	4.5	2.2	36
83	31.5	33.4	0.1	19.7	0.1	18.4	1.7	-90.1	-11.6	1.5	-0.1	2.2	6.8	2.3	50
83.5	37	27	0.1	12.7	0.1	15.3	1.5	-69	-9.8	1.3	21	2.2	5.4	2	37
84	31	35	0.1	20.6	0.1	21.2	1.9	-93.8	-15.8	2.1	-3.8	2.2	5.4	2.8	51
84	31.5	35.2	0.1	19.9	0.1	19	1.7	-92	-12.3	1.7	-2	2.2	6.7	2.4	31
84	33.5	35.3	0.1	17.9	0.1	18.1	1.5	-89.5	-9.6	1.4	0.5	2.2	8.5	2.1	39
84.5	30	35.6	0.2	22.5	0.1	15.2	1.7	-85.7	-17.4	1.9	4.3	2.2	-2.2	2.6	37
84.5	30.5	35.8	0.2	21.6	0.2	21	2	-92.7	-16	1.9	-2.7	2.2	5	2.8	39
85	37	28.9	0.2	12	0.2	15.5	1.7	-68	-16.5	1.7	22	2.2	-1	2.4	46
85.5	31	37.8	0.2	20.8	0.2	21.6	1.7	-86.6	-11.4	1.7	3.4	2.2	10.2	2.4	39
86	30.5	38.6	0.2	21.2	0.2	21.6	2	-85.7	-12.5	1.7	4.3	2.2	9.1	2.6	41
86.5	32.5	39.9	0.1	18.6	0.1	19.9	1.2	-74.5	-8.6	1.7	15.5	2.2	11.3	2.1	40
86.5	35.5	33.3	0.3	14.3	0.3	10.5	1.8	-58.6	-23.3	2	31.4	2.2	-12.8	2.7	51
87	27	38.5	0.2	33.4	0.1	2.4	3.1	-80.9	-52.3	3.5	9.1	2.2	-49.9	4.8	36
87	31	40.7	0.1	19.6	0.2	18.6	1.6	-79.9	-12.5	1.7	10.1	2.2	6.2	2.4	38
87	31.5	40.9	0.1	19	0.1	19.1	1.3	-76.8	-10.4	1.7	13.2	2.2	8.8	2.2	43
87.5	28.5	38.8	0.2	24.6	0.2	16.1	3	-94.7	-35.7	2.6	-4.7	2.2	-19.5	4	47
87.5	31.5	41.6	0.1	18.4	0.1	17.4	1.3	-76.7	-11.5	1.6	13.3	2.2	5.9	2.1	37
87.5	37	31.4	0.3	11.3	0.3	14	2	-74.3	-22.2	1.9	15.7	2.2	-8.2	2.8	44
88	31	42.1	0.1	18.5	0.1	15.2	1.4	-81.8	-13.7	1.5	8.2	2.2	1.5	2.1	45
88	31.5	42.4	0.1	17.8	0.1	16.3	1.3	-77.2	-11.9	1.5	12.8	2.2	4.4	2	41
88	32.5	42.2	0.1	16.7	0.1	18.4	1.5	-70.2	-10.6	1.4	19.8	2.2	7.8	2.1	50
88	33	42	0.2	16.3	0.2	19.5	1.7	-68.7	-10.7	1.6	21.3	2.2	8.7	2.3	41
88.5	27	38.6	0.3	33.6	0.3	18.3	4.7	-85	-108.2	7.6	5	2.2	-89.8	8.9	45
89	28	40.1	0.2	25.5	0.2	22.5	3.3	-86.2	-41.7	3.7	3.8	2.2	-19.1	4.9	45
89	37	33.3	0.4	10.8	0.4	15.5	1.5	-74.1	-24.4	2.7	15.9	2.2	-8.9	3.1	40
89.5	28	41.2	0.2	25	0.2	20.1	3.5	-81	-42.9	3.6	9	2.2	-22.8	5	43

89.5	29	41.7	0.1	21.3	0.1	14.9	2.2	-84.7	-29.2	2.6	5.3	2.2	-14.3	3.4	34
89.5	30.5	43.5	0.1	17.4	0.1	15.6	1.8	-79.1	-17.1	1.7	10.9	2.2	-1.5	2.4	44
90	28.5	41.8	0.1	22.2	0.1	11.4	2.4	-79	-36	2.8	11	2.2	-24.6	3.7	41
90.5	25.5	40.4	0.1	33.1	0.1	16.7	1.6	-43.4	-18.6	2.2	46.6	2.2	-1.9	2.7	40
90.5	28	41.7	0.2	23.3	0.2	7.8	2.6	-74.7	-42.9	2.8	15.3	2.2	-35.1	3.8	49
90.5	28.5	42.2	0.1	21.1	0.1	12.5	2.4	-78.1	-35.6	2.6	11.9	2.2	-23.1	3.6	45
90.5	36.5	36.4	0.3	10.7	0.3	23.8	2.1	-59.9	-20.9	2.7	30.1	2.2	2.9	3.5	41
91	25.5	40.3	0.1	31.8	0.1	13.3	2.1	-42.1	-19.5	1.6	47.9	2.2	-6.2	2.6	41
91	31	46.6	0.2	13.5	0.1	29.7	2.9	-79	-18.8	2.1	11	2.2	10.8	3.6	46
91	38.5	33.2	0.2	5.9	0.2	16.1	2.5	-69.4	-30.6	2.4	20.6	2.2	-14.5	3.5	44
91.5	27	40.6	0.3	25.3	0.3	7.4	4.5	-80.6	-62.6	2.6	9.4	2.2	-55.2	5.2	34
91.5	34	47.3	0.3	8.5	0.2	23.1	2.6	-63.1	-12.1	1.5	26.9	2.2	11	2.9	44
92.5	30	47.6	0.1	10.5	0.1	16.9	2.1	-67.1	-15.7	1.4	22.9	2.2	1.2	2.5	40
92.5	32	49.2	0.2	7.9	0.1	17	1.7	-65	-16.7	1.8	25	2.2	0.3	2.5	49
92.5	37.5	35.6	0.2	6.7	0.2	10.4	2.2	-62.9	-26.3	1.8	27.1	2.2	-15.9	2.9	42
93	32	49.7	0.2	6.7	0.1	16.1	1.5	-63.1	-15.5	1.8	26.9	2.2	0.6	2.4	45
93	32.5	49.6	0.2	6.3	0.2	15.9	1.5	-62.2	-14.1	1.7	27.8	2.2	1.8	2.2	49
93	40	31.3	0.1	2.2	0.1	7.7	1.3	-49.4	-13.6	1	40.6	2.2	-5.9	1.7	50
93.5	32	50.1	0.2	5.6	0.1	16.3	1.6	-60.4	-13.5	1.7	29.6	2.2	2.7	2.3	43
93.5	33	49.7	0.2	5.3	0.2	15.6	1.4	-56.5	-9.5	1.3	33.5	2.2	6.1	1.9	41
94	32.5	50.3	0.2	4.4	0.2	18	1.7	-54.9	-9.9	1.5	35.1	2.2	8.1	2.2	45
94.5	28.5	44.8	0.4	11.5	0.4	-4.5	2.7	-98.1	-71.8	4.1	-8.1	2.2	-76.3	4.9	41
95	37.5	35.9	0.1	3.1	0.1	8.3	1.3	-63.1	-18.8	1.7	26.9	2.2	-10.5	2.1	48
95.5	39	33.1	0.2	0.6	0.2	11.2	1.8	-53	-17.9	1.4	37	2.2	-6.7	2.2	42
96	27.5	41.1	0.4	12.6	0.4	16.8	4.1	-42.4	-57.4	3.8	47.6	2.2	-40.6	5.6	64
96	32.5	50.8	0.2	-0.1	0.2	16.5	1.7	-26.5	-14.7	1.7	63.5	2.2	1.8	2.4	47
96	38	35.3	0.1	1.5	0.1	9.9	1.2	-61.5	-19.3	1.8	28.5	2.2	-9.4	2.2	36
97	26.5	34.1	0.3	2.5	0.3	13.2	3.7	-27.7	-51.6	3.2	62.3	2.2	-38.4	4.9	45
97	32	49.8	0.2	-2.9	0.2	16.6	1.7	-14.2	-15.7	1.9	75.8	2.2	0.9	2.6	46
98	30.5	45.9	0.1	-8	0.1	20.6	1.7	-174.6	-11.2	1.8	-84.6	2.2	9.4	2.5	49

98.5	24.5	24.6	0.1	-10.3	0.1	26.1	3.4	-68.9	-26.7	2.5	21.1	2.2	-0.6	4.2	54
98.5	30.5	45.5	0.1	-9.2	0.1	22.5	1.7	-178.1	-10	1.8	-88.1	2.2	12.5	2.5	52
100	38	34.3	0.1	-2.5	0.1	16	2.7	-46	-30.7	2.2	44	2.2	-14.7	3.5	47
100	38.5	32.6	0.1	-3	0.1	9.2	2.2	-45.6	-27.9	1.9	44.4	2.2	-18.7	2.9	49
74.5	38.5	23.5	0.2	21.9	0.2	35.6	3.1	-94.5	-18.9	2.3	-4.5	2.1	16.7	3.9	42
75.5	33.5	29.2	0.2	29.1	0.2	9.8	2.7	-55.5	-33.9	1.7	34.5	2.1	-24.1	3.2	38
76	30.5	31.7	0.2	33.2	0.2	6.9	1.5	-64.2	-26.4	1.9	25.8	2.1	-19.5	2.4	29
76	31	31.2	0.2	32.2	0.2	6.2	1.5	-62.4	-27.8	2	27.6	2.1	-21.5	2.5	37
76	33	28.7	0.3	28.2	0.3	6.1	2.3	-46	-39.8	2.4	44	2.1	-33.7	3.4	53
76	35	26.2	0.1	23.6	0.1	11.5	2.1	-73.5	-35.4	2.6	16.5	2.1	-23.9	3.3	35
76.5	33	27.7	0.3	26.4	0.3	6	2.4	-43.6	-44.6	2.7	46.4	2.1	-38.6	3.7	36
77.5	40.5	29.2	0.1	14.9	0.1	4.9	1.5	-107.3	-28.2	2	-17.3	2.1	-23.2	2.5	58
80	42	30.4	0.1	10.4	0.2	12.1	3.2	-80.3	-37.7	2	9.7	2.1	-25.6	3.7	50
80.5	41	30.7	0.1	14	0.1	7.1	1.3	-88.1	-29	2.3	1.9	2.1	-21.8	2.7	36
81	31	30.6	0.1	20.5	0.1	17.3	2	-86	-19.2	1.8	4	2.1	-1.9	2.7	56
81	31.5	30.4	0.1	19.7	0.1	16.9	1.8	-90.8	-13.4	1.4	-0.8	2.1	3.5	2.2	51
82	33.5	32.1	0.1	17.6	0.1	17.3	1.3	-93.5	-7.8	1.3	-3.5	2.1	9.4	1.8	36
82	41.5	31.3	0.1	10.9	0.1	-0.7	1.9	-97.2	-38.6	2.1	-7.2	2.1	-39.3	2.8	43
82.5	33	32.8	0.1	18.1	0.1	17.4	1.2	-89.2	-8.6	1.4	0.8	2.1	8.8	1.8	33
82.5	33.5	32.9	0.1	17.6	0.1	17.5	1.2	-88.2	-8.7	1.3	1.8	2.1	8.8	1.8	35
83	31	33.2	0.1	20.4	0.1	15.5	1.7	-88.4	-15.9	1.6	1.6	2.1	-0.3	2.3	54
83	33	33.6	0.1	18.2	0.1	18	1.3	-89.9	-8.5	1.4	0.1	2.1	9.5	1.9	54
83.5	33	34.5	0.1	18.3	0.1	18.7	1.4	-90.8	-8.5	1.4	-0.8	2.1	10.2	2	47
83.5	33.5	34.5	0.1	17.8	0.1	18.1	1.4	-89.4	-9.3	1.4	0.6	2.1	8.8	1.9	46
84	27	37.1	0.3	37.4	0.3	4.3	2.3	-75.6	-47.8	3.3	14.4	2.1	-43.4	4	40
84	29	35.6	0.1	25	0.1	8.9	1.9	-77.5	-37.5	2.6	12.5	2.1	-28.5	3.3	53
84	29.5	34.9	0.2	23.7	0.1	11.8	1.7	-74.1	-25.5	2.2	15.9	2.1	-13.7	2.8	69
84	34	35	0.1	17.3	0.1	15.5	1.5	-82.7	-12	1.3	7.3	2.1	3.5	2	48
84.5	34.5	34.8	0.2	16.6	0.2	11.6	1.6	-73.6	-16.1	1.3	16.4	2.1	-4.5	2.1	40
85	28.5	36.5	0.1	26.2	0.1	8.8	2.6	-88	-44	2.7	2	2.1	-35.2	3.7	49

85	36	31.9	0.2	13.9	0.2	13.3	2	-56.5	-28.1	2.3	33.5	2.1	-14.8	3.1	47
85.5	34.5	35.4	0.2	16.4	0.2	10	1.6	-67.2	-18.3	1.4	22.8	2.1	-8.3	2.1	70
86	28	36.7	0.1	27.2	0.1	9.7	3.5	-73.4	-61.5	3.2	16.6	2.1	-51.7	4.7	38
86	31	38.8	0.2	20.5	0.2	22.2	1.7	-83.4	-10.5	1.6	6.6	2.1	11.7	2.4	54
86	33	38.8	0.2	18.4	0.2	19.5	1.3	-76.8	-10.3	1.7	13.2	2.1	9.3	2.2	55
86.5	28	37.3	0.1	26.3	0.2	14.7	3.5	-80.1	-49.3	2.9	9.9	2.1	-34.6	4.6	58
86.5	31	39.8	0.1	20.1	0.2	21.1	1.8	-81	-11.1	1.6	9	2.1	10	2.4	62
87	32	40.9	0.1	18.5	0.1	19.3	1.2	-73.4	-9.4	1.6	16.6	2.1	9.9	2.1	46
87.5	32	41.6	0.1	17.8	0.1	18.1	1.3	-72.6	-10.3	1.5	17.4	2.1	7.8	2	43
88	32	42.4	0.1	17.2	0.1	17.4	1.4	-72.7	-10.9	1.4	17.3	2.1	6.6	2	50
88	37.5	31.4	0.3	9.9	0.3	14.8	1.5	-73.3	-21.8	2.3	16.7	2.1	-7	2.7	43
88.5	26.5	39.3	0.2	34.4	0.2	8.5	1.6	-77.9	-41.6	3.7	12.1	2.1	-33.1	4	39
88.5	32	43.1	0.1	16.6	0.1	17.1	1.5	-72.4	-11.2	1.4	17.6	2.1	5.9	2	48
88.5	37.5	32.1	0.3	9.8	0.3	15.1	1.3	-72.5	-23	2.5	17.5	2.1	-7.9	2.8	44
89	27.5	40	0.2	28.3	0.2	23.1	3.5	-88.1	-58.8	4.5	1.9	2.1	-35.7	5.7	49
89	30	42.3	0.1	19.3	0.1	14	1.9	-84.8	-19.4	1.6	5.2	2.1	-5.4	2.5	33
89	32	43.8	0.1	15.9	0.1	18.2	1.7	-71.1	-12.1	1.5	18.9	2.1	6.2	2.2	42
89.5	28.5	41.2	0.1	23.1	0.1	14.2	2.2	-81.4	-32.2	2.5	8.6	2.1	-18	3.4	43
89.5	31.5	44.4	0.1	15.7	0.1	17.7	1.6	-74.2	-14.1	1.8	15.8	2.1	3.5	2.4	39
90	30.5	44.2	0.1	16.4	0.1	18.4	1.9	-78	-17.2	1.8	12	2.1	1.2	2.6	42
90.5	31	45.5	0.1	14.5	0.1	22.8	2.2	-77.8	-16.4	1.8	12.2	2.1	6.4	2.9	48
90.5	39.5	31.2	0.2	5.1	0.2	10.8	1.2	-62.9	-13.7	1.4	27.1	2.1	-2.9	1.8	40
92	32	48.7	0.1	9	0.1	19.1	2.1	-67.1	-18.3	1.9	22.9	2.1	0.8	2.8	39
92.5	37	36.4	0.2	7.2	0.2	16.5	2	-55.5	-22.7	2	34.5	2.1	-6.2	2.8	44
93.5	32.5	50	0.2	5.3	0.2	16.5	1.5	-60	-12.5	1.6	30	2.1	3.9	2.1	39
94	34.5	49	0.2	4.6	0.1	18.6	1.9	-44.1	-16.2	1.6	45.9	2.1	2.3	2.5	37
94.5	25.5	32.2	0.2	20	0.1	19.5	2	-6.3	-27.9	2.9	83.7	2.1	-8.4	3.5	43
94.5	39.5	32	0.1	1	0.1	15.3	1.9	-54.2	-16.4	1.3	35.8	2.1	-1.1	2.3	47
95	25	29	0.2	15.7	0.2	20.9	2.2	-20.3	-23.9	2.3	69.7	2.1	-3	3.2	33
95	28.5	44.9	0.4	12	0.4	-11.2	3.4	-93.6	-80.4	3.5	-3.6	2.1	-91.5	4.9	79

95	34	49.8	0.2	3.1	0.1	17.9	1.5	-30.2	-19.4	2.3	59.8	2.1	-1.5	2.8	41
95	38	35.1	0.1	2.4	0.1	8.9	1.2	-59.5	-20.9	1.7	30.5	2.1	-12	2.1	41
95.5	38	35.2	0.1	1.9	0.1	9	1.2	-61.1	-19.6	1.8	28.9	2.1	-10.6	2.1	43
96	25.5	30.7	0.3	9	0.3	31.4	3.1	-19.6	-18.2	1.8	70.4	2.1	13.2	3.6	33
96	37	37	0.1	3	0.1	12.3	1.7	-59.7	-18.3	1.4	30.3	2.1	-6.1	2.2	42
97	24.5	26.4	0.3	-2.3	0.3	22.4	3.2	-31.5	-45.7	4	58.5	2.1	-23.3	5.1	32
97	36.5	38.1	0.1	2.6	0.1	11.1	1.6	-56.3	-17.2	1.3	33.7	2.1	-6	2	53
97.5	28.5	40.6	0.2	-6.6	0.2	-0.6	2.2	-52	-49.5	2.7	38	2.1	-50.1	3.6	36
97.5	32	49.1	0.2	-3.9	0.2	18.5	1.8	-13.8	-15.9	1.8	76.2	2.1	2.5	2.6	41
97.5	36.5	38.2	0.1	2	0.1	9.6	1.4	-52.1	-18.8	1.5	37.9	2.1	-9.2	2	55
98	32	48.5	0.2	-4.7	0.2	21.2	1.9	-16.5	-16.1	1.9	73.5	2.1	5.2	2.7	33
98.5	32	47.9	0.2	-5.5	0.2	24.6	2.2	-18.1	-18.5	2.2	71.9	2.1	6.1	3.1	30
98.5	36.5	37.7	0.1	0.9	0.1	7.9	1.4	-47.7	-22	1.7	42.3	2.1	-14.1	2.2	37
72	34.5	27.5	0.1	28.7	0.1	0.6	1.4	-65.4	-27.6	1.5	24.6	2	-27	2	56
72.5	36.5	22.1	0.2	21.4	0.2	7.3	1.9	-74.3	-30.8	1.7	15.7	2	-23.6	2.5	46
73.5	36	23.9	0.2	23.1	0.2	6.4	1.4	-76.5	-25.7	1.6	13.5	2	-19.3	2.2	39
74.5	40.5	27.1	0.1	12.5	0.1	15.4	3.1	-87.4	-44.6	2.7	2.6	2	-29.1	4.1	70
75	30.5	31.4	0.2	34.3	0.2	7.9	0.9	-70.8	-19.9	1.7	19.2	2	-12.1	1.9	47
75.5	30.5	31.6	0.2	33.8	0.2	7.4	1.1	-67.7	-22.6	1.8	22.3	2	-15.3	2.1	62
75.5	38.5	26.5	0.1	21.9	0.1	28	2.3	-96.3	-15	1.9	-6.3	2	13	3	34
76	34	27.8	0.2	27	0.2	8	2.4	-57.3	-42.4	2.3	32.7	2	-34.4	3.4	42
76.5	39.5	28.9	0.1	18.5	0.1	-4.4	2	-99.1	-47.3	2.2	-9.1	2	-51.7	3	40
77	33.5	26.4	0.2	23.7	0.2	7.1	1.9	-44.5	-38.2	2.4	45.5	2	-31.1	3.1	42
77.5	31.5	29.6	0.3	28.1	0.3	13.6	3.4	-60.6	-60.6	4	29.4	2	-47	5.1	44
77.5	40	29	0.1	16.6	0.1	-0.3	1.5	-104.1	-35	1.9	-14.1	2	-35.3	2.4	60
78	41.5	29.5	0.1	12.7	0.1	11.1	2.6	-99.1	-39.9	2.7	-9.1	2	-28.9	3.8	44
80.5	36	26.1	0.1	16.3	0.1	11.1	1.3	-54.1	-12.2	1	35.9	2	-1.1	1.6	54
81.5	34	31.1	0.1	17.2	0.1	19.8	1.3	-84.8	-6.6	1.3	5.2	2	13.3	1.8	46
81.5	36.5	26	0.1	15	0.1	12.1	1.3	-60.6	-13	1.3	29.4	2	-0.9	1.8	37
82	34	31.9	0.1	17.2	0.1	19.4	1.3	-87.8	-8	1.3	2.2	2	11.4	1.9	40

82.5	34	32.7	0.1	17.1	0.1	18.3	1.4	-82.5	-9.7	1.4	7.5	2	8.6	1.9	36
83	33.5	33.7	0.1	17.7	0.1	17.7	1.3	-89.1	-9.2	1.3	0.9	2	8.6	1.9	50
83	34	33.5	0.1	17.2	0.1	17.5	1.4	-83.5	-10.6	1.3	6.5	2	6.9	1.9	52
83.5	34	34.2	0.1	17.2	0.1	16.6	1.4	-82.9	-11.3	1.3	7.1	2	5.3	1.9	40
84	37	27.7	0.1	12.4	0.1	16.1	1.5	-69.3	-11.5	1.3	20.7	2	4.5	2	53
84.5	37	28.4	0.2	12.2	0.2	16	1.5	-68.6	-13.7	1.4	21.4	2	2.3	2.1	44
87	32.5	40.7	0.1	18	0.1	19.4	1.2	-71.6	-9.7	1.6	18.4	2	9.7	2	49
87.5	32.5	41.5	0.1	17.4	0.1	18.8	1.3	-70.3	-10.1	1.5	19.7	2	8.7	1.9	40
88	27.5	38.4	0.1	29.7	0.1	7.9	3	-82.3	-58.5	3.3	7.7	2	-50.7	4.4	39
88	28	38.8	0.2	26.8	0.2	9.2	3.1	-85.6	-52.9	2.7	4.4	2	-43.7	4.2	53
88	33.5	41.4	0.2	15.8	0.2	21.4	1.5	-68.2	-12.2	1.7	21.8	2	9.1	2.3	28
89	28.5	40.5	0.1	23.6	0.1	15	2.3	-86.4	-31.6	2.3	3.6	2	-16.6	3.3	44
89.5	29.5	42.4	0.1	19.8	0.1	16.3	2	-84.5	-26.2	2.2	5.5	2	-9.9	3	35
89.5	33.5	44.2	0.2	13.1	0.2	24.3	1.7	-66.9	-14.7	2.2	23.1	2	9.6	2.8	35
90.5	30	44.6	0.1	16.4	0.1	22.3	2.4	-81.1	-22.1	2	8.9	2	0.2	3.1	39
90.5	39	31.6	0.2	5.4	0.2	14.6	1.6	-65.8	-21.2	1.9	24.2	2	-6.6	2.5	40
91	27.5	40.9	0.3	24.4	0.3	13.9	2.7	-74.8	-56.2	3.9	15.2	2	-42.3	4.8	44
91	29.5	44.9	0.1	16.4	0.1	18.6	2.3	-80	-23.6	1.9	10	2	-5	3	43
91	30.5	46.1	0.1	14.3	0.1	25.1	2.6	-78.3	-17.9	1.8	11.7	2	7.2	3.1	48
91	39.5	31.5	0.2	4.7	0.2	10.3	1.3	-58.8	-15.3	1.3	31.2	2	-5	1.8	35
91.5	30	46.4	0.1	13.9	0.1	18.2	2.1	-75.1	-18.8	1.7	14.9	2	-0.6	2.7	33
91.5	39.5	31.8	0.1	4.2	0.2	9.4	1.3	-54.4	-17.2	1.3	35.6	2	-7.8	1.8	40
92	31.5	48.7	0.1	9.8	0.1	19.6	1.8	-68.7	-18.2	2	21.3	2	1.3	2.6	42
92	34.5	46.5	0.3	7	0.2	28	2.6	-60	-14.7	1.4	30	2	13.4	3	40
92.5	29.5	46.7	0.2	11.3	0.1	17.5	2	-67.8	-18.1	1.3	22.2	2	-0.6	2.5	40
94.5	37.5	35.8	0.1	3.6	0.1	8.8	1.3	-60.3	-20.5	1.7	29.7	2	-11.6	2.1	44
95.5	33	50.8	0.2	1.5	0.2	17.9	1.5	-33.8	-15.2	1.8	56.2	2	2.7	2.4	44
96	38.5	34.3	0.1	0.9	0.1	9.2	1.2	-56.1	-19.2	1.6	33.9	2	-10.1	2	42
96.5	25.5	29.6	0.3	5	0.3	35.5	3.7	-21.6	-29.3	2.7	68.4	2	6.2	4.6	31
96.5	38	35.3	0.1	1.2	0.1	11.4	1.4	-59.6	-19.9	1.6	30.4	2	-8.5	2.1	39

97	23.5	25.6	0.2	-3.1	0.2	28	3.9	-32.4	-35	1.5	57.6	2	-7	4.3	35
97	25.5	28.3	0.3	0.7	0.3	34.6	4	-23.8	-59.7	5.4	66.2	2	-25.2	6.7	29
98.5	25	24.5	0.2	-11.1	0.2	32.7	3.4	-65.3	-25.5	2.5	24.7	2	7.2	4.2	47
99	31	46.6	0.2	-9.1	0.1	25.6	1.9	-4	-16	2.3	86	2	9.6	3	43
99	31.5	47.6	0.2	-7.7	0.2	28.2	2.4	-13.2	-21.1	2.4	76.8	2	7	3.4	45
99.5	31	46.1	0.2	-10.4	0.2	29.5	2.4	-5.8	-23.5	2.9	84.2	2	6	3.7	49
100	31	45.2	0.1	-12	0.1	31.3	2.5	-4.2	-23.1	2.8	85.8	2	8.2	3.8	51
72	35	26.4	0.1	26.9	0.1	-1.6	1.8	-71.1	-34	1.4	18.9	1.9	-35.5	2.2	48
72	36	23.3	0.1	23	0.1	3.1	2.3	-71.1	-37.8	1.6	18.9	1.9	-34.7	2.7	58
72	38.5	21.6	0.3	15.7	0.3	14.7	3.7	-126.1	-56.7	3.3	-36.1	1.9	-42	4.8	57
73	37	22	0.2	20.8	0.2	17	1.4	-88.8	-17.5	1.8	1.2	1.9	-0.5	2.3	33
73	38.5	21.8	0.2	18.8	0.2	22.2	1.9	-115.8	-45.7	4.2	-25.8	1.9	-23.5	4.6	41
73.5	37	22.6	0.2	21.3	0.2	17.2	1.1	-93.7	-12.3	1.8	-3.7	1.9	4.8	2.1	25
75	34	28.5	0.2	29.5	0.1	15.3	3	-69.3	-47.2	2.5	20.7	1.9	-31.9	4	31
75.5	34	28.5	0.2	28.6	0.2	13.5	2.9	-65.1	-46.1	2.3	24.9	1.9	-32.6	3.9	45
76	33.5	28.1	0.2	27.3	0.2	8	2.3	-48.3	-36.8	1.8	41.7	1.9	-28.8	2.9	52
77	40	29.1	0.1	16.2	0.1	-1.8	1.9	-100.4	-43.2	2	-10.4	1.9	-45	2.8	44
78.5	41.5	29.9	0.1	13.1	0.1	4.4	1.9	-96.8	-39.5	2.3	-6.8	1.9	-35.1	3	52
79.5	30.5	31	0.3	26.5	0.3	7.1	3.9	-67	-70.9	3.2	23	1.9	-63.9	5.1	49
80	41.5	30.5	0.1	12.5	0.1	6.9	2	-83.6	-36.6	2.3	6.4	1.9	-29.8	3	41
81	41	30.9	0.1	13.5	0.1	6.4	1.5	-87.4	-35.8	2.4	2.6	1.9	-29.5	2.8	33
81.5	30.5	31.6	0.1	21.4	0.1	10.1	1.8	-82.3	-32.9	2.2	7.7	1.9	-22.7	2.8	47
81.5	41	31	0.1	13.2	0.1	3.5	1.7	-89.3	-37	2.2	0.7	1.9	-33.6	2.7	47
83.5	29	35.1	0.1	25.1	0.1	9.7	1.8	-76.6	-47.2	2.8	13.4	1.9	-37.5	3.4	22
83.5	29.5	34.4	0.1	23.8	0.1	11.7	1.9	-72.5	-28.4	1.8	17.5	1.9	-16.6	2.6	36
84	30	34.8	0.2	22.5	0.1	15.5	1.8	-81.4	-21.9	1.9	8.6	1.9	-6.4	2.5	78
84	30.5	34.9	0.2	21.5	0.1	19.9	1.8	-88.9	-19.5	1.9	1.1	1.9	0.4	2.6	75
85	36.5	30.3	0.2	13	0.2	16.8	1.8	-62.3	-23.8	1.9	27.7	1.9	-6.9	2.6	38
85.5	27.5	36.7	0.1	33	0.1	3.8	3.5	-72.6	-76	4.2	17.4	1.9	-72.2	5.4	50
85.5	33.5	37.5	0.2	17.9	0.2	17.1	1.3	-77	-12.7	1.5	13	1.9	4.3	2	29

87	36	32.9	0.3	13.1	0.3	13.9	1.8	-64.9	-21.8	1.7	25.1	1.9	-7.9	2.4	34
87.5	27.5	38.1	0.1	30.1	0.1	0.7	2.9	-85.4	-62.6	3.1	4.6	1.9	-61.9	4.3	47
87.5	33	41.2	0.2	16.9	0.2	19.8	1.3	-69.4	-10.9	1.5	20.6	1.9	8.8	2	44
88.5	28	39.3	0.2	26.2	0.1	15.8	3.1	-84.1	-47.1	3	5.9	1.9	-31.2	4.3	43
89.5	30	43	0.1	18.5	0.1	16.7	1.9	-81.6	-22.1	1.8	8.4	1.9	-5.4	2.6	45
89.5	32	44.6	0.1	15	0.1	20.7	1.6	-70.5	-14.2	1.7	19.5	1.9	6.5	2.3	33
89.5	33	44.4	0.2	13.7	0.2	23.7	1.7	-67.4	-15	2	22.6	1.9	8.7	2.7	36
90	29	42.4	0.1	20.4	0.1	16.1	2.3	-84	-31.6	2.3	6	1.9	-15.6	3.2	43
90.5	29	43.1	0.1	19.3	0.1	16.9	2.6	-84.4	-31.3	2	5.6	1.9	-14.4	3.3	43
90.5	37	35.1	0.2	10.2	0.2	15.3	1.9	-68.4	-25.9	2	21.6	1.9	-10.6	2.8	49
91	39	32	0.2	5.1	0.2	13.3	1.7	-63.1	-22.7	1.7	26.9	1.9	-9.4	2.4	42
91.5	29.5	45.5	0.1	14.8	0.1	17.6	1.8	-75	-20.5	1.6	15	1.9	-2.9	2.5	36
91.5	31.5	48	0.1	11.1	0.1	22.9	2.1	-72.5	-19.8	2	17.5	1.9	3.2	2.9	46
92	29.5	46.2	0.1	13.1	0.1	17.3	1.7	-71.5	-18.7	1.4	18.5	1.9	-1.3	2.3	43
92	30	47	0.1	12.3	0.1	17	1.8	-71.5	-17.3	1.3	18.5	1.9	-0.3	2.2	43
92	31	48.4	0.1	10.6	0.1	19.9	1.7	-70.4	-18.8	2	19.6	1.9	1.1	2.5	49
92	38	34.7	0.2	6.3	0.2	11.7	2.2	-64.4	-28.5	1.5	25.6	1.9	-16.8	2.7	44
92	39.5	31.9	0.1	3.7	0.1	9.5	1.4	-51.7	-19.4	1.4	38.3	1.9	-9.8	1.9	43
92.5	28.5	45.1	0.1	13	0.1	19.8	2.5	-77.1	-30.1	2.2	12.9	1.9	-10.3	3.3	37
92.5	29	45.9	0.1	12	0.1	19.2	2.2	-70.2	-21.8	1.7	19.8	1.9	-2.7	2.7	41
92.5	39.5	31.7	0.1	3	0.1	11.7	1.7	-50.2	-21	1.5	39.8	1.9	-9.4	2.2	39
93	27	41	0.2	22.8	0.2	-1	3.8	-90.5	-71.5	2.6	-0.5	1.9	-72.5	4.6	43
93	39.5	31.6	0.1	2.5	0.1	13.3	1.7	-52.6	-19.1	1.3	37.4	1.9	-5.8	2.1	52
93.5	27.5	42.2	0.3	17.5	0.3	-1.1	3.4	-90.5	-65.4	2.6	-0.5	1.9	-66.5	4.3	40
93.5	37.5	35.7	0.2	4.9	0.2	10.7	1.6	-58.8	-25.2	1.7	31.2	1.9	-14.5	2.3	50
93.5	39.5	31.5	0.1	1.9	0.1	21.5	2.3	-55.2	-21.5	1.6	34.8	1.9	0	2.8	64
94	37.5	35.8	0.2	4.2	0.1	9.7	1.4	-57.7	-23.3	1.6	32.3	1.9	-13.6	2.1	60
94	38	35.1	0.1	3.4	0.1	10.7	1.5	-57.1	-25.4	1.7	32.9	1.9	-14.7	2.3	52
94	39.5	31.8	0.1	1.4	0.1	18.6	2	-55.2	-18.4	1.4	34.8	1.9	0.2	2.5	35
94.5	38	35.1	0.1	2.8	0.1	9.4	1.3	-57.9	-22.9	1.7	32.1	1.9	-13.5	2.2	45

95	38.5	34.2	0.1	1.6	0.1	10.6	1.3	-55.2	-20.6	1.5	34.8	1.9	-10	2	43
95	39	33.2	0.1	0.9	0.1	13.8	1.7	-53.4	-18.5	1.3	36.6	1.9	-4.7	2.1	43
95.5	37	36.8	0.1	3.3	0.1	12.6	1.6	-58.1	-18.9	1.4	31.9	1.9	-6.3	2.1	39
95.5	38.5	34.2	0.1	1.3	0.1	9.5	1.2	-55.8	-19.5	1.5	34.2	1.9	-10	2	47
96.5	32.5	50.3	0.2	-1.1	0.2	17.9	1.7	-21.4	-17.3	1.8	68.6	1.9	0.6	2.4	44
96.5	36.5	38.2	0.1	3	0.1	12.8	1.7	-54.6	-18	1.2	35.4	1.9	-5.2	2	45
96.5	39	33.1	0.1	0.1	0.1	8.6	1.3	-53.1	-20.6	1.5	36.9	1.9	-12	2	47
97	27	36.2	0.3	2.2	0.3	12.7	3.1	-37.6	-54.3	3.1	52.4	1.9	-41.6	4.3	56
97	38	35.3	0.1	0.9	0.1	12.4	1.7	-56.5	-21.9	1.5	33.5	1.9	-9.5	2.3	45
97.5	33.5	47.7	0.2	-0.8	0.2	22.7	2	-20.7	-21.1	1.9	69.3	1.9	1.6	2.8	41
98	39	32.5	0.1	-1.1	0.1	9.7	1.6	-49.9	-26.5	1.7	40.1	1.9	-16.7	2.4	37
99	24.5	25.7	0.1	-11.8	0.1	26.5	2.9	-77.8	-31	2.5	12.2	1.9	-4.5	3.8	49
99	25	25.7	0.1	-13.3	0.1	35.5	3.2	-75.5	-29.1	2.9	14.5	1.9	6.4	4.3	48
72	39	23.1	0.2	13.4	0.2	8.8	3.2	-125.8	-60.4	3.1	-35.8	1.8	-51.6	4.4	54
72.5	34.5	27.2	0.1	28.6	0.1	1.2	1.3	-62.7	-27	1.5	27.3	1.8	-25.8	1.9	36
72.5	38.5	21.6	0.3	17.4	0.3	21.3	2.6	-120.4	-52.2	4	-30.4	1.8	-30.9	4.7	43
73	34.5	26.8	0.1	28.5	0.1	1.6	1.3	-62.4	-28	1.5	27.6	1.8	-26.4	1.8	47
73.5	35.5	24.8	0.1	24.2	0.2	1.3	1.7	-71.2	-37.1	1.7	18.8	1.8	-35.8	2.4	42
74.5	34	28.3	0.1	29.9	0.1	10.2	2.1	-71.9	-39.2	2.2	18.1	1.8	-29	3.1	25
75	38.5	25.1	0.1	21.9	0.1	38.4	2.7	-95.8	-15.4	1.9	-5.8	1.8	23	3.3	71
76	39	28	0.1	20.6	0.1	10.2	1.9	-101.4	-36.6	2.2	-11.4	1.8	-26.5	2.9	42
76.5	33.5	27.2	0.2	25.5	0.2	6.9	2	-45.4	-39.2	2.1	44.6	1.8	-32.4	2.9	41
76.5	40	29.1	0.1	15.7	0.1	1.2	2.3	-98.3	-48.9	2.2	-8.3	1.8	-47.7	3.2	37
77.5	31	31.4	0.3	30.3	0.3	12.1	2.8	-59.9	-63.3	3.7	30.1	1.8	-51.1	4.6	43
78	31.5	29.2	0.3	26.2	0.3	15.7	3	-62.3	-51.6	3.2	27.7	1.8	-35.9	4.3	34
80.5	35	27.8	0.1	16.9	0.1	18.8	1.4	-66.9	-10.6	1.2	23.1	1.8	8.2	1.9	42
80.5	42	30.8	0.1	9.8	0.1	12.7	2.3	-77.9	-35	2	12.1	1.8	-22.3	3	45
81	42	31	0.1	9.3	0.1	9.1	1.8	-80	-32.9	1.9	10	1.8	-23.8	2.6	33
81.5	41.5	31.2	0.1	11	0.1	2.6	1.7	-90.5	-40.3	2	-0.5	1.8	-37.7	2.6	30
82.5	28	36	0.2	35.5	0.2	2.2	4	-76.2	-80.5	3.8	13.8	1.8	-78.4	5.5	33

82.5	30.5	32.4	0.1	21.3	0.1	8.5	1.6	-78.4	-26.8	1.6	11.6	1.8	-18.3	2.3	43
83	30.5	33	0.1	21.3	0.1	13.1	1.9	-82.2	-24	1.6	7.8	1.8	-10.9	2.5	62
83.5	30.5	33.9	0.1	21.4	0.1	19.1	2	-86.2	-22.3	1.8	3.8	1.8	-3.2	2.7	32
84	34.5	34.2	0.2	16.6	0.1	15.2	1.5	-73.5	-15.4	1.2	16.5	1.8	-0.1	1.9	57
84.5	28.5	36.2	0.1	26.4	0.1	5.9	2.3	-82.9	-54.4	2.7	7.1	1.8	-48.5	3.5	23
84.5	35	34	0.2	15.8	0.2	14.4	1.6	-67.5	-19.3	1.4	22.5	1.8	-4.9	2.1	43
85.5	28	36.8	0.1	29	0.1	3	3.3	-77	-71.6	3.2	13	1.8	-68.6	4.5	46
85.5	34	36.5	0.2	17.1	0.2	14.1	1.4	-71.8	-15.8	1.4	18.2	1.8	-1.7	2	43
86.5	33	39.6	0.2	17.9	0.2	19.6	1.1	-72.7	-11.5	1.6	17.3	1.8	8.1	2	47
86.5	35	34.8	0.3	14.9	0.2	14	1.5	-60.3	-21.6	1.7	29.7	1.8	-7.7	2.3	44
87	28	37.8	0.2	26.9	0.2	9.2	3.1	-89.9	-52.2	2.4	0.1	1.8	-43	3.9	42
87	33	40.4	0.2	17.5	0.2	19.8	1.1	-70.6	-11.5	1.6	19.4	1.8	8.3	2	43
88	37	32.1	0.3	11.1	0.3	14.8	1.3	-73.9	-22.7	1.9	16.1	1.8	-7.9	2.3	42
88.5	27.5	39	0.1	29	0.2	16	2.8	-83.6	-57.9	3.6	6.4	1.8	-41.9	4.6	36
88.5	34	41.4	0.3	14.5	0.2	24.5	1.5	-66.6	-14.9	1.9	23.4	1.8	9.7	2.4	34
88.5	37	32.6	0.3	11	0.3	15.4	1.2	-74.4	-23.5	2.2	15.6	1.8	-8.1	2.5	48
89.5	32.5	44.5	0.2	14.3	0.1	22.7	1.6	-68.3	-14.8	1.8	21.7	1.8	7.9	2.4	38
90	30	43.7	0.1	17.5	0.1	19.6	2	-80.6	-22.9	1.8	9.4	1.8	-3.3	2.7	40
90.5	29.5	44	0.1	17.7	0.1	19.8	2.4	-83.5	-26.9	1.9	6.5	1.8	-7.1	3.1	41
91	28	41.9	0.1	21.2	0.1	15.8	1.5	-73.9	-42.6	3.1	16.1	1.8	-26.8	3.5	45
91	29	43.9	0.1	17.8	0.1	17.2	2	-77.6	-26	1.8	12.4	1.8	-8.8	2.7	38
91.5	38.5	33.5	0.2	5.5	0.2	13.1	2.1	-65.6	-30.1	1.8	24.4	1.8	-16.9	2.8	41
91.5	39	32.3	0.2	4.7	0.2	12.5	1.8	-60	-23.9	1.5	30	1.8	-11.3	2.3	38
92	27	40.8	0.2	23.7	0.2	3.2	3.3	-92.4	-66.9	2.1	-2.4	1.8	-63.7	3.9	46
92	27.5	41.6	0.2	20.1	0.2	17.9	4.3	-90.6	-62.7	2.8	-0.6	1.8	-44.8	5.2	47
92	29	45.4	0.1	13.8	0.1	20.2	1.8	-73.1	-24.5	2.1	16.9	1.8	-4.2	2.8	40
92	30.5	47.8	0.1	11.5	0.1	18.9	1.7	-71.6	-18	1.7	18.4	1.8	0.9	2.4	49
93	37.5	35.7	0.2	5.8	0.2	11.8	1.8	-59.2	-25.9	1.6	30.8	1.8	-14.1	2.4	43
93.5	28	44	0.3	14.5	0.3	3.7	3.1	-94.2	-57.9	2.7	-4.2	1.8	-54.2	4	44
94.5	34.5	49.2	0.2	4.1	0.1	20.3	1.8	-35.9	-21	1.8	54.1	1.8	-0.7	2.6	43

94.5	37	37	0.1	4.1	0.1	11.9	1.3	-51.3	-20.6	1.5	38.7	1.8	-8.7	2	41
94.5	38.5	34.3	0.1	2	0.1	12.2	1.5	-54.5	-22.4	1.6	35.5	1.8	-10.2	2.2	46
95.5	28.5	44.8	0.3	13.6	0.3	-14.3	4.2	-76.8	-99.6	3.7	13.2	1.8	-113.9	5.6	58
95.5	33.5	50.2	0.2	1.9	0.1	18.5	1.4	-31.1	-19.2	2	58.9	1.8	-0.7	2.4	39
96	33	50.5	0.2	0.5	0.2	18.1	1.5	-28.1	-18	1.8	61.9	1.8	0.1	2.3	48
96.5	33	49.9	0.2	-0.4	0.2	19.5	1.7	-23.4	-19.8	1.8	66.6	1.8	-0.2	2.4	49
97	25	27.1	0.3	-1.1	0.3	28.5	2.9	-27.7	-55.3	4.6	62.3	1.8	-26.9	5.5	26
97	32.5	49.6	0.2	-2	0.2	19.4	1.7	-18	-19.3	1.7	72	1.8	0.1	2.4	47
97	33	49.3	0.2	-1.2	0.2	22	2	-19.5	-22.2	1.9	70.5	1.8	-0.2	2.8	42
97	39	33.1	0.1	-0.2	0.1	8.3	1.3	-51.4	-22.9	1.4	38.6	1.8	-14.6	1.9	44
97.5	32.5	49	0.2	-2.9	0.2	21.4	1.8	-17.1	-20.7	1.9	72.9	1.8	0.7	2.6	40
97.5	33	48.5	0.2	-1.8	0.2	23	2	-18.6	-22.2	2	71.4	1.8	0.8	2.8	38
97.5	38	35.3	0.1	0.5	0.1	12.5	1.8	-52.5	-24.1	1.3	37.5	1.8	-11.6	2.3	41
98	32.5	48.2	0.2	-3.6	0.2	23.1	1.8	-17.8	-20.4	1.9	72.2	1.8	2.7	2.6	32
98	33	47.6	0.2	-2.5	0.2	23.7	1.9	-17.9	-21.4	2	72.1	1.8	2.2	2.8	31
98	33.5	47	0.2	-1.5	0.2	23	1.9	-19.5	-21.2	1.9	70.5	1.8	1.8	2.7	33
98	36	39.2	0.1	1.6	0.1	13.7	1.4	-44.4	-22.5	1.8	45.6	1.8	-8.9	2.3	52
98.5	38	35	0.1	-0.7	0.1	13	2.1	-49.4	-25.8	1.3	40.6	1.8	-12.8	2.5	43
99	32	47.2	0.2	-6.3	0.1	29.4	2.4	-15.4	-23.9	2.3	74.6	1.8	5.5	3.3	42
99	36	38.5	0.1	0.4	0.1	16.3	1.9	-41.8	-23.5	1.6	48.2	1.8	-7.1	2.5	33
100	35	40.4	0.1	-1.1	0.1	17.8	1.9	-30.7	-25.3	1.8	59.3	1.8	-7.5	2.6	47
72	35.5	24.9	0.1	24.8	0.1	0.6	1.9	-72.3	-38.7	1.4	17.7	1.7	-38.1	2.3	44
72.5	35	26.1	0.1	26.8	0.1	-1.4	1.6	-68.1	-34.3	1.4	21.9	1.7	-35.6	2	46
73	39.5	24.8	0.3	13.9	0.3	21.6	3.7	-111.8	-70.6	4.3	-21.8	1.7	-49.1	5.7	49
73.5	34.5	26.7	0.1	28.2	0.1	1.5	1.4	-68.7	-31.4	1.5	21.3	1.7	-29.9	1.9	44
73.5	36.5	23.2	0.1	22.2	0.2	12.2	1.1	-85.5	-18.3	1.4	4.5	1.7	-6.1	1.8	37
75	40	28	0.1	14.4	0.1	16.6	2.6	-88.9	-45.5	2.8	1.1	1.7	-28.9	3.8	70
75.5	35	25.7	0.1	23.5	0.2	16.3	2.5	-77	-63.4	4	13	1.7	-47.1	4.7	39
75.5	40	28.6	0.1	14.5	0.1	11.4	2.4	-95.9	-47.4	2.6	-5.9	1.7	-35.9	3.6	40
76	34.5	27.1	0.1	25.7	0.1	8.8	2.2	-69.7	-58.4	3.3	20.3	1.7	-49.6	4.1	34

78	31	30.9	0.3	28.6	0.3	13.3	3.1	-62.6	-59.9	2.9	27.4	1.7	-46.6	4.3	43
80.5	35.5	26.9	0.1	16.6	0.1	15.3	1.3	-60.8	-12.3	1	29.2	1.7	3	1.6	50
81	34.5	29.5	0.1	17	0.1	22.3	1.3	-75.3	-8	1.2	14.7	1.7	14.3	1.8	42
82	30.5	32	0.1	21.3	0.1	8.1	1.5	-83.2	-29	1.7	6.8	1.7	-20.9	2.3	56
82	36.5	26.3	0.1	14.5	0.1	15.9	1.3	-66.7	-13.5	1.2	23.3	1.7	2.4	1.7	51
83.5	30	34	0.1	22.6	0.1	14.9	2	-78.4	-25.9	1.6	11.6	1.7	-11	2.5	39
83.5	34.5	33.6	0.1	16.6	0.1	17.4	1.4	-74.5	-14.2	1.2	15.5	1.7	3.3	1.9	31
84.5	27	37.3	0.3	37.7	0.3	5.3	2	-75.4	-60.6	3.6	14.6	1.7	-55.4	4.1	44
85.5	26.5	38.2	0.4	38.7	0.4	7.6	1.7	-75.4	-58	3.3	14.6	1.7	-50.4	3.7	42
86	34.5	35.8	0.2	16	0.2	13.6	1.4	-64.8	-19.3	1.4	25.2	1.7	-5.7	2	63
87.5	28	38.3	0.2	27.1	0.2	9	2.8	-90.1	-53.4	2.3	-0.1	1.7	-44.4	3.6	48
87.5	33.5	40.4	0.2	16.3	0.2	21.3	1.2	-68.7	-13.5	1.6	21.3	1.7	7.8	2	42
90	29.5	43.1	0.1	18.8	0.1	18.5	2	-83.3	-27.4	1.9	6.7	1.7	-8.9	2.8	40
90	33.5	45.1	0.2	12	0.2	24.6	1.3	-67.2	-15	1.9	22.8	1.7	9.5	2.3	37
91	28.5	42.8	0.1	19.2	0.1	16.9	1.5	-74.9	-30.2	2.2	15.1	1.7	-13.3	2.7	43
91	32.5	47.2	0.2	10.8	0.1	23.2	1.8	-68.6	-16.9	1.6	21.4	1.7	6.3	2.3	36
91	36	39.7	0.3	9.4	0.3	35	1.8	-50.4	-21.9	2.9	39.6	1.7	13.1	3.4	44
91.5	27.5	41.1	0.2	22.2	0.2	16.2	3.2	-79.2	-61.7	3.5	10.8	1.7	-45.5	4.7	34
91.5	28	42.3	0.1	18.9	0.1	18.6	1.7	-77.5	-36.2	2.7	12.5	1.7	-17.6	3.2	43
91.5	29	44.6	0.1	15.9	0.1	19	1.7	-74.4	-24.1	1.9	15.6	1.7	-5.1	2.6	38
91.5	30.5	47	0.1	13	0.1	21.4	2	-74.2	-18.8	1.6	15.8	1.7	2.6	2.5	35
91.5	31	47.6	0.1	12.1	0.1	23.4	2	-73.9	-19.6	1.8	16.1	1.7	3.8	2.7	40
92	28.5	44.3	0.1	15.1	0.1	21.4	1.9	-75.7	-27.4	2.1	14.3	1.7	-6	2.8	35
92	36.5	38.4	0.2	7.8	0.2	31.9	1.9	-47.2	-23.1	2.7	42.8	1.7	8.8	3.2	41
92	39	32.5	0.1	4.2	0.1	13.4	1.8	-57.7	-25.1	1.4	32.3	1.7	-11.7	2.3	47
92.5	27	41	0.1	23.6	0.2	5.4	3.7	-97.3	-70.4	2.1	-7.3	1.7	-65	4.3	48
92.5	38	34.9	0.2	5.6	0.1	13.2	2	-61.4	-28.2	1.4	28.6	1.7	-15	2.5	42
94	25.5	33.6	0.1	22.9	0.1	21	2.1	-8.2	-35.2	2.8	81.8	1.7	-14.2	3.4	43
94	37	37.1	0.2	4.6	0.2	13	1.3	-49.8	-23.4	1.7	40.2	1.7	-10.4	2.1	68
94	38.5	34.3	0.1	2.5	0.1	13.7	1.5	-55.2	-24.4	1.5	34.8	1.7	-10.7	2.2	41

94.5	25	29.4	0.1	18.9	0.1	19.2	2.2	-12.7	-36.8	2.5	77.3	1.7	-17.6	3.3	45
94.5	39	33.3	0.1	1.4	0.1	16.4	1.7	-53.2	-20.5	1.4	36.8	1.7	-4.1	2.2	49
95	29	46	0.3	8.1	0.2	-13.9	3	-91.8	-90.1	3.2	-1.8	1.7	-104	4.4	83
95	37	36.9	0.1	3.7	0.1	12.6	1.4	-54.3	-19.6	1.4	35.7	1.7	-7	2	44
95.5	25	29.3	0.2	11.6	0.2	30.3	2.2	-29.9	-19.9	2	60.1	1.7	10.5	3	28
95.5	34	49.3	0.2	2.4	0.2	19.5	1.5	-27.5	-25.6	2.2	62.5	1.7	-6	2.7	39
96.5	25	27.7	0.3	3.5	0.3	34.9	3.1	-29.7	-34.4	2.7	60.3	1.7	0.6	4.1	29
96.5	27	37.6	0.3	7.4	0.3	20.2	3.2	-37.3	-56.2	3.4	52.7	1.7	-36	4.5	62
96.5	38.5	34.2	0.1	0.6	0.1	9.7	1.2	-55.3	-20.4	1.4	34.7	1.7	-10.6	1.8	41
97	27.5	38.3	0.3	1.7	0.3	21.1	3.3	-43.2	-65.6	4.3	46.8	1.7	-44.5	5.3	55
97.5	36	39.4	0.1	2.2	0.1	14.4	1.3	-47.9	-19.5	1.5	42.1	1.7	-5.1	2	57
97.5	39	32.9	0.1	-0.6	0.1	8.5	1.4	-49.7	-25.2	1.5	40.3	1.7	-16.8	2.1	51
98	38	35.2	0.1	-0.1	0.1	12.4	1.9	-50.1	-25.5	1.2	39.9	1.7	-13.1	2.3	34
98.5	32.5	47.4	0.2	-4.3	0.2	24.9	1.9	-16.6	-21.8	2	73.4	1.7	3.1	2.8	30
98.5	33	46.8	0.2	-3.2	0.2	23.8	1.8	-16.1	-21.8	1.9	73.9	1.7	2	2.7	32
98.5	36	38.9	0.1	1	0.1	14.5	1.5	-42.4	-24.3	1.7	47.6	1.7	-9.8	2.3	39
98.5	38.5	33.6	0.1	-1.2	0.1	13.3	1.8	-49.3	-27.1	1.6	40.7	1.7	-13.7	2.3	38
99.5	33.5	44.4	0.1	-3	0.1	19.8	1.6	-12.7	-22.9	1.9	77.3	1.7	-3.1	2.5	34
99.5	35.5	39.5	0.1	-0.3	0.1	18.2	2	-36.5	-24.6	1.7	53.5	1.7	-6.5	2.6	46
100	33.5	43.4	0.1	-3.3	0.1	18.7	1.6	-12.3	-22.4	1.8	77.7	1.7	-3.7	2.4	39
100	34	42.8	0.1	-2.4	0.1	18	1.7	-17.6	-25	1.8	72.4	1.7	-7	2.5	39
73	35	25.7	0.1	26.5	0.1	0.1	1.6	-66.6	-36.7	1.5	23.4	1.6	-36.6	2.1	44
73	39	22.8	0.3	17.4	0.3	21.2	3.7	-111.8	-70.7	3.7	-21.8	1.6	-49.5	5.2	46
73.5	35	25.5	0.1	25.9	0.1	3.2	2.2	-67.8	-45.2	1.8	22.2	1.6	-42	2.8	44
73.5	39	23	0.3	18.9	0.3	23.8	3.8	-109.4	-69	3.5	-19.4	1.6	-45.2	5.1	38
74	39	23.4	0.2	20	0.2	27.8	3.6	-105.7	-60.4	3	-15.7	1.6	-32.6	4.7	45
76	40	28.9	0.1	15.1	0.1	4.8	2	-98	-48.5	2.3	-8	1.6	-43.7	3	34
79.5	29	36	0.2	35.6	0.2	12.1	2.1	-72.8	-66.9	3.8	17.2	1.6	-54.8	4.3	44
80.5	41.5	30.8	0.1	11.8	0.1	7.8	1.6	-84.1	-39.3	2.1	5.9	1.6	-31.6	2.7	36
81	36	26.5	0.1	15.9	0.1	14	1.2	-59.5	-13.7	1	30.5	1.6	0.3	1.5	44

82	28	36.2	0.2	35.4	0.2	-0.9	2.7	-75.8	-61.1	2.7	14.2	1.6	-62	3.8	40
82.5	34.5	32.2	0.1	16.6	0.1	21.6	1.4	-72.9	-12.9	1.3	17.1	1.6	8.7	1.9	47
83	28	36.1	0.2	34.4	0.2	10.1	3.8	-75.8	-81.2	3.4	14.2	1.6	-71.1	5.1	31
83	29.5	33.9	0.1	23.9	0.1	13.1	1.8	-68.5	-32	1.5	21.5	1.6	-18.9	2.4	39
83	30	33.2	0.1	22.6	0.1	11.3	1.8	-74.9	-29.9	1.4	15.1	1.6	-18.6	2.3	45
83	34.5	32.9	0.1	16.6	0.1	19.4	1.4	-73.7	-13.6	1.2	16.3	1.6	5.8	1.8	52
84.5	35.5	33.1	0.2	14.9	0.2	18.1	1.6	-62.9	-23.1	1.6	27.1	1.6	-5.1	2.3	45
86	33.5	38.1	0.2	17.5	0.2	18.2	1.1	-72.7	-14.4	1.5	17.3	1.6	3.8	1.9	56
88	34	40.3	0.2	15.1	0.2	23.5	1.3	-67.1	-15.2	1.7	22.9	1.6	8.2	2.2	34
89	36.5	34.7	0.3	11.1	0.2	16	1.3	-68.5	-19.5	1.4	21.5	1.6	-3.5	1.9	44
90	32	45.5	0.1	13.9	0.1	22	1.3	-71.7	-16.3	1.7	18.3	1.6	5.7	2.1	42
90.5	32	46.3	0.1	12.7	0.1	22.2	1.4	-72.3	-17.6	1.7	17.7	1.6	4.5	2.2	44
91	33	47	0.2	10.3	0.2	24	1.7	-67.3	-15	1.6	22.7	1.6	9.1	2.2	38
91	33.5	46.8	0.2	9.9	0.2	24.6	1.6	-65.8	-13.4	1.5	24.2	1.6	11.2	2.2	46
91.5	28.5	43.5	0.1	17.2	0.1	19.2	1.4	-75.3	-27.6	2	14.7	1.6	-8.4	2.5	43
92	38.5	33.7	0.1	5.1	0.1	13.9	2	-62.2	-29.1	1.5	27.8	1.6	-15.1	2.5	43
93	28	44.2	0.2	15.2	0.3	11.4	3	-93.6	-57	2.4	-3.6	1.6	-45.6	3.9	39
93	37	36.8	0.2	6.2	0.2	17.3	1.5	-53.2	-23.7	1.7	36.8	1.6	-6.4	2.3	43
93	38	35	0.2	4.9	0.1	13.3	1.8	-59.3	-27.6	1.4	30.7	1.6	-14.3	2.2	42
93	39	32.9	0.1	2.9	0.1	20.5	2.1	-55.3	-27.2	1.8	34.7	1.6	-6.8	2.7	49
93.5	35	47	0.2	4.8	0.2	25.1	2.1	-48	-24.3	1.6	42	1.6	0.8	2.7	46
93.5	37	37	0.2	5.3	0.2	15.4	1.3	-51.4	-23.8	1.7	38.6	1.6	-8.4	2.1	49
93.5	38	35.1	0.2	4.1	0.1	12.4	1.6	-58	-26.7	1.5	32	1.6	-14.3	2.2	51
93.5	38.5	34.4	0.1	3.1	0.1	15.6	1.7	-55.9	-27.1	1.7	34.1	1.6	-11.5	2.4	49
93.5	39	33.1	0.1	2.4	0.1	19.4	1.9	-54.7	-24.8	1.7	35.3	1.6	-5.4	2.5	50
94	39	33.2	0.1	1.9	0.1	17.9	1.7	-54.1	-22.4	1.5	35.9	1.6	-4.5	2.3	36
94.5	24.5	28	0.1	18.2	0.1	17.3	2.3	-20.7	-39.9	2.2	69.3	1.6	-22.5	3.2	42
95.5	29.5	46.1	0.2	2.5	0.1	-17.6	3.2	-84	-87.9	2.7	6	1.6	-105.5	4.2	50
96	25	28.6	0.2	7.5	0.2	35	2.6	-30.1	-24.9	2.1	59.9	1.6	10.1	3.4	33
96	36.5	38.3	0.1	3.4	0.1	16.7	1.7	-53	-19.8	1.1	37	1.6	-3.1	2	36

96.5	29.5	44.4	0.1	-3.2	0.1	-3.5	2.5	-62.7	-63	2.3	27.3	1.6	-66.5	3.4	25
97	28	40.2	0.3	0.9	0.3	30.3	5.1	-51.1	-105.4	5.2	38.9	1.6	-75.1	7.3	45
97	33.5	48.4	0.2	-0.3	0.2	22.1	1.7	-22.9	-21.1	1.7	67.1	1.6	1	2.4	46
97	38.5	34.2	0.1	0.3	0.1	10.1	1.3	-53.1	-22.6	1.2	36.9	1.6	-12.5	1.8	44
97.5	38.5	34.1	0.1	-0.1	0.1	10.9	1.5	-50.7	-24.9	1.2	39.3	1.6	-14	2	45
98	34	46.1	0.2	-0.5	0.1	23.3	1.8	-25.2	-21.4	1.8	64.8	1.6	1.9	2.5	41
98.5	33.5	46.2	0.2	-2.1	0.1	22.3	1.7	-17.6	-21.6	1.8	72.4	1.6	0.7	2.4	35
98.5	34	45.5	0.2	-1	0.1	22	1.8	-22.2	-23.2	1.8	67.8	1.6	-1.2	2.5	38
99	32.5	46.5	0.2	-4.9	0.1	26.7	2	-13.7	-24.6	2.1	76.3	1.6	2.1	2.9	35
99	33.5	45.3	0.2	-2.6	0.1	21.3	1.6	-15.1	-22.3	1.8	74.9	1.6	-1.1	2.4	34
99	34	44.6	0.1	-1.6	0.1	20.9	1.7	-20.6	-24.1	1.9	69.4	1.6	-3.2	2.5	36
99.5	34	43.7	0.1	-2	0.1	19.5	1.7	-18.9	-24.7	1.9	71.1	1.6	-5.1	2.5	44
100	33	43.8	0.1	-4.3	0.1	20.6	1.7	-8	-23.1	1.9	82	1.6	-2.5	2.5	41
100	34.5	41.7	0.1	-1.7	0.1	18.8	1.8	-24.5	-26.6	1.8	65.5	1.6	-7.7	2.6	41
73	35.5	24.7	0.2	24.2	0.2	0.2	1.6	-70.5	-42.2	1.8	19.5	1.5	-42	2.4	39
73	36.5	22.6	0.1	21.8	0.2	10.8	1.3	-80.3	-25.3	1.4	9.7	1.5	-14.5	1.9	32
73.5	39.5	25.2	0.2	15	0.2	24.2	3.8	-113.4	-73.1	3.5	-23.4	1.5	-48.9	5.1	26
75	35	25.4	0.1	24.3	0.2	10.5	1.8	-74.8	-57.5	3.1	15.2	1.5	-47	3.6	33
75.5	34.5	27	0.1	26.7	0.1	14.1	2.5	-75.1	-67	3.3	14.9	1.5	-52.9	4.2	47
80	29.5	33.9	0.2	31.9	0.2	16.6	3.6	-71.4	-80.7	3.9	18.6	1.5	-64.1	5.2	48
81	30.5	31	0.1	21.9	0.1	13.8	2.1	-77.1	-46.2	2.3	12.9	1.5	-32.4	3.1	60
81	41.5	31.1	0.1	11.2	0.1	6.3	1.5	-85.8	-40.6	2	4.2	1.5	-34.3	2.5	32
84	28	36.1	0.1	31.6	0.1	-2.8	3.9	-73.7	-93.4	3.6	16.3	1.5	-96.2	5.2	27
84	35	33.5	0.2	15.8	0.2	17.6	1.5	-67.9	-18.6	1.3	22.1	1.5	-0.9	1.9	42
84.5	27.5	36.7	0.2	35.5	0.2	6.6	2.7	-75.9	-94.1	5.3	14.1	1.5	-87.5	5.9	48
84.5	36.5	29.9	0.2	13.1	0.2	19.9	1.5	-64.8	-20.6	1.5	25.2	1.5	-0.7	2.1	40
85	27.5	36.8	0.2	34.2	0.2	6.1	2.6	-76.5	-85.1	4.4	13.5	1.5	-79	5.1	40
86	27.5	36.9	0.1	31.2	0.1	16.6	3.2	-73.9	-80.4	3.5	16.1	1.5	-63.8	4.6	43
86	34	37.1	0.2	16.7	0.2	16.6	1.2	-68.9	-17.1	1.3	21.1	1.5	-0.5	1.8	55
86.5	26.5	38.5	0.2	36.8	0.2	7.5	1.8	-78.1	-54.1	2.6	11.9	1.5	-46.6	3.2	60

86.5	27.5	37.6	0.1	30.1	0.1	12.7	2.8	-79.9	-71.5	3	10.1	1.5	-58.8	4.1	75
86.5	33.5	38.8	0.2	17.1	0.2	19.5	1	-70.6	-14.9	1.4	19.4	1.5	4.6	1.8	35
87	27.5	37.9	0.1	30	0.1	4	2.4	-84	-63.7	2.6	6	1.5	-59.7	3.6	43
87	33.5	39.6	0.2	16.7	0.2	20.6	1.1	-69.3	-14.4	1.5	20.7	1.5	6.2	1.9	38
87	35.5	34.4	0.3	13.6	0.2	16.4	1.3	-62.7	-21.4	1.5	27.3	1.5	-4.9	2	52
89	34	42	0.2	13.8	0.2	26.1	1.5	-62.9	-15.5	1.6	27.1	1.5	10.6	2.2	39
90	32.5	45.4	0.2	13.2	0.1	23.6	1.2	-69.1	-16.5	1.7	20.9	1.5	7.1	2.1	46
90	33	45.3	0.2	12.5	0.2	24.2	1.2	-68	-16	1.8	22	1.5	8.3	2.1	48
90.5	33.5	45.9	0.2	10.9	0.2	24.4	1.3	-66.8	-14.3	1.5	23.2	1.5	10.1	2	43
91.5	23	40.2	0.1	33.7	0.1	3.1	1	-33.2	-27	1.2	56.8	1.5	-23.9	1.5	43
92	28	43	0.1	16.8	0.1	19.8	2.2	-82.3	-40.6	2.3	7.7	1.5	-20.8	3.2	31
92.5	24	35	0.1	30.6	0.1	-2.2	1.6	-19.3	-48	1.6	70.7	1.5	-50.1	2.3	30
92.5	28	43.9	0.1	15.5	0.1	17.8	2.7	-88.5	-49.8	2.3	1.5	1.5	-32	3.5	35
92.5	38.5	34	0.1	4.5	0.1	15.8	1.9	-59.4	-28.5	1.4	30.6	1.5	-12.7	2.3	41
92.5	39	32.7	0.1	3.5	0.1	20.3	2.2	-56.6	-28.5	1.6	33.4	1.5	-8.1	2.7	39
93	27.5	42.7	0.2	19.1	0.3	8.2	3.4	-93.9	-66.6	2	-3.9	1.5	-58.4	3.9	42
93	35	46.4	0.2	5.4	0.2	26.6	2	-49.9	-20.9	1.5	40.1	1.5	5.7	2.6	41
93	38.5	34.2	0.1	3.9	0.1	16.9	1.9	-57.5	-28	1.5	32.5	1.5	-11.2	2.3	40
95	34.5	48.9	0.1	3.6	0.1	21.3	1.7	-29.4	-30.8	2.1	60.6	1.5	-9.5	2.8	39
96	33.5	49.6	0.2	1.1	0.2	19.5	1.4	-27.5	-21.6	1.7	62.5	1.5	-2.1	2.2	47
96.5	33.5	49	0.2	0.4	0.2	20.8	1.4	-25.3	-21.5	1.6	64.7	1.5	-0.7	2.1	46
97	29	42.6	0.2	-5.6	0.2	11	3.4	-54	-75.8	3	36	1.5	-64.8	4.5	34
97	36	39.6	0.1	2.7	0.1	14.3	1.3	-46.9	-19.8	1.2	43.1	1.5	-5.5	1.8	50
97.5	34	46.7	0.2	0	0.1	23.8	1.7	-26.7	-20.9	1.6	63.3	1.5	2.8	2.4	41
98	35.5	40.9	0.1	1.6	0.1	23	1.6	-40.2	-25	2	49.8	1.5	-2	2.6	50
98	38.5	33.8	0.1	-0.6	0.1	12.1	1.6	-49.6	-26.2	1.2	40.4	1.5	-14.1	2	45
99	33	45.9	0.2	-3.7	0.1	23.1	1.7	-13	-23.3	1.8	77	1.5	-0.2	2.5	36
99.5	31.5	46.9	0.1	-8.8	0.1	37.6	2.6	-10.8	-27.4	2.4	79.2	1.5	10.2	3.5	47
99.5	33	44.9	0.1	-4.1	0.1	22.3	1.6	-10.2	-24.1	1.8	79.8	1.5	-1.8	2.4	44
99.5	34.5	42.6	0.1	-1.2	0.1	20.8	1.7	-25.9	-28.1	2	64.1	1.5	-7.3	2.6	44

99.5	35	41	0.1	-0.7	0.1	20.9	1.8	-31.3	-28.1	1.9	58.7	1.5	-7.1	2.6	48
100	32.5	44.2	0.1	-5.5	0.1	27.3	2	-6.6	-28.4	2	83.4	1.5	-1.2	2.8	42
72.5	35.5	24.7	0.1	24.7	0.1	0.8	1.6	-70.3	-40.1	1.5	19.7	1.4	-39.3	2.1	50
72.5	36	23.3	0.1	22.8	0.2	3.7	1.7	-69.4	-39.3	1.6	20.6	1.4	-35.6	2.2	50
72.5	39	23.2	0.2	14.9	0.2	17.7	2.4	-120	-58.6	2.9	-30	1.4	-40.9	3.8	51
74	34.5	26.7	0.1	27.8	0.1	5.2	1.6	-73	-39	1.5	17	1.4	-33.7	2.2	38
74	35	25.5	0.1	25.4	0.1	4.8	1.7	-72.1	-46	1.7	17.9	1.4	-41.2	2.4	48
74	39.5	25.6	0.2	16.5	0.2	22.8	3.6	-110.8	-65.2	2.6	-20.8	1.4	-42.4	4.4	41
74.5	35	25.4	0.1	24.9	0.2	6.4	1.6	-74.3	-52.2	2.3	15.7	1.4	-45.9	2.8	31
76	39.5	28.9	0.1	18.1	0.1	5.3	1.9	-99.1	-57.8	2.3	-9.1	1.4	-52.4	3	39
80	30.5	30.7	0.2	24.8	0.2	13.4	2.7	-69.4	-65.9	2.7	20.6	1.4	-52.5	3.9	42
81	29	35.9	0.1	32.9	0.1	2.7	3	-68.6	-86.8	2.9	21.4	1.4	-84	4.2	40
81.5	34.5	30.3	0.1	16.8	0.1	23.4	1.2	-76.3	-9.6	1.1	13.7	1.4	13.8	1.7	40
82	34.5	31.3	0.1	16.7	0.1	24	1.3	-77.8	-10.7	1.1	12.2	1.4	13.3	1.7	42
82.5	30	32.8	0.1	22.7	0.1	8	1.6	-72.6	-33.7	1.4	17.4	1.4	-25.8	2.1	25
82.5	36.5	26.9	0.1	14.1	0.1	19	1.2	-62.7	-15.3	1.2	27.3	1.4	3.7	1.7	46
83.5	28	36.3	0.2	33.1	0.1	6.1	3.3	-74.5	-81.3	3.3	15.5	1.4	-75.2	4.7	59
83.5	35	32.7	0.1	15.9	0.1	20.2	1.4	-68	-17.9	1.2	22	1.4	2.3	1.8	27
84.5	36	31.5	0.2	14	0.2	19.9	1.5	-62	-24.3	1.5	28	1.4	-4.4	2.2	44
86.5	34.5	36.5	0.2	15.6	0.2	17.4	1.2	-64.5	-19.4	1.4	25.5	1.4	-2.1	1.9	32
87	35	35.7	0.3	14.3	0.2	18.1	1.2	-62.8	-21	1.6	27.2	1.4	-2.9	2	57
87.5	34	39.3	0.2	15.5	0.2	22.2	1.1	-67.5	-16.1	1.5	22.5	1.4	6	1.9	41
87.5	36	33.9	0.3	12.7	0.3	17.3	1.4	-65.7	-20.4	1.3	24.3	1.4	-3.1	1.9	44
88	36.5	33.3	0.3	11.7	0.2	16.5	1.2	-69.5	-20.2	1.3	20.5	1.4	-3.7	1.8	42
88.5	36.5	34	0.2	11.4	0.2	16.5	1.2	-69	-19.8	1.3	21	1.4	-3.3	1.7	49
89.5	34	43	0.2	12.8	0.2	26.7	1.4	-62.2	-15.5	1.5	27.8	1.4	11.2	2.1	35
90.5	32.5	46.3	0.2	12	0.1	23.5	1.3	-69.4	-17	1.6	20.6	1.4	6.6	2	42
90.5	33	46.2	0.2	11.4	0.1	24.1	1.2	-67.9	-15.8	1.6	22.1	1.4	8.3	2	44
91.5	36	40.6	0.2	8.4	0.2	35.1	1.4	-47.8	-23.2	2.5	42.2	1.4	12	2.8	44
92	24	37.3	0.1	31.9	0.1	-6.1	1.3	-17	-42.2	1.2	73	1.4	-48.3	1.8	36

92.5	27.5	42.4	0.1	19.6	0.2	16.4	3.5	-94.7	-65.5	1.9	-4.7	1.4	-49.2	3.9	45
92.5	35	45.7	0.2	6.2	0.2	30	1.8	-51.1	-19	1.5	38.9	1.4	11	2.3	44
93	24.5	33.9	0.1	27.8	0.1	-0.2	1.9	-21.9	-46.6	1.3	68.1	1.4	-46.8	2.3	46
93.5	25.5	35.1	0.2	25.5	0.2	14.1	2.2	-12.4	-42	2	77.6	1.4	-27.8	3	43
94	24.5	29.6	0.1	21	0.1	20	2.4	-18.7	-46.1	2	71.3	1.4	-26.1	3.1	39
94	25	31.2	0.1	21.9	0.1	22	2.3	-13.5	-44	2.2	76.5	1.4	-21.9	3.2	40
94	35	47.4	0.2	4.6	0.1	26.8	2	-43.7	-27.8	1.6	46.3	1.4	-1	2.7	46
94.5	36.5	38.5	0.2	4.4	0.1	19.8	1.6	-45.1	-26	1.5	44.9	1.4	-6.2	2.2	35
95.5	24	28.3	0.2	10.1	0.3	37.4	1.6	-42.3	-32.4	2.9	47.7	1.4	5	3.4	37
95.5	29	45.4	0.2	8.1	0.2	-16.4	3.4	-82	-103.8	2.6	8	1.4	-120.2	4.3	41
95.5	36.5	38.4	0.1	3.7	0.1	20	1.7	-50.9	-22.1	1.1	39.1	1.4	-2.2	2	42
96.5	24.5	26.9	0.3	2.6	0.2	35.8	2.7	-34	-41.7	2.5	56	1.4	-5.9	3.9	38
96.5	27.5	40	0.4	8.4	0.4	24.2	3.4	-45.6	-81.6	4.2	44.4	1.4	-57.3	5.2	63
96.5	28	41.5	0.3	8.8	0.3	15.4	3.6	-56.6	-113.9	5.1	33.4	1.4	-98.5	6.3	49
96.5	36	39.9	0.1	3.1	0.1	16.2	1.5	-45.7	-21.6	1.1	44.3	1.4	-5.4	1.8	42
98	23	25.8	0.2	-6.6	0.2	14.5	1.5	-54.2	-24.2	1.3	35.8	1.4	-9.7	1.9	37
98	34.5	44.8	0.1	0.3	0.1	26.3	1.7	-31.2	-23.8	1.8	58.8	1.4	2.5	2.5	46
98.5	34.5	44.3	0.1	-0.2	0.1	24.6	1.7	-28.8	-27.9	2	61.2	1.4	-3.3	2.6	40
98.5	35.5	40.5	0.1	1	0.1	26.6	1.9	-37.6	-28.4	2	52.4	1.4	-1.9	2.7	39
99	34.5	43.5	0.1	-0.7	0.1	22.7	1.7	-27	-29.2	2	63	1.4	-6.4	2.6	41
99	35	41.8	0.1	-0.1	0.1	24.2	1.8	-31.9	-31	2	58.1	1.4	-6.8	2.7	41
99	35.5	40	0.1	0.3	0.1	22.8	1.9	-36.5	-27.6	1.8	53.5	1.4	-4.8	2.6	36
99.5	32.5	45.4	0.1	-5.3	0.1	27.6	1.9	-10.2	-27.1	1.9	79.8	1.4	0.6	2.7	39
73	36	23.5	0.1	22.8	0.2	5.3	1.3	-71.7	-35.6	1.5	18.3	1.3	-30.3	1.9	35
74.5	39	24.4	0.1	20.3	0.1	36.8	2.8	-100.9	-45.6	2.3	-10.9	1.3	-8.8	3.6	47
75	34.5	26.8	0.1	27.3	0.2	11.8	2.2	-73.8	-60.8	2.4	16.2	1.3	-48.9	3.4	28
75.5	39	27.3	0.1	20.6	0.1	28.1	2	-100.9	-41.1	2.3	-10.9	1.3	-13	3	41
80	30	32.1	0.2	28.1	0.2	15.1	3.4	-70.8	-81	2.6	19.2	1.3	-65.9	4.3	31
81	35	28.5	0.1	16.6	0.1	21.7	1.2	-69.3	-11.8	0.9	20.7	1.3	9.8	1.5	47
81	35.5	27.5	0.1	16.2	0.1	18.8	1.2	-64.7	-13.8	0.9	25.3	1.3	5.1	1.5	42

81.5	28.5	36.5	0.2	34.5	0.2	0	2.4	-67.5	-75.9	2.8	22.5	1.3	-75.9	3.7	51
81.5	36	27.1	0.1	15.4	0.1	17.8	1.1	-63.5	-15.5	1	26.5	1.3	2.4	1.5	32
82	30	32.5	0.1	23.1	0.1	7	1.4	-77.7	-40.6	1.5	12.3	1.3	-33.6	2.1	52
82.5	29.5	33.5	0.1	24.5	0.1	12.3	1.6	-66.8	-39.5	1.6	23.2	1.3	-27.1	2.2	25
83	29	34.7	0.1	25.6	0.1	12.7	1.7	-70.8	-54.4	2.3	19.2	1.3	-41.7	2.9	28
83	35	32	0.1	15.9	0.1	22.4	1.4	-67.5	-17.3	1.1	22.5	1.3	5.1	1.8	55
83	36.5	27.7	0.1	13.8	0.1	21.4	1.3	-64.7	-16.9	1.2	25.3	1.3	4.6	1.8	19
83.5	36.5	28.5	0.1	13.5	0.1	22.5	1.3	-66	-17.9	1.2	24	1.3	4.6	1.8	33
84	28.5	35.9	0.1	27.3	0.1	8.3	2.3	-76.5	-71.9	2.6	13.5	1.3	-63.6	3.5	39
84	35.5	32.4	0.2	15	0.2	21	1.4	-64.2	-21.6	1.3	25.8	1.3	-0.6	1.9	39
84	36.5	29.3	0.1	13.3	0.1	21.6	1.3	-65.9	-18.8	1.2	24.1	1.3	2.8	1.8	51
84.5	28	35.9	0.1	29.7	0.2	5	3.1	-78.7	-116.6	3.9	11.3	1.3	-111.7	5	20
85	27	37.5	0.3	37.7	0.2	6.8	1.8	-74.4	-73	3.3	15.6	1.3	-66.2	3.6	41
85	28	36.4	0.1	29.6	0.1	10.6	2.8	-84.3	-86.8	3.4	5.7	1.3	-76.1	4.4	43
86.5	34	37.8	0.2	16.3	0.2	19	1	-67.8	-17.4	1.4	22.2	1.3	1.6	1.8	38
87	34	38.5	0.2	15.9	0.2	21.1	1	-67.2	-17.2	1.5	22.8	1.3	4	1.8	41
87	34.5	37.2	0.2	15.1	0.2	20.1	1.1	-64.9	-19.3	1.5	25.1	1.3	0.9	1.9	50
87.5	34.5	38	0.2	14.7	0.2	22	1.1	-65.6	-18.4	1.6	24.4	1.3	3.6	2	41
87.5	35.5	35.2	0.2	13.3	0.2	18.8	1.2	-63.4	-20.3	1.3	26.6	1.3	-1.5	1.8	45
90.5	36	38.3	0.3	10.4	0.2	33.4	1.7	-55.2	-19.1	1.5	34.8	1.3	14.3	2.3	42
91.5	23.5	39.6	0.1	33.2	0.1	-1.7	0.8	-28.6	-30.5	1.1	61.4	1.3	-32.3	1.3	41
94	36.5	38.8	0.2	4.8	0.2	20.4	1.4	-41.8	-29.2	1.7	48.2	1.3	-8.8	2.2	75
94.5	35	47.4	0.1	4.4	0.1	27.2	1.9	-38.4	-33.1	1.8	51.6	1.3	-5.9	2.6	44
95	24.5	28.2	0.2	15	0.2	26.6	1.8	-32.3	-28.6	2.1	57.7	1.3	-2	2.7	42
95	36.5	38.3	0.1	4.1	0.1	21.4	1.7	-48.8	-24	1.3	41.2	1.3	-2.6	2.1	44
95.5	24.5	28.3	0.2	10.7	0.2	34.3	1.7	-37.1	-30	2.2	52.9	1.3	4.3	2.9	33
96	24.5	27.6	0.2	6.5	0.2	37.6	2.2	-35.8	-34.7	2.4	54.2	1.3	2.9	3.3	37
96	34	48.5	0.2	1.7	0.1	21.2	1.3	-26.8	-26.2	1.7	63.2	1.3	-5	2.2	43
96.5	24	26.7	0.2	1.8	0.2	39.7	2.9	-32.5	-41.8	2	57.5	1.3	-2	3.7	39
96.5	34	47.8	0.2	1.1	0.1	22.5	1.4	-26.8	-24.2	1.5	63.2	1.3	-1.7	2	42

97	34	47.2	0.2	0.6	0.1	23.4	1.4	-27.1	-22.4	1.4	62.9	1.3	1.1	2	46
97.5	35.5	41.2	0.1	2	0.1	20.5	1.3	-41.1	-22.8	1.5	48.9	1.3	-2.2	2	54
98	35	43	0.1	1.1	0.1	29.5	1.7	-35.4	-26.5	2	54.6	1.3	3	2.6	43
98.5	35	42.5	0.1	0.5	0.1	27.2	1.7	-33.2	-30.7	2	56.8	1.3	-3.5	2.7	45
99.5	32	46.2	0.1	-6.8	0.1	37.8	2.4	-12.1	-29.8	2.2	77.9	1.3	7.9	3.2	41
74.5	34.5	26.8	0.1	27.4	0.1	7.6	1.7	-74	-49.3	1.8	16	1.2	-41.6	2.5	28
74.5	39.5	26.2	0.1	17.4	0.1	26.9	2.8	-102.6	-61.5	2.2	-12.6	1.2	-34.6	3.6	54
80.5	29.5	34.1	0.2	30.4	0.2	14.3	3.3	-70.9	-87.1	2.3	19.1	1.2	-72.8	4	36
80.5	30.5	30.7	0.2	23.3	0.2	15.4	2.3	-72.2	-60.4	2.3	17.8	1.2	-45	3.3	40
82	36	27.7	0.1	15.1	0.1	21.9	1.2	-66.4	-16.9	1.1	23.6	1.2	5	1.6	52
82.5	35	31.2	0.1	16	0.1	24	1.3	-67	-16.5	1.1	23	1.2	7.5	1.7	48
83	27.5	36.3	0.2	37.7	0.2	6.6	2.2	-77.3	-71.5	2.7	12.7	1.2	-64.9	3.5	49
83.5	35.5	31.6	0.1	15.1	0.1	22.7	1.3	-64.6	-20.6	1.2	25.4	1.2	2.1	1.8	26
84	36	31	0.1	14.2	0.1	22.7	1.3	-63.1	-23.3	1.3	26.9	1.2	-0.5	1.9	41
86	26.5	38.3	0.3	38.1	0.2	8.3	1.4	-76.6	-60.3	2.4	13.4	1.2	-52.1	2.8	43
88	34.5	38.7	0.2	14.3	0.2	23.4	1.1	-64.5	-17.9	1.4	25.5	1.2	5.4	1.8	36
88	36	34.7	0.2	12.3	0.2	18.4	1.1	-65.8	-19.4	1	24.2	1.2	-1	1.5	36
88.5	34.5	39.4	0.2	13.9	0.2	25.6	1.2	-62.5	-17.8	1.3	27.5	1.2	7.7	1.8	39
89.5	36	36.7	0.2	11.3	0.2	25.1	1.5	-60.5	-18	1	29.5	1.2	7.1	1.8	47
90	34	43.7	0.2	11.9	0.2	28	1.3	-61.4	-15.6	1.3	28.6	1.2	12.4	1.8	40
90	36	37.4	0.2	11	0.2	28.8	1.6	-57.7	-18.1	1.2	32.3	1.2	10.6	2	42
91	34	45.5	0.2	9.8	0.2	29.4	1.5	-61.2	-14.5	1.2	28.8	1.2	14.9	1.8	46
92.5	36.5	38.9	0.2	7	0.2	30.2	1.4	-45.7	-26.4	2.1	44.3	1.2	3.8	2.4	45
93.5	25	33.5	0.1	25.3	0.1	20.8	2.5	-14.5	-50.6	1.6	75.5	1.2	-29.8	3	44
94.5	23	27.8	0.1	17.1	0.1	29.6	1.5	-36.6	-20.8	1.7	53.4	1.2	8.8	2.2	36
95.5	23	27.2	0.2	8.6	0.2	49.3	2.8	-40.4	-39.5	2.7	49.6	1.2	9.9	3.8	43
95.5	34.5	48	0.1	3	0.1	22.8	1.5	-27.9	-35	1.8	62.1	1.2	-12.1	2.4	39
96	29.5	45.3	0.1	0.3	0.1	-9.7	2.7	-71.7	-90.1	2.4	18.3	1.2	-99.8	3.6	48
96	36	40.3	0.1	3.6	0.1	21.3	1.7	-45.3	-25	1.1	44.7	1.2	-3.7	2	38
96.5	23.5	26.5	0.2	1.1	0.2	52.1	3.5	-31.4	-40.3	1.6	58.6	1.2	11.8	3.9	40

97	28.5	41.7	0.2	-2.2	0.2	18.3	4.1	-58.1	-118.1	3.9	31.9	1.2	-99.8	5.7	36
97.5	23	25.8	0.2	-4.9	0.2	16.3	1.7	-47.9	-29.4	1.2	42.1	1.2	-13.1	1.9	31
97.5	34.5	45.2	0.1	0.8	0.1	26.7	1.5	-31.6	-23	1.5	58.4	1.2	3.7	2.2	48
97.5	35	43.3	0.1	1.5	0.1	26.3	1.4	-35.9	-24.6	1.5	54.1	1.2	1.7	2.1	48
100	31.5	45.6	0.1	-9.8	0.1	49.9	2.5	-7.1	-37.7	2.5	82.9	1.2	12.2	3.5	44
75	39	25.9	0.1	20.4	0.1	36.6	2.1	-100.1	-41.4	2.1	-10.1	1.1	-4.7	3	65
81	30	32.4	0.1	25	0.1	9.4	2.1	-72.9	-72	1.9	17.1	1.1	-62.6	2.9	47
81.5	30	32.4	0.1	23.8	0.1	6.8	1.6	-74.9	-55.4	1.8	15.1	1.1	-48.6	2.4	65
81.5	35	29.3	0.1	16.4	0.1	24.4	1.2	-71.3	-12.9	1	18.7	1.1	11.5	1.5	47
81.5	35.5	28.2	0.1	15.9	0.1	21.4	1.1	-67.4	-14.7	0.9	22.6	1.1	6.7	1.4	48
82	35	30.3	0.1	16.2	0.1	26	1.2	-72.7	-13.7	1	17.3	1.1	12.3	1.6	39
82.5	35.5	30	0.1	15.4	0.1	23.9	1.2	-63.5	-19.1	1	26.5	1.1	4.8	1.6	56
82.5	36	28.5	0.1	14.8	0.1	22.8	1.2	-61.4	-20.3	1.2	28.6	1.1	2.6	1.6	52
83	35.5	30.9	0.1	15.3	0.1	23.9	1.2	-64.2	-20.1	1.1	25.8	1.1	3.7	1.6	31
83	36	29.4	0.1	14.5	0.1	23.8	1.2	-62.6	-21.2	1.2	27.4	1.1	2.6	1.7	27
83.5	28.5	35.7	0.1	28.5	0.1	10.4	2.1	-76.2	-82.4	2.4	13.8	1.1	-71.9	3.2	34
83.5	36	30.3	0.1	14.4	0.1	24.2	1.3	-63.4	-22.3	1.2	26.6	1.1	1.9	1.8	31
88.5	36	35.4	0.2	11.9	0.2	19.8	1.1	-64.8	-18.8	0.9	25.2	1.1	1.1	1.4	46
89	36	36.1	0.2	11.5	0.2	21.3	1.2	-63.2	-18.4	0.9	26.8	1.1	2.9	1.5	38
90.5	34	44.6	0.2	10.8	0.2	29	1.3	-61.3	-15.3	1.2	28.7	1.1	13.7	1.7	40
91.5	34.5	44.7	0.2	8.7	0.2	34.9	1.6	-58.1	-15.8	1	31.9	1.1	19.2	1.9	44
92	35	44.3	0.2	7.5	0.2	33.6	1.4	-53.4	-17.7	1.2	36.6	1.1	15.9	1.9	46
92	35.5	43.1	0.2	7.3	0.2	33.7	1.2	-47.5	-21.6	1.7	42.5	1.1	12.1	2.1	42
92	36	41.2	0.2	7.5	0.2	34.5	1.2	-44.9	-25.7	2	45.1	1.1	8.8	2.3	43
93	36.5	39	0.2	6.2	0.2	27.3	1.3	-44.1	-28.2	1.8	45.9	1.1	-1	2.2	44
93.5	24.5	31.8	0.1	24.7	0.1	15.8	2.2	-20.7	-52.1	1.4	69.3	1.1	-36.4	2.6	41
93.5	35.5	44.3	0.2	5	0.2	30.4	1.7	-42.9	-30	1.6	47.1	1.1	0.4	2.3	46
93.5	36.5	39.1	0.2	5.4	0.2	23.8	1.3	-42.9	-29	1.7	47.1	1.1	-5.2	2.1	41
94	35.5	44.3	0.2	4.6	0.1	30.1	1.8	-41.8	-34.6	1.6	48.2	1.1	-4.5	2.5	46
94	36	41.3	0.2	4.7	0.2	26.5	1.6	-39.8	-35.1	1.7	50.2	1.1	-8.6	2.4	55

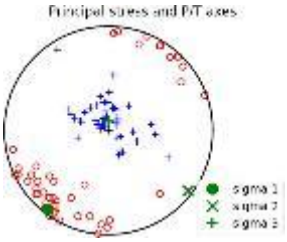
94.5	35.5	44.1	0.1	4.5	0.1	29.9	1.9	-40.1	-38.5	1.7	49.9	1.1	-8.6	2.6	43
94.5	36	40.9	0.2	4.5	0.1	25.6	1.7	-40.2	-35.2	1.7	49.8	1.1	-9.5	2.4	37
95	23.5	27.9	0.2	14.1	0.2	32.1	1.4	-39.3	-25.8	1.7	50.7	1.1	6.3	2.2	40
95	24	28.1	0.2	14.5	0.2	29.4	1.5	-36.5	-28.3	1.9	53.5	1.1	1.1	2.3	41
95	35	46.9	0.1	4.1	0.1	27.3	1.8	-34.4	-39.3	1.8	55.6	1.1	-12.1	2.6	40
95	36	40.7	0.1	4.3	0.1	27.3	1.8	-44.2	-30.9	1.3	45.8	1.1	-3.6	2.2	40
95.5	23.5	27.8	0.2	9.4	0.2	42.1	1.6	-40.4	-32.1	2.2	49.6	1.1	10	2.8	41
95.5	36	40.5	0.1	4	0.1	25.9	1.8	-45.2	-28.5	1.2	44.8	1.1	-2.6	2.1	37
96	24	27.4	0.2	5.8	0.2	40.7	1.9	-37.8	-40	2.4	52.2	1.1	0.7	3.2	40
96.5	23	26.4	0.2	0.2	0.2	39.5	2.5	-39.6	-40.7	1.6	50.4	1.1	-1.2	2.9	38
96.5	28.5	42.7	0.2	4.7	0.2	14	3.1	-59.5	-125.2	4	30.5	1.1	-111.2	5.1	39
97	23	26	0.2	-2.6	0.2	23.3	2	-43.3	-34.7	1.3	46.7	1.1	-11.4	2.3	37
97	35.5	41.6	0.1	2.5	0.1	20.4	1.3	-40	-24.1	1.2	50	1.1	-3.7	1.8	48
100	32	44.9	0.1	-7.2	0.1	43.9	2.3	-8	-36.8	2.2	82	1.1	7.1	3.2	43
75	39.5	27.3	0.1	17.4	0.1	29.9	2.2	-99.4	-63.9	2.3	-9.4	1	-34	3.2	61
75.5	39.5	28.3	0.1	17.6	0.1	20.3	2	-99	-65.3	2.4	-9	1	-45	3.2	38
80.5	30	32.3	0.2	26.6	0.2	13.3	2.5	-71.5	-78.1	1.9	18.5	1	-64.9	3.2	38
81	29.5	34.1	0.1	28.9	0.1	5.8	2.3	-70.1	-85.6	1.8	19.9	1	-79.8	2.9	50
81.5	29	35.3	0.1	31	0.1	4.1	1.9	-68.4	-85.7	2.2	21.6	1	-81.6	3	64
82	28.5	35.9	0.2	32.9	0.2	6.9	2.3	-71.2	-83.8	2.3	18.8	1	-76.8	3.3	39
82	29.5	33.4	0.1	25.5	0.1	8.3	1.4	-70.7	-58.2	1.8	19.3	1	-49.9	2.2	48
82	35.5	29.1	0.1	15.7	0.1	24.1	1.1	-69	-16	1	21	1	8.2	1.5	56
82.5	29	34.4	0.1	26.8	0.1	17	1.7	-65	-68.4	2.4	25	1	-51.4	2.9	25
83	28.5	35.6	0.1	29.7	0.1	11.6	2	-74	-89.9	2.4	16	1	-78.3	3.1	26
91.5	35.5	41.9	0.2	8.5	0.2	35.7	1.2	-51.8	-19.7	1.4	38.2	1	16	1.9	47
92.5	35.5	43.7	0.2	6.5	0.2	32.4	1.3	-45.7	-23.3	1.6	44.3	1	9	2	43
92.5	36	41.6	0.2	6.7	0.2	33	1.2	-43.3	-27.6	1.8	46.7	1	5.4	2.1	44
93	35.5	44.1	0.2	5.7	0.2	31	1.4	-43.9	-26.2	1.5	46.1	1	4.9	2.1	41
93	36	41.7	0.2	5.9	0.2	31	1.2	-41.8	-29.9	1.7	48.2	1	1.1	2	43
93.5	36	41.7	0.2	5.3	0.2	28.4	1.3	-40.8	-32	1.6	49.2	1	-3.6	2.1	42

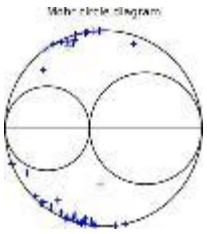
94	23	28.1	0.1	19.9	0.1	28.9	1.5	-26.8	-30.3	1.7	63.2	1	-1.4	2.1	49
94.5	23.5	27.9	0.1	17.4	0.1	25.9	1.4	-34.1	-27.7	1.5	55.9	1	-1.8	2	40
94.5	24	28.1	0.1	17.7	0.1	23.6	1.6	-30	-36.5	1.7	60	1	-12.9	2.2	44
95	23	27.6	0.1	13.1	0.2	36.1	1.6	-39.7	-27.7	1.8	50.3	1	8.4	2.4	49
95	35.5	43.6	0.1	4.3	0.1	29.7	1.8	-38.3	-40	1.6	51.7	1	-10.3	2.4	39
95.5	35	46	0.1	3.6	0.1	28.3	1.7	-32.9	-40.8	1.6	57.1	1	-12.5	2.3	37
95.5	35.5	43.3	0.1	3.9	0.1	29.3	1.7	-39.5	-35.9	1.3	50.5	1	-6.6	2.2	36
96	23	27.1	0.2	3.8	0.2	67.8	3.4	-37.4	-48.4	2.6	52.6	1	19.5	4.1	41
96	23.5	27.2	0.2	4.9	0.2	48.9	2.1	-37.6	-41.5	2.2	52.4	1	7.5	3	42
96	34.5	47.1	0.1	2.4	0.1	24.4	1.4	-28.8	-31.9	1.5	61.2	1	-7.5	2	39
96	35.5	42.8	0.1	3.4	0.1	25.8	1.6	-39.1	-31.6	1.1	50.9	1	-5.8	1.9	34
96.5	34.5	46.3	0.1	1.9	0.1	25.5	1.3	-29.9	-28.3	1.3	60.1	1	-2.7	1.9	40
96.5	35.5	42.2	0.1	3	0.1	22.4	1.4	-38.9	-27.7	1.1	51.1	1	-5.3	1.8	42
97	34.5	45.7	0.1	1.3	0.1	26.2	1.3	-30.7	-25	1.3	59.3	1	1.2	1.9	46
97	35	43.8	0.1	2	0.1	25.9	1.3	-35	-26.9	1.3	55	1	-0.9	1.8	42
82.5	28.5	35.6	0.1	31.3	0.1	12.8	2.1	-69.2	-90.5	2.4	20.8	0.9	-77.7	3.1	25
89.5	34.5	40.8	0.2	12.8	0.2	31.6	1.3	-58.7	-17.2	1	31.3	0.9	14.4	1.6	50
90	34.5	41.7	0.2	11.9	0.2	33.7	1.3	-58.1	-17.1	0.9	31.9	0.9	16.6	1.6	38
90	35.5	38.6	0.2	11.5	0.2	35.1	1.4	-57.2	-18.2	0.8	32.8	0.9	16.9	1.6	44
91	34.5	43.6	0.2	9.8	0.2	36.2	1.3	-58.2	-16.2	0.9	31.8	0.9	20	1.7	44
91	35.5	40.7	0.2	9.6	0.2	36.4	1.2	-54.6	-18.7	1.1	35.4	0.9	17.7	1.7	43
91.5	35	43.1	0.2	8.6	0.2	36.4	1.3	-55.1	-17.4	1	34.9	0.9	19	1.7	48
94	24	29	0.1	20.7	0.1	22.8	1.5	-25	-48.7	1.5	65	0.9	-25.8	2.1	43
96	29	44.5	0.1	6	0.1	1	3.5	-65.8	-126.9	2.6	24.2	0.9	-126	4.3	47
96	35	45.2	0.1	3	0.1	26.8	1.5	-33.7	-34.6	1.2	56.3	0.9	-7.7	1.9	39
96.5	29	43.5	0.2	0.4	0.1	7.4	2.8	-61.3	-110.2	2.4	28.7	0.9	-102.8	3.7	38
96.5	35	44.5	0.1	2.5	0.1	25.6	1.3	-34.2	-30.2	1.1	55.8	0.9	-4.6	1.7	42
81.5	29.5	33.7	0.1	27.2	0.1	5.1	1.5	-69.5	-76.5	1.7	20.5	0.8	-71.4	2.3	68
82	29	34.7	0.1	29	0.1	10.7	1.6	-68.7	-81.2	2.2	21.3	0.8	-70.5	2.7	43
90.5	34.5	42.5	0.2	10.9	0.2	34.8	1.2	-58.1	-16.6	0.8	31.9	0.8	18.2	1.5	44

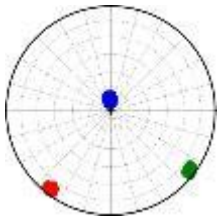
90.5	35.5	39.5	0.2	10.6	0.2	36.5	1.3	-56.4	-18.1	0.9	33.6	0.8	18.4	1.6	43
91	35	42	0.2	9.8	0.2	38.1	1.2	-56.4	-17.4	0.9	33.6	0.8	20.7	1.5	39
93	24	32.9	0.1	27.7	0.1	15.4	1.2	-23.6	-51.3	1.4	66.4	0.8	-35.9	1.8	43
93.5	24	30.8	0.1	24.4	0.1	21.1	1.3	-24.2	-53.4	1.3	65.8	0.8	-32.3	1.9	40
94	23.5	28.4	0.1	20.3	0.1	26.6	1.3	-26.6	-41.9	1.5	63.4	0.8	-15.3	1.9	48
90.5	35	40.9	0.2	10.8	0.2	37.7	1.2	-57	-17.5	0.8	33	0.7	20.3	1.4	46
92	23.5	37.7	0.1	32.1	0.1	7.8	1	-25.3	-56.6	1.2	64.7	0.7	-48.8	1.6	39
93.5	23.5	30	0.1	23.9	0.1	27.2	1.1	-22.8	-56	1.6	67.2	0.7	-28.8	1.9	42
92	23	38.4	0.1	32.6	0.1	19.4	1.5	-25.9	-69.8	1.4	64.1	0.6	-50.4	2.1	39
93	23.5	32.3	0.1	27.6	0.1	27.2	1	-20.4	-69.5	1.4	69.6	0.6	-42.3	1.8	43
92.5	23	35.4	0.1	30.2	0.1	31.6	1.5	-19.9	-82.3	1.1	70.1	0.5	-50.7	2	45
92.5	23.5	35.1	0.1	30.4	0.1	22.1	1.1	-22.2	-70.8	1.2	67.8	0.5	-48.7	1.7	44
93.5	23	29.6	0.1	23.1	0.1	29.8	1.2	-20.4	-64.9	1.1	69.6	0.5	-35.1	1.7	46
93	23	32.2	0.1	26.6	0.1	30.1	1.2	-19.4	-77.3	1	70.6	0.4	-47.2	1.6	31

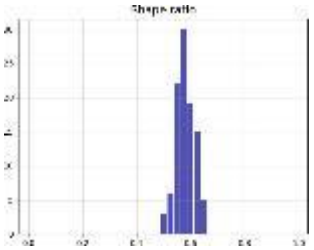
8.1.5. Figures – Stress inversion results

GRID ID = 11

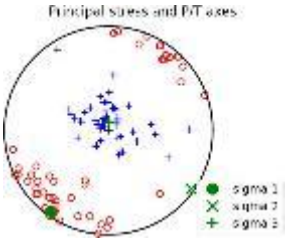


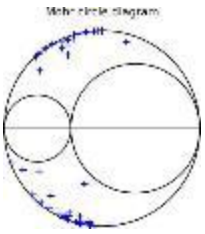


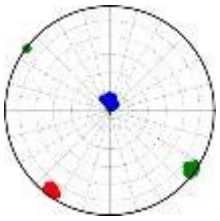


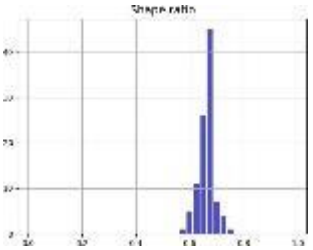


GRID ID = 12

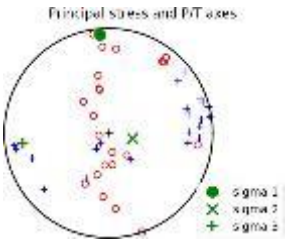


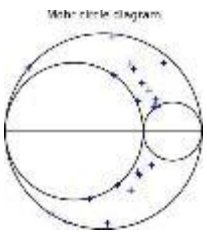


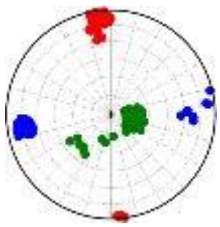


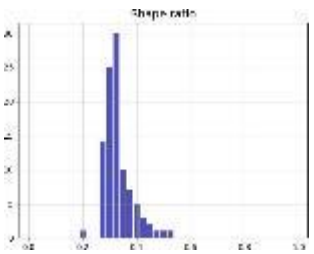


GRID ID = 13

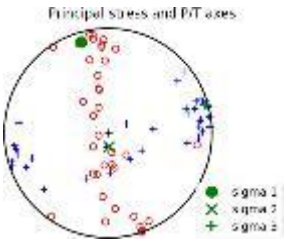


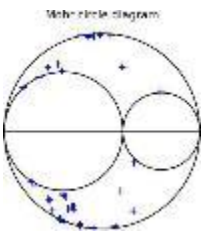


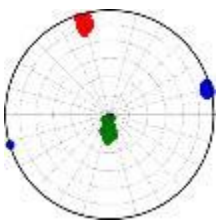


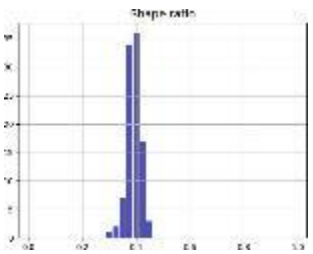


GRID ID = 14

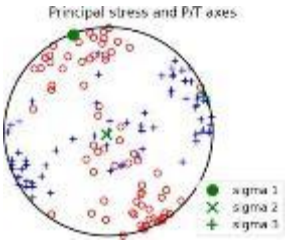


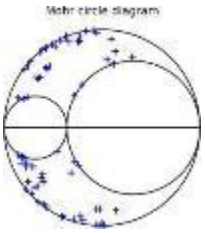


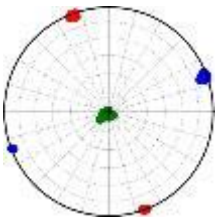


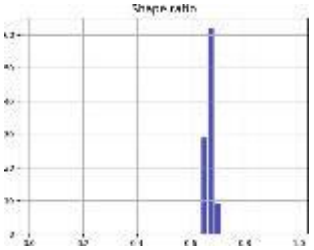


GRID ID = 15

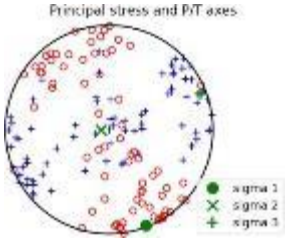


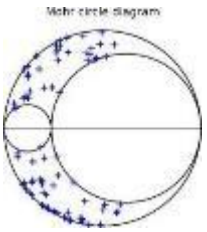


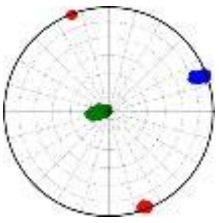


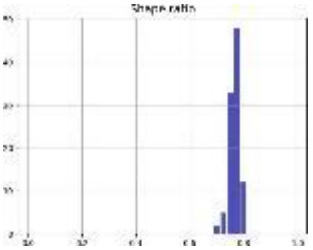


GRID ID = 16

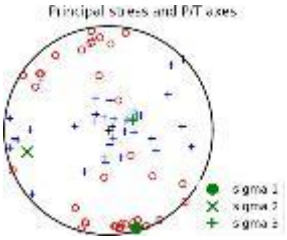


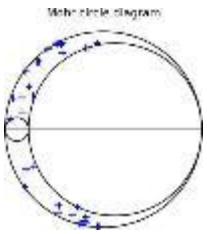


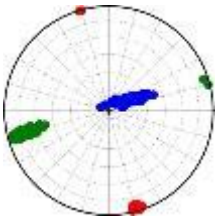


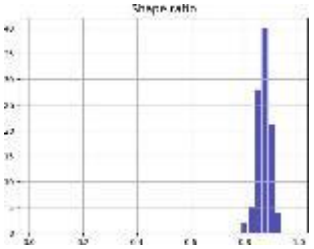


GRID ID = 17

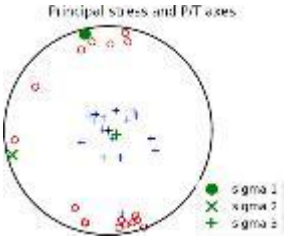


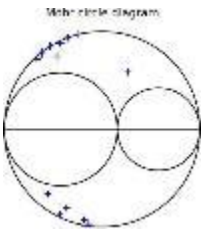


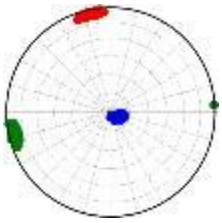


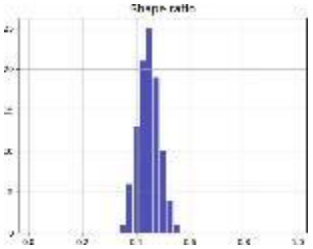


GRID ID = 18

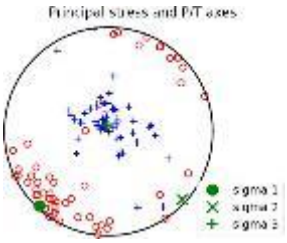


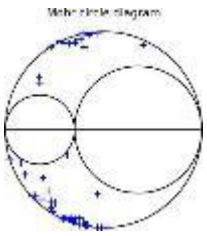


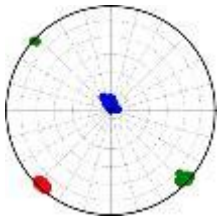


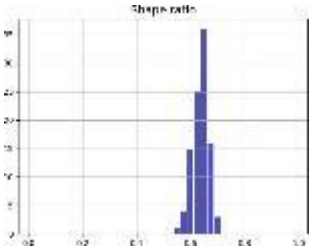


GRID ID = 30

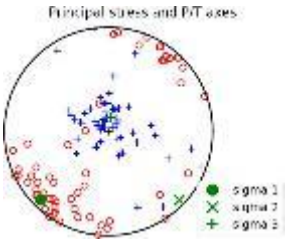


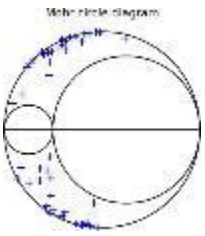


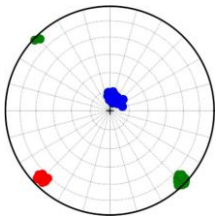


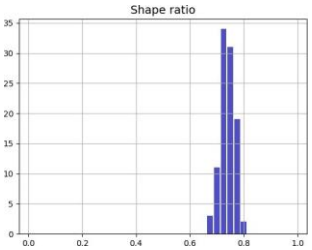


GRID ID = 31

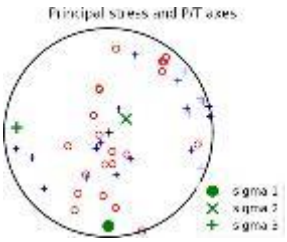


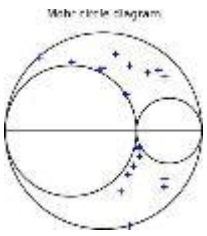


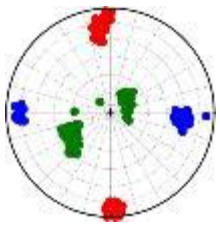


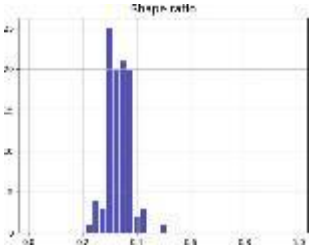


GRID ID = 32

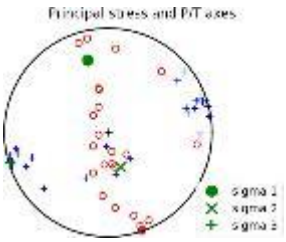


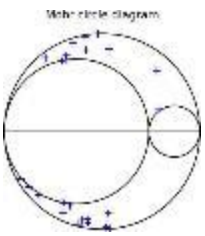


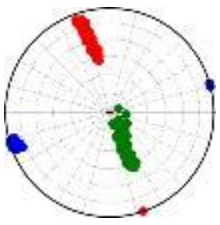


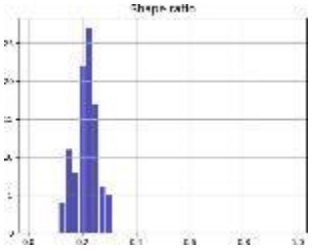


GRID ID = 33

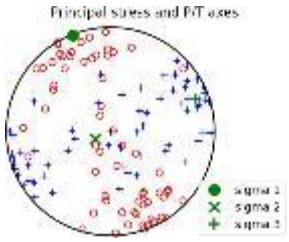


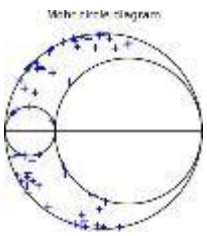


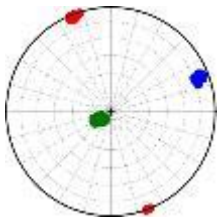




GRID ID = 34

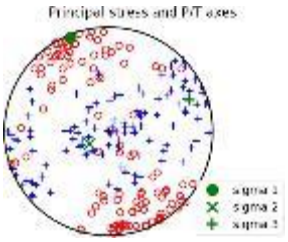


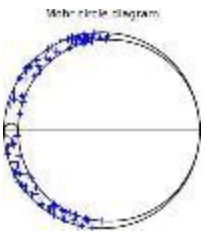


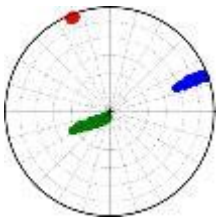


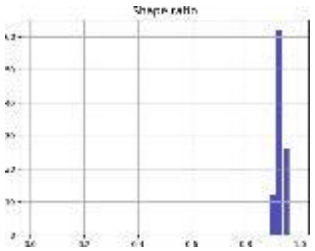


GRID ID = 35

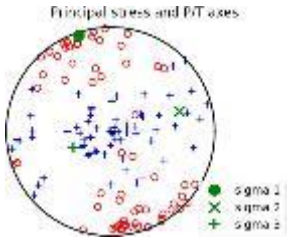


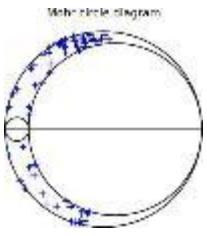


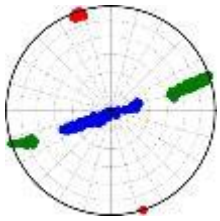


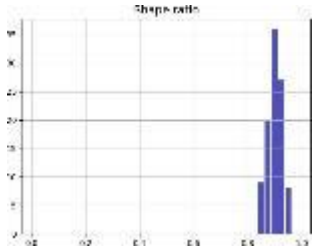


GRID ID = 36

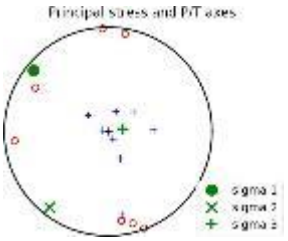


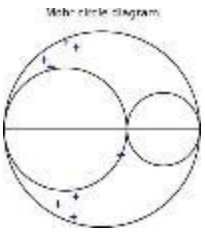


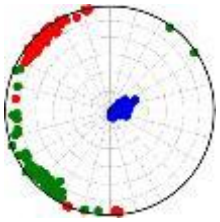


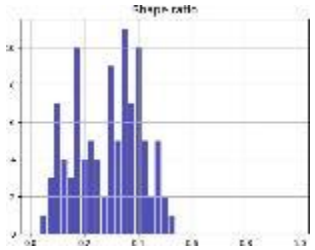


GRID ID = 37

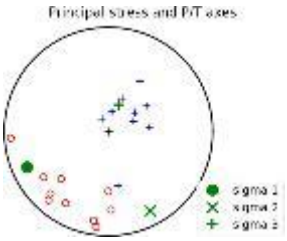


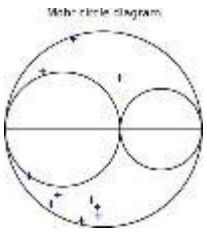


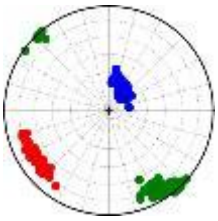


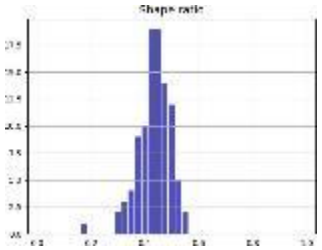


GRID ID = 48

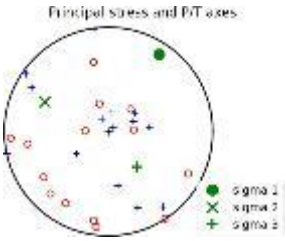


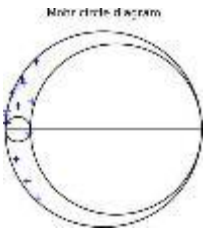


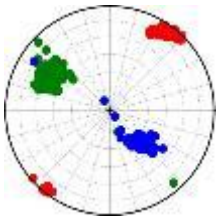


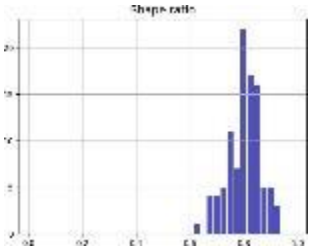


GRID ID = 49

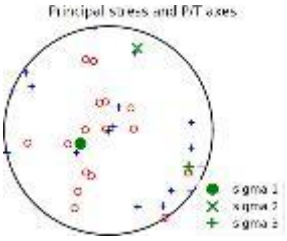


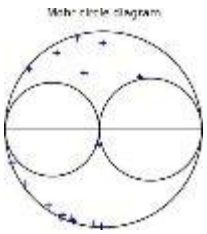


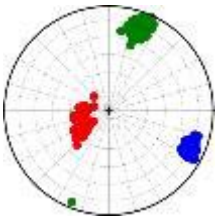


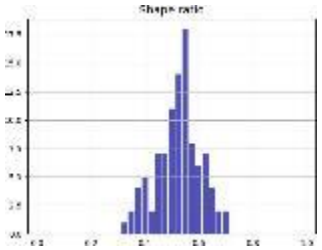


GRID ID = 50

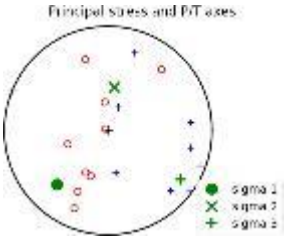


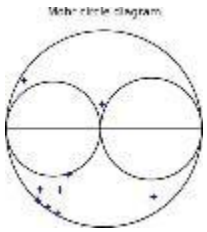


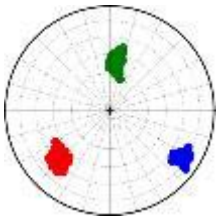


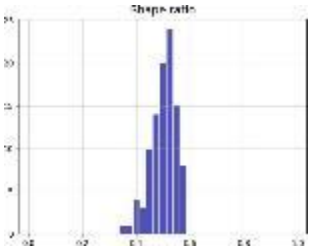


GRID ID = 51

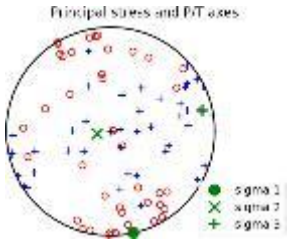


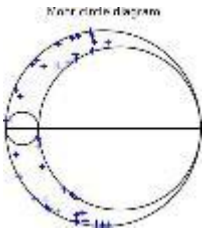


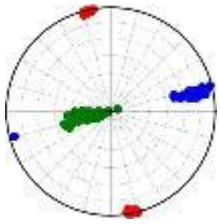


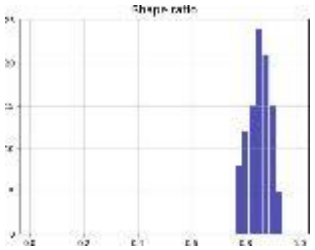


GRID ID = 53

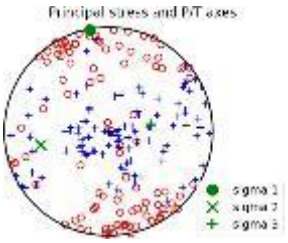


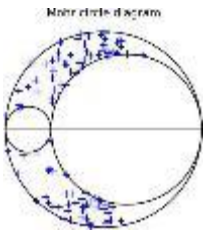


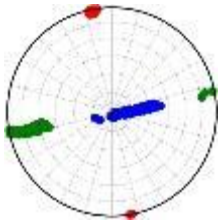


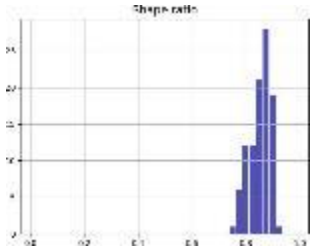


GRID ID = 54

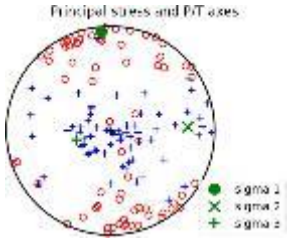


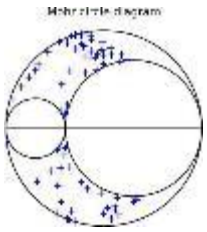


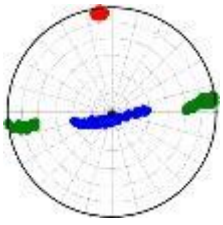


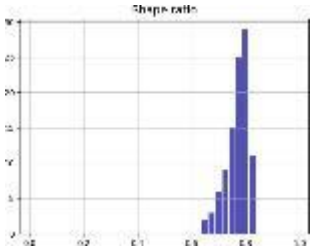


GRID ID = 55

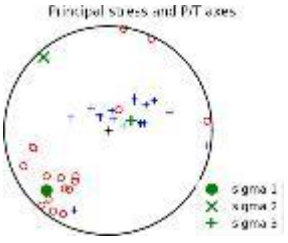


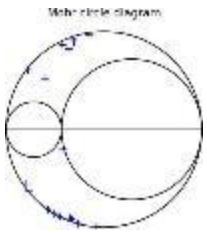


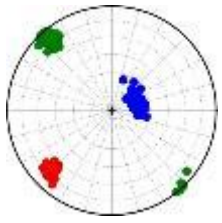


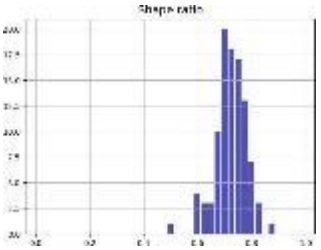


GRID ID = 66

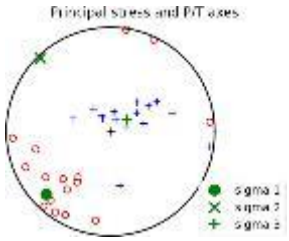


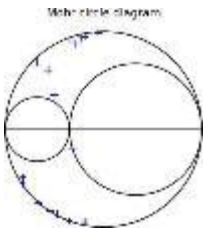


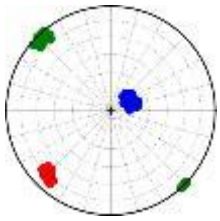


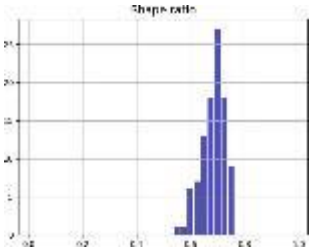


GRID ID = 67

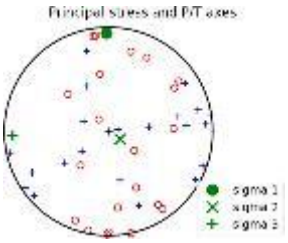


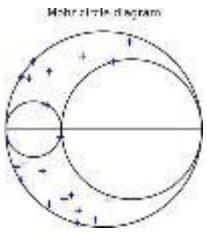


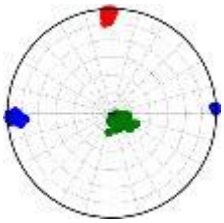


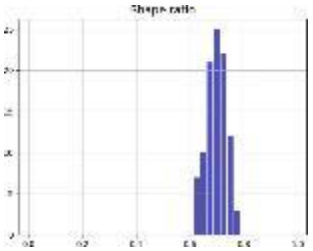


GRID ID = 72

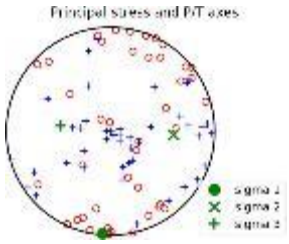


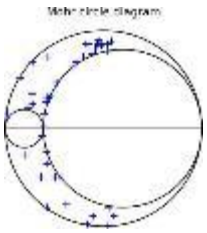


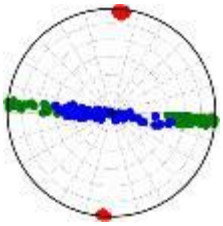


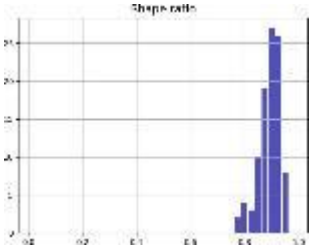


GRID ID = 73

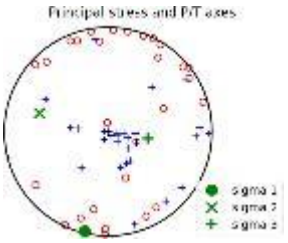


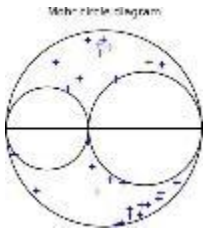


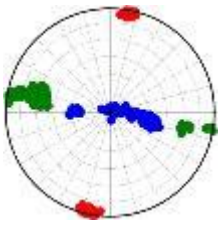


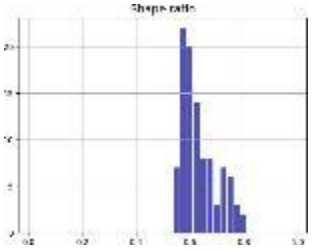


GRID ID = 74

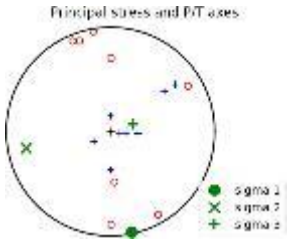


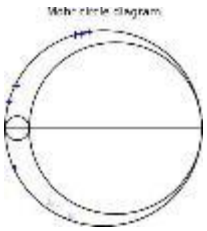


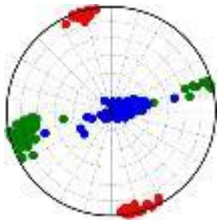


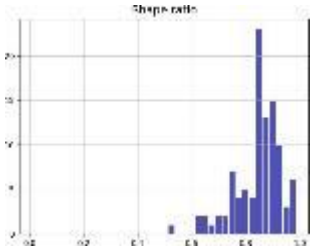


GRID ID = 75

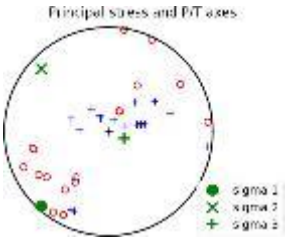


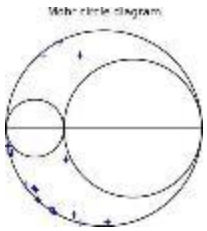


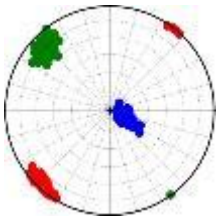


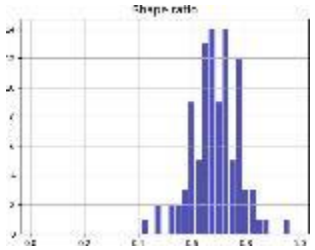


GRID ID = 85

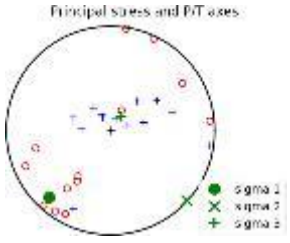


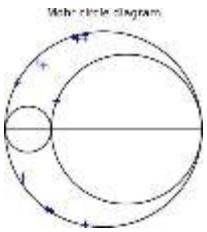


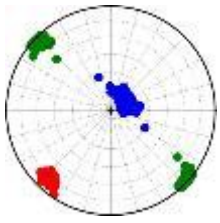


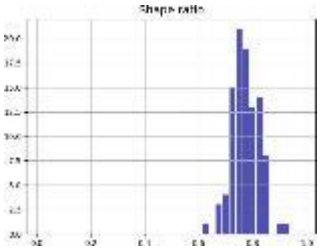


GRID ID = 86

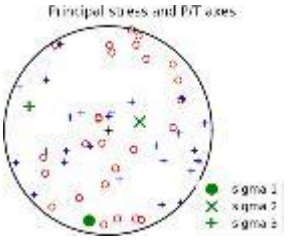


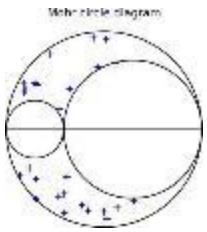


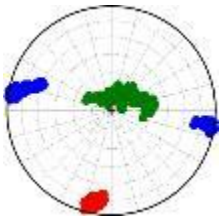


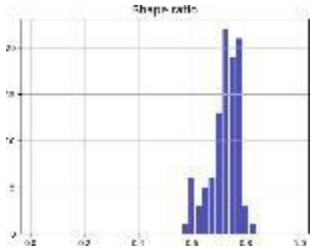


GRID ID = 91

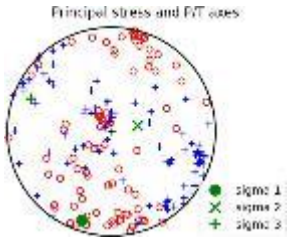


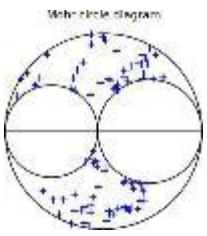


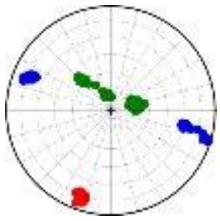


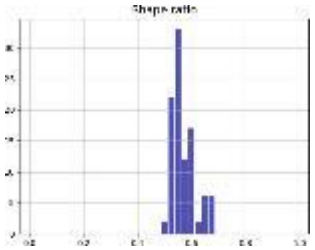


GRID ID = 92

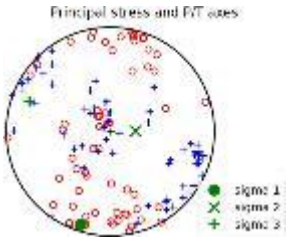


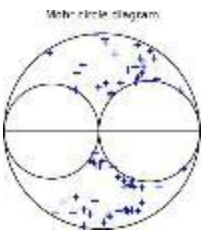


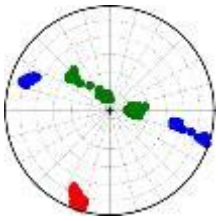


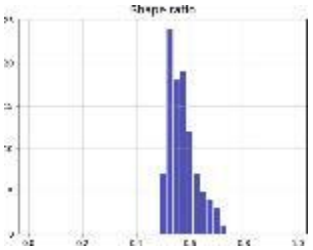


GRID ID = 93

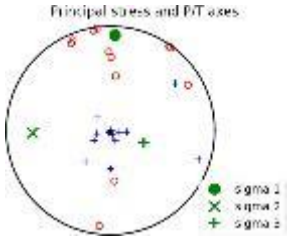


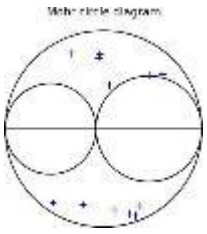


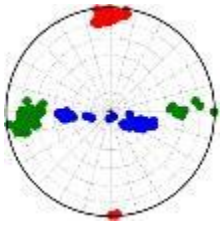


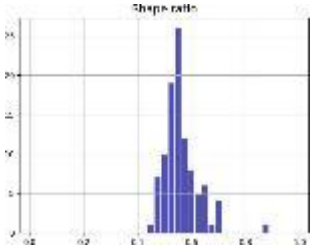


GRID ID = 94

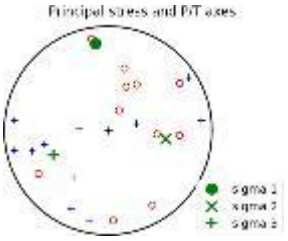


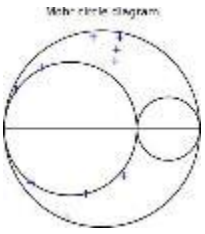


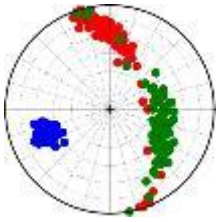


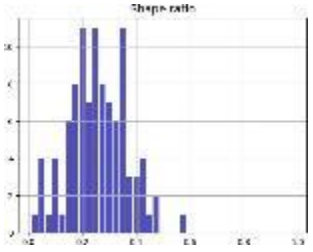


GRID ID = 104

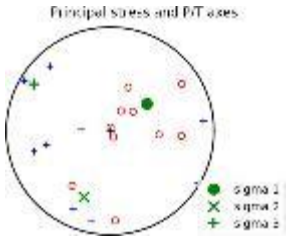


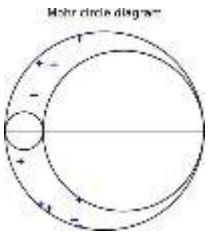


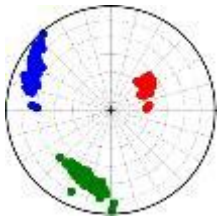


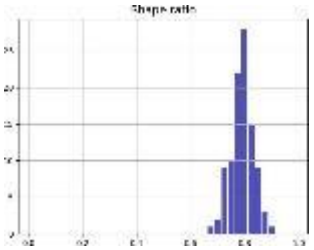


GRID ID = 105

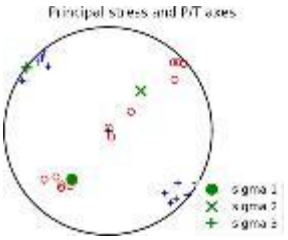


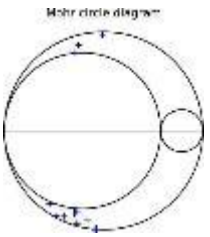


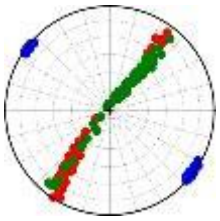


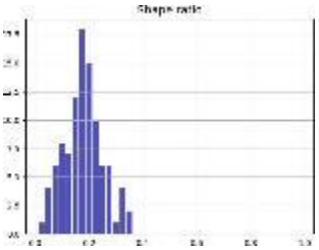


GRID ID = 106

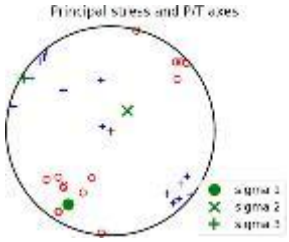


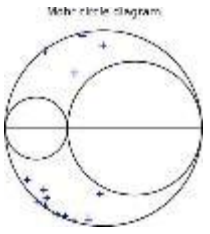


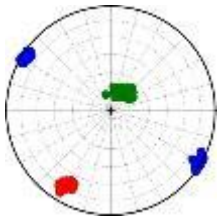


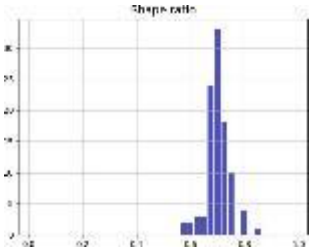


GRID ID = 107

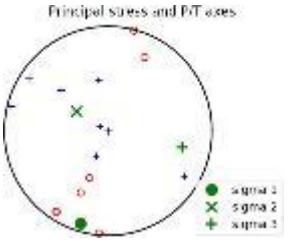


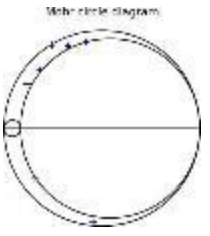


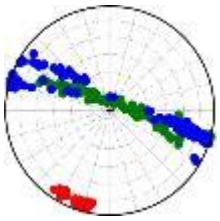


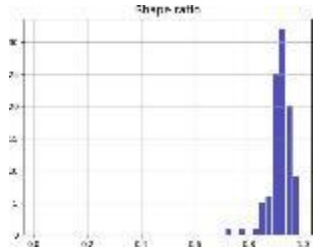


GRID ID = 108

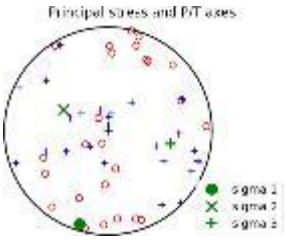


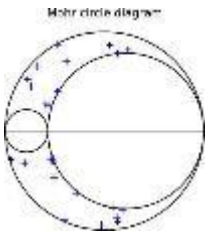


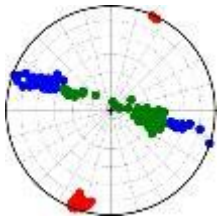


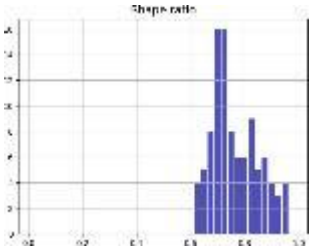


GRID ID = 110

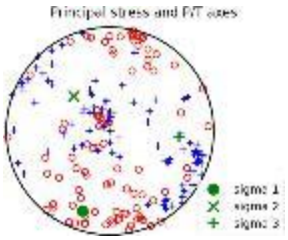


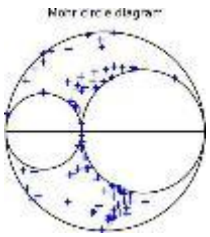


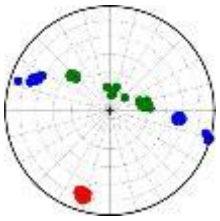


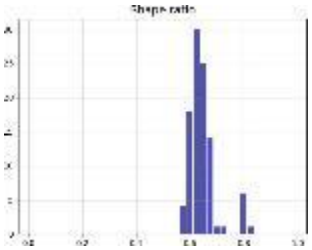


GRID ID = 111

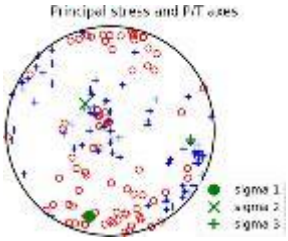


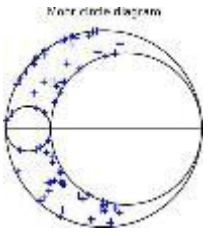


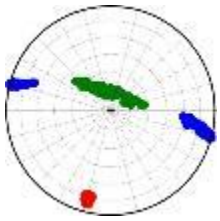


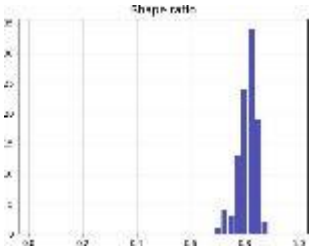


GRID ID = 112

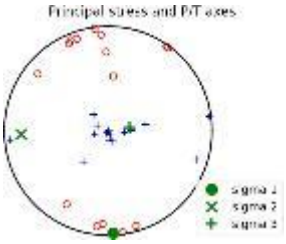


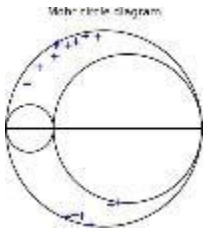


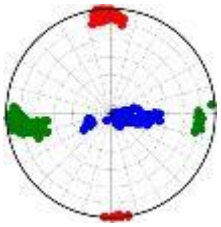


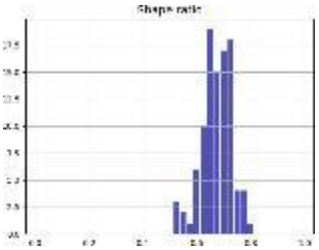


GRID ID = 113

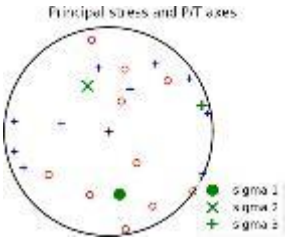


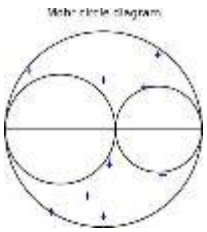


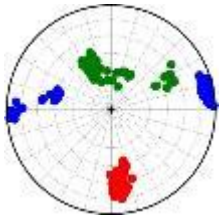


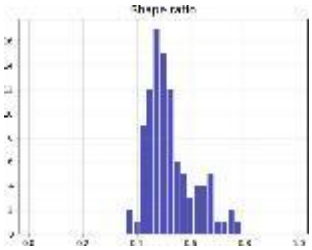


GRID ID = 122

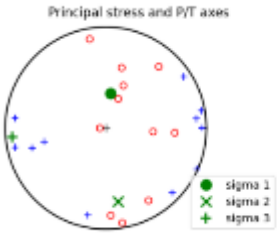


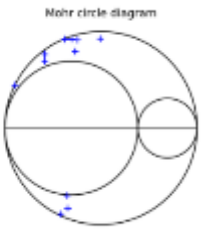


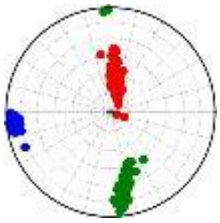


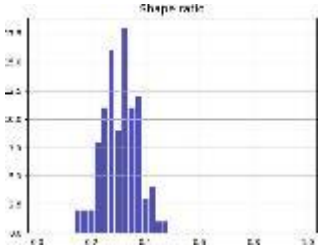


GRID ID = 123

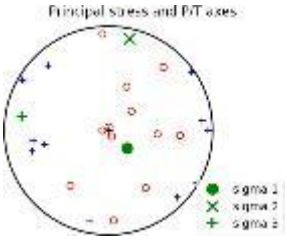


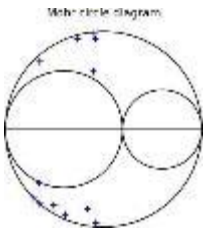


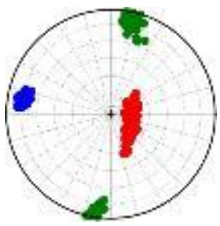


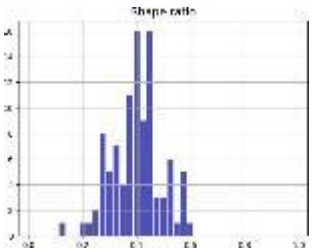


GRID ID = 124

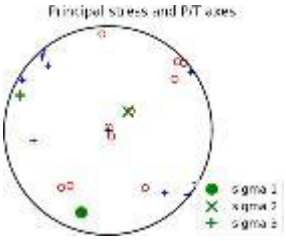


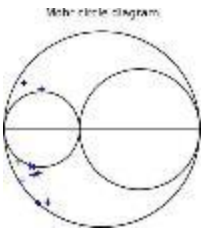


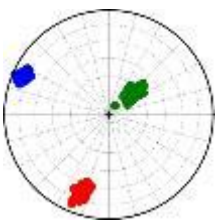


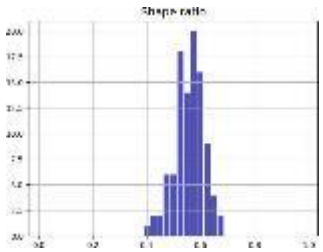


GRID ID = 125

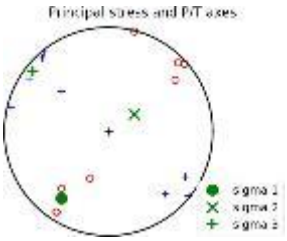


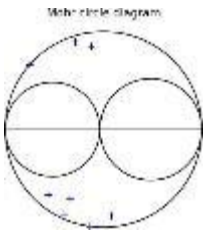


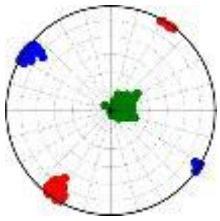


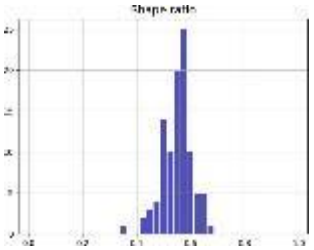


GRID ID = 126

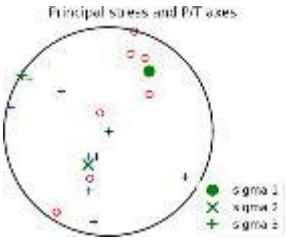


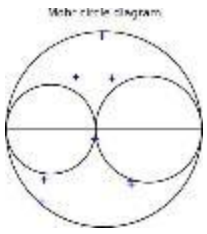


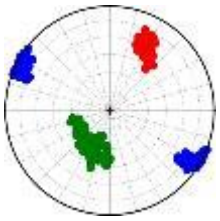


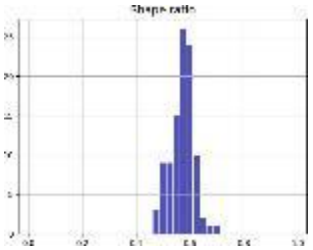


GRID ID = 127

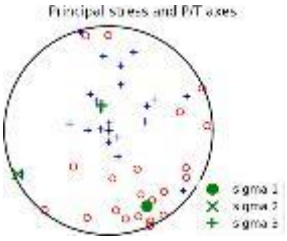


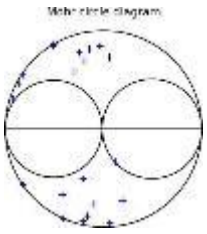


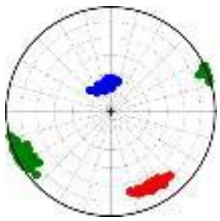


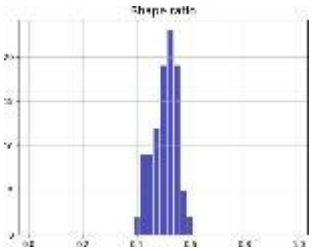


GRID ID = 130

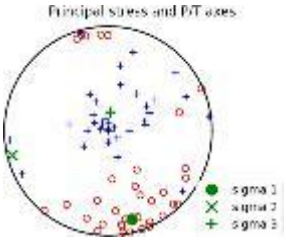


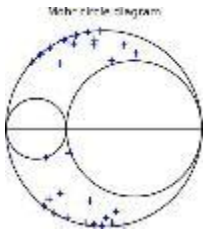


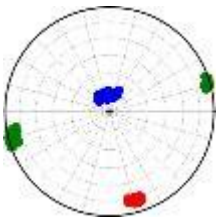


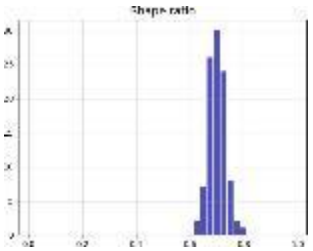


GRID ID = 131

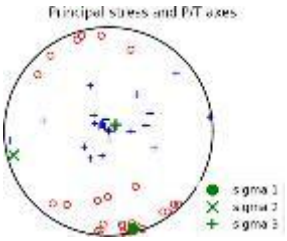


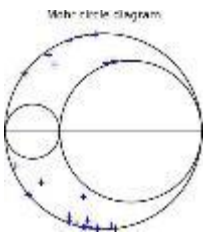


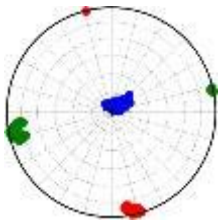


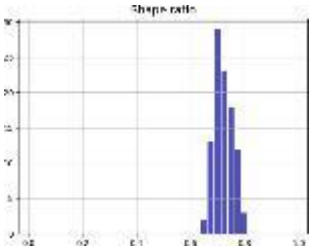


GRID ID = 132

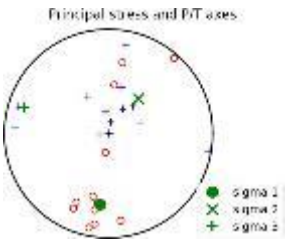


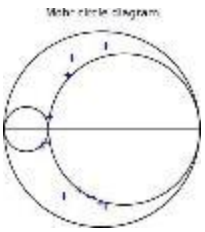


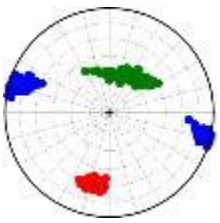


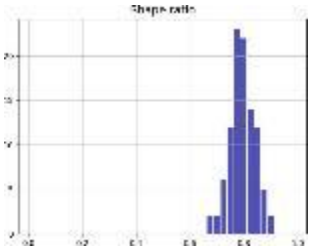


GRID ID = 139

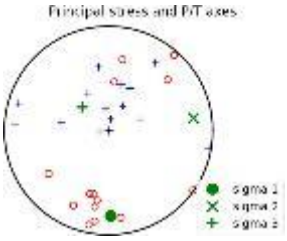


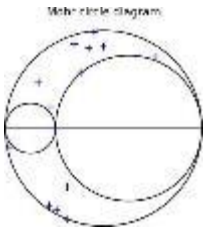


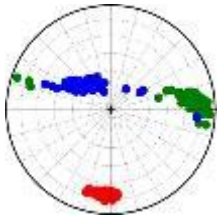


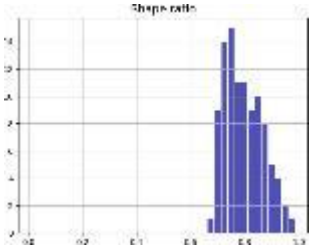


GRID ID = 140

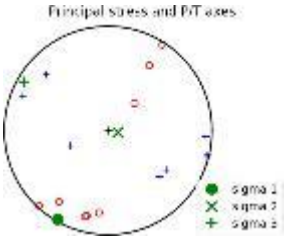


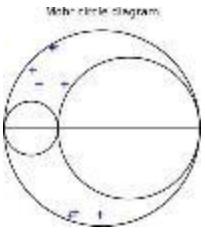


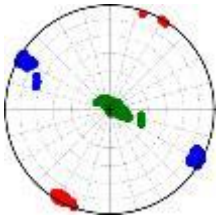


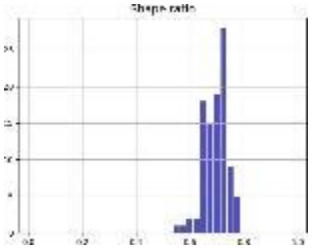


GRID ID = 145

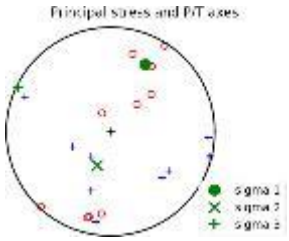


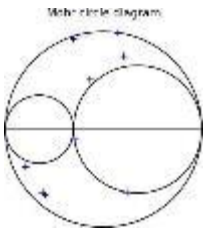


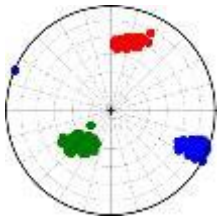


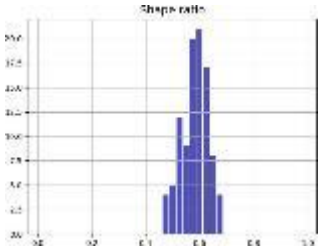


GRID ID = 146

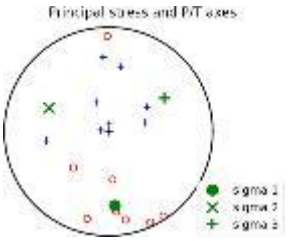


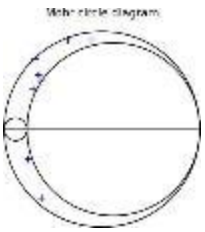


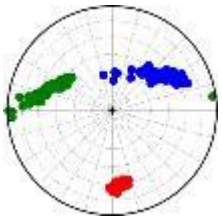


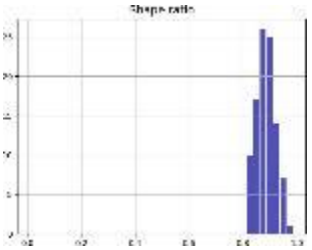


GRID ID = 149

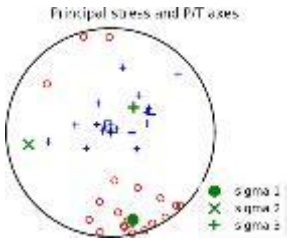


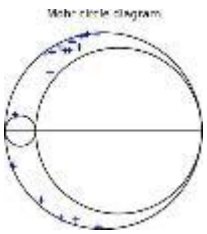


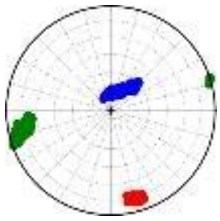


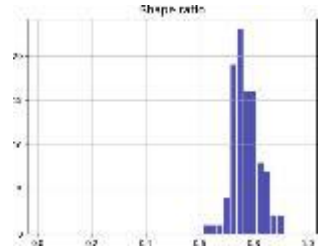


GRID ID = 150

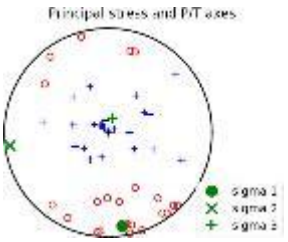


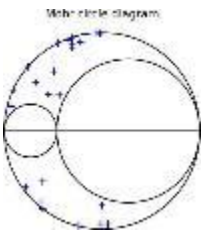


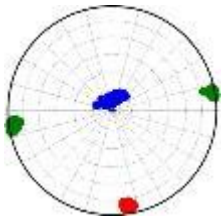


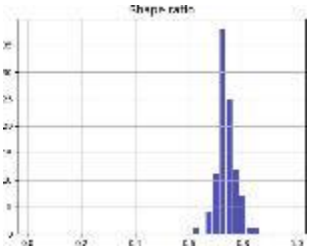


GRID ID = 151

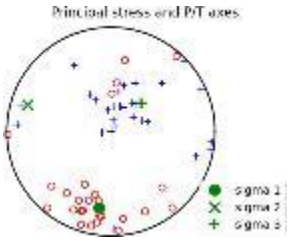


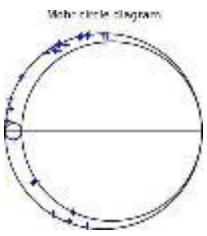


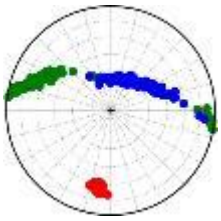


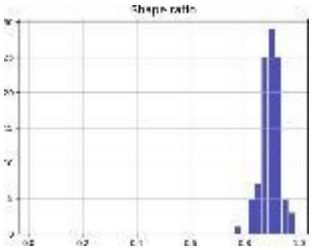


GRID ID = 158

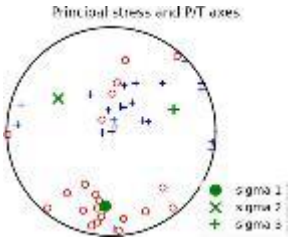


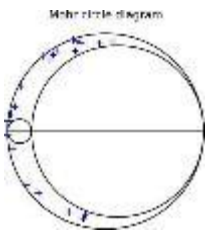


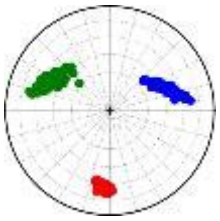


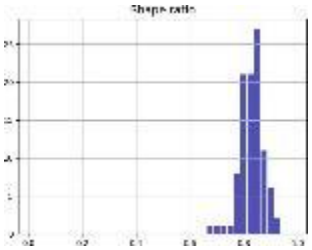


GRID ID = 159

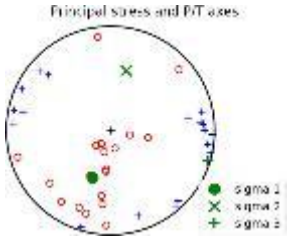


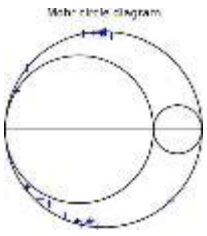


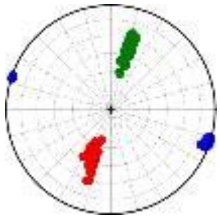


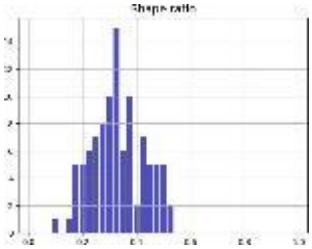


GRID ID = 163

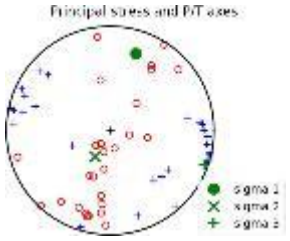


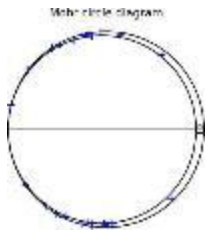


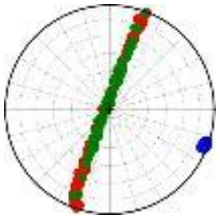




GRID ID = 164

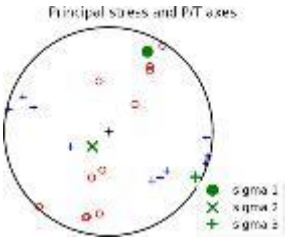


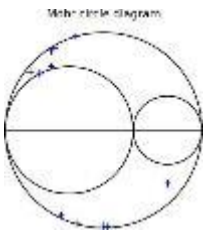


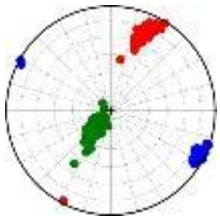


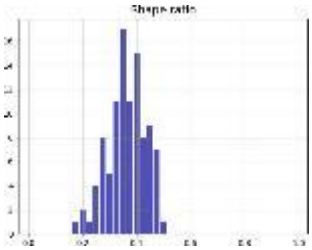


GRID ID = 165

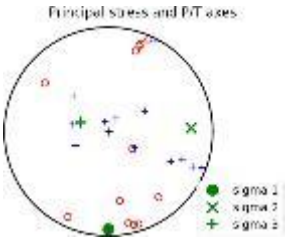


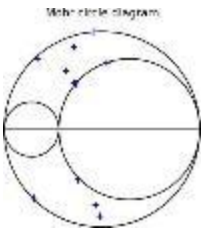


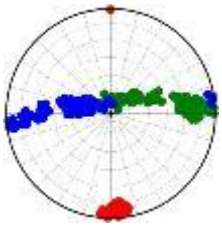


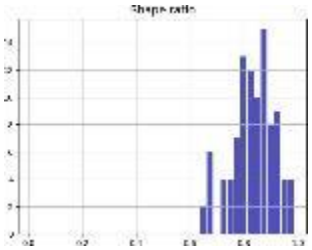


GRID ID = 170

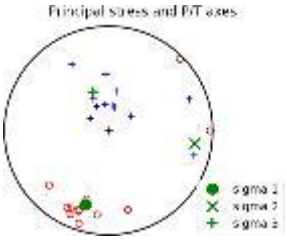


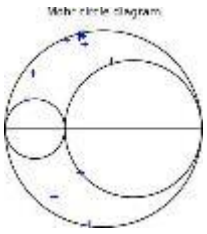


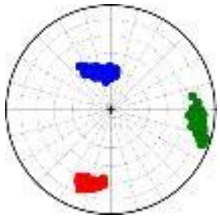


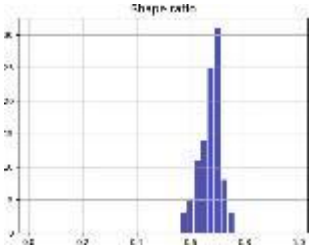


GRID ID = 176

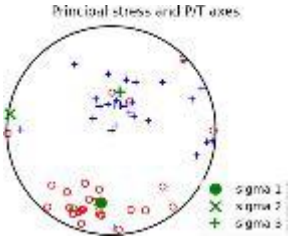


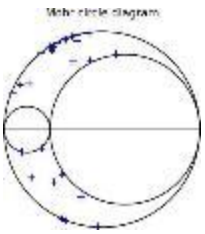


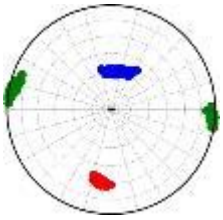


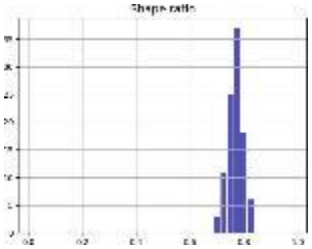


GRID ID = 177

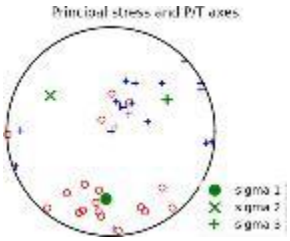


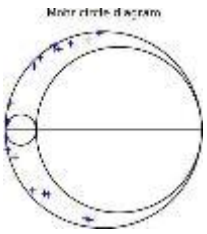


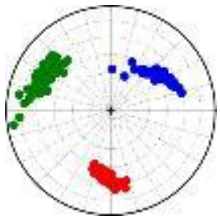


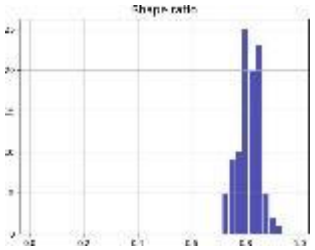


GRID ID = 178

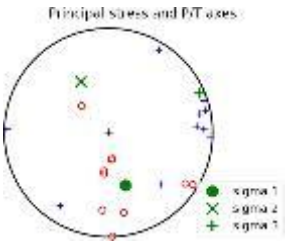


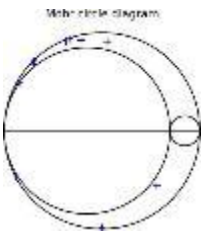


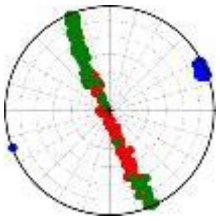


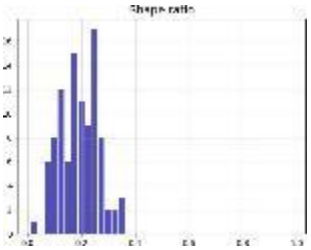


GRID ID = 181

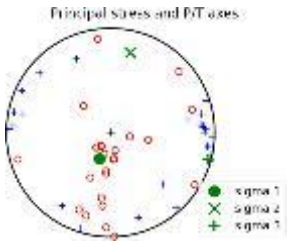


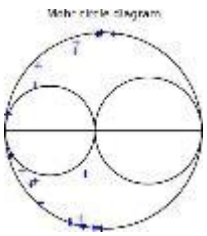


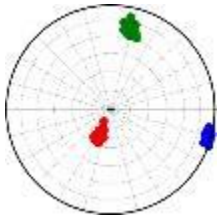


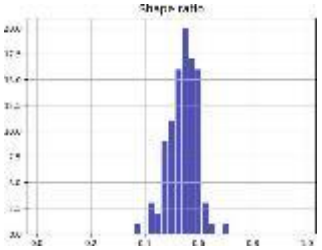


GRID ID = 182

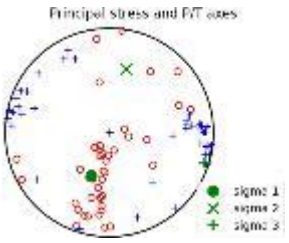


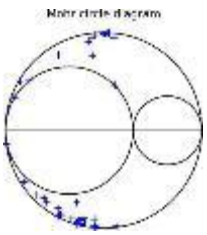


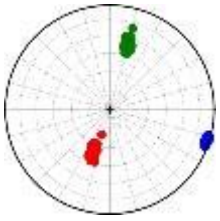


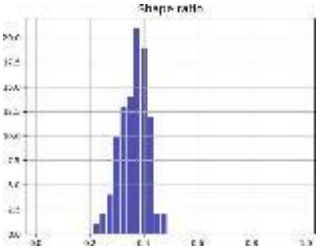


GRID ID = 183

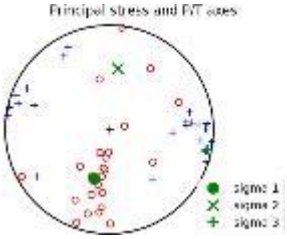


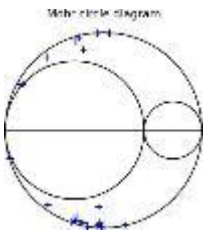


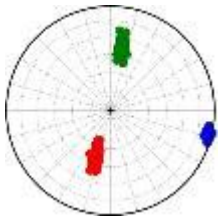


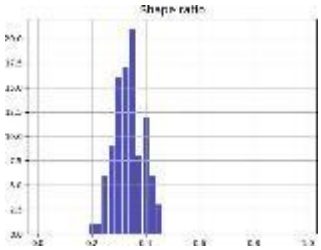


GRID ID = 184

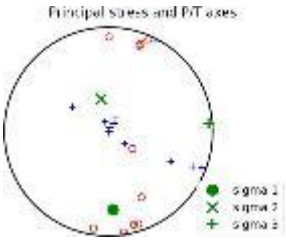


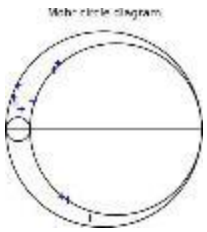


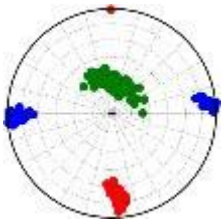


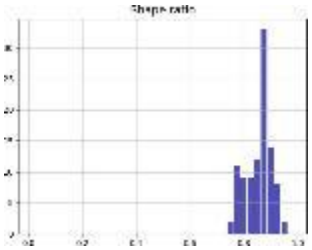


GRID ID = 189

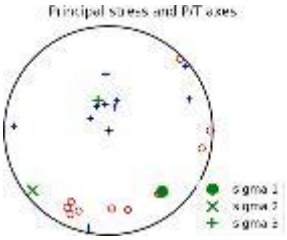


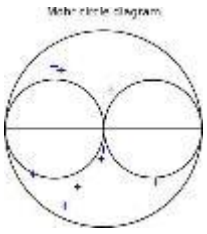


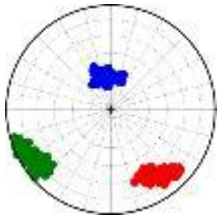


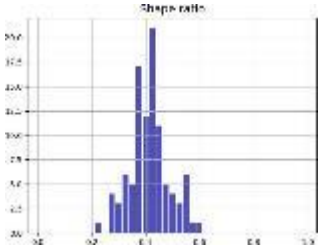


GRID ID = 195

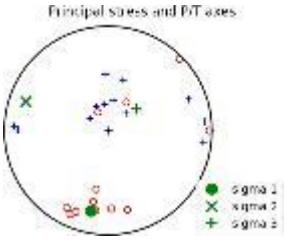


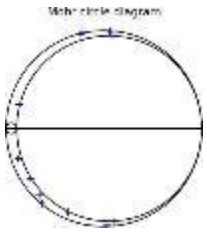


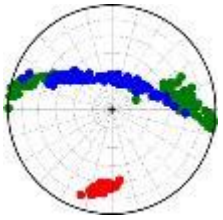


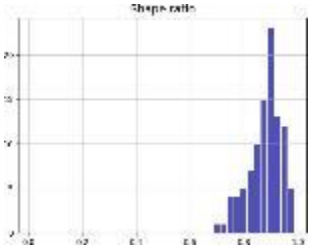


GRID ID = 196

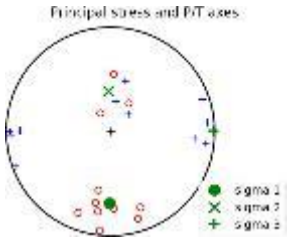


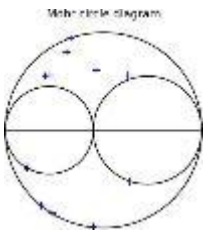


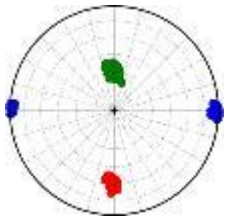


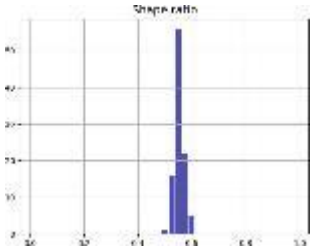


GRID ID = 197

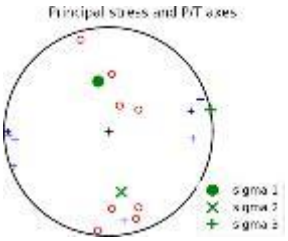


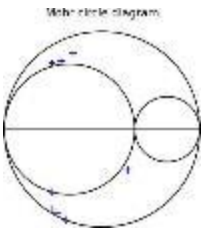


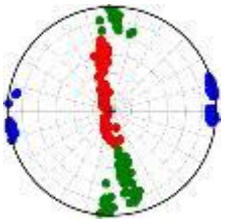


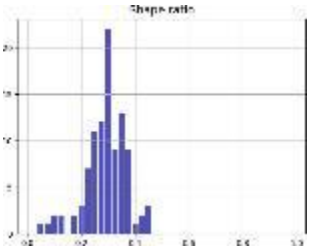


GRID ID = 198

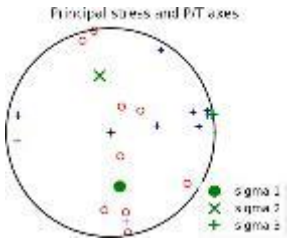


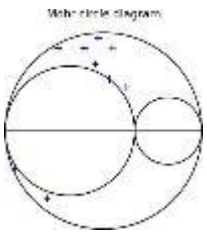


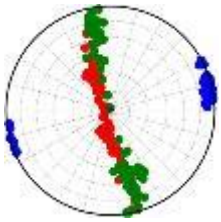


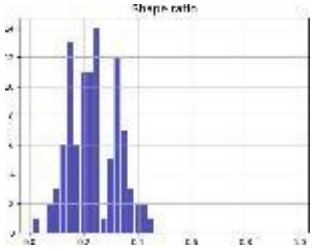


GRID ID = 199

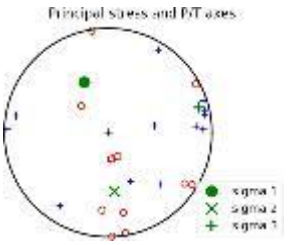


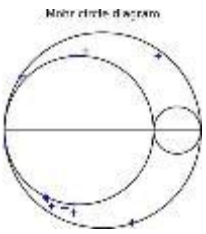


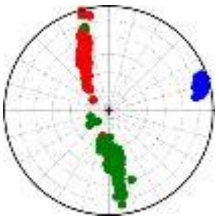


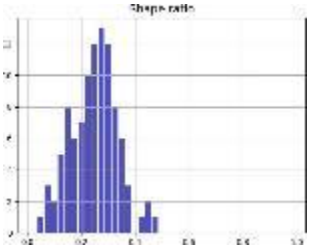


GRID ID = 200

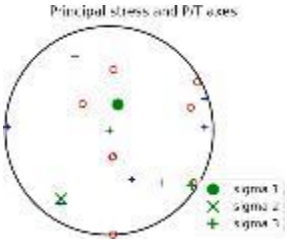


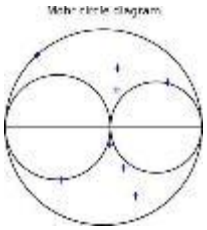


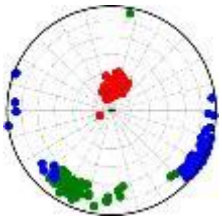


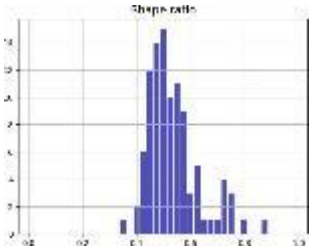


GRID ID = 201

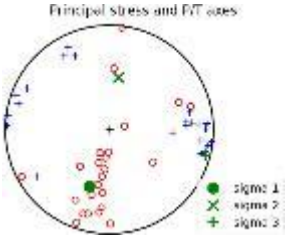


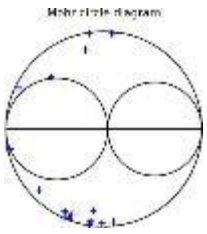


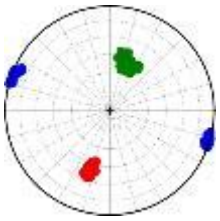


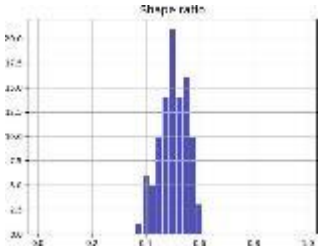


GRID ID = 202

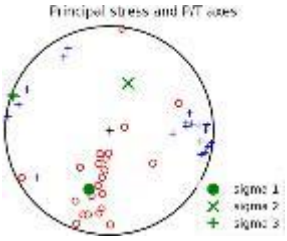


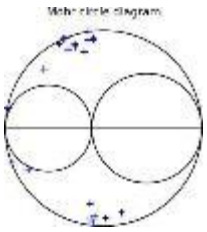


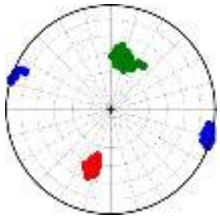


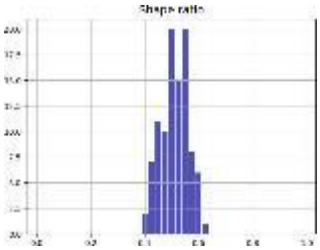


GRID ID = 203

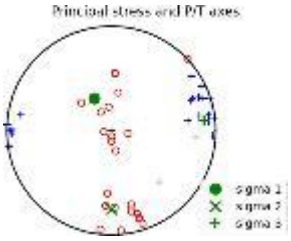


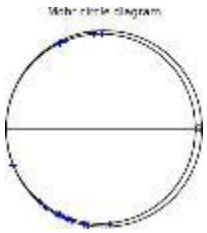


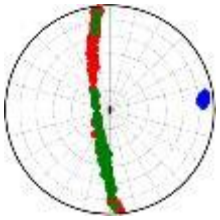


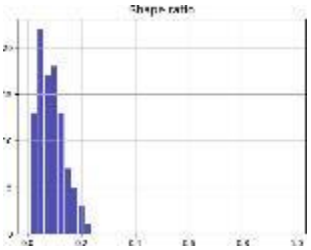


GRID ID = 216

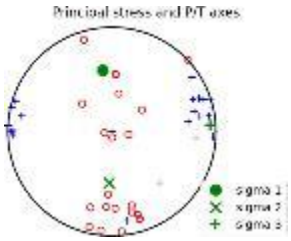


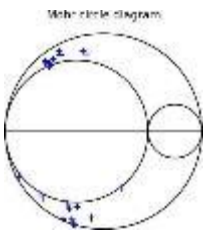


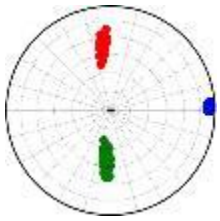


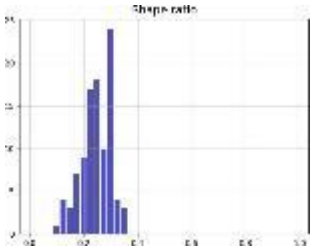


GRID ID = 217

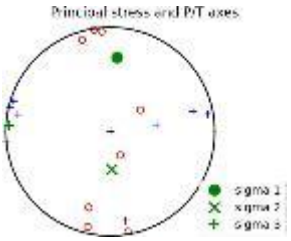


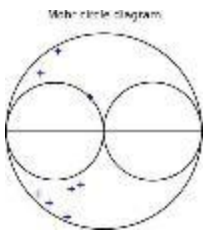


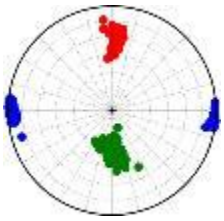


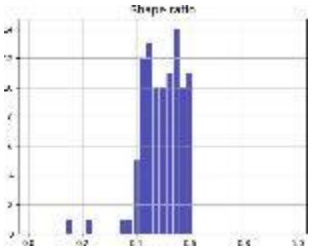


GRID ID = 218

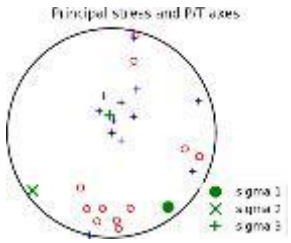


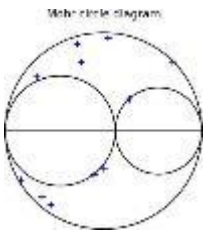


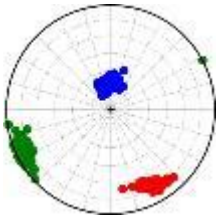


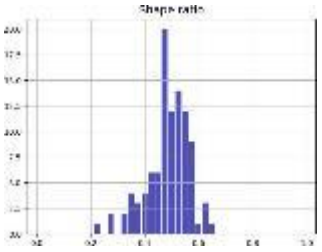


GRID ID = 227

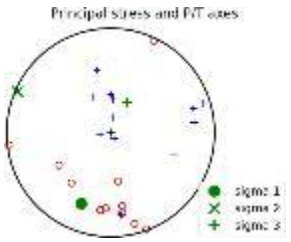


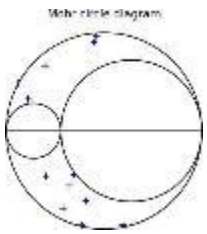


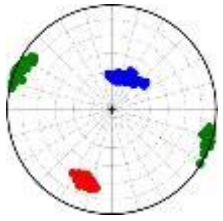


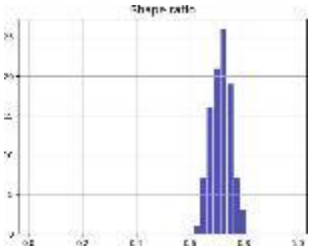


GRID ID = 232

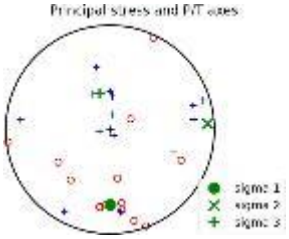


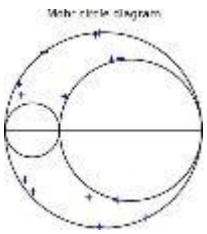


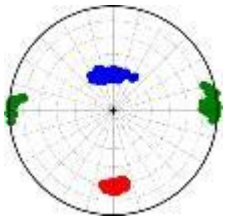


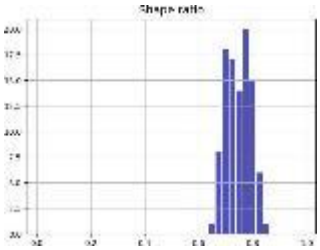


GRID ID = 233

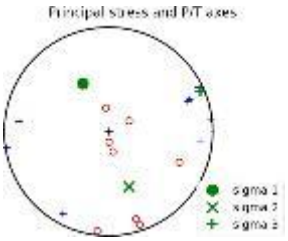


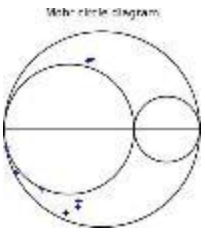


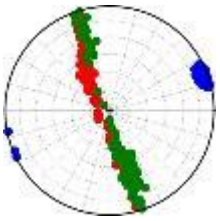


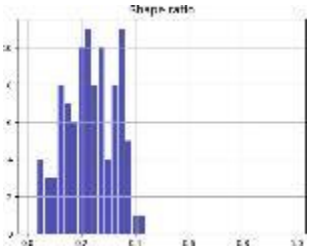


GRID ID = 234

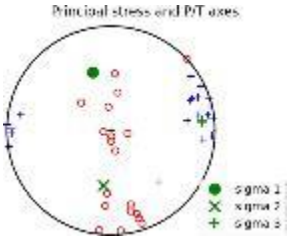


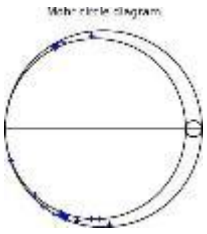


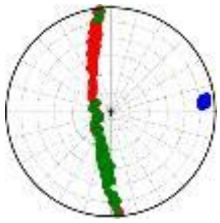


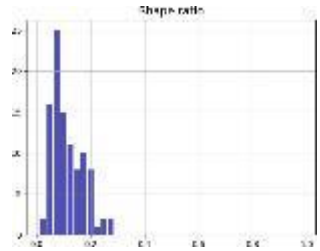


GRID ID = 235

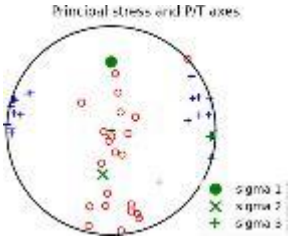


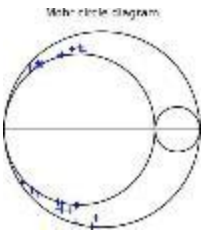


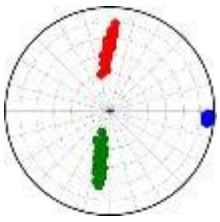


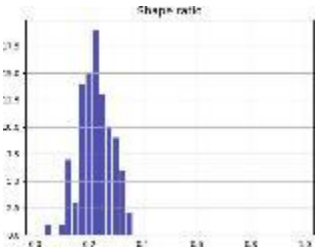


GRID ID = 236

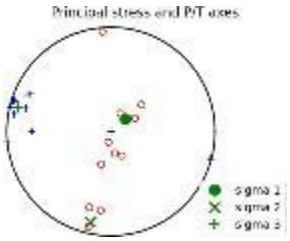


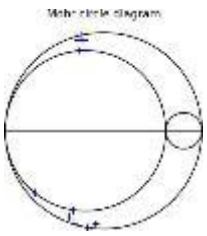


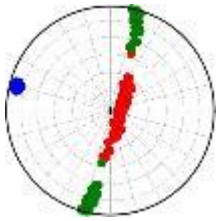


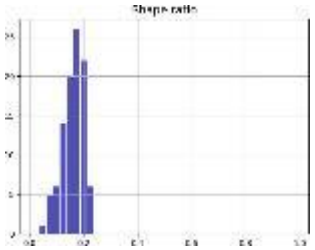


GRID ID = 237

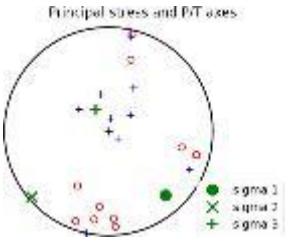


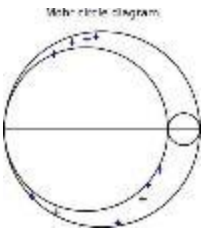


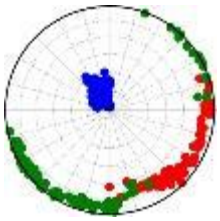


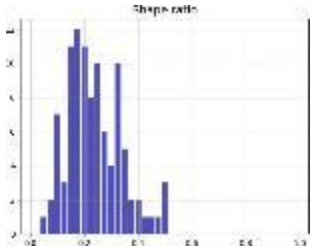


GRID ID = 246

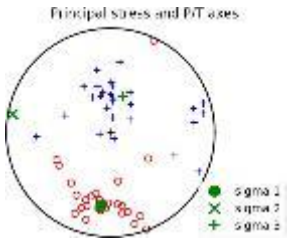


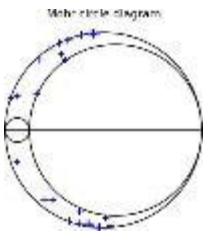


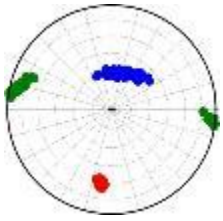


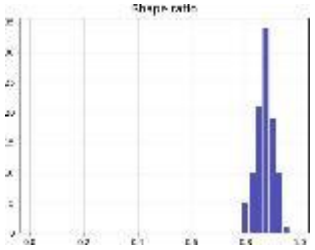


GRID ID = 251

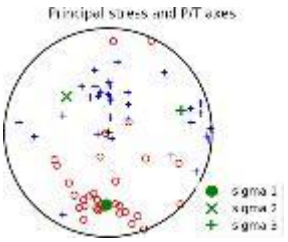


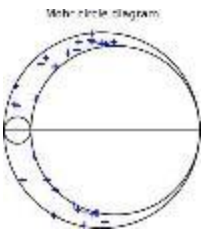


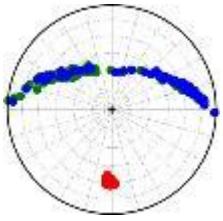


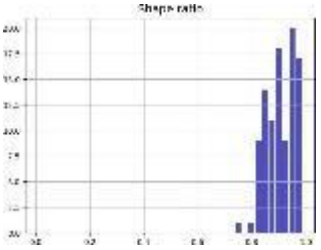


GRID ID = 252

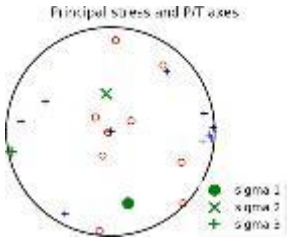


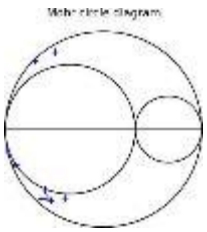


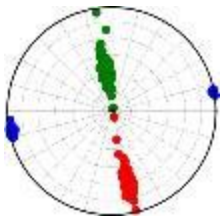


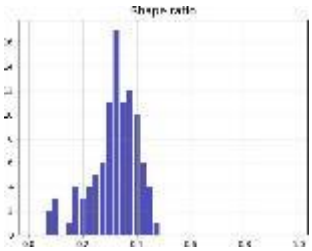


GRID ID = 253

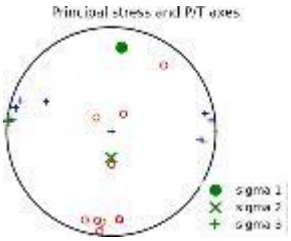


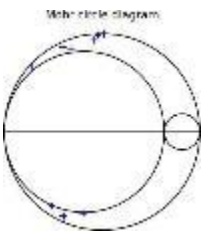


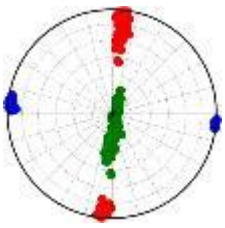


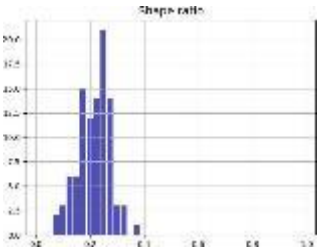


GRID ID = 254

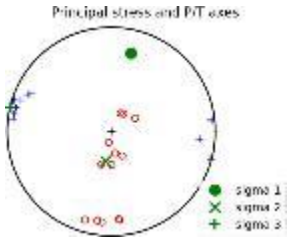


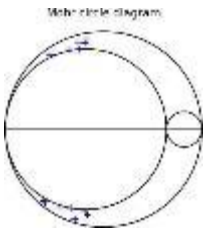


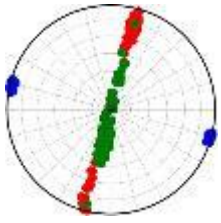


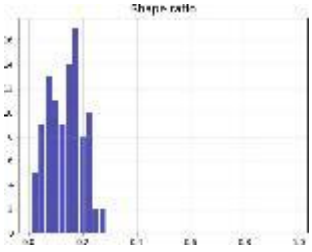


GRID ID = 255

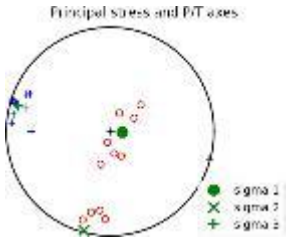


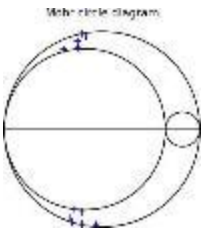


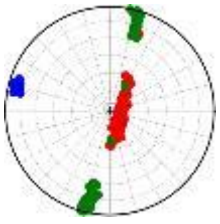


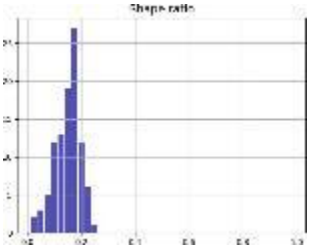


GRID ID = 256

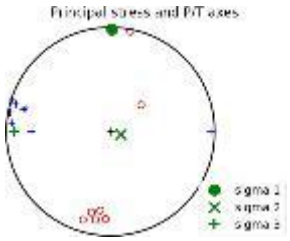


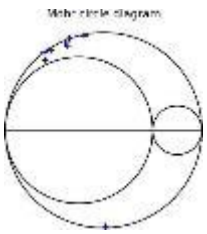


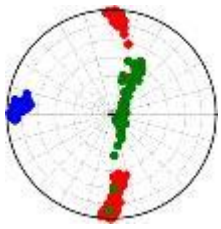


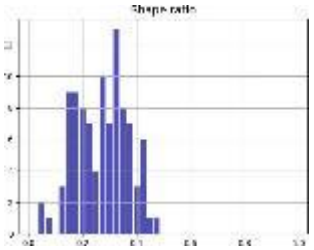


GRID ID = 257

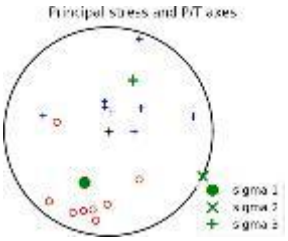


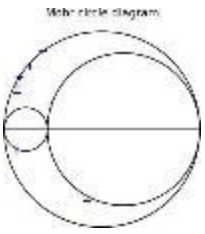


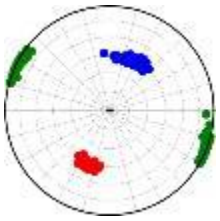


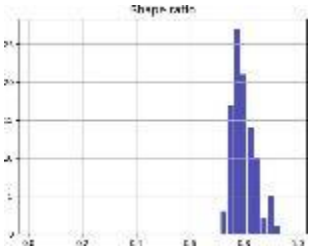


GRID ID = 269

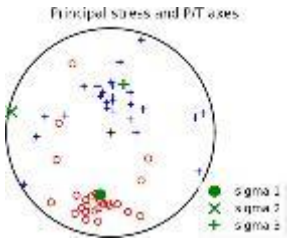


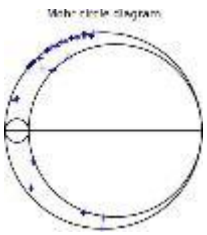


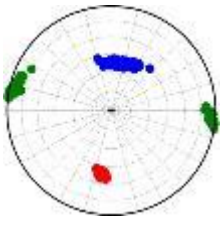


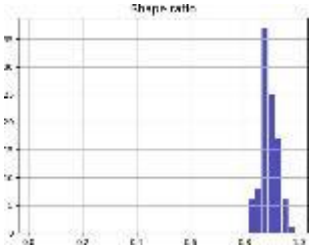


GRID ID = 270

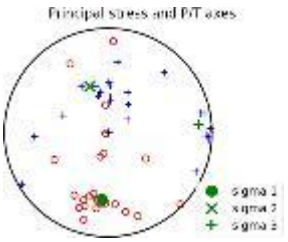


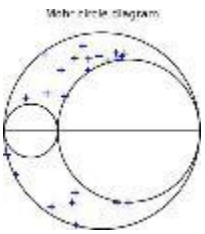


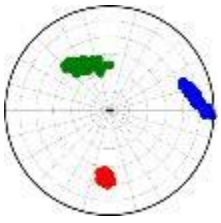


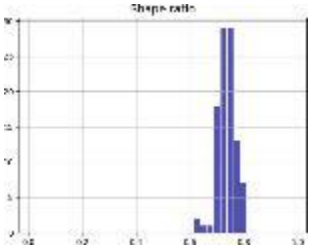


GRID ID = 271

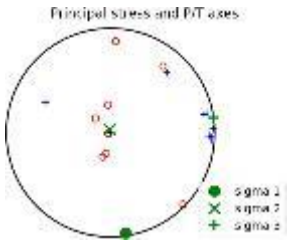


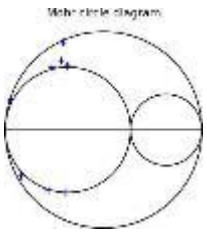


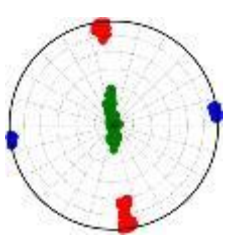


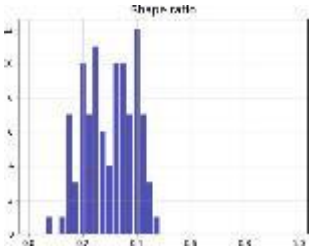


GRID ID = 272

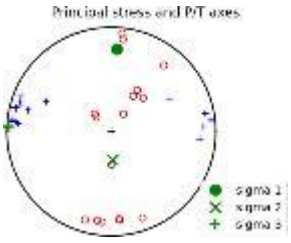


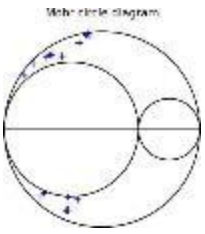


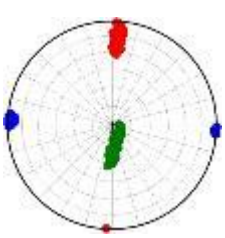


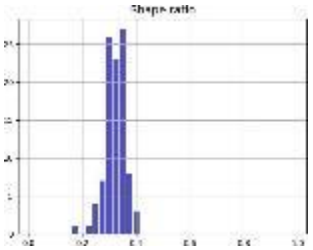


GRID ID = 273

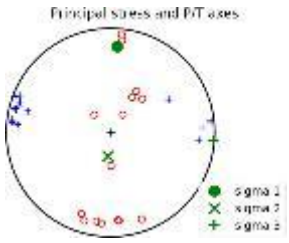


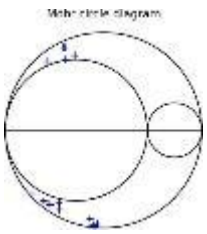


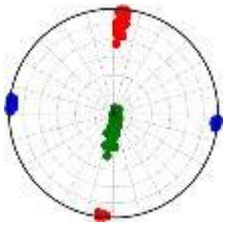


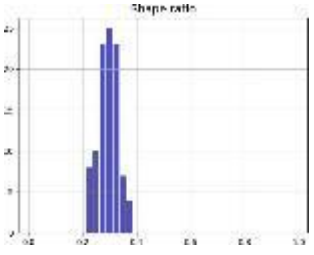


GRID ID = 274

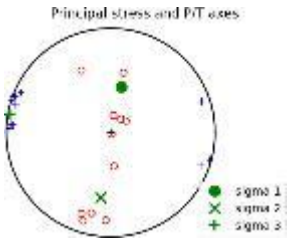


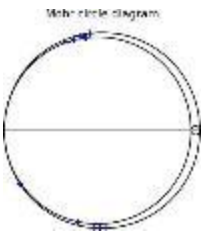


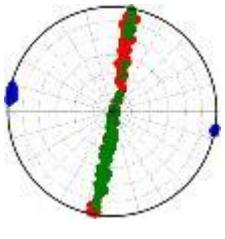


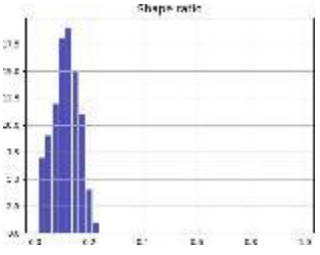


GRID ID = 275

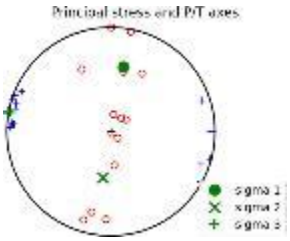


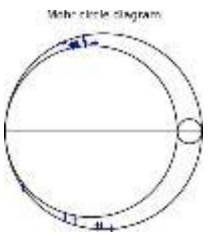


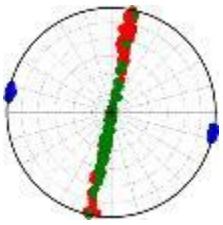


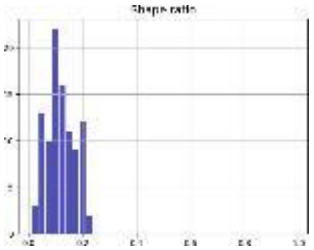


GRID ID = 276

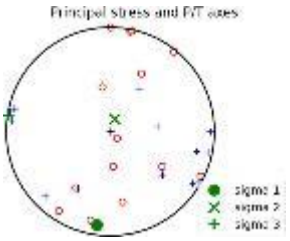


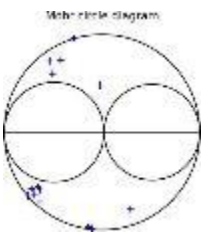


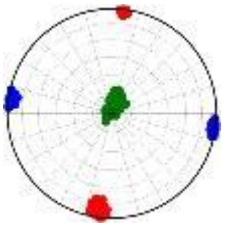


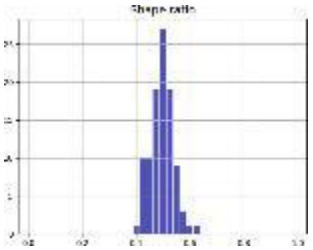


GRID ID = 277

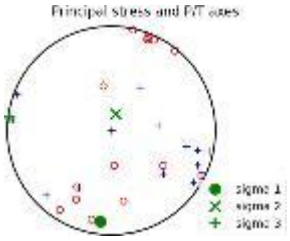


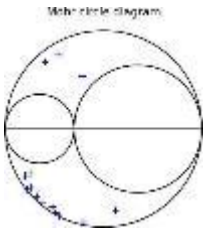


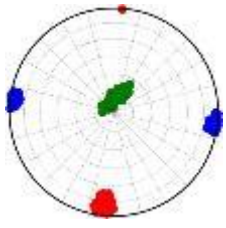


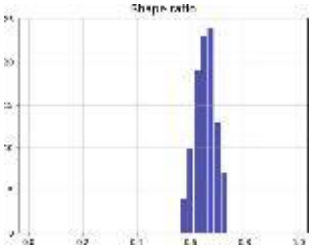


GRID ID = 278

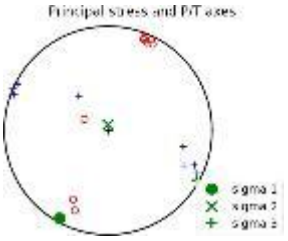


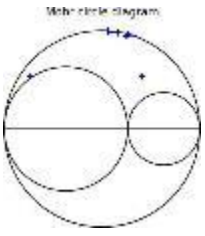


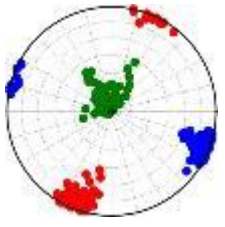


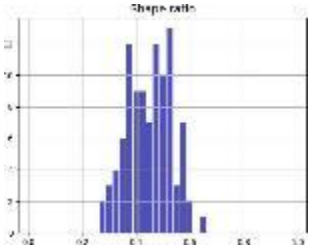


GRID ID = 279

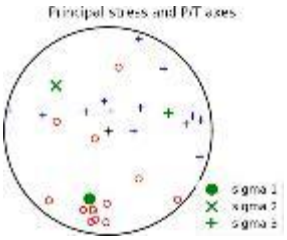


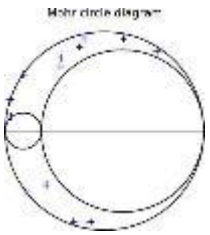


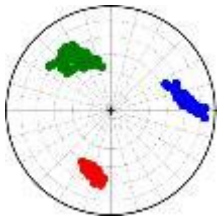


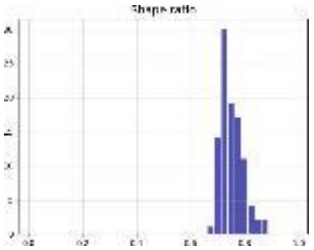


GRID ID = 288

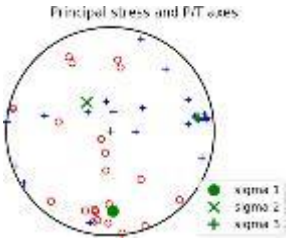


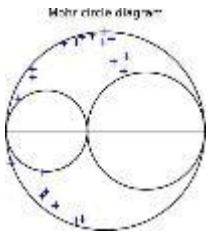


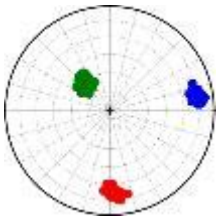


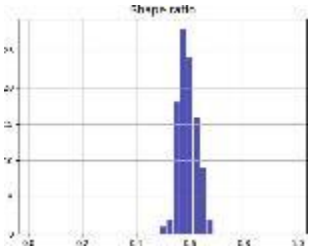


GRID ID = 289

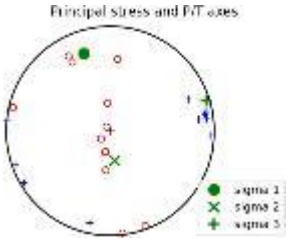


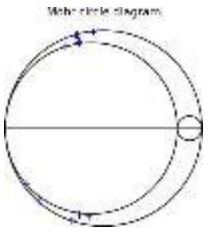


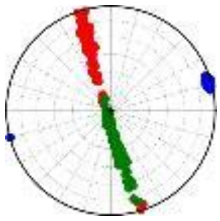


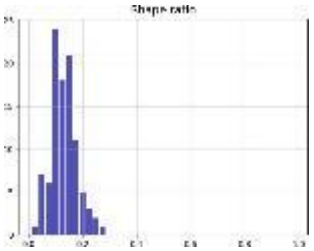


GRID ID = 290

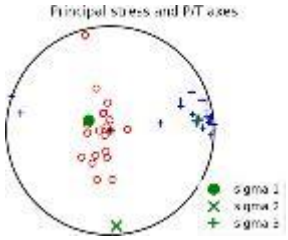


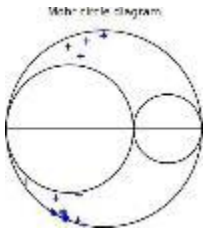


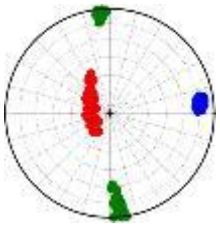


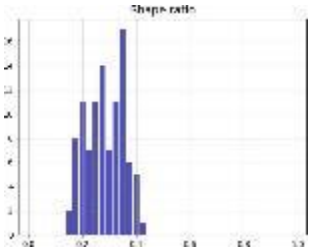


GRID ID = 291

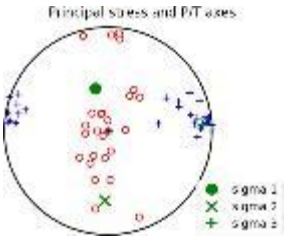


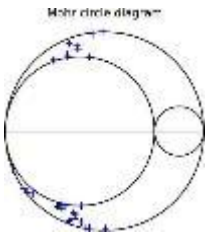


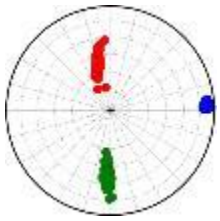


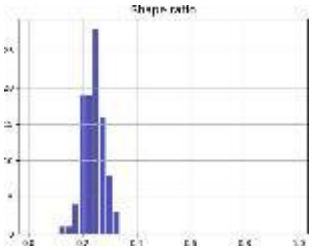


GRID ID = 292

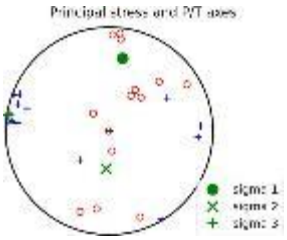


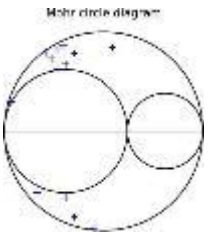


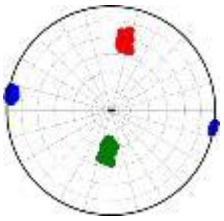


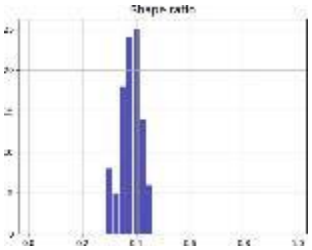


GRID ID = 293

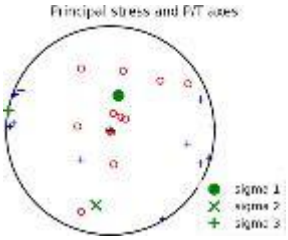


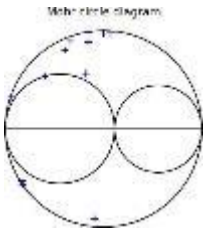


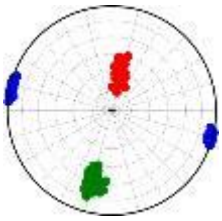


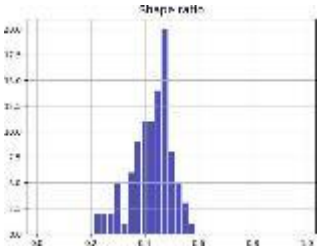


GRID ID = 294

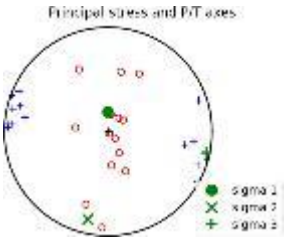


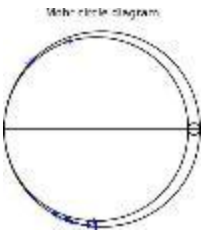


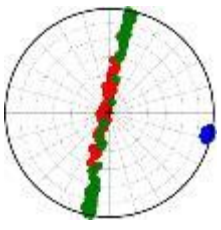


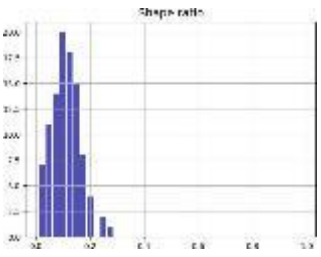


GRID ID = 295

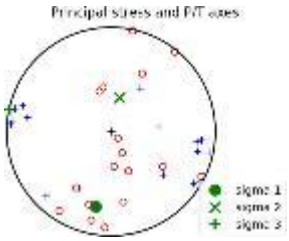


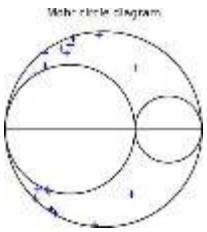


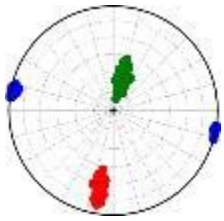


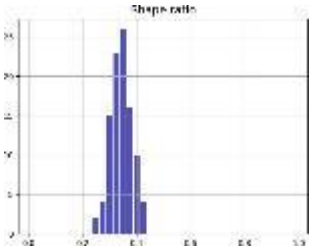


GRID ID = 296

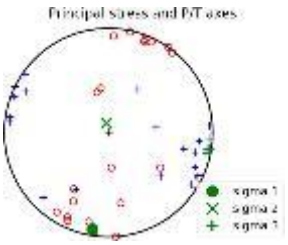


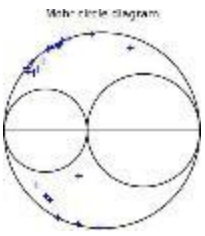


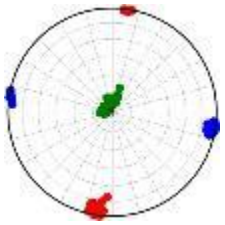


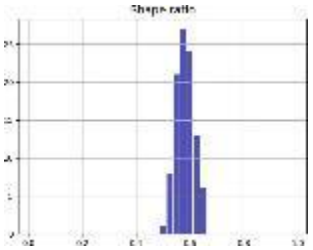


GRID ID = 297

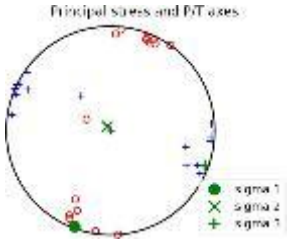


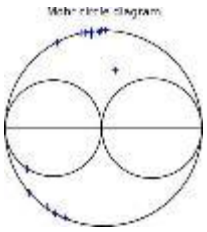


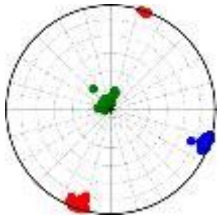


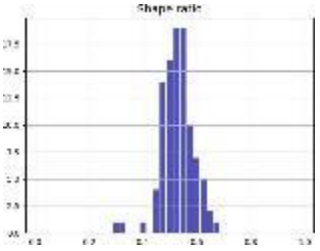


GRID ID = 298

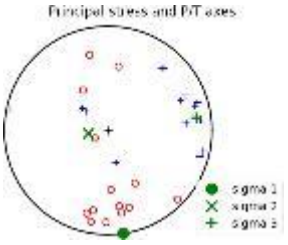


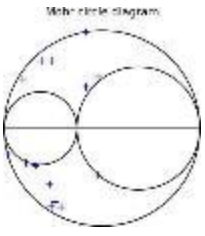


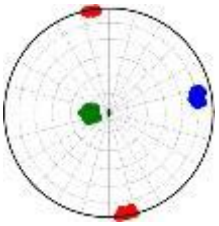


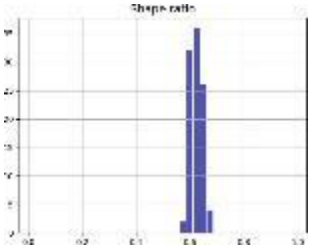


GRID ID = 307

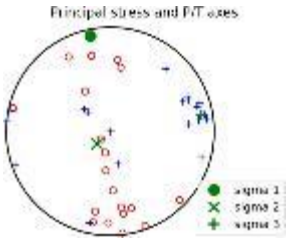


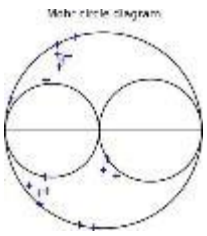


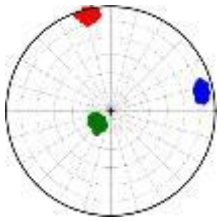


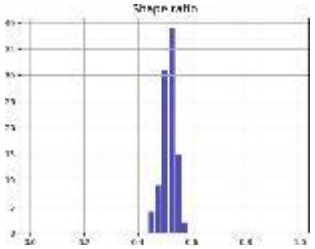


GRID ID = 308

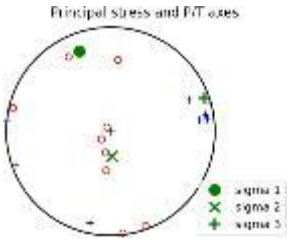


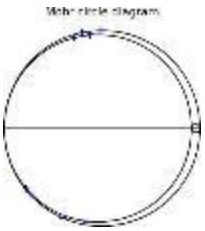


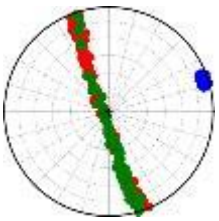


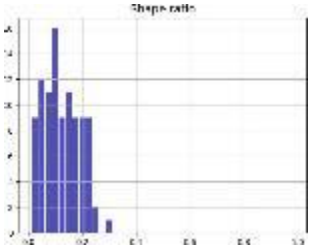


GRID ID = 309

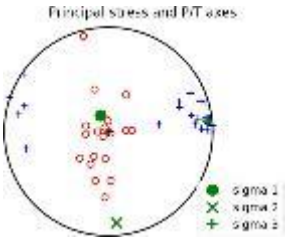


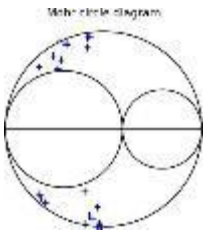


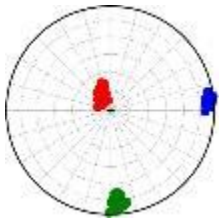


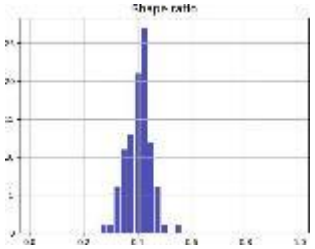


GRID ID = 310

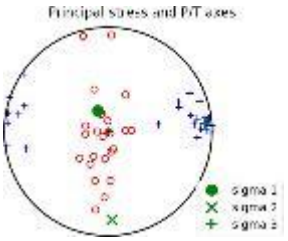


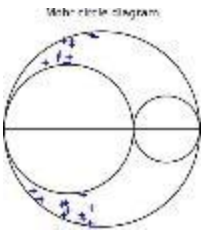


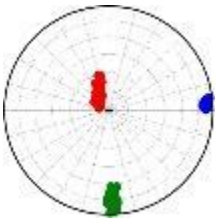


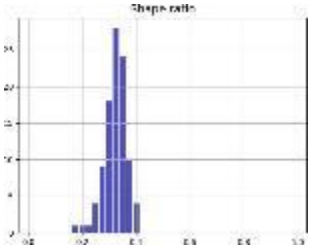


GRID ID = 311

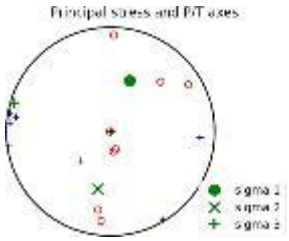


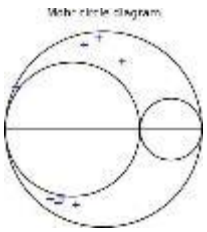


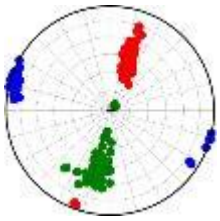


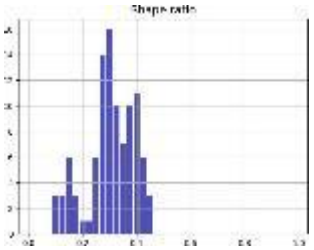


GRID ID = 312

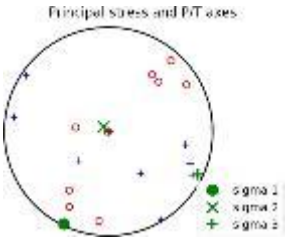


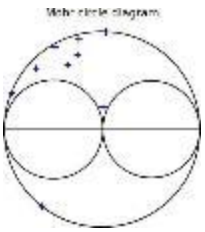


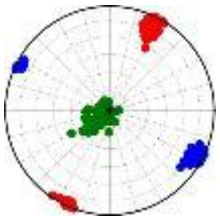


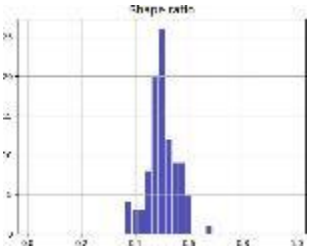


GRID ID = 313

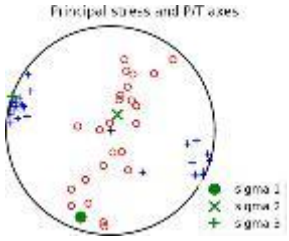


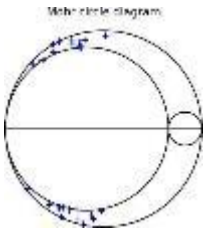


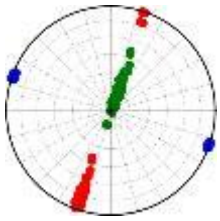


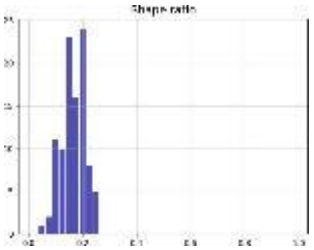


GRID ID = 314

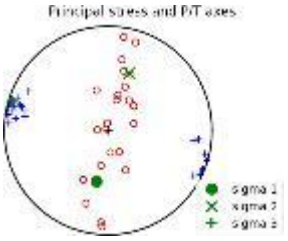


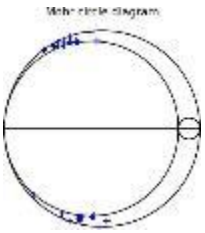


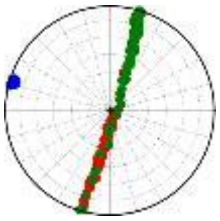


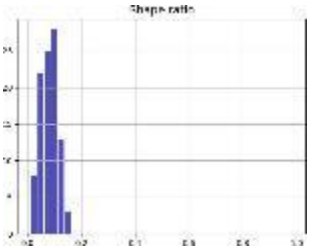


GRID ID = 315

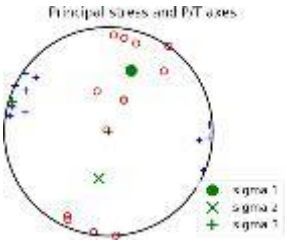


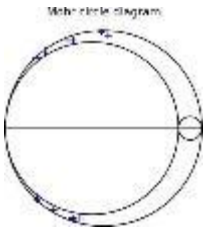


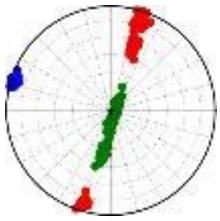


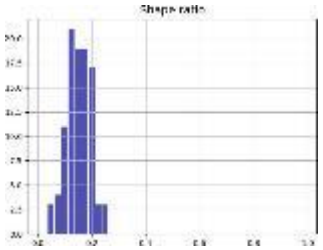


GRID ID = 316

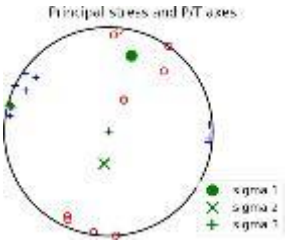


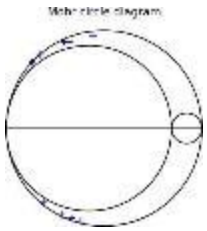


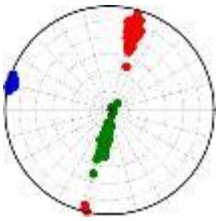


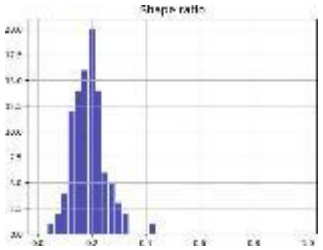


GRID ID = 317

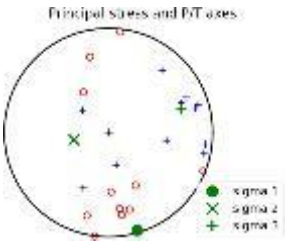


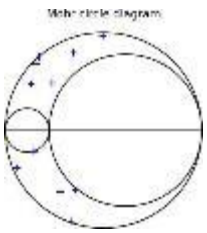


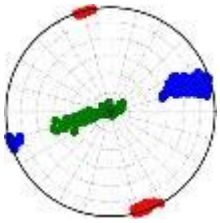


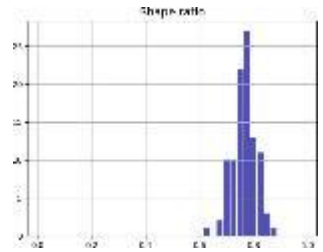


GRID ID = 326

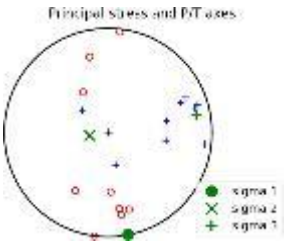


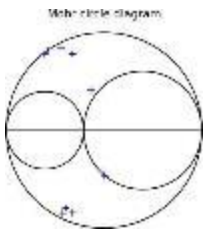


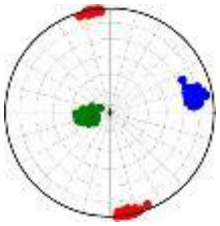


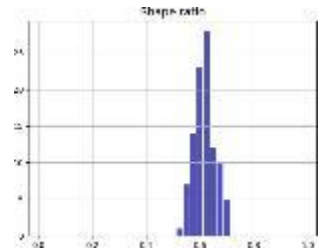


GRID ID = 327

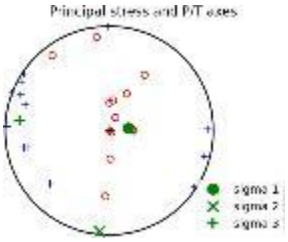


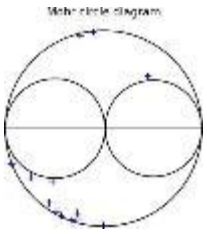


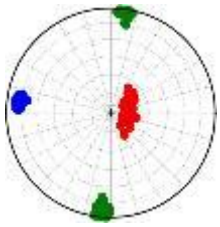


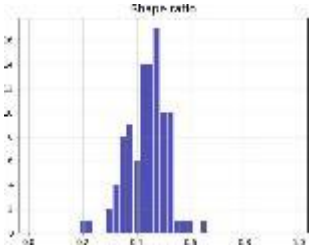


GRID ID = 329

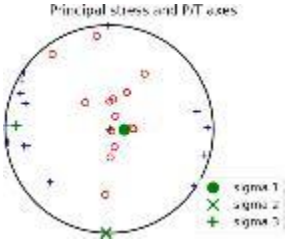


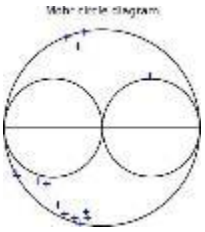


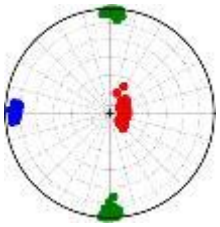


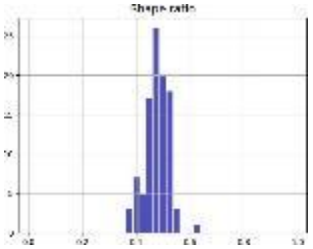


GRID ID = 330

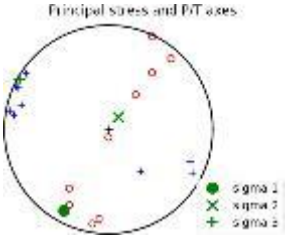


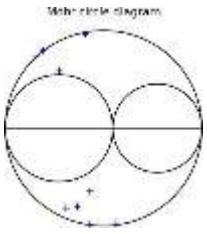


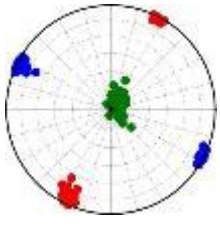


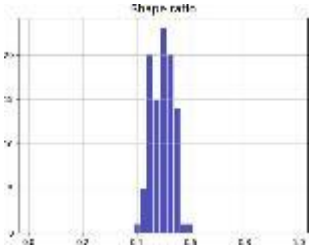


GRID ID = 332

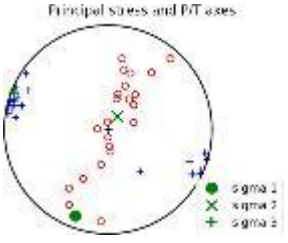


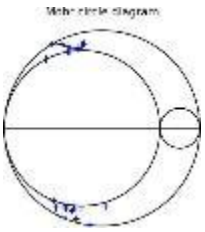


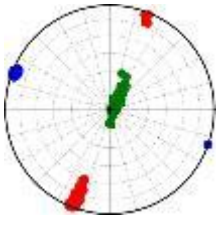


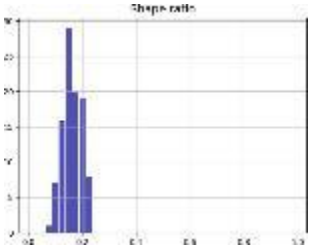


GRID ID = 333

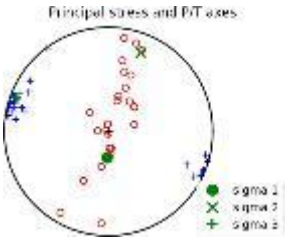


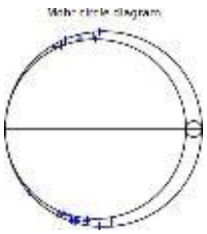


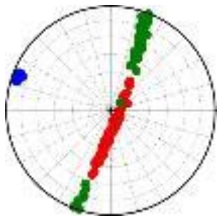


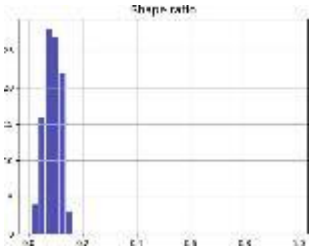


GRID ID = 334

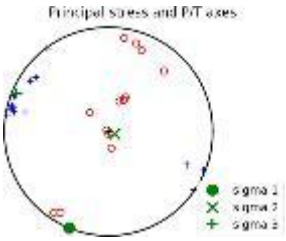


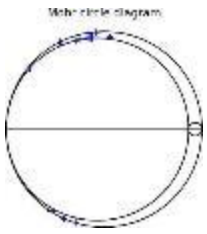


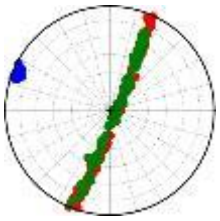


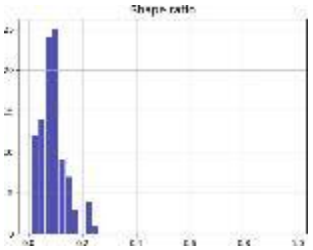


GRID ID = 335

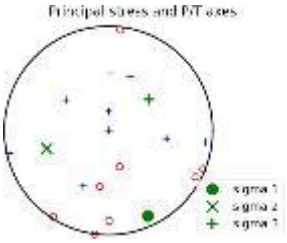


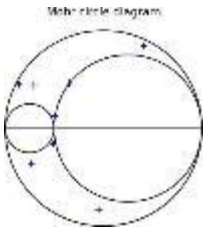


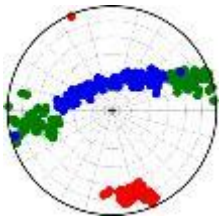


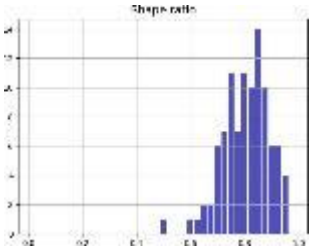


GRID ID = 345

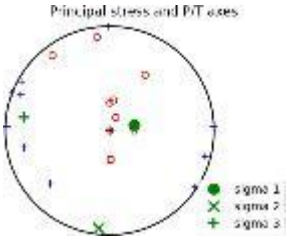


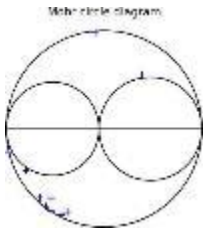


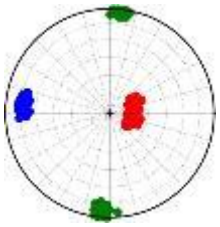


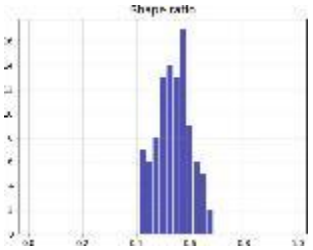


GRID ID = 348

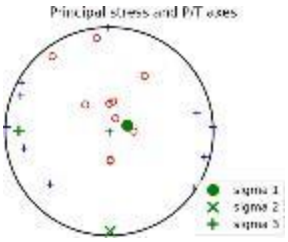


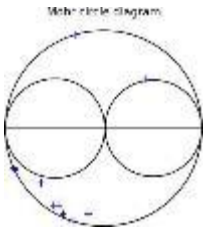


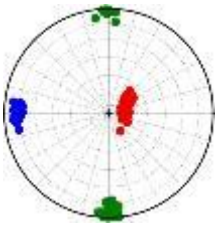


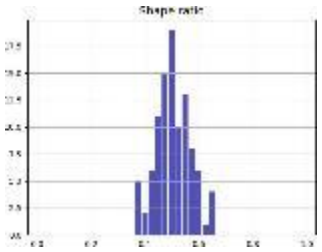


GRID ID = 349

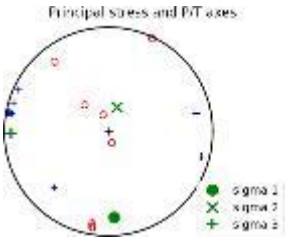


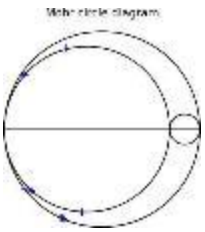


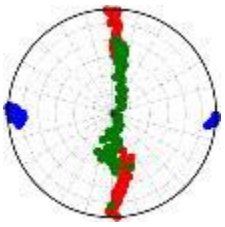


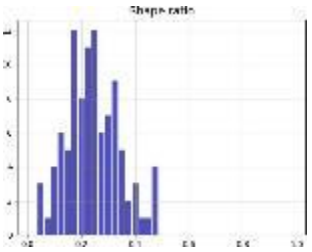


GRID ID = 350

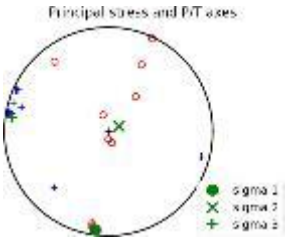


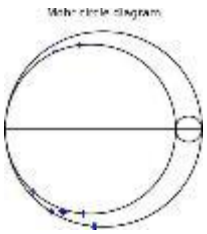


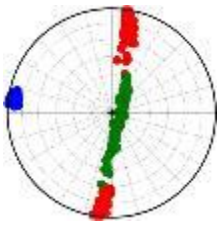


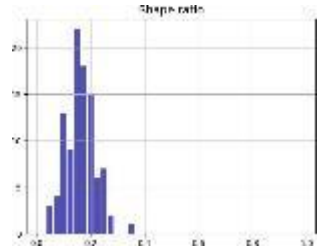


GRID ID = 351

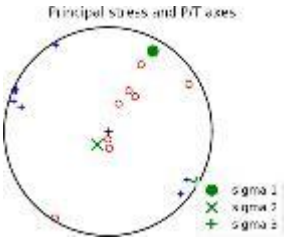


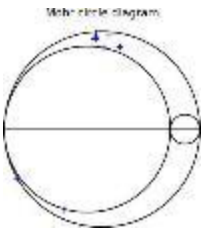


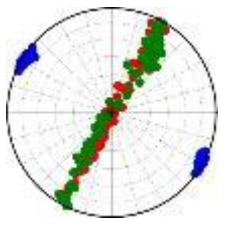


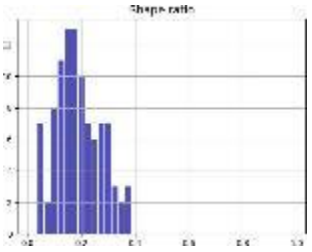


GRID ID = 352

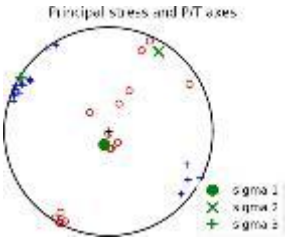


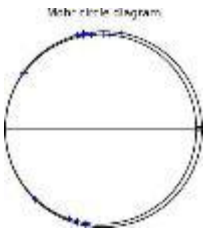


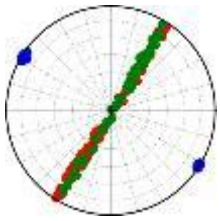


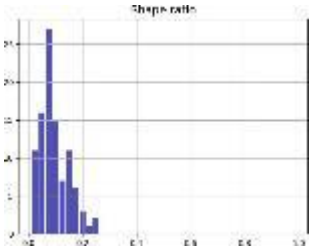


GRID ID = 353

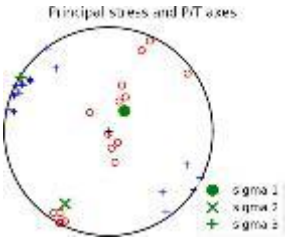


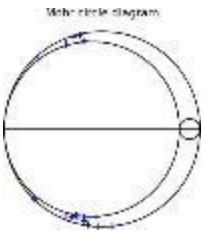


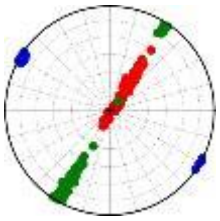


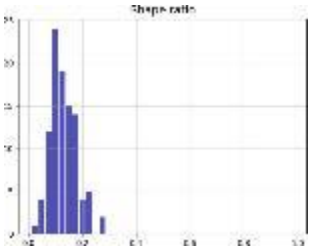


GRID ID = 354

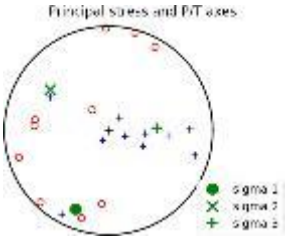


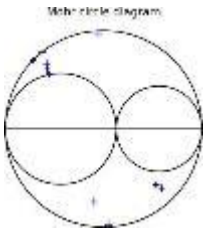


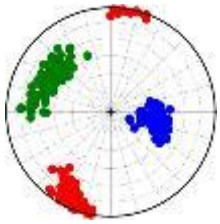


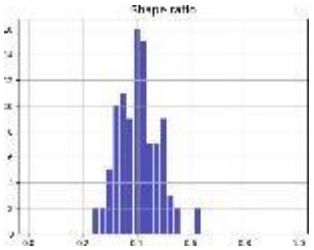


GRID ID = 361

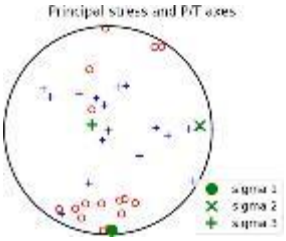


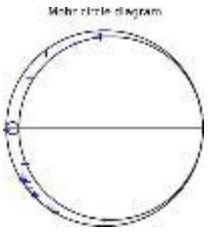


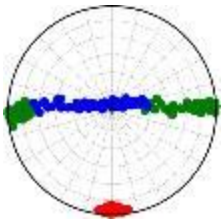


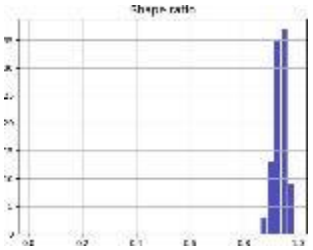


GRID ID = 362

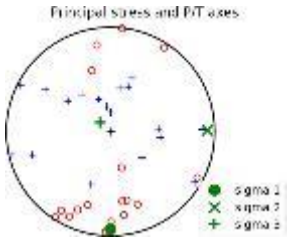


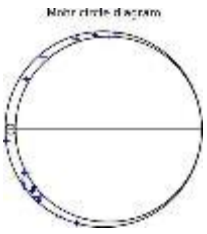


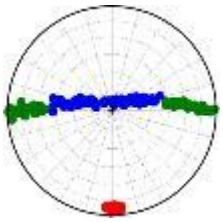


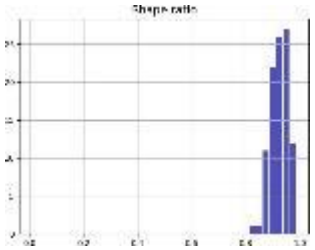


GRID ID = 363

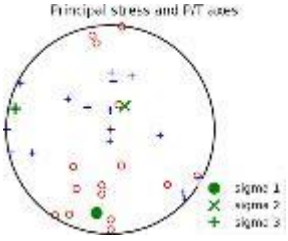


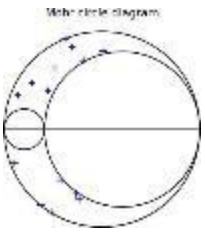


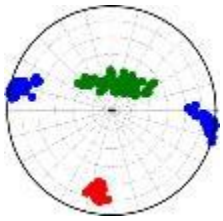


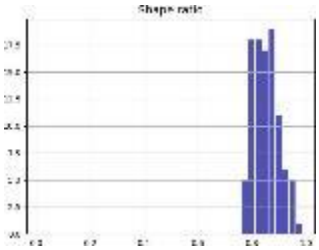


GRID ID = 364

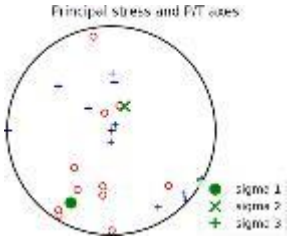


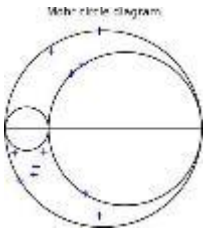


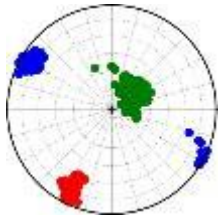


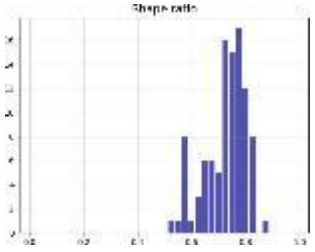


GRID ID = 365

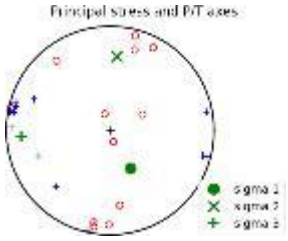


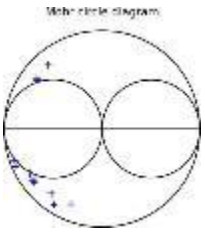


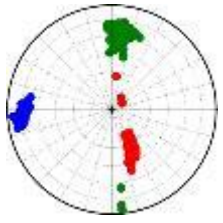


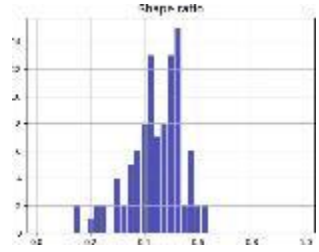


GRID ID = 369

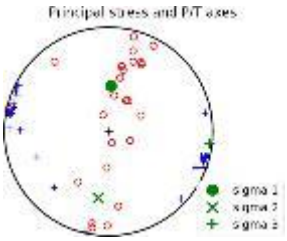


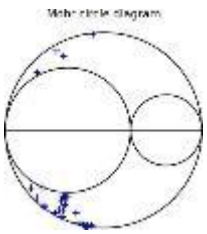


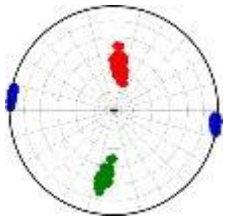


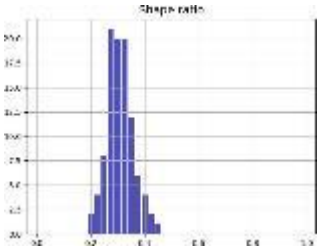


GRID ID = 370

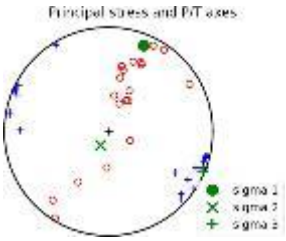


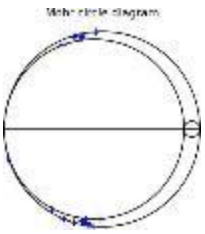


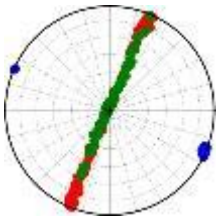


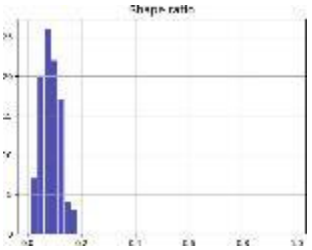


GRID ID = 371

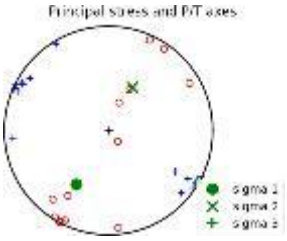


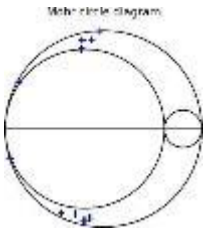


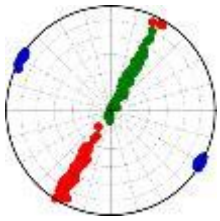


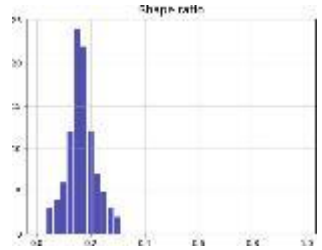


GRID ID = 372

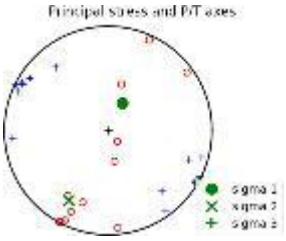


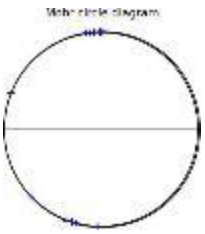


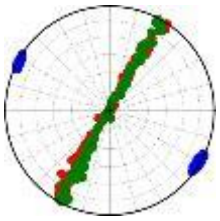


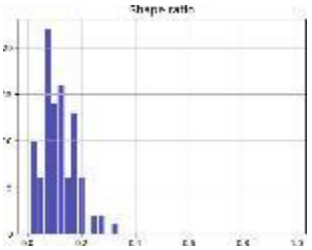


GRID ID = 373

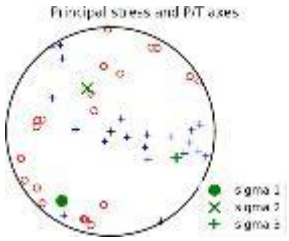


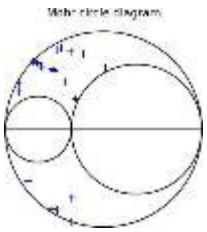


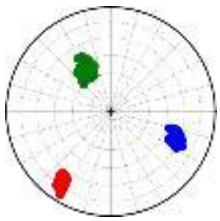


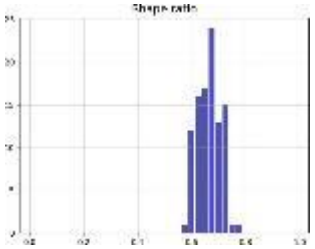


GRID ID = 380

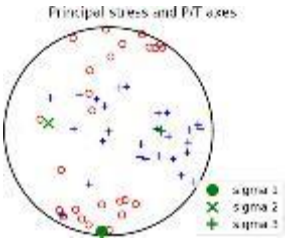


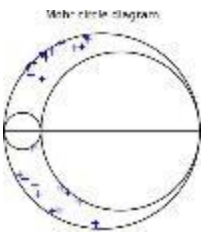


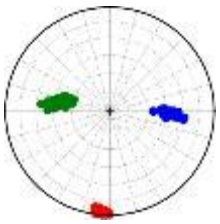


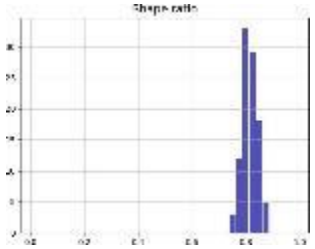


GRID ID = 381

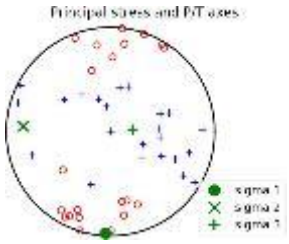


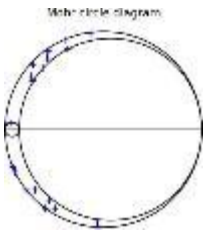


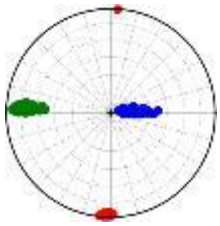


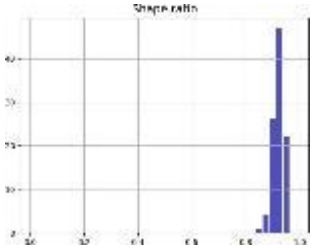


GRID ID = 382

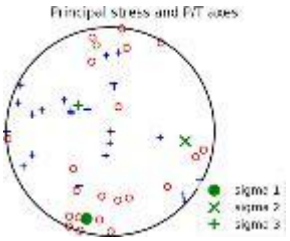


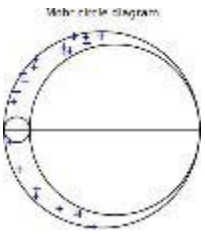


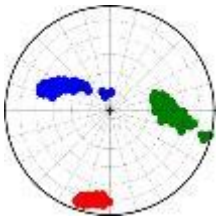


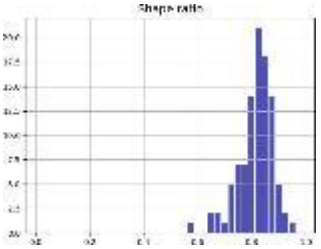


GRID ID = 383

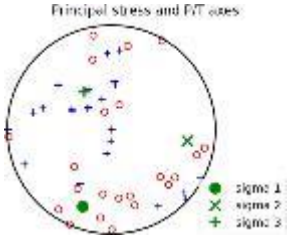


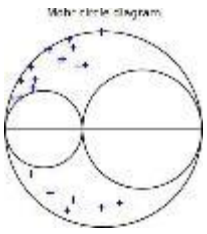


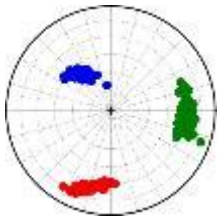


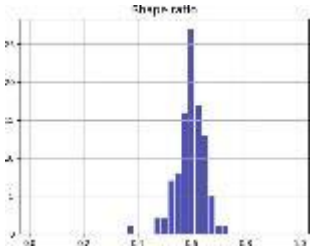


GRID ID = 384

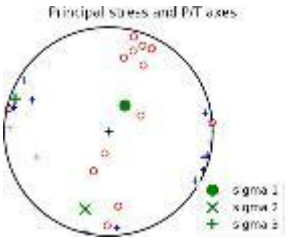


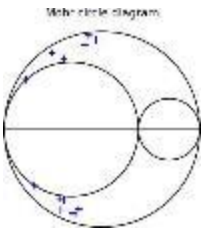


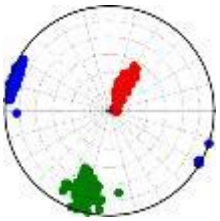


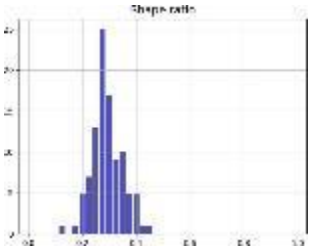


GRID ID = 388

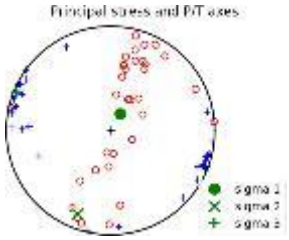


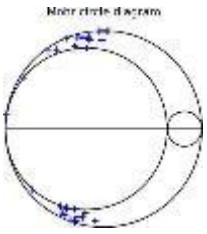


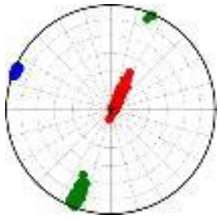


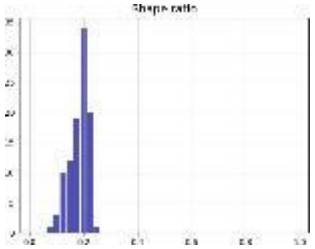


GRID ID = 389

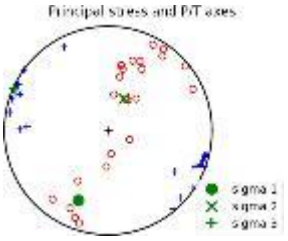


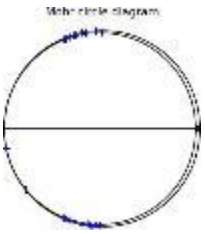


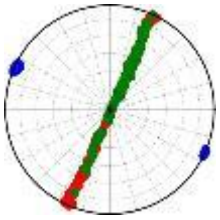


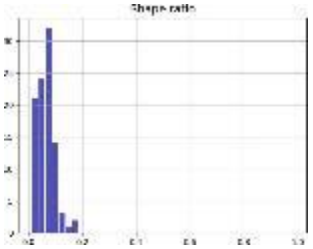


GRID ID = 390

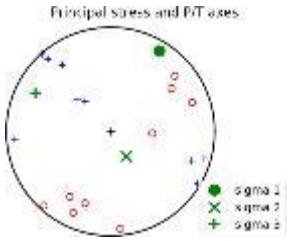


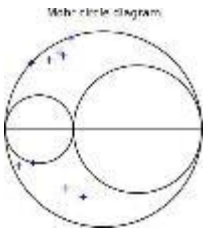


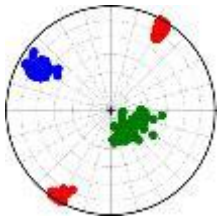


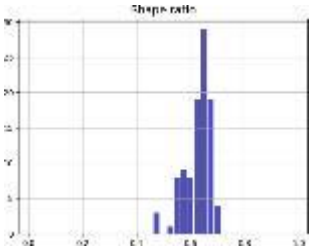


GRID ID = 392

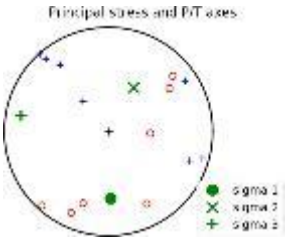


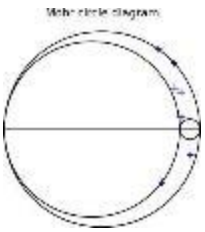


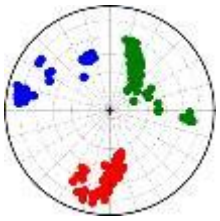


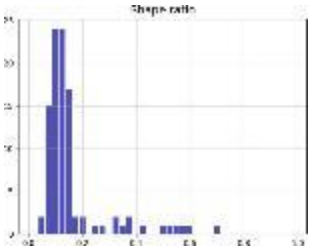


GRID ID = 393

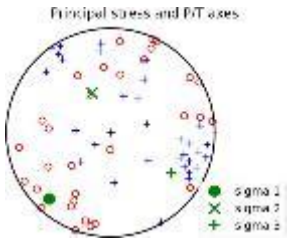


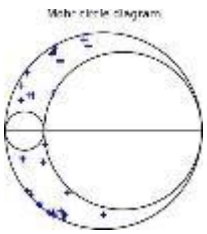


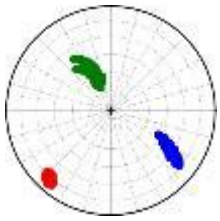


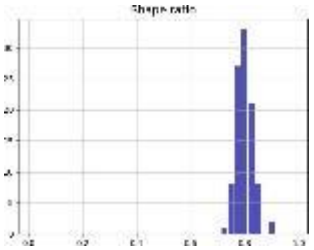


GRID ID = 399

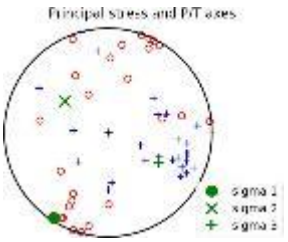


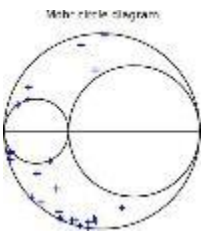


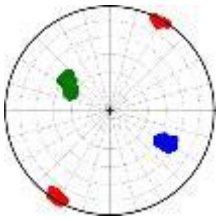


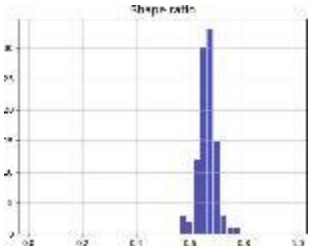


GRID ID = 400

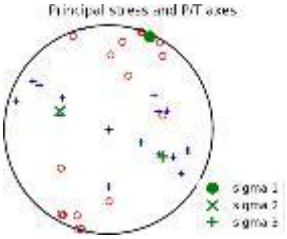


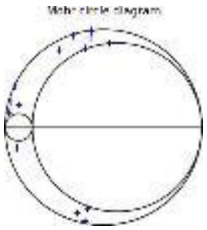


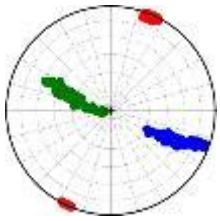


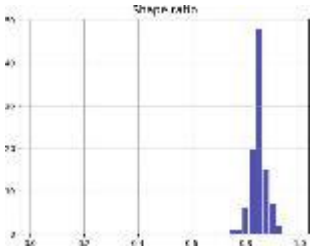


GRID ID = 401

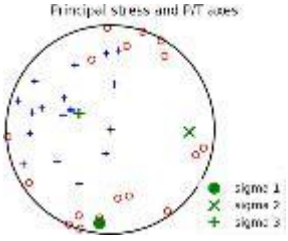


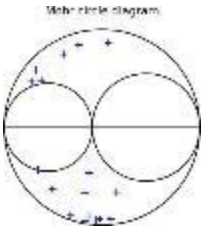


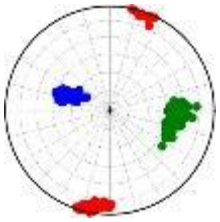


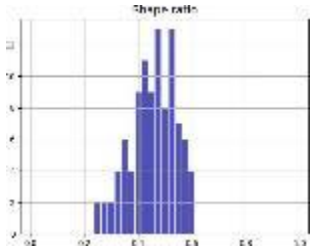


GRID ID = 402

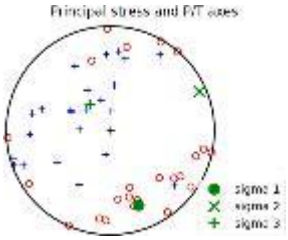


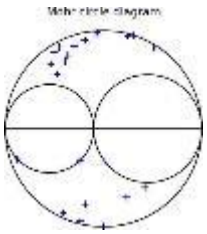


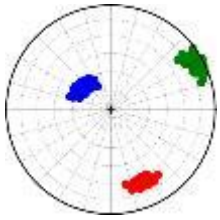


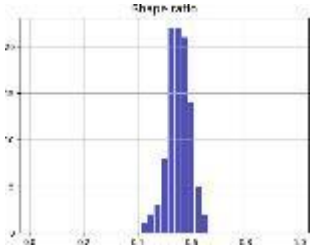


GRID ID = 403

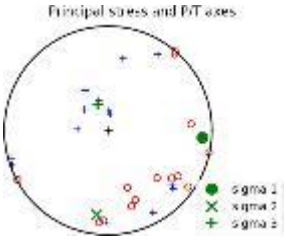


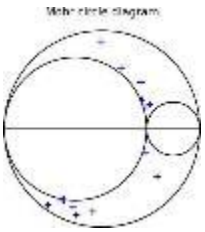


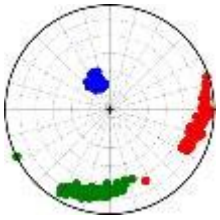


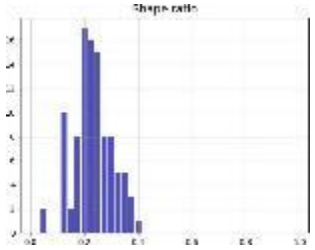


GRID ID = 404

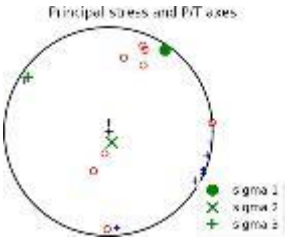


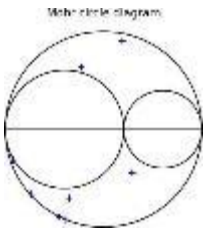


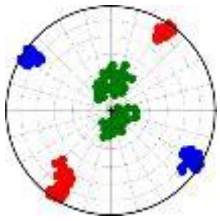


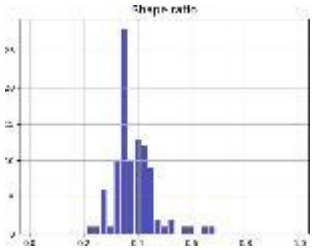


GRID ID = 407

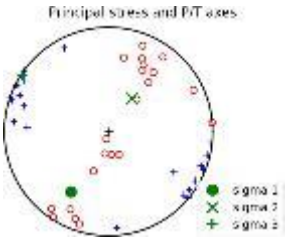


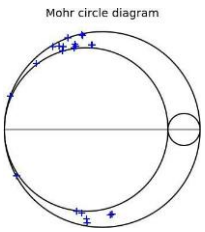


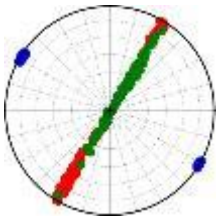


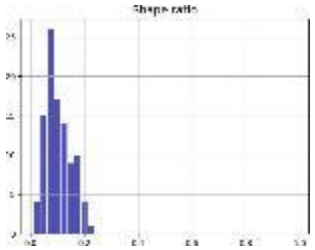


GRID ID = 408

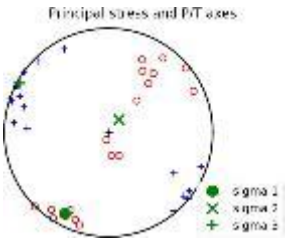


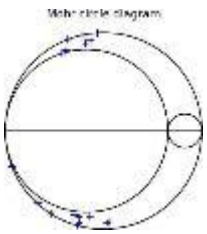


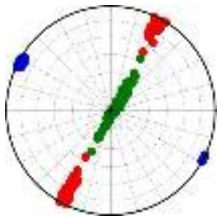


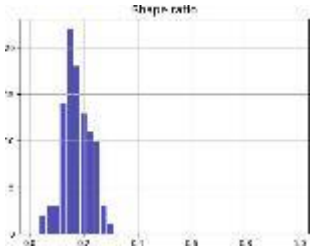


GRID ID = 409

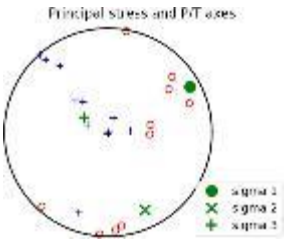


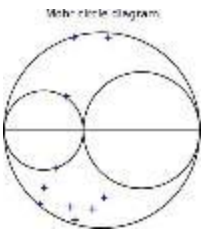


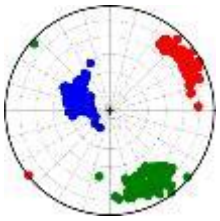


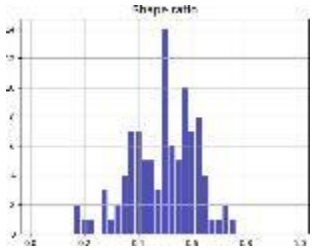


GRID ID = 411

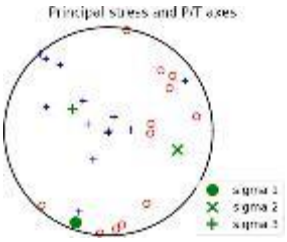


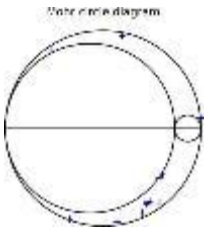


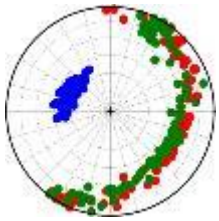


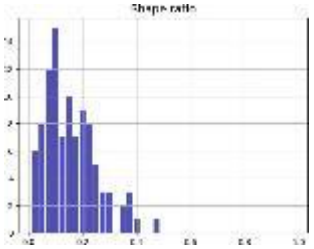


GRID ID = 412

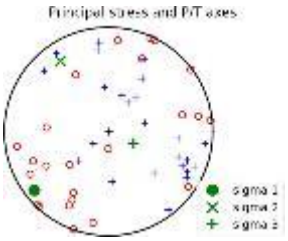


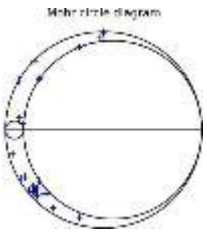


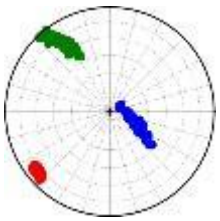


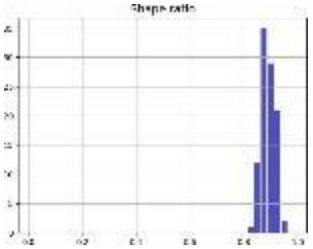


GRID ID = 418

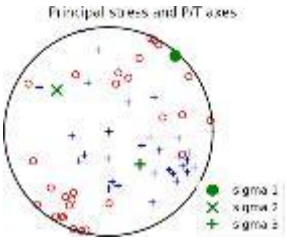


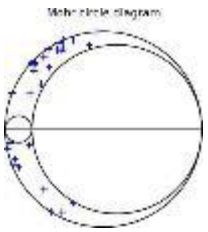


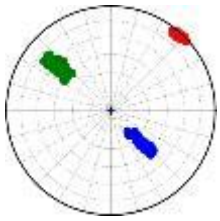


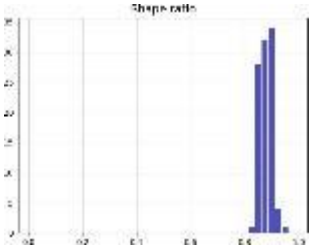


GRID ID = 419

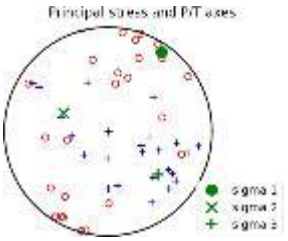


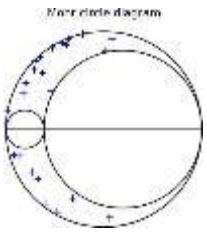


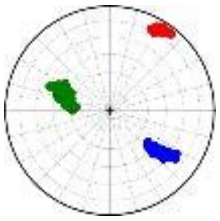


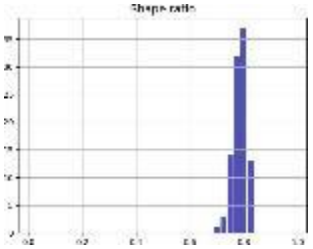


GRID ID = 420

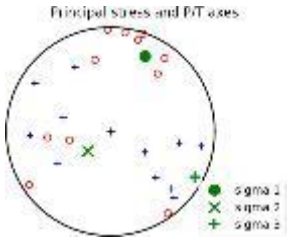


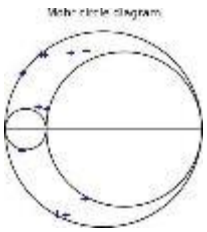


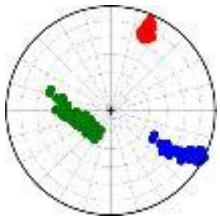


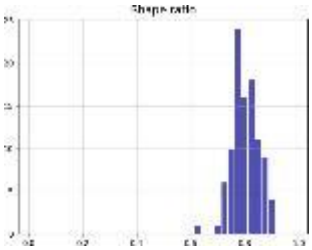


GRID ID = 421

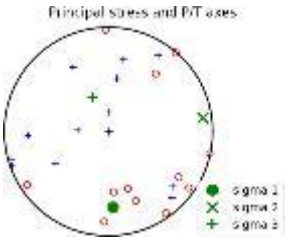


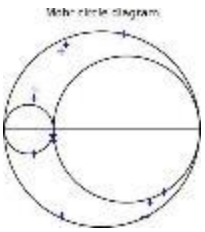


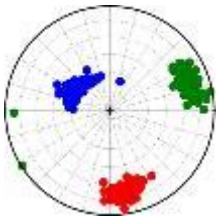


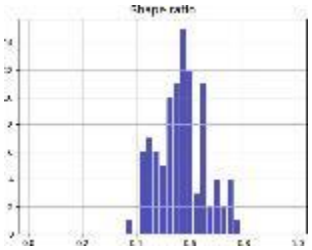


GRID ID = 422

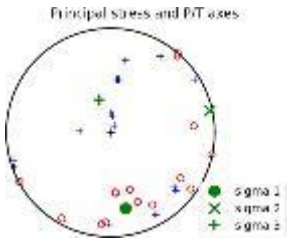


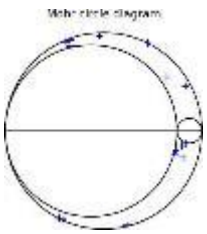


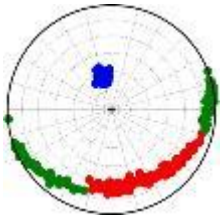


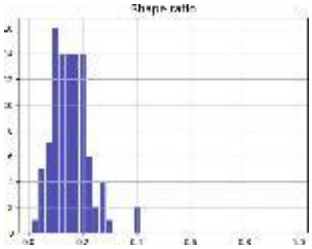


GRID ID = 423

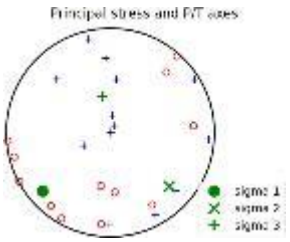


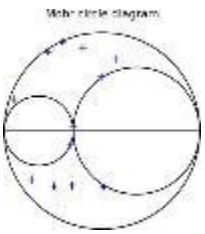


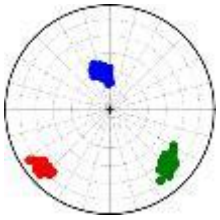


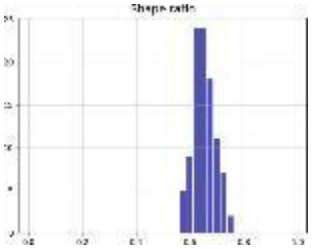


GRID ID = 424

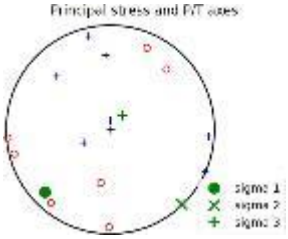


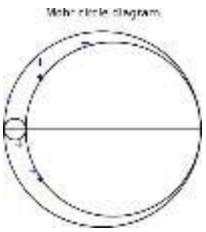


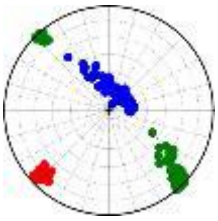


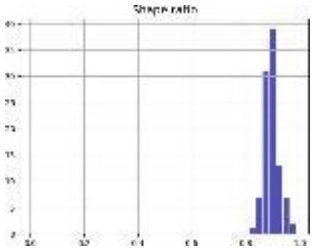


GRID ID = 425

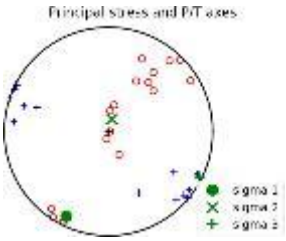


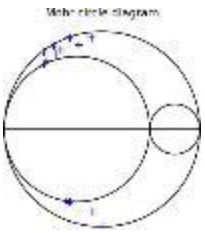


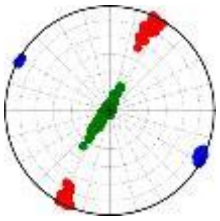


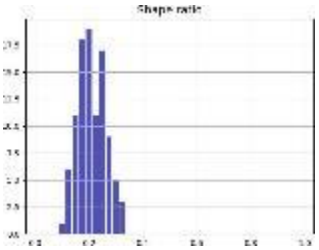


GRID ID = 427

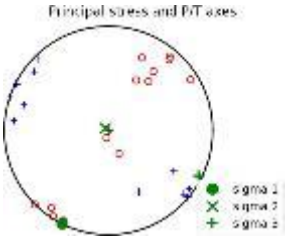


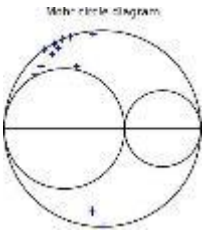


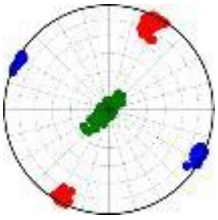


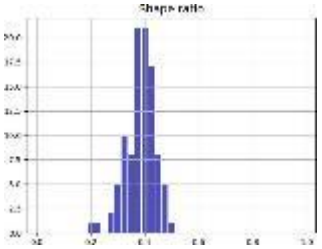


GRID ID = 428

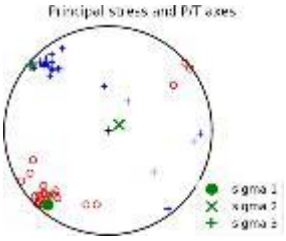


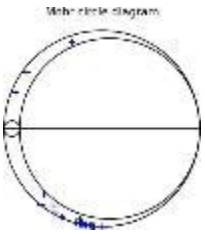


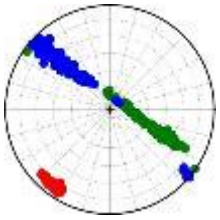


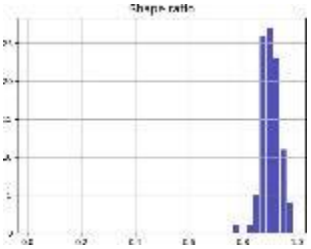


GRID ID = 437

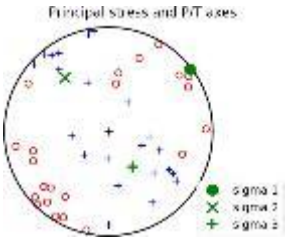


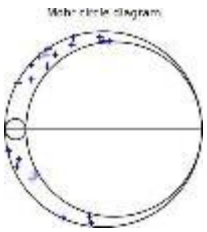


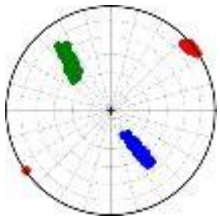


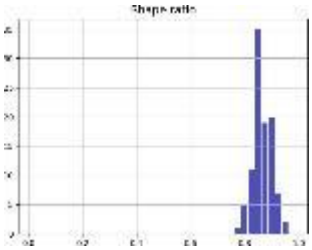


GRID ID = 438

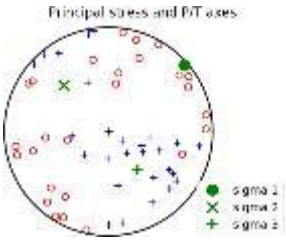


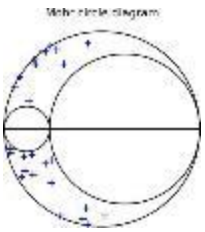


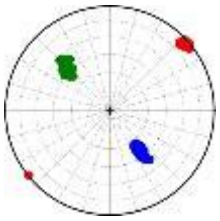


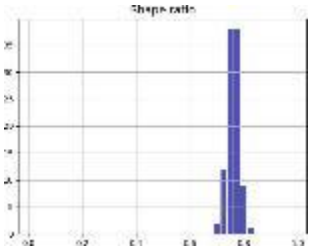


GRID ID = 439

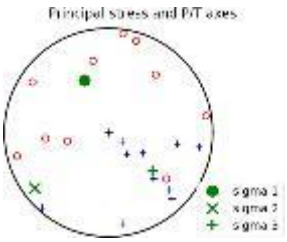


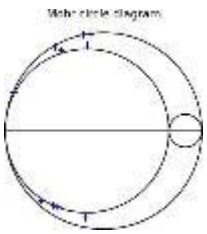


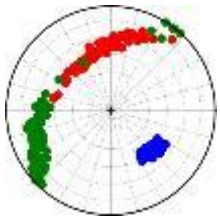


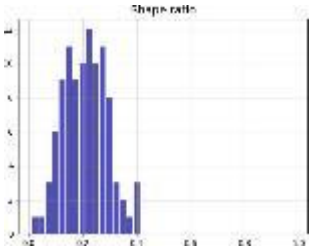


GRID ID = 440

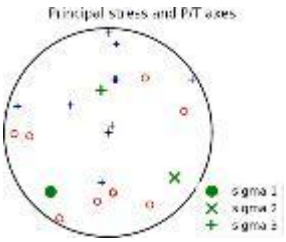


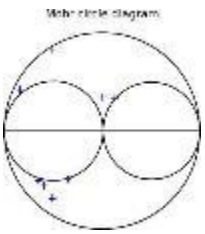


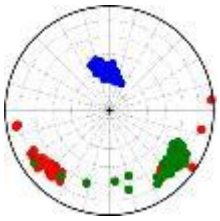


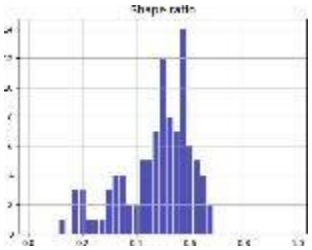


GRID ID = 442

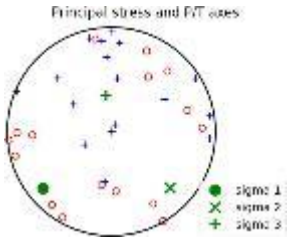


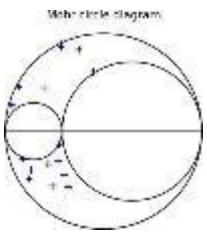


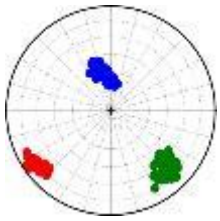


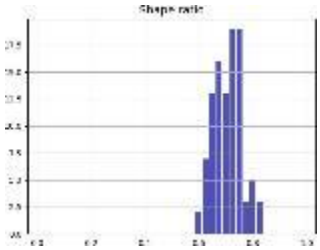


GRID ID = 443

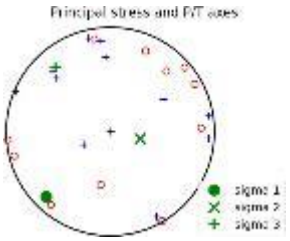


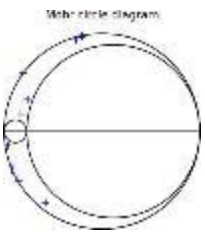


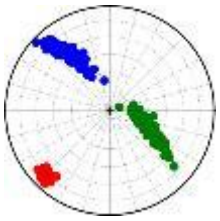


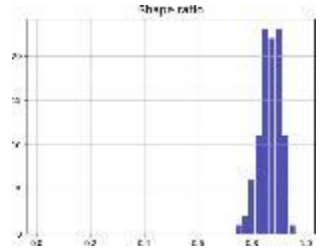


GRID ID = 444

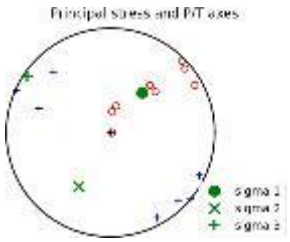


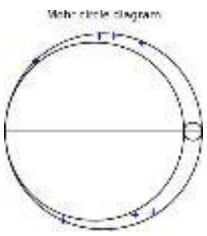


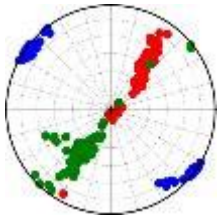


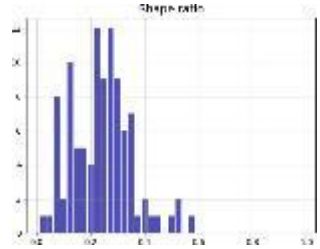


GRID ID = 445

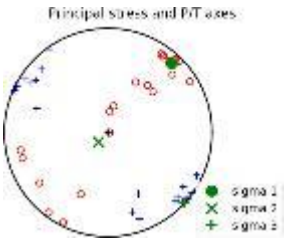


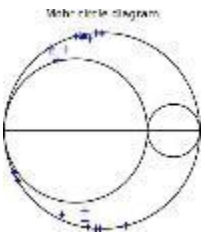


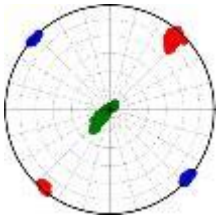


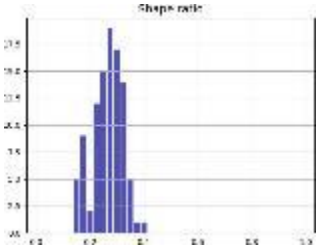


GRID ID = 446

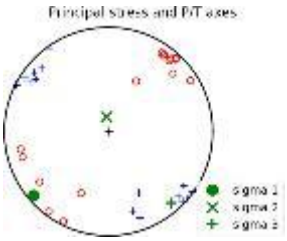


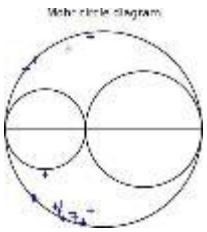


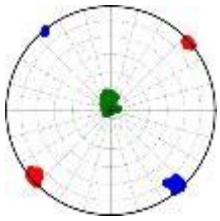


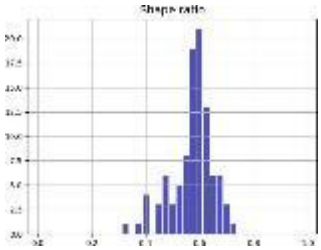


GRID ID = 447

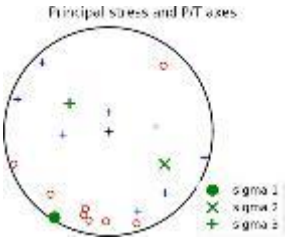


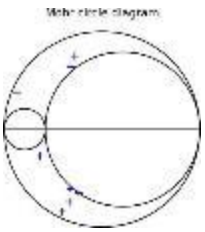


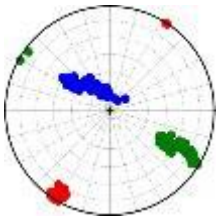


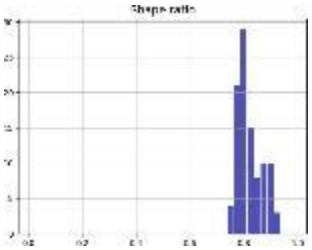


GRID ID = 450

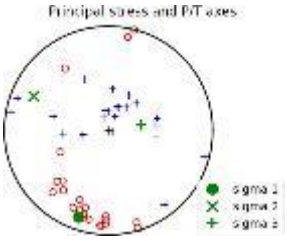


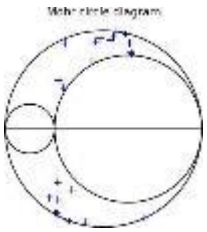


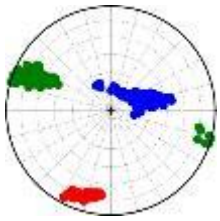


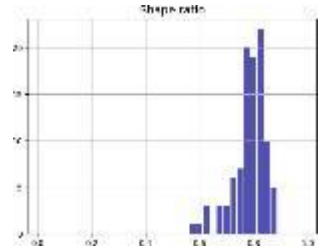


GRID ID = 451

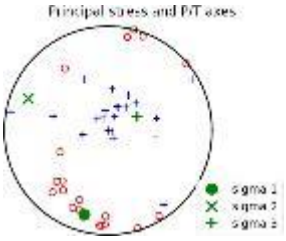


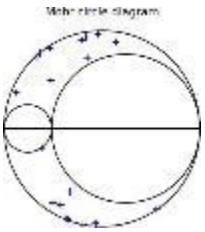


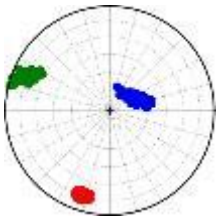


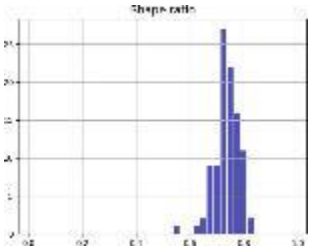


GRID ID = 452

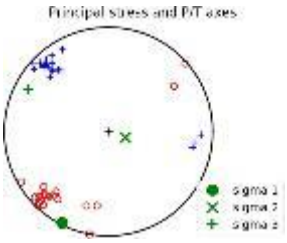


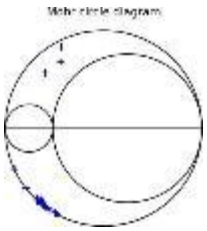


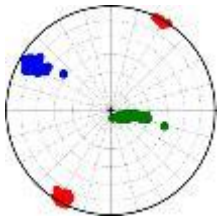


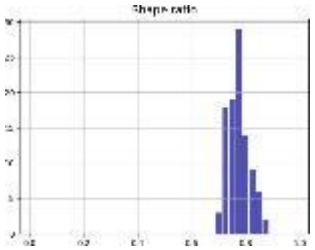


GRID ID = 456

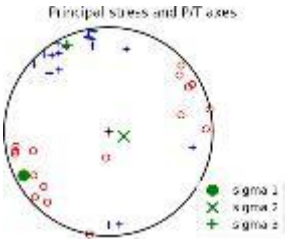


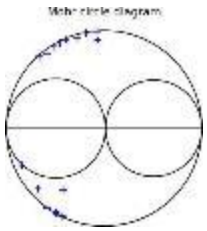


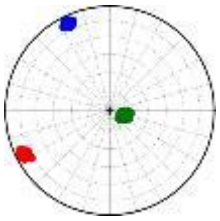


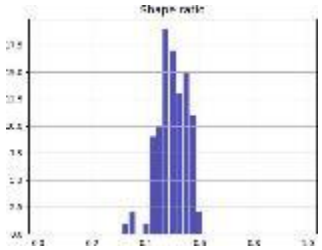


GRID ID = 457

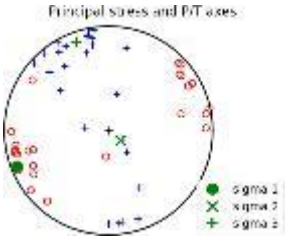


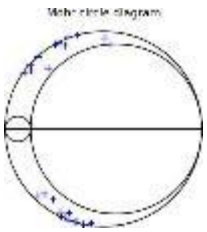


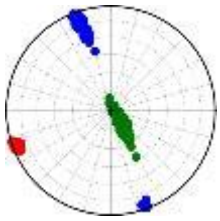


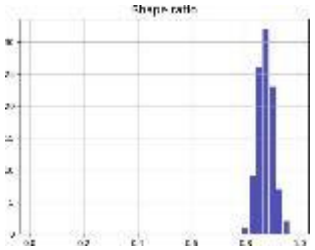


GRID ID = 458

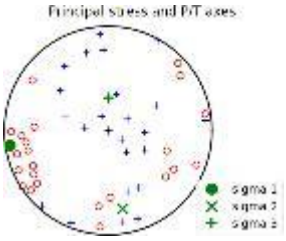


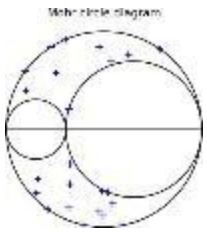


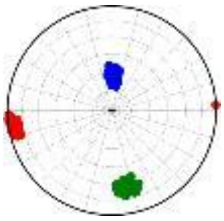


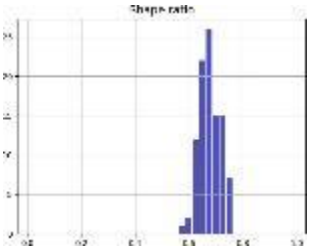


GRID ID = 459

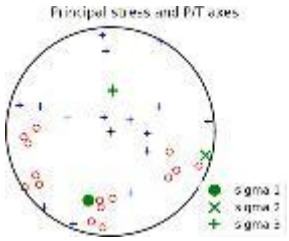


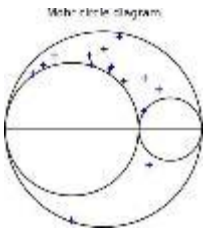


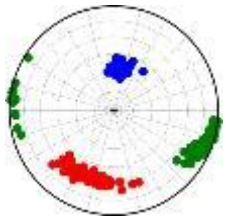


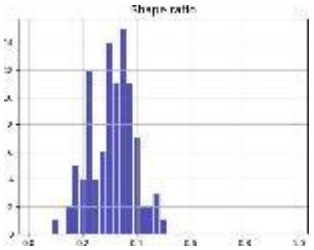


GRID ID = 460

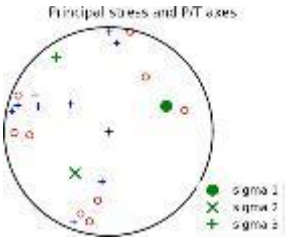


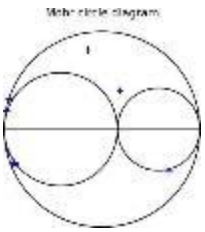


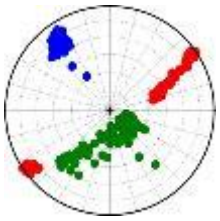


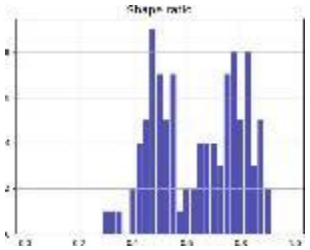


GRID ID = 461

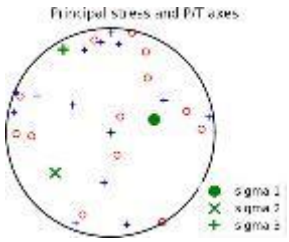


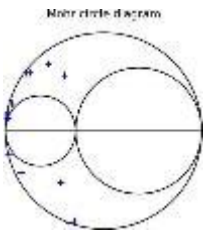


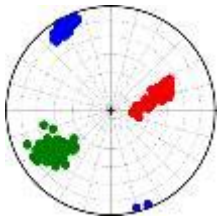


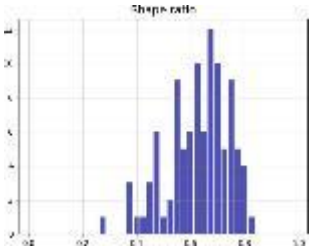


GRID ID = 462

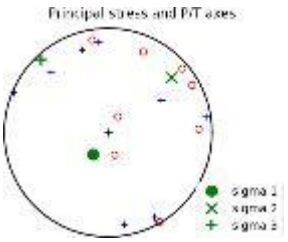


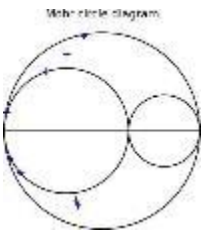


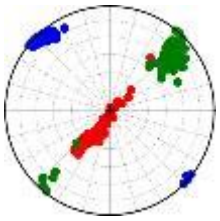


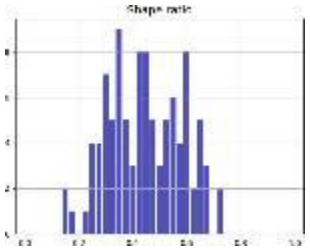


GRID ID = 463

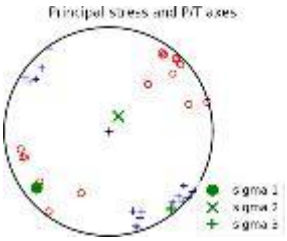


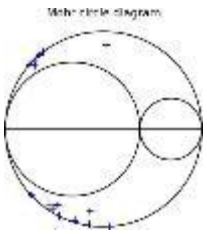


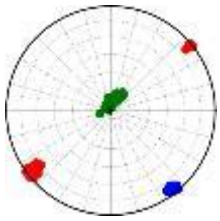


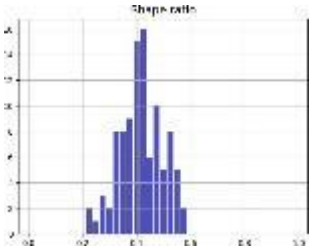


GRID ID = 465

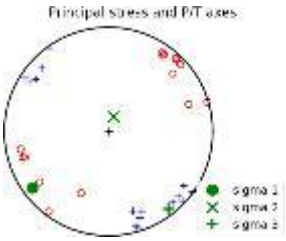


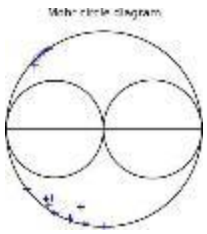


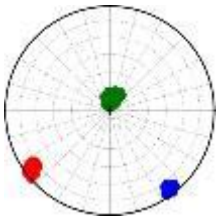


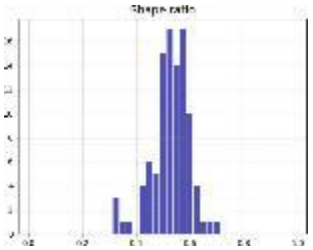


GRID ID = 466

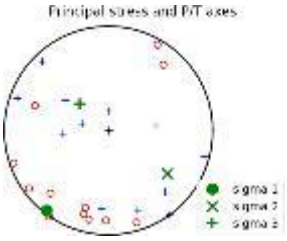


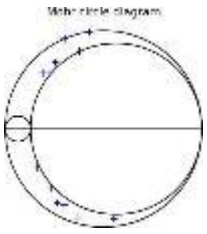


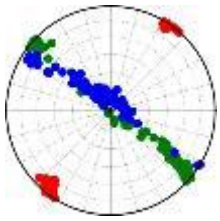


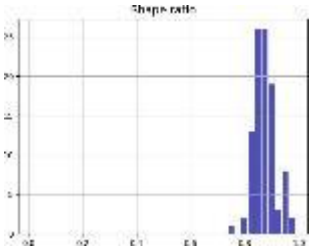


GRID ID = 469

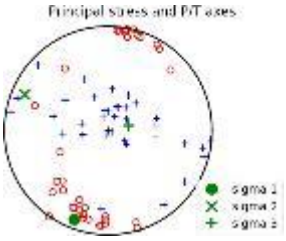


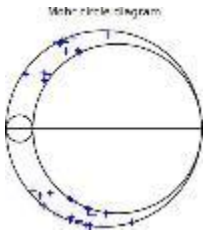


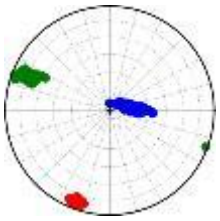


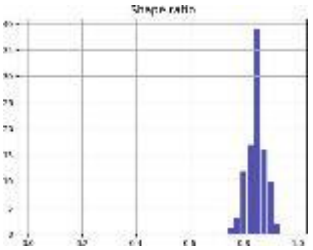


GRID ID = 470

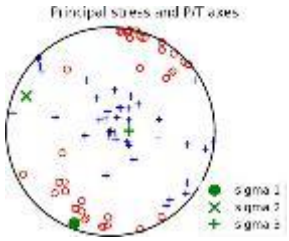


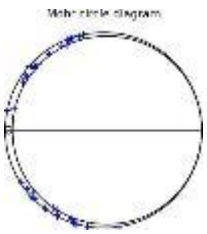


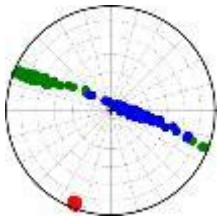


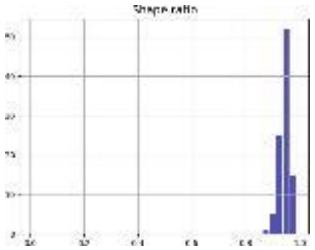


GRID ID = 471

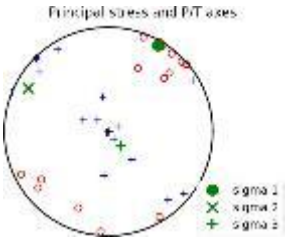


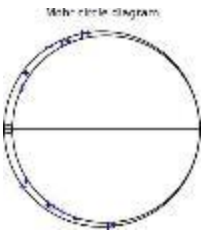


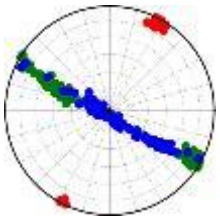


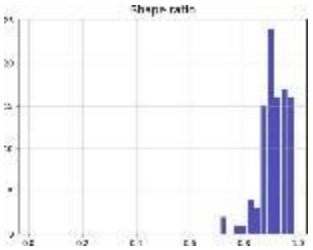


GRID ID = 472

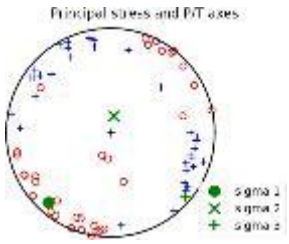


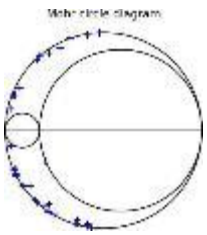


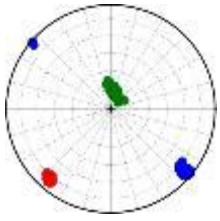


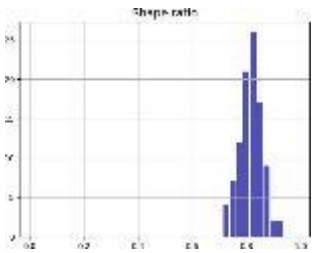


GRID ID = 476

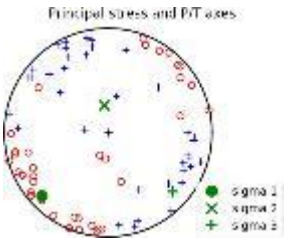


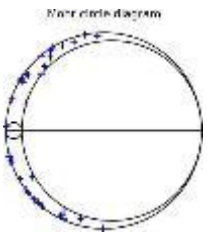


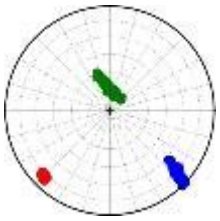


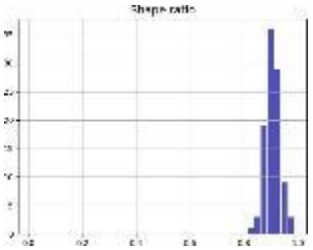


GRID ID = 477

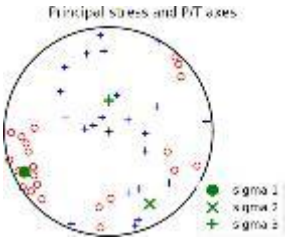


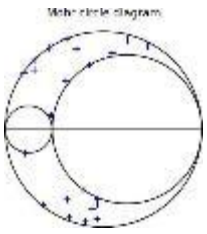


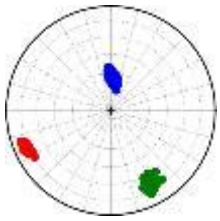


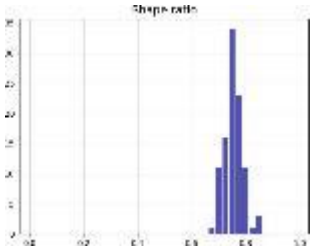


GRID ID = 478

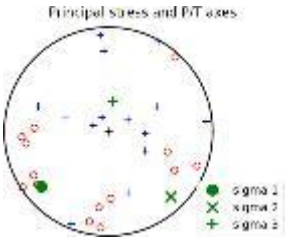


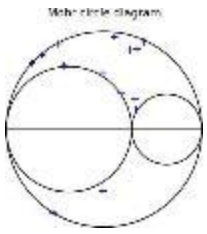


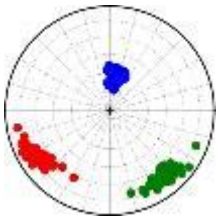


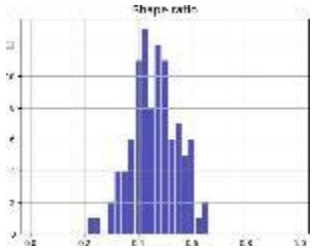


GRID ID = 479

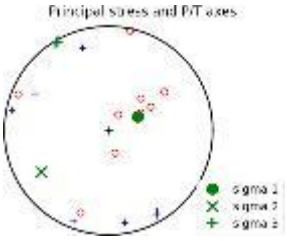


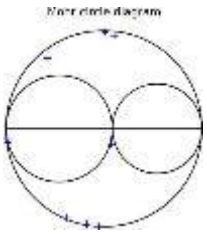


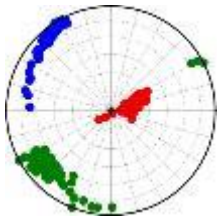


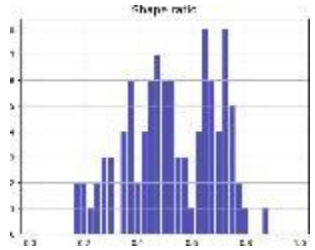


GRID ID = 481

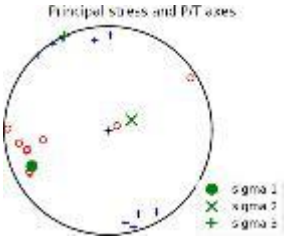


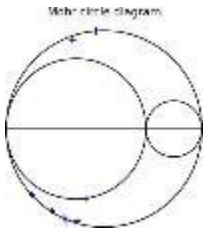


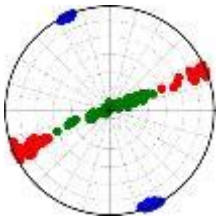


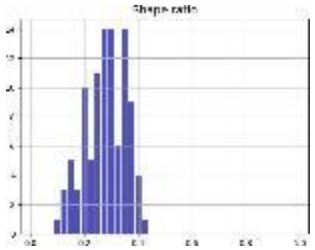


GRID ID = 486

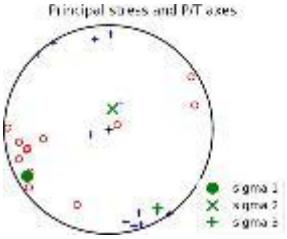


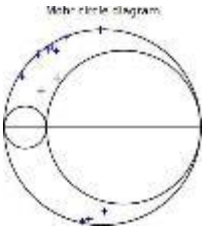


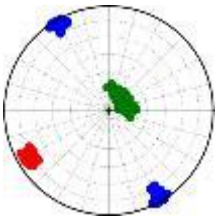


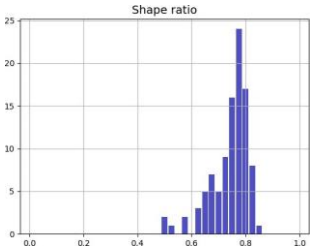


GRID ID = 487

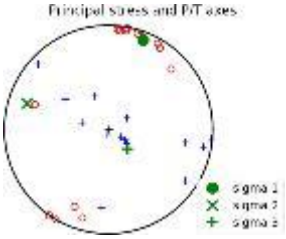


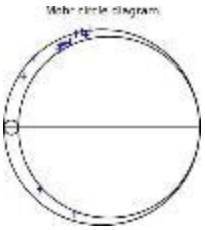


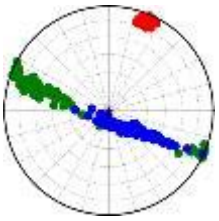


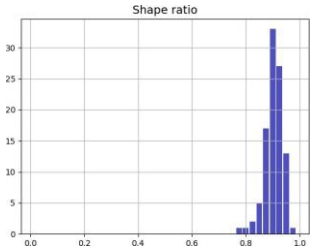


GRID ID = 489

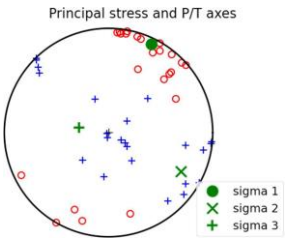


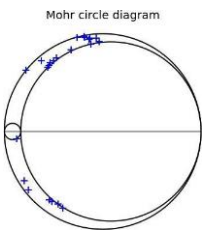


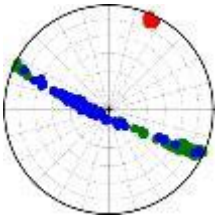


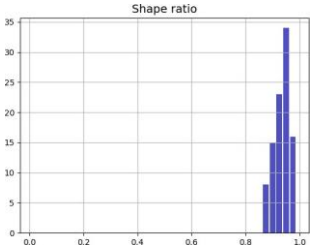


GRID ID = 490

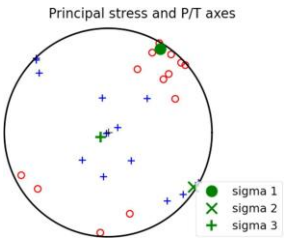


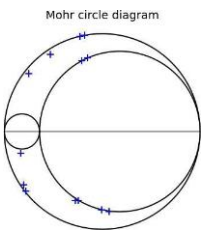


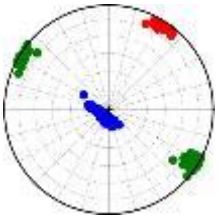


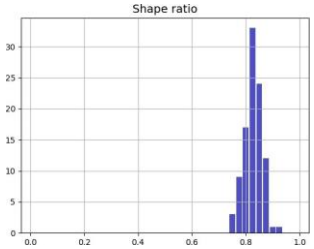


GRID ID = 491

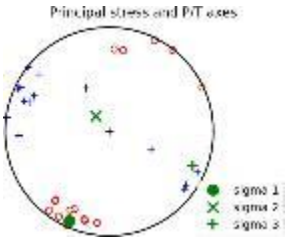


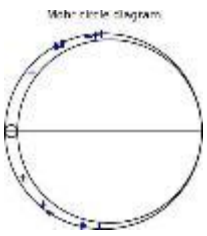


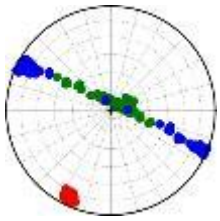


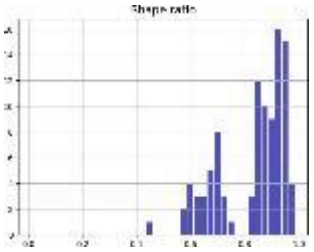


GRID ID = 494

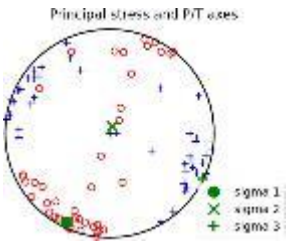


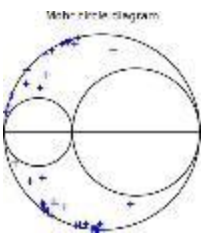


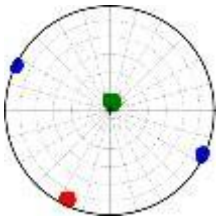


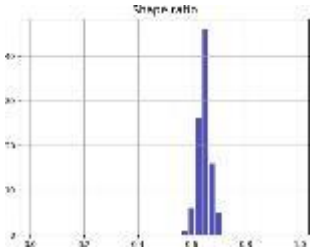


GRID ID = 495

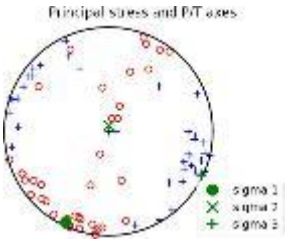


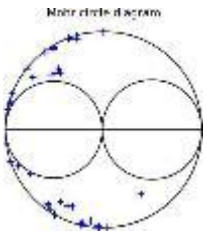


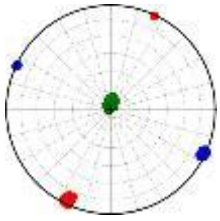


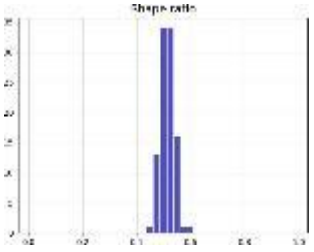


GRID ID = 496

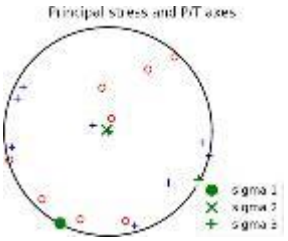


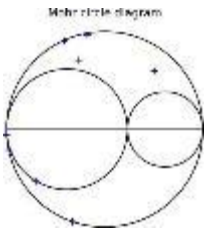


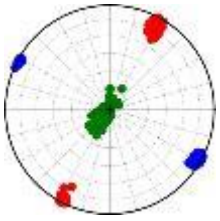


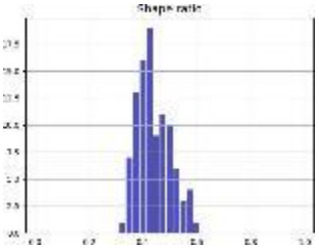


GRID ID = 497

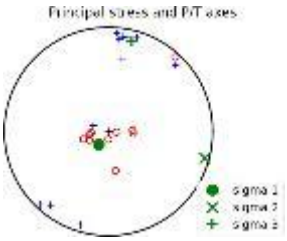


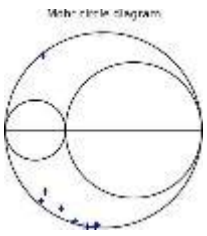


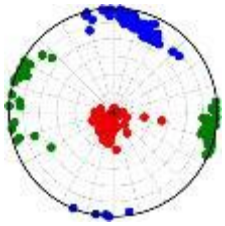


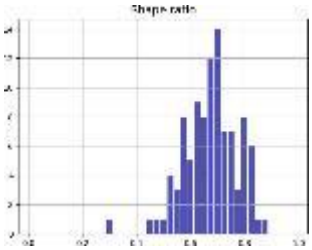


GRID ID = 498

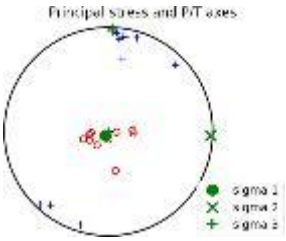


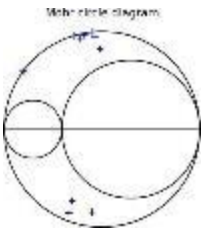


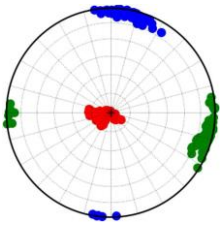


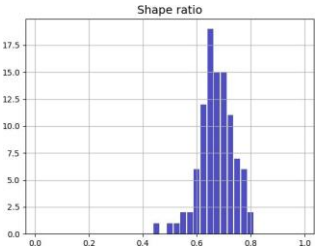


GRID ID = 499

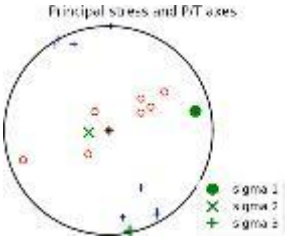


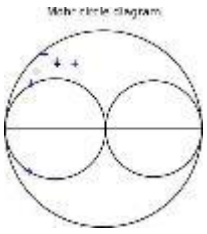


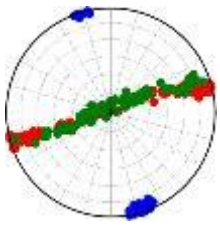


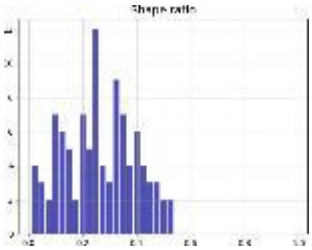


GRID ID = 500

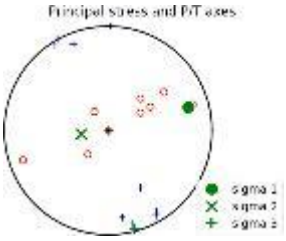


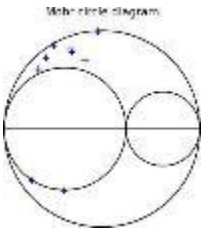


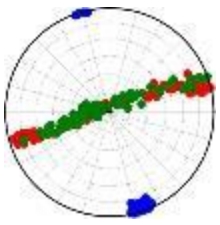


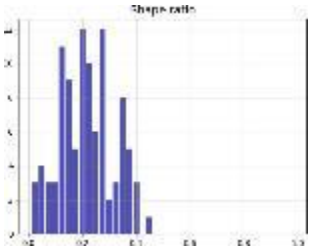


GRID ID = 501

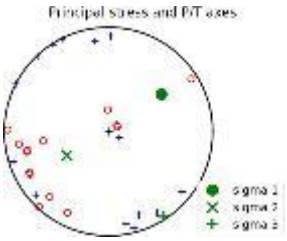


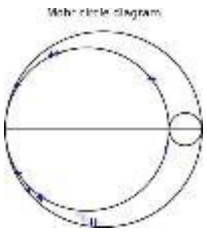


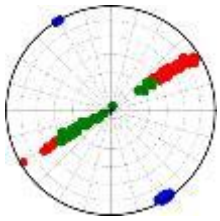


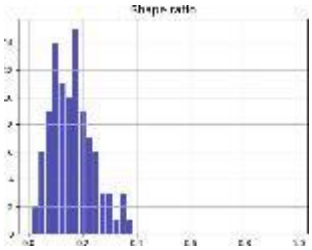


GRID ID = 505

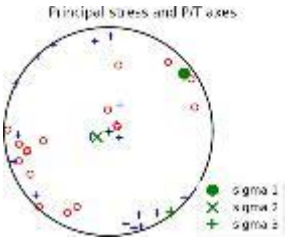


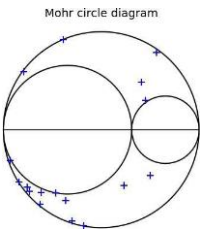


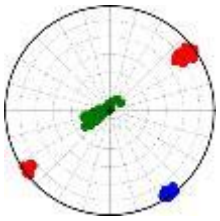


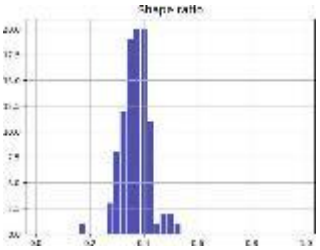


GRID ID = 506

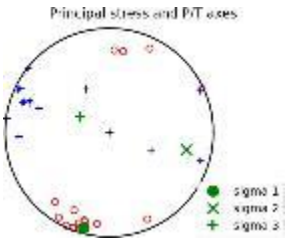


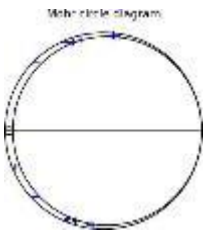


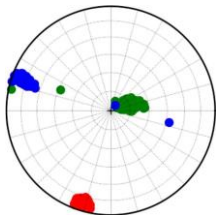


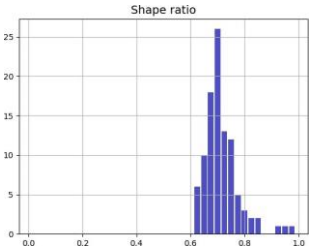


GRID ID = 513

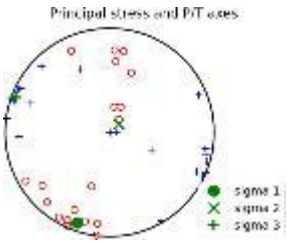


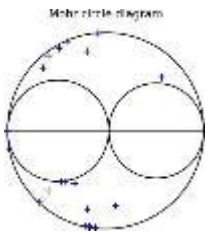


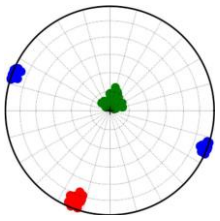


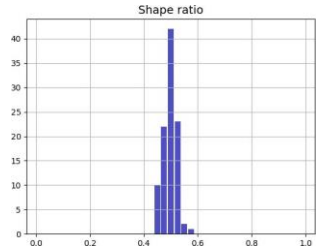


GRID ID = 514

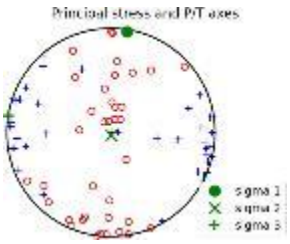


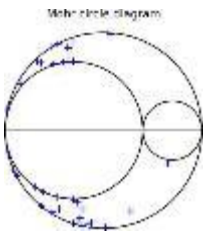


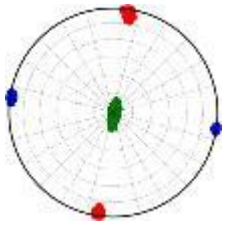


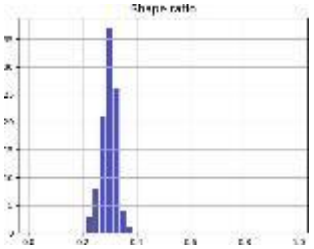


GRID ID = 515

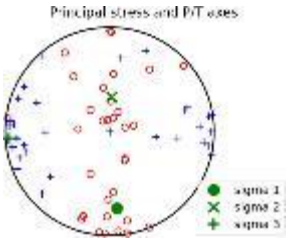


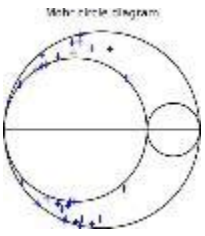


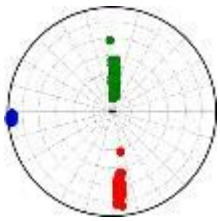


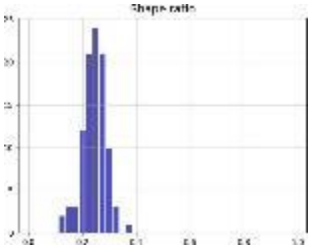


GRID ID = 516

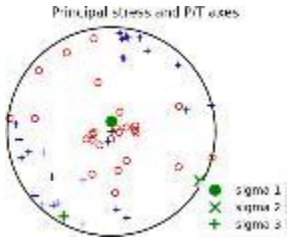


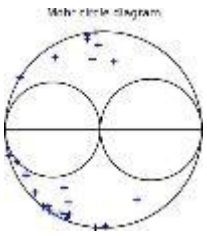


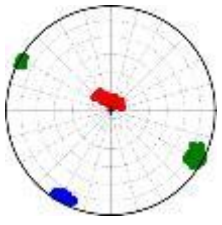


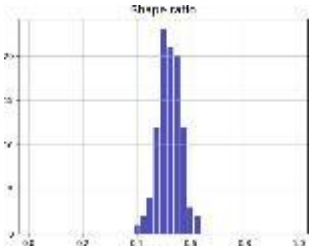


GRID ID = 517

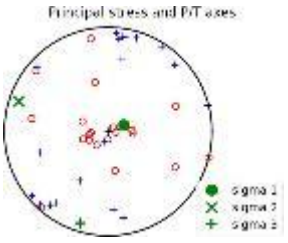


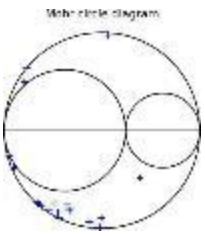


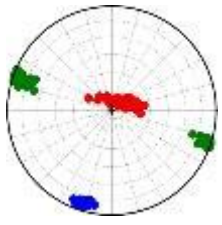


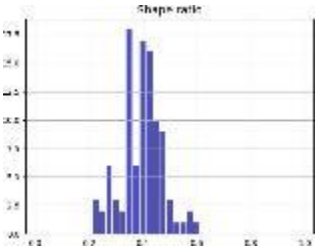


GRID ID = 518

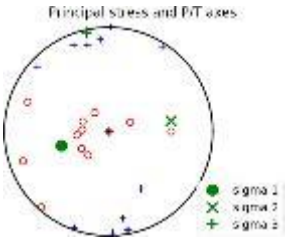


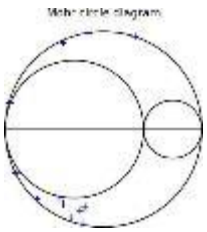


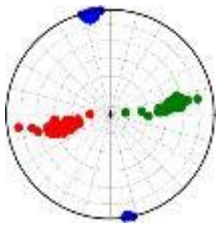


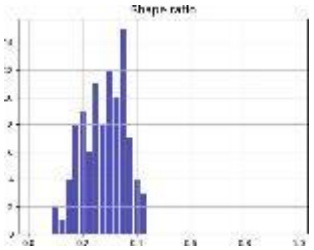


GRID ID = 519

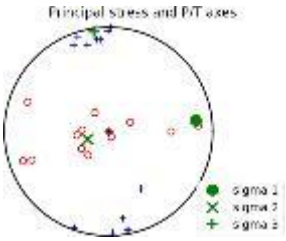


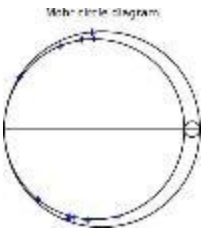


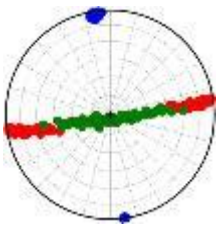


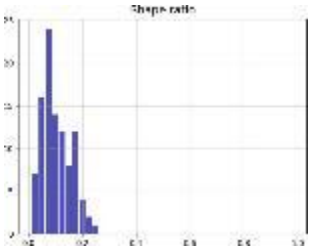


GRID ID = 520

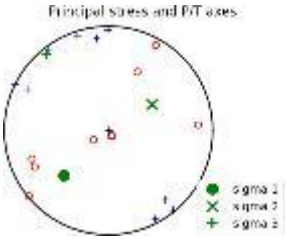


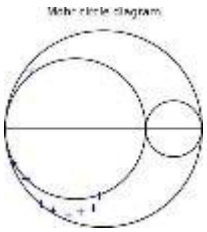


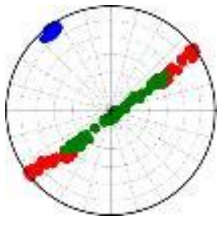


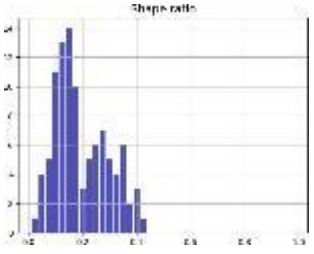


GRID ID = 521

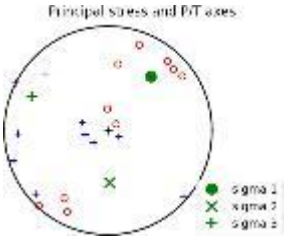


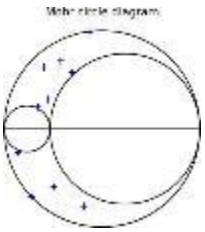


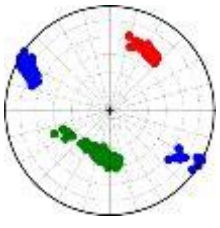


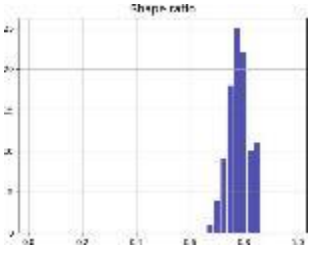


GRID ID = 525

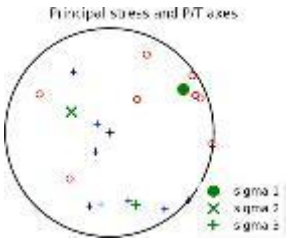


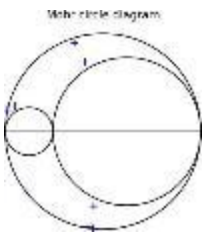


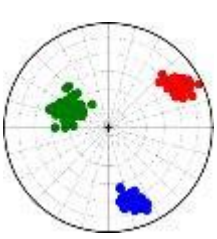


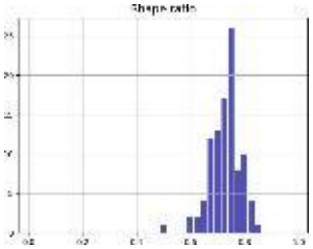


GRID ID = 527

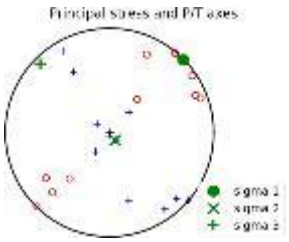


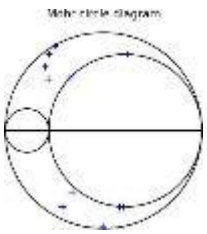


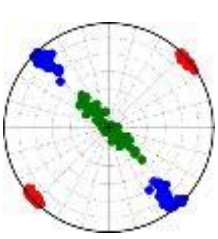


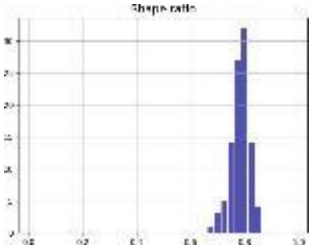


GRID ID = 528



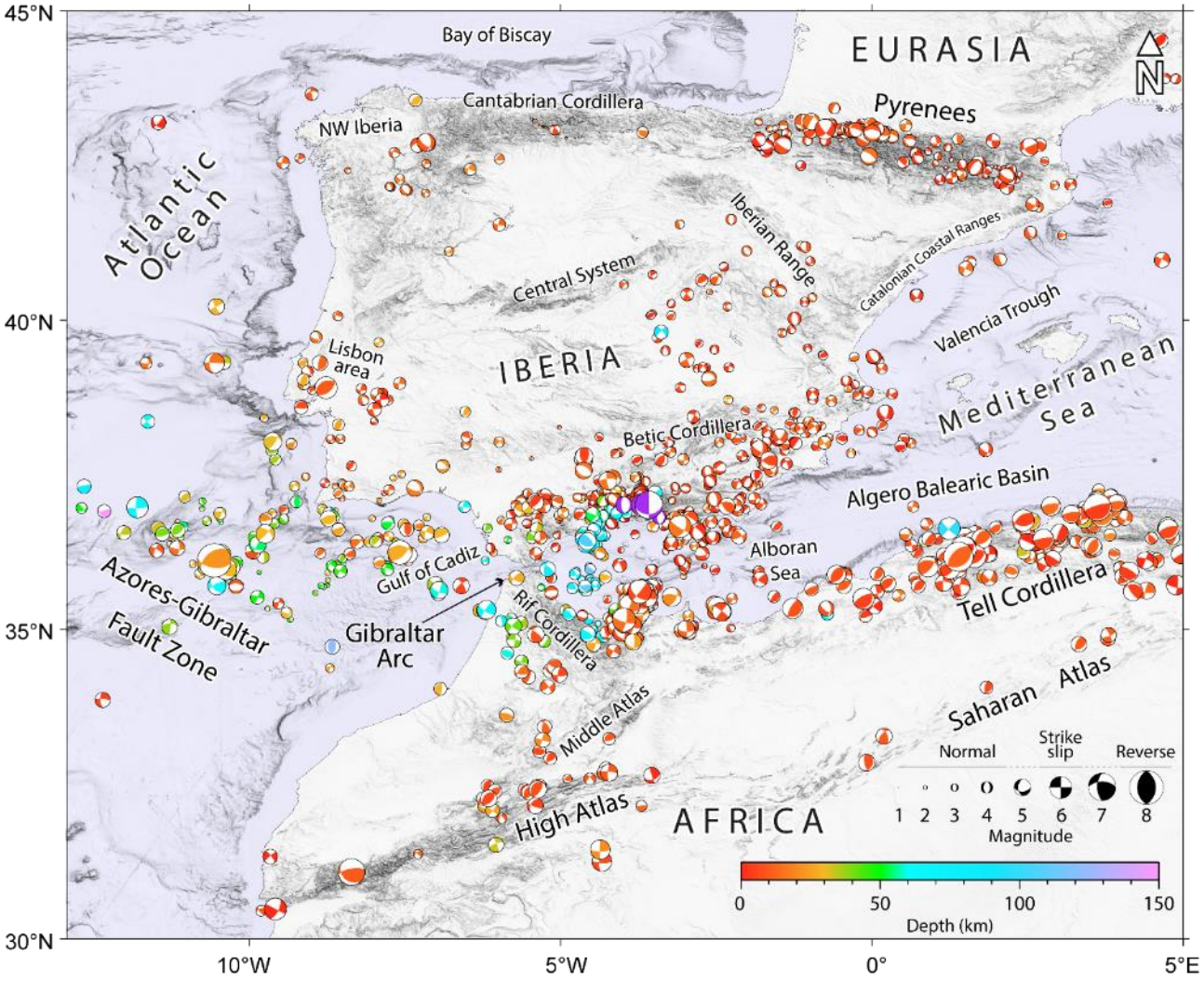






8.2. Supplementary material for Chapter 3

8.2.1. Image – Focal Mechanism Solutions



8.2.2. Table – Historical Earthquakes

Long.	Lat.	Mag	Date	Hour	Reference
(°)	(°)	(Mw)	(dd/mm/yyyy)	(hh:mm:ss)	
-6.00	35.00	6.4	1079	nan	Peláez et al. (2007)
-4.00	38.00	6.1	1169	nan	IGN (2022)
-11.00	36.00	7	22/02/1309	05:30:00	Martinez Solares & Mezcua (2002)
-9.20	38.70	6.7	1344	nan	Vilanova et al. (2007)
-10.00	36.50	6.7	24/08/1356	nan	Peláez et al. (2007)
3.05	36.77	7	03/01/1365	18:00:00	Hamdache et al. (2010)
0.70	42.70	6.2	03/03/1373	nan	Olivera et al. (2008)

-0.22	39.08	6.1	18/12/1396	12:00:00	IGN (2022)
2.33	42.30	6.5	02/02/1428	nan	Perea (2009)
-3.63	37.13	6.11	24/04/1431	14:00:00	LNEC (1986)
-5.47	37.38	6.1	05/04/1504	09:00:00	IGN (2022)
-1.87	37.23	6.1	09/11/1518	23:30:00	IGN (2022)
-2.67	36.97	6.5	22/09/1522	10:00:00	Peláez et al. (2007)
-9.00	38.95	6.9	26/01/1531	nan	Vilanova et al. (2007)
-2.73	37.53	6.1	30/09/1531	04:00:00	IGN (2022)
-5.33	34.00	6.4	23/05/1623	03:00:00	IGN (2022)
-4.57	34.26	6.7	11/05/1624	nan	Peláez et al. (2007)
0.04	42.58	6.1	21/06/1660	nan	Cara et al. (2008)
-4.77	36.66	6.8	09/10/1680	07:00:00	Goded et al. (2008)
3.10	36.70	7	03/02/1716	02:00:00	Hamdache et al. (2010)
-7.58	37.17	6.9	27/12/1722	17:30:00	Vilanova et al. (2007)
-12.50	39.00	7	12/10/1724	02:45:00	Alexandre, 1990
-9.36	30.26	6.4	1731	nan	Peláez et al. (2007)
-0.63	39.03	6.4	23/03/1748	06:30:00	IGN (2022)
-10.00	36.50	8.7	01/11/1755	10:16:00	Goded et al. (2008)
-9.38	36.80	6.7	31/03/1761	12:15:00	Peláez et al. (2007)
-7.00	36.00	6.7	12/04/1773	05:15:00	Peláez et al. (2007)
-0.60	35.70	6.7	09/10/1790	01:15:00	Peláez et al. (2007)
-3.58	36.08	6.7	13/01/1804	nan	Martinez Solares (2003)
-2.83	36.77	6.1	25/08/1804	08:25:00	IGN (2022)
0.10	35.40	6.4	01/03/1819	nan	Hamdache et al. (2010)
2.90	36.50	7	02/03/1825	07:00:00	Hamdache et al. (2010)
-0.68	38.08	6.7	21/03/1829	18:39:00	IGN (2022)
1.80	36.30	6.4	09/03/1856	nan	Hamdache et al. (2010)
-12.00	40.00	6.5	19/11/1857	08:25:00	LNEC (1986)
1.80	36.30	6.4	09/03/1858	04:30:00	Hamdache et al. (2010)
2.83	36.47	7.3	02/01/1867	07:13:00	Hamdache et al. (2010)

-6.92	36.85	6	20/10/1883	nan	Martinez Solares (2003)
-3.98	37.00	6.7	25/12/1884	21:08:00	IGN (2022)
4.67	35.84	6	03/12/1885	20:30:00	Harbi et al. (2010)
-9.00	38.20	7.1	11/11/1858	03:36:00	Vilanova et al. (2007)
1.80	36.50	7	15/01/1891	04:00:00	Hamdache et al. (2010)
4.68	36.62	6.4	13/01/1901	nan	Harbi et al. (2010)
-9.00	38.30	6.5	09/08/1903	22:10:00	Vilanova et al. (2007)
-5.60	35.50	6.4	21/01/1909	nan	IGN (2022)
3.69	36.14	6.5	24/06/1910	13:28:00	Ambraseys et al. (1991)
-11.80	35.50	6.3	11/07/1915	11:29:00	Vilanova et al. (2007)
3.10	36.97	6.2	24/12/1920	13:06:06	Hamdache et al. (2010)
1.30	36.30	7	22/08/1922	11:47:00	Hamdache et al. (2010)
4.95	35.75	6	12/02/1946	02:43:24	Hamdache et al. (2010)
3.20	37.00	6.3	25/10/1949	08:32:00	Hamdache et al. (2010)
4.03	36.70	6.8	08/07/1954	03:51:50	Hamdache et al. (2010)
1.60	36.40	6.2	29/05/1965	20:40:56	Hamdache et al. (2010)

Reference in Table	*Reference in extended version*
Alexandre, (1990)	Alexandre, P., 1990. Les séismes en Europe occidentale de 394 à 1259 Nouveau catalogue critique. Obersavoire R. Belg.
Ambraseys et al., (1991)	Ambraseys, N.N., Vogt, J., Adams, R.D., 1991. The Algerian earthquake of 24 June 1910: A case history. Tectonophysics 193, 205–213. https://doi.org/10.1016/0040-1951(91)90200-C
Cara et al., (2008)	Cara, M., Alasset, P.-J., Sira, C., 2008. Magnitude of Historical Earthquakes, from Macroseismic Data to Seismic Waveform Modelling: Application to the Pyrenees and a 1905 Earthquake in the Alps, in: Fréchet, J., Meghraoui, M., Stucchi, M. (Eds.), Historical Seismology, Modern Approaches in Solid Earth Sciences. Springer Netherlands, Dordrecht, pp. 369–384. https://doi.org/10.1007/978-1-4020-8222-1_18
Goded et al., (2008)	Goded, T., Buforn, E., Munoz, D., 2008. The 1494 and 1680 Malaga (Southern Spain) Earthquakes. Seismol. Res. Lett. 79, 707–715. https://doi.org/10.1785/gssrl.79.5.707
Hamdache et al., (2010)	Hamdache, M., Pelaez, J.A., Talbi, A., Casado, C.L., 2010. A Unified Catalog of Main Earthquakes for Northern Algeria from A.D. 856 to 2008. Seismol. Res. Lett. 81, 732–739. https://doi.org/10.1785/gssrl.81.5.732
Harbi et al., (2010)	Harbi, A., Peresan, A., Panza, G.F., 2010. Seismicity of Eastern Algeria: a revised and extended earthquake catalogue. Nat. Hazards 54, 725–747. https://doi.org/10.1007/s11069-009-9497-6
IGN, (2022)	IGN, 2022. Catálogo de terremotos. Centro Nacional de Información Geográfica (Ministerio de Transportes, Movilidad y Agenda Urbana), ES.
LNEC, (1986)	LNEC, 1986. A Sismicidade Histórica e a Revisão do Catálogo Sísmico. Laboratorio Nacional de Engenharia Civil, 189 pp.
Martínez-Solares and Mezcua-Rodríguez, (2002)	Martínez-Solares, J.M., Mezcua-Rodríguez, J., 2002. Catálogo sísmico de la Península Ibérica:(880 aC-1900). Dir. Gen. Instituto Geográfico Nac. DL 2002.
Martínez Solares, (2003)	Martínez Solares, J.M.M., 2003. Historical Seismicity of the Iberian Peninsula.
Olivera et al., (2008)	Olivera, C., Redondo, E., Lambert, J., Riera-Melis, A., Roca, A., 2008. Review of Historical Earthquakes in the Lower Middle Ages: Earthquakes of the XIV and XV Centuries in

	Catalonia (NE Spain), in: Fréchet, J., Meghraoui, M., Stucchi, M. (Eds.), Historical Seismology, Modern Approaches in Solid Earth Sciences. Springer Netherlands, Dordrecht, pp. 147–162. https://doi.org/10.1007/978-1-4020-8222-1_7
Pelaez et al., (2007)	Pelaez, J.A., Chourak, M., Tadili, B.A., Brahim, L.A., Hamdache, M., Casado, C.L., Solares, J.M.M., 2007. A Catalog of Main Moroccan Earthquakes from 1045 to 2005. Seismol. Res. Lett. 78, 614–621. https://doi.org/10.1785/gssrl.78.6.614
Perea, (2009)	Perea, H., 2009. The Catalan seismic crisis (1427 and 1428; NE Iberian Peninsula): Geological sources and earthquake triggering. J. Geodyn. 47, 259–270. https://doi.org/10.1016/j.jog.2009.01.002
Vilanova and Fonseca, (2007)	Vilanova, S.P., Fonseca, J.F.B.D., 2007. Probabilistic Seismic-Hazard Assessment for Portugal. Bull. Seismol. Soc. Am. 97, 1702–1717. https://doi.org/10.1785/0120050198

8.2.3. Table – Focal Mechanism Solutions

Long.	Lat.	h	Mag	TypeMag	Date	Hour	Strike	Dip	Rake	Reference	Method	TypeRef	Used for Inversion
(°)	(°)	(km)			(dd/mm/yyyy)	(hh:mm:ss)							
-8.8000	38.9000	010	6.0	Mw	23/04/1909	17:39:35	51	52	83	Setal2005a	Moment tensor inversion	Article	Yes
-3.1000	36.6500	016	6.1	Mw	16/06/1910	04:16:00	122	80	-137	Setal2003b	Moment tensor inversion	Article	Yes
-4.6500	37.5600	016	5.1	Mw	05/07/1930	23:11:44	123	39	-86	Batetal2010	Moment tensor inversion	Article	Yes
4.9000	35.7000	000	5.6	Mw	12/02/1946	02:43:00	100	70	12	MandC1991	Polarity	Article	Yes
-4.1950	37.4280	014	5.2	Mw	10/03/1951	10:38:28	177	66	-37	Batetal2008	Moment tensor inversion	Article	Yes
-4.2580	37.3900	016	5.3	Mw	19/05/1951	15:54:21	171	80	-20	Batetal2008	Moment tensor inversion	Article	Yes
-3.6000	37.0000	640	7.0	M	29/03/1954	06:16:05	87	32	-3	Buetal1991	Polarity	Article	No
1.4670	36.2830	000	6.7	Ms	09/09/1954	01:04:37	253	61	104	De1991	Polarity	Article	Yes
1.2410	36.6170	099	6.0	Ms	10/09/1954	05:44:00	44	90	-8	De1991	Polarity	Article	No
1.5000	36.3800	000	5.4	Mw	05/06/1955	14:56:16	172	56	-32	EMMA	Compilation	Catalog	Yes
-3.2300	35.5100	020	5.5	M	23/08/1959	22:21:30	276	70	137	MedandChe1992	Polarity	Article	Yes
2.5000	36.4000	000	5.1	Mw	07/11/1959	02:32:00	203	10	-1	V1986	Polarity	Article	Yes
4.2000	35.6000	005	5.5	Mw	21/02/1960	08:13:00	270	26	39	V1986	Polarity	Article	Yes
-9.6170	30.4500	000	6.0	MD	29/02/1960	23:40:14	27	65	0	Udetal1989	Polarity	Article	Yes
-6.6200	35.6900	005	4.9	M	05/12/1960	21:21:47	328	69	18	MedandChe1992	Polarity	Article	Yes
-10.6000	39.3000	015	5.7	Ms	26/12/1962	08:58:19	180	47	-3	Buetal1988a	Polarity	Article	Yes
-7.6100	36.2300	027	6.4	Mw	15/03/1964	22:30:00	277	43	131	Pondetal1999	Moment tensor inversion	Article	Yes
-5.4200	34.9000	008	5.0	M	15/11/1964	20:03:54	308	74	50	MedandChe1992	Polarity	Article	Yes

4.4200	35.6100	013	5.1	mb	01/01/1965	21:38:30	100	70	168	MandC1991	Polarity	Article	Yes
1.5000	36.3000	000	6.2	Mw	05/06/1965	00:00:00	281	64	-141	MandR2006	Compilation	Article	Yes
2.4400	36.2300	033	4.4	m	23/04/1967	09:30:22	302	55	129	V1986	Polarity	Article	Yes
0.0400	35.3600	000	4.8	m	13/07/1967	02:10:20	226	78	15	V1986	Polarity	Article	Yes
-0.7600	43.0900	005	5.7	Ml	13/08/1967	22:07:48	41	63	-19	Rigo2015	Compilation	Article	Yes
-6.0600	31.4900	033	4.7	mb	28/08/1967	21:15:36	248	75	171	MandC1991	Polarity	Article	Yes
-5.6600	35.0800	036	4.4	Mw	22/01/1968	07:19:00	121	48	159	EMMA	Compilation	Catalog	Yes
-4.5600	36.4800	091	4.3	MbLg	13/02/1968	18:57:33	239	90	80	CandB1994	Polarity	Article	No
-3.7300	35.2400	022	5.0	M	17/04/1968	09:12:00	83	70	-162	Buetal2004	Polarity	Article	Yes
-4.3400	34.8700	071	4.2	Mw	22/05/1968	14:01:00	229	28	136	EMMA	Compilation	Catalog	No
-3.7600	35.2800	005	4.6	MbLg	30/10/1968	11:41:56	20	84	145	CandB1994	Polarity	Article	Yes
-10.6000	36.1000	022	8.0	Ms	28/02/1969	02:40:34	231	47	54	Buetal1988a	Polarity	Article	Yes
-10.5000	36.2000	033	5.7	M	28/02/1969	04:25:37	242	52	70	M1985	Polarity	Article	Yes
0.7000	42.7000	005	4.0	Ml	11/03/1969	00:00:00	2	72	-99	Rigo2015	Compilation	Article	Yes
-10.3400	35.9900	037	5.5	Mw	05/05/1969	05:34:00	196	46	53	Pondetal1999	Moment tensor inversion	Article	Yes
-11.8400	36.9600	067	5.9	Mw	06/09/1969	14:30:36	179	78	5	Pondetal1999	Moment tensor inversion	Article	No
-10.4000	36.0000	015	5.1	Ms	24/12/1969	05:04:45	92	74	34	Buetal1988a	Polarity	Article	Yes
1.7000	42.5200	005	4.0	Ml	14/03/1970	00:00:00	270	79	108	Rigo2015	Compilation	Article	Yes
1.7100	42.5400	005	4.6	Ml	16/03/1970	00:00:00	290	82	135	Rigo2015	Compilation	Article	Yes
1.6600	42.4700	005	4.9	Ml	05/04/1970	00:00:00	216	55	-85	Rigo2015	Compilation	Article	Yes
-3.9000	34.8700	005	4.8	M	07/04/1970	09:16:00	244	64	151	Buetal2004	Polarity	Article	Yes
-5.2300	34.0500	011	4.6	M	02/07/1971	21:11:10	58	80	10	MedandChe1992	Polarity	Article	Yes
-11.2000	36.3000	015	4.7	Ms	18/04/1972	05:51:53	99	80	-155	Buetal1988a	Polarity	Article	Yes
-4.0700	36.0200	005	4.4	M	22/11/1972	00:00:00	234	50	-15	Buetal2004	Polarity	Article	Yes
-3.7000	36.9000	660	4.0	M	30/01/1973	02:36:00	303	37	-153	Buetal1991	Polarity	Article	No
-4.1700	34.6300	010	4.5	M	29/04/1973	14:37:00	212	90	1	Buetal2004	Polarity	Article	Yes
-1.8300	35.9200	008	3.9	M	24/08/1973	10:51:00	194	61	-16	BandB1999	Polarity	Article	Yes

4.4700	36.0600	008	4.9	m	24/11/1973	14:05:00	134	87	140	V1986	Polarity	Article	Yes
4.4000	36.1000	000	5.1	Mw	24/11/1973	15:22:00	200	90	-14	V1986	Polarity	Article	Yes
4.4700	36.1400	019	4.4	M	25/11/1973	04:20:00	240	72	88.9	Hatzetal1978	Polarity	Article	Yes
-4.1200	36.8700	060	4.1	MbLg	13/06/1974	04:20:08	78	72	-69	CandB1994	Polarity	Article	No
-3.6800	35.5800	005	4.3	M	14/07/1974	02:55:00	305	90	180	Buetal2004	Polarity	Article	Yes
-4.5900	36.4100	105	5.2	MbLg	07/08/1975	15:30:24	321	57	118	CandB1994	Polarity	Article	No
-1.7300	37.6500	009	4.2	mbLg	06/06/1977	10:49:12	64	50	-66	PS1998	Polarity	Article	Yes
-3.7300	35.1700	017	3.7	M	15/07/1977	05:41:50	211	70	155	MedandChe1992	Polarity	Article	Yes
-3.7300	35.1700	013	4.0	M	15/07/1977	23:58:00	211	70	-25	Buetal2004	Polarity	Article	Yes
-0.9900	43.0600	007	4.5	Ml	12/09/1977	00:00:00	267	75	127	Rigo2015	Compilation	Article	Yes
-6.9400	36.5100	030	4.8	Mw	14/08/1978	14:14:50	277	13	121	Pondetal1999	Moment tensor inversion	Article	Yes
-0.3600	43.0600	011	2.5	Ml	01/11/1978	00:00:00	317	16	93	Rigo2015	Compilation	Article	Yes
2.7000	42.8400	008	4.3	Ml	03/11/1978	00:00:00	286	52	49	Rigo2015	Compilation	Article	Yes
0.1900	33.2500	010	4.9	mb	11/12/1978	08:56:37	336	55	38	MandC1991	Polarity	Article	Yes
-5.2800	33.4000	012	4.5	M	17/01/1979	17:43:33	194	61	130	MedandChe1992	Polarity	Article	Yes
-4.2800	34.9300	005	4.3	M	24/02/1979	21:19:23	51	40	157	MedandChe1992	Polarity	Article	Yes
-3.7900	37.1600	005	4.1	MbLg	20/03/1979	21:53:56	316	78	-179	CandB1994	Polarity	Article	Yes
-4.0000	35.0300	005	4.0	Mw	21/04/1979	00:00:00	71	59	157	EMMA	Compilation	Catalog	Yes
-5.4200	36.9500	024	4.0	MbLg	01/05/1979	13:49:54	0	76	-122	CandB1994	Polarity	Article	Yes
-2.4600	37.6000	005	4.2	MbLg	14/05/1979	01:47:46	107	49	-40	CandB1994	Polarity	Article	Yes
-5.1900	32.8900	005	4.0	mb	16/06/1979	13:51:43	70	59	129	MandC1991	Polarity	Article	Yes
-3.5000	37.2000	060	4.5	M	20/06/1979	00:09:06	52	87	-102	Buetal1988b	Polarity	Article	No
-2.5200	40.6600	010	4.1	mbLg	30/06/1979	01:44:36	264	58	149	PS1998	Polarity	Article	Yes
-6.9600	34.0200	029	4.2	M	04/07/1979	14:24:53	4	70	74	MedandChe1992	Polarity	Article	Yes
-5.1900	32.8900	007	4.2	Mw	16/07/1979	00:00:00	192	47	44	EMMA	Compilation	Catalog	Yes
0.5400	43.1500	016	4.1	Ml	28/09/1979	00:00:00	276	72	174	Rigo2015	Compilation	Article	Yes
-0.7700	38.0100	020	4.3	MbLg	25/10/1979	15:29:49	59	81	-7	CandB1994	Polarity	Article	Yes
-4.3400	37.0600	040	4.0	MbLg	22/12/1979	23:45:12	210	64	-86	CandB1994	Polarity	Article	Yes
-4.9400	35.2900	033	4.0	M	10/02/1980	03:39:44	55	85	162	MedandChe1992	Polarity	Article	Yes
-0.0500	42.6500	015	5.1	Mw	29/02/1980	20:41:00	91	27	-122	CMT	Moment tensor inversion	Catalog	Yes

-0.3700	43.0700	006	3.3	Ml	02/03/1980	00:00:00	254	75	-146	Rigo2015	Compilation	Article	Yes
-0.3800	43.0800	005	3.2	Ml	03/03/1980	00:00:00	50	22	-118	Rigo2015	Compilation	Article	Yes
-0.3700	43.0700	005	3.1	Ml	04/03/1980	00:00:00	22	10	0	Rigo2015	Compilation	Article	Yes
-0.4000	43.0700	004	3.6	Ml	05/03/1980	00:00:00	266	73	-95	Rigo2015	Compilation	Article	Yes
-0.3700	43.0700	004	3.3	Ml	07/03/1980	00:00:00	139	52	-57	Rigo2015	Compilation	Article	Yes
-5.2300	35.9600	081	4.7	M	22/06/1980	23:18:33	304	66	45	MedandChe1992	Polarity	Article	No
-10.2500	35.6800	010	4.5	Mw	18/08/1980	00:00:00	88	33	-94	EMMA	Compilation	Catalog	Yes
1.3900	36.1600	012	7.3	M	10/10/1980	12:25:00	225	54	83	Ouyed et al. (1981)	Compilation	Article	Yes
1.4500	36.3000	010	5.5	Mw	10/10/1980	14:44:00	266	51	149	EMMA	Compilation	Catalog	Yes
1.6480	36.1670	005	6.2	Mw	10/10/1980	15:39:10	58	43	81	CMT	Moment tensor inversion	Catalog	Yes
1.4000	36.1300	010	5.5	Mw	10/10/1980	17:32:00	67	32	124	EMMA	Compilation	Catalog	Yes
1.6200	36.4000	010	5.5	Mw	10/10/1980	19:08:00	25	25	52	EMMA	Compilation	Catalog	Yes
1.6780	36.3780	005	5.5	Mw	13/10/1980	06:37:40	63	42	69	CMT	Moment tensor inversion	Catalog	Yes
1.6600	36.3300	010	5.1	Mw	13/10/1980	14:33:00	47	31	64	EMMA	Compilation	Catalog	Yes
1.6800	36.3500	010	5.1	Mw	14/10/1980	17:34:00	28	34	61	EMMA	Compilation	Catalog	Yes
1.4800	36.2470	008	2.7	Ml	17/10/1980	16:32:00	117	81	150	Ouyetal1983	Polarity	Article	Yes
1.4890	36.2070	007	2.8	Ml	18/10/1980	10:23:00	55	72	-11	Ouyetal1983	Polarity	Article	Yes
1.3990	36.1560	011	2.3	Ml	21/10/1980	21:32:00	129	41	163	Ouyetal1983	Polarity	Article	Yes
1.6360	36.2270	006	2.9	Ml	21/10/1980	22:47:00	223	64	46	Ouyetal1983	Polarity	Article	Yes
1.4710	36.2030	009	3.2	Ml	22/10/1980	16:06:00	287	59	144	Ouyetal1983	Polarity	Article	Yes
1.4900	36.4900	010	5.1	Mw	22/10/1980	16:23:00	30	11	66	EMMA	Compilation	Catalog	Yes
1.4620	36.2150	011	2.7	Ml	22/10/1980	22:38:00	204	53	8	Ouyetal1983	Polarity	Article	Yes
1.5790	36.2970	007	2.8	Ml	24/10/1980	15:37:00	86	76	-137	Ouyetal1983	Polarity	Article	Yes
1.4528	36.2240	007	2.7	Ml	24/10/1980	17:07:00	232	40	90	Yieletal1989	Polarity	Article	Yes
1.3832	36.1103	006	3.5	Ml	24/10/1980	21:59:00	221	60	65	Yieletal1989	Polarity	Article	Yes
1.6950	36.3630	004	3.3	Ml	24/10/1980	22:11:00	48	40	90	Yieletal1989	Polarity	Article	Yes
1.5635	36.2705	005	3.4	Ml	24/10/1980	23:31:00	219	50	115	Yieletal1989	Polarity	Article	Yes
1.6258	36.3790	006	2.4	Ml	25/10/1980	03:11:00	64	56	105	Yieletal1989	Polarity	Article	Yes
1.4008	36.0225	005	3.3	Ml	25/10/1980	03:46:00	270	90	180	Yieletal1989	Polarity	Article	Yes

1.5078	36.2077	005	3.2	MI	25/10/1980	04:23:00	202	56	48	Yieletal1989	Polarity	Article	Yes
1.6962	36.3402	007	2.8	MI	25/10/1980	11:42:00	258	70	88	Yieletal1989	Polarity	Article	Yes
1.3020	36.0513	008	2.4	MI	25/10/1980	15:55:00	91	70	135	Yieletal1989	Polarity	Article	Yes
1.4620	36.1650	005	2.7	MI	25/10/1980	17:05:00	212	57	54	Ouyetal1983	Polarity	Article	Yes
1.6217	36.3745	007	2.6	MI	25/10/1980	18:00:00	85	80	139	Yieletal1989	Polarity	Article	Yes
1.6737	36.3510	005	3.5	MI	25/10/1980	19:02:00	84	48	133	Yieletal1989	Polarity	Article	Yes
1.4198	36.2907	007	2.2	MI	25/10/1980	21:01:00	96	70	-164	Yieletal1989	Polarity	Article	Yes
1.4897	36.2567	008	2.1	MI	25/10/1980	21:53:00	62	81	153	Yieletal1989	Polarity	Article	Yes
1.4603	36.2055	007	3.1	MI	25/10/1980	23:34:00	16	54	71	Yieletal1989	Polarity	Article	Yes
1.5857	36.3138	007	2.1	MI	26/10/1980	00:26:00	329	81	6	Yieletal1989	Polarity	Article	Yes
1.6087	36.3250	004	3.2	MI	26/10/1980	02:54:00	226	63	57	Yieletal1989	Polarity	Article	Yes
1.6482	36.2442	007	3.1	MI	26/10/1980	05:54:00	269	62	120	Yieletal1989	Polarity	Article	Yes
1.5005	36.2282	004	2.6	MI	26/10/1980	13:11:00	185	52	35	Yieletal1989	Polarity	Article	Yes
1.6465	36.2607	007	2.6	MI	26/10/1980	17:24:00	236	60	63	Yieletal1989	Polarity	Article	Yes
1.6203	36.3755	006	2.6	MI	26/10/1980	22:27:00	19	80	-10	Yieletal1989	Polarity	Article	Yes
1.6957	36.3432	007	2.6	MI	26/10/1980	23:34:00	41	40	90	Yieletal1989	Polarity	Article	Yes
1.6050	36.3290	006	2.5	MI	27/10/1980	00:43:00	228	51	80	Yieletal1989	Polarity	Article	Yes
1.6367	36.3763	007	2.6	MI	27/10/1980	03:36:00	60	60	94	Yieletal1989	Polarity	Article	Yes
1.3555	36.0768	006	3.9	MI	27/10/1980	03:38:00	37	50	57	Yieletal1989	Polarity	Article	Yes
1.6863	36.2513	006	2.2	MI	27/10/1980	19:33:00	58	10	84	Yieletal1989	Polarity	Article	Yes
1.3625	36.0657	007	3.2	MI	27/10/1980	22:12:00	356	71	-159	Yieletal1989	Polarity	Article	Yes
1.7047	36.4130	007	3.6	MI	28/10/1980	00:18:00	264	80	150	Yieletal1989	Polarity	Article	Yes
1.6248	36.3268	007	2.6	MI	28/10/1980	03:26:00	20	63	39	Yieletal1989	Polarity	Article	Yes
1.5382	36.2640	006	2.0	MI	28/10/1980	03:45:00	25	50	57	Yieletal1989	Polarity	Article	Yes
1.4605	36.2142	005	2.5	MI	28/10/1980	10:07:00	316	56	73	Yieletal1989	Polarity	Article	Yes
1.6495	36.2527	008	2.4	MI	28/10/1980	10:26:00	100	70	137	Yieletal1989	Polarity	Article	Yes
1.3530	36.0790	006	3.0	MI	28/10/1980	13:07:00	21	80	-9	Ouyetal1983	Polarity	Article	Yes
1.5358	36.2373	007	2.6	MI	28/10/1980	13:30:00	239	60	85	Yieletal1989	Polarity	Article	Yes
1.6292	36.3567	006	3.0	MI	28/10/1980	20:09:00	53	86	166	Yieletal1989	Polarity	Article	Yes
1.6978	36.3465	005	3.5	MI	28/10/1980	21:44:00	255	58	115	Yieletal1989	Polarity	Article	Yes

1.4923	36.2042	006	1.9	Ml	28/10/1980	22:17:00	212	82	-92	Yieletal1989	Polarity	Article	No
1.7183	36.3363	005	4.2	Ml	29/10/1980	01:30:00	242	40	90	Yieletal1989	Polarity	Article	Yes
1.6232	36.3617	006	2.3	Ml	29/10/1980	02:01:00	152	70	-180	Yieletal1989	Polarity	Article	Yes
1.4373	36.2190	005	2.6	Ml	29/10/1980	04:45:00	193	60	63	Yieletal1989	Polarity	Article	Yes
1.6540	36.2000	006	2.2	Ml	29/10/1980	08:51:00	108	60	138	Ouyetal1983	Polarity	Article	Yes
1.5193	36.3113	009	2.3	Ml	29/10/1980	11:23:00	257	40	90	Yieletal1989	Polarity	Article	Yes
1.7000	36.2260	009	2.4	Ml	29/10/1980	12:00:00	217	71	34	Ouyetal1983	Polarity	Article	Yes
1.6722	36.3795	007	2.5	Ml	29/10/1980	20:50:00	89	72	127	Yieletal1989	Polarity	Article	Yes
1.6697	36.2787	005	2.5	Ml	29/10/1980	23:46:00	267	50	98	Yieletal1989	Polarity	Article	Yes
1.5550	36.2660	007	3.0	Ml	30/10/1980	11:30:00	248	30	142	Ouyetal1983	Polarity	Article	Yes
1.5340	36.3050	007	2.6	Ml	30/10/1980	15:40:00	59	54	95	Yieletal1989	Polarity	Article	Yes
1.6912	36.3650	004	3.7	Ml	30/10/1980	20:46:00	230	60	120	Yieletal1989	Polarity	Article	Yes
1.6912	36.3593	005	3.7	Ml	30/10/1980	23:38:00	244	50	105	Yieletal1989	Polarity	Article	Yes
1.5075	36.2213	007	3.5	Ml	31/10/1980	01:35:00	90	70	-131	Yieletal1989	Polarity	Article	Yes
1.6967	36.3467	005	3.5	Ml	31/10/1980	03:39:00	257	60	117	Yieletal1989	Polarity	Article	Yes
1.5047	36.2192	006	2.6	Ml	31/10/1980	11:23:00	356	58	-132	Yieletal1989	Polarity	Article	Yes
1.6240	36.3640	006	3.3	Ml	31/10/1980	14:41:00	150	74	1	Ouyetal1983	Polarity	Article	Yes
1.7050	36.2290	007	2.6	Ml	31/10/1980	20:02:00	118	60	124	Ouyetal1983	Polarity	Article	Yes
1.5070	36.2250	008	3.1	Ml	31/10/1980	20:51:00	254	48	56	Ouyetal1983	Polarity	Article	Yes
1.6270	36.3230	004	3.5	Ml	31/10/1980	21:00:00	235	56	59	Ouyetal1983	Polarity	Article	Yes
1.3850	36.0360	006	3.4	Ml	01/11/1980	07:45:00	355	55	-171	Ouyetal1983	Polarity	Article	Yes
1.3850	36.0370	006	2.6	Ml	01/11/1980	07:52:00	92	79	-150	Ouyetal1983	Polarity	Article	Yes
1.4000	36.1320	005	2.6	Ml	01/11/1980	10:33:00	196	60	56	Ouyetal1983	Polarity	Article	Yes
1.6330	36.3820	006	2.8	Ml	02/11/1980	03:27:00	195	47	33	Ouyetal1983	Polarity	Article	Yes
1.4650	36.2270	006	3.1	Ml	02/11/1980	05:09:00	305	66	133	Ouyetal1983	Polarity	Article	Yes
0.6300	36.3400	007	4.1	Mw	02/11/1980	05:21:00	351	84	180	EMMA	Compilation	Catalog	Yes
1.6330	36.3380	007	3.9	Ml	02/11/1980	05:21:00	351	84	0	Ouyetal1983	Polarity	Article	Yes
1.6180	36.3220	005	2.9	Ml	02/11/1980	08:53:00	249	46	169	Ouyetal1983	Polarity	Article	Yes
1.2950	36.0290	013	4.1	Ml	02/11/1980	15:56:00	57	57	131	Ouyetal1983	Polarity	Article	Yes
1.6360	36.3660	005	3.4	Ml	02/11/1980	17:51:00	199	50	29	Ouyetal1983	Polarity	Article	Yes

1.5760	36.2920	007	3.0	Ml	02/11/1980	19:25:00	82	89	-138	Ouyetal1983	Polarity	Article	Yes
1.7020	36.2230	010	3.5	Ml	03/11/1980	07:21:00	220	71	35	Ouyetal1983	Polarity	Article	Yes
1.3840	36.0680	007	3.4	Ml	03/11/1980	11:40:00	32	72	-11	Ouyetal1983	Polarity	Article	Yes
1.6600	36.3700	006	2.8	Ml	03/11/1980	20:36:00	234	48	40	Ouyetal1983	Polarity	Article	Yes
1.6350	36.2450	005	3.7	Ml	04/11/1980	09:16:00	229	47	43	Ouyetal1983	Polarity	Article	Yes
1.4500	36.1440	007	3.3	Ml	04/11/1980	16:29:00	303	70	174	Ouyetal1983	Polarity	Article	Yes
1.4580	36.1230	008	3.1	Ml	04/11/1980	17:40:00	285	62	156	Ouyetal1983	Polarity	Article	Yes
1.3840	36.1210	009	2.9	Ml	04/11/1980	17:50:00	206	54	37	Ouyetal1983	Polarity	Article	Yes
1.4960	36.2070	005	2.1	Ml	05/11/1980	03:00:00	291	54	148	Ouyetal1983	Polarity	Article	Yes
1.6320	36.3410	007	2.8	Ml	05/11/1980	12:32:00	84	87	6	Ouyetal1983	Polarity	Article	Yes
1.3950	36.0850	009	2.6	Ml	05/11/1980	20:17:00	356	64	-169	Ouyetal1983	Polarity	Article	Yes
1.6680	36.2530	005	2.4	Ml	06/11/1980	03:18:00	249	71	111	Ouyetal1983	Polarity	Article	Yes
1.6140	36.3650	005	2.9	Ml	06/11/1980	17:21:00	158	63	1	Ouyetal1983	Polarity	Article	Yes
1.3820	36.0710	008	3.1	Ml	06/11/1980	19:59:00	250	62	95	Ouyetal1983	Polarity	Article	Yes
1.4540	36.1660	006	3.6	Ml	06/11/1980	22:47:00	87	65	107	Ouyetal1983	Polarity	Article	Yes
1.5630	36.3170	006	3.0	Ml	07/11/1980	15:00:00	253	50	-152	Ouyetal1983	Polarity	Article	Yes
1.6650	36.3630	006	3.1	Ml	07/11/1980	17:47:00	334	70	-43	Ouyetal1983	Polarity	Article	Yes
1.6960	36.3160	006	3.2	Ml	07/11/1980	23:45:00	74	22	141	Ouyetal1983	Polarity	Article	Yes
1.6185	36.3550	004	2.3	Ml	08/11/1980	00:01:00	214	60	63	Yieletal1989	Polarity	Article	Yes
1.6333	36.4583	005	3.2	Ml	08/11/1980	04:16:00	191	70	-34	Yieletal1989	Polarity	Article	Yes
1.5033	36.2107	006	3.1	Ml	08/11/1980	04:40:00	231	45	111	Yieletal1989	Polarity	Article	Yes
1.4470	36.2000	005	5.3	Mw	08/11/1980	07:54:20	270	45	126	CMT	Moment tensor inversion	Catalog	Yes
1.6942	36.3702	006	3.2	Ml	08/11/1980	10:24:00	231	53	110	Yieletal1989	Polarity	Article	Yes
1.6897	36.4233	007	2.9	Ml	08/11/1980	19:09:00	270	90	0	Yieletal1989	Polarity	Article	Yes
1.3942	36.1387	006	3.0	Ml	08/11/1980	21:15:00	251	61	119	Yieletal1989	Polarity	Article	Yes
1.6280	36.3105	005	2.1	Ml	09/11/1980	02:03:00	268	50	78	Yieletal1989	Polarity	Article	Yes
1.4053	36.1300	007	3.1	Ml	09/11/1980	10:50:00	247	64	123	Yieletal1989	Polarity	Article	Yes
1.6247	36.3843	007	2.5	Ml	10/11/1980	00:30:00	65	45	83	Yieletal1989	Polarity	Article	Yes
1.6177	36.3678	005	2.4	Ml	10/11/1980	01:06:00	79	69	173	Yieletal1989	Polarity	Article	Yes
1.5400	36.2503	007	2.2	Ml	10/11/1980	02:29:00	264	51	126	Yieletal1989	Polarity	Article	Yes

1.6357	36.3680	008	3.2	MI	10/11/1980	02:47:00	63	50	82	Yieletal1989	Polarity	Article	Yes
1.5830	36.4430	007	3.4	MI	10/11/1980	03:35:00	285	86	171	Yieletal1989	Polarity	Article	Yes
1.3910	36.1270	006	2.8	MI	10/11/1980	06:36:00	211	58	61	Ouyetal1983	Polarity	Article	Yes
1.6330	36.3610	007	3.1	MI	10/11/1980	07:22:00	354	74	31	Yieletal1989	Polarity	Article	Yes
1.5140	36.2290	007	3.2	MI	10/11/1980	07:24:00	223	52	42	Ouyetal1983	Polarity	Article	Yes
1.4968	36.2277	005	2.7	MI	10/11/1980	08:20:00	187	70	30	Yieletal1989	Polarity	Article	Yes
1.6397	36.3763	007	3.2	MI	10/11/1980	09:02:00	92	67	163	Yieletal1989	Polarity	Article	Yes
1.3500	36.0150	008	3.3	MI	10/11/1980	10:43:00	97	84	-169	Ouyetal1983	Polarity	Article	Yes
1.4017	36.1288	006	3.2	MI	10/11/1980	14:40:00	235	50	71	Yieletal1989	Polarity	Article	Yes
1.6270	36.4547	006	2.4	MI	10/11/1980	17:18:00	16	80	30	Yieletal1989	Polarity	Article	Yes
1.3903	36.1240	006	3.5	MI	10/11/1980	21:08:00	193	51	56	Yieletal1989	Polarity	Article	Yes
1.6378	36.3160	005	3.5	MI	10/11/1980	22:28:00	237	70	87	Yieletal1989	Polarity	Article	Yes
1.5303	36.2403	005	2.8	MI	11/11/1980	08:23:00	226	45	90	Yieletal1989	Polarity	Article	Yes
1.6425	36.3157	007	2.0	MI	11/11/1980	08:34:00	291	68	111	Yieletal1989	Polarity	Article	Yes
1.6162	36.3358	006	2.5	MI	11/11/1980	12:40:00	99	60	109	Yieletal1989	Polarity	Article	Yes
1.4350	36.1570	008	3.6	MI	11/11/1980	20:32:00	28	67	46	Ouyetal1983	Polarity	Article	Yes
1.6782	36.3438	007	2.5	MI	12/11/1980	03:44:00	71	49	94	Yieletal1989	Polarity	Article	Yes
1.5003	36.2835	008	2.5	MI	12/11/1980	08:30:00	35	51	65	Yieletal1989	Polarity	Article	Yes
1.4135	36.1537	006	2.4	MI	12/11/1980	22:34:00	219	48	84	Yieletal1989	Polarity	Article	Yes
1.5575	36.2697	005	2.4	MI	12/11/1980	23:16:00	198	69	32	Yieletal1989	Polarity	Article	Yes
-11.7000	39.3000	015	4.0	MI	13/11/1980	00:00:00	358	54	-11	Boretal2001	Polarity	Article	Yes
1.6793	36.3598	004	2.3	MI	13/11/1980	00:21:00	268	59	97	Yieletal1989	Polarity	Article	Yes
1.6243	36.3358	008	2.4	MI	13/11/1980	08:59:00	53	50	57	Yieletal1989	Polarity	Article	Yes
1.5157	36.2112	005	2.2	MI	13/11/1980	15:49:00	302	30	-90	Yieletal1989	Polarity	Article	Yes
1.7167	36.2262	007	3.1	MI	13/11/1980	23:52:00	259	61	84	Yieletal1989	Polarity	Article	Yes
1.5588	36.3472	007	2.1	MI	14/11/1980	00:10:00	55	70	76	Yieletal1989	Polarity	Article	Yes
1.6250	36.2280	006	2.1	MI	14/11/1980	02:01:00	104	51	137	Ouyetal1983	Polarity	Article	Yes
1.4310	36.1463	007	2.3	MI	14/11/1980	07:33:00	310	81	-171	Yieletal1989	Polarity	Article	Yes
1.6835	36.3612	005	3.4	MI	14/11/1980	08:34:00	261	61	116	Yieletal1989	Polarity	Article	Yes
1.7258	36.2288	005	2.8	MI	14/11/1980	09:45:00	234	88	80	Yieletal1989	Polarity	Article	Yes

1.6373	36.2702	007	2.4	Ml	14/11/1980	14:38:00	58	35	90	Yieletal1989	Polarity	Article	Yes
1.4890	36.2350	010	2.5	Ml	14/11/1980	19:14:00	89	25	131	Ouyetal1983	Polarity	Article	Yes
1.6735	36.2233	006	3.6	Ml	15/11/1980	00:12:00	222	78	46	Yieletal1989	Polarity	Article	Yes
1.4900	36.2100	006	3.5	Mw	15/11/1980	00:43:00	58	50	26	EMMA	Compilation	Catalog	Yes
1.4885	36.2082	006	2.7	Ml	15/11/1980	05:43:00	317	80	140	Yieletal1989	Polarity	Article	Yes
1.6967	36.2440	008	2.9	Ml	15/11/1980	06:58:00	254	39	88	Yieletal1989	Polarity	Article	Yes
1.5500	36.2280	007	2.4	Ml	16/11/1980	04:07:00	237	58	121	Ouyetal1983	Polarity	Article	Yes
-5.6700	36.9200	027	4.3	MbLg	03/12/1980	22:16:27	114	68	32	CandB1994	Polarity	Article	Yes
1.3830	35.9750	005	5.3	Mw	05/12/1980	13:32:06	112	61	-179	CMT	Moment tensor inversion	Catalog	Yes
0.9000	36.0000	010	5.8	M	07/12/1980	17:37:10	277	40	140	Buetal2016	Compilation	Article	Yes
1.2520	35.9580	005	5.6	Mw	07/12/1980	17:37:10	277	40	140	CMT	Moment tensor inversion	Catalog	Yes
-5.8000	34.8500	001	3.8	M	02/01/1981	21:58:39	134	60	5	MedandChe1992	Polarity	Article	Yes
1.6520	36.4380	011	5.0	Mw	15/01/1981	04:25:17	181	53	29	CMT	Moment tensor inversion	Catalog	Yes
-4.7100	36.8500	005	4.0	MbLg	21/01/1981	20:38:39	33	53	44	CandB1994	Polarity	Article	Yes
1.7650	36.4500	011	5.6	Mw	01/02/1981	13:20:00	210	43	64	CMT	Moment tensor inversion	Catalog	Yes
1.3330	35.9630	026	5.2	Mw	14/02/1981	13:15:18	26	67	-18	CMT	Moment tensor inversion	Catalog	Yes
0.2100	38.4900	001	4.9	mbLg	05/03/1981	01:21:52	18	63	-46	PS1998	Polarity	Article	Yes
-3.9000	35.1300	005	4.0	M	20/03/1981	14:08:00	164	89	133	Bezzetal2012	Compilation	Article	Yes
-3.9800	35.1200	005	4.0	Mw	07/04/1981	00:00:00	83	59	162	EMMA	Compilation	Catalog	Yes
-0.4300	35.8900	016	4.2	MbLg	19/04/1981	19:29:36	198	57	-16	CandB1994	Polarity	Article	Yes
1.9500	42.9000	004	4.5	Ml	23/04/1981	00:00:00	176	70	174	Rigo2015	Compilation	Article	Yes
0.0700	43.0900	006	4.6	mbLg	19/07/1981	19:58:00	220	74	180	PS1998	Polarity	Article	Yes
-0.0300	43.1700	013	4.3	mbLg	28/09/1981	01:41:00	211	32	17	PS1998	Polarity	Article	Yes
-0.9800	43.2100	015	5.0	Ml	06/01/1982	16:32:50	210	81	-60	Rigo2015	Compilation	Article	Yes
-2.7500	40.6400	007	4.1	mbLg	23/02/1982	17:59:15	210	36	56	PS1998	Polarity	Article	Yes
-1.6900	42.8100	001	4.4	Ml	22/05/1982	00:00:00	70	60	-125	Rigo2015	Compilation	Article	Yes
-1.8100	42.8600	000	4.4	mbLg	22/06/1982	19:50:23	115	45	-173	PS1998	Polarity	Article	Yes
-0.2800	43.0700	008	4.3	mbLg	25/08/1982	20:59:00	0	27	-22	PS1998	Polarity	Article	Yes
-0.4200	43.0900	008	1.7	Ml	23/10/1982	00:00:00	277	73	-85	Rigo2015	Compilation	Article	No
-0.6100	43.0800	008	2.1	Ml	24/10/1982	00:00:00	63	82	54	Rigo2015	Compilation	Article	Yes

-0.3700	43.0700	005	2.0	Ml	30/10/1982	00:00:00	340	80	-53	Rigo2015	Compilation	Article	Yes
-0.5100	42.9200	004	2.1	Ml	31/10/1982	00:00:00	290	80	-27	Rigo2015	Compilation	Article	Yes
-0.8200	43.0800	013	1.9	Ml	01/11/1982	00:00:00	306	80	-123	Rigo2015	Compilation	Article	No
-0.7500	43.1500	015	1.5	Ml	03/11/1982	00:00:00	348	65	90	Rigo2015	Compilation	Article	No
-0.9700	43.1400	016	2.1	Ml	05/11/1982	00:00:00	171	83	52	Rigo2015	Compilation	Article	Yes
-0.3400	43.0500	004	2.1	Ml	11/11/1982	00:00:00	343	75	-29	Rigo2015	Compilation	Article	Yes
-0.6000	43.1000	005	1.6	Ml	15/11/1982	00:00:00	205	80	99	Rigo2015	Compilation	Article	No
1.4350	35.6770	007	5.2	Mw	15/11/1982	20:07:49	274	70	-169	CMT	Moment tensor inversion	Catalog	Yes
-1.2200	43.1700	004	1.8	Ml	22/11/1982	00:00:00	166	50	113	Rigo2015	Compilation	Article	No
-0.4500	43.1100	014	1.8	Ml	03/12/1982	00:00:00	124	53	-72	Rigo2015	Compilation	Article	No
-0.2400	43.1000	015	1.7	Ml	15/12/1982	00:00:00	121	70	-94	Rigo2015	Compilation	Article	No
0.5000	42.5500	005	4.0	Ml	24/12/1982	00:00:00	126	73	51	Rigo2015	Compilation	Article	Yes
-2.1500	36.4900	012	4.7	MbLg	06/01/1983	21:55:55	66	78	33	CandB1994	Polarity	Article	Yes
-2.2000	36.5500	006	4.4	MbLg	20/03/1983	06:59:13	266	62	-18	CandB1994	Polarity	Article	Yes
-0.4200	43.1100	007	4.0	Ml	06/06/1983	00:00:00	221	29	61	Rigo2015	Compilation	Article	Yes
2.2300	42.4300	004	3.9	Ml	20/07/1983	00:00:00	216	43	110	Rigo2015	Compilation	Article	Yes
-4.0000	37.0000	000	3.7	Mw	09/10/1983	00:00:00	270	46	-90	EMMA	Compilation	Catalog	Yes
-11.5000	43.2000	000	4.6	M	09/11/1983	00:00:00	136	48	-174	Galetal1993	Compilation	Article	Yes
-4.4900	34.7400	027	4.6	M	24/11/1983	20:55:32	272	74	157	MedandChe1992	Polarity	Article	Yes
0.1700	43.0200	012	4.5	Ml	23/02/1984	00:00:00	105	68	144	Rigo2015	Compilation	Article	Yes
-1.1200	43.2100	011	4.8	mbLg	25/02/1984	02:03:18	80	57	-18	PS1998	Polarity	Article	Yes
-3.7000	37.1200	006	5.0	Mw	24/06/1984	14:30:52	166	27	-79	Setal2003a	Moment tensor inversion	Article	Yes
-4.0000	36.8000	000	3.6	Mw	21/07/1984	00:00:00	280	28	33	EMMA	Compilation	Catalog	Yes
-4.1320	37.0450	039	3.2	m	06/08/1984	15:02:39	184	32	-163	V1986	Polarity	Article	Yes
-3.3400	36.8500	011	2.8	mb	26/08/1984	15:59:10	41	77	-134	Metal2006	Polarity	Article	Yes
-4.0000	36.7900	005	3.5	mb	31/08/1984	07:16:35	135	42	0	Balanetal2012	Polarity	Article	Yes
-2.3400	36.9800	009	5.0	mbLg	13/09/1984	04:34:10	275	47	51	PS1998	Polarity	Article	Yes
2.1700	42.1500	005	4.4	Ml	26/09/1984	00:00:00	344	75	180	Rigo2015	Compilation	Article	Yes
-4.2600	37.0500	011	3.0	mb	17/10/1984	13:45:26	69	41	75	Balanetal2012	Polarity	Article	Yes
-3.1000	36.1000	000	3.9	Mw	24/01/1985	00:00:00	312	28	-120	EMMA	Compilation	Catalog	Yes

0.2200	43.0400	010	4.1	Ml	08/02/1985	00:00:00	70	20	90	Rigo2015	Compilation	Article	Yes
-4.2100	37.1600	008	2.7	mb	12/02/1985	20:51:00	166	53	71	Balanetal2012	Polarity	Article	Yes
-4.2000	37.1500	005	2.8	mb	13/02/1985	22:39:58	3	30	7	Balanetal2012	Polarity	Article	Yes
-4.2000	37.1000	000	4.1	Mw	13/02/1985	23:38:02	306	22	-69	EMMA	Compilation	Catalog	Yes
-4.2000	37.1000	000	3.6	Mw	14/02/1985	01:01:42	338	16	-54	EMMA	Compilation	Catalog	Yes
-4.1500	37.1300	001	2.5	mb	14/02/1985	05:09:26	92	42	-53	Balanetal2012	Polarity	Article	Yes
-4.1500	37.1400	011	2.5	mb	15/02/1985	02:28:25	305	61	-7	Balanetal2012	Polarity	Article	Yes
-4.2000	37.1000	000	3.7	Mw	15/02/1985	07:34:54	115	44	-101	EMMA	Compilation	Catalog	Yes
-4.2500	37.1500	010	2.6	mb	15/02/1985	17:55:28	293	53	-65	Balanetal2012	Polarity	Article	Yes
-4.2000	37.1000	000	3.5	Mw	16/02/1985	02:36:41	297	51	-38	EMMA	Compilation	Catalog	Yes
-4.2200	37.1600	007	2.9	mb	17/02/1985	10:09:13	10	33	-23	Balanetal2012	Polarity	Article	Yes
-4.2100	37.1300	004	2.8	mb	21/02/1985	14:13:12	148	40	90	Balanetal2012	Polarity	Article	Yes
-4.2000	37.1000	000	3.8	Mw	23/02/1985	18:01:55	68	73	-120	EMMA	Compilation	Catalog	Yes
-4.2000	37.1000	000	3.6	Mw	25/02/1985	00:00:00	145	46	-99	EMMA	Compilation	Catalog	Yes
1.4000	35.6000	000	5.0	Mw	05/03/1985	15:37:00	225	54	83	MandR2006	Compilation	Article	Yes
-3.7000	37.2000	000	3.5	Mw	15/03/1985	00:00:00	266	6	68	EMMA	Compilation	Catalog	Yes
-3.7000	37.2000	000	3.5	Mw	07/04/1985	00:00:00	259	62	-113	EMMA	Compilation	Catalog	Yes
-2.8800	38.4300	005	4.2	MbLg	10/04/1985	00:36:01	298	67	-3	CandB1994	Polarity	Article	Yes
-4.7000	36.5000	000	3.8	Mw	08/05/1985	00:00:00	177	23	-124	EMMA	Compilation	Catalog	Yes
-3.7000	37.2000	000	2.7	M	24/05/1985	00:00:00	225	45	-111	V1986	Polarity	Article	Yes
-4.6400	37.7900	005	5.1	mbLg	26/05/1985	18:05:10	20	48	119	PS1998	Polarity	Article	Yes
-4.6400	37.7900	005	4.5	MbLg	26/05/1985	19:07:44	342	55	-110	CandB1994	Polarity	Article	Yes
-4.6000	37.7000	000	3.8	Mw	27/05/1985	00:00:00	108	44	-107	EMMA	Compilation	Catalog	Yes
-4.0000	37.1000	000	3.5	Mw	02/06/1985	00:00:00	286	89	107	EMMA	Compilation	Catalog	Yes
-4.4000	37.4000	000	3.8	Mw	16/06/1985	00:00:00	264	64	113	EMMA	Compilation	Catalog	Yes
-3.8000	37.0000	000	3.9	Mw	07/07/1985	00:00:00	213	11	-103	EMMA	Compilation	Catalog	Yes
-4.0200	36.8400	005	2.5	mb	10/07/1985	19:31:59	71	62	-12	Balanetal2012	Polarity	Article	Yes
-4.7000	37.8000	000	3.9	Mw	23/07/1985	00:00:00	32	22	153	EMMA	Compilation	Catalog	Yes
-3.6000	37.0000	000	3.5	Mw	01/08/1985	00:00:00	28	9	55	EMMA	Compilation	Catalog	Yes
-4.2000	36.8000	000	3.7	Mw	31/08/1985	00:00:00	311	63	83	EMMA	Compilation	Catalog	Yes

-3.7000	37.3000	000	3.4	Mw	08/09/1985	00:00:00	288	56	87	EMMA	Compilation	Catalog	Yes
-3.6500	37.3800	007	3.5	mbLg	14/09/1985	04:25:01	175	62	-80	PS1998	Polarity	Article	Yes
-3.8200	37.0200	005	3.0	mbLg	16/09/1985	22:25:09	239	40	-53	PS1998	Polarity	Article	Yes
-0.4400	43.0300	006	3.8	mbLg	30/09/1985	02:28:00	110	83	71	PS1998	Polarity	Article	Yes
1.3800	42.9300	013	3.8	Ml	02/10/1985	00:00:00	310	20	46	Rigo2015	Compilation	Article	Yes
-4.2200	37.0400	015	3.2	mb	02/10/1985	08:03:36	59	53	65	Balanetal2012	Polarity	Article	Yes
-5.0800	37.0200	020	3.7	mb	14/11/1985	22:21:23	241	16	76	Balanetal2012	Polarity	Article	Yes
-3.4000	37.7000	000	3.6	Mw	18/11/1985	00:00:00	137	25	-108	EMMA	Compilation	Catalog	Yes
-4.2000	36.7000	000	3.9	Mw	19/11/1985	00:00:00	330	63	-76	EMMA	Compilation	Catalog	Yes
-1.5760	38.5340	020	3.0	M	25/11/1985	20:56:00	179	49	34	RPandDV2001	Polarity	Article	Yes
-4.0100	37.0400	013	2.8	mb	09/12/1985	00:54:25	71	76	27	Balanetal2012	Polarity	Article	Yes
-4.3900	36.2200	020	4.1	mb	31/12/1985	04:20:46	180	41	-27	Balanetal2012	Polarity	Article	Yes
-4.1290	37.2230	031	3.7	m	13/01/1986	03:15:25	270	70	0	V1986	Polarity	Article	Yes
-3.7000	37.0500	003	3.3	mb	18/01/1986	06:47:48	138	13	119	Metal2006	Polarity	Article	Yes
-5.4280	32.1230	005	4.9	Mw	28/01/1986	20:01:29	212	42	16	CMT	Moment tensor inversion	Catalog	Yes
-3.0300	36.8700	010	2.5	mb	06/04/1986	15:20:39	313	45	108	Metal2006	Polarity	Article	Yes
-0.5100	43.0900	010	3.9	mbLg	19/04/1986	09:01:00	220	78	-140	PS1998	Polarity	Article	Yes
-3.7200	37.2200	005	4.0	mbLg	26/04/1986	00:12:01	170	57	79	PS1998	Polarity	Article	Yes
-4.2700	36.9700	007	2.8	mb	08/05/1986	21:04:34	16	53	65	Balanetal2012	Polarity	Article	Yes
-4.4000	38.1000	005	3.2	mbLg	08/05/1986	23:10:36	160	40	137	PS1998	Polarity	Article	Yes
-4.4830	36.6000	090	4.3	M	13/05/1986	00:19:00	335	36	-28	Buetal1997	Polarity	Article	No
-2.7300	39.2300	005	3.6	mbLg	13/05/1986	18:38:43	318	67	-165	PS1998	Polarity	Article	Yes
-2.6700	39.2300	005	3.0	mbLg	13/05/1986	20:24:19	50	79	-74	PS1998	Polarity	Article	Yes
-1.4500	39.7900	011	3.3	mbLg	14/05/1986	23:55:06	145	78	-13	PS1998	Polarity	Article	Yes
-4.1640	37.0770	008	3.9	m	30/05/1986	01:22:26	184	58	-66	V1986	Polarity	Article	Yes
-4.2600	37.0900	005	3.7	mbLg	30/05/1986	11:22:26	305	48	-129	PS1998	Polarity	Article	Yes
-3.7000	37.2000	000	3.8	Mw	05/06/1986	00:00:00	26	20	9	EMMA	Compilation	Catalog	Yes
-2.3180	38.7030	029	3.4	M	09/06/1986	23:05:00	245	81	-150	RPandDV2001	Polarity	Article	Yes
-1.4440	38.1120	007	3.5	M	21/06/1986	04:58:00	190	45	148	RPandDV2001	Polarity	Article	Yes
-2.0460	38.5220	009	3.1	M	21/06/1986	11:27:00	300	25	90	RPandDV2001	Polarity	Article	Yes

-3.6000	37.0100	011	2.6	mb	03/07/1986	06:24:32	279	57	114	Metal2006	Polarity	Article	Yes
-0.2400	38.7700	011	3.4	mbLg	05/07/1986	16:35:05	174	19	31	PS1998	Polarity	Article	Yes
-4.1200	37.0600	008	4.1	mb	17/07/1986	15:57:06	66	63	-62	Balanetal2012	Polarity	Article	Yes
-4.1600	37.0700	008	3.2	mb	18/07/1986	17:19:32	295	48	-38	Balanetal2012	Polarity	Article	Yes
-4.1400	37.0900	009	3.1	mb	19/07/1986	11:22:35	300	51	-77	Balanetal2012	Polarity	Article	Yes
-4.1400	37.0800	009	2.7	mb	20/07/1986	12:55:06	239	42	-90	Balanetal2012	Polarity	Article	Yes
-5.6600	37.0700	010	3.6	mb	04/08/1986	23:18:41	94	45	-86	Balanetal2012	Polarity	Article	Yes
-4.2000	37.0800	010	3.0	mb	13/08/1986	02:54:04	216	49	46	Balanetal2012	Polarity	Article	Yes
-3.2200	37.0700	009	3.0	mbLg	16/08/1986	18:10:40	250	42	-48	PS1998	Polarity	Article	Yes
-4.0700	37.1500	015	3.4	mb	29/08/1986	15:48:10	194	33	42	Balanetal2012	Polarity	Article	Yes
-4.0700	37.1500	011	2.2	mb	29/08/1986	16:00:02	93	90	30	Balanetal2012	Polarity	Article	Yes
-8.7500	36.8570	060	4.3	M	25/09/1986	06:31:50	7	70	-9	M1991	Compilation	Article	No
-3.6100	36.9900	013	3.0	mb	25/09/1986	14:40:29	15	66	137	Metal2006	Polarity	Article	Yes
-9.2800	37.0500	053	4.0	Mw	12/10/1986	00:00:00	181	59	91	EMMA	Compilation	Catalog	No
-4.1600	37.0900	009	4.3	mb	20/10/1986	03:03:23	325	53	-65	Balanetal2012	Polarity	Article	Yes
-8.7600	36.7800	030	4.9	Mw	20/10/1986	14:48:19	255	61	97	Setal2003a	Moment tensor inversion	Article	Yes
-1.3000	39.8400	005	3.2	mbLg	28/10/1986	06:48:09	287	53	-162	PS1998	Polarity	Article	Yes
-4.2300	37.0600	010	2.9	mb	04/11/1986	03:21:29	267	76	-27	Balanetal2012	Polarity	Article	Yes
-2.9700	36.8200	017	3.6	mb	05/11/1986	07:02:48	286	88	58	Metal2006	Polarity	Article	Yes
-0.6700	43.1600	008	3.6	Ml	03/12/1986	00:00:00	240	50	-151	Rigo2015	Compilation	Article	Yes
-1.2440	38.2310	015	3.7	M	19/12/1986	10:00:00	115	35	111	RPandDV2001	Polarity	Article	Yes
-3.6000	36.8300	008	2.6	mb	20/12/1986	14:28:29	106	84	-151	Metal2006	Polarity	Article	Yes
-3.6400	36.8400	009	2.6	mb	20/12/1986	14:46:12	122	84	-151	Metal2006	Polarity	Article	Yes
-3.6200	36.9700	015	2.2	mb	10/01/1987	00:42:47	33	75	143	Metal2006	Polarity	Article	Yes
1.3800	35.9100	010	5.1	Mw	26/01/1987	11:11:00	69	47	129	EMMA	Compilation	Catalog	Yes
-0.6500	43.1400	002	3.9	Ml	03/03/1987	00:00:00	222	74	38	Rigo2015	Compilation	Article	Yes
-3.4000	37.7300	006	4.3	mbLg	11/03/1987	00:36:40	235	48	119	PS1998	Polarity	Article	Yes
-3.6400	37.0300	012	2.0	mb	12/03/1987	17:45:39	242	43	-168	Metal2006	Polarity	Article	Yes
-4.1000	36.8500	060	3.5	mb	27/03/1987	09:38:00	231	16	64	MandR1997	Polarity	Article	No
0.1600	43.0500	013	3.6	Ml	13/04/1987	00:00:00	270	85	93	Rigo2015	Compilation	Article	Yes

-3.6100	36.8200	008	3.0	mb	15/05/1987	15:55:45	307	81	-31	Metal2006	Polarity	Article	Yes
-0.3800	43.1300	004	3.8	mbLg	26/05/1987	16:32:00	180	88	-71	PS1998	Polarity	Article	Yes
-8.0220	38.5450	008	4.4	M	04/06/1987	03:28:42	263	81	-160	M1991	Compilation	Article	Yes
-4.1200	36.9700	005	3.4	mb	05/06/1987	01:13:44	8	40	-61	Balanetal2012	Polarity	Article	Yes
-0.4100	43.0800	003	3.9	mbLg	26/06/1987	17:13:00	261	11	-114	PS1998	Polarity	Article	Yes
-5.1900	37.1000	008	3.7	mb	01/07/1987	21:48:05	274	82	-57	Balanetal2012	Polarity	Article	Yes
-7.9000	38.7000	000	4.4	Mw	04/07/1987	00:00:00	265	85	-160	EMMA	Compilation	Catalog	Yes
-1.0000	40.9500	005	3.4	mbLg	06/07/1987	04:32:25	3	73	-38	PS1998	Polarity	Article	Yes
-3.5400	36.9000	007	2.7	mb	20/07/1987	12:01:37	60	81	120	Metal2006	Polarity	Article	Yes
-5.9800	35.1200	069	3.9	mb	23/07/1987	11:57:00	226	20	-34	MandR1997	Polarity	Article	No
-9.1000	39.1600	005	4.0	Mw	05/08/1987	00:00:00	103	52	-130	EMMA	Compilation	Catalog	Yes
-5.1000	36.3100	001	3.4	mb	09/08/1987	01:14:22	247	68	-51	Balanetal2012	Polarity	Article	Yes
-4.0700	37.0100	010	3.0	mb	22/08/1987	21:58:54	234	76	4	Balanetal2012	Polarity	Article	Yes
1.5700	40.9300	008	4.2	mbLg	24/08/1987	18:43:00	254	45	-174	PS1998	Polarity	Article	Yes
-3.7000	37.0400	005	3.4	mb	10/09/1987	00:16:20	303	54	36	Metal2006	Polarity	Article	Yes
-1.7530	38.2910	006	3.0	M	14/09/1987	02:04:00	60	55	-64	RPandDV2001	Polarity	Article	Yes
-4.6900	37.1000	031	3.1	mb	25/09/1987	19:17:48	271	59	84	Balanetal2012	Polarity	Article	Yes
-3.2400	40.2600	005	3.2	mbLg	19/10/1987	12:54:42	45	55	-72	PS1998	Polarity	Article	Yes
-0.7600	42.9100	003	3.9	Ml	05/11/1987	00:00:00	14	65	-79	Rigo2015	Compilation	Article	Yes
-3.7000	43.0400	016	3.9	mbLg	07/11/1987	11:07:51	275	60	63	PS1998	Polarity	Article	Yes
-0.1800	43.0700	008	4.1	mbLg	11/11/1987	07:15:00	306	15	84	PS1998	Polarity	Article	Yes
-0.1700	43.1700	000	3.8	mbLg	12/11/1987	01:33:13	70	70	28	PS1998	Polarity	Article	Yes
-3.8800	35.4200	010	4.3	mb	09/12/1987	15:40:00	54	50	-58	MandR1997	Polarity	Article	Yes
-0.6100	43.4300	011	3.9	mbLg	15/12/1987	07:35:00	205	75	-74	PS1998	Polarity	Article	Yes
1.4300	42.3600	016	3.8	Ml	20/02/1988	00:00:00	312	51	-13	Rigo2015	Compilation	Article	Yes
2.2000	42.3400	008	3.8	Ml	16/03/1988	00:00:00	192	85	22	Rigo2015	Compilation	Article	Yes
-2.1000	37.1400	001	3.1	mbLg	20/03/1988	19:44:47	209	11	69	PS1998	Polarity	Article	Yes
-9.7000	31.3000	000	4.6	Mw	09/04/1988	00:00:00	230	84	-11	EMMA	Compilation	Catalog	Yes
-3.6080	37.1830	015	3.2	md	02/05/1988	10:51:00	67	90	90	Galetal1999	Polarity	Article	Yes
-1.0400	39.5400	002	3.2	mbLg	19/05/1988	21:16:30	306	73	-152	PS1998	Polarity	Article	Yes

-9.1600	38.9600	020	4.0	Mw	22/05/1988	00:00:00	285	38	-160	EMMA	Compilation	Catalog	Yes
-4.6020	36.4230	100	3.5	MbLg	30/05/1988	10:44:06	166	55	178	Serr1999	Polarity	Article	No
-5.4200	36.2100	008	4.1	Mw	08/07/1988	23:31:11	178	61	-159	Setal2003a	Moment tensor inversion	Article	Yes
-3.9650	36.9580	028	3.7	md	18/07/1988	20:32:00	248	70	90	Galetal1999	Polarity	Article	Yes
-3.8210	37.0890	011	2.9	md	25/07/1988	01:23:00	12	45	-101	Galetal1999	Polarity	Article	Yes
-7.1700	36.5500	028	4.5	Mw	25/07/1988	20:03:04	200	70	-7	Setal2003a	Moment tensor inversion	Article	Yes
-4.0600	37.0300	017	2.2	mb	04/08/1988	20:40:10	6	52	59	Balanetal2012	Polarity	Article	Yes
-3.7670	37.2070	002	3.9	MbLg	20/08/1988	13:03:03	135	90	90	Serretal1996	Polarity	Article	Yes
-3.7010	37.1810	017	3.9	M	20/08/1988	16:42:00	150	40	7	RPandDV2001	Polarity	Article	Yes
-4.4100	36.3520	090	3.0	MbLg	10/09/1988	10:27:13	197	56	-121	Serr1999	Polarity	Article	No
-3.7370	36.9900	011	2.7	md	15/09/1988	00:27:00	66	90	90	Galetal1999	Polarity	Article	Yes
-3.7370	36.9900	011	2.7	mb	15/09/1988	00:27:00	66	90	90	Serr1999	Polarity	Article	Yes
-3.5400	40.1000	002	3.0	M	28/09/1988	00:43:51	251	64	-45	Perezetal2022	Compilation	Article	Yes
-3.5400	40.1000	002	3.0	mbLg	28/09/1988	12:43:51	251	64	-46	PS1998	Polarity	Article	Yes
-3.5600	40.0800	002	3.1	M	04/10/1988	00:05:11	248	44	102	Perezetal2022	Compilation	Article	Yes
-3.5600	40.0800	002	3.1	mbLg	04/10/1988	13:05:11	248	44	102	PS1998	Polarity	Article	Yes
-4.4400	36.7700	003	2.4	mb	04/10/1988	13:20:57	217	11	68	Balanetal2012	Polarity	Article	Yes
-3.9900	35.4700	011	4.0	mb	05/10/1988	00:41:00	247	26	-58	MandR1997	Polarity	Article	Yes
-3.8600	35.5100	008	4.4	Mw	05/10/1988	00:42:11	137	59	-173	Setal2003a	Moment tensor inversion	Article	Yes
-4.5200	36.8400	002	2.3	mb	10/10/1988	13:37:51	251	37	77	Balanetal2012	Polarity	Article	Yes
-3.5800	40.0700	002	3.1	M	11/10/1988	00:15:29	219	29	82	Perezetal2022	Compilation	Article	Yes
-3.5800	40.0700	002	3.1	mbLg	11/10/1988	14:15:29	219	29	82	PS1998	Polarity	Article	Yes
-3.8950	37.0220	014	2.7	md	21/10/1988	12:05:00	163	65	-104	Galetal1999	Polarity	Article	Yes
-3.8470	37.0230	015	2.2	mb	22/10/1988	16:13:00	293	65	-90	Serr1999	Polarity	Article	Yes
-3.2400	40.0700	009	3.4	mbLg	24/10/1988	04:38:52	24	39	47	PS1998	Polarity	Article	Yes
2.4400	36.7800	006	5.2	Mw	29/10/1988	19:09:00	85	83	172	EMMA	Compilation	Catalog	Yes
2.7600	36.4400	006	5.8	Mw	31/10/1988	10:12:58	261	80	102	Setal2003a	Moment tensor inversion	Article	Yes
-3.8180	37.0420	010	2.6	mb	14/11/1988	11:20:00	135	70	-55	Serr1999	Polarity	Article	Yes
-4.2200	37.1700	012	2.1	mb	21/11/1988	07:09:31	227	22	26	Balanetal2012	Polarity	Article	Yes
-4.5660	36.3000	100	3.5	M	28/11/1988	19:54:29	205	5	-157	Buetal1997	Polarity	Article	No

-4.3380	36.8380	067	3.2	MbLg	01/12/1988	05:35:35	15	45	141	Serr1999	Polarity	Article	No
-3.6000	36.9500	009	2.7	mb	01/12/1988	16:13:53	196	76	-176	Metal2006	Polarity	Article	Yes
-4.1700	37.1300	005	2.7	mb	03/12/1988	02:40:59	340	36	31	Balanetal2012	Polarity	Article	Yes
-3.8350	37.0310	014	4.0	md	05/12/1988	20:12:00	100	58	127	Galetal1999	Polarity	Article	Yes
-3.8480	37.0240	013	3.2	md	06/12/1988	06:09:00	120	25	-95	Galetal1999	Polarity	Article	Yes
-3.8330	37.0150	002	3.1	MbLg	06/12/1988	06:09:16	120	25	-95	Serr1999	Polarity	Article	Yes
-3.8420	37.0290	015	3.8	md	06/12/1988	20:15:00	165	20	-76	Galetal1999	Polarity	Article	Yes
-3.8410	37.0070	015	3.4	M	07/12/1988	18:50:00	205	35	129	RPandDV2001	Polarity	Article	Yes
-4.6200	36.3400	082	4.5	mb	12/12/1988	06:40:00	315	50	5	MandR1997	Polarity	Article	No
-7.7600	42.1600	005	3.2	mbLg	12/12/1988	12:14:40	141	60	163	PS1998	Polarity	Article	Yes
-3.9270	37.0510	016	3.8	md	14/12/1988	17:00:00	315	80	-90	Galetal1999	Polarity	Article	Yes
-3.6740	37.0190	014	3.6	md	25/12/1988	13:56:00	322	75	-90	Galetal1999	Polarity	Article	Yes
-0.2900	39.4000	017	3.4	mbLg	28/12/1988	06:21:15	49	10	69	PS1998	Polarity	Article	Yes
-7.7500	42.1500	003	3.2	mbLg	30/12/1988	16:41:39	81	62	-171	PS1998	Polarity	Article	Yes
-3.8640	37.0190	023	2.4	md	05/01/1989	20:18:00	64	15	-39	Galetal1999	Polarity	Article	Yes
-3.8660	37.0160	023	2.9	md	05/01/1989	20:24:00	244	75	-90	Galetal1999	Polarity	Article	Yes
0.1700	43.0400	010	4.4	Ml	06/01/1989	00:00:00	276	75	-143	Rigo2015	Compilation	Article	Yes
-3.8580	37.0160	021	2.3	md	06/01/1989	06:33:00	45	25	-90	Galetal1999	Polarity	Article	Yes
-3.8580	37.0170	021	2.3	mb	06/01/1989	06:33:00	45	25	-90	Serr1999	Polarity	Article	Yes
0.1700	42.9900	011	4.4	mbLg	06/01/1989	19:33:00	50	45	21	PS1998	Polarity	Article	Yes
-4.2700	35.4700	005	3.1	mb	07/01/1989	14:43:11	345	56	48	Balanetal2012	Polarity	Article	Yes
-3.8070	37.0510	010	2.2	md	12/01/1989	13:34:00	131	45	-65	Galetal1999	Polarity	Article	Yes
-4.3300	37.0300	009	1.7	mb	13/01/1989	04:48:06	264	36	-54	Balanetal2012	Polarity	Article	No
2.6500	36.3900	002	5.0	Mw	12/02/1989	12:02:19	10	11	11	Setal2003a	Moment tensor inversion	Article	Yes
-4.0120	36.9930	000	3.4	MbLg	15/02/1989	00:04:04	123	65	0	Serr1999	Polarity	Article	Yes
-4.0470	36.9960	022	3.3	md	15/02/1989	01:54:00	45	45	-159	Galetal1999	Polarity	Article	Yes
-3.9900	37.0080	000	2.6	MbLg	15/02/1989	01:54:06	45	45	-159	Serr1999	Polarity	Article	Yes
-4.0430	36.9790	022	3.7	md	15/02/1989	04:04:00	123	65	0	Galetal1999	Polarity	Article	Yes
-4.0370	37.0010	016	2.1	md	15/02/1989	07:43:00	30	45	-152	Galetal1999	Polarity	Article	Yes
-4.0300	37.0100	013	2.1	mb	15/02/1989	07:43:14	116	51	17	Balanetal2012	Polarity	Article	Yes

-3.0900	38.9000	008	3.6	mbLg	20/02/1989	03:25:36	148	79	-33	PS1998	Polarity	Article	Yes
-5.1100	43.0800	005	3.7	mbLg	20/02/1989	20:52:28	310	70	28	PS1998	Polarity	Article	Yes
-8.9000	39.3000	012	4.7	Ml	08/04/1989	00:00:00	191	75	79	Boretal2001	Polarity	Article	Yes
-3.7000	36.8800	010	2.0	mb	26/04/1989	04:04:24	300	30	90	Metal2006	Polarity	Article	Yes
-4.5300	37.1500	006	3.4	mbLg	07/06/1989	00:12:48	270	76	159	PS1998	Polarity	Article	Yes
-4.6600	37.1200	002	3.1	mb	08/06/1989	04:19:54	102	43	-72	Balanetal2012	Polarity	Article	Yes
-4.7500	37.1200	016	3.4	mb	08/06/1989	04:48:56	112	57	-73	Balanetal2012	Polarity	Article	Yes
-7.7800	42.1600	011	3.2	mbLg	10/06/1989	07:15:08	329	58	-113	PS1998	Polarity	Article	Yes
-3.6860	37.0200	013	3.5	md	19/07/1989	04:30:00	321	75	-90	Galetal1999	Polarity	Article	Yes
-3.6900	37.0200	012	3.6	mb	19/07/1989	04:30:49	120	60	-90	Metal2006	Polarity	Article	Yes
-4.4330	36.6330	095	3.0	M	19/07/1989	10:49:34	296	79	86	Buetal1997	Polarity	Article	No
-3.8650	37.0780	008	2.6	MbLg	20/07/1989	20:24:50	30	85	-90	Serretal1996	Polarity	Article	Yes
-4.0400	37.0500	011	3.1	mb	25/07/1989	22:35:49	55	78	-78	Balanetal2012	Polarity	Article	Yes
-4.1400	36.6900	001	2.4	mb	08/08/1989	10:23:22	51	53	-65	Balanetal2012	Polarity	Article	Yes
-4.1100	37.0500	013	2.4	mb	17/08/1989	08:52:42	127	73	-58	Balanetal2012	Polarity	Article	Yes
-7.5200	42.1100	014	3.8	mbLg	30/08/1989	11:43:26	139	57	-97	PS1998	Polarity	Article	Yes
-8.6000	38.3000	025	4.0	Ml	23/09/1989	00:00:00	21	46	82	Boretal2001	Polarity	Article	Yes
-1.1500	41.2000	006	3.3	mbLg	24/09/1989	20:16:04	5	62	-49	PS1998	Polarity	Article	Yes
-3.6320	37.1160	013	3.5	md	07/10/1989	04:45:00	101	45	-101	Galetal1999	Polarity	Article	Yes
-3.6380	37.1050	003	3.2	MbLg	07/10/1989	04:45:11	101	45	-101	Serr1999	Polarity	Article	Yes
-3.8100	35.1500	006	2.0	mb	18/10/1989	18:11:00	180	40	-98	Hatzetal1993	Polarity	Article	Yes
-3.8500	35.2000	008	1.7	mb	19/10/1989	19:31:00	185	70	-14	Hatzetal1993	Polarity	Article	No
-3.9600	35.0800	006	2.7	mb	20/10/1989	13:07:00	20	70	-14	Hatzetal1993	Polarity	Article	Yes
-3.8600	35.1800	005	2.1	mb	21/10/1989	03:56:00	90	70	-153	Hatzetal1993	Polarity	Article	Yes
-3.8300	35.1600	007	1.7	mb	21/10/1989	11:00:00	145	30	-90	Hatzetal1993	Polarity	Article	No
-3.8300	35.1700	009	1.6	mb	23/10/1989	04:59:00	330	60	-90	Hatzetal1993	Polarity	Article	No
-4.0100	35.0600	009	1.8	mb	23/10/1989	06:41:00	220	60	161	Hatzetal1993	Polarity	Article	No
-3.8300	35.1600	008	1.4	mb	24/10/1989	13:28:00	160	20	-90	Hatzetal1993	Polarity	Article	No
-3.8600	35.1800	009	1.6	mb	25/10/1989	08:28:00	295	65	-168	Hatzetal1993	Polarity	Article	No
-3.8300	35.1600	008	1.3	mb	26/10/1989	11:29:00	160	20	-90	Hatzetal1993	Polarity	Article	No

-3.8300	35.1600	007	1.3	mb	29/10/1989	03:28:00	340	60	-100	Hatzetal1993	Polarity	Article	No
-3.8700	35.1700	009	1.3	mb	29/10/1989	05:25:00	95	70	-166	Hatzetal1993	Polarity	Article	No
-3.8700	35.1700	009	1.8	mb	29/10/1989	05:51:00	10	80	-27	Hatzetal1993	Polarity	Article	No
-3.8500	35.1700	008	1.8	mb	29/10/1989	09:27:00	340	45	-153	Hatzetal1993	Polarity	Article	No
2.4330	36.7480	005	6.0	Mw	29/10/1989	19:09:14	91	48	119	CMT	Moment tensor inversion	Catalog	Yes
2.4400	36.7400	010	5.2	Mw	29/10/1989	19:21:52	13	24	51	Pondetal1999	Moment tensor inversion	Article	Yes
-3.8700	35.1800	009	1.7	mb	30/10/1989	03:53:00	110	60	-161	Hatzetal1993	Polarity	Article	No
-3.8500	35.1700	010	1.3	mb	30/10/1989	04:25:00	45	70	-14	Hatzetal1993	Polarity	Article	No
-3.8200	35.1700	011	1.8	mb	31/10/1989	13:54:00	320	70	-90	Hatzetal1993	Polarity	Article	No
-8.7000	36.8000	040	4.5	M	02/11/1989	00:00:00	88	82	165	Boretal2001	Polarity	Article	Yes
-3.8700	35.1900	011	1.7	mb	02/11/1989	12:03:00	185	70	-14	Hatzetal1993	Polarity	Article	No
-3.8600	35.0300	009	1.3	mb	05/11/1989	20:58:00	275	70	-133	Hatzetal1993	Polarity	Article	No
-4.0400	35.0200	008	1.7	mb	07/11/1989	20:30:00	210	80	-27	Hatzetal1993	Polarity	Article	No
-3.8800	35.0600	009	3.3	mb	07/11/1989	21:05:00	350	70	-12	Hatzetal1993	Polarity	Article	Yes
-3.8700	35.0600	009	2.1	mb	07/11/1989	21:08:00	5	85	169	Hatzetal1993	Polarity	Article	Yes
-3.8700	35.0600	010	1.4	mb	07/11/1989	21:09:00	360	85	-116	Hatzetal1993	Polarity	Article	No
-3.8800	35.0600	008	1.9	mb	07/11/1989	21:21:00	185	70	-54	Hatzetal1993	Polarity	Article	No
-3.8800	35.0700	010	1.6	mb	07/11/1989	21:31:00	180	70	-68	Hatzetal1993	Polarity	Article	No
-3.8800	35.0700	008	1.4	mb	07/11/1989	21:44:00	330	20	-114	Hatzetal1993	Polarity	Article	No
-3.8800	35.0600	009	1.4	mb	07/11/1989	22:01:00	170	70	-87	Hatzetal1993	Polarity	Article	No
-3.8700	35.0600	010	1.7	mb	07/11/1989	23:13:00	170	85	-1	Hatzetal1993	Polarity	Article	No
-3.8700	35.0600	010	1.6	mb	08/11/1989	00:01:00	180	75	-19	Hatzetal1993	Polarity	Article	No
-3.8800	35.0600	010	2.0	mb	08/11/1989	00:04:00	185	70	-54	Hatzetal1993	Polarity	Article	Yes
-3.8700	35.0600	010	1.5	mb	08/11/1989	01:30:00	175	70	-38	Hatzetal1993	Polarity	Article	No
-3.8700	35.1700	007	1.6	mb	09/11/1989	07:25:00	10	70	-27	Hatzetal1993	Polarity	Article	No
2.3820	36.6070	002	1.6	Ml	09/11/1989	15:57:00	213	55	53	Ousetal2014	Polarity	Article	No
-3.9600	35.0900	008	1.7	mb	09/11/1989	19:54:00	95	50	8	Hatzetal1993	Polarity	Article	No
2.4180	36.6570	005	1.8	Ml	09/11/1989	22:17:00	220	71	34	Ousetal2014	Polarity	Article	No
2.3720	36.6240	004	1.6	Ml	09/11/1989	23:06:00	205	76	9	Ousetal2014	Polarity	Article	No
2.4350	36.6670	002	1.9	Ml	10/11/1989	01:20:00	295	60	173	Ousetal2014	Polarity	Article	No

-3.8600	35.0700	010	1.9	mb	10/11/1989	01:28:00	170	65	-74	Hatzetal1993	Polarity	Article	No
-3.8600	35.1600	009	1.5	mb	10/11/1989	02:05:00	30	80	0	Hatzetal1993	Polarity	Article	No
-3.9500	35.0900	006	1.8	mb	10/11/1989	02:55:00	185	80	153	Hatzetal1993	Polarity	Article	No
2.4550	36.6780	006	2.3	Ml	10/11/1989	06:33:00	305	65	172	Ousetal2014	Polarity	Article	Yes
2.3480	36.5910	008	1.9	Ml	10/11/1989	11:22:00	7	74	40	Ousetal2014	Polarity	Article	No
2.3810	36.6120	003	2.0	Ml	10/11/1989	12:44:00	197	82	13	Ousetal2014	Polarity	Article	Yes
2.3850	36.6080	003	1.7	Ml	10/11/1989	12:53:00	197	38	54	Ousetal2014	Polarity	Article	No
2.3440	36.6690	007	0.6	Ml	10/11/1989	18:55:00	48	51	104	Ousetal2014	Polarity	Article	No
2.3480	36.6130	006	1.1	Ml	10/11/1989	19:27:00	187	59	50	Ousetal2014	Polarity	Article	No
2.3840	36.6550	005	1.9	Ml	10/11/1989	20:14:00	212	47	58	Ousetal2014	Polarity	Article	No
2.3800	36.6400	004	2.2	Ml	10/11/1989	21:22:00	206	50	54	Ousetal2014	Polarity	Article	Yes
2.3790	36.6210	002	1.0	Ml	10/11/1989	21:30:00	218	44	68	Ousetal2014	Polarity	Article	No
2.3680	36.6040	002	1.3	Ml	10/11/1989	22:54:00	104	70	123	Ousetal2014	Polarity	Article	No
2.3760	36.6250	003	2.5	Ml	10/11/1989	23:39:00	108	61	144	Ousetal2014	Polarity	Article	Yes
2.3620	36.6240	004	1.8	Ml	11/11/1989	10:40:00	301	80	-151	Ousetal2014	Polarity	Article	No
2.3640	36.6170	003	1.6	Ml	11/11/1989	10:49:00	207	77	21	Ousetal2014	Polarity	Article	No
2.4080	36.6530	004	1.2	Ml	11/11/1989	13:57:00	229	55	53	Ousetal2014	Polarity	Article	No
-3.9500	35.0800	007	2.2	mb	11/11/1989	18:40:00	200	75	-19	Hatzetal1993	Polarity	Article	Yes
-3.9400	35.0800	006	2.0	mb	11/11/1989	19:59:00	200	80	-27	Hatzetal1993	Polarity	Article	Yes
2.3260	36.6110	009	1.4	Ml	12/11/1989	04:17:00	120	56	127	Ousetal2014	Polarity	Article	No
2.3510	36.6300	006	0.8	Ml	12/11/1989	07:33:00	122	76	136	Ousetal2014	Polarity	Article	No
2.3500	36.6190	008	1.4	Ml	12/11/1989	11:57:00	108	67	137	Ousetal2014	Polarity	Article	No
2.3430	36.6210	005	1.1	Ml	12/11/1989	12:33:00	174	62	35	Ousetal2014	Polarity	Article	No
2.3630	36.6820	010	2.3	Ml	12/11/1989	21:04:00	275	38	92	Ousetal2014	Polarity	Article	Yes
2.3750	36.6060	002	1.8	Ml	12/11/1989	22:03:00	210	48	45	Ousetal2014	Polarity	Article	No
2.3390	36.6550	006	1.9	Ml	12/11/1989	22:41:00	298	27	107	Ousetal2014	Polarity	Article	No
2.3550	36.6210	010	0.9	Ml	12/11/1989	23:11:00	217	38	42	Ousetal2014	Polarity	Article	No
2.3860	36.6480	005	1.4	Ml	13/11/1989	07:07:00	194	77	41	Ousetal2014	Polarity	Article	No
2.3860	36.6480	006	1.4	Ml	13/11/1989	08:07:00	176	34	48	Ousetal2014	Polarity	Article	No
2.3400	36.6110	004	0.6	Ml	13/11/1989	12:34:00	194	63	52	Ousetal2014	Polarity	Article	No

2.3450	36.6300	008	1.1	Ml	13/11/1989	18:11:00	210	54	53	Ousetal2014	Polarity	Article	No
2.3710	36.6620	006	1.8	Ml	13/11/1989	23:22:00	83	67	136	Ousetal2014	Polarity	Article	No
2.3490	36.6010	006	1.7	Ml	14/11/1989	03:13:00	185	58	24	Ousetal2014	Polarity	Article	No
2.3810	36.6050	002	1.5	Ml	14/11/1989	20:49:00	28	46	91	Ousetal2014	Polarity	Article	No
2.3570	36.6300	009	1.6	Ml	15/11/1989	07:04:00	346	83	-21	Ousetal2014	Polarity	Article	No
2.3610	36.6280	007	1.4	Ml	15/11/1989	16:13:00	100	44	132	Ousetal2014	Polarity	Article	No
-3.8600	35.1600	010	1.3	mb	15/11/1989	16:58:00	10	70	-27	Hatzetal1993	Polarity	Article	No
2.3220	36.6420	007	1.2	Ml	16/11/1989	00:26:00	350	28	89	Ousetal2014	Polarity	Article	No
2.3570	36.6290	008	1.9	Ml	16/11/1989	04:10:00	16	86	-2	Ousetal2014	Polarity	Article	No
2.3470	36.5890	007	1.1	Ml	17/11/1989	02:35:00	179	72	27	Ousetal2014	Polarity	Article	No
2.3850	36.6020	002	1.0	Ml	17/11/1989	02:49:00	48	62	96	Ousetal2014	Polarity	Article	No
2.4780	36.6770	007	2.4	Ml	17/11/1989	14:10:00	129	57	147	Ousetal2014	Polarity	Article	Yes
2.4810	36.6700	007	2.2	Ml	17/11/1989	14:22:00	270	47	118	Ousetal2014	Polarity	Article	Yes
2.3440	36.6170	005	0.7	Ml	17/11/1989	15:34:00	188	66	46	Ousetal2014	Polarity	Article	No
2.4650	36.6630	009	3.1	Ml	17/11/1989	15:59:00	285	53	148	Ousetal2014	Polarity	Article	Yes
2.3500	36.6230	007	1.3	Ml	17/11/1989	17:10:00	74	45	132	Ousetal2014	Polarity	Article	No
2.3730	36.6160	002	0.9	Ml	17/11/1989	23:47:00	227	66	67	Ousetal2014	Polarity	Article	No
2.3730	36.6200	002	0.5	Ml	18/11/1989	03:25:00	266	53	113	Ousetal2014	Polarity	Article	No
2.3760	36.5640	003	0.7	Ml	18/11/1989	13:34:00	169	66	13	Ousetal2014	Polarity	Article	No
2.3970	36.6350	005	0.6	Ml	18/11/1989	21:53:00	78	83	164	Ousetal2014	Polarity	Article	No
2.3640	36.6250	002	0.6	Ml	19/11/1989	01:31:00	258	53	94	Ousetal2014	Polarity	Article	No
2.3520	36.6170	006	0.4	Ml	19/11/1989	06:44:00	172	81	18	Ousetal2014	Polarity	Article	No
2.3870	36.6400	006	0.6	Ml	19/11/1989	16:41:00	55	56	107	Ousetal2014	Polarity	Article	No
2.3850	36.6480	005	2.5	Ml	19/11/1989	17:57:00	59	52	96	Ousetal2014	Polarity	Article	Yes
2.3520	36.6340	006	0.6	Ml	19/11/1989	19:30:00	249	55	111	Ousetal2014	Polarity	Article	No
2.3620	36.6070	002	0.4	Ml	19/11/1989	22:04:00	154	55	69	Ousetal2014	Polarity	Article	No
2.3810	36.6190	002	1.2	Ml	20/11/1989	02:27:00	41	39	99	Ousetal2014	Polarity	Article	No
-7.3700	37.2700	017	5.0	mbLg	20/12/1989	04:15:05	104	65	-115	PS1998	Polarity	Article	Yes
2.4800	36.7700	012	4.8	Mw	02/02/1990	09:31:00	259	39	63	EMMA	Compilation	Catalog	Yes
-4.5300	36.5660	068	3.4	M	06/02/1990	07:41:29	255	25	69	Buetal1997	Polarity	Article	No

2.5670	36.7320	027	5.2	Mw	09/02/1990	09:31:50	49	18	95	CMT	Moment tensor inversion	Catalog	Yes
-1.0400	42.9100	010	3.6	mbLg	28/02/1990	13:23:43	329	40	-122	PS1998	Polarity	Article	Yes
2.4900	36.5900	010	3.0	M	06/03/1990	07:45:00	75	75	-18.8	Sebai (1997)	nan	Article	Yes
-4.0000	37.0000	637	5.0	M	08/03/1990	01:37:12	0	28	-88	Buetal1997	Polarity	Article	No
2.4900	36.5800	008	4.6	M	11/03/1990	08:30:00	338	57	-44.5	Sebai (1997)	nan	Article	Yes
0.1600	38.2900	008	3.6	mbLg	29/03/1990	03:10:21	65	51	115	PS1998	Polarity	Article	Yes
-1.4300	43.1500	013	3.4	mbLg	01/04/1990	19:13:34	0	20	180	PS1998	Polarity	Article	Yes
2.4900	36.7900	014	4.3	Mw	12/04/1990	22:47:00	210	34	38	EMMA	Compilation	Catalog	Yes
-4.8300	35.6500	075	3.9	mb	13/04/1990	22:17:00	346	42	156	MandR1997	Polarity	Article	No
-4.2200	36.9700	008	2.0	mb	17/04/1990	01:02:40	133	81	-3	Balanetal2012	Polarity	Article	Yes
-1.1800	43.1100	012	2.4	Ml	26/04/1990	00:00:00	354	73	88	Rigo2015	Compilation	Article	Yes
-4.5220	36.5320	095	4.2	MbLg	02/05/1990	16:40:26	211	63	88	Serr1999	Polarity	Article	No
-11.6700	38.3500	068	4.4	Mw	26/05/1990	00:00:00	138	79	-12	EMMA	Compilation	Catalog	No
-0.5500	43.1000	007	2.4	Ml	30/05/1990	00:00:00	13	86	153	Rigo2015	Compilation	Article	Yes
-1.8300	43.2100	009	3.0	Ml	02/06/1990	00:00:00	295	52	-90	Rigo2015	Compilation	Article	Yes
-0.3100	43.1000	006	4.2	Ml	12/06/1990	00:00:00	92	46	104	Rigo2015	Compilation	Article	Yes
-1.0300	43.1000	020	1.5	Ml	16/06/1990	00:00:00	72	85	90	Rigo2015	Compilation	Article	No
-1.6600	42.7900	003	3.4	mbLg	19/06/1990	21:48:12	70	68	-44	PS1998	Polarity	Article	Yes
-1.3100	43.2900	015	1.5	Ml	28/06/1990	00:00:00	74	28	-90	Rigo2015	Compilation	Article	No
-3.8230	37.0960	013	3.2	md	01/07/1990	23:24:00	15	45	-114	Galetal1999	Polarity	Article	Yes
-1.3900	43.0600	011	1.5	Ml	05/07/1990	00:00:00	105	80	90	Rigo2015	Compilation	Article	No
-3.5400	40.7300	004	3.3	mbLg	07/07/1990	23:30:18	60	82	147	PS1998	Polarity	Article	Yes
-4.1000	37.0700	010	1.7	mb	11/07/1990	15:35:47	83	63	-3	Balanetal2012	Polarity	Article	No
-4.1600	37.1500	015	1.9	mb	18/07/1990	18:46:48	289	30	-90	Balanetal2012	Polarity	Article	No
-4.2800	37.1500	009	1.5	mb	18/07/1990	23:47:33	57	72	-84	Balanetal2012	Polarity	Article	No
-4.2800	37.1400	010	2.1	mb	19/07/1990	00:02:39	343	40	0	Balanetal2012	Polarity	Article	Yes
-4.2900	37.1400	010	2.4	mb	19/07/1990	00:16:05	26	14	45	Balanetal2012	Polarity	Article	Yes
-4.3100	37.1400	009	1.5	mb	19/07/1990	00:17:40	358	31	17	Balanetal2012	Polarity	Article	No
-4.3000	37.1400	009	1.6	mb	19/07/1990	00:30:16	280	51	-77	Balanetal2012	Polarity	Article	No
-1.5600	43.1200	012	2.1	Ml	20/07/1990	00:00:00	60	68	90	Rigo2015	Compilation	Article	Yes

-0.3800	43.0800	007	3.6	Ml	22/07/1990	00:00:00	90	90	90	Rigo2015	Compilation	Article	Yes
-0.5600	43.0600	003	3.6	Ml	24/07/1990	00:00:00	302	10	-110	Rigo2015	Compilation	Article	Yes
-1.1500	42.5000	000	3.6	mbLg	26/07/1990	16:29:34	120	45	-173	PS1998	Polarity	Article	Yes
1.0900	42.2700	000	3.7	mbLg	05/08/1990	21:32:00	20	77	-22	PS1998	Polarity	Article	Yes
-4.2400	37.1400	008	2.3	mb	04/09/1990	08:59:13	32	85	30	Balanetal2012	Polarity	Article	Yes
-4.0000	37.2400	009	1.6	mb	09/09/1990	19:02:29	126	82	-50	Balanetal2012	Polarity	Article	No
-4.1000	36.6400	008	1.5	mb	10/09/1990	19:24:07	282	74	82	Balanetal2012	Polarity	Article	No
-4.0000	37.2500	006	1.6	mb	11/09/1990	08:06:23	336	36	14	Balanetal2012	Polarity	Article	No
-4.0300	37.0800	015	2.0	mb	27/09/1990	07:58:30	323	90	42	Balanetal2012	Polarity	Article	Yes
-4.5450	35.9620	113	3.7	MbLg	28/09/1990	02:07:59	306	76	77	Serr1999	Polarity	Article	No
-4.4600	37.1400	007	3.5	mb	28/09/1990	03:51:37	327	72	87	Balanetal2012	Polarity	Article	Yes
-4.2300	37.0000	008	2.5	mb	01/10/1990	07:32:01	37	37	59	Balanetal2012	Polarity	Article	Yes
-3.6950	37.0120	012	3.2	md	14/10/1990	16:02:00	323	90	-90	Galetal1999	Polarity	Article	Yes
-3.9720	37.0520	000	2.4	MbLg	28/10/1990	07:33:43	215	90	90	Serr1999	Polarity	Article	Yes
-3.7000	36.9880	002	4.0	MbLg	07/11/1990	07:25:02	315	90	90	Serr1999	Polarity	Article	Yes
-3.6800	36.9900	013	2.2	mb	09/11/1990	15:51:19	187	81	-110	Metal2006	Polarity	Article	Yes
-3.7090	37.0040	013	3.1	md	10/11/1990	01:21:00	319	80	-90	Galetal1999	Polarity	Article	Yes
-3.6980	37.0070	006	2.7	MbLg	10/11/1990	01:21:54	319	80	-90	Serr1999	Polarity	Article	Yes
-4.0900	37.1000	017	2.8	mb	14/11/1990	15:43:34	211	79	-66	Balanetal2012	Polarity	Article	Yes
-4.0900	37.1000	019	2.4	mb	14/11/1990	20:34:46	159	85	-30	Balanetal2012	Polarity	Article	Yes
-3.9170	37.0630	013	2.5	mb	17/11/1990	18:34:00	46	35	-129	Serr1999	Polarity	Article	Yes
-4.5900	36.4100	085	3.4	M	18/11/1990	00:00:00	175	51	-30	Bezzetal2012	Compilation	Article	No
-7.6100	42.2800	017	3.6	mbLg	22/11/1990	04:33:14	38	68	-5	PS1998	Polarity	Article	Yes
-3.8600	36.9920	014	2.8	mb	23/11/1990	14:20:00	40	58	90	Serr1999	Polarity	Article	Yes
-2.8300	39.2100	002	3.0	mbLg	30/11/1990	21:52:12	336	79	-170	PS1998	Polarity	Article	Yes
-4.4400	37.0800	016	2.2	mb	17/12/1990	09:58:02	5	61	-28	Balanetal2012	Polarity	Article	Yes
-4.4200	37.0600	004	2.8	mb	23/12/1990	04:51:05	149	13	-51	Balanetal2012	Polarity	Article	Yes
-4.0200	37.0000	009	2.4	mb	24/12/1990	18:19:29	177	84	-40	Balanetal2012	Polarity	Article	Yes
-4.5100	37.0500	004	2.9	mb	25/12/1990	19:59:42	25	44	-60	Balanetal2012	Polarity	Article	Yes
-4.0600	36.9800	012	3.2	mb	02/01/1991	23:23:55	154	85	-9	Balanetal2012	Polarity	Article	Yes

-4.0500	36.9800	012	2.8	mb	28/01/1991	01:04:49	144	87	-9	Balanetal2012	Polarity	Article	Yes
-4.0300	37.1400	019	2.8	mb	09/02/1991	03:51:40	161	30	0	Balanetal2012	Polarity	Article	Yes
-5.4900	37.7500	015	2.0	mbLg	10/03/1991	11:17:06	10	65	62	PS1998	Polarity	Article	Yes
-4.2100	37.1400	016	2.0	mb	25/04/1991	19:16:32	112	83	-58	Balanetal2012	Polarity	Article	Yes
-4.0700	37.1400	005	3.2	mb	25/04/1991	19:23:26	351	41	12	Balanetal2012	Polarity	Article	Yes
-4.1700	37.1500	017	2.1	mb	25/04/1991	19:30:49	158	75	-73	Balanetal2012	Polarity	Article	Yes
-4.1300	37.1400	015	2.3	mb	25/04/1991	19:39:21	311	53	16	Balanetal2012	Polarity	Article	Yes
-4.0600	37.0500	015	1.6	mb	03/05/1991	17:16:02	143	90	50	Balanetal2012	Polarity	Article	No
-2.3100	39.2300	004	3.5	mbLg	30/05/1991	20:10:39	282	72	177	PS1998	Polarity	Article	Yes
-4.0300	37.0000	014	1.5	mb	31/05/1991	20:54:58	349	61	78	Balanetal2012	Polarity	Article	No
-10.4000	35.9000	006	4.8	M	15/06/1991	00:00:00	273	30	73	Buetal2004	Polarity	Article	Yes
-3.5810	37.0960	011	3.1	md	21/06/1991	21:23:00	334	85	-90	Galetal1999	Polarity	Article	Yes
-3.5230	37.0970	005	2.7	MbLg	21/06/1991	21:24:01	334	85	-90	Serr1999	Polarity	Article	Yes
-3.4600	37.1470	010	2.5	mb	06/07/1991	19:28:00	99	90	90	Serr1999	Polarity	Article	Yes
-3.9470	37.0770	003	3.1	MbLg	02/08/1991	08:57:54	70	45	-98	Serr1999	Polarity	Article	Yes
-3.7230	37.2430	004	3.0	MbLg	08/08/1991	03:31:58	15	70	-90	Serretal1996	Polarity	Article	Yes
-3.6430	36.9880	010	2.8	md	10/08/1991	09:34:00	150	90	90	Galetal1999	Polarity	Article	Yes
-3.6100	36.9500	011	2.8	mb	10/08/1991	09:34:51	315	80	131	Metal2006	Polarity	Article	Yes
-0.9600	38.8000	004	4.1	M	14/08/1991	10:32:09	314	72	-164	Buetal2004	Polarity	Article	Yes
-5.0400	38.2600	006	1.9	mbLg	22/08/1991	09:42:07	45	85	72	PS1998	Polarity	Article	No
-3.2800	36.8200	005	2.6	mb	24/08/1991	17:10:09	39	45	-135	Metal2006	Polarity	Article	Yes
-4.4830	36.8180	058	3.8	MbLg	25/08/1991	13:04:00	234	51	72	Serr1999	Polarity	Article	No
-5.5800	37.1600	005	2.9	mb	07/10/1991	00:06:59	344	55	47	Balanetal2012	Polarity	Article	Yes
-5.5500	37.1900	009	3.4	mb	07/10/1991	15:16:28	313	36	28	Balanetal2012	Polarity	Article	Yes
-5.5900	37.1700	007	3.1	mb	07/10/1991	15:23:35	326	39	37	Balanetal2012	Polarity	Article	Yes
-4.1500	37.1900	003	3.0	mb	24/10/1991	23:01:09	30	50	90	Balanetal2012	Polarity	Article	Yes
-3.9680	37.0880	003	3.0	MbLg	05/11/1991	01:55:50	33	35	138	Serr1999	Polarity	Article	Yes
-3.8530	37.0240	014	3.3	md	12/11/1991	06:45:00	45	35	-129	Galetal1999	Polarity	Article	Yes
-3.8100	37.0070	003	3.0	MbLg	12/11/1991	06:45:53	45	35	-129	Serr1999	Polarity	Article	Yes
0.9000	42.7300	007	2.9	Ml	02/12/1991	00:00:00	292	80	-135	Rigo2015	Compilation	Article	Yes

-3.7410	36.9210	016	3.1	md	10/12/1991	03:51:00	345	55	-135	Galetal1999	Polarity	Article	Yes
-3.7520	36.9130	004	2.9	MbLg	10/12/1991	03:51:34	345	55	-135	Serr1999	Polarity	Article	Yes
-4.5200	36.2700	006	3.1	mb	11/12/1991	11:45:22	0	57	40	Balanetal2012	Polarity	Article	Yes
2.0600	40.9800	012	4.2	mbLg	15/12/1991	11:50:00	261	20	-168	PS1998	Polarity	Article	Yes
-0.7900	39.4200	002	3.3	mbLg	21/12/1991	05:08:25	80	54	109	PS1998	Polarity	Article	Yes
-3.5840	37.0350	017	3.0	md	12/01/1992	04:39:00	337	80	-90	Galetal1999	Polarity	Article	Yes
-3.6250	36.9820	004	2.8	MbLg	12/01/1992	04:39:30	337	80	-90	Serr1999	Polarity	Article	Yes
1.9000	36.2000	010	4.7	M	19/01/1992	20:21:00	97	85	-169	Buetal2016	Compilation	Article	Yes
-2.3900	40.8600	001	3.4	mbLg	24/01/1992	09:49:32	55	70	-99	PS1998	Polarity	Article	Yes
-3.8900	37.1180	003	3.2	MbLg	28/01/1992	06:45:10	30	45	-118	Serr1999	Polarity	Article	Yes
-3.5900	37.1600	006	3.0	mb	07/02/1992	16:29:13	165	75	-90	Metal2006	Polarity	Article	Yes
1.8600	36.2100	000	5.1	Mw	19/02/1992	20:21:00	96	87	-168	EMMA	Compilation	Catalog	Yes
-2.5300	35.2700	008	4.8	M	12/03/1992	13:05:00	268	76	-161	Bezzetal2012	Compilation	Article	Yes
-4.4330	36.5170	064	3.7	Mw	14/03/1992	08:05:30	118	14	-123	Coca2003	Moment tensor inversion	Article	No
2.0600	42.2300	002	4.2	mbLg	19/03/1992	18:53:00	150	78	-40	PS1998	Polarity	Article	Yes
-3.8550	37.0980	024	3.3	MbLg	02/04/1992	00:59:55	23	45	-117	Serr1999	Polarity	Article	Yes
-9.8467	30.4200	009	3.7	MbLg	05/04/1992	21:16:38	250	53	29	CatMorr2008	Moment tensor inversion	Article	Yes
-2.5400	39.5200	005	3.4	mbLg	20/04/1992	02:08:26	340	60	-124	PS1998	Polarity	Article	Yes
-6.0200	37.5700	010	2.4	mbLg	19/05/1992	19:23:03	189	50	96	PS1998	Polarity	Article	Yes
-3.8720	37.0400	009	2.6	MbLg	28/05/1992	16:41:07	135	45	-58	Serr1999	Polarity	Article	Yes
1.2200	42.7900	012	3.1	Ml	25/07/1992	00:00:00	343	39	-125	Rigo2015	Compilation	Article	Yes
-0.8800	38.2600	016	3.0	mbLg	20/08/1992	03:38:55	230	46	-101	PS1998	Polarity	Article	Yes
2.3200	42.2700	000	2.8	Ml	24/08/1992	00:00:00	150	46	-43	Rigo2015	Compilation	Article	Yes
-4.4470	36.5970	071	3.5	MbLg	03/09/1992	09:43:27	299	41	-60	Serr1999	Polarity	Article	No
1.8600	42.4300	004	3.2	Ml	02/10/1992	00:00:00	193	35	153	Rigo2015	Compilation	Article	Yes
-4.3570	31.2200	007	5.6	Mw	23/10/1992	09:11:08	187	69	12	CMT	Moment tensor inversion	Catalog	Yes
-4.3830	31.4120	021	5.6	Mw	30/10/1992	10:44:01	90	72	176	CMT	Moment tensor inversion	Catalog	Yes
-1.8490	38.2700	006	3.2	M	06/11/1992	02:52:00	210	43	71	RPandDV2001	Polarity	Article	Yes
1.1500	35.7300	007	5.0	M	15/11/1992	00:00:00	274	70	-169	CMT	Moment tensor inversion	Catalog	Yes
-3.9680	36.9750	000	2.7	MbLg	22/11/1992	10:14:31	135	30	-117	Serr1999	Polarity	Article	Yes

1.0600	42.6500	009	3.1	Ml	15/12/1992	00:00:00	49	11	124	Rigo2015	Compilation	Article	Yes
-2.5500	35.3900	008	4.9	Mw	21/12/1992	09:02:00	224	10	-142	EMMA	Compilation	Catalog	Yes
-4.5100	36.6000	039	3.4	mb	21/12/1992	11:10:00	247	27	133	MandR1997	Polarity	Article	Yes
-4.5200	37.0100	002	2.9	mb	16/01/1993	03:55:02	257	57	76	Balanetal2012	Polarity	Article	Yes
-8.6000	36.6000	026	4.3	Ml	16/02/1993	03:11:00	17	33	34	Boretal2001	Polarity	Article	Yes
-4.0100	37.0500	007	1.9	mb	04/03/1993	08:11:14	339	59	-54	Balanetal2012	Polarity	Article	No
-3.5470	37.0970	002	2.9	MbLg	21/03/1993	08:17:38	76	23	-109	Serr1999	Polarity	Article	Yes
-3.5480	37.0870	003	2.9	MbLg	21/03/1993	09:55:26	76	23	-105	Serr1999	Polarity	Article	Yes
-3.4950	37.1040	010	3.3	MbLg	21/03/1993	10:01:00	76	23	-105	Serr1999	Polarity	Article	Yes
-4.0070	37.0530	003	2.9	MbLg	10/04/1993	07:59:08	34	40	-127	Serr1999	Polarity	Article	Yes
-6.3300	35.2900	030	4.2	mb	01/05/1993	00:22:00	15	24	-61	MandR1997	Polarity	Article	Yes
-4.3400	36.8200	056	4.0	M	01/05/1993	04:39:00	15	25	-60	Buetal2004	Polarity	Article	No
-2.5000	35.3600	027	5.3	Mw	05/05/1993	07:40:00	266	73	103	EMMA	Compilation	Catalog	Yes
-2.4200	35.2700	006	5.4	M	23/05/1993	07:40:56	308	86	4	BandB1999	Polarity	Article	Yes
-2.4300	35.2700	006	5.4	mb	23/05/1993	07:41:00	308	84	1	MandR1997	Polarity	Article	Yes
-0.8000	39.4300	002	3.3	mbLg	25/05/1993	07:07:13	301	76	-172	PS1998	Polarity	Article	Yes
-3.7270	37.1820	015	3.0	md	19/06/1993	23:11:00	128	35	90	Galetal1999	Polarity	Article	Yes
-8.3000	36.4000	015	4.4	Ml	22/06/1993	00:00:00	37	62	40	Boretal2001	Polarity	Article	Yes
-1.3000	38.2820	013	3.0	M	23/07/1993	03:59:00	210	70	-142	RPandDV2001	Polarity	Article	Yes
-4.0080	37.0930	000	2.7	MbLg	25/07/1993	14:35:09	86	20	-76	Serr1999	Polarity	Article	Yes
-3.4300	36.8000	663	4.4	M	31/07/1993	00:00:00	177	60	-91	Buetal2004	Polarity	Article	No
-1.0900	40.2900	005	3.4	mbLg	15/08/1993	22:32:25	314	89	-180	PS1998	Polarity	Article	Yes
-5.2900	37.0700	010	3.0	mb	29/08/1993	23:57:02	276	48	-86	Balanetal2012	Polarity	Article	Yes
-1.2550	38.4480	002	3.2	M	06/10/1993	13:49:00	202	53	-142	RPandDV2001	Polarity	Article	Yes
2.1300	42.4300	003	3.3	mbLg	08/10/1993	22:09:00	342	40	-111	PS1998	Polarity	Article	Yes
-1.3280	38.3130	007	3.5	M	19/10/1993	18:14:00	278	42	85	RPandDV2001	Polarity	Article	Yes
-1.5800	40.5900	005	3.2	mbLg	25/10/1993	00:16:06	224	51	-48	PS1998	Polarity	Article	Yes
-4.5570	36.7680	026	3.4	MbLg	26/10/1993	15:55:29	308	71	99	Serr1999	Polarity	Article	Yes
-1.6420	37.6860	011	3.4	M	03/11/1993	21:31:00	165	30	107	RPandDV2001	Polarity	Article	Yes
-4.4780	36.3520	059	3.8	MbLg	09/11/1993	00:22:32	223	60	86	Serr1999	Polarity	Article	No

-0.8200	38.2830	013	3.2	M	11/11/1993	02:05:00	159	37	23	RPandDV2001	Polarity	Article	Yes
0.0000	38.1800	008	3.7	mbLg	11/11/1993	07:33:24	146	31	-76	PS1998	Polarity	Article	Yes
-1.2600	38.4800	003	3.2	mbLg	05/12/1993	14:15:41	185	23	27	PS1998	Polarity	Article	Yes
-4.3900	36.9800	006	2.6	mb	10/12/1993	12:04:31	51	60	83	Balanetal2012	Polarity	Article	Yes
-4.3200	37.0000	008	2.6	mb	11/12/1993	01:40:57	274	75	85	Balanetal2012	Polarity	Article	Yes
-0.3420	37.8380	020	3.4	M	11/12/1993	02:51:00	325	66	-147	RPandDV2001	Polarity	Article	Yes
-5.0800	36.5100	007	3.0	mb	12/12/1993	18:43:27	266	55	-44	Balanetal2012	Polarity	Article	Yes
-3.9450	37.0120	003	3.6	MbLg	22/12/1993	20:11:38	117	55	-90	Serr1999	Polarity	Article	Yes
-2.9367	36.7800	008	4.8	Mw	23/12/1993	14:22:35	300	80	-120	Setal2001	Moment tensor inversion	Article	Yes
-3.0900	36.8100	019	3.3	mb	23/12/1993	14:34:50	327	37	-168	Metal2006	Polarity	Article	Yes
-2.9850	36.7383	002	3.6	Mw	23/12/1993	18:00:07	300	55	-120	Setal2001	Moment tensor inversion	Article	Yes
-3.0300	36.8100	010	2.8	mb	27/12/1993	20:01:59	262	56	-127	Metal2006	Polarity	Article	Yes
-3.0300	36.8500	009	2.1	mb	29/12/1993	00:06:14	45	87	-145	Metal2006	Polarity	Article	Yes
-2.9800	36.8500	010	2.6	mb	29/12/1993	04:42:06	284	81	58	Metal2006	Polarity	Article	Yes
-4.3750	36.5720	068	3.5	MbLg	01/01/1994	09:00:05	89	53	-119	Serr1999	Polarity	Article	No
-4.3700	36.5700	068	3.5	M	01/01/1994	18:15:00	60	71	-103	Bezzetal2012	Compilation	Article	No
-2.9700	36.7900	007	3.7	mbLg	03/01/1994	01:00:06	206	50	-23	PS1998	Polarity	Article	Yes
-2.8150	36.5717	002	4.9	Mw	04/01/1994	08:03:15	310	70	-130	Setal2001	Moment tensor inversion	Article	Yes
-2.8400	36.6000	009	3.5	mbLg	04/01/1994	08:47:28	235	81	-29	PS1998	Polarity	Article	Yes
-5.1500	37.0200	003	2.6	mb	04/01/1994	11:34:55	44	48	34	Balanetal2012	Polarity	Article	Yes
-2.8150	36.5717	002	4.9	Mw	05/01/1994	09:03:15	310	70	-130	Setal2001	Moment tensor inversion	Article	Yes
-2.8150	36.5717	002	4.9	Mw	06/01/1994	10:03:15	310	70	-130	Setal2001	Moment tensor inversion	Article	Yes
-2.8150	36.5717	002	4.9	Mw	07/01/1994	11:03:15	240	70	60	Setal2001	Moment tensor inversion	Article	Yes
-2.9500	36.8300	010	2.8	mb	08/01/1994	04:53:48	284	80	59	Metal2006	Polarity	Article	Yes
-3.0200	36.8200	010	2.1	mb	08/01/1994	16:15:45	137	61	-171	Metal2006	Polarity	Article	Yes
-3.9030	37.0470	004	3.6	M	08/01/1994	22:48:00	270	43	119	RPandDV2001	Polarity	Article	Yes
-2.8600	36.6100	013	3.1	mbLg	09/01/1994	16:01:36	305	40	143	PS1998	Polarity	Article	Yes
-2.8600	36.5600	006	3.4	mbLg	16/01/1994	15:55:03	135	40	-98	PS1998	Polarity	Article	Yes
-2.8500	36.6400	005	3.5	mbLg	16/01/1994	17:03:09	130	89	105	PS1998	Polarity	Article	Yes
-3.1650	37.2270	009	3.2	M	17/01/1994	05:50:00	50	55	-120	RPandDV2001	Polarity	Article	Yes

-4.3100	37.2900	008	3.3	mb	20/01/1994	06:32:37	82	80	53	Balanetal2012	Polarity	Article	Yes
-2.9800	36.8900	006	2.5	mb	22/01/1994	03:00:22	352	33	-178	Metal2006	Polarity	Article	Yes
-2.9800	36.8900	006	2.8	mb	22/01/1994	07:23:35	222	50	-3	Metal2006	Polarity	Article	Yes
-4.3200	37.2800	008	2.9	mb	25/01/1994	03:40:41	22	22	-26	Balanetal2012	Polarity	Article	Yes
-2.9100	36.8500	005	2.4	mb	25/01/1994	22:55:10	271	83	53	Metal2006	Polarity	Article	Yes
-2.8300	36.6500	003	3.7	mbLg	26/01/1994	16:16:45	200	89	105	PS1998	Polarity	Article	Yes
-4.3200	37.2900	007	2.9	mb	27/01/1994	21:21:50	16	53	-65	Balanetal2012	Polarity	Article	Yes
-4.2200	37.2700	009	2.8	mb	29/01/1994	17:05:03	335	63	63	Balanetal2012	Polarity	Article	Yes
-2.9600	36.8200	006	2.5	mb	31/01/1994	15:48:16	206	82	130	Metal2006	Polarity	Article	Yes
-2.8100	36.6700	010	3.4	mbLg	02/02/1994	06:03:06	50	80	106	PS1998	Polarity	Article	Yes
-2.8000	36.4900	011	3.7	mbLg	02/02/1994	18:03:40	160	47	165	PS1998	Polarity	Article	Yes
-2.9300	36.8900	004	2.1	mb	02/02/1994	23:20:43	101	67	104	Metal2006	Polarity	Article	Yes
-3.3300	39.5000	006	3.5	mbLg	06/02/1994	05:27:00	333	57	-123	PS1998	Polarity	Article	Yes
-2.9200	36.8900	005	2.6	mb	07/02/1994	06:13:22	262	51	-107	Metal2006	Polarity	Article	Yes
-4.4100	36.6230	062	2.9	MbLg	09/02/1994	18:31:32	116	14	2	Serr1999	Polarity	Article	No
-3.1790	37.2930	005	3.3	M	12/02/1994	03:36:00	165	56	-81	RPandDV2001	Polarity	Article	Yes
-2.6200	40.4500	016	2.5	mbLg	14/02/1994	12:03:50	60	34	116	PS1998	Polarity	Article	Yes
-4.3000	37.2800	007	2.6	mb	27/02/1994	05:51:37	43	32	15	Balanetal2012	Polarity	Article	Yes
-3.6240	37.1860	010	2.7	md	03/03/1994	13:09:00	171	57	90	Galetal1999	Polarity	Article	Yes
-3.9230	37.0470	004	2.9	MbLg	04/03/1994	10:00:23	118	85	90	Serr1999	Polarity	Article	Yes
-4.3700	36.9600	007	3.2	mbLg	05/03/1994	15:26:07	230	80	-105	PS1998	Polarity	Article	Yes
-1.8210	37.3310	005	3.0	M	11/03/1994	21:42:00	215	58	-88	RPandDV2001	Polarity	Article	Yes
-2.9700	36.8800	007	2.9	mb	12/03/1994	07:31:31	195	32	51	Metal2006	Polarity	Article	Yes
-4.1400	37.8300	008	3.4	mbLg	23/03/1994	15:10:31	46	83	99	PS1998	Polarity	Article	Yes
-2.8000	36.6200	006	3.5	mbLg	29/03/1994	14:29:02	21	42	-12	PS1998	Polarity	Article	Yes
-3.3600	36.6700	004	3.7	mbLg	29/03/1994	22:04:21	215	71	132	PS1998	Polarity	Article	Yes
-2.5100	37.0600	003	3.1	mbLg	30/03/1994	23:26:44	114	5	-106	PS1998	Polarity	Article	Yes
-2.9500	36.8900	004	2.6	mb	05/04/1994	03:15:15	254	36	-108	Metal2006	Polarity	Article	Yes
-2.0100	37.3700	002	3.9	mbLg	08/04/1994	04:00:04	4	40	-115	PS1998	Polarity	Article	Yes
-2.0400	37.3500	002	3.1	mbLg	08/04/1994	04:13:33	95	70	28	PS1998	Polarity	Article	Yes

-3.1000	41.5500	012	3.4	mbLg	13/04/1994	03:33:03	169	80	-65	PS1998	Polarity	Article	Yes
-7.3600	43.5600	029	4.2	mbLg	15/04/1994	13:26:19	225	58	82	PS1998	Polarity	Article	Yes
-3.6200	37.0300	014	2.5	mb	17/04/1994	11:40:40	91	41	-139	Metal2006	Polarity	Article	Yes
-1.9670	37.3090	021	3.6	M	19/04/1994	23:51:00	355	48	35	RPandDV2001	Polarity	Article	Yes
-2.0400	37.3500	001	3.2	mbLg	20/04/1994	21:23:38	250	48	119	PS1998	Polarity	Article	Yes
-2.9900	36.8800	007	2.6	mb	23/04/1994	12:59:04	328	36	-176	Metal2006	Polarity	Article	Yes
-2.0200	37.3600	002	3.2	mbLg	23/04/1994	17:53:59	190	46	-167	PS1998	Polarity	Article	Yes
-4.2200	37.2400	021	3.0	MbLg	04/05/1994	17:47:22	97	65	-90	Serr1999	Polarity	Article	Yes
-3.9100	35.3700	015	5.9	Mw	26/05/1994	08:27:00	112	48	-173	CMT	Moment tensor inversion	Catalog	Yes
-3.9967	35.2083	009	4.1	MbLg	26/05/1994	12:27:54	185	70	-50	CatMorr2008	Moment tensor inversion	Article	Yes
-3.9083	35.2600	016	3.5	MbLg	28/05/1994	03:32:03	180	50	-50	CatMorr2008	Moment tensor inversion	Article	Yes
-3.8933	35.2417	010	2.8	MbLg	29/05/1994	19:14:06	316	60	-168	CatMorr2008	Moment tensor inversion	Article	Yes
-3.9650	35.3017	011	3.4	MbLg	29/05/1994	23:45:07	199	82	-35	CatMorr2008	Moment tensor inversion	Article	Yes
-3.9917	35.1967	012	3.9	MbLg	01/06/1994	00:53:53	208	64	-54	CatMorr2008	Moment tensor inversion	Article	Yes
-3.9967	35.2367	011	4.6	MbLg	03/06/1994	08:57:39	190	55	30	CatMorr2008	Moment tensor inversion	Article	Yes
-0.3840	38.8870	020	3.1	M	07/06/1994	03:10:00	205	55	155	RPandDV2001	Polarity	Article	Yes
-3.9400	35.2433	009	3.4	MbLg	08/06/1994	03:08:32	8	80	-10	CatMorr2008	Moment tensor inversion	Article	Yes
-2.0400	36.9300	005	3.1	mbLg	12/06/1994	06:31:46	50	80	82	PS1998	Polarity	Article	Yes
-2.9700	36.8800	007	2.5	mb	19/06/1994	05:45:58	47	75	-132	Metal2006	Polarity	Article	Yes
-4.0100	37.0500	012	2.8	mb	20/06/1994	19:26:26	317	85	88	Balanetal2012	Polarity	Article	Yes
-6.9200	37.6300	023	4.3	mbLg	04/07/1994	13:38:47	83	48	-130	PS1998	Polarity	Article	Yes
-3.8200	36.5200	002	3.3	mbLg	13/07/1994	10:12:31	345	5	180	PS1998	Polarity	Article	Yes
-4.2250	37.0450	017	2.9	MbLg	22/07/1994	05:20:20	81	75	-90	Serr1999	Polarity	Article	Yes
-2.5100	36.9900	011	3.3	mbLg	24/07/1994	00:45:22	110	73	100	PS1998	Polarity	Article	Yes
-3.7000	37.0000	012	2.4	mb	26/07/1994	00:10:29	212	61	-173	Metal2006	Polarity	Article	Yes
-1.0600	38.1800	003	3.3	mbLg	04/08/1994	06:43:42	230	48	-145	PS1998	Polarity	Article	Yes
-3.4310	37.0960	009	2.6	md	08/08/1994	20:54:00	90	28	81	Galetal1999	Polarity	Article	Yes
-4.4500	37.1700	007	3.2	mb	10/08/1994	20:05:14	175	90	40	Balanetal2012	Polarity	Article	Yes
-7.2400	36.4600	025	3.5	mbLg	13/08/1994	16:25:18	290	40	-98	PS1998	Polarity	Article	Yes
-0.1420	35.4780	005	5.9	Mw	18/08/1994	01:13:07	40	23	70	CMT	Moment tensor inversion	Catalog	Yes

-1.2400	38.4930	005	3.6	MbLg	25/08/1994	05:15:51	174	39	64	Aletal	Polarity	Article	Yes
-7.7900	36.7200	024	3.3	mbLg	28/08/1994	13:43:12	90	80	-46	PS1998	Polarity	Article	Yes
-5.4000	36.8100	006	3.7	mbLg	06/09/1994	02:00:29	210	63	53	PS1998	Polarity	Article	Yes
-2.0900	38.0840	009	3.0	M	13/09/1994	21:06:00	135	62	159	RPandDV2001	Polarity	Article	Yes
-4.3200	37.0700	005	3.1	mbLg	23/09/1994	15:41:25	249	14	-160	PS1998	Polarity	Article	Yes
-7.8000	36.7000	052	4.3	Ml	24/09/1994	00:00:00	274	70	126	Boretal2001	Polarity	Article	No
4.6700	40.9700	009	4.8	Mw	24/09/1994	17:55:00	206	83	-8	FMHex20	Compilation	Catalog	Yes
2.5500	41.4100	010	4.2	mbLg	26/09/1994	05:38:00	30	30	-34	PS1998	Polarity	Article	Yes
-7.7700	36.7600	027	3.0	mbLg	26/09/1994	20:02:17	19	20	-12	PS1998	Polarity	Article	Yes
-6.1000	36.2300	017	3.0	mbLg	07/10/1994	12:51:17	241	31	104	PS1998	Polarity	Article	Yes
-3.7020	37.0000	016	2.8	md	24/10/1994	03:01:00	296	80	-90	Galetal1999	Polarity	Article	Yes
-2.3500	36.9800	003	4.0	mbLg	08/11/1994	00:17:35	341	17	60	PS1998	Polarity	Article	Yes
-4.0400	37.2300	013	2.6	mb	14/11/1994	14:31:06	143	77	38	Balanetal2012	Polarity	Article	Yes
-1.2710	38.4950	001	3.4	M	28/11/1994	07:30:00	85	20	85	RPandDV2001	Polarity	Article	Yes
-3.0040	37.2690	006	3.5	M	03/12/1994	18:42:00	285	55	-78	RPandDV2001	Polarity	Article	Yes
-3.5890	37.1480	012	3.2	md	06/12/1994	09:28:00	75	45	-125	Galetal1999	Polarity	Article	Yes
-3.8570	36.8980	007	2.9	md	23/12/1994	15:04:00	90	20	-62	Galetal1999	Polarity	Article	Yes
-3.0900	36.0700	001	3.3	mbLg	25/12/1994	12:04:28	169	72	-43	PS1998	Polarity	Article	Yes
-7.7900	36.4900	028	3.6	mbLg	26/12/1994	17:48:22	270	90	0	PS1998	Polarity	Article	Yes
-5.5600	36.7000	003	3.4	mb	07/01/1995	14:46:59	301	37	-40	Balanetal2012	Polarity	Article	Yes
-4.0700	37.8500	005	3.2	mbLg	25/01/1995	20:13:11	320	40	0	PS1998	Polarity	Article	Yes
-5.8200	36.8400	001	3.5	mb	06/02/1995	14:52:01	238	8	0	Balanetal2012	Polarity	Article	Yes
-5.9800	36.7500	015	3.0	mb	07/02/1995	01:58:02	3	48	48	Balanetal2012	Polarity	Article	Yes
-4.1100	35.2900	006	3.5	mb	10/02/1995	20:26:34	238	46	-49	Balanetal2012	Polarity	Article	Yes
-4.2100	36.9900	007	2.5	mb	23/02/1995	23:42:27	18	84	-72	Balanetal2012	Polarity	Article	Yes
-2.6400	37.3100	002	3.2	mbLg	25/02/1995	19:24:25	283	4	-117	PS1998	Polarity	Article	Yes
-7.4800	36.1000	014	3.7	mbLg	05/03/1995	23:46:22	285	40	-180	PS1998	Polarity	Article	Yes
-4.3400	36.8200	056	4.0	M	17/03/1995	13:36:56	100	85	-56	Buetal2004	Polarity	Article	No
-3.7900	37.1600	006	3.9	mbLg	17/03/1995	14:04:14	305	70	-99	PS1998	Polarity	Article	Yes
-2.1330	37.0780	006	3.9	M	18/03/1995	13:40:00	330	50	-110	RPandDV2001	Polarity	Article	Yes

-2.7900	39.6200	001	3.1	mbLg	29/03/1995	16:10:07	243	39	112	PS1998	Polarity	Article	Yes
-6.5300	38.1000	011	3.8	mbLg	30/03/1995	15:54:42	106	81	47	PS1998	Polarity	Article	Yes
-2.8530	38.3720	004	3.5	M	11/04/1995	06:42:00	45	40	62	RPandDV2001	Polarity	Article	Yes
-1.7830	38.5680	008	3.2	M	16/04/1995	13:59:00	215	80	-135	RPandDV2001	Polarity	Article	Yes
-1.7110	38.1730	005	3.0	M	25/04/1995	08:02:00	260	55	-105	RPandDV2001	Polarity	Article	Yes
-2.9700	36.8100	009	2.9	mb	25/04/1995	22:24:22	272	68	48	Metal2006	Polarity	Article	Yes
-2.8300	36.7300	006	3.1	mbLg	29/04/1995	07:37:41	96	30	78	PS1998	Polarity	Article	Yes
1.5100	40.8300	015	4.6	M	15/05/1995	15:37:00	207	83	3	PS1998	Polarity	Article	Yes
-3.0000	36.8200	010	3.2	mb	18/05/1995	23:13:05	358	40	-6	Metal2006	Polarity	Article	Yes
-3.8600	36.8700	006	3.0	mbLg	29/05/1995	16:21:26	320	74	-53	PS1998	Polarity	Article	Yes
-4.1900	37.2500	002	3.1	mbLg	06/06/1995	14:58:49	141	5	11	PS1998	Polarity	Article	Yes
-2.1700	36.9200	008	4.0	mbLg	07/06/1995	16:20:36	5	48	-35	PS1998	Polarity	Article	Yes
-3.8000	37.4500	014	3.4	mbLg	01/07/1995	03:29:07	230	66	109	PS1998	Polarity	Article	Yes
-3.8200	37.4500	020	3.6	mbLg	11/07/1995	18:27:34	285	55	163	PS1998	Polarity	Article	Yes
-4.3700	37.0400	009	3.2	mb	25/08/1995	19:58:07	245	78	-58	Balanetal2012	Polarity	Article	Yes
-4.1200	36.9400	012	2.1	mb	17/09/1995	14:42:22	190	88	-10	Balanetal2012	Polarity	Article	Yes
-4.0700	36.9400	001	3.0	mbLg	18/09/1995	05:14:41	343	20	-150	PS1998	Polarity	Article	Yes
0.3200	38.8000	006	3.8	mbLg	04/10/1995	02:06:07	150	60	-180	PS1998	Polarity	Article	Yes
-4.0500	36.2700	000	2.6	mb	04/10/1995	23:16:50	6	73	69	Balanetal2012	Polarity	Article	Yes
-4.3500	37.0100	005	2.5	mb	09/10/1995	08:30:07	301	41	41	Balanetal2012	Polarity	Article	Yes
-2.7200	36.4000	006	3.4	mbLg	09/11/1995	19:20:53	135	86	81	PS1998	Polarity	Article	Yes
-4.0000	40.5700	012	3.3	M	17/11/1995	00:11:48	305	45	-173	Perezetal2022	Compilation	Article	Yes
-4.0000	40.5700	012	3.3	mbLg	17/11/1995	15:11:48	296	58	174	PS1998	Polarity	Article	Yes
-4.3200	37.0200	052	3.6	M	18/11/1995	00:00:00	238	59	154	Buetal2004	Polarity	Article	No
-2.5300	36.9700	003	4.0	mbLg	18/11/1995	00:24:47	130	80	-46	PS1998	Polarity	Article	Yes
-4.3170	37.0170	052	3.6	MbLg	18/11/1995	08:23:38	226	58	67	Serr1999	Polarity	Article	No
-4.4900	37.0200	008	2.3	mb	23/11/1995	02:33:20	86	72	58	Balanetal2012	Polarity	Article	Yes
-1.2300	38.0000	002	4.1	mbLg	26/11/1995	05:39:40	35	87	86	PS1998	Polarity	Article	Yes
-1.2600	38.0200	001	3.7	mbLg	26/11/1995	06:25:05	235	72	-107	PS1998	Polarity	Article	Yes
-4.3800	37.1800	008	1.7	mb	27/11/1995	21:54:18	317	22	-63	Balanetal2012	Polarity	Article	No

-4.3700	37.1900	009	2.0	mb	27/11/1995	23:18:20	289	10	-90	Balanetal2012	Polarity	Article	Yes
-4.4000	37.1800	007	2.0	mb	27/11/1995	23:55:42	112	51	-77	Balanetal2012	Polarity	Article	Yes
-4.3780	36.6970	068	3.5	MbLg	28/11/1995	13:55:30	230	45	110	Serr1999	Polarity	Article	No
-0.7400	35.3200	008	4.7	Mw	29/11/1995	00:25:08	2	39	-42	Setal2003a	Moment tensor inversion	Article	Yes
-7.3200	42.8300	010	4.6	mbLg	29/11/1995	23:56:29	357	61	-148	PS1998	Polarity	Article	Yes
-7.3100	42.8200	010	3.8	mbLg	30/11/1995	02:20:34	336	47	-109	PS1998	Polarity	Article	Yes
-4.5230	36.8080	056	3.1	MbLg	05/12/1995	04:12:06	252	82	-85	Serr1999	Polarity	Article	No
-1.2700	38.0000	007	3.6	mbLg	06/12/1995	10:13:30	200	48	61	PS1998	Polarity	Article	Yes
-2.9500	36.9000	004	3.4	mb	13/12/1995	05:55:32	217	33	-101	Metal2006	Polarity	Article	Yes
-3.7600	37.4600	024	3.3	mbLg	18/12/1995	03:47:15	270	90	180	PS1998	Polarity	Article	Yes
-7.1700	42.8200	016	3.7	mbLg	24/12/1995	15:49:42	351	37	-145	PS1998	Polarity	Article	Yes
-4.3200	36.9500	007	2.2	mb	08/02/1996	14:12:46	10	75	1	Balanetal2012	Polarity	Article	Yes
2.5300	42.8000	008	5.3	mbLg	18/02/1996	01:45:45	150	45	173	PS1998	Polarity	Article	Yes
2.5500	42.7900	010	3.7	Ml	19/02/1996	00:00:00	320	77	88	Rigo2015	Compilation	Article	Yes
2.5100	42.7800	009	3.1	Ml	20/02/1996	00:00:00	306	44	72	Rigo2015	Compilation	Article	Yes
2.5400	42.7900	008	3.0	Ml	21/02/1996	00:00:00	50	61	-20	Rigo2015	Compilation	Article	Yes
2.5400	42.7900	009	3.5	Ml	22/02/1996	00:00:00	14	61	10	Rigo2015	Compilation	Article	Yes
2.5200	42.7900	009	3.6	Ml	23/02/1996	00:00:00	300	46	66	Rigo2015	Compilation	Article	Yes
-4.2400	37.0300	008	2.2	mb	24/02/1996	15:23:46	354	90	60	Balanetal2012	Polarity	Article	Yes
-4.3500	36.9400	009	2.1	mb	09/03/1996	13:01:03	91	79	72	Balanetal2012	Polarity	Article	Yes
-1.4120	37.8800	005	3.5	MbLg	22/03/1996	09:22:03	271	52	-132	Aletal	Polarity	Article	Yes
-4.3200	36.9500	008	2.1	mb	22/03/1996	17:55:02	165	80	28	Balanetal2012	Polarity	Article	Yes
4.7260	43.9140	006	3.6	Mw	25/03/1996	04:27:00	191	58	-29	FMHex20	Compilation	Catalog	Yes
-4.6600	37.6100	008	4.3	mb	16/04/1996	22:44:00	75	76	-179	MandR1997	Polarity	Article	Yes
-8.5440	37.1070	012	2.6	Ml	23/04/1996	00:00:00	301	90	-179	Bezzetal2012	Compilation	Article	Yes
-4.6700	35.2100	009	3.8	mb	18/06/1996	13:58:53	287	32	-86	Balanetal2012	Polarity	Article	Yes
-4.1900	37.0100	010	2.6	mb	20/06/1996	09:26:54	37	50	0	Balanetal2012	Polarity	Article	Yes
-4.2100	37.0000	009	2.8	mb	20/06/1996	18:33:22	169	45	-76	Balanetal2012	Polarity	Article	Yes
-4.1900	37.0000	008	2.0	mb	22/06/1996	02:43:41	56	51	-8	Balanetal2012	Polarity	Article	Yes
-4.4500	36.7100	068	3.9	M	22/06/1996	20:34:00	120	58	172	Bezzetal2012	Compilation	Article	No

-3.0000	36.8600	009	2.4	mb	23/06/1996	06:22:23	348	51	-15	Metal2006	Polarity	Article	Yes
-8.8180	37.3540	005	3.4	Ml	08/07/1996	00:00:00	81	90	179	Bezzetal2012	Compilation	Article	Yes
-8.4790	37.3390	009	2.2	Ml	17/07/1996	00:00:00	196	78	74	Bezzetal2012	Compilation	Article	Yes
-4.4000	36.9700	007	1.9	mb	02/08/1996	10:30:21	89	78	84	Balanetal2012	Polarity	Article	No
-1.4800	40.4700	010	4.0	Mw	03/08/1996	10:06:26	146	51	-56	Setal2003a	Moment tensor inversion	Article	Yes
-7.9420	37.0740	022	2.4	Ml	30/08/1996	00:00:00	39	65	102	Bezzetal2012	Compilation	Article	Yes
-1.6320	37.5700	010	4.4	Mw	02/09/1996	19:07:02	44	35	-8	Setal2003a	Moment tensor inversion	Article	Yes
2.8800	36.9800	014	5.5	Mw	04/09/1996	04:14:03	260	70	108	Setal2003a	Moment tensor inversion	Article	Yes
-3.3800	36.8100	007	2.4	mb	18/09/1996	21:25:15	158	32	-27	Metal2006	Polarity	Article	Yes
-4.3800	37.1800	014	2.5	mb	10/10/1996	01:37:12	13	73	-58	Balanetal2012	Polarity	Article	Yes
-4.3600	37.1800	008	2.1	mb	10/10/1996	12:15:21	183	84	40	Balanetal2012	Polarity	Article	Yes
-1.8700	37.4750	001	3.9	MbLg	22/10/1996	18:26:06	43	39	135	Aletal	Polarity	Article	Yes
-4.6500	36.5600	059	3.8	M	27/12/1996	00:00:00	60	60	49	Buetal2004	Polarity	Article	No
-3.7130	37.1540	012	3.9	Mw	28/12/1996	07:30:36	200	30	-36	Setal2003a	Moment tensor inversion	Article	Yes
-7.8000	38.7000	013	3.6	Ml	19/01/1997	00:00:00	101	59	172	Boretal2001	Polarity	Article	Yes
-3.8340	37.0260	016	4.3	Mw	24/02/1997	07:09:50	302	86	-90	Setal2003a	Moment tensor inversion	Article	Yes
-3.6700	37.0200	012	2.3	mb	27/02/1997	03:10:03	212	75	-12	Metal2006	Polarity	Article	Yes
-4.2300	36.9600	056	3.7	M	18/03/1997	00:00:00	43	34	87	Buetal2004	Polarity	Article	No
-4.3800	37.2100	013	2.5	mb	18/03/1997	14:30:55	303	41	-75	Balanetal2012	Polarity	Article	Yes
-4.0400	37.2400	015	2.8	mb	22/03/1997	00:00:00	182	17	44	Balanetal2012	Polarity	Article	Yes
-3.6800	37.0300	013	2.5	mb	02/05/1997	15:54:37	214	71	-156	Metal2006	Polarity	Article	Yes
-7.1900	42.8800	010	5.2	Mw	21/05/1997	23:50:43	129	61	-123	Setal2003a	Moment tensor inversion	Article	Yes
-7.1600	42.8600	008	4.8	Mw	22/05/1997	00:17:17	141	51	-112	Setal2003a	Moment tensor inversion	Article	Yes
-7.1700	42.8900	010	4.3	Mw	22/05/1997	05:06:50	159	52	-93	Setal2003a	Moment tensor inversion	Article	Yes
-7.7170	37.4370	027	2.7	Ml	11/06/1997	00:00:00	71	65	-153	Bezzetal2012	Compilation	Article	Yes
-4.3300	37.0600	009	3.1	mb	16/06/1997	13:02:35	80	54	37	Balanetal2012	Polarity	Article	Yes
-3.2350	36.3710	006	4.5	Mw	02/07/1997	09:38:41	134	68	-165	Setal2003a	Moment tensor inversion	Article	Yes
-3.2550	36.3670	010	4.4	Mw	02/07/1997	12:53:05	131	73	-167	Setal2003a	Moment tensor inversion	Article	Yes
-3.2430	36.3530	008	4.0	Mw	02/07/1997	17:33:05	135	63	-178	Setal2003a	Moment tensor inversion	Article	Yes
-3.2290	36.3620	010	4.0	Mw	03/07/1997	20:23:11	132	80	-161	Setal2003a	Moment tensor inversion	Article	Yes

-8.6560	37.3050	018	2.6	Ml	05/07/1997	00:00:00	276	90	-125	Bezzetal2012	Compilation	Article	Yes
1.1700	35.9400	010	4.7	mb	14/07/1997	15:49:51	23	45	56	RCMT	Moment tensor inversion	Catalog	Yes
2.7800	42.5700	006	3.2	Ml	07/08/1997	00:00:00	88	41	76	Rigo2015	Compilation	Article	Yes
-3.2380	36.4520	016	3.6	Mw	07/08/1997	19:17:26	212	82	20	Setal2003a	Moment tensor inversion	Article	Yes
-4.2700	36.9900	009	2.8	mb	15/08/1997	02:38:42	196	56	-53	Balanetal2012	Polarity	Article	Yes
-3.0900	36.8700	009	2.8	mb	18/08/1997	22:30:08	84	24	-90	Metal2006	Polarity	Article	Yes
-4.6900	36.4500	090	4.0	Mw	20/08/1997	02:44:00	43	14	38	IAG	Moment tensor inversion	Catalog	No
-3.7000	36.9900	016	2.7	mb	27/09/1997	10:09:52	253	27	-62	Metal2006	Polarity	Article	Yes
-3.0220	36.0130	004	3.8	Mw	13/10/1997	21:50:18	117	71	-133	Setal2003a	Moment tensor inversion	Article	Yes
4.8910	43.9060	006	3.6	Mw	09/02/1998	14:16:00	24	73	-102	FMHex20	Compilation	Catalog	Yes
-8.5310	37.3340	012	3.2	Ml	04/03/1998	00:00:00	93	72	179	Bezzetal2012	Compilation	Article	Yes
-4.3300	36.1700	029	3.5	mb	25/03/1998	05:04:12	28	84	-76	Balanetal2012	Polarity	Article	Yes
-1.7920	37.0120	008	3.9	Mw	06/04/1998	00:11:18	21	58	17	Setal2003a	Moment tensor inversion	Article	Yes
-4.2800	37.2200	014	2.7	mb	12/04/1998	09:51:56	31	82	-41	Balanetal2012	Polarity	Article	Yes
-4.2500	37.2100	009	2.7	mb	12/04/1998	11:09:01	328	83	-51	Balanetal2012	Polarity	Article	Yes
-4.2700	37.2200	015	3.1	mb	12/04/1998	12:36:01	261	9	-71	Balanetal2012	Polarity	Article	Yes
-4.2900	37.2200	015	3.2	mb	12/04/1998	12:52:39	21	70	-4	Balanetal2012	Polarity	Article	Yes
-4.2600	37.2100	012	2.5	mb	12/04/1998	12:58:34	42	75	-48	Balanetal2012	Polarity	Article	Yes
-4.3500	37.2200	010	3.6	mb	12/04/1998	13:10:36	199	84	40	Balanetal2012	Polarity	Article	Yes
-4.3100	37.2200	014	3.6	mb	12/04/1998	15:15:17	22	80	-2	Balanetal2012	Polarity	Article	Yes
-4.2500	37.2100	012	3.3	mb	12/04/1998	22:14:08	148	44	22	Balanetal2012	Polarity	Article	Yes
-4.2100	37.2100	011	2.6	mb	12/04/1998	22:35:37	304	75	81	Balanetal2012	Polarity	Article	Yes
-4.2500	37.2000	012	3.2	mb	13/04/1998	03:55:32	142	53	16	Balanetal2012	Polarity	Article	Yes
-4.2200	37.2000	011	2.8	mb	13/04/1998	04:44:58	307	76	82	Balanetal2012	Polarity	Article	Yes
-4.2700	37.2100	010	2.6	mb	13/04/1998	05:33:34	41	86	-48	Balanetal2012	Polarity	Article	Yes
-4.2400	37.2100	012	2.7	mb	13/04/1998	05:49:26	37	78	-28	Balanetal2012	Polarity	Article	Yes
-4.2600	37.2200	014	3.6	Mw	13/04/1998	05:55:41	346	61	-21	Setal2003a	Moment tensor inversion	Article	Yes
-4.2780	37.2200	014	3.6	Mw	13/04/1998	13:50:52	335	55	-20	Setal2003a	Moment tensor inversion	Article	Yes
-4.2500	37.2200	011	3.1	mb	13/04/1998	15:25:05	204	90	18	Balanetal2012	Polarity	Article	Yes
-4.2600	37.2100	012	3.1	mb	13/04/1998	17:59:38	259	10	-90	Balanetal2012	Polarity	Article	Yes

-4.2100	37.2200	012	3.5	Mw	14/04/1998	02:13:03	88	69	-145	Setal2003a	Moment tensor inversion	Article	Yes
-4.2400	37.2100	010	2.6	mb	14/04/1998	04:08:04	42	87	-20	Balanetal2012	Polarity	Article	Yes
-4.2400	37.2100	012	2.6	mb	14/04/1998	08:26:58	37	78	-28	Balanetal2012	Polarity	Article	Yes
-4.2600	37.2100	012	2.5	mb	15/04/1998	09:19:31	42	75	-48	Balanetal2012	Polarity	Article	Yes
-4.2000	37.2000	013	3.3	mb	17/04/1998	19:56:19	33	86	-25	Balanetal2012	Polarity	Article	Yes
-4.2000	37.1900	009	2.6	mb	18/04/1998	04:15:59	195	75	13	Balanetal2012	Polarity	Article	Yes
-4.2000	37.2000	012	3.0	mb	20/04/1998	05:06:11	278	84	40	Balanetal2012	Polarity	Article	Yes
-4.2200	37.2000	013	3.2	mb	20/04/1998	23:03:54	34	75	17	Balanetal2012	Polarity	Article	Yes
-4.2300	37.1000	004	2.6	mb	22/04/1998	09:43:39	48	32	-67	Balanetal2012	Polarity	Article	Yes
-4.2300	37.2100	012	2.5	mb	23/04/1998	18:26:04	136	89	1	Balanetal2012	Polarity	Article	Yes
-8.6480	36.9110	023	2.3	Ml	24/04/1998	00:00:00	332	90	36	Bezzetal2012	Compilation	Article	Yes
-4.2800	37.2500	013	3.0	mb	18/05/1998	06:19:02	128	79	-72	Balanetal2012	Polarity	Article	Yes
-3.6000	37.1800	010	3.1	mb	04/06/1998	17:38:16	70	25	-90	Metal2006	Polarity	Article	Yes
-3.6000	37.1900	010	2.5	mb	04/06/1998	19:28:51	158	70	-101	Metal2006	Polarity	Article	Yes
-3.5900	37.1900	010	3.0	mb	12/06/1998	06:31:41	123	40	180	Metal2006	Polarity	Article	Yes
-4.1300	37.0800	010	2.5	mb	17/07/1998	06:08:51	308	77	-12	Balanetal2012	Polarity	Article	Yes
-7.1700	42.8700	010	4.0	Mw	17/07/1998	08:29:04	152	62	-98	Setal2003a	Moment tensor inversion	Article	Yes
-1.6900	40.4500	020	3.6	Mw	25/07/1998	00:11:51	145	58	-83	Setal2003a	Moment tensor inversion	Article	Yes
-7.9000	38.8000	005	4.0	Ml	31/07/1998	00:00:00	95	70	180	Boretal2001	Polarity	Article	Yes
-4.2700	37.2100	013	3.1	mb	15/08/1998	16:03:42	253	49	57	Balanetal2012	Polarity	Article	Yes
-2.6430	36.9490	020	3.6	Mw	16/10/1998	09:46:46	85	54	131	Setal2003a	Moment tensor inversion	Article	Yes
-3.7760	34.8440	006	3.9	Mw	20/10/1998	23:47:03	116	54	-118	Setal2003a	Moment tensor inversion	Article	Yes
-0.2100	38.2100	008	3.7	Mw	14/11/1998	03:09:46	42	66	34	Setal2003a	Moment tensor inversion	Article	Yes
-3.7930	36.9900	008	4.1	Mw	18/11/1998	23:18:10	134	66	-63	Setal2003a	Moment tensor inversion	Article	Yes
-0.0970	35.4610	004	4.4	Mw	10/12/1998	17:01:09	79	24	145	Setal2003a	Moment tensor inversion	Article	Yes
-4.3700	35.7600	023	2.9	mb	30/12/1998	22:35:18	138	7	-56	Balanetal2012	Polarity	Article	Yes
-1.4900	38.1100	008	4.8	Mw	02/02/1999	13:45:17	41	69	-26	Setal2003a	Moment tensor inversion	Article	Yes
-1.5100	38.0800	003	4.1	mb	02/02/1999	17:13:18	150	58	143	Buetal2005	Polarity	Article	Yes
-1.5200	38.0600	003	4.3	mb	03/02/1999	02:02:30	333	47	-25	Buetal2005	Polarity	Article	Yes
-3.6700	37.0400	018	3.3	mb	11/02/1999	05:43:38	214	71	-156	Metal2006	Polarity	Article	Yes

-8.4750	37.2610	022	2.2	Ml	13/02/1999	11:25:39	46	88	-52	Cetal2004	Polarity	Article	Yes
-3.0300	36.8400	003	2.6	mb	21/03/1999	19:01:01	289	61	-174	Metal2006	Polarity	Article	Yes
-8.4750	37.3340	012	2.0	Ml	12/04/1999	11:40:39	186	81	-44	Cetal2004	Polarity	Article	Yes
-8.9600	39.7200	016	4.0	Mw	30/04/1999	09:00:35	348	51	-39	Setal2003a	Moment tensor inversion	Article	Yes
-2.7400	36.2100	006	3.9	Mw	29/05/1999	11:30:49	327	49	-36	Setal2003a	Moment tensor inversion	Article	Yes
-4.2200	36.9900	009	2.5	mb	04/06/1999	23:34:23	49	62	-11	Balanetal2012	Polarity	Article	Yes
-3.7300	37.2200	006	3.8	mb	07/06/1999	10:03:13	147	57	-62	Metal2006	Polarity	Article	Yes
-8.5510	37.3220	008	1.9	Ml	11/06/1999	23:54:39	347	79	-9	Cetal2004	Polarity	Article	No
-2.7400	36.2100	006	4.5	Mw	14/06/1999	00:00:00	327	49	-35	Setal2003a	Moment tensor inversion	Article	Yes
-2.1740	37.3380	008	3.7	Mw	14/06/1999	21:18:30	18	88	41	Setal2003a	Moment tensor inversion	Article	Yes
-4.0700	36.9900	009	2.5	mb	13/07/1999	10:38:52	195	27	62	Balanetal2012	Polarity	Article	Yes
-1.8300	42.8000	006	2.5	Ml	17/07/1999	00:00:00	330	65	-139	Ruiz2006	Polarity	Article	Yes
-4.0950	35.2430	010	3.9	Mw	18/07/1999	17:26:47	118	83	-149	Setal2003a	Moment tensor inversion	Article	Yes
-7.8690	37.1910	005	2.3	Ml	29/07/1999	04:01:39	178	61	-1	Cetal2004	Polarity	Article	Yes
-5.1690	35.5750	010	4.3	Mw	04/08/1999	09:02:54	263	55	-89	Setal2003a	Moment tensor inversion	Article	Yes
-1.6900	38.1800	006	3.8	Mw	14/08/1999	06:57:02	331	57	-169	Setal2003a	Moment tensor inversion	Article	Yes
0.6000	42.9000	010	4.2	Mw	04/10/1999	18:14:26	141	38	-48	Setal2003a	Moment tensor inversion	Article	Yes
-8.5620	37.3320	015	2.0	Ml	21/10/1999	14:46:39	184	87	-23	Cetal2004	Polarity	Article	Yes
-4.6300	35.6800	110	4.2	Mw	10/11/1999	13:10:12	146	35	150	IAG	Moment tensor inversion	Catalog	No
-1.2810	35.3210	008	5.7	Mw	22/12/1999	17:36:56	59	21	118	Setal2003a	Moment tensor inversion	Article	Yes
-5.0400	36.7600	005	2.8	mb	22/12/1999	19:12:25	275	48	-48	Balanetal2012	Polarity	Article	Yes
-2.9800	36.8500	005	3.3	mb	19/02/2000	20:05:09	117	75	-46	Metal2006	Polarity	Article	Yes
-7.3050	36.6700	019	3.7	Ml	27/03/2000	21:51:39	250	64	72	Cetal2004	Polarity	Article	Yes
-8.5970	37.2010	011	2.1	Ml	18/04/2000	19:43:39	210	81	-36	Cetal2004	Polarity	Article	Yes
-8.0560	36.7820	027	2.7	Ml	26/04/2000	12:06:39	356	80	23	Cetal2004	Polarity	Article	Yes
-3.1310	36.3620	016	3.6	Mw	27/05/2000	07:49:54	30	78	-13	Setal2003a	Moment tensor inversion	Article	Yes
-5.7400	36.9900	011	3.7	mb	14/06/2000	12:19:58	283	71	-52	Balanetal2012	Polarity	Article	Yes
1.3720	36.0220	004	4.5	Mw	02/07/2000	05:36:24	68	7	113	Setal2003a	Moment tensor inversion	Article	Yes
-7.9690	36.4480	006	4.1	Mw	05/07/2000	09:26:48	220	64	26	Setal2003a	Moment tensor inversion	Article	Yes
-4.0000	37.0600	013	2.8	mb	19/07/2000	02:28:33	190	30	-90	Balanetal2012	Polarity	Article	Yes

-7.3340	36.6460	021	2.7	Ml	30/07/2000	17:12:39	226	70	84	Cetal2004	Polarity	Article	Yes
-1.7700	37.6600	004	3.7	Mw	02/08/2000	09:01:39	54	62	102	Setal2003a	Moment tensor inversion	Article	Yes
-3.5470	35.9520	014	3.8	Mw	13/08/2000	23:17:59	130	75	-138	Setal2003a	Moment tensor inversion	Article	Yes
4.9720	36.1960	004	5.4	Mw	18/08/2000	18:15:06	238	88	95	Setal2003a	Moment tensor inversion	Article	Yes
-1.5830	35.5130	006	4.0	Mw	23/08/2000	00:42:06	45	19	99	Setal2003a	Moment tensor inversion	Article	Yes
-5.1200	34.3800	010	4.6	mb	27/09/2000	03:07:45	249	14	45	RCMT	Moment tensor inversion	Catalog	Yes
-1.1500	43.1300	013	1.9	Ml	23/10/2000	15:37:00	75	85	31	Ruiz2006	Polarity	Article	No
4.7730	36.6010	006	5.7	Mw	10/11/2000	20:10:53	251	70	97	Setal2003a	Moment tensor inversion	Article	Yes
4.7250	36.6180	004	4.9	Mw	10/11/2000	22:09:20	121	88	-98	Setal2003a	Moment tensor inversion	Article	Yes
4.8400	36.4700	010	4.5	mb	10/11/2000	23:16:28	238	45	122	RCMT	Moment tensor inversion	Catalog	Yes
4.7590	36.6580	004	5.2	Mw	16/11/2000	11:33:09	254	87	88	Setal2003a	Moment tensor inversion	Article	Yes
-3.7180	35.6310	006	3.9	Mw	28/11/2000	03:31:04	212	71	-54	Setal2003a	Moment tensor inversion	Article	Yes
-1.1700	43.0900	009	1.9	Ml	02/12/2000	00:00:00	165	40	-10	Ruiz2006	Polarity	Article	No
-1.5640	43.0970	008	2.8	Mw	10/12/2000	07:48:00	70	65	-90	FMHex20	Compilation	Catalog	Yes
-5.1700	35.8200	005	3.7	mb	13/12/2000	08:09:03	5	56	48	Balanetal2012	Polarity	Article	Yes
-1.0580	43.1320	016	2.7	Mw	18/01/2001	02:23:00	95	85	140	FMHex20	Compilation	Catalog	Yes
-1.4530	43.1310	018	3.3	Mw	01/02/2001	17:04:00	40	60	160	FMHex20	Compilation	Catalog	Yes
-1.3850	43.0160	009	3.5	Mw	03/02/2001	04:03:00	245	90	150	FMHex20	Compilation	Catalog	Yes
-1.6550	43.0980	012	2.8	Mw	10/02/2001	12:39:00	105	45	-31	FMHex20	Compilation	Catalog	Yes
-7.7000	42.7100	012	3.7	Mw	20/05/2001	01:39:10	285	80	-158	Setal2003a	Moment tensor inversion	Article	Yes
-1.7440	42.8770	000	2.5	Mw	02/06/2001	01:11:00	110	70	-10	FMHex20	Compilation	Catalog	Yes
-1.7440	42.8740	000	3.1	Mw	02/06/2001	02:33:00	110	70	-10	FMHex20	Compilation	Catalog	Yes
-3.9330	35.4970	008	4.0	Mw	08/06/2001	13:47:32	128	71	-157	Setal2003a	Moment tensor inversion	Article	Yes
-5.5400	34.2100	010	4.5	mb	28/06/2001	15:21:44	206	15	94	RCMT	Moment tensor inversion	Catalog	Yes
-2.2800	38.1500	008	3.7	Mw	16/07/2001	20:15:45	270	73	170	Setal2003a	Moment tensor inversion	Article	Yes
-4.1100	37.1100	019	3.0	mb	21/07/2001	00:02:02	98	82	50	Balanetal2012	Polarity	Article	Yes
-0.0800	38.8300	008	4.0	Mw	23/09/2001	04:33:48	49	89	-39	Setal2003a	Moment tensor inversion	Article	Yes
-0.1200	38.8300	005	3.4	Mw	23/09/2001	10:04:00	168	41	131	EMMA	Compilation	Catalog	Yes
-0.1400	38.8500	005	3.3	Mw	05/10/2001	00:50:00	193	44	118	EMMA	Compilation	Catalog	Yes
0.0720	43.0050	012	2.9	Mw	12/11/2001	00:00:00	96	87	-113	FMHex20	Compilation	Catalog	Yes

0.4600	37.9500	000	3.9	Mw	06/12/2001	13:24:00	49	26	57	EMMA	Compilation	Catalog	Yes
-0.3200	43.0740	011	2.8	Mw	05/01/2002	03:36:11	201	34	162	FMHex20	Compilation	Catalog	Yes
-0.3830	43.0770	008	2.5	Mw	05/01/2002	22:01:02	26	48	3	FMHex20	Compilation	Catalog	Yes
-0.0850	43.0000	008	2.8	Mw	13/01/2002	10:03:42	160	73	61	FMHex20	Compilation	Catalog	Yes
-2.5470	37.0910	010	4.7	Mw	04/02/2002	20:09:30	348	57	-88	Setal2003a	Moment tensor inversion	Article	Yes
-1.8600	42.9300	002	2.5	Mw	21/02/2002	10:21:00	70	70	10	FMHex20	Compilation	Catalog	Yes
-1.8350	42.9240	003	4.6	Mw	25/02/2002	12:41:00	150	75	-40	FMHex20	Compilation	Catalog	Yes
-1.8460	42.9250	002	2.9	Mw	26/02/2002	02:34:00	55	70	-140	FMHex20	Compilation	Catalog	Yes
-1.8330	42.9260	002	3.1	Mw	27/02/2002	06:13:00	40	75	-100	FMHex20	Compilation	Catalog	Yes
-1.8360	42.9270	002	3.3	Mw	27/02/2002	06:17:00	135	60	-70	FMHex20	Compilation	Catalog	Yes
-1.8330	42.9250	002	3.5	Mw	27/02/2002	08:44:00	75	65	-150	FMHex20	Compilation	Catalog	Yes
-1.8310	42.9240	002	2.6	Mw	27/02/2002	13:38:00	130	30	0	FMHex20	Compilation	Catalog	Yes
-1.8360	42.9230	001	3.3	Mw	27/02/2002	19:13:00	75	85	111	FMHex20	Compilation	Catalog	Yes
-1.8250	42.9260	002	3.1	Mw	03/03/2002	00:43:00	110	25	-70	FMHex20	Compilation	Catalog	Yes
-1.8460	42.9270	001	3.0	Mw	15/03/2002	08:20:00	10	70	100	FMHex20	Compilation	Catalog	Yes
-1.8480	42.9250	001	3.3	Mw	16/03/2002	03:44:00	110	50	-69	FMHex20	Compilation	Catalog	Yes
-1.8300	42.9180	002	2.9	Mw	18/03/2002	15:18:00	60	70	-120	FMHex20	Compilation	Catalog	Yes
-0.2310	43.0810	015	3.9	Mw	19/03/2002	00:00:00	197	43	143	FMHex20	Compilation	Catalog	Yes
-1.8270	42.9250	002	2.5	Mw	19/03/2002	09:28:00	145	70	-41	FMHex20	Compilation	Catalog	Yes
-8.2000	38.7000	013	3.7	Ml	20/03/2002	00:00:00	284	41	-149	Bezzetal2012	Compilation	Article	Yes
-0.3730	43.0650	004	2.9	Mw	22/03/2002	03:58:58	298	64	-118	FMHex20	Compilation	Catalog	Yes
-9.3600	37.9900	020	3.8	Mw	28/03/2002	04:09:23	255	72	132	Setal2006	Moment tensor inversion	Article	Yes
-0.1000	43.0500	013	1.5	Ml	10/04/2002	00:00:00	208	53	164	Rigo2015	Compilation	Article	No
-0.1010	43.0480	013	3.3	Mw	10/04/2002	19:17:55	208	53	165	FMHex20	Compilation	Catalog	Yes
-0.1900	43.0100	008	1.8	Ml	18/04/2002	00:00:00	101	74	105	Rigo2015	Compilation	Article	No
-0.1950	43.0120	009	2.5	Mw	18/04/2002	12:02:53	101	74	105	FMHex20	Compilation	Catalog	Yes
-0.1000	43.0500	014	2.3	Ml	22/04/2002	00:00:00	68	71	-9	Rigo2015	Compilation	Article	Yes
-0.1040	43.0470	014	2.7	Mw	22/04/2002	19:32:14	68	71	-9	FMHex20	Compilation	Catalog	Yes
-0.2270	43.0680	006	3.1	Mw	05/05/2002	00:00:00	308	90	51	FMHex20	Compilation	Catalog	Yes
-0.1160	43.0390	012	2.5	Mw	12/05/2002	06:40:00	351	81	-134	FMHex20	Compilation	Catalog	Yes

-0.0800	43.0700	015	1.1	Ml	15/05/2002	00:00:00	249	78	-166	Rigo2015	Compilation	Article	No
-0.0840	43.0740	015	2.5	Mw	15/05/2002	01:11:42	249	78	-168	FMHex20	Compilation	Catalog	Yes
0.1700	43.0200	011	1.4	Ml	16/05/2002	00:00:00	63	47	-100	Rigo2015	Compilation	Article	No
0.1740	43.0190	011	4.4	Mw	16/05/2002	04:12:00	63	47	-101	FMHex20	Compilation	Catalog	Yes
-0.1480	42.9210	009	4.5	Ml	16/05/2002	14:56:34	120	80	-105	Chevrot (2011)	Moment tensor inversion	Article	Yes
-0.1460	42.9280	008	4.2	Ml	16/05/2002	15:14:45	130	70	-90	Chevrot (2011)	Moment tensor inversion	Article	Yes
0.1400	42.9800	011	3.7	Ml	19/05/2002	00:00:00	121	75	-121	Rigo2015	Compilation	Article	Yes
0.1370	42.9810	011	4.4	Mw	19/05/2002	04:44:00	121	75	-121	FMHex20	Compilation	Catalog	Yes
-3.5900	37.0100	013	2.8	mb	20/06/2002	13:49:53	12	76	153	Metal2006	Polarity	Article	Yes
-3.7900	37.7300	002	3.7	mb	24/06/2002	04:26:52	60	45	90	SGandT2002	Polarity	Article	Yes
-3.7700	37.7300	003	3.4	mb	24/06/2002	10:50:06	246	49	111	SGandT2002	Polarity	Article	Yes
-4.0300	35.6300	014	3.8	Mw	27/06/2002	13:29:50	132	55	-143	Setal2006	Moment tensor inversion	Article	Yes
-3.9200	35.6300	018	4.2	Mw	06/07/2002	17:24:19	132	52	-135	Setal2006	Moment tensor inversion	Article	Yes
-1.8000	37.9000	004	4.5	M	06/08/2002	00:00:00	16	84	-11	Buetal2016	Compilation	Article	Yes
1.8260	37.8950	006	4.5	Mw	06/08/2002	06:16:19	119	68	-140	Setal2006	Moment tensor inversion	Article	Yes
-1.8200	37.9100	008	5.0	Mw	06/08/2002	06:16:19	119	68	-140	Benietal2007	Moment tensor inversion	Article	Yes
-1.8100	37.8900	006	3.9	Mw	06/08/2002	11:55:16	115	73	-122	Benietal2007	Moment tensor inversion	Article	Yes
-1.8100	37.8900	006	3.9	Mw	06/08/2002	11:55:17	115	73	-122	Setal2006	Moment tensor inversion	Article	Yes
-1.8300	37.9100	008	2.7	Mw	06/08/2002	19:25:06	328	40	-94	Buetal2005	Polarity	Article	Yes
-1.8200	37.8500	006	3.5	Mw	06/08/2002	19:25:07	153	50	-87	Buetal2005	Polarity	Article	Yes
-1.8400	37.8700	006	4.0	Mw	06/08/2002	23:09:08	188	90	-1	Buetal2005	Polarity	Article	Yes
-1.8000	37.9000	004	4.7	M	07/08/2002	00:00:00	25	84	-38	Buetal2016	Compilation	Article	Yes
-1.8300	37.8600	006	3.5	Mw	07/08/2002	00:43:56	120	74	-124	Benietal2007	Moment tensor inversion	Article	Yes
-1.8400	37.8600	006	4.0	Mw	07/08/2002	23:09:07	130	70	-122	Benietal2007	Moment tensor inversion	Article	Yes
-4.5600	36.4600	070	4.2	Mw	24/08/2002	00:00:00	96	21	165	RuizCetal2011	Compilation	Article	No
-4.5600	36.4600	070	4.2	Mw	24/08/2002	10:08:07	96	21	165	Setal2006	Moment tensor inversion	Article	No
-0.3940	43.0830	009	4.0	Ml	05/09/2002	20:42:15	130	5	-70	Chevrot (2011)	Moment tensor inversion	Article	Yes
-0.3960	43.0780	010	4.0	Mw	05/09/2002	20:49:11	291	87	-112	FMHex20	Compilation	Catalog	Yes
-5.2700	37.1600	004	4.1	Mw	15/09/2002	00:00:00	273	68	58	RuizCetal2011	Compilation	Article	Yes
-5.2700	37.1600	004	4.1	Mw	15/09/2002	20:54:19	273	68	58	Setal2006	Moment tensor inversion	Article	Yes

-7.4700	36.1900	006	5.0	Mw	10/12/2002	13:51:26	35	75	90	Setal2006	Moment tensor inversion	Article	Yes
-0.3640	43.0900	008	4.2	Ml	11/12/2002	20:09:51	130	45	-65	Chevrot (2011)	Moment tensor inversion	Article	Yes
-0.2720	43.0800	009	4.6	Ml	12/12/2002	17:59:50	175	30	-25	Chevrot (2011)	Moment tensor inversion	Article	Yes
2.9100	36.1300	002	4.9	Mw	01/01/2003	00:55:55	58	16	28	Setal2006	Moment tensor inversion	Article	Yes
-6.0000	41.5300	010	3.8	Mw	12/01/2003	15:56:35	277	78	-179	Setal2006	Moment tensor inversion	Article	Yes
-0.3330	43.0640	009	4.3	Ml	21/01/2003	18:01:00	120	45	-75	Chevrot (2011)	Moment tensor inversion	Article	Yes
-6.0100	41.5400	012	4.2	Mw	23/01/2003	10:13:18	102	88	165	Setal2006	Moment tensor inversion	Article	Yes
-4.7000	37.7400	012	4.2	Mw	24/01/2003	20:35:00	58	86	-176	Setal2006	Moment tensor inversion	Article	Yes
-3.8300	35.5800	012	4.0	Mw	15/02/2003	03:56:33	124	67	-171	Setal2006	Moment tensor inversion	Article	Yes
-3.5500	35.6700	004	4.8	Mw	18/02/2003	13:09:35	56	72	15	Setal2006	Moment tensor inversion	Article	Yes
-3.6100	35.6700	002	3.9	Mw	18/02/2003	13:59:29	81	72	49	Setal2006	Moment tensor inversion	Article	Yes
-3.4900	35.7300	004	4.0	Mw	19/02/2003	00:33:50	60	45	14	Setal2006	Moment tensor inversion	Article	Yes
-3.6200	35.6900	004	4.2	Mw	21/02/2003	11:46:37	48	51	0	Setal2006	Moment tensor inversion	Article	Yes
-3.6000	35.6900	002	3.8	Mw	21/02/2003	12:06:49	135	89	-136	Setal2006	Moment tensor inversion	Article	Yes
-3.5500	35.7000	004	3.7	Mw	22/02/2003	11:07:45	245	88	44	Setal2006	Moment tensor inversion	Article	Yes
2.2130	42.2920	009	4.4	Ml	26/02/2003	03:32:57	160	35	-70	Chevrot (2011)	Moment tensor inversion	Article	Yes
3.6300	36.9600	004	6.9	Mw	21/05/2003	18:44:20	52	13	69	Setal2006	Moment tensor inversion	Article	Yes
3.7020	36.8130	018	5.9	Mw	21/05/2003	18:51:00	72	20	82	BraunaandBer2005	Moment tensor inversion	Article	Yes
3.8850	36.9160	015	4.8	Mw	21/05/2003	22:04:00	76	17	86	BraunaandBer2005	Moment tensor inversion	Article	Yes
3.8140	36.9070	021	4.7	Mw	21/05/2003	23:18:00	93	23	82	BraunaandBer2005	Moment tensor inversion	Article	Yes
3.5000	36.9200	006	4.9	Mw	21/05/2003	23:23:43	247	71	99	Setal2006	Moment tensor inversion	Article	Yes
3.5750	36.6510	012	4.3	Mw	22/05/2003	01:39:00	37	21	68	BraunaandBer2005	Moment tensor inversion	Article	Yes
3.4600	36.6290	012	3.8	Mw	22/05/2003	01:55:00	69	25	87	BraunaandBer2005	Moment tensor inversion	Article	Yes
3.6300	37.0800	008	5.0	Mw	22/05/2003	03:14:03	51	19	83	Setal2006	Moment tensor inversion	Article	Yes
3.5650	36.8910	012	3.9	Mw	22/05/2003	04:29:00	44	21	96	BraunaandBer2005	Moment tensor inversion	Article	Yes
3.5700	36.9190	018	4.3	Mw	22/05/2003	04:45:00	31	24	68	BraunaandBer2005	Moment tensor inversion	Article	Yes

4.0650	36.7940	012	4.8	Mw	22/05/2003	06:27:00	17	68	-22	BraunaandBer2005	Moment tensor inversion	Article	Yes
3.8500	37.1400	006	4.6	Mw	22/05/2003	11:11:05	75	10	80	Setal2006	Moment tensor inversion	Article	Yes
3.5790	36.7380	012	4.2	Mw	22/05/2003	12:51:00	99	16	108	BraunaandBer2005	Moment tensor inversion	Article	Yes
3.9300	37.0300	012	5.0	Mw	22/05/2003	13:57:20	70	17	78	Setal2006	Moment tensor inversion	Article	Yes
3.7200	36.8220	009	4.3	Mw	23/05/2003	00:08:00	17	23	71	BraunaandBer2005	Moment tensor inversion	Article	Yes
4.0500	36.8110	015	4.2	Mw	24/05/2003	03:10:00	70	17	77	BraunaandBer2005	Moment tensor inversion	Article	Yes
3.6500	36.8880	015	4.4	Mw	24/05/2003	15:51:00	27	21	61	BraunaandBer2005	Moment tensor inversion	Article	Yes
3.9700	37.0400	006	4.8	Mw	24/05/2003	19:21:24	80	11	86	Setal2006	Moment tensor inversion	Article	Yes
3.7710	36.8350	012	3.9	Mw	24/05/2003	20:52:00	20	30	73	BraunaandBer2005	Moment tensor inversion	Article	Yes
3.5800	36.9400	010	5.7	Mw	27/05/2003	17:11:28	254	69	100	Setal2006	Moment tensor inversion	Article	Yes
3.2700	36.8800	006	4.7	Mw	28/05/2003	06:58:37	59	21	67	Setal2006	Moment tensor inversion	Article	Yes
3.4360	36.9410	009	4.4	Mw	28/05/2003	19:05:00	15	69	-39	BraunaandBer2005	Moment tensor inversion	Article	Yes
3.3600	36.8200	006	5.0	Mw	29/05/2003	02:14:59	95	53	-173	Setal2006	Moment tensor inversion	Article	Yes
3.4129	36.7522	032	4.9	Mw	29/05/2003	07:58:40	259	72	90	ETHZ	Moment tensor inversion	Catalog	Yes
3.4129	36.7522	032	4.8	Mw	30/05/2003	08:58:40	78	25	93	ETHZ	Moment tensor inversion	Catalog	Yes
4.0220	36.8350	006	4.2	Mw	01/06/2003	06:07:00	101	10	-80	BraunaandBer2005	Moment tensor inversion	Article	Yes
3.4600	36.7640	009	2.5	Ml	01/06/2003	06:44:00	297	53	119	Ayadetal2008	Polarity	Article	Yes
3.4280	36.7420	008	2.9	Ml	01/06/2003	09:00:00	318	22	133	Ayadetal2008	Polarity	Article	Yes
3.8390	36.8860	013	2.8	Ml	01/06/2003	12:02:00	350	55	84	Ayadetal2008	Polarity	Article	Yes
3.4600	36.8400	012	4.7	M	02/06/2003	00:00:00	261	61	88	Palano2013	Compilation	Article	Yes
3.4440	36.7610	008	2.3	Ml	02/06/2003	00:06:00	86	73	94	Ayadetal2008	Polarity	Article	Yes
3.7790	36.8970	016	2.7	Ml	02/06/2003	04:21:00	212	45	79	Ayadetal2008	Polarity	Article	Yes
3.7800	36.8940	016	2.8	Ml	02/06/2003	04:42:00	217	35	86	Ayadetal2008	Polarity	Article	Yes
3.6800	36.8610	017	2.7	Ml	02/06/2003	05:01:00	246	33	100	Ayadetal2008	Polarity	Article	Yes
3.5930	36.7670	010	3.1	Ml	02/06/2003	17:21:00	160	83	-131	Ayadetal2008	Polarity	Article	Yes

3.3690	36.7460	012	4.1	Mw	02/06/2003	22:30:00	85	29	93	BraunaandBer2005	Moment tensor inversion	Article	Yes
3.3990	36.7530	009	2.7	Ml	03/06/2003	18:48:00	341	16	112	Ayadetal2008	Polarity	Article	Yes
3.4630	36.7620	014	3.1	Ml	03/06/2003	21:37:00	56	69	73	Ousetal2014	Polarity	Article	Yes
3.4880	36.6470	011	3.0	Ml	04/06/2003	17:18:00	325	36	117	Ayadetal2008	Polarity	Article	Yes
3.4300	36.7390	008	2.9	Ml	05/06/2003	05:17:00	95	80	134	Ayadetal2008	Polarity	Article	Yes
3.4290	36.7430	010	2.8	Ml	05/06/2003	11:32:00	257	90	59	Ayadetal2008	Polarity	Article	Yes
3.4640	36.7400	012	3.0	Ml	05/06/2003	12:26:00	270	70	116	Ousetal2014	Polarity	Article	Yes
3.4210	36.7330	012	2.6	Ml	05/06/2003	14:06:00	246	75	62	Ousetal2014	Polarity	Article	Yes
3.4110	36.7060	012	2.0	Ml	05/06/2003	21:54:00	317	51	118	Ayadetal2008	Polarity	Article	Yes
3.5830	36.7920	012	2.7	Ml	07/06/2003	18:44:00	127	59	119	Ayadetal2008	Polarity	Article	Yes
3.8290	36.9790	015	2.5	Ml	09/06/2003	01:27:00	40	72	75	Ousetal2014	Polarity	Article	Yes
3.5850	36.7730	009	3.0	Ml	10/06/2003	08:44:00	186	34	46	Ousetal2014	Polarity	Article	Yes
3.7970	36.8900	015	3.0	Ml	10/06/2003	19:12:00	179	38	88	Ayadetal2008	Polarity	Article	Yes
3.4100	36.7080	011	3.4	Ml	12/06/2003	01:02:00	121	16	85	Ayadetal2008	Polarity	Article	Yes
4.0410	36.8860	014	2.9	Ml	14/06/2003	03:35:00	304	38	125	Ousetal2014	Polarity	Article	Yes
3.5870	36.7750	009	2.6	Ml	14/06/2003	14:38:00	280	53	120	Ousetal2014	Polarity	Article	Yes
3.7190	36.9330	010	2.6	Ml	14/06/2003	22:07:00	57	78	66	Ousetal2014	Polarity	Article	Yes
3.3980	36.6910	012	3.3	Ml	16/06/2003	20:08:00	311	50	114	Ousetal2014	Polarity	Article	Yes
3.3980	36.7810	011	3.1	Ml	16/06/2003	21:51:00	303	33	99	Ousetal2014	Polarity	Article	Yes
3.7280	36.8650	011	3.2	Ml	16/06/2003	23:58:00	302	45	114	Ousetal2014	Polarity	Article	Yes
4.0390	36.9060	016	3.6	Ml	17/06/2003	07:52:00	198	50	48	Ousetal2014	Polarity	Article	Yes
3.4110	36.7080	011	3.2	Ml	18/06/2003	00:58:00	126	8	78	Ayadetal2008	Polarity	Article	Yes
3.6090	36.8520	012	3.1	Ml	21/06/2003	04:17:00	233	8	125	Ayadetal2008	Polarity	Article	Yes
3.4380	36.7470	008	3.1	Ml	21/06/2003	05:06:00	290	34	128	Ousetal2014	Polarity	Article	Yes
3.5080	36.8190	013	3.1	Ml	21/06/2003	11:01:00	340	13	-129	Ayadetal2008	Polarity	Article	Yes
3.4150	36.7100	007	2.1	Ml	22/06/2003	15:16:00	260	60	113	Ousetal2014	Polarity	Article	Yes
3.4030	36.7010	010	2.3	Ml	22/06/2003	15:34:00	283	68	122	Ousetal2014	Polarity	Article	Yes
3.8260	36.9020	015	3.0	Ml	22/06/2003	17:17:00	173	80	-52	Ayadetal2008	Polarity	Article	Yes
3.8400	37.1300	012	4.7	M	23/06/2003	00:00:00	265	74	89	Palano2013	Compilation	Article	Yes
3.3940	36.7060	011	2.4	Ml	23/06/2003	03:45:00	260	77	115	Ousetal2014	Polarity	Article	Yes

3.7120	36.9230	012	4.1	Mw	23/06/2003	10:35:00	89	16	94	BraunaandBer2005	Moment tensor inversion	Article	Yes
3.3940	36.7950	011	2.7	Ml	24/06/2003	02:34:00	84	82	105	Ayadetal2008	Polarity	Article	Yes
3.3650	36.8070	010	2.4	Ml	24/06/2003	17:44:00	101	80	151	Ayadetal2008	Polarity	Article	Yes
3.7440	36.9310	011	2.9	Ml	26/06/2003	04:24:00	234	14	95	Ousetal2014	Polarity	Article	Yes
3.4380	36.7300	007	2.8	Ml	26/06/2003	08:04:00	253	54	89	Ousetal2014	Polarity	Article	Yes
3.4070	36.7470	010	3.1	Ml	26/06/2003	13:03:00	299	48	119	Ayadetal2008	Polarity	Article	Yes
3.7780	36.9330	014	2.9	Ml	26/06/2003	13:57:00	323	10	-160	Ayadetal2008	Polarity	Article	Yes
3.4000	36.6970	011	3.0	Ml	27/06/2003	01:45:00	255	83	116	Ousetal2014	Polarity	Article	Yes
3.4430	36.7680	009	2.8	Ml	27/06/2003	02:12:00	110	59	109	Ayadetal2008	Polarity	Article	Yes
3.5220	36.7370	012	2.2	Ml	27/06/2003	05:09:00	271	51	115	Ousetal2014	Polarity	Article	Yes
3.4070	36.7460	010	2.6	Ml	27/06/2003	15:55:00	7	67	63	Ayadetal2008	Polarity	Article	Yes
3.4080	36.7450	010	2.7	Ml	27/06/2003	23:43:00	203	87	-20	Ayadetal2008	Polarity	Article	Yes
3.4090	36.7310	008	2.6	Ml	28/06/2003	06:11:00	94	44	98	Ousetal2014	Polarity	Article	Yes
3.5880	36.7820	008	2.9	Ml	29/06/2003	09:40:00	296	41	108	Ousetal2014	Polarity	Article	Yes
3.6500	37.2400	021	4.1	M	05/07/2003	00:00:00	265	72	81	Palano2013	Compilation	Article	Yes
3.8290	36.5140	021	4.1	Mw	05/07/2003	20:03:00	111	20	115	BraunaandBer2005	Moment tensor inversion	Article	Yes
3.6490	37.2390	021	4.1	Mw	05/07/2003	20:03:33	111	20	115	ISC	Compilation	Catalog	Yes
3.9000	36.8700	009	4.5	M	06/07/2003	00:00:00	292	74	-87	Palano2013	Compilation	Article	Yes
3.9200	36.7370	009	3.9	Mw	06/07/2003	02:56:00	100	16	-101	BraunaandBer2005	Moment tensor inversion	Article	Yes
3.5300	36.7500	015	4.5	M	14/07/2003	00:00:00	265	70	97	Palano2013	Compilation	Article	Yes
3.5450	36.6120	015	3.9	Mw	14/07/2003	22:52:00	65	21	72	BraunaandBer2005	Moment tensor inversion	Article	Yes
-6.5700	36.9700	060	4.0	Mw	18/07/2003	00:00:00	96	82	160	Setal2005b	Moment tensor inversion	Article	No
-6.5700	36.9700	060	4.0	Mw	18/07/2003	21:23:15	189	70	9	Setal2006	Moment tensor inversion	Article	No
0.6300	38.0000	014	3.4	Mw	20/07/2003	13:12:05	12	85	-12	Setal2006	Moment tensor inversion	Article	Yes
-0.2800	38.9500	004	3.3	Mw	20/07/2003	21:09:08	148	76	-96	Setal2006	Moment tensor inversion	Article	Yes
-5.5600	36.9000	006	3.5	Mw	25/07/2003	00:00:00	29	40	82	RuizCetal2011	Compilation	Article	Yes
-5.5600	36.9000	006	3.5	Mw	25/07/2003	03:37:55	29	40	82	Setal2006	Moment tensor inversion	Article	Yes

-10.5600	35.6900	060	5.3	Mw	29/07/2003	05:31:26	243	72	41	Setal2006	Moment tensor inversion	Article	No
-3.7900	37.1400	012	3.8	Mw	10/09/2003	20:22:47	143	17	-55	Setal2024	Compilation	Article	Yes
-3.7900	37.1100	012	3.8	Mw	10/09/2003	20:22:47	289	76	-100	Setal2006	Moment tensor inversion	Article	Yes
0.0100	39.3900	008	4.2	Mw	16/09/2003	11:02:47	359	27	-40	Setal2006	Moment tensor inversion	Article	Yes
0.0100	39.3900	008	3.4	Mw	16/09/2003	20:19:48	175	58	-47	Setal2006	Moment tensor inversion	Article	Yes
0.0400	39.3900	008	4.3	Mw	21/09/2003	09:58:55	352	28	-45	Setal2006	Moment tensor inversion	Article	Yes
0.0100	39.4100	008	4.4	Mw	21/09/2003	10:34:16	148	64	-84	Setal2006	Moment tensor inversion	Article	Yes
3.5715	36.8707	018	4.0	Mw	12/10/2003	07:08:44	238	79	93	IGN	Moment tensor inversion	Catalog	Yes
-2.0700	37.7600	004	3.5	Mw	30/10/2003	01:12:03	58	29	97	Setal2006	Moment tensor inversion	Article	Yes
-2.6500	37.5300	008	4.1	Mw	16/11/2003	21:36:12	161	49	-100	Setal2006	Moment tensor inversion	Article	Yes
3.4300	36.9400	006	4.8	Mw	10/01/2004	18:38:15	119	86	-111	Setal2006	Moment tensor inversion	Article	Yes
-4.0000	35.1400	014	6.3	Mw	24/02/2004	02:27:46	11	72	-17	Setal2006	Moment tensor inversion	Article	Yes
-3.9800	35.1700	000	4.6	mb	24/02/2004	09:01:51	5	46	-11	RCMT	Moment tensor inversion	Catalog	Yes
-4.0800	35.1700	016	4.3	Mw	24/02/2004	11:04:44	123	67	-148	Setal2006	Moment tensor inversion	Article	Yes
-4.0800	35.0500	010	4.1	Mw	24/02/2004	16:42:12	11	68	-7	Setal2006	Moment tensor inversion	Article	Yes
-3.9100	35.0700	010	4.0	Mw	24/02/2004	18:53:02	106	49	-173	Setal2006	Moment tensor inversion	Article	Yes
-3.9500	35.1100	016	4.0	Mw	24/02/2004	20:37:02	97	74	-165	Setal2006	Moment tensor inversion	Article	Yes
-3.9300	35.1200	014	4.4	Mw	25/02/2004	05:21:14	0	69	-4	Setal2006	Moment tensor inversion	Article	Yes
-3.8600	35.0500	010	5.2	Mw	25/02/2004	12:44:54	108	73	-167	Setal2006	Moment tensor inversion	Article	Yes
-3.9400	35.1700	010	4.0	Mw	25/02/2004	16:33:28	117	73	-162	Setal2006	Moment tensor inversion	Article	Yes
-4.0600	35.1900	016	4.9	Mw	26/02/2004	12:07:03	13	75	-9	Setal2006	Moment tensor inversion	Article	Yes
-3.9900	35.1300	014	4.4	Mw	27/02/2004	00:59:00	102	71	-170	Setal2006	Moment tensor inversion	Article	Yes
-3.9600	35.1300	012	4.3	Mw	27/02/2004	03:12:36	10	73	-5	Setal2006	Moment tensor inversion	Article	Yes
-3.9200	35.1800	014	4.5	Mw	27/02/2004	16:50:42	110	80	-163	Setal2006	Moment tensor inversion	Article	Yes
-4.0100	35.0200	004	4.2	Mw	28/02/2004	16:29:25	36	35	23	Setal2006	Moment tensor inversion	Article	Yes
-3.8700	35.1400	012	4.4	Mw	02/03/2004	20:36:26	109	65	-167	Setal2006	Moment tensor inversion	Article	Yes
-4.0076	35.1715	012	3.8	Mw	04/03/2004	11:44:14	102	82	171	IGN	Moment tensor inversion	Catalog	Yes
-4.0100	35.0600	022	5.0	Mw	07/03/2004	06:37:52	93	81	-171	Setal2006	Moment tensor inversion	Article	Yes
-3.8984	35.1342	033	3.5	Mw	07/03/2004	10:30:06	189	84	16	IGN	Moment tensor inversion	Catalog	Yes
-4.0800	34.9100	006	4.0	Mw	10/03/2004	04:22:18	354	68	-50	Setal2006	Moment tensor inversion	Article	Yes

-4.0500	34.9200	006	4.9	Mw	12/03/2004	17:21:51	352	49	-62	Setal2006	Moment tensor inversion	Article	Yes
-4.2000	35.1100	012	3.9	Mw	15/03/2004	12:39:13	119	54	-148	Setal2006	Moment tensor inversion	Article	Yes
-4.2467	35.1642	009	3.9	Mw	18/03/2004	11:45:31	73	50	120	IGN	Moment tensor inversion	Catalog	Yes
-4.1500	35.0000	010	4.5	Mw	20/03/2004	09:37:26	119	56	-164	Setal2006	Moment tensor inversion	Article	Yes
-8.7100	36.0100	050	3.8	Mw	24/03/2004	00:59:10	297	76	224	Setal2006	Moment tensor inversion	Article	Yes
-3.9320	35.1184	004	1.7	MD	31/03/2004	17:40:44	119	83	-171	Vanetal2014	Polarity	Article	No
-3.9638	35.0985	009	1.7	MD	31/03/2004	20:15:38	277	82	176	Vanetal2014	Polarity	Article	No
-4.0900	35.0900	008	4.0	Mw	01/04/2004	00:25:35	28	53	14	Setal2006	Moment tensor inversion	Article	Yes
-3.9250	35.1174	008	2.1	MD	01/04/2004	01:33:54	283	79	-140	Vanetal2014	Polarity	Article	Yes
-3.9239	35.1211	011	1.5	MD	01/04/2004	12:36:22	285	81	165	Vanetal2014	Polarity	Article	No
-3.9487	35.1324	007	1.5	MD	02/04/2004	01:36:00	206	65	-7	Vanetal2014	Polarity	Article	No
-3.9472	35.1655	012	2.0	MD	02/04/2004	05:56:45	208	68	-12	Vanetal2014	Polarity	Article	Yes
-3.8411	35.0785	010	1.5	MD	02/04/2004	18:07:06	142	73	-153	Vanetal2014	Polarity	Article	No
-3.9244	35.1161	010	1.7	MD	02/04/2004	18:13:15	275	72	166	Vanetal2014	Polarity	Article	No
-3.9150	35.1127	004	1.8	MD	02/04/2004	19:27:35	215	79	6	Vanetal2014	Polarity	Article	No
-3.9186	35.2564	012	1.8	MD	02/04/2004	19:41:53	296	81	-172	Vanetal2014	Polarity	Article	No
-3.9718	35.0968	006	1.9	MD	02/04/2004	20:27:50	100	82	-163	Vanetal2014	Polarity	Article	No
-3.9542	35.1372	004	1.9	MD	02/04/2004	21:02:33	215	78	16	Vanetal2014	Polarity	Article	No
-3.9618	35.1325	004	2.8	MD	02/04/2004	21:43:00	303	82	172	Vanetal2014	Polarity	Article	Yes
-3.9188	35.2558	012	1.7	MD	03/04/2004	02:14:52	294	84	-179	Vanetal2014	Polarity	Article	No
-3.9165	35.1094	009	2.1	MD	03/04/2004	13:16:44	118	76	-157	Vanetal2014	Polarity	Article	Yes
-3.9269	35.1137	006	1.7	MD	03/04/2004	14:46:38	157	55	-131	Vanetal2014	Polarity	Article	No
-3.9758	35.0595	011	2.0	MD	03/04/2004	17:58:22	184	81	6	Vanetal2014	Polarity	Article	Yes
-3.9245	35.1156	010	1.6	MD	03/04/2004	19:24:22	332	41	-97	Vanetal2014	Polarity	Article	No
-3.9693	35.0292	006	1.6	MD	03/04/2004	19:45:25	290	82	166	Vanetal2014	Polarity	Article	No
-3.9204	35.1184	009	1.7	MD	03/04/2004	22:20:39	285	69	-165	Vanetal2014	Polarity	Article	No
-3.9869	35.0235	007	1.9	MD	04/04/2004	16:11:02	129	64	-169	Vanetal2014	Polarity	Article	No
-4.0678	35.1847	007	2.8	MD	04/04/2004	20:08:15	288	61	-165	Vanetal2014	Polarity	Article	Yes
-3.9155	35.1162	008	1.5	MD	04/04/2004	20:50:15	312	35	-104	Vanetal2014	Polarity	Article	No
-4.0619	35.1784	008	2.6	MD	04/04/2004	21:15:27	293	78	171	Vanetal2014	Polarity	Article	Yes

-3.9239	35.1194	008	0.9	MD	04/04/2004	22:30:49	127	83	-165	Vanetal2014	Polarity	Article	No
-3.9754	35.0973	006	1.6	MD	04/04/2004	23:13:51	128	74	-146	Vanetal2014	Polarity	Article	No
-3.9753	35.1604	009	1.5	MD	05/04/2004	00:12:48	145	75	-166	Vanetal2014	Polarity	Article	No
-3.9663	35.0570	006	2.8	MD	05/04/2004	00:26:01	122	70	-174	Vanetal2014	Polarity	Article	Yes
-3.9187	35.1129	010	1.4	MD	05/04/2004	01:11:40	266	67	-134	Vanetal2014	Polarity	Article	No
-3.9364	35.1219	008	1.4	MD	05/04/2004	01:51:21	155	46	-110	Vanetal2014	Polarity	Article	No
-3.9686	35.0568	006	2.5	MD	05/04/2004	02:41:50	123	73	-176	Vanetal2014	Polarity	Article	Yes
-3.9245	35.1135	010	2.5	MD	05/04/2004	03:01:53	109	71	-170	Vanetal2014	Polarity	Article	Yes
-3.9063	35.1188	008	1.7	MD	05/04/2004	04:40:58	294	80	-166	Vanetal2014	Polarity	Article	No
-3.9350	35.1177	010	1.9	MD	05/04/2004	06:15:45	257	45	-130	Vanetal2014	Polarity	Article	No
-3.9514	35.0947	010	1.8	MD	05/04/2004	06:29:19	131	62	-167	Vanetal2014	Polarity	Article	No
-3.9224	35.1332	010	1.8	MD	05/04/2004	07:01:33	271	49	-160	Vanetal2014	Polarity	Article	No
-3.9641	35.0556	006	1.7	MD	05/04/2004	09:53:58	126	66	171	Vanetal2014	Polarity	Article	No
-3.9658	35.0591	006	1.8	MD	05/04/2004	12:15:28	296	72	172	Vanetal2014	Polarity	Article	No
-3.9665	35.0753	009	1.4	MD	05/04/2004	15:12:17	288	71	-158	Vanetal2014	Polarity	Article	No
-3.9638	35.0585	006	1.8	MD	05/04/2004	16:23:25	326	58	-158	Vanetal2014	Polarity	Article	No
-3.9633	35.0459	004	3.4	MD	05/04/2004	16:28:10	284	82	-165	Vanetal2014	Polarity	Article	Yes
-3.9645	35.0443	004	1.6	MD	05/04/2004	16:34:25	319	82	-14	Vanetal2014	Polarity	Article	No
-3.7663	35.0592	007	1.9	MD	05/04/2004	16:43:52	148	55	-115	Vanetal2014	Polarity	Article	No
-3.9635	35.0420	004	2.5	MD	05/04/2004	18:54:41	143	73	-159	Vanetal2014	Polarity	Article	Yes
-3.7942	35.1167	004	1.6	MD	05/04/2004	19:31:48	353	54	-55	Vanetal2014	Polarity	Article	No
-3.9213	35.1137	007	2.4	MD	05/04/2004	21:28:51	292	74	-168	Vanetal2014	Polarity	Article	Yes
-3.9196	35.1108	007	1.4	MD	05/04/2004	21:34:42	288	84	-166	Vanetal2014	Polarity	Article	No
-3.9202	35.1131	007	2.1	MD	05/04/2004	22:42:53	286	70	-162	Vanetal2014	Polarity	Article	Yes
-3.9198	35.1127	007	1.0	MD	06/04/2004	00:56:56	289	69	-167	Vanetal2014	Polarity	Article	No
-4.1100	35.0500	006	4.2	Mw	06/04/2004	01:53:09	110	33	160	Setal2006	Moment tensor inversion	Article	Yes
-4.0511	35.1741	005	2.1	MD	06/04/2004	02:45:36	279	79	-166	Vanetal2014	Polarity	Article	Yes
-3.8719	35.1183	004	1.3	MD	06/04/2004	04:08:29	346	79	-16	Vanetal2014	Polarity	Article	No
-3.7342	35.0547	007	1.8	MD	06/04/2004	13:43:17	336	49	-66	Vanetal2014	Polarity	Article	No
-3.9687	35.0930	005	1.7	MD	06/04/2004	15:34:20	119	83	-175	Vanetal2014	Polarity	Article	No

-3.9213	35.1126	008	2.8	MD	06/04/2004	17:25:40	297	77	-171	Vanetal2014	Polarity	Article	Yes
-3.9221	35.1142	007	2.0	MD	06/04/2004	17:42:33	288	75	-165	Vanetal2014	Polarity	Article	Yes
-3.9227	35.1144	007	0.9	MD	06/04/2004	18:47:28	298	69	-159	Vanetal2014	Polarity	Article	No
-3.9239	35.1120	008	1.5	MD	06/04/2004	19:16:33	117	77	-169	Vanetal2014	Polarity	Article	No
-3.7407	35.0605	007	1.9	MD	06/04/2004	20:17:32	313	23	-99	Vanetal2014	Polarity	Article	No
-3.7249	35.0511	009	1.8	MD	06/04/2004	21:48:39	354	26	-62	Vanetal2014	Polarity	Article	No
-3.7923	35.1158	005	1.8	MD	06/04/2004	22:08:34	330	55	-75	Vanetal2014	Polarity	Article	No
-3.9809	35.0715	012	1.3	MD	06/04/2004	23:04:37	144	44	-126	Vanetal2014	Polarity	Article	No
-3.9236	35.1160	008	1.4	MD	06/04/2004	23:24:09	297	80	-166	Vanetal2014	Polarity	Article	No
-3.9219	35.1128	007	2.5	MD	06/04/2004	23:39:20	293	69	-168	Vanetal2014	Polarity	Article	Yes
-3.7275	35.0532	008	1.8	MD	07/04/2004	00:19:34	352	25	-67	Vanetal2014	Polarity	Article	No
-3.9496	35.1680	009	1.7	MD	07/04/2004	01:12:54	129	74	-168	Vanetal2014	Polarity	Article	No
-3.9019	35.0971	005	1.4	MD	07/04/2004	01:34:13	107	75	-137	Vanetal2014	Polarity	Article	No
-3.9024	35.0956	006	1.6	MD	07/04/2004	02:09:02	112	80	-153	Vanetal2014	Polarity	Article	No
-3.9152	35.1225	011	1.4	MD	07/04/2004	03:34:26	111	73	-161	Vanetal2014	Polarity	Article	No
-4.0455	35.1828	008	2.0	MD	07/04/2004	04:42:55	250	57	139	Vanetal2014	Polarity	Article	Yes
0.4250	35.5322	018	4.1	Mw	07/04/2004	06:07:25	65	72	-157	IGN	Moment tensor inversion	Catalog	Yes
-3.9658	35.1396	012	2.2	MD	07/04/2004	11:52:44	321	60	-112	Vanetal2014	Polarity	Article	Yes
-3.9215	35.1155	007	2.2	MD	07/04/2004	12:04:19	309	47	136	Vanetal2014	Polarity	Article	Yes
-3.9186	35.1155	008	1.5	MD	07/04/2004	12:49:44	302	76	156	Vanetal2014	Polarity	Article	No
-3.9597	35.1276	010	1.9	MD	07/04/2004	17:51:26	121	79	-161	Vanetal2014	Polarity	Article	No
-3.9145	35.1137	008	1.7	MD	07/04/2004	20:15:45	200	83	0	Vanetal2014	Polarity	Article	No
-3.9750	35.0767	010	1.3	MD	07/04/2004	20:18:12	288	67	152	Vanetal2014	Polarity	Article	No
-3.9019	35.0978	005	1.8	MD	08/04/2004	00:47:52	110	82	-153	Vanetal2014	Polarity	Article	No
-4.0296	35.1719	007	2.0	MD	08/04/2004	01:02:45	295	59	158	Vanetal2014	Polarity	Article	Yes
-3.9694	35.0282	006	1.9	MD	08/04/2004	02:09:37	132	72	-160	Vanetal2014	Polarity	Article	No
-3.9222	35.1211	009	1.8	MD	08/04/2004	14:22:56	300	75	-174	Vanetal2014	Polarity	Article	No
-3.9220	35.1204	008	1.9	MD	08/04/2004	14:39:40	306	79	-159	Vanetal2014	Polarity	Article	No
-3.7698	35.0394	006	1.7	MD	08/04/2004	16:20:27	287	52	-138	Vanetal2014	Polarity	Article	No
-3.9501	35.1348	006	1.8	MD	08/04/2004	17:00:36	11	72	-29	Vanetal2014	Polarity	Article	No

-3.9175	35.1087	008	1.7	MD	08/04/2004	17:21:14	116	77	-140	Vanetal2014	Polarity	Article	No
-3.9181	35.1082	007	1.9	MD	08/04/2004	17:47:07	298	78	170	Vanetal2014	Polarity	Article	No
-3.9339	35.1220	009	1.8	MD	08/04/2004	18:00:43	289	82	-172	Vanetal2014	Polarity	Article	No
-4.0465	35.1854	007	2.4	MD	08/04/2004	19:20:45	303	72	-163	Vanetal2014	Polarity	Article	Yes
-3.9487	35.1872	010	1.9	MD	08/04/2004	20:18:31	281	68	-164	Vanetal2014	Polarity	Article	No
-3.8119	35.0233	005	1.8	MD	08/04/2004	21:16:24	358	24	-57	Vanetal2014	Polarity	Article	No
-3.9296	35.1203	008	2.0	MD	08/04/2004	21:30:34	285	80	164	Vanetal2014	Polarity	Article	Yes
-3.9061	35.1207	009	1.1	MD	08/04/2004	21:32:36	279	64	-156	Vanetal2014	Polarity	Article	No
-3.8116	35.0245	005	1.8	MD	08/04/2004	22:22:47	339	52	-75	Vanetal2014	Polarity	Article	No
-3.7583	35.0215	008	1.7	MD	08/04/2004	22:31:08	299	55	-106	Vanetal2014	Polarity	Article	No
-3.8813	35.0843	002	1.5	MD	08/04/2004	23:06:15	207	84	7	Vanetal2014	Polarity	Article	No
-3.9142	35.0800	005	1.5	MD	08/04/2004	23:19:14	319	32	-99	Vanetal2014	Polarity	Article	No
-3.7626	35.0260	007	1.8	MD	08/04/2004	23:31:15	299	37	-133	Vanetal2014	Polarity	Article	No
-3.7931	35.0226	005	1.6	MD	09/04/2004	00:27:15	350	30	-71	Vanetal2014	Polarity	Article	No
-3.9695	35.1406	007	1.9	MD	09/04/2004	00:28:51	350	41	-102	Vanetal2014	Polarity	Article	No
-3.8121	34.9644	005	1.8	MD	09/04/2004	00:50:43	327	51	-85	Vanetal2014	Polarity	Article	No
-3.9665	35.0336	006	1.7	MD	09/04/2004	01:51:18	353	64	-73	Vanetal2014	Polarity	Article	No
-3.9819	35.1509	008	1.6	MD	09/04/2004	02:02:39	285	79	175	Vanetal2014	Polarity	Article	No
-3.8456	35.0813	008	1.7	MD	09/04/2004	03:08:18	128	75	-145	Vanetal2014	Polarity	Article	No
-3.7609	35.0229	001	1.6	MD	09/04/2004	03:14:00	315	80	159	Vanetal2014	Polarity	Article	No
-3.9166	35.1169	008	1.4	MD	09/04/2004	03:46:18	287	78	160	Vanetal2014	Polarity	Article	No
-3.9577	35.0715	010	1.6	MD	09/04/2004	04:09:56	274	62	166	Vanetal2014	Polarity	Article	No
-3.8952	35.0968	005	1.3	MD	09/04/2004	04:46:01	116	87	-169	Vanetal2014	Polarity	Article	No
-3.9227	35.1324	009	1.7	MD	09/04/2004	06:02:17	286	71	170	Vanetal2014	Polarity	Article	No
-3.9608	35.1157	005	1.5	MD	09/04/2004	06:11:32	307	87	167	Vanetal2014	Polarity	Article	No
-3.8400	35.0596	005	1.4	MD	09/04/2004	06:13:53	158	56	-105	Vanetal2014	Polarity	Article	No
-3.9356	35.1197	010	1.5	MD	09/04/2004	07:08:15	120	84	-169	Vanetal2014	Polarity	Article	No
-3.9156	35.1070	007	1.5	MD	09/04/2004	07:12:44	208	82	15	Vanetal2014	Polarity	Article	No
-4.0413	35.1864	005	2.5	MD	09/04/2004	07:24:00	131	59	-165	Vanetal2014	Polarity	Article	Yes
-4.0112	35.1653	009	1.9	MD	09/04/2004	07:45:49	128	72	-167	Vanetal2014	Polarity	Article	No

-3.8125	34.9671	004	2.0	MD	09/04/2004	08:40:32	343	30	-80	Vanetal2014	Polarity	Article	Yes
-3.9654	35.0348	005	1.8	MD	09/04/2004	10:46:20	244	57	82	Vanetal2014	Polarity	Article	No
-3.9239	35.1140	007	1.6	MD	09/04/2004	11:33:52	300	74	-179	Vanetal2014	Polarity	Article	No
-3.9164	35.0862	003	1.9	MD	09/04/2004	12:00:53	126	82	-160	Vanetal2014	Polarity	Article	No
-3.8479	35.0689	006	1.9	MD	09/04/2004	12:13:15	293	69	-163	Vanetal2014	Polarity	Article	No
-3.9216	35.1210	008	1.6	MD	09/04/2004	13:02:40	299	83	177	Vanetal2014	Polarity	Article	No
-3.9778	35.0387	006	1.7	MD	09/04/2004	13:24:36	226	81	19	Vanetal2014	Polarity	Article	No
-4.1235	35.2455	004	1.9	MD	09/04/2004	13:42:18	281	41	150	Vanetal2014	Polarity	Article	No
-3.9640	35.0391	005	2.0	MD	09/04/2004	14:11:58	106	80	-161	Vanetal2014	Polarity	Article	Yes
-3.9791	35.0677	006	1.9	MD	09/04/2004	14:34:07	265	75	-172	Vanetal2014	Polarity	Article	No
-3.9007	35.0881	006	1.7	MD	09/04/2004	14:36:34	327	79	-155	Vanetal2014	Polarity	Article	No
-3.9839	35.0259	007	1.7	MD	09/04/2004	14:54:20	128	75	-175	Vanetal2014	Polarity	Article	No
-3.9513	35.1376	012	1.8	MD	09/04/2004	15:39:47	348	56	-81	Vanetal2014	Polarity	Article	No
-3.9647	35.0410	004	1.7	MD	09/04/2004	19:13:58	123	84	-168	Vanetal2014	Polarity	Article	No
-3.9018	35.0982	005	1.5	MD	09/04/2004	19:30:43	116	82	-158	Vanetal2014	Polarity	Article	No
-3.9756	35.0956	006	1.5	MD	09/04/2004	19:37:06	301	82	148	Vanetal2014	Polarity	Article	No
-3.7718	35.0415	006	1.8	MD	09/04/2004	20:31:37	291	53	-133	Vanetal2014	Polarity	Article	No
-3.7740	35.0427	007	2.3	MD	09/04/2004	20:41:21	287	53	-139	Vanetal2014	Polarity	Article	Yes
-3.9489	35.0944	009	2.1	MD	09/04/2004	20:44:08	104	85	-170	Vanetal2014	Polarity	Article	Yes
-3.7700	35.0386	007	1.8	MD	09/04/2004	21:11:04	303	55	-164	Vanetal2014	Polarity	Article	No
-3.9461	35.1565	011	1.6	MD	09/04/2004	22:06:12	339	53	-83	Vanetal2014	Polarity	Article	No
-3.8529	35.1162	007	3.0	MD	09/04/2004	23:11:08	291	37	-127	Vanetal2014	Polarity	Article	Yes
-3.8535	35.1183	008	1.5	MD	09/04/2004	23:13:58	308	31	-96	Vanetal2014	Polarity	Article	No
-3.8538	35.1170	007	1.8	MD	09/04/2004	23:15:52	296	48	-134	Vanetal2014	Polarity	Article	No
-3.9805	35.0353	007	1.9	MD	10/04/2004	00:17:08	107	78	-153	Vanetal2014	Polarity	Article	No
-4.0394	35.1826	006	1.8	MD	10/04/2004	01:01:18	205	78	23	Vanetal2014	Polarity	Article	No
-3.9707	35.0398	006	1.5	MD	10/04/2004	01:04:41	302	79	168	Vanetal2014	Polarity	Article	No
-3.8523	35.1151	008	1.5	MD	10/04/2004	02:10:12	286	82	171	Vanetal2014	Polarity	Article	No
-3.9538	35.0707	010	1.2	MD	10/04/2004	02:16:01	289	84	162	Vanetal2014	Polarity	Article	No
-3.8112	34.9880	003	1.6	MD	10/04/2004	03:19:58	330	38	-87	Vanetal2014	Polarity	Article	No

-3.9658	35.0397	004	1.9	MD	10/04/2004	03:52:29	220	61	60	Vanetal2014	Polarity	Article	No
-3.9727	35.0886	005	1.6	MD	10/04/2004	07:25:49	344	33	-111	Vanetal2014	Polarity	Article	No
-3.9235	35.1143	009	1.6	MD	10/04/2004	07:42:17	126	61	-139	Vanetal2014	Polarity	Article	No
-3.9350	35.1202	009	1.9	MD	10/04/2004	09:04:51	128	74	-148	Vanetal2014	Polarity	Article	No
-3.9354	35.1201	010	1.7	MD	10/04/2004	11:12:52	133	77	-152	Vanetal2014	Polarity	Article	No
-4.0443	35.1759	007	2.0	MD	10/04/2004	11:45:03	167	68	20	Vanetal2014	Polarity	Article	Yes
-3.9170	35.1227	009	1.7	MD	10/04/2004	15:54:05	335	33	-107	Vanetal2014	Polarity	Article	No
-3.9175	35.1221	009	1.5	MD	10/04/2004	15:57:26	333	42	-128	Vanetal2014	Polarity	Article	No
-3.8519	35.0750	007	2.0	MD	10/04/2004	20:39:01	137	72	-169	Vanetal2014	Polarity	Article	Yes
-3.9237	35.1163	009	1.5	MD	10/04/2004	20:49:31	214	68	9	Vanetal2014	Polarity	Article	No
-3.9319	35.0809	007	1.6	MD	10/04/2004	22:50:58	117	81	-157	Vanetal2014	Polarity	Article	No
-3.9759	35.0797	010	1.5	MD	11/04/2004	04:35:11	314	37	-100	Vanetal2014	Polarity	Article	No
-3.9245	35.1203	008	1.3	MD	11/04/2004	06:06:20	227	61	21	Vanetal2014	Polarity	Article	No
-3.9717	35.0992	007	1.5	MD	11/04/2004	06:16:34	297	82	-163	Vanetal2014	Polarity	Article	No
-4.0180	35.2665	005	1.8	MD	11/04/2004	06:56:31	324	62	-154	Vanetal2014	Polarity	Article	No
-3.9246	35.1197	008	1.8	MD	11/04/2004	07:06:35	354	48	-87	Vanetal2014	Polarity	Article	No
-3.8379	35.0250	007	1.6	MD	11/04/2004	08:44:06	119	82	-126	Vanetal2014	Polarity	Article	No
-3.7828	35.0572	008	1.7	MD	11/04/2004	09:06:03	299	38	-133	Vanetal2014	Polarity	Article	No
-3.8377	35.0188	007	1.4	MD	11/04/2004	09:37:36	318	38	-144	Vanetal2014	Polarity	Article	No
-3.9358	35.0770	007	1.7	MD	11/04/2004	10:13:29	112	68	-171	Vanetal2014	Polarity	Article	No
-3.9328	35.1195	008	1.6	MD	11/04/2004	10:45:52	164	52	-142	Vanetal2014	Polarity	Article	No
-1.3800	37.6700	004	3.9	Mw	16/04/2004	19:23:25	335	82	-149	Setal2006	Moment tensor inversion	Article	Yes
-4.0231	35.1331	024	3.7	Mw	23/05/2004	00:29:44	99	77	165	IGN	Moment tensor inversion	Catalog	Yes
2.2230	42.2920	009	4.1	Ml	01/06/2004	16:50:18	155	35	-45	Chevrot (2011)	Moment tensor inversion	Article	Yes
-3.8800	34.9400	006	4.3	Mw	20/06/2004	22:47:05	122	47	-131	Setal2006	Moment tensor inversion	Article	Yes
-4.0700	35.1600	006	3.7	Mw	10/07/2004	17:57:16	358	62	-46	Setal2006	Moment tensor inversion	Article	Yes
1.0190	42.8900	009	3.9	Ml	18/07/2004	02:16:01	90	55	-160	Chevrot (2011)	Moment tensor inversion	Article	Yes
-3.8900	34.8700	006	3.8	Mw	14/08/2004	01:55:42	129	60	-115	Setal2006	Moment tensor inversion	Article	Yes
-1.4460	42.8340	008	5.2	Ml	18/09/2004	12:52:17	125	75	-70	Chevrot (2011)	Moment tensor inversion	Article	Yes
2.1700	42.3400	008	4.8	Ml	21/09/2004	15:48:04	120	65	-95	Chevrot (2011)	Moment tensor inversion	Article	Yes

-1.4590	42.8120	008	4.7	Ml	30/09/2004	13:09:06	100	60	-80	Chevrot (2011)	Moment tensor inversion	Article	Yes
-1.4320	42.8390	010	4.2	Ml	07/10/2004	06:16:29	105	85	-70	Chevrot (2011)	Moment tensor inversion	Article	Yes
-4.0600	35.0700	022	4.0	Mw	10/10/2004	08:13:59	284	85	170	Setal2006	Moment tensor inversion	Article	Yes
-3.3000	36.7000	018	3.8	Mw	06/11/2004	13:24:00	53	59	-117	EMSC	Compilation	Catalog	Yes
3.7550	37.0668	000	3.9	Mw	14/11/2004	01:48:33	277	61	82	ETHZ	Moment tensor inversion	Catalog	Yes
3.4500	36.8500	010	4.5	mb	01/12/2004	17:42:24	18	48	45	RCMT	Moment tensor inversion	Catalog	Yes
-2.9600	34.9500	008	4.9	Mw	02/12/2004	17:50:42	92	47	183	Setal2006	Moment tensor inversion	Article	Yes
-3.0000	34.9900	012	5.1	Mw	04/12/2004	10:30:00	93	61	189	Setal2006	Moment tensor inversion	Article	Yes
3.4411	36.7854	030	4.4	Mw	05/12/2004	08:31:00	284	83	114	IGN	Moment tensor inversion	Catalog	Yes
-3.0800	34.9700	012	4.5	Mw	09/12/2004	07:46:02	94	66	194	Setal2006	Moment tensor inversion	Article	Yes
-9.9800	36.2500	008	4.8	Mw	13/12/2004	14:16:11	257	83	119	Setal2006	Moment tensor inversion	Article	Yes
-3.0105	34.9487	000	3.9	Mw	29/12/2004	05:33:53	270	80	156	ETHZ	Moment tensor inversion	Catalog	Yes
-7.5500	36.6800	030	3.9	Mw	03/01/2005	11:34:16	79	68	111	Setal2006	Moment tensor inversion	Article	Yes
-1.7800	37.8800	010	4.8	Mw	29/01/2005	07:41:31	132	85	-153	Benietal2007	Moment tensor inversion	Article	Yes
-1.7000	38.0200	006	3.6	Mw	01/02/2005	23:53:56	120	68	-125	Benietal2007	Moment tensor inversion	Article	Yes
-1.7900	37.8200	010	4.2	Mw	03/02/2005	11:40:33	110	84	-136	Benietal2007	Moment tensor inversion	Article	Yes
-1.8000	37.8200	006	3.9	Mw	04/02/2005	01:09:41	109	82	-136	Benietal2007	Moment tensor inversion	Article	Yes
-2.9900	34.9500	003	4.4	Md	18/02/2005	00:00:00	43	67	164	Bensetal2011	Polarity	Article	Yes
-6.0100	38.0200	020	3.7	Mw	20/02/2005	13:26:01	315	76	177	Setal2006	Moment tensor inversion	Article	Yes
-2.9800	34.9300	006	4.4	Mw	22/03/2005	09:03:13	87	37	169	Setal2006	Moment tensor inversion	Article	Yes
-5.8800	34.6000	059	4.2	Md	26/05/2005	00:00:00	120	32	104	Bensetal2011	Polarity	Article	No
-1.5400	36.6500	006	3.8	Mw	30/06/2005	01:19:22	63	36	111	Setal2010	Moment tensor inversion	Article	Yes
-3.5400	35.7200	006	4.2	Mw	02/07/2005	12:58:07	236	74	60	Setal2010	Moment tensor inversion	Article	Yes
-3.5300	35.7100	006	3.9	Mw	06/07/2005	07:27:05	236	77	46	Setal2010	Moment tensor inversion	Article	Yes
-11.5300	36.2600	010	4.5	Mw	19/07/2005	08:04:43	204	68	-16	Setal2010	Moment tensor inversion	Article	Yes
0.6600	36.9700	016	3.8	Mw	20/07/2005	19:54:07	191	79	6	Setal2010	Moment tensor inversion	Article	Yes
-11.1900	36.5900	040	4.6	Mw	29/08/2005	09:38:54	52	57	99	Setal2010	Moment tensor inversion	Article	Yes
-4.0200	35.1300	016	3.8	Mw	24/10/2005	15:10:57	17	82	-14	Setal2010	Moment tensor inversion	Article	Yes
0.1760	43.0010	014	3.9	Mw	05/11/2005	00:30:00	65	11	3	FMHex20	Compilation	Catalog	Yes

-8.6100	40.0600	012	3.5	Mw	01/12/2005	20:02:06	284	85	-134	Setal2010	Moment tensor inversion	Article	Yes
1.4440	42.3390	002	3.8	Mw	27/12/2005	21:33:00	9	60	-46	FMHex20	Compilation	Catalog	Yes
-8.2300	38.8800	010	3.5	Mw	29/12/2005	04:25:44	104	68	173	Setal2010	Moment tensor inversion	Article	Yes
-8.2300	38.8800	008	3.7	Mw	29/12/2005	05:01:02	96	66	167	Setal2010	Moment tensor inversion	Article	Yes
-7.7100	36.1500	020	3.7	Mw	10/01/2006	10:57:40	110	78	150	Setal2010	Moment tensor inversion	Article	Yes
-6.5600	38.5100	026	3.7	Mw	22/01/2006	16:27:33	76	34	144	Setal2010	Moment tensor inversion	Article	Yes
-4.0100	35.0600	014	4.2	Mw	30/01/2006	07:58:13	128	63	-164	Setal2010	Moment tensor inversion	Article	Yes
-3.9769	34.9965	009	4.0	Mw	30/01/2006	18:16:57	117	87	-155	IGN	Moment tensor inversion	Catalog	Yes
-3.9769	35.1174	006	3.7	Mw	22/02/2006	01:01:12	187	85	10	IGN	Moment tensor inversion	Catalog	Yes
-1.6100	37.7100	002	3.5	Mw	08/03/2006	09:04:14	242	68	82	Setal2010	Moment tensor inversion	Article	Yes
-1.2500	40.0200	006	4.3	Mw	10/03/2006	19:33:17	179	46	-78	Setal2010	Moment tensor inversion	Article	Yes
-4.9800	36.8700	022	3.9	Mw	11/03/2006	13:43:07	243	88	-170	Setal2010	Moment tensor inversion	Article	Yes
-5.0400	36.8300	014	3.7	Mw	26/03/2006	18:15:40	151	70	5	Setal2010	Moment tensor inversion	Article	Yes
3.8100	34.8900	010	4.7	mb	02/04/2006	06:44:31	67	78	-169	RCMT	Moment tensor inversion	Catalog	Yes
-1.0800	38.1700	008	3.7	Mw	05/04/2006	17:22:00	253	75	7	Setal2010	Moment tensor inversion	Article	Yes
-9.1700	39.3000	026	3.6	Mw	15/04/2006	19:52:31	55	47	85	Setal2010	Moment tensor inversion	Article	Yes
-9.0300	43.6600	010	4.2	Mw	23/04/2006	05:31:36	167	85	-35	Setal2010	Moment tensor inversion	Article	Yes
-6.4800	42.4400	020	4.1	Mw	10/06/2006	06:18:45	203	63	6	Setal2010	Moment tensor inversion	Article	Yes
-10.4700	35.9300	050	4.7	Mw	21/06/2006	00:51:16	122	57	152	Setal2010	Moment tensor inversion	Article	Yes
-9.5700	35.4000	008	3.8	Mw	07/07/2006	13:13:03	279	68	178	Setal2010	Moment tensor inversion	Article	Yes
0.7400	35.6900	006	4.5	Mw	23/07/2006	20:17:13	61	39	113	Setal2010	Moment tensor inversion	Article	Yes
0.6800	35.8100	008	3.9	Mw	23/07/2006	23:07:00	76	29	95	Setal2010	Moment tensor inversion	Article	Yes
3.8000	34.8400	010	4.7	mb	07/08/2006	10:59:45	62	71	-180	RCMT	Moment tensor inversion	Catalog	Yes
-9.9100	35.5000	050	4.4	Mw	10/08/2006	09:16:07	21	83	8	Setal2010	Moment tensor inversion	Article	Yes
-12.3751	36.8978	150	4.3	Mw	20/09/2006	06:53:18	256	81	66	IGN	Moment tensor inversion	Catalog	No
-0.0030	43.0280	010	5.1	Ml	17/11/2006	18:19:51	105	35	-80	Chevrot (2011)	Moment tensor inversion	Article	Yes
0.0030	43.0120	007	3.3	M	18/11/2006	20:34:00	122	30	-74	FMHex20	Compilation	Catalog	Yes
0.0000	43.0120	007	3.0	M	18/11/2006	22:17:00	137	29	-60	FMHex20	Compilation	Catalog	Yes
-0.0060	43.0230	008	2.8	M	19/11/2006	05:10:00	299	40	-90	FMHex20	Compilation	Catalog	Yes

-0.0100	43.0220	008	3.3	M	19/11/2006	13:16:00	260	65	-86	FMHex20	Compilation	Catalog	Yes
-0.0080	43.0190	008	2.9	M	20/11/2006	04:01:00	104	70	-72	FMHex20	Compilation	Catalog	Yes
-0.0060	43.0260	009	2.8	M	22/11/2006	13:55:00	249	55	-90	FMHex20	Compilation	Catalog	Yes
-0.0010	43.0210	008	2.9	M	02/12/2006	06:23:00	285	28	-90	FMHex20	Compilation	Catalog	Yes
-0.1100	43.0210	009	4.0	Ml	16/12/2006	08:17:01	105	35	-120	Chevrot (2011)	Moment tensor inversion	Article	Yes
0.9100	36.4500	008	4.5	Mw	16/12/2006	19:34:34	62	17	114	Setal2010	Moment tensor inversion	Article	Yes
3.3300	34.7400	010	4.8	mb	30/12/2006	23:50:48	61	41	123	RCMT	Moment tensor inversion	Catalog	Yes
-5.3900	37.1100	010	3.6	Mw	02/01/2007	12:19:26	135	79	-174	Setal2010	Moment tensor inversion	Article	Yes
-5.3300	37.1600	014	3.6	Mw	02/01/2007	15:00:47	136	71	-152	Setal2010	Moment tensor inversion	Article	Yes
-3.7700	37.1900	006	3.7	Mw	04/01/2007	23:32:32	303	53	-62	Setal2010	Moment tensor inversion	Article	Yes
-3.5507	32.6147	000	4.9	Mw	30/01/2007	04:38:41	74	44	-179	ETHZ	Moment tensor inversion	Catalog	Yes
-10.4100	35.9600	030	5.9	Mw	12/02/2007	10:35:00	246	64	51	Buetal2016	Compilation	Article	Yes
-8.8600	36.9300	032	3.6	Mw	10/04/2007	19:46:28	178	64	-22	Doetal2013	Moment tensor inversion	Article	Yes
2.5400	36.1600	016	4.4	Mw	08/05/2007	06:56:34	137	84	-133	Setal2010	Moment tensor inversion	Article	Yes
-6.2600	35.2900	059	4.6	Md	18/05/2007	00:00:00	161	7	-26	Bensetal2011	Polarity	Article	No
-2.9800	40.4100	008	4.2	M	07/06/2007	00:42:09	225	75	179	Perezetal2022	Compilation	Article	Yes
-3.6300	37.0600	012	3.4	Mw	09/06/2007	07:15:16	188	38	-55	Setal2010	Moment tensor inversion	Article	Yes
-5.6500	34.3000	015	4.5	Md	23/06/2007	00:00:00	97	55	136	Bensetal2011	Polarity	Article	Yes
-5.4400	37.0700	008	4.4	Mw	30/06/2007	03:53:45	81	45	123	Setal2010	Moment tensor inversion	Article	Yes
-5.4200	37.0800	008	3.6	Mw	30/06/2007	11:29:35	103	58	158	Setal2010	Moment tensor inversion	Article	Yes
-12.0600	36.5500	034	4.5	Mw	01/07/2007	19:03:14	98	65	148	Doetal2013	Moment tensor inversion	Article	Yes
-5.3100	33.1900	020	4.7	Mw	11/08/2007	20:45:58	106	87	171	Setal2010	Moment tensor inversion	Article	Yes
-2.9900	39.3500	012	4.7	Mw	12/08/2007	07:47:05	335	85	6	Setal2010	Moment tensor inversion	Article	Yes
2.7300	36.1200	014	4.1	Mw	21/08/2007	14:58:42	15	65	-18	Daboetal2021	Others	Article	Yes
2.7700	36.0300	004	4.4	Mw	22/08/2007	18:08:33	23	57	-1	Setal2010	Moment tensor inversion	Article	Yes
-8.6240	36.0320	038	3.0	Ml	03/09/2007	03:07:18	-84	90	-97	Silva2017	Polarity	Article	Yes
-1.8800	37.3200	008	3.4	Mw	03/09/2007	13:21:16	26	73	18	Setal2010	Moment tensor inversion	Article	Yes
2.7000	36.2000	021	3.8	Mw	04/09/2007	14:41:00	223	89	4	EMSC	Compilation	Catalog	Yes
-10.8310	35.8860	025	3.7	Ml	06/09/2007	06:44:31	8	82	-41	Silva2017	Polarity	Article	Yes

-3.4900	35.6800	004	4.4	Mw	08/09/2007	16:41:30	259	64	78	Setal2010	Moment tensor inversion	Article	Yes
-9.7700	36.5640	041	3.4	Ml	09/09/2007	03:16:41	7	26	-21	Silva2017	Polarity	Article	Yes
-5.4700	37.0800	012	3.6	Mw	14/09/2007	03:45:06	65	35	107	Setal2010	Moment tensor inversion	Article	Yes
-5.4700	37.0800	008	3.6	Mw	14/09/2007	03:46:49	51	54	97	Setal2010	Moment tensor inversion	Article	Yes
-9.6360	36.7010	040	3.6	Ml	14/09/2007	17:40:26	8	38	9	Silva2017	Polarity	Article	Yes
-10.3740	35.8710	043	3.1	Ml	17/09/2007	02:34:05	120	68	155	Silva2017	Polarity	Article	Yes
-5.4300	37.0100	008	3.9	Mw	18/09/2007	23:20:42	52	34	103	Setal2010	Moment tensor inversion	Article	Yes
-10.5070	35.8450	048	2.7	Ml	22/09/2007	00:07:45	81	53	138	Silva2017	Polarity	Article	Yes
-3.9300	37.0500	006	3.5	Mw	01/10/2007	00:39:56	107	62	-120	Setal2010	Moment tensor inversion	Article	Yes
-9.8000	36.6280	040	2.5	Ml	04/10/2007	19:25:19	48	83	-161	Silva2017	Polarity	Article	Yes
-11.3440	36.5510	034	2.8	Ml	05/10/2007	04:00:22	129	77	-59	Silva2017	Polarity	Article	Yes
-9.9060	36.4700	039	2.2	Ml	10/10/2007	14:45:08	160	42	98	Silva2017	Polarity	Article	Yes
-11.3210	36.3670	032	2.5	Ml	20/10/2007	05:34:52	139	48	-114	Silva2017	Polarity	Article	Yes
-9.9530	36.4360	032	2.4	Ml	21/10/2007	07:38:48	138	86	158	Silva2017	Polarity	Article	Yes
-10.7910	37.0570	045	2.9	Ml	23/10/2007	06:20:23	31	28	138	Silva2017	Polarity	Article	Yes
-10.4000	35.8280	033	2.1	Ml	28/10/2007	00:50:27	133	58	-172	Silva2017	Polarity	Article	Yes
-8.7780	35.6970	046	2.1	Ml	01/11/2007	15:41:43	116	87	98	Silva2017	Polarity	Article	Yes
-8.8920	36.2150	014	3.7	Ml	06/11/2007	23:09:54	197	31	53	Geisetal2010	Polarity	Article	Yes
-10.5270	35.8740	017	2.5	Ml	07/11/2007	14:25:31	29	60	-1	Silva2017	Polarity	Article	Yes
-8.9170	36.2090	008	2.2	Ml	07/11/2007	14:28:01	250	82	-21	Geisetal2010	Polarity	Article	Yes
-9.7780	36.5790	041	2.1	Ml	13/11/2007	11:05:08	75	78	-141	Silva2017	Polarity	Article	Yes
-0.0020	43.0210	008	4.0	Ml	15/11/2007	13:47:35	130	60	-60	Chevrot (2011)	Moment tensor inversion	Article	Yes
-10.3830	35.8770	040	2.5	Ml	17/11/2007	07:54:52	88	35	138	Silva2017	Polarity	Article	Yes
-4.5040	36.3850	080	3.7	mb	20/11/2007	06:27:13	9	76	-27	Sanetal2019	Polarity	Article	No
-10.2180	35.7050	032	3.3	Ml	23/11/2007	04:28:58	90	78	-179	Silva2017	Polarity	Article	Yes

-10.1740	35.7070	033	2.3	Ml	23/11/2007	19:52:31	27	51	40	Silva2017	Polarity	Article	Yes
-9.7590	36.6190	043	2.7	Ml	25/11/2007	00:23:13	24	66	-21	Silva2017	Polarity	Article	Yes
-10.6320	36.1100	032	2.1	Ml	25/11/2007	23:46:39	69	78	138	Silva2017	Polarity	Article	Yes
-11.3120	36.3760	030	2.4	Ml	03/12/2007	12:28:22	53	28	-1	Silva2017	Polarity	Article	Yes
-9.7870	36.6210	042	2.2	Ml	04/12/2007	07:04:21	78	67	-172	Silva2017	Polarity	Article	Yes
-9.7840	36.5510	042	2.2	Ml	04/12/2007	19:31:15	127	56	-121	Silva2017	Polarity	Article	Yes
-7.6750	36.4140	033	2.7	Ml	06/12/2007	18:22:58	97	10	-21	Silva2017	Polarity	Article	Yes
-9.8150	36.4900	039	2.5	Ml	12/12/2007	05:13:28	22	90	78	Silva2017	Polarity	Article	Yes
-9.7680	36.6680	047	3.1	Ml	13/12/2007	05:36:09	73	89	-142	Silva2017	Polarity	Article	Yes
-6.2600	32.1200	026	4.1	Md	18/12/2007	00:00:00	276	32	-107	Bensetal2011	Polarity	Article	Yes
-9.8580	36.4280	041	2.1	Ml	27/12/2007	08:11:38	32	68	-113	Silva2017	Polarity	Article	Yes
-10.3790	35.8130	045	3.2	Ml	27/12/2007	20:20:40	18	78	18	Silva2017	Polarity	Article	Yes
-8.5330	36.1330	040	3.3	Ml	01/01/2008	14:00:40	28	50	94	Silva2017	Polarity	Article	Yes
-0.4570	35.6890	011	4.7	Mw	09/01/2008	22:24:04	235	39	88	Bouhetal2022	Moment tensor inversion	Article	Yes
-9.9400	36.4700	046	4.4	Mw	11/01/2008	00:21:45	40	74	30	Doetal2013	Moment tensor inversion	Article	Yes
-9.9180	36.4450	044	3.0	Ml	11/01/2008	01:35:27	33	90	78	Silva2017	Polarity	Article	Yes
-9.9170	36.4440	042	2.3	Ml	11/01/2008	06:53:04	158	61	-46	Silva2017	Polarity	Article	Yes
-10.8000	36.9390	043	2.4	Ml	12/01/2008	19:11:37	90	79	118	Silva2017	Polarity	Article	Yes
-3.9400	35.1200	008	4.1	Md	21/01/2008	00:00:00	200	70	-9	Bensetal2011	Polarity	Article	Yes
-10.9480	36.0430	029	2.9	Ml	24/01/2008	03:15:39	105	58	178	Silva2017	Polarity	Article	Yes
-5.3600	33.0100	006	4.3	Md	25/01/2008	00:00:00	80	40	69	Bensetal2011	Polarity	Article	Yes
3.4700	36.8300	010	4.6	mb	01/02/2008	07:33:40	101	83	-173	RCMT	Moment tensor inversion	Catalog	Yes
-11.2520	36.5130	031	3.2	Ml	03/02/2008	04:52:36	0	26	58	Silva2017	Polarity	Article	Yes
-8.8370	35.6760	039	2.5	Ml	04/02/2008	15:44:02	33	48	78	Silva2017	Polarity	Article	Yes
-2.2000	36.9900	012	4.2	Mw	06/02/2008	17:53:01	12	84	5	Setal2010	Moment tensor inversion	Article	Yes
-8.9720	35.5730	042	2.4	Ml	13/02/2008	17:30:36	107	38	58	Silva2017	Polarity	Article	Yes

-10.5590	35.8730	049	2.8	Ml	15/02/2008	07:37:05	0	10	-126	Silva2017	Polarity	Article	Yes
-8.6030	35.8540	042	2.0	Ml	21/02/2008	10:10:58	48	58	-171	Silva2017	Polarity	Article	Yes
-10.4160	35.8010	044	2.7	Ml	23/02/2008	16:37:34	148	32	134	Silva2017	Polarity	Article	Yes
-10.3070	35.8500	047	3.1	Ml	24/02/2008	22:53:22	99	58	-179	Silva2017	Polarity	Article	Yes
-9.2200	42.6200	010	3.5	Mw	25/02/2008	15:29:53	76	69	146	Setal2010	Moment tensor inversion	Article	Yes
-10.3090	35.8470	047	2.4	Ml	27/02/2008	02:50:51	93	78	158	Silva2017	Polarity	Article	Yes
-11.1370	36.4750	040	2.7	Ml	27/02/2008	05:19:18	107	75	118	Silva2017	Polarity	Article	Yes
-0.9000	37.9500	004	3.5	Mw	02/03/2008	04:03:52	298	73	113	Setal2010	Moment tensor inversion	Article	Yes
-9.9460	36.4220	041	2.7	Ml	02/03/2008	21:58:00	29	78	-1	Silva2017	Polarity	Article	Yes
-10.7880	35.9790	052	2.4	Ml	05/03/2008	23:34:53	15	54	-82	Geisetal2010	Polarity	Article	No
-9.8900	36.4030	044	2.9	Ml	06/03/2008	12:33:52	160	77	-50	Silva2017	Polarity	Article	Yes
-7.8810	36.0340	036	3.5	Ml	06/03/2008	16:35:41	50	48	30	Silva2017	Polarity	Article	Yes
-10.2810	35.8630	042	2.2	Ml	10/03/2008	00:40:44	115	62	-121	Silva2017	Polarity	Article	Yes
-8.8780	35.6870	051	2.7	Ml	13/03/2008	03:37:59	38	59	38	Silva2017	Polarity	Article	No
-9.8240	36.5340	041	2.2	Ml	13/03/2008	03:53:32	136	51	-21	Silva2017	Polarity	Article	Yes
-9.9940	36.3370	039	2.1	Ml	14/03/2008	06:37:03	46	54	18	Silva2017	Polarity	Article	Yes
-10.4910	36.7180	048	2.1	Ml	19/03/2008	08:10:13	50	82	57	Silva2017	Polarity	Article	Yes
-10.5110	36.7920	044	3.0	Ml	19/03/2008	18:11:24	30	48	-21	Silva2017	Polarity	Article	Yes
-9.7420	35.3200	037	2.3	Ml	20/03/2008	17:55:52	0	45	-128	Silva2017	Polarity	Article	Yes
-10.4120	35.8510	047	2.2	Ml	21/03/2008	16:01:41	76	62	71	Geisetal2010	Polarity	Article	Yes
-10.3920	35.7620	042	2.6	Ml	27/03/2008	15:26:51	99	88	138	Silva2017	Polarity	Article	Yes
-11.1980	36.3410	027	2.8	Ml	01/04/2008	13:05:13	40	48	-21	Silva2017	Polarity	Article	Yes
-9.9140	36.4910	044	3.8	Ml	02/04/2008	00:46:26	26	52	58	Silva2017	Polarity	Article	Yes
-9.8130	36.5860	044	2.0	Ml	06/04/2008	23:44:12	160	81	-25	Silva2017	Polarity	Article	Yes

-9.3760	35.1440	044	2.5	Ml	11/04/2008	22:51:40	138	15	58	Silva2017	Polarity	Article	Yes
-9.8390	36.3370	044	3.3	Ml	12/04/2008	14:36:33	18	51	55	Silva2017	Polarity	Article	Yes
-9.3100	37.3000	030	3.6	Mw	14/04/2008	03:33:08	201	77	-19	Doetal2013	Moment tensor inversion	Article	Yes
-9.9440	36.4470	025	2.1	Ml	14/04/2008	08:00:52	120	28	-141	Silva2017	Polarity	Article	Yes
-9.9470	36.4460	033	2.3	Ml	16/04/2008	20:33:44	73	56	98	Silva2017	Polarity	Article	Yes
-11.2440	36.5930	031	2.8	Ml	21/04/2008	16:52:10	49	75	78	Silva2017	Polarity	Article	Yes
-10.7340	36.7210	041	2.4	Ml	22/04/2008	03:26:18	40	80	56	Silva2017	Polarity	Article	Yes
-9.7670	36.6640	044	3.1	Ml	25/04/2008	13:36:15	20	47	40	Silva2017	Polarity	Article	Yes
-9.8780	35.9050	046	2.0	Ml	26/04/2008	08:27:51	81	36	98	Silva2017	Polarity	Article	Yes
-3.4600	39.7100	006	3.6	Mw	28/04/2008	05:25:05	42	89	-140	Setal2010	Moment tensor inversion	Article	Yes
-8.7720	35.7840	034	2.2	Ml	28/04/2008	23:51:44	30	76	29	Silva2017	Polarity	Article	Yes
-11.2780	36.2770	033	2.2	Ml	29/04/2008	05:52:08	107	58	-141	Silva2017	Polarity	Article	Yes
-1.7000	38.1500	008	3.4	Mw	30/04/2008	22:30:40	324	73	165	Setal2010	Moment tensor inversion	Article	Yes
0.2220	42.9600	012	3.8	Ml	03/05/2008	12:14:21	145	70	-50	Chevrot (2011)	Moment tensor inversion	Article	Yes
-11.1930	36.7180	021	2.4	Ml	05/05/2008	00:44:17	68	35	35	Silva2017	Polarity	Article	Yes
-10.7310	36.1430	021	3.9	Ml	07/05/2008	15:12:39	76	48	118	Silva2017	Polarity	Article	Yes
-4.7620	35.9390	089	2.7	mb	08/05/2008	16:57:33	338	50	-90	Sanetal2019	Polarity	Article	No
-10.7700	35.9700	050	3.9	Mw	10/05/2008	16:33:09	360	77	-88	Setal2010	Moment tensor inversion	Article	Yes
-0.1770	43.0280	010	4.2	Ml	18/05/2008	01:57:21	100	35	-75	Chevrot (2011)	Moment tensor inversion	Article	Yes
-10.4760	35.9490	045	2.9	Ml	22/05/2008	18:12:31	38	86	-31	Geisetal2010	Polarity	Article	Yes
-9.8000	36.5210	046	2.3	Ml	23/05/2008	11:39:10	37	48	18	Silva2017	Polarity	Article	Yes
-9.9640	36.3920	043	3.1	Ml	29/05/2008	23:27:41	60	74	56	Silva2017	Polarity	Article	Yes
-9.9130	36.4260	035	2.1	Ml	05/06/2008	11:34:02	128	88	101	Silva2017	Polarity	Article	Yes
-0.5760	35.8690	008	5.4	Mw	06/06/2008	20:02:57	215	50	84	Bouhetal2022	Moment tensor inversion	Article	Yes
-0.6300	35.8300	006	4.2	Mw	06/06/2008	22:48:23	62	17	117	Setal2010	Moment tensor inversion	Article	Yes
-8.7740	35.9010	032	2.5	Ml	11/06/2008	14:40:31	92	67	-177	Silva2017	Polarity	Article	Yes

-4.5830	34.9050	064	4.8	mb	13/06/2008	11:27:42	60	36	31	Sanetal2019	Polarity	Article	No
-9.9710	36.3090	042	1.9	Ml	13/06/2008	22:42:18	328	20	-75	Silva2017	Polarity	Article	No
-0.4200	39.0200	006	3.3	Mw	15/06/2008	20:55:24	164	45	-101	Setal2010	Moment tensor inversion	Article	Yes
-10.1900	35.6910	032	2.5	Ml	16/06/2008	20:03:42	92	38	-177	Silva2017	Polarity	Article	Yes
1.1500	36.1900	008	4.5	Mw	18/06/2008	13:23:58	38	32	77	Setal2010	Moment tensor inversion	Article	Yes
-9.9960	36.1850	042	2.6	Ml	22/06/2008	16:37:23	160	47	-41	Silva2017	Polarity	Article	Yes
-9.9110	36.4650	032	2.0	Ml	26/06/2008	07:06:38	42	90	29	Silva2017	Polarity	Article	Yes
-9.9200	36.4310	034	1.9	Ml	30/06/2008	14:49:31	133	68	138	Silva2017	Polarity	Article	No
-9.9270	36.5100	042	2.5	Ml	04/07/2008	03:11:33	28	58	-1	Silva2017	Polarity	Article	Yes
-0.4060	43.0840	016	4.1	Ml	16/07/2008	20:33:33	155	80	-5	Chevrot (2011)	Moment tensor inversion	Article	Yes
-9.8900	36.2400	060	3.9	Mw	17/07/2008	19:22:07	20	51	62	Setal2010	Moment tensor inversion	Article	No
-10.7220	36.7390	038	3.4	Ml	18/07/2008	07:12:41	7	78	2	Silva2017	Polarity	Article	Yes
-8.5280	36.0360	054	2.4	Ml	19/07/2008	12:51:52	10	12	-141	Silva2017	Polarity	Article	No
-0.4200	39.0100	006	3.7	Mw	21/07/2008	02:30:03	155	41	-120	Setal2010	Moment tensor inversion	Article	Yes
2.5840	41.8730	011	4.4	Ml	22/07/2008	22:36:32	25	55	-5	Chevrot (2011)	Moment tensor inversion	Article	Yes
-0.9800	35.6400	010	4.4	Mw	24/07/2008	17:19:52	60	18	85	Setal2010	Moment tensor inversion	Article	Yes
-4.6870	35.7970	088	2.9	mb	28/07/2008	02:16:35	229	60	-90	Sanetal2019	Polarity	Article	No
3.0600	41.3700	014	3.4	Mw	16/08/2008	10:21:20	50	66	37	Setal2010	Moment tensor inversion	Article	Yes
1.0500	36.4500	004	3.8	Mw	24/08/2008	20:52:44	56	14	103	Setal2010	Moment tensor inversion	Article	Yes
-0.5000	35.9000	069	4.2	Mw	25/08/2008	02:15:00	81	80	-169	EMSC	Compilation	Catalog	No
-6.9790	35.6190	059	5.2	mb	09/09/2008	13:36:40	21	83	-19	Sanetal2019	Polarity	Article	No
-0.9000	38.2700	004	3.7	Mw	14/09/2008	14:03:39	148	51	160	Setal2010	Moment tensor inversion	Article	Yes
-4.4490	36.7150	070	4.0	mb	17/09/2008	05:27:18	183	51	-8	Sanetal2019	Polarity	Article	No
-0.3350	43.0370	009	3.8	Ml	18/09/2008	12:55:49	115	55	-95	Chevrot (2011)	Moment tensor inversion	Article	Yes
-5.8900	33.5900	022	4.5	Md	28/09/2008	00:00:00	80	21	66	Bensetal2011	Polarity	Article	Yes
-5.4100	37.0400	004	4.6	Mw	02/10/2008	04:02:54	45	73	97	Doetal2013	Moment tensor inversion	Article	Yes
-5.4300	37.0200	012	3.9	Mw	02/10/2008	04:05:06	54	39	92	Setal2010	Moment tensor inversion	Article	Yes
-5.4300	37.0600	006	3.4	Mw	02/10/2008	05:14:19	44	45	109	Setal2010	Moment tensor inversion	Article	Yes
-5.4000	37.0600	016	3.2	Mw	02/10/2008	09:22:14	87	66	166	Setal2010	Moment tensor inversion	Article	Yes

-5.4100	37.0600	012	3.5	Mw	08/10/2008	16:04:47	211	69	24	Setal2010	Moment tensor inversion	Article	Yes
-2.5700	36.4900	006	3.7	Mw	20/10/2008	09:46:11	16	73	-42	Setal2010	Moment tensor inversion	Article	Yes
-2.5600	36.4700	014	4.3	Mw	21/10/2008	03:28:53	112	62	-174	Setal2010	Moment tensor inversion	Article	Yes
-2.5900	36.4700	014	4.3	Mw	21/10/2008	05:55:46	114	72	-168	Setal2010	Moment tensor inversion	Article	Yes
-2.5200	36.4700	014	3.8	Mw	21/10/2008	12:50:56	21	75	-11	Setal2010	Moment tensor inversion	Article	Yes
-2.5700	36.4700	014	4.0	Mw	26/10/2008	00:51:22	22	79	-12	Setal2010	Moment tensor inversion	Article	Yes
-2.5700	36.4700	006	4.4	Mw	07/11/2008	11:02:51	128	57	-148	Setal2010	Moment tensor inversion	Article	Yes
-7.5000	36.6000	009	4.4	Mw	04/12/2008	13:18:00	170	61	78	EMSC	Compilation	Catalog	Yes
1.5800	36.3800	004	4.0	Mw	17/01/2009	11:22:26	75	48	106	Maretal2015	Moment tensor inversion	Article	Yes
-0.2620	43.0610	002	4.2	Mw	09/02/2009	08:38:00	264	30	-89	FMHex20	Compilation	Catalog	Yes
-8.5700	38.0700	013	3.4	Mw	17/02/2009	16:00:05	28	74	-5	Doetal2013	Moment tensor inversion	Article	Yes
-4.5410	36.3970	084	3.2	mb	01/04/2009	12:56:10	9	76	-27	Sanetal2019	Polarity	Article	No
-1.1600	38.2400	010	3.9	Mw	15/04/2009	15:42:25	319	78	169	Maretal2015	Moment tensor inversion	Article	Yes
-9.6700	36.8600	025	3.3	Mw	22/05/2009	23:58:08	45	73	56	Doetal2013	Moment tensor inversion	Article	Yes
0.7200	36.2400	006	4.0	Mw	11/06/2009	05:42:15	56	21	112	Maretal2015	Moment tensor inversion	Article	Yes
-4.6280	35.7640	099	2.6	mb	15/06/2009	08:21:46	339	61	78	Sanetal2019	Polarity	Article	No
-4.5000	36.8460	053	4.6	mb	05/07/2009	14:15:01	21	50	0	Sanetal2019	Polarity	Article	No
-10.2500	36.0600	050	4.3	Mw	05/07/2009	15:50:57	93	53	94	Maretal2015	Moment tensor inversion	Article	Yes
-5.9700	31.9200	010	3.6	Ml	06/07/2009	12:00:27	314	64	-134	ElMoudetal2023	Polarity	Article	Yes
-7.8100	35.9500	050	4.1	Mw	18/08/2009	06:56:00	284	72	-142	Maretal2015	Moment tensor inversion	Article	Yes
-2.5360	35.9490	002	3.5	Mw	29/08/2009	06:53:00	240	67	68	Greetal2015	Polarity	Article	Yes
-2.9090	36.5710	009	2.9	Mw	03/09/2009	11:36:00	221	67	46	Greetal2015	Polarity	Article	Yes
-7.8250	36.0000	050	3.8	Mw	08/09/2009	00:04:00	232	41	-75	Greetal2015	Polarity	Article	Yes
-3.0380	35.8470	012	2.7	Mw	18/09/2009	17:22:00	18	30	-178	Greetal2015	Polarity	Article	Yes
-4.7940	35.8770	069	3.8	mb	19/09/2009	07:23:56	76	67	20	Sanetal2019	Polarity	Article	No
-2.2770	35.0020	004	3.2	Mw	20/09/2009	11:13:00	160	75	-48	Greetal2015	Polarity	Article	Yes
-4.5750	35.8040	093	2.8	Mw	25/09/2009	16:37:00	282	76	27	Greetal2015	Polarity	Article	No
-3.9670	35.1040	030	3.0	Mw	03/10/2009	13:51:00	205	35	-30	Greetal2015	Polarity	Article	Yes
-2.9650	36.0890	013	2.8	Mw	06/10/2009	14:00:00	127	73	58	Greetal2015	Polarity	Article	Yes
-3.0340	35.9560	006	3.4	Mw	12/10/2009	12:03:00	103	44	22	Greetal2015	Polarity	Article	Yes

-3.0090	36.4200	012	2.8	Mw	12/10/2009	14:06:00	66	38	-22	Greetal2015	Polarity	Article	Yes
-3.7290	35.3380	004	2.8	Mw	13/10/2009	09:35:00	235	64	56	Greetal2015	Polarity	Article	Yes
-2.3355	40.2135	011	3.3	Mw	14/10/2009	16:16:33	228	71	-157	IGN	Moment tensor inversion	Catalog	Yes
0.2000	43.0210	013	4.0	Mw	15/10/2009	22:27:00	312	35	-61	FMHex20	Compilation	Catalog	Yes
-2.7010	36.0100	002	2.4	Mw	23/10/2009	13:02:00	58	62	11	Greetal2015	Polarity	Article	Yes
-3.3280	36.2470	009	2.8	Mw	28/10/2009	17:21:00	172	38	-47	Greetal2015	Polarity	Article	Yes
-4.3100	36.4990	085	3.7	Mw	30/10/2009	07:01:00	295	73	71	Greetal2015	Polarity	Article	No
-4.3710	36.5100	091	4.1	mb	30/10/2009	07:01:04	322	40	0	Sanetal2019	Polarity	Article	No
1.7500	36.5000	006	4.2	Mw	02/11/2009	07:28:31	41	22	83	Maretal2015	Moment tensor inversion	Article	Yes
-3.8200	37.0500	026	4.0	Mw	05/11/2009	05:39:55	100	28	-83	Maretal2015	Moment tensor inversion	Article	Yes
-3.0620	36.0250	009	2.1	Mw	12/11/2009	02:58:00	58	34	-42	Greetal2015	Polarity	Article	Yes
-3.0630	36.0260	008	2.3	Mw	12/11/2009	03:25:00	271	56	-53	Greetal2015	Polarity	Article	Yes
-4.6680	35.6430	072	3.4	mb	25/11/2009	01:42:46	277	44	-60	Sanetal2019	Polarity	Article	No
-4.6410	35.6940	102	2.7	mb	09/12/2009	00:11:03	285	61	42	Sanetal2019	Polarity	Article	No
-0.0900	32.8200	008	5.0	Mw	14/12/2009	06:41:12	29	27	128	Maretal2015	Moment tensor inversion	Article	Yes
-9.7800	36.5300	030	5.4	Mw	17/12/2009	01:37:47	43	83	38	Maretal2015	Moment tensor inversion	Article	Yes
-0.1100	35.2000	004	4.2	Mw	21/12/2009	02:45:04	75	71	104	Maretal2015	Moment tensor inversion	Article	Yes
-5.7700	34.8000	040	4.5	Mw	21/01/2010	16:57:06	274	81	-13	Maretal2015	Moment tensor inversion	Article	Yes
-5.2800	34.7900	040	4.1	Mw	14/02/2010	22:14:30	33	70	-92	Maretal2015	Moment tensor inversion	Article	Yes
-8.4200	36.2080	011	3.9	Ml	05/03/2010	17:10:50	105	40	135	Custetal2016	Polarity	Article	Yes
-4.8860	35.2300	069	4.2	mb	07/03/2010	16:35:13	86	28	43	Sanetal2019	Polarity	Article	No
-7.9510	39.6340	029	3.5	Ml	22/03/2010	12:06:59	95	85	-170	Custetal2016	Polarity	Article	Yes
-7.6130	38.9700	014	4.1	Ml	27/03/2010	13:37:52	190	80	5	Custetal2016	Polarity	Article	Yes
-9.7690	36.7690	020	4.2	Mw	31/03/2010	03:12:03	80	69	65	Custetal2016	Moment tensor inversion	Article	Yes
0.3190	42.9730	013	4.3	Ml	01/04/2010	01:36:39	110	25	-90	Chevrot (2011)	Moment tensor inversion	Article	Yes
-3.6900	37.0000	620	6.3	Mw	11/04/2010	22:08:06	55	24	-44	Maretal2015	Moment tensor inversion	Article	No
-6.2150	35.2990	070	5.4	mb	22/04/2010	01:24:00	215	80	17	Sanetal2019	Polarity	Article	No
-6.2310	35.2790	068	5.1	mb	22/04/2010	01:42:47	99	30	90	Sanetal2019	Polarity	Article	No
-1.4040	42.8900	001	4.0	Mw	07/05/2010	19:14:00	273	63	-90	FMHex20	Compilation	Catalog	Yes
4.1400	35.9200	002	5.4	Mw	14/05/2010	12:29:23	241	80	102	Maretal2015	Moment tensor inversion	Article	Yes

4.1100	35.9200	006	4.7	Md	14/05/2010	15:13:13	88	85	-177	Yelletal2014	Polarity	Article	Yes
4.0000	35.9700	015	4.5	mb	14/05/2010	23:43:25	338	82	3	RCMT	Moment tensor inversion	Catalog	Yes
4.0900	35.9700	009	4.0	Md	15/05/2010	00:00:40	273	58	93	Yelletal2014	Polarity	Article	Yes
4.1300	35.8700	008	4.3	Mw	16/05/2010	03:51:30	44	28	134	Maretal2015	Moment tensor inversion	Article	Yes
4.0500	35.8400	006	5.1	Mw	16/05/2010	06:52:42	45	32	95	Maretal2015	Moment tensor inversion	Article	Yes
4.0900	35.9700	009	4.0	Md	16/05/2010	09:46:01	292	71	127	Yelletal2014	Polarity	Article	Yes
4.0900	35.9500	008	4.1	Md	19/05/2010	23:59:50	283	49	108	Yelletal2014	Polarity	Article	Yes
4.1200	35.9500	008	4.0	Md	21/05/2010	12:16:18	85	89	168	Yelletal2014	Polarity	Article	Yes
-4.4920	36.2650	081	3.3	mb	22/05/2010	08:04:40	313	80	80	Sanetal2019	Polarity	Article	No
4.1400	35.9200	004	5.5	Mw	23/05/2010	13:28:17	92	18	62	Maretal2015	Moment tensor inversion	Article	Yes
4.0900	35.9100	005	4.1	Md	23/05/2010	23:39:54	7	85	-26	Yelletal2014	Polarity	Article	Yes
4.1500	35.9500	008	4.2	Mw	24/05/2010	21:00:42	345	49	19	Maretal2015	Moment tensor inversion	Article	Yes
4.1100	35.9200	006	4.1	Md	24/05/2010	23:48:25	3	89	-35	Yelletal2014	Polarity	Article	Yes
4.1100	35.9100	005	4.5	Md	25/05/2010	13:05:09	3	87	-14	Yelletal2014	Polarity	Article	Yes
4.1100	35.9000	006	4.2	Md	26/05/2010	17:49:44	12	73	5	Yelletal2014	Polarity	Article	Yes
4.1100	35.9100	006	4.3	Md	26/05/2010	20:47:39	179	89	25	Yelletal2014	Polarity	Article	Yes
-2.2600	35.4800	014	3.8	Mw	28/05/2010	15:55:04	22	73	1	Maretal2015	Moment tensor inversion	Article	Yes
4.1200	35.9400	005	4.2	Md	30/05/2010	04:48:30	55	51	40	Yelletal2014	Polarity	Article	Yes
4.1100	35.9200	007	4.6	Md	31/05/2010	16:05:03	23	89	-10	Yelletal2014	Polarity	Article	Yes
-4.6140	35.6220	055	4.2	mb	10/06/2010	12:37:50	204	70	-4	Sanetal2019	Polarity	Article	No
-4.5480	35.8110	085	3.0	mb	14/06/2010	12:23:04	264	30	0	Sanetal2019	Polarity	Article	No
-6.2000	36.6200	040	3.5	Mw	21/06/2010	15:22:05	192	53	45	Maretal2015	Moment tensor inversion	Article	Yes
3.9000	36.2000	012	3.9	Mw	01/07/2010	03:29:00	93	60	87	EMSC	Compilation	Catalog	Yes
-2.3100	36.5700	008	4.2	Mw	05/07/2010	10:38:11	185	87	9	Maretal2015	Moment tensor inversion	Article	Yes
-2.3800	36.6900	010	4.0	Mw	06/07/2010	14:44:05	79	65	169	Maretal2015	Moment tensor inversion	Article	Yes
-2.3700	36.6900	012	3.7	Mw	06/07/2010	20:34:00	354	88	-33	Maretal2015	Moment tensor inversion	Article	Yes
-2.3400	36.5500	008	3.5	Mw	10/07/2010	19:12:33	84	68	176	Maretal2015	Moment tensor inversion	Article	Yes
-2.3700	36.7000	020	3.7	Mw	10/07/2010	19:18:02	208	53	30	Maretal2015	Moment tensor inversion	Article	Yes
-7.6960	42.7120	015	3.4	Ml	18/07/2010	22:38:28	125	70	-145	Custetal2016	Polarity	Article	Yes
-10.3400	35.9340	031	3.9	Mw	23/07/2010	12:45:17	107	76	129	Custetal2016	Moment tensor inversion	Article	Yes

-7.7170	36.2350	010	3.9	Mw	25/07/2010	20:24:41	313	80	-138	Custetal2016	Moment tensor inversion	Article	Yes
-6.0800	32.3600	010	4.4	Mw	05/08/2010	18:54:16	53	36	82	Maretal2015	Moment tensor inversion	Article	Yes
-6.1560	36.3060	000	3.4	Ml	25/08/2010	08:29:03	350	70	-85	Custetal2016	Polarity	Article	Yes
-4.2080	36.9290	063	3.7	mb	30/08/2010	02:58:26	40	53	-65	Sanetal2019	Polarity	Article	No
-2.9600	35.2000	022	3.9	Mw	05/09/2010	03:33:47	215	87	17	Maretal2015	Moment tensor inversion	Article	Yes
-3.7200	32.1200	012	3.8	Mw	08/09/2010	10:32:49	260	87	71	Maretal2015	Moment tensor inversion	Article	Yes
-1.1170	43.1600	016	4.0	Mw	14/09/2010	12:07:00	277	72	-81	FMHex20	Compilation	Catalog	Yes
-2.5800	36.7100	026	3.7	Mw	12/10/2010	07:20:49	204	77	17	Maretal2015	Moment tensor inversion	Article	Yes
-4.6420	36.4890	052	2.9	mb	15/10/2010	21:00:53	40	40	0	Sanetal2019	Polarity	Article	No
-2.6511	36.6856	006	3.6	Mw	04/11/2010	05:10:20	27	79	-46	IGN	Moment tensor inversion	Catalog	Yes
-2.5900	36.7200	012	4.1	Mw	04/11/2010	12:02:01	213	68	-2	Maretal2015	Moment tensor inversion	Article	Yes
-4.4140	36.4410	090	2.7	mb	10/11/2010	19:15:09	70	62	-11	Sanetal2019	Polarity	Article	No
-0.1910	43.0340	006	3.8	Mw	14/11/2010	22:13:00	321	68	-86	FMHex20	Compilation	Catalog	Yes
-9.1300	37.4580	020	3.1	Ml	27/11/2010	07:14:51	145	50	-110	Custetal2016	Polarity	Article	Yes
-12.7400	36.9500	050	3.8	Mw	29/11/2010	23:57:27	66	44	16	Maretal2015	Moment tensor inversion	Article	Yes
-3.4000	39.8000	087	4.5	Mw	17/12/2010	22:15:00	225	76	-22	EMSC	Compilation	Catalog	No
-4.3850	36.5040	091	3.6	mb	28/12/2010	11:18:19	121	80	-28	Sanetal2019	Polarity	Article	No
-4.4020	36.6700	084	3.6	mb	30/12/2010	00:33:38	276	81	70	Sanetal2019	Polarity	Article	No
-3.9580	36.7820	062	2.7	mb	06/01/2011	23:54:11	29	90	130	Sanetal2019	Polarity	Article	No
-4.5360	36.5730	071	3.1	mb	18/01/2011	04:40:17	285	83	19	Sanetal2019	Polarity	Article	No
-4.4610	35.6960	082	3.6	mb	09/02/2011	11:37:22	41	77	-16	Sanetal2019	Polarity	Article	No
-6.1200	32.0500	026	4.5	Mw	14/02/2011	06:04:55	38	84	-4	Maretal2015	Moment tensor inversion	Article	Yes
-4.3960	36.5190	088	3.2	mb	27/02/2011	07:10:29	24	71	36	Sanetal2019	Polarity	Article	No
-4.5760	35.1490	079	3.7	mb	01/03/2011	10:26:27	282	80	80	Sanetal2019	Polarity	Article	No
-7.1960	42.0550	017	3.1	Ml	15/03/2011	08:49:54	280	85	-170	Custetal2016	Polarity	Article	Yes
-8.4290	37.3040	019	3.6	Mw	26/03/2011	07:36:00	113	78	177	Neretal2024	Moment tensor inversion	Article	Yes
-1.0800	41.1800	010	3.8	Mw	08/04/2011	15:07:12	127	33	-141	Maretal2015	Moment tensor inversion	Article	Yes
3.6000	37.1000	111	4.6	Mw	13/04/2011	18:36:00	138	66	-117	EMSC	Compilation	Catalog	No
-8.4510	42.4200	014	2.6	Ml	22/04/2011	19:01:38	150	55	-10	Custetal2016	Polarity	Article	Yes
-4.9100	32.5600	012	3.3	Ml	01/05/2011	04:50:34	225	50	50	ElMoudetal2023	Polarity	Article	Yes

-6.5460	37.9760	014	3.4	Ml	02/05/2011	23:30:10	205	60	-5	Custetal2016	Polarity	Article	Yes
-1.6800	37.7100	006	4.6	Mw	11/05/2011	15:05:12	127	62	129	Maretal2015	Moment tensor inversion	Article	Yes
-1.6700	37.7200	006	5.2	Mw	11/05/2011	16:47:25	121	55	135	Maretal2015	Moment tensor inversion	Article	Yes
-1.6900	37.7200	004	3.9	Mw	11/05/2011	20:37:44	216	63	22	Maretal2015	Moment tensor inversion	Article	Yes
-12.4000	33.8400	005	4.7	mb	11/05/2011	23:23:35	178	64	-12	RCMT	Moment tensor inversion	Catalog	Yes
-0.1900	43.0240	008	3.6	Mw	14/05/2011	10:25:00	308	62	-76	FMHex20	Compilation	Catalog	Yes
-8.0260	38.3560	004	3.0	Ml	22/05/2011	13:06:38	355	55	-20	Custetal2016	Polarity	Article	Yes
-4.5010	36.4580	079	3.1	mb	22/06/2011	01:42:15	30	64	56	Sanetal2019	Polarity	Article	No
-1.0200	38.3400	014	3.9	Mw	10/07/2011	22:54:21	118	78	163	Maretal2015	Moment tensor inversion	Article	Yes
-4.1430	36.7950	064	3.7	mb	27/08/2011	07:54:50	40	61	-6	Sanetal2019	Polarity	Article	No
-4.4890	34.9770	064	3.1	mb	29/09/2011	20:44:30	246	67	20	Sanetal2019	Polarity	Article	No
-7.1850	42.5260	013	3.3	Mw	01/10/2011	07:14:38	175	57	-2	Custetal2016	Moment tensor inversion	Article	Yes
-1.7954	37.8157	009	3.5	Mw	02/10/2011	13:11:45	25	74	-23	IGN	Moment tensor inversion	Catalog	Yes
0.5100	38.0700	006	3.8	Mw	13/10/2011	11:15:51	146	51	134	Maretal2015	Moment tensor inversion	Article	Yes
-1.9400	37.3100	016	3.7	Mw	24/10/2011	23:35:24	291	80	162	Maretal2015	Moment tensor inversion	Article	Yes
-5.8710	36.4330	052	2.9	mb	05/11/2011	18:22:34	240	90	180	Sanetal2019	Polarity	Article	No
-5.3310	35.6610	052	2.9	mb	06/11/2011	05:45:11	279	53	-65	Sanetal2019	Polarity	Article	No
-9.8000	38.4030	028	3.1	Ml	22/11/2011	10:35:12	165	55	25	Custetal2016	Polarity	Article	Yes
-7.3200	31.3400	013	3.4	Ml	26/12/2011	04:33:54	225	55	0	ElMoudetal2023	Polarity	Article	Yes
-4.4450	36.2900	074	2.7	mb	10/01/2012	06:38:28	150	82	50	Sanetal2019	Polarity	Article	No
-0.7229	35.2291	072	4.1	Mw	15/01/2012	13:45:40	139	62	-95	IGN	Moment tensor inversion	Catalog	No
-6.2360	36.0960	059	3.1	mb	29/01/2012	19:57:12	218	67	20	Sanetal2019	Polarity	Article	No
-3.0420	37.7400	016	3.9	Mw	31/01/2012	14:36:22	93	71	-168	Moetal2015	Moment tensor inversion	Article	Yes
-5.6500	34.4600	040	4.3	Mw	18/02/2012	00:28:27	200	88	8	Maretal2015	Moment tensor inversion	Article	Yes
0.8529	36.4160	039	4.2	Mw	05/03/2012	02:45:23	194	57	45	IGN	Moment tensor inversion	Catalog	Yes
-0.6400	35.8300	004	4.3	Mw	21/03/2012	06:41:58	220	79	108	Maretal2015	Moment tensor inversion	Article	Yes
0.8800	36.6900	012	4.1	Mw	24/03/2012	05:50:03	81	59	-158	Maretal2015	Moment tensor inversion	Article	Yes
0.5400	36.5200	014	4.2	Mw	25/03/2012	02:45:24	8	41	4	Maretal2015	Moment tensor inversion	Article	Yes
4.5900	36.1000	010	4.6	mb	05/04/2012	04:56:21	217	43	75	RCMT	Moment tensor inversion	Catalog	Yes
-4.5410	35.7540	099	3.2	mb	10/04/2012	19:22:56	278	76	27	Sanetal2019	Polarity	Article	No

-4.4640	35.7530	092	3.4	mb	12/04/2012	19:41:28	126	61	78	Sanetal2019	Polarity	Article	No
-2.6400	36.4800	006	4.2	Mw	18/04/2012	09:47:25	201	62	-44	Maretal2015	Moment tensor inversion	Article	Yes
-2.6300	36.5000	006	3.6	Mw	18/04/2012	11:10:37	204	53	-33	Maretal2015	Moment tensor inversion	Article	Yes
1.6560	36.5340	009	4.9	Mw	25/04/2012	03:18:18	10	85	1	Abbeetal2016	Others	Article	Yes
-7.7860	37.2420	012	3.7	Mw	03/05/2012	14:16:24	179	83	-1	Custetal2016	Moment tensor inversion	Article	Yes
-5.8150	35.1720	055	3.5	mb	12/05/2012	09:54:50	301	70	79	Sanetal2019	Polarity	Article	No
-4.5620	36.0000	097	3.1	mb	16/05/2012	11:19:56	22	71	7	Sanetal2019	Polarity	Article	No
1.8400	34.0400	006	4.2	Mw	18/05/2012	13:12:12	49	27	127	Maretal2015	Moment tensor inversion	Article	Yes
-12.7000	37.3000	081	4.5	Mw	01/06/2012	11:00:00	258	79	91	EMSC	Compilation	Catalog	No
-10.5100	36.8600	031	4.1	Mw	05/06/2012	05:09:50	20	70	30	Custetal2016	Moment tensor inversion	Article	Yes
-6.8180	41.1130	024	3.4	Ml	19/06/2012	22:05:47	125	60	175	Custetal2016	Polarity	Article	Yes
-2.9400	34.9100	012	4.0	Mw	04/07/2012	07:44:15	87	57	177	Maretal2015	Moment tensor inversion	Article	Yes
0.9700	36.0800	012	3.7	Mw	15/07/2012	02:05:07	90	39	120	Maretal2015	Moment tensor inversion	Article	Yes
-4.4180	35.0780	063	2.6	mb	13/08/2012	13:13:12	180	50	-90	Sanetal2019	Polarity	Article	No
-4.3940	36.5820	076	2.5	mb	04/09/2012	00:29:56	62	66	33	Sanetal2019	Polarity	Article	No
-2.9200	36.6000	010	3.6	Mw	06/09/2012	04:24:50	96	57	158	Maretal2015	Moment tensor inversion	Article	Yes
-8.7000	34.7000	123	4.6	Mw	23/09/2012	12:17:00	8	49	97	EMSC	Compilation	Catalog	No
-8.3900	37.6280	007	3.6	Mw	24/09/2012	21:52:50	36	72	81	Custetal2016	Moment tensor inversion	Article	Yes
4.5000	36.4600	008	4.0	Mw	10/10/2012	06:14:40	307	62	61	Maretal2015	Moment tensor inversion	Article	Yes
-0.2050	42.9910	006	3.9	Mw	13/10/2012	04:33:00	342	29	-57	FMHex20	Compilation	Catalog	Yes
-2.8900	35.0300	006	4.0	Mw	27/11/2012	08:51:33	171	28	-77	Maretal2015	Moment tensor inversion	Article	Yes
-0.2132	43.0932	006	4.1	Mw	30/12/2012	23:35:01	293	71	-94	IGN	Moment tensor inversion	Catalog	Yes
-8.7370	34.3540	025	3.3	Mw	19/01/2013	17:53:00	19	87	24	Neretal2024	Moment tensor inversion	Article	Yes
-3.2900	38.0200	002	3.7	Mw	05/02/2013	21:24:13	274	59	-168	Moetal2015	Moment tensor inversion	Article	Yes
-5.4800	36.4700	040	4.1	Mw	19/03/2013	03:11:31	81	49	43	Maretal2015	Moment tensor inversion	Article	Yes
-1.8000	42.8200	006	3.8	Mw	23/03/2013	02:57:39	142	85	5	Maretal2015	Moment tensor inversion	Article	Yes
-1.7900	37.8300	022	3.9	Mw	04/04/2013	02:27:14	11	75	-2	Maretal2015	Moment tensor inversion	Article	Yes
-1.7000	37.8800	022	3.4	Mw	07/04/2013	05:45:00	273	86	148	Maretal2015	Moment tensor inversion	Article	Yes
-1.7100	42.7300	004	3.9	Mw	20/04/2013	15:58:21	47	78	-124	Maretal2015	Moment tensor inversion	Article	Yes

-5.5300	32.3400	008	4.6	Ml	27/04/2013	09:21:26	35	52	90	ElMoudetal2023	Polarity	Article	Yes
0.0800	35.6000	006	4.4	Mw	02/05/2013	18:55:35	166	83	32	Maretal2015	Moment tensor inversion	Article	Yes
-0.0570	42.9800	002	3.6	Mw	13/05/2013	12:40:00	112	73	-72	FMHex20	Compilation	Catalog	Yes
-6.2600	32.2400	009	4.5	Ml	27/05/2013	20:07:10	237	60	84	ElMoudetal2023	Polarity	Article	Yes
-5.3900	32.3900	008	5.2	Ml	31/05/2013	08:46:26	32	63	90	ElMoudetal2023	Polarity	Article	Yes
-5.3800	32.4300	005	4.9	Ml	31/05/2013	14:46:03	70	15	90	ElMoudetal2023	Polarity	Article	Yes
-0.6320	43.0510	011	3.8	Mw	07/06/2013	10:07:00	139	45	-47	FMHex20	Compilation	Catalog	Yes
-0.7000	38.0900	014	3.3	Mw	13/06/2013	13:24:22	320	75	163	Maretal2015	Moment tensor inversion	Article	Yes
-8.1000	36.4000	031	3.7	Mw	21/06/2013	18:40:13	67	58	78	Custetal2016	Moment tensor inversion	Article	Yes
-5.3400	32.4100	014	4.5	Ml	25/06/2013	13:09:55	28	58	90	ElMoudetal2023	Polarity	Article	Yes
-5.6300	37.1000	004	3.2	Mw	04/07/2013	17:25:04	136	34	-151	Maretal2015	Moment tensor inversion	Article	Yes
3.0200	36.5500	002	5.1	Mw	17/07/2013	03:00:56	45	9	113	Maretal2015	Moment tensor inversion	Article	Yes
-4.1500	35.2700	004	4.2	Mw	08/08/2013	07:05:25	348	40	-94	Maretal2015	Moment tensor inversion	Article	Yes
-2.8600	36.3300	020	3.5	Mw	14/08/2013	19:24:13	217	84	0	Maretal2015	Moment tensor inversion	Article	Yes
0.7142	40.3805	003	3.5	Mw	24/09/2013	00:21:50	132	88	-155	IGN	Moment tensor inversion	Catalog	Yes
0.7080	40.3849	015	3.9	Mw	29/09/2013	22:15:48	132	62	-139	IGN	Moment tensor inversion	Catalog	Yes
0.7150	40.3821	006	3.9	Mw	30/09/2013	02:21:16	33	70	-26	IGN	Moment tensor inversion	Catalog	Yes
0.7129	40.3914	003	4.2	Mw	01/10/2013	03:32:44	131	70	-158	IGN	Moment tensor inversion	Catalog	Yes
0.7044	40.3990	003	4.1	Mw	02/10/2013	23:06:49	35	75	-28	IGN	Moment tensor inversion	Catalog	Yes
0.7205	40.4031	003	4.1	Mw	02/10/2013	23:29:29	128	87	-134	IGN	Moment tensor inversion	Catalog	Yes
0.7121	40.3932	012	3.8	Mw	04/10/2013	08:49:48	135	71	-151	IGN	Moment tensor inversion	Catalog	Yes
0.7164	40.3876	003	3.5	Mw	04/10/2013	09:55:19	216	86	19	IGN	Moment tensor inversion	Catalog	Yes
-9.8180	36.1510	035	4.1	Mw	19/10/2013	00:19:16	353	73	-115	Custetal2016	Moment tensor inversion	Article	Yes
-3.2600	38.0200	008	3.4	Mw	19/10/2013	15:54:21	205	68	5	Maretal2015	Moment tensor inversion	Article	Yes
-3.2600	38.0200	008	3.2	Mw	19/10/2013	17:31:54	193	85	-30	Moetal2015	Moment tensor inversion	Article	Yes
-9.4390	35.2510	030	3.9	Mw	23/10/2013	13:57:29	106	82	-129	Custetal2016	Moment tensor inversion	Article	Yes
-6.9920	35.5670	070	4.6	Mw	16/12/2013	07:06:23	115	85	134	Custetal2016	Moment tensor inversion	Article	No
-4.3000	35.8300	030	4.0	Mw	23/12/2013	06:12:49	289	54	119	Maretal2015	Moment tensor inversion	Article	Yes
-2.9800	36.5100	004	3.8	Mw	29/12/2013	10:50:37	342	21	-157	Maretal2015	Moment tensor inversion	Article	Yes
-0.1960	43.0100	003	3.6	Mw	03/01/2014	16:51:00	317	63	-78	FMHex20	Compilation	Catalog	Yes

-7.5820	37.4970	022	3.0	Mw	20/01/2014	17:59:28	249	72	-157	Custetal2016	Moment tensor inversion	Article	Yes
3.6400	36.8200	013	4.5	mb	22/02/2014	19:30:34	94	54	-164	RCMT	Moment tensor inversion	Catalog	Yes
-2.8243	36.5548	006	4.0	Mw	24/02/2014	14:24:52	105	86	142	IGN	Moment tensor inversion	Catalog	Yes
-5.0400	34.2500	006	4.8	Mw	11/03/2014	12:27:06	94	76	162	Custetal2016	Moment tensor inversion	Article	Yes
-6.2000	32.4500	005	4.1	Ml	12/03/2014	12:27:09	30	50	90	ElMoudetal2023	Polarity	Article	Yes
-9.4780	36.9160	009	3.5	Mw	13/03/2014	08:56:42	50	73	63	Custetal2016	Moment tensor inversion	Article	Yes
-3.7100	36.9500	013	3.6	Mw	25/03/2014	00:20:10	69	45	-106	Setal2024	Moment tensor inversion	Article	Yes
-0.0070	43.0150	005	4.6	Mw	29/04/2014	07:03:00	115	60	-69	FMHex20	Compilation	Catalog	Yes
-6.1800	32.2400	006	5.0	Ml	12/05/2014	03:53:21	45	50	90	ElMoudetal2023	Polarity	Article	Yes
-5.6000	32.3800	006	4.3	Ml	19/05/2014	12:09:28	30	55	90	ElMoudetal2023	Polarity	Article	Yes
0.2633	35.7074	030	3.7	Mw	22/05/2014	02:57:42	237	79	105	IGN	Moment tensor inversion	Catalog	Yes
0.2590	35.7250	007	4.7	Mw	22/05/2014	05:22:03	254	36	117	Bouhetal2022	Moment tensor inversion	Article	Yes
-3.5584	35.9382	006	4.0	Mw	02/06/2014	07:02:09	135	73	-142	IGN	Moment tensor inversion	Catalog	Yes
-3.9600	36.8800	060	4.0	Mw	09/07/2014	18:36:23	66	43	28	Maretal2015	Moment tensor inversion	Article	No
-5.5200	36.9800	030	3.3	Mw	13/07/2014	04:38:53	239	80	144	Maretal2015	Moment tensor inversion	Article	Yes
-2.9469	35.0170	138	4.6	Mw	31/07/2014	17:14:24	177	78	-164	IGN	Moment tensor inversion	Catalog	No
3.2050	36.8510	010	5.3	Mw	01/08/2014	04:11:18	101	17	109	Bouhetal2022	Moment tensor inversion	Article	Yes
3.1920	36.8530	009	3.9	Md	01/08/2014	04:20:19	184	69	51	Yelletal2019	Polarity	Article	Yes
3.1870	36.8500	011	4.3	Md	01/08/2014	04:26:42	246	81	110	Yelletal2019	Polarity	Article	Yes
3.1920	36.8480	009	3.6	Md	01/08/2014	04:34:27	262	84	128	Yelletal2019	Polarity	Article	Yes
3.1820	36.8380	010	3.5	Md	01/08/2014	08:37:17	250	72	96	Yelletal2019	Polarity	Article	Yes
3.1810	36.8450	009	3.2	Md	03/08/2014	01:29:23	241	71	74	Yelletal2019	Polarity	Article	Yes
3.1950	36.8380	013	2.7	Md	06/08/2014	06:33:51	245	62	113	Yelletal2019	Polarity	Article	Yes
3.1820	36.8440	013	4.0	Md	09/08/2014	10:19:44	295	87	20	Yelletal2019	Polarity	Article	Yes
-4.1348	35.3007	042	4.3	Mw	09/08/2014	15:45:49	12	85	-7	IGN	Moment tensor inversion	Catalog	Yes
3.1710	36.8380	013	2.5	Md	11/08/2014	06:19:19	351	33	62	Yelletal2019	Polarity	Article	Yes
3.1860	36.8540	011	3.0	Md	11/08/2014	22:36:40	200	60	90	Yelletal2019	Polarity	Article	Yes
3.1790	36.8410	013	3.3	Md	19/08/2014	01:52:56	183	62	11	Yelletal2019	Polarity	Article	Yes
-5.5400	36.9600	030	4.3	Mw	19/08/2014	13:38:24	322	71	8	Maretal2015	Moment tensor inversion	Article	Yes
0.2605	35.6592	030	3.5	Mw	22/08/2014	00:22:48	2	68	-35	IGN	Moment tensor inversion	Catalog	Yes

-3.5798	37.9679	003	3.5	Mw	14/09/2014	03:36:54	165	77	-29	IGN	Moment tensor inversion	Catalog	Yes
-2.7028	36.7022	018	3.4	Mw	09/10/2014	19:52:59	200	88	7	IGN	Moment tensor inversion	Catalog	Yes
-11.3200	35.0210	038	4.8	Mw	03/11/2014	03:39:44	269	52	169	Custetal2016	Moment tensor inversion	Article	Yes
3.4400	36.3800	010	4.3	mb	15/11/2014	01:13:00	218	44	96	RCMT	Moment tensor inversion	Catalog	Yes
2.9700	36.4900	010	4.7	mb	19/12/2014	11:06:00	61	14	99	RCMT	Moment tensor inversion	Catalog	Yes
3.0200	36.4400	010	4.7	mb	23/12/2014	08:00:21	40	32	80	RCMT	Moment tensor inversion	Catalog	Yes
3.0500	36.4200	010	4.5	mb	23/12/2014	08:59:00	90	34	99	RCMT	Moment tensor inversion	Catalog	Yes
3.0100	36.5100	012	4.7	mb	26/12/2014	17:55:18	49	23	78	RCMT	Moment tensor inversion	Catalog	Yes
3.0100	36.5100	010	4.6	mb	01/02/2015	20:06:36	39	32	79	RCMT	Moment tensor inversion	Catalog	Yes
2.2469	35.9168	015	4.4	Mw	06/02/2015	23:02:46	96	58	77	IGN	Moment tensor inversion	Catalog	Yes
-2.6273	39.0475	014	4.7	Mw	23/02/2015	16:16:31	78	64	-114	IGN	Moment tensor inversion	Catalog	Yes
-2.9400	34.9700	010	4.4	mb	06/03/2015	04:01:51	188	64	-25	RCMT	Moment tensor inversion	Catalog	Yes
-8.5460	37.3490	009	3.3	Mw	22/07/2015	04:35:00	84	85	168	Neretal2024	Moment tensor inversion	Article	Yes
-1.2795	38.3648	003	3.2	Mw	30/07/2015	04:23:41	32	66	59	IGN	Moment tensor inversion	Catalog	Yes
-2.2726	41.6274	011	3.7	Mw	05/08/2015	16:26:52	179	45	-90	IGN	Moment tensor inversion	Catalog	Yes
-7.0380	35.7120	036	4.9	mb	17/09/2015	15:11:45	130	87	-170	Cabiecetal2020	Moment tensor inversion	Article	Yes
-4.1200	37.1100	040	3.7	Mw	10/10/2015	05:05:29	85	39	-172	Setal2024	Moment tensor inversion	Article	Yes
-5.7310	35.8140	027	4.7	mb	20/10/2015	20:15:25	221	67	30	Cabiecetal2020	Moment tensor inversion	Article	Yes
-8.5240	37.3260	020	3.3	Mw	21/10/2015	08:39:00	216	50	88	Neretal2024	Moment tensor inversion	Article	Yes
3.1942	42.1954	006	4.0	Mw	29/10/2015	00:37:47	29	84	13	IGN	Moment tensor inversion	Catalog	Yes
-5.4066	36.6995	028	3.8	Mw	07/11/2015	18:11:58	1	75	-44	IGN	Moment tensor inversion	Catalog	Yes
-7.1770	36.8000	031	3.0	mbLg	18/11/2015	13:13:15	250	61	150	Cabiecetal2020	Moment tensor inversion	Article	Yes
-3.1812	36.8040	017	3.9	Mw	23/11/2015	08:02:11	83	77	130	IGN	Moment tensor inversion	Catalog	Yes
-9.4810	36.7710	043	3.6	mbLg	03/01/2016	06:05:10	133	71	-110	Cabiecetal2020	Moment tensor inversion	Article	Yes
-4.9359	42.9454	011	1.4	Mw	18/01/2016	00:21:57	67	48	-79	Lopezetal2018	Polarity	Article	No
-3.7600	35.6310	012	5.1	Mw	21/01/2016	13:47:19	125	68	-162	Setal2020	Moment tensor inversion	Article	Yes
-9.9000	36.3560	054	5.0	mb	23/01/2016	15:35:12	210	87	52	Cabiecetal2020	Moment tensor inversion	Article	No
-3.7480	35.5950	006	6.3	Mw	25/01/2016	04:22:00	131	51	-177	Setal2020	Moment tensor inversion	Article	Yes
-3.7353	35.6035	015	4.5	Mw	25/01/2016	04:34:20	226	87	7	Buetal2017	Moment tensor inversion	Article	Yes
-3.8400	35.5200	010	4.5	mb	25/01/2016	05:03:45	131	80	-171	RCMT	Moment tensor inversion	Catalog	Yes

-3.7750	35.6390	006	5.2	Mw	25/01/2016	05:54:03	99	50	-170	Setal2020	Moment tensor inversion	Article	Yes
-3.7450	35.3750	008	5.2	Mw	25/01/2016	06:10:40	15	81	-25	Setal2020	Moment tensor inversion	Article	Yes
-3.8230	35.5410	012	4.0	Mw	25/01/2016	08:15:27	286	75	-170	Setal2020	Moment tensor inversion	Article	Yes
-3.8210	35.5070	008	3.9	Mw	25/01/2016	08:25:04	11	59	12	Setal2020	Moment tensor inversion	Article	Yes
-3.8410	35.5500	008	4.3	Mw	25/01/2016	09:06:13	122	50	-175	Setal2020	Moment tensor inversion	Article	Yes
-3.8520	35.4550	006	3.7	Mw	25/01/2016	11:29:20	148	60	-89	Setal2020	Moment tensor inversion	Article	Yes
-3.7120	35.6720	004	4.8	Mw	25/01/2016	14:52:41	253	72	92	Setal2020	Moment tensor inversion	Article	Yes
-3.8440	35.5340	018	4.1	Mw	25/01/2016	16:02:42	35	61	-1	Setal2020	Moment tensor inversion	Article	Yes
-3.8320	35.5560	012	4.2	Mw	25/01/2016	18:17:32	198	87	16	Setal2020	Moment tensor inversion	Article	Yes
-3.8380	35.5010	006	4.3	Mw	26/01/2016	01:16:45	107	33	129	Setal2020	Moment tensor inversion	Article	Yes
-3.8420	35.5450	002	4.3	Mw	26/01/2016	23:15:23	115	85	-122	Setal2020	Moment tensor inversion	Article	Yes
-3.5640	35.5310	006	4.5	Mw	27/01/2016	06:32:04	41	42	71	Setal2020	Moment tensor inversion	Article	Yes
-5.2827	43.1207	015	1.1	Mw	27/01/2016	07:17:25	10	18	78	Lopezetal2018	Polarity	Article	No
-3.8230	35.4840	004	4.2	Mw	27/01/2016	21:57:47	126	36	157	Setal2020	Moment tensor inversion	Article	Yes
-3.8210	35.5300	004	4.4	Mw	27/01/2016	22:10:35	96	23	169	Setal2020	Moment tensor inversion	Article	Yes
-3.8550	35.4400	016	3.8	Mw	27/01/2016	22:52:56	19	82	-1	Setal2020	Moment tensor inversion	Article	Yes
-3.8570	35.5170	010	4.2	Mw	28/01/2016	19:48:50	39	63	9	Setal2020	Moment tensor inversion	Article	Yes
-3.7820	35.6660	010	3.8	Mw	31/01/2016	04:54:50	283	76	-169	Setal2020	Moment tensor inversion	Article	Yes
-3.0895	36.5839	003	4.5	Mw	31/01/2016	16:25:28	196	43	-68	Buetal2017	Moment tensor inversion	Article	Yes
-3.8100	35.5290	016	4.1	Mw	01/02/2016	23:50:48	42	66	29	Setal2020	Moment tensor inversion	Article	Yes
-3.8290	35.4570	004	3.8	Mw	05/02/2016	09:04:58	101	70	-162	Setal2020	Moment tensor inversion	Article	Yes
-11.1140	36.6400	056	3.9	Mw	07/02/2016	14:57:58	188	39	14	Cabiecetal2020	Moment tensor inversion	Article	No
-5.2551	43.1187	013	1.3	Mw	18/02/2016	11:37:36	91	58	93	Lopezetal2018	Polarity	Article	No
-5.4859	43.2574	021	1.3	Mw	20/02/2016	19:20:39	35	57	-72	Lopezetal2018	Polarity	Article	No
-3.6030	35.5890	006	5.1	Mw	22/02/2016	03:46:03	256	64	102	Setal2020	Moment tensor inversion	Article	Yes
-3.6080	35.6530	004	4.3	Mw	22/02/2016	04:14:29	245	69	92	Setal2020	Moment tensor inversion	Article	Yes
-3.6420	35.6600	004	3.9	Mw	22/02/2016	06:43:02	56	19	99	Setal2020	Moment tensor inversion	Article	Yes
-3.6230	35.6700	004	4.4	Mw	23/02/2016	08:46:00	49	20	62	Setal2020	Moment tensor inversion	Article	Yes
-3.6420	35.6280	016	4.3	Mw	23/02/2016	10:12:32	111	67	-156	Setal2020	Moment tensor inversion	Article	Yes
-3.7720	35.4170	014	4.7	Mw	03/03/2016	11:36:25	278	65	-178	Setal2020	Moment tensor inversion	Article	Yes

-3.8160	35.4580	018	3.7	Mw	05/03/2016	21:00:30	89	65	-167	Setal2020	Moment tensor inversion	Article	Yes
-3.7340	35.4490	004	3.5	Mw	07/03/2016	02:38:19	101	62	173	Setal2020	Moment tensor inversion	Article	Yes
-3.6720	35.6740	006	3.8	Mw	09/03/2016	23:04:19	86	28	139	Setal2020	Moment tensor inversion	Article	Yes
-3.6240	35.4980	004	4.6	Mw	09/03/2016	23:46:07	248	70	88	Setal2020	Moment tensor inversion	Article	Yes
-3.6750	35.6430	004	5.0	Mw	11/03/2016	04:16:47	68	17	103	Setal2020	Moment tensor inversion	Article	Yes
-3.6920	35.6810	010	3.8	Mw	11/03/2016	09:40:19	191	83	37	Setal2020	Moment tensor inversion	Article	Yes
-3.6070	35.5500	004	3.9	Mw	12/03/2016	09:20:00	87	24	96	Setal2020	Moment tensor inversion	Article	Yes
-3.6550	35.6120	004	4.8	Mw	12/03/2016	15:04:05	75	21	85	Setal2020	Moment tensor inversion	Article	Yes
-3.6800	35.6090	004	4.8	Mw	12/03/2016	15:17:11	244	64	91	Setal2020	Moment tensor inversion	Article	Yes
-3.7850	35.3260	006	4.1	Mw	13/03/2016	20:54:02	13	75	-25	Setal2020	Moment tensor inversion	Article	Yes
-3.6510	35.6010	004	5.2	Mw	15/03/2016	04:40:38	48	35	54	Setal2020	Moment tensor inversion	Article	Yes
-3.7110	35.2880	012	4.7	Mw	16/03/2016	16:27:33	353	62	-86	Setal2020	Moment tensor inversion	Article	Yes
-3.6440	35.5220	004	3.6	Mw	16/03/2016	19:43:09	330	55	-38	Setal2020	Moment tensor inversion	Article	Yes
-3.6030	35.5210	004	3.7	Mw	16/03/2016	23:10:46	87	33	138	Setal2020	Moment tensor inversion	Article	Yes
3.2900	36.4000	010	4.3	mb	24/03/2016	08:06:19	65	41	172	RCMT	Moment tensor inversion	Catalog	Yes
-5.4294	43.2229	018	2.0	Mw	25/03/2016	03:23:16	135	40	98	Lopezetal2018	Polarity	Article	Yes
-3.5317	36.6470	023	3.9	Mw	25/03/2016	12:05:35	45	82	138	IGN	Moment tensor inversion	Catalog	Yes
-3.5750	35.5460	004	3.8	Mw	25/03/2016	22:28:48	47	26	56	Setal2020	Moment tensor inversion	Article	Yes
-3.7400	35.3100	002	3.8	Mw	27/03/2016	23:56:21	178	87	-43	Setal2020	Moment tensor inversion	Article	Yes
-3.6600	35.5610	004	3.5	Mw	29/03/2016	22:53:59	79	29	111	Setal2020	Moment tensor inversion	Article	Yes
-3.7970	35.4760	014	4.0	Mw	02/04/2016	14:48:04	131	70	-160	Setal2020	Moment tensor inversion	Article	Yes
-3.6140	35.5380	004	3.8	Mw	05/04/2016	17:39:03	97	32	139	Setal2020	Moment tensor inversion	Article	Yes
-3.6030	35.6390	008	3.6	Mw	06/04/2016	03:17:47	46	41	71	Setal2020	Moment tensor inversion	Article	Yes
-3.8170	35.4640	016	4.1	Mw	08/04/2016	07:10:06	29	78	-5	Setal2020	Moment tensor inversion	Article	Yes
3.5800	36.2970	012	4.9	Mw	10/04/2016	17:48:53	161	72	22	Bouhetal2022	Moment tensor inversion	Article	Yes
-5.8244	36.6862	010	4.1	Mw	10/05/2016	17:18:48	265	78	157	IGN	Moment tensor inversion	Catalog	Yes
-0.6574	43.1720	013	3.8	Mw	11/05/2016	10:45:53	113	54	-58	IGN	Moment tensor inversion	Catalog	Yes
3.4810	36.3270	007	4.6	Mw	16/05/2016	09:19:05	191	51	46	Bouhetal2022	Moment tensor inversion	Article	Yes
3.5520	36.3360	012	5.1	Mw	28/05/2016	23:54:53	215	55	99	Bouhetal2022	Moment tensor inversion	Article	Yes
3.5200	36.2500	010	4.4	mb	29/05/2016	05:23:10	1	41	34	RCMT	Moment tensor inversion	Catalog	Yes

-3.8010	35.4700	016	3.7	Mw	30/05/2016	22:03:49	191	83	-10	Setal2020	Moment tensor inversion	Article	Yes
3.5200	36.3300	015	4.4	mb	31/05/2016	17:35:14	34	33	84	RCMT	Moment tensor inversion	Catalog	Yes
-5.2751	43.1294	012	1.0	Mw	05/06/2016	08:49:11	57	64	-39	Lopezetal2018	Polarity	Article	No
-3.6520	35.5890	004	3.8	Mw	06/06/2016	03:03:27	133	89	-157	Setal2020	Moment tensor inversion	Article	Yes
2.9393	42.1816	013	3.4	Mw	10/06/2016	06:57:52	27	74	24	IGN	Moment tensor inversion	Catalog	Yes
-5.2587	43.1283	012	1.2	Mw	30/06/2016	09:37:24	68	48	-153	Lopezetal2018	Polarity	Article	No
-7.9414	36.0623	022	4.1	Mw	01/08/2016	03:48:52	254	60	80	IGN	Moment tensor inversion	Catalog	Yes
-10.4419	39.3079	034	4.4	Mw	19/08/2016	11:44:18	98	87	95	IGN	Moment tensor inversion	Catalog	Yes
-11.4394	36.5272	040	4.5	Mw	25/08/2016	01:33:27	78	68	92	IGN	Moment tensor inversion	Catalog	Yes
-5.2828	43.1276	013	0.9	Mw	26/08/2016	00:44:40	68	79	-139	Lopezetal2018	Polarity	Article	No
-5.3675	43.1677	017	1.2	Mw	02/09/2016	21:34:14	68	52	-43	Lopezetal2018	Polarity	Article	No
-2.5960	37.4922	015	3.8	Mw	25/09/2016	07:33:55	5	77	-38	IGN	Moment tensor inversion	Catalog	Yes
-5.3226	43.1420	014	1.0	Mw	27/09/2016	04:58:30	85	57	-141	Lopezetal2018	Polarity	Article	No
-5.3015	43.1468	012	1.2	Mw	30/10/2016	14:07:09	137	57	138	Lopezetal2018	Polarity	Article	No
3.9900	35.9800	010	4.3	mb	05/11/2016	20:43:25	20	56	0	RCMT	Moment tensor inversion	Catalog	Yes
-5.2024	43.1005	012	1.7	Mw	03/12/2016	11:12:48	130	40	98	Lopezetal2018	Polarity	Article	No
-4.9345	42.9579	008	1.2	Mw	16/12/2016	20:54:40	70	38	-81	Lopezetal2018	Polarity	Article	No
-5.4548	43.2148	017	1.2	Mw	28/01/2017	03:34:02	88	77	-1	Lopezetal2018	Polarity	Article	No
-5.4554	43.2156	017	1.4	Mw	28/01/2017	12:05:10	42	18	-28	Lopezetal2018	Polarity	Article	No
-5.3095	43.1268	015	1.0	Mw	11/02/2017	06:03:11	132	39	158	Lopezetal2018	Polarity	Article	No
1.3330	42.3600	012	3.4	Mw	20/02/2017	11:09:39	0	90	-18	FMHex20	Compilation	Catalog	Yes
-1.5690	42.9199	011	4.2	Mw	10/03/2017	06:43:37	160	82	28	IGN	Moment tensor inversion	Catalog	Yes
-1.6125	42.9399	005	3.4	Mw	10/03/2017	15:21:24	359	73	-40	IGN	Moment tensor inversion	Catalog	Yes
2.6834	41.8259	013	3.5	Mw	15/04/2017	11:04:36	350	73	-83	IGN	Moment tensor inversion	Catalog	Yes
0.1440	42.9700	008	3.4	Mw	26/04/2017	15:12:09	20	10	-167	FMHex20	Compilation	Catalog	Yes
0.0420	42.9930	010	3.2	Mw	08/05/2017	02:08:26	130	45	-34	FMHex20	Compilation	Catalog	Yes
-3.9400	37.0600	013	3.5	Mw	18/05/2017	10:07:55	94	69	-99	Setal2024	Moment tensor inversion	Article	Yes
-3.8500	37.1000	018	3.4	Mw	29/06/2017	22:32:37	168	31	-56	Setal2024	Moment tensor inversion	Article	Yes
1.8000	35.8400	020	4.4	mb	08/07/2017	10:42:52	37	56	-5	RCMT	Moment tensor inversion	Catalog	Yes

-1.8081	35.7930	005	4.7	Mw	11/07/2017	03:18:18	225	78	19	IGN	Moment tensor inversion	Catalog	Yes
1.8800	35.8200	010	4.9	mb	11/07/2017	03:18:19	35	69	-14	RCMT	Moment tensor inversion	Catalog	Yes
-3.5600	37.0000	011	3.5	Mw	31/07/2017	23:16:55	211	31	-33	Setal2024	Moment tensor inversion	Article	Yes
-9.1672	39.0311	028	4.0	Mw	17/08/2017	06:44:57	202	60	101	IGN	Moment tensor inversion	Catalog	Yes
-0.9641	40.3625	017	3.3	Mw	21/08/2017	03:10:13	132	46	-97	IGN	Moment tensor inversion	Catalog	Yes
-8.6030	37.1890	019	3.5	Mw	11/09/2017	18:09:00	240	43	100	Neretal2024	Moment tensor inversion	Article	Yes
-5.0754	37.0566	012	4.0	Mw	05/10/2017	11:55:13	115	74	113	IGN	Moment tensor inversion	Catalog	Yes
-0.9595	38.7155	003	3.7	Mw	04/12/2017	08:47:19	326	81	-170	IGN	Moment tensor inversion	Catalog	Yes
2.5680	36.3830	004	4.7	Mw	02/01/2018	20:59:38	197	43	30	Bouhetal2022	Moment tensor inversion	Article	Yes
-7.9739	38.7925	011	4.3	Mw	15/01/2018	11:51:40	5	88	-23	IGN	Moment tensor inversion	Catalog	Yes
-1.4193	37.9778	010	3.9	Mw	02/03/2018	19:08:22	267	80	63	IGN	Moment tensor inversion	Catalog	Yes
-3.2482	37.8505	008	3.5	Mw	22/03/2018	14:12:04	292	88	160	IGN	Moment tensor inversion	Catalog	Yes
-3.2496	37.8618	013	3.5	Mw	24/03/2018	00:41:12	186	86	11	IGN	Moment tensor inversion	Catalog	Yes
-3.2391	37.8632	010	3.6	Mw	07/04/2018	01:42:41	189	81	10	IGN	Moment tensor inversion	Catalog	Yes
0.0800	35.8800	010	4.4	mb	23/04/2018	15:48:52	55	32	120	RCMT	Moment tensor inversion	Catalog	Yes
-3.2378	37.8490	011	3.3	Mw	24/04/2018	01:53:09	168	87	-39	IGN	Moment tensor inversion	Catalog	Yes
-11.0809	37.1327	032	4.0	Mw	26/04/2018	03:33:55	229	62	86	IGN	Moment tensor inversion	Catalog	Yes
-5.3431	36.4692	011	4.2	Mw	26/04/2018	11:13:21	174	83	35	IGN	Moment tensor inversion	Catalog	Yes
-2.1876	38.0654	009	3.6	Mw	26/05/2018	18:58:16	271	70	103	IGN	Moment tensor inversion	Catalog	Yes
-4.5500	32.5600	010	4.0	mb	04/06/2018	22:11:43	221	72	-19	RCMT	Moment tensor inversion	Catalog	Yes
-4.2800	37.1400	018	3.5	Mw	17/06/2018	07:47:34	257	63	159	Setal2024	Moment tensor inversion	Article	Yes
0.3390	42.9730	016	3.8	Mw	06/08/2018	20:49:00	292	81	-89	FMHex20	Compilation	Catalog	Yes
-0.9523	38.2491	011	4.2	Mw	13/08/2018	14:40:05	236	86	-30	IGN	Moment tensor inversion	Catalog	Yes
-7.6974	42.7059	011	3.5	Mw	21/08/2018	00:28:57	299	79	-138	IGN	Moment tensor inversion	Catalog	Yes
-10.5665	40.2162	029	4.9	Mw	04/09/2018	06:12:55	242	90	-170	IGN	Moment tensor inversion	Catalog	Yes
-9.6151	37.7362	036	3.9	Mw	01/10/2018	05:51:59	39	54	62	IGN	Moment tensor inversion	Catalog	Yes
-3.7500	37.2500	003	3.9	Mw	09/10/2018	07:41:53	148	20	-100	Setal2024	Moment tensor inversion	Article	Yes
0.1526	39.2114	011	3.8	Mw	17/10/2018	02:51:33	211	90	9	IGN	Moment tensor inversion	Catalog	Yes
-3.2481	37.8581	012	3.7	Mw	18/10/2018	17:57:44	101	87	172	IGN	Moment tensor inversion	Catalog	Yes

-4.6000	34.8800	060	4.4	mb	16/02/2019	04:35:34	82	38	105	RCMT	Moment tensor inversion	Catalog	No
-5.2873	36.9962	019	4.0	Mw	13/03/2019	02:41:37	84	87	-158	IGN	Moment tensor inversion	Catalog	Yes
-0.4855	38.0741	003	3.8	Mw	24/03/2019	16:16:08	102	53	104	IGN	Moment tensor inversion	Catalog	Yes
1.2845	42.3032	007	4.0	Mw	03/04/2019	15:29:52	170	90	3	IGN	Moment tensor inversion	Catalog	Yes
-1.6414	37.5365	005	3.6	Mw	22/06/2019	20:00:02	47	88	15	IGN	Moment tensor inversion	Catalog	Yes
-2.6097	37.3874	004	4.2	Mw	29/06/2019	19:26:55	318	50	-95	IGN	Moment tensor inversion	Catalog	Yes
-7.9993	36.4037	035	4.1	Mw	16/07/2019	13:31:58	50	75	118	IGN	Moment tensor inversion	Catalog	Yes
-5.2479	37.0416	007	3.8	Mw	15/09/2019	22:30:40	228	85	29	IGN	Moment tensor inversion	Catalog	Yes
-5.2780	37.0740	013	3.7	Mw	18/09/2019	13:38:53	241	76	35	IGN	Moment tensor inversion	Catalog	Yes
-5.2529	37.1657	010	3.6	Mw	24/09/2019	00:46:35	231	79	29	IGN	Moment tensor inversion	Catalog	Yes
-5.2555	36.9798	010	3.5	Mw	30/09/2019	18:27:03	210	88	5	IGN	Moment tensor inversion	Catalog	Yes
2.0410	42.4595	009	2.0	Ml	16/10/2019	11:23:57	140	70	-90	Ruiz2023	Polarity	Article	Yes
2.3752	42.3530	008	2.5	Ml	18/10/2019	02:29:47	150	45	-140	Ruiz2023	Polarity	Article	Yes
-5.2931	36.9835	012	4.5	Mw	25/10/2019	09:35:48	256	89	171	IGN	Moment tensor inversion	Catalog	Yes
4.6382	44.5269	001	4.8	Mw	11/11/2019	10:52:45	220	45	82	FMHex20	Compilation	Catalog	Yes
-4.2400	32.6600	010	5.1	mb	17/11/2019	08:39:09	184	76	-12	RCMT	Moment tensor inversion	Catalog	Yes
-4.3200	32.6500	010	4.5	mb	17/11/2019	14:39:08	277	58	-176	RCMT	Moment tensor inversion	Catalog	Yes
1.0173	42.5357	008	2.7	Ml	08/12/2019	04:08:27	345	15	-60	Ruiz2023	Polarity	Article	Yes
1.2767	42.5947	006	2.2	Ml	21/12/2019	12:17:11	25	40	-100	Ruiz2023	Polarity	Article	Yes
1.9240	42.4803	007	1.9	Ml	25/12/2019	20:34:03	105	70	-100	Ruiz2023	Polarity	Article	No
1.9432	42.2890	002	1.2	Ml	28/12/2019	01:47:03	120	50	-80	Ruiz2023	Polarity	Article	No
2.0220	42.4797	011	1.4	Ml	31/12/2019	23:29:03	225	20	0	Ruiz2023	Polarity	Article	No
-2.3569	36.9558	017	3.7	Mw	01/01/2020	09:09:46	87	86	163	IGN	Moment tensor inversion	Catalog	Yes
1.7127	42.4488	009	1.3	Ml	23/01/2020	16:38:33	160	60	-40	Ruiz2023	Polarity	Article	No
1.7807	42.4440	008	1.5	Ml	10/02/2020	00:11:48	135	45	-90	Ruiz2023	Polarity	Article	No
1.7813	42.4440	008	1.6	Ml	13/02/2020	20:29:07	145	45	-80	Ruiz2023	Polarity	Article	No
-4.2900	32.7200	010	4.5	mb	16/02/2020	21:56:54	19	72	17	RCMT	Moment tensor inversion	Catalog	Yes
0.1000	39.3426	002	3.7	Mw	23/03/2020	04:42:57	183	77	-43	IGN	Moment tensor inversion	Catalog	Yes
1.8010	42.4880	003	2.7	Ml	29/03/2020	10:52:33	140	40	-70	Ruiz2023	Polarity	Article	Yes
2.6683	41.8324	005	3.5	Mw	08/05/2020	12:47:44	88	75	-119	IGN	Moment tensor inversion	Catalog	Yes

1.8015	42.4812	004	1.0	Ml	15/05/2020	01:37:22	150	35	-70	Ruiz2023	Polarity	Article	No
1.8482	42.3095	005	1.4	Ml	26/05/2020	10:35:34	135	55	-90	Ruiz2023	Polarity	Article	No
1.8462	42.3128	006	1.6	Ml	26/05/2020	11:04:21	135	60	-90	Ruiz2023	Polarity	Article	No
1.8478	42.3117	006	1.9	Ml	26/05/2020	11:07:29	120	55	-120	Ruiz2023	Polarity	Article	No
1.1912	42.4635	011	1.9	Ml	17/06/2020	11:13:12	140	35	-160	Ruiz2023	Polarity	Article	No
1.8173	42.3472	010	1.8	Ml	26/06/2020	03:13:54	160	65	-80	Ruiz2023	Polarity	Article	No
-5.1900	34.3100	010	4.5	mb	01/07/2020	06:06:40	276	39	60	RCMT	Moment tensor inversion	Catalog	Yes
1.8025	42.4833	004	1.4	Ml	08/07/2020	19:53:07	200	50	-60	Ruiz2023	Polarity	Article	No
-3.7500	35.5100	010	4.3	mb	25/07/2020	12:12:57	170	52	-41	RCMT	Moment tensor inversion	Catalog	Yes
1.8165	42.3440	011	2.1	Ml	29/07/2020	13:54:23	345	25	-80	Ruiz2023	Polarity	Article	Yes
1.8190	42.3470	011	2.7	Ml	29/07/2020	21:05:05	155	65	-90	Ruiz2023	Polarity	Article	Yes
1.9900	36.6300	010	4.2	mb	08/08/2020	23:00:31	44	33	73	RCMT	Moment tensor inversion	Catalog	Yes
1.8165	42.3458	011	1.9	Ml	12/08/2020	17:28:47	160	65	-80	Ruiz2023	Polarity	Article	No
1.6195	42.3797	010	2.3	Ml	13/08/2020	01:16:30	20	15	-30	Ruiz2023	Polarity	Article	Yes
-1.4878	42.8478	003	4.1	Mw	30/08/2020	05:57:57	35	69	145	IGN	Moment tensor inversion	Catalog	Yes
-1.4713	42.8360	003	4.5	Mw	30/09/2020	22:02:31	149	84	-60	IGN	Moment tensor inversion	Catalog	Yes
-1.4895	42.8253	003	3.5	Mw	30/09/2020	22:54:14	128	66	-58	IGN	Moment tensor inversion	Catalog	Yes
-1.5023	42.8446	004	4.0	Mw	30/09/2020	23:37:31	47	90	-141	IGN	Moment tensor inversion	Catalog	Yes
-1.4778	42.8255	003	4.4	Mw	01/10/2020	00:21:38	232	85	-149	IGN	Moment tensor inversion	Catalog	Yes
-5.4104	36.6147	033	4.1	Mw	16/10/2020	00:58:52	18	89	-69	IGN	Moment tensor inversion	Catalog	Yes
-1.8741	37.9945	005	3.8	Mw	09/11/2020	00:46:19	143	88	-129	IGN	Moment tensor inversion	Catalog	Yes
1.9935	42.4710	006	2.0	Ml	20/11/2020	10:20:37	85	70	-150	Ruiz2023	Polarity	Article	Yes
-3.7300	37.2200	006	3.6	Mw	02/12/2020	23:09:09	153	46	-74	Setal2024	Moment tensor inversion	Article	Yes
-3.7100	37.2200	005	4.3	Mw	23/01/2021	11:15:24	140	36	-95	Setal2024	Moment tensor inversion	Article	Yes
-3.7000	37.2100	005	4.1	Mw	26/01/2021	21:36:33	123	37	-109	Setal2024	Moment tensor inversion	Article	Yes
-3.7000	37.2100	005	4.1	Mw	26/01/2021	21:44:18	123	39	-103	Setal2024	Moment tensor inversion	Article	Yes
-3.7100	37.2100	005	4.4	Mw	26/01/2021	21:54:55	114	40	-115	Setal2024	Moment tensor inversion	Article	Yes
-3.7200	37.2200	007	3.6	Mw	28/01/2021	18:06:28	126	41	-115	Setal2024	Moment tensor inversion	Article	Yes
-3.7200	37.2200	007	4.4	Mw	28/01/2021	18:49:49	123	36	-111	Setal2024	Moment tensor inversion	Article	Yes
-3.7000	37.2100	007	3.6	Mw	28/01/2021	19:28:19	108	40	-123	Setal2024	Moment tensor inversion	Article	Yes

-3.6900	37.2200	007	3.4	Mw	28/01/2021	21:29:04	124	41	-112	Setal2024	Moment tensor inversion	Article	Yes
-9.0265	38.8519	008	3.1	Mw	18/03/2021	09:51:36	52	73	121	IGN	Moment tensor inversion	Catalog	Yes
-3.6783	35.3931	006	3.9	Mw	17/04/2021	09:51:29	6	84	-21	IGN	Moment tensor inversion	Catalog	Yes
-3.6635	35.4957	009	4.1	Mw	28/04/2021	12:40:51	14	85	-13	IGN	Moment tensor inversion	Catalog	Yes
-3.6167	35.4227	005	4.3	Mw	01/05/2021	22:10:06	13	85	-12	IGN	Moment tensor inversion	Catalog	Yes
-3.6494	35.4672	005	4.0	Mw	11/05/2021	16:52:03	9	74	-31	IGN	Moment tensor inversion	Catalog	Yes
-3.6089	35.4855	009	4.0	Mw	14/05/2021	06:54:58	14	82	-15	IGN	Moment tensor inversion	Catalog	Yes
-7.4867	42.0982	010	3.6	Mw	20/05/2021	22:35:32	5	49	-63	IGN	Moment tensor inversion	Catalog	Yes
-3.6549	35.4490	007	4.1	Mw	21/05/2021	11:10:55	2	76	-21	IGN	Moment tensor inversion	Catalog	Yes
-3.6901	35.3674	007	4.1	Mw	23/05/2021	06:18:39	4	80	-18	IGN	Moment tensor inversion	Catalog	Yes
-3.6981	35.4417	005	4.2	Mw	23/05/2021	06:42:15	7	81	-20	IGN	Moment tensor inversion	Catalog	Yes
-3.6537	35.4143	004	4.0	Mw	27/05/2021	22:55:43	11	84	-24	IGN	Moment tensor inversion	Catalog	Yes
-3.6428	35.4843	005	4.7	Mw	19/06/2021	03:23:06	8	85	-12	IGN	Moment tensor inversion	Catalog	Yes
-3.6385	35.4346	005	4.0	Mw	22/06/2021	14:54:33	16	89	-16	IGN	Moment tensor inversion	Catalog	Yes
-3.6789	35.4397	010	4.3	Mw	11/07/2021	11:40:03	15	82	-21	IGN	Moment tensor inversion	Catalog	Yes
-3.6204	35.4474	005	4.3	Mw	30/07/2021	08:38:53	12	86	-14	IGN	Moment tensor inversion	Catalog	Yes
-3.6350	35.4144	005	4.5	Mw	30/07/2021	08:58:51	6	84	-21	IGN	Moment tensor inversion	Catalog	Yes
-3.6597	35.4978	005	4.2	Mw	30/07/2021	09:13:03	279	89	-167	IGN	Moment tensor inversion	Catalog	Yes
1.6600	36.3100	010	4.3	mb	31/07/2021	02:01:45	14	49	1	RCMT	Moment tensor inversion	Catalog	Yes
-3.6069	35.4734	015	4.0	Mw	01/08/2021	10:48:19	6	77	-18	IGN	Moment tensor inversion	Catalog	Yes
-3.6928	35.4886	005	4.0	Mw	02/08/2021	14:06:10	11	76	-20	IGN	Moment tensor inversion	Catalog	Yes
-3.6241	35.4648	005	4.4	Mw	07/08/2021	04:19:16	13	86	-19	IGN	Moment tensor inversion	Catalog	Yes
-3.5447	35.3843	006	4.0	Mw	08/08/2021	05:50:39	1	90	-21	IGN	Moment tensor inversion	Catalog	Yes
-3.7300	37.1900	004	4.5	Mw	12/08/2021	21:25:12	128	61	-67	Setal2024	Moment tensor inversion	Article	Yes
-3.6202	35.4545	006	5.1	Mw	28/08/2021	11:20:50	14	82	-13	IGN	Moment tensor inversion	Catalog	Yes
-3.6148	35.4594	005	4.0	Mw	28/08/2021	12:09:43	8	73	-32	IGN	Moment tensor inversion	Catalog	Yes
-3.6538	35.4355	005	4.1	Mw	01/09/2021	12:51:59	356	87	-33	IGN	Moment tensor inversion	Catalog	Yes
-3.6333	35.4570	007	4.0	Mw	19/09/2021	00:31:48	359	77	-14	IGN	Moment tensor inversion	Catalog	Yes
-3.7363	35.5881	005	3.8	Mw	24/09/2021	00:31:27	101	84	-153	IGN	Moment tensor inversion	Catalog	Yes
1.4525	42.5182	005	3.6	Mw	11/10/2021	08:23:15	154	65	-117	IGN	Moment tensor inversion	Catalog	Yes

-1.4938	42.8111	001	4.1	Mw	11/10/2021	20:45:25	39	86	105	IGN	Moment tensor inversion	Catalog	Yes
-5.2831	36.9868	021	4.2	Mw	19/10/2021	17:43:32	169	86	-5	IGN	Moment tensor inversion	Catalog	Yes
-3.6643	35.4126	007	3.8	Mw	23/10/2021	19:54:02	360	81	-18	IGN	Moment tensor inversion	Catalog	Yes
-3.6287	35.4363	013	4.4	Mw	14/11/2021	04:48:27	4	75	-26	IGN	Moment tensor inversion	Catalog	Yes
-3.6654	35.4292	007	3.9	Mw	14/11/2021	04:53:20	81	90	-178	IGN	Moment tensor inversion	Catalog	Yes
-3.9071	35.1483	005	4.5	Mw	23/12/2021	01:54:26	162	64	-82	IGN	Moment tensor inversion	Catalog	Yes
-3.6736	35.4549	005	4.0	Mw	30/12/2021	15:28:20	234	84	13	IGN	Moment tensor inversion	Catalog	Yes
-7.6271	36.3276	020	4.1	Mw	01/01/2022	21:03:49	112	89	156	IGN	Moment tensor inversion	Catalog	Yes
-3.6527	35.5291	015	4.1	Mw	05/01/2022	09:11:52	50	81	-16	IGN	Moment tensor inversion	Catalog	Yes
-4.2400	33.2100	010	4.2	mb	24/01/2022	07:11:39	212	33	50	RCMT	Moment tensor inversion	Catalog	Yes
-9.4919	42.5481	012	4.1	Mw	27/01/2022	14:44:07	98	83	163	IGN	Moment tensor inversion	Catalog	Yes
-3.6646	35.4665	005	4.0	Mw	06/02/2022	06:17:06	53	87	-10	IGN	Moment tensor inversion	Catalog	Yes
-3.6906	35.4125	005	4.0	Mw	06/02/2022	09:59:38	15	85	-25	IGN	Moment tensor inversion	Catalog	Yes
-3.6339	35.4061	005	4.1	Mw	09/04/2022	03:55:21	360	85	-10	IGN	Moment tensor inversion	Catalog	Yes
-3.6191	35.4866	012	4.2	Mw	14/05/2022	22:34:53	182	83	16	IGN	Moment tensor inversion	Catalog	Yes
-3.6145	35.4975	008	5.3	Mw	20/05/2022	12:35:50	99	80	169	IGN	Moment tensor inversion	Catalog	Yes
-3.6643	35.4732	005	4.1	Mw	20/05/2022	20:11:28	109	77	152	IGN	Moment tensor inversion	Catalog	Yes
-3.6213	35.3537	005	4.4	Mw	29/05/2022	20:15:26	85	87	-167	IGN	Moment tensor inversion	Catalog	Yes
-3.6415	35.3615	001	4.6	Mw	02/06/2022	12:55:13	267	90	153	IGN	Moment tensor inversion	Catalog	Yes
-3.6488	35.3625	009	4.2	Mw	06/06/2022	17:57:47	353	86	-20	IGN	Moment tensor inversion	Catalog	Yes
-2.0214	41.1176	012	3.6	Mw	23/06/2022	12:56:38	150	47	-83	IGN	Moment tensor inversion	Catalog	Yes
-0.4400	35.8500	010	4.6	mb	26/06/2022	19:17:50	360	80	2	RCMT	Moment tensor inversion	Catalog	Yes
-3.5972	35.4868	006	3.9	Mw	09/07/2022	23:10:16	19	85	-23	IGN	Moment tensor inversion	Catalog	Yes
-3.6009	35.4584	013	4.3	Mw	20/07/2022	14:11:45	17	88	-28	IGN	Moment tensor inversion	Catalog	Yes
-3.6361	35.4647	003	3.9	Mw	29/07/2022	22:51:48	25	77	-24	IGN	Moment tensor inversion	Catalog	Yes
-3.6094	35.4619	003	4.1	Mw	03/08/2022	21:19:58	103	84	-164	IGN	Moment tensor inversion	Catalog	Yes
-3.6078	35.5333	005	4.2	Mw	10/08/2022	18:33:15	21	77	-14	IGN	Moment tensor inversion	Catalog	Yes
-8.5681	35.9280	045	4.3	Mw	14/08/2022	20:20:46	120	87	172	IGN	Moment tensor inversion	Catalog	Yes
-3.6557	35.4640	009	4.0	Mw	23/08/2022	17:46:04	3	72	-34	IGN	Moment tensor inversion	Catalog	Yes
-3.6231	35.5404	016	4.1	Mw	14/09/2022	05:17:40	196	89	22	IGN	Moment tensor inversion	Catalog	Yes

-2.0946	37.7923	006	3.7	Mw	16/09/2022	12:26:12	96	86	174	IGN	Moment tensor inversion	Catalog	Yes
-11.5054	36.6184	033	4.5	Mw	19/09/2022	16:30:44	55	65	96	IGN	Moment tensor inversion	Catalog	Yes
-4.0400	37.1600	011	3.5	Mw	29/09/2022	09:14:45	18	56	-112	Setal2024	Moment tensor inversion	Article	Yes
-3.6143	35.4391	005	4.0	Mw	04/10/2022	15:37:20	277	83	157	IGN	Moment tensor inversion	Catalog	Yes
-3.6335	35.4386	005	4.7	Mw	04/10/2022	15:39:31	355	87	-11	IGN	Moment tensor inversion	Catalog	Yes
-3.6404	35.4457	003	4.1	Mw	16/10/2022	07:32:17	355	85	-11	IGN	Moment tensor inversion	Catalog	Yes
-4.0698	35.2360	013	4.1	Mw	21/10/2022	12:45:59	112	79	-160	IGN	Moment tensor inversion	Catalog	Yes
-3.6025	35.4012	005	3.9	Mw	04/11/2022	22:26:52	3	84	-7	IGN	Moment tensor inversion	Catalog	Yes
2.9800	36.3400	010	4.5	mb	12/11/2022	13:32:14	315	37	-167	RCMT	Moment tensor inversion	Catalog	Yes
-3.6064	35.4271	005	4.3	Mw	18/11/2022	23:32:42	197	74	17	IGN	Moment tensor inversion	Catalog	Yes
-3.6375	35.4870	003	4.3	Mw	30/11/2022	11:07:02	352	83	-28	IGN	Moment tensor inversion	Catalog	Yes
-1.8990	37.1063	009	4.0	Mw	31/12/2022	07:05:54	343	78	-20	IGN	Moment tensor inversion	Catalog	Yes
-3.8533	34.7801	025	5.0	Mw	07/01/2023	08:12:26	0	75	-61	IGN	Moment tensor inversion	Catalog	Yes
-9.6721	37.9002	037	4.2	Mw	07/01/2023	18:41:06	233	60	80	IGN	Moment tensor inversion	Catalog	Yes
-2.4654	38.0139	013	3.5	Mw	03/02/2023	00:09:23	292	86	-154	IGN	Moment tensor inversion	Catalog	Yes
-0.6555	38.6845	014	3.8	Mw	30/07/2023	04:11:04	309	87	-168	IGN	Moment tensor inversion	Catalog	Yes
3.7926	41.8900	005	3.4	Mw	20/08/2023	20:22:20	78	51	94	IGN	Moment tensor inversion	Catalog	Yes
0.7327	42.6228	004	4.1	Mw	28/08/2023	17:42:04	280	54	-126	IGN	Moment tensor inversion	Catalog	Yes
-8.3900	31.0500	010	6.9	mb	08/09/2023	22:11:00	130	30	136	RCMT	Moment tensor inversion	Catalog	Yes
-8.7275	38.0656	009	3.3	Mw	15/09/2023	23:49:54	111	68	-156	IGN	Moment tensor inversion	Catalog	Yes
-6.0079	42.6071	017	3.6	Mw	30/09/2023	12:46:42	96	66	130	IGN	Moment tensor inversion	Catalog	Yes
-3.6193	35.4502	013	4.5	Mw	15/03/2024	20:17:47	24	85	-15	IGN	Moment tensor inversion	Catalog	Yes
0.1198	43.0054	011	3.9	Mw	21/05/2024	09:23:33	310	70	-90	IGN	Moment tensor inversion	Catalog	Yes
-3.5865	35.5289	007	4.1	Mw	27/05/2024	00:40:25	116	76	164	IGN	Moment tensor inversion	Catalog	Yes
-9.6588	38.0265	031	5.3	Mw	26/08/2024	04:11:38	32	70	55	IGN	Moment tensor inversion	Catalog	Yes
-2.9714	36.7941	011	3.7	Mw	02/09/2024	08:25:52	309	49	-107	IGN	Moment tensor inversion	Catalog	Yes
-5.7851	35.0348	042	5.0	Mw	10/02/2025	22:48:42	219	78	11	IGN	Moment tensor inversion	Catalog	Yes
-9.2110	38.5726	007	4.4	Mw	17/02/2025	13:24:03	216	24	36	IGN	Moment tensor inversion	Catalog	Yes

Reference in Table	*Reference in extended version*
Abbeetal2016	Abbes, K., Dorbath,L., Dorbath, C., Djeddi, M., Ousadou, F., Maouche, S., Benkaci, N., Slimani, A., Larbes, S. and Bouziane, D. (2016). The Beni Haoua, Algeria, Mw 4.9 earthquake: source parameters, engineering, and seismotectonic implications. Journal of Seismology, 20, 655-667.
Aletal	Alfaro, P., Rueda, J., Delgado, J., Estevez, A., López Casado, C., & Giner, J. (1999). Sismotectónica de la Cuenca del Bajo Segura. 1. Asamblea Hispano-Portuguesa de Geodesia y Geofísica.
Ayadetal2008	Ayadi, A., Dorbath, C., Ousadou, F., Maouche, S., Chikh, M., Bounif, M. A., & Meghraoui, M. (2008). Zemmouri earthquake rupture zone (Mw 6.8, Algeria): Aftershocks sequence relocation and 3D velocity model. Journal of Geophysical Research: Solid Earth, 113(B9).
Balanetal2012	Balanya, J. C., Crespo-Blanc, A., Díaz-Azpiroz, M., Expósito, I., Torcal, F., Pérez-Peña, V., & Booth-Rea, G. (2012). Arc-parallel vs back-arc extension in the Western Gibraltar arc: Is the Gibraltar forearc still active?. Geológica Acta: an international earth science journal, 10(3), 249-263.
BandB1999	Bezzeghoud, M., & Buforn, E. (1999). Source parameters of the 1992 Melilla (Spain, MW= 4.8), 1994 Alhoceima (Morocco, MW= 5.8), and 1994 Mascara (Algeria, MW= 5.7) earthquakes and seismotectonic implications. Bulletin of the Seismological Society of America, 89(2), 359-372.
Batetal2008	Batlló, J., Stich, D., Palombo, B., Macia, R., & Morales, J. (2008). The 1951 M w 5.2 and M w 5.3 Jaén, southern Spain, earthquake doublet revisited. Bulletin of the Seismological Society of America, 98(3), 1535-1545.
Batetal2010	Batlló, J., Stich, D., Macià, R., & Morales, J. (2010). Moment tensor inversion for the 5 July 1930 Montilla earthquake (southern Spain). Seismological Research Letters, 81(5), 724-731.
Benietal2007	Benito, B., Capote, R., Murphy, P., Gaspar-Escribano, J.M., Martínez-Díaz, J.J., Tsige, M., Stich, D., García-Mayordomo, J., García Rodríguez, M.J., Jiménez, M.E., Insua-Arévalo, J.M., Álvarez-Gómez, J.A. and Canora, C. (2007). An overview of the damaging and low magnitude M w 4.8 La Paca earthquake on 29 January 2005: Context, seismotectonics, and seismic risk implications for southeast Spain. Bulletin of the Seismological Society of America, 97(3), 671-690.
Bensetal2011	Bensaid, I., Buforn, E., Cherkaout, T.E., Medina, F. and Hahou, Y. (2011). New fault-plane solutions of Moroccan earthquakes for the 2005-2008 period. Bulletin de l'Institut Scientifique, Rabat, section Sciences de la Terre, 33, 47-52.
Bezzetal2012	Bezzeghoud, M., Borges, J.F., Caldeira, B., 2012. Fontes sísmicas ao longo da fronteira de placas tectónicas entre os Açores e a Argélia: um modelo sismotectónico. Escolar Editora (volume Geologia de Portugal. chapter III.9).
Boretal2001	Borges, J. F., Fitas, A. J., Bezzeghoud, M., & Teves-Costa, P. (2001). Seismotectonics of Portugal and its adjacent Atlantic area. Tectonophysics, 331(4), 373-387.
Bouhetal2022	Bouhadad, Y., Benfedda, A., Maouche, S., Bezzeghoud, M., & Meghraoui, M. (2022). Seismicity of northern Algeria: performance of local networks. Mediterranean Geoscience Reviews, 4(4), 389-406.
BraunaandBer2005	Braunmiller, J., & Bernardi, F. (2005). The 2003 Boumerdes, Algeria earthquake: Regional moment tensor analysis. Geophysical Research Letters, 32(6).
Buetal1988a	Buforn, E., Udias, A., & Colombas, M. A. (1988). Seismicity, source mechanisms and tectonics of the Azores-Gibraltar plate boundary. Tectonophysics, 152(1-2), 89-118.
Buetal1988b	Buforn, E., Udías, A., & Mezcua, J. (1988). Seismicity and focal mechanisms in south Spain. Bulletin of the Seismological Society of America, 78(6), 2008-2024.
Buetal1991	Buforn, E., Udias, A., & Madariaga, R. (1991). Intermediate and deep earthquakes in Spain. Source Mechanism and Seismotectonics, 375-393.

Buetal1997	Buforn, E., Coca, P., Udías, A., & Lasa, C. (1997). Source mechanism of intermediate and deep earthquakes in southern Spain. Journal of Seismology, 1, 113-130.
Buetal2004	Buforn, E., Bezzeghoud, M., UdÍas, A., & Pro, C. (2004). Seismic sources on the Iberia-African plate boundary and their tectonic implications. Pure and applied geophysics, 161, 623-646.
Buetal2005	Buforn, E., Benito, B., De Galdeano, C. S., Del Fresno, C., Muñoz, D., & Rodríguez, I. (2005). Study of the damaging earthquakes of 1911, 1999, and 2002 in the Murcia, Southeastern Spain, region: seismotectonic and seismic-risk implications. Bulletin of the Seismological Society of America, 95(2), 549-567.
Buetal2016	Buforn, E., Udías, A., & Pro, C. (2016). Source mechanism studies of earthquakes in the Ibero-Maghrebian region and their tectonic implications. Journal of Seismology, 20(4), 1075-1088.
Buetal2017	Buforn, E., Pro C., Sanz de Galdeano, C., Cantavella, J.V., Cesca, S., Caldeira, B., Udías, A. and Mattesini, M. (2017). The 2016 south Alboran earthquake (Mw= 6.4): A reactivation of the Ibero-Maghrebian region?. Tectonophysics, 712, 704-715.
Cabiecetal2020	Cabieces, R., Buforn, E., Cesca, S., & Pazos, A. (2020). Focal parameters of earthquakes offshore Cape St. Vincent using an amphibious network. Pure and Applied Geophysics, 177, 1761-1780.
CandB1994	Coca, P., & Buforn, E. (1994). Mecanismos focales en el Sur de España: Periodo 1965-1985. Estudios Geológicos, 50(1-2), 33-45.
CatMorr2008	Medina, F. (2008). Catalogue of focal mechanisms of Moroccan earthquakes for the period 1959-2007. Documents de l'Institut Scientifique, Rabat, 23.
Cetal2004	Carrilho, F., Teves-Costa, P., Morais, I., Pagarete, J., & Dias, R. (2004). GEOALGAR Project: first results on seismicity and fault-plane solutions. pure and applied geophysics, 161, 589-606.
Chevrot (2011)	Chevrot, S., Sylvander, M., & Delouis, B. (2011). A preliminary catalog of moment tensors for the Pyrenees. Tectonophysics, 510(1-2), 239-251.
CMT	Ekström, G., Nettles, M., & Dziewoński, A. M. (2012). The global CMT project 2004–2010: Centroid-moment tensors for 13,017 earthquakes. Physics of the Earth and Planetary Interiors, 200, 1-9. / https://www.globalcmt.org/
Coca2003	Coca, P. (2003). Métodos para la inversión del tensor momento sísmico. Terremotos del Sur de España. PhD thesis, Universidad Complutense de Madrid, Spain, 300 pp.
Custetal2016	Custódio, S., Lima, V., Vales, D., Cesca, S., & Carrilho, F. (2016). Imaging active faulting in a region of distributed deformation from the joint clustering of focal mechanisms and hypocentres: Application to the Azores–western Mediterranean region. Tectonophysics, 676, 70-89.
Daboetal2021	Dabouz, G., Beldjoudi, H., Delouis, B., Boulahia, O., Mohammedi, Y., & Yelles-Chaouche, A. (2021). The 2007 Medea seismic sequence, North-Central Algeria: source parameters, stress tensor, and static stress changes. Pure and Applied Geophysics, 178(9), 3313-3337.
De1991	Dewey, J. W. (1991). The 1954 and 1980 Algerian earthquakes: implications for the characteristic-displacement model of fault behavior. Bulletin of the Seismological Society of America, 81(2), 446-467.
Doetal2013	Domingues, A., Custodio, S., & Cesca, S. (2013). Waveform inversion of small-to-moderate earthquakes located offshore southwest Iberia. Geophysical Journal International, 192(1), 248-259.
ElMoudetal2023	Moudnib, L. E., Timoulali, Y., Nouayti, A., El Abbassi, M., Bouka, M., Nouayti, N., & Mhammdi, N. (2023). Seismotectonic model of High-Middle Atlas Junction (Morocco) derived from earthquake focal mechanism and stress tensor analysis. Modeling Earth Systems and Environment, 9(2), 2407-2423.
EMMA	Vannucci, G., & Gasperini, P. (2004). The new release of the database of Earthquake Mechanisms of the Mediterranean Area (EMMA version 2). Annals of Geophysics, 47, 307–334.

EMSC	https://www.emsc-csem.org/Earthquake_data/tensors.php / https://seismicportal.eu/mtws/
ETHZ	Braunmiller, J., Kradolfer, U., Baer, M., & Giardini, D. (2002). Regional moment tensor determination in the European–Mediterranean area—initial results. Tectonophysics, 356(1-3), 5-22. / http://seismo.ethz.ch/mt/
FMHex20	Mazzotti, S., Aubagnac, C., Bollinger, L., Coca Oscanoa, K., Delouis, B., Do Paco, D., Doubre, C., Godano, M., Jomard, H., Larroque, C., Laurendeau, A., Masson, F., Sylvander, M., & Trilla, A. (2021). FMHex20: An earthquake focal mechanism database for seismotectonic analyses in metropolitan France and bordering regions. BSGF-Earth Sciences Bulletin, 192(1), 10.
Galetal1993	Galindo-Zaldívar, J., González-Lodeiro, F., & Jabaloy, A. (1993). Stress and palaeostress in the Betic-Rif cordilleras (Miocene to the present). Tectonophysics, 227(1-4), 105-126.
Galetal1999	Galindo-Zaldívar, J., Jabaloy, A., Serrano, I., Morales, J., González-Lodeiro, F., & Torcal, F. (1999). Recent and present-day stresses in the Granada Basin (Betic Cordilleras): Example of a late Miocene-present-day extensional basin in a convergent plate boundary. Tectonics, 18(4), 686-702.
Geisetal2010	Geissler, W. H., Matias, L., Stich, D., Carrilho, F., Jokat, W., Monna, S., IbenBrahim, A., Mancilla, F., Gutscher, M.-A., Sallares, V., & Zitellini, N. (2010). Focal mechanisms for sub-crustal earthquakes in the Gulf of Cadiz from a dense OBS deployment. Geophysical Research Letters, 37(18).
Greetal2015	Grevemeyer, I., Gràcia, E., Villaseñor, A., Leuchters, W., & Watts, A. B. (2015). Seismicity and active tectonics in the Alboran Sea, Western Mediterranean: Constraints from an offshore-onshore seismological network and swath bathymetry data. Journal of Geophysical Research: Solid Earth, 120(12), 8348-8365.
Hatzetal1978	Hatzfeld, D. (1978). Etude Sismotectonique de la Zone de Collision Ibero-Maghrebine. PhD thesis, Université Scientifique et Médicale de Grenoble, France, 281 pp.
Hatzetal1993	Hatzfeld, D., Caillot, V., Cherkaoui, T. E., Jebli, H., & Medina, F. (1993). Microearthquake seismicity and fault plane solutions around the Nekor strike-slip fault, Morocco. Earth and Planetary Science Letters, 120(1-2), 31-41.
IAG	https://iagpds.ugr.es/investigacion/proyectos/moment-tensor-catalogue
IGN	Rueda, J., & Mezcua, J. (2005). Near-real-time seismic moment-tensor determination in Spain. Seismological research letters, 76(4), 455-465. / https://www.ign.es/web/en/ign/portal/tensor-momento-sismico
ISC	https://www.isc.ac.uk/iscbulletin/search/fmechanisms/
Lopezetal2018	López-Fernández, C., Fernández-Viejo, G., Olona, J., & Llana-Fúnez, S. (2018). Intraplate seismicity in northwest Iberia along the trace of the Ventaniella fault: a case for fault intersection at depth. Bulletin of the Seismological Society of America, 108(2), 604-618.
M1985	Moreira, V. S. (1985). Seismotectonics of Portugal and its adjacent area in the Atlantic. Tectonophysics, 117(1-2), 85-96.
M1991	Moreira, V.S. (1991). Historical seismicity and seismotectonics of the area situated between the Iberian Peninsula, Morocco, Selvagens and Azores Islands, en Seismicity, Seismotectonics and Seismic Risk of the Ibero-Maghrebian Region, J. Mezcua y A. Udías (Editors), Monografía 8, IGN, Madrid, 213-225.
MandC1991	Medina, F., & Cherkaoui, T. E. (1991). Focal mechanisms of the Atlas earthquakes, and tectonic implications. Geologische Rundschau, 80(3), 639-648.
MandR1997	Mezcua, J., & Rueda, J. (1997). Seismological evidence for a delamination process in the lithosphere under the Alboran Sea. Geophysical Journal International, 129(1), F1-F8.
MandR2006	Mezcua, J., & Rueda, J. (2006). Sismicidad, sismotectónica y evolución geodinámica de la Península Ibérica. Física de la Tierra, 18, 137-155.

Maretal2015	Martín, R., Stich, D., Morales, J., & Mancilla, F. (2015). Moment tensor solutions for the Iberian-Maghreb region during the IberArray deployment (2009–2013). Tectonophysics, 663, 261-274.
MedandChe1992	Medina, F., & Cherkaoui, T. E. (1992). Mécanismes au foyer des séismes du Maroc et des régions voisines (1959-1986). Conséquences tectoniques. Eclogae Geol. Helv, 85(2), 433-457.
Metal2006	Martínez-Martínez, J. M., Booth-Rea, G., Azañón, J. M., & Torcal, F. (2006). Active transfer fault zone linking a segmented extensional system (Betics, southern Spain): Insight into heterogeneous extension driven by edge delamination. Tectonophysics, 422(1-4), 159-173.
Moetal2015	Morales, J., Azañón, J. M., Stich, D., Roldán, F. J., Pérez-Peña, J. V., Martín, R., Cantavella, J.V., Martín, J.B., Mancilla, F., & González-Ramón, A. (2015). The 2012–2013 earthquake swarm in the eastern Guadalquivir basin (South Spain): A case of heterogeneous faulting due to oroclinal bending. Gondwana Research, 28(4), 1566-1578.
Neretal2024	Neres, M., Camargo, G., Soares, A., Custódio, S., Bos, M., Vales, D., & Terrinha, P. (2024). Monchique alkaline magmatic intrusion (SW Iberia): Geophysical modeling and relationship with active seismicity and hydrothermalism. Tectonophysics, 888, 230426.
Ousetal2014	Ousadou, F., Dorbath, L., Ayadi, A., Dorbath, C., & Gharbi, S. (2014). Stress field variations along the Maghreb region derived from inversion of major seismic crisis fault plane solutions. Tectonophysics, 632, 261-280.
Ouyed et al. (1981)	Ouyed, M., Meghraoui, M., Cisternas, A., Deschamps, A., Dorel, J., Frechet, J., Gaulon, R., Hatzfeld, D., & Philip, H. (1981). Seismotectonics of the El Asnam earthquake. Nature, 292(5818), 26-31.
Ouyetal1983	Ouyed, M., Yielding, G., Hatzfeld, D., & King, G. C. P. (1983). An aftershock study of the El Asnam (Algeria) earthquake of 1980 October 10. Geophysical Journal International, 73(3), 605-639.
Palano2013	Palano, M., González, P. J., & Fernández, J. (2013). Strain and stress fields along the Gibraltar Orogenic Arc: Constraints on active geodynamics. Gondwana Research, 23(3), 1071-1088.
Perezetal2022	Pérez-López, R., Ramos, A., & Giner-Robles, J. L. (2022). Stress and strain analysis and induced seismicity in geological gas storage (Yela, Spain). Journal of Structural Geology, 161, 104662.
Pondetal1999	Pondrelli, S., Ekström, G., Morelli, A., & Primerano, S. (1999). Study of source geometry for tsunamigenic events of the Euro-Mediterranean area. In international Conference on Tsunamis (Vol. 297, p. 307). UNESCO books Paris.
PS1998	Proyecto Sigma (1998). Análisis del estado de esfuerzos tectónicos, reciente y actual a partir de poblaciones de fallas y mecanismos focales de terremotos. Metodología y aplicación a la Península Ibérica. Colección Otros Documentos, CSN, Madrid.
RCMT	Pondrelli, S. (2002). European-Mediterranean Regional Centroid-Moment Tensors Catalog (RCMT). / https://rcmt2.bo.ingv.it/
Rigo2015	Rigo, A., Vernant, P., Feigl, K. L., Goula, X., Khazaradze, G., Talaya, J., Morel, L., Nicolas, J., Baize, S., Chéry, J., & Sylvander, M. (2015). Present-day deformation of the Pyrenees revealed by GPS surveying and earthquake focal mechanisms until 2011. Geophysical Journal International, 201(2), 947-964.
RPandDV2001	Rodríguez-Pascua, M. A., & De Vicente, G. (2001). Estado de esfuerzos actual en la Cordillera Bética Oriental. Boletín Geológico y Minero, 112 (4).
Ruiz2006	Ruiz, M., Gallart, J., Díaz, J., Olivera, C., Pedreira, D., López, C., González-Cortina, J. M., & Pulgar, J. A. (2006). Seismic activity at the western Pyrenean edge. Tectonophysics, 412(3-4), 217-235.
Ruiz2023	Ruiz, M., Diaz, J., Canari, A., Ortuño, M., & Vergés, J. (2023). Seismic activity at the eastern Pyrenean termination. Tectonophysics, 862, 229977.

RuizCetal2011	Ruiz-Constán, A., Galindo-Zaldívar, J., Pedrera, A., Celerier, B., & Marín-Lechado, C. (2011). Stress distribution at the transition from subduction to continental collision (northwestern and central Betic Cordillera). Geochemistry, Geophysics, Geosystems, 12(12).
Sanetal2019	Santos-Bueno, N., Fernández-García, C., Stich, D., Mancilla, F. D. L., Martín, R., Molina-Aguilera, A., & Morales, J. (2019). Focal mechanisms for subcrustal earthquakes beneath the Gibraltar Arc. Geophysical Research Letters, 46(5), 2534-2543.
Sebai (1997)	Sebai-Yahia, O. (1997). Analyse sismologique des séismes récents du Sahel d'Alger. Master thesis, Université des Sciences et de la Technologie Houari Boumediene, Algeria, 178 pp
Serr1999	Serrano, I. (1999). Distribución espacial de la sismicidad en las Cordilleras Béticas-Mar de Alborán. PhD thesis, Universidad de Granada. 225 pp.
Serretal1996	Serrano, I., Morales, J., Vidal, F. y Torcal. F. (1996). Mecanismos focales en la cuenca de Granada. Homenaje en honor al profesor Fernando de Miguel Martínez, Universidad de Granada, I.A.G.P.D.S., 619-640.
Setal2001	Stich, D., Alguacil, G., & Morales, J. (2001). The relative locations of multiplets in the vicinity of the Western Almería (southern Spain) earthquake series of 1993–1994. Geophysical Journal International, 146(3), 801-812.
Setal2003a	Stich, D., Ammon, C.J. and Morales, J. (2003). Moment tensor solutions for small and moderate earthquakes in the Ibero-Maghreb region. Journal of Geophysical Research, 108, B3, 2148
Setal2003b	Stich, D., Batlló, J., Morales, J., Macià, R., & Dineva, S. (2003). Source parameters of the Mw= 6.1 1910 Adra earthquake (southern Spain). Geophysical Journal International, 155(2), 539-546.
Setal2005a	Stich, D., Batlló, J., Macià, R., Teves-Costa, P., & Morales, J. (2005). Moment tensor inversion with single-component historical seismograms: The 1909 Benavente (Portugal) and Lambesc (France) earthquakes. Geophysical Journal International, 162(3), 850-858.
Setal2005b	Stich, D., Mancilla, F. D. L., & Morales, J. (2005). Crust-mantle coupling in the Gulf of Cadiz (SW-Iberia). Geophysical Research Letters, 32(13).
Setal2006	Stich, D., Serpelloni, E., de Lis Mancilla, F., & Morales, J. (2006). Kinematics of the Iberia–Maghreb plate contact from seismic moment tensors and GPS observations. Tectonophysics, 426(3-4), 295-317.
Setal2010	Stich, D., Martín, R., & Morales, J. (2010). Moment tensor inversion for Iberia–Maghreb earthquakes 2005–2008. Tectonophysics, 483(3-4), 390-398.
Setal2020	Stich, D., Martín, R., Morales, J., López-Comino, J. Á., & Mancilla, F. D. L. (2020). Slip partitioning in the 2016 Alboran Sea earthquake sequence (Western Mediterranean). Frontiers in Earth Science, 8, 587356.
Setal2024	Stich, D., Morales, J., López-Comino, J. Á., Araque-Pérez, C., Azañón, J. M., Dengra, M. Á., Ruiz, M., & Weber, M. (2024). Seismogenic structures and active creep in the Granada Basin (S-Spain). Tectonophysics, 230368.
SGandT2002	Sanchez-Gomez, M., and F. Torcal (2002), Recent tectonic activity on the south margin of the Guadalquivir basin, between Cabra and Quesada towns (provinces of Jaen and Cordoba, Spain), in I Centenario del Observatorio de Cartuja, Abstract book, pp. 59–60, Inst. Andaluz de Geofis., Univ. de Granada, Granada, Spain.
Silva2017	Silva, S., Terrinha, P., Matias, L., Duarte, J. C., Roque, C., Ranero, C. R., Geissler, W. H., & Zitellini, N. (2017). Micro-seismicity in the Gulf of Cadiz: Is there a link between micro-seismicity, high magnitude earthquakes and active faults?. Tectonophysics, 717, 226-241.
Udetal1989	Udías, A., Buforn, E. and Ruiz de Gauna, J. (1989). Catalogue of focal mechanisms of european earthquakes. Department of Geophysics, Universidad Complutense, Madrid.
V1986	Vidal Sanchez, F. (1986). Sismotectónica de la región Béticas-Mar de Alborán. PhD thesis, Universidad de Granada, Spain,

Vanetal2014	van Der Woerd, J., Dorbath, C., Ousadou, F., Dorbath, L., Delouis, B., Jacques, E., Tapponier, P., Hahou, Y., Menzhi, M., Frogneux, M., & Haessler, H. (2014). The Al Hoceima Mw 6.4 earthquake of 24 February 2004 and its aftershocks sequence. Journal of Geodynamics, 77, 89-109.
Yelletal2014	Yelles-Chaouche, A. K., Abacha, I., Semmane, F., Beldjoudi, H., & Djellit, H. (2014). The Beni-Ilmane (north-central Algeria) earthquake sequence of May 2010. Pure and Applied Geophysics, 171, 1283-1298.
Yelletal2019	Yelles-Chaouche, A., Khelif, M. F., Haned, A., Chami, A., Aidi, C., Beldjoudi, H., Kherroubi, A., & Benaissa, Z. (2019). The Algiers (north central Algeria) earthquake of August 1st, 2014 M w 5.5 in the Algiers Bay tectonic context. Journal of Seismology, 23, 287-302.
Yieletal1989	Yielding, G., Ouyed, M., King, G. C. P., & Hatzfeld, D. (1989). Active tectonics of the Algerian Atlas mountains—evidence from aftershocks of the 1980 El Asnam earthquake. Geophysical journal international, 99(3), 761-788.

8.2.4. Table – Stress Inversion Results

Long.	Lat.	N_FMS	σ_1 trend	σ_1 plunge	σ_2 trend	σ_2 plunge	σ_3 trend	σ_3 plunge	Shape ratio (R)	σ_{Hmax}
(°)	(°)		(°)	(°)	(°)	(°)	(°)	(°)		(°)
-7.25	43.25	8	352.27	1.39	256.61	76.19	82.61	13.73	0.4	172.47
-2.25	43.25	17	143.52	75.84	279.2	10.23	10.97	9.68	0.67	104.56
-1.75	43.25	39	98.68	60.84	270.71	28.92	2.58	3.39	0.44	93.55
-1.25	43.25	32	98.15	54.43	271.51	35.39	3.75	3.14	0.58	95.16
-0.75	43.25	46	135.12	60.93	298.8	28.08	32.51	6.92	0.87	130.25
-0.25	43.25	84	123.96	72.86	295.04	16.95	25.8	2.51	0.77	117.65
0.25	43.25	52	68.19	87.23	298.25	1.78	208.19	2.12	0.79	117.95
2.25	43.25	8	9.39	33.05	273.6	8.81	170.57	55.5	0.52	19.76
-7.25	42.75	12	163.28	33.43	338.21	56.47	71.74	2.34	0.36	162.17
-2.25	42.75	17	143.52	75.84	279.2	10.23	10.97	9.68	0.67	104.56
-1.75	42.75	40	97.05	63.15	270.88	26.72	2.13	2.48	0.41	92.74
-1.25	42.75	34	94.95	60.77	275.58	29.23	185.43	0.27	0.47	95.35
-0.75	42.75	46	137.64	62.03	303.92	27.29	36.85	5.67	0.81	132.11
-0.25	42.75	84	124.63	74.08	293.17	15.62	24.01	3.01	0.74	115.9
0.25	42.75	56	119.59	85.61	297.28	4.38	27.3	0.18	0.78	117.34
0.75	42.75	13	256.33	70.47	132.85	11.07	39.66	15.88	0.39	127.5
1.25	42.75	17	328.49	59.07	158.11	30.57	65.6	4.24	0.81	151.82
1.75	42.75	24	344.67	66.93	129.08	19.1	223.46	12.44	0.65	139.99
2.25	42.75	22	9.62	52.44	131.55	22.14	234.38	28.63	0.82	177.53

2.75	42.75	10	15.14	27.34	278.26	13.05	165.37	59.22	0.91	15.94
-7.75	42.25	9	331.57	18.77	174.95	69.68	64.14	7.5	0.2	153.67
-7.25	42.25	9	321.95	27.71	154.98	61.67	54.81	5.44	0.23	144.28
1.25	42.25	14	329.91	58.39	140.48	31.26	233.04	4.21	0.8	146.69
1.75	42.25	24	23.6	75.03	135.81	5.77	227.23	13.77	0.48	138.66
2.25	42.25	19	18.04	78.23	137.76	5.9	228.82	10.15	0.48	139.82
2.75	42.25	8	332.23	22.85	179.88	64.56	66.75	10.59	0.68	153.82
-1.25	40.75	8	159.92	48.37	337.13	41.59	68.36	1.39	0.54	158.9
-3.75	40.25	9	173.17	34.61	278.24	20.64	33.02	48.05	0.76	167.05
-3.25	40.25	10	123.29	38.12	215.3	2.55	308.54	51.76	0.74	121.89
-1.25	40.25	8	151.03	52.55	330.93	37.45	60.97	0.05	0.66	151
0.75	40.25	8	0.04	33.51	175.47	56.41	268.65	2.11	0.6	179.36
-3.75	39.75	8	192.96	21.05	98.67	11.01	342.75	66	0.61	16.13
-3.25	39.75	11	140.63	25.32	241.14	21.08	6.03	56.02	0.84	138.5
-9.25	39.25	8	301.37	1.3	33.06	52.54	210.37	37.43	0.38	120.86
-8.75	39.25	8	301.37	1.3	33.06	52.54	210.37	37.43	0.38	120.86
-2.75	39.25	9	333.08	23.55	134.12	65.26	239.94	7.16	0.27	150.68
-0.75	39.25	9	334.45	28.57	149.69	61.34	243.36	2	0.52	153.86
-0.25	39.25	15	7.43	48.8	132.44	26.66	238.48	28.83	0.48	160.75
0.25	39.25	11	343.27	18.59	96.36	49.38	239.86	34.59	0.42	156.37
-8.25	38.75	10	323.91	3.56	57.42	44.48	230.3	45.3	0.5	142.71
-7.75	38.75	10	319.9	14.09	176.05	72.73	52.38	9.78	0.28	141.7
-2.75	38.75	9	325.28	40.58	115.24	45.31	221.53	15.51	0.65	138.93
-2.25	38.75	9	141.42	54.75	316.66	35.16	48.24	2.24	0.52	139.08
-1.75	38.75	11	87.37	15.57	178.77	5.01	286.12	73.61	0.6	86.32
-1.25	38.75	14	169.23	23.49	70.78	18.68	306.16	59.25	0.52	177.5
-0.75	38.75	12	358.69	5.73	115.75	77.56	267.57	11.01	0.1	177.68
-0.25	38.75	12	340.35	16.84	88.21	45.37	235.75	39.8	0.41	153.41
0.25	38.75	8	340.12	14.78	245.2	18.03	107.18	66.36	0.58	163.4
-8.25	38.25	8	322.06	4.47	57.86	52.32	228.64	37.32	0.54	140.84

-3.25	38.25	11	131.44	4.63	23.27	75.44	222.58	13.77	0.8	131.66
-2.75	38.25	10	301.21	13.95	180.52	64.05	36.8	21.42	0.81	122.19
-2.25	38.25	27	335.02	12.72	114.26	73.4	242.63	10.48	0.46	153.72
-1.75	38.25	44	349.01	27.25	117.92	50.65	244.45	26.02	0.55	162.39
-1.25	38.25	34	10.01	12.72	115.63	50.04	270.18	37.11	0.38	4.86
-0.75	38.25	18	196.79	9.86	89.42	59.8	292.14	28.23	0.8	17.67
-0.25	38.25	8	161.28	10.58	47.4	65.23	255.63	22.12	0.56	163.08
-8.75	37.75	14	151.67	0.66	246.73	82.58	61.59	7.39	0.66	151.64
-8.25	37.75	12	325.84	1.94	230.43	70.25	56.54	19.65	0.63	146.08
-4.75	37.75	15	315.54	32.84	107.48	53.82	216.63	13.49	0.53	130.69
-4.25	37.75	25	128.6	6.11	2.6	79.68	219.5	8.29	0.78	128.8
-3.75	37.75	19	139.71	9.61	16.87	72.66	232.18	14.29	0.89	139.98
-3.25	37.75	17	329.02	18.34	146.48	71.64	238.77	0.76	0.2	148.81
-2.75	37.75	15	86.25	83.9	320.61	3.56	230.3	4.94	0.33	140.14
-2.25	37.75	38	340.42	23.6	122.32	60.96	243.26	15.93	0.31	155.34
-1.75	37.75	53	348.12	16.74	113.01	62.26	251.34	21.45	0.65	165.87
-1.25	37.75	30	12.13	22.69	131.23	49.31	267.17	31.71	0.63	7.2
-0.75	37.75	11	15.61	3.89	115.33	68.06	284.07	21.56	0.59	15.03
-9.25	37.25	9	150.7	8.13	7.47	79.88	241.56	5.97	0.66	151
-8.75	37.25	19	147.66	3.85	13.28	84.5	237.92	3.92	0.8	147.71
-8.25	37.25	20	139.93	2.78	31.99	81.03	230.35	8.52	0.86	139.99
-7.75	37.25	8	120.8	18.98	334.5	67.54	214.84	11.56	0.47	123.01
-5.75	37.25	37	306.48	24.03	212.84	8.1	105.51	64.48	0.75	127.96
-5.25	37.25	42	306.66	20.38	211.1	14.62	87.91	64.52	0.74	128.78
-4.75	37.25	69	328.1	18.51	117.24	68.7	234.66	10.18	0.7	147
-4.25	37.25	216	345.45	82.87	130.2	5.83	220.61	4.09	0.48	130.99
-3.75	37.25	239	207.33	81.93	112.49	0.69	22.4	8.05	0.75	112.09
-3.25	37.25	118	231.62	75.65	114.4	6.68	22.89	12.65	0.88	98.04
-2.75	37.25	47	258.41	73.79	352.37	1.15	82.71	16.17	0.8	174.78
-2.25	37.25	31	144.39	20.16	340.44	69.09	236.35	5.31	0.62	145.19

-1.75	37.25	27	163.22	10.88	49.92	64.08	257.95	23.22	0.75	164.27
-1.25	37.25	9	356.11	36.92	236.49	33.33	118.51	35.5	0.56	10.58
2.75	37.25	15	318.91	13.17	51.47	10.83	179.7	72.82	0.71	137.84
3.25	37.25	56	339.46	4.51	69.68	2.85	191.86	84.66	0.72	159.37
3.75	37.25	65	340.34	1.84	70.57	7.11	235.88	82.65	0.72	160.25
4.25	37.25	21	146.22	2.42	55.8	9.7	250.11	80	0.6	146.48
-11.75	36.75	9	143.31	12.1	343.09	77.16	234.22	4.22	0.62	143.67
-11.25	36.75	17	150.74	5.68	16.53	81.88	241.32	5.78	0.83	150.84
-10.75	36.75	14	154.9	4.97	44.6	75.94	246.06	13.12	0.88	155.04
-10.25	36.75	37	144.15	4.48	43.04	67.86	235.93	21.63	0.77	144.51
-9.75	36.75	36	143.5	4.78	41.96	67.31	235.45	22.13	0.76	143.93
-8.75	36.75	9	139.98	7.89	37.44	57.45	234.83	31.34	0.84	140.58
-8.25	36.75	17	148.69	3.48	56.38	33.54	243.91	56.23	0.69	149.32
-7.75	36.75	16	161.98	6.98	70.12	14.87	276.4	73.51	0.68	162.79
-7.25	36.75	10	133.47	8.41	230.78	40.72	34.01	48.05	0.83	132.65
-5.75	36.75	44	309.69	22.62	212.94	15.75	91.04	61.92	0.83	131.16
-5.25	36.75	49	302.36	24.26	203.32	19.22	79.06	58.23	0.72	126.09
-4.75	36.75	63	332.38	15.62	171.52	73.52	63.82	5.14	0.73	152.78
-4.25	36.75	204	338.83	85.61	129.11	3.81	219.26	2.17	0.64	129.51
-3.75	36.75	234	218.61	80.89	105.92	3.54	15.4	8.39	0.8	103.05
-3.25	36.75	141	220.77	72.17	330.58	6.22	62.44	16.64	0.77	161.1
-2.75	36.75	84	340.52	6.88	229.47	71.44	72.65	17.15	0.2	162.2
-2.25	36.75	35	150.44	1.84	246.03	71.71	59.83	18.19	0.44	150.11
-1.75	36.75	10	153.78	23.09	331.18	66.89	63.38	0.94	0.67	153.63
1.25	36.75	88	323.38	3.77	231.7	24.05	61.74	65.62	0.96	143.44
1.75	36.75	87	323.82	2.68	233.34	10.17	68.39	79.48	0.95	143.84
2.25	36.75	23	337.06	8.09	239.18	43.97	75.21	44.9	0.85	157.75
2.75	36.75	40	336.89	10.53	244.26	13.88	102.88	72.45	0.83	157.41
3.25	36.75	97	337.78	4.55	68.16	4.77	204.3	83.4	0.7	157.61
3.75	36.75	100	337.18	2.08	67.47	7.88	232.53	81.84	0.69	157.06

4.25	36.75	25	146.71	0.65	56.58	11.71	239.84	78.27	0.56	146.81
-11.75	36.25	9	143.31	12.1	343.09	77.16	234.22	4.22	0.62	143.67
-11.25	36.25	17	332.3	7.28	167.44	82.46	62.55	1.95	0.81	152.35
-10.75	36.25	36	342.74	0.51	252	55.23	73.1	34.77	0.95	162.75
-10.25	36.25	62	150.27	1.12	250.57	83.77	60.15	6.13	0.93	150.26
-9.75	36.25	36	145.35	0.54	52.73	78.26	235.46	11.73	0.76	145.38
-8.75	36.25	12	154.04	6.75	247.25	25.35	50.22	63.64	0.74	153.14
-8.25	36.25	17	174.69	7.88	267.09	16.84	60.55	71.3	0.94	174.55
-7.75	36.25	20	182.75	12.51	89.93	12.51	316.35	72.16	0.77	3.58
-7.25	36.25	14	144.32	11.7	238.85	20.9	26.91	65.78	0.89	143.83
-5.75	36.25	11	331.63	19.4	226.01	37.41	83.16	46.18	0.79	154.22
-5.25	36.25	10	333.12	52.61	202.68	26.37	99.65	24.46	0.69	171.72
-4.75	36.25	10	171.72	17.12	274.1	34.83	60.17	50.01	0.13	155.16
-4.25	36.25	12	165.74	26.15	328.6	62.81	72.31	6.94	0.6	164.2
-3.75	36.25	12	156.52	75.15	343.64	14.74	253.17	1.76	0.65	162.45
-3.25	36.25	42	172.16	22.17	338.85	67.28	80.23	4.72	0.23	170.62
-2.75	36.25	57	343.4	0.63	250.08	79.21	73.52	10.78	0.29	163.49
-2.25	36.25	26	335.41	17.01	196.54	67.89	69.69	13.69	0.43	157.89
0.75	36.25	12	330.83	14.3	234.36	23.87	89.08	61.7	0.85	151.81
1.25	36.25	166	329.2	5.72	238.23	9.66	89.44	78.74	0.95	149.26
1.75	36.25	166	330.39	5.67	60.69	3.02	178.62	83.57	0.95	150.38
2.25	36.25	29	339.49	9.76	243.85	29.76	85.7	58.37	0.92	159.84
2.75	36.25	31	341.43	9.77	236.87	55.6	77.75	32.61	0.91	161.86
3.25	36.25	43	337.43	5.21	68.24	8.79	217.09	79.76	0.69	157.08
3.75	36.25	55	332.07	5.43	62.6	5.61	198.25	82.18	0.75	151.89
4.25	36.25	28	324.75	8.54	57.77	19.35	212.09	68.71	0.84	144.23
4.75	36.25	10	333.13	21.79	76.36	29.8	212.77	51.67	0.87	151.58
-10.75	35.75	27	161.46	1.28	253.01	50.44	70.41	39.53	0.89	161.39
-10.25	35.75	33	161.5	6.45	261.9	57.93	67.56	31.26	0.86	161.08
-9.75	35.75	12	166.19	26.89	330.15	62.18	72.82	6.61	0.58	164.6

-9.25	35.75	10	169.83	8.49	263.34	22.33	60.3	65.95	0.87	169.38
-8.75	35.75	13	162.94	14.31	259.12	22.91	43.54	62.54	0.6	159.51
-8.25	35.75	10	170.04	12.86	268.48	32.73	61.58	54.22	0.53	165.69
-7.75	35.75	9	180.01	25.99	72.97	30.99	302.09	47.45	0.86	2.32
-4.75	35.75	8	119.35	13.15	241.28	66.17	24.6	19.5	0.68	117.88
-4.25	35.75	44	345.75	24.81	168.17	65.17	76.17	0.92	0.46	166
-3.75	35.75	136	339.66	22.29	154.04	67.61	248.85	1.98	0.74	159.43
-3.25	35.75	106	337.71	18.81	159.82	71.17	67.93	0.64	0.76	157.77
-2.75	35.75	19	38.08	67.42	299.19	3.68	207.68	22.24	0.49	115.73
-2.25	35.75	12	325.84	34.57	111.76	50.24	223.55	17.17	0.69	141.22
-0.75	35.75	8	314.65	14.56	140.68	75.37	45.03	1.47	0.67	134.78
-0.25	35.75	12	316.93	16.73	183.8	66.26	51.99	16.34	0.84	137.76
0.25	35.75	12	317.83	22.04	202.28	46.81	64.25	34.91	0.91	138.9
0.75	35.75	12	317.05	6.87	55.99	52.23	221.85	36.92	0.83	136.43
1.25	35.75	81	336.28	6.21	245.48	7.34	106.15	80.36	0.93	156.34
1.75	35.75	81	338.04	8.87	247.64	2.59	141.5	80.76	0.94	158.07
2.25	35.75	9	344.34	15.83	76.41	7.24	190.2	72.52	0.79	163.76
3.75	35.75	21	323.01	9.8	232.33	3.89	120.94	79.44	0.68	143.33
4.25	35.75	26	328.83	9.69	237.63	7.02	112.26	78	0.8	149.14
-9.75	35.25	9	143.93	48.93	336.29	40.4	241.03	6.15	0.23	150.21
-4.25	35.25	131	336.83	16.78	153.56	73.19	246.56	0.91	0.4	156.66
-3.75	35.25	225	337.7	18.16	155.21	71.83	247.46	0.74	0.62	157.6
-3.25	35.25	108	335.85	17.06	177.88	71.68	67.84	6.47	0.85	156.17
-2.75	35.25	18	307.39	30.99	122.32	58.91	216.04	2.25	0.73	126.95
0.25	35.25	10	317.83	11.15	190.11	72.15	50.6	13.76	0.81	138.35
-5.75	34.75	8	24.7	0.79	294.31	26.45	116.29	63.54	0.64	24.86
-5.25	34.75	8	354.25	14.03	254.68	33.63	103.47	52.8	0.71	176.8
-4.25	34.75	94	334.52	11.15	155.03	78.85	64.54	0.1	0.38	154.53
-3.75	34.75	94	334.61	13.26	153.17	76.73	244.54	0.32	0.4	154.56
-3.25	34.75	13	315.75	25.94	175.74	57.59	54.87	18.04	0.56	139.98

-2.75	34.75	11	152.47	41.2	299.79	43.87	46.92	17.03	0.1	137.89
-5.75	32.75	9	327.43	0.63	57.61	15.76	235.22	74.23	0.51	147.29
-5.25	32.75	10	159.87	7.36	250.56	5.3	15.98	80.92	0.43	158.94
-5.75	32.25	11	325.13	1.52	58.98	68.41	234.53	21.53	0.56	144.89

8.2.5. Table – σ_{Hmax} directions

Lon.	*Lat.*	σ_{Hmax}	*Type*	*Reference*	*FMS source*
(°)	(°)	(°)			
-7.250	43.250	172	Stress inversion	This study	
-2.250	43.250	105	Stress inversion	This study	
-1.750	43.250	94	Stress inversion	This study	
-1.250	43.250	95	Stress inversion	This study	
-0.750	43.250	130	Stress inversion	This study	
-0.250	43.250	118	Stress inversion	This study	
0.250	43.250	118	Stress inversion	This study	
2.250	43.250	20	Stress inversion	This study	
-7.250	42.750	162	Stress inversion	This study	
-2.250	42.750	105	Stress inversion	This study	
-1.750	42.750	93	Stress inversion	This study	
-1.250	42.750	95	Stress inversion	This study	
-0.750	42.750	132	Stress inversion	This study	
-0.250	42.750	116	Stress inversion	This study	
0.250	42.750	117	Stress inversion	This study	
0.750	42.750	128	Stress inversion	This study	
1.250	42.750	152	Stress inversion	This study	
1.750	42.750	140	Stress inversion	This study	
2.250	42.750	178	Stress inversion	This study	
2.750	42.750	16	Stress inversion	This study	
-7.750	42.250	154	Stress inversion	This study	
-7.250	42.250	144	Stress inversion	This study	

1.250	42.250	147	Stress inversion	This study	
1.750	42.250	139	Stress inversion	This study	
2.250	42.250	140	Stress inversion	This study	
2.750	42.250	154	Stress inversion	This study	
-1.250	40.750	159	Stress inversion	This study	
-3.750	40.250	167	Stress inversion	This study	
-3.250	40.250	122	Stress inversion	This study	
-1.250	40.250	151	Stress inversion	This study	
0.750	40.250	179	Stress inversion	This study	
-3.750	39.750	16	Stress inversion	This study	
-3.250	39.750	139	Stress inversion	This study	
-9.250	39.250	121	Stress inversion	This study	
-8.750	39.250	121	Stress inversion	This study	
-2.750	39.250	151	Stress inversion	This study	
-0.750	39.250	154	Stress inversion	This study	
-0.250	39.250	161	Stress inversion	This study	
0.250	39.250	156	Stress inversion	This study	
-8.250	38.750	143	Stress inversion	This study	
-7.750	38.750	142	Stress inversion	This study	
-2.750	38.750	139	Stress inversion	This study	
-2.250	38.750	139	Stress inversion	This study	
-1.750	38.750	86	Stress inversion	This study	
-1.250	38.750	178	Stress inversion	This study	
-0.750	38.750	178	Stress inversion	This study	
-0.250	38.750	153	Stress inversion	This study	
0.250	38.750	163	Stress inversion	This study	
-8.250	38.250	141	Stress inversion	This study	
-3.250	38.250	132	Stress inversion	This study	
-2.750	38.250	122	Stress inversion	This study	
-2.250	38.250	154	Stress inversion	This study	

-1.750	38.250	162	Stress inversion	This study	
-1.250	38.250	5	Stress inversion	This study	
-0.750	38.250	18	Stress inversion	This study	
-0.250	38.250	163	Stress inversion	This study	
-8.750	37.750	152	Stress inversion	This study	
-8.250	37.750	146	Stress inversion	This study	
-4.750	37.750	131	Stress inversion	This study	
-4.250	37.750	129	Stress inversion	This study	
-3.750	37.750	140	Stress inversion	This study	
-3.250	37.750	149	Stress inversion	This study	
-2.750	37.750	140	Stress inversion	This study	
-2.250	37.750	155	Stress inversion	This study	
-1.750	37.750	166	Stress inversion	This study	
-1.250	37.750	7	Stress inversion	This study	
-0.750	37.750	15	Stress inversion	This study	
-9.250	37.250	151	Stress inversion	This study	
-8.750	37.250	148	Stress inversion	This study	
-8.250	37.250	140	Stress inversion	This study	
-7.750	37.250	123	Stress inversion	This study	
-5.750	37.250	128	Stress inversion	This study	
-5.250	37.250	129	Stress inversion	This study	
-4.750	37.250	147	Stress inversion	This study	
-4.250	37.250	131	Stress inversion	This study	
-3.750	37.250	112	Stress inversion	This study	
-3.250	37.250	98	Stress inversion	This study	
-2.750	37.250	175	Stress inversion	This study	
-2.250	37.250	145	Stress inversion	This study	
-1.750	37.250	164	Stress inversion	This study	
-1.250	37.250	11	Stress inversion	This study	
2.750	37.250	138	Stress inversion	This study	

3.250	37.250	159	Stress inversion	This study	
3.750	37.250	160	Stress inversion	This study	
4.250	37.250	146	Stress inversion	This study	
-11.750	36.750	144	Stress inversion	This study	
-11.250	36.750	151	Stress inversion	This study	
-10.750	36.750	155	Stress inversion	This study	
-10.250	36.750	145	Stress inversion	This study	
-9.750	36.750	144	Stress inversion	This study	
-8.750	36.750	141	Stress inversion	This study	
-8.250	36.750	149	Stress inversion	This study	
-7.750	36.750	163	Stress inversion	This study	
-7.250	36.750	133	Stress inversion	This study	
-5.750	36.750	131	Stress inversion	This study	
-5.250	36.750	126	Stress inversion	This study	
-4.750	36.750	153	Stress inversion	This study	
-4.250	36.750	130	Stress inversion	This study	
-3.750	36.750	103	Stress inversion	This study	
-3.250	36.750	161	Stress inversion	This study	
-2.750	36.750	162	Stress inversion	This study	
-2.250	36.750	150	Stress inversion	This study	
-1.750	36.750	154	Stress inversion	This study	
1.250	36.750	143	Stress inversion	This study	
1.750	36.750	144	Stress inversion	This study	
2.250	36.750	158	Stress inversion	This study	
2.750	36.750	157	Stress inversion	This study	
3.250	36.750	158	Stress inversion	This study	
3.750	36.750	157	Stress inversion	This study	
4.250	36.750	147	Stress inversion	This study	
-11.750	36.250	144	Stress inversion	This study	
-11.250	36.250	152	Stress inversion	This study	

-10.750	36.250	163	Stress inversion	This study	
-10.250	36.250	150	Stress inversion	This study	
-9.750	36.250	145	Stress inversion	This study	
-8.750	36.250	153	Stress inversion	This study	
-8.250	36.250	175	Stress inversion	This study	
-7.750	36.250	4	Stress inversion	This study	
-7.250	36.250	144	Stress inversion	This study	
-5.750	36.250	154	Stress inversion	This study	
-5.250	36.250	172	Stress inversion	This study	
-4.750	36.250	155	Stress inversion	This study	
-4.250	36.250	164	Stress inversion	This study	
-3.750	36.250	162	Stress inversion	This study	
-3.250	36.250	171	Stress inversion	This study	
-2.750	36.250	163	Stress inversion	This study	
-2.250	36.250	158	Stress inversion	This study	
0.750	36.250	152	Stress inversion	This study	
1.250	36.250	149	Stress inversion	This study	
1.750	36.250	150	Stress inversion	This study	
2.250	36.250	160	Stress inversion	This study	
2.750	36.250	162	Stress inversion	This study	
3.250	36.250	157	Stress inversion	This study	
3.750	36.250	152	Stress inversion	This study	
4.250	36.250	144	Stress inversion	This study	
4.750	36.250	152	Stress inversion	This study	
-10.750	35.750	161	Stress inversion	This study	
-10.250	35.750	161	Stress inversion	This study	
-9.750	35.750	165	Stress inversion	This study	
-9.250	35.750	169	Stress inversion	This study	
-8.750	35.750	160	Stress inversion	This study	
-8.250	35.750	166	Stress inversion	This study	

-7.750	35.750	2	Stress inversion	This study	
-4.750	35.750	118	Stress inversion	This study	
-4.250	35.750	166	Stress inversion	This study	
-3.750	35.750	159	Stress inversion	This study	
-3.250	35.750	158	Stress inversion	This study	
-2.750	35.750	116	Stress inversion	This study	
-2.250	35.750	141	Stress inversion	This study	
-0.750	35.750	135	Stress inversion	This study	
-0.250	35.750	138	Stress inversion	This study	
0.250	35.750	139	Stress inversion	This study	
0.750	35.750	136	Stress inversion	This study	
1.250	35.750	156	Stress inversion	This study	
1.750	35.750	158	Stress inversion	This study	
2.250	35.750	164	Stress inversion	This study	
3.750	35.750	143	Stress inversion	This study	
4.250	35.750	149	Stress inversion	This study	
-9.750	35.250	150	Stress inversion	This study	
-4.250	35.250	157	Stress inversion	This study	
-3.750	35.250	158	Stress inversion	This study	
-3.250	35.250	156	Stress inversion	This study	
-2.750	35.250	127	Stress inversion	This study	
0.250	35.250	138	Stress inversion	This study	
-5.750	34.750	25	Stress inversion	This study	
-5.250	34.750	177	Stress inversion	This study	
-4.250	34.750	155	Stress inversion	This study	
-3.750	34.750	155	Stress inversion	This study	
-3.250	34.750	140	Stress inversion	This study	
-2.750	34.750	138	Stress inversion	This study	
-5.750	32.750	147	Stress inversion	This study	
-5.250	32.750	159	Stress inversion	This study	

-5.750	32.250	145	Stress inversion	This study	
-5.890	33.590	12	Individaul earthquake FMS	This study	Bensaid et al. (2011)
-10.600	39.300	128	Individaul earthquake FMS	This study	Bufforn et al. (1988)
-4.357	31.220	138	Individaul earthquake FMS	This study	CMT
-4.383	31.412	317	Individaul earthquake FMS	This study	CMT
-11.320	35.021	145	Individaul earthquake FMS	This study	Custodio et al. (2016)
-9.700	31.300	185	Individaul earthquake FMS	This study	EMMA
-12.700	37.300	348	Individaul earthquake FMS	This study	EMSC
-8.700	34.700	93	Individaul earthquake FMS	This study	EMSC
-3.551	32.615	309	Individaul earthquake FMS	This study	ETHZ
4.638	44.527	136	Individaul earthquake FMS	This study	FMHex20
4.670	40.970	162	Individaul earthquake FMS	This study	FMHex20
-11.500	43.200	6	Individaul earthquake FMS	This study	Galindo et al. (1993)
-10.567	40.216	107	Individaul earthquake FMS	This study	IGN
-6.060	31.490	115	Individaul earthquake FMS	This study	Medina and Cherkaoui (1991)
0.190	33.250	277	Individaul earthquake FMS	This study	Medina and Cherkaoui (1991)
-0.090	32.820	264	Individaul earthquake FMS	This study	Martin et al. (2015)
-5.230	34.050	12	Individaul earthquake FMS	This study	Medina and Cherkaoui (1992)
1.510	40.830	161	Individaul earthquake FMS	This study	Proyecto Sigma (1998)
-4.320	32.650	145	Individaul earthquake FMS	This study	RCMT
-12.400	33.840	133	Individaul earthquake FMS	This study	RCMT
3.800	34.840	289	Individaul earthquake FMS	This study	RCMT
3.810	34.890	291	Individaul earthquake FMS	This study	RCMT
3.330	34.740	305	Individaul earthquake FMS	This study	RCMT
-4.240	32.660	140	Individaul earthquake FMS	This study	RCMT
-8.390	31.050	358	Individaul earthquake FMS	This study	RCMT
-1.281	35.321	303	Individaul earthquake FMS	This study	Stich et al. (2003)
1.826	37.895	332	Individaul earthquake FMS	This study	Stich et al. (2006)
-9.617	30.450	339	Individaul earthquake FMS	This study	Udias et al. (1989)
-9.316	41.750	147	Indiviudal borehole breakout	Heidbach et al. (2016)	

-9.264	39.903	142	Indiviudal borehole breakout	Heidbach et al. (2016)	
-9.206	40.116	140	Indiviudal borehole breakout	Heidbach et al. (2016)	
-9.134	40.026	147	Indiviudal borehole breakout	Heidbach et al. (2016)	
-9.129	41.134	110	Indiviudal borehole breakout	Heidbach et al. (2016)	
-9.113	41.713	139	Indiviudal borehole breakout	Heidbach et al. (2016)	
-9.047	38.638	91	Indiviudal borehole breakout	Heidbach et al. (2016)	
-9.031	39.936	49	Indiviudal borehole breakout	Heidbach et al. (2016)	
-8.953	38.343	150	Indiviudal borehole breakout	Heidbach et al. (2016)	
-8.417	39.900	165	Indiviudal borehole breakout	Heidbach et al. (2016)	
-4.120	42.740	59	Indiviudal borehole breakout	Heidbach et al. (2016)	
-3.870	42.830	135	Indiviudal borehole breakout	Heidbach et al. (2016)	
-3.367	42.826	28	Indiviudal borehole breakout	Heidbach et al. (2016)	
-2.930	42.310	36	Indiviudal borehole breakout	Heidbach et al. (2016)	
-2.850	42.390	47	Indiviudal borehole breakout	Heidbach et al. (2016)	
-2.840	42.430	39	Indiviudal borehole breakout	Heidbach et al. (2016)	
-1.124	44.150	145	Indiviudal borehole breakout	Heidbach et al. (2016)	
-1.065	44.602	117	Indiviudal borehole breakout	Heidbach et al. (2016)	
-0.990	44.468	172	Indiviudal borehole breakout	Heidbach et al. (2016)	
-0.989	44.841	122	Indiviudal borehole breakout	Heidbach et al. (2016)	
-0.922	44.566	157	Indiviudal borehole breakout	Heidbach et al. (2016)	
-0.885	44.478	154	Indiviudal borehole breakout	Heidbach et al. (2016)	
-0.850	41.830	0	Indiviudal borehole breakout	Heidbach et al. (2016)	
-0.100	41.640	76	Indiviudal borehole breakout	Heidbach et al. (2016)	
1.375	40.827	18	Indiviudal borehole breakout	Heidbach et al. (2016)	
1.712	40.961	3	Indiviudal borehole breakout	Heidbach et al. (2016)	
1.980	41.170	17	Indiviudal borehole breakout	Heidbach et al. (2016)	
2.197	41.119	36	Indiviudal borehole breakout	Heidbach et al. (2016)	
2.334	41.211	158	Indiviudal borehole breakout	Heidbach et al. (2016)	
2.374	41.443	2	Indiviudal borehole breakout	Heidbach et al. (2016)	
2.950	41.630	52	Indiviudal borehole breakout	Heidbach et al. (2016)	

3.300	41.710	33	Indiviudal borehole breakout	Heidbach et al. (2016)	
3.300	41.730	53	Indiviudal borehole breakout	Heidbach et al. (2016)	
4.700	44.850	140	Indiviudal borehole breakout	Heidbach et al. (2016)	
-7.350	39.830	149	Inversion of fault-slip data observed on planes of a variety of trends	Heidbach et al. (2016)	
-6.940	33.827	21	Inversion of fault-slip data observed on planes of a variety of trends	Heidbach et al. (2016)	
-6.863	33.883	175	Inversion of fault-slip data observed on planes of a variety of trends	Heidbach et al. (2016)	
-6.683	34.088	72	Inversion of fault-slip data observed on planes of a variety of trends	Heidbach et al. (2016)	
-6.680	33.848	166	Inversion of fault-slip data observed on planes of a variety of trends	Heidbach et al. (2016)	
-6.110	38.990	97	Inversion of fault-slip data observed on planes of a variety of trends	Heidbach et al. (2016)	
-5.687	34.054	178	Inversion of fault-slip data observed on planes of a variety of trends	Heidbach et al. (2016)	
-5.182	34.106	1	Inversion of fault-slip data observed on planes of a variety of trends	Heidbach et al. (2016)	
-5.100	39.290	175	Inversion of fault-slip data observed on planes of a variety of trends	Heidbach et al. (2016)	
-5.077	34.092	179	Inversion of fault-slip data observed on planes of a variety of trends	Heidbach et al. (2016)	
-4.965	34.092	17	Inversion of fault-slip data observed on planes of a variety of trends	Heidbach et al. (2016)	
-4.500	41.330	172	Inversion of fault-slip data observed on planes of a variety of trends	Heidbach et al. (2016)	
-4.050	38.980	150	Inversion of fault-slip data observed on planes of a variety of trends	Heidbach et al. (2016)	
-4.040	38.930	14	Inversion of fault-slip data observed on planes of a variety of trends	Heidbach et al. (2016)	
-3.620	42.300	101	Inversion of fault-slip data observed on planes of a variety of trends	Heidbach et al. (2016)	
-2.700	41.450	106	Inversion of fault-slip data observed on planes of a variety of trends	Heidbach et al. (2016)	
-2.470	41.350	59	Inversion of fault-slip data observed on planes of a variety of trends	Heidbach et al. (2016)	
-2.060	40.790	165	Inversion of fault-slip data observed on planes of a variety of trends	Heidbach et al. (2016)	

-1.930	41.240	110	Inversion of fault-slip data observed on planes of a variety of trends	Heidbach et al. (2016)	
-8.646	41.964	118	Paleo-focal mechanism, P-axis measured at 30° to fault in plane of slip vector	Heidbach et al. (2016)	
-8.568	41.964	9	Paleo-focal mechanism, P-axis measured at 30° to fault in plane of slip vector	Heidbach et al. (2016)	
-7.859	40.315	140	Orientation from fault altitude and primary sense of offset	Heidbach et al. (2016)	
-7.070	41.270	170	Orientation from fault altitude and primary sense of offset	Heidbach et al. (2016)	
1.982	41.458	20	Orientation from fault altitude and primary sense of offset	Heidbach et al. (2016)	
3.300	43.630	80	Testing of pre-existing fractures (HTPF technique) stress magnitudes from inversion of tests over a depth interval	Heidbach et al. (2016)	
-6.730	40.880	163	Overcoring or other strain relief measurement	Heidbach et al. (2016)	
-6.610	41.120	151	Overcoring or other strain relief measurement	Heidbach et al. (2016)	
4.317	44.450	135	Overcoring or other strain relief measurement	Heidbach et al. (2016)	

Reference in Table	*Reference in extended version*
Bensaid et al. (2011)	Bensaid, I., Buforn, E., Cherkaout, T.E., Medina, F. and Hahou, Y. (2011). New fault-plane solutions of Moroccan earthquakes for the 2005-2008 period. Bulletin de l'Institut Scientifique, Rabat, section Sciences de la Terre, 33, 47-52.
Bufforn et al. (1988)	Buforn, E., Udias, A., & Colombas, M. A. (1988). Seismicity, source mechanisms and tectonics of the Azores-Gibraltar plate boundary. Tectonophysics, 152(1-2), 89-118.
CMT	Ekström, G., Nettles, M., & Dziewoński, A. M. (2012). The global CMT project 2004–2010: Centroid-moment tensors for 13,017 earthquakes. Physics of the Earth and Planetary Interiors, 200, 1-9. / https://www.globalcmt.org/
Custodio et al. (2016)	Custódio, S., Lima, V., Vales, D., Cesca, S., & Carrilho, F. (2016). Imaging active faulting in a region of distributed deformation from the joint clustering of focal mechanisms and hypocentres: Application to the Azores–western Mediterranean region. Tectonophysics, 676, 70-89.
EMMA	Vannucci, G., & Gasperini, P. (2004). The new release of the database of Earthquake Mechanisms of the Mediterranean Area (EMMA version 2). Annals of Geophysics, 47, 307–334.
EMSC	https://www.emsc-csem.org/Earthquake_data/tensors.php / https://seismicportal.eu/mtws/

ETHZ	Braunmiller, J., Kradolfer, U., Baer, M., & Giardini, D. (2002). Regional moment tensor determination in the European–Mediterranean area—initial results. Tectonophysics, 356(1-3), 5-22. / http://seismo.ethz.ch/mt/
FMHex20	Mazzotti, S., Aubagnac, C., Bollinger, L., Coca Oscanoa, K., Delouis, B., Do Paco, D., Doubre, C., Godano, M., Jomard, H., Larroque, C., Laurendeau, A., Masson, F., Sylvander, M., & Trilla, A. (2021). FMHex20: An earthquake focal mechanism database for seismotectonic analyses in metropolitan France and bordering regions. BSGF-Earth Sciences Bulletin, 192(1), 10.
Galindo et al. (1993)	Galindo-Zaldívar, J., González-Lodeiro, F., & Jabaloy, A. (1993). Stress and palaeostress in the Betic-Rif cordilleras (Miocene to the present). Tectonophysics, 227(1-4), 105-126.
Heidbach et al. (2016)	Heidbach, O., M. Rajabi, K. Reiter, M.O. Ziegler, and the WSM Team (2016): World Stress Map Database Release 2016. GFZ Data Services, doi:10.5880/WSM.2016.001
IGN	Rueda, J., & Mezcua, J. (2005). Near-real-time seismic moment-tensor determination in Spain. Seismological research letters, 76(4), 455-465. / https://www.ign.es/web/en/ign/portal/tensor-momento-sismico
Medina and Cherkaoui (1991)	Medina, F., & Cherkaoui, T. E. (1991). Focal mechanisms of the Atlas earthquakes, and tectonic implications. Geologische Rundschau, 80(3), 639-648.
Martin et al. (2015)	Martín, R., Stich, D., Morales, J., & Mancilla, F. (2015). Moment tensor solutions for the Iberian-Maghreb region during the IberArray deployment (2009–2013). Tectonophysics, 663, 261-274.
Medina and Cherkaoui (1992)	Medina, F., & Cherkaoui, T. E. (1992). Mécanismes au foyer des séismes du Maroc et des régions voisines (1959-1986). Conséquences tectoniques. Eclogae Geol. Helv, 85(2), 433-457.
Proyecto Sigma (1998)	Proyecto Sigma (1998). Análisis del estado de esfuerzos tectónicos, reciente y actual a partir de poblaciones de fallas y mecanismos focales de terremotos. Metodología y aplicación a la Península Ibérica. Colección Otros Documentos, CSN, Madrid.
RCMT	Pondrelli, S. (2002). European-Mediterranean Regional Centroid-Moment Tensors Catalog (RCMT). / https://rcmt2.bo.ingv.it/
Stich et al. (2003)	Stich, D., Ammon, C.J. and Morales, J. (2003). Moment tensor solutions for small and moderate earthquakes in the Ibero-Maghreb region. Journal of Geophysical Research, 108, B3, 2148
Stich et al. (2006)	Stich, D., Serpelloni, E., de Lis Mancilla, F., & Morales, J. (2006). Kinematics of the Iberia–Maghreb plate contact from seismic moment tensors and GPS observations. Tectonophysics, 426(3-4), 295-317.
Udias et al. (1989)	Udías, A., Buforn, E. and Ruiz de Gauna, J. (1989). Catalogue of focal mechanisms of european earthquakes. Department of Geophysics, Universidad Complutense, Madrid.

8.2.6. Table – GNSS Networks used for velocity field computation

Network Id	*Country*	*Web address*
EUREF	Europe	https://www.epncb.oma.be/
RGP	France	https://rgp.ign.fr/
RENEP	Portugal	https://renep.dgterritorio.gov.pt/
SERVIR	Portugal	https://www.igeoe.pt/index.php?id=45
ARAGEA	Spain	https://gnss.aragon.es/

BIZKAIA	Spain	https://www.bizkaia.eus/es/gnss-bizkaia
CANTABRIA	Spain	https://gnss.cantabria.es/
CATNET	Spain	https://catnet-ip.icgc.cat/
ERVA	Spain	https://icv.gva.es/es/web/icv-erva/
EUSKADI	Spain	https://www.gps2.euskadi.eus/
GALNET	Spain	http://cartogalicia.com/galnet2/
GIPUZKOA	Spain	https://b5m.gipuzkoa.eus/web5000/en/geodesy/gipuzkoa-gnss-network
IGN	Spain	https://www.ign.es/web/ign/portal/gds-gnss-estaciones-permanentes
ITACYL	Spain	http://gnss.itacyl.es/
LARIOJA	Spain	https://iderioja.larioja.org/servicios/red-de-estaciones-gnss
RAP	Spain	https://www.juntadeandalucia.es/institutodeestadisticaycartografia/rap/nodos
REP	Spain	http://www.rep-gnss.es/
REGAM	Spain	https://sitmurcia.carm.es/regam-presentacion
RGAN	Spain	https://www.navarra.es/es/web/rgan
RGAPA	Spain	http://rgapa.cartografia.asturias.es/
SONEL	Worldwide	https://www.sonel.org/

8.2.7. Table – GNSS velocities

ID	Long.	Lat.	E IRTF14	N IRTF14	E Eu	N Eu	E Afr	N Afr	E Adj.	N Adj.	Reference	Used for strain
	(°)	(°)	(mm/yr)	(mm/yr)	(mm/yr)	(mm/yr)	(mm/yr)	(mm/yr)	(mm/yr)	(mm/yr)		
3CAN_GPS	-3.7016	40.6136	18.39	16.12	-0.71	-0.41	3.93	-2.60	0.10	0.15	This study	Yes
ABAN_GPS	-1.0537	38.1751	19.25	17.22	-0.91	0.78	3.51	-1.68	0.06	0.07	This study	Yes
ACIN_GPS	-1.4368	40.4089	18.57	16.11	-1.01	-0.35	3.57	-2.77	0.07	0.07	This study	Yes
ACNS_GPS	-6.3521	41.7001	17.75	16.78	-0.57	0.2	4.21	-1.72	0.08	0.08	This study	Yes
ADAX_GPS	-1.0556	43.7108	18.45	15.97	-0.38	-0.47	4.38	-2.93	0.14	0.17	This study	Yes
AGDE_GPS	3.4664	43.2964	19.79	15.70	-0.03	-0.51	4.57	-3.41	0.09	0.12	This study	Yes
AGDS_GPS	3.4743	43.3127	19.74	15.78	-0.07	-0.42	4.52	-3.33	0.06	0.07	This study	Yes
AGEN_GPS	0.6115	44.1725	18.81	16.31	-0.23	-0.05	4.51	-2.68	0.08	0.12	This study	Yes
AGRD_GPS	-1.9305	41.8490	19.48	16.13	0.35	-0.34	5.03	-2.71	0.15	0.13	This study	Yes

AGUE_GPS	-8.4469	40.5756	17.48	16.76	-0.74	0.16	4.00	-1.55	0.08	0.07	This study	Yes
AICI_GPS	-1.0144	43.3336	18.90	16.15	-0.03	-0.29	4.71	-2.75	0.08	0.18	This study	Yes
AIGL_GPS	3.5813	44.1214	19.58	15.80	-0.06	-0.4	4.58	-3.31	0.06	0.10	This study	Yes
AIRM_GPS	-1.1286	37.8065	18.92	16.28	-1.31	-0.17	3.08	-2.62	0.08	0.08	This study	Yes
AJAL_GPS	-2.2736	41.2161	18.71	15.80	-0.51	-0.69	4.13	-3.02	0.08	0.11	This study	Yes
ALAC_GPS	-0.4812	38.3389	19.58	16.22	-0.65	-0.2	3.77	-2.72	0.07	0.05	This study	Yes
ALBA_GPS	-1.8564	38.9779	18.32	15.98	-1.52	-0.49	2.98	-2.87	0.08	0.09	This study	Yes
ALBM_GPS	2.1524	43.9472	18.95	16.43	-0.45	0.15	4.22	-2.63	0.51	0.21	This study	Yes
ALBO_GPS	-3.0342	35.9399	17.44	17.54	-2.88	1.02	1.44	-1.24	0.09	0.09	This study	Yes
ALC1_GPS	-0.1440	41.0569	19.16	15.86	-0.5	-0.54	4.08	-3.09	0.07	0.07	This study	Yes
ALCA_GPS	-0.8608	37.7308	19.86	17.07	-0.44	0.63	3.95	-1.84	0.06	0.07	This study	Yes
ALCO_GPS	-0.4735	38.6980	19.41	16.47	-0.74	0.05	3.70	-2.47	0.07	0.06	This study	Yes
ALCX_GPS	-8.8729	38.7853	17.94	16.75	-0.68	0.14	3.96	-1.51	0.07	0.06	This study	Yes
ALGC_GPS	-5.4442	36.1111	16.09	17.30	-3.78	0.72	0.60	-1.29	0.10	0.06	This study	Yes
ALIA_GPS	-0.7032	40.6709	19.21	15.83	-0.44	-0.6	4.13	-3.09	0.07	0.07	This study	Yes
ALME_GPS	-2.4594	36.8525	18.29	15.92	-1.92	-0.58	2.44	-2.90	0.06	0.06	This study	Yes
ALMO_GPS	-4.1803	38.7055	17.95	15.89	-1.53	-0.66	3.00	-2.80	0.08	0.31	This study	Yes
ALOR_GPS	4.1402	39.9344	20.52	15.90	-0.18	-0.26	4.19	-3.23	0.06	0.06	This study	Yes
ALSA_GPS	-2.1644	42.8916	18.29	16.89	-0.53	0.41	4.22	-1.94	0.10	0.12	This study	Yes
AMAR_GPS	-7.2279	38.2087	17.48	16.96	-1.58	0.36	2.99	-1.47	0.07	0.07	This study	Yes
AMUR_GPS	-3.0036	43.0562	18.56	16.32	-0.06	-0.19	4.72	-2.45	0.12	0.10	This study	Yes
ANDU_GPS	-4.0303	38.0404	18.61	16.67	-1.06	0.13	3.43	-2.03	0.07	0.08	This study	Yes
APBI_GPS	-3.0450	43.3517	18.65	16.19	0.12	-0.32	4.92	-2.58	0.34	0.39	This study	Yes
ARAC_GPS	-6.5654	37.8939	17.58	16.92	-1.67	0.33	2.85	-1.57	0.08	0.08	This study	Yes
ARAJ_GPS	-3.6125	40.0253	17.48	16.29	-1.79	-0.24	2.82	-2.44	0.11	0.10	This study	Yes
ARAN_GPS	-3.6125	40.0253	17.48	16.29	-1.79	-0.24	2.82	-2.44	0.11	0.10	This study	Yes
ARAS_GPS	-1.1016	39.9450	19.24	15.96	-0.51	-0.48	4.03	-2.94	0.09	0.10	This study	Yes
ARIB_GPS	-1.2621	42.9351	18.60	16.12	-0.39	-0.33	4.34	-2.77	0.08	0.07	This study	Yes
ARMH_GPS	2.7660	43.2419	19.66	15.69	-0.03	-0.56	4.58	-3.39	0.10	0.10	This study	Yes
ARRA_GPS	-8.9611	38.4928	17.03	16.41	-1.65	-0.2	2.97	-1.84	0.07	0.07	This study	Yes

ARRD_GPS	-9.0794	38.9829	17.79	16.76	-0.74	0.15	3.91	-1.48	0.08	0.08	This study	Yes
ARSP_GPS	-5.0828	40.2068	18.25	16.10	-0.7	-0.46	3.95	-2.51	0.07	0.08	This study	Yes
ARUF_GPS	-0.4311	43.0995	18.92	16.15	-0.19	-0.26	4.52	-2.78	0.13	0.13	This study	Yes
ASTO_GPS	-6.0547	42.4572	17.89	16.55	-0.29	-0.03	4.53	-1.98	0.07	0.18	This study	Yes
AUCH_GPS	0.5807	43.6495	19.12	15.96	-0.05	-0.41	4.66	-3.03	0.06	0.06	This study	Yes
AUMO_GPS	3.2836	44.7218	19.47	15.94	0.04	-0.28	4.72	-3.16	0.10	0.09	This study	Yes
AURI_GPS	4.9489	43.7066	19.93	15.08	-0.08	-1.03	4.49	-4.07	0.08	0.14	This study	Yes
AVEL_GPS	0.7505	41.8816	19.07	14.80	-0.56	-1.56	4.04	-4.20	0.09	0.10	This study	Yes
AVI2_GPS	-4.6782	40.6638	18.32	15.99	-0.59	-0.57	4.08	-2.66	0.17	0.19	This study	Yes
AVIL_GPS	-4.6793	40.6511	18.19	16.58	-0.72	0.02	3.95	-2.07	0.08	0.08	This study	Yes
AVIS_GPS	-7.8895	39.0566	17.22	17.00	-1.5	0.4	3.13	-1.36	0.09	0.09	This study	Yes
AVLS_GPS	-5.9058	43.5661	17.46	17.16	-0.45	0.58	4.44	-1.38	0.09	0.08	This study	Yes
AYOR_GPS	-1.0592	39.0613	19.21	15.46	-0.75	-0.98	3.73	-3.44	0.09	0.10	This study	Yes
AZAR_GPS	-4.0232	39.8714	19.06	15.98	-0.17	-0.56	4.44	-2.72	0.13	0.11	This study	Yes
AZIL_GPS	-6.6156	31.9338	15.74	18.52	-4.85	1.92	-0.76	0.03	0.21	0.20	This study	Yes
BADA_GPS	-6.9893	38.8937	17.63	17.29	-1.3	0.69	3.31	-1.16	0.08	0.10	This study	Yes
BAHA_GPS	-9.1016	30.0527	15.82	18.18	-4.8	1.57	-0.81	-0.07	0.23	0.21	This study	Yes
BAIA_GPS	-8.0340	41.1643	17.55	16.73	-0.59	0.13	4.18	-1.62	0.08	0.07	This study	Yes
BAIO_GPS	-8.8463	42.1194	17.83	16.83	0.1	0.23	4.96	-1.43	0.10	0.07	This study	Yes
BAND_GPS	-7.9717	42.0331	18.10	16.03	0.18	-0.57	5.01	-2.32	0.41	0.64	This study	Yes
BANN_GPS	4.1563	44.3692	19.62	15.82	-0.07	-0.34	4.56	-3.31	0.04	0.04	This study	Yes
BARA_GPS	-2.7111	43.0659	18.43	16.00	-0.24	-0.5	4.53	-2.79	0.13	0.15	This study	Yes
BARC_GPS	-6.9844	42.4156	17.66	16.38	-0.35	-0.21	4.49	-2.07	0.07	0.07	This study	Yes
BARN_GPS	4.1692	44.6682	19.87	15.93	0.25	-0.23	4.89	-3.20	0.73	0.82	This study	Yes
BARY_GPS	0.6719	43.0357	19.35	16.00	0.01	-0.36	4.68	-2.99	0.06	0.06	This study	Yes
BAUB_GPS	3.9670	43.8769	19.76	15.69	-0.01	-0.48	4.60	-3.43	0.17	0.23	This study	Yes
BBFH_GPS	-4.3010	35.0814	14.34	15.51	-5.95	-1.04	-1.67	-3.17	0.38	0.40	This study	Yes
BCL1_GPS	2.1657	41.3418	20.05	15.41	0.02	-0.87	4.55	-3.65	0.09	0.08	This study	Yes
BCLN_GPS	2.0042	41.4054	19.77	15.87	-0.21	-0.42	4.32	-3.18	0.12	0.07	This study	Yes
BEAR_GPS	-8.2792	42.4723	17.60	16.85	-0.14	0.25	4.73	-1.47	0.09	0.07	This study	Yes

BEJA_GPS	-7.8729	38.0129	17.44	17.18	-1.55	0.58	3.01	-1.19	0.08	0.07	This study	Yes
BEJE_GPS	-7.8654	37.9983	18.01	16.88	-0.99	0.28	3.57	-1.49	0.10	0.07	This study	Yes
BELL_GPS	1.4011	41.5996	19.51	16.01	-0.31	-0.32	4.25	-3.02	0.10	0.09	This study	Yes
BENA_GPS	-8.1267	37.2324	16.92	16.93	-2.22	0.32	2.29	-1.41	0.07	0.07	This study	Yes
BERG_GPS	-0.0973	40.6115	20.02	15.95	0.24	-0.45	4.79	-3.00	0.15	0.12	This study	Yes
BEUD_GPS	2.6757	42.2557	19.39	15.90	-0.52	-0.35	4.04	-3.18	0.14	0.08	This study	Yes
BIAZ_GPS	-1.5369	43.4720	19.03	16.37	0.23	-0.09	5.00	-2.50	0.05	0.05	This study	Yes
BIDA_GPS	-1.7979	43.3364	19.06	16.22	0.28	-0.25	5.04	-2.63	0.08	0.10	This study	Yes
BINE_GPS	0.2959	41.8482	19.34	15.81	-0.22	-0.57	4.40	-3.16	0.07	0.07	This study	Yes
BLGU_GPS	-0.8007	42.9583	18.86	15.75	-0.21	-0.68	4.50	-3.16	0.09	0.10	This study	Yes
BMNT_GPS	0.9773	43.8774	19.36	15.97	0.17	-0.38	4.88	-3.04	0.28	0.28	This study	Yes
BMTR_GPS	-2.0327	33.9864	16.16	19.07	-4.73	2.58	-0.58	0.22	0.24	0.21	This study	Yes
BONA_GPS	3.3923	39.6137	20.38	16.13	-0.26	-0.08	4.12	-2.98	0.07	0.07	This study	Yes
BORB_GPS	-7.4625	38.8103	18.59	16.60	-0.27	0	4.33	-1.80	0.10	0.07	This study	Yes
BORR_GPS	-0.0832	39.9052	20.25	16.00	0.31	-0.4	4.81	-2.96	0.11	0.07	This study	Yes
BOSS_GPS	0.6540	44.7159	18.69	15.85	-0.22	-0.51	4.55	-3.14	0.17	0.29	This study	Yes
BRAG_GPS	-8.4289	41.5533	17.00	16.84	-0.96	0.24	3.85	-1.47	0.10	0.08	This study	Yes
BRGA_GPS	-8.4128	41.5646	16.92	16.38	-1.04	-0.22	3.77	-1.93	0.10	0.09	This study	Yes
BRGN_GPS	-6.7639	41.8074	17.95	16.84	-0.26	0.25	4.53	-1.63	0.08	0.08	This study	Yes
BRJA_GPS	-1.5261	41.8349	18.79	15.80	-0.42	-0.66	4.24	-3.07	0.07	0.07	This study	Yes
BUIT_GPS	-3.6369	41.0006	19.03	16.38	0.01	-0.15	4.68	-2.35	0.11	0.10	This study	Yes
BUNO_GPS	-8.7806	43.2730	17.36	16.38	-0.06	-0.22	4.87	-1.89	0.17	0.17	This study	Yes
BUOS_GPS	-3.0680	41.5881	18.14	15.77	-0.84	-0.74	3.85	-3.00	0.10	0.14	This study	Yes
BURG_GPS	-3.6868	42.3470	18.14	16.68	-0.53	0.15	4.23	-2.04	0.07	0.08	This study	Yes
CAAL_GPS	-2.5476	37.2211	18.42	16.01	-1.7	-0.49	2.70	-2.80	0.10	0.09	This study	Yes
CABO_GPS	-0.6984	37.6309	19.66	17.32	-0.69	0.89	3.69	-1.60	0.10	0.15	This study	Yes
CABR_GPS	-4.4242	37.4680	18.16	16.12	-1.57	-0.43	2.88	-2.55	0.14	0.10	This study	Yes
CACE_GPS	-6.3418	39.4789	18.15	16.66	-0.75	0.07	3.88	-1.85	0.05	0.05	This study	Yes
CALA_GPS	-1.2986	40.9214	19.08	15.99	-0.4	-0.46	4.20	-2.90	0.22	0.16	This study	Yes
CALH_GPS	-1.9950	42.2950	18.71	16.04	-0.3	-0.44	4.41	-2.80	0.08	0.07	This study	Yes

CAMI_GPS	-8.8377	41.8786	17.00	16.76	-0.8	0.16	4.04	-1.50	0.08	0.08	This study	Yes
CANT_GPS	-3.7981	43.4720	18.07	16.44	-0.28	-0.09	4.55	-2.27	0.07	0.06	This study	Yes
CAPA_GPS	3.5090	43.2864	19.40	16.33	-0.43	0.13	4.17	-2.78	0.20	0.23	This study	Yes
CAPT_GPS	-0.2567	44.2952	18.84	16.22	0	-0.18	4.78	-2.72	0.09	0.07	This study	Yes
CARA_GPS	-1.9677	38.0459	18.92	15.76	-1.11	-0.72	3.32	-3.09	0.07	0.06	This study	Yes
CARC_GPS	-1.4408	42.3782	18.92	15.61	-0.17	-0.85	4.52	-3.27	0.07	0.09	This study	Yes
CARG_GPS	-0.9739	37.5966	19.16	17.53	-1.15	1.09	3.23	-1.38	0.11	0.08	This study	Yes
CAS0_GPS	-2.9138	42.5438	17.95	16.38	-0.82	-0.13	3.93	-2.40	0.09	0.08	This study	Yes
CASC_GPS	-9.4185	38.6934	17.37	16.63	-1.17	0.02	3.47	-1.58	0.05	0.05	This study	Yes
CASO_GPS	-5.3424	43.1819	17.96	16.61	-0.16	0.04	4.69	-1.98	0.06	0.07	This study	Yes
CASS_GPS	2.9042	41.8829	20.05	16.02	0.01	-0.22	4.54	-3.07	0.10	0.07	This study	Yes
CATU_GPS	-5.5388	38.7304	18.00	16.68	-1.23	0.11	3.33	-1.90	0.07	0.08	This study	Yes
CATY_GPS	-1.6397	41.3528	18.94	15.72	-0.37	-0.74	4.27	-3.14	0.07	0.07	This study	Yes
CAUS_GPS	1.6150	44.1816	18.88	16.20	-0.36	-0.11	4.35	-2.83	0.06	0.06	This study	Yes
CAZA_GPS	-5.7598	37.9379	18.08	16.92	-1.31	0.34	3.21	-1.64	0.07	0.13	This study	Yes
CAZE_GPS	1.0861	43.2069	18.58	16.47	-0.8	0.13	3.87	-2.54	0.15	0.14	This study	Yes
CBRA_GPS	-7.5122	39.8190	17.70	16.92	-0.9	0.32	3.78	-1.48	0.07	0.08	This study	Yes
CBRN_GPS	-5.4105	43.4167	17.72	16.69	-0.32	0.12	4.54	-1.89	0.12	0.11	This study	Yes
CCEX_GPS	-6.3779	39.4723	17.66	15.78	-1.23	-0.81	3.40	-2.72	0.10	0.16	This study	Yes
CDJ2_GPS	-0.5299	44.7288	18.66	16.16	-0.01	-0.26	4.80	-2.77	0.12	0.17	This study	Yes
CDRD_GPS	-6.5381	40.5900	17.80	16.41	-0.78	-0.18	3.93	-2.08	0.08	0.08	This study	Yes
CEBR_GPS	-4.3678	40.4534	18.18	16.41	-0.84	-0.14	3.81	-2.26	0.09	0.10	This study	Yes
CEPI_GPS	2.2488	43.1025	19.47	15.75	-0.16	-0.53	4.47	-3.31	0.21	0.25	This study	Yes
CERC_GPS	-8.7132	37.7898	17.01	16.95	-1.89	0.34	2.67	-1.33	0.12	0.06	This study	Yes
CERV_GPS	-1.9432	42.0074	18.77	15.91	-0.32	-0.56	4.37	-2.93	0.08	0.13	This study	Yes
CEU1_GPS	-5.3064	35.8920	15.28	16.91	-4.66	0.34	-0.30	-1.69	0.07	0.07	This study	Yes
CEUT_GPS	-5.3113	35.8961	15.08	17.01	-4.86	0.44	-0.50	-1.59	0.15	0.16	This study	Yes
CHAV_GPS	-7.4727	41.7518	17.39	17.50	-0.7	0.9	4.10	-0.90	0.09	0.09	This study	Yes
CHER_GPS	-1.5501	43.3216	18.71	16.53	-0.12	0.07	4.63	-2.34	0.29	0.22	This study	Yes
CHRN_GPS	4.8618	43.8814	19.92	15.66	-0.03	-0.45	4.55	-3.49	0.03	0.04	This study	Yes

CIEZ_GPS	-1.3809	38.2332	19.20	16.89	-0.89	0.43	3.54	-1.99	0.07	0.07	This study	Yes
CLTR_GPS	-3.7564	38.8203	18.80	16.60	-0.73	0.07	3.80	-2.12	0.18	0.21	This study	Yes
CNAR_GPS	-6.5413	43.1658	17.59	16.62	-0.3	0.03	4.57	-1.87	0.08	0.07	This study	Yes
COBA_GPS	-4.7211	37.9156	18.12	16.06	-1.45	-0.5	3.04	-2.59	0.10	0.11	This study	Yes
COIM_GPS	-8.4180	40.2059	18.01	17.98	-0.32	1.38	4.40	-0.33	0.12	0.20	This study	Yes
CORC_GPS	-9.1904	42.9447	17.50	16.59	0.07	-0.01	4.99	-1.64	0.08	0.07	This study	Yes
CORI_GPS	-6.5196	39.9816	17.88	16.79	-0.86	0.2	3.81	-1.70	0.08	0.10	This study	Yes
CORU_GPS	-8.4028	43.3665	17.04	16.99	-0.43	0.39	4.50	-1.32	0.07	0.07	This study	Yes
CORZ_GPS	-0.2398	43.1824	18.95	16.36	-0.17	-0.04	4.53	-2.58	0.10	0.12	This study	Yes
COVI_GPS	-7.5092	40.2749	17.89	17.02	-0.59	0.42	4.12	-1.38	0.10	0.16	This study	Yes
CRAI_GPS	-9.1333	39.3942	17.19	16.32	-1.22	-0.29	3.46	-1.92	0.07	0.06	This study	Yes
CRAL_GPS	0.3672	43.1284	19.04	16.03	-0.22	-0.35	4.47	-2.95	0.06	0.07	This study	Yes
CRDB_GPS	-4.7878	37.8774	18.27	16.29	-1.3	-0.27	3.19	-2.35	0.06	0.06	This study	Yes
CRNA_GPS	-1.2215	41.3363	19.25	15.69	-0.14	-0.76	4.48	-3.20	0.07	0.07	This study	Yes
CRNH_GPS	-9.1354	39.4070	17.58	16.68	-0.83	0.07	3.86	-1.56	0.09	0.10	This study	Yes
CRT1_GPS	-0.9793	37.6066	19.47	17.89	-0.83	1.45	3.55	-1.02	0.08	0.12	This study	Yes
CRTG_GPS	-0.9954	37.6062	18.90	17.11	-1.4	0.67	2.98	-1.80	0.16	0.15	This study	Yes
CRVC_GPS	-1.8686	38.1146	18.93	15.98	-1.1	-0.5	3.33	-2.87	0.08	0.13	This study	Yes
CSOS_GPS	0.4856	42.5119	18.50	16.24	-0.93	-0.13	3.72	-2.74	0.10	0.07	This study	Yes
CSTN_GPS	1.5001	43.5278	19.12	16.39	-0.26	0.07	4.42	-2.64	0.07	0.09	This study	Yes
CUBX_GPS	-0.5664	44.8689	18.74	15.84	0.11	-0.58	4.93	-3.08	0.04	0.04	This study	Yes
CUE1_GPS	-2.1397	40.0728	18.60	15.72	-0.93	-0.76	3.64	-3.11	0.08	0.14	This study	Yes
CURA_GPS	2.8551	44.1997	19.42	15.86	-0.06	-0.38	4.61	-3.22	0.25	0.26	This study	Yes
DEBD_GPS	-3.0553	33.9187	16.42	18.24	-4.32	1.72	-0.15	-0.54	0.24	0.22	This study	Yes
DENI_GPS	0.1037	38.8348	20.23	16.19	0.01	-0.2	4.44	-2.78	0.12	0.08	This study	Yes
EBRE_GPS	0.4924	40.8209	19.63	15.93	-0.21	-0.44	4.34	-3.06	0.05	0.05	This study	Yes
EDVD_GPS	-8.4843	40.9127	16.67	16.06	-1.46	-0.54	3.31	-2.24	0.11	0.10	This study	Yes
EIVI_GPS	1.4069	38.9512	20.02	16.23	-0.41	-0.1	3.99	-2.80	0.08	0.10	This study	Yes
EJEA_GPS	-1.1299	42.1259	18.84	16.00	-0.38	-0.44	4.30	-2.89	0.07	0.06	This study	Yes
EJID_GPS	-2.8036	36.7527	17.89	15.32	-2.29	-1.19	2.08	-3.47	0.14	0.14	This study	Yes

ELCI_GPS	-2.6182	42.5149	18.63	16.04	-0.2	-0.46	4.54	-2.76	0.06	0.07	This study	Yes
ELGE_GPS	-2.4864	43.1371	18.73	16.37	0.03	-0.12	4.81	-2.44	0.09	0.06	This study	Yes
ELHA_GPS	-5.3647	33.6668	15.91	17.76	-4.51	1.18	-0.32	-0.84	0.28	0.21	This study	Yes
ELVA_GPS	-7.1594	38.8794	18.37	16.90	-0.53	0.3	4.08	-1.53	0.12	0.10	This study	Yes
EMAZ_GPS	-3.4114	43.2425	18.30	15.93	-0.19	-0.59	4.62	-2.81	0.11	0.12	This study	Yes
ENTR_GPS	-8.4739	39.4712	17.95	16.80	-0.56	0.19	4.11	-1.50	0.11	0.11	This study	Yes
EPSH_GPS	-0.4482	42.1191	19.13	15.75	-0.22	-0.66	4.43	-3.18	0.09	0.08	This study	Yes
ERFD_GPS	-4.1868	31.5487	16.42	19.24	-4.62	2.69	-0.60	0.54	0.24	0.23	This study	Yes
ESC1_GPS	-4.1269	40.5783	18.48	16.41	-0.55	-0.13	4.10	-2.28	0.08	0.09	This study	Yes
ESCO_GPS	0.9757	42.6936	19.20	16.12	-0.28	-0.23	4.36	-2.89	0.05	0.05	This study	Yes
ESTE_GPS	-2.0244	42.6515	18.56	15.84	-0.35	-0.64	4.38	-3.00	0.07	0.07	This study	Yes
EVOR_GPS	-7.9044	38.5681	17.67	17.24	-1.18	0.64	3.42	-1.12	0.07	0.14	This study	Yes
FAJ1_GPS	-7.9217	40.1491	17.74	17.45	-0.69	0.85	4.01	-0.91	0.07	0.07	This study	Yes
FAJA_GPS	-7.9217	40.1491	17.74	17.45	-0.69	0.85	4.01	-0.91	0.07	0.07	This study	Yes
FAJP_GPS	2.0258	43.2074	19.27	16.04	-0.29	-0.25	4.35	-3.01	0.11	0.10	This study	Yes
FARO_GPS	-7.9375	37.0164	17.06	16.69	-2.17	0.08	2.33	-1.67	0.06	0.06	This study	Yes
FCOA_GPS	-7.1442	41.0819	17.65	16.87	-0.68	0.28	4.07	-1.56	0.07	0.07	This study	Yes
FENO_GPS	2.0296	43.1572	19.51	16.33	-0.06	0.04	4.57	-2.72	0.24	0.28	This study	Yes
FERY_GPS	-1.2488	44.6460	18.44	15.92	-0.11	-0.53	4.72	-2.96	0.14	0.33	This study	Yes
FILF_GPS	2.4171	42.5603	19.63	16.11	-0.16	-0.16	4.43	-2.96	0.14	0.10	This study	Yes
FJCP_GPS	2.7949	43.0482	19.08	15.96	-0.67	-0.29	3.94	-3.12	0.07	0.07	This study	Yes
FLRC_GPS	3.5945	44.3253	19.25	15.62	-0.34	-0.58	4.31	-3.49	0.07	0.07	This study	Yes
FONS_GPS	-7.0669	43.1293	17.60	16.49	-0.2	-0.1	4.69	-1.95	0.07	0.07	This study	Yes
FORM_GPS	1.4288	38.7053	20.10	16.24	-0.39	-0.09	4.00	-2.79	0.07	0.07	This study	Yes
FRAG_GPS	0.3242	41.5095	19.23	16.11	-0.41	-0.27	4.18	-2.87	0.08	0.07	This study	Yes
FSTH_GPS	-3.8632	35.1750	16.30	18.00	-4.04	1.46	0.23	-0.72	0.13	0.13	This study	Yes
FUDE_GPS	-4.8057	43.1536	17.96	16.16	-0.28	-0.4	4.56	-2.47	0.10	0.11	This study	Yes
FVFI_GPS	-8.3205	38.7205	17.79	17.61	-0.94	1	3.68	-0.71	0.10	0.10	This study	Yes
GAIA_GPS	-8.5891	41.1060	17.29	16.78	-0.76	0.18	4.02	-1.51	0.06	0.08	This study	Yes
GAJN_GPS	4.2097	43.9018	19.74	15.69	-0.08	-0.47	4.53	-3.44	0.26	0.24	This study	Yes

GARD_GPS	0.3109	44.8376	18.79	16.05	-0.02	-0.33	4.77	-2.92	0.19	0.10	This study	Yes
GARR_GPS	1.9140	41.2929	19.75	15.96	-0.24	-0.34	4.29	-3.09	0.06	0.06	This study	Yes
GERN_GPS	-2.6787	43.3174	18.41	16.04	-0.2	-0.46	4.59	-2.75	0.08	0.07	This study	Yes
GIBR_GPS	-5.3650	36.1482	14.03	18.27	-5.84	1.7	-1.46	-0.33	0.31	0.31	This study	Yes
GIRO_GPS	2.8551	42.0416	19.63	15.70	-0.36	-0.54	4.18	-3.39	0.10	0.08	This study	Yes
GLRA_GPS	4.5241	44.8393	19.63	15.71	-0.02	-0.42	4.62	-3.43	0.09	0.08	This study	Yes
GRA1_GPS	-3.5964	37.1899	18.45	15.95	-1.49	-0.58	2.92	-2.78	0.11	0.07	This study	Yes
GRAU_GPS	0.3407	42.1915	19.07	15.97	-0.41	-0.41	4.22	-3.01	0.08	0.06	This study	Yes
GRIB_GPS	-8.6417	39.0405	17.58	17.05	-1.01	0.44	3.64	-1.24	0.08	0.07	This study	Yes
GROV_GPS	-8.8645	42.4980	17.01	17.83	-0.61	1.23	4.27	-0.43	0.07	0.06	This study	Yes
GRSL_GPS	-6.8771	43.2256	17.75	16.34	-0.06	-0.25	4.83	-2.11	0.08	0.09	This study	Yes
GUA0_GPS	-3.1675	40.6338	18.61	16.30	-0.59	-0.22	4.04	-2.46	0.12	0.10	This study	Yes
GUAR_GPS	-7.2664	40.5365	17.60	16.86	-0.86	0.26	3.87	-1.56	0.07	0.07	This study	Yes
GUDI_GPS	-7.1250	42.0591	17.66	16.88	-0.42	0.29	4.40	-1.55	0.08	0.10	This study	Yes
GUIJ_GPS	-5.6778	40.5467	18.02	16.72	-0.73	0.14	3.96	-1.84	0.07	0.06	This study	Yes
HEBR_GPS	-5.1312	33.3327	15.98	17.91	-4.55	1.34	-0.38	-0.71	0.21	0.23	This study	Yes
HENA_GPS	-3.3840	40.4886	18.40	16.04	-0.79	-0.48	3.84	-2.71	0.07	0.08	This study	Yes
HERR_GPS	-5.0500	39.1814	18.15	16.51	-1.06	-0.06	3.52	-2.11	0.07	0.07	This study	Yes
HOLA_GPS	3.2216	43.9698	19.41	15.84	-0.2	-0.38	4.45	-3.26	0.14	0.13	This study	Yes
HUE1_GPS	-6.8337	37.1320	16.77	17.16	-2.62	0.56	1.86	-1.31	0.12	0.10	This study	Yes
HUEL_GPS	-6.9203	37.2000	17.35	17.13	-2.01	0.53	2.48	-1.33	0.07	0.06	This study	Yes
HULV_GPS	-6.9135	37.2803	17.55	16.91	-1.79	0.31	2.70	-1.55	0.06	0.06	This study	Yes
HUOV_GPS	-1.9421	37.4016	19.41	16.75	-0.77	0.27	3.62	-2.10	0.06	0.07	This study	Yes
IBIZ_GPS	1.4490	38.9113	20.20	15.84	-0.24	-0.49	4.15	-3.19	0.09	0.06	This study	Yes
ICOL_GPS	0.6847	39.8985	19.50	15.70	-0.59	-0.66	3.90	-3.30	0.10	0.11	This study	Yes
IEJA_GPS	-0.4060	40.5257	19.48	16.11	-0.26	-0.3	4.29	-2.83	0.09	0.08	This study	Yes
IFR1_GPS	-5.1255	33.5139	16.41	17.02	-4.08	0.45	0.10	-1.60	0.08	0.08	This study	Yes
IFRN_GPS	-5.1085	33.5396	16.24	17.04	-4.25	0.47	-0.07	-1.58	0.09	0.10	This study	Yes
IGEL_GPS	-2.0411	43.3064	18.71	16.59	-0.03	0.11	4.74	-2.25	0.06	0.11	This study	Yes
IGP0_GPS	-9.1585	38.7260	16.83	16.43	-1.75	-0.18	2.89	-1.80	0.13	0.09	This study	Yes

ILLE_GPS	-3.8322	40.1251	18.37	16.53	-0.83	-0.01	3.79	-2.18	0.20	0.13	This study	Yes
IMZR_GPS	-9.5212	30.5956	16.01	17.54	-4.43	0.93	-0.40	-0.66	0.18	0.17	This study	Yes
ISGN_GPS	-4.5483	34.9322	15.75	15.00	-4.53	-1.56	-0.26	-3.66	0.92	0.99	This study	Yes
ISPS_GPS	-2.5536	43.3544	18.57	17.16	-0.06	0.67	4.73	-1.64	0.09	0.10	This study	Yes
JACA_GPS	-0.7265	42.5673	18.58	15.88	-0.6	-0.55	4.08	-3.04	0.07	0.07	This study	Yes
JERE_GPS	-6.7794	38.3201	17.57	16.56	-1.54	-0.03	3.02	-1.91	0.08	0.09	This study	Yes
JORD_GPS	2.9982	39.3149	20.48	15.97	-0.15	-0.27	4.22	-3.13	0.07	0.07	This study	Yes
JUM1_GPS	-1.3256	38.5021	19.44	16.14	-0.6	-0.31	3.85	-2.75	0.06	0.07	This study	Yes
JUMI_GPS	-1.3272	38.4712	19.31	15.84	-0.74	-0.61	3.71	-3.05	0.06	0.12	This study	Yes
KBGA_GPS	-6.8905	32.8340	16.15	18.49	-4.21	1.89	-0.05	0.03	0.21	0.21	This study	Yes
KTMA_GPS	-4.8021	34.9867	13.43	16.70	-6.8	0.14	-2.51	-1.94	0.54	0.58	This study	Yes
LACA_GPS	2.7276	43.6810	19.49	15.89	-0.09	-0.36	4.55	-3.19	0.06	0.14	This study	Yes
LACO_GPS	1.1297	43.2513	18.88	16.14	-0.49	-0.2	4.18	-2.87	0.11	0.12	This study	Yes
LAGO_GPS	-8.6684	37.0989	17.02	17.04	-2.06	0.43	2.45	-1.25	0.07	0.05	This study	Yes
LANT_GPS	-2.9809	42.7154	18.44	16.24	-0.27	-0.27	4.49	-2.53	0.07	0.08	This study	Yes
LAOU_GPS	-5.1553	35.3950	14.19	16.42	-5.89	-0.15	-1.57	-2.19	0.21	0.22	This study	Yes
LARE_GPS	-3.4466	43.4046	18.01	16.05	-0.43	-0.47	4.39	-2.69	0.11	0.07	This study	Yes
LAVA_GPS	0.2999	44.1757	19.63	16.13	0.65	-0.25	5.40	-2.84	0.27	0.38	This study	Yes
LAZK_GPS	-2.1869	43.0346	18.67	16.25	-0.11	-0.23	4.65	-2.58	0.06	0.07	This study	Yes
LBRD_GPS	-0.5278	44.6814	18.67	16.09	-0.01	-0.33	4.79	-2.84	0.05	0.05	This study	Yes
LBUG_GPS	0.9211	44.9454	19.10	16.08	0.19	-0.27	4.97	-2.92	0.06	0.07	This study	Yes
LCAU_GPS	-1.0755	44.9782	18.49	16.35	0	-0.09	4.83	-2.54	0.06	0.04	This study	Yes
LEBR_GPS	-6.0819	36.9224	17.31	17.04	-2.26	0.45	2.19	-1.49	0.10	0.07	This study	Yes
LEIR_GPS	-8.7948	39.7315	17.38	16.74	-1	0.13	3.69	-1.53	0.07	0.07	This study	Yes
LEIT_GPS	-1.9142	43.0820	18.28	16.37	-0.54	-0.1	4.21	-2.47	0.07	0.07	This study	Yes
LEIX_GPS	-8.8053	39.7273	17.02	16.75	-1.36	0.14	3.33	-1.52	0.13	0.07	This study	Yes
LEMZ_GPS	-2.9024	43.4138	18.73	16.67	0.19	0.16	4.99	-2.11	0.16	0.16	This study	Yes
LENA_GPS	-5.8248	43.1496	17.41	16.90	-0.63	0.32	4.23	-1.65	0.09	0.08	This study	Yes
LEON_GPS	-5.6510	42.5884	17.59	16.32	-0.63	-0.25	4.19	-2.24	0.07	0.08	This study	Yes
LESA_GPS	4.6841	43.5607	19.77	15.67	-0.22	-0.45	4.35	-3.47	0.30	0.28	This study	Yes

LGAR_GPS	0.3789	44.2974	18.27	16.34	-0.69	-0.04	4.06	-2.64	0.05	0.05	This study	Yes
LLEI_GPS	0.5963	41.6293	19.49	15.95	-0.17	-0.42	4.42	-3.04	0.07	0.07	This study	Yes
LLER_GPS	-6.0107	38.2368	17.82	16.56	-1.45	-0.02	3.09	-1.98	0.07	0.07	This study	Yes
LLIV_GPS	1.9731	42.4781	19.57	15.86	-0.15	-0.43	4.44	-3.19	0.11	0.08	This study	Yes
LOSA_GPS	-2.1952	42.5679	18.40	16.28	-0.5	-0.2	4.23	-2.55	0.08	0.08	This study	Yes
LOZO_GPS	-3.6268	40.9335	18.21	15.66	-0.83	-0.87	3.84	-3.07	0.11	0.10	This study	Yes
LUAR_GPS	-6.5281	43.5473	17.37	16.73	-0.42	0.14	4.48	-1.76	0.08	0.09	This study	Yes
LUGO_GPS	-7.5447	42.9931	17.36	16.67	-0.38	0.07	4.51	-1.72	0.07	0.07	This study	Yes
LUVI_GPS	4.0959	43.6924	19.76	15.68	-0.08	-0.48	4.51	-3.45	0.09	0.11	This study	Yes
MAD2_GPS	-4.2496	40.4292	18.32	15.99	-0.73	-0.56	3.92	-2.69	0.05	0.05	This study	Yes
MADR_GPS	-4.2496	40.4292	18.32	15.99	-0.73	-0.56	3.92	-2.69	0.05	0.05	This study	Yes
MAFR_GPS	-9.3261	38.9345	16.85	16.02	-1.65	-0.59	3.01	-2.20	0.10	0.16	This study	Yes
MALA_GPS	-4.3935	36.7261	16.89	15.01	-3.02	-1.54	1.38	-3.66	0.15	0.21	This study	Yes
MALL_GPS	2.6246	39.5526	19.84	16.04	-0.67	-0.22	3.73	-3.04	0.05	0.05	This study	Yes
MAR1_GPS	-8.0181	31.6652	15.90	18.52	-4.54	1.91	-0.44	0.16	0.20	0.19	This study	Yes
MARE_GPS	2.4343	41.5285	19.78	15.93	-0.25	-0.34	4.27	-3.14	0.09	0.07	This study	Yes
MATA_GPS	2.4289	41.5399	19.71	15.68	-0.32	-0.59	4.21	-3.39	0.14	0.14	This study	Yes
MAZA_GPS	-1.3105	37.5935	19.22	17.81	-1.03	1.36	3.36	-1.08	0.07	0.08	This study	Yes
MBLD_GPS	-4.6336	32.7694	16.11	19.18	-4.62	2.62	-0.50	0.52	0.24	0.23	This study	Yes
MDAR_GPS	-3.5322	34.9701	16.74	19.60	-3.7	3.07	0.55	0.86	0.22	0.23	This study	Yes
MDNR_GPS	-5.0487	41.8888	18.09	16.83	-0.43	0.27	4.33	-1.79	0.10	0.10	This study	Yes
MDPM_GPS	-3.4836	42.9413	18.42	16.52	-0.13	0	4.65	-2.22	0.06	0.08	This study	Yes
MELI_GPS	-2.9516	35.2812	17.02	18.47	-3.45	1.96	0.81	-0.31	0.08	0.08	This study	Yes
MELR_GPS	-8.1304	39.6949	17.55	16.90	-0.97	0.3	3.72	-1.44	0.07	0.06	This study	Yes
MENC_GPS	3.8312	40.0006	20.62	15.90	-0.01	-0.29	4.37	-3.22	0.08	0.07	This study	Yes
MEQU_GPS	0.3036	41.3786	19.24	15.90	-0.43	-0.48	4.15	-3.07	0.07	0.07	This study	Yes
MER2_GPS	-3.6301	40.3894	17.83	15.91	-1.34	-0.62	3.29	-2.82	0.12	0.09	This study	Yes
MERI_GPS	-6.3485	38.9163	17.86	17.20	-1.18	0.61	3.41	-1.31	0.07	0.11	This study	Yes
MERT_GPS	-7.6600	37.6465	17.50	17.19	-1.62	0.59	2.91	-1.20	0.07	0.07	This study	Yes
MESS_GPS	-8.2447	37.8346	17.26	17.06	-1.71	0.45	2.85	-1.27	0.07	0.07	This study	Yes

MIBR_GPS	-2.9384	42.6804	18.66	16.36	-0.07	-0.15	4.69	-2.42	0.14	0.08	This study	Yes
MIMZ_GPS	-1.2283	44.2006	18.80	16.34	0.13	-0.11	4.93	-2.55	0.05	0.05	This study	Yes
MIRA_GPS	-7.1862	41.5168	17.71	16.72	-0.5	0.13	4.28	-1.71	0.07	0.07	This study	Yes
MLGA_GPS	-4.4354	36.7156	16.63	15.56	-3.27	-0.99	1.13	-3.11	0.06	0.07	This study	Yes
MNTP_GPS	3.8691	43.6462	19.56	15.70	-0.25	-0.48	4.35	-3.42	0.11	0.14	This study	Yes
MOFR_GPS	-5.4624	37.1207	17.24	16.61	-2.39	0.04	2.06	-1.98	0.10	0.08	This study	Yes
MOGA_GPS	-6.7135	41.3426	17.65	16.85	-0.7	0.26	4.06	-1.62	0.08	0.07	This study	Yes
MOLH_GPS	2.3409	43.7203	19.29	16.05	-0.2	-0.22	4.45	-3.02	0.10	0.11	This study	Yes
MORA_GPS	-1.9988	38.2475	19.05	16.06	-0.93	-0.42	3.52	-2.78	0.12	0.10	This study	Yes
MOST_GPS	-3.8630	40.3241	18.32	15.33	-0.83	-1.21	3.80	-3.38	0.19	0.22	This study	Yes
MOTA_GPS	-2.8700	39.5032	18.09	15.91	-1.44	-0.6	3.11	-2.87	0.08	0.08	This study	Yes
MOTR_GPS	-3.5205	36.7548	16.94	14.83	-3.11	-1.7	1.27	-3.91	0.07	0.06	This study	Yes
MSGT_GPS	1.6294	42.8796	19.18	15.98	-0.38	-0.33	4.25	-3.06	0.07	0.05	This study	Yes
MSLA_GPS	-4.1844	34.4317	16.18	16.91	-4.27	0.36	-0.04	-1.78	0.22	0.22	This study	Yes
MTDM_GPS	-0.4849	43.8828	18.71	16.26	-0.19	-0.15	4.57	-2.67	0.06	0.06	This study	Yes
MTLS_GPS	1.5507	44.1625	18.92	16.01	-0.31	-0.31	4.40	-3.02	0.32	0.61	This study	Yes
MTP2_GPS	3.8641	43.6388	19.77	15.75	-0.04	-0.43	4.56	-3.37	0.10	0.09	This study	Yes
MTPL_GPS	3.8648	43.6374	19.85	15.72	0.04	-0.46	4.64	-3.40	0.05	0.05	This study	Yes
MULA_GPS	-1.4488	38.0411	18.98	16.09	-1.14	-0.37	3.28	-2.79	0.07	0.08	This study	Yes
MUNI_GPS	-0.8074	41.0303	18.94	15.94	-0.6	-0.49	3.99	-2.97	0.07	0.07	This study	Yes
MUR1_GPS	-1.1225	37.9902	19.59	16.65	-0.6	0.2	3.81	-2.25	0.06	0.06	This study	Yes
MURC_GPS	-1.1247	37.9922	19.65	16.90	-0.54	0.45	3.87	-2.00	0.06	0.07	This study	Yes
MVEL_GPS	-8.6791	40.1811	17.27	16.81	-1.02	0.21	3.71	-1.47	0.14	0.26	This study	Yes
MYRG_GPS	-5.2635	42.1684	18.27	16.66	-0.14	0.09	4.64	-1.94	0.08	0.06	This study	Yes
NARB_GPS	2.9726	43.1983	19.73	15.85	-0.01	-0.39	4.59	-3.24	0.07	0.07	This study	Yes
NAVA_GPS	-5.5451	39.8949	17.65	16.64	-1.29	0.07	3.35	-1.94	0.08	0.08	This study	Yes
NIME_GPS	4.3569	43.8286	19.62	15.81	-0.24	-0.34	4.35	-3.32	0.10	0.12	This study	Yes
ODEM_GPS	-8.6313	37.5987	17.37	17.04	-1.59	0.43	2.95	-1.25	0.10	0.10	This study	Yes
OLM1_GPS	-4.6839	41.2856	18.34	16.27	-0.41	-0.29	4.30	-2.38	0.12	0.11	This study	Yes
OLME_GPS	-4.6839	41.2856	18.04	16.62	-0.71	0.06	4.00	-2.03	0.07	0.07	This study	Yes

ONOR_GPS	-6.8214	40.6071	18.09	16.62	-0.43	0.03	4.29	-1.84	0.10	0.10	This study	Yes
ORIN_GPS	-0.6744	43.2309	18.92	16.27	-0.11	-0.15	4.62	-2.65	0.13	0.14	This study	Yes
ORON_GPS	-1.6087	43.1393	18.73	16.30	-0.14	-0.16	4.61	-2.56	0.06	0.08	This study	Yes
ORUS_GPS	-3.2211	40.2876	19.01	16.11	-0.26	-0.41	4.35	-2.65	0.17	0.13	This study	Yes
OSCA_GPS	-0.4138	42.1395	18.92	15.75	-0.43	-0.66	4.22	-3.19	0.12	0.12	This study	Yes
OSUN_GPS	-5.0952	37.2323	17.60	16.22	-2.07	-0.35	2.38	-2.40	0.14	0.10	This study	Yes
OUCA_GPS	-7.8665	31.2066	15.67	17.53	-4.89	0.92	-0.83	-0.84	0.11	0.11	This study	Yes
OUZS_GPS	-5.5392	34.8504	15.05	18.38	-5.09	1.8	-0.80	-0.20	0.30	0.31	This study	Yes
PACO_GPS	-9.2949	38.6943	17.31	16.27	-1.25	-0.34	3.38	-1.95	0.16	0.14	This study	Yes
PAIA_GPS	-8.4515	39.5373	17.20	16.93	-1.3	0.33	3.38	-1.38	0.22	0.15	This study	Yes
PALA_GPS	-7.8707	42.8734	17.36	16.75	-0.35	0.15	4.54	-1.61	0.07	0.07	This study	Yes
PALC_GPS	-2.9324	37.7023	17.79	15.79	-2.15	-0.72	2.28	-2.99	0.07	0.07	This study	Yes
PALE_GPS	-4.5575	42.0078	18.42	16.73	-0.17	0.18	4.59	-1.93	0.06	0.07	This study	Yes
PALI_GPS	4.8105	43.3760	19.73	15.98	-0.33	-0.14	4.23	-3.17	0.04	0.06	This study	Yes
PALM_GPS	-8.9034	38.5715	17.49	16.78	-1.18	0.17	3.44	-1.48	0.11	0.12	This study	Yes
PAMP_GPS	-1.6362	42.8060	18.45	16.25	-0.5	-0.21	4.23	-2.61	0.10	0.09	This study	Yes
PANE_GPS	-4.5833	43.3250	18.01	16.69	-0.22	0.14	4.61	-1.96	0.07	0.07	This study	Yes
PARC_GPS	-9.2949	38.6943	17.31	16.27	-1.25	-0.34	3.38	-1.95	0.16	0.14	This study	Yes
PARD_GPS	2.8235	43.4314	19.54	15.95	-0.12	-0.29	4.51	-3.13	0.06	0.07	This study	Yes
PAS2_GPS	-1.9315	43.3218	18.60	16.29	-0.16	-0.18	4.61	-2.55	0.07	0.06	This study	Yes
PASA_GPS	-1.9315	43.3218	18.60	16.29	-0.16	-0.18	4.61	-2.55	0.07	0.06	This study	Yes
PAYR_GPS	2.3398	43.5514	19.34	16.49	-0.2	0.22	4.45	-2.58	0.15	0.41	This study	Yes
PCO1_GPS	-8.5600	41.9122	17.27	16.69	-0.57	0.09	4.27	-1.60	0.13	0.11	This study	Yes
PCOU_GPS	-8.5600	41.9122	16.25	16.74	-1.59	0.14	3.25	-1.55	0.13	0.11	This study	Yes
PDBC_GPS	-5.2001	40.8998	18.62	15.81	-0.13	-0.76	4.57	-2.79	0.15	0.17	This study	Yes
PEN1_GPS	-7.1755	40.1701	17.68	16.98	-0.89	0.38	3.81	-1.45	0.07	0.07	This study	Yes
PENA_GPS	-4.1196	41.5922	18.87	16.27	0.09	-0.27	4.81	-2.42	0.09	0.07	This study	Yes
PERP_GPS	2.8821	42.6892	19.98	15.80	0.13	-0.44	4.71	-3.29	0.09	0.06	This study	Yes
PEYR_GPS	0.2157	43.6313	18.64	16.27	-0.46	-0.11	4.26	-2.70	0.15	0.13	This study	Yes
PLAN_GPS	1.9870	41.4185	19.65	15.80	-0.33	-0.49	4.21	-3.25	0.08	0.09	This study	Yes

PNAV_GPS	-3.9899	40.7855	18.15	15.95	-0.86	-0.59	3.81	-2.75	0.19	0.14	This study	Yes
PORT_GPS	-7.4329	39.2910	17.74	16.81	-1.01	0.21	3.63	-1.60	0.07	0.07	This study	Yes
POZO_GPS	-4.8493	38.3835	18.14	16.25	-1.3	-0.31	3.22	-2.39	0.09	0.08	This study	Yes
PRAC_GPS	1.1879	44.5094	18.59	15.58	-0.48	-0.75	4.26	-3.43	0.20	0.23	This study	Yes
PSBR_GPS	-6.6369	42.0512	18.18	16.94	0.01	0.35	4.81	-1.54	0.07	0.07	This study	Yes
PUEC_GPS	3.3144	43.6934	20.00	15.86	0.31	-0.35	4.93	-3.24	0.21	0.12	This study	Yes
PUYO_GPS	-0.9135	43.5270	18.69	16.23	-0.21	-0.2	4.53	-2.68	0.13	0.15	This study	Yes
PVAR_GPS	-8.7382	41.3905	17.34	16.75	-0.61	0.15	4.20	-1.52	0.06	0.07	This study	Yes
PZNA_GPS	3.4133	43.4477	19.56	15.90	-0.21	-0.31	4.40	-3.21	0.06	0.06	This study	Yes
QINT_GPS	-3.0337	41.9853	18.76	15.84	-0.13	-0.67	4.59	-2.93	0.06	0.06	This study	Yes
QNTO_GPS	-0.4969	41.4256	19.07	15.82	-0.44	-0.6	4.17	-3.11	0.07	0.07	This study	Yes
RABT_GPS	-6.8543	33.9981	15.76	17.63	-4.35	1.03	-0.10	-0.84	0.05	0.05	This study	Yes
REUS_GPS	1.1685	41.1700	19.48	16.17	-0.4	-0.17	4.14	-2.85	0.06	0.07	This study	Yes
RIAN_GPS	-5.0061	42.9758	17.94	16.81	-0.3	0.25	4.52	-1.81	0.08	0.07	This study	Yes
RIAZ_GPS	-3.4808	41.2756	18.34	16.14	-0.64	-0.38	4.04	-2.60	0.11	0.12	This study	Yes
RIBA_GPS	-7.0357	43.5366	18.00	16.14	0.31	-0.45	5.22	-2.30	0.07	0.08	This study	Yes
RIBE_GPS	-5.0670	43.4645	18.54	16.83	0.44	0.27	5.30	-1.78	0.08	0.07	This study	Yes
RICH_GPS	-4.5348	32.2552	16.91	18.47	-3.94	1.91	0.14	-0.20	0.23	0.22	This study	Yes
RIO1_GPS	-2.4261	42.4643	18.51	16.01	-0.37	-0.48	4.36	-2.80	0.07	0.07	This study	Yes
RIOS_GPS	-5.0487	41.8887	17.97	16.88	-0.55	0.32	4.21	-1.74	0.09	0.08	This study	Yes
RNAN_GPS	-4.4117	43.2961	17.93	16.70	-0.34	0.15	4.49	-1.97	0.06	0.06	This study	Yes
ROAG_GPS	-6.2063	36.4634	16.05	16.49	-3.61	-0.1	0.81	-2.03	0.10	0.09	This study	Yes
ROAP_GPS	-6.2063	36.4643	15.98	16.71	-3.68	0.12	0.74	-1.81	0.10	0.08	This study	Yes
RODI_GPS	-7.5903	42.2988	17.57	16.97	-0.35	0.37	4.49	-1.42	0.11	0.10	This study	Yes
RON1_GPS	-5.1475	36.7222	16.76	16.28	-3.02	-0.29	1.40	-2.33	0.10	0.11	This study	Yes
RONC_GPS	-0.9547	42.8100	18.87	16.12	-0.21	-0.32	4.50	-2.78	0.10	0.10	This study	Yes
ROND_GPS	-5.1435	36.7541	16.41	16.86	-3.36	0.29	1.06	-1.75	0.08	0.08	This study	Yes
S0RI_GPS	-2.4705	41.7622	18.88	15.75	-0.17	-0.74	4.52	-3.06	0.01	0.01	This study	Yes
SABI_GPS	-0.3621	42.5153	19.01	15.84	-0.26	-0.57	4.42	-3.10	0.07	0.07	This study	Yes
SAFQ_GPS	2.8625	43.9592	19.04	15.75	-0.5	-0.49	4.15	-3.34	0.22	0.34	This study	Yes

SAGR_GPS	-8.9596	37.0220	16.96	17.17	-2.09	0.56	2.42	-1.09	0.07	0.06	This study	Yes
SALA_GPS	-5.4959	40.9451	18.05	16.45	-0.63	-0.12	4.08	-2.13	0.07	0.06	This study	Yes
SALI_GPS	-0.7785	37.8349	19.70	16.74	-0.59	0.31	3.80	-2.18	0.10	0.07	This study	Yes
SALS_GPS	-6.2561	43.4060	17.88	16.91	0	0.33	4.88	-1.60	0.08	0.09	This study	Yes
SALX_GPS	-8.6195	33.1624	15.02	19.06	-5	2.45	-0.78	0.76	0.23	0.24	This study	Yes
SANA_GPS	-1.9392	42.3397	19.14	16.11	0.13	-0.36	4.84	-2.73	0.09	0.07	This study	Yes
SANG_GPS	-1.2869	42.5795	18.88	16.03	-0.19	-0.42	4.51	-2.85	0.10	0.09	This study	Yes
SANM_GPS	-4.3763	40.3583	18.55	16.37	-0.49	-0.18	4.15	-2.30	0.06	0.06	This study	Yes
SARR_GPS	-0.8120	40.1404	19.05	15.80	-0.71	-0.63	3.83	-3.12	0.07	0.07	This study	Yes
SAUV_GPS	4.4669	44.2554	19.63	15.67	-0.15	-0.47	4.46	-3.47	0.03	0.04	This study	Yes
SBAR_GPS	2.1743	41.9801	19.52	15.78	-0.36	-0.5	4.20	-3.28	0.09	0.13	This study	Yes
SCAC_GPS	-8.6926	38.0188	16.82	16.94	-2.02	0.33	2.55	-1.34	0.09	0.08	This study	Yes
SCDA_GPS	3.2675	44.7945	19.32	15.79	-0.09	-0.43	4.59	-3.31	0.04	0.05	This study	Yes
SCOA_GPS	-1.6817	43.3952	18.50	16.19	-0.29	-0.27	4.48	-2.67	0.07	0.10	This study	Yes
SENE_GPS	2.4121	44.7025	19.45	16.30	0.18	0.03	4.89	-2.77	0.63	0.43	This study	Yes
SETE_GPS	3.6991	43.3976	19.79	15.81	-0.05	-0.38	4.55	-3.30	0.05	0.06	This study	Yes
SEVI_GPS	-5.9715	37.3457	17.71	17.18	-1.78	0.6	2.70	-1.36	0.13	0.12	This study	Yes
SFER_GPS	-6.2056	36.4644	15.95	16.56	-3.71	-0.03	0.71	-1.96	0.06	0.05	This study	Yes
SGIL_GPS	4.4337	43.6770	19.44	15.84	-0.47	-0.3	4.11	-3.30	0.06	0.06	This study	Yes
SGVA_GPS	-4.1203	40.9493	18.47	16.29	-0.47	-0.25	4.21	-2.40	0.09	0.06	This study	Yes
SINE_GPS	3.0154	39.6459	20.39	16.02	-0.17	-0.22	4.22	-3.08	0.09	0.10	This study	Yes
SIRO_GPS	-5.7919	43.4116	17.70	16.70	-0.27	0.13	4.60	-1.85	0.09	0.09	This study	Yes
SLVT_GPS	3.2683	43.9198	19.42	15.87	-0.21	-0.35	4.43	-3.23	0.08	0.05	This study	Yes
SMAM_GPS	-7.3596	39.3133	17.88	16.88	-0.88	0.28	3.77	-1.53	0.07	0.06	This study	Yes
SMAN_GPS	-7.7520	38.4592	17.65	16.80	-1.25	0.2	3.34	-1.58	0.10	0.09	This study	Yes
SMAR_GPS	-8.2937	39.4228	17.64	16.36	-0.92	-0.24	3.75	-1.96	0.08	0.09	This study	Yes
SMDV_GPS	-4.3763	40.3583	18.55	16.37	-0.49	-0.18	4.15	-2.30	0.06	0.06	This study	Yes
SNT1_GPS	-8.5517	42.8854	17.44	17.07	-0.13	0.47	4.77	-1.22	0.08	0.11	This study	Yes
SNTG_GPS	-8.5888	42.8753	17.16	16.74	-0.41	0.14	4.49	-1.55	0.07	0.07	This study	Yes
SOBE_GPS	-7.5868	42.4626	17.33	17.01	-0.55	0.41	4.31	-1.38	0.07	0.07	This study	Yes

SONA_GPS	1.5168	41.9922	19.56	15.87	-0.19	-0.45	4.39	-3.16	0.11	0.06	This study	Yes
SONS_GPS	-3.9640	39.6754	18.43	16.03	-0.86	-0.51	3.73	-2.67	0.05	0.05	This study	Yes
SOPU_GPS	-3.1542	43.2769	18.34	16.47	-0.19	-0.04	4.61	-2.29	0.08	0.07	This study	Yes
SOR1_GPS	1.1328	42.3745	19.23	16.04	-0.36	-0.3	4.26	-2.97	0.07	0.10	This study	Yes
SOUR_GPS	2.4350	42.7275	19.90	15.49	0.15	-0.78	4.74	-3.58	0.17	0.40	This study	Yes
SOUS_GPS	2.0271	44.8746	18.81	15.99	-0.34	-0.3	4.40	-3.06	0.05	0.07	This study	Yes
SPAB_GPS	-4.3517	39.5459	18.48	16.31	-0.77	-0.24	3.82	-2.36	0.11	0.10	This study	Yes
SRNA_GPS	-0.1627	41.7932	19.33	15.78	-0.15	-0.62	4.47	-3.17	0.07	0.07	This study	Yes
SROM_GPS	-2.4572	42.2340	18.85	17.02	-0.08	0.53	4.63	-1.79	0.07	0.41	This study	Yes
STBX_GPS	4.1969	44.2594	19.53	15.91	-0.2	-0.25	4.43	-3.22	0.05	0.09	This study	Yes
STEM_GPS	-8.6854	39.2407	19.17	16.94	0.64	0.33	5.30	-1.34	0.32	0.32	This study	Yes
STGR_GPS	4.5738	44.1853	20.03	15.73	0.21	-0.4	4.82	-3.41	0.09	0.19	This study	Yes
STMR_GPS	4.4216	43.4491	19.53	15.77	-0.43	-0.37	4.14	-3.37	0.05	0.06	This study	Yes
STSX_GPS	-0.5671	43.7763	19.26	15.86	0.35	-0.56	5.10	-3.07	0.28	0.18	This study	Yes
STVD_GPS	-6.0143	42.0740	18.21	16.11	-0.08	-0.47	4.72	-2.42	0.09	0.09	This study	Yes
T3RR_GPS	2.0230	41.5628	19.43	15.50	-0.52	-0.79	4.02	-3.55	0.13	0.12	This study	Yes
TABU_GPS	-7.5676	41.1162	17.47	16.84	-0.78	0.24	3.99	-1.55	0.07	0.07	This study	Yes
TAFA_GPS	-1.6767	42.5209	18.62	15.99	-0.39	-0.47	4.32	-2.87	0.07	0.07	This study	Yes
TALR_GPS	-5.2354	39.0351	18.14	16.69	-1.07	0.12	3.51	-1.91	0.08	0.08	This study	Yes
TALV_GPS	-4.9429	39.9473	18.02	16.58	-1.02	0.02	3.61	-2.05	0.21	0.17	This study	Yes
TARI_GPS	-5.6026	36.0085	15.31	17.45	-4.56	0.87	-0.18	-1.13	0.18	0.15	This study	Yes
TARR_GPS	1.1661	41.6574	18.79	15.52	-0.98	-0.82	3.60	-3.50	0.12	0.10	This study	Yes
TAVI_GPS	-7.6409	37.1323	16.92	17.15	-2.33	0.55	2.16	-1.24	0.07	0.07	This study	Yes
TERU_GPS	-1.1243	40.3505	19.32	15.70	-0.33	-0.74	4.23	-3.20	0.07	0.07	This study	Yes
TETN_GPS	-5.3630	35.5617	14.87	16.83	-5.14	0.26	-0.80	-1.77	0.08	0.06	This study	Yes
TLIA_GPS	1.4806	43.5614	19.21	16.05	-0.16	-0.27	4.52	-2.98	0.05	0.05	This study	Yes
TLMF_GPS	1.3751	43.5746	19.15	16.13	-0.19	-0.2	4.49	-2.89	0.06	0.05	This study	Yes
TLSE_GPS	1.4809	43.5607	19.46	15.86	0.09	-0.46	4.77	-3.17	0.03	0.04	This study	Yes
TLSG_GPS	1.4850	43.5497	19.17	16.10	-0.2	-0.22	4.48	-2.93	0.08	0.10	This study	Yes
TLVR_GPS	-6.7841	38.8662	17.71	16.87	-1.26	0.28	3.34	-1.60	0.14	0.12	This study	Yes

TMAD_GPS	-6.7695	41.7967	17.77	16.15	-0.45	-0.44	4.35	-2.32	0.12	0.11	This study	Yes
TNDR_GPS	-2.0030	33.0313	16.70	18.16	-4.39	1.67	-0.30	-0.69	0.23	0.22	This study	Yes
TNIN_GPS	-5.9584	35.3508	15.87	17.93	-4.09	1.34	0.25	-0.62	0.17	0.19	This study	Yes
TORO_GPS	-5.3910	41.5225	17.89	16.43	-0.66	-0.14	4.08	-2.16	0.07	0.06	This study	Yes
TORR_GPS	-0.6809	37.9753	19.38	16.76	-0.89	0.33	3.50	-2.17	0.07	0.06	This study	Yes
TOUL_GPS	1.4808	43.5608	19.15	16.09	-0.22	-0.23	4.46	-2.94	0.18	0.22	This study	Yes
TRAM_GPS	2.8916	39.8184	20.26	15.95	-0.24	-0.29	4.16	-3.14	0.07	0.06	This study	Yes
TRLV_GPS	-4.0556	43.3556	18.48	16.71	0.15	0.17	4.98	-1.98	0.08	0.08	This study	Yes
TRNH_GPS	-0.7514	44.2138	17.63	15.91	-1.13	-0.52	3.65	-3.00	0.28	0.24	This study	Yes
TRRA_GPS	-8.2192	38.2909	17.44	17.12	-1.42	0.51	3.17	-1.21	0.10	0.10	This study	Yes
TRUJ_GPS	-5.8556	39.4798	17.23	16.93	-1.76	0.35	2.86	-1.62	0.09	0.09	This study	Yes
TRVG_GPS	-4.0504	43.3375	18.15	16.73	-0.19	0.19	4.64	-1.96	0.16	0.14	This study	Yes
TUDE_GPS	-1.6034	42.0486	18.82	15.78	-0.32	-0.68	4.36	-3.09	0.06	0.08	This study	Yes
UCA1_GPS	-6.2119	36.5317	16.57	16.63	-3.07	0.04	1.35	-1.89	0.08	0.08	This study	Yes
UJAE_GPS	-3.7817	37.7878	18.51	16.63	-1.26	0.09	3.20	-2.09	0.08	0.14	This study	Yes
UNME_GPS	-0.3256	43.3216	18.96	16.31	-0.11	-0.1	4.61	-2.63	0.05	0.07	This study	Yes
UPNA_GPS	-1.6356	42.8009	18.63	16.26	-0.32	-0.2	4.41	-2.60	0.10	0.09	This study	Yes
UTIE_GPS	-1.2086	39.5687	19.15	15.91	-0.67	-0.54	3.85	-2.98	0.07	0.06	This study	Yes
VALA_GPS	-4.7083	41.7025	18.13	16.58	-0.51	0.02	4.23	-2.06	0.06	0.06	This study	Yes
VALC_GPS	-7.2483	39.4076	17.60	16.57	-1.15	-0.03	3.49	-1.85	0.07	0.12	This study	Yes
VALE_GPS	-0.3376	39.4808	19.26	15.98	-0.73	-0.43	3.75	-2.96	0.10	0.07	This study	Yes
VBLO_GPS	-6.3251	42.9394	18.34	16.14	0.35	-0.44	5.20	-2.37	0.08	0.07	This study	Yes
VCIA_GPS	-0.3439	39.4357	19.41	16.07	-0.59	-0.34	3.89	-2.87	0.07	0.06	This study	Yes
VCRD_GPS	-3.8497	43.2459	18.37	15.76	-0.03	-0.77	4.78	-2.95	0.33	0.21	This study	Yes
VDGO_GPS	-4.0105	42.5160	17.95	16.79	-0.61	0.25	4.16	-1.91	0.07	0.11	This study	Yes
VEG1_GPS	-7.0490	43.4666	17.57	16.68	-0.14	0.09	4.77	-1.76	0.13	0.11	This study	Yes
VEGA_GPS	-7.0488	43.4665	17.22	16.64	-0.49	0.05	4.42	-1.80	0.11	0.11	This study	Yes
VERI_GPS	-7.4606	41.9298	17.67	16.64	-0.38	0.04	4.44	-1.76	0.07	0.06	This study	Yes
VIAR_GPS	-3.0125	38.1676	18.30	15.75	-1.52	-0.76	2.95	-3.03	0.06	0.06	This study	Yes
VICA_GPS	-3.0829	38.1176	18.11	15.78	-1.71	-0.74	2.76	-2.99	0.10	0.08	This study	Yes

VIGO_GPS	-8.8131	42.1840	17.16	16.68	-0.56	0.08	4.30	-1.59	0.05	0.05	This study	Yes
VILA_GPS	-7.6827	43.2992	17.45	16.71	-0.18	0.11	4.73	-1.67	0.07	0.07	This study	Yes
VILH_GPS	-2.8414	38.7512	18.18	14.90	-1.53	-1.61	2.97	-3.89	0.22	0.19	This study	Yes
VILL_GPS	-3.9520	40.4436	18.43	16.10	-0.67	-0.44	3.97	-2.60	0.06	0.11	This study	Yes
VISE_GPS	-7.9063	40.6533	17.24	17.12	-1.06	0.52	3.68	-1.24	0.09	0.07	This study	Yes
VISN_GPS	4.9492	44.3199	19.70	15.66	-0.16	-0.45	4.44	-3.49	0.04	0.06	This study	Yes
VISX_GPS	-7.9260	40.6450	17.52	16.69	-0.78	0.09	3.96	-1.67	0.08	0.06	This study	Yes
VITO_GPS	-2.6726	42.8401	18.42	17.21	-0.32	0.71	4.44	-1.58	0.16	0.11	This study	Yes
VJOI_GPS	-0.1984	38.5300	20.15	15.58	-0.09	-0.83	4.33	-3.37	0.11	0.13	This study	Yes
VNAN_GPS	-5.6294	42.3167	18.00	16.78	-0.3	0.21	4.50	-1.79	0.12	0.14	This study	Yes
VNOV_GPS	-8.4570	38.6786	17.84	16.90	-0.88	0.29	3.74	-1.41	0.06	0.06	This study	Yes
VROB_GPS	0.1559	40.8726	19.35	16.10	-0.41	-0.29	4.15	-2.87	0.07	0.08	This study	Yes
VRSA_GPS	-7.4139	37.1918	17.02	16.77	-2.26	0.17	2.24	-1.64	0.09	0.10	This study	Yes
VTGD_GPS	-6.4333	41.0088	18.12	16.57	-0.37	-0.02	4.37	-1.93	0.10	0.08	This study	Yes
VTRO_GPS	-2.8467	42.1747	18.21	15.55	-0.66	-0.95	4.06	-3.23	0.14	0.13	This study	Yes
XIXO_GPS	-5.7019	43.5701	18.08	16.63	0.13	0.06	5.01	-1.93	0.12	0.10	This study	Yes
YEB1_GPS	-3.0902	40.5238	18.52	16.16	-0.72	-0.35	3.90	-2.61	0.08	0.08	This study	Yes
YEBE_GPS	-3.0886	40.5249	18.57	16.04	-0.67	-0.47	3.95	-2.73	0.05	0.05	This study	Yes
ZAGO_GPS	-5.5313	34.1580	14.99	17.14	-5.3	0.56	-1.06	-1.44	0.18	0.19	This study	Yes
ZAR1_GPS	-5.8983	30.4154	15.87	19.20	-5.14	2.61	-1.18	0.64	0.22	0.21	This study	Yes
ZARA_GPS	-0.8822	41.6334	18.81	15.84	-0.57	-0.59	4.06	-3.07	0.05	0.05	This study	Yes
ZFRA_GPS	-6.4100	38.4260	17.84	16.48	-1.31	-0.11	3.25	-2.02	0.07	0.07	This study	Yes
ZGZA_GPS	-0.8762	41.6523	19.05	15.87	-0.33	-0.56	4.30	-3.04	0.08	0.09	This study	Yes
ZMRA_GPS	-5.7392	41.5068	17.19	16.30	-1.3	-0.28	3.45	-2.26	0.11	0.08	This study	Yes
ZUER_GPS	-0.7904	41.8664	19.13	16.14	-0.21	-0.29	4.43	-2.77	0.07	0.07	This study	Yes
ABKD_GPS	2.3098	36.5347	19.74	17.14	-1.35	0.86	2.86	-1.93	0.12	0.11	Bougrine et al. (2019)	Yes
ABSD_GPS	4.1986	35.4346	18.38	18.05	-3.24	1.88	0.85	-1.09	0.15	0.11	Bougrine et al. (2019)	Yes
ABZH_GPS	3.0333	36.7961	20.33	16.98	-0.83	0.74	3.38	-2.12	0.08	0.1	Bougrine et al. (2019)	Yes

ADCK_GPS	3.448	34.9115	17.35	18.09	-4.24	1.88	-0.17	-1.03	0.12	0.12	Bougrine et al. (2019)	Yes
ADJF_GPS	3.0982	34.215	17.13	19.05	-4.53	2.81	-0.5	-0.05	0.12	0.14	Bougrine et al. (2019)	Yes
AFDJ_GPS	2.5758	35.4014	17.5	18.11	-3.86	1.84	0.27	-0.97	0.13	0.12	Bougrine et al. (2019)	Yes
AFRS_GPS	4.451	34.7238	17.68	18.27	-4.11	2.12	-0.08	-0.88	0.13	0.12	Bougrine et al. (2019)	Yes
AKDR_GPS	3.4143	36.6508	19.83	18.7	-1.42	2.49	2.77	-0.41	0.17	0.4	Bougrine et al. (2019)	Yes
AKET_GPS	3.8908	36.0539	20.7	18.71	-0.75	2.53	3.39	-0.42	0.87	0.4	Bougrine et al. (2019)	Yes
ATKJ_GPS	4.1243	36.4427	19.34	17.7	-2.07	1.53	2.08	-1.44	0.21	0.24	Bougrine et al. (2019)	Yes
CAEK_GPS	4.8734	35.5645	17.6	17.8	-4.1	1.68	-0.03	-1.36	0.23	0.3	Bougrine et al. (2019)	Yes
CTCH_GPS	4.6514	36.4299	20.08	18.75	-1.42	2.62	2.71	-0.4	0.3	0.25	Bougrine et al. (2019)	Yes
EADB_GPS	1.5613	34.8582	17.88	18.57	-3.42	2.25	0.71	-0.47	0.12	0.1	Bougrine et al. (2019)	Yes
EASA_GPS	1.5438	34.1522	17.9	18.19	-3.53	1.86	0.55	-0.85	0.17	0.16	Bougrine et al. (2019)	Yes
EBGR_GPS	1.9357	35.5624	16.51	16.87	-4.71	0.57	-0.55	-2.19	0.22	0.27	Bougrine et al. (2019)	Yes
EECH_GPS	1.3451	36.1601	17.54	17.87	-3.47	1.54	0.75	-1.16	0.11	0.14	Bougrine et al. (2019)	Yes
EMHD_GPS	2.9505	36.2091	17.94	17.36	-3.32	1.12	0.85	-1.74	0.16	0.11	Bougrine et al. (2019)	Yes
ESKN_GPS	0.8274	34.5512	18.28	17.93	-2.96	1.57	1.16	-1.08	0.25	0.2	Bougrine et al. (2019)	Yes
ETJN_GPS	2.1164	33.5002	16.93	18.03	-4.71	1.74	-0.7	-1.04	0.29	0.41	Bougrine et al. (2019)	Yes
EZEA_GPS	2.3057	34.8667	17.39	18.42	-4.03	2.14	0.08	-0.65	0.17	0.2	Bougrine et al. (2019)	Yes
OAIN_GPS	0.1714	36.0109	18.63	17.66	-2.21	1.27	2.03	-1.31	0.24	0.21	Bougrine et al. (2019)	Yes
OAIR_GPS	0.7353	33.406	17.36	18.22	-4.08	1.85	-0.04	-0.79	0.18	0.13	Bougrine et al. (2019)	Yes
OASF_GPS	-0.6066	32.7843	17.26	17.55	-4.09	1.12	-0.06	-1.38	0.34	0.25	Bougrine et al. (2019)	Yes

OBBL_GPS	-1.5042	34.7076	17.85	19.11	-2.98	2.64	1.21	0.23	0.34	0.49	Bougrine et al. (2019)	Yes
OBHM_GPS	-0.4792	34.4185	16.96	18.25	-4.09	1.83	0.05	-0.69	0.25	0.21	Bougrine et al. (2019)	Yes
ODJA_GPS	-0.1592	35.3442	17.97	18.33	-2.95	1.92	1.25	-0.63	0.18	0.14	Bougrine et al. (2019)	Yes
OKHE_GPS	0.0585	34.1464	17.58	17.21	-3.61	0.81	0.5	-1.76	0.23	0.27	Bougrine et al. (2019)	Yes
OKHM_GPS	0.2965	33.869	16.99	17.57	-4.3	1.18	-0.21	-1.41	0.24	0.28	Bougrine et al. (2019)	Yes
OLHC_GPS	-1.5119	35.2488	17.23	18.42	-3.49	1.96	0.74	-0.46	0.17	0.14	Bougrine et al. (2019)	Yes
ORAN_GPS	-0.5778	35.7074	18.27	17.41	-2.51	0.98	1.73	-1.52	0.09	0.09	Bougrine et al. (2019)	Yes
OTSS_GPS	-0.7939	35.2817	14.99	17.56	-5.84	1.12	-1.62	-1.36	0.77	0.21	Bougrine et al. (2019)	Yes
ALFE_GPS	-8.0612	37.1588	17.09	17.14	-2.08	0.53	2.42	-1.21	0.19	0.13	Cabral et al. (2017)	Yes
ALPO_GPS	-8.3852	37.1044	16.87	17.24	-2.26	0.63	2.25	-1.08	0.22	0.15	Cabral et al. (2017)	Yes
ATAL_GPS	-8.7188	37.087	17.09	17.18	-1.98	0.57	2.53	-1.1	0.29	0.18	Cabral et al. (2017)	Yes
BARR_GPS	-8.1626	37.1243	17.4	17.3	-1.76	0.69	2.74	-1.04	0.19	0.15	Cabral et al. (2017)	Yes
CATA_GPS	-8.7484	37.1268	15.9	17.54	-3.16	0.93	1.36	-0.74	0.3	0.2	Cabral et al. (2017)	Yes
CERR_GPS	-8.9376	37.0476	17.41	16.7	-1.64	0.09	2.88	-1.56	0.28	0.17	Cabral et al. (2017)	Yes
CHLB_GPS	-8.8	37.236	16.7	15.87	-2.32	-0.74	2.2	-2.4	0.2	0.15	Cabral et al. (2017)	Yes
CTEL_GPS	-8.5545	37.2066	16.9	17.04	-2.17	0.43	2.34	-1.26	0.28	0.17	Cabral et al. (2017)	Yes
DELG_GPS	-8.5681	37.1252	17.26	16.12	-1.83	-0.49	2.68	-2.18	0.21	0.14	Cabral et al. (2017)	Yes
ESPA_GPS	-8.8469	37.3399	16.81	17.15	-2.18	0.54	2.35	-1.12	0.3	0.24	Cabral et al. (2017)	Yes
FOIA_GPS	-8.5962	37.3158	16.96	16.64	-2.08	0.03	2.45	-1.65	0.16	0.09	Cabral et al. (2017)	Yes
FONT_GPS	-8.4976	37.1575	16.98	16.87	-2.11	0.26	2.4	-1.43	0.26	0.16	Cabral et al. (2017)	Yes

GUIN_GPS	-8.2473	37.1786	17.23	17.26	-1.9	0.65	2.61	-1.07	0.19	0.14	Cabral et al. (2017)	Yes
MALH_GPS	-8.8548	37.2349	17.7	16.13	-1.31	-0.48	3.21	-2.14	0.24	0.15	Cabral et al. (2017)	Yes
MOSQ_GPS	-8.2296	37.1167	16.72	17.59	-2.43	0.98	2.07	-0.74	0.2	0.16	Cabral et al. (2017)	Yes
MTLD_GPS	-8.6289	37.1835	15.85	16.27	-3.22	-0.34	1.3	-2.02	0.2	0.14	Cabral et al. (2017)	Yes
MTQM_GPS	-8.8669	37.1578	16.02	16.72	-3.01	0.11	1.51	-1.55	0.29	0.18	Cabral et al. (2017)	Yes
PEFU_GPS	-8.7398	37.3675	16.71	16.78	-2.29	0.17	2.24	-1.5	0.19	0.13	Cabral et al. (2017)	Yes
PELA_GPS	-7.9617	37.3071	17.67	16.64	-1.48	0.04	3.03	-1.72	0.23	0.18	Cabral et al. (2017)	Yes
PTAT_GPS	-8.9315	37.0023	16.88	16.79	-2.18	0.18	2.33	-1.47	0.28	0.18	Cabral et al. (2017)	Yes
STEO_GPS	-8.7283	37.5476	16.6	16.73	-2.36	0.12	2.19	-1.55	0.14	0.07	Cabral et al. (2017)	Yes
ZIMB_GPS	-8.3068	37.2401	16.81	16.73	-2.3	0.12	2.22	-1.59	0.21	0.14	Cabral et al. (2017)	Yes
CARB_GPS	-1.88	37.01	19.18	17.38	-1.1	0.9	3.26	-1.47	0.2	0.2	Echeverria et al. (2013)	Yes
CUCO_GPS	-2.09	37.18	19.11	17	-1.09	0.52	3.28	-1.84	0.2	0.2	Echeverria et al. (2013)	Yes
ESPU_GPS	-1.5900	37.8700	19.19	16.30	-0.95	-0.17	3.46	-2.57	0.20	0.20	Echeverria et al. (2013)	Yes
GANU_GPS	-1.4200	37.6600	19.96	17.28	-0.25	0.82	4.14	-1.60	0.20	0.20	Echeverria et al. (2013)	Yes
HUEB_GPS	-2.23	37	18.11	16.6	-2.11	0.11	2.26	-2.23	0.3	0.3	Echeverria et al. (2013)	Yes
HUER_GPS	-1.94	37.35	19.01	17.2	-1.18	0.72	3.2	-1.65	0.3	0.3	Echeverria et al. (2013)	Yes
MAJA_GPS	-1.1800	37.6200	19.42	17.26	-0.84	0.81	3.54	-1.64	0.20	0.20	Echeverria et al. (2013)	Yes
MELL_GPS	-1.8300	37.5900	19.19	16.20	-0.97	-0.27	3.43	-2.66	0.20	0.20	Echeverria et al. (2013)	Yes
MOJA_GPS	-1.8600	37.1300	18.67	17.58	-1.58	1.1	2.78	-1.27	0.30	0.30	Echeverria et al. (2013)	Yes
MONT_GPS	-1.5200	37.4400	19.58	17.68	-0.66	1.22	3.72	-1.20	0.20	0.20	Echeverria et al. (2013)	Yes

PANI_GPS	-1.7000	37.3300	19.56	16.78	-0.68	0.31	3.70	-2.08	0.30	0.30	Echeverria et al. (2013)	Yes
PUAS_GPS	-2.09	37.4	18.67	16.71	-1.48	0.23	2.91	-2.13	0.2	0.3	Echeverria et al. (2013)	Yes
PURI_GPS	-1.6400	37.5400	19.14	17.69	-1.06	1.22	3.33	-1.18	0.20	0.20	Echeverria et al. (2013)	Yes
RELL_GPS	-2.06	36.84	18.98	17.28	-1.3	0.8	3.05	-1.56	0.2	0.2	Echeverria et al. (2013)	Yes
TERC_GPS	-1.6400	37.7400	19.10	16.00	-1.06	-0.47	3.35	-2.87	0.20	0.20	Echeverria et al. (2013)	Yes
GATA_GPS	-2.061	36.835	18.99	17.43	-1.29	0.95	3.06	-1.41	0.2	0.2	Echeverria et al. (2015)	Yes
AREZ_GPS	-1.9405	37.8354	18.63	16.2	-1.45	-0.28	2.97	-2.65	0.21	0.2	Garate et al. (2015) UB solution	Yes
ASIN_GPS	-0.0987	42.5166	19.01	16.13	-0.31	-0.27	4.36	-2.82	0.18	0.19	Garate et al. (2015) UB solution	Yes
BENI_GPS	-6.3186	32.3768	15.85	16.79	-4.7	0.2	-0.58	-1.73	0.19	0.26	Garate et al. (2015) UB solution	Yes
CABU_GPS	-6.47	43.569	17.77	16.28	-0.02	-0.3	4.87	-2.21	0.19	0.27	Garate et al. (2015) UB solution	Yes
CAST_GPS	-6.5321	38.1227	17.5	16.95	-1.7	0.36	2.84	-1.54	0.21	0.21	Garate et al. (2015) UB solution	Yes
CIER_GPS	-6.2807	41.9411	18.05	17	-0.22	0.42	4.57	-1.51	0.2	0.24	Garate et al. (2015) UB solution	Yes
EPCU_GPS	-2.1465	40.0795	18.05	16.03	-1.47	-0.45	3.1	-2.8	0.4	0.38	Garate et al. (2015) UB solution	Yes
ERRA_GPS	-4.4561	31.9388	16.42	17.73	-4.5	1.17	-0.45	-0.94	0.19	0.19	Garate et al. (2015) UB solution	Yes
FUEN_GPS	-0.8854	42.3602	19.18	15.97	-0.02	-0.46	4.65	-2.94	0.18	0.19	Garate et al. (2015) UB solution	Yes
LIJA_GPS	-5.4038	36.9062	16.97	15.21	-2.72	-1.36	1.71	-3.38	0.35	0.36	Garate et al. (2015) UB solution	Yes

LNDA_GPS	-2.5783	42.96	18.46	16.63	-0.26	0.13	4.5	-2.17	0.18	0.21	Garate et al. (2015) UB solution	Yes
LOBE_GPS	-5.1104	40.2204	18.42	16.09	-0.52	-0.48	4.13	-2.52	0.27	0.27	Garate et al. (2015) UB solution	Yes
LOJA_GPS	-4.1064	37.1073	16.92	15.7	-2.95	-0.85	1.47	-3	0.2	0.37	Garate et al. (2015) UB solution	Yes
MAIL_GPS	-6.2237	40.5692	17.56	16.38	-1.08	-0.2	3.62	-2.14	0.19	0.19	Garate et al. (2015) UB solution	Yes
NEVA_GPS	-3.3856	37.0626	18.3	15.72	-1.71	-0.81	2.69	-3.03	0.2	0.2	Garate et al. (2015) UB solution	Yes
PALM_GPS	-3.5623	36.809	17.11	14.75	-2.92	-1.78	1.46	-3.99	0.19	0.19	Garate et al. (2015) UB solution	Yes
PILA_GPS	-1.2894	38.2543	18.94	17.25	-1.16	0.8	3.27	-1.64	0.19	0.18	Garate et al. (2015) UB solution	Yes
REIN_GPS	-4.1771	43.0459	17.98	16.77	-0.41	0.23	4.4	-1.91	0.19	0.2	Garate et al. (2015) UB solution	Yes
RUBI_GPS	-4.1966	38.6093	18.45	16.06	-1.05	-0.49	3.47	-2.63	0.2	0.2	Garate et al. (2015) UB solution	Yes
TAZA_GPS	-3.9964	34.2295	16.22	18.52	-4.3	1.97	-0.09	-0.19	0.27	0.22	Garate et al. (2015) UB solution	Yes
TGIL_GPS	-3.3026	38.0342	18.61	15.9	-1.19	-0.62	3.28	-2.85	0.2	0.2	Garate et al. (2015) UB solution	Yes
TIOU_GPS	-7.2452	30.9236	15.49	17.57	-5.22	0.96	-1.2	-0.86	0.37	0.34	Garate et al. (2015) UB solution	Yes
TRIA_GPS	-7.2414	42.7148	17.29	17.09	-0.59	0.5	4.28	-1.33	0.17	0.19	Garate et al. (2015) UB solution	Yes
UCMT_GPS	-0.4722	40.3638	20.34	15.9	0.57	-0.52	5.12	-3.03	0.37	0.29	Garate et al. (2015) UB solution	Yes
0002_GPS	2.1	42.23	19.73	15.64	-0.08	-0.65	4.5	-3.42	0.32	0.32	Rigo et al. (2015)	Yes

0003_GPS	2.17	42.34	19.47	15.88	-0.32	-0.4	4.26	-3.18	0.29	0.29	Rigo et al. (2015)	Yes
0004_GPS	2.32	42.32	19.38	15.78	-0.45	-0.5	4.13	-3.29	0.32	0.32	Rigo et al. (2015)	Yes
0005_GPS	2.26	42.23	19.6	15.92	-0.24	-0.36	4.34	-3.14	0.31	0.31	Rigo et al. (2015)	Yes
0007_GPS	2.52	42.17	20.04	15.83	0.14	-0.43	4.7	-3.24	0.31	0.31	Rigo et al. (2015)	Yes
0008_GPS	2.53	42.26	19.99	15.65	0.11	-0.61	4.67	-3.42	0.31	0.31	Rigo et al. (2015)	Yes
0009_GPS	2.33	41.99	19.89	15.68	-0.02	-0.59	4.54	-3.39	0.31	0.31	Rigo et al. (2015)	Yes
0010_GPS	2.59	42.08	20.14	15.97	0.2	-0.29	4.76	-3.11	0.31	0.31	Rigo et al. (2015)	Yes
0011_GPS	2.8	42.19	20.2	15.64	0.25	-0.61	4.8	-3.44	0.31	0.31	Rigo et al. (2015)	Yes
0013_GPS	2.82	42.4	19.88	16.07	-0.02	-0.18	4.54	-3.02	0.33	0.32	Rigo et al. (2015)	Yes
0014_GPS	2.27	42.12	20.04	15.77	0.17	-0.51	4.74	-3.29	0.31	0.31	Rigo et al. (2015)	Yes
0102_GPS	2.29	42.54	19.82	16.07	0.05	-0.21	4.64	-2.99	0.3	0.3	Rigo et al. (2015)	Yes
0103_GPS	2.5	42.38	19.34	16.22	-0.51	-0.04	4.07	-2.85	0.29	0.29	Rigo et al. (2015)	Yes
0105_GPS	2.52	42.8	19.67	15.57	-0.08	-0.69	4.52	-3.5	0.32	0.32	Rigo et al. (2015)	Yes
0107_GPS	2.58	42.64	19.73	15.63	-0.07	-0.63	4.52	-3.45	0.31	0.31	Rigo et al. (2015)	Yes
0108_GPS	2.64	42.48	19.81	16.41	-0.04	0.15	4.54	-2.67	0.33	0.34	Rigo et al. (2015)	Yes
0109_GPS	2.68	42.73	19.15	16.07	-0.65	-0.18	3.94	-3.01	0.3	0.31	Rigo et al. (2015)	Yes
0110_GPS	2.76	42.88	19.72	15.75	-0.06	-0.5	4.54	-3.33	0.32	0.32	Rigo et al. (2015)	Yes
0111_GPS	2.72	42.62	19.3	15.73	-0.53	-0.52	4.05	-3.35	0.32	0.32	Rigo et al. (2015)	Yes
0112_GPS	2.87	42.51	19.81	16.35	-0.08	0.11	4.49	-2.74	0.3	0.31	Rigo et al. (2015)	Yes
ARD0_GPS	-2.1	42.25	18.16	16.77	-0.84	0.29	3.87	-2.06	0.32	0.32	Rigo et al. (2015)	Yes

ARG0_GPS	-0.53	43.54	18.86	16.05	-0.12	-0.37	4.62	-2.88	0.32	0.32	Rigo et al. (2015)	Yes
ASCO_GPS	1.86	42.72	18.84	15.57	-0.8	-0.73	3.81	-3.48	0.32	0.32	Rigo et al. (2015)	Yes
ASPI_GPS	0.33	42.94	19.03	15.82	-0.26	-0.56	4.41	-3.15	0.3	0.3	Rigo et al. (2015)	Yes
ATC0_GPS	-1.19	43.33	18.61	16.61	-0.29	0.17	4.46	-2.28	0.31	0.32	Rigo et al. (2015)	Yes
AYER_GPS	-0.72	42.29	19.3	16.16	0.05	-0.27	4.72	-2.76	0.35	0.35	Rigo et al. (2015)	Yes
AYG0_GPS	-2.05	42.66	19.15	15.98	0.25	-0.5	4.98	-2.86	0.32	0.32	Rigo et al. (2015)	Yes
BEL0_GPS	-1.62	43.05	18.6	16.78	-0.29	0.32	4.45	-2.08	0.31	0.32	Rigo et al. (2015)	Yes
BEN0_GPS	0.47	42.11	19.1	15.93	-0.43	-0.44	4.2	-3.05	0.3	0.3	Rigo et al. (2015)	Yes
BGRN_GPS	0.13	43.06	18.48	15.85	-0.75	-0.54	3.94	-3.11	0.33	0.34	Rigo et al. (2015)	Yes
BGS0_GPS	0.1	42.91	18.82	15.93	-0.44	-0.46	4.24	-3.03	0.33	0.32	Rigo et al. (2015)	Yes
BOHO_GPS	-1.01	43.1	18.88	16.06	-0.11	-0.38	4.61	-2.84	0.34	0.34	Rigo et al. (2015)	Yes
BOR0_GPS	-0.4	42.56	19.05	15.74	-0.2	-0.67	4.48	-3.2	0.31	0.32	Rigo et al. (2015)	Yes
BOUI_GPS	2.44	43	19.51	15.71	-0.18	-0.56	4.43	-3.36	0.31	0.31	Rigo et al. (2015)	Yes
CAAR_GPS	0.01	42.42	19.58	15.94	0.22	-0.45	4.87	-3.02	0.34	0.34	Rigo et al. (2015)	Yes
CAR0_GPS	-1.62	42.33	18.63	15.84	-0.44	-0.62	4.26	-3.02	0.31	0.32	Rigo et al. (2015)	Yes
COUP_GPS	1.07	43.14	18.68	15.84	-0.71	-0.5	3.96	-3.17	0.32	0.32	Rigo et al. (2015)	Yes
DUH0_GPS	-0.32	43.71	19.23	15.97	0.26	-0.44	5	-2.97	0.32	0.32	Rigo et al. (2015)	Yes
EMBU_GPS	-0.72	42.63	18.33	15.75	-0.84	-0.68	3.85	-3.17	0.39	0.4	Rigo et al. (2015)	Yes
ETXA_GPS	-1.78	42.8	18.32	16.29	-0.6	-0.18	4.13	-2.56	0.34	0.35	Rigo et al. (2015)	Yes
FUE0_GPS	-0.88	42.36	18.8	16.24	-0.41	-0.19	4.27	-2.67	0.32	0.32	Rigo et al. (2015)	Yes

ISSA_GPS	-0.79	43.02	19.3	16.3	0.24	-0.13	4.96	-2.61	0.34	0.35	Rigo et al. (2015)	Yes
JAUT_GPS	-0.34	43.03	18.32	16.56	-0.82	0.15	3.88	-2.38	0.35	0.36	Rigo et al. (2015)	Yes
LHRZ_GPS	1.39	42.81	19.57	15.49	0.04	-0.84	4.67	-3.54	0.3	0.3	Rigo et al. (2015)	Yes
LIE0_GPS	-1.32	42.63	19.06	16.26	0.01	-0.19	4.71	-2.62	0.31	0.32	Rigo et al. (2015)	Yes
MARC_GPS	0.16	43.53	18.94	15.92	-0.17	-0.47	4.54	-3.05	0.35	0.37	Rigo et al. (2015)	Yes
MCA0_GPS	3.02	43.6	19.15	16.07	-0.51	-0.16	4.12	-3.02	0.29	0.3	Rigo et al. (2015)	Yes
MGA0_GPS	1.64	42.94	18.8	16.06	-0.75	-0.25	3.89	-2.98	0.3	0.3	Rigo et al. (2015)	Yes
MRTE_GPS	0.75	42.92	18.79	16.23	-0.59	-0.13	4.07	-2.77	0.32	0.33	Rigo et al. (2015)	Yes
NEN0_GPS	0.7	43.36	18.96	16.18	-0.3	-0.18	4.39	-2.81	0.32	0.33	Rigo et al. (2015)	Yes
PANT_GPS	-0.24	42.76	19.26	15.73	0.03	-0.68	4.71	-3.21	0.34	0.35	Rigo et al. (2015)	Yes
PER0_GPS	-0.02	42.05	19.56	16.13	0.11	-0.27	4.75	-2.83	0.32	0.32	Rigo et al. (2015)	Yes
PLAB_GPS	0.95	42.71	19.72	15.81	0.25	-0.54	4.89	-3.2	0.33	0.32	Rigo et al. (2015)	Yes
POM0_GPS	-0.83	43.63	19.2	16.14	0.31	-0.29	5.06	-2.77	0.32	0.32	Rigo et al. (2015)	Yes
PPY0_GPS	1.71	42.64	20.78	16.3	1.15	-0.01	5.76	-2.74	0.33	0.3	Rigo et al. (2015)	Yes
QUI0_GPS	2.15	42.87	19.56	15.9	-0.1	-0.38	4.51	-3.16	0.31	0.3	Rigo et al. (2015)	Yes
RGS0_GPS	2.63	43.16	19.88	15.55	0.19	-0.71	4.81	-3.53	0.29	0.29	Rigo et al. (2015)	Yes
RIEB_GPS	1.34	43.06	19.4	15.78	-0.06	-0.55	4.59	-3.24	0.3	0.3	Rigo et al. (2015)	Yes
RON0_GPS	-0.98	42.74	19.01	16.33	-0.08	-0.11	4.62	-2.57	0.32	0.32	Rigo et al. (2015)	Yes
RPE0_GPS	2.53	43.42	19.03	15.51	-0.57	-0.75	4.06	-3.56	0.31	0.31	Rigo et al. (2015)	Yes
SEIX_GPS	1.13	42.87	19.43	15.65	-0.04	-0.69	4.61	-3.36	0.33	0.32	Rigo et al. (2015)	Yes

SEPE_GPS	-0.41	42.25	19.9	15.74	0.58	-0.67	5.24	-3.2	0.37	0.35	Rigo et al. (2015)	Yes
SERR_GPS	0.71	42.56	19.58	15.42	0.12	-0.94	4.76	-3.57	0.32	0.32	Rigo et al. (2015)	Yes
SOMP_GPS	-0.55	42.8	18.5	15.88	-0.66	-0.54	4.04	-3.05	0.34	0.34	Rigo et al. (2015)	Yes
TRMO_GPS	0.1	42.73	18.66	16.01	-0.64	-0.38	4.03	-2.95	0.31	0.31	Rigo et al. (2015)	Yes
TRON_GPS	0.31	42.31	19.03	15.38	-0.42	-1	4.22	-3.59	0.32	0.32	Rigo et al. (2015)	Yes
UNC0_GPS	-1.19	42.33	18.69	16.11	-0.46	-0.34	4.22	-2.78	0.33	0.33	Rigo et al. (2015)	Yes
UNZU_GPS	-1.63	42.66	19.17	15.79	0.19	-0.67	4.9	-3.07	0.36	0.36	Rigo et al. (2015)	Yes
VCGE_GPS	2.82	43.04	19.77	15.4	0.02	-0.85	4.62	-3.68	0.31	0.31	Rigo et al. (2015)	Yes
VGR0_GPS	-2.53	42.31	18.17	16.38	-0.73	-0.11	3.99	-2.42	0.31	0.31	Rigo et al. (2015)	Yes
ACOR_GPS	-8.3989	43.3644	20.65	16.62	3.18	0.02	8.11	-1.69	0.05	0.05	This study	No
AIO2_GPS	-1.0592	39.0614	18.49	16.36	-1.47	-0.08	3.01	-2.54	0.16	0.20	This study	No
AION_GPS	-2.5325	34.5879	15.17	17.21	-5.52	0.71	-1.31	-1.60	0.73	0.69	This study	No
ALBX_GPS	2.1368	43.9342	18.25	15.19	-1.15	-1.09	3.52	-3.87	0.89	0.46	This study	No
ALC2_GPS	-0.1453	41.0579	20.08	15.60	0.42	-0.8	5.00	-3.35	0.19	0.18	This study	No
ALDA_GPS	-2.3319	42.7544	18.58	15.51	-0.24	-0.98	4.50	-3.31	0.06	0.11	This study	No
ALHA_GPS	-1.4467	37.8042	20.81	14.46	0.63	-2	5.04	-4.42	0.12	0.20	This study	No
ALM1_GPS	-2.4850	36.8322	18.15	19.13	-2.06	2.63	2.30	0.32	0.18	0.25	This study	No
ALMZ_GPS	-2.5390	41.5031	19.87	17.24	0.77	0.74	5.44	-1.56	0.22	0.18	This study	No
AND2_GPS	-4.0298	38.0404	18.60	16.49	-1.07	-0.05	3.42	-2.21	0.11	0.12	This study	No
ARDU_GPS	-3.7426	41.6658	17.35	16.58	-1.48	0.05	3.23	-2.14	0.13	0.07	This study	No
ARES_GPS	-1.1341	44.7640	19.55	16.38	1.01	-0.06	5.84	-2.51	0.15	0.12	This study	No
AVL1_GPS	-5.9131	43.5579	17.59	15.07	-0.32	-1.51	4.57	-3.47	0.12	0.11	This study	No
BEA2_GPS	3.1367	42.5153	20.84	15.60	0.9	-0.63	5.46	-3.50	0.17	0.31	This study	No
BECE_GPS	-7.1580	42.8560	20.05	17.72	2.2	1.13	7.06	-0.71	0.08	0.08	This study	No
BEJR_GPS	-5.7485	40.3959	17.65	17.81	-1.13	1.23	3.55	-0.75	0.12	0.14	This study	No

BOTI_GPS	-7.6581	41.6929	16.60	16.10	-1.47	-0.5	3.33	-2.28	0.33	0.24	This study	No
BUJA_GPS	-0.1525	41.4941	19.38	15.89	-0.18	-0.51	4.43	-3.06	1.60	0.87	This study	No
CESS_GPS	-0.1774	44.7429	19.13	21.89	0.39	5.49	5.19	2.94	0.25	0.41	This study	No
CORX_GPS	-8.7367	43.1872	16.65	17.60	-0.8	1	4.12	-0.67	0.10	0.12	This study	No
CREU_GPS	3.3156	42.3189	20.54	16.13	0.52	-0.09	5.07	-2.97	0.05	0.06	This study	No
CRNO_GPS	-7.8664	43.7378	17.05	15.78	-0.42	-0.82	4.52	-2.58	0.11	0.08	This study	No
CRPO_GPS	-5.1097	41.2140	18.70	15.36	0.01	-1.2	4.73	-3.25	0.11	0.16	This study	No
ELCH_GPS	-0.6646	38.2627	20.05	14.21	-0.16	-2.22	4.25	-4.72	1.17	1.36	This study	No
ESPI_GPS	-8.6434	40.9760	15.97	15.00	-2.11	-1.6	2.67	-3.28	0.23	0.23	This study	No
ESTR_GPS	-7.5854	38.8466	16.74	16.37	-2.09	-0.23	2.52	-2.02	0.16	0.26	This study	No
FJC2_GPS	2.7949	43.0482	17.18	15.37	-2.57	-0.88	2.04	-3.71	0.20	0.26	This study	No
FRRL_GPS	-8.3382	43.4614	19.86	17.58	2.41	0.98	7.34	-0.73	0.11	0.09	This study	No
GRAN_GPS	-3.5953	37.1902	18.60	16.56	-1.34	0.03	3.07	-2.17	0.36	0.50	This study	No
GRSF_GPS	-3.3967	34.2157	14.82	18.08	-5.8	1.55	-1.61	-0.67	1.01	0.83	This study	No
HOND_GPS	-1.7980	43.3848	19.07	15.68	0.3	-0.79	5.07	-3.17	0.27	0.29	This study	No
IGEO_GPS	-9.1136	38.7783	18.47	15.93	-0.1	-0.68	4.53	-2.31	0.11	0.23	This study	No
IGNE_GPS	-3.7095	40.4458	18.80	15.53	-0.34	-1	4.29	-3.19	0.08	0.08	This study	No
KAST_GPS	-2.9657	43.2503	20.09	17.56	1.52	1.05	6.31	-1.21	0.10	0.10	This study	No
LAGU_GPS	1.9684	44.1455	19.22	14.69	-0.1	-1.6	4.60	-4.36	0.26	0.30	This study	No
LAMU_GPS	1.5677	44.6477	20.72	15.81	1.61	-0.5	6.34	-3.22	0.12	0.13	This study	No
LAUZ_GPS	1.1052	44.2471	18.56	15.35	-0.56	-0.99	4.17	-3.66	0.14	0.27	This study	No
LERM_GPS	-3.7568	42.0267	18.38	15.66	-0.36	-0.87	4.38	-3.06	0.30	0.17	This study	No
LNGS_GPS	-8.5301	43.3465	15.57	15.87	-1.88	-0.73	3.05	-2.42	0.16	0.36	This study	No
LOD1_GPS	3.3317	43.7747	17.82	14.75	-1.85	-1.46	2.77	-4.35	0.36	0.50	This study	No
LOR1_GPS	-1.7137	37.6566	24.21	12.75	4.05	-3.72	8.45	-6.11	0.23	0.29	This study	No
LOR2_GPS	-1.6996	37.6579	25.60	11.61	5.43	-4.86	9.84	-7.25	0.24	0.25	This study	No
LORC_GPS	-1.6868	37.6539	25.01	12.29	4.84	-4.18	9.24	-6.57	0.38	0.34	This study	No
MAD1_GPS	-3.6861	40.4073	18.22	16.62	-0.94	0.09	3.69	-2.10	0.14	0.16	This study	No
MAL1_GPS	2.6375	39.5602	20.03	14.11	-0.48	-2.15	3.92	-4.97	0.13	0.19	This study	No
MIRP_GPS	0.6929	43.7366	20.95	15.04	1.78	-1.32	6.49	-3.95	0.20	0.15	This study	No

MLLL_GPS	-2.9285	35.2907	16.43	17.59	-4.04	1.08	0.22	-1.19	0.23	0.16	This study	No
MOLI_GPS	-1.8793	40.8412	20.62	13.85	1.23	-2.62	5.84	-5.00	0.14	0.21	This study	No
MORE_GPS	-0.1015	40.6180	19.56	15.05	-0.21	-1.35	4.33	-3.90	0.20	0.20	This study	No
MZAN_GPS	-1.2242	44.1985	18.47	16.25	-0.2	-0.2	4.60	-2.64	0.09	0.10	This study	No
OLOT_GPS	2.5100	42.1430	19.65	16.74	-0.26	0.48	4.30	-2.33	0.37	0.40	This study	No
OVIE_GPS	-5.8553	43.3593	18.17	15.85	0.2	-0.73	5.07	-2.70	0.24	0.27	This study	No
PDB1_GPS	-5.2025	40.9019	16.52	17.76	-2.23	1.19	2.47	-0.84	0.17	0.13	This study	No
PENI_GPS	0.3589	40.3957	18.39	16.81	-1.52	0.43	3.00	-2.17	0.15	0.18	This study	No
PIMI_GPS	0.1427	42.9364	20.47	12.68	1.21	-3.71	5.89	-6.28	0.16	0.23	This study	No
PONF_GPS	-6.5818	42.5511	17.76	15.56	-0.29	-1.03	4.55	-2.92	0.08	0.13	This study	No
PUIG_GPS	1.8705	42.4157	18.50	18.03	-1.22	1.73	3.38	-1.02	0.40	0.35	This study	No
RIA1_GPS	-3.4803	41.2787	18.76	15.98	-0.22	-0.54	4.46	-2.76	0.16	0.10	This study	No
RIOJ_GPS	-2.5021	42.4580	18.74	14.52	-0.13	-1.97	4.60	-4.29	0.23	0.39	This study	No
RRMT_GPS	-6.9196	33.9582	14.75	16.58	-5.36	-0.02	-1.11	-1.88	0.33	0.33	This study	No
SALD_GPS	-4.7429	42.5199	18.55	15.48	0.13	-1.08	4.93	-3.16	0.08	0.09	This study	No
SEV1_GPS	-6.0022	37.4109	18.61	16.02	-0.86	-0.56	3.62	-2.52	0.10	0.11	This study	No
SJAC_GPS	-8.7348	40.6602	15.99	16.47	-2.16	-0.13	2.60	-1.81	0.10	0.06	This study	No
SMA2_GPS	-7.7521	38.4593	19.35	18.85	0.45	2.25	5.04	0.47	1.93	1.72	This study	No
SORI_GPS	-2.4705	41.7622	18.80	15.95	-0.25	-0.54	4.44	-2.86	0.16	0.15	This study	No
STS2_GPS	-0.5675	43.7764	18.67	16.52	-0.24	0.1	4.51	-2.41	0.38	0.76	This study	No
SURI_GPS	-2.4693	41.7639	18.23	15.87	-0.82	-0.62	3.87	-2.94	0.11	0.12	This study	No
TAR0_GPS	-5.6027	36.0086	14.62	20.25	-5.25	3.67	-0.87	1.67	0.24	0.15	This study	No
TAR2_GPS	-5.6069	36.0341	27.73	20.40	7.87	3.82	12.25	1.82	0.64	0.37	This study	No
TAVX_GPS	-7.6496	37.1214	19.90	17.01	0.65	0.41	5.14	-1.38	0.33	0.14	This study	No
TOR0_GPS	-0.6804	37.9754	20.25	15.73	-0.02	-0.7	4.37	-3.20	0.37	0.31	This study	No
TRRG_GPS	1.2132	41.0790	18.05	14.64	-1.86	-1.7	2.68	-4.38	0.13	0.13	This study	No
TUD1_GPS	-1.6034	42.0486	18.61	15.89	-0.53	-0.57	4.15	-2.98	0.11	0.13	This study	No
VREA_GPS	-7.7374	41.3097	17.01	17.63	-1.15	1.03	3.63	-0.74	0.41	0.16	This study	No
VRGH_GPS	-0.1984	43.7184	19.03	15.40	0.03	-1	4.77	-3.55	0.34	0.24	This study	No
VRO1_GPS	0.1560	40.8736	19.40	14.88	-0.36	-1.51	4.20	-4.09	0.17	0.18	This study	No

XIX1_GPS	-5.6984	43.5581	18.61	15.57	0.66	-1	5.54	-2.99	0.22	0.19	This study	No
YEB2_GPS	-3.0876	40.5238	18.30	16.43	-0.94	-0.08	3.68	-2.34	0.24	0.25	This study	No
EBNH_GPS	1.5588	36.5213	21.71	19.05	0.74	2.73	4.98	0.01	1.34	1.28	Bougrine et al. (2019)	No
EKMS_GPS	0.6636	36.2143	13.12	19.39	-7.76	3.02	-3.52	0.39	0.50	0.69	Bougrine et al. (2019)	No
OJGS_GPS	0.9775	35.5052	17.42	22.86	-3.66	6.51	0.53	3.85	0.47	0.82	Bougrine et al. (2019)	No
OSDA_GPS	0.1169	34.8243	20.57	22.58	-0.5	6.18	3.66	3.61	1.40	3.28	Bougrine et al. (2019)	No
ALJI_GPS	-5.6494	36.5299	13.59	16.87	-6.15	0.29	-1.73	-1.7	2.51	0.66	Garate et al. (2015) UB solution	No
PYG0_GPS	0.4600	42.7700	16.51	17.54	-2.85	1.17	1.81	-1.44	1.09	1.11	Rigo et al. (2015)	No

Reference in Table	*Reference in extended version*
Bougrine et al. (2019)	Bougrine, A., Yelles-Chaouche, A. K., & Calais, E. (2019). Active deformation in Algeria from continuous GPS measurements. Geophysical Journal International, 217(1), 572-588.
Cabral et al. (2017)	Cabral, J., Mendes, V. B., Figueiredo, P., da Silveira, A. B., Pagarete, J., Ribeiro, A., Dias, R., & Ressurreição, R. (2017). Active tectonics in Southern Portugal (SW Iberia) inferred from GPS data. Implications on the regional geodynamics. Journal of Geodynamics, 112, 1-11.
Echeverria et al. (2013)	Echeverria, A., Khazaradze, G., Asensio, E., Gárate, J., Dávila, J. M., & Suriñach, E. (2013). Crustal deformation in eastern Betics from CuaTeNeo GPS network. Tectonophysics, 608, 600-612.
Echeverria et al. (2015)	Echeverria, A., Khazaradze, G., Asensio, E., & Masana, E. (2015). Geodetic evidence for continuing tectonic activity of the Carboneras fault (SE Spain). Tectonophysics, 663, 302-309.
Garate et al. (2015) UB solution	Garate, J., Martin-Davila, J., Khazaradze, G., Echeverria, A., Asensio, E., Gil, A. J., de Lacy, M. C., Armenteros, J. A., Ruiz, A. M., Gallastegui, J., Alvarez-Lobato, F., Ayala, C., Rodríguez-Caderot, G., Galindo-Zaldívar, J., Rimi ., & Harnafi, M. (2015). Topo-Iberia project: CGPS crustal velocity field in the Iberian Peninsula and Morocco. GPS Solutions, 19, 287-295.
Rigo et al. (2015)	Rigo, A., Vernant, P., Feigl, K. L., Goula, X., Khazaradze, G., Talaya, J., Morel, L., Nicolas, J., Baize, S., Chéry, J., & Sylvander, M. (2015). Present-day deformation of the Pyrenees revealed by GPS surveying and earthquake focal mechanisms until 2011. Geophysical Journal International, 201(2), 947-964.

8.3. Supplementary material for Chapter 4

8.3.1. Table – Stress2GRID results – Geological (SS) vs Geodetic strain (GPS)

Lon	*Lat*	*SS_count*	*FSP_count*	ε_{Hmax} *SS*	*STD* ε_{Hmax} *SS*	ε_{Hmax} *GPS*	*dazi* ε_{Hmax} *GPS*	ε_{Hmax} *angular diff.*
15.267	37.871	1	1	127		154.7	1.4	27.70
15.156	37.964	2	3	111.92	33.62	137.7	2.1	25.78
15.045	38.056	3	14	70.54	25.09	115.9	1.2	45.36
15.159	38.054	6	21	111	44.40	123.3	1.1	12.30
15.387	38.049	1	6	68		130.4	1.2	62.40
15.501	38.046	2	20	104.26	34.83	129.4	1.2	25.14
15.728	38.041	1	7	115		132.6	2	17.60
15.048	38.146	3	6	32.11	29.77	106.8	0.7	74.69
15.162	38.144	4	14	117.82	6.99	116.1	0.8	1.72
15.276	38.141	1	6	124		117.1	0.9	6.90
15.39	38.139	2	42	131.79	17.89	130	0.9	1.79
15.504	38.136	2	28	150.06	7.85	131.4	1.2	18.66
15.618	38.134	2	5	115.92	6.02	134	1.3	18.08
15.732	38.131	2	10	117.95	8.05	130.5	1.6	12.55
15.393	38.229	2	42	135.89	18.04	118.6	0.8	17.29
15.507	38.226	1	17	126		129.2	1.2	3.20
15.621	38.224	3	28	130.08	10.62	125.7	1.1	4.38
15.735	38.221	3	20	130.84	10.29	127.3	1.4	3.54
15.849	38.218	4	60	149.57	15.18	125	1.4	24.57
15.963	38.215	5	39	121.8	6.94	122.3	1.8	0.50
16.077	38.212	1	6	109		116.1	2.5	7.10
15.739	38.311	1	4	152		119.5	1.2	32.50
15.853	38.308	5	64	152.56	14.74	118.6	1.6	33.96
15.967	38.305	3	17	121.17	7.89	116.8	1.7	4.37
16.082	38.302	2	10	123.11	7.52	111.3	2.3	11.81
15.857	38.398	1	3	147		113.3	1.7	33.70
16.086	38.391	2	14	133.78	2.15	107.5	2.4	26.28
15.975	38.485	1	2	70		107.7	2.1	37.70
16.09	38.481	2	9	108.81	26.02	104.1	3.1	4.71

15.979	38.575	1	48	24		102.9	2.5	78.90
16.209	38.568	5	8	144.57	24.85	109.6	3.6	34.97
16.098	38.661	2	10	54.09	53.46	108.9	4.1	54.81
16.213	38.658	3	6	105		111	4.5	6.00
16.217	38.748	1	4	124		125.1	5.5	1.10
16.332	38.745	1	6	114		120.5	5.6	6.50
16.221	38.838	2	18	118.19	3.00	129.1	5.1	10.91
16.337	38.835	2	18	117.49	2.96	120.1	7.8	2.61
16.226	38.928	2	21	164.3	11.52	129.2	6.7	35.10
16.456	38.921	3	25	178.97	6.52	101.8	4.6	77.17
16.571	38.917	1	1	2		100.3	2	81.70
16.23	39.018	3	26	162.05	12.15	113.4	6.3	48.65
16.461	39.011	4	24	171.19	4.10	98	3.1	73.19
16.576	39.007	2	14	162		100.1	2.1	61.90
16.807	39	1	6	92		98.4	1.4	6.40
16.119	39.111	2	20	151.27	43.78	114.2	6.8	37.07
16.235	39.108	5	65	138.08	30.42	108.5	5.6	29.58
16.35	39.105	1	11	104		101.6	4.2	2.40
16.007	39.205	1	6	113		108.8	3.1	4.20
16.123	39.202	6	64	96.41	19.65	102.1	6.2	5.69
16.239	39.198	6	74	118.15	8.71	105.8	5.7	12.35
16.355	39.195	6	87	93.76	5.44	103.4	5	9.64
16.012	39.295	1	5	118		101.9	5	16.10
16.127	39.292	10	126	95.62	23.79	95.1	4.9	0.52
16.243	39.288	6	86	107.94	14.43	95.4	5.2	12.54
16.359	39.285	8	100	95.49	11.85	105.8	4.5	10.31
16.938	39.266	1	3	50		111.6	1.7	61.60
16.132	39.382	9	121	107.05	16.20	84.3	5.6	22.75
16.248	39.378	5	42	78.78	14.33	99.2	6.3	20.42
16.364	39.375	8	91	105.38	28.18	102.2	5.5	3.18

16.944	39.356	1	3	50		113.7	3.6	63.70
16.136	39.472	8	71	103.66	19.22	86.2	5.7	17.46
16.252	39.468	7	57	96.09	22.95	93	4.5	3.09
16.368	39.465	9	47	90.9	15.37	107.2	4.9	16.30
15.907	39.568	1	13	71		86.7	5	15.70
16.024	39.565	6	42	95.61	25.48	82.2	7.3	13.41
16.14	39.562	8	66	99.29	28.24	81.6	6.4	17.69
16.257	39.558	4	43	27.11	44.16	88.6	5.6	61.49
16.373	39.555	1	9	8		96.6	6.3	88.60
16.605	39.547	1	8	32		124.2	23.1	87.80
15.795	39.661	3	24	49.19	44.38	55.9	2.9	6.71
15.911	39.658	4	37	70.86	40.16	79	7.4	8.14
16.028	39.655	8	70	136.95	38.41	79.3	6.4	57.65
16.144	39.652	3	22	115.65	13.92	78.1	4.7	37.55
16.261	39.648	6	49	46.27	26.65	86	6.6	39.73
16.377	39.645	2	9	37.47	2.97	85.8	7.5	48.33
16.61	39.637	1	8	32		108.9	10.6	76.90
16.032	39.745	2	15	99.5	7.48	65.5	5.4	34.00
16.149	39.742	3	13	103.03	10.97	68	5.4	35.03
16.265	39.738	10	63	65.62	26.68	75.9	5.5	10.28
15.919	39.838	10	34	90.27	12.57	50.4	6	39.87
16.036	39.835	11	98	31.69	44.93	50.9	5.4	19.21
16.153	39.832	14	75	106.22	51.79	55.2	4.7	51.02
16.27	39.828	14	122	60.52	9.60	63.2	4.9	2.68
16.387	39.825	2	8	136.14	36.58	66.6	8.2	69.54
15.806	39.931	1	10	57		42.5	3.8	14.50
15.923	39.928	10	33	86.31	8.88	39.4	4.9	46.91
16.04	39.925	13	129	93.97	31.15	42.9	4	51.07
16.157	39.922	23	164	149.62	56.61	52.5	3.8	82.88
16.274	39.919	1	6	97		57.4	4.7	39.60

15.693	40.024	2	290	61.2	8.01	51.1	1.6	10.10
15.81	40.021	11	362	58.38	31.99	39.3	2.4	19.08
15.927	40.018	9	93	18.51	29.46	39.1	3.4	20.59
16.045	40.015	4	71	40.7	29.93	40.8	3.6	0.10
16.162	40.012	2	22	40.63	10.56	38.5	4.7	2.13
15.579	40.117	5	42	41.54	31.44	59.5	1.8	17.96
15.697	40.114	8	62	59.62	21.98	54.7	2.6	4.92
15.814	40.111	1	29	56		44.4	2.9	11.60
15.931	40.108	4	63	70.15	15.64	39.2	2.7	30.95
16.049	40.105	1	26	83		28.8	3.6	54.20
15.465	40.21	2	8	39.71	8.02	62.3	2	22.59
15.583	40.207	4	14	22.97	32.61	60.9	1.7	37.93
15.7	40.204	8	47	45.48	23.56	59.7	2.1	14.22
15.818	40.202	4	11	42.58	4.98	56.4	3.1	13.82
15.935	40.199	3	21	63.63	21.14	42.7	3.6	20.93
15.351	40.303	1	3	61		67.9	4.5	6.90
15.469	40.3	6	29	38.58	24.43	62.8	1.9	24.22
15.587	40.297	2	6	52.85	6.43	60.3	1.8	7.45
15.704	40.295	11	73	54.35	22.29	57.3	1.9	2.95
15.822	40.292	12	118	43.39	14.91	54.6	4	11.21
15.939	40.289	7	67	48.93	22.79	53.8	10.8	4.87
16.057	40.285	2	2	40		49.5	8.9	9.50
16.292	40.279	1	5	172		54.9	9.1	62.90
15.472	40.39	4	12	27.1	17.01	66.6	2.6	39.50
15.59	40.387	8	60	39.21	23.93	60.6	1.8	21.39
15.708	40.385	12	71	48.79	33.21	60.6	1.8	11.81
15.826	40.382	12	100	32.89	26.22	57.3	2.6	24.41
15.944	40.379	3	39	48.76	40.16	57.2	4.4	8.44
16.061	40.376	4	29	65.16	14.38	59.4	5.9	5.76
16.297	40.369	1	5	172		59.5	6.8	67.50

15.358	40.483	5	57	33.78	21.21	55.9	2.2	22.12
15.476	40.48	9	90	45.88	23.85	55.1	2.4	9.22
15.594	40.478	8	89	45.57	23.15	54.5	1.7	8.93
15.712	40.475	5	26	33.09	40.51	56.1	1.7	23.01
15.83	40.472	1	5	5		55.7	2.6	50.70
15.948	40.469	4	30	79.18	22.09	51.9	2.9	27.28
16.066	40.466	3	23	72.61	34.49	55	4.2	17.61
15.243	40.575	2	6	165.47	3.70	95.3	3.1	70.17
15.361	40.573	6	41	13.51	18.92	68.9	2.9	55.39
15.479	40.57	13	440	23.75	21.26	50.8	2.1	27.05
15.597	40.568	4	26	70.38	42.15	47.3	1.5	23.08
15.715	40.565	2	3	54		47.8	1.8	6.20
15.834	40.562	3	11	54		50.2	1.9	3.80
15.952	40.559	4	31	66.7	15.90	48.8	2.5	17.90
16.07	40.556	1	6	51		51.7	3.4	0.70
15.246	40.665	2	4	36		71.7	1.8	35.70
15.364	40.663	14	177	12.6	36.31	55.1	1.7	42.50
15.482	40.66	17	101	34.56	18.49	50.4	1.6	15.84
15.601	40.658	5	36	38.64	9.10	46.4	1.5	7.76
15.13	40.758	1	4	110		66.7	1.2	43.30
15.249	40.756	3	60	18.18	48.02	64.5	1.1	46.32
15.367	40.753	7	86	17.48	20.62	54.3	1.3	36.82
15.486	40.751	7	36	11.64	10.82	48.6	1.4	36.96
15.604	40.748	3	3	39.98	26.55	44.2	1.7	4.22
14.896	40.852	2	12	55		57	1.2	2.00
15.015	40.85	4	17	34.87	19.25	62.7	1.3	27.83
15.133	40.848	5	60	26.24	23.26	63.1	1.1	36.86
15.252	40.846	3	50	40.74	17.75	54.8	1.2	14.06
15.371	40.843	1	1	13		52.4	1.2	39.40
15.489	40.841	3	12	10.62	2.94	48	1.4	37.38

15.608	40.838	1	1	105		43.1	2.1	61.90
14.899	40.942	4	16	44.16	34.04	52.2	2	8.04
15.017	40.94	4	6	26.55	35.73	51.7	2.3	25.15
14.546	41.128	2	17	22.09	19.78	13.6	5.2	8.49
14.665	41.126	1	4	47		32.3	3.2	14.70
14.548	41.218	5	45	12.75	14.71	33.7	5.7	20.95
14.668	41.217	7	37	24.24	24.55	41.2	2.6	16.96
14.787	41.215	2	8	65.48	35.68	44.2	1.5	21.28
14.907	41.213	1	5	49		45.4	1.2	3.60
14.311	41.311	1	16	169		59.7	3.1	70.70
14.431	41.31	1	7	78		51.5	3.5	26.50
14.551	41.308	2	12	30.52	15.86	47	3.1	16.48
14.67	41.307	3	14	174.49	25.68	45.4	1.9	50.91
14.909	41.303	1	5	49		47.6	1.2	1.40
13.954	41.405	2	23	22.71	7.50	50.4	1.4	27.69
14.194	41.403	6	38	171.21	39.32	54.7	1.8	63.49
14.313	41.402	1	16	169		53.4	3.2	64.40
14.553	41.398	1	12	7		47	2.1	40.00
12.996	41.499	1	4	46		56.6	7.3	10.60
13.836	41.496	2	29	37.48	5.43	51	1.8	13.52
13.955	41.495	5	68	32.15	8.30	50.6	1.6	18.45
14.075	41.494	2	5	12.85	14.59	52.8	1.9	39.95
14.195	41.493	5	29	31.43	11.87	52.6	2.1	21.17
14.315	41.492	6	85	21.29	21.39	50.4	2.7	29.11
14.435	41.49	3	46	27.05	20.73	44.3	2.4	17.25
14.555	41.489	2	20	178.61	9.52	43.7	2.2	45.09
13.116	41.589	3	26	49.47	8.15	53.9	6.4	4.43
13.236	41.589	2	22	19.91	13.73	45.8	4.7	25.89
14.317	41.582	3	42	21.19	20.54	49.2	2.5	28.01
13.116	41.68	2	17	31.45	2.97	58.8	4.6	27.35

13.237	41.679	4	25	17.17	12.99	55.9	4.2	38.73
13.357	41.679	2	12	10.09	19.06	54	4.6	43.91
13.237	41.769	6	53	36.46	21.36	55.1	3.3	18.64
13.357	41.769	1	8	34		57.1	3.7	23.10
13.598	41.768	1	8	40		52.9	3.1	12.90
13.719	41.767	2	21	49.45	10.09	52.4	2.1	2.95
13.839	41.767	2	25	35.63	7.49	50.3	2	14.67
13.959	41.766	2	23	30.57	8.74	51.2	1.5	20.63
14.08	41.765	2	11	70.4	20.14	51.7	1.9	18.70
13.117	41.86	1	2	17		54.1	4.3	37.10
13.358	41.859	1	3	26		50.4	2.6	24.40
13.478	41.859	2	38	56.5	1.50	49.6	2.4	6.90
13.599	41.858	2	37	46.24	8.02	54	2.5	7.76
13.72	41.858	3	26	46.92	23.25	56.4	2	9.48
13.84	41.857	5	55	45.62	13.27	54.5	2.1	8.88
14.081	41.855	7	55	62.19	25.31	50.5	1.5	11.69
14.202	41.854	2	25	90.07	12.69	49	1.9	41.07
13.358	41.949	6	52	31.09	12.40	42.2	2.6	11.11
13.479	41.949	3	29	49.65	6.17	51.5	3.1	1.85
13.6	41.948	3	26	39.89	2.93	57.8	2.7	17.91
13.721	41.948	9	101	47.89	14.00	61.6	2	13.71
13.841	41.947	3	44	58.95	17.98	62.2	1.8	3.25
13.962	41.946	1	6	42		54.1	1.5	12.10
14.083	41.945	5	41	59.99	16.64	52.3	1.4	7.69
12.996	42.04	3	16	50.95	10.17	47.7	4.3	3.25
13.238	42.04	3	17	20.48	24.25	47.8	2.1	27.32
13.359	42.04	3	44	17.4	11.94	48	2.2	30.60
13.48	42.039	7	50	165.34	16.59	55.2	1.5	69.86
13.601	42.039	7	46	31.88	34.17	59.7	1.5	27.82
13.722	42.038	4	30	57.14	11.05	62.8	1.9	5.66

13.843	42.037	1	5	64		65.2	1.7	1.20
13.964	42.036	2	9	2.92	16.36	57.3	1.7	54.38
14.084	42.035	3	38	26.22	28.95	50.9	1.4	24.68
12.875	42.13	4	27	44.25	22.24	49.4	5	5.15
12.996	42.13	4	28	38.64	17.82	42.8	2.5	4.16
13.117	42.13	2	4	50.22	10.82	47.7	1.8	2.52
13.238	42.13	3	15	58.48	27.22	46.6	2	11.88
13.359	42.13	3	34	22.93	16.99	54.5	1.7	31.57
13.481	42.129	17	208	12.19	27.00	60.2	1.5	48.01
13.602	42.129	8	48	33.9	57.03	69.3	1.3	35.40
13.723	42.128	4	38	37.13	11.25	69.5	1.4	32.37
13.844	42.127	5	79	36.86	11.62	69.7	1.4	32.84
13.965	42.126	4	65	0.88	22.80	67.2	2	66.32
14.086	42.125	1	21	59		57.5	2.7	1.50
12.632	42.22	1	3	21		62.2	8.8	41.20
12.754	42.22	1	3	21		57.1	6.3	36.10
12.996	42.22	2	12	44.55	12.99	45.2	2.2	0.65
13.117	42.22	4	25	17.28	31.62	46.5	2.2	29.22
13.239	42.22	1	4	55		43.4	2.3	11.60
13.36	42.22	6	67	44.44	7.66	56.3	1.8	11.86
13.481	42.219	6	65	39.38	6.18	63.7	1.5	24.32
13.602	42.219	3	15	24.99	10.08	65.4	1.3	40.41
13.724	42.218	9	65	30.54	11.13	71.7	1.3	41.16
13.845	42.217	3	35	39.49	4.08	75.2	1.3	35.71
13.966	42.216	2	30	160.37	6.01	71.7	2	88.67
12.996	42.311	3	22	40.94	7.79	47.9	2.3	6.96
13.118	42.311	4	33	31.81	33.04	43.4	2	11.59
13.239	42.31	1	8	44		44	2	0.00
13.36	42.31	5	36	50.26	9.55	45.5	2.8	4.76
13.482	42.31	4	32	33.27	14.29	56.4	1.9	23.13

13.603	42.309	5	40	42.44	12.99	64.8	1.3	22.36
13.725	42.308	4	27	45.81	14.61	72.3	1.2	26.49
12.874	42.401	1	2	83		45.6	2.4	37.40
12.996	42.401	1	23	28		45.8	2.4	17.80
13.118	42.401	4	26	34.08	3.22	41.4	1.7	7.32
13.239	42.401	8	86	35.6	10.10	41.3	1.7	5.70
13.361	42.4	11	104	39.33	12.54	31.9	7.4	7.43
13.483	42.4	9	60	30.02	13.82	52.2	1.8	22.18
13.604	42.399	5	40	20.38	9.53	59.1	1.5	38.72
13.726	42.399	5	32	29.39	6.40	66.5	1.5	37.11
13.847	42.398	1	16	23		69.4	1.5	46.40
12.509	42.49	3	40	48.98	10.86	34.3	3.6	14.68
12.631	42.49	1	11	27		34.6	4.1	7.60
12.874	42.491	1	2	83		42.8	2.3	40.20
12.996	42.491	1	23	28		41.2	1.9	13.20
13.118	42.491	3	22	32.99	17.29	37	1.7	4.01
13.24	42.491	9	113	43.04	14.48	39.8	1.6	3.24
13.361	42.49	7	89	40.94	14.79	58.6	2	17.66
13.483	42.49	2	10	14		58.1	1.7	44.10
13.605	42.489	1	12	29		55.4	1.6	26.40
13.727	42.489	1	4	33		65.3	2	32.30
12.508	42.58	1	15	69		35.5	3.1	33.50
12.63	42.58	4	42	33.96	15.12	35.7	3.1	1.74
12.996	42.581	1	15	26		42.1	2	16.10
13.118	42.581	1	18	40		45.4	1.7	5.40
13.24	42.581	5	41	74.13	29.66	48.9	1.7	25.23
13.362	42.581	4	56	55.56	9.20	59.6	1.4	4.04
12.507	42.67	2	17	54.92	2.47	35.2	4.3	19.72
12.63	42.671	1	8	52		38.1	2.8	13.90
12.996	42.671	1	5	50		49.3	1.7	0.70

13.118	42.671	9	129	48.88	8.36	49.6	1.5	0.72
13.24	42.671	5	46	62.77	24.04	53.9	1.3	8.87
13.362	42.671	2	10	59.93	8.84	58.4	1.5	1.53
12.384	42.76	3	35	55.26	6.23	40.2	3.4	15.06
12.507	42.76	1	8	59		48.5	4.4	10.50
12.996	42.761	1	9	48		48.7	1.5	0.70
13.118	42.761	9	90	54.49	15.63	53	1.2	1.49
13.241	42.761	8	177	57.74	13.36	56	1.5	1.74
12.506	42.85	3	28	37.8	9.68	51.7	3.3	13.90
13.119	42.851	4	40	55.86	9.31	55.9	1.2	0.04
13.241	42.851	19	282	53.43	14.37	59.9	1.5	6.47
12.383	42.94	1	8	69		58.3	3.7	10.70
12.873	42.942	2	19	38.66	10.62	56	1.4	17.34
12.996	42.942	5	47	44.44	9.53	57.3	1.2	12.86
13.119	42.942	5	33	51.07	6.36	59.9	1.4	8.83
13.241	42.941	6	42	54.07	17.37	60.3	1.5	6.23
12.382	43.03	1	8	69		61.6	3.1	7.40
12.873	43.032	5	34	54.81	12.51	60.2	1.6	5.39
12.996	43.032	1	10	31		62.3	1.3	31.30
13.119	43.032	2	11	46.14	7.16	64.1	1.6	17.96
13.242	43.031	1	9	79		64.2	1.6	14.80
12.873	43.122	1	8	50		63	1.4	13.00
11.641	43.204	1	3	48		48.6	2.8	0.60
12.257	43.21	2	13	38.66	8.36	107.9	50.7	69.24
12.38	43.21	4	41	44.23	4.48	132.9	11.6	88.67
12.256	43.3	3	25	68.02	13.27	12.9	4.5	55.12
12.379	43.3	3	34	33.71	14.69	24.2	5	9.51
12.626	43.301	2	48	46.19	1.99	58.4	1.7	12.21
13.119	43.302	1	8	60		70.6	2.2	10.60
12.378	43.391	1	12	34		38.4	2.8	4.40

12.502	43.391	2	25	49.98	3.46	49	1.7	0.98
12.625	43.392	3	64	44.53	1.95	60.2	1.9	15.67
12.996	43.392	1	9	55		66.1	2.1	11.10
13.12	43.392	2	17	57.03	2.46	69.6	3.7	12.57
12.13	43.479	1	16	49		27.4	2.3	21.60
12.129	43.569	2	22	39.02	7.12	28.4	1.9	10.62
12	43.838	1	7	50		39.6	1.6	10.40
11.75	43.926	2	18	23.35	18.58	36.2	1.5	12.85
11.874	43.927	1	12	48		40.7	1.5	7.30
11.999	43.929	2	13	88.88	35.23	45.4	1.5	43.48
11.373	44.012	2	15	43.53	7.54	38.2	1.9	5.33
11.498	44.013	2	23	27.11	6.07	33.3	2	6.19
11.748	44.016	2	18	26.36	18.60	36.5	1.7	10.14
10.247	44.081	1	16	50		50.3	2.4	0.30
10.372	44.084	2	16	70		50.4	2.6	19.60
11.121	44.098	2	17	5.88	17.56	27.1	1.7	21.22
11.371	44.102	1	7	51		37	1.9	14.00
10.118	44.168	1	7	13		49.6	3.3	36.60
10.243	44.171	2	23	25.71	18.31	46.3	2.4	20.59
10.368	44.174	2	16	73.88	2.09	48.3	2.4	25.58
10.743	44.182	3	27	119.89	10.95	31	2.4	88.89
10.868	44.184	1	8	124		29.8	1.8	85.80
11.118	44.188	1	13	164		33.4	1.9	49.40
9.863	44.252	2	16	44.69	19.49	42.9	4.1	1.79
9.988	44.255	1	9	31		44.3	3.9	13.30
10.615	44.269	4	42	38.2	4.74	32	2.5	6.20
10.74	44.272	3	33	90.78	43.20	29.2	2	61.58
9.733	44.338	1	5	64		34.8	3.4	29.20
9.859	44.342	4	31	63.4	5.24	40.8	3.4	22.60
9.984	44.345	3	27	39	19.38	45.1	3.4	6.10

10.109	44.348	1	9	9		41.5	2.7	32.50
10.611	44.359	2	18	35.8	4.00	41.8	3.7	6.00
11.364	44.372	1	15	56		91.4	4	35.40
11.489	44.373	1	15	56		101	3	45.00
9.854	44.432	1	5	32		43.8	3.1	11.80
9.979	44.435	2	14	45.5	14.80	44.8	3.1	0.70

8.3.2. Table – Stress2GRID results – Geological (SS) vs Seismological strain (FM)

Lon	*Lat*	*ε_{Hmax} FM*	*STD ε_{Hmax} FM*	*Depth min FM*	*Depth max FM*	*Mw min FM*	*Mw max FM*	*NUM FM*	*SS count*	*FSP count*	*ε_{Hmax} SS*	*STD ε_{Hmax} SS*	*ε_{Hmax} angular diff.*
9.854	44.432	20.00		5.1	10	4.3	5.4	4	1	5	32.00		12.00
10.118	44.168	16.76	8.24	5.1	10	4.3	5.4	4	1	7	13.00		3.76
10.243	44.171	13.09	6.51	5.1	10	4.3	5.4	4	2	23	25.71	18.31	12.62
10.74	44.272	58.00		10	10	4.2	4.6	2	3	33	90.78	43.20	32.78
11.121	44.098	53.47	9.49	5	7	4.2	4.9	2	2	17	5.88	17.56	47.59
11.373	44.012	26.00		5	10	4.2	4.7	3	2	15	43.53	7.54	17.53
11.489	44.373	61.00		8	9	3.44	4.94	2	1	15	56.00		5.00
11.498	44.013	19.44	4.38	8	9	3.44	4.94	2	2	23	27.11	6.07	7.67
11.748	44.016	16.00		6	15	3.41	4.2	5	2	18	26.36	18.60	10.36
11.75	43.926	29.85	1.82	6	15	3.41	4.2	5	2	18	23.35	18.58	6.50
11.874	43.927	35.17	12.50	6	15	3.41	4.6	8	1	12	48.00		12.83
11.999	43.929	56.69	16.33	5	7	3.74	4.6	4	2	13	88.88	35.23	32.19
12	43.838	43.11	14.49	5	7	4	4.6	4	1	7	50.00		6.89
12.129	43.569	67.41	12.20	10	10	4.4	4.7	2	2	22	39.02	7.12	28.39
12.379	43.3	51.32	2.27	3	9	3.17	4.46	4	3	34	33.71	14.69	17.61
12.38	43.21	51.05	2.49	3	9	3.17	4.46	4	4	41	44.23	4.48	6.82
12.502	43.391	39.10	1.38	9	10	3.9	4.2	2	2	25	49.98	3.46	10.88
12.507	42.67	95.00		8	10	3.37	4.2	3	2	17	54.92	2.47	40.08
12.508	42.58	95.00		8	10	3.37	4.2	3	1	15	69.00		26.00

12.625	43.392	37.41	2.02	8	10	3.4	4.2	3	3	64	44.53	1.95	7.12
12.626	43.301	41.18	12.98	8	14	3.4	5.6	4	2	48	46.19	1.99	5.01
12.63	42.58	173.00		8	10	3.37	4.2	3	4	42	33.96	15.12	40.96
12.63	42.671	178.79	9.48	8	10	3.37	4.2	3	1	8	52.00		53.21
12.873	42.942	41.02	9.38	10	11.6	3.9	5.6	20	2	19	38.66	10.62	2.36
12.873	43.122	57.94	11.41	2.6	10	3.15	5.9	7	1	8	50.00		7.94
12.873	43.032	46.30	10.49	5.5	11.6	3.15	5.9	17	5	34	54.81	12.51	8.51
12.874	42.401	15.07	13.67	10	10	4.2	4.4	2	1	2	83.00		67.93
12.996	42.671	52.00		5	16	3.26	5.8	14	1	5	50.00		2.00
12.996	42.942	55.90	15.81	7	10	3.23	5.85	34	5	47	44.44	9.53	11.46
12.996	42.311	27.00		10	10	4.2	4.4	2	3	22	40.94	7.79	13.94
12.996	42.401	12.24	13.71	10	10	4.2	4.4	2	1	23	28.00		15.76
12.996	42.761	74.45	21.63	5	16	3.26	5.8	14	1	9	48.00		26.45
12.996	43.032	58.29	10.59	7	10.2	3.05	5.6	33	1	10	31.00		27.29
12.996	42.491	180.00		10	10	4.2	4.4	2	1	23	28.00		28.00
12.996	43.392	88.00		8	8	3.3	4.57	8	1	9	55.00		33.00
13.118	42.761	65.71	20.49	6	16	3.03	6.5	72	9	90	54.49	15.63	11.22
13.118	42.671	63.30	8.56	8	13	3.14	5.96	25	9	129	48.88	8.36	14.42
13.118	42.581	60.89	4.06	10	12	3.32	4.2	6	1	18	40.00		20.89
13.119	42.851	64.40	19.06	6	16	3.06	6.5	65	4	40	55.86	9.31	8.54
13.119	43.032	58.30	11.00	7	9	3.05	4.8	33	2	11	46.14	7.16	12.16
13.119	42.942	66.48	13.00	7	11	3.05	5.85	46	5	33	51.07	6.36	15.41
13.12	43.392	88.00		8	8	3.6	4.57	4	2	17	57.03	2.46	30.97
13.238	42.13	50.00		10	10	4.4	6.3	2	3	15	58.48	27.22	8.48
13.238	42.04	50.00		17	17	4.08	4.3	2	3	17	20.48	24.25	29.52
13.239	42.31	52.11	4.97	10	10	4.4	6.3	2	1	8	44.00		8.11
13.239	42.401	62.60	10.11	9	14	3.35	5.02	12	8	86	35.60	10.10	27.00
13.24	42.671	60.68	11.60	7	13	3.12	5.96	57	5	46	62.77	24.04	2.09
13.24	42.491	58.34	9.12	9	15	3.27	5.49	23	9	113	43.04	14.48	15.30
13.24	42.581	58.61	9.06	7	14	3.12	5.49	51	5	41	74.13	29.66	15.52

13.241	42.761	64.87	20.73	6	13	3.03	5.96	52	8	177	57.74	13.36	7.13
13.241	42.941	65.31	9.34	7	11	3.1	3.81	14	6	42	54.07	17.37	11.24
13.241	42.851	65.79	21.43	6	13	3.06	5.38	39	19	282	53.43	14.37	12.36
13.242	43.031	61.29	4.69	7	9	3.3	3.86	3	1	9	79.00		17.71
13.359	42.13	50.00		10	15	3.46	5.5	5	3	34	22.93	16.99	27.07
13.359	42.04	50.00		17	17	4.08	4.3	2	3	44	17.40	11.94	32.60
13.36	42.31	61.90	13.69	9	15	3.46	6.3	14	5	36	50.26	9.55	11.64
13.36	42.22	59.42	1.96	9	15	3.46	6.3	14	6	67	44.44	7.66	14.98
13.361	42.49	53.46	12.90	9	17	3.27	5.49	34	7	89	40.94	14.79	12.52
13.361	42.4	58.75	15.09	9	15	3.35	6.3	22	11	104	39.33	12.54	19.42
13.362	42.581	56.92	11.25	7	17	3.12	5.49	37	4	56	55.56	9.20	1.36
13.362	42.671	56.45	13.34	7	13	3.12	4.76	20	2	10	59.93	8.84	3.48
13.478	41.859	47.00		17	17	4.08	4.3	2	2	38	56.50	1.50	9.50
13.479	41.949	44.54	1.15	17	17	4.08	4.3	2	3	29	49.65	6.17	5.11
13.48	42.039	44.00		17	17	4.08	4.3	2	7	50	165.34	16.59	58.66
13.481	42.219	52.62	7.18	10	15	3.46	5.5	5	6	65	39.38	6.18	13.24
13.482	42.31	60.52	15.56	10	15	3.46	5.5	8	4	32	33.27	14.29	27.25
13.483	42.49	31.74	22.86	10	10	3.9	4.3	2	2	10	14.00		17.74
13.483	42.4	66.65	20.23	10	10	4	5.2	4	9	60	30.02	13.82	36.63
13.598	41.768	53.87	3.52	11	16	3.42	4.9	3	1	8	40.00		13.87
13.599	41.858	40.51	15.65	10	17	4.08	4.43	3	2	37	46.24	8.02	5.73
13.6	41.948	45.00	0.82	10	17	4.08	6.6	3	3	26	39.89	2.93	5.11
13.601	42.039	44.57	0.50	10	17	4.3	6.6	2	7	46	31.88	34.17	12.69
13.602	42.219	47.00		10	15	3.46	5.5	5	3	15	24.99	10.08	22.01
13.719	41.767	41.18	13.90	8	16	3.42	4.9	3	2	21	49.45	10.09	8.27
13.72	41.858	19.96	7.81	8	10	4.4	4.9	2	3	26	46.92	23.25	26.96
13.721	41.948	24.14	17.78	10	10	4.4	6.6	2	9	101	47.89	14.00	23.75
13.839	41.767	45.86	14.59	5	10	4.7	5.8	3	2	25	35.63	7.49	10.23
13.84	41.857	23.94	21.33	8	17	4.8	5.4	3	5	55	45.62	13.27	21.68
13.954	41.405	61.00		5	10	4.7	4.7	2	2	23	22.71	7.50	38.29

13.955	41.495	61.00		5	10	4.7	4.7	2	5	68	32.15	8.30	28.85
13.959	41.766	42.49	23.25	10	17	4.7	5.8	4	2	23	30.57	8.74	11.92
14.431	41.31	35.17	6.02	11	11	4.3	5.1	2	1	7	78.00		42.83
14.553	41.398	29.48	6.74	10	11	4.3	5.1	3	1	12	7.00		22.48
14.555	41.489	38.76	6.41	10	11	3.64	4.25	2	2	20	178.61	9.52	40.15
15.015	40.85	38.00		10	10	4.9	5	2	4	17	34.87	19.25	3.13
15.017	40.94	67.00		10	15	4.9	5.2	3	4	6	26.55	35.73	40.45
15.133	40.848	38.00		10	10	4.9	5	2	5	60	26.24	23.26	11.76
15.159	38.054	134.00		9	12	3.4	4.5	3	6	21	111.00	44.40	23.00
15.162	38.144	120.68	13.30	9	12	3.4	4.5	3	4	14	117.82	6.99	2.86
15.249	40.756	42.00		10	10	4.9	5	2	3	60	18.18	48.02	23.82
15.252	40.846	52.35	5.96	10	10	4.9	5	2	3	50	40.74	17.75	11.61
15.276	38.141	120.11	7.64	9	10	3.4	4.3	2	1	6	124.00		3.89
15.361	40.573	20.00		5	10	3.14	5.3	4	6	41	13.51	18.92	6.49
15.364	40.663	26.49	10.24	5	10	3.14	5.3	4	14	177	12.60	36.31	13.89
15.367	40.753	36.88	6.13	5	14	3.14	5.3	5	7	86	17.48	20.62	19.40
15.371	40.843	40.85	4.84	10	10	4.9	6.8	3	1	1	13.00		27.85
15.387	38.049	101.00		9	10	3.4	4.3	2	1	6	68.00		33.00
15.39	38.139	101.00		9	10	3.4	4.3	2	2	42	131.79	17.89	30.79
15.482	40.66	41.76	13.28	5	10	3.33	5.3	5	17	101	34.56	18.49	7.20
15.486	40.751	46.76	6.08	5	10	3.14	4.9	5	7	36	11.64	10.82	35.12
15.489	40.841	48.00		5	10	3.14	4.9	5	3	12	10.62	2.94	37.38
15.504	38.136	101.00		8	17	3.37	3.72	2	2	28	150.06	7.85	49.06
15.601	40.658	44.00		10	10	4.3	4.9	2	5	36	38.64	9.10	5.36
15.604	40.748	45.14	1.81	10	10	4.3	4.9	2	3	3	39.98	26.55	5.16
15.704	40.295	52.00		10	10	4.7	5.6	2	11	73	54.35	22.29	2.35
15.708	40.385	52.00		10	10	4.7	5.6	2	12	71	48.79	33.21	3.21
15.732	38.131	3.05	33.14	8	17	3.37	3.72	2	2	10	117.95	8.05	65.10
15.735	38.221	96.00		8	17	3.37	3.72	2	3	20	130.84	10.29	34.84
15.739	38.311	150.00		8	17	3.37	3.72	2	1	4	152.00		2.00

15.81	40.021	131.00		10	10	4.6	5.6	3	11	362	58.38	31.99	72.62
15.818	40.202	39.00		10	10	4.7	5.6	2	4	11	42.58	4.98	3.58
15.822	40.292	39.00		10	10	4.7	5.6	2	12	118	43.39	14.91	4.39
15.849	38.218	97.12	35.15	8	17	3.37	3.72	2	4	60	149.57	15.18	52.45
15.919	39.838	68.00		10	15	4.6	5.3	2	10	34	90.27	12.57	22.27
15.923	39.928	117.43	30.84	10	15	4.6	5.3	2	10	33	86.31	8.88	31.12
15.927	40.018	89.86	64.11	10	10	4.6	5.6	3	9	93	18.51	29.46	71.35
15.931	40.108	52.03	4.90	10	10	4.7	5.6	2	4	63	70.15	15.64	18.12
15.935	40.199	39.00		10	10	4.7	5.6	2	3	21	63.63	21.14	24.63
15.939	40.289	39.00		10	10	4.7	5.6	2	7	67	48.93	22.79	9.93
15.963	38.215	150.00		8	17	3.37	3.72	2	5	39	121.80	6.94	28.20
16.024	39.565	116.00		9	10	4.26	4.6	2	6	42	95.61	25.48	20.39
16.036	39.835	65.98	4.28	3	15	4.3	5.3	3	11	98	31.69	44.93	34.29
16.04	39.925	63.40	5.44	10	15	4.3	5.3	2	13	129	93.97	31.15	30.57
16.045	40.015	48.16	5.35	10	10	4.7	5.6	2	4	71	40.70	29.93	7.46
16.049	40.105	55.00		10	10	4.7	5.6	2	1	26	83.00		28.00
16.09	38.481	139.67	3.30	10	15	3.39	3.66	2	2	9	108.81	26.02	30.86
16.127	39.292	113.33	14.56	10	12	4.4	4.6	2	10	126	95.62	23.79	17.71
16.132	39.382	118.90	12.18	9	10	4.26	4.6	2	9	121	107.05	16.20	11.85
16.153	39.832	65.82	4.41	3	10	4.3	4.4	2	14	75	106.22	51.79	40.40
16.157	39.922	61.58	5.44	3	10	4.3	4.4	2	23	164	149.62	56.61	88.04
16.209	38.568	137.12	3.22	10	15	3.39	3.66	2	5	8	144.57	24.85	7.45
16.217	38.748	121.00		10	15	4.1	6.8	2	1	4	124.00		3.00
16.221	38.838	133.83	21.33	10	15	4.1	6.8	2	2	18	118.19	3.00	15.64
16.243	39.288	105.99	14.12	9	12	4.26	4.6	3	6	86	107.94	14.43	1.95
16.248	39.378	104.70	13.64	9	12	4.26	4.6	3	5	42	78.78	14.33	25.92
16.355	39.195	102.00		11	15	3.52	4.5	2	6	87	93.76	5.44	8.24
16.359	39.285	99.54	1.15	11	15	3.52	4.5	2	8	100	95.49	11.85	4.05
16.364	39.375	99.00		11	15	3.52	4.5	2	8	91	105.38	28.18	6.38
16.576	39.007	115.00		8	10	3.83	4.3	3	2	14	162.00		47.00

8.3.3. Table – Stress2GRID results – Geodetic (GPS) vs Seismological strain (FMS)

Lon	*Lat*	*ε_{Hmax} FM*	*STD ε_{Hmax} FM*	*Depth min*	*Depth max*	*Mw min*	*Mw max*	*NUM FM*	*ε_{Hmax} azi*	*dazi ε_{Hmax}*	*ε_{Hmax} angular diff.*
14.695	37.702	163.00		5	10	3.44	4.6	3	172.10	1.70	9.10
14.808	37.7	163.00		5	10	3.44	4.6	3	138.90	1.90	24.10
14.13	37.799	7.00		6	6	3.34	3.53	2	17.50	0.90	10.50
14.244	37.798	8.73	4.24	6	6	3.34	3.53	2	16.70	0.90	7.97
14.357	37.797	19.00		5	8	3.44	4.6	4	11.00	0.70	8.00
14.47	37.795	0.98	8.48	5	10	3.44	4.6	3	10.30	0.80	9.32
14.584	37.794	163.00		5	10	3.44	4.6	3	8.00	0.90	25.00
14.697	37.792	3.72	14.26	5	10	3.44	4.6	3	176.30	1.10	7.42
14.811	37.79	13.00		7.4	7.5	4	4.7	2	165.80	1.50	27.20
14.245	37.888	7.00		6	6	3.34	3.53	2	12.80	1.00	5.80
14.359	37.887	8.79	6.26	5	8	3.44	4.6	4	16.00	1.20	7.21
14.472	37.885	3.91	6.16	5	10	3.44	4.6	4	10.30	0.80	6.39
14.586	37.884	163.00		5	10	3.44	4.6	4	9.30	0.80	26.30
14.813	37.88	13.00		7.4	7.5	4	4.7	2	163.20	0.90	29.80
14.474	37.975	5.00		5	10	3.44	4.6	4	15.60	1.10	10.60
14.702	37.972	180.00		7.4	7.5	4	4.7	2	173.90	1.50	6.10
14.815	37.97	180.00		7.4	7.5	4	4.7	2	166.50	1.50	13.50
14.704	38.062	176.00		7.4	7.5	4	4.7	2	87.10	3.90	88.90
14.818	38.06	177.59	1.96	7.4	7.5	4	4.7	2	117.40	4.80	60.19
15.159	38.054	134.00		9	12	3.4	4.5	3	123.30	1.10	10.70
15.387	38.049	101.00		9	10	3.4	4.3	2	130.40	1.20	29.40
15.956	38.035	143.00		8	14	3.37	3.91	2	129.00	2.40	14.00
16.069	38.032	143.00		8	14	3.37	3.91	2	124.60	2.20	18.40
14.82	38.15	137.22	0.97	10	10	4.6	4.7	2	92.70	1.10	44.52
14.934	38.148	137.04	1.00	10	10	4.6	4.7	2	101.50	1.00	35.54
15.162	38.144	120.68	13.30	9	12	3.4	4.5	3	116.10	0.80	4.58

15.276	38.141	120.11	7.64	9	10	3.4	4.3	2	117.10	0.90	3.01
15.39	38.139	101.00		9	10	3.4	4.3	2	130.00	0.90	29.00
15.504	38.136	101.00		8	17	3.37	3.72	2	131.40	1.20	30.40
15.732	38.131	3.05	33.14	8	17	3.37	3.72	2	130.50	1.60	52.55
15.846	38.128	179.39	12.21	8	14	3.37	3.91	2	125.60	1.80	53.79
15.959	38.125	150.00		8	14	3.37	3.91	2	127.90	2.20	22.10
16.073	38.122	143.00		8	14	3.37	3.91	2	123.90	2.70	19.10
14.937	38.238	136.00		10	10	4.6	4.7	2	96.10	0.80	39.90
15.165	38.234	99.51	5.06	9	12	4.3	4.5	2	111.70	0.70	12.19
15.279	38.231	98.00		9	10	3.4	4.3	2	118.10	0.80	20.10
15.735	38.221	96.00		8	17	3.37	3.72	2	127.30	1.40	31.30
15.849	38.218	97.12	35.15	8	17	3.37	3.72	2	125.00	1.40	27.88
15.963	38.215	150.00		8	17	3.37	3.72	2	122.30	1.80	27.70
15.739	38.311	150.00		8	17	3.37	3.72	2	119.50	1.20	30.50
15.628	38.403	150.00		8	17	3.37	3.72	2	110.50	1.00	39.50
15.743	38.401	150.00		8	17	3.37	3.72	2	111.70	1.20	38.30
16.314	38.385	140.00		10	15	3.39	3.66	2	104.90	3.20	35.10
16.429	38.381	140.00		10	15	3.39	3.66	2	109.60	2.80	30.40
16.09	38.481	139.67	3.30	10	15	3.39	3.66	2	104.10	3.10	35.57
16.204	38.478	138.44	3.50	10	15	3.39	3.66	2	105.30	3.10	33.14
16.319	38.475	140.00		10	15	3.39	3.66	2	107.60	3.60	32.40
16.094	38.571	138.45	3.50	10	15	3.39	3.66	2	104.00	3.30	34.45
16.209	38.568	137.12	3.22	10	15	3.39	3.66	2	109.60	3.60	27.52
15.065	38.686	162.00		9	12	4.3	4.5	2	95.90	1.30	66.10
15.18	38.684	162.00		9	12	4.3	4.5	2	101.80	1.20	60.20
14.952	38.778	148.00		9	12	4.3	4.5	2	96.30	0.90	51.70
15.067	38.776	162.00		9	12	4.3	4.5	2	95.20	0.90	66.80
15.182	38.774	162.00		9	12	4.3	4.5	2	100.60	2.50	61.40
15.757	38.761	63.00		10	15	4.1	6.8	2	103.90	1.50	40.90
15.872	38.758	63.00		10	15	4.1	6.8	2	106.50	1.50	43.50

15.987	38.755	142.00		10	15	4.1	6.8	2	108.30	1.90	33.70
16.102	38.751	139.08	22.92	10	15	4.1	6.8	2	116.40	3.50	22.68
16.217	38.748	121.00		10	15	4.1	6.8	2	125.10	5.50	4.10
14.955	38.868	148.00		9	12	4.3	4.5	2	97.60	0.90	50.40
15.761	38.851	63.00		7	15	4.1	6.8	3	103.00	1.40	40.00
15.876	38.848	63.00		7	15	4.1	6.8	3	106.60	1.50	43.60
15.991	38.845	142.00		7	15	4.1	6.8	3	109.00	1.90	33.00
16.106	38.841	149.41	17.44	7	15	4.1	6.8	3	112.70	3.50	36.71
16.221	38.838	133.83	21.33	10	15	4.1	6.8	2	129.10	5.10	4.73
16.576	39.007	115.00		8	10	3.83	4.3	3	100.10	2.10	14.90
16.692	39.004	115.00		8	10	3.83	4.3	3	98.50	1.80	16.50
16.581	39.097	82.56	28.40	8	10	3.83	4.3	3	98.70	2.80	16.14
16.697	39.094	96.14	26.04	8	10	3.83	4.3	3	95.30	2.30	0.84
17.158	39.077	180.00		8	10	3.83	4.3	3	113.90	1.20	66.10
17.274	39.073	180.00		8	10	3.83	4.3	3	117.30	1.40	62.70
16.355	39.195	102.00		11	15	3.52	4.5	2	103.40	5.00	1.40
16.47	39.191	102.00		10	10	4.2	4.3	2	104.50	3.40	2.50
16.586	39.187	101.25	19.49	10	10	4.2	4.3	2	100.90	2.60	0.35
16.702	39.184	109.00		8	10	3.83	4.3	3	99.30	2.60	9.70
17.048	39.171	176.00		8	10	3.83	4.3	3	107.50	1.30	68.50
17.164	39.167	176.00		8	10	3.83	4.3	3	115.80	0.50	60.20
17.28	39.163	180.00		8	10	3.83	4.3	3	125.00	1.20	55.00
16.127	39.292	113.33	14.56	10	12	4.4	4.6	2	95.10	4.90	18.23
16.243	39.288	105.99	14.12	9	12	4.26	4.6	3	95.40	5.20	10.59
16.359	39.285	99.54	1.15	11	15	3.52	4.5	2	105.80	4.50	6.26
16.475	39.281	101.33	1.25	11	15	3.52	4.5	2	104.70	3.70	3.37
17.054	39.261	176.00		8	10	3.83	4.3	3	109.60	1.10	66.40
17.17	39.257	176.00		5	14	3.62	4.8	2	117.90	0.60	58.10
15.203	39.404	105.00		10	15	4.6	5.3	2	87.70	0.90	17.30
16.132	39.382	118.90	12.18	9	10	4.26	4.6	2	84.30	5.60	34.60

16.248	39.378	104.70	13.64	9	12	4.26	4.6	3	99.20	6.30	5.50
16.364	39.375	99.00		11	15	3.52	4.5	2	102.20	5.50	3.20
15.206	39.494	105.00		10	15	4.6	5.3	2	86.40	1.10	18.60
15.904	39.478	116.00		9	10	4.26	4.6	2	79.70	3.00	36.30
16.02	39.475	116.00		9	10	4.26	4.6	2	77.00	6.40	39.00
16.024	39.565	116.00		9	10	4.26	4.6	2	82.20	7.30	33.80
16.727	39.634	167.00		5	14	3.62	4.8	2	104.50	3.60	62.50
16.843	39.63	162.96	4.92	5	14	3.62	4.8	2	105.00	2.90	57.96
16.732	39.724	157.00		5	14	3.62	4.8	2	104.40	3.10	52.60
16.848	39.72	157.92	2.90	5	14	3.62	4.8	2	105.60	2.70	52.32
15.919	39.838	68.00		10	15	4.6	5.3	2	50.40	6.00	17.60
16.036	39.835	65.98	4.28	3	15	4.3	5.3	3	50.90	5.40	15.08
16.153	39.832	65.82	4.41	3	10	4.3	4.4	2	55.20	4.70	10.62
15.923	39.928	117.43	30.84	10	15	4.6	5.3	2	39.40	4.90	78.03
16.04	39.925	63.40	5.44	10	15	4.3	5.3	2	42.90	4.00	20.50
16.157	39.922	61.58	5.44	3	10	4.3	4.4	2	52.50	3.80	9.08
15.81	40.021	131.00		10	10	4.6	5.6	3	39.30	2.40	88.30
15.927	40.018	89.86	64.11	10	10	4.6	5.6	3	39.10	3.40	50.76
16.045	40.015	48.16	5.35	10	10	4.7	5.6	2	40.80	3.60	7.36
15.931	40.108	52.03	4.90	10	10	4.7	5.6	2	39.20	2.70	12.83
16.049	40.105	55.00		10	10	4.7	5.6	2	28.80	3.60	26.20
15.818	40.202	39.00		10	10	4.7	5.6	2	56.40	3.10	17.40
15.935	40.199	39.00		10	10	4.7	5.6	2	42.70	3.60	3.70
15.704	40.295	52.00		10	10	4.7	5.6	2	57.30	1.90	5.30
15.822	40.292	39.00		10	10	4.7	5.6	2	54.60	4.00	15.60
15.939	40.289	39.00		10	10	4.7	5.6	2	53.80	10.80	14.80
15.708	40.385	52.00		10	10	4.7	5.6	2	60.60	1.80	8.60
15.361	40.573	20.00		5	10	3.14	5.3	4	68.90	2.90	48.90
15.364	40.663	26.49	10.24	5	10	3.14	5.3	4	55.10	1.70	28.61
15.482	40.66	41.76	13.28	5	10	3.33	5.3	5	50.40	1.60	8.64

15.601	40.658	44.00		10	10	4.3	4.9	2	46.40	1.50	2.40
15.249	40.756	42.00		10	10	4.9	5	2	64.50	1.10	22.50
15.367	40.753	36.88	6.13	5	14	3.14	5.3	5	54.30	1.30	17.42
15.486	40.751	46.76	6.08	5	10	3.14	4.9	5	48.60	1.40	1.84
15.604	40.748	45.14	1.81	10	10	4.3	4.9	2	44.20	1.70	0.94
15.015	40.85	38.00		10	10	4.9	5	2	62.70	1.30	24.70
15.133	40.848	38.00		10	10	4.9	5	2	63.10	1.10	25.10
15.252	40.846	52.35	5.96	10	10	4.9	5	2	54.80	1.20	2.45
15.371	40.843	40.85	4.84	10	10	4.9	6.8	3	52.40	1.20	11.55
15.489	40.841	48.00		5	10	3.14	4.9	5	48.00	1.40	0.00
15.017	40.94	67.00		10	15	4.9	5.2	3	51.70	2.30	15.30
15.136	40.938	38.00		10	15	4.9	5.2	3	52.20	1.30	14.20
15.255	40.936	50.61	8.90	10	15	4.9	5.2	3	51.70	1.20	1.09
15.374	40.933	38.92	11.39	10	15	4.5	6.8	4	48.70	1.40	9.78
15.493	40.931	62.00		10	15	4.5	6.8	4	50.00	1.80	12.00
14.901	41.032	67.00		10	15	4.9	5.2	3	50.00	2.20	17.00
15.02	41.03	67.00		10	15	4.9	5.2	3	48.70	2.00	18.30
15.377	41.023	27.00		10	15	4.5	6.8	4	50.80	1.50	23.80
15.496	41.021	62.00		10	15	4.5	6.8	4	55.30	1.90	6.70
13.953	41.315	54.00		5	10	4.7	4.7	2	50.80	1.60	3.20
14.072	41.314	54.00		11	11	4.3	5.1	2	54.60	1.70	0.60
14.431	41.31	35.17	6.02	11	11	4.3	5.1	2	51.50	3.50	16.33
13.954	41.405	61.00		5	10	4.7	4.7	2	50.40	1.40	10.60
14.433	41.4	36.32	5.88	11	11	4.3	5.1	2	45.60	2.60	9.28
14.553	41.398	29.48	6.74	10	11	4.3	5.1	3	47.00	2.10	17.52
14.672	41.397	25.00		10	11	3.64	4.25	2	46.60	1.80	21.60
13.955	41.495	61.00		5	10	4.7	4.7	2	50.60	1.60	10.40
14.555	41.489	38.76	6.41	10	11	3.64	4.25	2	43.70	2.20	4.94
14.675	41.487	38.12	6.50	10	11	3.64	4.25	2	53.70	2.00	15.58
13.717	41.587	61.00		11	16	3.42	4.9	2	53.80	2.40	7.20

13.837	41.586	61.00		5	10	4.7	4.7	2	53.00	2.00	8.00
14.557	41.579	38.14	6.50	10	11	3.64	4.25	2	52.10	2.70	13.96
14.677	41.577	37.29	6.52	10	11	3.64	4.25	2	62.10	3.00	24.81
13.477	41.679	58.00		11	16	3.42	4.9	2	48.10	3.30	9.90
13.597	41.678	57.60	0.80	11	16	3.42	4.9	2	49.90	2.80	7.70
13.838	41.676	55.62	14.90	5	10	4.7	4.7	2	53.50	1.90	2.12
13.958	41.676	64.00		10	17	4.7	5.8	4	51.90	2.10	12.10
12.755	41.769	44.00		10	10	4.2	4.4	2	124.60	8.00	80.60
13.598	41.768	53.87	3.52	11	16	3.42	4.9	3	52.90	3.10	0.97
13.719	41.767	41.18	13.90	8	16	3.42	4.9	3	52.40	2.10	11.22
13.839	41.767	45.86	14.59	5	10	4.7	5.8	3	50.30	2.00	4.44
13.959	41.766	42.49	23.25	10	17	4.7	5.8	4	51.20	1.50	8.71
15.284	41.747	36.00		10	11	3.64	4.25	2	34.40	2.00	1.60
15.404	41.744	36.00		10	11	3.64	4.25	2	39.20	2.40	3.20
12.755	41.86	44.00		10	10	4.2	4.4	2	132.90	9.10	88.90
12.875	41.86	44.00		10	10	4.2	4.4	2	138.00	7.80	86.00
13.478	41.859	47.00		17	17	4.08	4.3	2	49.60	2.40	2.60
13.599	41.858	40.51	15.65	10	17	4.08	4.43	3	54.00	2.50	13.49
13.72	41.858	19.96	7.81	8	10	4.4	4.9	2	56.40	2.00	36.44
13.84	41.857	23.94	21.33	8	17	4.8	5.4	3	54.50	2.10	30.56
13.961	41.856	30.80	28.21	13	17	4.8	5.4	2	52.70	1.70	21.90
12.875	41.95	167.00		10	10	4.2	4.4	2	129.10	11.00	37.90
12.996	41.95	167.00		10	10	4.4	6.3	2	64.20	11.00	77.20
13.479	41.949	44.54	1.15	17	17	4.08	4.3	2	51.50	3.10	6.96
13.6	41.948	45.00	0.82	10	17	4.08	6.6	3	57.80	2.70	12.80
13.721	41.948	24.14	17.78	10	10	4.4	6.6	2	61.60	2.00	37.46
13.238	42.04	50.00		17	17	4.08	4.3	2	47.80	2.10	2.20
13.359	42.04	50.00		17	17	4.08	4.3	2	48.00	2.20	2.00
13.48	42.039	44.00		17	17	4.08	4.3	2	55.20	1.50	11.20
13.601	42.039	44.57	0.50	10	17	4.3	6.6	2	59.70	1.50	15.13

13.238	42.13	50.00		10	10	4.4	6.3	2	46.60	2.00	3.40
13.359	42.13	50.00		10	15	3.46	5.5	5	54.50	1.70	4.50
13.36	42.22	59.42	1.96	9	15	3.46	6.3	14	56.30	1.80	3.12
13.481	42.219	52.62	7.18	10	15	3.46	5.5	5	63.70	1.50	11.08
13.602	42.219	47.00		10	15	3.46	5.5	5	65.40	1.30	18.40
11.66	42.303	32.00		8	10	3.37	4.2	3	33.50	3.80	1.50
11.782	42.304	32.00		8	10	3.37	4.2	3	55.30	6.80	23.30
12.996	42.311	27.00		10	10	4.2	4.4	2	47.90	2.30	20.90
13.239	42.31	52.11	4.97	10	10	4.4	6.3	2	44.00	2.00	8.11
13.36	42.31	61.90	13.69	9	15	3.46	6.3	14	45.50	2.80	16.40
13.482	42.31	60.52	15.56	10	15	3.46	5.5	8	56.40	1.90	4.12
11.78	42.394	32.00		8	10	3.37	4.2	3	56.70	5.20	24.70
12.874	42.401	15.07	13.67	10	10	4.2	4.4	2	45.60	2.40	30.53
12.996	42.401	12.24	13.71	10	10	4.2	4.4	2	45.80	2.40	33.56
13.239	42.401	62.60	10.11	9	14	3.35	5.02	12	41.30	1.70	21.30
13.361	42.4	58.75	15.09	9	15	3.35	6.3	22	31.90	7.40	26.85
13.483	42.4	66.65	20.23	10	10	4	5.2	4	52.20	1.80	14.45
12.996	42.491	180.00		10	10	4.2	4.4	2	41.20	1.90	41.20
13.24	42.491	58.34	9.12	9	15	3.27	5.49	23	39.80	1.60	18.54
13.361	42.49	53.46	12.90	9	17	3.27	5.49	34	58.60	2.00	5.14
13.483	42.49	31.74	22.86	10	10	3.9	4.3	2	58.10	1.70	26.36
12.386	42.579	95.00		8	10	3.37	4.2	3	41.50	3.70	53.50
12.508	42.58	95.00		8	10	3.37	4.2	3	35.50	3.10	59.50
12.63	42.58	173.00		8	10	3.37	4.2	3	35.70	3.10	42.70
13.118	42.581	60.89	4.06	10	12	3.32	4.2	6	45.40	1.70	15.49
13.24	42.581	58.61	9.06	7	14	3.12	5.49	51	48.90	1.70	9.71
13.362	42.581	56.92	11.25	7	17	3.12	5.49	37	59.60	1.40	2.68
13.484	42.58	122.00		10	10	3.9	4.3	2	60.10	1.70	61.90
13.606	42.579	122.00		10	10	3.9	4.3	2	59.30	2.10	62.70
11.897	42.666	32.00		3	9	3.17	4.46	4	37.00	3.40	5.00

12.019	42.667	32.00		8	10	3.37	4.2	3	45.10	4.00	13.10
12.385	42.67	95.00		8	10	3.37	4.2	3	43.60	3.30	51.40
12.507	42.67	95.00		8	10	3.37	4.2	3	35.20	4.30	59.80
12.63	42.671	178.79	9.48	8	10	3.37	4.2	3	38.10	2.80	39.31
12.752	42.671	179.13	9.80	8	10	3.37	4.2	3	37.10	2.20	37.97
12.996	42.671	52.00		5	16	3.26	5.8	14	49.30	1.70	2.70
13.118	42.671	63.30	8.56	8	13	3.14	5.96	25	49.60	1.50	13.70
13.24	42.671	60.68	11.60	7	13	3.12	5.96	57	53.90	1.30	6.78
13.362	42.671	56.45	13.34	7	13	3.12	4.76	20	58.40	1.50	1.95
13.485	42.67	122.00		7	13	3.12	4.76	20	59.90	1.70	62.10
11.895	42.756	32.00		3	9	3.17	4.46	4	38.30	3.50	6.30
12.017	42.757	32.00		3	9	3.17	4.46	4	40.70	5.10	8.70
12.874	42.761	73.00		5	10	4.2	5.6	15	47.80	1.50	25.20
12.996	42.761	74.45	21.63	5	16	3.26	5.8	14	48.70	1.50	25.75
13.118	42.761	65.71	20.49	6	16	3.03	6.5	72	53.00	1.20	12.71
13.241	42.761	64.87	20.73	6	13	3.03	5.96	52	56.00	1.50	8.87
13.363	42.761	68.00		8	9	3.52	3.73	2	56.10	1.50	11.90
11.649	42.844	11.00		3	9	3.17	4.46	4	32.60	2.90	21.60
11.771	42.845	11.00		3	9	3.17	4.46	4	37.90	3.60	26.90
12.629	42.851	85.00		10	11.6	3.9	4.4	4	53.10	2.70	31.90
12.751	42.851	85.00		10	11.6	3.9	4.4	4	50.00	1.60	35.00
12.874	42.851	46.71	13.99	5	10	4.2	5.6	15	50.30	1.40	3.59
12.996	42.851	56.41	21.40	5	16	3.26	6.5	31	54.60	1.40	1.81
13.119	42.851	64.40	19.06	6	16	3.06	6.5	65	55.90	1.20	8.50
13.241	42.851	65.79	21.43	6	13	3.06	5.38	39	59.90	1.50	5.89
13.364	42.851	62.96	1.00	8	9	3.52	3.73	2	59.90	1.80	3.06
11.647	42.934	11.00		3	9	3.17	4.46	4	38.60	3.30	27.60
11.769	42.935	11.00		3	9	3.17	4.46	4	44.10	4.10	33.10
12.751	42.941	40.24	9.09	10	11.6	3.9	4.4	4	56.30	1.70	16.06
12.873	42.942	41.02	9.38	10	11.6	3.9	5.6	20	56.00	1.40	14.98

12.996	42.942	55.90	15.81	7	10	3.23	5.85	34	57.30	1.20	1.40
13.119	42.942	66.48	13.00	7	11	3.05	5.85	46	59.90	1.40	6.58
13.241	42.941	65.31	9.34	7	11	3.1	3.81	14	60.30	1.50	5.01
13.364	42.941	126.00		8	9	3.52	3.73	2	61.30	2.10	64.70
13.487	42.941	126.00		8	9	3.52	3.73	2	60.80	3.30	65.20
12.75	43.031	48.48	13.04	2.6	11.6	3.9	5.9	13	57.90	1.50	9.42
12.873	43.032	46.30	10.49	5.5	11.6	3.15	5.9	17	60.20	1.60	13.90
12.996	43.032	58.29	10.59	7	10.2	3.05	5.6	33	62.30	1.30	4.01
13.119	43.032	58.30	11.00	7	9	3.05	4.8	33	64.10	1.60	5.80
13.242	43.031	61.29	4.69	7	9	3.3	3.86	3	64.20	1.60	2.91
13.365	43.031	126.00		7	9	3.3	3.86	3	61.70	2.70	64.30
13.487	43.031	126.00		8	9	3.52	3.73	2	51.20	4.60	74.80
12.504	43.121	69.26	3.94	13	16	4.6	4.6	2	55.10	2.60	14.16
12.627	43.121	66.43	4.42	8	16	4.6	5.1	4	55.50	1.50	10.93
12.75	43.122	60.35	9.99	2.6	10	4.2	5.9	9	57.90	1.50	2.45
12.873	43.122	57.94	11.41	2.6	10	3.15	5.9	7	63.00	1.40	5.06
12.996	43.122	57.60	7.01	8	8	3.3	4.57	8	66.90	1.40	9.30
13.119	43.122	54.60	6.49	8	8	3.6	4.57	4	68.30	1.50	13.70
10.902	43.193	24.00		10	15	4.1	4.6	2	36.30	2.00	12.30
11.025	43.195	24.00		5	10	4.2	4.7	3	34.50	1.90	10.50
12.38	43.21	51.05	2.49	3	9	3.17	4.46	4	132.90	11.60	81.85
12.503	43.211	54.15	17.94	14	16	4.6	5.6	2	51.80	3.70	2.35
12.626	43.211	66.33	13.28	10	16	4.2	5.6	5	56.70	1.80	9.63
12.75	43.212	62.18	7.49	10	10	4.2	5.1	4	60.40	1.50	1.78
12.873	43.212	54.00		2.6	10	3.15	5.9	7	64.90	1.20	10.90
10.899	43.283	24.00		10	15	4.1	4.6	2	35.40	1.70	11.40
11.022	43.285	24.00		5	10	4.2	4.7	3	35.00	1.60	11.00
12.379	43.3	51.32	2.27	3	9	3.17	4.46	4	24.20	5.00	27.12
12.502	43.301	43.29	6.47	3	14	3.76	5.6	6	47.00	3.30	3.71
12.626	43.301	41.18	12.98	8	14	3.4	5.6	4	58.40	1.70	17.22

12.749	43.302	34.00		10	10	4.2	5.1	4	64.50	1.50	30.50
12.996	43.302	88.00		8	8	3.3	4.57	8	66.80	1.30	21.20
12.502	43.391	39.10	1.38	9	10	3.9	4.2	2	49.00	1.70	9.90
12.625	43.392	37.41	2.02	8	10	3.4	4.2	3	60.20	1.90	22.79
12.996	43.392	88.00		8	8	3.3	4.57	8	66.10	2.10	21.90
13.12	43.392	88.00		8	8	3.6	4.57	4	69.60	3.70	18.40
12.377	43.481	49.43	22.07	2	8	3.56	4	2	38.70	2.50	10.73
12.501	43.481	44.97	21.49	2	8	3.56	4	2	45.00	2.10	0.03
10.147	43.538	63.00		10	15	4.1	4.6	2	42.00	4.50	21.00
11.138	43.558	58.00		5	10	4.2	4.7	3	31.30	1.90	26.70
11.261	43.56	58.00		5	10	4.2	4.7	3	33.20	1.90	24.80
12.005	43.568	74.00		10	10	4.4	4.7	2	31.40	2.60	42.60
12.129	43.569	67.41	12.20	10	10	4.4	4.7	2	28.40	1.90	39.01
10.143	43.628	53.72	16.09	10	15	4.1	4.6	2	44.30	3.50	9.42
10.267	43.631	43.24	17.95	10	15	4.1	4.6	2	45.80	3.00	2.56
11.135	43.648	58.00		5	10	4.2	4.7	3	29.40	2.40	28.60
11.259	43.65	58.00		5	10	4.2	4.7	3	32.40	2.00	25.60
12.127	43.659	56.52	13.86	10	10	4.4	4.7	2	34.80	1.70	21.72
12.251	43.66	46.00		10	10	4.4	4.7	2	31.80	2.40	14.20
13.368	43.662	28.00		6	17	3.09	4.6	2	138.20	1.90	69.80
13.492	43.661	28.00		6	17	3.09	4.6	2	134.40	1.60	73.60
10.263	43.721	28.00		10	15	4.1	4.6	2	43.80	2.70	15.80
12.002	43.748	40.00		5	7	4	4.6	4	34.10	1.60	5.90
12.126	43.749	35.10	7.77	7	11	4	4.4	2	40.60	1.70	5.50
12.25	43.75	23.00		7	11	4	4.4	2	35.30	2.20	12.30
13.369	43.752	37.48	32.32	6	17	3.09	4.6	2	137.50	1.70	79.98
13.493	43.752	81.61	38.59	6	17	3.09	4.6	2	131.60	1.10	49.99
11.876	43.837	45.13	12.12	6	7.8	4.2	4.6	4	37.20	1.40	7.93
12	43.838	43.11	14.49	5	7	4	4.6	4	39.60	1.60	3.51
12.125	43.839	24.00		7	11	4	4.4	2	45.90	1.50	21.90

12.249	43.84	23.00		7	11	4	4.4	2	51.10	1.70	28.10
13.494	43.842	99.00		6	17	3.09	4.6	2	131.90	1.00	32.90
11.75	43.926	29.85	1.82	6	15	3.41	4.2	5	36.20	1.50	6.35
11.874	43.927	35.17	12.50	6	15	3.41	4.6	8	40.70	1.50	5.53
11.999	43.929	56.69	16.33	5	7	3.74	4.6	4	45.40	1.50	11.29
10.999	44.006	60.00		5	7	4.2	4.9	2	28.70	2.20	31.30
11.124	44.008	40.00		5	7	4.2	4.9	2	28.90	2.10	11.10
11.249	44.01	31.45	5.47	5	10	4.2	4.7	3	34.30	2.30	2.85
11.373	44.012	26.00		5	10	4.2	4.7	3	38.20	1.90	12.20
11.498	44.013	19.44	4.38	8	9	3.44	4.94	2	33.30	2.00	13.86
11.623	44.015	19.04	4.27	8	9	3.37	4.94	3	31.40	1.70	12.36
11.748	44.016	16.00		6	15	3.41	4.2	5	36.50	1.70	20.50
11.873	44.017	33.00		6	15	3.41	4.6	8	42.20	2.00	9.20
10.122	44.078	17.96	7.79	5.1	10	4.3	5.4	2	54.40	2.90	36.44
10.497	44.086	26.91	15.94	10	15	3.67	4.3	2	46.00	2.20	19.09
10.622	44.089	50.69	21.53	10	16	4.3	4.6	3	37.80	1.80	12.89
10.746	44.091	42.46	17.67	12	16	4.4	4.6	2	34.30	2.00	8.16
10.996	44.096	60.00		5	7	4.2	4.9	2	26.70	1.70	33.30
11.121	44.098	53.47	9.49	5	7	4.2	4.9	2	27.10	1.70	26.37
11.246	44.1	34.69	4.44	5	10	4.2	4.7	2	30.00	1.70	4.69
11.496	44.103	18.93	4.23	8	9	3.44	4.94	2	35.20	2.00	16.27
11.621	44.105	18.79	4.17	8	9	3.37	4.94	3	32.10	2.00	13.31
11.746	44.106	16.00		8	9	3.37	4.94	3	34.60	2.00	18.60
10.118	44.168	16.76	8.24	5.1	10	4.3	5.4	4	49.60	3.30	32.84
10.243	44.171	13.09	6.51	5.1	10	4.3	5.4	4	46.30	2.40	33.21
10.493	44.177	0.45	11.48	14	15	3.57	3.67	2	40.60	2.70	40.15
10.618	44.179	19.67	34.16	12	15	3.57	4.4	3	33.00	2.10	13.33
10.239	44.261	9.00		5.1	10	4.3	5.4	4	43.40	2.40	34.40
10.489	44.267	66.00		14	15	3.57	3.67	2	40.40	3.70	25.60
10.74	44.272	58.00		10	10	4.2	4.6	2	29.20	2.00	28.80

10.865	44.274	27.74	22.54	10	10	4.2	4.6	2	28.90	2.00	1.16
10.99	44.276	13.00		10	10	4.2	4.6	2	27.90	1.80	14.90
11.492	44.283	61.00		8	9	3.44	4.94	2	76.30	4.90	15.30
10.36	44.354	66.00		5.1	10	4.3	5.4	4	45.00	2.90	21.00
10.486	44.357	66.00		14	15	3.57	3.67	2	43.80	3.90	22.20
10.862	44.364	13.00		10	10	4.2	4.6	2	36.90	2.40	23.90
11.489	44.373	61.00		8	9	3.44	4.94	2	101.00	3.00	40.00
9.728	44.428	20.00		6	10.5	3.23	4.6	4	38.30	3.20	18.30
9.854	44.432	20.00		5.1	10	4.3	5.4	4	43.80	3.10	23.80
9.346	44.507	46.00		6	10.5	3.23	4.3	3	28.50	5.10	17.50
9.472	44.511	46.00		6	10.5	3.23	4.6	4	38.00	4.70	8.00
9.724	44.518	20.00		6	10.5	3.23	4.6	4	48.00	2.90	28.00
9.849	44.522	20.00		6	10.5	3.23	4.6	4	46.50	3.00	26.50
9.341	44.597	31.51	13.16	6	10.5	3.23	4.3	3	32.00	5.40	0.49
9.467	44.601	30.88	44.37	6	10.5	3.23	4.6	4	42.50	6.20	11.62
9.593	44.605	112.00		6	10.5	3.23	4.6	4	49.40	4.60	62.60
9.336	44.687	25.15	4.78	0	7	3.23	4	3	45.40	7.70	20.25
9.462	44.691	29.17	58.10	0	8	3.23	4.6	4	53.10	6.40	23.93
9.588	44.695	112.00		0	8	3.23	4.6	4	55.40	4.50	56.60
9.33	44.777	28.00		0	7	3.23	4	3	60.40	8.00	32.40
8.188	44.827	64.00		0	7	3.23	4	3	157.10	9.40	86.90
8.314	44.832	64.00		0	7	3.23	4	3	158.90	7.30	85.10
8.44	44.837	43.00		0	7	3.23	4	3	153.70	8.90	69.30
8.566	44.841	43.00		0	7	3.23	4	3	155.90	11.60	67.10
8.18	44.917	64.00		0	7	3.23	4	3	142.30	13.20	78.30
8.307	44.922	64.00		0	7	3.23	4	3	142.90	10.40	78.90
8.433	44.927	43.00		0	7	3.23	4	3	138.60	10.10	84.40
8.56	44.931	43.00		0	7	3.23	4	3	119.20	10.70	76.20